II INTERNATIONAL CONFERENCE ONRADIOECOLOGICAL CONCENTRATION PROCESSES
II INTERNATIONAL CONFERENCE 50 years later

Persson, Bertil R; Holm, Elis; Garcia-Tenorio, Rafael ; Manjón , Guillermo

2016

II INTERNATIONAL CONFERENCE ON RADIOECOLOGICAL CONCENTRATION PROCESSES

(50 years later)

Seville, Spain, November 2016

BOOK OF PROCEEDINGS

II INTERNATIONAL CONFERENCE ON RADIOECOLOGICAL CONCENTRATION PROCESSES

(50 years later)

Seville, Spain, November 2016

BOOK OF PROCEEDINGS

II INTERNATIONAL CONFERENCE ON RADIOECOLOGICAL CONCENTRATION PROCESSES

(50 years later)

Seville, Spain, November 2016

BOOK OF PROCEEDINGS

Editors:
Rafael Garcia-Tenorio (University of Sevilla)
Elis Holm (University of Gothemburg)
Guillermo Manjón (University of Sevilla)

Conference hosted by Centro Nacional de Aceleradores (CNA), Seville, Spain

INDEX

A9.-Radioactive Contamination Evolution for Thirty Years in Mushrooms Samples Imported by Spain following the Chernobyl Nuclear Accident
M E. Veiga, J Castro and R. Basante (Spain)

A10.-Polonium ^{210}Po and radiolead ^{210}Pb in edible mushrooms collected in Northern Poland
K. Szymanska, D.I. Struminska-Parulska, G. Krasinska, B. Skawercz and J. Falandysz (Poland)

A11.-^{137}Cs Activity Concentration in Potatoes from a Greek Contaminated Area after the Chernobyl Accident
D Dimitrellou and H Papaefthymiou (Greece)

A12.-Uranium (^{238}U) and polonium (^{210}Po) isotopes in mosses and lichens samples From Sobieszewo Island
A.Boryło, G Romańczyk, D. I. Strumińska-Parulska and B. Skwarzec (Poland)

A13.- Uranium in Polish mushrooms from *Leccinum* (Gray) genus
K Szymańska, D I Strumińska-Parulska, B Skwarzec and J Falandysz (Poland)

A14.-Behaviour of ^{137}Cs during biodegradation of contaminated biomass
J. Mihalic, J. Corisco and M.J. Madruga (Portugal)

A15 .-Distribution of the ^{210}Pb and ^{210}Po activity concentration in morphological moss body parts
M. Długosz-Lisiecka (Poland)

A16.- Re-Examination of ^{137}Cs Depth Profiles in Undisturbed Soils in Northern Germany
A. Anesiadou, P. Kaiser, G. Kirchner, M. E. Souti and H. W. Fischer (Germany)

B - Terrestrial-wildlife and food chain

B1.-Analysis and Modelling of Radioecological Concentration Processes in the food chain Lichen-Reindeer-Man
B.R.R. Persson (Sweden)

B2.-Cesium-137 in reindeer and Sami herders- - 50 years of studies
L. Skuterud, M.A. Ytre-Eide, T.H.Hevroy and H. Torring (Norway)

B3.-Radionuclides Accumulation in Antartic Birds
K M. Szufa, J W. Mietelski and A.M..Olech (Poland)

B4.-Summing Internal and External exposures from the Chernobyl Fallout to Hunters Using Regional Ecological Transfer Factors
C L. Rääf, M Isaksson ,M. Jonsson, A.Mamour, M. Tondel and R. Wålinder (Sweden)

B5.-Organ distribution of ^{210}Po and ^{137}Cs in lynx (*Lynx lynx*), wolverine (*Gulogulo*) and wolves (*Canis lupus*)
R: Gjelsvik, E. Holm, J. A. Kålås and B.R.R.Persson (Norway)

C - Terrestrial- Semipalatinsk

C1.-The particle size distribution of radioisotopes in soils at fallout traces of nuclear explosions
A.M. Kabdyrakova, A.T. Mendubaev and S.N. Lukashenko (Kazakhstan)

C2.-Speciation of Artificial Radionuclides in Soils of Semipalatinsk Test Site
A Y. Kunduzbayeva, A.M. Kabdyrakova and S. N. Lukashenko (Kazakhstan)

C3.-Transfer of radionuclides to plants of natural ecosystems at the Semipalatinsk Test Site
N.V. Larionova and S.N.Lukasenko (Kazakhstan)

C4.-Peculiarities of Radionuclides build-up by Fruit and Berry Crops
T.E.Kozhahanov, S.N.Lukashenko and N.V. Larionova (Kazakhstan)

C5.-Investigation of distribution of radioactive contamination in the water objects of the Semipalatinsk test site
A.K. Aidarkhanova and S.N. Lukashenko (Kazakhstan)

C6.-Parameters of transfer $^{239+240}$Pu, ^{241}Am, ^{137}Cs, ^{90}Sr and ^{3}H into body of Farm Animals and Poultry at the Semipalatinsktest site condition
Zh.Baigazinov, S.N. Lukashenko, A Panitskiy, S Karataev, S Baigazy and A Mamyrbaeva (Kazakhstan)

C7.-Assessment of Tritium Distribution and Mechanisms of its Formation in the STS Snowcover
D.Turchenko, S Lukashenko and O Lyahova (Kazakhstan)

C8.-Assessing Distribution of Tritium Speciation in Soils of Radiation Dangerous Sites at the Semipalatinsk Test Site
Z B Serzhanova, A K Aidakhanovav and S N Lukashenko (Kazakhstan)

C9.-Regularities of Tritium Distribution in Soil in Venues of surface nuclear tests in the territory of Semipalatinsk Test Site Territory
L V Timonova, O N Lyakhova and S N. Lukashenko (Kazakhstan)

C10.-Non-Radiation factors of Hazard at STS
V.V. Romanenko, S.B. Subbotin, S.N. Lukashenko and V.I. Suprunov (Kazakhstan)

C11- Results of areal radiological survey of the territory adjacent to the "Atomic lake"
A.O.Aidarhanov, S.N. Lukashenko, M.A. Umarov and Y.Y. Yakovenko (Kazakhstan)

D- Marine

D1.-Concentration of Radionuclides in Marine Organisms
F. P. Carvalho (Portugal)

D2.-Bioaccumulation and trophic transfer in marine food chains – An example from the northern Arabian Gulf
S. Uddin and, M. Behbahani (Kuwait)

D3.-Activity Levels of ^{210}Po in Marine Organisms Consumed in South of Spain
I Diaz-Francés, G Manjón and R García-Tenorio (Spain)

D4.-A New Approach to Process Planktonic Foraminifera for Radiocarbon Measurements
R Guerra, F.J Santos and R García-Tenorio (Italy)

D5.-Pacific Proving grounds radioisotope imprint in sediments from equatorial Western Pacific and Indonesian throughflow
D. Pittauer, S. Tims, P. Roos, M. Froelich, J. Qiao and H.W. Fischer (Germany)

D6.-Health and Environmental Risk Assessment of the Dumped Russian Submarine K-27 in the Arctic
A Hosseini, I Amundsen, J Bartnicki, J E Brown, M Dowdall, J E Dyve, M Karcher, F Kauker, H Klein, O C Lind, B Salbu, R. Schnur and W Standring (Norway)

E - Terrestrial/Marine - Fukushima

E1.-Radioactive and stable cesium isotopes in Fukushima forests
V.Yoshenko, T. Takase, K. Nanba, Y.Onda and A. Konoplev (Japan)

E2.- Effective Half-lives of Radiocesium in Different Japanese Tree Species
K Tagami, S Uchida and NIshi (Japan)

E3.- ^{90}Sr in Japanese soil samples After the Fukushima Nuclear Accident
N. Kavasi, S. K. Sahoo and T. Aono (Japan)

E4.-Behavior of radiocesium from arthropods in different trophic levels after the Fukushima Daiichi Nuclear Power Plant accident: Chronological changes from 2012 to 2015
S. Tanaka, T. Adati, T. Takahashi and S. Takahashi (Japan)

E5.-Measurement of Environmental Radioactivity Using a Cumulative Gamma Radiation Dosimeter: A Challenge in detecting Regional Characteristics of Landscapes
T Yoshihara, ' A Kominato, Y Nagao, N Kawachi, S Hashida, N Suzui, Y Yin and S Fujimaki (Japan)

E6.-Reconstruction of radiocesium levels in Fukushima coastal organisms. Best practice for planning emergency monitoring
Y. Tateda, D. Tsumune and T. Aono (Japan)

E7.-Concentration Ratios of Radionuclides in Marine Organisms around Japan
T Aono, M Fukuda, S. Yamazaki, Y Ito, T Ishimaru and J Kanda (Japan)

F - NORM

F1.-Identification and classification of key processes ruling environmental behaviour of radionuclides released from NORM industry
B. Michalik (Poland)

F2.-Environmental behaviour of radionuclides from uranium mining and milling activities
F.P.Carvalho, J.M.Oliveira and M.Malta (Portugal)

F3.-Dispersion, transfer and Risk of NORM and metals due to construction in U-bearing minerals
L. Skipperud, H-C.Teien, K.E. Tollefsen and F.M. Woersted (Norway)

F4.-Environmental Impact of some NORM Industries in Mexico
D Mandujano-García, M Sosa, J Mantero and R García-Tenorio (México)

F5.-Radioactivity levels in scales generated from crude oil production in Ghanna
R.Garcia-Tenorio, J.Mantero, G.Manjón, I, Vioque and D. Kpeglo (Spain)

F6.-Heavy Mineral Sands Deposits and Accumulation of Radionuclides in Foods
F.P. Carvalho, J.M. Oliveira and M. Malta (Portugal)

G - EMERGING ISSUES
(Hot-particles, New radionuclides, new technologies)

G1.-Particles as concentrated sources related to uptake and radiological dose in mammals
M. P. Johanssen, E. Caffrey, D.P.Child, R. Collins, M.A.C. Hotchicks, N. Howell, T. E. Payne, A. Ikeda-Ohno and L. Mokhber-Shalin (Australia)

G2.-Characterisation of Radionuclides in Uranium Mine Tailings with Synchrotron-based Hard X-ray Microprobe Techniques
S Mihok, K Lange, A Lanzirotti and J Brown (Canada)

G3.-Accelerator Mass Spectrometry (AMS) in Radioecology
M. García-León (Spain)

G4.-^{129}I, ^{236}U, ^{239}Pu and ^{240}Pu profiles in a peatbog from the Southern Hemisphere
E. Chamizo, J M. López-Gutierrez, E. Holm and R. García-Tenorio (Spain)

G5.-Survey of Iodine-129 in soil from South Korea
H Kim, J.M Lim, Y.Y Ji, W Lee, K.H Chung, and M J Gang (Korea)

G6.-First Results of Uranium-236 in the South-Atlantic Ocean
M López-Lora, E Chamizo, O Blinova, M Rožmarić, D. C. Louw and I Levy (Spain)

G7.-^{129}I in the environment
J.M. Lopez-Gutierrez (Spain)

H - Aquatic Systems

H1.-Study of plutonium redistribution in a raised peat bog following a fire.
M. Sáez-Muñoz, E. Holm, J. Mantero, R. Thomas, S. Martorell and R. García-Tenorio (Spain)

H2.-Depth distributions of bomb-derived and Chernobyl-derived radiocesium in sediment sinks and their applications in reconstructing changes in erosion rates
V. Golosov, D. Walling, M. Ivanov and A. Sharifullin (Russia)

H3.- Redistribution of ^{137}Cs from an Ash Landfill to a Nearby lake
S. Erhs, M. Eriksson, S. Eriksson, P. Andersson and M. Huss (Sweden)

H4.-Uranium Concentration in the Sandy-Clayey Aquifer
A.Marlov (Russia)

H5.-Factors influencing the distribution of weapon-test plutonium alpha-emitters on the whole-basin of a lake
I. Vioque, G. Manjón and R. García-Tenorio (Spain)

H6.-^{210}Pb and ^{137}Cs as tracers of recent sedimentary processes in two tropical water reservoirs
M. Diaz-Asencio, J.A. Corcho, H. Cartas, A.Pulido, C. Betancourt, E.Alvarez, Y. Labaut, C. Alonso-Hernández and M. Seisdedo (Cuba)

H7.-^{226}Ra, ^{228}Ra, ^{40}K and ^{137}Cs Activity Concentrations in a sediment core of a Reservoir Affected by Acid Mining Drainage
E.G. San Miguel, C.R. Cánovas, M. Casas-Ruiz and J.P.Bolívar (Spain)

H8.- Distribution coefficients water sediment for uranium and polonium in the Moulouya River (eastern Morocco), a river affected by abandoned mines of lead and zinc
J. Galván, I. Diaz, G.Manjón, J.Mantero, I.Vioque, S. Chakiri and R. García-Tenorio (Spain)

H9.-Evidence of Change in ^{210}Pb Atmospheric Flux in the Oualidia Lagoon Inferred from Sediment Radiometric Dating
A Laissaoui, N. Mejjad, O. El Hammoumi, A. Benkdad, A. Fekri and M. Ghazi (Morocco)

H10.-^{234}Th as a proxy for determination of scavenging rates in a Coastal zone: its measurement with a proportional counter
E. Cuesta, R.L. Lozano, E.G. San Miguel, M. Casas-Ruiz and J. P. Bolívar (Spain)

H11.- ^{222}Rn concentrations and disolved ionic species in spring wáter from an arid región at the east of Chihuaua, Mexixo
A.Cervantes-Trejo, A. Covarrubias, A. Pinedo, G. Manjón and M. Rentería (Mexico)

H12.-Behaviour of Natural radionuclides in the karst aquifer system of sierra de Gádor (Almeria, SE Spain)
J. L. Guerrero, A. Vallejo, J C Cerón, F. Martos, A. Pulido and J. P. Bolívar (Spain)

I - Atmosphere

I1.-EURDEP and REMdb tools for the sake of Radioecological science opportunities
M.A.Hernandez-Ceballos, K. Bogucarskis, T. Tollefsen, G. Cinelli, L. de Felice, E. Nweke, P.V. Tognoli, S. Vanzo and M. de Cort (Italy)

I2.- Deposition Patterns of Atmospheric ^{7}Be, ^{210}Pb, and ^{40}K in Coast of West Mediterranean Sea, Malaga, Spain
C. Dueñas, E. Gordo, S. Cañete , E. Liger, M. Pérez and M. Cabello (Spain)

I3.-Winter Extremes of Beryllium-7 Surface Concentrations in Northern Europe
J Ajtic, V Djurdjevic, M A. Hernández-Ceballos and E Brattich (Serbia)

I4.-Events Affecting Levels of Gross Alpha and Gross Beta Activities and Heavy Metals Composition of Airborne Particulate Samples
E Liger, C Dueñas, E Gordo, S Cañete, M Cabello and M Pérez (Spain)

I5.-Soil CO_2 Monitoring under a Cool-Temperate Forest Site in Winter in Hokkaido, Japan
T Nakamura, K Okamoto, K Umegaki and R Fujiyoshi (Japan)

J - Modelling

J1.-An overview of marine modelling activities in IAEA Modaria program: lessons learnt from the Baltic Sea and Fukushima scenarios
R. Periañez, R. Bezhenar, I.Brovchenko, C. Duffa, M. Iojspe, K.T. Jung, T. Kobayashi, F. Lamego, V. Maderich, B.I.Min, H.Nies, I. Osvath, I. Outola, M. Psaltaki, K.S. Suh and G. de With (Spain)

J2.-Radioecological Informatics and Modelling of Polonium-210 and Caesium-137 in top pedrators
B.R.R.Persson, R.Gjaelsvik, J.A. Kalas, J. Asbrink and E. Holm (Sweden)

J3.-Considerations of application of ecological thermodynamics to radionuclide transfer parameters
V. Kangasniemi and A.T.K. Ikonen (Finland)

J4.-Implementation of a food chain sub-module into a model for radioecological assessments in the coastal waters around Iceland
M. Iosjpe, M. Isaksson, R. Thomas, O. Halldorsson, P. Roos, K. Logemann, G. Jonsson, H.P. Joensen and V. Soulanen (Norway)

J5.-Radioecological sensitivity of Aegean Sea
G. Eleftheriou and M. Iojspe (Norway)

J6.-A Three-Dimensional Numerical Model Describing the ^{137}Cs Behaviour in Coastal Waters: Model Verification and Validation
V Bacchi and P Tossi (France)

J7.-Modeling ^{131}I distribution in a tidal river
M.E. Souti and H.W. Fischer (Germany)

J8.-Comprehensive and Systematic Knowledge Quality Assessment as a Tool for Model Qualification
A. T. K. Ikonen and V Kangasniemi, (Finland)

J9.- Developing operational models to trace marine radioactive contamination of lower- and mid-trophic level organisms
I.Senina, P. Lehodey and A. Cochon (France)

J10.- New approach for simulation of particle dynamics and trace metal interactions in the ocean
E. Ceballos-Romero, M. Villa and F. de Soto (Spain)

K - Radiochemistry and Instrumentation

K1.-Application of modern AC system in HPGe γ-spectrometry for the detection limit lowering of the radionuclides in air filters
M. Długosz-Lisiecka (Poland)

K2.-Fully Automated System for Monitoring ^{99}Tc in Radioactive Residues Using a Selective Resin and UV-Vis On-Line Detection
M Villar, A Borràs, F Vega, V Cerdà and L Ferrer (Spain)

K3.-Study of the Dynamic Lixiviation of ^{226}Ra from Phosphogypsum by an Automatic System Previous Radiometric Detection
M Rodas, A Borràs, R. García-Tenorio, J M Estela,V Cerdà and L Ferrer (Spain)

K4.-Sedactiv 1.0: A Cosmic Veto Gamma Spectrometry Setup for Sediment Samples
D Pittauer, D Höweling, M Pérez Mayo, B Hettwig and H W. Fischer (Germany)

K5.-Testing a CeBr$_3$ γ ray Spectrometer for Radiological Environmental Monitoring
R Idoeta, M Herranz, N Alegria and F Legarda (Spain)

K6.-Evaluation of radiochemical methods for Thorium Isotopes Determination in Environmental and Industrial Samples by Alpha-Spectrometry
J.C.Lozano, M.Herranz, J.P.Bolívar and R.García-Tenorio (Spain)

L - Miscellaneous

L1.- Aspects of caesium-137 transport by microalgae *Chlamydomonas reinhardtii* related with potassium
J A Gil Corisco (Portugal)

L2.-Influence of Radioecological Parameters on the Dose Rate in Urban Environments After a Release of Radioactive Substances
Y Hinrichsen (Denmark)

L3.-Analysis of Transgenerational alterations in Mitochondrial Activity in three generations of Crustacean *Daphnia Magna* flowing acute parentalexposure to γ-Irradiation
E.Sarapultseva, D.V. Uskalova and N.B. Savina (Russia)

L4.- Plant Bioassays for Environment Monitoring Around Facilities for Radioactive Waste Treatment
A A Oudalova, S A Geras'kin, S V Pyatkova and S M Kiselev (Russia)

L5.-Polonium ^{210}Po and radiolead ^{210}Pb in calcium and magnesium supplements
D. I. Strumińska-Parulska and B. Skwarzec (Poland)

L6.-How to get 16-19 years old students interested in radiation physics
P Törnquist, H B.L. Pettersson (Sweden)

M – LAST SUBMISSIONS

M1.- The dissolved polonium in groundwaters from spas of southeast Brazil
D.M. Bonotto and A.M.M. Oliveira (Brazil)

M2.- Measurement of ^{236}U at the GEOTRACES East Pacific Zonal Transect
M. Villa, E.Chamizo, M. Lopez-Lora, T. Kenna, N. Casacuberta, P. Masqué and M. Christi (Switzerland)

M3.- Levels of natural radionuclides in water and sediments from mining lakes in Sweden
J. Mantero, R. Thomas,M. Isaksson, C. Rääf, S. Perez-Moreno, E. Forssell-Aronsson, E. Holm and R. García-Tenorio (Spain)

II International Conference on Radioecological Concentration Processes (50 years later)

Seville, 6th-9th November 2016

Editorial

R.García-Tenorio[1]*, E. Holm[2] and G.Manjón[1]

[1]University of Seville, Department of Applied Physics, ETSA, Avenida Reina Mercedes 2, 41012 Seville, Spain
[2]Department of Medical Radiation Physics, Gothenburg University, Gothenburg, Sweden

Abstract

In this editorial a summary of the main contributions and outcomes of the conference celebrated in Seville about Radioecological Concentration processes during six intense sessions is given. It was quite remarkable in addition to the good quality of the communications presented, the active participation of the delegates and the good working atmosphere created during the conference as well as the participation of a good set of young researchers that will construct the future of the radioecology. In addition, it was possible to obtain as a main conclusion of the conference that the radioecology is in good health with a set of emerging new topics under development.

Introduction

From the 6th to the 9th of November 2016, in the meeting hall of Centro Nacional de Aceleradores (University of Seville, Seville, Spain) took place the "II International Conference on Radioecological Concentration Processes (50 years later)" under the joint organization of the Universities of Seville (Spain) and Gothenburg (Sweden). With this event, the organization try to commemorate the fifty years anniversary of the first Radioecological Concentration Processes Conference hold in Stockholm, which is recognized as an extremely important event which contributed to the birth of the modern radioecology: In the pioneer 1966 conference, more than 100 communications were presented and a good number of participants played afterwards an essential role in the development and growing of the radioecology as scientific discipline.

The first conference had as a main motivation the dissemination of the radioecological studies appearing at that time associated to the nuclear weapon tests performed by USA and the former USSR at the end of the 1950s or beginning of the 1960s. Since then, a lot of anthropogenic emissions of radioactivity (provoked or accidental) have occurred, being remarkable at the dates of this II edition the 30 years passed since the Chernobyl accident and the 5 years passed from the Fukushima accident. In addition, the emergence of new analytical techniques has made possible to extend the radioecological studies to new radionuclides and environmental compartments.

With this II edition of the Conference, the promotors have tried to obtain information about the actual status of the radioecology over the world, to evaluate the advances reached during the last years and to plan the development of some priority research lines to be followed along the first half of the XXI century. Just thinking in the future of the radioecology, special efforts were devoted to stimulate the active participation, through presentation of communications, of young researchers.

---

*Corresponding author, E-mail: gtenorio@us.es

The response of the radioecology community to the conference can be qualified as very positive. A total of 152 delegates coming from 35 different countries participated in the conference in a very active way because more than 160 communications were presented, distributed in 6 intense sessions. A total of 6 invited lectures, 40 oral presentations and 120 poster communications formed the scientific program of the conference.

The scientific content of the Conference

Between the invited lectures presented we can start the presentation of the scientific content of the conference by highlighting two of them. The first one was given by professor Elis Holm (Sweden) presenting an evaluation of the radioecological studies performed at the time of the first edition of the conference, 50 years ago, and remarking some pioneer radioecological studies performed at these dates, while the second one was given by Professor Francois Brechignac (France), secretary of the International Union of Radioecology (IUR), which exposed the perspectives and priority lines to be followed by the Radioecology in the XXI century: The past and the future of the radioecology was then exposed, immersed in a huge number of communications that have allowed to obtain a well-defined picture of the actual status of this scientific discipline.

As anecdotic information, we can indicate that in this II edition have participated two delegates that attended and presented communications in the Ist edition: Professors Rudolph Alexakhin (Russia) and Bertil Persson (Sweden). Both delegates, in several speeches distributed along the conference, transmitted to the participants, and based in their experience, their vision about the actual situation of the radioecology and the main problems that have this discipline nowadays.

The communications presented at the conference can be classified in different sections according with their thematic, doing easier their exposition and discussion. In each section the more representative communications (from the point of view of the authors of this document) will be shown, trying to remark emerging research lines existing nowadays.

Obviously in the conference were presented communications that can be put in the frame of historically well-defined lines of research in radioecology: Works analyzing radionuclides transfer soil-plant in ecosystems or contaminant situations not well analyzed until now, works analyzing transfers to the trophic chain and to the wildlife, etc were presented and the main contributions are compiled in Table 1.

Tabla 1	First Author
Analysis and modelling of radioecological concentration processes in the food chain lichen - reindeer – man	Bertil Persson (Sweden)
Comparison of radiocesium root uptake by leguminous andnon-leguminous herbaceous plants	Shigeo Uchida (Japan)
Transfer parameters for ICRP´S reference animals and plants in terrestrial mediterranean ecosystems	F.Javier Guillén (Spain)
TJØTTA – ICRP reference site in Norway	H.Torring (Norway)
Assessment of anthropogenic radionuclides in tundra of high arctic environment	A.Cwanek (Poland)
Caesium-137 in norwegian reindeer and sámi herders – 50 years of studies	L. Skuterud (Norway)
Radionuclides accumulation in antarctic birds	K.M. Szufa (Poland)
Organ distribution of ^{210}Po and ^{137}Cs in lynx (*Lynx lynx*), wolverine (*Gulogulo*) and wolves (*Canis lupus*)	R. Gjesvik (Norway)
Concentration of radionuclides in marine organisms	F.P.Carvalho (Portugal)

In this section can be located also the elevated number of communications presented in association with the Fukushima accident. Within this frame about 30 communications (the majority lead by the 20 Japanese scientists attending to the conference) were presented with contributions in the fields of terrestrial and marine radioecology as well as evaluating the impact of the accident in the wildlife. Some of these works are compiled in Table 2.

Table 2	Main Author
Land use, Controls Fate and Transport of Radionuclides in Fukushima in the terrestrial environment	Y. Onda (Japan)
Radioactive and stable cesium isotopes in Fukushima forests	V. Yoshenko (Japan)
Effective half-lives of radiocesium in different Japanese tree species	K. Tagami (Japan)
Radiostrontium isotopes in Japan after the Fukushima nuclear accident	N. Kavasi (Japan)
The impact of recent releases from the Fukushima nuclear accident on the marine environment	N. Cascuberta (Switzerland)
Reconstruction of radiocesium levels in Fukushima coastal organisms: best practice for planning emergency monitoring	Y. Tateda (Japan)
Bioaccumulation of radiocesium in marine fish; pre- and post- Fukushima data records	M. Johanssen (Australia)
Distribution of $^{239+240}$Pu concentrations and ^{240}Pu/^{239}Pu atom ratios in surface seawaters of theNorth Pacific Ocean	M. Yamada (Japan)
Concentration ratios of radionuclide in marine organisms around Japan	T. Aono (Japan)
Behaviour of radiocesium from arthropods in different trophic levels after the Fukushima power plant accident: chronological changes from 2012 to 2015	S. Tanaka (Japan)
Dosimetry method of animals affected by Fukushima Nuclear Plant accident	G. Hayashi (Japan)

The radioecological studies associated to ecosystems affected by nuclear accidents or contaminated by weapon tests were not only centered in the previously detailed, associated to the Fukushima accident. They were also presented, for example, studies in areas affected by the weapon tests carried out in the Pacific by USA in the years 1950-60 and in zones affected by Bristish nuclear weapon tests in Australia, as well as it was presented the evaluation of the impact generated in their surroundings by a nuclear submarine dumped in the Artic Ocean. Some of these works are compiled in Table 3.

In this Table are also compiled 3 or the 15 presented radioecological works carried out in Semipalatinsk (Kazakhstan), region where the former Soviet Union carried out an elevated number of atmospheric and underground weapon tests. In the conference a complete description of the radiological works carried out by Institute of Radiation Safety and Ecology, Kurchatov, Kazakhstan (leaded by Prof. Lukshenko) was disseminated being presented for the first time for example hundreds of results concerning transfer soil to plant in Semiplatinsk and the results obtained in the same area about the distribution of the antropogenic contamination remaining in the soils of the contaminated area as a function of the grain size.

Table 3	Main autor
A Comparison of remediation strategies after the Kyshtym, Chernobyl and Fukushina Daiichi accidents	**S. Fesenko (IAEA)**
Pacific proving grounds imprint in the Indonesian throughflow sediments	**D. Pittauer (germany)**
Health and environmental risk assessment of the dumped Russian submarine K-27 in Arctic	**A.Hosseini (Norway)**
Distribution of artificial radionuclides in particle-size fractions of soil on fallout plumes of nuclear explosions	**Kabdyrakova (Kazajistan)**
Transfer of radionuclides to plants of natural ecosystems at the Semipalatinsk Test Site	**Larionova (Kazajistán)**
Parameters of radionuclides transfer into bodies of wild animals inhabiting nuclear weapons testing venues	**Panitskiy (Kazajistán)**

During the conference, on the other hand, it has been evidenced clearly the existence of a series of emerging working lines in the field of radioecology. These emerging lines are the following:

a)Radioecology and NORM. Once the dosimetric studies designed and performed to evaluate the occupational and public doses associated to the extraction (mining) or the processing (industries) of NORM materials (materials enriched in natural radionuclides) have been established, are growing the studies devoted to the evaluation of the radioactive impact due to the mentioned mining and industrial activities in their surrounding environmental compartments. The existence in these cases of a radioactive contamination source that can be quite well characterized, is allowing to gain much information about the behavior of several natural radionuclides in the environment.

In this emerging research line an elevated number of communications have been presented. Some of the most representative ones are compiled in Table 4. These studies have not been limited exclusively to evaluate the environmental radioactive impact generated by the traditional mining of uranium, being also analyzed the environmental radioactive impact due to some non-uranium NORM industries such as the devoted ones to the production of phosphoric acid or to the extraction and processing of oil and gas . In addition it has been also analyzed the environmental radioactive impact due to the performance of big civil constructions (a traffic tunnel for example) in an area enriched in natural radionuclides.

Table 4	Main Author
Environmental behaviour of radionuclides from uranium mining and milling activities	**Oliveira (Portugal)**
Uptake of natural radionuclides to edible vegetables from contaminated soil	**Smodis (Slovenia)**
Dispersion and Transfer of NORM & metals due to construction in U-bearing minerals	**Skipperud (Norway)**
A review on the natural radionuclides behaviour in an estuary affected by mining activities and fertilizers industries; the case of "Ría de Huelva"	**Bolivar (Spain)**
Environmental impact of some NORM industries in Mexico	**Mandujano (Mexico)**
Radioecological and Environmental impact of produced water discharged from a shallow water offshore petroleum field	**Kpeglo (Ghana)**

b) Radioecology and hot-particles: It is well known by the scientific community working in radioecology the fact that in defined zones of the world affected by nuclear accidents, controlled releases or weapon tests, the existing radioactive contamination is present mostly in particulate form. In many cases, these particles have a refractory behavior being inhibited the transfer of radionuclides to the surrounding environmental compartments.

A proper evaluation of the radioecological behavior of this form of radioactive contamination needs of a detailed knowledge of the composition, morphology and chemical state of these particles, known commonly as "hot particles". These particles can be found in areas affected by the Chernobyl accident, in areas affected by nuclear weapon tests (Semipalatinsk, Nevada, Maralinga, etc), in areas affected by the accidental dispersion of Pu due to aircrafts accidents (Palomares, Thule), in releases from nuclear reprocessing plants (Sellafied, Dounrey,Mayak, etc) and even in some releases of NORM industries.

In this conference have been presented several communications related to radioactive particles, being the most representative ones compiled in Table 5. Between them, we can highlight, a) the invited lecture given by Prof. Brit Salbu (Norway) where the challenges associated to the presence of radioactive particles in the environment were presented and discussed, and b) the communication presented by Dr. Ole-Christian Lind (Norway) about the impact in biota of these particles, in particular when are incorporated by ingestion.

Table 5	Main author
Challenges associated with radioactive particles in the environment	**Salbu (Norway)**
Particles as concentrated sources related to uptake and radiological dose in mammals	**Johansen (Australia)**
Retention of particle associated radionuclides in biota	**Lind (Norway)**
Hot particles studies by ion beam analysis (IBA) techniques and accelerator mass spectrometry (AMS) at CAN	**Jimenez-Ramos (Spain)**
Characterization of radionuclides in uranium mine tailings with synchrotron based hard X-ray microprobe techniques	**Mihok (Canada)**

C) Radioecology, new analytical techniques and new radionuclides: The consolidation of two mass spectrometric techniques, the accelerator (AMS) and the high resolution inductively coupled (ICPMS-HR) mass spectrometric techniques have allowed to reach limits of detection so low than new anthropogenic radionuclides with very long half-lives can be evaluated wit high precision in several environmental compartment, opening new research lines in radioecology. Communications centered in the determination of radionuclides such as I-129, U-236, Np-237, etc in several environmental compartments have been presented in the conference, and are compiled in Table 6. Radionuclides as I-129 and U-236 are starting to play a relevant role in fields such as Oceanography due to its conservative behavior and because their main sources are known with enough detail.

In this subject, we can highlight the communication presented by Prof. García-León (University of Seville). In this communication it was performed a detail evaluation of the role of the Accelerator Mass Spectrometry Technique (AMS) in Radioecology, showing as examples some relevant works done recently in Radioecology with basis in the use of AMS.

Tabla 6	Main Author
Accelerator mass Spectrometry (AMS) in Radioecology	**García-León (Spain)**
^{129}I concentrations in the south hemisphere: North Atlantic versus Southern Ocean	**Lopez-Gutierrez (Spain)**
Analysis of Pu isotopes and Np-237 in seawater by AMS	**Levy (IAEA)**
Iodine-129 in soil from Korea	**Kim (South Korea)**
First results of Uranium-236 in the South-Atlantic Ocean	**Lopez-Lora Spain)**
^{135}Cs activity and ^{135}Cs/^{137}Cs atomic ratio in Japanese environmental samples before and after the Fukushima Daiichi Nuclear Power Plant accident	**Yang (Japan)**
Measurement of ^{236}U at the Geotraces East Pacific Zonal Transect	**Villa (Spain)**

On the other hand, in the conference were presented communications related with the use of natural and/or artificial radionuclides in sedimentological studies and in the estimation of erosion rates. ^{210}Pb, ^{137}Cs and $^{239+240}$Pu profiles in lacustrine and marine sediment cores have been used as essential tools to establish sedimentation rates in the analyzed ecosystems and to evaluate for example in them the evolution of contaminants such as metals and pesticides during the last 50-100 years, while determinations of artificial radionuclides with different sources (fallout, Chernobyl, Fukushima) in various terrestrial systems have allowed to show the utility of these radionuclides to

evaluate erosion rates and redistribution of particulate matter. Representative communications in this research line have been compiled in Table 7, together with other communications showing the role of different natural and artificial radionuclides as tracers of atmospheric processes.

Table 7	Main Author
Depth distributions of bomb-derived and Chernobyl-derived radiocesium in sediment sinks and their application in reconstructing changes in erosion rates	Golosov (Russia)
Cesium-137 wash-off associated with soil erosion on various land uses in Fukushima	Wakiyama (Japan)
Factors influ encing the distribution of weapon-test plutonium alpha emitters on the whole basin of a lake	Vioque (Spain)
Records of plutonium fallout in tropical coastal marine sediments	Corcho (Switzerland)
Atmospheric Deposition Flux of radioisotopes in Krakow, southern Poland during years 2005-2015.	Nalichowska (Poland)
[7]Be activity concentration during heatwave events in Spain	Hernandez (EU)
Events affecting levels of gross alpha and gross beta activities and heavy metals composition of airborne particulate samples	Liger (Spain)
Winter extremes of berylium-7 surface concentrations in Northern Europe	Ajtic (Serbia)

We will finish indicating that a big fraction of the experimental work carried out in Radioecology are focused to obtain parameters, transfer coefficients and concentration factors to be implemented in models which are developed to study the dispersion, behavior and routes followed by the radionuclides in different environmental compartments. For that reason, a conference in Radioecology cannot be considered complete if there are not included communications devoted to show the advances in modeling and the results obtained through their application. Some communications compiled under the epigraph of Modeling are indicate in Table 8, being particularly interesting to highlight the work presented by Dr. Periañez summarising the results obtained in the implementation of various radioecological models developed by the scientific community for studying the dispersion of contaminants in the marine environment. The results obtained through the application of these models to the study of the dispersión of ^{137}Cs in the Pacífic due to the Fukushima accident has shown the necessity to increase the efforts in an improvement and validation of the models, and to enhance the coordination between the modelers and experimentalists.

Table 8	Main Author
Overview of marine modelling activities in IAEA Modaria Program: Lessons learn from the Baltic Sea and Fukushima Scenarios	Periañez (Spain)
Implementation of a food chain sub-module into a model for radioecological assessments in the coastal waters around Iceland: effects on kinetic modelling of bioaccumulation processes.	Iojspe (Norway)
Considerations of application of ecological thermodynamics to radionuclide transfer parameters	Ikonen (Finland)
Modelling of Cs-137 input into the sediment and its vertical distribution within the sediment of a shallow eutrophic lake.	Putyrskaya (Germany)

Dissemination of the communications presented in the Conference

Once the conference has finished, the promoters have had in front of them one final task: the dissemination of the main results and works presented in the conference.

The book of proceedings that the reader has now in his hands is the first product generated. This book is edited by the University of Seville, Department of Physics, in paper and electronic versions, being formed for around 100 extended abstracts (maximum 8 pages including tables and figures)

In addition, a special issue devoted to the conference will be published in the international journal more representative in radioecology: Journal of Environmental Radioactivity (Elsevier). This special issue will be formed by near 20 papers corresponding to different communications presented in the conference. With this special issue, we pretend to transmit to the scientific community and to future generations a picture about the status of the Radioecology 50 years after the celebration of the pioneer first edition of the Radioecological Concentration Processes Conference.

A – TERRESTRIAL

Tjøtta – ICRP Reference site in Norway

H. Thørring[*], J. E. Brown and A. Hosseini

Norwegian Radiation Protection Authority, P.O. Box 55, NO-1332 Østerås, Norway

Abstract

An ICRP reference site in Norway has been identified and described, namely the island of Tjøtta in the northern part of the country. The data gathered concern all 12 ICRP Reference animals and plants (RAPs), including different life-stages for frogs (eggs, tadpoles and juvenile/adult frogs). The data presented concern whole-body concentration ratios (CRs) for up to 54 stable and radioactive elements in selected RAPs from all three ecosystems specified by the ICRP – terrestrial, freshwater and marine.

Introduction

The ICRP system for environmental protection is centred on the concept of "Reference Animals and Plants" (RAP) (ICRP, 2008). These are essentially a limited number of animals and plants to be used as the basis for systematically relating exposure to dose, and then dose (or dose rate) to different types of effect, for organisms that are characteristic of different types of natural environments. The ICRP have also selected a number of radioisotopes of 40 elements that have originally been considered priorities for collation of data (ICRP, 2009).

To ensure internal consistency in relation to derivation of element specific transfer, it was recommended that smaller 'Reference sites', in different countries, should be identified – where samples of RAPs, and their different life stages, should be collected and analysed (ICRP, 2009).

The aim of the present work, in the project "TRAP", was to:
- Identify and describe a suitable reference site in Norway
- Identify species that may represent RAPs
- Sample RAPs, including life stages as far as practicable and environmental media for the organisms' habitat with a view to covering terrestrial, marine and freshwater ecosystems
- Analyse stable elements in RAPs (including accumulating organs/body parts and gonads where practicable) and environmental media in accordance with the prioritized list specified by the ICRP
- Derive whole body CRs accounting for factors such as home range where appropriate

Materials and Methods

Reference site and sampling
Tjøtta was selected as a suitable reference site in Norway based on previous studies in connection with Chernobyl fallout in the area. The presence of a local research centre including an agricultural meteorological station was also considered an advantage particularly in relation to sampling / fieldwork. Tjøtta is an 11.3 km^2 island in the municipality of Alstahaug in Nordland County. The island is rather flat, with the highest point being Kalvberghaugen (77 m). The area is well mapped

---

[*] Corresponding author, e-mail: havard.thorring@nrpa.no

and comprises of agricultural and pasture land, marshland, other open areas, and forests – mainly deciduous or mixed (Fig.1, area A). Several lakes and ponds are also found on the island – the largest being the shallow lake Storvatnet. At Tjøtta, suitable candidates were found for all RAPs except Trout (*Salmonidae*). Therefore, an additional river reference area in the same municipality (Alstahaug) was included to cover the whole RAP spectrum (Fig. 1, Area B). This river is 4–10 m wide with deep pools and small waterfalls, and originates in the "Seven Sisters" mountains, flowing through marshlands, mixed forest and agricultural areas.
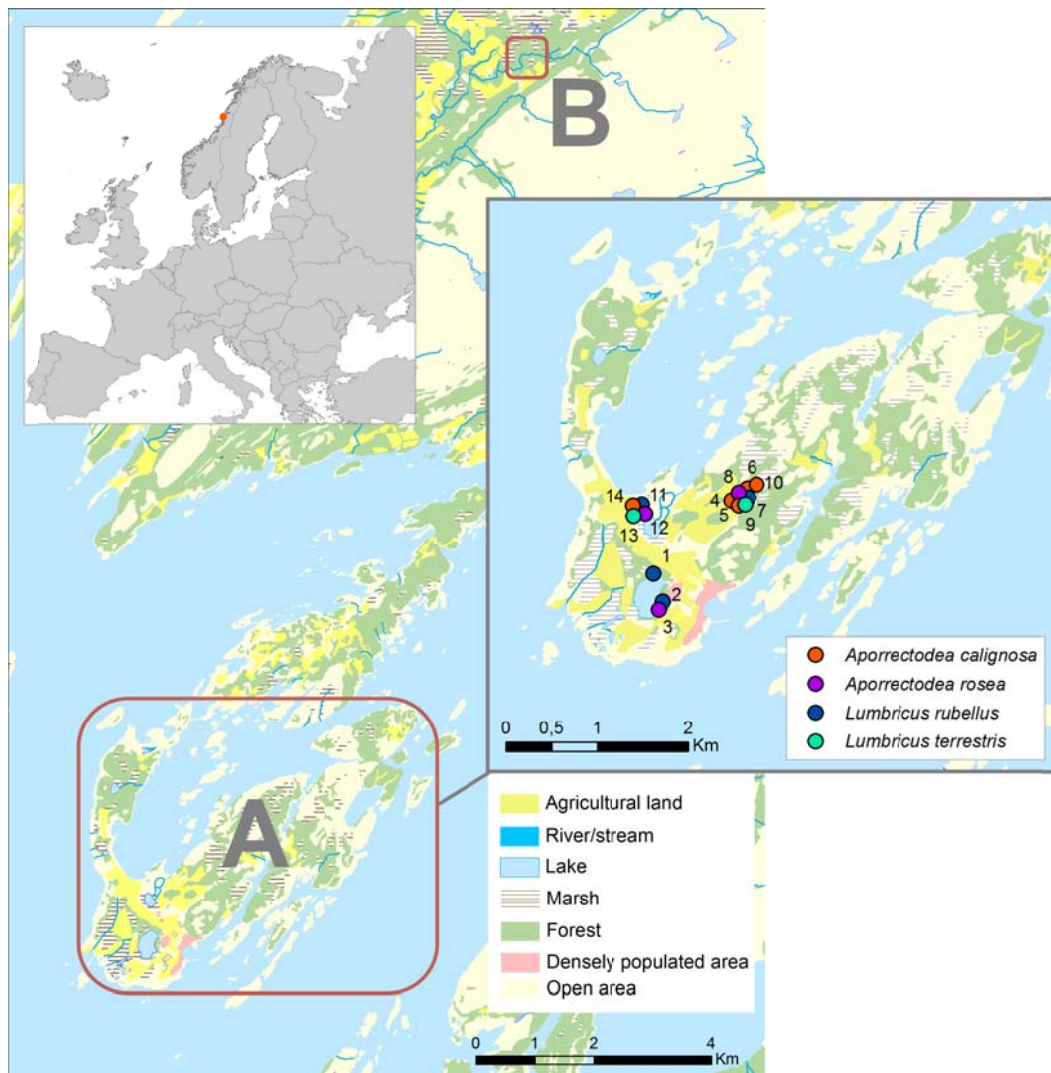
Figure 1. *The two areas constituting the Tjøtta reference site. Sampling localities shown for earthworms (example).*

All sampling was done in 2011–2012. At different locations within areas A and B, an appropriate number of specimens/samples of biota, representing each of the 12 RAPs, were collected along with corresponding samples of soil, freshwater or sea water (depending on type of RAP). Around 10 specimens or composite samples were gathered for each RAP (earthworm localities are shown in Fig. 1, as an example). For frogs, spawn of eggs and tadpoles were also considered in addition to juvenile/adult frogs. In general, muscles (M), bone (B), liver (L) and gonads (G) were sampled from individual vertebrates. From crabs, all soft tissues (including claw muscles) were pooled and referred to as "soft tissue" (ST) samples, and the carapace plus parts of shells from claws and legs were categorised as "hard tissues" (HT) samples. The various species sampled are summarised in Table 1.

Table 1. *Overview of species sampled in the TRAP project*

Ecosystem	RAP (Family)	Species (Latin)	Species (English)
Terrestrial	*Poaceae*	*Deschampsia flexuosa*	Wavy hair grass
	Pinaceae	*Picea sitchensis*	Sitka spruce
		Pinus sylvestris	Scots pine
	Lumbricidiae	*Lumbricus rubellus*	Red earthworm
		Aporrectodea rosea	Rosy-tipped worm
		Aporrectodea calignosa	Grey worm
		Lumbricus terrestris	Common earthworm
	Apidea	*Apis mellifera*	Western honey bee
	Muridae	*Mus musculus*	House mouse
	Cervidae	*Alces alces*	Moose
Freshwater	*Anatidae*	*Anas crecca*	Eurasian teal
		Anas platyrhynchos	Mallard
		Aythya fuligula	Tufted duck
	Ranidae	*Rana temporaria*	Common frog
	Salmonidae	*Salmo trutta*	Brown trout
Marine	*Fucaceae*	*Fucus vesiculosus*	Bladder wrack
	Cancridae	*Cancer pagurus*	Edible crab
	Pleuronectidae	*Pleuronectes platessa*	Plaice

Sample treatment and quantitative analyses

Plants and brown algae were dried (50 °C, 2 days), and subsequently homogenised using a mill/grinder. The rest of the biota samples were freeze-dried. Each individual dried sample was homogenised using a mill/grinder, kept separate in terms of location/specimen and – where applicable – type of organ. Soil samples comprised of the upper 0–10 cm layer. For each locality, one composite sample was prepared by mixing five sub-samples of soil. The wet soil samples were dried (40°C, 4–6 days – depending on moisture content), homogenised and sieved (2 mm). pH and LOI (loss on ignition) were determined. Regarding freshwater and seawater, three samples were mixed to a pooled sample per locality. A small portion of the bulk sample was taken out for measuring pH and salinity (seawater) and conductivity (freshwater). The remaining part of the bulk sample was vacuum filtered (0.45μm), and acidified (pH <2) for conservation.

Approximately 0.25 g sample material was digested in nitric acid (ultrapure) under high pressure and temperature using an UltraClave. All soil and biota samples were diluted – using deionised water from a MilliQ apparatus – to 0.6M HNO_3. Water samples were acidified to a total strength of 0.1M HNO_3 using concentrated nitric acid (ultrapure). All samples were analysed by sector field inductively coupled plasma mass spectrometry (ICP-MS). The elements determined are shown in Figure 2.


Figure 2. *Elements, shown in red, determined using ICP-MS. Bold font elements are those on the ICRP list. Ir and Pt were generally below detection limit and are therefore shown in grey.*

Grass (*Poaceae*), pine (*Pinaceae*), bees (*Apidea*) and soil samples were also analysed using HPGe gamma spectrometry to determine radionuclides such as ^{137}Cs, ^{40}K and ^{226}Ra. To allow for ingrowth of ^{222}Rn and progeny in connection with Ra determination, containers were sealed using aluminium foil and left for 3 weeks prior to radionuclide determination.

Further treatment of data

For vertebrates, element concentrations in muscle, bone and liver were used to derive whole-body concentration ratios (CR)[1]. The contribution of different organs/tissues to CR for different elements were also determined. In most cases, one sample of a particular RAP was linked with a soil or water sample from a specific locality. However, for some of the RAPs soil or water data from more than one locality had to be used for all individual samples – e.g. to reflect large home ranges as in the cases of Moose (*Cervidae*) and Bees (*Apidae*).
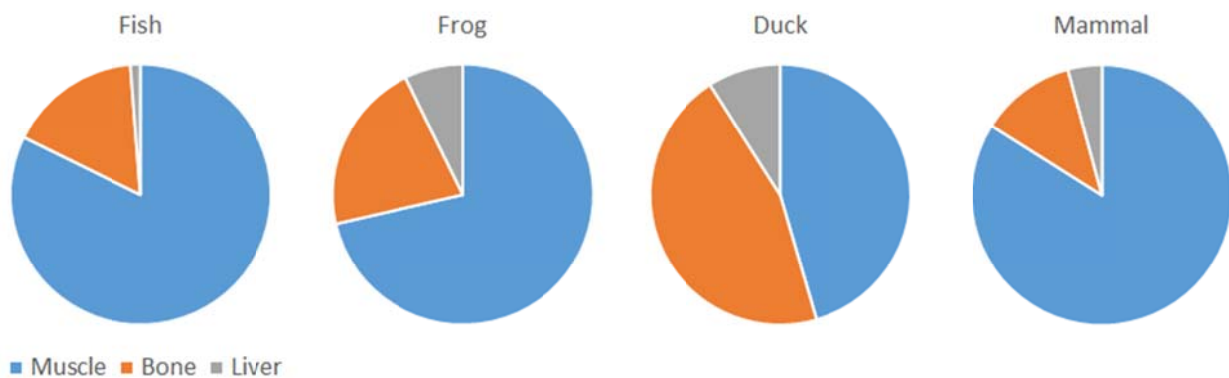
Figure 3. Relative mass of organs or tissues used to estimate the whole body concentration in vertebrates

Results and Discussion

All results from TRAP are available in the report by Thørring et al. (2016). In the following, a few examples will be provided – two from each type of ecosystem (i.e. terrestrial, freshwater and marine). For the sake of simplicity, geometric means (GM) and geometric standard deviations (GSD) have been used throughout. Detailed discussions on findings or identification of important parameters for CR variability etc. are beyond the scope of the present work. However, results for selected elements will be briefly discussed:

- Alkali metals (K, Rb, Cs),
- Alkaline earth metals (Ca, Sr, Ba, Ra),
- Rare earth elements (i.e. lanthanides + Sc, Y, Lu)
- Actinides (U, Th).

Other elements of particular importance for a specific RAP are also considered. For vertebrates, information will be provided regarding which organ/tissue contributes the most to a specific CR. Note that this contribution depends on both fresh weight concentrations in relevant tissues and the relative mass of various organs (Fig. 3).

---

[1] Fresh weight concentration of an element in an animal/plant divided by the concentration of the same element in soil (dry), freshwater or seawater (depending on type of organism)

Terrestrial RAPs

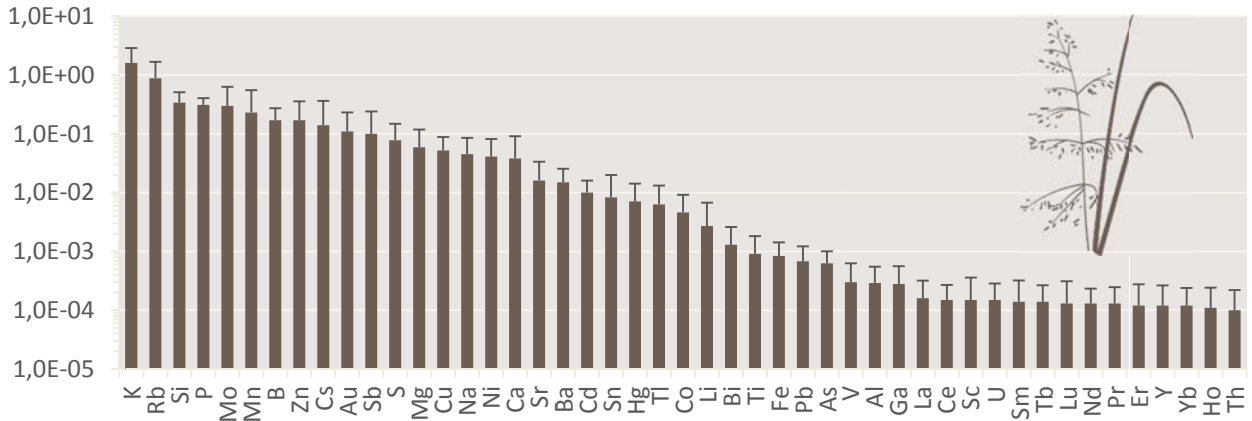Grass and earthworms were selected as examples of the terrestrial RAPs.

Figure 4. *Concentration ratio (FW grass / DW soil) – Geometric mean with GSD (n=10)*

For grass (Fig. 4), transfer of alkali metals are generally high, particularly K. The CR of stable Cs (0.14) is approximately an order of magnitude lower than for K. The geometric mean CR of radioactive Cs-137 mainly from the Chernobyl accident is slightly higher than for the stable analogue (0.27). The variability is, however, considerably higher for stable Cs. Regarding alkaline earth metals, the geometric mean transfer of Ca, Sr and Ba is quite similar – 0.038, 0.016 and 0.015, respectively. Ra-226, determined using gamma spectrometry, shows slightly higher geometric mean CR than its biogeochemical analogue Ba (0.026), but this difference may well be attributable to methodological issues (e.g. due to the low levels of Ra-226). Furthermore, soil concentrations of Ra-226 pertain to total content, whereas Ba refers to the acid soluble fraction. In general, the transfer of rare earths and actinides are very low (CR $<2 \times 10^{-4}$). Consequently, surface contamination from soil can be an important additional source to plant contamination from these elements.
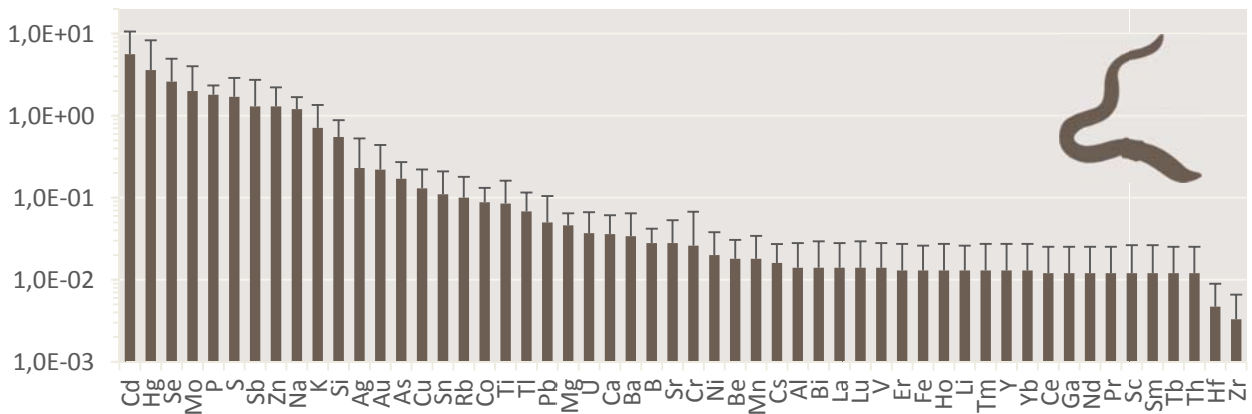
Figure 5. *Concentration ratio (FW earthworm / DW soil) – Geometric mean with GSD (n=14)*

Note the very high CRs of toxic heavy metals such as Cd and Hg – 5.6 and 3.6, respectively for earthworms (Fig. 5). Uptake of alkali metals decrease in the order: K (0.71), Rb (0.10), Cs (0.016), whereas CRs for alkaline earths seems to be quite similar for Ca, Sr and Ba (0.028–0.036). The CRs of rare earths and actinides range between 0.012 (Th)–0.037 (U), which is the same order of magnitude as e.g. Cs and Sr. In fact, most element CRs range between 0.01–0.1. Residual soil (not properly flushed out from the gastro-intestinal tract) may have had an influence on the results for earthworms.

Frogs and Trout were selected as examples for freshwater RAPs.
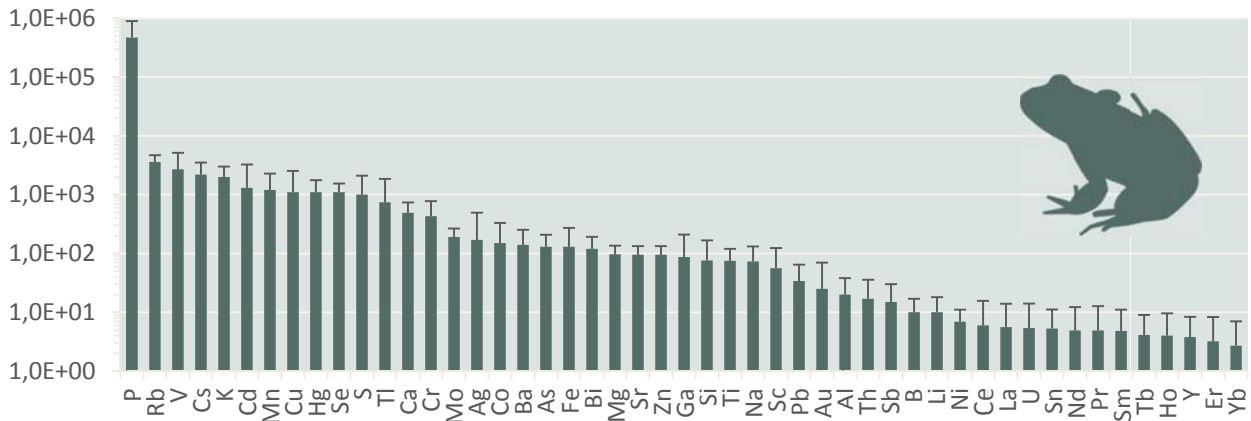
Figure 6. *Concentration ratio (FW frog / freshwater) – Geometric mean with GSD (n=9)*

For frogs, the CR for P is more than 100 times higher than the next ranked element CR (Fig. 6). CRs of most alkali elements are high, decreasing in the order Rb (3600), Cs (2200) and K (2000). Alkaline earth CRs are lower: Ca (490), Ba (140) and Sr (95). The geometric mean CR of most rare earths and actinides lies in the range 2.7–17. However, the CR of Sc is slightly higher (56). Bone concentration is particularly important for Ca, but also for Sr, Mn, Ba, P, Pb, U, Li, Na and Sc. Liver is the main contributor to the CRs of Cu, Ag and Cd.
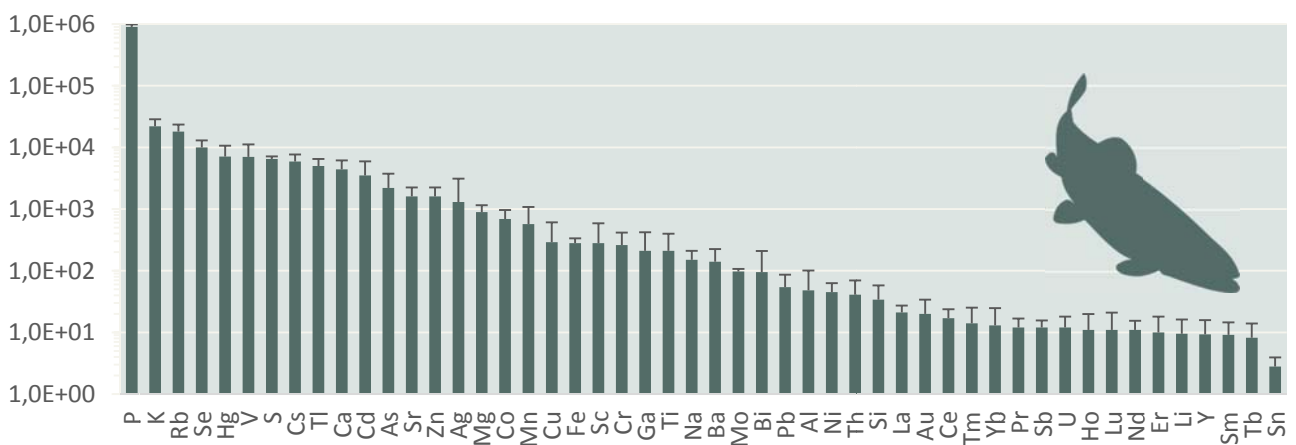
Figure 7. *Concentration ratio (FW trout / freshwater) – Geometric mean with GSD (n=10)*

Relatively high CRs for P are also observed for trout (Fig. 7). CRs of K, Rb and Cs are also high – 22 000, 18 000 and 5900, respectively. Lower, but still high, CRs for alkaline earths – decreasing in the order Ca (4400), Sr (1600) and Ba (140). The geometric mean CR of rare earths (Sc excluded) and actinides lies in the range 8.2–41. For Sc the CR seems to be higher (280), as was the case for frogs. Concentrations in bone constitute the main contributor to the whole body CR for Ca, Sr, Ba, Mn, U, Pb, Cd, Cr, Y and Zn (with decreasing importance). Liver concentrations contributed most to the CRs of Ag, Cu, La, Ce, Nd, Pr and Sc. Lower atomic number lanthanides (La, Ce, Nd, Pr) tend to be more concentrated in liver, whereas those with the highest atomic number are mainly found in muscles (Tm, Yb). For the in-between elements Er, Ho, Sm and Tb, none of the three tissues contributed more than 50% to the whole body CR.

Marine RAPs

Brown seaweed and plaice were selected as examples for marine RAPs.
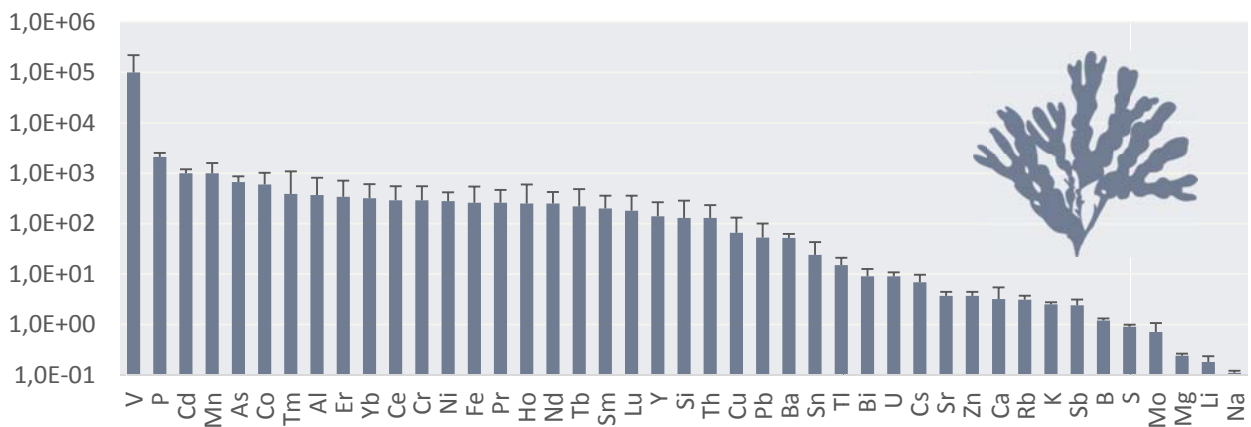
Figure 8. *Concentration ratio (FW brown seaweed / seawater) – Geometric mean with GSD (n=10)*

For seaweed (Fig. 8), the CR of most rare earths and actinides lies in the range 130–390, an exception being U where the respective value is only 9.0. CRs of alkali and alkaline earth elements are generally low (due to the high levels usually found in seawater), with CRs <10 for K, Rb, Ca, Sr and Cs, while Ba is slightly higher (52). Note that the CR of V is 50 times higher than the next ranked element CR (P).
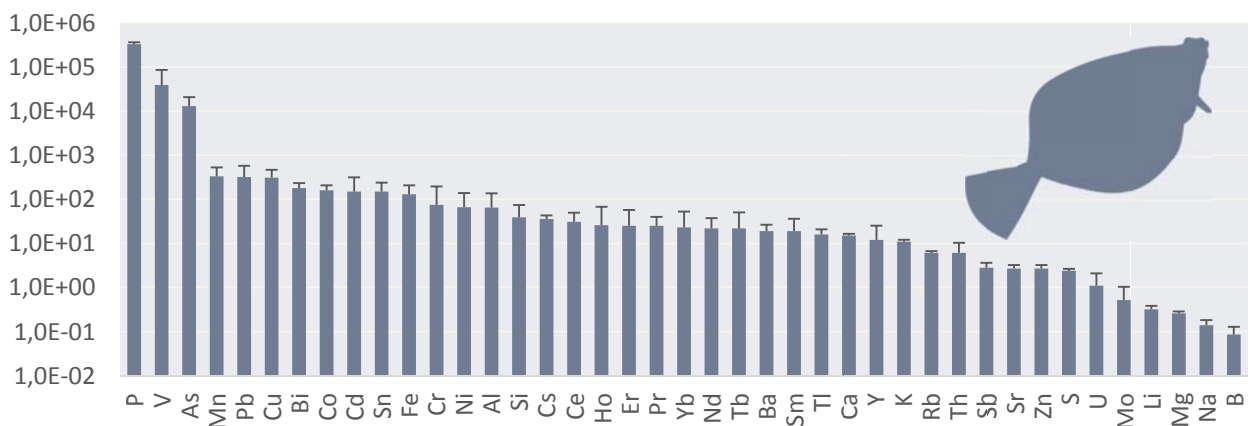
Figure 9. *Concentration ratio (FW plaice / seawater) – Geometric mean with GSD (n=10)*

For plaice (Fig. 9), the geometric mean CR of rare earths lies in the range 12–31, while actinides show even lower values – 1.1 and 6.1 for U and Th, respectively. CRs of most alkali and alkaline earth elements are also relatively low, with CRs decreasing in the order Cs (36), Ba (19), Ca (15), K (11), Rb (6.1) and Sr (2.7). Note the gap between P, V, As and the other elements. Concentration in bone is the most important contributor to the whole body CR for elements Ca, Sr, Ba, Mn, U, V, Li and P (with decreasing importance). The liver concentration is most important for Cd, only. For the rest of the elements muscle concentration dominates the CR.

Conclusions

• An ICRP reference site in Norway has been identified and described

• The data gathered concern all 12 ICRP Reference Animals and Plants (RAPs), including different life-stages for frogs (eggs, tadpoles and juvenile/adult frogs)

• Whole-body concentration ratios (CRs) for up to 54 elements were provided for terrestrial and freshwater RAPs and up to 43 elements for marine RAPs. Still, important elements on the ICRP list were – for various reasons – not a part of our study. The list of those not determined includes trans-uranium elements (Am, Cf, Cm, Np, Pu), Cl, I, Po and Tc.

• Comparison of results from TRAP with data from similar investigations in other areas within or outside Norway was beyond the scope of the work presented here. However, site-specific CR values from the present study will be compared with other available CR data e.g. through the work within the ongoing EC-COMET project (Contract Number: Fission-2012-3.4.1-604794). Thus, the datasets collated from Tjøtta and other related sites will potentially serve as 'points of reference' consistent with other components of the ICRP's nascent system on environmental protection.

References

ICRP (2008). Environmental protection: the concept and use of reference animals and plants. ICRP Publication 108. Ann. ICRP 38 (4–6).

ICRP (2009). Environmental Protection: Transfer Parameters for Reference Animals and Plants. ICRP Publication 114, Ann. ICRP 39(6).

Thørring H, Brown JE, Aanensen L, Hosseini A (2016). Tjøtta – ICRP reference site in Norway (Summary report of the TRAP project). StrålevernRapport 2016:9. Østerås: Statens strålevern. http://www.nrpa.no/filer/2617d93958.pdf

Transfer parameters for ICRP's Reference Animal and Plants in terrestrial Mediterranean ecosystems

J. Guillén[*a], *N. A. Beresford*[b,c], *A. Baeza*[a],*M. Izquierdo*[d], *M.D. Wood*[c], *A. Salas*[a], *A. Muñoz-Serrano*[a], *J.M. Corrales-Vázquez*[e] *and J.G. Muñoz-Muñoz*[a]

[a] LARUEX, Dpt. Applied Physics, Faculty of Veterinary Sciences, University of Extremadura, Avda. Universidad, s/n, 10003, Cáceres, Spain.

[b] NERC Centre for Ecology & Hydrology, Lancaster Environment Centre,.Bailrigg, Lancaster LA1 4AP, UK

[c]School of Environment and Life Sciences, University of Salford, Manchester, M5 4WT, UK

[d] School of Biosciences, Faculty of Science, University of Nottingham, Sutton Bonington Campus, Leicestershire, LE12 5RD, UK

[e] Department of Experimental Sciences and Mathematics Teaching, University of Extremadura, Avda. Universidad, s/n, 10003, Cáceres, Spain

Abstract

An international system for the radiological protection of the environment (or non-human biota) has been suggested by the International Commission on Radiological Protection (ICRP) based on the use of Reference Animals and Plants (RAPs). Transfer parameters are required for the RAPs to enable the estimation of organism radionuclide contents, and hence internal dose rates, within environmental assessments. However, transfer values specifically for the taxonomic families as defined for the RAPs are often sparse and can be extremely site-dependent. There is a considerable geographical bias within the available data, with few data for Mediterranean ecosystems. In the present work, stable element concentrations in selected terrestrial RAPs, and the corresponding whole-body concentration ratios, CR_{wo}, were determined in two different Mediterranean ecosystems: a pinewood and a dehesa (grassland with sparse tree cover). The RAPs considered in the pinewood ecosystem were Pine Tree and Wild Grass; whereas in the dehesa ecosystem those considered were Deer, Rat, Earthworm, Bee, Frog and Wild Grass. The estimated CR_{wo} values are compared to those reported in international compilations and databases in this paper.

Introduction

Radiological protection of the environment has evolved from an anthropocentric point of view ('if man is adequately protected, so is the environment') (ICRP, 1977, 1991) to recommendations that the environment is assessed in its own right (ICRP 2008a). The concept of Reference Animals and Plants (RAP) has been proposed by the ICRP (ICRP 2008b) in order to develop a similar methodology to the Reference Man conceptused in human radiological protection models that have been developed to assess radiation exposure of animals and plants (e.g. Brown et al., 2016, USDoE, 2002,Copplestone et al., 2003). Concentration ratios, CR_{wo}, are often used in such models (Beresford et al. 2008) to predict activity concentrations in wildlife assuming that there is equilibrium between the whole organism (RAP) and the appropriate medium (e.g. soil in the case of terrestrial ecosystems).These estimated whole-body activity concentrations are then used in the calculation of internal dose. There are many gaps in the CR_{wo} data for element-RAP combinations considered in ICRP (2009), even for some radiologically significant elements (e.g. iodine). CR_{wo}

---

values are also known to be highly site specific which contributes to the large variation observed within the available data, and there are also biases in the available data (Wood et al., 2013). The data for RAPs used in ICRP (2009), are predominantly from Europe and North America with significant contributions from Japan and Australia; they are mainly from temperate and artic ecosystems (Howard et al., 2013).

The goal of this study was to determine CR_{wo} values for terrestrial RAPs (Earthworm, Bee, Rat, Frog, Deer, Duck, Wild Grass and Pine Tree[1]) collected in Mediterranean ecosystems for 32 elements (Ag, Al, As, B, Ba, Be, Ca, Cd, Co, Cr, Cs, Cu, Fe, I, K, Li, Mg, Mn, Mo, Na, Ni, P, Pb, Rb, S, Sr, Ti, Tl, U, V and Zn). The main sampling site was a dehesa, which is a typical Mediterranean semi-natural grassland with sparse tree cover, mainly holm oaks (*Quercus ilex*). As there was no pine tree in the dehesa, a pinewood located in the vicinity was also selected. Pine Tree wood and Wild Grass were collected from this second site. The CR_{wo} values for these Mediterranean ecosystems were compared with values reported in temperate climates (Barnett et al., 2014; Copplestone et al., 2013).

Materials and Methods

Sampling sites

Two locations were selected for sampling terrestrial RAPs in the province of Cáceres, western Spain, in the surroundings of Monfragüe National Park: a dehesa and a pinewood (Figure 1). The climate is dry sub-humid (hot summer Mediterranean climate), with an annual average temperature of 16°C and a hot summer. The Dehesa extends over more than 4600 ha. It serves as hunting reserve, mainly for red deer (*Cervus elaphus*) and wild boar (*Sus scrofa*). Soil texture was silt-loam with a pH 6.5 at the dehesa. As no pine trees were present in the Dehesa, a pinewood, located about 16 km away, was selected. It is a natural pinewood with no management. Wild grass and pine tree were sampled at this location. The texture of Pinewood site soil was loamy-sand with a pH 5.2.

Table 1 lists the representative species of RAPs sampled at the Dehesa and Pinewood sites. Rat, Deer, Wild Grass and Pine Tree were collected in different seasons during 2014/15. Individual vertebrate RAPs were skinned and different tissues were separated: muscle, bone, liver, kidney and thyroid. As the thyroid gland for Rat and Frog was too small to isolate, an area around it was selected and classified as thyroid. Prior to analysis, biota samples were freeze-dried and stored in a dry place, ground using a nitrogen mill and then acid digested.

Soil samples (0–10 cm) were collected in the Dehesa and Pinewood at with the same time as Wild Grass and Pine Tree sampling. For each season at each site 6 soil samples were collected from a 500 m^2 area and combined to form a composite sample for subsequent analysis. Samples were sieved, and fractionsgreater than 2 mm were discarded, samples were then homogenized and oven dried (c. 60°C).

---

[1] We have included Duck and Frog, as they inhabit terrestrial ecosystems,but acknowledge that some ICRP publications (e.g. ICRP 2009) consider them in the freshwater environment only.
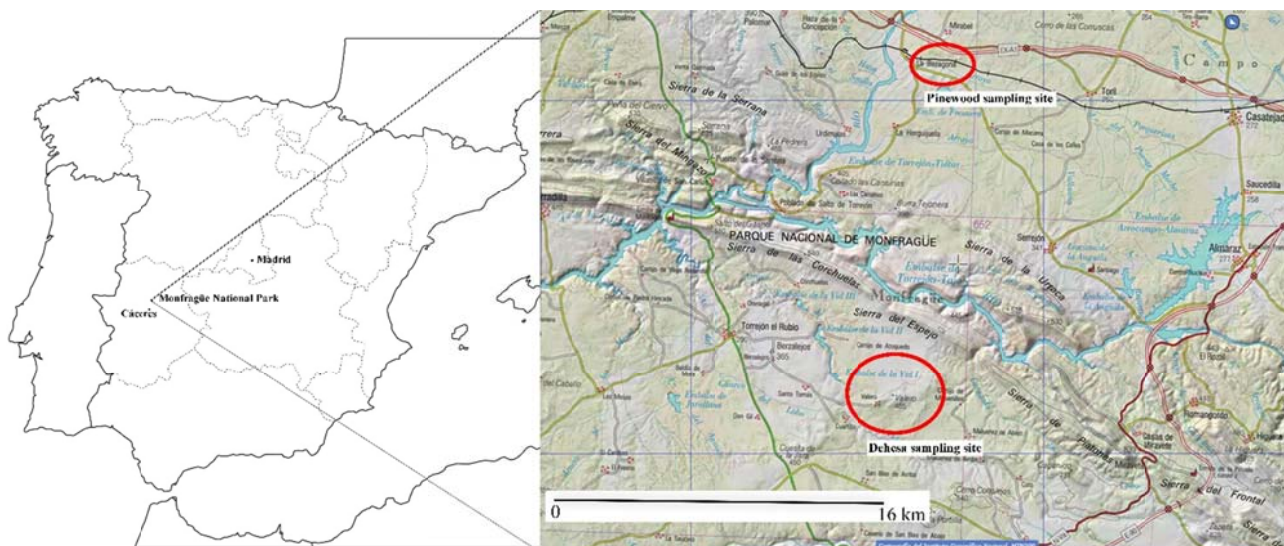
Figure 1.*General location of the Dehesa and Pinewood sampling sites.*

RAP	Family as defined in ICRP (2008b)	Family/Species sampled	Sampling Site
Earthworm	*Lumbricidae*	*Lumbricidaespp.*	Dehesa
Bee	*Apidea*	*Apis mellifera*	
Frog	*Ranidae*	*Pelophylaxperezi*	
Rat	*Muridae*	*Apodemussylvaticus*	
Deer	*Cervidae*	*Cervuselaphus*	
Duck	*Anatidae*	*Anasplatyrhynchos*	
Wild Grass	*Poceae*	*Briza minor*	Dehesa and pinewood
Pine Tree	*Pinaceae*	*Pinuspinaster*	Pinewood

Table 1.*Representative species of terrestrial RAPs sampled from the Dehesa and Pinewood sites.*

ICP-MS analysis.

Soil digestion (c.0.2 g) was undertaken by adding concentrated HF, HNO_3 and $HClO_4$ (2.5:2:1 mL), and heating to 160°C overnight. Plant and animal tissues were acid digested with microwave oven at 140 ℃ for 20 min. with: a) 6 mL *Primar* grade HNO_3 for plants, or b) HNO_3, MilliQ ultrapure water and 30% v/v H_2O_2 (3:2:2 mL) for animal tissues. Alkaline extraction with tetramethylammonium hydroxide (TMAH) was used to determine iodine content in the samples. Iodine analyses were carried out in thyroid samples and if enough mass was available (greater than 0.3 g dry matter (DM)) in the other sample types. For soils, aliquots of 1 g were weighed into polypropylene tubes and 10 mL of 10% TMAH were added. The soil suspensions were heated at 90°C for 24 h, and then centrifuged at 3500 rpm for 30 min.

Multi-element analysis of diluted solutions was undertaken by ICP-MS. Sample processing was undertaken using Qtegra™ software (Thermo-Fisher Scientific) utilizing external cross-calibration between pulse-counting and analogue detector modes when required.Iodine analysis was undertaken separately, using a 1% TMAH matrix for standards and samples.

Detection limits were calculated as threetimes the standard deviation of the reagent blanks for each extraction form and sample type. Blank samples and Certified Reference Materials (NIST SRM 2711a (Montana soil), NIST 1573a (tomato leaves), NIST 1577c (bovine liver) were digested and prepared in a similar manner to check the accuracy and precision of the digestion and analysis methods.

Results and Discussion

The whole-body concentrations for Rat, Frog, Deer and Duck were calculated assuming that the tissues analyzed (thyroid, liver, kidney, meat and bone) represented the whole animal (an approach taken by Barnett et al. (2014) in a similar study). In order to estimate Deer whole organism concentrations, fresh mass percentages of the whole-body for each tissue were assumed to be the same as roe deer collected in a UK site (Barnett et al., 2014).

CR_{wo} is defined as the ratio between the equilibrium activity concentration of a radionuclide in an organism and in the corresponding medium (ICRP 2009). In the existing models and data compilations CR_{wo} values are presented by element assuming the same value for all isotopes (of that element) including stable isotopes (eq. 1) (Copplestone et al. 2013). So, here for stable elements CR_{wo} is:

$$CR_{wo} = \frac{Concentration\ element\ X\ in\ whole\ body\ RAP\ (mg\,/\,kg\ FM)}{Concentration\ element\ X\ in\ soil\ (mg\,/\,kg\ DM)} \quad (1)$$

The soil used for the calculation of Deer CR_{wo} values in this study was the mean value of all soils analyzed in dehesa, because red deer (*Cervus elaphus*) range freely over the dehesa. As only one individual of duck was available, the corresponding CR_{wo} values should be considered to give an approximate order of magnitude.

For comparative purposes, a selection of alkali (K, Rb, and Cs), alkaline earth (Ca, Sr and Ba), heavy metal (Cd, Pb and U) elements, together with I, P, and Fe have been used. The I CR_{wo} values for Rat and Frog should be considered as provisional, as an area around the thyroid was sampled. Figures 2 and 3 show the comparison of the CR_{wo} values for these elements from the present study with those reported for a temperate climate site in the UK (Barnett et al., 2014) and in the online wildlife transfer database (WTD) described by Copplestone et al. (2013). The latter was used for the elaboration of ICRP 114 (ICRP, 2009). Here we use an updated version of the WTD (see Brown et al. 2016). Although the UK data (Barnett et al., 2014) is included in the WTD database, we also make specific comparison with that study because we adopted the protocols from it and applied them to the Mediterranean ecosystem. The variation of CR_{wo} values for some elements (ratio between standard deviation and mean value) was in the range 6 - 170 % for RAPs collected in different seasons. This may suggest a seasonal variation of the CR_{wo} values and needs further analysis (Guillén et al., 2016).

Phosphorus generally presented the highest CR_{wo} value of all analyzed elements for all the RAPs considered. Deer and Bee presented the highest P CR_{wo} value, followed by Rat, Frog and Duck, which were similar, and by Wild Grass, Earthworm and Pine Tree. Note the WTD does not contain any CR_{wo} values relating P in organisms to soil concentrations.

When considering elements from a single column in the periodic table, alkali (K, Rb and Cs) or alkaline earth (Ca, Sr and Ba), the CR_{wo} values decrease with increasing atomic number for all RAPs (see Fig. 2 and 3). Similar trends can be seen in reported CR_{wo} ranges for Earthworm, Bee, Deer at a UK site (Barnett et al., 2014).

The Rb, Sr, Cd, Fe and U values for Earthworm (see Fig. 2a) were within the WTD ranges. The Ca value was slightly higher than at the UK site and in the WTD, probably due to a lower Ca concentration in analyzed Spanish soils, while Cs and Ba were slightly lower, but within the same order of magnitude.

Bee CR_{wo} values were generally 1 – 2 orders of magnitude higher than those reported for the UK site and WTD database (see Fig. 2b).

The Rb, Ca, Sr and Pb CR_{wo} values for Rat were within the ranges reported in the WTD (see Fig. 2c). The K, Ba and Fe were higher. The Cs mean value was slightly higher than the UK site range, but within the WTD range.
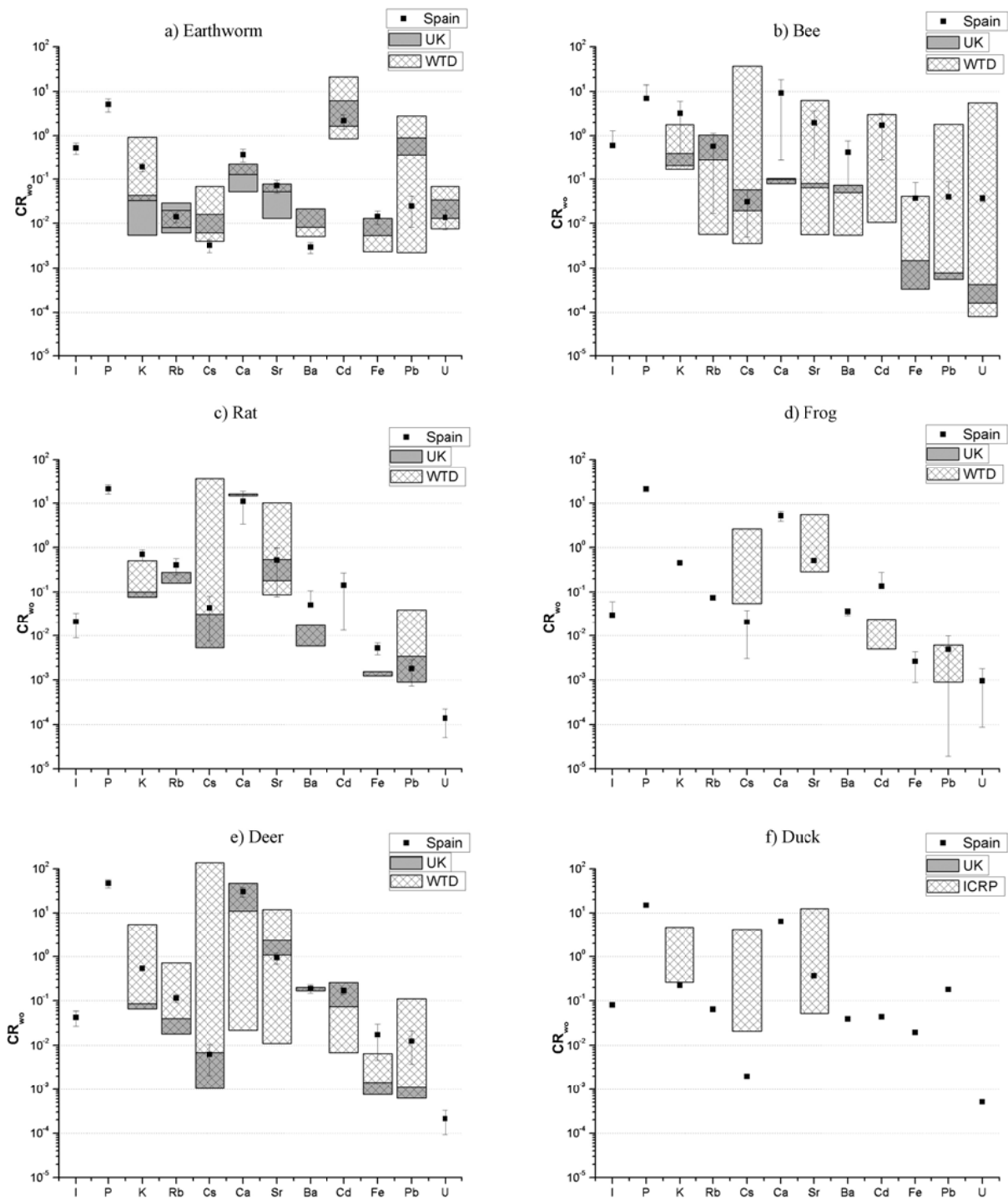
Figure 2. *Mean value and standard deviation of CR_{wo} values for I, P, K, Rb, Cs, Ca, Sr, Ba, Cd, Fe, Pb and U in Spain, and ranges reported in the UK site (Barnett et al., 2014) and online database, WTD, (Copplestone et al., 2013) for animal RAPs: a) Earthworm, b) Bee, c) Rat, d) Frog, e) Deer and f) Duck.*
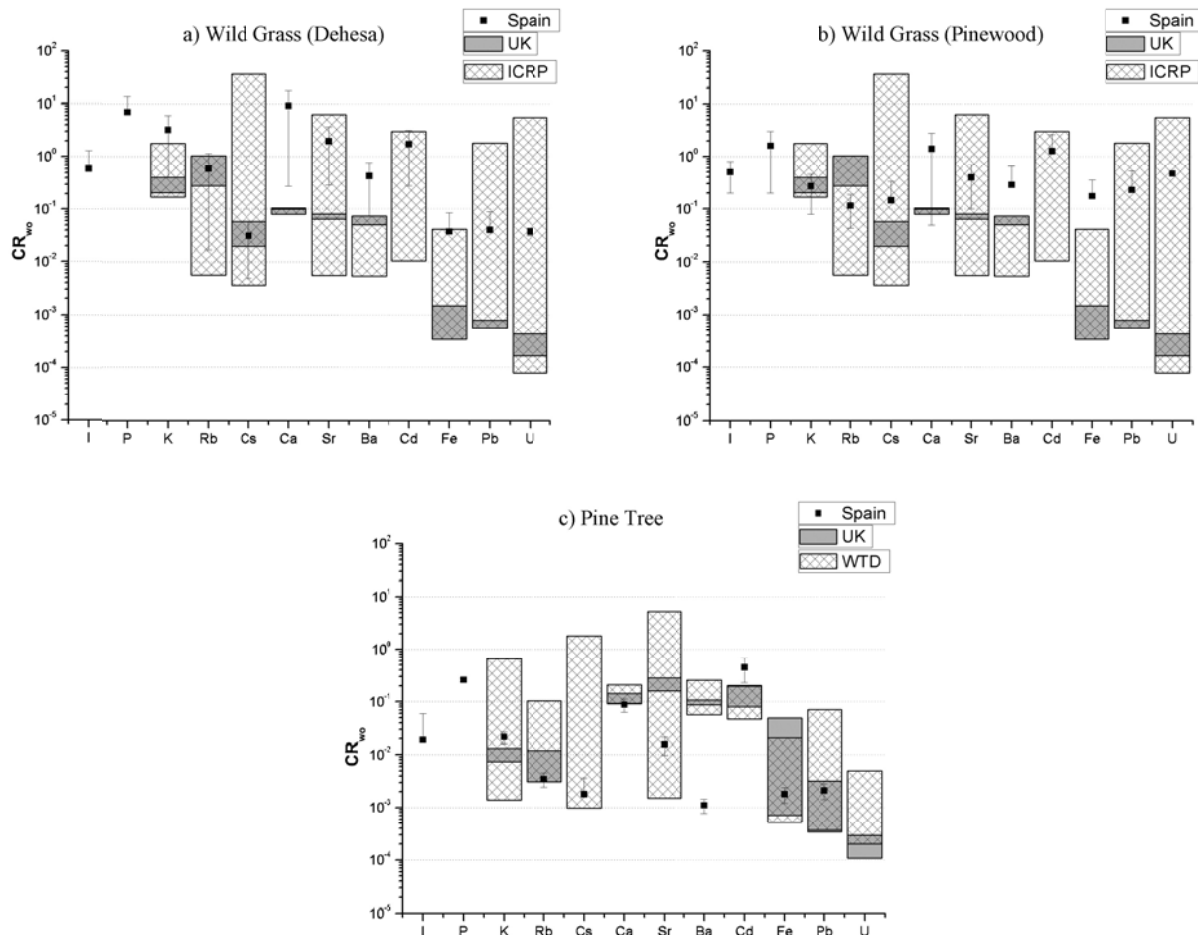
Figure 3. *Mean value and standard deviation of CR_{wo} values for I, P, K, Rb, Cs, Ca, Sr, Ba, Cd, Fe, Pb and U in Spain, and ranges reported in the UK site (Barnett et al., 2014) and online database, WTD, (Copplestone et al., 2013) for vegetal RAPs: a) Wild Grass (Dehesa; b) Wild Grass (Pine Wood) and c) Pine Tree.*

Reported CR_{wo} values for Frog were limited to Cs, Sr and Pb in the WTD database (Fig. 2d). The Sr and Pb values were within the range reported in the WTD. The Cs was lower, but within the same order of magnitude as the lower part of the WTD range.

The Cs, Ca, Sr, Ba and Cd CR_{wo} values for Deer were similar to those reported in the UK site and WTD database (see Fig. 2e). The K, Rb and Pb values were about one order of magnitude higher than the UK site range, but within the WTD range. The Fe mean value was one order of magnitude higher than the WTD range. The Cs CR_{wo} values at the dehesa site were one order of magnitude lower than the ^{137}Cs CR_{wo} range reported in the UK site was 0.01 – 0.12, but similar to the stable Cs values (0.001 – 0.0069) (Barnett et al., 2014).

Figure 3a and 3b show the Wild Grass CR_{wo} values from the Dehesa and Pinewood sampling sites. The K, Rb, Ca and Sr values for the Dehesa site were approximately one order of magnitude higher than in Pinewood site; while Cs, Fe, Pb and U were about one order of magnitude higher in the Pinewood site than in Dehesa. The Ca, Sr and Ba values (for both sites) were one order of magnitude higher than UK site range, and only Sr was within the WTD range. For Ca, it may be attributed to a lower Ca concentration in Spanish soils. The Cd, Fe, Pb and U values were about 2 orders of magnitude higher than UK site range, but within the WTD range (with the exception of Fe at Pinewood, which was about one order of magnitude higher). The Cs CR_{wo} value for the Dehesa site was within stable Cs range reported in the WTD, and for a UK site (Barnett et al., 2014).

Pine Tree CR_{wo} values were usually $1 – 2$ orders of magnitude lower than for Wild Grass. The Rb, Ca, Fe and Pb CR_{wo} values for Pine Tree were within the ranges reported for the UK site and WTD (see Fig. 3c). The K and Sr values were within the range reported in the WTD. The Cd values were above the WTD range but within the same order of magnitude; while Ba values were about $1 – 2$ orders of magnitude lower. The stable Cs CR_{wo} were within the ^{137}Cs range 0.001-0.0014 at the UK site (Barnett et al., 2014).

Conclusions

The transfer parameters databases used to derive transfer parameters for commonly used assessment approaches have some short-comings: a) there is a lack of CR_{wo} data for many RAP-element combinations; and b) there is geographical and climate bias. In this paper, soil and organism elemental concentrations and the corresponding CR_{wo} values were reported for species representative of the ICRP RAPs collected in Mediterranean ecosystems.

- CR_{wo} data for 30 elements and 8 terrestrial RAPs in Mediterranean ecosystems were presented, including amongst the first data available for I and P for terrestrial RAPs.

- For some elements, it can be observed that the CR_{wo} mean value (annual) was lower than the standard deviation, suggesting a possible seasonal variation, which requires further research comparing across different seasons.

- Regarding some alkali (K, Rb and Cs) and alkali earth (Ca, Sr and Ba) elements, the CR_{wo} show a decreasing trend with increasing atomic number.

References

1. Barnett, C.L., Beresford, N.A., Walker, L.A., Baxter, M., Wells, C., Copplestone, D., 2014. Transfer parameters for ICRP reference animals and plants collected from a forest ecosystem. Radiat. Environ. Biophys. 53,125–149

2. Beresford, N.A., Barnett, C.L., Brown, J., Cheng, J-J. Copplestone, D., Filistovic, V., Hosseini, A., Howard, B.J., Jones, S.R., Kamboj, S., Kryshev, A., Nedveckaite, T., Olyslaegers, G., Saxén, R., Sazykina, T., Vives i Batlle, J., Vives-Lynch, S., Yankovich, T. and Yu, C. 2008. Inter-comparison of models to estimate radionuclide activity concentrations in non-human biota. Radiat. Environ. Biophys., 47, 491–514.

3. Brown, J.E.,Alfonso, B., Avila, R., Beresford, N.A., Copplestone, D., Hosseini, A., 2016. A new version of the ERICA tool to facilitate impact assessments of radioactivity on wild plants and animals J. Environ. Radioactiv. 153, 141-148.

4. Copplestone, D.,Wood, M. D., Bielby, S., Jones, S. R.,Vives i Batlle, J.,Beresford, N.A., 2003. Habitat Regulations for Stage 3 Assessments: Radioactive Substances Authorisations. R&D Technical Report P3-101/Sp1a. Environment Agency, Bristol.

5. Copplestone, D.C., Beresford, N.A., Brown, J., Yankovich, T., 2013.An International database of radionuclide concentration ratios for wildlife: development and uses. J. Environ. Radioactiv. 126, 288-298.

6. Howard, B.J., Beresford, N.A., Copplestone, D., Telleria, D., Proehl, G., Fesenko, S., Jeffree, R., Yankovich, T., Brown, J., Higley, K., Johansen, M., Mulye, H., Vandenhove, H., Gashchak, S., Wood, M.D., Takata, H., Andersson, P., Dale, P., Ryan, J., Bollhöfer, A., Doering, C., Barnett, C.L., Wells, C., 2013. The IAEA Handbook on Radionuclide Transfer to Wildlife. J. Environ. Radioact. 121, 55–74

7. Guillén J., Beresford N. A., Baeza A., Wood M. D., Salas A., Izquierdo M., Muñoz-Serrano A., Young S., Corrales-Vázquez J.M., Muñoz-Muñoz J.G. 2016. Seasonal variation of concentration ratios ICRP's Reference Animals and Plants in terrestrial Mediterranean ecosystems. Póster presentation at II

International Conference on Radiological contentration Processess (50 years later), 6th - 9th November 2016, Seville, Spain.

8. ICRP, 1977. Recommendations of the International Commission on Radiological Protection. ICRP Publication 26. Annals of the ICRP 1(3).
9. ICRP, 1991. The 1990 Recommendations of the International Commission on Radiological Protection. ICRP Publication 60. Annals of the ICRP 21(1–3).
10. ICRP, 2008a. Nuclear Decay Data for Dosimetric Calculations. ICRP Publication 107. Annals of the ICRP 38(3).
11. ICRP, 2008b. Environmental Protection - the Concept and Use of Reference Animals and Plants. ICRP Publication 108. Annals of the ICRP 38 (4-6).
12. ICRP, 2009. Environmental Protection: Transfer Parameters for Reference Animals and Plants. Strand, P., Beresford, N.A., Copplestone, D., Godoy, J., Jianguo, L., Saxén, R., Yankovich, T., Brown. J. Annals of the ICRP: Publication 114, 39, 6.
13. USDoE, United States Department of Energy., 2002. A Graded Approach for Evaluating Radiation Doses to Aquatic and Terrestrial Biota. DOE-STD-1153-2002, Dept. Energy, Washington, D.C.
14. Wood, M.D., Beresford, N.A., Howard, B.J., Copplestone, D., 2013. Evaluating summarised radionuclide concentration ratio datasets for wildlife. J.Environ.Radioactiv.126, 314-325.

Acknowledgement

Comparison of radiocesium root uptake by leguminous and non-leguminous herbaceous plants

*S. Uchida and K. Tagami

National Institutes for Quantum and Radiological Science and Technology (QST) -
National Institute of Radiological Sciences (NIRS), Anagawa 4-9-1, Inage-ku, Chiba 263-8555, Japan

Abstract

Transfer of radiocesium from soil to plant is an important factor for radiation dose assessments. After the Fukushima Daiichi Nuclear Power Plant (FDNPP) accident, food monitoring results showed slightly high radiocesium concentrations in soybean than other crops, such as brown rice; however, details has not been reported yet. In this study, therefore, we compared the concentrations of ^{137}Cs in red clover and mixture of several grass species obtained at the same sampling ground affected by the FDNPP fallout to check their ^{137}Cs concentration differences. It was found that the aggregated transfer factor for red clover was 8.9×10^{-4} and significantly lower value of 2.7×10^{-4} was observed for mixed grass species in 2013-2015.

Introduction

After the Fukushima Nuclear Power Plant (FDNPP) accident, radiocesium concentrations in soybeans tended to be higher than those in brown rice (Figure 1) (data from Ministry of Health, Labour and Welfare, 2016). Before the accident, even under equilibrium conditions, we found that ^{137}Cs and stable Cs transfer factors from soil to soybean were higher than those to brown rice in Japan (not published). In the outside Japan, similarly, a greenhouse experiment showed that ^{137}Cs concentrations in soybean beans were higher than that in wheat grain (Adriano et al., 1984); however, in IAEA TRS 472 (2010), similar soil-to-crop transfer factors were listed for leguminous fodder and grass (stems and shoots of cereals). High potassium demand in soybean seeds may affect this Cs concentration differences; however, because soybean and paddy rice were grown under different conditions, not only due to the plant physiology but also the soil management might affect the Cs concentrations in these crops. In this study, therefore, we measured leguminous and grass species grown under the same conditions to compare the ability of Cs uptake from soil.
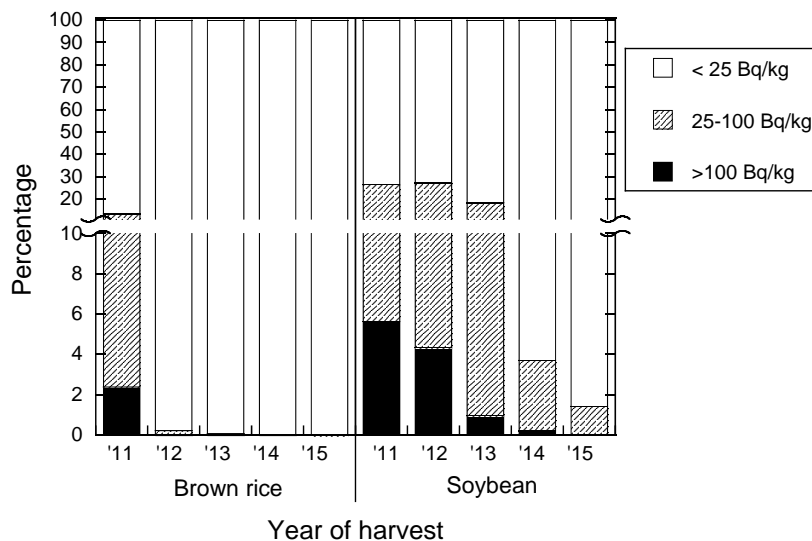
Figure 1. Percentages of brown rice and soybean products with radiocesium ($^{134+137}$Cs) concentrations in three categories (<25 Bq/kg, 25-100 Bq/kg or >100 Bq/kg) in 2011-2015 in Fukushima Prefecture.

---

* Corresponding author, E-mail: uchida.shigeo@qst.go.jp

Materials and Methods

The collection site was the QST-NIRS campus in Chiba Prefecture located about 220 km south from the FDNPP; the site had received radioactivity fallout released by the nuclear accident mainly in March to April 2011. The fallout amount has been given as about 14.8 kBq m^{-2} of ^{137}Cs (Ishii et al., 2013) and we found arithmetic mean ^{137}Cs concentration in each year ranged from 9.9-13.5 kBq m^{-2} in 2011-2014 (Tagami & Uchida, 2015). Two leguminous species, red clover (*Trifolium pratense*) and narrow-leaved vetch (*Vicia sativa*) were found in the ground, and also grass species, such as *Eragrostis ferruginea*, and *Paspalum thunbergii* Kunth ex Steud. were found on the same ground. These samples were collected in 2012-2015. Other plant species were also collected for comparison, that is, knotweed (*Fallopia japonica*), mugwort (*Artemisia indica* var. *maximowiczii*) and field horsetail (*Equisetum arvense*). Number of samples were 2-10 each year for each plant species.

Immediately after collection, plant samples were transferred to a laboratory and then weighed. Except for field horsetail, each tissue was washed with tap water to remove dust from the surface; this was done in a washing bowl by changing the water 5 times, and then, finally, the samples were rinsed with reverse osmosis water. All samples were oven-dried to a constant weight at 80˚C in an electric oven for at least 2 d to decrease the sample volume and to calculate water contents of samples. Each oven-dried sample was pulverized and mixed well, and then transferred to a 100-mL plastic container.

Radioactivity concentration in each sample was measured by a Ge detector system (Seiko EG&G) using 50,000-200,000 s counting interval. Potassium-40 (^{40}K, natural abundance: 0.0117%) was also measured to understand total K distribution.

Results and Discussion

Comparison of ^{137}Cs and ^{40}K concentration rank in five plant species

After the Fukushima accident, ^{137}Cs concentration decreases with time in herbaceous plants (e.g., Tagami & Uchida, 2015). Therefore, it was difficult to compare the ^{137}Cs concentrations with ^{40}K which were already in an equilibrium condition in the study ground. Thus we simply ranked the geometric mean ^{137}Cs concentrations in each year and the rank was compared with ^{40}K rank (average of 2012-2015). Figure 2 shows the results; ^{137}Cs concentration rank for Glass spp. kept low from 2012 to 2015, while that for red clover showed became higher. The averaged ^{40}K concentrations were, however, similar for red clover and grass spp. Thus potassium demand might be similar for both plant species, however, interestingly, ^{137}Cs concentration in red clover were always higher in 2012-2015. Similar results were reported by Kobayashi et al. (2014) for phytoremediation of agricultural fields in Fukushima. In our study, in 2015, the geometric means of ^{137}Cs concentrations in red clover and grass spp. were 16 and 7.0 Bq/kg-dry, respectively. The difference was only about two times, therefore, using leguminous plants for radiocesium removal from soil would not be practical for remediation purposes.

If plant mass of red clover was smaller than that of grass spp. then the total ^{137}Cs absorbed by plant might be comparable. However, unfortunately, when we measured the masses of these plants, red clover was 0.46 kg-dry/m^2 and grass spp. was 0.47 kg-dry/m^2 (at August 15, 2016); no difference was observed. Thus the ^{137}Cs concentration difference was not due to the mass dilution effect.
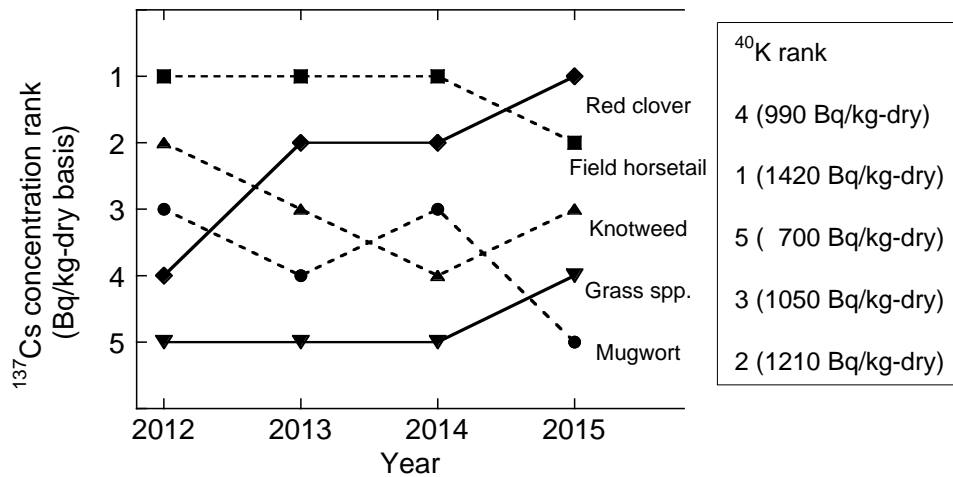
Figure 2. *Comparison of rank of ^{137}Cs and ^{40}K concentrations in five plant species collected in the same sampling ground (QST-NIRS) in 2012-2015.*

Effective half-lives

^{137}Cs concentration changes in red clover plus narrow-leaved vetch are plotted in Figure 3 and also the concentration was fitted with a two-component exponential decline curve. The short and long effective half-lives for other plant species (grass spp., mugwort, and field horsetail) are summarized in Table 1. The calculated long effective half-lives of ^{137}Cs in herbaceous plants collected at QST-NIRS ranged from 3.5-11.3 y. Using the previously reported data by Komamura et al. (2006), effective half-lives of ^{137}Cs in grains of brown rice and wheat collected throughout Japan were calculated and the values were from 9.7-14.3 y. Thus, the ^{137}Cs from Fukushima fallout almost reached to an apparent equilibrium condition (note: the condition did not mean to be in equilibrium with stable Cs conditions in soil). Since the decreasing rates of ^{137}Cs concentrations in herbaceous plants slows, it was assumed that ^{137}Cs in leguminous would kept higher than grass spp. for a long time.
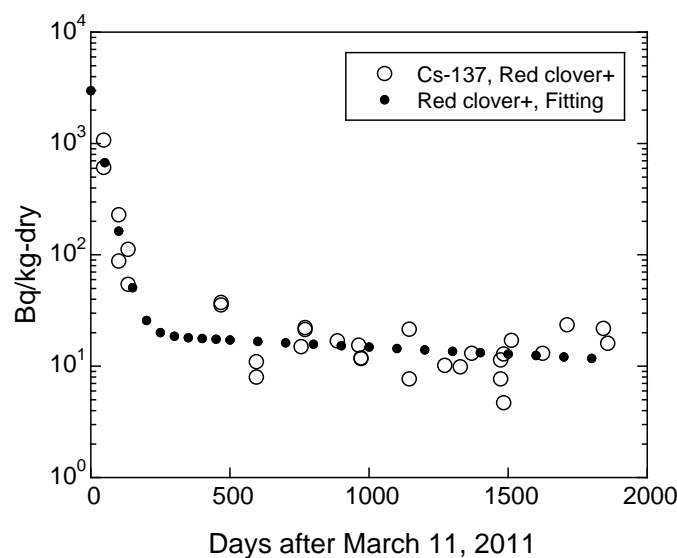
Figure 3. *^{137}Cs concentrations in leguminous plants (red clover and narrow-leaved vetch) collected at QST-NIRS campus and the results of two-component exponential decline curve fitting results.*

Table 1. *Effective half-lives ($T_{eff}s$) of ^{137}Cs observed after the Chernobyl and Fukushima nuclear accident in tree tissues observed in Japan.*

Plant	Short effective half life, y	Long effective half life, y	Comment
Red clover + narrow-leaved vetch	0.06	6.5	
Grass spp.	0.18	11.3	This study
Mugwort	0.22	3.5	
Field horsetail	-	3.5	
Brown rice and wheat grains	-	9.7-14.3	Data from Komamura et al., 2006

Then, why leguminous plants have ability to uptake ^{137}Cs higher than grass spp. is in question. Joner et al. (2004) reported arbuscular mycorrhizal fungi did not contribute to the radiocesium transfer from soil to plants. Interestingly, Mengel & Steffens (1985) reported that K^+ uptake per unit root fresh weight, root surface and root length were significantly higher for red clover than rye-grass. From these results, provably because not due to arbuscular mycorrhizal fungi contribution, but because higher ^{40}K uptake ability by red clover, red clover would concentrate ^{137}Cs in soil more than grass spp. could. However, the root uptake mechanisms of K and Cs were not clarified yet so that more studies are necessary to understand the ^{137}Cs concentration mechanisms by leguminous plants.

Conclusions

We measured ^{137}Cs concentrations in leguminous and non-leguminous herbaceous plants in 2012-2015 collected from the same sampling field. It was found that ^{137}Cs concentrations in red clover samples were the highest among the plant species we observed in this study in 2015. Thus, it was not due to the field management system but the ^{137}Cs uptake ability by leguminous plant species affected the ^{137}Cs differences. Since the long effective half-lives of showed 3.5-11.3 y, the trend would not change for a long time. Unfortunately, however, we could not identify why leguminous plants can take up ^{137}Cs higher than other plant species. Further studies are needed to clarify the radiocesium uptake mechanisms by leguminous plant species.

Acknowledgement

References

Adriano, D.C., McLeod, K.W., Ciravolo, T.G., 1984. Long-term root uptake of radiocesium by several crops. J. Plant Nutr. 7, 1415-1432.

IAEA, 2010. Handbook of Parameter Values for the Prediction of Radionuclide Transfer in Terrestrial and Freshwater Environments. Technical Report Series No. 472. IAEA, Vienna.

Ishii, N., Tagami, K., Takata, H., Fujita, K., Kawaguchi, I., Watanabe, Y., Uchida, S., 2013. Deposition in Chiba Prefecture, Japan of Fukushima Daiichi nuclear power plant fallout. Health Phys. 104, 189-194.

Joner, E.J., Roos, P., Jansa, J., Frossard, E., Leyval, C., Jakobsen, I., 2004. No significant contribution of arbuscular mycorrhizal fungi to transfer of radiocesium from soil to plants. Appl. Environ. Microbiol. 70, 6512-6517.

Kobayashi, D., Okouchi, T., Yamagami, M., Shinano, T., 2014. Verification of radiocesium decontamination from farmlands by plants in Fukushima. J. Plant Res 127, 51-56.

Komamura, M., Tsumura, A., Yamaguchi, N., Kihou, N., Kodaira, K., 2006. Monitoring ^{90}Sr and ^{137}Cs in rice wheat and soil in Japan from 1959-2000. Miscellaneous publication of National Institute for Agro-Environmental Sciences, No.28. ISSN 0912-7542. NIAES, Tsukuba.

Mengel, K., Steffens, D., 1985. Potassium uptake of rye-grass (*Lolium perenne*) and red clover (*Trifolium pratense*) as related to root parameters. Biol. Fert. Soils 1, 53-58.

Ministry of Health, Labour and Welfare, 2016. Levels of Radioactive Contaminants in Foods Tested in Respective Prefectures. Available at: http://www.mhlw.go.jp/english/topics/2011eq/index_food_radioactive.html (accessed 14.10.16.).

Tagami, K. Uchida, S., 2015. Effective half-lives of ^{137}Cs in giant butterbur and field horsetail, and the distribution differences of potassium and ^{137}Cs in aboveground tissue parts. J. Environ. Radioact. 141, 138-145.

Lessons Learnt from Ten Years Investigations of Site-Specific Partitioning Coefficients (K_d) and Concentration Factors (CR)

Ulrik Kautsky, [1] *Sara Grolander* [3]*, Mats Tröjbom*[4] *Peter Saetre* [1]
Sara Nordén [1]*, Rodolfo Avila* [2]

[1] SKB, Swedish Nuclear Fuel and Waste Mngmt. Co. Sweden, ulrik.kautsky@skb.se
[2] Facilia AB, Sweden
[3] Kemakta Konsult AB, Sweden
4 Mats Tröjbom Konsult AB

Abstract

Normally radio-ecological models require solid/liquid partition coefficients (Kd) and organism/media concentration ratios (CR) to able to estimate concentrations in organisms and fate of radionuclides in the biosphere. These concentrations in organisms are used to estimate dose to organisms or to humans consuming the organisms. SKB has performed ten years of site investigation at two potential sites for a final repository of spent fuel in Sweden. Among many other measurements the concentrations of more than 40 elements has been measured in a wide variety environments mainly with ICP-MS methods. Samples have been taken from soil, sediments, plants (including algae), wild animals with different life history and position in trophic levels as well as water from the habitats (marine, lake, rivers, mires and soils). With different methods, site specific Kd and CR values for each element and media or organism have been calculated. Both best estimates (BE) and parameters for probabilistic density functions (PDF) have been used and compared with internationally published values. Many of estimates show correlations with other environmental parameters measured simultaneously (e.g pH, redox conditions, organic matter).

Generally the results show that if sufficient samples are obtained the variation is considerable less than previously published for some elements, but also that for some elements BE can be more than an order of magnitude different from published values.

It is beneficial to have site specific BE for Kd and CR, because correlations to the sites chemistry and ecosystem function are handled in a consistent way for all parameters in the model. There are however also difficulties to handle site data when matched pairs and samples are scarce. Some examples of how this can be handled are discussed.

Keywords: partition coefficient, K_d, concentrations ratios, on site field measurements, stable natural isotopes, ICP-MS,

Introduction

In assessments, most radio-ecological models require solid/liquid partition coefficients (K_d) and organism/media concentration ratios (CR) to be able to estimate concentrations in organisms and fate of radionuclides in the biosphere. These concentrations in organisms are used to estimate dose to organisms or to humans consuming the organisms.

Data can be obtained from international databases (e.g. Beresford et al., 2008; Hosseini et al., 2008; IAEA, 2010; ICRP, 2009) and/or collected from a specific site (e.g. Finnish and Swedish siting programme). Site-specific data are preferred to make estimates for a site during current situations. For assessments of e.g. nuclear wastes repositories the period of assessment requires periods up to 1 million years and datasets from sites analogues to expected future situations are used.

The Swedish Nuclear Fuel Waste Management Co. (SKB) submitted an application for deep repository for spent nuclear fuel 2011, and in 2014 an application for a repository for operational low level waste. These safety assessments required a intensive site characterisation programme over a ten years period (Kautsky et al., 2013). Among many other datasets biogeochemical data were obtained from a variety of surface ecosystems for a large number of elements. From this

dataset solid/liquid partition coefficients (K_d) and organism/media concentration ratios (CR) were calculated and compared with existing data (Tröjbom et al., 2013). These parameters are then used in the radionuclide transport model for the biosphere to estimate dose to humans and non-human biota (e.g. Avila et al., 2013)

In this paper the dataset is exemplified and some lessons learned discussed.

Materials and Methods

The interdisciplinary site investigations were performed during 2001-2011 at two potential sites, Forsmark and Laxemar, for the selection of a final repository of spent fuel in Sweden, The site descriptive model described the ecosystems, hydrology, soils and sediments, chemistry in detail for the different ecosystems; freshwater, (Andersson(ed), 2010), marine (Aquilonius(ed), 2010) and terrestrial (Löfgren(ed), 2010).

Among many other measurements the concentrations of more than 40 elements were measured in a wide variety of environments mainly with ICP-MS methods (c.f. Tröjbom et al., 2013). Samples were taken from soils, sediments, plants (including algae), wild animals with different life history and position in trophic levels as well as water from the habitats (marine, lake, rivers, mires and soils). For the assessment of low level waste (SKB, 2014) K_d values for selected agricultural soils and CRs for crops (cereal) were measured (Sheppard et al., 2011).

Site-specific K_d and CR values for each element and media or organism were calculated (Tröjbom et al., 2013). Both best estimates (BE) and parameters for probabilistic density functions (PDF) were used and compared with internationally published values (Beresford et al., 2008; Hosseini et al., 2008; IAEA, 2010; ICRP, 2009).

The radionuclide transport model (Saetre et al., 2013) has 9 K_d parameters for soils and 2 for particulate matter. Each of these 11 K_d parameters data for the 31 elements included in the safety assessment gives in total 341 unique K_d parameter values to be selected and justified.

The model also needs concentration factors (CR) for 16 types of organisms, for example fishes, algae, cray fish, terrestrial vegetation, mushrooms, terrestrial herbivores and different crops. In total 496 specific CR values were necessary for the model. Additionally, another 1302 CR values were necessary for the assessment of dose to non-human biota (Saetre et al., 2013).

A database was created including site-specific data and available literature data. Fixed criteria were used for data selection which ensured a traceable, systematic and transparent data selection process (Tröjbom et al., 2013).

For K_d parameter most of the cases are parametrised using site-specific data with exception of metals as Ac, Am, Cm, Np, Pd, Po, Pu and Tc where site-specific data were not available. Site-specific data for an element regarded as analogue are used when possible. For some of these elements that is not natural occurring it is not possible to measure site-specific data and gap filling methods, like element analogues are required.

Results and Discussion

For many of elements the estimated K_d values showed variation between soil types. A clear difference of K_d values between soil type with high organic content and those with low organic content were found (Sohlenius et al., 2013). K_d values were strongly affected by pH, organic content and clay content. For most elements the K_d values decreased with decreasing pH and clay content, thus the mobility of metals is higher in soils with lower pH and low clay content. The effect of carbon content on K_d values was both positive and negative as shown in *Figure 1* where K_d values for caesium and uranium are plotted against organic content of the soils in figure A and B respectively. For caesium K_d values are low for soils with high organic content while the opposite is true for uranium. The effect of pH on K_d values for nickel and radium are plotted in figure C and D

respectively. The mobility decreases with increasing pH. The results confirm that K_d values are highly dependent on the soil type and chemical conditions and that site-specific measurements of each soil type included in the model is needed in order to assess the mobility of each element.
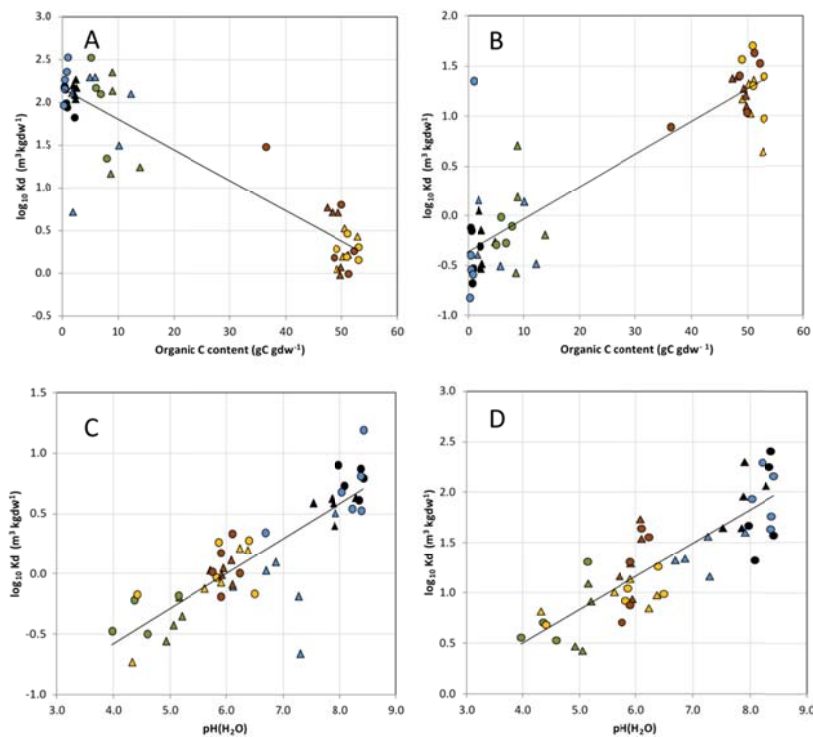
Figure 1 *K_d values for A. Cesium, B. Uranium, C. Nickel and D. Radium plotted against organic content and pH. The color of the symbols represents the different soil types, black clayey till, blue glacial clay, green clay gyttja, yellow cultivated peat, brown wetland peat and the shape of the symbol represent different sampling depths, triangle 20 cm depth circle 50 cm depth.(from Tröjbom et al. 2013).*

Site-specific data shows that if sufficient samples are obtained, the variation is considerable less than previously published for some elements, but also that BE can be more than an order of magnitude different from published values. In

Figure 2 this is illustrated by comparing the geometric means, 5th and 9th percentile from site-specific measurement of K_d in till to reported data for mineral soil and sand from IAEA 2010. There are cases were these two data source do not overlap at all, as for example for calcium (Ca), holmium (Ho), samarium (Sm), tin (Sn) and lead (Pb) in all these cases the site-specific K_d values are higher than the literature data. The variation in reported data from IAEA (2010) is large in some cases as for example for torium (Th) and uranium (U) where the site-specific data fall within the large range of literature data but the geometric mean differs with more than one order of magnitude from value reported by IAEA (2010). Site data for Th is higher than literature data while the opposite is true for U.

The estimates of site-specific concentration ratios (CR) show similar patterns as site-specific K_d, e.g. lower variation for site data, for some elements non overlapping ranges with published data and systematic deviations from published literature values (Tröjbom et al., 2013). Moreover the concentrations in organisms reveal informative relationships between component in the ecosystem and common features for similar species in different ecosystems. For an example the variation of CR is less than order of magnitude for fish in different habitats (lakes or coastal area) and at the different sites (Figure 3.)
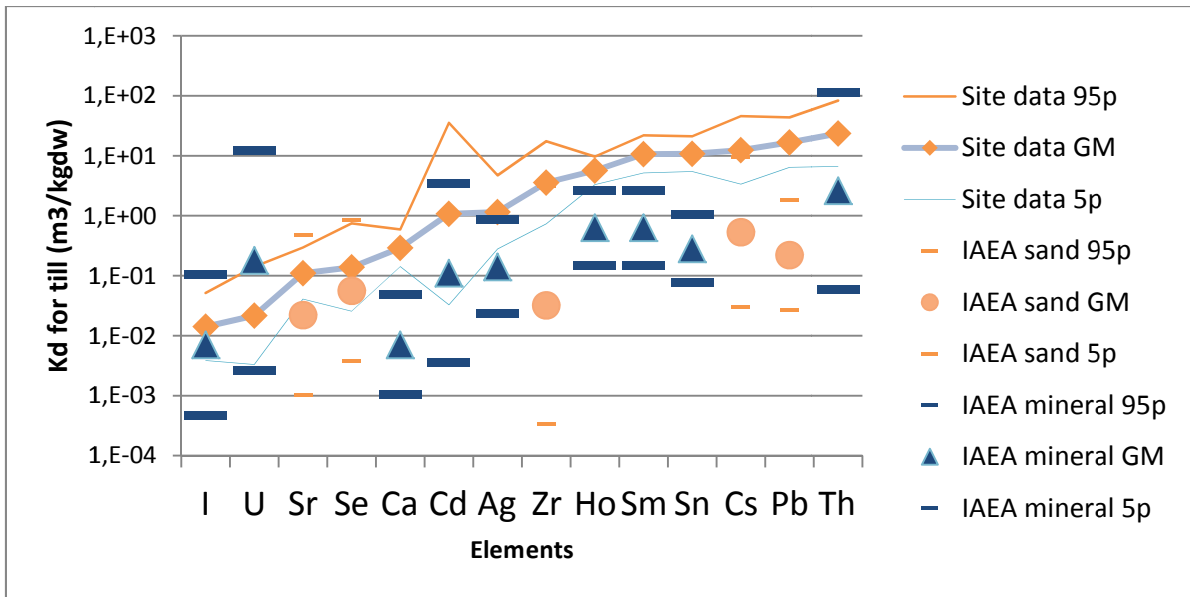
Figure 2 *The site-specific K_d values for deep layer of till in Forsmark are compared to literature data reported for mineral and sandy soils in IAEA 2010. The geometric mean (GM) and 5 percentile (5p) and 95 percentile (95p) is shown for each element and datasource. In many cases the differences between the data sources are large. Adapted from Tröjbom et al 2013.*
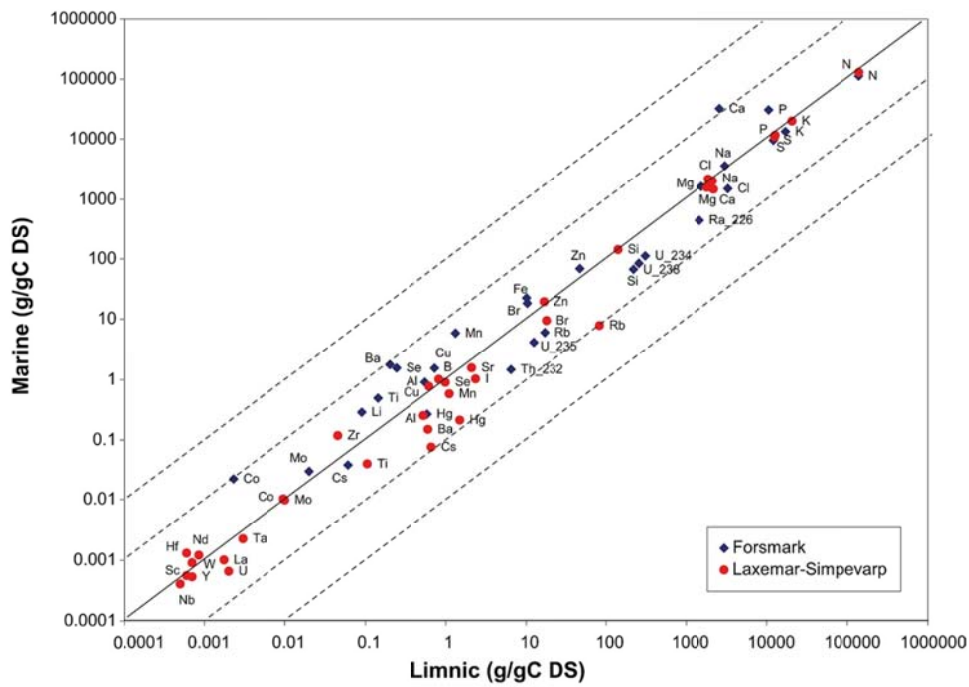
Figure 3 *Comparision of median values of concentrationratios for different elements in sampled fish from freshwater (x-axix) and the Baltic Sea at the two sites, lines shows magnitude of deviation from 1:1 correlation. Adapted from Tröjbom et al 2013.*

The results from the comparative analysis illustrate the importance of site-specific data to be able to predict the mobility and uptake of elements under site-specific conditions. Moreover site data can capture correlations between soils and soil/water chemistry as well ecosystem type in a consistent way, since they are observations from the same system.

Even if there is large site-specific database, data gaps are still common. This is handled using different data gap filling methods as described in detail by Tröjbom et al (2013). A common method is to use analogues for elements with similar chemical properties It is assumed that the selected data are representative for the missing data. A good understanding of local chemical conditions is necessary to select appropriate analogues. For example, the presence of calcite and relict marine ions as sulphate, SO_4^{2-}, will affect analogues for alkaline earth metals (calcium, strontium, barium and radium) in different ways. Ca and Sr will likely precipitate with calcite and therefore these two elements will behave similar in the calcite rich environment at the site. Ba and Ra are less likely to co-precipitate with calcite, instead barium precipitates as barite ($BaSO_4$) (Jaremalm et al., 2013).

Another method that has been used to select element analogues is thermodynamic modelling. For the redox sensitive elements neptunium (Np) and plutonium (Pu) thermodynamic modelling based on groundwater samples is used to predict the dominating oxidation state. K_d values for iron and manganese are used as redox indicators to determine which oxidation state that is dominating and which analogue that is most likely to best represent the redox sensitive element in different environments.

In other cases, the number of samples are low, which gives difficulties to define the variation (as PDF) of the parameters. The geometric standard deviation (GSD) of all elements for a group of similar parameters is used to identify the range of GSD to be expected for a parameter with few samples (Tröjbom et al., 2013). This method ensures that the PDF is not underestimated due to few samples.

Conclusions

Site-specific data are important since these normally have lower variation and sometimes significantly different best estimates from the reported literature data. The site-investigations ensure that K_d and CR values are reported for the same local chemical environment and correlations and relationships between these parameters are included in the model. The knowledge gained from the site investigations can be used to fill data gaps by use of suitable elements analogues for the specific geochemical condition prevailing at the site.

A database is necessary to efficiently handle the large number of parameters and data sources and also to facilitate data analysis and evaluations. The database ensures traceability and consistent parameterisation methods. Even if data handling is automatized in the database it is important with manual control and evaluation to identify inconsistency in parameter values. The manual evaluation has ensured that elements with similar properties have similar K_d and CR values.

Moreover, the detailed database can be used in future re-evaluations or alternatives approaches replacing traditional K_d values or CR .

References

Andersson(ed), E., 2010. The limnic ecosystems at Forsmark and Laxemar-Simpevarp. Svensk Kärnbränslehantering AB, Stockholm, Sweden, p. 578.

Aquilonius(ed), K., 2010. The marine ecosystems at Forsmark and Laxemar-Simpevarp. SR-Site Biosphere. Svensk Kärnbränslehantering AB, Stockholm, Sweden, p. 504.

Avila, R., Kautsky, U., Ekström, P.-A., Åstrand, P.-G., Saetre, P., 2013. Model of the long-term transport and accumulation of radionuclides in future landscapes. Ambio 42, 497-505.

Beresford, N.A., Barnett, C.L., Howard, B.J., Scott, W.A., Brown, J.E., Copplestone, D., 2008. Derivation of transfer parameters for use within the ERICA Tool and the default concentration ratios for terrestrial biota. Journal of Environmental Radioactivity 99, 1393-1407.

Hosseini, A., Thørring, H., Brown, J.E., Saxén, R., Ilus, E., 2008. Transfer of radionuclides in aquatic ecosystems – Default concentration ratios for aquatic biota in the Erica Tool. Journal of Environmental Radioactivity 99, 1408-1429.

IAEA, 2010. Handbook of parameter values for the prediction of radionuclide transfer in terrestrial and freshwater environments. International Atomic Energy Agency, Vienna.

ICRP, 2009. Environmental Protection: Transfer Parameters for Reference Animals and Plants. ICRP Publication 114. Ann. ICRP 39.

Jaremalm, M., Köhler, S., Lidman, F., 2013. Precipitation of barite in the biosphere and its consequences for the mobility of Ra in Forsmark and Simpevarp. Svensk Kärnbränslehantering AB, Stockholm.

Kautsky, U., Lindborg, T., Valentin, J., 2013. Humans and ecosystems over the coming millennia - overview of a biosphere assessment of radioactive waste disposal in Sweden. Ambio 42, 383–392.

Löfgren(ed), A., 2010. The terrestrial ecosystems at Forsmark and Laxemar-Simpevarp. SR-Site Biosphere. Svensk Kärnbränslehantering AB, Stockholm, Sweden, p. 444.

Saetre, P., Nordén, S., Keesmann, S., Ekström, P.-A., 2013. The biosphere model for radionuclide transport and dose assessment in SR-PSU. , . Svensk Kärnbränslehantering AB, Stockholm, p. sohisso.

Sheppard, S., Sohlenius, G., Omberg, L.-G., Borgiel, M., Grolander, S., Nordén, S., 2011. Solid/liquid partition coefficients (Kd) and plant/soil concentration ratios (CR) for selected soils, tills and sediments at Forsmark. Svensk Kärnbränslehantering AB, Stockholm, Sweden.

SKB, 2014. Safety analysis for SFR Long-term safety. Main report for the safety assessment SR-PSU. Svensk Kärnbränslehantering AB.

Sohlenius, G., Saetre, P., Nordén, S., Grolander, S., Sheppard, S., 2013. Inferences about radionuclide mobility in soils based on the solid/liquid partition coefficients and soil properties. Ambio 42, 414-424.

Tröjbom, M., Grolander, S., Raguz, V., Nordén, S., 2013. Kd and CR used for transport calculations in the biosphere in SR-PSU. Svensk Kärnbränslehantering AB, Stockholm.

Seasonal variation of concentration ratios for ICRP's Reference Animal and Plants in terrestrial Mediterranean ecosystems

*J. Guillén[*a], N. A. Beresford[b,c], A. Baeza[a], M. Izquierdo[d], M.D. Wood[c], A. Salas[a], A. Muñoz-Serrano[a], J.M. Corrales-Vázquez[e] and J.G. Muñoz-Muñoz[a]*

[a] LARUEX, Dpt. Applied Physics, Faculty of Veterinary Sciences, University of Extremadura, Avda. Universidad, s/n, 10003, Cáceres, Spain.

[b] NERC Centre for Ecology & Hydrology, Lancaster Environment Centre, Bailrigg, Lancaster LA1 4AP, UK

[c] School of Environment and Life Sciences, University of Salford, Manchester, M5 4WT, UK

[d] School of Biosciences, Faculty of Science, University of Nottingham, Sutton Bonington Campus, Leicestershire, LE12 5RD, UK

[e] Department of Experimental Sciences and Mathematics Teaching, University of Extremadura, Avda. Universidad, s/n, 10003, Cáceres, Spain

Abstract

The International Commission on Radiological Protection (ICRP) have proposed a system for the radiological protection of the environment based on the use of Reference Animals and Plants (RAPs).Seasonal variation may be important in all climatic types.In the case of Mediterranean ecosystem, seasonal variations may influence the transfer of elements in a different way than in temperate ecosystems. This is because the strong variation in temperature and precipitation can significantly alter the availability of nutrients in the ecosystem. In the present work, variation of whole organism concentration ratios, CR_{wo}, was determined for several stable elements (I, Li, Be, B, Na, Mg, Al, P, S, K. Ca, Ti, V, Cr, Mn, Fe, Co, Ni, Cu, Zn, As, Se, Rb, Sr, Mo, Ag, Cd, Cs, Ba, Tl, Pb and U) in selected terrestrial RAPs in two different Mediterranean ecosystems: a pinewood and a dehesa (grassland with disperse tree cover). For this paper the RAPs considered in the pinewood ecosystem were Pine Tree and Wild Grass; whereas in the dehesa ecosystem those considered were Deer, Rat and Wild Grass. Seasonal variation was observed to be likely site-dependent, and depended on the element-RAP combination.

Introduction

The ICRP have proposed a system for the radiological protection of the environment based on the concept of Reference Animals and Plants (RAPs) (ICRP 2008).There are different models in the literature to assess the dose rate to RAPs. Most of them, such as ERICA (Brown et al., 2016), RESRAD-BIOTA (USDoE, 2002), R&D128/SP1a (Copplestone et al., 2001; 2003) use a quasi-equilibrium approach to estimate the activity concentration in organisms and consequently their internal dose rate.Concentration ratios, CR_{wo}, are used in such models (Beresford et al. 2008) to predict activity concentrations in wildlife assuming that there is equilibrium between the whole organism (RAP) and the appropriate medium (e.g. soil in the case of terrestrial ecosystems). There is a lack of CR_{wo} data (ICRP, 2009) for many element-RAP combinations. CR_{wo} values are also likely to be highly site specific which contributes to the large variation observed within the

---

available data,much of which originates from Europe andNorth America, mainly for temperate and artic ecosystems (Howard et al., 2013). As the CR_{wo} values are defined for quasi-equilibrium approach, it is assumed to be approximately constant throughout the year. However, seasonal variation of radionuclide transfer has been previously reported with an increase in radionuclide uptake from November to February for Mediterranean grazing-land ecosystems (Baeza et al., 2001). The alternation between hot dry seasons (mainly summer) and cold wet seasons (mainly winter) reflectsvariation innutrient availability in each season.Seasonal variation of transfer and element concentration inbees in Spain have also been reported (Gutiérrez et al., 2015). This seasonal pattern contrast to that observed in temperate ecosystems following the Chernobyl accident where radiocaesium concentrations in grazing animals and herbaceous vegetation was highest during summer months (see Beresford et al. 1996).

The goal of this study is to analyze the seasonal variation of CR_{wo} values for some terrestrial RAPs (Rat, Deer, Wild Grass and Pine Tree) collected in Mediterranean ecosystems for 32 elements (Ag, Al, As, Ba, Be, Ca, Cd, Co, Cr, Cs, Cu, Fe, I, K, Li, Mg, Mn, Mo, Na, Ni, P, Pb, Rb, Sr, Ti, Tl, U, V and Zn). The main sampling site was a Dehesa, which is a typical Mediterranean semi-natural grassland with disperse tree cover, mainly holm oaks. As there was no pine tree at this location, a Pinewood located in the vicinity was also selected. Pine Tree wood and Wild Grass were collected from this second site.

Materials and Methods

Sampling sites

Two locations were selected for sampling terrestrial RAPs in the province of Cáceres, western Spain, in the surroundings of Monfragüe National Park: a dehesa and a pinewood (Figure 1) (Guillén et al., 2016). The climate is dry sub-humid (Csa in Köppen classification), with annual average temperature of 16ºC and hot summer. The Dehesa extends over more than 4,600 ha.It serves as hunting reserve, mainly for red deer (*Cervuselaphus*) and wild boar (*Susscrofa*). Soil texture was silt-loam with a pH 6.5 at the Dehesa. As no pine treeswere present in the selected Dehesa, a Pinewood located about 16 km from Dehesa sitewas selected. It isa natural pinewood with no management. Wild grass and pine tree were sampled at this location. The texture of Pinewood site soil was loamy-sand with a pH 5.2.

Table 1 lists the representative species of RAPs sampled at the Dehesa and Pinewood sites. Rat, Deer, Wild Grass and Pine Tree were collected in different seasons (summer, autumn, winter and spring) during 2014/15. No Deer was sampled in spring, because it was close season.Individuals for vertebrate animals were skinned and different tissues were separated: muscle, bone, liver, kidney and thyroid. In summer no Deer thyroid was possible to collect, and therefore data for summer are not shown. Wild Grass collected in summer was very dry, with a dry content of about 77 % and higher. As the Rat thyroid gland was too small to isolate it directly, the area of tissue around it was sampled. Prior to analysis, biota samples were freeze-dried and stored in a desicator, ground using a nitrogen mill and then acid digested.

Soil samples(0 – 10 cm) were collected in the Dehesa and Pinewood at the same time as Wild Grass and Pine Tree sampling. For each season at each site 6 soil samples were collected from a 500 m^2 area and combined to form a composite sample for subsequent analysis. Samples were sieved, and fractions greater than 2 mm were discarded. Soil samples were then homogenized and oven dried (c. 60°C).

ICP-MS analysis.

Soil digestion (about 0.2 g) was undertaken by adding concentrated HF, HNO_3 and $HClO_4$ (2.5:2:1 mL), and heating to 160°C overnight. Plant and animal tissues were acid digested with

microwave oven at 140 ºC for 20 min. with: a) 6 mL *Primar* grade HNO_3 for plants, or b) HNO_3, MilliQ ultrapure water and 30% v/v H_2O_2 (3:2:2 mL) for animal tissues. Alkaline extraction with tetramethylammonium hydroxide (TMAH) was used to determine iodine content in the samples. Iodine analyses were carried out in thyroids samples and if enough mass was available (greater than 0.3 g dry matter (DM)) in the other sample types. For soils, aliquots of 1 g were weighed into polypropylene tubes and 10 mL of 10% TMAH were added. The soil suspensions were heated at 90°C for 24 h, and then centrifuged at 3500 rpm for 30 min.
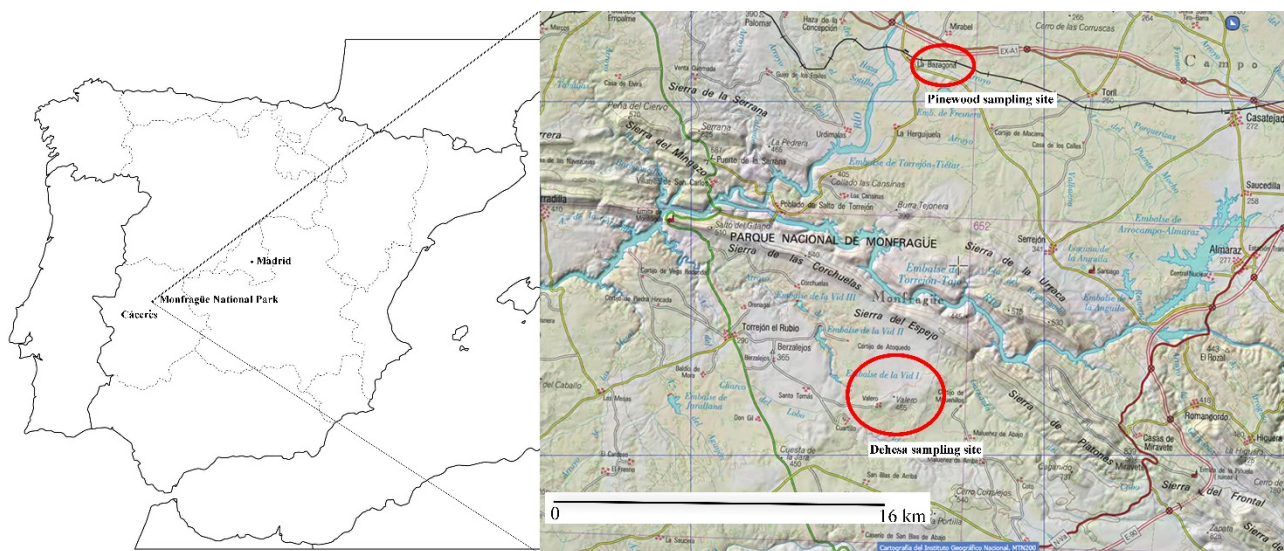
Figure 1.*General location of the Dehesa and Pinewood sampling sites.*

RAP	Family	Family/Species sampled	Sampling Site
Rat	*Muridae*	*Apodemussylvaticus*	Dehesa
Deer	*Cervidae*	*Cervuselaphus*	
Wild Grass	*Poceae*	*Briza minor*	Dehesa and Pinewood
Pine Tree	*Pinaceae*	*Pinuspinaster*	Pinewood

Table 1.*Representative species of terrestrial Reference Animals and Plants sampled from the Dehesa and Pinewood sites in different seasons (summer, autumn, winter and spring).*

Multi-element analysis of diluted solutions was undertaken by ICP-MS. Sample processing was undertaken using Qtegra™ software (Thermo-Fisher Scientific) utilizing external cross-calibration between pulse-counting and analogue detector modes when required.Iodine analysis was undertaken separately, using a 1% TMAH (tetramethylammonium hydroxide) matrix for standards and samples.

Detection limits were calculated as 3 times the standard deviation of the reagent blanks for each extraction form and sample type. Blank samples and Certified Reference Materials (CRM) NIST SRM 2711a Montana soil, NIST 1573a Tomato Leaves, NIST 1577c Bovine Liver were digested and prepared in a similar manner to check the accuracy and precision of the digestion and analysis methods.

Results and Discussion

The whole-body concentrations for Rat and Deer were calculated assuming that the tissues analyzed (thyroid, liver, kidney, meat and bone) represented the whole animal (an approach taken by Barnett et al. (2014) in a similar study). For Deer, fresh mass percentages of the whole-body for each tissue were assumed to be the same as roe deer collected in the UK (Barnett et al., 2014).

CR_{wo} is defined as the ratio between the equilibrium activity concentration of a radionuclide in an organism and the corresponding medium (ICRP 2009). In the existing models and data compilations CR_{wo} values are present by element assuming the same value for all isotopes (of that element) including stable isotopes (eq. 1) (Copplestone et al. 2013) so here CR_{wo} is defined as:

$$CR_{wo} = \frac{Concentration\ element\ X\ in\ whole\ body\ RAP\ (mg\,/\,kg\ FM)}{Concentration\ element\ X\ in\ soil\ (mg\,/\,kg\ DM)} \quad (1)$$

For comparative purposes, a selection of alkali (K, Rb, and Cs), alkaline earth (Ca, Sr and Ba), heavy metal (Pb) elements, and I and P have been used. Figure 2 shows the CR_{wo} variation for Rat in the period summer 2014 - winter 2015.A maximum in autumn can be observed for P, Rb and Pb within the same order of magnitude, and for Ca, Sr, Ba and Cs. Iodine concentrations were under detection limits in autumn, but the CR_{wo} in winter and spring were about one order of magnitude higher than the detection limits. The I CR_{wo} values should be considered as provisional at the moment, as they require some additional verification.

Figure 3 shows the CR_{wo} seasonal variation for Deer. It showed a lower degree of seasonal variation compared to Rat. A slight increase in autumn can be observed in P, Ca, Sr, Ba, which may be related to the antler generation;antlers are formed by bone tissue, shed annually in spring and regenerated again at the beginning of autumn. Antlers have been reported to bioaccumulate ^{90}Sr, and stable alkaline earth elements (Ca, Mg and stable Sr) (Baeza et al., 2011).Antler generation may be responsible for the autumn maximum in CR values for these elements in Deer, due to the need for nutrients required for their growth. This need was also reported in the traslocation of these elements from bone to antlers (Baxter et al., 1999). The CR_{wo} for Pb presented a variation about one order of magnitude, with a minimum in autumn. However, the Cs CR_{wo} values in autumn and winter increased compared to those in summer. The K CR_{wo} presented minimal variations, about 7 % variation over the mean value, due to its homeostatic behaviour.

Figure 4 shows the seasonal variation of CR_{wo} for Wild Grass at the Dehesa and Pinewood sampling sites. It can be observed that there is no similar trend for all radionuclides, suggesting that seasonal variations may be related to nutrient and water seasonal variations in each site. In the Dehesa site, a maximum in autumn can be observed for most elements, with variations of 1-2 orders of magnitude across the year. In the Pinewood site, this trend (maximum value in autumn) was only observed for P and Ca, which may be related to the nutrient availability. The rest of elements showed a decreasing trend in Pinewood site, with maximum values in summer.

Figure 5 shows the seasonal variation of CR_{wo} for Pine Tree. It presented the smallest seasonal variability of the RAPs analyzed, the variation was kept in the same order of magnitude. The P CR_{wo} values presented the same variation as the other RAPs analyzed, a maximum value in autumn. The Cs CR_{wo} presented a variation about one order of magnitude, but it was under detection limit in summer and spring.
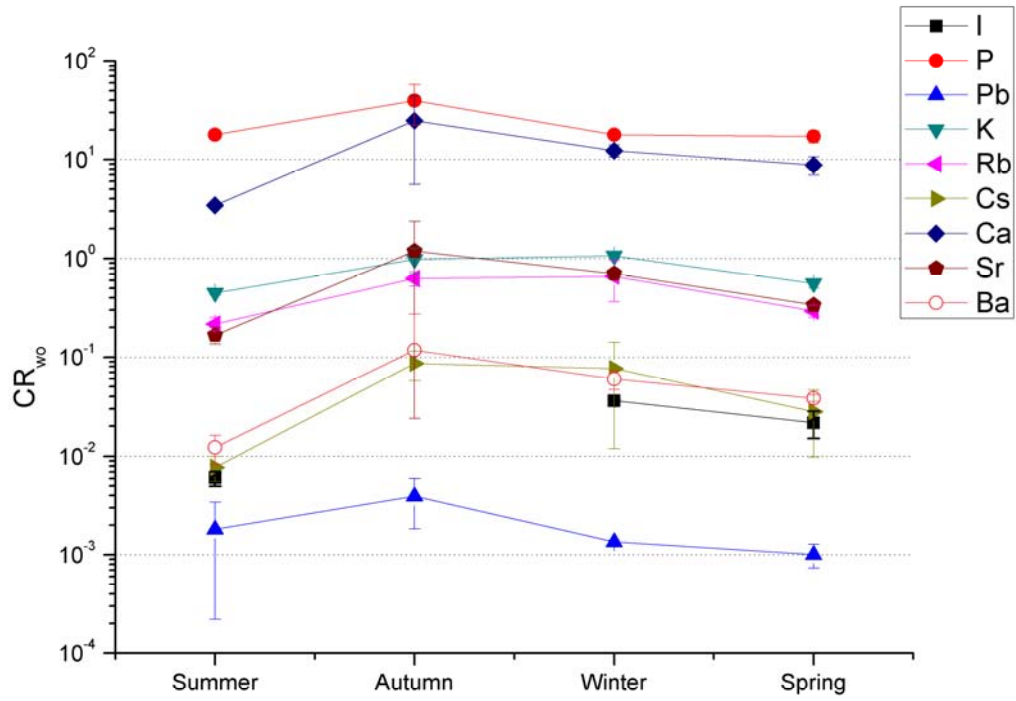
Figure 2.*Seasonal variation of CR$_{wo}$ values for I, P, Pb, K, Rb, Cs, Ca, Sr and Ba for Rat.*
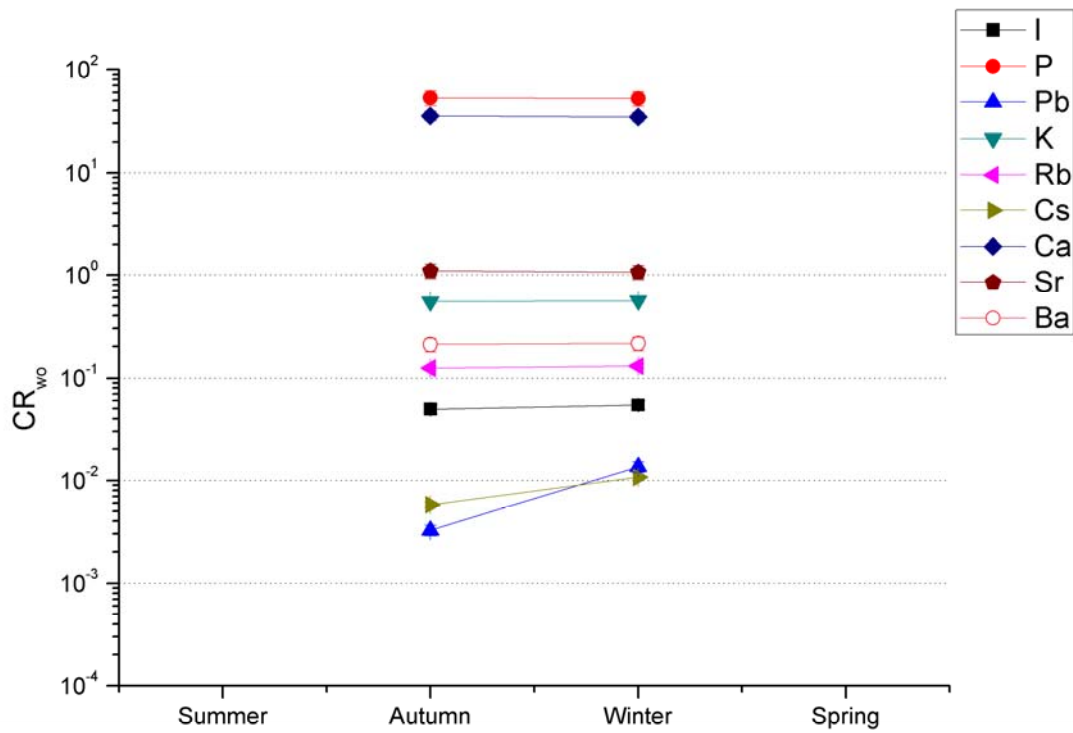
Figure 3.*Seasonal variation of CR$_{wo}$ values for I, P, Pb, K, Rb, Cs, Ca, Sr and Ba for Deer.*
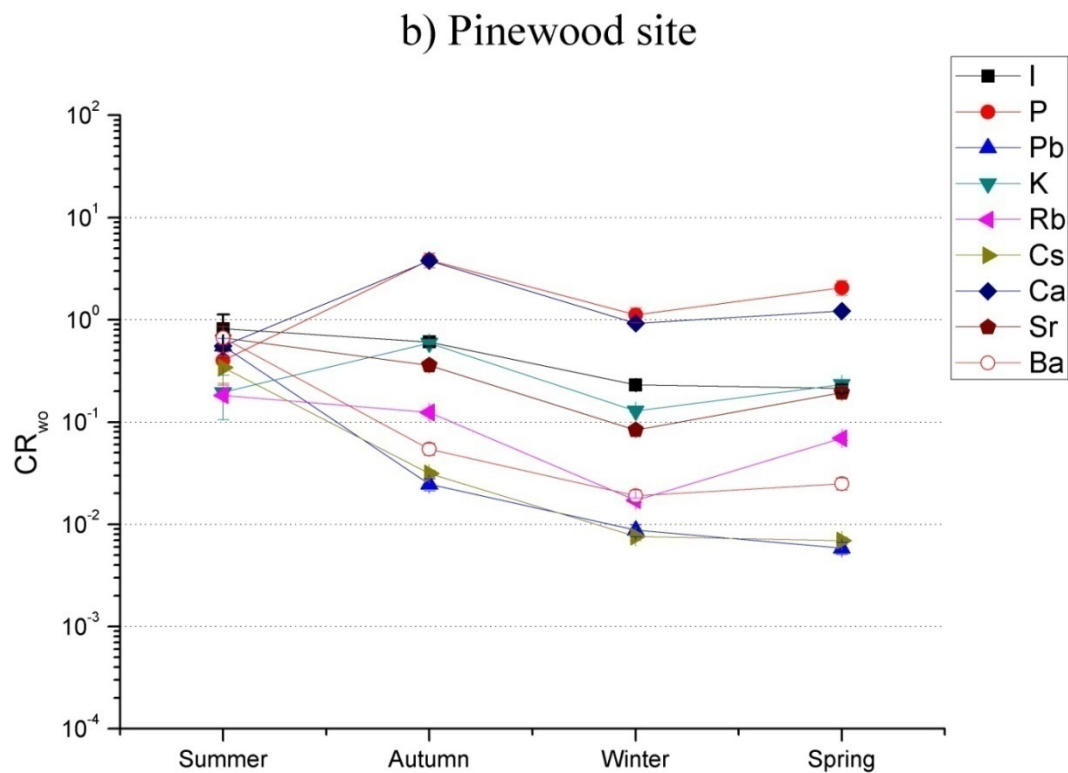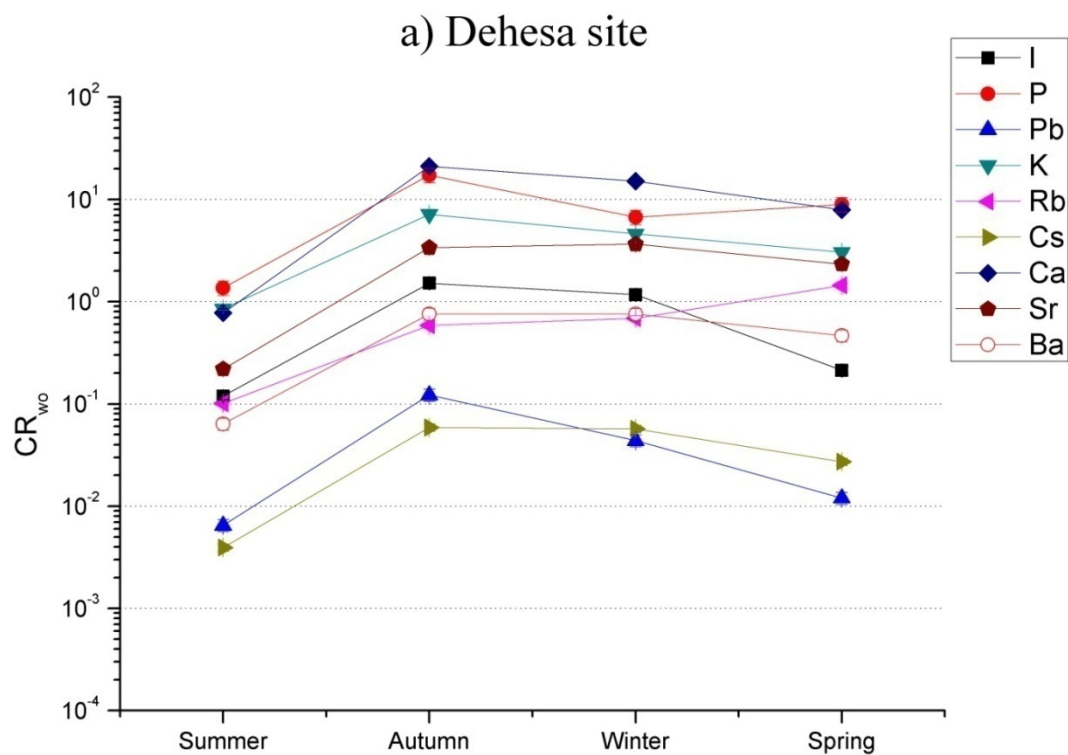
Figure 4. *Seasonal variation of CR$_{wo}$ values for I, P, Pb, K, Rb, Cs, Ca, Sr and Ba for Wild Grass sampled in a) Dehesa site and b) Pinewood site.*
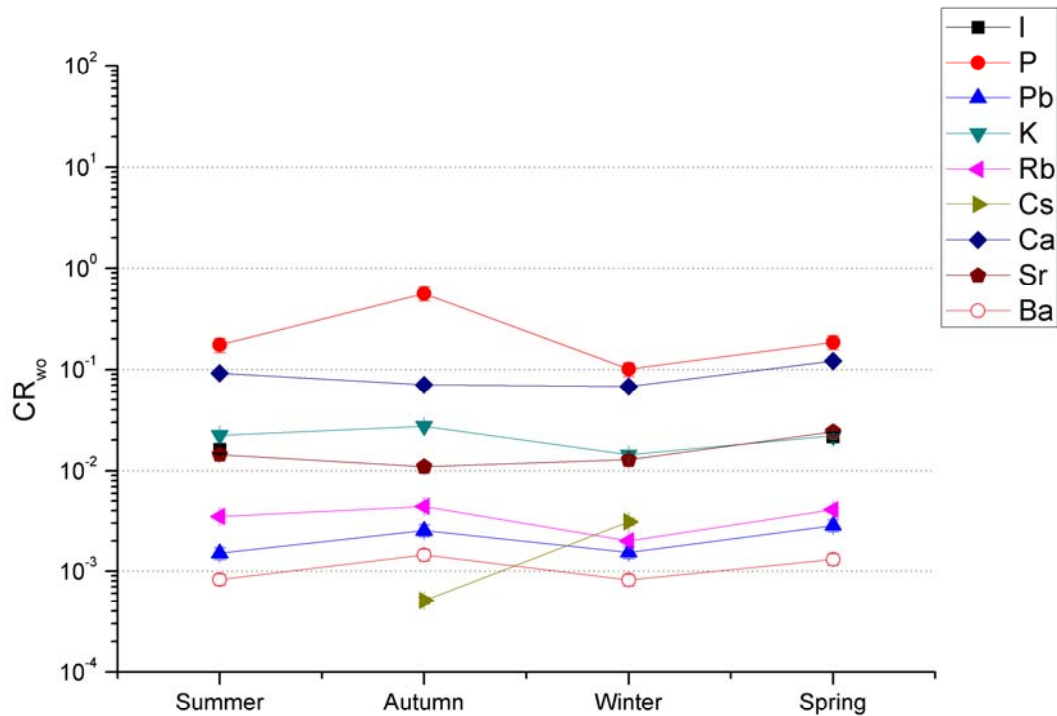
Figure 5. Seasonal variation of CR_{wo} values for I, P, Pb, K, Rb, Cs, Ca, Sr and Ba for Pine Tree.

Conclusions

The seasonal variation of CR_{wo} values for different elements (I P, Pb, K, Rb, Cs, Ca, Sr and Ba) was analyzed for different RAPs (Rat, Deer, Wild Grass and Pine Tree) in two Mediterranean ecosystems (Dehesa and Pinewood).

- Seasonal variations up to 1 - 2 orders of magnitude were observed.

- This variation was not the same for all elements and RAPs.

- Seasonal variation is likely to be site dependent, as for most elements the seasonal variation in Wild Grass was different in the Dehesa and Pinewood ecosystems, maybe related to nutrient and water availability.

- However, the seasonal variation for P was the same for all RAPs and sites, showing a maximum value in autumn.A similar trend was observed for Ca in all RAPs, except for Pine Tree.

References

1. Baeza, A., Paniagua, J., Rufo, M., Guillén, J., Sterling, A., 2001. Seasonal variations in radionuclide transfer in a Mediterranean grazing-land ecosystem. J. Environ. Radioactiv. 55, 283-302.

2. Baeza, A., Vallejo, A., Guillén, J., Salas, A., Corbacho, J.A., 2011.Antlers of *Cervuselaphus* as biomonitors of ^{90}Sr in the environment. J.Environ. Radioactiv.102, 311-315

3. Barnett, C.L., Beresford, N.A., Walker, L.A., Baxter, M., Wells, C., Copplestone, D., 2014. Transfer parameters for ICRP reference animals and plants collected from a forest ecosystem. Radiat.Environ.Biophys. 53, 125–149

4. Baxter, B.J., Andrews R.N., Barrel G.K., 1999. Bone turnover associated with antler growth in red deer (*Cervuselaphus*). Anat. Rec. 256(1), 14-19

5. Beresford, N.A., Barnett, C.L., Crout, N.M.J. & Morris, C. 1996. Radiocaesium variability within sheep flocks: Relationships between the ^{137}Cs activity concentrations of individual ewes within a flock and between ewes and their progeny. Sci. Tot. Environ., 177, 85-96. http://dx.doi.org/10.1016/0048-9697(95)04863-4

6. Beresford, N.A., Barnett, C.L., Brown, J., Cheng, J-J. Copplestone, D., Filistovic, V., Hosseini, A., Howard, B.J., Jones, S.R., Kamboj, S., Kryshev, A., Nedveckaite, T., Olyslaegers, G., Saxén, R., Sazykina, T., VivesiBatlle, J., Vives-Lynch, S., Yankovich, T. and Yu, C. 2008. Inter-comparison of models to estimate radionuclide activity concentrations in non-human biota. Radiat. Environ. Biophys., 47, 491–514.

7. Brown, J.E., Alfonso, B., Avila, R., Beresford, N.A., Copplestone, D., Hosseini, A., 2016. A new version of the ERICA tool to facilitate impact assessments of radioactivity on wild plants and animals J.Environ.Radioactiv. 153, 141-148.

8. Copplestone, D.,Bielby, S., Jones, S.R., Patton, D., Daniel, P.,Gize, I., 2001. Impact Assessment of Ionising Radiation on Wildlife. R&D Publication 128. Environment Agency, Bristol.

9. Copplestone, D.,Wood, M. D.,Bielby, S., Jones, S. R., Vives i Batlle, J., Beresford, N.A., 2003. Habitat Regulations for Stage 3 Assessments: Radioactive Substances Authorisations. R&D Technical Report P3-101/Sp1a. Environment Agency, Bristol.

10. Copplestone, D.C., Beresford, N.A., Brown, J., Yankovich, T., 2013.An International database of radionuclide concentration ratios for wildlife: development and uses. J.Environ.Radioactiv. 126, 288-298.

11. Guillén, J., Beresford, N.A., Baeza, A., Izquierdo M., Wood, M.D., Salas, A., Muñoz-Serrano, A., Corrales-Vázquez, J.M., Muñoz-Muñoz.J.G., 2016. Transfer parameters for ICRP's Reference Animals and Plants in terrestrial Mediterranean ecosystems. Presentation at the II International Conference on Radiological concentration Processess (50 years later), 6th - 9th November 2016, Seville, Spain.

12. Gutiérrez. M., Molero.R., Gaju. M., van der Steen.J., Porrini.C., Ruiz. J.A., 2015.Assessment of heavy metal pollution in Córdoba (Spain) by biomonitoring foraging honeybee. Environ. Monit. Assess. 187,651

13. Howard, B.J., Beresford, N.A., Copplestone, D., Telleria, D., Proehl, G., Fesenko, S., Jeffree, R., Yankovich, T., Brown, J., Higley, K., Johansen, M., Mulye, H., Vandenhove, H., Gashchak, S., Wood, M.D., Takata, H., Andersson, P., Dale, P., Ryan, J., Bollhöfer, A., Doering, C., Barnett, C.L., and Wells, C., 2013. The IAEA Handbook on Radionuclide Transfer to Wildlife. J. Environ. Radioact. 121, 55–74

14. ICRP, 2008. Environmental Protection - the Concept and Use of Reference Animals and Plants. ICRP Publication 108. Annals of the ICRP 38 (4-6).
15. ICRP, 2009. Environmental Protection: Transfer Parameters for Reference Animals and Plants. Strand, P., Beresford, N.A., Copplestone, D., Godoy, J., Jianguo, L., Saxén, R., Yankovich, T., Brown. J. Annals of the ICRP: Publication 114, 39, 6.
16. USDoE, United States Department of Energy, 2002. A Graded Approach for Evaluating Radiation Doses to Aquatic and Terrestrial Biota. DOE-STD-1153-2002, Dept. Energy, Washington, D.C-.

Acknowledgement

Site-specific soil to plant concentration ratios for wild berries

J. Kuusisto, L. Parviainen and K. Riekki

Posiva Oy, Olkiluoto 27160 Eurajoki, Finland

Abstract.

Posiva is building a final disposal facility for spent nuclear fuel and low and intermediate level operational waste at Eurajoki in Southwestern Finland. Currently Posiva is preparing for the operational license application where Posiva needs to show that disposal is safe and no harm to humans or environment will be caused; this is done mainly in the safety case. Part of the safety case is the biosphere assessment in which the transportation of radionuclides in the future surface environment is modelled and radiological impacts of the disposal facility are assessed. Because biosphere assessment is done for the actual disposal site, site specific data must be acquired. Site specific concentration data of soils and vegetation is used to model the element storages and fluxes as part of the characterisation of ecosystems for modelling. In the biosphere assessment the future humans are assumed to consume the natural products at the site, and be potentially exposed to radioactive contaminants.

In this study the soil to plant concentration ratios are derived for some wild berry species typical for Finnish nature and diet: buckthorn, blueberry, lingonberry and strawberry. The studies were located at the disposal site and at the reference area around the site which is selected to have similar properties as the disposal site itself. The berry samples were analysed for the chemical concentrations with ICP-MS analysis method. For some of the berry sampling plots, extensive soil study has been carried out. The concentration ratios from soil to berries were calculated and the results are presented for the most important nuclides for the biosphere assessment which are Ag, Cl, Cs, I, Mo, Nb, Ni, Pd, Pb, Se, Sn and Sr.

Introduction

Olkiluoto Island on the west coast of Finland has been selected as the repository site for spent nuclear fuel (Posiva, 2013, p. 9). For the operational license Posiva has to prove that the disposal is safe for humans and environment and all the studies related to the work comprise the so called safety case. Part of the safety case is the biosphere assessment in which the transportation of radionuclides in the future surface environment is modelled and radiological impacts of the disposal facility are assessed. Because biosphere assessment is done for the actual disposal site, site specific data must be acquired (Radiation and Nuclear Safety Authority, 2013). Site specific concentration data of soils and vegetation is used to model the element storages and fluxes as part of the characterisation of ecosystems for modelling. In the biosphere assessment the future humans are assumed to consume the natural products at the site and potentially expose to radioactive contaminants. It is assumed that present diet of humans will remain same in the future (Radiation and Nuclear Safety Authority, 2013). In order to fulfil the requirements of authorities and to perform comprehensive safety assessment it is also important to research transportation of radionuclides and uptake in wild berries as being one essential expose route for humans and animals.

In Finland and especially in rural areas, wild berries have been a nutritionally valuable natural resource (Tikkanen, 2015). Finnish wild berries contain a lot of vitamins, trace elements and fibre together with flavonoids, phenol acids, lignans and tannins. (Roininen & Mokkila, 2007). Especially the sea buckthorn is famous for its high amounts of vitamin C (Chen, et al., 1990; Suryakumar & Gupta, 2011). Blueberry and lingonberry are among the most important forest products in Finland where they are collected typically for household consumption but also for sale (Roininen & Mokkila, 2007, pp. 12-13). For example, in 2011 54% of all Finnish households were engaged in picking berries and the total harvest of blueberries was 14.3 million kg and for lingonberries 16.3 million kg (Vaara, et al., 2013). As wild berries are part of human nutrition, they are also major source of food for many herbivores. Thus in the sense of safety assessment it is important to study all routes of radionuclides in food chains.

Figure 1. Common wild berry species in Finland. A) blueberry (Vaccinium myrtillus), B)Lingonberry (Vaccinium vitis-idaea), C) strawberry (Fragaria vesca) and D) sea buckthorn (Hippophae rhamnoides). Photo D taken by Ville Kangasniemi (2012).

Wild berries like blueberry and lingonberry and strawberry together with sea-buckthorn (*Figure 1*) are very common species currently at Olkiluoto Island and they are also assumed to be the dominant species in the future as the climax stage forests; *myrtillus* type (MT) and *vaccinium* type (VT) in Finnish classification system favours growth of blueberry and lingonberry (Kuusipalo, 1996, pp. 37-47).

In this study the soil to plant concentration ratios for the most important elements for the biosphere assessment (Ag, Cl, Cs, I, Mo, Nb, Ni, Pd, Pb, Se, Sn and Sr (Posiva, 2016)) were calculated with two different methods for blueberry (*Vaccinium myrtillus*), lingonberry (*Vaccinium vitis-idaea*), sea-buckthorn (*Hippophae rhamnoides*) and strawberry (*Fragaria vesca*) (*Figure 1*). Finally a concise analysis was done about the variation of CRs between the two methods and for different wild berry species.

Materials and Methods

Sampling

The sampling of common sea-buckthorn (*Hippophae rhamnoides*) was done twice, first in August 2011 and second time in October 2012 at Viasvesi that belongs to the reference area of biosphere assessment in Satakunta province (*Figure 2*). The sampling area was located near the sea shore that was relatively stark and partly growing reed. The soil samples were also taken at same time as the berry samples at the same area. The top soil at Viasvesi was very coarse grained sandy soil.

The sampling of other wild berries was done in the Olkiluoto Island during years 2011 and 2012 (*Figure 2*). Matching soil samples for calculating concentration ratios were found only for two blueberry and lingonberry[1] samples and one for strawberry. For these berries there is long gap between the dates when the berry samples were collected (2011 - 2012) and when the soil samples (2008) were acquired. The soil samples weren't also acquired exactly from same place as the berry samples, but they were either 100m or 200m range from the berry sample points.

---

[1] Collected from several sampling points due to limited amount of berries from one sampling point
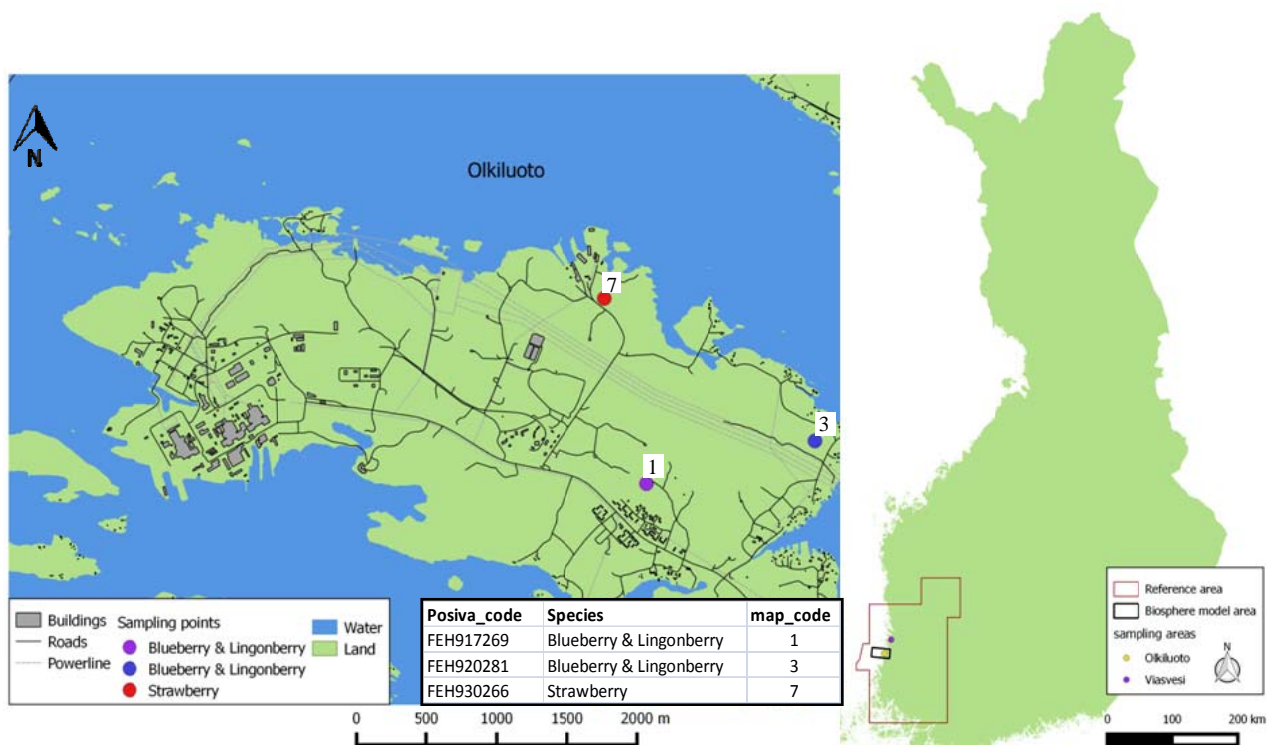
Figure 2. Sample points of blueberry, lingonberry and strawberry at Olkiluoto. The table in bottom right corner represents the corresponding codes Posiva uses and codes used on the map. (National Land Survey of Finland: maastotietokanta 2015, downloaded 1/2016, Projection: ETRS-TM35FIN).

Analytical methods

All berry samples were analysed by ALS Scandinavia, Sweden. Berry samples were freeze dried before analysis and when sample amount was sufficient, a separate DS 105°C was carried out for determining dry matter content. For these samples the final results was recalculated and reported in unit µg/kg DS 105°C. "Total" element analysis was carried after digestion of freeze dried and homogenised samples in a microwave oven with HNO_3 and HF (trace). Element concentrations were analysed with ICP-SFMS. Soil samples were also analysed by ALS. Dried (105 C) soil samples were digested with $LiBO_2$ fusion and HNO_3/HF together with NH_4Ac solutions. The concentrations were analysed with ICP-SFMS or ICP-AES. The concentrations digested with HNO_3/HF and $LiBO_2$ were used to calculate the "total" CRs and the NH_4Ac method for calculating the "bioavailable" CRs. The "total" refers in this case to the all available elements and the "bioavailable" to the amount of elements the plants could uptake.

Soil-to-plant concentrations ratios (CR)

CRs are commonly used in describing migration of radionuclides and uptake in plants in cases that the actual activity concentrations of the reference organisms are not available. The concentrations could be estimated by multiplying the concentrations in the reference media with the appropriate CR. (Brown, et al., 2003). In general, all isotopes of an element are assumed to have the same CR value, because uptake is a process generally unaffected by small deviations in atomic mass or nuclear emissions (Sheppard, et al., 2011, pp. 8-9). CR is basically the ratio of concentration of an element in specific part of the plant divided by the by the concentration in the solid phase of soil (e.g. Brown, et al., 2003; Vera Tome, et al., 2003; Howard, et al., 2013).

The ratio is often expressed as:

$CR_{b,i} = C_{b,i} / C_{soil,i}$ Where:

$CR_{b,i}$ = Concentration ratio for reference organism b and radionuclide i (dimensionless);

$C_{b,i}$ = Activity concentration of radionuclide i in whole body of reference biota (Bq kg^{-1}, fresh or dry weight);

C_{soil} = Activity concentration of radionuclide i in surface soil (Bq kg^{-1} dry weight)

In this study CRs were calculated dividing the concentration in berries (µg/kg DW) by concentrations of soil (µg/kg DW). Some of the concentrations results were below the limit of quantification, but the results were still used in the calculations of CRs. In cases where the concentrations in berries were below LOQ, the value used was the LOQ itself but if the concentrations in soil were below LOQ then LOQ/2 was used to ensure that CR values are not underestimated and they stay on the conservative side. There was also uncertainty in the concentration results for Pd due the interference in the ICP-SFMS. In these cases if the measured value was above LOQ then the measured value was used in calculations, but if the value was below LOQ then the value of LOQ itself was used. All measurements below LOQs in certain sample are listed in table 1.

Higher CR values indicate higher uptake in vegetation and vice versa (Sheppard, et al., 2009, p. 4). It needs to be recognised that CRs describe the uptake of elements in steady state conditions assuming that uptake will linearly increase or decrease proportionally to the changes in substrate concentrations. This assumption could be considered valid for non-essential elements, which are migrated via diffusion (passive process) governed by concentration differences (Raguz, et al., 2013; Vera Tome, et al., 2003). For essential elements that the uptake is active the assumption of linearity is not very realistic because the uptake of essential elements will decrease at certain level when need for element is satisfied and the active uptake does not increase more even if the substrate concentration continues increase. (Tuovinen, et al., 2016; Vera, et al., 2003). However, despite the assumption of linearity isn't valid in all cases, it is still possible to select the conservative parameter values for radionuclide transport modelling.

Results and Discussion

Generally, the CRs for sea buckthorn vary highly among the key elements and the bioavailable CRs are clearly higher for all elements (*Figure 3*). Temporal variability of bioavailable CRs is moderate for almost all elements and high only for Ag, I, Pd and Sn. The total CRs vary generally less than bioavailable CRs because the bioavailable concentrations comprise the most mobile portion of total element concentrations and they are harder to determine. Contrary to the high CRs of bioavailable concentrations the distribution coefficient (*Kd*) values are typically lower than *Kd* - values calculated with total values.
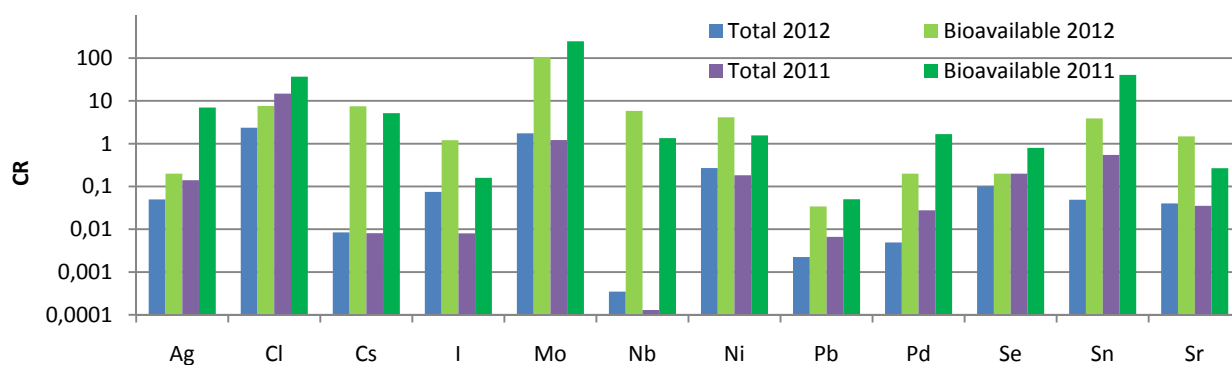
*Figure 3. Total and bioavailable CRs of sea buckthorn (Hippophae rhamnoides) at Viasvesi in years2011 & 2012.*Only total CRs for Cl and Mo reach higher values than the equilibrium level (CR = 1), but the majority of the bioavailable CRs reach the value of 1 with the exception of Pb and Se. It can be seen from the figure 3 that some elements like Cl and Mo which are very mobile in most conditions (Kabata - Pendias & Mukherjee, 2007, p. 433; Söderlund, et al., 2011, pp. 61 - 66) get also highest CRs. The mobility of Cl and Mo is found to be very high in sandy soils as they follow well the movement of water. The big differences between total and bioavailable CRs for Nb are caused mainly due that the extremely low concentrations in berries but the total concentrations soil is high and bioavailable low. This refers that Nb has typically very high *Kd* - value which means that is very immobile in soils (Söderlund, et al., 2014).

The variability of lingonberry CRs is also high and the bioavailable ratios are higher than total ratios (
Figure 4). The highest total and bioavailable CRs were calculated for Mo, Cl and Cs at sample point 1. At sample point 3 Mo has also highest bioavailable CR but Cl has highest total CR. Spatial variability of the total CRs at sample points 1 and 3 is lower than variation of bioavailable CRs.

Figure 4. *Total and bioavailable CRs for lingonberry (Vaccinium vitis-idaea) at Olkiluoto sample points 3(A) and 1(B) (Figure 2). In A there was no NHAc (bioavailable) data from soil samples for Sn and the concentratiosn for strontium were determined with ICP-AES method as the other concentrations were measured with ICP-SFMS. Total CR of Nb at sample point 1 was below 0,0001 and not shown in this figure.*

For lingonberry at sample point 3 only the bioavailable CRs for Mo, Ni and Sr reached values higher than 1. At sample point 1 bioavailable CRs for Cl, Cs, Mo and Sn were above equilibrium level. However, only the total CR for chlorine was higher than 1.

For blueberry at same sample points (3 and 1) the CRs varied almost identical to the lingonberry (*Figures 4 & 5)*. This similarity is mostly explained with the same soil properties for the same sample points (Figure 2) and the similarity of the wild berry species. Mo got highest total and bioavailable CRs at sample point 3. At sample point 1 the highest total CRs were calculated for Cl

and highest bioavailable values for Mo. The total CRs of Mo at sample point 3 was slightly higher than in the sample point 1 but for the bioavailable CRs the situations was opposite.
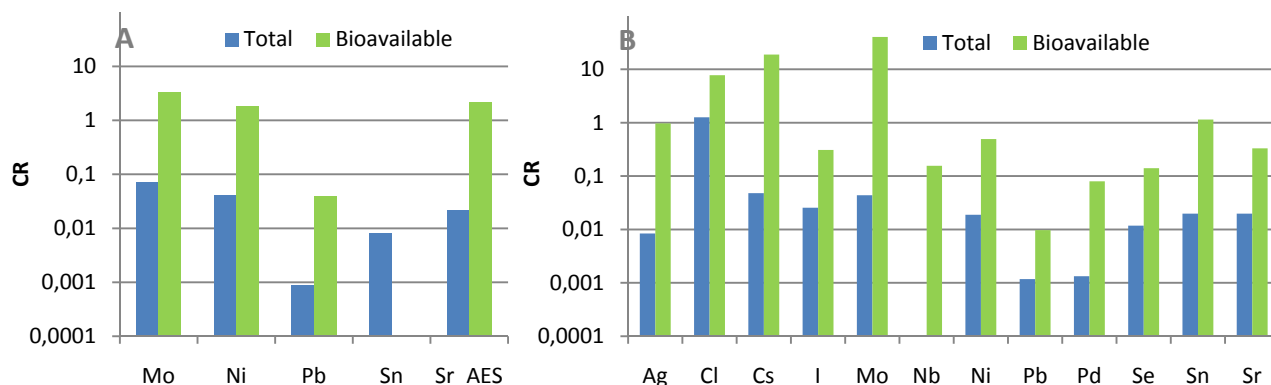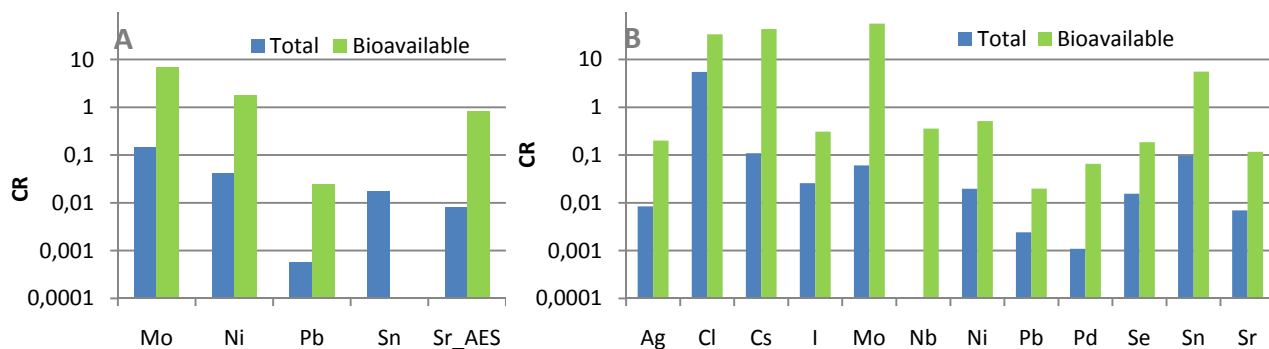

Figure 5. Total and bioavailable CRs for blueberry (Vaccinium myrtillus) at Olkiluoto sample points 3(A) and 1(B) (Figure 2). In A there was no NHAc (bioavailable) data from soil samples for Sn and the concentratiosn for strontium were determined with ICP-AES method as the other concentrations were measured with ICP-SFMS. The CRs of sample point 3 (A) are calculated from average values of 2011 and 2012 berry samples. Total CR of Nb at sample point 1 was below 0,0001 and not shown in this figure.
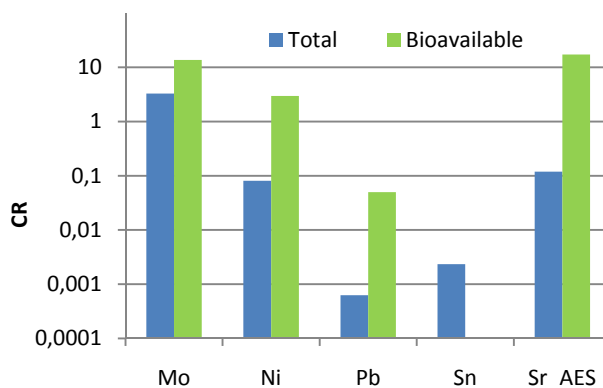
Figure 6. Total and bioavailable CRs for strawberry (Fragaria vesca) at Olkiluoto sample point 7 (Figure 2). In A there was no NHAc (bioavailable) data from soil samples for Sn and the concentratiosn for strontium were determined with ICP-AES method as the other concentrations were measured with ICP-SFMS.

For strawberry the total and bioavailable CRs were highest for Mo and Sr. Only for strawberry together with the sea buckthorn, the total CRs of Mo were higher than one. Also the CRs for Sr were clearly higher than for blueberry, lingonberry and sea buckthorn. Generally, the total (and bioavailable) CRs for sea buckthorn were certainly higher than ratios of lingonberry and blueberry. The CRs of strawberry were also higher than CRs of lingonberry and blueberry with the exception of Sn. It is also important to recognize that bioavailable CRs get unrealistic high values in many cases as the element concentrations analyzed with NH_4Ac extraction are extremely low.

Even though the soils were not studied comprehensively in this research the results still support the earlier findings that CRs differ among soil properties (Greger, 2004). The linearity assumption was also tested with data of sea buckthorn due the most valid soil results (*Figure 7*). These results reasonably support the assumption of linear relationship and removing the essential elements (Cl, Mo and Ni) had no significant effect on R^2 values. Using the bioavailable concentrations of soils seem to represent linearity better than the total concentrations. However, these results of linearity are only directional as the amount of samples is low and many of the concentration were below limit of quantifications (*Table 1*). The approach in this study also ignores the specific behaviour of different elements in varying concentration ranges.
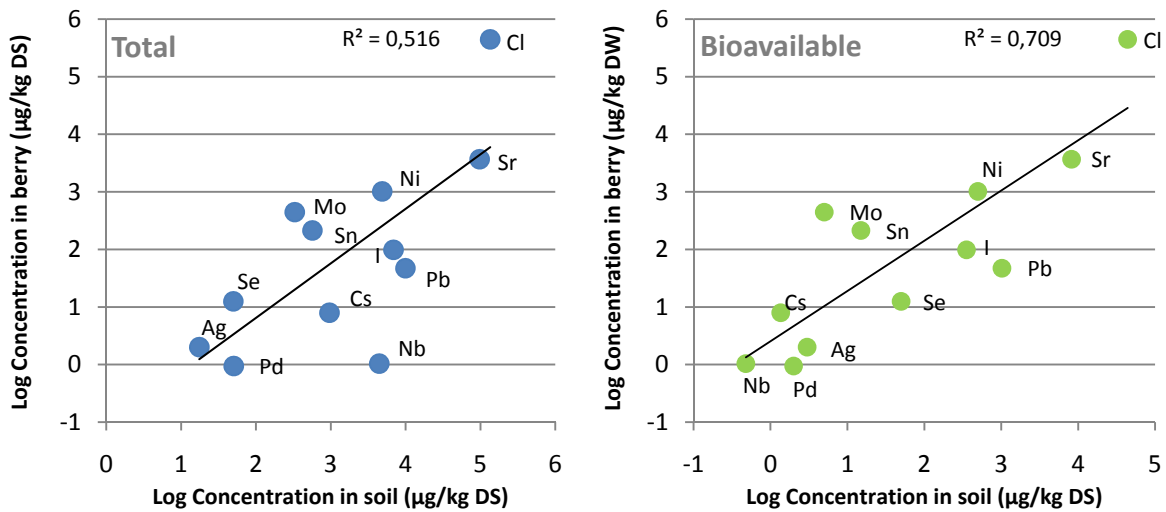
Figure 7. Total and bioavailable concentrations in soil vs. concentrations in sea bucthorn berries and best fit lines. The values were calculated as averages from the measured concentrations form years 2011 and 2012 at Viasvesi.

The CR's for other berries than sea-buckthorn are after all more unreliable because the soil samples were not taken at the same time and not from the exactly same location as the berry samples. This is important to bring out because the temporal changes in concentrations in soils and berries can be significant. Also many of the concentrations were below limit of quantification (*Table 1*) which increases uncertainty in the interpretation of results.

Table 1. List of element concentration below LOQs in the corresponding samples.

Sample	Elements
Sea buckthorn berries 2012	Ag, Pd*, Se
Total Soil for sea buckthorn	Pd*, Se
Bioavailable Soil for sea buckthorn	Ag, Mo, Nb, Pd*, Se, Sn
Sea buckthorn berries 2011	I, Se
Total Soil for sea buckthorn	Cl, Pd*
Bioavailable Soil for sea buckthorn	Ag, Cl, Mo, Pd, Se, Sn
Lingonberry	Ag, I, Pd*
Total Soil for lingonberry and blueberry at sp1 and 2008 sp3 in brackets	Pd* (Sn)
Bioavailable Soil for lingonberry blueberry at sp1 and sp3 in brackets	Ag, Cl, Mo, Pd*, Se (Ni)
Blueberry 2012	Ag, I, Pd*
Blueberry 2011	Ag, I, Pd*
Strawberry	Ag, Pd*
Total Soil for strawberry	Mo, Sn
Bioavailable Soil for strawberry	Ni

* Unreliable due interference, ALS classify these results unaccredited

Conclusions

The transfer of many elements from soil to plants is strongly influenced by soil characteristics. The variation of CRs between different elements is remarkably high. CRs of lingonberry and blueberry were very similar in same sample points, but the CRs of the sea buckthorn were clearly higher. According to the results of this study at least Mo and Cl could be considered as accumulators as their CRs are above equilibrium level in many cases. Generally, CRs derived from NH_4Ac extraction concentrations were clearly higher than CRs calculated from total concentrations. Thus, using these bioavailable CRs in radionuclide transportation models would lead to more conservative results in safety assessments. The bioavailable concentrations might also support the assumption of linear relationship in transfer model better than using total digestion (HNO_3/HF). The main contribution of this study is to complement the site-specific data for the biosphere assessment of spent nuclear fuel repository.

References

Brown, J. et al., 2003. *Handbook for Assessment of the Exposure of Biota to Ionising Radiation from Radionuclides in the Environment,* s.l.: Framework for Assessment of Environmental Impact.

Chen, Y. et al., 1990. Chemical composition and characteristics of sea buckthorn fruit and its oil. *Chem.Ind.For.Prod.,* Issue 10, pp. 163-175.

Greger, M., 2004. *TR-04-14, Uptake of nuclides by plants,* Stockholm, Sweden: SKB,Svensk Kärnbränslehantering AB.

Howard, B. ym., 2013. The IAEA handbook on radionuclide transfer to wildlife. *Journal of Environmental Radioactivity,* Issue 121, pp. 55-74.

Kabata - Pendias, A. & Mukherjee, A. B., 2007. *Trace Elements from Soil to Human.* New York: Springer-Verlag Berlin Heidelberg.

Kuusipalo, J., 1996. *Suomen metsätyypit.* Rauma: Kirjapaino Oy West Point.

Posiva, 2013. *Safety Case for the Disposal of Spent Nuclear Fuel at Olkiluoto - Biosphere Assessment 2012,* Eurajoki, Finland: Posiva Oy.

Radiation and Nuclear Safety Authority, 2013. *STUKLEX: Ydinjätteiden loppusijoitus, YVL D.5.*

Raguz, V. et al., 2013. Plant uptake of elements in soil and pore water: Field observations versus model assumptions. *Journal of Environmental Management,* Issue 126, pp. 147-156.

Roininen, K. & Mokkila, M., 2007. *Selvitys marjojen ja marjasivuvirtojen hyödyntämispotentiaalista Suomessa,* Espoo, Finland: SITRA & VTT.

Sheppard, S., Long, J. & Sanipelli, B., 2009. *Field measurements of the trasfer factors for iodine and other trace elements,* Toronto, Ontario: NWMO.

Sheppard, S. et al., 2011. *Solid/liquid partition coefficients (Kd) and plant/soil concentration ratios (CR) for selected soils, tills and sediments at Forsmark,* Stockholm, Sweden: Svensk Kärnbränslehantering AB (SKB).

Suryakumar, G. & Gupta, A., 2011. Medicinal and therapeutic potential of Sea buckthorn (Hippophae rhamnoides L.). *Journal of Ethnopharmacology,* Issue 138, p. 268– 278.

Söderlund, M. et al., 2011. *Sorption of Iodine, Chlorine, Technetium and Cesium in Soils,* Eurajoki, Finland: Posiva Oy.

Söderlund, M. et al., 2014. *Distribution Coefficients of Caesium, Chlorine, Iodine, Niobium, Selenium and Technetium on Olkiluoto Soils,* Eurajoki, Finland: Posiva Oy.

Tikkanen, I., 2015, May 24-29. *Challenges in the supply and consumption of wild berries in Finland. Paper presented at The 17th IBFRA Conference: "Sustainable forest management in an era of global changes".* Rovaniemi, Finland, University of Eastern Finland, Faculty of Social Sciences and Business Studies, Business School.

Tuovinen, T. et al., 2016. Transfer of elements relevant to nuclear fuel cycle from soil to borealplants and animals in experimental meso- and microcosms. *Science of the Total Environment,* Issue 539, p. 252–261.

Vaara, M., Saastamoinen, O. & Turtiainen, M., 2013. Changes in wild berry picking in Finland between 1997 and 2011. *Scandinavian Journal of Forest Research,* Issue 28, pp. 586-595.

Vera Tome, F., Blanco, R. M. P. & Lozano, J. C., 2003. Soil-to-plant transfer factors for natural radionuclides and stable elements in a Mediterranean area. *Journal of Environmental Radioactivity,* Issue 65, pp. 161-175.

Air to grass transfer of iodine - estimation of dry and wet deposition rates, velocities, and mass interception factors for a postulated accidental scenario

Karunakara N.[1], Ujwal P.[1], Yashodhara I.[1], Sudeep Kumara K.[1], Geetha P. V.[2], Dileep B. N.[3], Joshi P. James[3] and Ravi P. M.[4]

[1]Center for Advanced Research in Environmental Radioactivity (CARER)
[2]Nuclear Power Corporation of India Limited, Anushaktinagar, Mumbai – 400 094
[3]Environmental Survey Laboratory, Kaiga Generating Station, Kaiga-581 400
[4]Health Physics Division, Bhabha Atomic Research Centre, Trombay, Mumbai – 400 085
(Corresponding Author: Email: drkarunakara@gmail.com; Phone: 0824-2287733)

Abstract

Air to grass radionuclide transfer parameters such as dry and wet deposition rates, velocities, and mass interception factors are important basic input parameters for the estimation of radiation dose to the public around a nuclear power plant. We have carried out a study on air to grass transfer of iodine for a postulated emergency situation. A walk-in environmental chamber was designed and fabricated with facilities for exposing the plants grown in pots to controlled levels of radionuclides/stable elements. The temperature, humidity, and airflow inside the environmental chamber can be controlled to required values. The chamber has the facility for generating artificial rainfall. Grass grown in pots was kept inside the environmental chamber. Stable iodine (elemental form) was sublimed and injected into the environmental chamber suddenly to generate known concentration of iodine in the air inside the chamber. This simulated an accidental release of iodine to the environment. The concentration of iodine in the air inside the chamber was monitored continuously by drawing air from the environmental chamber through a bubbling setup (bubbling air through 1% sodium carbonate solution) and the iodine was then separated chemically and the concentration was measured by UV-VIS spectrometry. The concentration of iodine inside the chamber was monitored for every 30 min. The grass was exposed to iodine for 3 h after which the leaves were sampled and analysed for iodine concentration. From the concentration values of iodine in air and grass - the dry deposition rate, deposition velocity, and mass interception rates were estimated. The dry deposition velocity of iodine varied in the range of 0.5×10^{-5}–3.3×10^{-5} m s^{-1} with a mean value of 1.7×10^{-5} m s^{-1}. The mass interception factor varied in the range of 0.25-13 m^2 kg^{-1} with a mean value of 4.2 m^2 kg^{-1} with respect to fresh weight. The wet deposition velocity varied in the range of 0.6×10^{-4}-6.7×10^{-4} m s^{-1} with a mean value of 2.2×10^{-4} m s^{-1}. The mass interception factor for wet deposition varied in the range of 0.6-10.3 m^2 kg^{-1} with a mean value of 2.6 m^2 kg^{-1}. The experiments conducted using the environmental chamber provided valuable data on the air to grass transfer of iodine, which will be very important for the estimation of concentration of iodine in the grass in case of any emergency around a nuclear facility.

1.0   Introduction

In the case of emergency release form a nuclear power plant, the radioisotopes of iodine, cesium, and strontium are regarded as important as they are environmentally mobile and transfer readily to foodstuffs. During the short initial phase of release of the radioactivity (0 to 2 months), ^{131}I ($T_{1/2}$=8 days) is the most important radionuclide as it rapidly transfers to milk, leading to significant thyroid dose to those consuming the milk, especially infant and children. This is because radioiodine released to the environment is intercepted by plant surfaces that are then grazed by dairy cows. The ingested radioiodine is completely absorbed in the gut and then rapidly transferred to the milk. Hence, from the radiological viewpoint, considerable attention should be paid to the levels and behaviour of radioiodine in the environment.

Air to grass radionuclide transfer parameters such as dry and wet deposition rates, velocities, and mass interception factors are important basic input parameters for the estimation of radiation dose to the public around a nuclear power plant. Therefore, site-specific data on air to grass transfer

are important for a quick evaluation of the environmental contamination, during both normal and abnormal operational phases of a nuclear facility.

A detailed study on air to grass and grass to cow milk transfer of iodine was carried out by us in Kaiga region of South West Coast of India, where a nuclear power plant with 4 reactors of 220 MWe each is in operation. Kaiga is situated in the valley of the Western Ghats, about 60 km inland from Karwar, a town on the west coast of India. A site specific study was essential for the Kaiga region because of several important features of this region. It has a unique topography - it is bounded by steep hills with dense forest which is a natural habitat for a variety of plants that play a significant role in the environmental transport of radionuclides (Joshy et al., 2011). The annual rainfall is well over 4000 mm y^{-1} and this rainfall is higher when compared to the rainfall received by the other nuclear power stations of India. The local breed cows of this region have very low milk yield, often < 1.5 L d^{-1}. They are fed with little or no nutrient rich supplement feed and their dietary requirement is met mainly by grazing the pastures grown naturally in the large open grass fields. The villages around Kaiga have moderate population. The main cultivation is rice and different types of vegetables.

In this paper we report the result of laboratory experiments on air to grass dry and wet deposition rates, velocities, and mass interception factors. The experiments were carried out on grass grown in a walk-in type environmental chamber and exposing the grass to sudden release of stable iodine concentrations.

2.0   Materials and Methods

Dry and wet deposition rates of ^{131}I on grass have been reported after the Chernobyl accident (IAEA, 1994). But, under normal operational conditions of a nuclear power reactor, ^{131}I is not present in measurable concentration in the environmental matrices around the power plant. This makes the estimation of dry and wet deposition rates in the field impossible. Therefore, the only option available in such situations is to conduct laboratory experiments on air to grass under simulated conditions. For this a walk-in type environmental chamber with a working area of 2 m x 2 m x 2 m was designed. The chamber, made of stainless steel, has facility for (i) controlling the atmospheric parameters (temperature and humidity) (ii) for exposing the plants grown in pots to controlled concentrations of stable iodine, and (iii) artificial rainfall, (iv) ports for air sampling, injection of stable iodine vapours, etc.

2.1   Experiments on air to grass transfer for iodine - studies using the environmental chamber

Grass grown in experimental pots was kept inside the environmental chamber. Elemental iodine was sublimed suddenly inside the chamber to generate known concentration of iodine in air inside the chamber. This simulated an accidental release of iodine to the environment. The experimental arrangement for exposing the grass to iodine inside the environmental chamber is shown in Fig. 1. The environmental parameters such as humidity and temperature were controlled by required values. The concentration of iodine in the air inside the chamber was monitored continuously by drawing air from inside the environmental chamber through the bubbling setup consisting of 1% sodium carbonate solution. The iodine was then separated chemically and the concentration was measured by UV-VIS spectrometry (Karunakara et al, 2012). The concentration inside the chamber was monitored every 30 min and the mean value of concentration was taken as the representative concentration. The exposure time of grass inside the chamber varied between 3 to 4 h.

Measurements of dry deposition rate on ground surface was performed by placing stainless steel trays, of known surface area, on the bottom surface inside the chamber during spike condition.

At the end of the experiment the iodine deposited on the trays was collected by washing it with sodium carbonate solution and the concentration of iodine was measured as mentioned earlier. From the obtained concentration (mg m^{-2}) the deposition rate on the ground was calculated as under:

$$d_i = C_d / T \qquad \qquad \text{.... (1)}$$

where d_i - the deposition rate (mg m^{-2}), C_d is the total deposited Iodine concentration per unit area of tray (mg m^{-2}), and T is the time duration of deposition.

The dry deposition of iodine on grass was determined by considering the surface area of both sides of the grass leaves available for deposition. After exposing the grass to the iodine deposition inside the chamber, the leaves were collected and analsyed. For the grass used in this study the surface area of leaves per unit mass of leaves is found to be 46.4 m^2 kg^{-1} (fresh weight) and 9.9 m^2 kg^{-1} (dry weight). The deposition velocity (m s^{-1}) is the coefficient of dry/wet deposition rate and elemental concentration in air (mg.m^{-3}) and it is calculated as under:

$$V_d = d_i / C_a \qquad \qquad \text{.... (2)}$$

where V_d - is the dry/wet deposition velocity, d_i is the dry/wet deposition rate (mg.m^{-2}.s^{-1}), C_a is the iodine concentration in air (mg m^{-3})

The mass interception factor (α) (m^2. kg^{-1}) is the fraction of total concentration of radionuclide deposited on ground by the dry/wet deposition process, intercepted by the unit mass of grass/pasture and it is an important factor in the estimation of air to grass transfer of radionuclides. It was calculated by using the following equation:

$$\alpha = C_g / C_d \qquad \qquad \text{.... (3)}$$

where C_g – concentration in grass leaves (mg.kg^{-1}), C_d – total iodine concentration deposited per unit area of ground/tray (mg m^{-2}) .

As in the case of dry deposition, wet deposition was also measured both on the grass as well as on the stainless steel trays. Grass grown in pots was kept inside the chamber and iodine was injected to the chamber as outlined above and then artificial rainfall was created for a known time. The rain time was maintained for about 10 min, which corresponds to about 300 mm rain/day. The actual annual rainfall in the South West Coast of India is about 3500 – 5000 mm/year, spread over about 5 months. The simulated rainfall is deliberately maintained higher than the actual rainfall in Kaiga since it was important to simulate the extreme conditions. The higher simulated rainfall would yield a higher wet deposition rate of iodine and since the aim is to find out the air to grass transfer of iodine for emergency condition it was felt that simulating an extreme rainfall condition is appropriate.

3.0 Results and Discussion

Table 1 presents the results of dry deposition of iodine on the grass leaves for a simulated emergency situation. The dry deposition velocity on the grass leaves varied in the range of 0.5x10^{-5} to 3.3x10^{-5} m s^{-1} with a mean value of 1.7x10^{-5} m s^{-1} (column 5). The values reported in the literature on dry deposition velocity are also presented in the table for comparison. It may be noted that literature values vary in several orders of magnitude, from 10^{-7} to 10^{-2} m s^{-1}. Experiments conducted under the present study yielded consistent results, all in the order of 10^{-5}. The mass interception factors for iodine for grass are presented in column 6 and 7 of Table 1, with respect to fresh weight and dry weight of the grass leaves, respectively. The mass interception factor varied in the range of 0.25-13 m^2 kg^{-1} with a mean value of 4.2 m^2 kg^{-1} with respect to fresh weight. In all these experiments, the temperature of the air inside in the environmental chamber was maintained either at 20, 25 or 30°C, which is the representative ambient temperature for the South West Coast

of India. The air circulation inside the chamber was deliberately switched off to minimize the plate-out of the iodine on the walls of the chamber.

In Table 2 the results of the wet deposition rates of iodine on grass leaves for different rainfall rates are presented. The rainfall rates are given in column 3 and the wet deposition rates and deposition velocities are presented in column 5 and 6. The mass interception factors with respect to fresh and dry weights of the grass are presented in column 7 & 8. It may be noted from the mean values presented at the bottom of the table that wet deposition rates and deposition velocities is higher by an order of magnitude when compared to the dry deposition rates and deposition velocities. However, it is interesting to note that the mass interception factors for the grass remained nearly the same in both the cases of dry and wet deposition.

As mentioned earlier, experiments were also carried out to estimate the dry and wet deposition rates and deposition velocities of iodine on plain ground surface. The data on this aspect will be important to estimate the deposition of iodine on the soil. This information is useful to estimate the soil to grass transfer of iodine. In these experiments, instead of using the grass grown in pots, stainless steel trays were kept on the floor of the environmental chamber and the iodine present in air was allowed to deposit on it. The results of these experiments are presented in Tables 3 and 4 for dry and wet deposition, respectively. It may be noted from column 4, Table 3 that the deposition rate on the tray is of an order of magnitude higher when compared to that on grass. This is obvious because grass intercepts only a fraction of the iodine depositing from air and this interception mainly depend on the leaf morphology. From Table 4 it may be noted that the wet deposition rate on the tray is of an order of magnitude higher than that observed in the case of grass.

The experiments conducted using the environmental chamber provided valuable data on the air to grass transfer of iodine, which will be very important for the estimation of concentration of iodine isotopes in the grass in case of any emergency release of radioactivity from a nuclear facility. These data along with the data on grass to milk transfer coefficient values would of immense importance in the estimation of ingestion of iodine radioisotopes by the population and the radiation dose to the public.

4.0 Conclusions

The study has generated data on air to grass transfer of iodine for a postulated emergency release of iodine from a nuclear facility. The important conclusions drawn from the study are :
- The mass interception factor of iodine, measured using the environmental chamber, varied in the range of 0.25-13 m^2 kg^{-1} with a mean value of 4.2 m^2 kg^{-1} with respect to the fresh weight of the grass leaves. These values are derived using the large size environmental chamber with temperature varying in the range of 20-30°C.
- The wet deposition rate and deposition velocity of iodine is higher by an order of magnitude when compared to the dry deposition rates and deposition velocities. However, the mass interception factors for grass remained nearly the same both in the cases of dry and wet deposition of iodine.
- The experiments conducted using the environmental chamber provided valuable data on the air to grass transfer of iodine and this will serve as valuable input for the estimation of ingestion of iodine radioisotopes by the population and the resulting radiation dose to the public.

References

Chamberlain, A.C. and Chadwick, R.C. 1966. Transfer of iodine from atmosphere to ground. Tellus (Online library), Vol. 18, Issue 2-3, 226-237.

Handge, P., Hoffmann, F. O., 1974. The necessity for environmental surveillance in the evaluation of nuclear power plant sites. IAEA-SM-180/29.

Hansen, H. S., Andersson, I., 1994. Transfer of ^{137}Cs to cow's milk in the Nordic countries. IN Nordic Radioecology: the transfer of radionuclides through Nordic Ecosystems to Man. Amsterdam, Elsevier, pp. 197-210.

International Atomic Energy Agency (IAEA), 1994. Handbook of Parameter Values for the Prediction of Radionuclide Transfer in Temperate Environments. Technical Reports Series No. 364.

Joshi, R. M, James, J. P. Dileep, B. N., Mulla, R. M., Reji, T. K., Ravi, P. M., Hegde, A. G., Sarkar, P. K., 2011. Transfer coefficient of ^{137}Cs from feed to cow milk in tropical region kaiga, India. Radiation Protection Dosimetry, 1–7.

Karunakara N, Ujwal U P, Yashodhara I, Somashekarappa H M, Balakrishna K M, Geetha P V, Dileep B N and Ravi P M. 2012. Studies on transfer factors and transfer coefficients of Iodine, Cesium and Strontium in air→ grass→ cow→ milk pathway and estimation of radiation dose specific to Kaiga region. Final Report of the NPCIL sponsored research project. University Science Instrumentation Centre, Mangalore University, Mangalagangothri –574199, India.

Singhal., R. K., Narayanan, U. and Gurg, R. P. 2004. Estimation of deposition velocities ^{85}Sr, ^{131}I, ^{137}Cs on Spinach, Radish and Bean leaves in a tropical region in a simulated fallout conditions. Water, air and soil pollution, 158 (1-4), 181-192

Wershofen, H., Aumann, D.C. Dry deposition velocity of Iodine 129 onto grass as obtained by field measurements in the environment of a nuclear fuel reprocessing plant. J. Radioanal. Nucl. Chem., Letters 137 /5/ 373-379 (1989).

Table 1. *Results of laboratory experiments on dry deposition on grass leaves*

Sl. No.	Temp (°C)	Iodine Conc. in air (mg m^{-3})	Deposition rate on grass leaves (mg.m^{-2} d^{-1})	Deposition velocity on grass leaves (m s^{-1})	Mass interception factor (α) (m^2 kg^{-1}) (fresh wt.)	Mass interception factor (α) (m^2 kg^{-1}) (dry wt.)
1.	20	313.5	345	1.2×10^{-5}	7.7	30.4
2.	20	688.8	486	0.8×10^{-5}	4.5	19.8
3.	25	783.8	1643	2.5×10^{-5}	13	60
4.	25	720	1243	2.0×10^{-5}	0.25	1.1
5.	30	1045	1168	1.3×10^{-5}	1.5	8.4
6.	30	2258.5	1160	0.6×10^{-5}	3.3	14.5
7.	30	3278	861	0.5×10^{-5}	1.0	4.2
8.	30	355.5	1055	3.3×10^{-5}	0.86	4.4
9.	30	598.5	1147	2.2×10^{-5}	0.33	1.2
10.	30	416.5	972	2.7×10^{-5}	0.56	3.2
11.	30	450	597	1.5×10^{-5}	13	56
		Range	345-1643	$0.5 \times 10^{-5} - 3.3 \times 10^{-5}$	0.25-13	1.1-60
		Mean	971	1.7×10^{-5}	4.2	18.5

Literature values reported on deposition velocity (m s^{-1}) for comparison

^{131}I (Chamberlain and Chadwick, 1966)	5.4×10^{-3} (grass)
^{129}I (Wershofen and Aumann, 1989)	5.8×10^{-3} (pasture grass)
^{131}I (Handge and Hoffman, 1974)	10^{-5} -10^{-2} (grass land)
^{131}I, (Singhal *et al*. 2004)	5.4×10^{-7} (on Bean leaves using environmental chamber)

Table 2. *Results of laboratory experiments of wet deposition on grass leaves*

Sl. No.	Temp (°C)	Rainfall rate (mm for 10 min)	Iodine Conc. In air (mg m^{-3})	Wet deposition rate on grass leaves (mg m^{-2} d^{-1})	Wet deposition velocity on grass leaves (m s^{-1})	Mass interception factor (α) (m^2 kg^{-1}) (w.r.t. fresh wt.)	Mass interception factor (α) (m^2 kg^{-1}) (w.r.t. dry wt.)
1.	20	1.0	484	3331	0.8×10^{-4}	0.6	2.5
2.	25	3.2	318	3227	1.1×10^{-4}	5.0	23.5
3.	25	4.6	620	1758	3.2×10^{-4}	10.3	45
4.	30	3.0	511	16898	3.7×10^{-4}	3.1	14.4
5.	30	6.8	230	5206	2.5×10^{-4}	2.1	9.2
6.	30	6.5	489	3818	0.9×10^{-4}	1.4	6.8
7.	30	5.1	120	7003	6.7×10^{-4}	2.1	8.5
8.	30	3.7	1380	14492	1.0×10^{-4}	1.7	8.3
9.	30	10.3	1512	9874	0.8×10^{-4}	0.6	3
10.	30	8	292.5	4138	1.6×10^{-4}	0.99	5.5
11.	30	6.8	309	10138	3.7×10^{-4}	2.3	11.7
12.	30	4.6	793.5	4213	0.6×10^{-4}	1.3	6.9
			Range	1758-16898	$0.6 \times 10^{-4} - 6.7 \times 10^{-4}$	0.6-10.3	2.5-45
			Mean	8326	2.2×10^{-4}	2.6	12.1

Table 3. Results of laboratory experiments on dry deposition on ground surface

Sl. No.	Temp (°C)	Average air Concentration in chamber (mg m^{-3})	Deposition rate on tray (mg.m^{-2} d^{-1})	Deposition velocity on tray (m s^{-1})
1.	20	313	840	1.8×10^{-5}
2.	20	689	1139	1.8×10^{-5}
3.	25	784	2234	1.8×10^{-5}
4.	25	720	4654	7.4×10^{-5}
5.	30	450	505	1.2×10^{-5}
6.	30	753	128	2.0×10^{-6}
7.	30	315	449	1.2×10^{-5}
8.	30	330	629	2.4×10^{-5}
9.	30	1045	6385	6.6×10^{-5}
10.	30	2258	3723	1.1×10^{-5}
11.	30	3278	9520	5.0×10^{-5}
12.	30	355	11049	3.6×10^{-4}
13.	30	598	41379	8.0×10^{-4}
14.	30	416	13726	3.8×10^{-4}
Range		313-3278	128-41379	$0.2 \times 10^{-5} - 80 \times 10^{-5}$
Mean		879	6883	13.17×10^{-5}

Table 4. Results of laboratory experiments on wet deposition on ground surface

Sl. No.	Temp (°C)	Average air Concentration in chamber (mg m^{-3})	Deposition rate on tray (mg.m^{-2} d^{-1})	Deposition velocity on tray (m s^{-1})
1.	20	484	62956	1.4×10^{-3}
2.	25	318	6334.2	2.3×10^{-4}
3.	25	620	18155	3.3×10^{-4}
4.	30	230	26066	1.3×10^{-3}
5.	30	489	25850	6.1×10^{-4}
6.	30	150	35028	6.7×10^{-3}
7.	30	120	26657	2.4×10^{-3}
8.	30	51	53926	1.1×10^{-3}
9.	30	1380	80028	6.6×10^{-4}
10.	30	1512	139048	1.1×10^{-3}
11.	30	293	34466	1.3×10^{-3}
12.	30	309	39873	1.4×10^{-4}
13.	30	793.5	28217	4.1×10^{-4}
Range		51-1512	6334-139048	$0.14 \times 10^{-3} - 6.7 \times 10^{-3}$
Mean		554	44354	1.36×10^{-3}

Fig. 1. (a) A view of environmental chamber with grass grown in it (b) grass exposed to stable iodine concentration by injecting it in elemental form.

Assessment of anthropogenic radionuclides in tundra of the High Arctic environment

Anna Cwanek[1], Jerzy W. Mietelski[1], Edyta Łokas[1], Maria A. Olech [2]

[1]Institute of Nuclear Physics, Polish Academy of Sciences, Cracow, Poland
[2]Institute of Botany, Jagiellonian University, Cracow, Poland

Abstract

This paper present results of gamma, beta and alpha spectrometry measurements for lichens and mosses from 13 sites of vast Arctic coastal zone: Western Greenland, lands along the Northwest Passage and Labrador, Canada. The activity concentration of ^{134}Cs, ^{137}Cs for 103 samples and of ^{90}Sr, $^{238, 239+240}$Pu, ^{241}Am in case of 25 samples were determined. The level of radioactive contamination is relatively low. On the basis of contamination with ^{137}Cs it was observed that mosses accumulate pollution with higher efficiency than lichens. The global fallout seems to be the dominant source of radioactive pollution in whole study area except Nome, Alaska. There were found traces of ^{134}Cs and the ratios of ^{134}Cs/^{137}Cs is about 1 (March 2011), what suggest Fukushima fallout origin in Alaska.

Introduction

A few individual features make Arctic extremely sensitive to contamination. Special attention should be paid to the relatively short food chains, efficient transfer of contaminants between different organisms forming these chains and close relationship with the terrestrial and marine ecosystems (Dowdall et al., 2003). Moreover, observed warming temperature, changes in precipitation type and amount may contribute to the increase mobility of radionuclidesin the Arctic environment (AMAP, 2010).

On the radioecological point of view important issue is the accumulation of pollutants by dominant representatives of Arctic tundra - lichens and mosses. The lack of vax cuticle and root systems causes that lichens and mosses have the uptake of nutrients from the atmosphere and surface water together with inherent contaminants. Furthermore a relatively slow growth rates and long lifespan results in the incorporation of large amounts of impurities in the intracellular structure with time (Dowdall et al., 2005). This is a potential threat for local ecosystems that are exposed to penetration of toxic radioactive elements through the food chain.

The main aim of presented study is the assessment of contamination level of artificial radioisotopes such as: $^{238,239+240}$Pu, ^{241}Am, ^{90}Sr, ^{134,137}Cs and identification their origin in lichens and mosses from Western Arctic territory. In addition the comparative analysis of radioactivity accumulation properties and selectionof species with the highest accumulation efficiency were made.
The global fallout is taking into account as the main sources of mentioned artificial radioactive isotopes. It could be slightly modified by expected influence of the explosion carried out in Arctic nuclear training ground at Novaya Zemlya. Additionally there areconsidered the impact of Chernobyl fallout (1986), Fukushima fallout (2011), crash of Boeing B-52 with nuclear bombs on board near the Thule Base, Greenland (1968) and Kosmos 954 satellite crashover the Great Slave Lake in Northern Canada(1978).

Because of the research material comes mainly from coastal zone, radioactive contamination transported by ocean currents may also play significant role.Thus discharges from nuclear fuel

reprocessing plants at Sellafield and Cap de la Hague into the Irish Sea and the English Channel, respectively, or those released as a result storage of radioactive waste by the USSR in theArctic seas are taking into consideration as well.Thanks to characteristic values of isotopic ratios it will be possible to distinguish contamination from these sources from the global fallout.

The described research is the part of larger project (No. 2015/17/N/ST10/03121).

Materials and Methods

Samples

The research material includes 103 labeled species of lichens and mosses from coastal zone of the Western Arctic territory (Table 1). Samples were collected during two scientific expeditions in 2012 and 2013 by one of us (M.A.O.).

Table 1. Locations and date of sampling with species of lichens and mosses

No.	Location	Date of sampling	Species of lichens	Species of mosses
1	Illulisat 1 Greenland	08.08.2012	*Cetrariacucullata Cetrariadelicei Cetrariaislandica Cetrarianivalis Cladonia mitis Sphaerophorusglobosus Stereocaulonalpinum*	*Sanioniauncinata Racomintriumlanuginosum*
2	Ilullisat 2 Greenland	09.08.2012	*Alectoriaochroleuca Cetrariacucullata Cetrariadelicei Cetrariaislandica Cetrarianivalis Cladonia mitis Stereocaulonalpinum*	*Dicranumelongatum Polytrichastrumalpinum*
3	Upernavik Greenland	14.08.2012	*Cetrariacucullata Cetrariadelicei Cetrariaislandica Cetrarianivalis Cladonia mitis Sphaerophorusglobosus Stereocaulonalpinum*	*Dicranumelongatum Polytrichastrumalpinum Racomintriumlanuginosum*
4	Resolute Canadian Arctic	21.08.2012	*Certariatilesi Thamnoliavermicularis*	*Aulacomniumpalustre Sanioniauncinata*
5	Boothia Canadian Arctic	23.08.2012	*Cetrarianivalis Cetrariatilesi Cladonia mitis Thamnoliavermicularis*	*Sanioniauncinata*
6	Gjøa Haven Bay Canadian Arctic	25.08.2012	*Cetrariacucullata Cetrariadelicei Cetrarianivalis Cetrariatilesi Thamnoliavermicularis*	*Sanioniauncinata*

7	Bernard Harbour Canadian Arctic	30.08.2012	*Cetrariacucullata* *Cetrariadelicei* *Cetrarianivalis* *Cetrariatilesi* *Thamnoliavermicularis*	*Aulacomniumpalustre* *Sanioniauncinata* *Syntrychiaruralis*
8	Herschel Island Canadian Arctic	10.09.2012	*Alectoriaochroleuca* *Cetrariacucullata* *Cetrarianivalis* *Thamnoliavermicularis*	*Aulacomniumpalustre* *Sanioniauncinata*
9	Nome, Alaska USA	21.09.2012	*Alectorianigricans* *Cetrariacucullata* *Cetrariadelicei* *Cetrarianivalis* *Cetrariatilesi* *Cladonia mitis* *Cladoniafurcata* *Stereocaulonalpinum* *Thamnoliavermicularis*	*Dicranumelongatum* *HylocomiumSplendens* *Racomitriumcanescens*
10	Nuuk 1 Greenland	11.07.2013	*Cetrariacucullata* *Cetrariaislandica* *Cetrarianivalis* *Cladonia mitis* *Parmeliasaxatilis* *Sphaerophorusglobosus* *Stereocaulonalpinum*	*Dicranumelongatum* *Polytrichastrumalpinum* *Racomitriumlanuginosum* *Sanioniauncinata*
11	Nuuk 2 Greenland	21.07.2013	*Cetrarianivalis* *Cladonia mitis* *Sphaerophorusglobosus*	
12	Qeqertarsuatsiaat Greenland	29.07.2013	*Cetrariadelicei* *Cetrariaislandica* *Cetrarianivalis* *Cladonia mitis* *Sphaerophorusglobosus* *Stereocaulonalpinum*	*Dicranumelongatum* *Polytrichastrumalpinum* *Racomitriumlanuginosum*
13	Battle Harbour Labrador, Canada	07.08. 2013	*Alectoriaochroleuca* *Alectorianigricans* *Cetrariadelicei* *Cetrariaislandica* *Cetrarianivalis* *Cladonia mitis* *Parmeliasaxatilis* *Stereocaulonalpinum* *Sphaerophorusglobosus* *Thamnoliavermicularis*	*Racomitriumlanuginosum*

Methods

Experimental part of research was made in Environmental Radioactivity Laboratory of the Institute of Nuclear Physics PAS, Cracow, Poland. There were used gamma-, alpha- and beta-ray spectrometers. It was necessary to extract Pu isotopes, ^{241}Am and ^{90}Sr, thus the sequential radiochemical procedure was applied.

First of all each sample was homogenized and dried at 70 ^{0}C over 24 h. Afterwards there were made measurements on low-background spectrometers with HPGe detectors. Activity concentrations of ^{134}Cs and ^{137}Cs were calculated.

The next step was radiochemical analysis. It was done for 25 samples only. After ashing in 600 ^{0}C there were added radioactive tracers (^{85}Sr, ^{242}Pu, ^{243}Am) in order to determine chemical recovery of the procedure. The radiochemical treatments starts with completely wet mineralization using concentrated acids (HF, HNO$_3$, HCl) and small addition of H$_3$BO$_3$. Finally sample solution was converted to 1 M HNO$_3$. Plutonium was separated in columnsfilled with anion exchange resin DOWEX 1x8 (ion-exchange pressure chromatography) (Mietelski, Wąs, 1995; Mietelski, et al., 1999).^{90}Sr was extract using column filled with Sr-resin. The purified Sr solution of 5 mL of 0.5 M HNO$_3$ was transferred into a LSC vials followingby determination of ^{85}Sr recovery by means of gamma-sectrometry. Then, after 2 weeks to achieve equilibration between^{90}Sr and ^{90}Y, Sr solution was mixed with 15 mL of Gold Star LT2 scintillation cocktail and measured using1414 - 003 Wallac Guardian liquid scintillation spectrometer (Mietelski, Vajda, 1997; Mietelski, 1998). Before nest separation it was necessary to dispose of matrix components, thus co-precipitation with CaC$_2$O$_4$ at pH ~ 3 and then co-precipitation with Fe(OH)$_3$ at pH ~ 9 were made. The resultant precipitate (containing Am) was re-dissolved in 4 M HNO$_3$ and passed through the TEVA (Triskem) resin; it allowed to repurificate Am fraction from traces of Th. Finally, americium was removed using a conventional methanol-acid standard procedure on Dowex 1x8 resin (Mietelski et al., 1997; Łokas et al., 2010).

Activity concentrations for plutonium, americium isotopes were determined using alpha spectrometers (Silena Alpha Quattro, Ortec Alpha Duo or Canberra 7401; all equipped with Canberra or Ortec ion - implanted silicon detectors). All alpha sources were prepared using NdF$_3$micro-coprecipitation method (Sill, 1987).

Analysis quality was evaluated through the determination of radionuclides activity concentrations of IAEA Reference Materials (IAEA – 447, IAEA – 330). The results agreed well with recommended values. Blank samples made of reagents were also analysed. Average results for blanks were used for background corrections.

Results and Discussion

There were described initial results in this section.All values are calculate on dry weight and decay correction was calculated on the date of sampling.
The results of gamma spectrometry measurements are presented in Figure 1. The activity concentration of ^{137}Cs are ranging from 5.3 ± 0.8Bq/kg to 293±27 Bq/kg and do not show any clear tendency. The maximum and minimum values were observed in Greenland. Labrador, Bernard Harbour, Hershel Island, Northwest Canada and Nome, Alaska seem to be polluted in the slightest, because of quite low activity concentrations as well as only some results are above detection limit. There can be noticed differences between mosses and lichen accumulation properties for radiocesium; in general activity concentration of Cs–137 was lower for lichens than mosses.*Sanioniauncinata*and *Cetrariadelicei*are species of moss and lichen, respectively, with the highest content of radiocaesium.
Traces of ^{134}Cs were found in case of four lichens coming from Nome, Alaska only. Received values of activity concentration are on level of several Bg/kg. The^{134}Cs/^{137}Cs isotopic ratios are ranging from 0.8 ± 0.2 to 1.1 ± 0.3 (decay corrected to March 2011), whereas ^{134}Cs/^{137}Cs activity ratio equals 1.033 ± 0.006 (decay corrected to March 2011) represent FDNPP derived radiocesium signature (Yang et al, 2016). Therefore it points to clear Fukushima fallout origin of radioactive

contaminations in samples from Nome, Alaska. For the remaining study area derivation of cesium isotopes is unclear at this time.
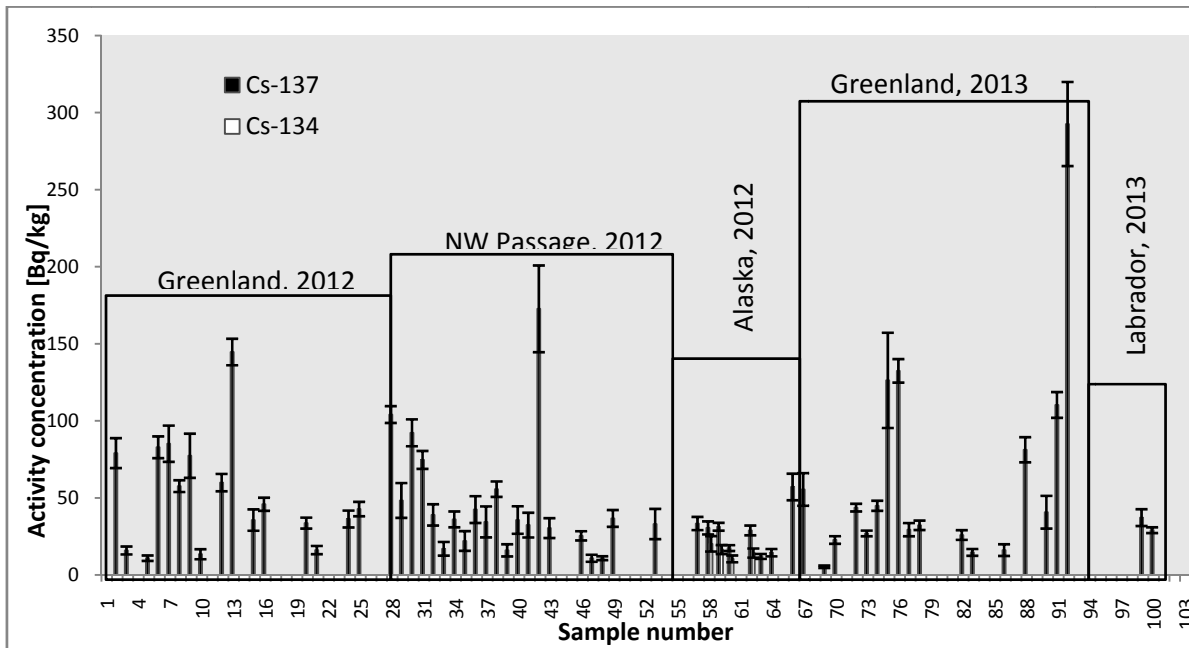
Figure 1.*Result of gamma spectrometry measurement.The empty spaces on the graph means activity concentrations are below the detection limit.*

Only several results of activity concentration for artificial radionuclides separated in radiochemical procedures followed by alpha-ray spectrometry and/or liquid scintillation spectrometry have been obtained so far. The activity concentrations of ^{90}Sr do not exceed 10 Bq/kg except two cases coming from NW Passage territory, Canada, when the values reached85 ± 8 Bq/kg and 24 ± 2 Bq/kg. There is no known reason such high content of Sr–90 at the moment.

The activity concentrations for alpha emitters revealed maxima equal to 4.7± 0.1 Bq/kg for $^{239+240}$Pu, 0.128± 0.009 Bq/kg for ^{238}Pu and 3.0± 0.2 Bq/kg for^{241}Am. These highest values were found in the Northwest Passage territory, Canada. According to Figure 2 it can be noticed that contaminations of Pu isotopes and ^{241}Am come mainly from the global fallout. Determination of possible participation of other sources require further investigations.
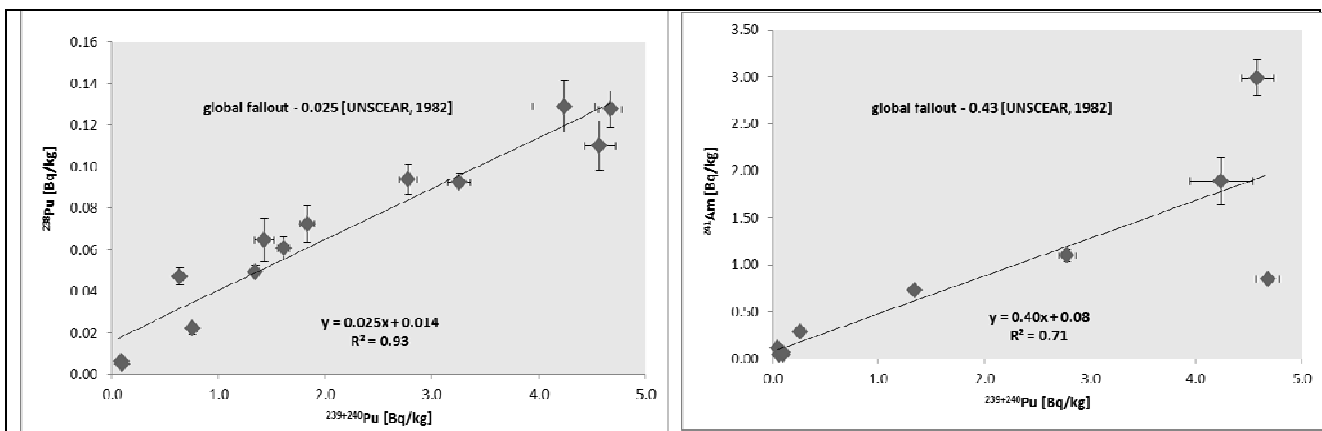
Figure 2.*Correlation between ^{238}Pu and$^{239+240}$Pu (on the left) and between ^{241}Am and ^{239*240}Pu)on the right). Fit is the regressionline,fitting coefficients were placed on graphs. There have been shown mean values of considered isotopic ratios charcteristic for the global fallout[UNSCEAR, 1982].*

Conclusions

The received results allow noticing that the level of radioactive contamination in study area is relatively low. Cs-137 was found in all considered area wherein its origin is unknown at this time. Only for Nome, Alaska traces of ^{134}Cs are the clear evidence of Fukushima fallout. The mosses accumulate radiocesium with higher efficiency than lichens. The highest activity concentration of ^{137}Cs was found in Greenland for moss sample - *Sanioniauncinata* - and equals about 300 Bq/kg. The highest content of ^{90}Sr occur in Canadian Arctic (Boothia, Gjoa Haven), sources are not known at the moment. The maximum of activity concentration of Pu isotopes and Am-241 are on level of single Bq/kg and they were found in Canadian Arctic. The global fallout seems to be the most likely sources of artificial alpha emitters in considered area.

References

AMAP, 2010, AMAP Assesment 2009: Radioactivity in the Arctic. Arctic Monitoring and AssesmentProgramme.

Dowdall, M., Gerald, S., Lind, B., 2003. Gamma-emitting natural and anthropogenic radionuclides in the terrestial environment of Kongsfjord, Svalbard. Sci. Total Environ.305, 229-240.

Dowdall, M., Gwynn, J.P., Moran, C., Davids, C., O'Dea, J., Lind, B., 2005. Uptake of radionuclides by vegetation at a High Arctic location. Environ. Pollut. 133, 327-332.

Yang, G., Tazoe, H., Yamada, M., 2016. ^{135}Cs activity and ^{135}Cs/^{137}Cs atom ratio in environmental samples before and after the Fukushima Daiichi Nuclear Power Plant accident. Sci. Rep. 6:24119, doi: 10.1038/srep24119.

Łokas, E., Mietelski, J.W., Kleszcz, K., Tomankiewicz, E.,2010.A sequential procedure for determining ^{238}Pu, $^{239+240}$Pu, ^{241}Am, ^{90}Sr, U and Th activities in soils and peats from Spitsbergen. Nukleonika. 55(2),195-199.

Mietelski, J.W., Vajda N.,1997.Chernobyl Sr-90 in bilberries from Poland. J.Radioanal. Nucl. Chem. 222(1-2), 183-187.

Mietelski, J.W., Wąs B., 1995. Plutonium from Chernobyl in Poland, Applied Radiation and Isotopes, 46: 1203-1211.

Mietelski, J.W., Wąs, B., 1997. Americium, curium and rare earths radionuclides in forest litter samples from Poland. Appl. Radiat.Isot. 48(5), 705-713.

Mietelski, J.W., Dorda, J., Wąs, B., 1999. Pu-241 in samples of forest soil from Poland, Appl. Radiat. Isot. 51, 435-447.

Mietelski, J.W., 1998. Transuranic elements and Sr-90 in samples from forests of Poland, a review. Nukleonika, 43(4), 449-458.

Sill, C.W., 1987. Precipitation of actinides as fluorides or hydroxides for high-resolution alpha spectrometry.Nucl. Chem. Waste Manage. 7, 201.

UNSCEAR,1982. Ionizing Radiation Sources and Biological Effects; Raport to the General Assembly with annexes, UN Pub.

Acknowledgement

Radioactive Contamination Evolution for Thirty Years in Mushrooms Samples Imported by Spain Following the Chernobyl Nuclear Accident

Mª Elena Veiga Ochoa[1], Jesús Castro Catalina[1], Rosa Basante Pol[2]

1 Health Research Institute Carlos III.Environmental Health National Centre. Madrid, Spain.
2 Department of Pharmacy and Pharmaceutical Technology. Complutense University of Madrid. Madrid, Spain

Abstract

Following the accident at the Chernobyl nuclear power station on 26 April 1986, considerable quantities of radioactive elements were released into the atmosphere. European Union Council developed own regulations in order to ensure health protection of European consumers, to imported food from countries affected by the radioactive cloud. The radioecological study of mushrooms samples should provide information about their absorption capacity of radionuclides and its life cycle in an exchange between soil and vegetation.
The highest percentage of fungi species growing in forests and wooded areas analyzed comes from former third countries like Bulgaria, Romania, Hungary, Poland and Yugoslavia and third countries like Russia, Ukraine, Turkey and Macedonia.
The aim is to study the significant radioactive contaminants as cesium 137 in edible mushrooms analyzed by gamma-ray spectrometry.
The contamination depends on genre of mushrooms and the country of origin. However it would be valuable knowing the region of country of each imported food. Bulgaria has the greatest number of samples contaminated; otherwise some *Cantharellus* species show the highest level of cesium.
The activity and the number of contaminated samples decays over time, although there has been an increase in imported food since the approval of Commission Regulation (EC) No 1661/1999 of 27 July 1999, that recommends a greater control of them.

Introduction

After the Chernobyl accident in April 1986 considerable quantities of radioactive elements were released into the atmosphere. European Union Council developed own regulations in order to ensure health protection of European consumers (Council Regulation (EEC) No 1707/86 of 30 May 1986),(Council Regulation (EC) No 1048/2009 of 23 October) regarding the food imported from other countries affected by the radioactive cloud.

There has been an increase in imported mushrooms since the approval of new regulation (Commission Regulation (EC) No 1661/1999 of 27 July 1999) that recommends a greater control on them, because repeated cases of non-compliance with the maximum permitted levels of radioactive contamination have been recorded in consignments of certain types of mushrooms imported from a number of third countries.

Mushrooms, due to their ability to accumulate cesium isotopes, represent an important pathway to the food chain for radioactivity arising from radioactive fallout from the

accident (Malinowska *et al.,* 2006). Furthermore, mycorrhizal mushrooms accumulate Cesium 137 more than saprophytes (Baeza *et al.,* 2004)

Materials and Methods

Samples, coming from Slavic and Central European countries and Turkey, were controled by Foreign Health Services of Spanish Government, between 1986 and 2016. The study took into account the following mushrooms genre: *Boletus, Lactarius, Morchella, Craterellus, Calocybe, Cantharellus, Marasmius* and *Tricholoma*.
The samples are finely crushed, homogenized and put into Marinelli beakers according to the available geometries. Time counting depends on the amount of sample, type of detector and geometry employed. Reference materials used are supplied by reference laboratories, such as CIEMAT and IAEA.
Gamma spectrometry was carried out using a germanium HPGe with 1.80 keV resolution for the 1332 keV ^{60}Co peak and a peak-to-Compton ratio of 64.2:1, and a broad energy germanium with a 1.91 keV resolution at 1332 keV^{60}Co line.

Results and Discussion

It is known that mushrooms have the ability to accumulate cesium isotopes. Among the soil organisms, fungi were the most effective accumulators of radiocesium when the soil is contaminated (Calmon *et al.,* 2009).
During last 30 years, we have analyzed 1100 samples of mushrooms whose origin has been European countries and third countries that now most of them belong to EU. We have assessed the level of contamination and the difference in the absorption of Cesium by fungi according to their living habits. Saprophytes species live on organic substrate and decompose it by excreting extracellular enzymes, but symbiotic fungi form a mutual association with the fine root system of trees. This symbiosis is called mycorrhizal and is essential for both partners in forest ecosystems (Kammerer et al 1994).
In agreement with different studies, we have also observed that mycorrhizal mushrooms accumulate ^{137}Cs more than saprophytes (Kalac, 2001; Heinrich, 1992; Guillitte*et al*.1994)
The activity of cesium 137 found in mycorrhizal species belonging to *Cantharellaceae* family is given in Figure 1 with respect to *Cantharelluscibarius*
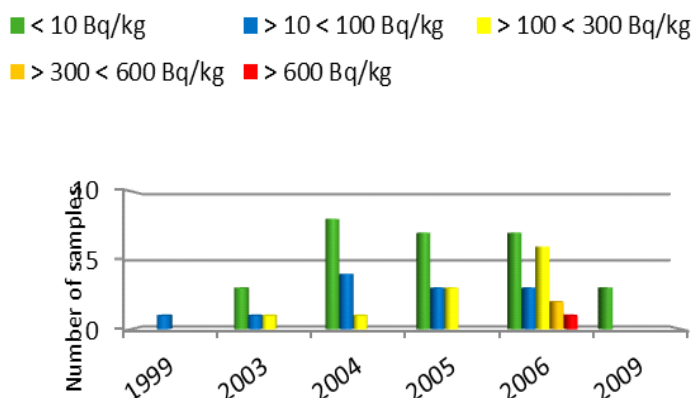
Figure 1.Cantharelluscibarius.Activity concentration of Cs-137 (Bq/kg)

The Figures 2 and 3 show the activity of cesium 137 in *Cantharelluslutescens* and *C. tubaeformis*, respectively.
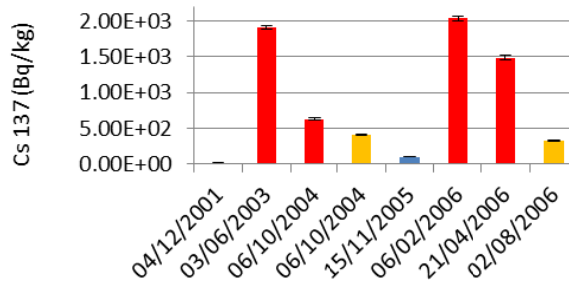
Figure 2.Cantharelluslutescens.Activity concentration of Cs 137 (Bq/kg)

The countries of origin of *Cantharelluslutescens* are Bulgaria, Romania, Turkey, Lithuania and Serbia and all the samples of *C. tubaeformis* come from Bulgaria.
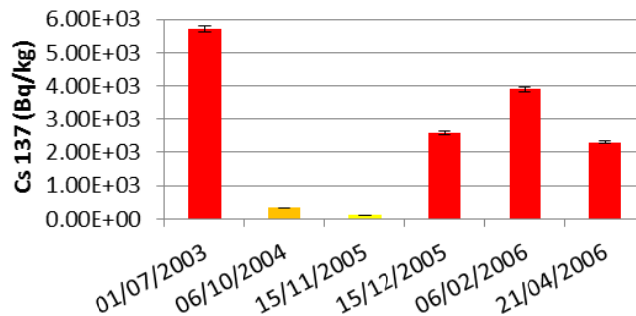
Figure 3. Cantharellustubaeformis. Activity concentration of Cs 137 (Bq/kg)

The activity concentration of ^{137}Cs concerning mycorrhizal species such as *C. lutescens* and *C. tubaeformis* has shown the highest contamination. The maximum level was found in a sample of *C. tubaeformis* from Bulgaria (5,710 ± 100 Bq/kg).
Up to 79 samples of *Craterrelluscornucopiodes* (*Cantharellaceae* family) have been analyzed coming from Turkey, Bulgaria and Serbia.Their activity concentration of ^{137}Cs is shown in Figure 4 and the levels are lower than other species' levels of the*Cantharellaceae* family. Only one samplefrom Bulgaria exceeded the maximum permitted levels of cesium 137 (821 ± 33.6 Bq/kg).

Figure 4.Craterelluscornucopiodes. Activity concentration of Cs 137 (Bq/kg)

The results of *Boletus spp* (symbiotic fungi) are shown in Figure 5. The countries of origin of *Boletus* are mainly, Bulgaria y Romania and only one sample from Romania exceeded the permitted level of cesium 137 (654 ± 30.8 Bq/kg).
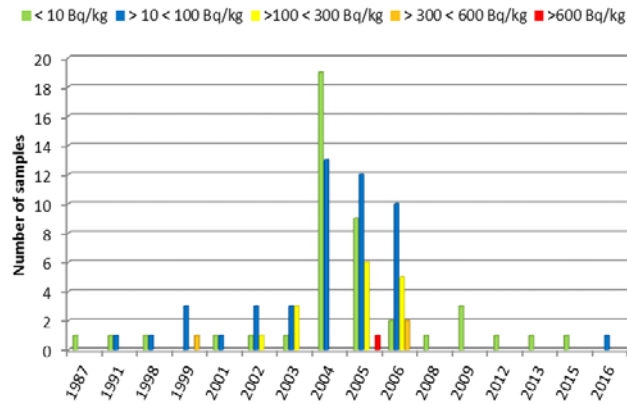
Figure 5. Boletus spp. Activity concentration of Cs 137 (Bq/kg)

Nevertheless, *Lactariusdeliciosus*, despite it being a mycorrhizal species, the level of cesium is much less than the other mycorrhizal species. The highest contamination level (43.3 ± 4.8 Bq/kg) of cesium 137 was observed in a sample from Bulgaria (Figure 6).
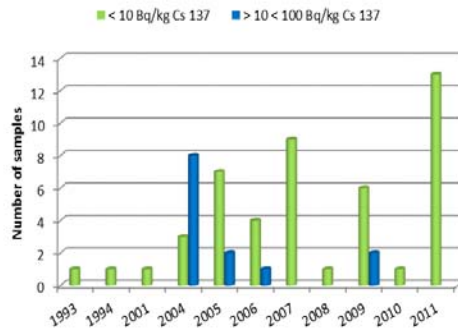
Figure 6.Lactariusdeliciosus. Activity concentration of Cs 137 (Bq/kg)

One of the saprophyte species analyzed is *MarasmiusOreades* which comes from Bulgaria and Macedonia. A number of 173 samples of *Morchellaspp,* also saprophyte fungi, have been assessed. The figure 7 shows the concentration of ^{137}Cs of *Marasmiusoreades* (a) and *Morchellaspp* (b)

(a)   (b)
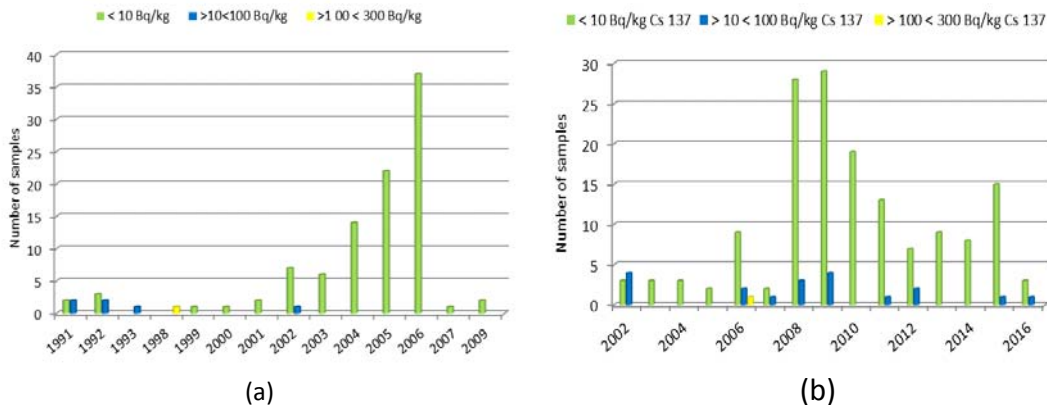
Figure 7.Activity concentration of Cs 137 (Bq/kg) Marasmiusoreades (a) and Morchellaspp (b)

The activity concentration of ^{137}Cs in saprophyte *Calocybegambosum,* was very small, ranging from 0.9 ± 0.4 Bq/kg to 10.7 ± 1.33 Bq/kg just as *Tricholomaspp*, whose values range from 0.54 ± 0.12 Bq/kg to 4.77 ± 0.74 Bq/kg, Figure 8

(a)   (b)
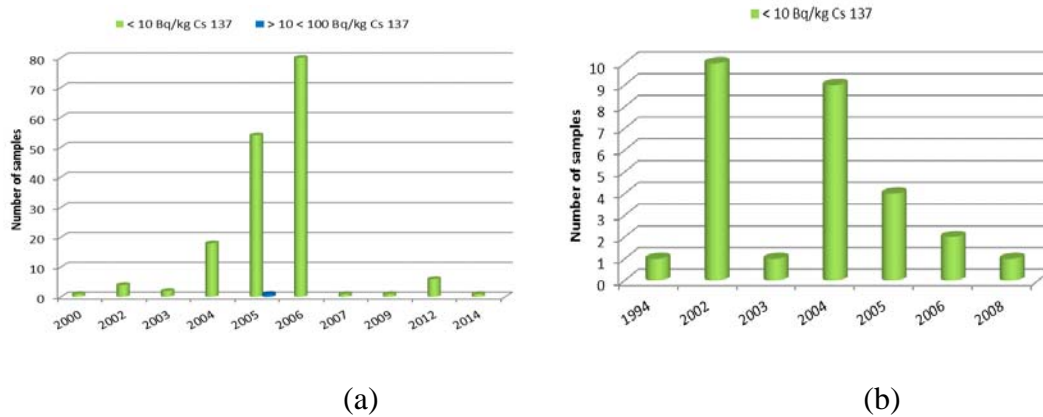
Figure 8.Activity concentration of Cs 137 (Bq/kg)Calocybegambosum (a) and Tricholomaspp (b)

The countries of origin of *Calocybegambosum* and *Tricholoma*samples are Bulgaria and Macedonia.

Conclusions

The species that have presented greater contamination in ^{137}Cs have been C*antharellusspp* and *boletus spp*, both mycorrhizal species, focusing that the most contamination in mushrooms comes from Southern Slavic countries. It is striking that *Lactariusdeliciosus*, despite being mycorrhizal species has not presented significant contamination regardless of origin country. Nevertheless, there has not beena direct relationship between contamination level of different species and their countries of origin.

We can emphasize that the customs offices control has been effective for the health protection of European consumers.

References

Baeza A et al. *Radiocaesium and natural gamma emitters in mushrooms collected in Spain*. The Science of the Total Environment (2004) 318, 59-71.

Calmon et al. *Transfer parameter values in temperate forest ecosystems: a review.*Journa of EnvironmntalRadiaoctivity (2009) 100, 757-766.

Council Regulation (EEC) No 1707/86 of 30 May 1986 on the conditions governing imports of agricultural products originating in third countries following the accident at the Chernobyl nuclear power-station.OJ No L 146/88 31.5.1986http://eur-lex.europa.eu/legal-content/EN/TXT/PDF/?uri=CELEX:31986R1707&from=EN

Commission Regulation (EC) No 1661/1999 of 27 July 1999 laying down detailed rules for the application of Council Regulation (EEC) No 737/90 on the conditions governing imports of agricultural products originating in third countries following the accident at the Chernobyl nuclear power-station. OJ No L 197/17 29.7.1999. http://eur-lex.europa.eu/legal-content/EN/TXT/PDF/?uri=CELEX:31999R1661&from=ES

Council Regulation (EC) No 1048/2009 of 23 October 2009 amending Regulation (EC) No 733/2008 on the conditions governing imports of agricultural products originating in third countries following the accident at the Chernobyl nuclear power station. OJ No L 290/4 6.11.2009.
http://eurlex.europa.eu/legalcontent/EN/TXT/PDF/?uri=CELEX:32009R1048&from=EN

Guillite, O, Meli, J, Wallberg L. *Biological pathways of radionuclides originating from the Chernobyl fallout in a boreal forest ecosystem* The Science of the Total Environment (1994) 157, 207-215.

Heinrich, G. *Uptake and transfer factors of Cs 137 by mushrooms.*Radiation and Environmental Biophysics (1992) 31, 39-49.

Kalac, *A review of edible mushroom radioactivity.*Food chemistry (2001) 75, 29-35.

Kammerer L, Hiersche L, Wirth E. *Uptake radiocaesium by different species o mushrooms.* Journal of Environmental Radioactivity (1994) 23, 135-150.

Malinowska, E, Szefer, P, Bojanowski R. *Radionuclides content in Xerocomusbadius and other commercial mushrooms from several regions of Poland.* Food Chemistry (2006) 97, 19-24.

Polonium [210]Po and radiolead ^{210}Pb in edible mushrooms collected in northern Poland

Karolina Szymańska, Dagmara Ida Strumińska-Parulska, Grażyna Krasińska, Bogdan Skwarzec, Jerzy Falandysz

University of Gdańsk, Faculty of Chemistry, Analytics and Environmental Radiochemistry Department, WitaStwosza 63, 80-308 Gdańsk

Abstract

The aim of the project was [210]Po and ^{210}Pb determination in caps and stems of mushrooms from *Leccinumpseudoscabrum*, *Leccinumaurantiacum*, *Leccinumvulpinum*, *Leccinumduriusculum* and *Leccinumquercinum* collected in northern Poland. The average [210]Po concentration in mushrooms caps and stems ranged from 0.85 ± 0.09 Bq·kg^{-1} in *Leccinumquercinum* stem to 10.77 ± 0.47 Bq·kg^{-1} in *Leccinumpseudoscarbum* cap. Analysis of [210]Po concentrations in mushrooms showed its higher values in caps in comparison to stems. The studies showed interspecies differences in polonium and radiolead accumulation among all analyzed species.

Introduction

Natural radioactive elements are present in very low concentrations in earth's crust. Human activities, such as oil and gas exploration, mining or coal burning in power plants can enhance their content. Technologically Enhanced Naturally Occurring Radioactive Materials (TENORM) consist of materials, usually industrial wastes or by-products enriched with radioactive elements found in the environment, such as uranium, thorium and potassium and any of their decay products, such as radium and radon, polonium and radiolead (Bem, 2005). Also the accident at the Chernobyl nuclear power plant (April 1986), and the following radioactive contamination of most European territory, initiated extensive research on the environment, including mushrooms (Heinrich, 1992). There were many papers written about cesium ^{137}Cs accumulation in the environment, wild plants, berries and mushrooms as well (Gruter, 1964; Gruter, 1971; Gwynn et al., 2013). But the studies on [210]Po and ^{210}Pb, much harder to conduct, were not carried out on such large scale (Guillen and Baeza, 2014).

Polonium [210]Po ($T_{1/2}$=138.4 days) and radiolead [210]Pb ($T_{1/2}$=22.2 years) appear at the end of the decay-chain of uranium [238]U and are radio-ecologically interesting natural elements to investigate due to their significant radiotoxic characteristics (Heiserman, 1997; Persson and Holm, 2011). These radionuclides are introduced into the biosphere through various routes of terrestrial and marine pathways and continuously deposited from the atmosphere in association with aerosols (Persson and Holm, 2011). [210]Po and ^{210}Pb are, together with radon and potassium, the natural radioactive material delivering the highest natural dose to living organisms (Bem, 2005).

Mushrooms absorb heavy metals from the environment such as mercury, chrome and cadmium. Previous studies have shown radionuclides (e.g. polonium, uranium, plutonium) are accumulated in green plants and mushrooms as well. Radioactive elements are taken either from the soil, through the mycelium or directly from the entire surface gathered in the fruiting bodies. After the Chernobyl accident radioactive contamination of the environment has grown considerably (Kalač, 2000; Kalač, 2012). The fruiting bodies of mushrooms are generally considered as

absorbing mineral constituents, including heavy metals and radionuclides. They could be used as environmental biomonitoring indicators to evaluate the level of the environment contamination as well as the quality of the ecosystem (Skwarzec and Jakusik, 2003). The activity concentrations of ^{210}Po and ^{210}Pb in mushrooms were higher comparing to other groundcover plants (Kostianen, 2007). Mushroom species have different retain capacities of ^{210}Po and ^{210}Pb (Skwarzec and Jakusik, 2003; Malinowska et al., 2006; Guillen et al., 2009). Previous studies on King Bolete (*Boleusedulis* Bull) showed the values of ^{210}Po concentration in caps were higher in comparison to its levels in stems (from 1.02 to 2.05; mean value 1.44) (Skwarzec and Jakusik, 2003). The highest activity concentration of ^{210}Pb in samples of Finnish mushrooms was detected in Red-banded Cortinarius (*Cortinariusarmillatus*(Fr) Fr), (16.2 Bq kg^{-1} dry biomass; db) while the lowest in Foxy Bolete (*Leccinumvulpinum*Watling) (1.38 Bq kg^{-1}db) (Vaarama et al., 2009).Mushrooms also influence natural radionuclides migration in soil and food chains (Ibrahim and Whicker, 1987; Calmon et al., 2009). Many species of wild edible mushrooms adsorb and bioaccumulate mercury, chromium, silver, cadmium as well as radionuclides, i.e. cesium, strontium, polonium, radiolead, uranium, plutonium (Gentili et al., 1991; Falandysz et al., 1994; Falandysz et al., 2002; Falandysz et al., 2003; Falandysz et al., 2012; Zhang et al., 2013; Guillen and Baeza, 2014).

Materials and Methods

Fruiting bodies of wild edible mushrooms and topsoil samples (0-10 cm layer) underneath the fruiting bodies were collected from distantly distributed forested places across Pomerania (northern Poland). All mushroom samples, after the removal of plant and soil using plastic knife, were separated into caps and stems, sliced and oven dried at 65°C to constant weight and further ground in porcelain mortar to fine powder. The soil samples, free of any visible organisms, small stones, sticks and leaves were dried at 65°C to constant mass. Next, the soil samples were ground in a porcelain mortar and sieved through a pore size of 2 mm plastic sieve.

About 2 g of soil and 5 g of mushrooms were digested using 65% nitric acid (HNO$_3$) and 36% hydrochloric acid (HCl) with a ^{209}Po (9 mBq) spike added as a yield tracer. Further the samples were mineralized in hot aqua regia about 5 days to receive clear color of the solution, and then evaporated. The dry residue was dissolved in 25 ml of 0.5 M HCl and 0.5 g of ascorbic acid (C$_6$H$_8$O$_6$) was added to reduce iron Fe^{3+} to Fe^{2+}, then the solution was transferred to PTFE vessels equipped with silver sheet bottom disc. Polonium was autodeposited at 90 °C for 4 hours. ^{210}Po activity was measured using an alpha spectrometer equipped with semiconductor silicon detectors and a 450 mm^2 active surface barrier (Alpha Analyst S470, Canberra-Packard, USA). Polonium samples were measured for 1-3 days (Skwarzec, 1995; 1997; 2010). Activity concentration of ^{210}Pb in analyzed samples was calculated indirectly via its daughter ^{210}Po activity measurement. All samples after the first ^{210}Po deposition were stored for 6 months to allow for ^{210}Po increment from ^{210}Pb. The deposition of ^{210}Po on silver disc was repeated and the activities of ingrowing ^{210}Po were measured in alpha spectrometer (Alpha Analyst S470, Canberra-Packard). The measurement of a single sample took 1-4 days and ^{210}Po activity in analyzed samples was corrected for decay to the day of polonium deposition (time of separation ^{210}Po from ^{210}Pb). ^{210}Pb activity at the time of sample collection was calculated using the simplified form of the Bateman equation (Skwarzec, 1997; 2010). The ^{210}Po and ^{210}Pb yield in the analyzed mushroom and soil samples ranged from 95 to 100%.

The results of ^{210}Po and ^{210}Pb concentrations were given with standard deviation (SD) calculated for 95% confidence intervals. The accuracy and precision of the radiochemical method were positively evaluated using IAEA reference materials (IAEA-414; IAEA-384) and both estimated at less than 5%.

Results and Discussion

The results of average ^{210}Po and ^{210}Pb activity concentrations in analyzed mushrooms samples from Pomerania (northern Poland) are presented in Table 1. The highest ^{210}Po activity concentrations were in cap of *L. pseudoscabrum* from Borkowo (10,9±0,1Bq kg^{-1}d.w.), while the lowest were measured in stem of *L. pseudoscabrum* from Złotów (0,79±0,06Bq kg^{-1}d.w.). In case of ^{210}Pb results its highest activity concentrations were determined in cap of *L. pseudoscabrum* from Borkowo (4.92±0.09Bq kg^{-1}d.w.). Observed differences could be a result of disparities in topsoil, dry atmospheric fallout (mineral particles from dusty soils covering the surface of plants and ground, gravitationally deposited), and bioaccumulation levels. Almost all mushrooms have been collected in forests, which were semi-natural ecosystems and differed from agricultural cultivated lands; its soils were multilayer, hemi-organic and mineral. Mushrooms and microbes biological activities effect on long-term radionuclides retention in organic layers of forest soil and the soil represents the major reservoir of radionuclides - thus they can be easily available for mushrooms and mycelium located in organic layers. Among the soil samples, the highest activity concentrations of ^{210}Po and ^{210}Pb were noticed in Borkowo (89.1±2.9 and 59.7±2.3Bq kg^{-1}),while the lowest is Wysokie (both 1.66±0.02 Bq kg^{-1}d.w.). High values of ^{210}Po and ^{210}Pb activities found in Borkowo could depend on soil fertility – high moisture and radionuclides bonding by organic matter. ^{210}Po and ^{210}Pb activity concentrations in analyzed topsoil were highly differentiated, in some cases an order of magnitude higher than those in mushrooms.

Conclusions

The studies showed that edible wild mushrooms, *Leccinum* accumulate ^{210}Po and ^{210}Pb at different level and this process depends on soil type and atmospheric fallout. The highest ^{210}Po and ^{210}Pb activity concentrations were found in mushrooms collected in from Borkowo (*L. pseudoscabrum*) which fertile soil contained the highest activity concentrations of ^{210}Po and ^{210}Pb also. But we found ^{210}Po and ^{210}Pb activity concentrations in mushrooms did not reflect their concentrations in topsoil thus ^{210}Po and ^{210}Pb were not selectively bioaccumulated by.

References
Bem, H., 2005. Radioaktywność w środowisku naturalnym. PAN, Łódź 2005.
Falandysz, J., Bona, H., Danisiewicz, D., 1994.Silver content of wild grown mushrooms from Northern Poland. Z LebensmUntersForsch 199:222-224. doi:10.1007/BF01193449
Falandysz, J., Gucia, M., Skwarzec,B., Frankowska, A., Klawikowska, K., 2002.Total mercury in mushrooms and underlying soil substrate from the Borecka Forest, Northeastern Poland. ArchEnvironContaminToxicol 42:145-154. doi:10.1007/s00244-001-0026-1
Falandysz, J., Gucia, M., Brzostowski, A., Kawano M., Bielawski L., Frankowska A., Wyrzykowska B., 2003.Content and bioconcentration of mercury in mushrooms from northern Poland. Food. AdditContam 20:247-253. doi:10.1080/0265203021000057485
Falandysz, J., Kowalewska, I., Nnorom, I.C., Drewnowska, M., Jarzyńska G., 2012.Mercury in Red Aspen Boletes (*Leccinumaurantiacum*) mushrooms and the soils. J Environ Sci Health A 47:1695-1700. doi:10.1080/10934529.2012.687277
Gruter, H., 1964.VerhalteneinheimischerPilzartengegeniiberdemSpaltprodukt[137]Cs. ZeitschrLebensmusFrosch 123(4):173-179.
Gruter, H., 1971. Radioactive fission product ^{137}Cs in mushrooms in W. Germany during 1963-1970. Health Phys 20:655-666.

Gwynn, J., Nalbandyan, A., Rudolfsen G., 2013.^{210}Po, ^{210}Pb, ^{40}K and ^{137}Cs in edible wild berries and mushrooms and ingestion doses to man from high consumption rates of these wild foods. J Environ Radioact 116:34–41. doi:10.1016/j.jenvrad.2012.08.016

Guillen, J., Baeza, A., Ontalba, M.A., Miguez, M.P., 2009.^{210}Pb and stable lead content in fungi: its transfer from soil. Sci Total Environ 407:4320-4326. doi:10.1016/j.scitotenv.2009.03.025

Guillen, J., Baeza, A., 2014. Radioactivity in mushrooms: A health hazard Food Chem 154:14-25. doi:10.1016/j.foodchem.2013.12.083

Heinrich, G., 1992. Uptake and transfer factors of ^{137}Cs by mushrooms. RadiatEnvironBiophys 31:39-49. doi: 10.1007/BF01211511

Heiserman, D.L., 1997. Księga pierwiastków chemicznych. Prószyński i S-ka, Warszawa 1997.

Kalač, P., 2012. Radioactivity of European wild growing edible mushrooms, Nova Science Publ, Hauppauge.

Kalač, P., Svoboda, L., 2000. A review of trace element concentrations in edible mushrooms. Food Chem 69:273–281. doi:10.1016/S0308-8146(99)00264-2

Kostiainen, E., 2007.^{123}Cs in Finnish wild berries, mushrooms and game meat in 2000-2005. Boreal Environ Res 12(1):23-28. ttp://www.borenv.net/BER/pdfs/ber12/ber12-023.pdf

Malinowska, E., Szefer, P., Bojanowski, R., 2006.Radionuclides content in Xerocomusbadius and other commercial mushrooms from several regions of Poland. Food Chem 97(1):19–24. doi:10.1016/j.foodchem.2005.02.048

Persson, B.R.R., Holm E., 2011. Polonium-210 and lead-210 in the terrestrial environment: a historical review. J EnvironRadioact 102:420-429. doi:10.1016/j.jenvrad.2011.01.005

Skwarzec, B., 1995 Polon, uran i pluton w ekosystemie południowego Bałtyku. Rozprawy i monografieInstytutuOceanografii PAN, Sopot.

Skwarzec, B., 1997. Radiochemical methods for the determination of polonium, uranium and plutonium in environment. Chem Anal 42:107-115.

Skwarzec, B., Jakusik, A., 2003.^{210}Po bioaccumulation by mushrooms from Poland. J Environ Monit 5:791-794.

Skwarzec, B., 2010. Determination of radionuclides in aquatic environment (ed) Analytical measurement in aquatic environments. Tylor & Francis PE, 241-258.

Zhang, D., Zhang, Y., Morawska, E., Bielawski, L., Krasińska, G., Drewnowska, M., Pankavec, S., Szymańska, K., Falandysz, J., 2013.Trace elements in *Leccinumscabrum* mushrooms and topsoil from Kłodzka Dale in SudetyMontains, Poland, J Mt Sci 10(4):621-627. doi:10.1007/s11629-013-2384-3

Table 1. Concentration of ^{210}Po and ^{210}Pb in mushrooms collected in northern Poland.

Species Samplingsite	Activity concentration Bq kg^{-1}d.w.				Activity concentration in topsoil Bq kg^{-1}d.w.	
	Cap		Stem		Soil	
	^{210}Po	^{210}Pb	^{210}Po	^{210}Pb	^{210}Po	^{210}Pb
L. pseudoscabrum Sławno	2.44±0.02	2.44±0.02	2.44±0.02	2.44±0.02	2.44±0.02	2.44±0.02
	0.71±0.06	0.48±0.01	1.95±0.07	1.26±0.09		33.1±1.3
	2.49±0.03	1.32±0.07	1.71±0.09	1.00±0.05		26.0±1.0
	2.70±0.04	0.90±0.04	3.21±0.18	0.71±0.09		26.0±1.0
	2.59±0.04	1.20±0.06	1.85±0.08	1.21±0.08		33.9±2.1
	2.63±0.02	0.89±0.05	2.72±0.07	1.14±0.11		25.2±1.2
L. pseudoscabrum Złotów	2.52±0.03	1.47±0.06	0.79±0.06	0.68±0.06	2.71±1.09 3.53±1.01	9.51±1.43
L. pseudoscabrum Borkowo	10.9±0.1	4.92±0.09	1.02±0.06	0.67±0.07	89.1±2.9	59.2±2.0
	2.21±0.04	1.66±0.07	1.84±0.05	0.92±0.06	38.9±1.9	59.7±2.3
	1.75±0.01	0.96±0.04	9.03±0.47	3.57±0.19		33.4±1.8
L. quercinum Gdynia	1.95±0.04	0.79±0.05	1.69±0.07	1.13±0.13	23.4±1.7	22.7±1.4
	1.74±0.03	0.86±0.03	1.16±0.08	0.57±0.07	31.4±1.6	17.4±1.9
	1.04±0.04	0.34±0.01	0.84±0.04	0.48±0.06	18.3±1.5	8.77±1.21
	0.74±0.01	0.48±0.01	1.12±0.11	0.59±0.07	12.1±1.8	14.0±1.6
	1.45±0.02	0.64±0.03	1.11±0.09	0.64±0.09		8.13±1.09
L. auratiacum Parchowo	6.04±0.03	1.05±0.01	4.08±0.08	1.01±0.08	27.6±1.0	22.4±1.0
	4.39±0.04	0.83±0.01	5.29±0.19	2.31±0.09	97.8±2.7	65.5±2.0
	5.16±0.02	0.65±0.03	3.04±0.04	0.94±0.04	65.4±2.9	64.0±2.3
	6.2±0.04	1.57±0.12	2.54±0.05	0.98±0.03	40.4±2.0	28.4±1.9
	4.1±0.11	1.17±0.09	3.61±0.13	1.40±0.06	28.3±1.4	14.1±1.0
L. auratiacum Trzechowo	1.69±0.04	0.68±0.04	2.20±0.01	1.17±0.09	8.98±1.02	6.01±1.03
	0.67±0.03	0.58±0.03	4.33±0.11	1.53±0.08	8.73±1.04	6.01±1.44
	2.18±0.03	1.05±0.07	5.36±0.03	2.16±0.09	7.46±1.11	6.77±1.43
L. auratiacum Orzechowo	1.01±0.03	0.49±0.04	1.67±0.07	0.84±0.07	25.5±1.0	16.5±1.7
	0.92±0.05	0.34±0.01	0.74±0.03	0.45±0.06	47.5±1.4	30.0±1.8
	1.81±0.04	0.31±0.01	0.93±0.01	0.36±0.05	31.1±1.4	4.53±1.09
		0.54±0.04		0.97±0.09		22.5±1.6
L. vulpinum Sulęczyno	2.15±0.05	0.93±0.02	1.83±0.04	1.01±0.04	10.0±1.0	9.53±1.04
	2.75±0.03	1.53±0.09	2.63±0.21	1.48±0.07	5.39±1.01	4.60±1.06
	1.99±0.01	1.01±0.07	1.21±0.39	1.92±0.08	8.45±1.09	7.28±1.21
	1.70±0.03	1.13±0.06	2.20±0.44	0.90±0.06	8.19±1.02	5.35±1.36
		1.90±0.09		2.10±0.12	9.42±1.06	7.42±1.20
L. vulpinum Złotów	1.92±0.02	1.76±0.10	1.91±0.05	1.32±0.07	9.40±1.07	7.23±1.09
	1.77±0.03	1.04±0.06	1.64±0.06	0.99±0.08	16.5±1.1	11.2±1.7
	1.59±0.02		1.50±0.11		6.87±1.32	
L. duriusculum Wysokie	3.16±0.03	2.44±0.21	1.21±0.26	1.20±0.07	21.1±1.4	18.2±1.7
	1.68±0.02	1.68±0.02	1.68±0.02	1.68±0.02	1.68±0.02	1.68±0.02
	1.66±0.02	1.66±0.02	1.66±0.02	1.66±0.02	1.66±0.02	1.66±0.02
	1.76±0.04	1.76±0.04	1.76±0.04	1.76±0.04	1.76±0.04	1.76±0.04
	1.97±0.03	1.97±0.03	1.97±0.03	1.97±0.03	1.97±0.03	1.97±0.03

^{137}Cs activity concentration in potatoes from a Greek contaminated area after the Chernobyl accident

D. Dimitrellou and H.Papaefthymiou *

University of Patras, Department of Chemistry, GR-265 00 Rio- Patras, Greece

Abstract

The Chernobyl nuclear power plant accident, released massive amounts of radioactive materials into the atmosphere. It is estimated that 7.0×10^4 TBq of ^{137}Cs was released in the atmosphere and more than half of the emitted ^{137}Cs, carried by wind, was transported throughout Europe. Greece is one of the countries where the impact of the Chernobyl accident was great due to weather conditions in the period of the accident. ^{137}Cs was transferred in soil and directly to plant surfaces by wet and dry deposition and in turn contaminated crops which are used for food. The sampling area was Trikala, due to the fact that high amounts of ^{137}Cs were deposited after the nuclear accident at Chernobyl at this area, which in conjunction with the vertical movement of the ground, has resulted in the entry of the root system of the plant potato. The ^{137}Cs concentration in potato samples of Trikala region ranged from undetectable levels up to 20.3 ± 1.6 Bq/kg, while the activity of ^{40}K concentrations were between 6.80 ± 0.63 kBq/kg and 15.1 ± 0.89 kBq/kg. The transfer factor (TF) of soil-potato system was also determined and Trikala region showed the highest average value of transfer factor (TF) for ^{137}Cs compared to other Greek regions.

Introduction

It is known that, as for naturally occurring radionuclides, the man-made radionuclides introduced into soil are incorporated metabolically into plants. In addition to root uptake, direct deposition may occur on foliar surfaces resulting also in absorption by the plants and in turn contaminated crops which are used for food. The majority of the radiation dose to humans from artificial environmental radioactivity comes from ^{137}Cs via, mainly, by the consumption of natural food products, i.e. fish, mushrooms and potatoes.

This work reports the activity concentrations of ^{137}Cs in potato samples collected from the Prefecture of Trikala, which was one of the most contaminated Greek areas from the Chernobyl accident (Figure 1). The activity concentrations of the natural radionuclide ^{40}K in the examined potato samples are also presented.

Soil to plant transfer factors (TFs) of ^{137}Cs and ^{40}K were also determined for a number of potato samples. The transfer factor is a value used to evaluate the impact of radioactive release to the environment in various studies. It accounts for the uptake of radionuclides via the root, since soil is a long-term reservoir for plant contamination and the ingestion of contaminated plants contribute to large extent to the dose to human beings. It is defined as the ratio of units of radioactivity per unit mass dry crop divided by the units of radioactivity per unit of mass dry soil (Knatko et al., 2000).

Materials and Methods

Samples

A number of potato samples were collected by hand from the study area during 2013. The collected samples were washed, unpeeled and the edible part was cut in small pieces. Each sample (about 0.5 kg) was dried at 100°C for 24h and then washed at 450°C. Soil cores (5-cm diameter and

25 cm depth) were taken at each place that a potato sample was sampled. The soil samples, after removing roots and pebbles were dried, passed through a 2 mm sieve and then were dried at104°C for 24h. Finally, all samples were transferred to standard counting cups, weighed and sealed tightly.

Radiometric technique

The activity concentration measurements of ^{137}Cs in the potato and soil samples were performed by means of a high resolution γ-ray spectrometry set-up combined with a Canberra HPGe detector.The detector, with an energy resolution of 1.9 keV at the 1.33 MeV of ^{60}Co gamma-ray and a relative efficiency of 25 %, was connected to an 8k computerised ACCUSPEC MCA installation and appropriate electronics. The IAEA GANNAS software was used for data analysis. The activities of ^{40}K and ^{137}Cs were directly determined using their photopeaks at 1460.8 and 661.7 keV, respectively.
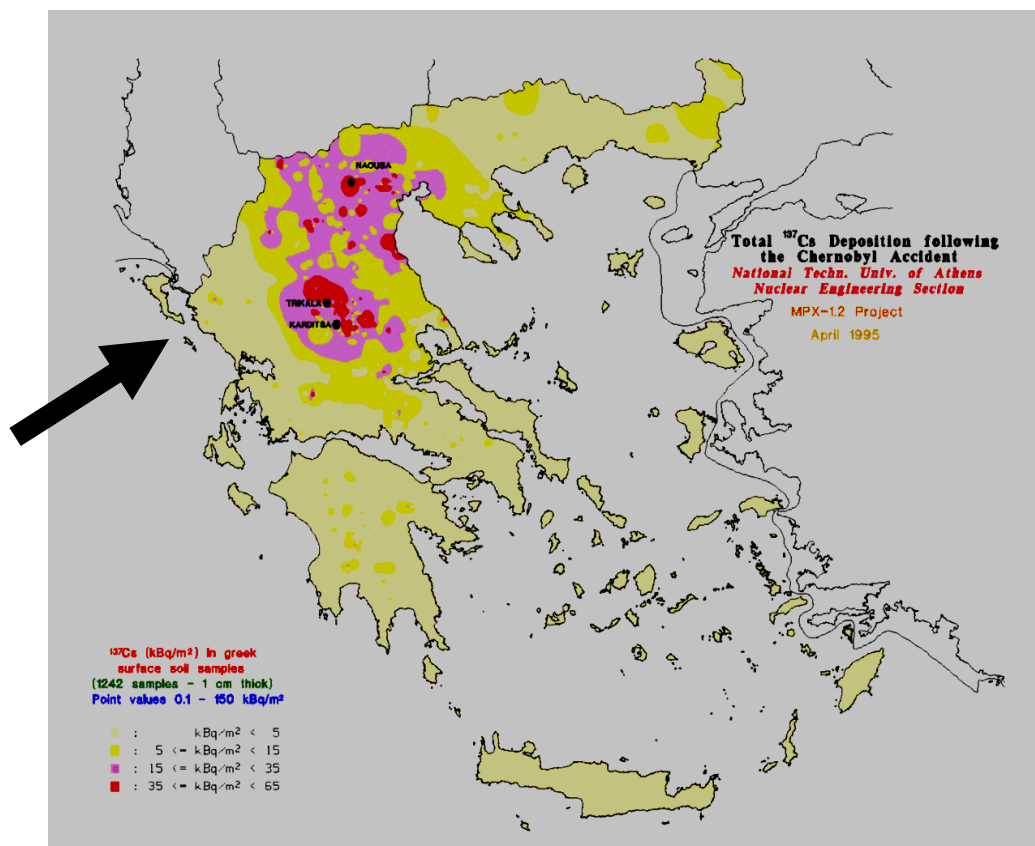
Figure1. Distribution of ^{137}Cs at Greece region after the Chernobyl accident (EUR, 12254 EN Report, 1989).

Results and Discussion

Root uptake of radionuclides by plants depends upon their vertical distribution inthe actual rooting zone in soil. The ^{137}Cs activity concentration in the top soil layer (0-20 cm) of examined area during the sampling period, ranged in the interval 3-280Bq/kg. The ^{137}Cs activity concentrations in the examined potato samples from Trikala area ranged from undetectable amounts up to 20.3 ± 1.6 Bq/kg, with an average concentration value of 6.28± 5.94 Bq/kg. The highest value

of[137]Cs activity concentration (20.3 ± 1.6 Bq/kg) was recorded in the P2 potato sample in Trikala region. Unfortunately, there are no other similar works in Greece in order to compare our results. Furthermore, similar works in other countries are also limited. It is worth noting that, the values presented in this work are comparable to the activity concentration of ^{137}Cs in potato samples collected at 1992 in Russia which had an average value at 19 Bq/kg (Fresenko et al. 1995). Also,the highest value is much greater than the highest ^{137}Cs activity concentration in potatoes measured in Croatia 2005 which was 0.055 ± 0.023 Bq/kg (Franić et al. 2007). These differences could be attributed, on the one hand, in the different sampling chronologies and on the other hand in the different weather conditions that prevailed during and after the Chernobyl accident. Moreover, the soil characteristics play also an important role in the vertical distribution of [137]Cs.

The activity concentration of [40]K in potato samples ranged from 6800 ± 632Bq/kg to 15090 ± 892 Bq/kg. The fluctuations in the values of the [40]K concentrations depend on variety and different soil management conditions of each region.

Table 1.*Concentrations of[137]Cs and[40]K at soilsamplesfrom Trikala region.*

SampleCode	[137]Cs (Bq/kg)	[40]K (Bq/kg)
P2	20.3 ± 1.6	15090± 892
P3	6.33 ± 0.65	8934 ± 528
P7	12.5 ± 1.3	11486 ± 682
P8	3.81 ± 0.52	8698 ± 516
P9	8.17 ± 1.3	11057 ± 651
P10	5.02 ± 0.76	8229 ± 531
P11	0.51 ± 0.40	6800 ± 632
P12	5.56 ± 0.58	10748 ± 634
P13	UDL	9034 ± 534
P14	14.8 ± 1.3	10056 ± 595
P16	UDL	8466 ± 980
P17	5.60 ± 0.92	10090 ± 1001
P18	13.0 ± 1.7	7383 ± 854
P20	UDL	10920 ± 1101
P21	3.61 ± 0.54	8539 ± 506
PX1	UDL	8354 ± 506
PX5	7.07 ± 0.98	7217 ± 835

[137]Cs and [40]K concentrations in soil and potato samples were used for the determination of transfer factors (TFs) from soil in potato from the relationship:

TF = Concentration in potato (Bq/kg dry weight of the radionuclide) / Concentration in soil (Bq/kg dry weight of the radionuclide)

In the literature this relationship is also known as the relative concentration factor (relative concentration factor) (Eisenbud, 1973) or as plant-soil concentration ratio CR (Kathreen, 1984). The TF values of radionuclides vary enormously. The main factors which cause this variability for any particular radionuclide are the type of crop and type of soil. The length of time the radionuclide has been in the soil is also important, particularly for [137]Cs. Other factors are crop variety, agricultural

practice (especially fertilization) and differences in the weather during the growing season (not overall climate). Soil properties that are likely to affect TF values include mineralogical and particle size distribution, organic matter content, pH and fertility. Cation exchange capacity is also important since Cs and K are cations (Cs^+ and K^+) (IAEA-TECDOC-1497).

The average transfer factor (TF) for ^{137}Cs at Trikala region was calculated to be 0.014.Eisenbud (1973) indicates that the TF of ^{137}Cs from the soil in plants is ranging from 0.01 to 1, while Kathreen (1984) notes 0.01 as a typical concentration ratio of the plant-soil for ^{137}Cs. The TF values for ^{137}Cs in the examined samples are within these limits. Tsukada and Nakamura (1999) indicated that the transmission factor values for potato samples are ranging from 0.0037 to 0.16.

The average transfer factor (TF) for ^{40}K at Trikala region was calculated to be 0.288, with no significant difference among the samples.

In this study, the concentrations of ^{137}Cs and ^{40}K in the upper soil layer is considered to be representative of those in the whole soil layer, due to the homogeneous distribution of the same root system for arable crops, to a depth of 20 cm.

Conclusions

The activity concentration of ^{137}Cs in potato samples ranged from undetectable amounts up to 20.3 Bq/kg, with an average concentration value of 6.28 ±5.94 Bq/kg. The activity concentration of ^{40}K in potato samples ranged from 6800 to 15090 Bq/kg. The average transfer factor (TF) for ^{40}K at Trikala region was calculated to be 0.288, whereas the average TF of ^{137}Cs from soil to potato samples was found to be in the range given by other researchers.

References

Eisenbud, M., 1973. Environmental radioactivity (2nd ed.). New York: Academic Press.

Fesenko, S.V., Pakhomov, A.Yu, Pasternak, A.D., Goryaenov, V.A., Fesenko, G.A.,Panov, A.V., 2004. Regularities of change in ^{137}Cs activity concentrations in the long term after the accident at the Chernobyl.NPP. Rad. Biol.Radioecol., 44, 35–49.

Franić, Z., Petrinec, B., Marović, G. and Franić, Z., 2007.Radiocaesium activity concentrations in potatoes in Croatia after the Chernobyl accident and dose assessment. J. Environ. Sci. Health, 42(2), 211–217.

IAEA-TECDOC-1497, 2006.Classification of soil systems on the basis of transfer factors of radionuclides from soil to reference plants, IAEA.

Kathreen, R., 1984. Radioactivity in the environment: Sources, distribution and surveillance. Chur: Harwood Academic Publishers.

Knantko, V.A., Ageets, V.U., Shmigelskaya, I.V., Ivashkevich, I.I., 2000. Soil-to-potato transfer of ^{137}Cs in an area of Belarus: regression analysis of the transfer factor against ^{137}Cs deposition and soil characteristics. J.Environ.Radioact. 48, 171–181.

Letho,J., Vaaramaa, K.,Leskinen, A., 2013. ^{137}Cs, $^{239,240}Pu$ and ^{241}Am in boreal forest soil and their transfer into wild mushrooms and berries. J. Environ.Radioact.116, 124–132.

Tsukada, H., Hasegawa, H., Hisamatsu, A., Yamasaki, S., 2002. Transfer of ^{137}Cs and stable Cs from paddy soil to polished rice in Aomori, Japan. J. Environ.Radioact.59, 351–363.

Uranium (^{238}U) and polonium (^{210}Po) isotopes in mosses and lichens samples from Sobieszewo Island

A.Boryło, G. Romańczyk, D. I. Strumińska-Parulska, B. Skwarzec

Department of Analytical and Environment Radiochemistry,Faculty of Chemistry, University of Gdańsk, WitaStwosza63, 80-308 Gdańsk, Poland

Abstract

In the study, the activities of polonium ^{210}Po and uranium ^{234}U, ^{238}U radionuclides in moss and lichen samples were determined using alpha spectrometry. Different lichens and mosses were collected around the Sobieszewo Island (northern Poland) and investigated for potential use as biomonitors for ^{210}Po and ^{238}U deposition. Mosses and lichens have a high efficiency in capturing ^{210}Po and ^{238}U from atmospheric fallout. The obtained results showed that ^{210}Po, ^{238}U concentrations are changing in analyzed thallophytes samples depending on the type of thallus.

Introduction

The lichen is a composite organism that arises from algae or cyanobacteria (or both) living among filaments of fungus in a symbiotic relationship. The combined life form has properties that are very different from the properties of its component organisms. Lichens come in many colors,sizes, and forms. The properties are sometimes plant-like,but lichens are not plants. Lichens may have tiny, leaf less branches (fruticose), flat leaf-like structures (foliose),flakes that lie on the surface like peeling off paint (crustose) or other growth forms (Fałtynowicz&Wawrzoniak, 2003; Raghukumar, 2012). As mentioned above lichens grow in a wide range of shapes and forms. The shape of a lichen is usually determined by the organization of the fungal filaments. The non reproductive tissues, or vegetative body parts, are called the thallus. Lichens are grouped by thallus type, since the thallus is usually the most visually prominent part of the lichen. Thallus growth forms typically correspond to a few basic internal structure types. Common groupings of lichen thallus growth forms are: fruticose, foliose, leprose, gelatinous, filamentous, byssoid and structureless. Due to the lack of root system, they depend on surface absorption of nutrients and accumulate fallout radionuclides from atmosphere. In these plants, the accumulation degree is much higher than invascular plants growing in the same habitats (Sert et al., 2011). Lichen sare well known to accumulate and retain a variety of contaminants, particularly heavy metals and radionuclides (Nash and Wirth, 1988; Garty et al., 2003; Loppi et al., 2003). The obtained results concerning the differences between mosses and lichens as accumulation biomonitors depend on the species and the environment of the researched area. There is rich literature on the use of lichens and mosses as bio-monitors of atmospheric contamination,the organisms are also good radionuclide bioaccumulators (e.g. were used to assess radionuclide fallout after the Chernobyl accident) (Barci, 1988;Seaward et al., 1988; Mihok et al., 1989; Byazrov et al., 1993; Hofmann et al., 1993; Triulzi et al., 1996; Sawidis et al., 1997; Conti &Cecchetti, 2001; Kirchner &Daillant, 2002; Golubev et al., 2005; Rapport S, 2012). The aim of the study was to determinate of ^{210}Po, ^{234}Uand ^{238}U concentration and value of the activity ratio between ^{234}U and ^{238}U as well as to show differences between kind of thallus, individual species and sampling sites taking into account seasonal changes. In order to examine impact of seasons on observed concentration values, partial results from our previous work was included.

Materials and Methods

The mosses sampled including *Dicranumscoparium* and *Pleuroziumschreberi* were collected in spring and autumn 2009 from Sobieszewo Island near the phosphogypsum waste heap in Wiślinka (northern Poland). The lichen samples including *Leprariaincana*, *Lecanoracarpinea*, *Everniaprunastri*, *Pseudeverniafurfuracea* and *Platismatiaglauca* were collected in spring and autumn 2011 from Sobieszewo Island, too. Five positions where mosses and lichens were collected were marked along the area of Sobieszewo Island. The selected green part of mosses and lichens was dried in the air in a well-ventilated area. Dry moss and lichen samples (about 1–2 g) were mineralized using concentrated acids HNO_3 and HCl in a volume ratio of 2:1. Following the same procedure, blank samples were analyzed. Before radiochemical analysis, each sample was enriched with about 25 and 50 mBq of ^{209}Po and ^{232}U as yield tracers, respectively. After evaporation, the dry residue was dissolved in 20 ml of 0.5 M HCl and, after the addition of ascorbic acid to reduce Fe^{3+}, the solution was transferred to teflon (PTFE) vessels equipped with a silver sheet bottom. Polonium was autodeposited at 90 ^{0}C for 4 h on silver discs. After polonium electrodeposition the sample was evaporated and the dry residue was dissolved in 60 ml of 8 M HNO_3. The solution was introduced into a column filled with anion exchange resins AG 1–X 8 (50–100 mesh). The column then was washed with 90 ml of 8 M HNO_3, and the uranium fraction contained also iron, alkaline earth elements were dissolved in 10 ml of 9 M HCl and introduced into a column filled with anion exchange resins AG 1–X 8 (100–200 mesh). The column was washed with 60 ml of 9 M HCl (in order to remove Cs, Sr, Ra, Ni), and next, U, Fe, Co and Cu retained by the resin were washed with 60 ml of 0.5 M HCl. Eluent was evaporated and dissolved in 10 ml of 1 M $(NH_4)_2SO_4$ (pH 1.5). In order to separate and purify uranium from Fe, Co and Cu, the solution was introduced into a column filled with anion exchange resins AG 1–X 8 (100–200 mesh), and washed with 60 ml of 1 M solution $(NH_4)_2SO_4$ (pH 1.5) and 50 ml of 10 M HCl subsequently, and next uranium adsorbed by resins was eluted with 50 ml of 0.5 M HCl. The solution containing uranium was evaporated and dry residue was mineralized with 2 ml of 1:1 mixture of concentrated HNO_3 and HCl. After evaporation, residue was dissolved in 5 ml of 0.75 M $(NH_4)_2SO_4$ (pH 2) and transferred into cell and the electrolysis was carried out on steel disc during 90 min at a constant current of 1.0 A (Skwarzec; 1997; 2009; Boryło et al., 2012; Boryło 2013). The activities of ^{210}Po, ^{234}U, and ^{238}U in moss and lichen samples were measured using an alpha spectrometer (Alpha Analyst S470) equipped with semiconductor silicon detectors and 300 mm^2 active surface barrier. Minimum detectable activity (MDA) was calculated as 0.1 mBq for ^{210}Po and 0.3 mBq for ^{238}U. Polonium samples were measured for 3 days and ^{210}Po activity was calculated on the time of electrodeposition on silver discs. Uranium samples were measured for 2–7 days. The accuracy and precision of the radiochemical methods were within 10 % based on an international laboratory comparison using International Atomic Energy Agency reference materials. The polonium and uranium recoveries in analyzed samples ranged between 70 and 95 %. The results of ^{210}Po, ^{234}U, and ^{238}U concentrations in analyzed samples are given with standard deviation (SD) calculated for a 95 % confidence interval (±2 r). The obtained results of polonium and uranium radionuclide concentration in analyzed moss and lichen samples are given as an average of four experiments conducted for each sample.

Results and Discussion

^{210}Po concentrations in moss samples were between 133±1 and 501±17 Bq kg^{-1}, while ^{238}U concentration ranged from 1.36±0.13 to 3.87±0.10 Bq kg^{-1}. The higher concentrations of ^{210}Po and ^{238}U were measured in mosses collected in autumn than spring (from 133±1 to 427±15
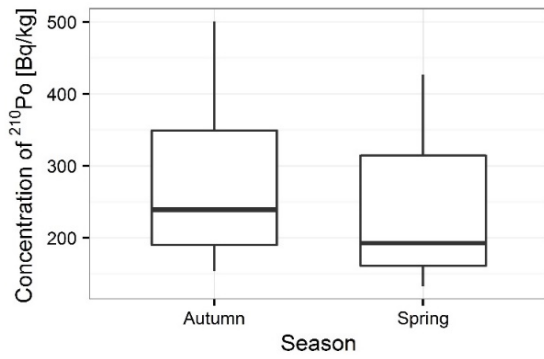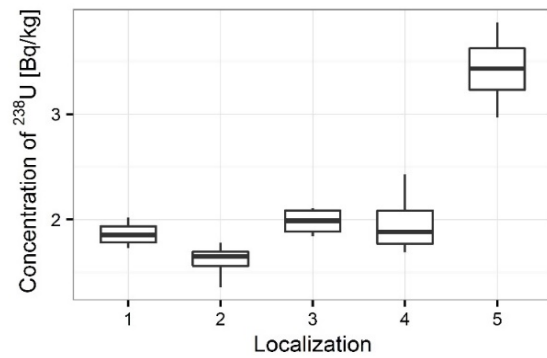
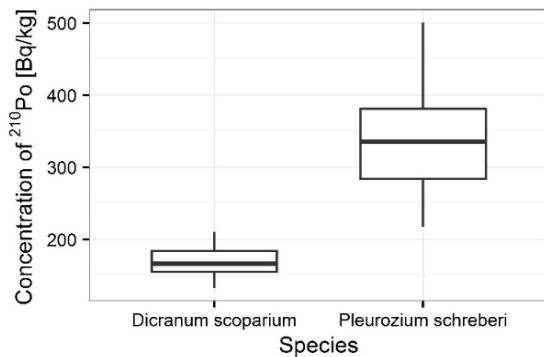***Figure 1.*** *Seasonal concentrations of* ^{210}*Po in analyzed moss samples.*
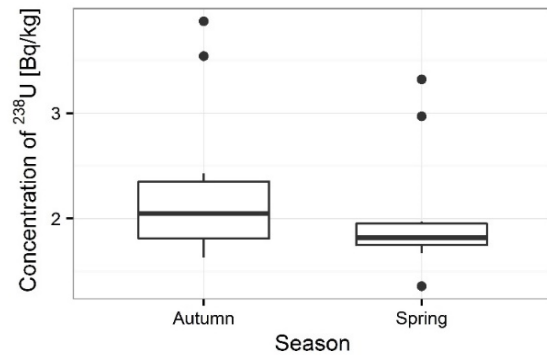
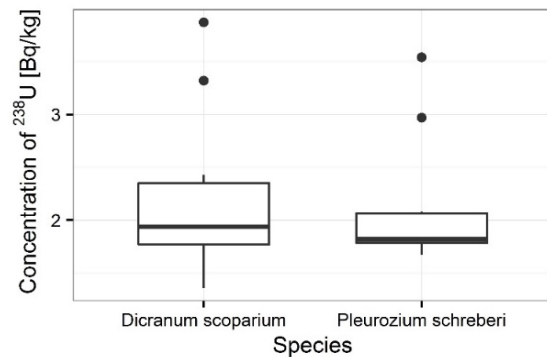***Figure 2.*** *Seasonal concentrations of* ^{238}*U in analyzed moss samples.*
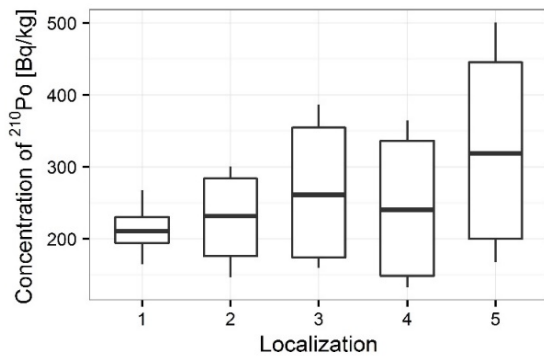
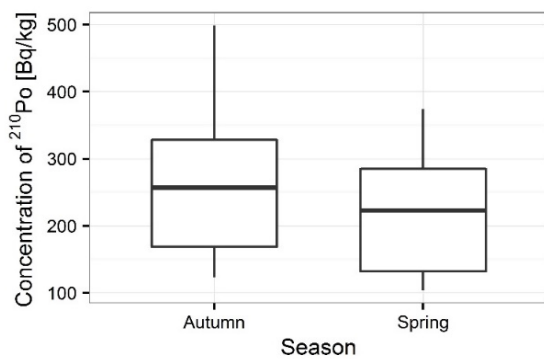***Figure 3.*** *Concentration of* ^{210}*Po for moss samples collecting sites.*

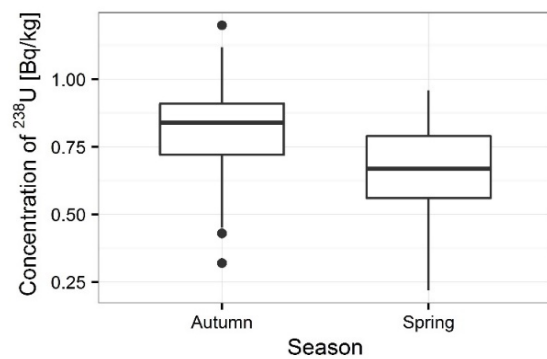***Figure 4.*** *Concentration of* ^{238}*U for moss samples collecting sites.*

Figure 5. *Concentration of* ^{210}*Po in analyzed moss species.*

Figure 6. *Concentrations of* ^{238}*U in analyzed moss species.*

Figure 7. *Seasonal concentrations of* ^{210}*Po in analyzed lichen samples.*

***Figure 8.*** *Seasonal concentrations of* ^{238}*U in analyzed lichen samples.*

Bq kg^{-1} in spring (Boryło et al, 2012) and from 154±3 to 501±17 Bq kg^{-1} in autumn for ^{210}Po; from 1.36±0.13 to 3.32±0.11 Bq kg^{-1} in spring (Boryło et al., 2012) and from 1.63±0.12 to 3.87±0.10 Bq kg^{-1} in autumn for ^{238}U). (Figs. 1, 2). Performed statistical analysis did not confirm the significant differences between the concentrations of ^{210}Po and ^{238}U in spring and autumn (ANOVA, p=0.380 for ^{210}Po and Kruskal–Wallis test, p=0.257 for ^{238}U). The highest ^{210}Po and ^{238}U concentrations in moss samples were observed for two sampling sites: 3 and 5; (Figs. 3, 4). Statistical analysis of ^{210}Po and ^{238}U concentrations in moss samples between collection sites shows significant differences only for ^{238}U (ANOVA, p\0.001), while no significant differences were found for ^{210}Po (ANOVA, p=0.850). The values of the activity ratio between ^{234}U and ^{238}U isotopes in analyzed moss samples were close to one (from 0.97 ± 0.05 to 1.02 ± 0.08).

The statistical analysis shows significant differences between ^{210}Po content in individual mosses species (ANOVA, p\0.001). There were not significant differences between ^{238}U content in analyzed mosses species (Kruskal–Wallis, p=0.705). The higher ^{210}Po concentration was observed in samples of *P. schreberi*, where its average concentration was 342±26 Bq kg^{-1} respectively, the smaller concentration was measured in *D. scoparium* samples (171±8 Bq kg^{-1}) (Fig. 5). The average ^{238}U concentration in *P. schreberi* and *D. scoparium* samples was respectively 2.12±0.20 mg kg^{-1} and 2.22±0.25 mg kg^{-1} (Fig. 6).

^{210}Po concentration in lichen samples collected from Sobieszewo Island was in the range between 104±2 to 499±10 Bq kg^{-1}, while ^{238}U concentration ranged from 0.22±0.06 to 1.12±0.10 Bq kg^{-1}. The results of polonium ^{210}Po concentrations clearly varied depending on the season (ANOVA, p\0.001). The slightly higher values of ^{210}Po concentration were measured, similar as in moss samples, in samples collected in autumn (from 123±3 to 546±9 Bq kg^{-1}), smaller in samples collected in spring (from 104±2 to 406±9 Bq kg^{-1}) (Fig. 7). ^{238}U and total uranium concentration in moss and lichen samples from Sobieszewo Island was varied. The small ^{238}U concentration was observed for spring, definitely higher for autumn. The obtained results of the statistical analysis showed significant seasonal differences, too (ANOVA, p\0.001). The similar effect was noticed for ^{238}U. The average concentration of ^{238}U in lichen samples was 0.66±0.04 mg kg^{-1} for spring and 0.82±0.04 mg kg^{-1} for autumn (Fig. 8). Performed statistical analysis shows significant differences between the activities of ^{238}U in lichen samples and seasons (ANOVA, p = 0.004). Thus lichen samples accumulate ^{210}Po and ^{238}U from the atmosphere throughout the year, wherein the higher ability of accumulation is observed in autumn, while the lower in spring. This effect can suggest that the morphology of lichens vary with seasons. As in the case of moss samples, the highest ^{210}Po and ^{238}U concentrations were measured near the positions of samples collection 3 and 5 (Figs. 9, 10). The position number three is situated in the vicinity of Orle settlements belonging to Sobieszewo Island, whereas position number five is situated near Świbno. There were significant differences in concentrations of ^{238}U in lichen samples among the five areas (ANOVA, p = 0.018), while statistically significant differences were not observed while for ^{210}Po (ANOVA, p = 0.766). The similar effect was observed in moss samples, too.

The higher values of ^{210}Po and ^{238}U concentrations in sites 3 and 5 are likely to be related to the location of sampling sites. The sources of analyzed radionuclides in the analyzed species of mosses and lichens in these areas are probably various industrial branches in Gdańsk agglomeration (the petroleum refinery Lotos SA, ''Remontowa'' Shipyard SA, Gdańsk Power Station, thermal power station in Gdan´sk, the ''Siarkopol'' plant, the lightweight aggregate ''Pollytag SA'') (Boryło et al., 2012). This conclusion can be drawn from the resultingconcentration distribution, and, what is important, based on the direction and strength of winds, which were measured in three points (Świbno, Rębiechowo, Port Północny) in the vicinity of Gdansk agglomeration (Boryło et al., 2012). The winds blowing from the southwest could have carried pollutants to site 3, and winds coming from the south could have
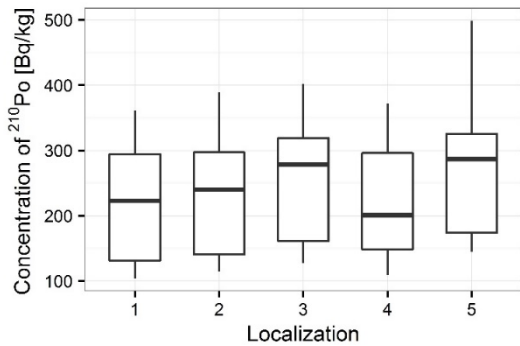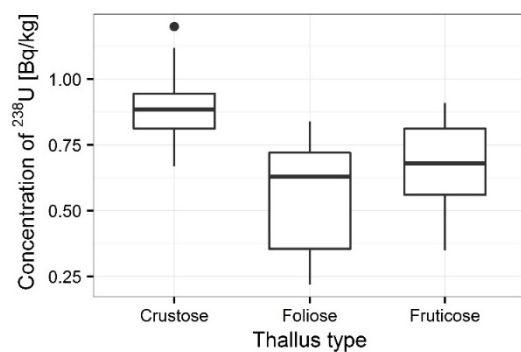
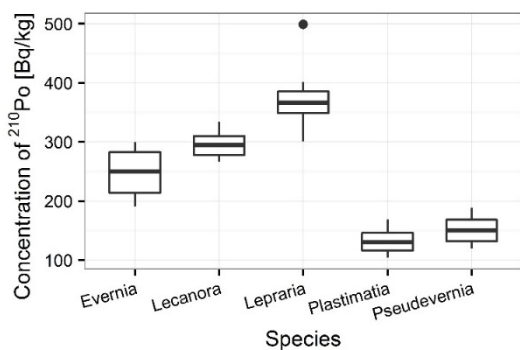**Figure 9.**Concentration of ^{210}Po for lichen samples collecting sites.
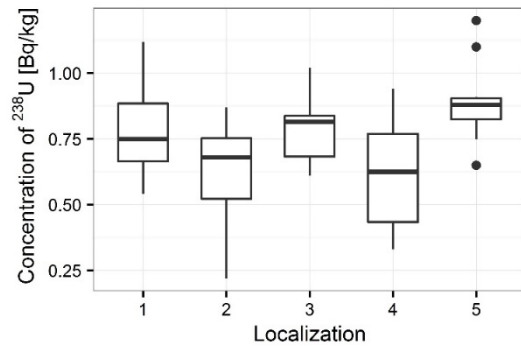
Figure 10. Concentration of ^{238}U for lichen samples collecting sites.
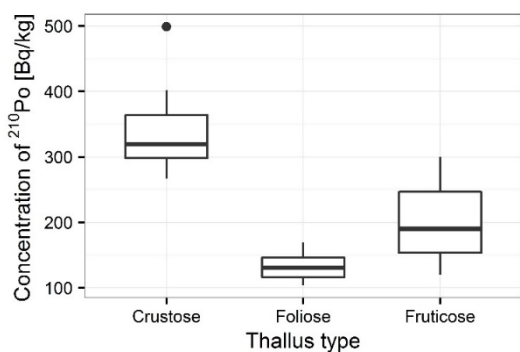
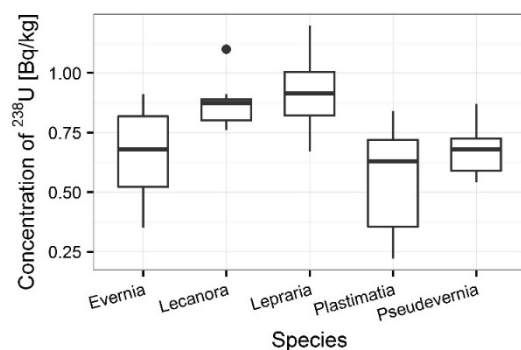**Figure 11.**Concentration of ^{210}Po in analyzed lichen thallus types.

Figure 12. Concentration of ^{238}U in analyzed lichen thallus types.

Figure 13. Concentration of ^{210}Po in analyzed lichen species.

Figure 14. Concentration of ^{238}U in analyzed lichen species.

driven pollutants to site 5 (near phosphogypsum stockpile in Wiślinka). Such factors as the wind direction, its velocity and humidity have an impact an radionuclides'content in the environment and can be used to diagnose a long-term atmospheric contamination with polonium and uranium and to identify the contamination source (Golubev et al., 2005).

Some of the biomonitoring studies throughout the world indicated that the concentrations of various elements in lichens and mosses are inversely correlated with the distance from pollution sources (Dillman, 1996; Fernandez et al., 2007). Contrary to other studies in this research, it has been found that relationships between distance from the plant and contamination in mosses and lichens are directly correlated. Our research was carried out at the moment, when phosphogypsum stockpile in Wiślinka was still working. ^{210}Po were

measured in individual lichen species given kind of thallus for analyzed organisms.The highest ^{210}Po bioaccumulation capacity was observed in organisms built from crustose thallus(e.g. *L. incana and L. carpinea*), where the average concentration of analyzed radionuclide was334±13 Bq kg^{-1} (Fig. 11). The smaller ^{210}Po bioaccumulation capacity was measured in organisms built from fruticose thallus (e.g. *E. prunastri and P. furfuracea*), where the average ^{210}Po concentration was 200±13 Bq kg^{-1})(Fig. 11). The smallest average ^{210}Po concentration (133±7 Bq kg^{-1}) was measured in organisms built from foliose thallus (e.g. *P. glauca*) (Fig. 11). The observed differences between ^{210}Po bioaccumulation capacity and kind of thallus have also been confirmed statistically using ANOVA (p\0.001). Significant statistical differences based on ANOVA were also found for the characterizing thallus of thallophyte in the case of ^{238}U (p\0.001). The highest ^{238}U bioaccumulation was observed for lichens with crustose thallus (with the average value 0.89±0.03 mg kg^{-1}), slightly smaller for lichens with fruticose thallus (with the average value 0.67±0.03 mg kg^{-1}), and thesmallest for lichens with foliose thallus (with the average value 0.56±0.07 mg kg^{-1}) (Fig. 12). Statistically significant difference was also confirmed by ANOVA between the concentration of ^{210}Po and ^{238}U indifferent species of lichens (ANOVA, p\0.001 for ^{210}Po and ^{238}U). The observed changes between individual speciesare presented in Figs. 13 and 14. The differences observed in ^{210}Po and ^{238}U concentrations in lichen samples are the results of differences in accumulation properties of species. The average ^{210}Po concentration in lichen samples was 370±18 Bq kg^{-1} for *L. incana*, 297±7 Bq kg^{-1} for *L. carpinea*, 248±13 Bq kg^{-1} for *E. prunastri*, 151±7 Bq kg^{-1} for *P. furfuracea* and 133±7 Bq kg^{-1}for *P. glauca* (Fig. 13). The average ^{238}U concentration in *L. incana* and *L. carpinea* samples was respectively 0.91±0.06 and 0.87±0.03 mg kg^{-1}, in *E. prunastri* and in *P. furfuracea* samples 0.66±0.06 and 0.68±0.04 mg kg^{-1} respectively, whereas in *P. glauca* samples it was 0.56±0.07 mg kg^{-1} (Fig. 14). The values of the activity ratios of ^{234}U/^{238}U in lichen and moss samples are between 0.97±0.05 and 1.03±0.08, which indicates that the main source of polonium and uranium in the analyzed area is air dry atmospheric fallout which contains phosphogypsum particles from the phosphogypsum waste heap in Wiślinka.

Conclusions

The polonium and uranium content in lichen and moss samples as well as isotopic ratios ^{234}U/^{238}U was measured by alfa-spectrometer technique. The results of the presented survey suggest that the lichens and mosses can be good indicators of polonium and uranium contamination in environment. The present results also proved that the higher polonium and uranium content were determined for mosses than lichens. ^{210}Po concentrations were found higher than ^{238}U concentrations at all sampling stations. The highest polonium and uranium concentrations were found at the sampling sites 3 and 5. The observed highest distribution of polonium and uranium can be explained by the type of lichens thalli. The highest polonium and uranium concentrations were characterized for crustose thallus, the smaller for fruticose thallus, the smallest for foliose thallus. The results for polonium and uranium concentrations indicated great differences between analyzed species of organisms. Also, the polonium and uranium concentrations in all moss and lichen species were very diverse. The ability of accumulation of polonium and uranium isotopes by mosses and lichens makes them useful as bio-indicators of environmental radioactive contamination. The differences observed in ^{210}Po and ^{238}U concentrations in lichen and moss samples could be linked to the differences in accumulation properties of species and the sampling sites as it is shown as shows in the article there were significant differences in concentrations of ^{210}Po and ^{238}U among the sampling sites, kind of thalli as well as seasonsand individual mosses and lichens characteristics.

References

Fałtynowicz, W., Wawrzoniak, J., 2003.Forest condition in Poland in 2003. Biblioteka Monitoringu Środowiska, Warszawa.

Raghukumar CH (ed) (2012) Biology of marine fungi. Springer, Berlin.

Sert, E., Uğur, A., Őzden, B., Sas¸ M.M., Camgőz, B. 2011. Biomonitoring of [210]Po and ^{210}Pb using lichens and mosses around coal-fired power plants in Western Turkey. J. Environ.Radioact. 102, 535–542.

Nash, T.H., Wirth, V., 1988. Lichens, bryophytes and air quality. Bibliotheca Lichenologica. J Cramer, Berlin.

Garty, J., Tomer, S., Levin, T., Lehr, H., 2003. Lichens as biomonitors around a coal-fired power station in Israel. Environ. Res. 91, 186–198.

Loppi, S., Riccobono, F., Zhang, Z.H., Savic, S., Ivanov, D., Pirintsos, S.A., 2003. Lichens as biomonitors of uranium in the Balkan area. Environ.Pollut. 125, 277–280.

Barci, G., Dalmasso, J., Ardisson, G., 1988. Chernobyl fallout measurements in some Mediterranean biotas. Sci. Total. Environ. 70, 73–387.

Seaward, M.R.D., Heslop, J.A., Green, D., Bylinska, E.A., 1988. Recent levels of radionuclides in lichens from southwest Poland withparticular reference to cesium-134 and cesium-137. J. Environ.Radioact. 7(2), 123–130.

Mihok, S., Schwartz, B., Wiewel, A.M., 1989.Bioconcentration of fallout ^{137}Cs by fungi and red-backed voles *(Clethrionomysgarperi)*. Health Phys. 57(6), 959–966.

Hofmann, W., Attarpour, N., Letter, H., Turk, R., 1993. [137]Cs concentrations in lichens before and after the Chernobyl accident.Health Phys. 64(1), 70–73.

Triulzi, C., Marzano, F.N., Vaghi, M., 1996.Important alpha, beta and gamma-emitting radionuclides in lichens and mosses collected in different world areas. Ann.Chim. 86(11–12), 699–704.

Sawidis, T., Heinrich, G., Chettri, M.K., 1997. Cesium-137 monitoring using lichens from Macedonia, northern Greece. Can. J. Bot.75(12), 2216–2223.

Conti, M.E., Cecchetti, G., 2001. Biological monitoring: lichens as bioindicators of air pollution assessment—a review. Environ.Pollut. 114, 471–492.

Byazrov, L.G., Arkhireeva, A.I., Tarasov, O.V., 1993. Ekologiche skiyeposledstviya radioaktiv nogozagryazneniya na YuzhnomUrale. (Ecological Impact of Radioactive Contamination in South Ural). Nauka, Moskow.

Golubev, V., Golubeva, V.N., Krylov, N.G., Kuznetsova, V.F., Mavrin, S.V., Aleinikov, A.Y., Hoppes, W.G., Surano, K.A., 2005. On monitoring anthropogenic airborne uranium concentrations and [235]U/[238]U isotopic ratio by lichen bio-indicator technique. J. Environ.Radioact. 84, 333–342.

Kirchner, G., Daillant, O., 2002. The potential of lichens as longtermbiomonitors of natural and artificial radionuclides. Environ.Pollut. 120, 145–150.

Rapport S., 2012. Polonium-210 and other radionuclides in terrestrial, freshwater and brackish environments, Norvegian Radiation Protection Authority 3.

Boryło,A., Nowicki,W., Olszewski,G.,Skwarzec, B., 2012.Polonium ([210]Po), uranium ([234]U, [238]U) isotopes and trace metals in mossesfrom Sobieszewo Island, northern Poland. J. Environ. Sci. HealthPart A.47(12), 1831–1842.

Boryło, A., 2013. Determination of uranium isotopes in environmentalsamples. J.Radioanal.Nucl. Chem. 295(1), 621–631.

Skwarzec, B., 1997. Radiochemical methods for the determinationof polonium, radiolead, uranium and plutonium in environmentalstudies. Chem. Anal. 42, 107–113.

Skwarzec, B., 2009. Determination of radionuclides in aquaticenvironment. In: Namies´nik J, Szefer P (eds) Analytical measurementin aquatic environments. Tylor & Francis, London,p 241-248.

Dillman, K.L., 1996. Use of the lichen *Rhizoplacamelanophthalma* as a biomonitor in relation to phosphate refineries near Pocatello, Idaho. Environ.Pollut. 92, 91–96.

Fernandez, J.A., Aboal, J.R., Real, C., Carballeira, A., 2007. A new moss biomonitoring method for detecting sources of small scale pollution. Atmos Environ. 41, 2098–2110.

Uranium in Polish mushrooms from *Leccinum* (Gray) genus

Szymańska K., Strumińska-Parulska D., Skwarzec B., Falandysz J.

University of Gdańsk, Faculty of Chemistry, Analytics and Environmental Radiochemistry Chair, WitaStwosza 63, 80-308 Gdańsk, Poland

Abstract

The aim of the project was uranium determination in soil, caps and stem of mushrooms from *Leccinum* (Gray) genus collected in Pomorskie, northern Poland. In our research naturally occurring ^{234}U, ^{235}U and ^{238}U were determined. The average activity concentration of uranium ^{234}U in mushrooms caps and stems ranged from 0.097 to 0.432 mBq·g^{-1}d.w., in case of ^{235}U the activities were from 0.007 to 0.069 mBq·g^{-1}d.w. and for ^{238}U the activities ranged from 0.087 to 0.576 mBq·g^{-1}d.w. Obtained results could indicate that sampling sites were slightly contaminated with radioactive products of uranium fuel, probably from the accident at Chernobyl nuclear power plant.

Introduction

Natural radioactive elements, such as uranium, thorium and potassium and any of their decay products, such as radium and radon, polonium and radiolead,are present in very low concentrations in earth's crust. Human activities, such as oil and gas exploration, mining or coal burning in power plants can enhance their contentin the environment (Bem, 2005). Also the accident at the Chernobyl nuclear power plant (April 1986), and the following radioactive contamination of most European territory, initiated extensive research on the environment, including mushrooms (Heinrich, 1992). There were many papers written about cesium ^{137}Cs accumulation in the environment, wild plants, berries and mushrooms as well (Gruter, 1964; Gruter, 1971; Gwynn et al., 2013).

Uranium is a silvery-white metal in the actinide series of periodic table. Uranium has six known isotopes with half-lives varying from 69 years to 4.5 billion years. The most common isotopes in natural uranium are ^{235}U (about 0.7%) and ^{238}U (about 99.3%) and they occur naturally in low concentrations in soil, rock, and water, and is commercially extracted from uranium-bearing minerals such as uraninite(Heiserman, 1997).

Mushrooms are highly effective bioaccumulators of heavy metals. Fungi contain a lot of water (75-90%) and many species of wild edible mushrooms adsorb and bioaccumulate mercury, chromium, silver, cadmium as well as radionuclides, i.e. cesium, strontium), polonium, radiolead, uranium, plutonium (Gentili et al., 1991; Falandysz et al., 2002; Falandysz et al., 2003; Falandysz et al., 2012; Zhang et al., 2013; Guillen and Baeza, 2014). Radioactive elements are taken either from the soil, through the mycelium or directly from the entire surface gathered in the fruiting bodies. After the Chernobyl accident radioactive contamination of the environment has grown considerably. Mushrooms typically grow in forests and fields, but almost all ecosystems will favor their growth in the correct substrate medium (Kalač, 2000). They could be used as environmental biomonitoring indicators to evaluate the level of the environment contamination as well as the quality of the ecosystem (Skwarzec and Jakusik, 2003). Mushroom species have different retain capacities of radionuclides (Skwarzec and Jakusik, 2003; Malinowska et al., 2006; Guillen et al., 2009). Mushrooms also influence natural radionuclides migration in soil and food chains (Ibrahim and Whicker, 1987; Calmon et al., 2009).

Materials and Methods

Fruiting bodies of wild edible mushrooms and topsoil samples (0-10 cm layer) underneath the fruiting bodies were collected from distantly distributed forested places across Pomerania (northern Poland) – Sławno, Złotów and Gdynia. All mushroom samples, after the removal of plant and soil using plastic knife, were separated into caps and stipes, sliced and oven dried at 65°C to constant weight and further ground in porcelain mortar to fine powder. The soil samples, free of any visible organisms, small stones, sticks and leaves were dried at 65°C to constant mass. Next, the soil samples were ground in a porcelain mortar and sieved through a pore size of 2 mm plastic sieve.

About 2 g of soil and 5 g of mushrooms were digested using 65% nitric acid (HNO_3) and 36% hydrochloric acid (HCl) with a ^{232}U (32.5 mBq) spike added as a yield tracer. The cold mineralization took 7 days. Further the samples were mineralized in hot aqua regia about 5 days to receive clear color of the solution, and then evaporated. Uranium after separation on Dowex anion-exchange resins, were electrolyzed on stainless steel discs (Skwarzec, 2010). The activities of ^{234}U, ^{235}U and ^{238}U were measured using alpha spectrometry with semiconductor silicon detectors (Canberra-Packard, USA).The minimum detectable activity (MDA) for uranium was 0.3 mBq at 2 days counting time. The accuracy and precision of the radiochemical methods were estimated as better than 7% by participation in intercomparison exercises and analysis of IAEA reference materials. The uranium yield in analyzed samples ranged between 70-96% (Skwarzec, 2010). The results of ^{234}U, ^{235}U and ^{238}U activities are given with standard deviation (SD) calculated for 95% confidence intervals (2σ).

Results and Discussion

The results of uranium activity determination in analyzed mushrooms samples from Pomerania (northern Poland) were presented in Table 1. The highest ^{234}U, ^{235}U and ^{238}U activity concentrations were in cap of *L.pseudoscabrum* collected in Sławno– 0.432±0.056; 0.065±0.022 and 0.576±0.06Bq·kg^{-1}d.w. respectively, while the lowest ^{234}U, ^{235}U and ^{238}U were measured in caps of mushrooms *L. quercinum* collected in Gdynia 0.097±0.010; 0.017±0.004 and 0.090±0.009Bq·kg^{-1}d.w. Observed differences could be a result of disparities in topsoil, mineral particles from dusty soils covering the surface of plants and ground, gravitationally deposited, bioaccumulation levels. Almost all mushrooms have been collected in forests, which were semi-natural ecosystems and differed from agricultural cultivated lands; its soils were multilayer, hemi-organic and mineral. Mushrooms and microbes biological activities effect on long-term radionuclides retention in organic layers of forest soil and the soil represents the major reservoir of radionuclides - thus they can be easily available for mushrooms and mycelium located in organic layers. Among the soil samples, the highest activity concentrations of uranium^{234}U, ^{235}U and ^{238}U were noticed in Gdynia: 27.7±0.4; 0.894±0.066 and 23.6±0.3 Bq·kg^{-1}. The highest values of uranium activities found in Gdynia could depend on soil fertility – high moisture and radionuclides bonding by organic matter. Uranium activity concentrations in analyzed topsoil were highly differentiated, in some cases an order of magnitude higher than those in mushrooms.

Conclusions

The studies showed that edible wild mushrooms from *Leccinum* accumulate low value uranium at different level and this process depends on soil type. The highest uranium activity concentrations were found in mushrooms collected in Sławno (*L. pseudoscabrum*) which fertile soil contained the lowest activity concentrations of uranium. We found low uranium

activity concentrations in mushrooms did not reflect their concentrations in soil thus uranium does not bioaccumulate in mushrooms.

Acknowledgments

References

Bem, H., 2005. Radioaktywność w środowisku naturalnym. PAN, Łódź 2005.

Falandysz, J., Gucia, M., Skwarzec, B., Frankowska, A., Klawikowska, K., 2002. Total mercury in mushrooms and underlying soil substrate from the Borecka Forest, Northeastern Poland. ArchEnvironContaminToxicol 42:145-154. doi:10.1007/s00244-001-0026-1

Falandysz, J., Gucia, M., Brzostowski, A., Kawano M., Bielawski L., Frankowska A., Wyrzykowska B., 2003. Content and bioconcentration of mercury in mushrooms from northern Poland. Food. AdditContam 20:247-253. doi:10.1080/0265203021000057485

Falandysz, J., Kowalewska, I., Nnorom, I.C., Drewnowska, M., Jarzyńska G., 2012. Mercury in Red Aspen Boletes (*Leccinumaurantiacum*) mushrooms and the soils. J Environ Sci Health A 47:1695-1700. doi:10.1080/10934529.2012.687277

Gruter, H., 1964. VerhalteneinheimischerPilzartengegeniiberdemSpaltprodukt[137]Cs. ZeitschrLebensmusFrosch 123(4):173-179.

Gruter, H., 1971. Radioactive fission product ^{137}Cs in mushrooms in W. Germany during 1963-1970. Health Phys 20:655-666.

Gwynn, J., Nalbandyan, A., Rudolfsen G., 2013. [210]Po, ^{210}Pb, [40]K and ^{137}Cs in edible wild berries and mushrooms and ingestion doses to man from high consumption rates of these wild foods. J Environ Radioact 116:34–41. doi:10.1016/j.jenvrad.2012.08.016

Guillen, J., Baeza, A., Ontalba, M.A., Miguez, M.P., 2009. [210]Pb and stable lead content in fungi: its transfer from soil. Sci Total Environ 407:4320-4326. doi:10.1016/j.scitotenv.2009.03.025

Guillen, J., Baeza, A., 2014. Radioactivity in mushrooms: A health hazard Food Chem 154:14-25. doi:10.1016/j.foodchem.2013.12.083

Heinrich, G., 1992. Uptake and transfer factors of ^{137}Cs by mushrooms. RadiatEnvironBiophys 31:39-49. doi: 10.1007/BF01211511

Heiserman, D.L., 1997. Księga pierwiastków chemicznych. Prószyński i S-ka, Warszawa, pp.99-103.

Kalač, P., Svoboda, L., 2000. A review of trace element concentrations in edible mushrooms. Food Chem 69:273–281. doi:10.1016/S0308-8146(99)00264-2

Malinowska, E., Szefer, P., Bojanowski, R., 2006. Radionuclides content in Xerocomusbadius and other commercial mushrooms from several regions of Poland. Food Chem 97(1):19–24. doi:10.1016/j.foodchem.2005.02.048

Skwarzec, B., 1995 Polon, uran i pluton w ekosystemie południowego Bałtyku. Rozprawy i monografieInstytutuOceanografii PAN, Sopot.

Skwarzec, B., 1997. Radiochemical methods for the determination of polonium, uranium and plutonium in environment. Chem Anal 42:107-115.

Skwarzec, B., Jakusik, A., 2003. [210]Po bioaccumulation by mushrooms from Poland. J Environ Monit 5:791-794.

Skwarzec, B., 2010. Determination of radionuclides in aquatic environment (ed) Analytical measurement in aquatic environments. Tylor & Francis PE, 241-258.

Zhang, D., Zhang, Y., Morawska, E., Bielawski, L., Krasińska, G., Drewnowska, M., Pankavec, S., Szymańska, K., Falandysz, J., 2013. Trace elements in *Leccinumscabrum* mushrooms and topsoil from Kłodzka Dale in SudetyMontains, Poland, J Mt Sci 10(4):621-627. doi:10.1007/s11629-013-2384-3

Table 1. *Values of uranium activity concentrations in mushrooms and soil collected in northern Poland*

Sampling site *Species*	Activity concentration Bq kg^{-1}d.w.						Activity concentration in topsoil Bq kg^{-1}d.w.		
	Cap			Stem					
	^{234}U	^{235}U	^{238}U	^{234}U	^{235}U	^{238}U	^{234}U	^{235}U	^{238}U
Sławno *Leccinumpseudo scabrum*	0.157±0.036	0.016±0.012	0.157±0.04	0.210±0.015	0.023±0.05	0.181±0.01	5.88±0.25	0.205±0.047	5.88±0.25
	0.432±0.056	0.065±0.022	0.576±0.06	0.226±0.014	0.013±0.003	0.238±0.01	5.26±0.36	1.71±0.21	6.35±0.39
	0.186±0.016	0.014±0.004	0.163±0.01	0.259±0.025	0.027±0.008	0.248±0.02	8.19±0.68	0.281±0.125	8.02±0.67
				0.425±0.039	0.043±0.012	0.383±0.04	6.50±0.19	0.275±0.038	6.66±0.19
				0.259±0.029	0.069±0.015	0.147±0.022	5.92±0.23	0.189±0.040	5.12±0.21
				0.442±0.040	0.058±0.015	0.380±0.037	7.37±0.34	0.289±0.066	8.31±0.35
Złotów *Leccinum pseudoscabrum*	0.092±0.009	0.015±0.004	0.087±0.009	0.091±0.010	0.018±0.004	0.106±0.010	2.69±0.188	0.236±0.056	3.03±0.199
Gdynia *Leccinumquerci num*	0.133±0.015	0.032±0.008	0.090±0.013	0.140±0.014	0.010±0.004	0.147±0.022	7.72±0.50	0.261±0.092	8.80±0.54
	0.190±0.018	0.007±0.004	0.160±0.017	0.215±0.024	0.019±0.007	0.188±0.036	9.69±0.45	0.407±0.093	9.86±0.46
	0.097±0.010	0.017±0.004	0.090±0.009				12.2±0.6	0.496±0.120	13.3±0.6
	0.106±0.014	0.025±0.007	0.097±0.013				12.5±0.3	0.545±0.061	11.9±0.3
	0.109±0.015	0.013±0.005	0.116±0.016				27.7±0.4	0.894±0.066	23.6±0.3

Behavior of ^{137}Cs during biodegradation of contaminated biomass

Ján Mihalík, Jose Corisco, Maria José Madruga

Centro de Ciências e Tecnologias Nucleares (C2TN), Instituto Superior Técnico, Universidade de Lisboa, Campus Tecnológico e Nuclear, Bobadela, Portugal, e-mail: jmihalik@ctn.tecnico.ulisboa.pt.

Keywords: biomass, radiocesium, composting, biodegradation, leachability

Introduction

Bench scale experiments of composting of biomass contaminated by ^{137}Cs are being carried out. The goal is to determinate the leachability of radiocesium present in biomass during the biodegradation process.

The radionuclide behaviour in plant detritus is a poorly investigated phenomenon. Depending on the conditions, Shaw et al. (2004) found that radiocesium in biomass is mainly associated with the exchangeable fraction which results in 35% loss of Cs due to water passing through compost. When they reduced water volume only 1% of Cs was taken off the compost. Very similar results were reached by Jouve and Schulte (1991). Moreover, they recorded that in anaerobic conditions up to 50 % of Cs was released from compost. Mihalik et al. (2014) examining peat showed that 27 years after Chernobyl accident the 18% of all ^{137}Cs is still bioavailable.

Methods

In this study we will examine the behaviour of ^{137}Cs during composting of biomass contaminated in two ways: a) external contamination of leaves, b) internal contamination through root absorption. The alphalpha plants (*Medicago sativa*) were used for experiments.

After the harvesting, the biomass cut to small pieces was placed in a 500 ml vessel in which the composting process is running. During the following two months the leachate was collected and analysed on ^{137}Cs by gamma spectrometry. Final detritus was washed with water in order to release remaining ^{137}Cs.

Results

The table 1 shows that the majority of ^{137}Cs was leachable with water. While the cumulative ^{137}Cs activity of the eluents from externally contaminated biomass reached 20 %, in the internally contaminated biomass it was almost 50 %. It was quite surprise result because the expectation was that Cs applied on the leaves is more leachable. Finally, the same procedures led to a bit higher activities in biomass residuum of the trial of the external contamination than of the internal contamination.

Due to a presence of high weight organic molecules in the eluates we were interested of their role in the ^{137}Cs transport from the biomass. The majority of ^{137}Cs was associated with humic acids-like (HAL) compounds which were confirmed by the size exclusion chromatography and precipitation of humic acids.

The binding to HAL could result in a high mobility of ^{137}Cs when the compost eluents reache soil or surface water due to elimination of Cs adsorption on clay minerals.

Table 1: The quantity of ^{137}Cs released in the various steps during experiments.

		External contamination		Internal contamination	
		Bq	%	Bq	%
Biodegradation	Σ eluates (n 15/11)	194 ± 19	20	1.1 ± 0.1	47
Centrifugation	water fraction	406 ± 9	40	0.69 ± 0.03	20
	1st washing – water fraction	166 ± 5	17	0.57 ± 0.03	16
	2nd washing – water fraction	142 ± 4	14	0.27 ± 0.02	11
	Σ		91		94
	Solid residuum	193 ± 14	20	0.14 ± 0.02	6.1

Conclusion

The most important consequences coming from the presented investigation target on the emergency situation after a nuclear accident. If the plant biomass is contaminated by ^{137}Cs fallout, very early, since the beginning of biodegradation, the activity will be measurable in eluents. The good practice should be, do not leave contaminated biomass on fields if soil should be protected. From another point of view, the activity of ^{137}Cs in collected biomass decreases in a few months on an acceptable level if this biomass is composted under controlled conditions. So, taking in account this consideration eventually, biomass could be suitable used.

Distribution of the ^{210}Pb and ^{210}Po activity concentration in morphological moss parts

M. Długosz-Lisiecka*

Technical University of Lodz, Institute of Applied Radiation Chemistry, Wróblewskiego 15, 90-924 Łódź

Abstract

Radionuclide concentration analysis of the total moss body gave often relatively different results than analysis each different morphological parts. Therefore, first order kinetic model has been used for ^{210}Po and ^{210}Pb transport to the three mosses body components. Activity concentrations of ^{210}Po and ^{210}Pb radionuclides in various morphological parts of mosses were measured. The highest content of both radionuclides was detected in rhizoid parts of the moss species *Pleurozium schreberi*. A significant excess of the activity concentration of ^{210}Po in relation to the ^{210}Pb radionuclide in the rhizoid system was observed. Comparison of the ^{210}Po specific activities in the moss leaves from unpolluted and urban sites allows an estimation of the additional unsupported ^{210}Po activity in urban air.

Introduction

The concentrations of ^{210}Pb and ^{210}Po in plants are correlated with the annual radioactive dry and wet deposition rate (Persson, 2014, Długosz-Lisiecka and Wróbel, 2014). In contrast to natural radionuclides coming from ^{222}Rn decay in the air, most of the anthropogenically originating ^{210}Pb and ^{210}Po radionuclides (equation 1) are discharged and deposited seasonally on the ground and plants in the vicinity of their emission sites (Długosz et al. 2010; Długosz-Lisiecka, 2015 a,b, 2016).

$$^{210}Pb_{22.3\,years} \rightarrow ^{210}Bi_{5.03\,days} \rightarrow ^{210}Po_{138\,days} \tag{1}$$
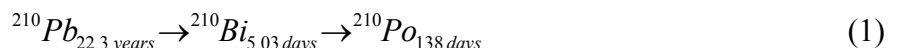
The accumulation of ^{210}Pb and ^{210}Po in the moss body is generally characterized by two distinct processes: bioadsorption from dry or wet precipitation or from soil and then internal transport. First rapid metal uptake with a passive ion exchange process is occurring on the cell walls until a steady state conditions are reached, then it is followed by a slower linear accumulation. This second, slow step is considered decisive for the final total metal uptake by the moss cells. For characterization of the dynamics of the metal bioaccumulation in moss body plant three compartment model has been applied (Boquete et al., 2014; Brumelis and Brown,1997). For each compartment first order kinetic equation was used for analyzing the ^{210}Pb and ^{210}Po radionuclides transport in the mosses (Ghaemian,1979; González and Pokrovsky, 2014, Sert et al. 2011, Ugur et al. 2003; Ugur et al.2004).

Level of ^{210}Po and ^{210}Pb activity concentration in the various moss body parts depends on several factors; eg. initial both radionuclides content in the local environment and its activity ratios in the air and in the soil and the time which plays a significant role in internal transport of metals (Koz and Cevik,2014; Nadeem, et al., 2016).

---

*Corresponding author, E-mail: mdlugosz@mitr.p.lodz.pl

Materials and Methods

Samples

Sampling sites were selected in two fields: the first in Lodz city center and the second in an unpolluted forest located tens of km from the residential region.

There is a significant environmental contrast between these regions. The urban air contains a mixture of radionuclides arising from several sources, e.g. coal power plants, natural ^{222}Rn exhalation, and the resuspension of soil. Mosses from the urban region are exposed to additional environmental **stresses**, such as high levels of sulfur or nitrogen oxides. Samples collected in the second location can be treated as clean environmental background samples**.**

The family of *Pleurozium* mosses are one of the most widespread moss families in the region of central Poland. The experimental material was separated from foreign plants with pincers. After cleaning and drying at room temperature, each sample was weighed and prepared for radiometric analysis (Steinnes, 1995). The samples of *Pleurozium schreberi* mosses were divided into three parts: stems leaves, stems, and rhizoids. The sample weights ranged from 1 up to a maximum of 2g.

Radiometric technique

The ^{210}Pb activities were determined by nondestructive gamma spectrometry analysis. The selected material was compacted in the form of thin discs with a diameter of approx. 5 cm and a thickness of 2 mm. These prepared samples were analyzed by a γ-ray spectrometer with anticoincidence mode using an 80,000sec. acquisition time (Długosz-Lisiecka, 2016). The low background conditions achieved by the addition of the active shield and the long measurement time resulted in a relative error of less than 10% in environmental samples.

After instrumental ^{210}Pb analysis, a radiochemical ^{210}Po separation technique was applied before counting this radionuclide with α-spectrometry. Each sample was placed in a beaker filled with 2 and 5 ml of concentrated HNO_3 and HCl, respectively. In order to calculate the ^{210}Po separation efficiency, a known activity of its ^{209}Po isotope (NIST 4326a) was added to each sample as a marker. After digestion, the samples were evaporated and the dry residues were dissolved in 70 ml of 1M HCl. Prior to the spectrometry measurement, the ^{210}Po and ^{209}Po present in the solution were separated by spontaneous deposition on silver discs. The activities of ^{210}Po and ^{209}Po were determined using an alpha spectrometry system with a PIPS (CANBERRA) detector. Details of the method used have been described elsewhere (Długosz et al., 2010). The relative measurement error of these assays ranged from4 to 6%.

Results and Discussion

The plants from the polluted sites (from the urban region) were generally smaller, with fewer branches and smaller leaves, and therefore had less surface area available for the uptake of atmospheric pollutants than the plants from the relatively unpolluted region. Preliminary studies showed some interesting regularities, independent of the sampling site or season of collection. Both the ^{210}Po and ^{210}Pb radionuclides' specific activities and their ratios (Fig.1) were different, depending on the part of the moss examined.
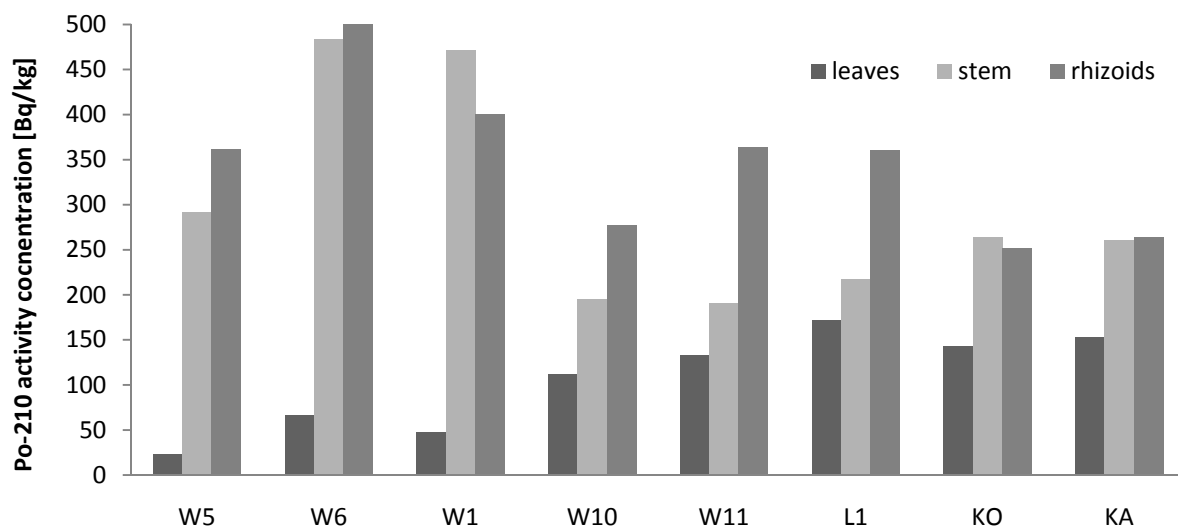
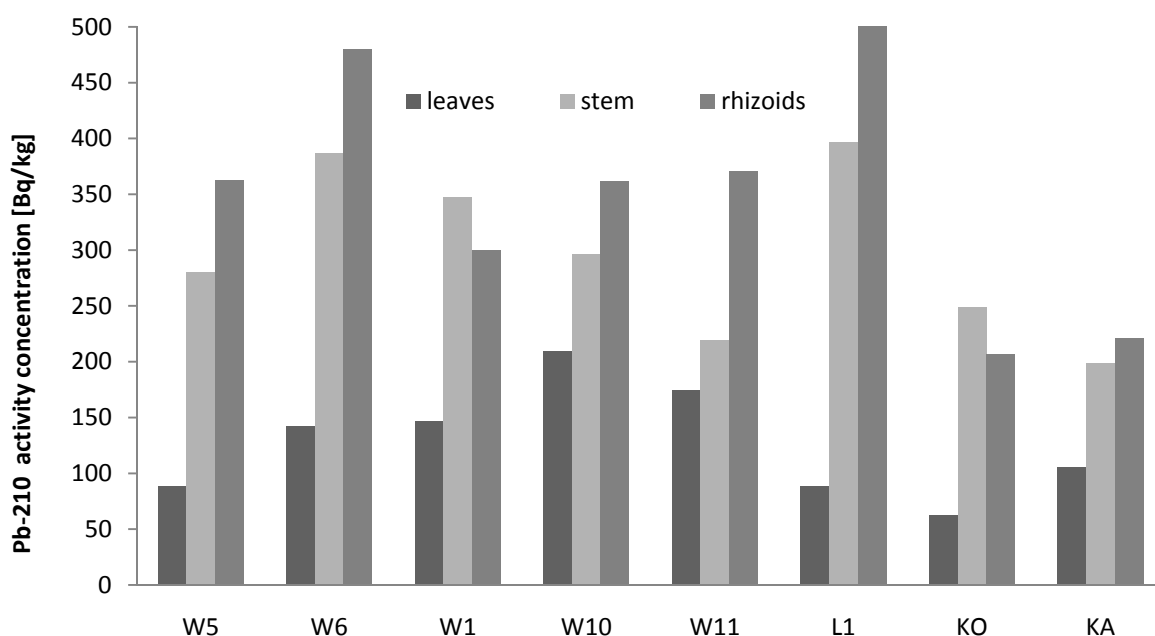***Figure 1.*** *^{210}Po activity concentrations in different parts of the moss.*

Figure 2. *^{210}Pb activity concentrations in different parts of the moss.*

The W1, W5, and W6 samples were taken during the summer, while samples W10 and W11 were taken in winter, all from a deep forest area. The ^{210}Pb and ^{210}Po radionuclides' activity concentrations in the surface layer of soil at this site were basically in radioactive equilibrium and equal to 26±4Bq/kg.

Three remaining samples, L1, KO, and KA, were taken from the city center, located near coal power plants and close to domestic heating systems. A higher ^{210}Pb and ^{210}Po activity concentration in the local environment was confirmed by an analysis of surface soil, where 84±15 Bq/kg of 210Pb (also in radioactive equilibrium with ^{210}Po) was detected.

The relatively small difference between ^{210}Po and ^{210}Pb metal accumulation can be explained, in part, by the fact that the two metals have different affinities to the binding centers of the different parts of the moss.

The most interesting fact observed in Fig.1 and Fig. 2 is that particular fragments of the moss have different abilities to storage these two radionuclides. Rhizoids and stems have the greatest likelihood of accumulating nutrient components, including metals. Radionuclides initially adsorbed on the leaves from the air are partially washed out to the surface soil, from there they are finally transported into the moss part. Changes in the seasonal concentrations of ^{210}Po in the different parts of the moss can be also be confirmed by Fig.1.In the summer (samples W5, W6, and W1),the average ^{210}Po to ^{210}Pb activity ratio in the leaves reaches a value of 0.3, whereas the same ratios for stems or rhizoids exceed a value of 1.2, but in winter (samples W10 and W11) the ratios for the leaves are doubled. The observed changes are related to the contribution of different sources of both isotopes, their adsorption and washing out processes, and additionally the transportation of the components within the plant.

Average 50% of the ^{210}Po and ^{210}Pb radionuclides' activity is stored in the rhizoids, while the remaining part of the activity is deposited in the stems and leaves. Vertical transport down from the leaves via the stem to the rhizoids is more effective than in the opposite direction (rhizoids-stem-leaves). These results are consistent with an analysis of lead uptake experiments, carried out under in vivo and in vitro conditions (Ghaemian N., 1979).

The low values of the ^{210}Po/^{210}Pb activity ratios in the summer leaves from the unpolluted area, close to the values found in atmospheric aerosols, suggests that the moss leaves can be good bioindicators of direct fresh atmospheric pollution.

The values that are higher than 1 for this radionuclide ratio in the leaves from the polluted urban atmosphere indicate an additional, anthropogenic flux of ^{210}Po (Długosz-Lisiecka, 2016). The bioaccumulation of ^{210}Po from the soil to the moss profile by rhizoids seems to be similar to that of the ^{210}Pb radionuclide, and generally these processes are much slower (especially in winter); ^{210}Po growth from ^{210}Pb decay should be taken into account for stem and rhizoids. Rhizoids adsorb metals mostly from the surface ground phase, where the ^{210}Po/^{210}Pb ratio is on average ~ 1, as both radionuclides are practically in secular equilibrium.

Therefore stems and rhizoids, where activity concentrations are several times higher than in leaves, can be used for the estimation of general long term pollution levels in the local environment.
Dependaly on the initial ^{210}Po/^{210}Pb activity ratio in the local environment dynamic of ^{210}Po accumulation change in the wide range. In case of secular equilibrium between ^{210}Po and ^{210}Pb, (typical for soil) from city dynamic of ^{210}Po activity stabilize after a half year. In case of ^{210}Po/^{210}Pb =0.1, (typical for clean atmosphere) a steady state of the passive processes can be obtain after even 2 years.

As it can be seen mathematical descrition of all processes occur in the moss body after absorption of the metals is a quite complicated and depends on the speed of various passive processes. However linear correlation between ^{210}Po and ^{210}Pb should be obtain. A pilot study confirm this assumption.

Conclusions

^{210}Po accumulated in the moss body parts comes from natural ^{222}Rn exhalation from the ground or results from human activity and has been named supported and unsupported, respectively. Concentration distributions in a significant change with the change of seasonal shares emission sources and transport of minerals within the plant. The pollutants accumulated in the moss tissues come from sources atmospheric. Increasing of ^{210}Po and ^{210}Pb in vertical moss body profile

confirm significant contribution of ^{210}Po activity ingrowth from ^{210}Pb decay and aging of the moss tissue. First order kinetic of ^{210}Po bioaccumulation in each of the morphological moss parts can be used as a method of ^{210}Po source identification in the air.

References

Boquete, M.T., Aboal, J.R., Carballeira, A., Fernández, J.A., 2014. Effect of age on the heavy metal concentration in segments of Pseudoscleropodium purum and the biomonitoring of atmospheric deposition of metals, Atmospheric Environment, 86, 28-34.

Brumelis, G.and Brown, D. H. 1997. Movement of metals to new growing tissue in the moss Hylocomium splendens (Hedw.) BSG, Annals of Botany 79, 679–686.

Długosz-Lisiecka, M., Wróbel, J., 2014. Use of moss and lichen species to identify ^{210}Po contaminated regions, Environ Sci Process Impacts., 16,12, 2729-33.

Długosz-Lisiecka, M., 2015a. Excess of Polonium-210 activity in the surface urban atmosphere. Part 1. Fluctuation of the 210Po excess in the air, Environ. Sci.: Processes Impacts, 17, 2,458-464.

Długosz-Lisiecka, M., 2015b. Excess of Polonium-210 activity in the surface urban atmosphere. Part 2. Origin of ^{210}Po excess Environ. Sci.: Processes Impacts, 17, 2,465-470.

Długosz, M., Grabowski, P., Bem, H., 2010. ^{210}Pb and ^{210}Po radionuclides in urban air in Lodz city, Poland, Journal of Radioanalytical and Nuclear Chemistry, 289, 719-725.

Długosz-Lisiecka, M., 2016. The sources and fate of ^{210}Po in the urban air: a review, Environment International, 94, 325–330.

Ghaemian, N.,1979. Lead uptake and its effects upon moss metabolism, Doctoral dissertation, University of Aberdeen,

González, A.G., Pokrovsky, O.S., 2014. Metal adsorption on mosses: Toward a universal adsorption model, Journal of Colloid and Interface Science, 415, 169–178.

Koz, B., Cevik, U.,2014. Lead adsorption capacity of some moss species used for heavy metal analysis, Ecological Indicators 36, 491–494.

Nadeem, R., Manzoor, Q., Iqbal, M., Nisar, J., 2016. Biosorption of Pb(II) onto immobilized and native Mangifera indica waste biomass, Journal of Industrial and Engineering Chemistry 35, 185–194.

Persson, B.,2014. ^{210}Po and ^{210}Pb in the Terrestrial Environment, CAES 2, 1, 22-37.

Sert, E., Uğur, A., Özden, B., Murat Saç, M., Camgöz, B., 2011. Biomonitoring of ^{210}Po and ^{210}Pb using lichens and mosses around coal-fired power plants in Western Turkey, Journal of Environmental Radioactivity, 102, 535-542.

Uğur A., Özden, B., Saç, M. M., Yener, G, 2003. Biomonitoring of ^{210}Po and ^{210}Pb using lichens and Moses around a uraniferous coal-fired power plant in western Turkey, Atmospheric Environment 37, 2237–2245.

Uğur,, A., Özden, B., Saç, M. M., Yener, G., Altınbaş, Ü., Kurucu, Y., Bolca, M., 2004. Lichens and mosses for correlation between trace elements and ^{210}Po in the areas near coal-fired power plant at Yatağan, Turkey, Journal of Radioanalytical and Nuclear Chemistry, 259, 1, 87–92.

Acknowledgements

Re-examination of ^{137}Cs Depth Profiles in Undisturbed Soils in Northern Germany

*A.Anesiadou[*1], P. Kaiser[2], G. Kirchner[2], M. E. Souti[1], H. W. Fischer[1]*

* Aikaterini Anesiadou, E-mail: aanesiad@uni-bremen.de

[1]Institute of Environmental Physics, University of Bremen, Germany
[2]Hamburg University, Germany

Abstract

^{137}Cs vertical soil distribution is being re-examined in two different undisturbed regions of Northern Germany. First sampling had been performed between 1992 and 1994 in the two regions and the second was implemented in 2014, all of them providing vertical soil cores with a depth of more than 70 cm. A detection threshold of 0.04 Bq/kg has been achieved from the measuring procedure in relation to one of the deepest soil samples. Vertical profiles of the two regions are quite different, probably as a result of their different soil types. In the first sampling site, ^{137}Cs migration seems to be a slow process, something that was not primarily observed in the second site. Convection dispersion equation has been used as an attempt to model the vertical migration of the radionuclide, returning thus far non - meaningful results and hence it is still under investigation.

Introduction

Radioactive ^{137}Cs was deposited in the Earth's surface globally due to nuclear weapon fallout (1945 - 1963). Concerning Europe, ^{137}Cs levels were later increased after the Chernobyl accident (April 1986). Fukushima disaster (March 2011) also contributed to that increase, but only by a minor amount with respect to Chernobyl, while more specifically this contribution shall be negligible for soils in Northern Germany (Pittauerova et al., 2011).

Radioactive ^{137}Cs enters the soil by dry deposition and precipitation scavenging and depending on its migration rate it can be available for plant uptake and/or groundwater contamination. Its vertical profile knowledge, hence, is crucial in identifying radioactive fallout in soils and in predicting the transfer to human food chains.

The objective of this study is the re-examination of ^{137}Cs vertical distribution originating from the Chernobyl accident and nuclear weapons fallout at two undisturbed soils in Northern Germany sampled first in 1992 (Kirchner, 1998) and 1994 (Kirchner, unpublished data) and later in 2014 at the same locations. Additionally, a model will be applied to represent the transport of ^{137}Cs in the soil

Materials and Methods

Sampling regions

The two undisturbed sampling locations, in Sandkrug and Fischerhude are located around 45 km west and 30 km east of Bremen respectively, as shown in figure 1. The type of soil in Sandkrug could be described as sandy, while the one in Fischerhude as peaty.

At each region two vertical soil profiles have been sampled with an approximate distance of 60 cm from each other, having a depth of 72 cm and 82 cm in Sandkrug and Fischerhude respectively, separated in soil layers of 2 cm.

Since this work is an on-going Master thesis project and time available is limited and in addition to the limited time available for measurement in the gamma detectors of the laboratory, only one soil core of each region has been and is still being measured.

Figure 1. *The two sampling sites (open street map).*

Experimental procedure

Soil profiles, after being sampled and transported in the radioactivity laboratory, have been dried in a drying oven of 105 oC for about 4 to 7 days and sieved in order to exclude roots, leaves and obtain a homogenized sample.

Afterwards, depending on the mass of the samples - which ranged from 130.9 to 1143.9 gr - either a Marinelli beaker or a plastic bottle geometry has been used for their measurement. In each case, samples have been measured by gamma-ray spectrometry, using high purity Ge semiconductor detectors of 50% relative efficiencies and Pb shielding of 10 cm. Measuring time has varied depending on the sample´s depth. As in deeper soil layers where ^{137}Cs concentration is lower, longer measurement time is needed for the radionuclide to be measured above detection limit. Up until now, regarding some of the deeper soil layers, measuring times of about 6 days have been achieved.

Model for transport of ^{137}Cs

All activity distributions measured have been fitted as a first approach to the well-known convection dispersion equation (CDE) that takes into account dispersion, convection and sorption phenomena in soil, assuming linear sorption equilibrium of caesium in liquid and soil. The solution of CDE used in this study is (Kirchner, 1998):

$$C(y,t) = \sum_{j=1}^{n} C_{0j} \cdot e^{-\lambda(t_j)} \left[\frac{e^{-(y-ut_j)^2/4D(t_j)}}{\sqrt{\pi D(t_j)}} - \frac{u}{2D} e^{yu/D} \, erfc \left(\frac{y+u(t_j)}{2\sqrt{D(t_j)}} \right) \right]$$

where C is the total activity concentration, C_{0j} is the initial deposition, λ is the radioactive decay constant, y is the depth and tj is related to the time period between the radioactive fallout incident and the sampling date. D and u are the effective dispersion coefficient and convective velocity of the radionuclide considered.
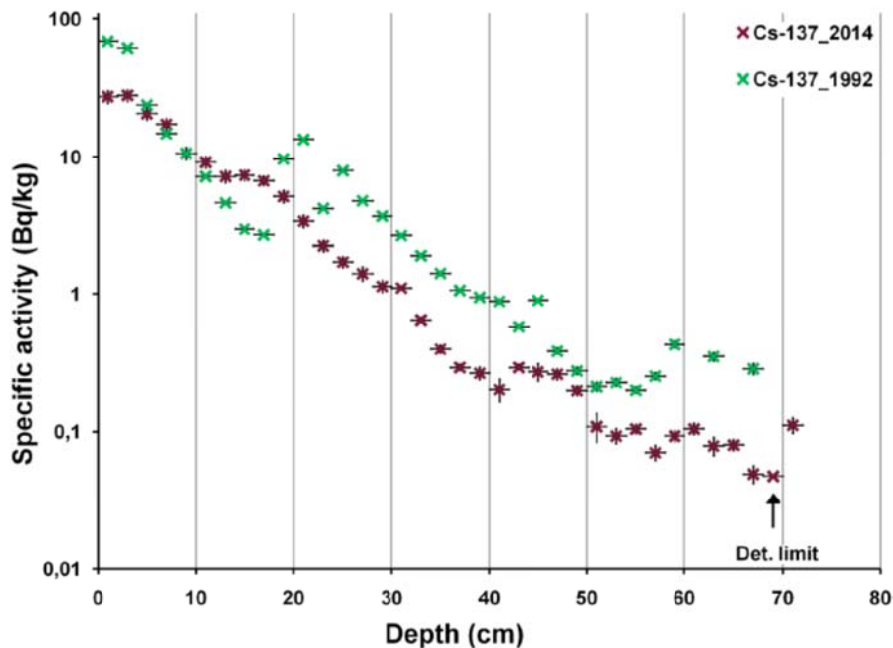
Results and Discussion

Sandkrug (sandier)

Depth distributions

The research of the acquired soil samples regarding this region has been implemented in cooperation with Paul Kaiser (Kaiser, 2016).

Previous and recent depth distributions of ^{137}Cs are shown in figure 2, where the decrease of specific activities with increasing depths can be firstly observed.

Figure 2. *Depth distributions of ^{137}Cs in Sandkrug in 1992 and 2014. Logarithmic scale is being used for specific activities in order to show the features found at greater depths that would not be visible in a linear one.*

^{137}Cs inventories are also calculated giving approximately 6084 ± 51 Bq/m^2 for the 1992 core and 4394 ± 149 Bq/m^2 for the 2014 core. Taking into account decay correction, a total inventory of 3679 ± 30 Bq/m^2 would have been expected. This, however, does not even roughly agree with the observation and hence raises question marks regarding the ^{137}Cs excess.

In the older vertical profile, activity concentrations of Chernobyl fallout are still present in the first 2 cm of soil, while the weapon fallout related ^{137}Cs shows maxima at around 20 cm depth (Kirchner 1998). Regarding the recent core, most of the core's inventory is still present in the uppermost 15 cm indicating slow migration of ^{137}Cs in the soil profile. A first maximum seems to be present near the surface at the first 5 cm for which, as a first hypothesis and in combination to the inventories discrepancy mentioned above, is assumed that there might exist additional contribution from other sources such as erosion or redistribution processes. A possible second maximum seems to exist at around 15 cm and thereafter as depth increases, activity values get lower displaying peak-like features at around 5 cm.

Model Performance

There has been a first attempt to fit the solution of CDE to the data taking into account both Chernobyl and Weapon fallout contribution as follows: C_{total} (y, t) = C_{Ch} (y, t_1, u, D) + C_{Wf} (y, t_2, u, D). The outcome of this, however, yielded non - physically meaningful values for the fitted parameters u and D. Therefore, as a second approach and bearing in mind that u and D have been found to be different between Chernobyl and Weapon fallout in some studies (e.g. Bossew & Kirchner, 2004, Iurian et al., 2014), the solution of CDE has been fitted as follows: C_{total} (y, t) = C_{Ch} (y, t_1, u_1, D_1) + CWf (y, t_2, u_2, D_2). Results of this fitting although ranging in reasonable values, presented unreasonable difference between u_1 and u_2 and the curve fitting outcome was considered unsuccessful.

Fischerhude (peatier)

Results regarding this sampling site are not completed yet, as the low activity of the deeper soil layers requires very long measurement times in order to achieve results with acceptable uncertainties.

Depth distributions of this region are demonstrated in Fig.3, revealing decreasing specific activities with respect to increasing depths and with one prominent peak not near the surface, but at a depth of around 15 cm and 20 cm for the cores sampled at 1994 and 2014 respectively.

Moreover, ^{137}Cs inventories have been calculated as 11566 ± 145 Bq/m^2 related to the older core and 3834 ± 32 Bq/m^2 related to the up to now measured and analysed soil core of 2014. A total inventory of about 7309 ± 92 Bq/m^2 would have been expected in the re-examined core only if reduction due to radioactive decay is taken into account. An implication of ^{137}Cs escape arises in combination to the fact that 95 % of the inventory of so far measured soil core (0 – 48 cm) lies in the first 25 cm

The first maximum in the older core is located not in the uppermost soil layers, implying a convective dominated transport. The aforementioned peak shall be connected to the Chernobyl fallout and it seems to have migrated by around 5 cm downward in the time period between the two sampling dates. This region is characterised of soil with high organic content which would have possibly implied retention of ^{137}Cs at the surface (Al-Masri, 2006). This retention, however, was not observed in our case.
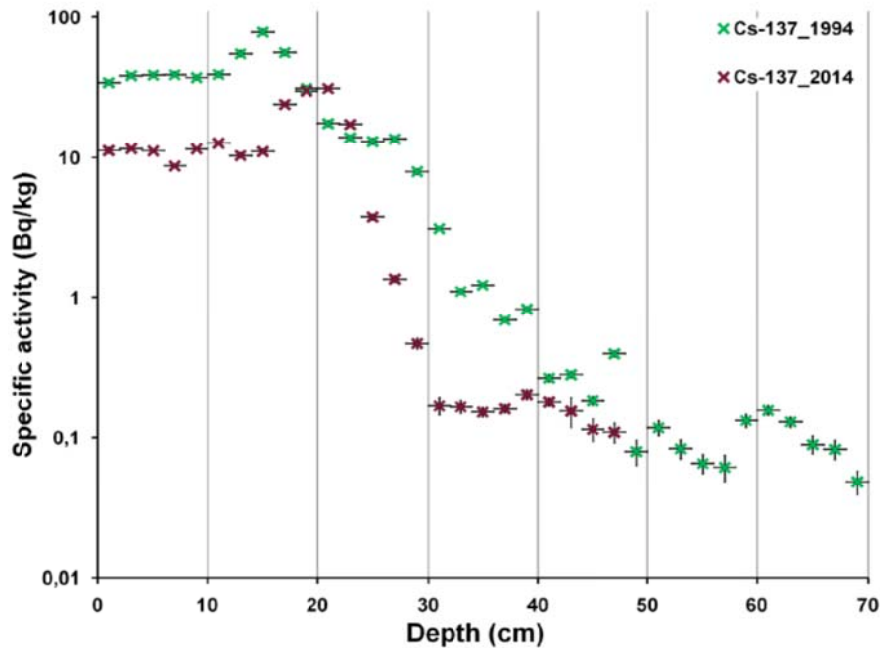
Figure 3. Depth distributions of ^{137}Cs in Fischerhude in 1994 and 2014.

Regarding this region there has been an attempt to fit CDE to the data, but it has not beensuccessful up to now.

Difference between regions

Vertical distributions in the two regions are non – similar to each other, with the most significant difference being that unlike in Fischerhude, in Sandkrug the high activity concentrations of ^{137}Cs have been found in the top soil layers. This could be explained by different physical and chemical parameters depending on the properties of soil.

Conclusions

Results up to now concerning Sandkrug, show that migration of ^{137}Cs is a slow process with most of its activity still found in the top 15 cm, while in Fischerhude vertical soil profile revealed greater ^{137}Cs downward migration. This leads us to the deduction, which is in agreement with (Bossew & Kirchner, 2004), that the difference of the soil type of these regions is one factor determining the migration fate of this radionuclide.

Modelling approaches are still in progress for both sampling sites and their results are up to this time under investigation; a conclusion, hence, could not be drawn yet. One of the ideas initially, as regards Sandkrug, is to fit a third peak to the data and check whether the assumption of an additional source would be meaningful and present a better fitting outcome.

References

Al-Masri, M.S., (2006). Vertical distribution and inventories of ^{137}Cs in the Syrian soils of the eastern Mediterranean region. J. Environ. Radioact. 86, 187-198.

Bossew, P., Kirchner, G., (2004). Modelling the vertical distribution of radionuclides in soil. Part 1: the convection - dispersion equation revisited. J. Environ. Radioact. 73, 127-150.

Iurian, A.R., Mabit, L., Cosma, C., (2014). Uncertainty related to input parameters of ^{137}Cs soil redistribution model for undisturbed fields. J. Environ. Radioact. 136, 112-120.

Kaiser, P., (2016). Gammaspektroskopie zum Nachweis von Cs-137 Aktivitäten und deren vertikale Verteilung in Bodenprofilen. Bachelor thesis, University of Hamburg. (https://www.znf.uni-hamburg.de/studium/qualifikationsarbeiten/archiv-qualifikationsarbeiten.html, 2016)

Kirchner, G., (1998). Modeling the migration of fallout radionuclides in soil using a transfer function model. Health Physics 74 (1), 78-85.
Pittauerova, D., Hettwig, B., Fischer, H.W., (2011). Fukushima fallout in Northwest German environmental media. J. Environ. Radioact. 102, 877-880.
https://www.openstreetmap.de/karte.html, 2016.

B – TERRESTRIAL WILDLIFE AND FOOD CHAIN

Analysis and modelling of radioecological concentration processes in the food chain lichen - reindeer – man

Bertil R.R. Persson,

Lund University, Medical Radiation Physics, 22185 Lund, Sweden.
E-mail: bertil_r.persson@med.lu.se

Abstract

This presentation deals with analysis and modelling of the natural radionuclides[210]Pb and [210]Po in the food-chain lichen, reindeer, man and predators. The analysis and modelling of [210]Po and ^{137}Cs in lynx (*Lynx lynx*), wolverine (*Gulo gulo*) and wolves (*Canis lupus*) will be presented separately in "*Radioecological Informatics and Modelling of Polonium-210 and Caesium-137 in top predators*" (Persson et al., 2016).

By using the methods of Partial Least Square regression (PLSR) the atmospheric deposition of ^{210}Pb and [210]Po is predicted at various locations (Persson, 2016). Dynamic modelling of the activity concentration with differential equations is matched to coincide with sample data. Reindeer lichen consumption, gastrointestinal absorption and organ distribution is derived from information in the literature. The results of dynamic modelling the transfer of ^{210}Pb and [210]Po to reindeer meat, liver and bone from lichen consumption is compared with measurements of samples collected in Sweden and Finland during 1966-1971.

The dynamic modelling of ^{210}Pb and [210]Po activity concentration in various organs of manis matched to coincide with that of samples collected from reindeer breeders in Sweden and Finland during 1966-1971. The activity concentration of ^{210}Pb in the skeleton is modelled by using the results of studying the kinetics of lead in skeleton and blood in lead-workers after end of occupational exposure. The result of modelling ^{210}Pb and [210]Po activity in skeleton is compared with samples of teeth from reindeer-breeders and autopsy bone samples in Finland.

Introduction

At the first international radioecology conference 25-29 April 1966, in Stockholm, Sweden, I presented a study concerning the transfer of [55]Fe in the food chain lichen-reindeer-man (Persson, 1966). Today 50 years later, I will present analysis and modelling of the natural radioactive ^{210}Pb and [210]Po in the same food-chain. The analysis and modelling of [210]Po and ^{137}Cs in lynx (*Lynx lynx*), wolverine (*Gulo gulo*) and wolves (*Canis lupus*) will be presented separately in "*Radioecological Informatics and Modelling of Polonium-210 and Caesium-137 in top predators*"(Persson et al., 2016).

By using the methods of Partial Least Square regression (PLSR) modelling the atmospheric deposition of[210]Pb and [210]Po published from various locations is applied to predict the activity deposition at the reindeer herding districts in Sweden and Finland (Persson, 2016).

The radioecological pathways considered in the present terrestrial model are displayed in Figure 1 with the compartments of the food chain lichen-reindeer-man indicated by a dashed line. The dynamic modelling of the activity concentration in the various compartments is implemented by a system of linear differential equations, one for the activity concentration A_i of each compartment (i) in the food chain.

$$dA_i/dt = \mathcal{F}(A_{i-1})[input] - \mathcal{F}(A_i)[output]$$

Data about reindeer lichen consumption, gastrointestinal absorption and organ distribution is derived from information in the literature. The values of the parameters are matched so that the final result coincide with those of collected sample data. The results of dynamic modelling the transfer of ^{210}Pb and ^{210}Po to reindeer meat, liver and bone from lichen consumption is compared with measurements of samples collected in Sweden and Finland during 1966-1971.
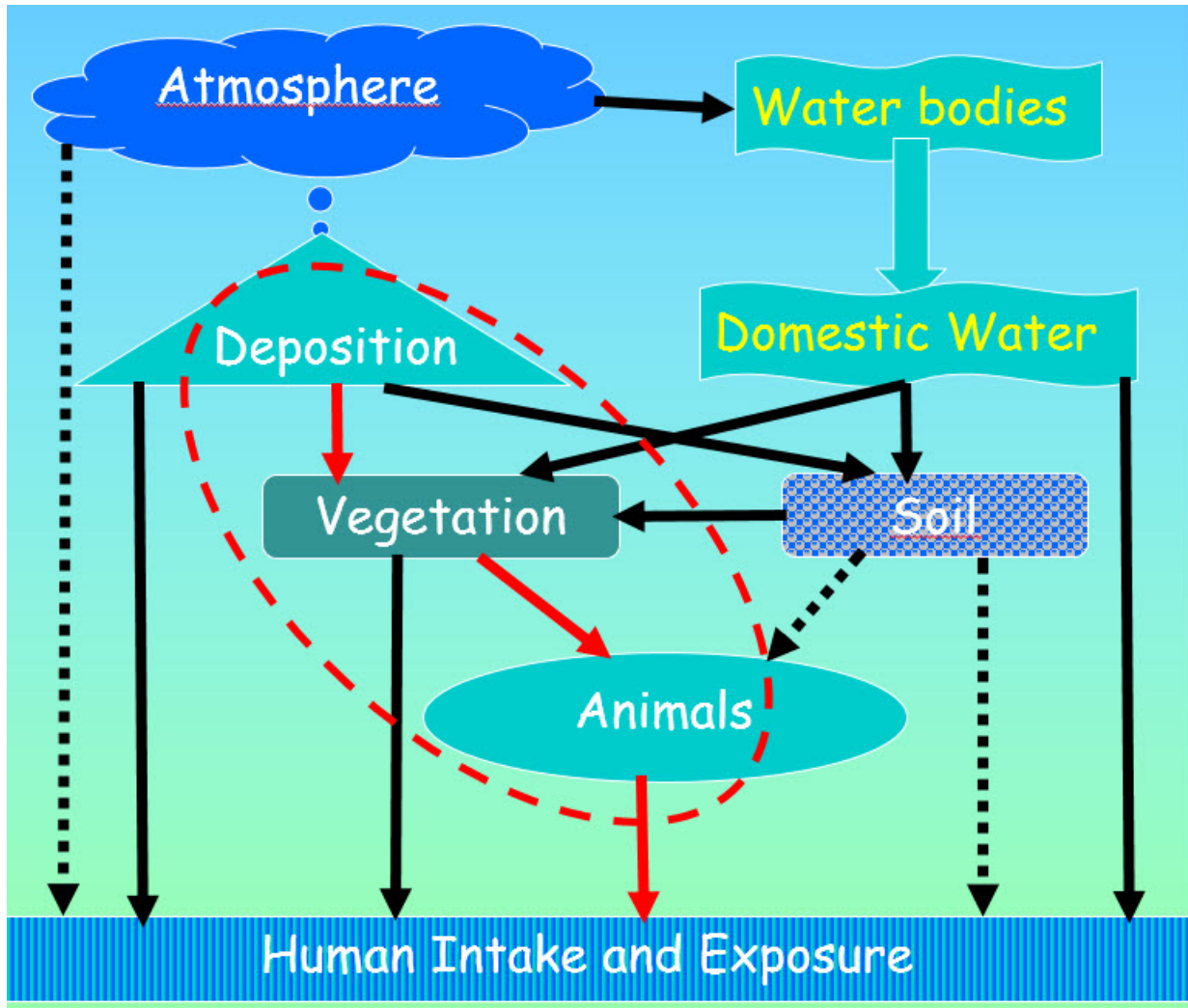
Figure 1. Model of the terrestrial radioecological pathways.

Materials and Methods

Model for lichen

By using the methods of Partial Least Square regression (PLSR) information about the local atmospheric deposition DR of ^{210}Pb and ^{210}Po is derived from deposition data elsewhere (Persson, 2016). The input of activity concentration "ACL(t)" in the top-layer of the vegetation lichen "L" is described with the annual rate of radionuclide deposition $DR(t)$ (Bq.m^{-2}.a^{-1}) converted to dry mass of lichen by the factor $fmaL$ (kg$_{dw}$·m^{-2}), and assuming that *Interception fraction* IF is equal to one for lichen. The output is described by the bio-elimination rate constant from Lichen k$_L$, and the decay constant of radionuclide in question.

The annual activity concentration change in the lichen that is grazed by the reindeer is described by the equation:

$$\frac{dACL(t)}{dt} = DR(t) \cdot fmaL \cdot IF - ACL(t) \cdot (kL + \lambda) \; ;$$

$$(\text{Bq.m}^{-2}.\text{a}^{-1}) \cdot (\text{kg}_{dw}.\text{m}^{-2}) - (\text{Bq.kg}_{dw}^{-1}) \cdot (\text{a}^{-1}) = (\text{Bq.kg}_{dw}^{-1}. \text{a}^{-1})$$
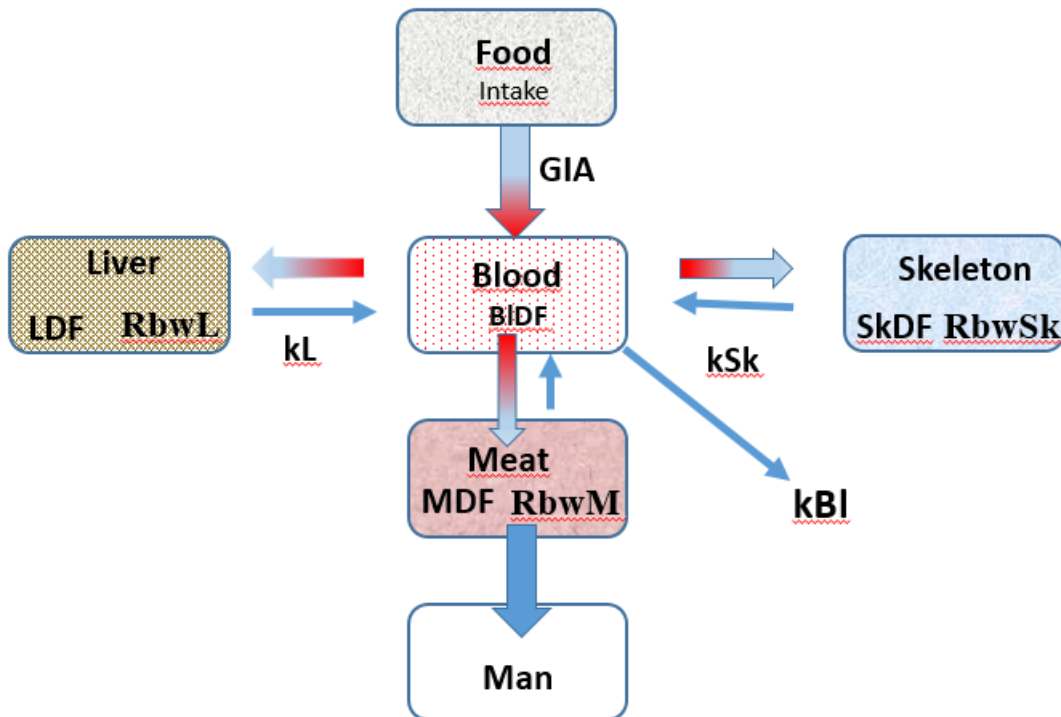
Model for reindeer and man

The activity concentration in the tissue or organ in question is described by a model displayed in *Figure 2*.

Figure 2. *Compartment model of the transfer of radionuclides by food-intake in animals and man.*

The intake rate of lichen per bodyweight of reindeer is IRdL ($\text{kg}_{dw}.\text{a}^{-1}.\text{kg}_{bw}^{-1}$), and the activity concentration in Lichen ACL. Thus the rate of consumed radioactivity is IRdL $\cdot$ ACL($\text{kg}_{dw}.\text{a}^{-1}.\text{kg}_{bw}^{-1}$). The gastrointestinal absorption is GIA, and the fraction of absorbed activity that is distributed to the tissue or organ O is ODF. The conversion to activity concentration in the organ in question is made by the factor BO ($\text{kg}_{bw}.\text{kg}_{fw}^{-1}$). The elimination of the activity from the organ depends on the radioactivity decay constant of the radionuclide in question λ and the elimination rate from organ O is kO. The annual activity concentration change in the organ O in question of the reindeer is described by the following equation.

$$\frac{dACO(t)}{dt} = \text{IRdL} \cdot ACL(t) \cdot GIA \cdot \text{ODF} \cdot BO - \text{ACO}(t) \cdot (kO + \lambda);$$

$(\text{kg}_{dw}.\text{a}^{-1}.\text{kg}_{bw}^{-1}) \; (\text{Bq.kg}_{dw}^{-1}) \; (\text{kg}_{bw} \, \text{kg}_{fw}^{-1}) - (\text{Bq.kg}_{dw}^{-1})(\text{a}^{-1}) = [\text{Bq.kg}_{fw}^{-1}\cdot\text{a}^{-1}]$

3

Results and Discussion

Dynamic Modelling of ^{210}Po in reindeer meat:

The average value of ^{210}Pb in samples of fresh reindeer meat collected in central Sweden and northern Scandinavia varies between 250 and 600 mBq/kg$_{f.w.}$ with an average of 360±50mBq/kg$_{f.w}$ and the average value of ^{210}Po varies between 2.8 and 13.3 Bq/kg$_{f.w.}$ with an average of about 9 Bq/kg$_{f.w.}$(Kauranen and Miettinen, 1969; Kauranen et al., 1971; Persson, 1972; Persson, 1970; Persson et al., 1974; Skuterud et al., 2005).

The activity concentration "ACRM(t)" of ^{210}Po in reindeer from Inari Finland is modelled with the ^{210}Pb average activity concentration of 263 ± 42 Bq.kg$_{dw}^{-1}$ of lichen samples (Kauranen and Miettinen, 1969), and the parameters in *Table 1*.

Table 1. *Modelling parameters of ^{210}Po in Reindeer meat "RM" in Inari area.*

Reindeer meat	IRL	GIA	RMDF	BRM	kRM	^{210}Pb	^{210}Po
ACRM(t) Bq.kg$_{fw}^{-1}$	kg$_{dw}$.a^{-1}.kg$_{bw}^{-1}$			kg$_{bw}$ kg$_{fw}^{-1}$	a^{-1}	a^{-1}	a^{-1}
Meat ^{210}Po	3	0.4	0.084	2.4	6.2	0.0311	1.828

Data from humans consuming reindeer meat containing ^{210}Po indicated a GIA value of about 0.3–0.7 (Hill, 1965; Kauranen and Miettinen, 1967; Ladinska. et al., 1973; Thomas et al., 2001) and the value of 0.5 is recommended to Po in foodstuffs (ICRP, 1993). A GIA value of 0.4 for reindeer consuming lichen is considered in the model. The fraction of ^{210}Po activity that is distributed to the meat RMDF is estimated to 0.084, and the ratio of reindeer body mass versus mass of muscle tissue BRM is 2.4 (kg$_{bw}$ kg$_{fw}^{-1}$).The elimination rate constant of ^{210}Po (T$_{½}$ =50 d) from muscle tissue in reindeer is kM = 6.2 (a^{-1}) (Henricsson and Persson, 2012).

The ingrowth of ^{210}Po from ^{210}Pb as a function of time T(months) is estimated by the equation:

$$[ACPo(T)] = [ACPb(T=0)] \cdot 1.017 \cdot [e^{-0.03 \cdot T} - 0.0363 \cdot e^{-50.5 \cdot T} - e^{-1.83 \cdot T}]$$

As seen in **Figure 3** the ingrowth of ^{210}Po from ^{210}Pb present in reindeer meat quite low compared to the ^{210}Po due to intake.
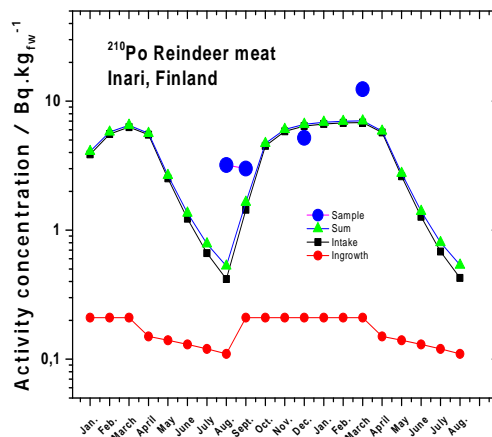
Figure 3 ^{210}Po in reindeer meat from Inari Finland. The blue circles are reported sample values (***Kauranen and Miettinen, 1969***)

Modelling ^{210}Po in Reindeer liver from Inari area (Kauranen 1969)

Due to the short halftime of ^{210}Po compared to ^{210}Pb the timescale for modelling of ^{210}Po is taken to months instead of years. The ^{210}Po activity in green food intake during the summer period April-September is also considered.

The monthly intake rate of lichen by reindeer, per kg of body weight (80 kg_{bw}), during Oct-March "ILRd", is estimated to 0.4 ($kg_{dw}.a^{-1}.kg_{bw}^{-1}$). The activity concentration of ^{210}Po in Lichen PoACL during this period is estimated to 270 ($Bq.kg_{dw}^{-1}$).

The monthly intake rate of green food "G" by reindeer per kg of body weight (80 kg_{bw}) during April –Sept. "IGRd" is estimated to 0.4 ($kg_{dw}.a^{-1}.kg_{bw}^{-1}$). The activity concentration of ^{210}Po in green food PoACG during this period is estimated to = 9 ($Bq.kg_{dw}^{-1}$). For modelling the intake of ^{210}Po in reindeer GIA = 0.4 is considered here. The fraction of GI-absorbed ^{210}Po activity that goes to the liver is estimated to SkDF = 0.022 and the elimination rate kRL = 0.53 (month^{-1}) (Fellman et al., 1994; Henricsson and Persson, 2012).

Table 2. Modelling parameters of ^{210}Po in Reindeer liver "RL" in Inari area.

Reindeer Liver	IRL IRG	GIA	RLDF	BRL	kRL	^{210}Pb	^{210}Po
ACRL(t)Bq.kg_{fw}^{-1}	$kg_{dw}.a^{-1}.kg_{bw}^{-1}$			$kg_{bw} kg_{fw}^{-1}$	month^{-1}	month^{-1}	month^{-1}
^{210}Po intake	0.4	0.4	0.022	120	0.53	0.0026	0.15

Due to the high accumulation of ^{210}Pb in the liver to about 28 $Bq.kg_{fw,}$ and faster kinetics of $^{210}Po$the ingrowth of ^{210}Po become as high as 6.2 $Bq.kg_{fw}$.
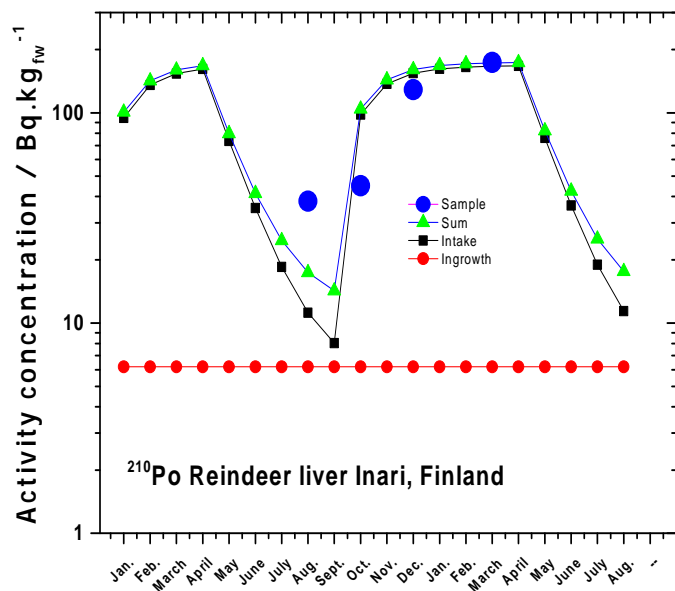
*Figure 4 ^{210}Po in reindeer liver from Inari Finland. The blue circles are reported sample values (**Kauranen and Miettinen, 1969**)*

Modelling ^{210}Po in Reindeer bone from Inari area (Kauranen 1969)

The lichen and green food intake and the GIA values is the same as above. The fraction of absorbed ^{210}Po activity that is distributed to the skeleton is estimated to RBDF = 0.09 and the elimination rate from bone kRB= 0.53 (month^{-1}) (Fellman et al., 1994; Henricsson and Persson, 2012).

Table 3 *Modelling parameters of ^{210}Po in Reindeer bone "RB" in Inari area*

Reindeer bone	IRL IRG	GIA	RBDF	BRB	kRB	^{210}Pb λ	^{210}Po λ
ACRdb(t)	kg$_{dw}$.month^{-1}.kg$_{bw}$$^{-1}$			kg$_{bw}$ kg$_{fw}$$^{-1}$	month^{-1}	month^{-1}	month^{-1}
^{210}Po intake	0.4	0.2	0.09	20	0.53	0.0026	0.15

Due to the high accumulation of ^{210}Pb in the skeleton of about 170 Bq.kg$_{fw}$ the ingrowth of ^{210}Po become quite high. But due to the more rapid kinetics of ^{210}Po the activity of the ingrown ^{210}Po become about 40 Bq.kg$_{fw}$.
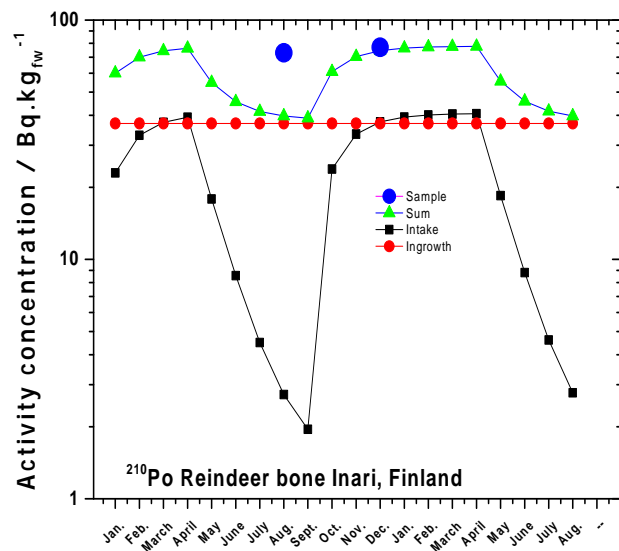
Figure 5 *^{210}Po in reindeer liver from Inari Finland. The blue circles are reported sample values (**Kauranen and Miettinen, 1969**)*

Modelling of ^{210}Po activity concentration in human blood (Kauranen 1969)

The activity concentration of ^{210}Po in human blood was modelled using the parameters in ***Table 4***

Table 4 *Modelling parameters of ^{210}Po in human blood "bl" in Inari area*

Man		ACRdm(t)	IMRd	GIA	blDF	Obl	kbl	^{210}Pb	^{210}Po
blood	Po	Sample ave. 0.5 Bq.kg$_{fw}$$^{-1}$	0.27	0.26	0.13	12.25	0.15	0.0026	0.15

Figure 6 *Activity concentration in blood from reindeer herders at Inari, Finland. Samples average 1966 = 0.5 bq.kg$_{fw}$$^{-1}$(**Kauranen and Miettinen, 1969**)*
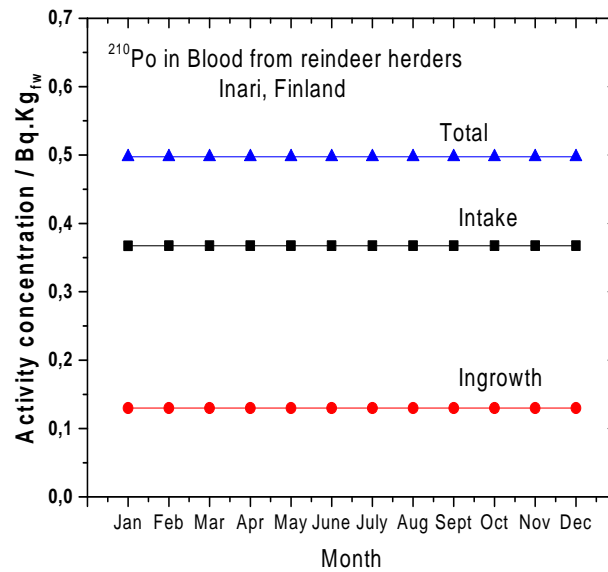
Modelling of ^{210}Po activity concentration in human skeleton (Kauranen 1969)

The activity concentration in human skeleton of reindeer herders from Inari area Finland, is modelled by using values of the various parameters given in **Table 5.**

The ingrowth of ^{210}Po from ^{210}Pb in the skeleton is estimated by the equation applying the $[PbACsk]$ value 5.8 Bq.kg$_{fw}$$^{-1}$.

$$\frac{d[PoACsk(t)]}{dt} = \lambda_{Po} \cdot [PbACsk] - (ksk + \lambda_{Po}) \cdot [PoACsk(t)]$$

Where $[PoACsk]$ is the activityconcentration of ^{210}Po in skeleton (Bq.kg$_{fw}$$^{-1}$).

Table 5 *Modelling parameters of ^{210}Po in human skeleton "Sk"in Inari area*

Man	ACRdm(t)	IMRd	GIA	skDF	Bsk	ksk	^{210}Pb	^{210}Po
Intake	6.5 Bq.kgdw	kg$_{dw}$.month^{-1}.kg$_{bw}$$^{-1}$			kg$_{bw}$ kg$_{fw}$$^{-1}$	month^{-1}	month^{-1}	month^{-1}
skeleton	Samples ^{210}Po 4.8 Bq.kg$_{fw}$$^{-1}$ ^{210}Pb 5.8 Bq.kg$_{fw}$$^{-1}$	0.27	0.26	0.13	20	0.15	0.0026	0.15
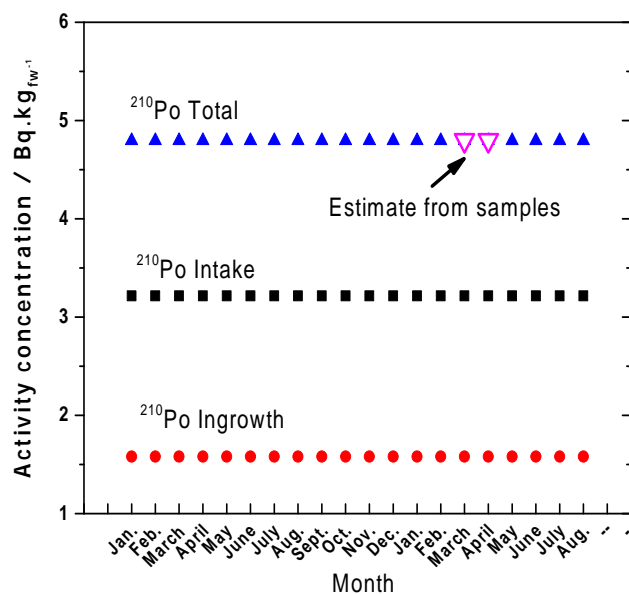
Figure 7 *²¹⁰Po-activity concentration in skeleton from reindeer herders at Inari, Finland. Values from autopsy Samples values shown in triangles* ²¹⁰Po = 4.8 Bq.kg$_{fw}^{-1}$ *(**Kauranen and Miettinen, 1969**)*

Conclusions

The transfer of ²¹⁰Pb and ²¹⁰Po in the food-chain Lichen-reindeer-man has been considered as an example of dynamic modelling of radioecological concentration processes. The differential equations in the model apply various parameters such as *Interception fraction* "IF",and bio-elimination rate constants that can be generalized to other vegetation pathways. The equations for animals and man involves gastrointestinal absorption "GIA", the distribution fraction "DF" of radionuclide that is distributed to the various organs, andthe ratio of body mass versus mass of organ in question "BO " (kg$_{bw}$ kg$_{fw}^{-1}$). Also these parameters can be generalized and used for various subjects. The dynamic modelling can be used, when only few samples are available, to predict the temporal and seasonal variation of the radioactivity concentration of various compartments.

References

Fellman, A., Ralston, L., Hickman, D., Ayres, L., Cohen, N., 1994. Polonium metabolism in adult female baboons. Radiation Research 137, 238-250.

Henricsson, F., Persson, B.R.R., 2012. Polonium-210 in the bio-sphere: bio-kinetics and biological effects, in: Guillén Gerada, J. (Ed.), Radionuclides: Sources, Properties and Hazards. Nova Science Publishers, Inc., Hauppauge NY 11788-3619, p. 28.

Hill, C.R., 1965. Polonium-210 in man. Nature 208, 423-&.

ICRP, 1993. Age-dependent doses to members of the public from intake of radionuclides: Part 2 ingestion dose coefficients. Annals of ICRP 23.

Kauranen, P., Miettinen, J.K., 1967. 210Po and 210Pb in environmental samples in Finland, in:m Aberg, B., Hungate, F.P. (Eds.), Radioecological Concentration Processes. Pergamon press, Oxford:, pp. 257–280.

Kauranen, P., Miettinen, J.K., 1969. [210]Po and ^{210}Pb in Artic Food Chain and Natural radiation exposure of Lapps. Health Phys. 16, 287-295.

Kauranen, P., Miettinen, J.K., Pullianinen, E., 1971. Polonium-210 and lead-210 in some terrestrial animals in Finland. Ann. Zoo. Fennici 8, 318-323.

Ladinska., L.A., Parfenov, Y.D., Popov, D.K., Fedorova, A.V., 1973. Pb-210 and po-210 content in air, water, foodstuffs, and human body. Archives of Environmental Health 27, 254-258.

Persson, B., 1966. Iron-55 from fallout in Lichen Reindeer and lapps, in: W., H.F., Åberg, B.(Eds.), Radioecological Concentration Processes. Pergamon Press, Oxford, Stockhoilm, Sweden.

Persson, B.R., 1972. Lead-210, Polonium-210, and stable Lead in the Food-Chain lichen Reindeer and man, in: Adms, J.A.S., Lowder W. M., Gesell T. F. (Eds.), The Natural Radiation Environment II, Rice University , Houston, Texas, USA, pp. 347-367.

Persson, B.R.R., 1970. [55]Fe, ^{90}Sr, [134]Cs, ^{137}Cs and ^{210}Pb in the Biosphere. Radiological Health Aspects of the Environmental Contamination from Radioactive Materials in Northern Sweden (PhD thesis), Radiation Physics. Lund University, Lund, Sweden.

Persson, B.R.R., 2016. Global distribution of [7]Be, ^{210}Pb and, [210]Po in the surface air (with Appenix A-E). Acta Scientiarum Lundensia 2015, 1-51.

Persson, B.R.R., Gjelsvik, R., Kålås, J.A., Åsbrink, J., Holm, E., 2016 Radioecological Informatics and Modelling of Polonium-210 and Caesium-137 in top predators., in: García-Tenorio, R., Holm, E. (Eds.), II international conference on radioecological concentration processes (50 years later) Seville (Spain), November, 6th-9th, 2016

Persson, B.R.R., Holm, E., Lidén, K., 1974. Radiolead (Pb-210) and stable lead in lichen Cladonia-alpestris. Oikos 25, 140-147.

Skuterud, L., Gwynn, J.P., Gaare, E., Steinnes, E., Hove, K., 2005. Sr-90, Po-210 and Pb-210 in lichen and reindeer in Norway. Journal of Environmental Radioactivity 84, 441-456.

Thomas, P.A., Fisenne, I., Chorney, D., Baweja, A.S., 2001. Human absorption and retention of polonium-210 from caribou meat. Radiation Protection Dosimetry 97, 241-250.

Caesium-137 in Norwegian reindeer and Sámi herders – 50 years of studies

L. Skuterud*, M. A. Ytre-Eide, T.H. Hevrøy and H. Thørring

Norwegian Radiation Protection Authority, PO Box 55, 1332 Østerås, Norway

Abstract

Radiocaesium in Norwegian reindeer and reindeer herders has been studied for 50 years, and will probably be studied for many years still because of the persistent contamination levels. This paper gives an overview of the studies carried out, and of the levels and time-trends observed. In addition, it gives a brief summary of the consequences of the Chernobyl fallout for reindeer herders in central and southern Norway: On the need for the exceptionally high intervention level for ^{137}Cs in reindeer meat of 6,000 Bq/kg, and on the need for developing remedial measures. Without the various actions implemented, it has been estimated that average ingestion doses would have reached 10 mSv/year the first 1-2 years. The intervention level was reduced to 3,000 Bq/kg in 1994 and has been maintained at this level partly to alleviate the practical consequences for the reindeer herders. In case the limit will be reduced in the future, and because the previous remedial measures are not applicable any longer, a dynamic model tool is presented that may help the herders assess optimum times for slaughter, depending on the ^{137}Cs deposition levels in their vast pastures.

Introduction

The discovery of the unexpected high concentrations of ^{137}Cs in Swedish reindeer herders in 1961 (Lidén, 1961), triggered studies on transfer of radionuclides in the lichen – reindeer – human food-chain in several Arctic countries, and the topic was thoroughly discussed at the First International Conference on Radioecological Concentration Processes. In Norway, the systematic monitoring of reindeer herders commenced relatively late, in 1965.

However, contrary to the situation in most of the other countries, the studies were still ongoing in Norway when the 1986 Chernobyl accident happened, and the annual whole-body monitoring campaign had just been completed. The ^{137}Cs contamination in Norway in the 1960s was not high enough to lead to any measures to reduce exposure, and the studies of reindeer and reindeer herders therefore served only as monitoring and documentation of levels and trends. A completely different situation arose from the Chernobyl fallout in the affected areas in central and southern Norway.

Average radiocaesium (^{134}Cs and ^{137}Cs) concentrations in reindeer meat reached 50-60,000 Bq/kg in several herds, with 150,000 Bq/kg as the maximum observed in individual samples (Strand et al., 1992). With the knowledge of the time-trends of the levels from the 1960s onwards, Norwegian health authorities in autumn 1986 chose to raise the permissible/intervention level for radiocaesium in marketed reindeer meat to 6,000 Bq/kg, because: "A maintained intervention level of 600 Bq/kg will [...] result in production for condemnation and uneasiness among reindeer herders in the coming years. A despondent atmosphere, apathy and defection of young people will come forward in reindeer husbandry and the Sámi community [...]. If the limit is not raised, these problems will last for many years and can thereby threaten the Sámi lifestyle and culture, irrespective of monetary compensation" (Press release, 1986).

However, actions including dietary advice were developed to help the reindeer herders themselves, with their high reindeer meat consumption, obtain reindeer meat with contamination levels below the permissible level for basic foodstuffs of 600 Bq/kg.

---

* Corresponding author, E-mail: Lavrans.Skuterud@nrpa.no

Whole-body monitoring was carried out both as a survey of ingestion doses to the reindeer herders, and as an aid to validate the reindeer herders' own actions to reduce their radiocaesium intake. The permissible level for radiocaesium in reindeer meat in Norway was reduced to 3,000 Bq/kg in 1994, and has been maintained at this level since.

The significant contamination problems caused by the Chernobyl fallout triggered studies on measures to reduce contamination levels in reindeer meat (e.g., Hove et al., 1991)), and on transfer and time-trends of radiocaesium in reindeer (e.g., Pedersen et al., 1995)). It was quickly realized that condemnation was an unsatisfactory and expensive countermeasure, and alternatives were therefore needed. Live monitoring of animals prior to slaughter (Brynildsen & Strand, 1994) became an appreciated tool that enabled slaughtering only animals that would be accepted for human consumption. The others could e.g. be clean fed instead of being condemned.

Figure 1. Map of study areas and ^{137}Cs deposition in Norway (interpolated ^{137}Cs values from Backe et al. (1986)).

The considerable small-scale variability in Chernobyl deposition across the vast reindeer grazing areas did for many years prevent any detailed studies on the transfer of radiocaesium from lichens, or soil and plants, to reindeer in the affected areas. It also limited the applicability of radioecological models in the management of the Chernobyl consequences. However, the last years' development of GPS tracking devices and technology for free-ranging animals has significantly changed this situation. This paper will summarize findings and experiences from the pre- and post-Chernobyl studies on transfer of radiocaesium in the food-chain to reindeer and humans in Norway, and present some results from an ongoing modelling activity.

Materials and Methods

Studies areas and population groups

When the studies were initiated in the 1960s, the Kautokeino area in northern Norway (Fig. 1) was selected because of the population size and the important role of reindeer herding in the area. Northern Norway was also relevant because of the proximity to the USSR's test site at Novaya Zemlya. However, later studies showed that the fallout was largest in areas of high and frequent precipitation (which does not include Kautokeino) and there was no strong evidence of elevated fallout in northern Norway due to tests at Novaya Zemlya (Bergan, 2002).

The Chernobyl fallout was significantly higher in central and southern than northern Norway. The South Sámi is an ethnic minority in this area, living scattered over large areas. Due to differences in deposition levels, and consequently the different needs for remedial measures, the participants in our studies are grouped according to where their reindeer graze, in the Snåsa or Røros regions respectively (Fig. 1). Skuterud & Thørring (2012, 2015) give more details on the number of participants in the studies in Kautokeino and central Norway, on the various whole-body monitoring techniques applied during the years, and summarizes some results of dietary surveys.

Studies and modelling of radiocaesium in plants, lichens and reindeer

Prior to the Chernobyl accident, we know of no systematic studies of transfer of radiocaesium to reindeer in Norway. However, samples of reindeer meat were obtained in Kautokeino in connection
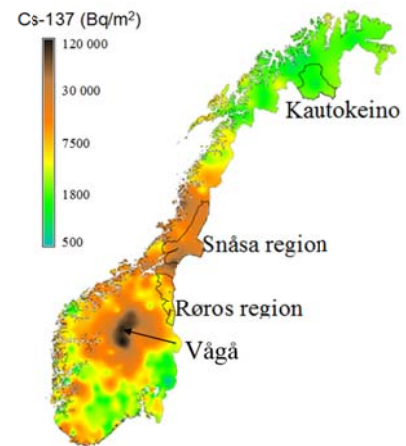
with the whole-body monitoring campaigns (Westerlund et al., 1987), and continued after 1986. In the Chernobyl affected areas monitoring of reindeer became a routine every time the herders rounded up their herds for slaughter, and most of the measurements from the years that followed are stored in a database.

The Vågå herd (owned by a non-Sámi reindeer company) was one of the reindeer herds most affected by the Chernobyl fallout (Fig.1) and has been the subject of various studies during the years. The herd counts about 2000 animals in winter (before calving), and uses a pastureland of 1357 km^2 (see Skuterud et al. (2005) for more details). A detailed aerial survey of the ^{137}Cs deposition in the area was carried out in 2011 (Baranwal et al., 2011). Mostly for the herders' own interest, but also for our scientific use, 15-20 of the Vågå reindeer have for some years carried GPS collars (Telespor AS) with an online mapping service showing their positions, and were positions can be downloaded. Thus, combining the positions and the deposition maps gives a record of the ^{137}Cs levels were the individual reindeer have grazed. We use these levels to estimate ^{137}Cs concentrations in plants and lichens across the pastureland, based on determined correlations between ^{137}Cs deposition levels and concentrations in various plant and lichen species sampled in the area as part of this project and previously (Skuterud et al., 2005; Rosén et al., 2012; Thørring et al., 2012; Skuterud et al., 2014). The plants and lichens then comprise a seasonally varying diet, which is fed to a model reindeer. The reindeer model is based on (Åhman, 2007), but with the diet separated into the components: Lichens, grasses, herbs and woody plants (based on information in Gaare & Staaland (1994)). Our model has been developed in python. Model estimates are validated through results of live monitoring of GPS collared reindeer during the autumn and winter round up and slaughter of the Vågå herd.

Results and Discussion

Radiocaesium levels and trends in reindeer and herders

Although the Partial Nuclear Test Ban Treaty in 1963 put an end to most of the atmospheric nuclear testing, the studies around the Arctic showed that the concentrations in reindeer herders still increased. The studies in Kautokeino commenced when the ^{137}Cs levels probably were at their highest (Fig.2), and from there on the concentrations declined with half-lives of about 6 years in reindeer herders and 6.7 years in reindeer meat until March 1986 (Skuterud & Thørring, 2015). The Chernobyl fallout resulted in a doubling of concentrations observed the year before. From these peaks the levels again declined, with half-times of 7−8 years. The effective half-time in herders during 1987−2010 is longer than during 1965−1986, potentially because societal changes in Kautokeino resulted in a reduction in reindeer meat consumption during the first decade of the studies (Skuterud & Thørring, 2015).

The ^{137}Cs concentrations in herders in central Norway did not peak in 1987, and show no clear maximum year (Fig.2). This probably
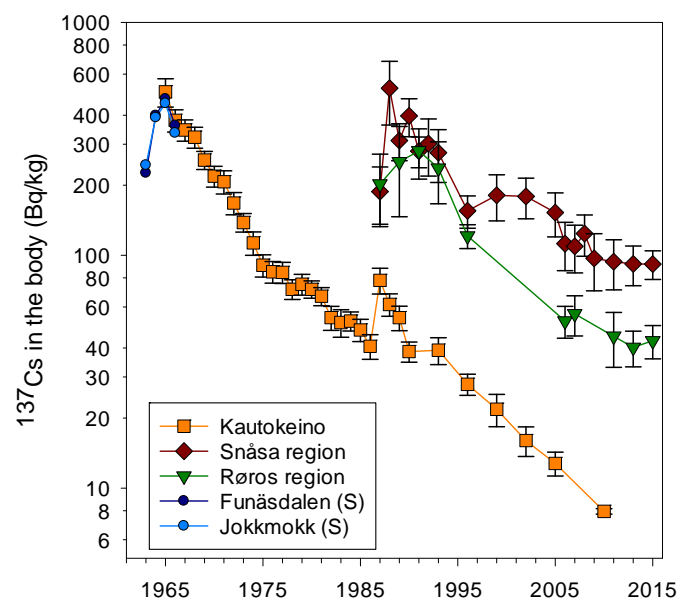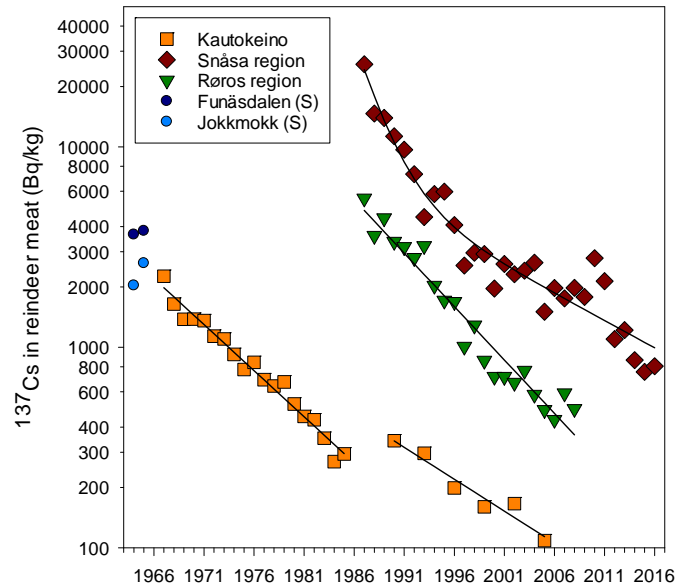

Figure 2. *Cs-137 concentrations in Sámi reindeer herders (mean±SE). Data from Sweden (S) (from Lidén & Gustafsson (1967)) included to illustrate the peak in 1965.*

reflects the various measures introduced to reduce the intake, the cautious intake by the reindeer herders, and that humans need more than a year on a contaminated diet to reach 'equilibrium' concentrations. Furthermore, a comparison of whole-body levels in central Norway after Chernobyl and in Kautokeino in the 1960s shows that the significantly higher Chernobyl fallout (Fig.1) was not similarly reflected in the herders' bodies.

The most successful and applied countermeasures in reindeer husbandry have been "early slaughtering" and clean feeding, supplemented by live monitoring. Early slaughtering implies slaughtering in August/September instead of during winter (the traditional slaughtering season). This was effective because radiocaesium concentrations in reindeer increased considerable during autumn when the diet changed from green vegetation to more contaminated lichens (Fig.4). Clean feeding implied a more untraditional change to reindeer husbandry, since the otherwise free-ranging animals had to be fenced and fed. Some herders also avoided slaughtering reindeer after they grazed in areas known to cause higher contamination levels.

In addition to the mentioned measures, which were aimed at the traded reindeer meat, the reindeer herders took several measures to limit their own radiocaesium intake. The dietary advice gave guidelines regarding intake of the most contaminated products, depending on their activity concentrations, and included some examples on how to prepare food to reduce the radiocaesium content. Many of the herders nevertheless reduced their reindeer meat consumption because of the contamination, and ten years after the accident still one third of the population

Figure 3. *Cs-137 concentrations in reindeer meat. Data from Sweden (S) included as in Fig.2.*
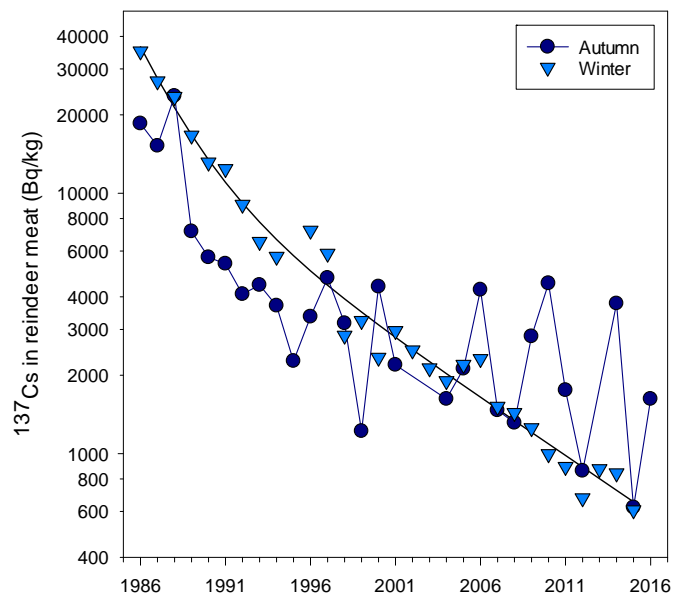
Figure 4. *Cs-137 concentrations in reindeer in Vågå in autumn and winter (mean values; for details about the data see (Skuterud et al., 2005).*

took this measure (Mehli et al., 2000). By 2005, none of the respondents answered that they had reduced reindeer meat intake because of the Chernobyl fallout, but 24% of them used various other measures to reduce radiocaesium intake (Skuterud & Thørring, 2012). The most common measure was to use live monitoring to select low-contaminated reindeer for their own consumption. Particularly long clean feeding periods for reindeer for their own consumption has also been applied.

The estimated effective ^{137}Cs half-times in reindeer meat in central and southern have varied through the years, and with the areas studied. Previous studies suggested that ^{137}Cs concentrations declined much slower some 15-20 years after the accident (Skuterud et al., 2005; Skuterud &

Thørring, 2012). This can be observed as a 'plateau' in Vågå about 2001-2006 (Fig.4) and in Snåsa until about 2011 (Fig.3). Thereafter the concentrations are again declining with current estimates of effective half-times about 7 and 11 years in Vågå and Snåsa, respectively (cf. fitted regression lines in Figs.3 and 4).

   An analysis of potential whole-body concentrations and ingestion doses from ^{137}Cs in the absence of any countermeasures, based on observed radiocaesium levels in reindeer meat and estimated traditional reindeer meat consumption, showed that average ingestion doses were reduced by about 90 % in the most affected area the first years after the accident (Fig. 5). Until 2009 the integrated dose was reduced by about 73 % to an integrated dose of about 17 mSv (Skuterud & Thørring, 2012).
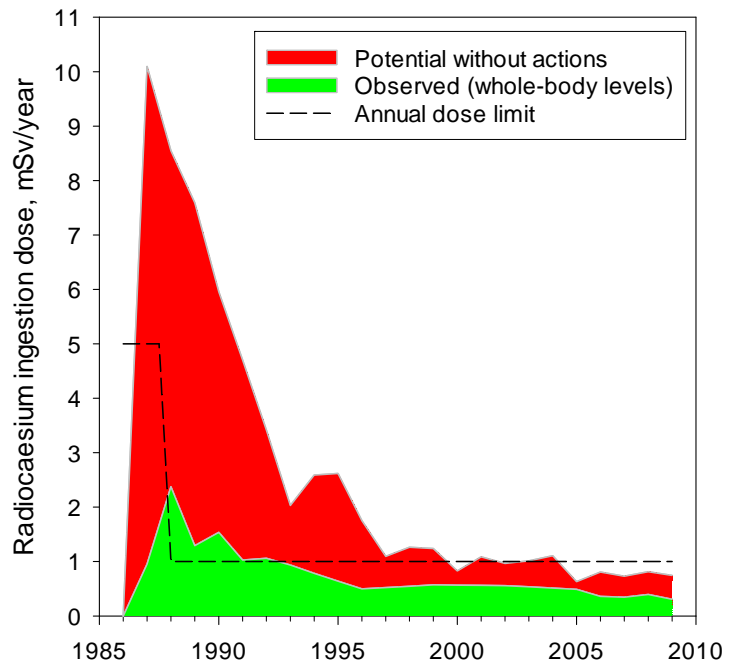
Figure 5 *Estimated radiocaesium ingestion doses (sum of ^{134}Cs and ^{137}Cs) based on observed whole-body levels (green line/area), and a scenario without any actions after Chernobyl (adapted from Skuterud & Thørring (2012)).*

Long-term transfer and reindeer modelling

Fig.4 illustrates that the considerable difference in radiocaesium levels in reindeer in autumn and winter gradually disappeared, because of the steadier decline in concentrations in lichens than in plants and fungi. The highest concentrations in reindeer the last years have been observed in autumns with abundant fungi. Otherwise, differences in concentrations in autumn and winter are no longer significant. This is reflected in the non-significant differences in observed ^{137}Cs concentrations in plants and lichens sampled in the area during the last 15 years (Skuterud et al., 2005; Rosén et al., 2012; Thørring et al., 2012; Skuterud et al., 2014). Table 1 summarizes this as the "transfer factors" used to estimate ^{137}Cs concentration in the model reindeer's diet based on the deposition levels where they have roamed.

   Some initial modelling results for the Vågå herd based on the results in Table 1 are shown in Fig.6. The estimated values are generally a little lower than the observed, and the current model does not successfully reproduce the range of measured ^{137}Cs concentrations in individual reindeer.

   Even though ^{137}Cs levels in diet components

Table 1. *Cs-137 concentrations in reindeer's diet components relative to the soil deposition levels (mean ± SD, 10^{-2} m^2/kg). For plants, this equals the aggregated transfer coefficient, T_{ag}.*

Diet group	Arithmetic mean ± SD	Number of samples (N)
Lichens	1.7 ± 1.9	23
Graminoids	1.4 ± 1.4	55
Woody plants	1.2 ± 1.8	87
Herbs	2.6 ± 4.8	37

are similar, seasonal differences in intake and metabolism/biological half-time in reindeer causes some increase in ^{137}Cs levels in reindeer from summer to winter. However, the differences in model results for individual reindeer during summer and late autumn 2015 (see Fig.6), which merely reflects differences in deposition levels were the animals have grazed, suggest that these deposition

differences have larger impacts on reindeer ^{137}Cs levels than season. These differences might become important to the reindeer herders if the permissible level for radiocaesium in reindeer meat in Norway is reduced from the current 3,000 Bq/kg level.
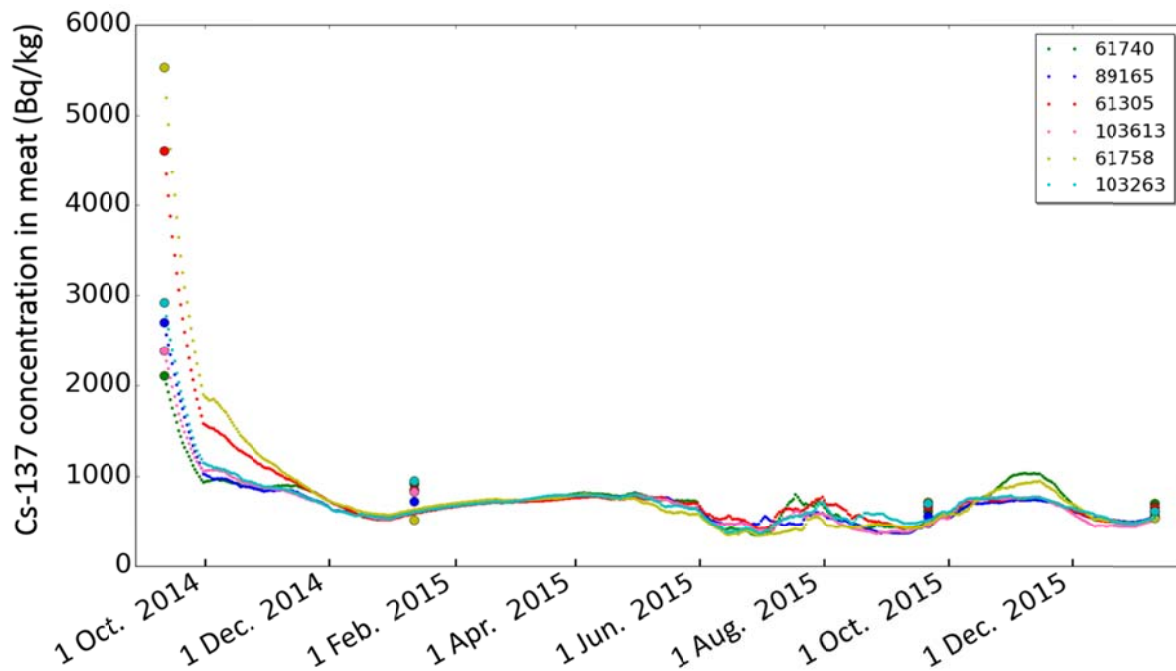
Figure 6. Observed (dots) and modelled (dotted lines) ^{137}Cs concentrations in individual Vågå reindeer during Sep. 2014 – Jan. 2016. Observed levels in Sep. 2014 served as start values in the model (legend gives animal/GPS id.).

Summary and conclusions

Radiocaesium in Norwegian reindeer and reindeer herders has been studied for 50 years, and will probably be studied for many years still because of the persistent contamination levels. While the levels of ^{137}Cs from the nuclear weapons tests in reindeer and herders were relatively low and declined steadily to levels of no concern for food safety, post-Chernobyl levels in several reindeer herds in central and southern Norway remain above the general permissible level for basic foodstuffs in Europe of 600 Bq/kg. A higher limit is still maintained in Norway partly to reduce the practical consequences for the reindeer herders. Whole-body monitoring of herders will probably continue as long as control of reindeer is needed. If the permissible level for ^{137}Cs in reindeer meat is reduced, new management options might be needed as the former "early slaughtering" is not applicable any longer. The dynamic reindeer model presented gives promising results as a tool to assist reindeer herders in assessing optimum times for slaughter, depending on the ^{137}Cs deposition levels in their pastures. Model improvements are underway, and we are currently also analysing further lichen samples from fieldwork last September.

References

Backe S, Bjerke H, Rudjord AL, Ugletveit F (1986). Cesium fallout in Norway after the Chernobyl accident. Østerås, National Institute of Radiation Hygiene, SIS rapport 1986:5 (in Norwegian), 50 pp.

Baranwal VC, Ofstad F, Rønning JS, Watson RJ (2011). Mapping of caesium fallout from the Chernobyl accident in the Jotunheimen area. Trondheim, Norway, Geological Survey of Norway (NGU), Report 2011.062, 26 pp.

Bergan T (2002). Radioactive fallout in Norway from atmospheric nuclear weapons tests. Journal of Environmental Radioactivity 60: 189-208.

Brynildsen LI, Strand P (1994). A rapid method for the determination of radioactive caesium in live animals and carcasses, and its practical application in Norway after the Chernobyl nuclear reactor accident. Acta Veterinaria Scandinavica 35: 401-408.

Gaare E, Staaland H (1994). Pathways of fallout radiocaesium via reindeer to man. In: Dahlgaard, H (ed). Nordic radioecology. The transfer of radionuclides through Nordic ecosystems to man. Amsterdam, Elsevier: p. 303-334.

Press release by the Norwegian Directorate of Health and Ministry of Agriculture 20 November 1986: The intervention level for radioactivity in meat of semi-domestic reindeer and game changed to 6000 Bq per kg (in Norwegian),.

Hove K, Staaland H, Pedersen Ø (1991). Hexacyanoferrates and bentonite as binders of radiocaesium in reindeer. Rangifer 11(2): 43-48.

Lidén K (1961). Cesium 137 burdens in Swedish laplanders and reindeer. Acta Radiol. 56: 237-240.

Lidén K, Gustafsson M (1967). Relationships and seasonal variation of ^{137}Cs in lichen, reindeer and man in Northern Sweden 1961-1965. In: Åberg B, Hungate FP (eds). Radioecological Concentration Processes. Proceedings of an International Symposium held in Stockholm 25-29 April, 1966. Oxford, Pergamon Press: 193-208.

Mehli H, Skuterud L, Mosdøl A, Tønnessen A (2000). The impact of Chernobyl fallout on the Southern Saami reindeer herders of Norway in 1996. Health Physics 79(6): 682-690.

Pedersen Ø, Hove K, Staaland H (1993). Seasonal variation and effective halflife of ^{137}Cs in semi-domestic reindeer grazing mountain pasture contaminated by deposition from the Chernobyl accident. In: Strand P, Holm E (eds). Environmental Radioactivity in the Arctic and Antarctic. Østerås, Norway, Norwegian Radiation Protection Authority, p.303-304.

Rosén K, Villanueva J-LG, Sundell-Bergman S, Solatie D, Kostiainen E, Turtiainen T, Roos P, Pálsson SE, Skuterud L, Thørring H, Skipperud L, Popic JM (2012). Natural Radionuclides in Meadow and Pasture land in the Nordic countries. NKS-265.

Skuterud L, Gaare E, Eikelmann IM, Hove K, Steinnes E (2005). Chernobyl radioactivity persists in reindeer. Journal of Environmental Radioactivity 83(2): 231-252.

Skuterud L, Thørring H (2012). Averted doses to Norwegian Sami reindeer herders after the Chernobyl accident. Health Physics 102(2): 208-216.

Skuterud L, Thørring H (2015). Fallout ^{137}Cs in Reindeer Herders in Arctic Norway. Environmental Science & Technology 49(5): 3145-3149.

Skuterud L, Thørring H, Ytre-Eide MA (2014). Use of total ^{137}Cs deposition to predict contamination in feed vegetation and reindeer 25 years after Chernobyl. ICRER 2014 – Third International Conference on Radioecology and Environmental Radioactivity, 7-12 September 2014, Barcelona, Spain, http://radioactivity2014.pacifico-meetings.com/

Staaland H, Garmo TH, Hove K, Pedersen Ø (1995). Feed selection and radiocesium intake by reindeer, sheep and goats grazing alpine summer habitats in southern Norway. Journal of Environmental Radioactivity 29(1): 39-56.

Strand P, Selnæs TD, Bøe E, Harbitz O, Andersson-Sørlie A (1992). Chernobyl fallout: Internal doses to the Norwegian population and the effect of dietary advice. Health Physics 63(4): 385-392.

Thørring H, Skuterud L, Steinnes E (2012). Distribution and turnover of ^{137}Cs in birch forest ecosystems: influence of precipitation chemistry. J Environ Radioact 110: 69-77.

Westerlund EA, Berthelsen T, Berteig L (1987). Cesium-137 body burdens in Norwegian Lapps, 1965-1983. Health Physics 52(2): 171-177.

Åhman B (2007). Modelling radiocaesium transfer and long-term changes in reindeer. Journal of Environmental Radioactivity 98(1-2): 153-165.

Radionuclides accumulation in Antarctic birds.

K. M. Szufa[1]*, J. W. Mietelski[1] and A. M. Olech [2,3]

1 The Henryk Niewodniczański Institute of Nuclear Physics, Polish Academy of Sciences, Poland,
2 Institute of Botany, Jagiellonian University, Zdzisław Czeppe Department of Polar Research and Documentation, Poland.
3 Institute of Biochemistry and Biophysics, Polish Academy of Sciences, Department of Antarctic Biology, Poland

Abstract

Antarctic ecosystem is not very diverse because of its extreme climatic conditions, however it is unique in the world. Thus protection of southern polar environment and attempts to understand it better seems to be significant. Nowadays there are numerous research stations on the Antarctic where various environmental studies are carried out. Even though accumulation of natural and artificial radionuclides has not been explored enough so far, especially accumulation in Antarctic animals. Anthropogenic radioisotopes over Antarctica originated mainly from global fallout due to nuclear weapon tests. Additionally ^{238}Pu level is increased by burnup of an American satellite (energized by an on-board plutonium system SNAP-9A) that took place over Madagascar.

Samples of bones, soft tissues and feathers of Antarctic birds (*Pygoscelis adeliae*, *Pygoscelis papua*, *Pagodroma nivea* and *Macronectes giganteus*) were studied. No bird was hunted purposely. Remains of the animals were collected during the Polish Antarctic Expeditions in the years 2002-2010. Gamma emitting isotopes (^{137}Cs and ^{40}K) were determined by low background gamma spectrometry with an HPGe detector. Then plutonium, americium, uranium, thorium and strontium where chemically separated. $^{239+240}$Pu, ^{238}Pu, ^{241}Am, ^{230,232}Th, ^{234,238}U where measured using alpha spectrometers with silicon detectors whereas ^{90}Sr was measured using Liquid Scintillation Counters.

Introduction

From 1945 to 1998 nuclear weapons tests entered into the atmosphere radioactive pollutions which spread over the entire surface of globe. Despite of the fact that the overwhelming majority of those explosions were carried out on northern hemisphere from 1957 to 1963 radioactive contamination of lands around the South Pole is detectable. Additionally in 1964 plutonium level on southern hemisphere was increased by reentry and burnup of an American satellite energized by an on-board plutonium system SNAP-9A that took place over Madagascar. Around 0.629 PBq of Plutonium was released then. As a consequence isotopic activity ratio ^{238}Pu/$^{239+240}$Pu is higher for southern hemisphere than that for northern hemisphere.

Laboratory of Environmental Radioactivity in Institute of Nuclear Physics in Cracow have been conducting Antarctic research for many years. This activity has resulted in several publications and many scientific projects i.a. participation in BIOTAS (Biological Investigation of Terrestrial Antarctic Systems) (Mietelski et al., 2000). Current investigation on accumulation of artificial (^{137}Cs, ^{90}Sr, $^{238,239+240}$Pu, ^{241}Am) and natural (^{40}K, ^{230,232}Th, ^{234,238}U) radionuclides in Antarctic environment is a continuation and somehow summary of above-mentioned activity. One of the main motivations to carry on Antarctic exploration was big diversity of plutonium ratios in marine samples revealed in previous studies (Mietelski at al., 2008). This variability may be due to the inflow of masses of water from other locations and organisms migration which can bring plutonium

---

* katarzyna.szufa@ifj.edu.pl

with different ratios, other than those already reported for the Antarctic (Desideri et al. 2003, Marzano et al. 2000).

Presented results reflect only initial part of the project proceeded currently in Laboratory of Environmental Radioactivity in Institute of Nuclear Physics in Cracow. Whole work comprises other marine samples (algae, bones and tissues of seals, fish) and also terrestrial samples (mosses, lichens, soil) collected within four decades (1980-2015) and in general is aimed to enlarge and improve radioecological research of Antarctic region, provide a better understanding of radioisotopes transport among elements of Antarctic environment and examine time dependent variability of radionuclides activities and doses absorbed by Antarctic biota in 35 years.

Materials and Methods

Samples

Research material comes from various localizations on King George Island (Fig.1) which is a part of South Shetland Archipelago located at 62°0′S 58°0′W, south of the Falkland Islands and north of the Antarctic Peninsula and the Schirmacher Oasis (Fig.1.) which is situated at 70°45′30″S, 11°38′40″E in East Antarctica, and is elevated on average for about 100 m.a.s.l. Samples were obtained during the Polish Antarctic Expeditions in the years 2002-2010. In detail: bones, soft tissues(containing feathers), feathers alone and egg shells of Antarctic birds: *Pygoscelis adeliae, Pygoscelis papua, Pagodroma nive, Macronectes giganteus* were analyzed. No bird was hunted purposely, the research material was collected in the form of the remains of animals found *post mortem*. Various species of birds were identified by biologist specialists.

Figure 1. *Places fo sampling: 1 – the Schirmacher Oasis, 2 – King George Island*

Radiometric technique

Samples were ashed at 400 ºC in a muffle oven, then soft tissues containing feathers were separated from bones if needed and mechanical homogenization in mortar was done. Next measurements by high resolution low-background gamma-ray spectrometer with an HPGe detector to determine activity levels of ^{137}Cs and ^{40}K were performed. Afterwards samples were ashed again but this time in 600 ºC to dispose of remaining carbon (at this temperature ceasium escapes) and sequential radiochemical procedures were executed – separation of alpha (^{241}Am, $^{238,239+240}$Pu, ^{230,232}Th, ^{234,238}U) and beta (^{90}Sr) emitting radionuclides. At the very beginning ^{243}Am, ^{85}Sr, ^{229}Th, ^{232}U tracers were added which allows determination of radiochemical technic efficiency (eventual loss of material during carrying out procedures is possible).

Samples of soft tissues and feathers were digested with boiling mixture of concentrated HF, HNO$_3$, HCl, H$_3$BO$_3$ acids, bones and egg shells were dissolved in 6M HCl. Plutonium and thorium were separated by anion-exchange with Dowex-1 during passing the column according to procedure applied at Department of Nuclear Physical Chemistry, Institute of Nuclear Physic (Mietelski et al. 1995; 1999), americium by anion-exchange with Dowex-1 and mineral acids' solutions and methanol (Mietelski et al. 1997), uranium also by anion-exchange with Dowex-1 but with 9M HCl acid. As a consequence sources of alpha emitting radionuclides were prepared by NdF$_3$ coprecipitation method and measured by alpha spectrometers with silicon detectors (Sill, 1987). Separation of ^{90}Sr was accomplished in Sr-resin column (Mietelski et al, 1997; 1998). Determination of strontium activity was done by using Liquid Scintillation Counter.

In the close future selected plutonium sources will be dissolved in ultra-pure acids, purified and subsequently measured by mass spectrometer MC ICPMS Neptun in order to determine ^{240}Pu/^{239}Pu ratio. Spectrometer MC ICPMS Neptun allows identifying abundance of isotopes on level of nanograms.

Data accomplished will be analyzed in terms of dosimetry and radiological protection using widely accepted approaches to derive benchmarks for environmental risk assessment (DOE-STD-1153-2002; Larsson 2008; Brown et al. 2008) and software systems: ERICA Tool and RESRAD Biota dedicated to doses for biota.

Results and Discussion

Since project is still in progress not all samples were measured consequently presented data is incomplete. Nonetheless some trends may be recognized.

The highest activity concentrations were reveled in soft tissues for ^{40}K with maximal and minimal values 2.1 kBq/kg and 0.3 kBq/kg respectively. At the same time no ^{137}Cs was detected in any sample, likewise in none sample ^{90}Sr was discovered.

When it comes to alpha emitting radionuclides higher levels were found for natural radioactivity. Maximal ^{230}Th and ^{232}Th (around 3 Bq/kg) were observed in soft tissues, some tracers of thorium (several dozens of mBq/kg) were in egg shells. Uranium isotopes were reveled in both bones and tissues samples and range from 0.11 to 1.16 Bq/kg and 0.17 to 1.19 Bq/kg for ^{238}U and ^{234}U respectively. In case of Pu and Am isotopes only soft tissues samples were above detection limits.

Correction for eventual input of ^{228}Th (5423 eV) to ^{238}Pu count rate was applied. Determination of ^{238}Pu/$^{239+240}$Pu ratio was possible in two samples. For the first sample – penguin sample (*Pygoscelis*

adeliae) ratio is equal to 0.19 (Fig.2) which is close to results obtained for terrestrial samples (Mietelski et al., 2000, 2008), for the second – petrel sample (*Pagodroma nive)* the value is significantly lower, on 0.08 level (Fig.3), which is closer to characteristic value for the lower latitudes.
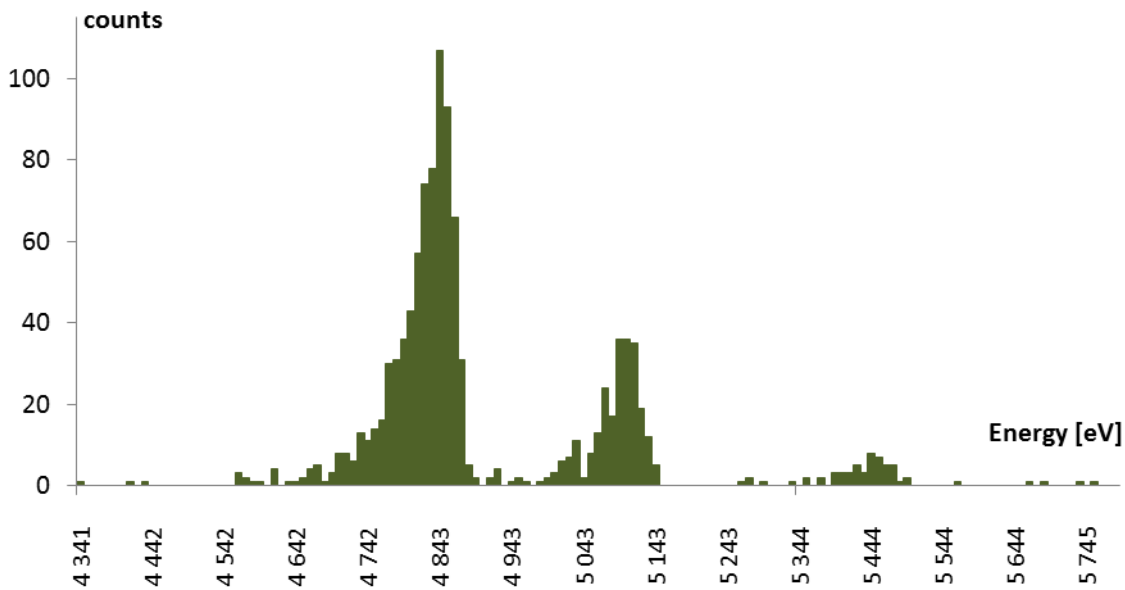
Figure 2. Plutonium alpha-spectra of penguin sample (Pygoscelis adeliae).
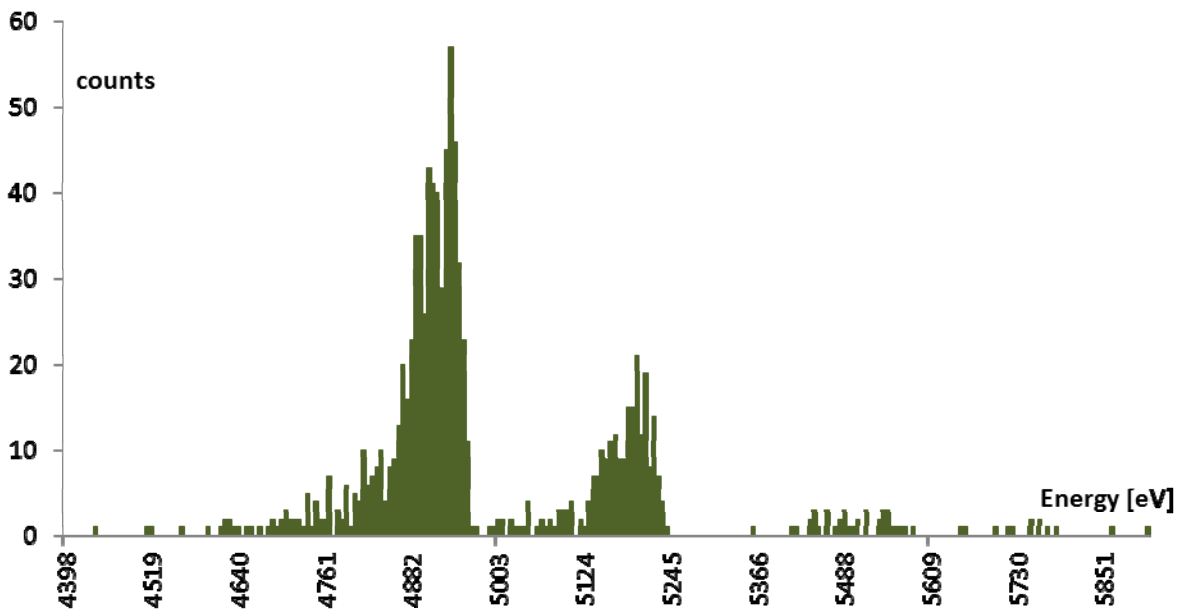
Figure 3. Plutonium alpha-spectra of petrel sample (Pagodroma nive).

Conclusions

Due to small number of so far analyzed samples it is difficult to make general statements about Antarctic marine ecosystem. Despite this fact some findings were done. Results obtained show that soft tissues (samples of soft tissues comprise also feathers) accumulate natural and artificial radionuclides better then bones, egg shells and feathers alone. In case of ^{40}K that is predictable because muscles are enriched in potassium. ^{238}Pu was discovered only in 2 samples of soft tissues

where plutonium ratios are very different. That may indicate various contribution of global fallout and plutonium from satellite accident (SNAP 9A) to contamination Antarctic marine organisms which can migrate to distant places (with other plutonium ratios). All results for ceasium and strontium which are below MDC may indicate intensive washout of these elements from birds bodies.

References

Brown, J.E., Alfonso, B., Avila, R., Beresford, N.A., Copplestone, D., Prohl, G., Ulanovsky, A., 2008. The ERICA Tool. J. Environ. Radioact. 99, 1371-1383.

Desideri, D., Giuliani,S., Testa, C.,Triulzi1, C. 2003. ^{90}Sr, ^{137}Cs, ^{238}Pu, $^{239+240}$Pu and ^{241}Am levels in terrestrial and marine ecosystems around the Italian base in Antarctica. J. Radioanal. Nucl. Chem. 258, 221-225.

DOE-STD-1153-2002 A Graded Approach for Evaluating Radiation Doses to Aquatic and Terrestrial Biota

Larsson, C.M. 2008. An overview of the ERICA Integrated Approach to the assessment and management of environmental risks from ionizing contaminants. J. Environ. Radioact. 99, 1364-1370

Marzano, F.N., Fiori, F., Jia, G., Chiantore, M. 2000. Anthropogenic radionuclides bioaccumulation in Antarctic marine fauna and its ecological relevance. Polar Biol. 23, 753-758.

Mietelski, J.W., Gaca, P., Olech, M.A. 2000. Radioactive cantaminations od lichens and mosses collected in South Shetlands anf Antarctic Penisula. J. Radioanal. Nucl. Chem. 245, 527-537.

Mietelski, J.W., Olech, M.A., Sobiech-Matura, K., Howard, B.J., Gaca, P., Zwolak, M., Błażej, S., Tomankiewicz ,E. 2008. ^{137}Cs, ^{40}K, ^{238}Pu, $^{239+240}$Pu and ^{90}Sr in biological samples from King George Island (Southern Shetlands) in Antarctica. Polar Biol. 31, 1081-1089.

Mietelski, J.W., Dorda, J., Wąs, B., 1999. Pu-241 in samples of forest soil from Poland. Appl. Radiat. Isot. 51. 435-447.

Mietelski, J.W., Wąs, B., 1995. Plutonium from Chernobyl in Poland. Appl. Radiat. Isot. 46, 1203-1211.

Mietelski, J.W. 1998. Transuranic elements and Sr-90 in samples from forests of Poland, Nukleonika. 43. 449-458.

Mietelski, J.W., Wąs, B., 1997. Americium, curium and rare earths radionuclides in forest litter samples from Poland, Appl. Radiat. Isot, 48, 705-713.

Sill, C.W. 1987. Precipitation of actinides as fluorides or hydroxides for high resolution alpha spectrometry. Nucl. Chem. Waste. Man. 7, 201-215.

Acknowledgements

Summing internal and external exposures from Chernobyl fallout to hunters using regional ecological transfer factors

C. L. Rääf[1]*, M. Isaksson[2], M. Jönsson[1], A. Mamour[2], M. Tondel[3], R. Wålinder[3]

[1]Medical Radiation Physics, Department of Translational medicine, Malmö, Lund University, Sweden.
[2]Department of Radiation Physics, Institute of Clinical Sciences, Sahlgrenska Academy, University of Gothenburg, Sweden.
[3]Occupational and Environmental Medicine, Department of Medical Sciences, University of Uppsala, Sweden.

Abstract

The projected life-time effective doses from the Chernobyl fallout to hunters in Sweden living in the most affected counties have been estimated. The external exposures have been estimated using data from digital ^{137}Cs deposition maps provided by the Swedish Geological survey, combined with a number of dose conversion and correction factors. The internal exposures have been estimated using previously determined transfer factors between the county average of the ^{137}Cs deposition and the resulting time-integrated body burdens of the radionuclide in hunters. The corresponding internal effective dose contribution from ^{134}Cs was calculated assuming the same transfer and a correction for the shorter physical half-life of the radionuclide (2.07 a compared with 30.2 a for ^{137}Cs). In addition to the contribution from the two principal Cs radionuclides, the corresponding contribution from short-lived fission products were estimated as well. The summed effective doses to the hunter family members being originally exposed in 1986 typically ranged from 1 to 9 mSv. The method used in this study can potentially also be used for estimating the exposure in an epidemiological study hypothesizing excess cancer incidence in hunters and their family members.

Introduction

The aim has been to estimate the summed external and internal effective doses from the Chernobyl fallout of ^{134}Cs and ^{137}Cs to the hunters and their families, who were one of the most affected communities in Scandinavia (e.g. Ågren, 1998, Rääf et al., 2006). This aim includes testing and modification of existing models for radioecological transfer and external dose rate to residents in affected areas regarding i.) existing exposures, ii.) future events when epidemiological studies may be necessary, iii.) prospective management of emergency preparedness.

Materials and Methods

Samples

The three counties in Sweden with the highest average surface equivalent deposition of ^{137}Cs in 1986 were selected for this study: Gävleborg (X in figure 1: 13.4 kBq m^{-2}), Uppsala (C in figure 1: 15.4 kBq m^{-2}) and Västernorrland county (Y in Figure 1: 28.4 kBq m^{-2}), respectively. However, local variations in the ^{137}Cs deposition ranged from 2.6 to 42.5 kBq m^{-2}. Ten hunters per county were randomly selected from the Swedish hunting registry in 1986 and matched to the fallout map using their dwelling coordinates. From the population registry we retrieved the family members, in total 85 individuals, with information on year of birth, sex, county and deposition of ^{137}Cs at their residential addresses.

---

* Corresponding author, E-mail: Christopher.raaf@med.lu.se

Figure 1. *County average surface equivalent deposition of ^{137}Cs in Sweden. In the map are also indicated the three counties of the studied hunter cohort.*
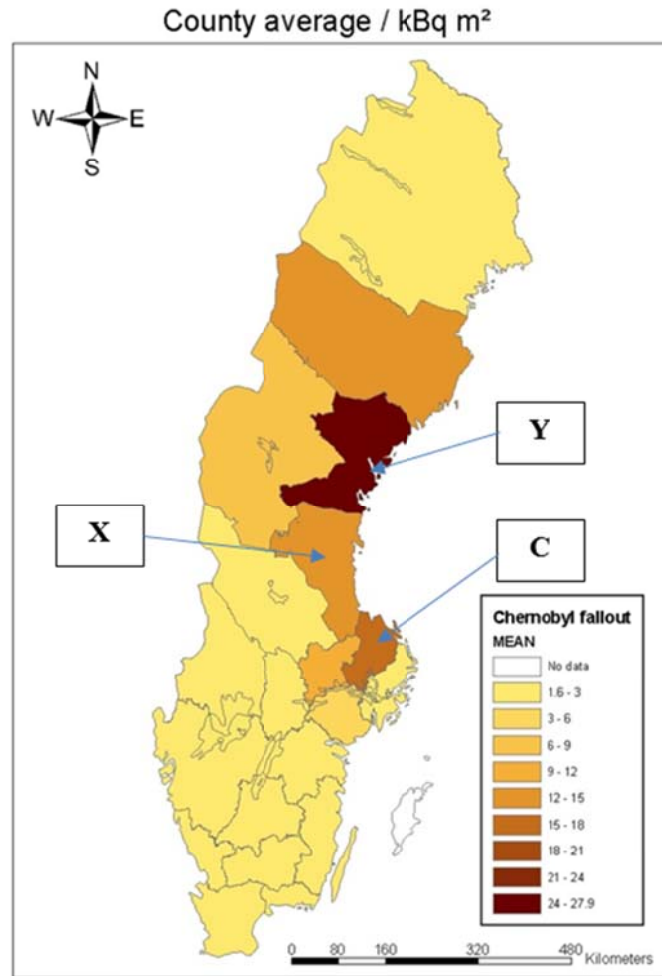
Models

The internal exposures have been estimated using previously determined transfer factors between the county average of the ^{137}Cs deposition and the resulting time-integrated body burdens of the radionuclide in hunters (Rääf et al., 2006b). In Eqn 1 is given an analytical expression of the time-integrated aggregate transfer. $T_{ag,int}$, used to relate the county average deposition of ^{137}Cs, A_{esd}, with the corresponding whole-body concentration of the radionuclide, c(t) (Bq kg^{-1}).

$$a_{Cs\text{-}137}(t) = A_{esd}(County) \cdot T_{ag}(t) \cdot k_s = A_{esd}(County) \cdot T_{ag,peak} \cdot [(1 - e^{-(\ln2/t1.1)\cdot(t-1986.33)}) \cdot (0.9 \cdot e^{-(\ln2/1.2)(t-1986.33)} + 0.11 \cdot e^{-(\ln2/30)\cdot(t-1986.33)}] \cdot k_s \qquad 1$$

Where A_{esd}(County) is the mean surface equivalent deposition of ^{137}Cs in the studied county (Bq m^{-2}), t is the time passed since 1 May 1986 in y, k_s is a correction factor accounting for the sex difference in the observed transfer of Cs to man between males and females, and $T_{ag,peak}$ is the empirical peak transfer for the particular population category, found to be 29.3 (Bq kg^{-1})/(kBq m^{-2}) from reassessment of Rääf et al., 2006b.

Once the activity concentration is established the internal effective dose can be estimated using relationships given by e.g. Leggett et al., 1984. The method is similar to one used in Rääf et al., 2006b.The corresponding internal effective dose contribution from [134]Cs was calculated assuming the same transfer and a correction for the shorter physical half-life of the radionuclide (2.07 a compared with 30.2 a for ^{137}Cs).

The external dose rates, $\dot{E}(t)$, were determined using a digital fallout map based on aerial measurements by the Geological Survey of Sweden (Byström, 2000), combined with a time-pattern modulation factor, $r(t)$, described in Jönsson et al., 2017. The external exposure was divided into the contribution obtained from outdoor and indoor occupancy, respectively (Eq. 2);

$$\dot{E}(t)=(\dot{K}(t)_{Cs\text{-}137} + \dot{K}(t)_{Cs\text{-}134})\cdot[F_{snow}\cdot F_{rot}\cdot F_{out} + F_{snow}\cdot F_{rot}\cdot F_{sh}\cdot(1\text{-} F_{out})] \qquad 2$$

where, $\dot{K}(t)_{Cs\text{-}134}$, and $\dot{K}(t)_{Cs\text{-}137}$, (mGy y^{-1}) are the air kerma rate contributions from the ground deposition of [134]Cs and ^{137}Cs, respectively, at the place pf residence of hunting households, as retrieved from the digital ^{137}Cs surface equivalent deposition map described earlier. F_{snow} is the correction factor for the shielding effect of regular snow layer for gamma emitting radionuclides in the photon energy range from 600 to 800 keV. F_{rot} (mSv/mGy) is the conversion factor between effective dose rate and the air kerma for a rotational symmetric gamma emission field (ICRP, 2010). F_{out} is the fraction of time spent indoors, and finally F_{sh} is a shielding factor taking into account the attenuation of the gamma fluence from the surrounding ground deposition. The values attached to these factors are described in more detail in Jönsson et al., 2017.

The models enable prediction and projection over long-term periods. However, these predictions cannot take into account changes in hunting patterns that drastically change the transfer factor used in Eq. 1. Using Eqs 1-2 we obtained the predicted life-time effective dose (mSv) from the year 1986 assuming an average life expectancy of 79.9 years for men and 83.7 years for women.

Results and Discussion

The projected life-time effective dose from the Chernobyl fallout to the hunter family members being originally exposed in 1986, combining external and internal exposures typically ranged from 1 to 9 mSv (Figure 2).

For a member of a hunter household in the most affected areas in Sweden, the average life-time effective dose attributed to the Chernobyl fallout can be up to 10 mSv if the individual was newly born or infant in 1986 at the event of the accident. Given the higher radiobiological sensitivity for infants and adolescent it can be assumed that the aforementioned young members of hunting households are the most exposed in Sweden from the Chernobyl fallout, except for members of the reindeer herding communities (e.g. Rääf et al., 2006a). However, based on c. 300,000 hunting permits being issued annually (Swedish Environmental Protection Agency, 2016), and an average household size of 2.8 as found in the sample of this study, the hunting community in Sweden is significantly larger (up to 1 million) than the reindeer herding community (<10,000), and the collective doses may therefore be larger for the former group.

Figure 2. *Histogram plots of life time effective doses to a sample of hunter family members during the period 1986 to 2016 in three Swedish counties.*
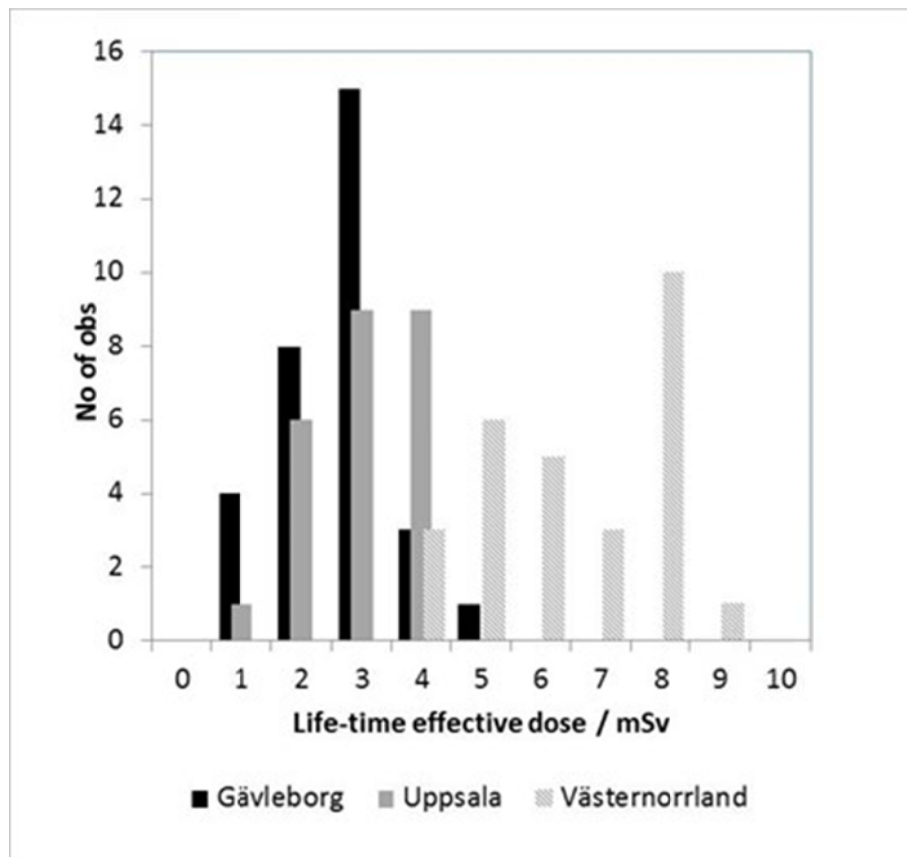
Conclusions

The summed effective doses to the hunter family members being originally exposed in 1986 typically ranged from 1 to 9 mSv. The method used in this study can potentially also be used for estimating the exposure in an epidemiological study hypothesizing excess cancer incidence in hunters and their family members. Summing external and internal effective doses according to the proposed model will also provide estimations of effective doses to various subpopulations, both for existing exposure situations and as a planning tool for emergency preparedness.

References

Ågren G. Seasonal and long-term variations in ^{137}Cs among adults from Swedish hunter families. Radiat Prot Dosimetry. 2001;93(1):49-53.

Andersson P. Strålmiljön i Sverige. SSI rapport 2007:02. [in Swedish]. Stockholm; Swedish Radiation Protection Authority 2007.

Byström S. Cesium-137 beräknat ur flygmätningar utförda av SGU/SGAB från och med 1986 tom 2000, på uppdrag av SSI; Statens strålskyddsinstitut. Report to Swedish Radiation Protection Authority, Project: SSI P1075.98, SGU dnr 08-783/98. Uppsala, Sweden: Swedish Geological Airborne Division; 2000. [in Swedish].

International Commission on Radiological Protection ICRP. Conversion Coefficients for Radiological Protection Quantities for External Radiation Exposures. ICRP Publication 116. Ann. ICRP 2010;40:(2-5).

Jönsson M. Tondel M. Isaksson M. Finck R. Wålinder R. Mamour A. Rääf C. Modelling the decrease in ambient dose rate from the Chernobyl fallout using data from the Swedish municipality measurement system (manuscript in preparation).

Leggett R. Eckerman K. Dunning D. Christy M. Crawford-Brown D. Williams L. Dose rates to organs as a function of age following internal exposure to radionuclides. Washington. DC: Division of Facility Operations. Office of Nuclear Regulatory Research. U.S. Nuclear Regulatory Commission; Report Nureg/CR-3245 ORNL/TM-8265; 1984.

Rääf CL. Hubbard L. Falk R. Ågren G. Vesanen R. Ecological half-time and effective dose from Chernobyl debris and from nuclear weapons fallout of 137Cs as measured in different Swedish populations. Health Phys. 2006a May;90(5):446-58.

Rääf CL. Hubbard L. Falk R. Ågren G. Vesanen R. Transfer of ^{137}Cs from Chernobyl debris and nuclear weapons fallout to different Swedish population groups. Sci Total Environ. 2006b Aug 15;367(1):324-40.

Organ distribution of ^{210}Po and ^{137}Cs in lynx (*Lynx lynx*), wolverine (*Gulo gulo*) and wolves (*Canis lupus*)

Runhild Gjelsvik[1]*, Elis Holm[2], John Atle Kålås[3] and Bertil Persson[4]

Norwegian Radiation Protection Authority, PO Box 55, NO-1332 Østerås Norway[1]
Department of Medical Radiation Physics, Gothenburg University, Gothenburg Sweden[2]
Norwegian Institute for Nature Research, PO Box 5685 Sluppen, NO-7485 Trondheim, Norway[3]
Department of Medical Radiation Physics, Lund University, Barngatan 2, SE-22185, Lund, Sweden[4]

Abstract

Big predators in northern Scandinavia are exposed to radioactive radiation from natural and anthropogenic sources. Lynx (*Lynx lynx*), wolverine (*Gulo gulo*) and wolf (*Canis lupus*) take up ^{210}Po and ^{137}Cs from different prey species. To investigate the distribution of ^{210}Po and ^{137}Cs in different tissues and blood, samples were collected from 28 wolves from Sweden, 16 lynx, and 16 wolverine from Norway. Concentration of ^{210}Po and ^{137}Cs in wolf were analysed in muscle, liver and kidney tissue in addition to blood. Samples of liver from lynx and wolverine were analysed for ^{210}Po and for ^{137}Cs in muscle and liver. The activity concentrations of ^{210}Po in wolves were higher for liver and kidney than muscle and blood. The opposite pattern were found for ^{137}Cs with higher concentration in muscle than liver, kidney and blood. For wolves, strong correlations were obtained between different tissues and blood for both the investigated radionuclides (p<0.002). Not surprisingly, levels of ^{137}Cs in lynx and wolverine were higher in muscle than liver. For both species, a strong correlation between ^{137}Cs concentration in muscle and liver were found (p<0.001).

Introduction

Wild animals are exposed to radioactive radiation both from natural and anthropogenic sources. In Europe, the most important natural sources of such radiation to wild and semi domestic animals is ^{210}Po ($T_{1/2}$ = 138 d) which originates from deposition of ^{210}Pb from precipitation or exhaled from the ground as ^{222}Rn. The deposition of ^{210}Pb depends on surrounding land area, amount of uranium in the ground and precipitation. The deposition is also dependent on rainfall, distance from sea and local emanation of ^{222}Rn. The annual deposition of ^{210}Pb in Scandinavia is approximately 55 Bq m^{-2}. At 62° N in Sweden the integrated areal concentration of ^{210}Po, which is the granddaughter product of ^{210}Pb ($T_{1/2}$ = 22.3 a) via Bi, has been estimated to 2000 Bq m^{-2} (Persson, 1970, 1972) assuming radioactive equilibrium.

The most important anthropogenic radionuclide in Scandinavia is now ^{137}Cs, which was deposited just after the Chernobyl accident in 1986. Total deposition of ^{137}Cs in Norway and Sweden were approximately 2300 ± 200 TBq (Bache et al. 1987) and 4.25 PBq (Edvarson, 1991). The radioactivity was deposited in central and southern parts of Norway and Sweden. In Scandinavia, the deposition of ^{134}Cs and ^{137}Cs varied between 1000-50000 Bq m^{-2}. Areas with rainfall in the following days after the accident received most radioactive fallout (Edvarson, 1991). The northern part of Norway and Sweden suffered less from the Chernobyl accident, but these areas got deposition from nuclear tests during the 1950-1960. Most of the fallout from these atmospheric testing ended up in northern part of Norway or in areas with heavy precipitation like the west coast of Norway. The deposition from nuclear tests in Scandinavia was about 2500 Bq m^{-2} in 1963. Almost all ^{134}Cs has decayed while considerable amount of ^{137}Cs (T ½ =30.2 y), still remains in the ecosystems.

^{210}Po as well as ^{137}Cs accumulate in the food chain. Especially reindeer are known to contain enhanced concentrations of radiocaesium and polonium in soft tissues after feeding on lichen during the winter (Lidèn and Gustafsson, 1967, Persson, 1970, 1972, Åhman et al. 2004). Concentration of ^{210}Po and ^{137}Cs in wild and domestic animals are a result of the presence of these radionuclides in the environment, trophical level, food consumption and animal behaviour (Dietz et al. 2000, Skuterud et al. 2005). Since many studies of concentration of radioactivity in different tissues focus on consequences to human health, the investigated species are domestic and game animals (Fuma et al. 2016, Potter et al. 1989, Åhman et al. 2004) in addition to marine molluscs and fish (Carvalho 2011, Cherry et al. 1994, Khan et al. 2014, Marsico et al. 2014,). In addition, numerous papers are published on distribution of different metals in kidney, liver and muscle tissue from domestic and game animals (Gašparík 2016, Jarzyńska and Falandysz 2011), but less on big predators (Kauranen 1971).

Eurasian lynx (*Lynx lynx*), wolverine (*Gulo gulo*) and wolves (*Canis lupus*) are on the top of the food chain in the sub-arctic environment in Scandinavia. Here we describe activity concentrations of ^{210}Po and ^{137}Cs in different tissues of muscle, liver, kidney and blood in lynx, wolverine and wolf, and investigated any relationship between the concentrations in these tissues. In wolf, analyse of ^{210}Po and ^{137}Cs were carried out on liver, muscle, kidney and blood. For lynx and wolverine, liver samples were analysed for ^{210}Po and liver and muscle samples for ^{137}Cs.

Materials and Methods

Samples
Wolves (N=28) were collected in Sweden by licenced hunting or traffic accident during the months January to March 2010-2011. The wolves were collected over a large area (Figure 1). Samples of muscle, liver, kidney and blood were obtained from the National Veterinary Institute, Uppsala, Sweden after storing at -20 ^{0}C. Muscle and liver samples of lynx (N=16) and wolverine (N=16) from Norway were collected from ordinary licenced hunting, trapping or claim selection in 2011. The animals were from north to south of Norway (Figure 1). The Norwegian Institute for Nature Research (NINA) organized the sampling and samples were stored frozen at - 20° C until analyses. Detailed information about the sex, age and area, see Gjelsvik et al. 2014.

Radiometric technique
Concentration of ^{137}Cs in muscle and liver samples of lynx and wolverine were analysed by use of a Wizard 2480 (PerkinElmer) gamma counter by Norwegian Institute for Nature Research. The ^{137}Cs analyses in different wolf organs were carried out at Lund University in Sweden by HpGe gamma spectrometry and NaI. Concentration of ^{210}Po in blood and different wolf tissues were analysed in Sweden. The samples were prepared by drying at 80° C for approximately 30 h and grinding. The dry weights of liver samples as percentages of the wet weight were obtained. The blood samples were wet ashed directly (Henricsson et al., 2011). ^{210}Po was analysed by alpha spectrometry (ion implanted Si detectors) after wet ashing and spontaneous deposition on silver discs. ^{209}Po was used as radiochemical yield determinant (Henricsson et al., 2011). Samples of wolves were analysed by similar methods at Lund University. In the first nine samples of wolves, ^{210}Pb was also analysed. This was done by dry incineration of a larger amount of sample where Po evaporates. After waiting for about six months, the build up ^{210}Po from ^{210}Pb was analysed. The ingrowth rate gives the concentration of ^{210}Pb. For all animals, the ^{210}Po and ^{137}Cs concentrations were decay corrected to date of death. The samples at lynx and wolverine were analysed in Norway by Norwegian Radiation

Protection Authority. They were prepared at the same way as wolf tissue samples, except from drying at 60 $^{\circ}$ C.

Statistical analysis
Because the type of data we here present rarely are normal distributed and often suffered by lack of homogeneity of variance we use non-parametric statistics (Spearman rank correlation) to test for relationship between concentration of ^{210}Po and ^{137}Cs in liver, muscle, kidney and blood from the investigated species.
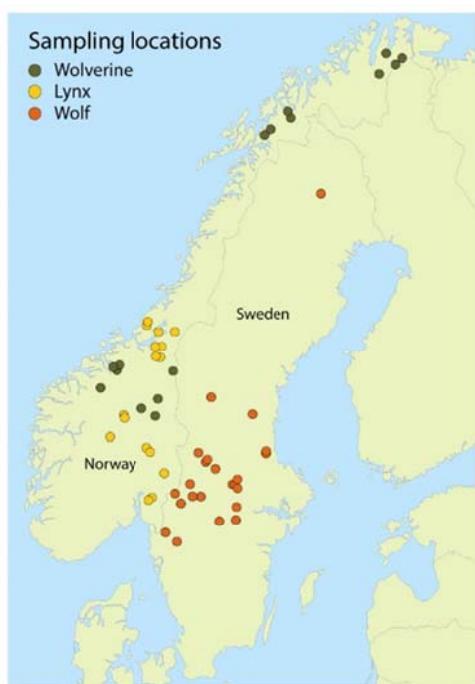
Figure 1. Sampling location of wolverine and lynx in Norway and wolf in Sweden during the years 2010-2011.

Results and Discussion

The activity concentrations of ^{210}Po in wolves were higher for liver (range 20-523 Bq kg^{-1} d.w.) and kidney (range 24-942 Bq kg^{-1} d.w.) than muscle (range 1-43 (Bq kg^{-1} d.w.) and blood (range 2-54 Bq l^{-1}). The concentrations of ^{210}Po in liver from lynx and wolverine ranged from 16-211 Bq/kg d.w. For ^{137}Cs the concentrations in wolves were in the order muscle (range 70-8410 Bq/kg d.w.), liver (range 36-4050 Bq/Kg d.w.), kidney (range (31-3456 Bq/kg d.w.) and blood (range 4-954 Bq l^{-1}). Same pattern were found for lynx and wolverine with high concentrations in muscle (range 53-10260 Bq kg^{-1} d.w.) and liver (range 22-13393 Bq kg^{-1} d.w., Figure 2). For all species, a strong correlation between ^{137}Cs concentration in muscle and liver were found (Spearman's rank correlation; wolf: $r_s = 0.969$, N = 28, p<0.000. Lynx: $r_s = 0.918$, N = 16, p<0.000. Wolverine: $r_s = 0.935$, N = 16, p<0.000, Figure 3).

For wolves, strong correlations were obtained between concentration in liver, muscle, kidney and blood for both the investigated radionuclides (^{137}Cs in wolf. Spearman's rank correlations. Liver vs kidney: $r_s = 0.967$, N = 28, p<0.000. Kidney vs blood: $r_s = 0.660$, N = 17, p<0.004. Kidney vs blood: $r_s = 0.660$, N = 17, p<0.004. Liver vs blood: $r_s = 0.782$, N = 17, p<0.000. Muscle vs kidney: $r_s = 0.948$, N = 28, p<0.000. Muscle vs blood: $r_s = 0.766$, N = 17, p<0.000, Figure 4. ^{210}Po in wolf. Spearman's rank correlations. Liver vs kidney: $r_s = 0.833$, N = 28, p<0.000. Liver vs muscle: $r_s = 0.718$, N = 27, p<0.000. Liver vs blood: $r_s = 0.499$, N = 25, p<0.011. Kidney vs muscle: $r_s = 0.800$,

N = 27, p<0.000. Muscle vs blood: r_s = 0.602, N = 24, p<0.002. Kidney vs blood: r_s = 0.602, N = 24, p<0.016, Figure 5).
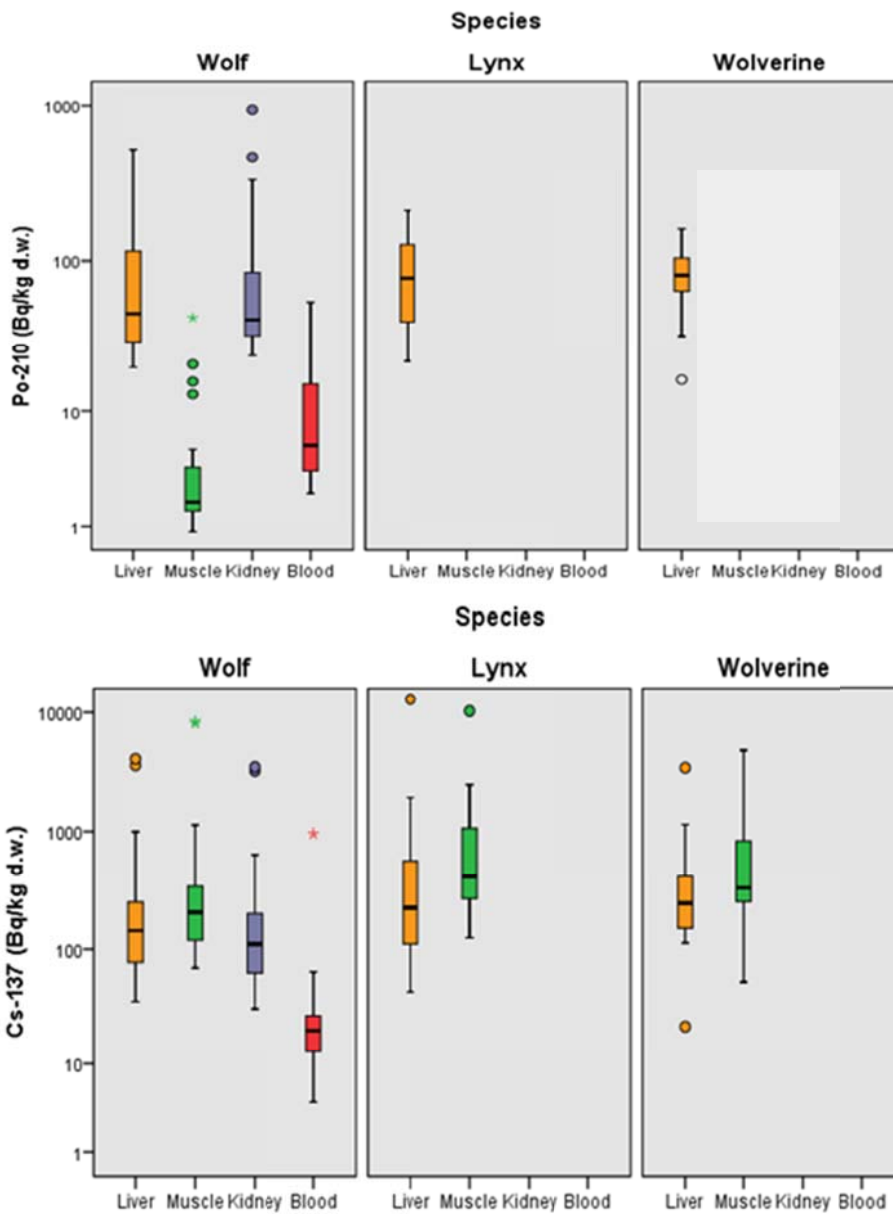
Figure 2. Concentrations of ^{210}Po and ^{137}Cs in liver, muscle, kidney and blood from wolf, lynx and wolverine. Boxplot shows mean, median, outliers, 25 and 75 quartiles.
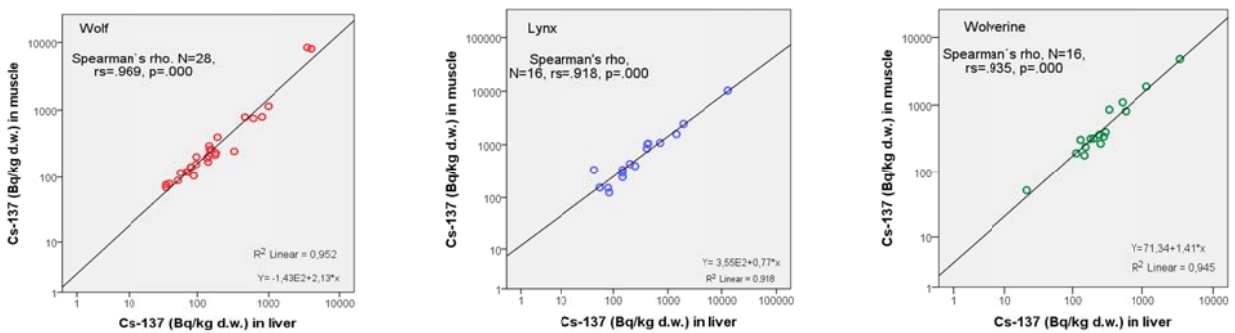
Figure 3. Concentration of ^{137}Cs in muscle correlated with concentration of ^{137}Cs in liver from wolf, lynx and wolverine.
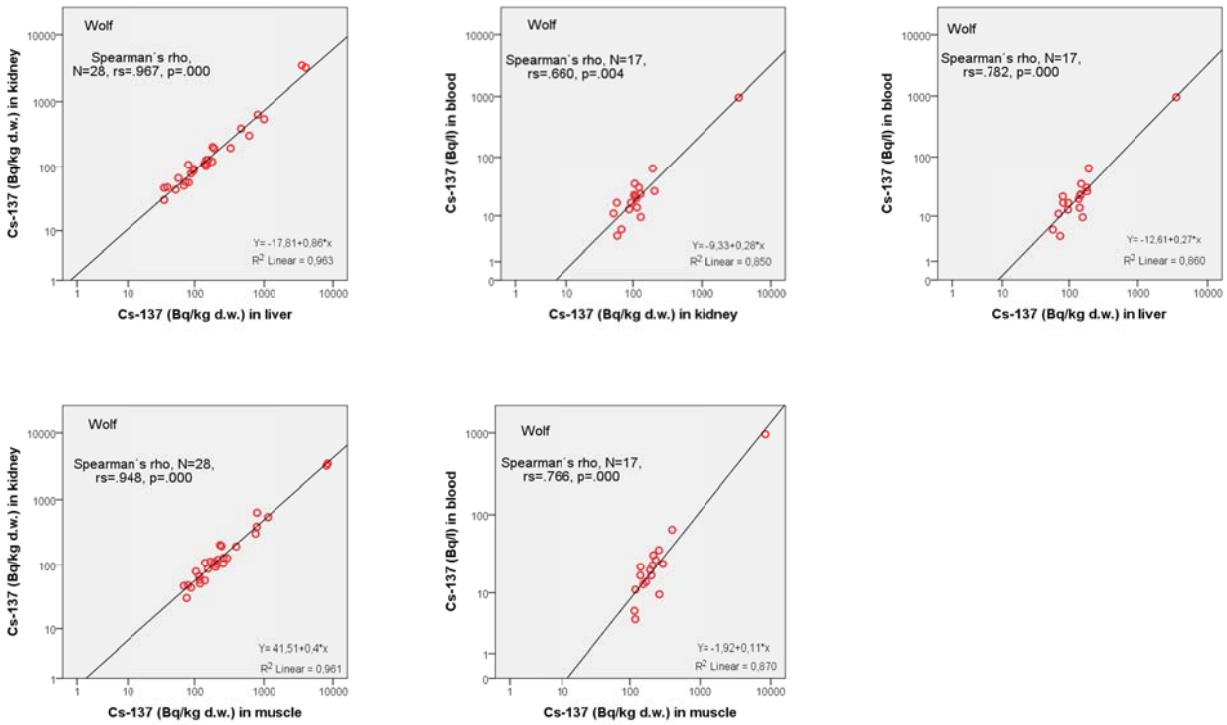
Figure 4. *Concentration of ^{137}Cs in tissue of kidney, liver, muscle and blood correlated with the concentration of ^{137}Cs in the studied tissues and blood from wolf.*
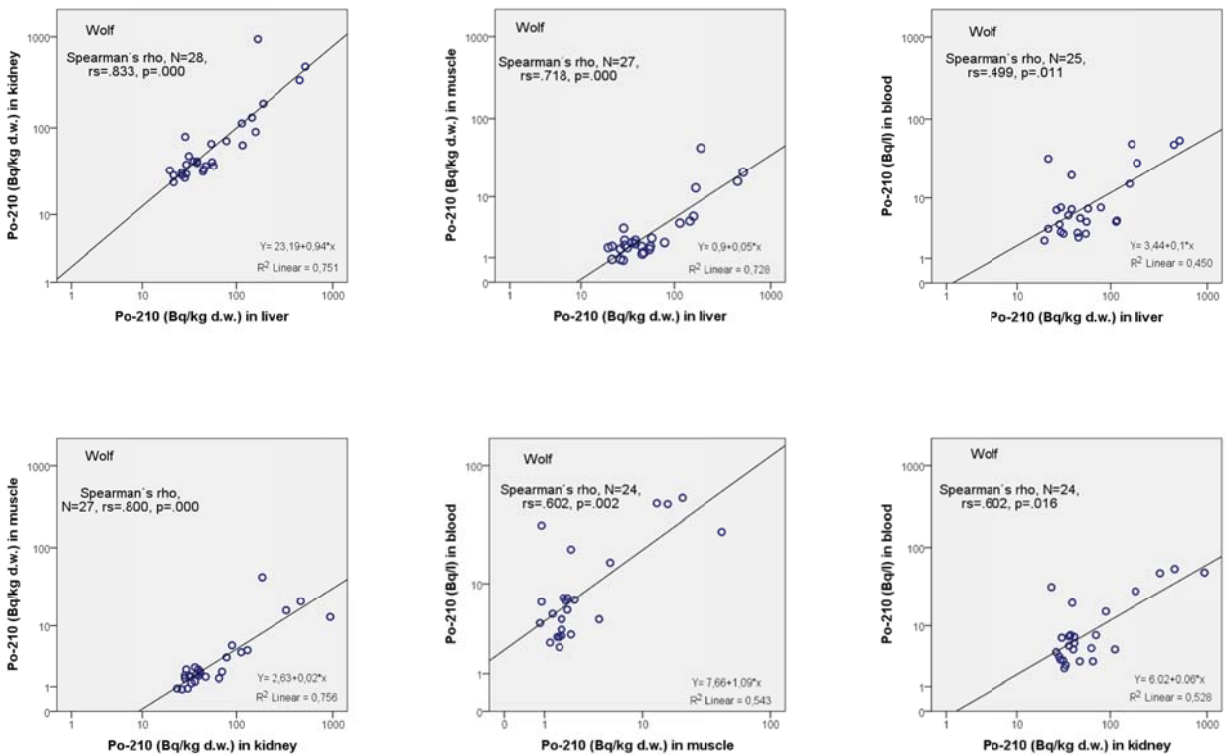
Figure 5. *Concentration of ^{210}Po in tissue of kidney, liver, muscle and blood correlated with the concentration of ^{210}Po in the studied tissues and blood from wolf.*

Conclusions

Big predators like lynx, wolverine and wolf, take up ^{210}Po and ^{137}Cs from different prey species. The natural and artificial radionuclide are differently distributed in the muscle, liver, kidney and blood. Concentrations of ^{210}Po were higher for liver and kidney than muscle and blood. The opposite pattern was found for ^{137}Cs in muscle, with highest levels in the muscle. Strong correlations were obtained between activity of ^{210}Po and ^{137}Cs in different tissues and blood. The correlations makes it possible to calculate the levels of ^{210}Po and ^{137}Cs in different tissues based on analyses of one sample. When working with wild animals, another advantage of the results is to take a blood sample and release the animal back into the wild.

References

Bache S., Bjerke, H., Rudjord, AL., Ugletveit, F., 1987. Fall-out patters in Norway after the Chernobyl accident estimated from soil samples. Radiation Protection Dosimetry 18, 105-107

Carvalho, F. P., 2011. Polonium (210 Po) and lead (210 Pb) in marine organisms and their transfer in marine food chains. Journal of environmental radioactivity, 102(5), 462-472.

Cherry, R. D., Heyraud, M., & Rindfuss, R., 1994. Polonium-210 in teleost fish and in marine mammals: interfamily differences and a possible association between polonium-210 and red muscle content. Journal of environmental radioactivity, 24(3), 273-291.

Dietz, R., Riget, F., Cleemann, M., Aarkrog, A., Johansen, P., & Hansen, J. C., 2000. Comparison of contaminants from different trophic levels and ecosystems. Science of the Total Environment, 245(1), 221-231.

Edvarson K., 1991. Fallout over Sweden from the Chernobyl Accident. In: The Chernobyl fallout in Sweden, Ed. L. Moberg. The Swedish Radiation Protection Institute, Stockholm, Sweden, pp 47-65.

Gašparík, J., Binkowski, Ł. J., Jahnátek, A., Šmehýl, P., Dobiaš, M., Lukáč, N. & Massanyi, P., 2016. Levels of Metals in Kidney, Liver, and Muscle Tissue and their Influence on the Fitness for the Consumption of Wild Boar from Western Slovakia. Biological Trace Element Research, 1-9.

Gjelsvik, R., Holm, E., Kålås, J. A., Persson, B., & Åsbrink, J., 2014. Polonium-210 and Caesium-137 in lynx (*Lynx lynx*), wolverine (*Gulo gulo*) and wolves (*Canis lupus*). Journal of environmental radioactivity, 138, 402-409.

Jarzyńska, G., & Falandysz, J., 2011. Selenium and 17 other largely essential and toxic metals in muscle and organ meats of Red Deer (*Cervus elaphus*) —consequences to human health. Environment international, 37(5), 882-888.

Henricsson F., Ranebo Y., Holm E., Roos P., 2011. Aspects on the analysis of ^{210}Po. Journal of Environmental Radioactivity 80, 415-419.

Kauranen, P., Miettinen, J., & Pulliainen, E., 1971. Polonium-210 and lead-210 in some terrestrial animals in Finland. Annales Zoologici Fennici, 8(2), 318-323. Retrieved from http://www.jstor.org/stable/23731624

Lidèn K., Gustafsson M., 1967. Relationship and seasonal variation of Cs-137 in lichen, reindeer and man in Northern Sweden 1961-1965. In Radioecological Concentration Processes. Eds Åberg and Hungate. Proc. Int Symp. Stockholm Sweden, 1966, Pergamon press, pp. 193-208.

Marsico, E. T., Ferreira, M. S., São Clemente, S. C., Gouvea, R. C. S., Jesus, E. F. O., Conti, C. C. & Kelecom, A. G. A. C., 2014. Distribution of Po-210 in two species of predatory marine fish from the Brazilian coast. Journal of environmental radioactivity, 128, 91-96.

Khan, M. F., Wesley, S. G., & Rajan, M. P., 2014. Polonium-210 in marine mussels (bivalve molluscs) inhabiting the southern coast of India. Journal of environmental radioactivity, 138, 410-416.

Persson, R.B.R., 1970. ^{55}Fe, ^{90}Sr, ^{134}Cs, ^{137}Cs, and ^{210}Po in the biosphere: radiological health aspects of the environmental contamination from radioactive materials in northern Sweden. PhD thesis, Medical Radiation Physics, Lund University, Lund, Sweden

Persson, R.B.R., 1972. Lead-210, Polonium-210, and stable lead in the food-chain lichen reindeer and man. In: Adams, J.A.S., Lowder, W.M., Gesell, T.F. (Eds.). The Natural Radiation Environment II. Rice University, Houston, Texas, USA, pp. 347-367

Potter, C. M., Brisbin, I. L., McDowell, S. G., & Whicker, F. W., 1989. Distribution of 137 Cs in the American coot (*Fulica americana*). Journal of environmental radioactivity, 9(2), 105-115.

Fuma, S., Kubota, Y., Ihara, S., Takahashi, H., Watanabe, Y., Aono, T. & Yoshida, S., 2016. Radiocaesium contamination of wild boars in Fukushima and surrounding regions after the Fukushima nuclear accident. Journal of Environmental Radioactivity, 164, 60-64.

Skuterud L., Gaare E., Kvam T., Hove K., Steinnes E., 2005. Concentrations of ^{137}Cs in lynx (*Lynx lynx*) in relation to prey choice. Journal of Environmental Radioactivity 80, 125-138.

Åhman, B., Wright, S. M., & Howard, B. J., 2004. Radiocaesium in lynx in relation to ground deposition and diet. Radiation and environmental biophysics, *43*(2), 119-126.

C – TERRESTRIAL

SEMIPALATINSK

The Particle size distribution of radioisotopes in soils at fallout traces of nuclear explosions

A.M. Kabdyrakova[*], A.T. Mendubaev, S.N. Lukashenko

Branch «Institute of Radiation safety and Ecology» of the National Nuclear Center of the Republic of Kazakhstan, 2, Krasnoarmeyskaya st., 071100 Kurchatov, Kazakhstan

Abstract

The paper presents results of the research of ^{137}Cs, ^{90}Sr, ^{241}Am and $^{239+240}$Pu distribution in particle size fractions of soil on the traces of radioactive fallouts from surface nuclear explosions conducted at the Semipalatinsk Test Site (STS). The researches have been carried out on the plumes of nuclear tests with various yields and extension. The fractions of definite size enriched with artificial radionuclides were found in the investigated soils. The dimensions of enriched fractions revealed at different traces were as follows 1000-500 µm, 500-250 µm, 40-8 µm and <1 µm. Enriched coarse fractions having the grain size larger than 250 µm were frequently found on the short plumes and their enrichment grade reached 5 times. Fine fractions, enriched with radionuclides were found along the plumes in even more remote areas. Their enrichment grade varied within two orders of magnitude, with the maximum enrichment of 12 times.

Introduction

Radioactive fallouts from the nuclear explosions occur due to forming radioactive particles, those are further transported with air flows and fall out on the ground. One of the main characteristics of radioactive particles determining the scale and the level of environmental radioactive contamination along with radiation and physicochemical characteristics, is their dispersibility. The dimensions of radioactive particles determine their distribution in the atmosphere and the distances from the epicenter at that will fallout (Izrael and Sutkin, 1967; Izrael 1973; Loborev et al, 1997). Distribution of radionuclides in the particle site fractions of soil can make it possible to reveal peculiarities of radioactive fallouts' plumes formation and to characterize radioactive contamination of the soil cover due to nuclear tests.

Research methods and materials

Objects of research.

As the objects of research the plumes of the following tests carried out at the STS were chosen:

− surface explosion without significant nuclear energy emission (hydronuclear experiments). The object conventionally named «R» is located at the «P2-M» site;
− surface nuclear explosion allegedly with the yield of 1.2 kT (assumed date 30.10.1962). The object conventionally named «V-1» is located at the «Experimental Field» site;
− surface nuclear explosion with the yield of 140 kT (29.08.1949).

The length of researched sites was 0.6, 3.2 and 150 km respectively.

[**]Corresponding author, E-mail: kabdyrakova@nnc.kz

Sampling.
5 cm depth topsoil samples were collected along the middle of the trace with increasing distance from the explosion epicenter. At the trace of explosion carried out 29.08.1949 samples were also collected in lateral direction from the middle towards to the periphery. Thus sampling points were arranged in longitudinal and cross profiles (lines). Two cross profiles were laid at the distance of 15 km and 120 km from the explosion epicenter respectively.

Fractions separation.
To separate off the particle size fractions of soil two methods were used sequentially: «wet» sieving and sedimentation. Using «wet» sieving method the following fractions were separated: 1000-500; 500-250; 250-100; 100-63, 63-40 μm. using sedimentation method the following fractions were separated: 40-8 μm, 8-5 μm, 5-1 μm and< μm.

Radionuclide analyses.
The content of artificial radionuclides was determined in soil samples and particle size fractions. Activity concentration of ^{137}Cs and ^{241}Am were determined using Canberra GX-2020 gamma-spectrometer with semiconductor detector. ^{90}Sr activity concentration was determined by direct measuring via «Progress-BG» beta-spectrometer (Russia). However, if activity concentration of the radionuclide was below the detection limit (100 Bq/kg) a radiochemical analysis was carried out using «TRICARB 3100 TR» liquid-scintillation spectrometer with the energy range of 2000 keV. Radiochemical extraction of ^{90}Sr, as well as $^{239+240}$Pu consisted of several steps as follows: extraction of radionuclides from the soil matrix via either leaching or complete combustion, cleaning from interfering radionuclides, preparation sources for counting and measuring activity of radioisotopes. Activity of $^{239+240}$Pu in counting sources were measured using «Alpha – Analyst» alpha-spectrometer with semiconductor detector («CANBERRA», USA) with the energy range 3,6 – 6,0 MeV, the maximal energy resolution of 23 keV, and the maximal alpha-radiation registration efficiency of 25 %.

Results and discussion

The particle-size composition of soils.
The mass percentage (ω, %) of the total weight of dry sample was determined for each particle size fraction of soil. The Table
Table1 presents the results of particle size analysis of soil samples collected at the research objects/

Table1. Mass percentage of the particle-size fractions of soils, %

Object	Fraction, μm								
	1000-500	500-250	250-100	100-63	63-40	40-8	8-5	5-1	<1
R	17.9	15.9	18.3	5.1	4.5	14.5	7.7	10.5	4.1
V-1	19.6	16.1	19.1	4.2	2.6	14.8	7.2	9.9	4.4
1949	18.2	23.0	21.7	4.8	4.0	10.0	5.8	7.3	3.5

Results show that the particle-size composition of soils from the researched objects is similar. Coarse particles (sand) larger than 100 μm in size and silt fraction 40-8 μm in size dominate in soils. The mass of other fractions, including clay fraction (<1 μm) is much lower.

Concentration of artificial radionuclides in soil.
The level of soil contamination with radionuclides at the traces of hydronuclear test and surface test of the 1962 are high. Specific activity of ^{241}Am and $^{239+240}$Pu vary from n×10^2 to n×10^5 Bq/kg, while for ^{137}Cs and ^{90}Sr this range lies within n×10^1 to n×10^4 Bq/kg. As the rule, soils in the

epicentral area are contaminated to the highest extent. With increasing distance from the epicenter activity concentration of radionuclides decrease.

Contamination level of the soil at the trace of surface explosion of the 1949 is lower in several orders of magnitude than at the other plumes. Activity concentration of ^{137}Cs, ^{241}Am and $^{239+240}$Pu ranges within $n \times 10^0$ to $n \times 10^1$ Bq/kg.

Distribution of radionuclides in the particle size fractions.

Enrichment factor (E$_f$) was used for quantitative assessment of ^{137}Cs, ^{241}Am, $^{239+240}$Pu and ^{90}Sr distribution in the particle size fractions of soil. This value is determined as a ratio of specific activities of a radionuclide in fraction ($A_{sp.}^{fr.}$) and in soil ($\overline{A}_{sp.}^{s}$): E$_f$=$A_{sp.}^{fr.}/\overline{A}_{sp.}^{s}$. This parameter serves as an index of enrichment or depletion of particle size fractions in respect to average concentration of radionuclides in soil. E$_f$>1 means that fraction is enriched by radionuclides, while E$_f$<1 means that the fraction is depleted by radioisotopes. The results are presented in the tables (Tables 2-4)

Table2. Enrichment factors of particle size fractions of soil on the trace «R» for various radionuclides

Fraction, μm	^{137}Cs		^{90}Sr		^{241}Am		$^{239+240}$Pu	
	range	average	range	average	range	average	range	average
1000-500	0,2-0,6	0,5	0,1-0,3	0,1	0,1-0,9	0,5	0,03-0,06	0,05
500-250	1,6-2,8	2,1	1,3-3,4	2,4	1,1-3,3	2,1	2,1-5,1	3,0
250-100	0,8-1,3	1,1	0,2-1,5	0,8	0,6-1,8	1,2	0,5-0,9	0,8
100-63	0,5-0,7	1,0	0,1-1,1	0,6	0,4-0,9	0,7	0,3-1,0	0,8
63-40	0,2-1,2	0,6	0,1-0,8	0,4	0,3-1,2	0,7	0,2-1,0	0,5
40-8	0,4-1,0	0,6	0,1-0,6	0,4	0,5-1,5	1,0	0,3-1,3	0,9
8-5	0,5-0,9	0,6	0,1-0,4	0,3	0,4-1,3	0,9	0,3-1,5	0,8
5-1	0,9-1,3	1,1	0,03-0,8	0,3	0,3-1,2	0,8	0,3-1,1	0,8
<1	1,3-2,6	1,9	0,2-1,1	0,6	0,2-1,1	0,8	0,2-0,9	0,6

According to results, there a non-uniform distribution of radionuclides in particle size fractions of soil takes place at the trace of hydronuclear test and its character is identical for all the radionuclides under research. The dimensions of fraction enriched with radionuclides to the greatest extent ranges within 500-250 μm. Other fractions are depleted by radionuclides or enriched insignificantly. An exception is ^{137}Cs, which is also concentrated within the fraction of <1 μm.

The character of radionuclides distribution remains stable all along the plume length.

Table 3. Enrichment factors of soil particle size fractions on the plume «V-1» for various radionuclides

Fraction, μm	^{137}Cs		^{90}Sr		^{241}Am		$^{239+240}$Pu	
	range	average	range	average	range	average	range	average
1000-500	1,8-3,7	2,8	1,5-3,8	2,9	1,8-2,8	2,0	1,2-3,0	2,2
500-250	0,9-2,5	1,5	1,0-2,4	1,5	0,4-1,8	1,0	0,5-2,1	1,2
250-100	0,1-0,9	0,4	0,1-0,8	0,4	0,1-0,9	0,4	0,1-0,9	0,4
100-63	0,3-0,7	0,5	0,2-0,7	0,4	0,3-1,5	0,7	0,5-1,0	0,7
63-40	0,2-0,7	0,4	0,1-0,6	0,4	0,1-2,0	0,7	0,2-0,9	0,5
40-8	0,2-0,6	0,3	0,2-0,5	0,4	0,5-1,7	1,2	0,3-1,8	1,0
8-5	0,3-0,5	0,4	0,2-0,5	0,4	0,2-1,7	0,7	0,3-1,4	0,6
5-1	0,3-0,6	0,5	0,1-0,8	0,4	0,3-0,9	0,5	0,2-0,7	0,4
<1	0,4-0,8	0,5	0,2-1,1	0,5	0,2-12,9	2,6	0,1-9,8	2,2

The data presented in the table (Table 3) also shows non-uniform character of radionuclides distribution at the plume V-1. The coarse fractions with soil particles sized from 1000 to 250 μm are enriched with radionuclides to the highest extent. All the other fractions are depleted by radionuclides. However within the area of the plume, located at the distance of 2-3 km to the epicenter, the fraction of <1 μm becomes enriched with radionuclides ^{241}Am and $^{239+240}$Pu sharply. The values of <1 μm fraction enrichment factors at this area exceed 10. In general, except for this fact, the character of radionuclides distribution remains stable all along the trace.

Table 4. Enrichment factors of soil particle size fractions on the trace of the 1949 for various radionuclides

Fraction, μm	Longitudinal profile				Cross-profile			
	^{137}Cs		^{241}Am		^{137}Cs		^{241}Am	
	range	average	range	average	range	average	range	average
1000-500	0,3-2,9	0,9	0,1-2,5	0,7	0,4-3,9	0,8	0,01-0,9	0,5
500-250	0,3-1,4	0,8	0,1-3,8	1,0	0,4-1,4	0,6	0,03-3,6	0,8
250-100	0,3-1,4	0,8	0,3-1,6	0,7	0,5-1,1	0,7	0,1-1,5	0,7
100-63	0,4-5,2	1,5	0,1-7,4	1,4	0,6-2,2	1,1	0,1-1,9	0,8
63-40	0,4-6,1	2,1	0,1-7,2	2,0	0,5-6,1	1,9	0,2-7,2	2,1
40-8	0,6-11,0	3,1	1,7-16,5	5,0	0,6-11,0	2,7	0,5-16,5	4,8
8-5	0,9-13,0	3,8	0,2-14,9	3,8	1,0-13,0	3,7	0,2-14,9	4,1
5-1	1,1-12,3	4,1	0,1-10,3	2,0	1,3-12,6	4,4	0,1-10,3	3,0
<1	1,4-13,8	5,0	0,1-2,1	0,9	1,8-15,7	5,7	0,1-4,4	1,8

Unlike two objects mentioned above, there are different character of distribution ^{137}Cs and ^{241}Am in soil fractions at the trace of explosion carried out in 1949. ^{137}Cs is concentrated in fine soil fractions less than 40 μm large. At that, with decrease in dimensions of soil fractions, their enrichment factor grows achieving the maximum in <1 μm soil fraction.

In their turn 100 to 5 μm large soil particles are enriched with ^{241}Am radionuclide. The highest enrichment factor was found for the particles with dimensions of 40-8 μm.

The fractions with soil particles, sized less than 40 μm have a wide range of enrichment factor values. High enrichment factor values exceeding 10, can be found in the most remote points at the distance of 120-150 km to the epicenter. This can be indication of the fact that distant parts of the trace are mainly formed by fine particles fallouts.

In general there are almost no significant differences between the characters of radionuclides' distribution in longitudinal and cross profiles. However, at the closest cross profile located in the distance of 15 km to the epicenter, at the periphery of the trace the enrichment of coarse fractions with size exceeding 500 μm rises a little.

Therefore according to results of research, at all the researched traces of radioactive fallouts from surface nuclear explosions, some definite fractions with predominant enrichment by radionuclides were found. Probably the size of the most enriched fractions corresponds to the dispersion of substances of fallouts which formed the radioactive trace.

Conclusion

As the result of research of radionuclides' distribution in particle size fractions of soil at the various traces of surface nuclear tests carried out at the Semipalatinsk Test Site the following peculiarities of radioactive contamination were found:
   - the fractions with some definite size where the most of radionuclides' activity is concentrated can be found in soils at the traces of radioactive fallouts;
   - the highest activity of radionuclides at the trace of hydronuclear explosion is concentrated in 500-250 μm soil fractions;

- at the trace of a nuclear explosion with the yield of 1.2 kT the most of radionuclides' activity is concentrated in soil particles with size from 250 to 1000 μm;
- at the trace of 140 kT yield nuclear explosion having length over 150 km the highest ^{137}Cs and ^{241}Am activities are concentrated in fractions with particles size <1 μm and 40-8 μm respectively.

References

Izrael, Yu.A.,Sutkin, E.D., 1967. Gamma emission of radioactive fallouts. Atomizdat, Moscow (in Russian)

Izrael, Yu.A.,1973. Isotopic composition of radioactive fallouts. Hydrometeoizdat, Leningrad (in Russian)

Loborev, V.M. et al, 1997. Physics of nuclear explosion,Vol 1, in: Bochkarev M.V. et al. Radioactive contamination of the atmosphere and the Earth surface. Nauka. Phyzmatlit. Moscow. pp. 277-330 (in Russian)

Speciation of artificial radionuclides in soils of Semipalatinsk Test Site

A.Ye. Kunduzbayeva[*], A.M. *Kabdyrakova, S.N. Lukashenko*

Institute of Radiation Safety and Ecology, National Nuclear Center of the Republic of Kazakhstan, Kurchatov city, Kazakhstan

Abstract

The paper presents study data on speciation of artificial radionuclides ^{137}Cs, $^{239+240}$Pu, ^{241}Am and ^{90}Sr in soils of major testing areas of STS ("Experimental Field", "Degelen", "4a" and "Atomic" lake site) and in conventionally "background" territories of STS. Regularities in radionuclide distribution in STS soils have been identified depending on the nature of radionuclide contamination in the soil cover.

Introduction

One parameter widely used in integrated radioecological studies is speciation of radionuclides in soils. Speciation of radionuclides is applied to estimate the bioavailability prediction and migration ability of radionuclides (migration in the food chain, wash-out by surface and ground water) in soils, as a scientific basis for choice justification to select a remediation technique for contaminated area etc. [1, 2].

A unique peculiarity of STS territory that determines scientific interest in it, are sites located there (testing areas, conventionally "background" STS territories) of different levels and nature of radioactive contamination (type of test, mechanism of how radioactive particles are formed) in the soil cover. The purpose of this research is to reveal peculiarities of distribution in speciation of ^{137}Cs, ^{90}Sr, $^{239+240}$Pu artificial radionuclides in soils of STS depending on the nature of radioactive contamination in the soil cover. In the course of research, the main testing areas of STS and conventionally "background" STS territories were studied. The paper makes a comprehensive assessment and systematization of data acquired in the course of previous research for the purpose of defining a single whole picute of the state and peculiarities of radionuclide distribution in STS soils differentiated by mechanism of how radioactive contamination is formed. This approach enhances capabilities of applications for results obtained. Findings obtained at STS can be applied in assessing and predicting radionuclide behavior in soils of contaminated territories having similar mechanisms of how radioactive contamination is formed (areas in the zone impacted by atomic industry and power engineering sites (routine operations, emergency emissions), nuclear test sites, zones impacted by fallout plumes from nuclear explosions etc.

Materials and Methods

Targets of research

The targets of research are the main testing areas of STS ("Experimental Field", "Degelen", "4a", "Atomic" lake site) and conventionally "background" territories of STS (Figure 1).

---

[*]Corresponding author, E-mail: kunduzbaeva@nnc.kz
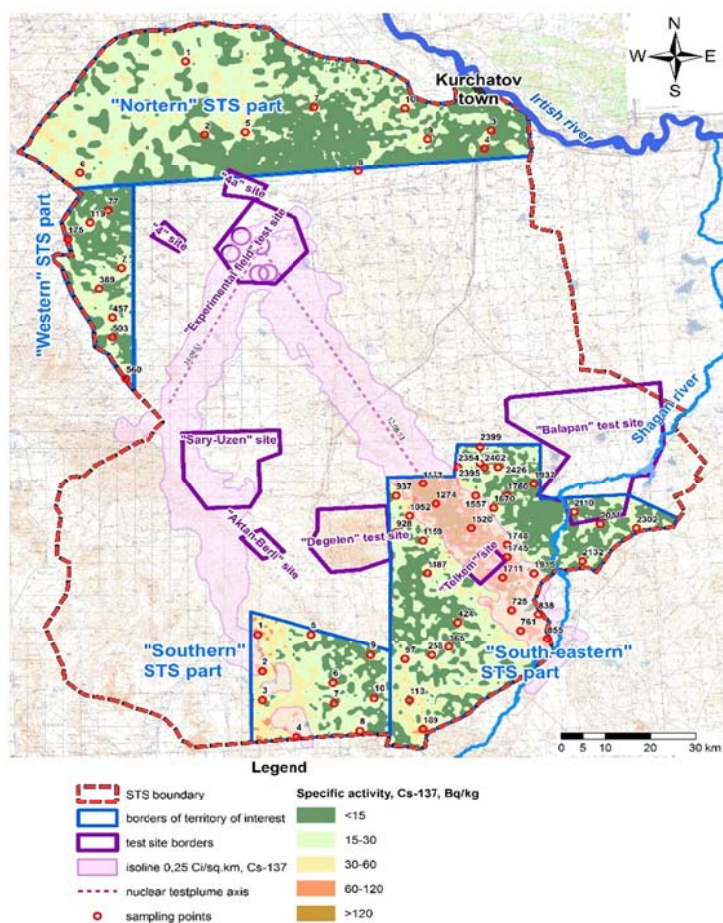
Figure 1. *Location diagram of STS targets of research*

Studies of the "Experimental Field" ground were conducted at ground zeros of surface nuclear tests. 2 to 4 research areas were laid out at each epicentral spot. In total, about 30 soil samples were studied [3].

STS conventionally background territories were studied the case of the "northern", "western", "south-eastern" and "southern" parts of STS. Radioactive contamination in the "northern" and "western" territories was due to global fallout. The territory of the "south-eastern" and "southern" part were impacted by passing fallout plumes of surface nuclear tests. Soil was sampled at points of elevated radionuclide concentration as well as in the zone of fallout plumes from surface nuclear tests [4].

The "Atomic" lake site is the result of industrial nuclear explosion by with soil ejected (excavation explosion). The area of maximum radioactive contamination was selected for the research – the one along the direction of fallout plume from the basic wave [5]. Soil samples were sequentially collected at a distance of 60 to 400 m from one another with distance from the crater ridge of the "Atomic" lake.

In "Degelen" testing area, studies were conducted on near-mouth grounds of tunnels 176 and 177 of water seepage, where contamination is determined by carry-over of radioactive contamination into the daylight surface with tunnel water [6,7]. Sampling was made along the stream flow bed with distance from the tunnel entry.

Contamination in "4a" area is determined by testing radiological warfare agents (liquid and powder-like). 10 spots of maximum radioactive contamination were explored. Soil samples were taken at points of maximum radionuclide concentration [8].

At site soil sampling was made at a depth of 0-5 cm by "envelope" (in "Degelen" area – pointwise at 0-20 cm).

Research procedure for speciation of radionuclides in soil.

Study of radionuclide speciation in soils was conducted by sequential extraction as modified by Pavlovskaya F.I. Water-soluble (H2O), exchangeable (1M CH3COONH4, pH=6.8), mobile (1M HCl) and tightly bound (soil after extraction) forms were determined [9]. The procedure was modified by adding an intermediate stage of determining fractions of organically bound radionuclides by 0.1N NaOH solution based on the technique developed by Tyurin I.V. [10]. The ratio of soil and leaching solution was 1:5. Radionuclide concentration in extracts obtained and soil after extraction was determined in accordance with certified procedures [11,12,13]. The analytical bias did not exceed 20 %.

Results and Discussion

[137]Cs radionuclide

[137]Cs concentration in STS soil is predominantly in a tightly bound form which is typical of this radionuclide (Fig 2). Low mobility of ^{137}Cs trace amount in soils is due to specific adsorption which occurs in interaction of many clay minerals with crystal lattice (similar to potassium) [14].

In spite of low mobility of ^{137}Cs in soils, the procedure applied has identified concentration of soluble forms that provide for its different bioavailability in soils. On the "Experimental Field" ground the lowest concentration of exchangeable and mobile forms can be observed, concentration of mobile form at the rest of sites is roughly at the same level. Maximum concentration of ^{137}Cs exchangeable form is observed in soils of "4a" area where [90]Cs water-soluble form was reliably determined.
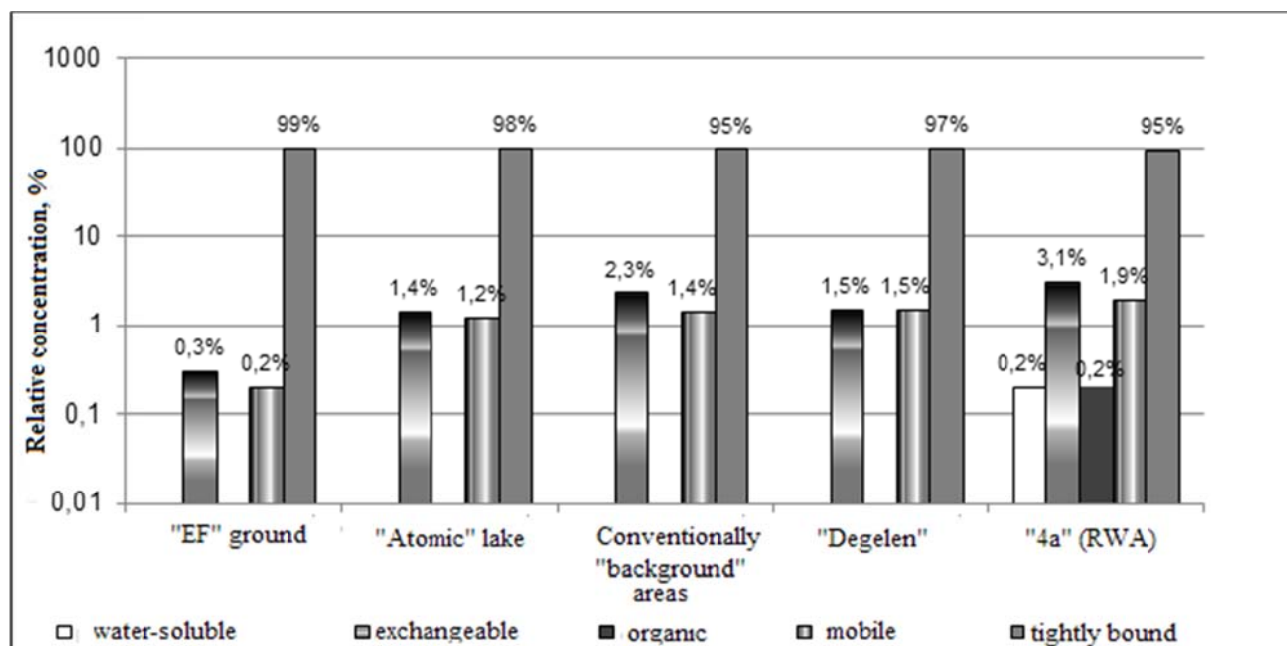
Figure 2. *Findings of ^{137}Cs radionuclide*

$^{239+240}$Pu radionuclide

Peculiarity in $^{239+240}$Pu behavior is its stable concentration as part of organic fraction. Under STS conditions concentration of organic form along with mobile one of the radionuclide reflects different mobilities of $^{239+240}$Pu in soils of sites in question (Figure 3). Elevated concentration of $^{239+240}$Pu exchangeable form is observed in conventionally "background" territories of STS and in "Degelen" area.
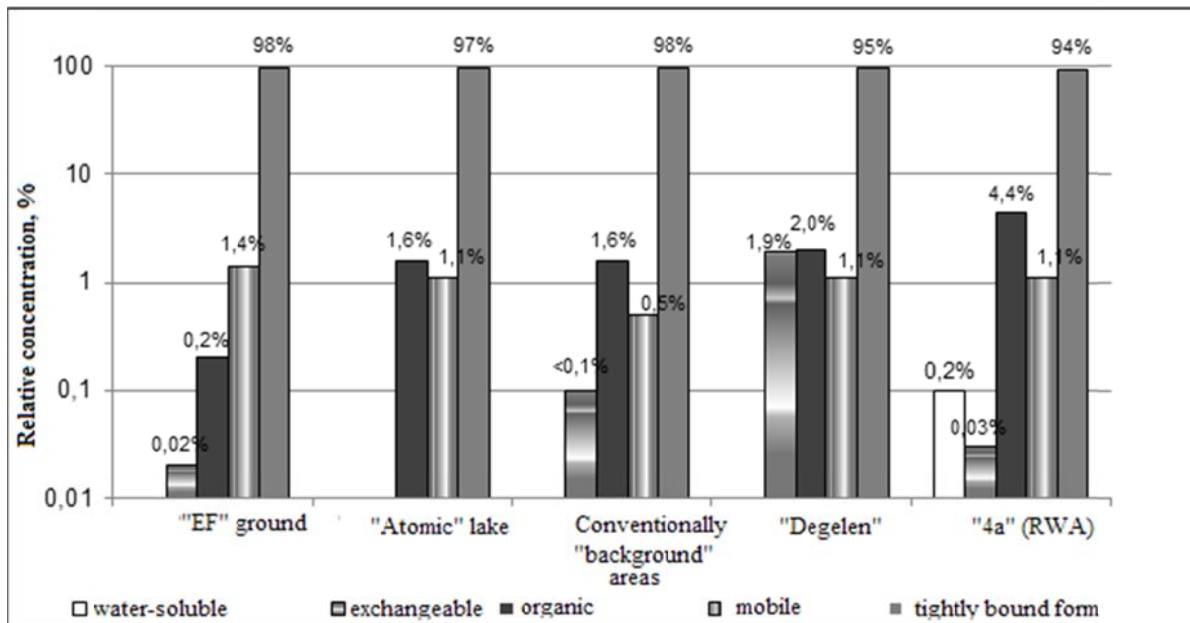
Figure 3. Findings of $^{239+240}$Pu radionuclide

In "4a" area, quantitative concentration of water-soluble form and maximum concentration of organic form of $^{239+240}$Pu was determined.

^{241}Am radionuclide

^{241}Am should be noted to have predominantly concentration in its mobile and tightly bound forms the ratio of which varies with a target of research. The lowest parameter values for bioavailability were determined in soils of the "Experimental Field" ground (Figure 4).
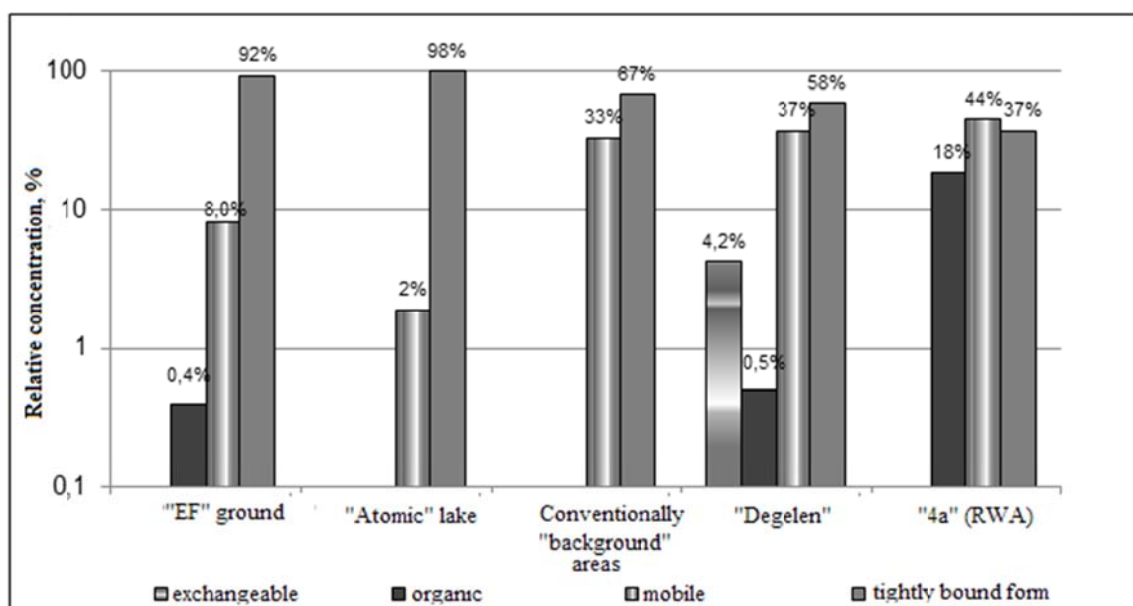
Figure 4. Findings of ^{241}Am radionuclide

Depending on a target of research, small amount of Am organic form is also observed with maximum value in "4a" area as well as its exchangeable form in "Degelen" area.

^{90}Sr radionuclide
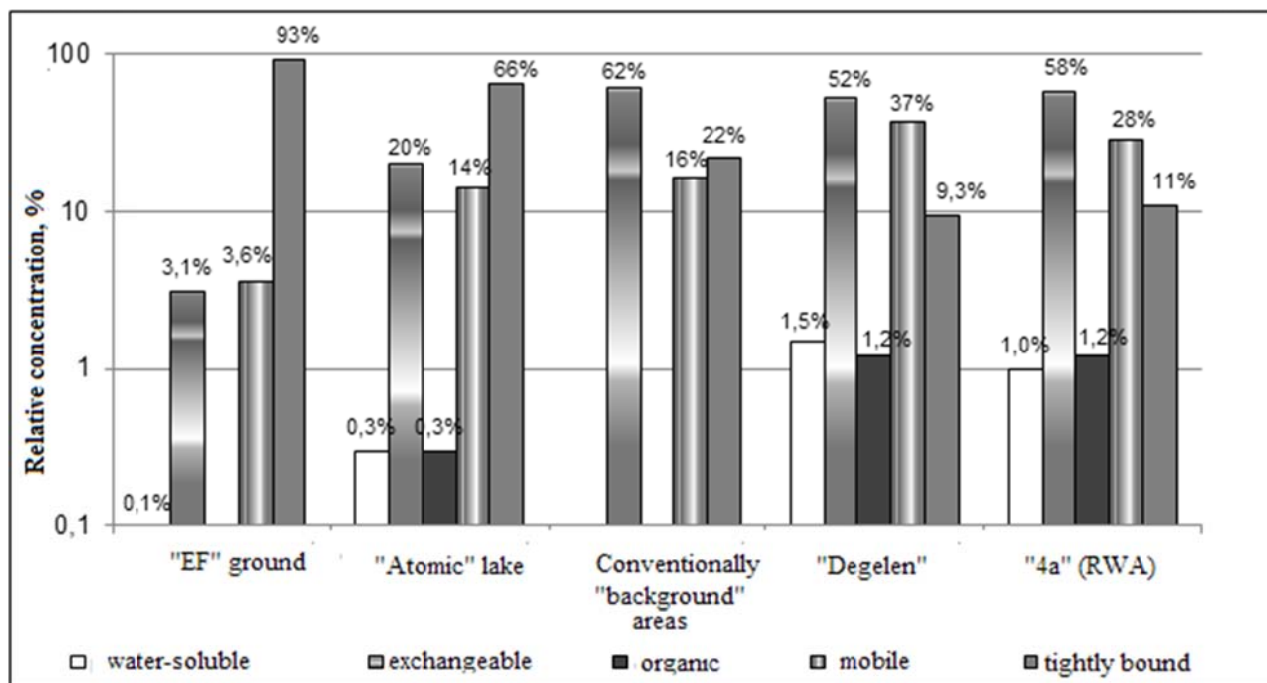
Figure 5. Findings of ^{90}Sr radionuclide

^{90}Sr radionuclide in STS soils is characterized by maximum mobility parameters. The lowest concentration of ^{90}Sr soluble forms was determined in soils of "Experimental Field" ground. ^{90}Sr concentration was found in its water-soluble form and organic form of maximum values in soils of "Degelen" and "4a" areas. Maximum concentrations of ^{90}Sr exchangeable form was determined in soils of "Degelen" and «4a" areas, in conventionally "background" STS territories (Figure 5).

Conclusions

Speciation of the major artificial radionuclides ^{137}Cs, ^{90}Sr, $^{239+240}$Pu and ^{241}Am has been determined in soils of STS of different levels and nature of radioactive contamination in the soil cover. Peculiarities of radionuclide speciation have been identified for each target of research. It was found that radionuclide speciation distribution in STS soils depends on the nature of radioactive contamination in the soil cover (mechanism of how radioactive particles are formed).

The lowest mobility and bioavailability of radionuclides has been found on the "Experimental Field" ground and at the "Atomic" lake which is determined by mechanism peculiarities of how radioactive particles are formed during surface and excavation explosions. The highest bioavailability of radionuclides is determined in soils of RWA test venues ("4a" area); zones impacted by radioactive stream flows of "Degelen" area and in conventionally "background" territories of STS of which sorption mechanism of radioactive contamination in soil particles is characteristic.

In STS soils ^{137}Cs and $^{239+240}$Pu radionuclides, irrespective of a sampling point and the nature of radionuclide contamination in soils, are mainly available in their tightly bound forms. The

main forms of ^{241}Am in STS soils are mobile and tightly bound one. An increase in ^{241}Am mobility was observed in soils of "Degelen" area, RWA test area and in conventionally "background" territories. ^{241}Am tightly bound form predominates in soils of testing areas where surface nuclear tests were conducted including those of excavation ones.

Distribution of ^{90}Sr radionuclide speciation in STS soils in nonuniform and depends on mechanisms of how soil radioactive contamination is formed (radioactive particles). A tendency has been revealed in conventionally "background" territories of STS toward a decrease in parameters of ^{90}Sr bioavailability in areas adjacent to fallout "plumes" from nuclear tests and directly in zones of "plumes". A tendency toward higher mobility of ^{90}Sr is observed at "Atomic" lake site (excavation explosion) with increasing distance from the ground zero of an explosion.

Research results allow it to use ^{90}Sr speciation under STS conditions along with basic parameters as diagnosing sign to characterize radioactive contamination in background territories and identify fallout plumes from surface nuclear tests.

References

1. Speciation of radionuclides in the environment / B.Salbu, L.Skipperud // Journal of Environmental Radioactivity. – 2009. – No.100. – P. 281-282.
2. Jeffrey R. Bacon. Is there a future for sequential chemical extraction / Jeffrey R. Bacon, Christine M. Daidson // Analyst. – 2008. - No.133. - P. 25 - 46.
3. **Kunduzbayeva, A.Ye.** Speciation of artificial radionuclides in soils of "Experimental Field" ground. / A.Ye. Kunduzbayeva., S.N.Lukashenko, R.Yu. Magasheva // Proceedings of the National Nuclear Center of the Republic of Kazakhstan over 2011-2012. /edited by S.N. Lukashenko. – Vol.2. - Issue 4. - Pavlodar: Dom Pechati, 2013. – P. 181-208.
4. Topical issues in radioecology of Kazakhstan [Optimizing explorations of Semipalatinsk test site territories for the purpose of transferring them to the economic turnover] / under the guidance of. Lukashenko S.N.- Issue 5. – Pavlodar: Dom Pechati, 2015. – 500 p.
5. Isotopic composition of radioactive fallout / Yu. A. Israel. – L.: Gidrometeoizdat, 1973. – 109 p.
6. **Kadyrzhanov, К.К.** Peculiarities in the composition, speciation and distribution of radionuclides in different STS testing areas / K.K. Kadyrzhanov, S. Khazhekber, I.V. Kazachevsky, V.P. Solodukhin, S.N. Lukashenko // NNCRK bulletin. – 2000. - Issue 3. - P. 15-21.
7. **Logachyov, V.A.** Nuclear tests in USSR: present radioecological state of test sites. / Corporate authors under the guidance of prof. V. A. Logachyov - M.: Publishing House AT, 2002. - 639 p.
8. **Kunduzbayeva, A.Ye.** Speciation of artificial radionuclides in soils of a testing area of warfare radiological agents. / A.Ye. Kunduzbayevaa, A.Yu. Osintsev. S.N. Lukashenko, R.Yu. Magasheva // Proceedings of the National Nuclear Center of the Republic of Kazakhstan over 2011-2012. / edited by S.N. Lukashenko. – Vol.2. – Issue 4. – Pavlodar: Dom Pechati, 2013. – P. 167-180.
9. **Pavlotskaya, F.I.** Migration of radioactive products of global fallout in soils. / F.I. Pavlotskaya. – M.: Atomizdat, 1974. – 215 p.
10. **Ponomaryova, V. V.** Humus and soil formation (methods and study results) / V.V. Ponomaryova, T.A. Plotnikova. - L.: Nauka, 1980. – 222 p.
11. Activity of radionuclidesв in bulk samples. Measurement procedure with a gamma-spectrometer: MP 2143-91. - Intr. 1998-06-02. – Reg. No.5.06.001.98. – M.: SPA VNIIFTRI, 1991. - 17 p.
12. Instruction and guidelines to assess radiation situation in the contaminated territory. USSR Goskomgidromet, 17.03.89.
13. Measurement procedure of activities for such radionuclides as plutonium-238, plutonium-239+plutonium-240 in counting samples prepared from environmental samples. M.: FSUE SPA V.G. Khlopin Radium Institute.
14. **Prokhorov, V.M.** Migration of radioactive contamination in soils. / Edited by R.M. Aleksakhin. – M.: Energoizdat, 1981. - 98 p.

Transfer of Radionuclides to Plants of Natural Ecosystems at the Semipalatinsk Test Site

Larionova N.V., Lukashenko S.N.

Institute of Radiation Safety and Ecology, Kurchatov, Kazakhstan

Semipalatinsk Test Site (STS) was one of the largest test sites for nuclear tests conducting (Fig. 1). Each type of tests has been characterized by some definite amount and composition of radionuclides and their distribution.
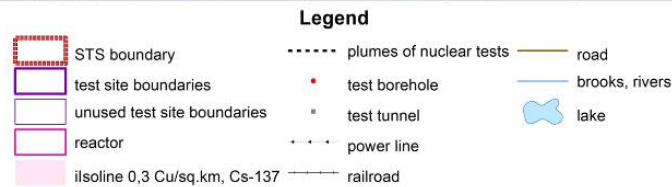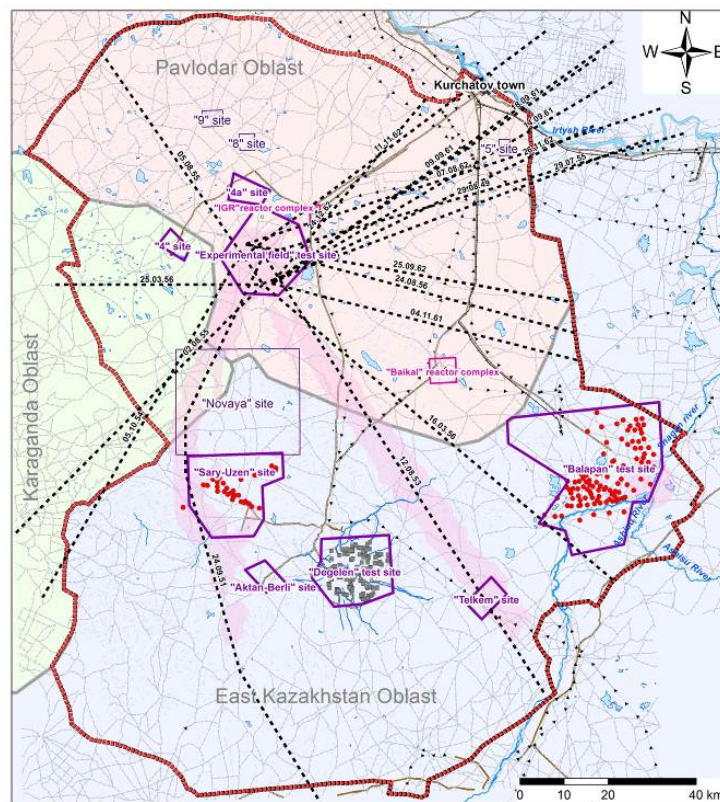
Fig. 1. Semipalatinsk Test Site (STS)

The largest input into radioactive contamination of the STS was made as a result of surface nuclear testing at the «Experimental field» site. Surface tests were cause of formation of

significant «plumes» of radioactive fallouts. The other type of contamination can be observed at the «Degelen» site. This site was used for underground nuclear tests in tunnels. Till today radionuclides are migrated from tunnels with water streams which are reason of the radioactive contamination of large areas around.

Two sites of STS - «4» and «4a» - were used for testing of warfare radioactive agents and they have unique radionuclides ratio in soil. Specific activity of ^{90}Sr here reaches several millions of Bq per kg, while concentration of other radionuclides is much lower. As a result of different types of tests there is different speciation of radionuclides at the STS. This, in turn, could lead to formation of artificial radionuclides with different bioavailability. However 90 % of the STS territories are characterized as areas with background levels of concentration of radionuclides.

Research on levels of radioactive contamination and accumulation parameters of artificial radionuclide's in plants were performed at all know sites of the STS, characterized by different types of radioactive contamination. Subjects of research were plant of meadow and steppe ecosystems, light-chestnut and meadow soils.

Ranges of radionuclides specific activity in soils are shown at table 1.

Table 1. Range of radionuclides specific activity in soils

Territory	Specific activity of radionuclides in soil, Bq/kg			
	^{137}Cs	^{90}Sr	$^{239+240}$Pu	^{241}Am
epicenters of the aboveground nuclear	$n*10^1$ - $n*10^3$	<100 - $n*10^4$	$n*10^2$ - $n*10^6$	$n*10^1$ - $n*10^5$
«plumes» of radioactive fallout	$n*10^1$ - $n*10^2$	$n*10^1$ - $n*10^3$	$n*10^{-1}$ - $n*10^2$	$n*10^{-1}$ - $n*10^1$
conditionally «background» areas	$n*10^{-1}$ - $n*10^1$	$n*10^{-1}$ - $n*10^1$	<1 - $n*10^1$	<1 - $n*10^{-1}$
zones of radioactive streamflows	$n*10^1$ - $n*10^5$	$n*10^2$ - $n*10^5$	$n*10^1$ - $n*10^4$	<1 - $n*10^2$
places of former tests of WRA	<4 - $n*10^2$	$n*10^4$ - $n*10^6$	-	-

Maximal concentration of transuranic radionuclides were found for epicenters of the aboveground nuclear testing, ^{137}Cs – for zones of radioactive stream flows, ^{90}Sr – for places of former tests of warfare radioactive agent.

Transfer factor was calculated and used as the main indicator of plants radioactive contamination. The table 2 shows arithmetical mean, range of values and number of cases in the different zones analyzed.

The distribution of transfer factors are shown in Figure 2 in the form of logarithms. As a result of consolidation of all data a comprehensive picture of concentration ^{137}Cs, ^{90}Sr, ^{241}Am and $^{239+240}$Pu in vegetative cover at the territory of the Semipalatinsk Test Site have been obtained (Fig. 2).

Table 2. Values of transfer factor (Tf) for investigated territories of the STS

Investigated territory	Tf			
	^{137}Cs	^{90}Sr	$^{239+240}$Pu	^{241}Am
Epicenters of the aboveground nuclear testing	0,0061 (n=72) 0,00023-0,07	0,065 (n=67)	0,0060 (n=66) 0,000011-0,13	0,0019 (n=73) 0,000004-0,064
«Plumes» of radioactive fallout	0,035 (n=42) 0,0012-0,30	0,097 (n=6) 0,014-0,2	0,0044 (n=7) 0,0014-0,0084	0,027 (n=28) 0,00050-0,42
Conditionally «background» areas	0,057 (n=41) 0,003-0,3	0,48 (n=17) 0,071-1,73	0,036 (n=33) 0,0019-0,21	0,041 (n=10) 0,0043-0,11
Zones of radioactive streamflow	1,1 (n=134) 0,0014-16	2,3 (n=138) 0,1-29	0,021 (n=32) 0,00016-0,13	<0,1 (n=31)
Places of former tests of WRA	0,023 (n=7) 0,018-0,03	6,6 (n=15) 0,74-49	-	-
in the numerator – arithmetical mean, in brackets – number of cases in the denominator – range of values				
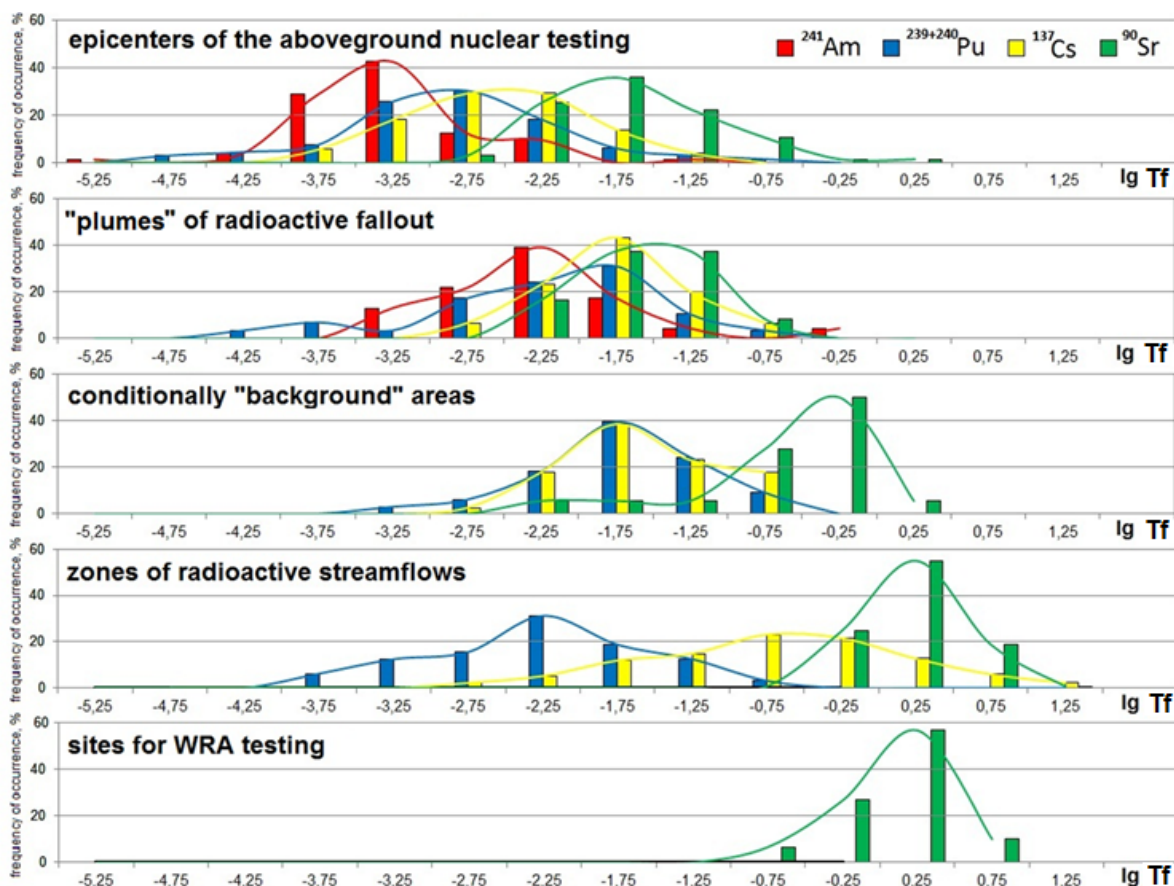
Fig. 2. Distribution of lg transfer factors (Tf) values for ^{241}Am, $^{239+240}$Pu, ^{137}Cs and ^{90}Sr for studied STS lands

Minimal transfer factors for all radionuclides had been found in epicenters of surface nuclear tests, a bit higher transfer factors had been found at «plumes» of radioactive fallouts and background territories. Zones of radioactive streams and places where warfare radioactive agents had been tested have maximal transfer factors.

Certain differences are observed for individual species of plants and soils, which are characterized by different physico-chemical properties. Specific peculiarities of plants cause differences in accumulation of radionuclide ^{137}Cs from 2 to 10 times, ^{90}Sr – from 2 to 6 times, $^{239+240}$Pu from 2 to 3 times, ^{241}Am – from 2 to 5 times.

The biggest differences were found in transfer factors for territories with different radionuclide contamination. These differences were for ^{137}Cs to 71 times, for ^{90}Sr to 74 times, for $^{239+240}$Pu to 14 times, for ^{241}Am to 11 times. Radionuclides by their ability to be accumulated by plants form the following range: ^{90}Sr – ^{137}Cs – $^{239+240}$Pu – ^{241}Am.

The received Tf could be used for development of methods on decrease radionuclide concentration in vegetation cover; to take decisions to hold remediation works; for assess of radioactive level of foods contamination and population dose.

Peculiarities of Radionuclide Build-up by Fruit and Berry Crops

T.E. Kozhahanov[*]*, S.N. Lukashenko, N.V. Larionova*

Institute of Radiation STFety and Ecology NNC RK, Krasnoarmeyskaya St. 2,
071100, Kurchatov city, Kazakhstan

Abstract

Solving problems related to farming in radioactively contaminated territories, takes a leading place in an action plan aimed at reduction of radionuclide concentrations in crop products. As of today, in the global practice transfer of artificial radionuclides into crop plants is well- studied, however, transfer of artificial radionuclides into fruit and berry crops still remains understudied.

This paper presents results of full-scale experiment of many years with fruit and berry crops raised under conditions of soil highly contaminated with radionuclides, first of all, with transuranium elements. The paper only covered one pathway of radionuclides into plants – that is consuming elements from soil with roots. Targets of research were 5 species of fruit and berry crops: codling, cherry-tree, plum- tree, raspberry and black currant.

As a result, quantitative parameters of ^{241}Am, ^{137}Cs, ^{90}Sr, $^{239+240}$Pu radionuclides transfer were found and their distribution in various parts of fruit and berry crops studied. Mean geometric values have been obtained for accumulation factors of radionuclides of interest. Accumulation dynamics of artificial radionuclides have been determined in leaves of fruit and berry crops for one crop season as well as several sequential years.

Keywords: Semipalatinsk test site (STS), radioactive contamination, radionuclides, plants, fruit and berry crops, transfer factors (TF),

Introduction

Consuming farm products of elevated concentrations of radioactive substances remains one of the major exposure sources to population residing or performing their economic activities in a radioactively contaminated territory. For that reason, quality of farm products to be obtained in territories exposed to radioactive contamination, is an important topical issue as of today.

This paper deals with findings of peculiarities of ^{137}Cs, ^{241}Am, ^{90}Sr and $^{239+240}$Pu accumulation in fruit and berry crops (apple-tree, cherry-tree, raspberry, plum-tree and black currant) when raise under conditions of radioactive contamination in the territory of the Semipalatinsk test site (STS) in venues of nuclear surface explosions.

Individual research was conducted to study transfer of transuranic elements from soil to fruit trees and the radionuclide distribution in separate plant bodies in different parts of the Earth [1,2,3,4,5,6]. IAEA has generalized all significant results from global studies on transfer of radionuclides from soil to plants and they are presented in a special handbook [7]. Despite that migration and transfer processes of individual radionuclides to fruit and berry products are quite well studied in the global practice, accumulation nature of ^{241}Am and $^{239+240}$Pu for these plants, still remains understudied. At our baseline for STS territory, information on radionuclide migration in the soil-fruit and berry crops system was not available.

Targets of research were fruit and berry crops of 5 species related to 3 different groups: the pomaceous (apple-tree), the drupaceous (cherry –tree and plum-tree) and berries (raspberry and black currant).

This paper aimed at the study of artificial radionuclides peculiarities accumulated by fruit and berry crops under conditions of radioactive contamination.

Research tasks:

1. To obtain quantitative parameters for radionuclide transfer from soil to fruit and berry crops;
2. To establish the nature of radionuclide distribution in various herb bodies;
3. To determine the dynamics of radionuclide build-up for one crop season as well as several sequential years.

Materials and Methods

The research was implemented by performing field, office, laboratory works and by analyzing findings. Based on dosimetric measurements (of β-particle flux density and equivalent dose rate (EDR)), an area was selected to station a pilot plot. Targets of research were 5 types of fruit and berry crops: codling (*Málus sylvéstris*), cherry-tree (*Prúnus cerásus*), plum-tree (*Prúnus doméstica*), raspberry (*Rúbus idáeus*) and black currant (*Ríbes nígrum*). Plants of interest were planted in the autumn-spring period of 2011-2012 for the apple-tree, cherry-tree and plum-tree as 2-year saplings, and for raspberry and black currant – as annual shoots.

System of farming included the following activities: agrotechnical (spring plowing of the plot, preparing holes to plant tree saplings, removing weedage), reclamative (artificial irrigation) and agrotechnical farming techniques (applying organic types of fertilizers).

As the main edible plant parts were ripening, fruits and berries were sampled (July), final sampling of aboveground parts of experimental plants was made in September. Plant samples, first of all leaves, were taken as composite samples, i.e. from trees and bushes of the lower, middle and upper parts of the leafy krone. In order to determine dynamics of radionuclide accumulation for 3 crops of interest: raspberry, cherry-tree and the apple-tree, plant samples were collected for one crop season (May to August), every 30 days. Once sampled in the field or in vitro, plant samples were divided by vegetative organs and weighed raw. Plant samples were placed in polyethylene bags and were furnished with data sheets [8]. Soil was sampled in duplication with that of plants (at five points of the experimental lot) at a depth of 0-25 cm. Further, middle soil samples were obtained by quartering for each experimental plot.

Specific activities of ^{137}Cs and ^{241}Am radionuclides was determined for soil and plants with a gamma-spectrometer "Canberra GX-2020", those of ^{90}Sr and $^{239+240}$Pu – using radiochemical isolation followed by measuring with a beta-spectrometer TRI-CARB 2900 TR and alpha-spectrometer Canberra (mod. 7401) respectively. To determine ^{90}Sr, a beta-spectrometer "Progress" was also applied. Concentrations of ^{137}Cs, ^{241}Am, ^{90}Sr and $^{239+240}$Pu radionuclides in plants were determined in ash followed by conversion on dry basis. Transfer factors (TF) were calculated to assess parameters of radionuclides transfer from soil to plants – the ratio of radionuclide concentration in unit mass of plants and soil respectively [9].

Results and Discussion

Values of activity concentration of ^{241}Am, ^{137}Cs, ^{90}Sr, $^{239+240}$Pu radionuclides in the soil of interest (0-25 cm layer) were 980 Bq/kg, 160 Bq/kg, 50 Bq/kg and 5500 Bq/kg respectively. For all plants of interest values of specific activities of radionucldies (on dry weight) vary for ^{241}Am - 0.3 to 71 Bq/kg, ^{137}Cs – 0.2 to 6.2 Bq/kg, ^{90}Sr – 12.0 to 99.7 Bq/kg and и $^{239+240}$Pu – 1.0 to 74.6 Bq/kg. Overall, for each organ of crops studied, TF for ^{90}Sr was $n \times 10^{-1}$, ^{241}Am, ^{137}Cs and $^{239+240}$Pu – $n \times 10^{-3}$- $n \times 10^{-2}$. Thus, TF of ^{90}Sr for plants of interest proved to be 1-2 orders of magnitude higher than TF for other radionuclides. It was determined that values obtained for radionuclides TF in crops of interest are commensurable with the international ones, however, for black currant fruits, mean values of TF of ^{241}Am $(1,7 \times 10^{-2})$ turned out a factor of 10 higher than those of maximum TF known.

It was found that accumulation for different species varies (leaves): ^{137}Cs – black currant $\geq$ raspberry $\geq$ plum-treec > cherry-tree > apple-tree; ^{90}Sr – apple-tree $\geq$ black currant $\geq$ cherry-tree > raspberry> plum-tree; ^{241}Am - raspberry > cherry-tree > apple-tree > black currant > plum-tree; $^{239+240}$Pu - raspberry > apple-tree > cherry-tree > black currant.

Mean values of radionuclide TF were obtained for aboveground parts (leaves) of fruit and berry crops. TF of ^{241}Am for leaves of apple-tree, cherry-tree, raspberry, black currant and plum-tree were 1.9×10^{-2}, 2.2×10^{-2}, 3.3×10^{-2}, 1.7×10^{-2} and 1.6×10^{-2} respectively. TF of ^{137}Cs for leaves of apple-tree, cherry-tree, raspberry, black currant and plum-tree were 7.0×10^{-3}, 1.0×10^{-2}, 1.3×10^{-2}, 1.4×10^{-2} and 1.2×10^{-2} respectively. ^{90}Sr TF for leaves of apple-tree, cherry-tree, raspberry, black currant and plum-tree were 6.7×10^{-1}, 6.4×10^{-1}, 6.0×10^{-1}, 6.5×10^{-1} and 3.8×10^{-1} respectively. $^{239+240}$Pu TF for leaves of apple-tree, cherry-tree, raspberry, black currant were 1.3×10^{-2}, 6.8×10^{3}, 2.7×10^{-2} and 1.5×10^{-3} respectively.

For plants of interest according to data over one year of research (the fourth year), distribution nature of ^{241}Am and ^{137}Cs radionuclides was determined in various organs of aboveground parts. In most cases, ^{137}Cs accumulation in fruits and berries proved to be higher than that in leaves and branches (apple-tree, cherry-tree, black currant), however, for raspberry the lowest accumulation of ^{137}Cs is observed in berries. ^{241}Am distribution in aboveground organs of plants has shown that in some cases it is higher in leaves, and in other cases - for branches in cases reviewed, at that, the least accumulation is characteristic of fruits (berries) in each case under review. Based on findings of radionuclide distribution in various organs of fruit and berry crops, descending accumulation series were drawn up:
1) ^{137}Cs – fruits > leaves > branches (apple-tree, cherry-tree, black currant), leaves > branches $\geq$ fruits (raspberry), branches > leaves (plum-tree);
2) ^{241}Am – leaves > branches > fruits (apple-tree, raspberry, black currant and plum-tree) and branches > leaves > fruits (cherry-tree).

To assess the dynamics of radionuclide accumulation for one crop period May through August, there were 2 different species of fruit and berry crops selected that related to essentially different biological groups: the pomaceous (apple-tree) and the drupaceous (cherry-tree). Data obtained indicates that radionuclide accumulation takes place differently in various phases. Thus, for the apple-tree from blossoming to fruit ripening, ^{137}Cs concentration in leaves decreases, and after the fruiting stage is completed (growth of fruits) it increases insignificantly. ^{241}Am radionuclide accumulation in leaves of the apple-tree from fruiting and to the end of sprout growth gradually rises. For cherry-tree, ^{137}Cs build-up goes down from blooming stage and to the time sprouts stop growing. Maximum concentration of ^{241}Am in leaves of cherry-tree is observed in the blooming stage, and after blooming until fruit growth, it decreases followed by insignificant increase in the phase when sprouts stop growing.

^{137}Cs TF data for the apple-tree, cherry-tree and raspberry turned out to be close in value and vary slightly for a few years which may indicate the absence of relationship between ^{137}Cs accumulation and plant ages. By its accumulation feature ^{90}Sr for apple-tree, raspberry and cherry-tree one can mention insignificant increase in the radionuclide for leaves of the apple-tree and some decrease in ^{90}Sr accumulation on the 2nd and 3rd year of plant development for cherry-tree and raspberry leaves. However, as is the case with ^{137}Cs, no clear dependency of ^{90}Sr accumulation for fruit and berry plants, as time passed, was established.

The most distinct picture of radionuclide accumulation nature for a long period (4 years) has been obtained for apple-tree, raspberry and black currant for ^{241}Am. Thus, steady increase of ^{241}Am concentration in leaves of plants for several years running, is observed for apple-tree, black currant and raspberry. The exception is cherry-tree for which there is no such dynamics of the radionuclide accumulation. Maximum accumulation of ^{241}Am radionuclide for 4-year periods can be observed in very crops (black currant and raspberry).

Conclusions

1. It was found that obtained values of radionuclides TF for crops of interest are commensurable with international ones, however, for currants, TF values were obtained that exceed world data for ^{241}Am by a factor of 10.
2. Accumulation for different species of varies: ^{137}Cs - black currant≥ raspberry ≥ plum-tree > cherry-tree > apple-tree; ^{90}Sr - apple-tree ≥ black currant≥ cherry-tree > raspberry > plum-tree; ^{241}Am - raspberry > cherry-tree > apple-tree > black currant> plum-tree; $^{239+240}$Pu - raspberry > apple-tree > cherry-tree > currant.
3. It was found that radionuclides distribution in organs of species studied is of non-uniform nature: ^{137}Cs – fruits> leaves > branches (apple-tree, cherry-tree and currant), leaves > branches ≥ fruits (raspberry), branches > leaves (plum-tree); ^{241}Am – leaves > branches > fruits (apple-tree, raspberry, black currant and plum-tree) and branches > leaves > fruits (cherry-tree).
4. It was determined that during one crop season, maximum concentration of ^{137}Cs in leaves of apple-tree and cheery-tree falls on blooming stage, and that of ^{241}Am – on the stasis stage of the apple-tree and cherry-tree blooming stage.
5. On the whole, there has been no clear accumulation dependency for ^{137}Cs and ^{90}Sr radionuclides identified in fruit and berry plants with the course of time. Insignificant decrease of ^{90}Sr accumulation, as time passed, can be observed in leaves of cherry-tree and on the contrary, increase in ^{90}Sr accumulation in leaves of apple-tree and cherry-tree.
6. Steady growth was found in ^{241}Am accumulation for several years in leaves of apple-tree, currant and raspberry.

1　Velasco, H., Cid, A.S., Anjos, R.M., Zamboni, C.B., Rizzotto, M., Valladares, D.L., Juri Ayub, J. // Journal of Environmental Radioactivity. Feb. 2012, Volum 104, P. 64-70.
2　Joshy P. James, B.N. Dileep, P.M. Ravi and other Soil to leaf transfer factor for the radionuclides ^{226}Ra, ^{40}K, ^{137}Cs and ^{90}Sr at Kaiga region, India // Journal of Environmental Radioactivity. – 2011. - Volume 102 – Issue 12 – P. 1070-1077.
3　Al-Oudat, M. , Asfary, A.F., Mukhalallti, H., Al-Hamwi, A., Kanakri, S. Transfer factors of ^{137}Cs and ^{90}Sr from soil to trees in arid regions // Journal of Environmental Radioactivity. - 2006 - Volume 90 - Issue 1 – P. 78-88.
4　M.S. Al-Masri, B. Al-Akel, A. Nashawani, Y. Amin, K.H. Khalifa, F. Al-Ain // Journal of Environmental Radioactivity. - 2008 – Volume 99 – Issue 2 – P. 219-436.
5　F.Carini, G.Bengtsson Post-deposition transport of radionuclides in fruit // Journal of Environmental Radioactivity. - 2001 – Volume 52 – Issue 2-3 – P. 215-236.
6　C.J Atkinson, A.D Webster The influence of the development of temperate fruit tree species on the potential for their uptake of radionuclides// Journal of Environmental Radioactivity. - 2001 – Volume 52 – Issue 2-3 – P. 131-146
7　Handbook of Parameter Values for the Prediction of Radionuclide Transfer in Terrestrial and Freshwater Environments / Technical Reports Series No. 472. – Vienna: IAEA, 2010.
8　Instruction and guidelines for terrestrial survey of radiation situation in the contaminated territory: approved by the Interagency Commission for Radiation Monitoring of Natural Environment under USSR Goskomgidromet. – M., 1989.
9　Annenkov B.N. Fundamentals of agricultural radiobiology / B.N. Annenkov, Ye.V. Yudintseva. – Moscow, 1991. – P. 56-83.

Investigation of distribution of radioactive contamination in the water objects of the Semipalatinsk test site

A.K. Aidarkhanova, S.N. Lukashenko

Institute of Radiation Safety and Ecology, National Nuclear Center of the Republic of Kazakhstan, Krasnoarmeyskaya 2, 071100 Kurchatov, Kazakhstan

Abstract

This paper provides research data on levels and character of radionuclide contamination distribution in the «water- sediments» system of objects of the Semipalatinsk test site (STS) and adjacent territories. As the research objects there were chosen water reservoirs and streamflows of «Experimental Field», «Balapan», «Degelen», «Telkem» and adjacent territories as well as the Shagan and Irtysh rivers. At selected objects conjugate samples of water and bottom sediments were taken. Collected samples were used to determine concentration of artificial radionuclides ^{90}Sr, $^{239+240}$Pu, ^{241}Am, ^{137}Cs and ^{152}Eu. As a result of research carried out transfer factors (TF) were calculated that allowed assessment of expected levels of radioactive contamination in water objects. The research carried out has shown that most of technogenic radionuclides (except in some cases of ^{90}Sr) in the «water-sediments» system accumulated in sediments.

Introduction

Surface water is vital to man in performing their economic activities; therefore assessing radionuclide contamination in surface water in the territory of the former Semipalatinsk test site (STS) is a top-priority issue.

Surface water of STS are presented as the following types of sites:
- water objects of technogenic origin;
- water objects of naturally occurring;
- stream flows.

Water objects of technogenic origin in the territory of testing areas («Experimental Field», "Balapan", "Telkem") are generally craters filled with water and formed due to surface or excavation explosions conducted. Water objects of naturally occurring are small-area natural lakes the bulk of which dry up by the middle of summer. The main stream flows of STS territory are streams in "Degelen" area and Shagan river, which flows along the boundary of "Balapan" area and goes beyond the STS border.

Bottom sediments play a crucial role in forming hydrochemical regime of water and in functioning of ecosystems of reservoir and stream flows [1, 2, 3]. The bulk of contaminants entering water objects is adsorbed by mineral and organic particles, deposits at the bottom and is accumulated in sediments [4, 5]. Therefore, a crucial source of information on the state of aquatic ecosystems can be contamination of sediments.

Accumulation capability of sediments with respect to radionuclides is quantitatively characterized by a transfer factor (TF) which is calculated as the ratio of radionuclide concentration in sediments to that of in water [6]. The physical meaning of TF is that it shows the transfer degree of radionuclides from water to sediments: the higher TF, the more intense this transfer is. According to

numerous literature sources, TF values, on average, decrease $n\times10^5$ to $n\times10^0$ for radionuclides in the series of $^{239,240}Pu>^{137}Cs>^{90}Sr$ [7, 8, 9 ,10]. According to data from IAEA, recommended TF to sediments of the ocean coast for the following elements are: Am – 2×10^6, Pu – 1×10^5, Cs – 4×10^3 and Sr – 8×10^0 [11, p. 18-21].

Materials and Methods

Research objects

Research objects were surface water and stream flows of STS territory shown in Figure 1.
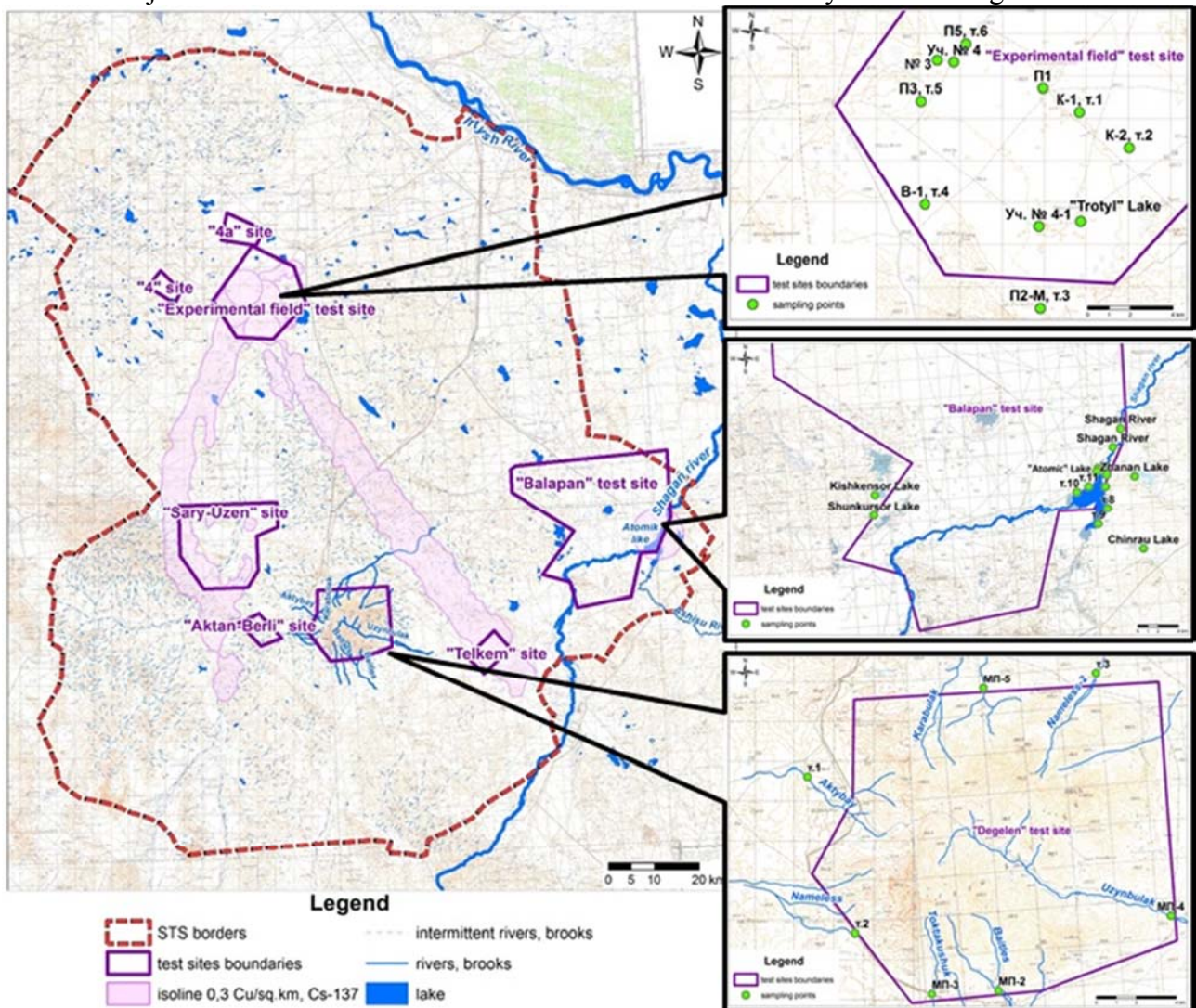
Figure 1. Surface water of STS territory.

Water objects on the "Experimental Field" ground are craters of different diameter formed as a result of air and surface tests, filled with water and overgrown in common reed (*Phragmites australis*). Overall, this ground numbers 10 water objects like that.

The "Atomic" lake and "Telkem-1", "Telkem-2" are water objects formed as a result of excavation explosions of soil ejection which aimed at creation of artificial reservoirs.
"Atomic" lake was formed as a result of the 15.01.65 explosion of 140 kt yield at the confluence of Shagan and Ashchisu rivers which resulted in a crater of more than 100 m deep and 400 diameter that was filled with water. A water reservoir was formed in the southern and southeastern direction

from the embankment around the "Atomic" lake. The water reservoir area changed and in 2015 it was about 9 km^2.

In the southeastern part of STS, two underground nuclear tests were conducted with soil ejected: a single explosion at "Telkem-1" (21.10.1968) and a coyote one (consisting of three linearly arranged charges) – "Telkem-2" (12.11.1968). Craters formed were filled with water and formed the lakes "Telkem-1" of 90 m diameter and 15 m deep and "Telkem-2", a prolate-shaped lake of 120 m long, 60 wide and 10 m.

Shagan river is the main surface stream flow within STS. It flows along the eastern border of "Balapan", goes beyond STS and the left bank tributary of Irtysh river. Within STS the riverbed is about 50 km long. The discharge of the river in the summer period is 3 m^3 per minute. Being shallow, Shagan is characterized by low flow rate, branchings, dead end backwaters, bogged up banks [12]. Based on previous research conducted by the Institute of Radiation Safety and Ecology, high ^{3}H concentration was registered and repeatedly corroborated in the region of 5 km away from the "Atomic" lake. So, this paper deals with a section of Shagan river from the "Atomic" lake as far as 5 km.

Streams in "Degelen" testing area such as Uzynbulak, Karabulak, Toktakushuk and Baitles, located in the zone impacted by tunnel stream flows, are also of some interest. The largest water source of all the streams at Degelen mountain massif is Uzynbulak. The valley of Uzynbulak stream extending for about 20 km away, has the largest catchment area. About 50 tunnels are adjacent to the stream itself and its tributaries [13]. At the sampling point, at the boundary of Degelen area the stream width is about 1 m, depth is 0.5 m. Streams Toktakushuk and Baitles are located in the southern part of Degelen testing area. Toktakushuk has no tributaries. Baitles stream forms two main tributaries, a third left-side one flows into the main bed beyond the mountain massif. The extent of Toktakushuk stream valley is about 10–12 km, that of Baitles over 15 km. Karabulak stream is located in the northern part of the area and consists of two tributaries, a third tributary flows into the main bed beyond the mountain massif. The total extent of the stream is some 30 km, within Degelen area - some 4 km. Sampling points around these streams were at the boundary of Degelen testing area where the width of beds was about 0.5 m, depth – 20-25 cm.

Samples

For research, duplicate water and sediment samples were collected from sites. Sediments were sampled at a depth of 0 – 10 cm. Water was samples from a ground layer of 0 – 15 cm. Water samples of 10 l were taken from STS sites. All of the samples were delivered to the laboratory in the shortest possible time. Samples of sediments were transferred for analysis. Water samples were filtered and preserved by concentrated nitric acid to pH=2. A preserved sample was stored prior to analysis but for 30 days at the longest [14, 15].

Radiometric technique

Concentration of technogenic radionuclides ^{90}Sr, $^{239+240}$Pu, ^{241}Am, ^{137}Cs was determined in samples collected.
γ-spectrometric measurements to determine concentrations of ^{241}Am and ^{137}Cs were carried out in sediments after drying [16]. ^{90}Sr concentration was determined by β-spectrometric measurements for daughter ^{90}Y following prior radiochemical isolation. $^{239+240}$Pu concentration was determined be means of α-spectrometric analysis following prior extraction and chromotographic separation and electrolytic precipitation. [17]

[241]Am concentration was determined in 10 l water samples by γ-spectrometric measurements. Then, samples were concentrated be means of co-precipitation technique. [137]Cs concentration was determined by γ-spectrometric measurements after co-precipitation with copper hexacyanoferrate. [90]Sr concentration was determined by β-spectrometric measurements for daughter ^{90}Y following prior co-precipitation with calcium carbonate and radiochemical separation. [239+240]Pu concentration was determined be means of α-spectrometric analysis after it was previously co-precipitated with ferrum hydroxide (III), extraction and chromatographic separation and electrolytic precipitation [18].

Results and Discussion

Concentrations of technogenic radionuclide in water samples and sediments of water objects and stream flows in STS territory as well as their transfer factors (TF) are presented in Table 1 and 2 respectively.

According to findings TF depend on a type of a water object. As previously noted, type 1 includes water objects of technogenic origin in the territories of "Experimental Field", "Sary-Uzen", "Telkem" testing areas and the "Atomic" lake. These are craters formed due to surface or excavation explosions and filled with water. Their depths vary from 10 to 80 m. These water objects (except for the "Atomic" lake) have no tributaries and are drainless, i.e. in fact water does not intermix. As far as the "Atomic" lake is concerned, based on the earlier research [19] it was proved that even with a tributary available, changes occur only in the surface layer of 15-20 m, bottom layers remain unchanged. Very high TF are characteristic of such water objects even for such a mobile radionuclide as [90]Sr: for [239+240]Pu TF values are some 1.0×10^8 to 7.5×10^2, for [137]Cs – $>1.3 \times 10^6$ to 3.5×10^2, for [90]Sr – 1.3×10^4 to 2.0×10^1.

Type 2 includes water objects of naturally occurring: natural lakes that do not have any tributaries either being drainless. The depth of these lakes do not exceed 1.5-2 m. Most of natural lakes in the test site territory dries up by the middle of summer. Nevertheless, TF for these water objects are also very high: for [239+240]Pu TF values vary about from $>1.5 \times 10^6$ to $>4.3 \times 10^3$, for [137]Cs – $>1.5 \times 10^5$ to 3.2×10^3, for [90]Sr – $>2.6 \times 10^3$ to 4×10^1.

Type 3 includes stream flows: streams of Degelen area and Shagan river. Low TF values were obtained for these sites: for [239+240]Pu TF values vary from some $>1.5 \times 10^5$ to 2.7×10^2, for [137]Cs – $>1.5 \times 10^3$ to $>9 \times 10^2$, for [90]Sr – 1.5×10^2 to 4.8×10^0. This is due to the fact that water in this system is a mobile dynamic medium which does not allow radionuclides to be fully accumulated in sediments.

Conclusions

Despite that TF for different technogenic radionuclides differ by several orders of magnitude for various types of water objects on average from $n \times 10^4$ to $n \times 10^2$, it is significantly higher than 1. This is indicative that most of radionuclides of interest in the "water – sediments" system are concentrated in sediments. The only exception is ^{90}Sr for which a TF was obtained in some cases equal to $n \times 10^0$, which indicated a uniform ^{90}Sr distribution in the "water – sediments" system. In this case, when numerical values of this radionuclide concentration in sediments are obtained, it becomes necessary to determine its concentration in water.

Thus, the condition of sediments is the most informative indicator in radioecological assessment of a water object.

References

1 Handbook for Sediment Quality Assessment, Simpson S.L., Batley G.E., Chariton A.A. et al., Bangor, CSIRO, 2005. – 117 p.

2 Man-made contamination in river ecosystems /Edited by Rainin V. N., Vinogradova G.N. - M.: Nauchny mir, 2002. – 140 p.

3 Tomilina I.I., Komov V.T. Bottom sediments as a target of toxicity research (review) // Biology of inland water, 2002. - № 2. – P. 20-26.

4 Mizandrontsev I.B. Chemical processes in bottom sediments of water bodies / I.B. Mizandrontsev. - Novosibirsk: Nauka, 1990. - 176 p.

5 Handbook of Parameter Values for the Prediction of Radionuclide Transfer in Terrestrial and Freshwater Environments, Technical Reports Series No. 472, IAEA, Vienna, 2010.

6 ICRU Report 65. Quantities, Units and Terms in Radioecology. J. ICRU. vol. 1, 2, 2002

7 Pirnach L.S. Radioactive contamination in sediments of a ChNPP heat sink. II. ^{137}Cs, ^{241}Am, ^{90}Sr distribution in soil solid phase // Nuclear physics and power engineering: Radiobiology and radioecology, Vol. 12, № 4, 2011.

8 Tereshchenko N.N. Leading role by bottom sediments in redistribution of plutonium in Black Sea region ecosystems. Наукові праці: науково-методичний журнал. Серія: Техногенна безпека.– Миколаїв: Вид-во ЧДУ ім. Петра Могили, 2011.– т.169, вип.157.– С.63-70.

9 Tereshchenko N.N., Polikarpov G.G., Krylova T.A. Role of barriers at the Black Sea with respect to $^{239+240}$Pu, ^{137}Cs, ^{90}Sr – the major technogenic dose-forming radionuclides in the post-Chernobyl period // Ecosystems, their optimization and protection. Issue 7, 2012. – p. 243-250.

10 Levina S.G., Akleyev A.V., Deryagin V.V., Udachin V.N., Korman G.G., Sutyagin A.A., Mukhametshina L.F. Peculiarities of long-lived radionuclide and trace elements accumulation in soils of water collecting areas at lakes Bolshoy and Malyy Igish in the post-accident period (middle part of EURP) // radiation safety issues –2009. – №1. - P. 63-72.

11 Sediment Distribution Coefficients and Concentration Factors for Biota in the Marine Environment, Technical Reports Series No. 422, IAEA, Vienna (2004).

12 Aidarkhanov A.O. State of Shagan river ecosystem and the main mechanisms of how it is formed/ A.O. Aidarkhanov, S.N. Lukashenko, S.B. Subbotin [et al.]. // Topical issues in radioecology of Kazakhstan [Proceedings of the Institute of Radiation Safety and Ecology over 2007 – 2009.] / under the guidance of Lukashenko S.N. – Pavlodar: Dom Pechati, 2010. – Issue 2. – P. 9-56.

13 Panitsky A.V. Characteristic features of radioactive contamination in natural environment components of stream flow ecosystems in tunnels of Degelen mountain massif / A.V. Panitsky, S.N. Lukashenkko, R.Yu. Magasheva // Topical issues of radioecology in Kazakhstan [Proceedings of the Institute of Radiation Safety and Ecology over 2007 – 2009] / under the guidance of Lukashenko S.N. – Pavlodar: Dom Pechati, 2010. – Issue 2. – P. 57-102.

14 GOST 24481-80. Potable water. Sampling. - Appr.1980-29-12. № 6043. - M.: Izdatelstvo standartov,1993. -5 p.

15 Collection and Preparation of Bottom Sediment Samples for Analysis of Radionuclides and Trace Elements, IAEA-TECDOC-1360, IAEA, Vienna, 2003.

16 RK MP 2143-91 "Activity of radionuclides in bulk samples. Measurement procedure with a gamma-spectrometer". - Intr. 1998-06-02. – Reg. No. № 5.06.001.98. - M.: SPA VNIIFTRI, 1991. - 18 p.

17 Procedure to determine plutonium – (239+240), strontium-90 and americium-241 isotopes in environmental sites (soil, plants, natural waters). № 06-7-98 dated March 4, 1998 – Almaty: Almaty SE "TSSMS"(Centre of Standardization, Metrology and Certification), 1998.

18 Procedure to determine ^{239,240}Pu, ^{90}Sr and ^{137}Cs artificial radionuclides in natural waters by concentration. – INP NNC RK, registration No.0307/3 dated 5.04.2001.

19 Aktayev M.R., Lukashenko S.N., Aidarkhanov A.O. Nature of radioactive contamination with artificial radionuclides of the Shagan river and "Atomic" lake / Meeting in St. Petersburg: Fourth International Conference, Dedicated to N.W. Timofeeff-Ressovsky and His Scientific School "Modern Problems of Genetics, Radiobiology, and Evolution", St. Petersburg, 2-6 June 2015: Abstracts, Papers by Young Scientists. – Dubna: JINR, 2015. – 272 p.

Table 1. Contents of radionuclides in sediments and water of reservoirs, and transfer factors

	Sampling point	Specific activity ^{137}Cs, Bq/kg		TF	Specific activity ^{90}Sr, Bq/kg		TF	Specific activity $^{239+240}$Pu, Bq/kg		TF
		Sediment	Water		Sediment	Water		Sediment	Water	
«Experimental field»	Site № 3	$(4,7\pm0,9)\cdot10^3$	< 0,04	>$1,2\cdot10^5$	$(3,5\pm0,5)\cdot10^4$	75 ± 7	$4,7\cdot10^2$	$(1,1\pm0,1)\cdot10^4$	$(1,7\pm0,3)\cdot10^{-2}$	$6,5\cdot10^5$
	Site № 4	$(9,3\pm1,9)\cdot10^4$	$2,8\pm0,2$	$3,3\cdot10^4$	$(4,2\pm0,6)\cdot10^3$	$(2,4\pm0,2)\cdot10^2$	$1,8\cdot10^1$	$(3,0\pm0,2)\cdot10^6$	$(2,9\pm0,5)\cdot10^{-2}$	$1,0\cdot10^8$
	P1	$(1,2\pm0,2)\cdot10^3$	< 0,01	>$1,2\cdot10^5$	14 ± 2	$1,1\pm0,2$	$1,3\cdot10^1$	$(1,7\pm0,2)\cdot10^3$	$(1,0\pm0,2)\cdot10^{-2}$	$1,7\cdot10^5$
	K-1, p.1	14 ± 3	< 0,01	>$1,4\cdot10^3$	14 ± 2	$(3,0\pm0,4)\cdot10^{-2}$	$4,7\cdot10^2$	21 ± 5	$(2,3\pm0,4)\cdot10^{-2}$	$9,1\cdot10^2$
	K-2, p.2	18 ± 4	< 0,02	>$9,0\cdot10^2$	55 ± 8	$0,08\pm0,01$	$6,8\cdot10^2$	$(1,2\pm0,2)\cdot10^2$	$(0,6\pm0,2)\cdot10^{-2}$	$2,0\cdot10^4$
	«Trotyl» Lake	$8,1\pm1,6$	< 0,01	>$8,1\cdot10^2$	280 ± 40	$(2,2\pm0,3)\cdot10^{-2}$	$1,3\cdot10^4$	$(6,3\pm1,0)\cdot10^2$	$(2,5\pm0,3)\cdot10^{-2}$	$2,5\cdot10^4$
	Site № 4-1	81 ± 16	< 0,01	>$8,1\cdot10^3$	17 ± 3	$0,09\pm0,01$	$1,9\cdot10^2$	$(1,2\pm0,1)\cdot10^3$	$(0,7\pm0,2)\cdot10^{-2}$	$1,7\cdot10^5$
	P2-M, p.3	$6,9\pm1,7$	< 0,02	>$3,5\cdot10^2$	8 ± 1	$0,08\pm0,01$	$1,0\cdot10^2$	$(9,3\pm0,6)\cdot10^2$	$(5,0\pm0,2)\cdot10^{-1}$	$1,8\cdot10^3$
	B-1, p.4	$(1,3\pm0,3)\cdot10^4$	< 0,01	>$1,3\cdot10^6$	$(6,9\pm1,0)\cdot10^2$	$2,5\pm0,4$	$2,7\cdot10^2$	$(1,3\pm0,1)\cdot10^5$	$(1,1\pm0,1)\cdot10^{-1}$	$1,2\cdot10^6$
	P3, p.5	<1,4	< 0,03	-	$2,8\pm0,7$	$1,4\pm0,2$	2	$7,5\pm1,7$	$(1,0\pm0,2)\cdot10^{-2}$	$7,5\cdot10^2$
	P5, p.6	$(1,0\pm0,2)\cdot10^4$	< 0,01	>$1,0\cdot10^6$	$(1,1\pm0,2)\cdot10^3$	$1,0\pm0,2$	$1,1\cdot10^3$	$(1,9\pm0,2)\cdot10^4$	$(2,3\pm0,4)\cdot10^{-2}$	$8,3\cdot10^5$
«Atomic» Lake		$(5,3\pm1,1)\cdot10^3$	< 0,01	>$5,3\cdot10^5$	$(3,1\pm0,5)\cdot10^3$	$0,29\pm0,04$	$1,1\cdot10^4$	$(5,3\pm0,4)\cdot10^3$	$(0,6\pm0,3)\cdot10^{-3}$	$8,8\cdot10^6$
Telkem-1		$(2,2\pm0,2)\cdot10^3$	< 0,03	>$7,3\cdot10^4$	$(5,2\pm0,8)\cdot10^2$	$(2,0\pm0,2)\cdot10^2$	2,6	$(9,9\pm0,5)\cdot10^4$	$(4,7\pm0,9)\cdot10^{-2}$	$2,1\cdot10^6$
Telkem-2		$(2,1\pm0,2)\cdot10^3$	< 0,03	>$7,0\cdot10^4$	$(4,0\pm0,6)\cdot10^2$	$(1,3\pm0,1)\cdot10^2$	3,1	$(9,8\pm0,6)\cdot10^4$	$(1,0\pm0,1)\cdot10^{-1}$	$9,8\cdot10^5$

Table 1. Contents of radionuclides in sediments and water of streams, and transfer factors

	Sampling point	Specific activity ^{90}Sr, Bq/kg		TF	Specific activity $^{239+240}$Pu, Bq/kg		TF
		Sediment	Water		Sediment	Water	
Shagan River		44 ± 7	$0,9\pm0,1$	$4,8\cdot10^1$	17 ± 4	< $1,1\cdot10^{-4}$	>$1,5\cdot10^5$
"Degelen"	Karabulak	210 ± 30	$1,4\pm0,2$	$1,5\cdot10^2$	99 ± 10	$(6,8\pm0,9)\cdot10^{-3}$	$1,5\cdot10^4$
	Toktakuchuk	13 ± 2	$0,09\pm0,01$	$1,4\cdot10^2$	$1,6\pm0,5$	$(6,0\pm1,3)\cdot10^{-3}$	$2,7\cdot10^2$
	Baitles	100 ± 20	$1,3\pm0,2$	$7,7\cdot10^1$	$8,6\pm1,2$	$(6,4\pm0,9)\cdot10^{-3}$	$1,3\cdot10^3$
	Uzynbulak	55 ± 8	$1,0\pm0,2$	$5,5\cdot10^1$	$2,8\pm0,8$	$(5,7\pm0,8)\cdot10^{-3}$	$5,0\cdot10^2$

Parameters of transfer $^{239+240}$Pu, ^{241}Am, ^{137}Cs, ^{90}Sr and ^{3}H into body of farm animals and poultry at the Semipalatinsk Test Site condition

Zh. Baigazinov[*]*, S. Lukashenko, A. Panitskiy, S. Karataev,*
S. Baigazy, A. Mamyrbaeva

Institute of Radiation Safety and Ecology NNC RK, Department of integrated Ecosystem studies,
Krasnoarmeyskaya st. 2, 071100 Kurchatov, Kazakhstan

As the result of operation of Semipalatinsk Test Site (STS) for the period from 1949 to 1989 local spots with high concentrations of radionuclides in environment were formed at its territory. After it was officially closed, inhabitants of the nearby localities have actively started performing unauthorized economic activities. As the result, nowadays there is approximately 100 farming enterprises continuously performing cattle-breeding works out of control. The types of cattle breeding operations typical for this area are, cattle breeding and horse breeding at extensive steppe lands.

It is commonly known, that the transfer of radionuclides into cattle breeding products can be determined by multiple factors, including the level and the character of pasture lands contamination, type of animals' diet and its components, types, age and productivity of animals, technology of their management etc. (Alexakhin, 1992). The world-wide available knowledge on transfer of ^{137}Cs and ^{90}Sr into cattle-breeding and poultry products is extensive enough (Sirotkin, 1991, Green, 2003). However, most of it was obtained in laboratory conditions or the territories contaminated as the result of radiation accidents [Fesenko, 2009], those differ from the STS territory both in character of radioactive contamination and natural-climatic conditions. Only singular works were dedicated to transfer of artificial radionuclides (Pu, Am) and ^{3}H into cattle and poultry products (Averin, 2014, Buldakov, 1968), In some cases there is no data available (IAEA, 2010).

The main contributors to the environmental contamination at the STS territory are ^{137}Cs, ^{90}Sr, $^{239+240}$Pu, ^{241}Am and ^{3}H. At that if high activities of radionuclides ^{137}Cs, ^{90}Sr, $^{239+240}$Pu and ^{241}Am present directly at the territory of the test sites («Experimental Field», «Degelen», «4a» and ect.) increased activity of ^{3}H can be found in water sources beyond these sites and beyond the STS (Lyakhova, 2008).

The foregoing information has identified the relevance of this study, the purpose of which was to study the distribution and parameters of radionuclides' transfer into bodies of some species of farm animals and birds under the STS conditions. In particular:

1. to study the dynamics of transfer and distribution of $^{239+240}$Pu, ^{241}Am, ^{137}Cs and ^{90}Sr radionuclides in organs and tissues of farm animals;

2. to determine the parameters of $^{239+240}$Pu, ^{241}Am, ^{137}Cs and ^{90}Sr radionuclides' transfer from forage and soil from the epicenters of surface nuclear tests and radioactive streamflows' zones, as well as from water into organs and tissues of various species (sheep and horses) and ages (mares and fillies) of farm animals:

---

[*] Corresponding author, E-mail: baigazinov@nnc.kz

3. to study the parameters of ^{3}H transfer into poultry products (chicken meat and eggs), sheep breeding products (meat) and horse breeding products (milk) for various terms of its entry with environmental components (air, water, forage);

4. to assess a possibility of cattle breeding activities at the STS territory.

As the objects of research the animals most widely spread and typical for this region (small cattle, black cattle, horses) and farm birds (laying hens) were chosen. Sheep were represented by two-year wethers of Kazakh fat-tailed coarse wool breed ("Edilbaevskaya"), with the living weight of 51±3 kg (the total of 6 groups, 5 heads in each). Horses are represented by typical for this region outbred (mixtures of Kazakh horses) breeding mares aged from 10 to 12 and one-year old fillies, with the living weight of 350–400 kg and 150–200 kg respectively (2 groups with 2 heads in each.). Farm birds are represented by laying hens aged of 1,5 years (3 groups, 18 heads each). Animals and birds in the groups were similar in health condition, exterior and body type characteristics and productivity.

All the researches were carried out in summer time keeping the animals and laying hens in confinedness. Some individual groups of birds and animals were fed with contaminated forage and soil, collected at the territory of the epicenter of surface test and the zones of radioactive streamflows, watered with contaminated water, in some case radionuclide-containing solutions were added to the forage.

Terms of keeping sheep on contaminated forage – 7, 14, 28, 56, 112 days, horses – 56 days, laying hens – 1, 3, 7, 14, 21, 28, 36, 50, 55 days. At the end of each period, animals and birds were slaughtered. The following parts were sampled for analysis: liver, kidneys, lungs, heart, spleen, crural muscle, bone tissue, broadtail fat, wool, skin, tongue and brain. To control the entry of radionuclides into bodies of animals and birds for the whole period of the experiment each day the amount of consumed forage, soil and water were registered and also samples of vegetation, soil and water were collected according to the scheme of the experiment. After that the samples were subjected to spectrometric measurements.

The radionuclides of interest were $^{239+240}$Pu, ^{241}Am, ^{137}Cs , ^{90}Sr and ^{3}H. Samples of organs and tissues of small cattle were measured via gamma-spectrometer (for ^{137}Cs, ^{241}Am) as a raw substance. Organs and tissues of fetuses and the bone tissue of mature animals were preliminarily ashed (380°C). After that the ashes were measured using spectrometer with semiconductor Ge-based detector by CANBERRA.

Specific activity of $^{239+240}$Pu in samples was determined using radiochemical extraction methods with subsequent measurement via "Alpha Analyst" alpha-spectrometer by "Canberra". The detection limit for $^{239+240}$Pu was 0,1 Bq/kg. Error in measurements mainly did not exceed 30%. The method of ^{90}Sr determination is based on transferring strontium isotopes into solution, extraction of chemically pure strontium isotopes, two week accumulation of Y-90 and measuring its activity using «TriCarb-3100» liquid-scintillation spectrometer. The quality control of analytical results was provided by RK GSO 72/IAEA -134 measurements (body of a shell). The deviations between measurement results of samples and the standard sample satisfy the requirements of the measurement technique used and did not exceed 20% for all intervals of values.

Samples (plants, milk, eggs, muscle) for determining tritium content in free water (HTO) of bio objects were prepared using distillation method. The first condensate amount of 10 ml was removed, and the next 5 ml were taken for analysis. A scintillator was added to the analytical sample, after that it was measured via TriCarb 2900 TR liquid scintillation spectrometer. Samples for determining concentration of organically bound tritium (OCT) were prepared using PerkinElmer 307 automated device. For the measurement purpose Quantulus 1220 spectrometer was used. The time needed for measuring each sample was 120 minutes. The error in measurements did not exceed 10%.

As a result of this work the following conclusions were obtained:

1. It has been revealed that in lasting intake of $^{239+240}$Pu, ^{241}Am, ^{137}Cs and ^{90}Sr by sheep bodies, their concentrations in the main depositing organs (for $^{239+240}$Pu and ^{241}Am – liver, bone tissue, for ^{137}Cs –   muscular tissue, for ^{90}Sr – bone tissue) increase for 16 weeks. Significant slowdown in the growth of activities of $^{239+240}$Pu, ^{241}Am, ^{137}Cs and ^{90}Sr occurs in other organs and tissues after 2 and 4 weeks' intake by a body.

2. It was found that $^{239+240}$Pu, ^{241}Am, ^{137}Cs and ^{90}Sr in organs and tissues of sheep with the equilibrium state of radionuclides in a body, is in a certain quantitative ratio. Concentration of ^{137}Cs, $^{239+240}$Pu, ^{241}Am and ^{90}Sr radionuclides in the most accumulating organs (for ^{137}Cs – thigh muscles, for $^{239+240}$Pu, ^{241}Am – liver, for ^{90}Sr – bone tissue), exceed concentrations in the least accumulating organs (for ^{137}Cs – tail fat, for $^{239+240}$Pu, ^{241}Am, ^{90}Sr – thigh muscles) of up to 45, 200, 250 and 560 times, respectively.

3. It was found that with increasing activity of ^{90}Sr in the wool, its activity is characterized by an increase in the sheep's bone tissue. Thus, this dependency allows it to make a life-animal estimate of ^{90}Sr concentration in a body.

4. In the course of research it was determined that T_f of $^{239+240}$Pu, ^{137}Cs and ^{90}Sr into organs and tissues of sheep at intake of radionuclides by bodies of animals with various sources (forage, water, soil) differ. At that, the highest bioavailability of ^{137}Cs in a body is observed at intake with forage, the least – with soil. It was also determined that T_f of ^{137}Cs into mutton when feeding animals vegetation from venues of surface nuclear tests is down to three times lower than if they are fed vegetation from places of radioactive stream flows. T_f of $^{239+240}$Pu into mutton at intake with vegetation (grassland and steppe), on average, is 6 times higher than T_f at intake with soil from the zone of radioactive stream flow and is 150 times higher than T_f at intake with soil from the ground zero of surface explosion. T_f of ^{90}Sr into mutton at intake with water is higher than that at intake of the radionuclide with forage and soil up to 2 and 4 times, respectively.

5. Study of $^{239+240}$Pu, ^{241}Am, ^{137}Cs and ^{90}Sr distribution in horses' and fruits' bodies showed that radionuclide distribution is more uniform in fruits' bodies than in mares'. It was determined that ^{137}Cs and ^{90}Sr are more transferred into organs and tissues of one year mares than those of adult ones (10 years) up to 1.6 and 3.6 times respectively, for $^{239+240}$Pu and ^{241}Am no significant difference was identified. With lasting intake of $^{239+240}$Pu, ^{241}Am, ^{137}Cs and ^{90}Sr by horses' bodies, T_f of radionuclides in the main depositing organs (for $^{239+240}$Pu and ^{241}Am – liver, for ^{137}Cs – muscular tissue, for ^{90}Sr – bone tissue) is higher with radioactive solution added to forage than that with soil up to 40, 60, 500 and 1.4 times respectively.

6. It was determined that with lasting intake of ^{3}H by laying hens' bodies with various sources (with air, water and grass meal), in the first 2 weeks HTO concentration rises both in muscular tissue and hen's eggs. Next, dynamic equilibrium of this radionuclide concentration comes in these products. OBT (organically bound tritium) concentration dynamics in muscular tissue at intake with water and grass meal is different. At intake with water, equilibrium state takes place 4 weeks later whereas at intake with grass meal, no equilibrium state has been revealed at the lapse of 8 weeks. It was found that at lasting intake of ^{3}H with water, HTO concentration ratio in muscular tissue and that of HTO in hen eggs do not exceed – 1, at intake with air – 4, at intake with grass meal – 6. OBT concentration ratio and that of HTO in muscular tissue of hens (OBT/HTO) at intake with water, atmospheric air and grass meal were 0.09 and 0.7 respectively.

7. Findings have shown that T_f of ^{3}H into mutton at intake with water will not exceed 1.1×10^{-2} l/day, at intake with vegetation – 1.5×10^{-1}. ^{3}H is most transferred into mare milk with forage than water. It was determined that reduced ^{3}H concentration in mare milk after lasting intake of the radionuclide with hay will be twice slower than at intake with potable water.

8. Animal and poultry products obtained in the STS territory outside testing areas will mostly conform to the hygienic standard "Sanitary-epidemiological requirements for radiation safety" of the Republic of Kazakhstan. The exception is Shagan river and water sources flowing beyond

"Degelen" area. When animals are grazed, these areas may have the intake of elevated ^{3}H concentrations by products.

References

Beresford, N.A., Howard, B.J., Mayes, R.W., Lamb, C.S., 2008. The transfer of radionuclides from saltmarsh vegetation to sheep tissues and milk. Journal of Environmental Radioactivity 98, 36–49.

Alexakhin R.M, Vasilyev A.V., Dikarev V.G., 1992. Agricultural radioecology. Ecology, Moscow, p.400 (in Russian).

Averin V.S., 1986. Americium and plutonium in agro-ecosystems. The Chernobyl disaster in 1986: monograph. Gomel RRUE MOE RB "Institute of Radiology", 2014. Gomel. p. 176 (in Russian).

Buldakov L.A., 1969. Kinetics of ^{239}Pu exchange and biological effect. Issues of plutonium toxicology, Atomizdat, Moscow.

Fesenko, S., Isamov, N., Howard, B.J., Beresford, N.A., Barnett, C.L., Sanzharova, N., Voigt, G., 2009. Review of Russian language studies on radionuclide behaviour in agricultural animals: part 3. Transfer to muscle. Journal of Environmental Radioactivity 100, 215–231.

Fesenko, S., Isamov, N., Howard, B.J., Beresford, N.A., Barnett, C.L., Sanzharova N., Voigt, G., 2009. Review of Russian-language studies on radionuclide behaviour in agricultural animals: part 4. Transfer to poultry animals: 3. Transfer to muscle. Journal of Environmental Radioactivity 100. 815–822.

Green, N., Woodman, R.F.M., 2003. Recommended transfer factors from feed to animal products. NRPB-W40. National Radiological Protection Board, Chilton.

International Atomic Energy Agency (IAEA), 2010. Handbook of Parameter Values for the Prediction of Radionuclide Transfer in Terrestrial and Freshwater Environments. TRS 472. International Atomic Energy Agency, Vienna.

Lyakhov O., Lukashenko S.N., Umarov M.A., Aidarkhanov S.A., 2008. Study the nature of distribution of tritium in the atmosphere of the ecosystem of the watercourse gallery №176 site "Delegen". Vestnik NNC. Vol. 3 (35), p. 52.

Sirotkin A.N., 1992. Release of radionuclides in animal products. Agricultural Radioecology. Nauka, 1991, Moscow, p. 106-115.

International Atomic Energy Agency (IAEA), 2014. Transfer of Tritium in the Environment after Accidental Releases from Nuclear Facilities. TRS 1738. International Atomic Energy Agency, Vienna.

Johansen, M.P., Child, D.P., Caffrey, E.A, Davis, E., Harrison, J.J., Hotchkis, M.A., Ikeda-Ohno, A., Thiruvoth, S., Twining, J.R., Beresford, N.A., 2016. Accumulation of plutonium in mammalian wildlife tissues following dispersal by accidental-release tests. Journal of Environmental Radioactivity 151, 387-394.

Howard, B.J., Beresford, N.A., Barnett, C.L., Fesenko, S., 2009. Quantifying the transfer of radionuclides to food products from domestic farm animals. Journal of Environmental Radioactivity 100, 767–773.

Howard, B.J., Beresford, N.A., Barnett, C.L., Fesenko, S., 2009. Radionuclide transfer to animal products: revised recommended transfer coefficient values. Journal of Environmental Radioactivity 100, 263–273.

Assessment of Tritium Distribution and Mechanisms of its Formation in the STS Snowcover

D.Turchenko[*]*, S.Lukashenko, O.Lyakhova*

Branch «Institute of Radiation Safety and Ecology» of the NNC RK, Krasnoarmeiskaya 2, 071100, Kurchatov, Kazakhstan

Abstract

The paper presents the results of investigation of tritium content in the layers of snow located in the stream beds of the "Degelen" massif contaminated with tritium. The objects of investigation were creek watercourses Karabulak, Uzynbulak, Aktybai located beyond the "Degelen" site. We studied the spatial distribution of tritium relative to the bed of watercourses and defined the borders of the snow cover contamination. In the center of the creek watercourses the snow contamination in the surface layer is as high as 40 kBq/kg. The main mechanisms causing tritium transfer in snow were examined and identified. The most important mechanism of tritium transfer in the streams is tritium emanation from ice or soil surface.

Introduction

Many investigations devoted to studying artificial radionuclide migration to the environment both on the territory of the experimental site "Degelen" and beyond it have been carried out. Among the most hazardous artificial radionuclides, such as ^{137}Cs, ^{90}Sr, $^{239+240}$Pu, and ^{3}H (tritium) present in this ecosystem, tritium has the highest migration rate. In [1, 2] high tritium concentrations in surface and ground waters as well as in the components of the ecosystem (animals, plants, atmospheric air) were registered. The tritium concentration in the surface waters of the streams on the site Degelen goes up from tens to hundreds of thousands of Bq/L, and the lengths of streambeds of some streams exceed ten kilometers, therefore they go beyond the territory of the Degelen massif.

A comparative analysis of the tritium concentration in the ecosystem components showed that the main contribution to the ecosystem contamination is made by the streams located on the territory of the "Degelen" massif. No information on tritium concentration in the snow cover on the contaminated areas was obtained before this study.

In different climatic periods of snow accumulation, the tritium inflow may be caused by the two main transfer mechanisms:

- tritium inflow from the atmosphere as a result of transfer of snow particles or condensation of water vapor on snow particles during precipitations.
- tritium emanation from soil or ice cover.

Over 130 underground nuclear explosions (UNE) of various types and yields were made at Semipalatinsk Test Site, including 106 UNEs at «Balapan» site, 24 UNEs at «Saty-Uzen» site. UNEs were aimed at nuclear weapons invention and modification, and for peaceful purposes as well. Each UNE contributed to tritium accumulation in gopher cavity. Increased concentrations of

---

[*] Corresponding author, E-mail: turchenko@nnc.kz

tritium were found in UNE venues (warfare boreholes at «Balapan» site) in particular in atmospheric and soil air [4], as well as some insignificant extraction gases from the soil cover [5].

As expected, the main sources of tritium emanation to the environment are surface and ground waters of the STS, nevertheless epicentral zones of UNE boreholes at «Balapan» and «Sary-Uzen» sites, can be potential sources of tritium entry to the environment.

The work presented here included the following stages:

− study of levels and character of tritium distribution in the snow cover in STS streamflows;
− study of mechanisms of tritium entry into snow cover.

Materials and Methods

Samples

To estimate the spatial distribution of tritium, the research profiles perpendicular to the water flow were made on the streams. The points of the research profile were located on the right and left sides of the stream. The center of the profile was located in the center of the streambed, the distance between the examined points was 50m, and the depth of sampling was 0–10, 10–20 and 20–30cm.

Tritium distribution beyond the testing sites of the STS was assessed as follows: at the distance of 0-10 km from «Degelen» site (southern and southeastern direction), in inhabited localities adjacent to the STS, UNE venues at «Balapan» site and at the «Experimental Field» site. To study mechanisms of tritium entry into snow cover researches were carried out as follows: at the streamflows of «Degelen» and «Balapan» site the dynamics changes in tritium concentration in the snow cover layers was researched, and in UNE venues tritium content was determined in snow and soil.

To study mechanisms of tritium entry into snow cover at the sites 1355 and 1010 areal survey of tritium content in the snow cover was carried out. In 2011 and 2012 snow cover on the borehole 1355 was sampled by 1x1km grid, with the distance between survey points of 100 m. The center of the grid was near the wellhead. To get more detailed information on tritium content in the snow cover, in 2013 the snow cover was sampled at the boreholes 1355, 1010 of «Balapan» site and 1003 of «Sary-Uzen» site by 0,5x0,5 km grid with 50 m interval. Snow cover was sampled layerwise at the depth of 0-10 (top layer) and 10-20 cm (bottom layer). When total snow layer was less than 20 cm, snow sampling was made at the depth of 0-10 cm and the remaining depth till the bottoming surface. Snow cover thickness was measured via dipstick.

Radiometric technique

The snow cover thickness was measured with a measuring bar.
To determine tritium concentration, the snow samples were placed in the polyethylene bag and thawed to a liquid state. The samples were then placed in 20 mL plastic vessels. In order to remove mechanical admixtures, the melted snow samples were filtered by the filters "Whatman 589/3". The obtained filtered sample was placed in a 20 mL plastic cavity, and a scintillation cocktail in proportion 3:12 mL was added.
To determine the specific activity of tritium in the snow samples we used a liquid scintillation spectrometer TriCarb 2900 TR and the standard technique of measurements [3].

Results and Discussion

Study of levels and character of tritium distribution in the snow cover

Figure 1 shows spatial tritium distribution relative to the streambed of the Uzynbulak, Karabulak, Baytles stream.
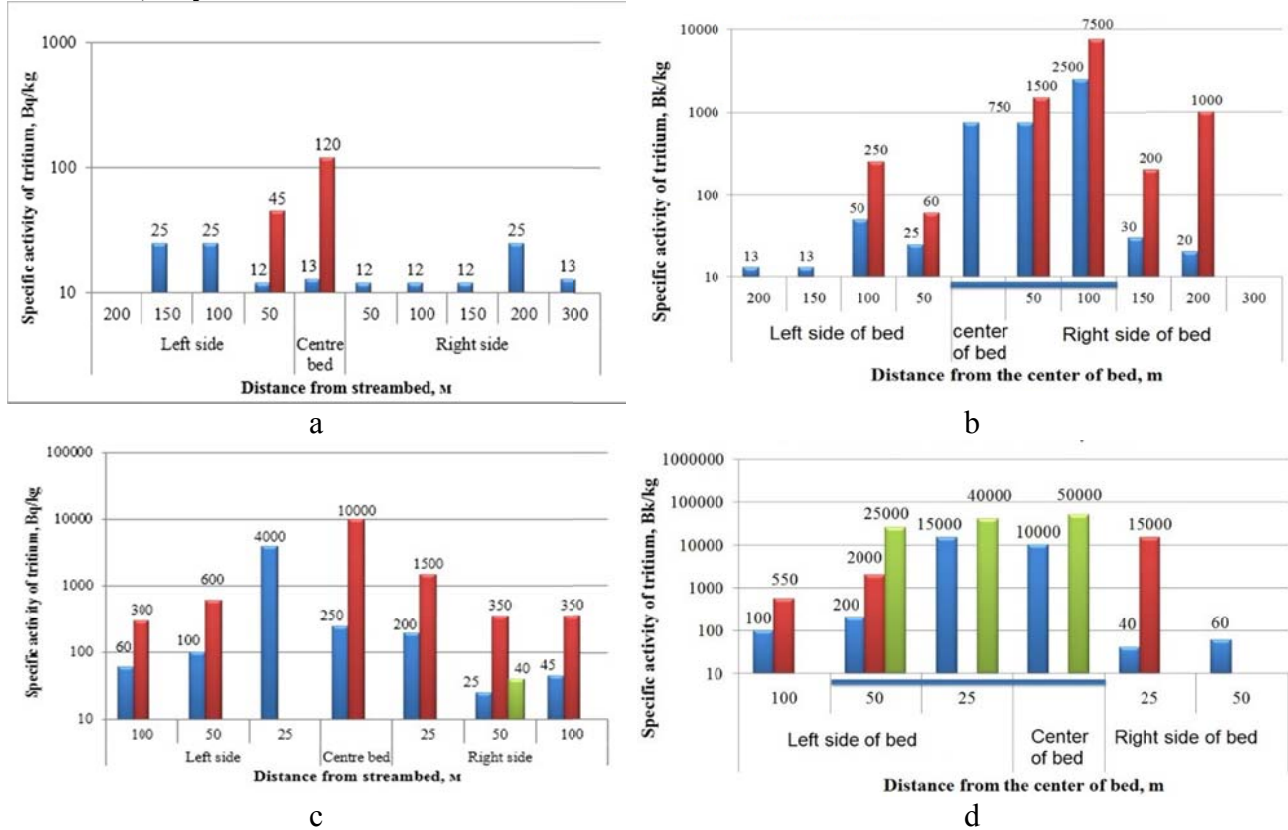
Figure 1. Spatial distribution of tritium in the snow cover in the tributaries of the Uzynbulak, Karabulak, Baytles stream: a) stream Karabulak in December; b) stream Karabulak in March, c) stream Baitles, d) stream Uzynbulak.

Maximal tritium concentrations of 40 kBq/kg were registered in the center of the streambeds (on the ice surface) and in the near-ground layer of the snow cover beyond the ice cover.

Thus, the results of investigations show that the snow cover of the streams Karabulak, Uzynbulak, and Baytles can contain quite high tritium concentrations. The tritium is not distributed uniformly among the layers: in most cases in the near-ground layer its concentration is higher than that in the surface layer.

In order to estimate tritium distribution in depth of snow cover, the ratio of tritium concentrations in the near-ground layer to that in the surface snow layer was calculated. In calculations, if the numerical values of tritium concentration were absent, the value of minimal detected activity was taken as the numerical value. An analysis of the results of tritium concentration in the near-ground and surface snow layer showed that the ratio of tritium concentrations varied from 0.70 to 0.66. The obtained average ratio of tritium concentration can be used for rough estimation of tritium concentration in the near-ground and surface snow layer if its concentration in the other layer of the snow cover is known. As the distance from the center of the streambed in the perpendicular direction increases, at a distance of 200-300m tritium concentration in the near-ground and surface snow layer decreases to its background values.

Figure 2 shows spatial distribution of tritium as a function of distance from all studied streams. For each case (stream) the tritium concentration is normalized to the maximal value. The

approximation curve in figure 2 shows the dependence of tritium contamination on the distance from the streambeds.
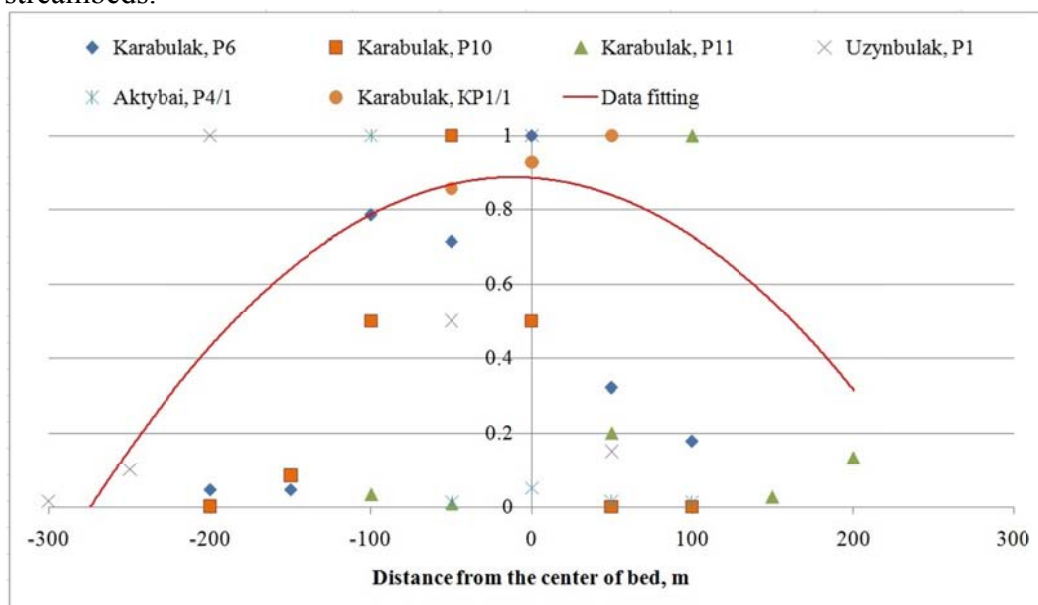
Figure 2. Spatial distribution of tritium as a function of distance from the studied streams, the distribution is normalized to the maximal value of tritium contamination.

Maximal levels of contamination with tritium (up to 20-40 kBq/kg) are, on average, located at a distance not more than 100-200m from the streambed center and are limited by the streambed. As the distance from the streambed in the perpendicular direction increases, the tritium concentration in the snow cover falls to the background values.

A comparison of the results in the surface and near-ground layers of the snow cover on the streambeds shows that in all cases maximal tritium concentrations were registered in the near-ground layer of the snow cover, and could reach 40 kBq/kg. This fact shows that the main source of tritium contamination is the stream; the mechanism of tritium transfer to the snow cover depends on the underlying surface, namely, tritium emanation from the surface of the soil or ice cover.

Study of mechanisms of tritium entry into snow cover

Figure 3 shows data (generalized for the period from 2011 to 2013) on tritium content in the surface and the bottom layer of the snow cover at the warfare boreholes 1355 and 1010 of «Balapan» site. Provided concentrations of tritium in the snow cover include all accumulated data for the winter period from 2011 to 2013. Data massif obtained for the borehole 1355 for 2011-2013 was plotted on the map, at that in corresponding points of the grid, average value was calculated for each layer. For convenient presentation, processing and plotting the data, tritium detection limit in the snow cover was taken as an integer value (for example, <11 = 11).

Researches carried out have revealed sites with increased tritium concentrations in the snow cover. As a rule, maximum concentrations of tritium in snow are observed at the wellhead of boreholes 1355 and 1010, in some cases achieving 400 Bq/kg. It should be noted also, that maximum concentrations of tritium in snow were found not only at the wellhead, but also 200-300 away from the nuclear test epicenter southward (see. Figure 3, b).

Comparing data for the bottom and the top snow cover layer revealed that tritium concentration in the bottom layer is higher than in the top layer. This fact proofs an assumption made before on tritium entry (emanation) from soil.
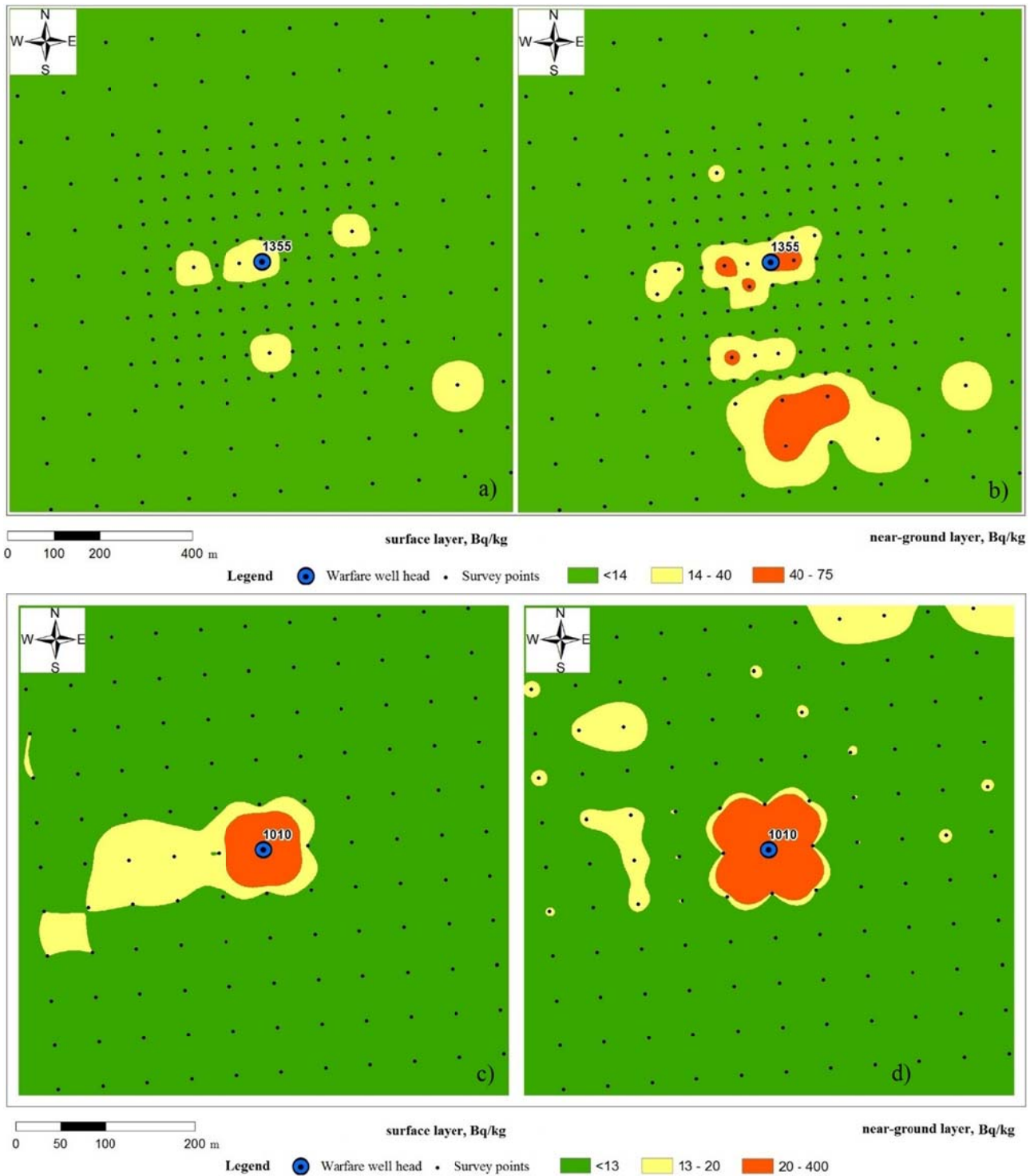
Figure 3. Tritium content in the snow cover of warfare boreholes: a) borehole 1355 top layer; b) borehole 1355 bottom layer; c) borehole 1010 top layer a; d) borehole 1010 bottom layer.

Detailed areal surveys of the snow cover in the borehole 1355 allowed to reveal sites with increased tritium concentrations in the bottom layer of snow. Maximum concentrations of tritium in the snow cover not exceeding 75 Bq/kg were found near and at the distance of 200 m southwards the wellhead. In the borehole 1010 maximum concentration of tritium of 400 Bq/kg was also found in the bottom snow layer, near the well head. It should be noted also, that tritium concentration in the bottom layer of snow exceeds concentration in the top layer of snow, that also proofs previous opinion about emanation of tritium from the soil cover.

Conclusions

The results of investigations enable us to make a conclusion that the snow cover of "Degelen" mountain range may have quite high tritium concentrations both in the near-ground and surface snow cover. Highest levels of contamination with tritium are, on average, located at a distance of 100-200m from the streambed center and are limited by the streambed, reaching the values comparable to tritium concentrations in the stream water. As the distance from the streambed increases, the tritium concentration in the snow cover falls to the background values.

The obtained complex data show that in the "Degelen" massif there are 2 main mechanisms of tritium penetration to the snow cover:
- Condensation of tritium-containing water vapors on snow particles in the moment of snowfall, which gives tritium concentrations in the snow cover layers not more than 60 Bq/kg;
- Tritium emanation from the underlying surface of the soil or ice cover, and tritium redistribution from the near-ground to the surface layer of the snow cover.
-

Nevertheless, an issue of the origin of tritium in snow cover remains open: tritium enters the top soil layer from either UNE gopher cavity or a closely-spaced water-bearing layer. For more detailed research of mechanisms of tritium entry into the snow cover, at peri-portal sites of warfare boreholes it is necessary to carry out additional works to study geological structure and chemical composition if the soil cover at various depths from the bottoming surface. Besides that additional researches of snowcover need to be carried out at «Balapan» site, allowing to assess global fallout background of tritium from atmosphere for this area.

This research shows that tritium at the STS is distributed in much larger scales, than we expected before. This method can be successfully used in identification of underground test venues. The method developed is cheap enough and easy to be implemented.

References

1. *Subbotin S.B.* Subterranean migration of artificial radionuclides beyond Degelen massif / Subbotin S.B., Lukashenko S.N., Kashirskii V.M., Yakovenko Yu.Yu., Bakhtin L.V. // Current Issues in radiology of Kazakhstan [Collection works of the Institute of Radiation Safety and Ecology for 2007-2009] / Sup. by Lukashenko S.N. – V.2. – Pavlodar: Printing House, 2010. – 527 pp.: illustration.- appendix.: p. 518. - ISBN 978-601-7112-32-5. – [in Russian]
2. *Lyakhova O.N.* Research on tritium concentration in environmental objects on the territory of Degelen test site/ Lyakhova O.N., Lukashenko S.N., Umarov M.A., Aidarkhanov A.O.// NNC RK Bulletin. – 2007. Vol.4. – pp.80-86. – [in Russian]
3. Water quality – determination of tritium activity concentration – liquid scintillation counting method: ISO 9698-1989.
4. Lyakhova O.N. Tritium as an indicator of nuclear tests locations/ O.N. Lyakhova, S.N. Lukashenko, N.V. Larionova, S.B. Subbotin // Topical Issues In Radioecology of Kazakhstan [Proceedings of the National Nuclear Center of Kazakhstan for 2010г.] / under guidance of S.N. Lukashenko –V. 2. - Issue 3. – Pavlodar: Dom Pechati, 2011. – C. 121-142. - ISBN 978-601-7112-53-0.
5. Romanenko V.V. Investigation of the gas presence at "Balapan" site / S.B. Subbotin , S.N. Lukashenko, L.V. Chernova// Topical Issues In Radioecology of Kazakhstan [Proceedings of the National Nuclear Center of Kazakhstan for 2010г.] / under guidance of S.N. Lukashenko – V. 2. – Issue 3. – Pavlodar:Dom Pechati, 2011. – C. 275– 294.

Assessing distribution of tritium speciation in soils of radiation hazardous sites at the Semipalatinsk test site

Serzhanova Z.B., Aidarkhanovav A.K.,Lukashenko S.N.

Institute of Radiation Safety and Ecology, NNC RK, 071100, Kurchatov city, Kazakhsatn

Abstract

The article presents results on determination of tritium speciation (^{3}H) in soils of "Degelen" and "Balapan" areas located in the territory of the Semipalatinsk test site (STS). These area are different in mechanism of how tritium contamination was formed in soils. It was found that the main ^{3}H speciation in test venues of STS in soils are: ^{3}H in surface-adsorbed water, ^{3}H in interlayer water, hydroxyl ^{3}H, organically bound ^{3}H and crystally bound ^{3}H. Findings give an idea of contamination mechanisms as well as an assessment of migration capability and bioavailability of ^{3}H.

Introduction

Tritium – one of hydrogen isotopes is one of the most commonly spread technogenic radionuclides in the STS territory. Tritium concentration both in water and soil at some spots of STS can reach a few hundreds of thousands Bq/kg. This notwithstanding, ^{3}H speciation in soil in venues of nuclear tests, being the major parameter to characterize its migration processes, has hardly been studied. Lack of such information calls for the study of ^{3}H speciation in soil for the purpose of further predicting its behavior in the natural environment.

It is known that hydrogen in soil minerals may be contained as part of free water and in the structure of crystal lattice. A distinctive feature of each form is a different binding force with soil. Free water contains hydrogen in surface-adsorbed and interlayer water. Chemically (hydroxyl) and organically bound hydrogen are bound forms included in the crystal lattice structure (Lopez-Galindo, A., et al., 2008), (Betekhin, A.G., 1950), (Pushkaryov, A.V., et al., 2007).

As ^{3}H is one of hydrogen isotopes, it is assumed that soils contain ^{3}H in the same forms as hydrogen.

Bound forms also include less known ^{3}H in a crystally bound form (tightly bound). A possibility that such form exists can be stated considering that ^{3}H can be recovered (accumulated) on light elements as a result of activation reaction that took place at the moment of explosions, for example nuclear reactions like:

$$^6Li_3 + n \rightarrow {}^4He_2 + {}^3H \quad \text{(Lyakhova, O.N., 2011)}$$
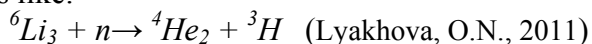
Thus, the main speciation of ^{3}H in soil is ^{3}H in surface-adsorbed water and ^{3}H in the interlayer water which free water of soils contains. Hydroxyl, organically bound and crystally bound ^{3}H are ^{3}H bound forms.

Targets of research

In order to determine ^{3}H speciation in soil, RHS (radiation hazardous sites) located in the STS territory were selected as research areas – these are "Degelen" and "Balapan" testing areas. Elevated ^{3}H concentration is observed in these areas both in water and soils (Republican Budget Program Report 008, 2015).

Degelen area. According to results of previous radioecological studies in Degelen area, it was established that the most significant sources of contamination are currently tunnel stream flows. Long-term monitoring studies have shown that ^{3}H carry-over with tunnel water from tunnel

cavities still continues. ^{3}H concentration in water both within the area and beyond it significantly exceeds intervention levels (Semipalatinsk test site. Present state: popular science edition, edited by Lukashenko, S.N., 2008).

"Balapan" area.

Research was carried out in two areas – in the region of Shagan river and near the "Atomic" lake.

Shagan river. During radioecological studies of STS aquatic environment, contamination at Shagan river with nuclear debris was discovered. The main radioactive contaminant is ^{3}H. Maximum values of ^{3}H tritium specific activity are established in the region of 5 km away from the "Atomic" lake and are in the order of 400 000 Bq/kg, which is over 50 times higher than allowable levels. With distance from the "Atomic" lake ^{3}H concentration in the water of Shagan river significantly decreases and at the confluence with Irtysh river ^{3}H concentration in the water is not more than 100-200 Bq/kg (Aidarkhanov, A.O., et al., 2010.).

"Atomic" lake. The most significant contamination of the territory close to the crater of the "Atomic" lake occurred due to the 1965 excavation explosion in borehole 1004. The aim was to create water reservoir in arid regions of the former USSR, particularly, in Kazakhstan. As a result of the explosion, 30-40% of radionuclides fell in the zone of soil banks from the "recovered" amount including ^{3}H too.

As a result of research carried out, it was found that maximum values of ^{3}H concentration in soil are observed in the zone of soil banks beyond which they go down to background values (Research report (final) edited by Ptitskaya, L.D., 2003).

Research methodology

Methodology to determine ^{3}H speciation consisted in stepwise extraction of each form. ^{3}H speciation contained in free water was determined using distillation at different temperatures. Thus, ^{3}H in surface-adsorbed water was nearly fully isolated from soil when heated up to 110°C. For ^{3}H isolation, a sample in interlayer water was heated up to 300°C. Tritium bound forms were determined by two-stage autoclave decomposition of intermediate calcination for the purpose of removing organically bound ^{3}H. Autoclave decomposition was based on acid oxidative mineralization of soil in a sealed closed volume on exposure to temperature and pressure. The course of experiment is schematically presented below (Fig. 1).
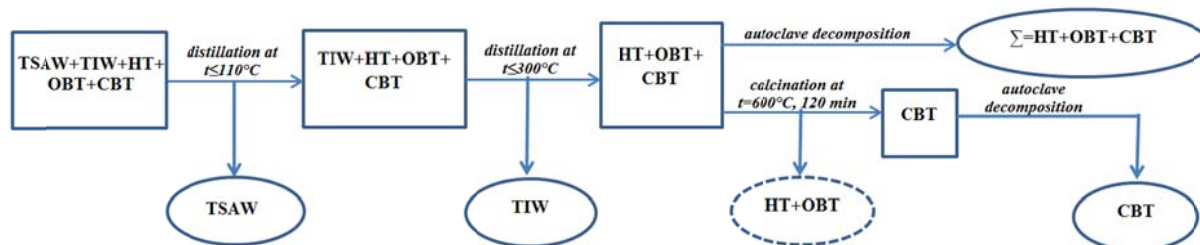
where TSAW - ^{3}H in surface-adsorbed water;
   TIW - ^{3}H in interlayer water;
   HT –hydroxyl ^{3}H;
   OBT –organically bound ^{3}H;
   CBT – crystally bound ^{3}H.

Figure 1. *Procedure of experiment to determine ^{3}H speciation*

In samples obtained, ^3H concentration was determined in accordance with the certified procedure (ISO 9698 (E), 1989.). ^3H specific activity was determined by liquid scintillation spectrometer TriCarb 2900 TR.

^3H specific activity was estimated per mass of the original sample (kg) given the distillate volume formed.

Results and discussion

As a result of experimental works on determination of ^3H speciation in soils of "Degelen" and "Balapan" areas, it was found that distribution of ^3H speciation in non-uniform. Such distribution is associated with mechanism of ^3H formation and entry into this site. Results are shown in Table 1.

Table 1. Distribution of ^3H speciation in surface soil

#	Sampling place	Sampling point	^3H specific activity, Bq/kg			
			^3H surface-adsorbed water	^3H in interlayer water	Hydroxyl ^3H + OBT	CBT
1	"Degelen"	Karabulak stream	4400±440	2100±210	230±120	<120
2		Baitles stream	10300±1000	4100±420	<120	<120
3		Uzynbulak stream	2200±210	1700±160	<120	<120
4		р. Актыбай	2000±200	1300±130	<120	<120
5		Bezymyannyy stream	2300±250	1050±100	420±120	190±20
6		Toktakushuk stream	6800±600	4000±370	<120	<120
7		Bezymyannyy stream 2	1970±180	350±40	<120	<120
8	"Balapan"	Shagan river, p.1	10000±900	-	560±120	<120
9		Shagan river, p.2	28000±2500	15500±1200	2400±200	<120
10		Shagan river, p.3	650±120	60±10	430±120	250±120
11		"Atomic" lake, p.1	850±80	5500±560	11000±1100	730±120
12		"Atomic" lake, p.2	750±70	1100±420	11000±1200	700±120
13		"Atomic" lake, p.3	1700±170	3200±320	4400±500	710±120

- no speciation observed

"Degelen" testing area. As it follows from results, speciation in free water predominates in soils of this area. Its concentration is in the order of 85-98 %, the remaining part is bound ^3H forms - 2 to 15%.

Thus, findings suggest that predominating ^3H speciation in free water, soils of "Degelen" area is associated with its entry to the site by ^3H carry-over with surface water from tunnels.

Shagan river. It follows from findings that speciation in free water predominate in soils of Shagan river – 60-95%. One of the points registered concentration of crystally bound tritium in the amount significantly higher than at others.

Obtained results suggest that predominant ^3H speciation contained in free water in soils of Shagan river is related to the inflow of contaminated ground water in this area.

"Atomic" lake. It follows from obtained results that concentration of bound forms dominated in soils of the "Atomic" lake, in particular, organically bound and hydroxyl ^3H. Their percentage totaled over 50%.

Predominance of bound ^3H forms in soils of the "Atomic" lake is probably related to characteristic features of a nuclear explosion (excavation test) in this area, as a result of which soil contamination with ^3H took place.

Conclusion

As a result of works performed, it was found that ^3H forms in free water prevail in places of contaminated ground water inflow. That is Shagan riverbed and "Degelen" testing area. Soils of these spots exhibit high ^3H concentration in surface-adsorbed water being the most available form. ^3H transfer is possible in these spots not only to plants but also to water and air.

Bound forms of ^3H predominate in epicentral areas of venues of nuclear tests. The "Atomic" lake is one of such spots where organically bound ^3H predominated. Organically bound ^3H is the available form for plants which is the reason why ^3H is in vegetation at the "Atomic" lake.

Obtained results suggest that availability of some or other ^3H speciation is probably related to its formation and intake mechanisms.

References

Aidarkhanov, A.O., et al., 2010. Ecosystem condition of Shagan river and the main mechanisms of how it is formed. Topical issues in radioecology of Kazakhstan, Proceedings of the Institute of Radiation Safety and Ecology over 2007-2009, 9-55.

Betekhin, A.G., 1950. Mineralogy. Moscow, 76-78.

ISO 9698 (E), 1989. Water Quality e Determination of Tritium Activity Corresponding to a Given Concentration e Liquid Scintillation Counting Method.

Lopez-Galindo, A., et al., 2008. Tritium redistribution between water and clay minerals. Applied Clay Science, 151-159.

Lyakhova, O.N., 2011. Tritium as a tracer in venues of nuclear tests. NNC RK bulletin, issue № 3, 125–129.

Pushkaryov, A.V., et al., 2007. Kinetics of isotope-hydrogen exchange in a bentonite-sand mixture Institute of Environmental Geochemistry: collected papers. Kiev, issue 15, 27-36.

Republican Budget Program Report 008, 2015. Radiation Safety Assurance in the territory of the Republic of Kazakhstan", measure 1 "Safety assurance at the former Semipalatinsk test site: information report. IRSE NNC RK, Kurchatov.

Research report (final) edited by Ptitskaya, L.D., 2003. Assessing radiological situation and monitoring in the territory of the Semipalatinsk test site and adjacent territories. IRSE NNC RK, Kurchatov.

Semipalatinsk test site. Present state: popular science edition, edited by Lukashenko, S.N., 2008. Dom Pechati. Pavlodar, 10-11.

Regularities of tritium distribution in soil in venues of surface nuclear tests in the territory of Semipalatinsk test site

L.V.Timonova[*], O.N.Lyakhova, S.N. Lukashenko

Branch «Institute of Radiation Safety and Ecology» of the NNC RK, Kurchatov city, Kazakhstan

Introduction

Taking into account various nature of tests conducted on the "Experimental Field" ground, each site of explosions conducted has their characteristic features of radionuclide contamination. As of today large dataset already been collected on radionuclide concentration in soil on this ground but there is no available information on tritium concentration (^{3}H). To get a complete idea of radiation situation on the "Experimental Field" ground, soil was additionally studied for ^{3}H.

The aim of this paper is to determine the level and nature of ^{3}H distribution in soil in venues of surface nuclear explosions on the "Experimental Field" ground.

Materials and Methods

Research areas

Research areas were sites of supposed epicenter of explosions as well as those located with distance from epicenter.
Schematic location of research areas on the "Experimental Field" ground is presented in Figure 1

Figure 1. Schematic location of research areas on the "Experimental Field" ground

---
[*] L.V.Timonova, E-mail:Timonova@nnc.kz

Research methodology

Taking into account that ^3H could have been formed during nuclear tests in the same way as ^{152}Eu, due to neutron activation reaction, soil was sampled in points of maximum ^{152}Eu concentration. Soil sampling depth was 0-10 cm.

Geographycal coordinates were determined in each point (longitude and latitude) with a GPS navigator GARMIN, exposure dose rate (EDR) and density of β-particle flux were also measured using MKS-AT6130 dosimeter-radiometer.

All of the samples taken were prepared by autoclave decomposition (Operating Instruction 03-02-03). ^3H specific activity was determined by beta-spectrometric analysis (ISO 9698 (E)).

Results and Discussion

The research carried out has shown that ^3H is present in soil of venues of surface nuclear tests in significant quantities. The Figures 2, 3 and 4 presents results of ^3H concentration in soil.

P-1 site

Soil sampling at P-1 site was made both at epicenter and with distance from it along the ray extending for 2000 m.

^3H concentration level in soil varied from <150 to 71000 Bq/kg. The analysis of findings showed that maximum ^3H concentration is at the point of the epicenter

a   b
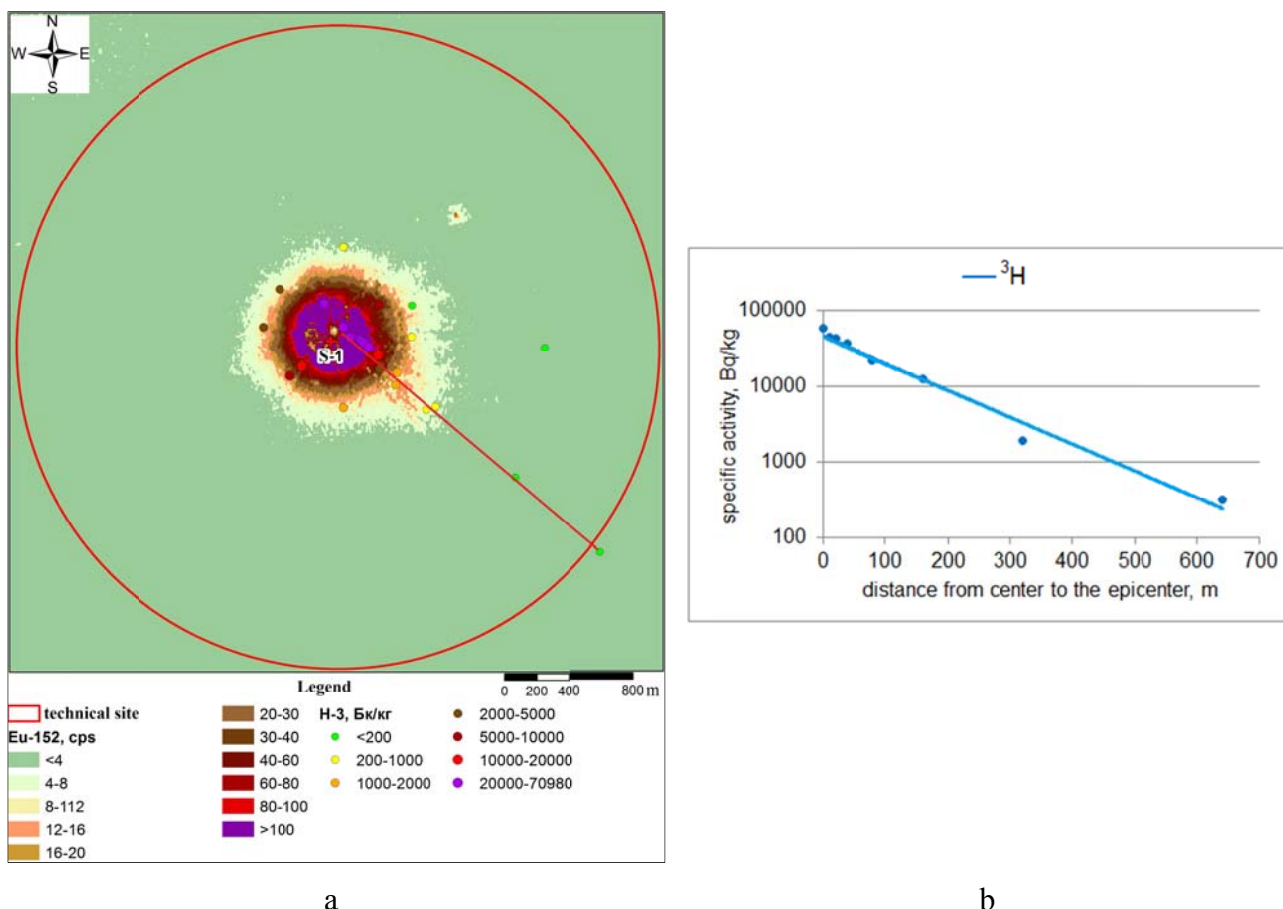
Figure 2. *Level of ^3H concentration and distribution at P-1*

In the course of researching into ^{3}H distribution with distance from the epicenter of explosion, it has been revealed that with increase in distance specific activity of ^{3}H in soil is significantly reduced

P-2, P-7 sites

At P-2, P-7 sites the highest values of tritium contamination in soil is registered at sites 1 and 4. At these sites ^{3}H specific activity was 7 600 and 11 200 Bq/kg respectively. At sites 2 and 5 ^{3}H concentration in soil reached some 5 000 Bq/kg. The rest of the sites exhibit lower level of tritium contamination – down to 4 000 Bq/kg. At sites 16 and 19, no ^{3}H concentration has been revealed.

a   b
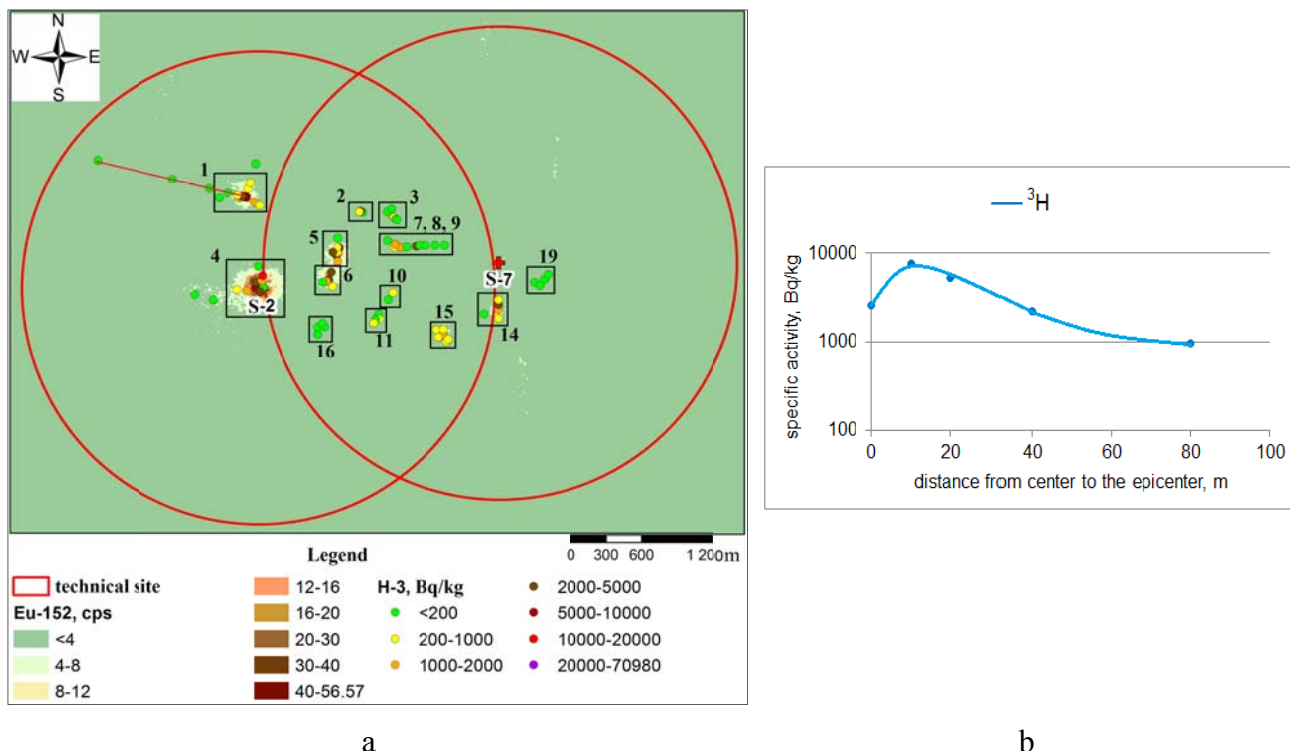
Figure 3. *Level of ^{3}H concentration and distribution at P-2, P-7 sites*

^{3}H distribution in soil with distance from the epicenter of explosion was researched at site 1 along the ray of 1 300 m.

Findings have shown that ^{3}H tritium is non-uniformly distributed. At a distance of 10 m from the epicenter, there is elevated ^{3}H concentration, and then it decreases. Thus, ^{3}H activity peak has been identified. An assumption was made that the reason could be soil ejection in this direction at the moment of explosion and maximum ^{3}H concentration in soil is shifted from the epicenter in the direction of supposed ejection.

P-3, P-5 sites

Maximum ^{3}H tritium specific activity in these territories is identified at spot 1, P-3 site and spot 8, P-5 site. According to data obtained, ^{3}H specific activity in soil at these spots was in the order of 20 000 Bq/kg.
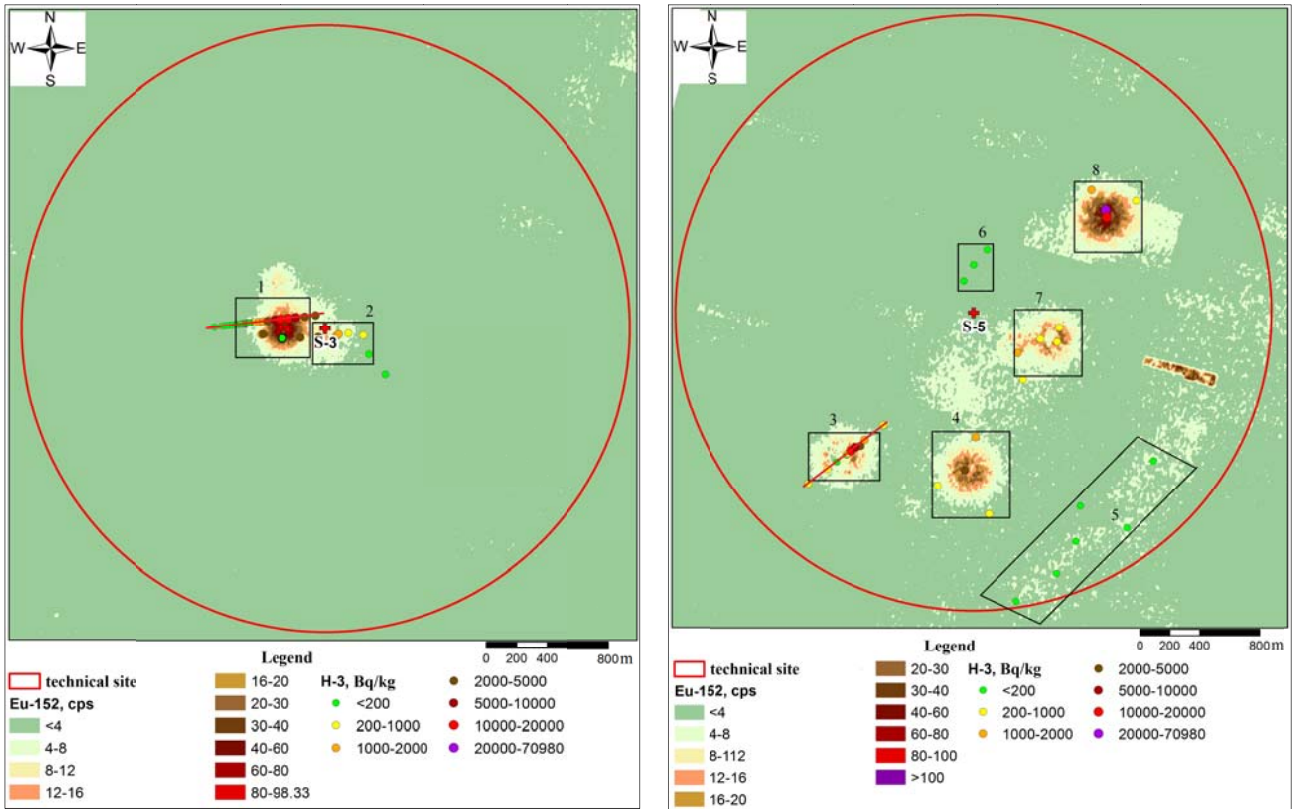
Figure 4. *³H concentration level at P-3, P-5 sites*

At spot 2 of P-3 site, ³H specific activity in soil ranged from <150 to 2 500 Bq/kg.

At spots 3, 4 and 7 of P-5 site, ³H concentration level in soil varied from <150 to 18 000 Bq/kg. No ³H concentration is revealed at spots 5 and 6.

Nature of ³H distribution with distance from epicenter of explosions was researched at spot 1, P-3 site and spot 3, P-5 site. Soil was sampled along rays laid in both directions from epicenter of explosions. Research results are shown in figures
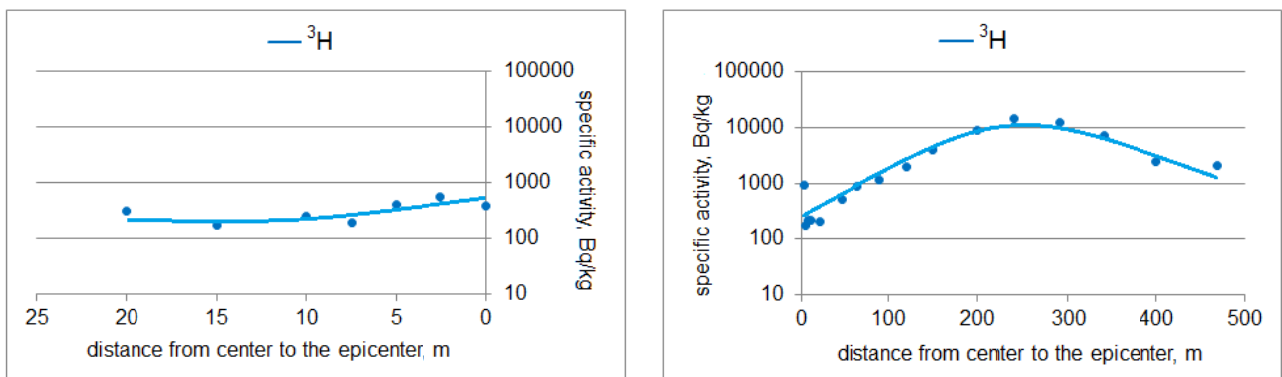
a. Distribution of ³H on the left from the ground zero	*b. Distribution of ³H on the right from the ground zero*

Figure 5. *³H distribution in soil with distance from the ground zero of explosion at P-3 site (spot 1)*
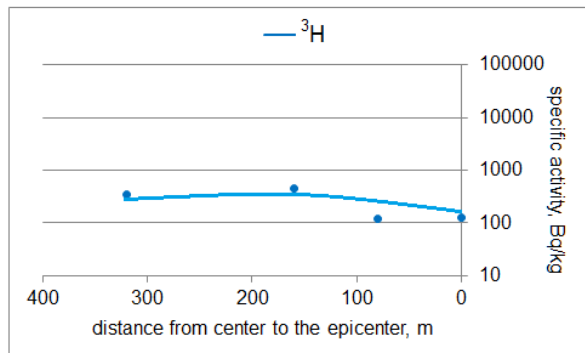
*a. Distribution of ^3H on the left from the
ground zero*
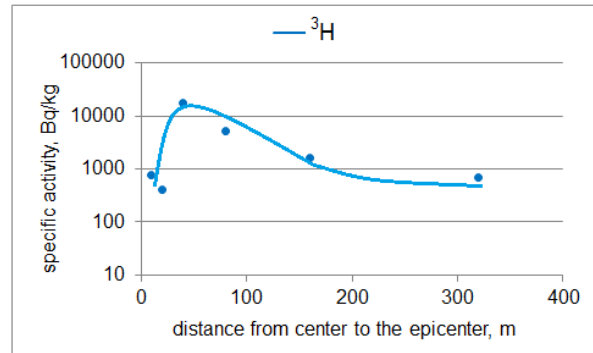
*b. Distribution of ^3H and on the right from the
ground zero*

Figure 6. ^3H *distribution with distance from the ground zero of explosion P-5 site (spot 3)*

The analysis of findings has shown that in both cases ^3H distribution with distance from the epicenter is virtually uniform on the left. On the right from the epicenter, ^3H concentration in soil initially rises and then decreases.

Conclusions

Based on findings from the "Experimental Field" ground it was found that soil contains ^3H in significant quantities. Maximum ^3H concentration in soil is 71 000 Bq/kg registered at P-1 site. The lowest ^3H concentration level in soil is observed at P-2, P-7, P-3 and P-5 sites. Probably, this is associated with types of tests conducted, explosion yield and other related conditions.

References

ISO 9698 (E), 1989. Water quality – Determination of Tritium Activity Corresponding to a Given Concentration – Liquid Scintillation Counting Method.

Operating Instruction 03-02-03 (A). Sample preparation for elemental analysis by autocalve decomposition. – Kurchatov: IRSE NNC RK, 2011. – P.12.

Non-radiation factors of hazard at STS

V.V. Romanenko, S.B. Subbotin, S.N. Lukashenko, V.I. Suprunov

Institute of Radiation Safety and Ecology, National Nuclear Center of Republic of Kazakhstan,
Krasnoarmeyskaya str., 2, 071100 Kurchatov, Republic of Kazakhstan

Abstract

As from the date of Semipalatinsk Test Site (STS) shut-down, impact of nuclear explosions on the environment began to be studied. Those activities were related to the study of the existing radiation situation. It became obvious during the research that there are other hazardous processes not related to ionizing radiation, which are the consequence of other nuclear effects from tests (Subbotin and Lukashenko, 2010; Lukashenko et al, 2009).
This paper has researched into signs of long-term geothermal activity development in ground zero zones after underground nuclear explosions (UNE).

Introduction

There are several grounds at STS where various tests were conducted (Mikhailov et al, 1997). UNE in vertical mines were conducted in testing areas "Balapan" and "Sary-Uzen" (Bocharov et al, 1989; Logachyov, 1997) (Figure 1).
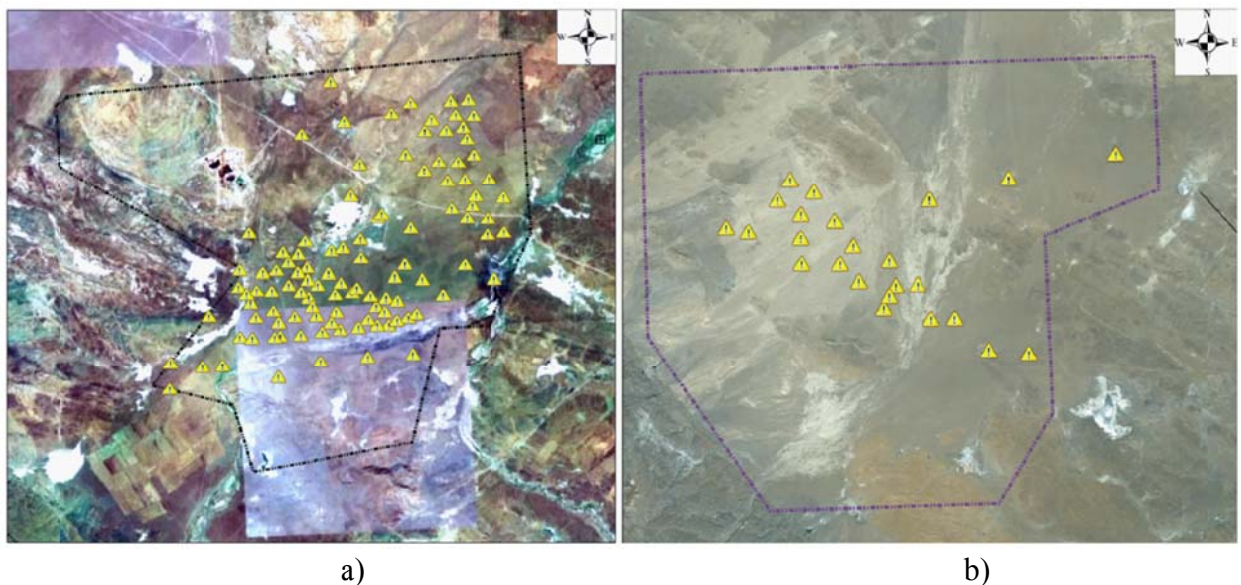
a) b)
Figure 1. *Location diagram of "warfare" holes in testing areas of STS a) "Balapan", b) "Sary-Uzen"*

Some of warfare boreholes (roughly 12 %) in the territories of those sites have cave-in occurrences (craters and others) that were formed at different times –some of them during tests, others – far later after tests. Most of warfare holes are characterized by no disturbance of the daylight surface. Therefore, the cavity formed because of UNE remains at a quasi-stable state until nowadays. At the same time, ground zero zones of a number of boreholes exhibit some cave-in occurrences (Figure 2).

Figure 2. "Balapan" site. General view of ground zero zones of UNE as cave-in occurrences were developing

There were a few cases of spontaneous gas inflammation and their stable combustion for many days. The most powerful disastrous show of gas presence in the territory happened in April of 1992 in "Balapan" testing area, at the near-mouth spot of warfare borehole "Glubokaya" (UNE conducted in 1977). In April of 1992, a sudden funnel-like earth surface subsidence (a cave in) took place next to the mouth of this warfare borehole. Formation of the surface subsidence was accompanied by explosion and fire. At present, the crater formed is of over 200 m diameter and is 20 m deep. This event can be estimated as a local phenomenon of disastrous nature. This happened 15 years later after a nuclear explosion was conducted in this hole. Thus, we have encountered the necessity to research into stability of UNE cavities and security in testing areas (Figure 3).

Figure 3. General view of ground zero zone at "Glubokaya" hole

Research methods of long-term post-explosion effects

It should be noted that during UNE, effervescence from some warfare borehole could be observed. Gas was observed to self-ignite a few times and burned steadily for many days.
Gas emission is one of signs shown by long-term underground gas generation processes in rocks. Additional indirect sign of such processes is the presence of thermal anomaly (Busygin et al, 1996; Izrael, 1974; Nifontov et al, 1965; Taylar, 1973).

Research into long-term post-explosion effects were divided into three areas:
1. Determining "critical" warfare boreholes;
2. Assessing special configuration of gas release;
3. Assessing existing thermal anomalies.

Results and discussion

Determining "critical" warfare boreholes

Samples were collected from soil gas close to 106 warfare boreholes in "Balapan" testing area and 24 warfare boreholes in "Sary-Uzen" area. Storage tanks (10 l polyethylene canisters with sampling tubes) to sample gas from soil were placed at 2 points next to each warfare borehole.

Points of disturbed relief of technogenic nature (cracks, craters), closest to the warfare borehole head were regarded as preferable.

Samples of soil air were made by means of storage tanks (10 l polyethylene canisters furnished with branch pipes for air sampling). Tightness was achieved by burying a tank down to 5-7 cm and compacting soil adjacent to its walls. Duration of gases accumulation was at least 24 hours. After 24 hours accumulation gas mixture was sampled from storage tanks.

Storage tanks were placed at points remote from borehole heads to gather information on background values of gas concentration. Points for gathering of background datum were arranged at a distance of 0.3 – 37.3 km from warfare borehole heads.

Since gas leak is one of sings of long-term destruction processes, activities to determine potentially hazardous warfare boreholes were performed based on data on gas release and thermal anomaly.

Background concentrations

Gas concentrations at points for gathering of background datum are shown in Table 1. Most of concentrations are below the level of minimal detection.

# of control point	Background gas concentrations					
	CO_2	CO	H_2S	CH_4	SO_2	H_2
1	<0,002	<0,0002	<4-E6	<0,02	<3,5E-6	<0,001
2	<0,002	<0,0002	<4-E6	<0,02	<3,5E-6	<0,001
3	<0,002	<0,0002	<4-E6	<0,02	<3,5E-6	<0,001
4	<0,002	<0,0002	<4-E6	<0,02	<3,5E-6	<0,001
5	<0,002	<0,0002	<4-E6	<0,02	<3,5E-6	<0,001
6	<0,002	<0,0002	<4-E6	0,8±0,16	<3,5E-6	<0,001
7	<0,002	<0,0002	<4-E6	<0,02	<3,5E-6	<0,001
8	<0,002	<0,0002	<4-E6	<0,02	<3,5E-6	0,10±0,02
9	<0,002	<0,0002	<4-E6	<0,02	<3,5E-6	0,10±0,02
10	<0,002	<0,0002	<4-E6	<0,02	<3,5E-6	<0,001
11	<0,002	<0,0002	<4-E6	<0,02	<3,5E-6	<0,001
12	<0,002	<0,0002	<4-E6	<0,02	<3,5E-6	0,120±0,024
13	<0,002	<0,0002	<4-E6	<0,02	<3,5E-6	<0,001

Table 1. *Background gas concentrations*

"Balapan" testing area

Gas was sampled from heads of 106 warfare boreholes in this area. Numerical values for CO_2 concentrations were at 53 warfare boreholes which is equal to the half of the total (50%), methane concentration – 22 boreholes (20%), hydrogen – 84 boreholes (79%). Carbon oxide, hydrogen sulphide and sulphur oxide concentrations were lower than the detection level of equipment used.

Warfare boreholes of gas release: 1010, 1086, 1053, 1223, 1201, 1234, 1236, 1309, 1315, 1316, 1318, 1322, 1323, 1325, 1326, 1328, 1331, 1340, 1355, 1421, "Glubokaya" (Subbotin and Lukashenko, 2010).

"Sary-Uzen" testing area

Gas was sampled from heads of 24 warfare boreholes here. Numerical values of CO_2 concentrations were obtained for 22 warfare boreholes (93%), methane – 3 (11%). Warfare boreholes of gas release: 102, 104 and 111 (Lukashenko et al, 2010; Romanenko et al, 2010).

Data comparison for testing areas has shown that maximum methane concentration in soil of "Balapan" and "Sary-Uzen" are practically equal but that of carbon and hydrogen dioxide differ by 6-7 times (Table 2).

Gas	Test site "Balapan" Cmax, %	Test site "Sary-Uzen" Cmax, %	c_B / c_{SU}
CO_2	0,34	0,05	7
CH_4	0,79	0,75	1
H_2	0,36	0,06	6

Table 2. *Maximum gas concentrations in "Sary-Uzen" and "Balapan" testing areas*

Thus, in "Sary-Uzen" and "Balapan" areas warfare boreholes have been discovered having gas release traces that indicate continuation of post-explosive processes to date.

Assessing configuration of gas anomalies

The cavity from the underground nuclear explosion (UNE) is not absolutely airtight.
Presence of technogenic effects, zone of intense fracturing, cone of collapse and other tectonic disturbances make it permeable to air. This enables a thermal convection of gases from the nuclear explosion cavity with the daylight surface (Busygin et al, 1997). Elevated gas release in these regions is supposed to be an expected effect owing to the presence of a great number of cracks. Evidently, elevated gas release means technogenic effects from UNEs in the bowels.

Gas release after UNEs was researched at 3 warfare borehole heads of "Balapan" testing area.
Warfare boreholes 1010, 1220 and 1315 with signs of post-explosion activity (gas emission and daylight surface cave in) were selected for research conduction.
Sampling was made using a sampler with a sampling tube. A 1 m blast hole was drilled at each measurement point.

Results from warfare borehole 1315 were used as an example (Figure 4).
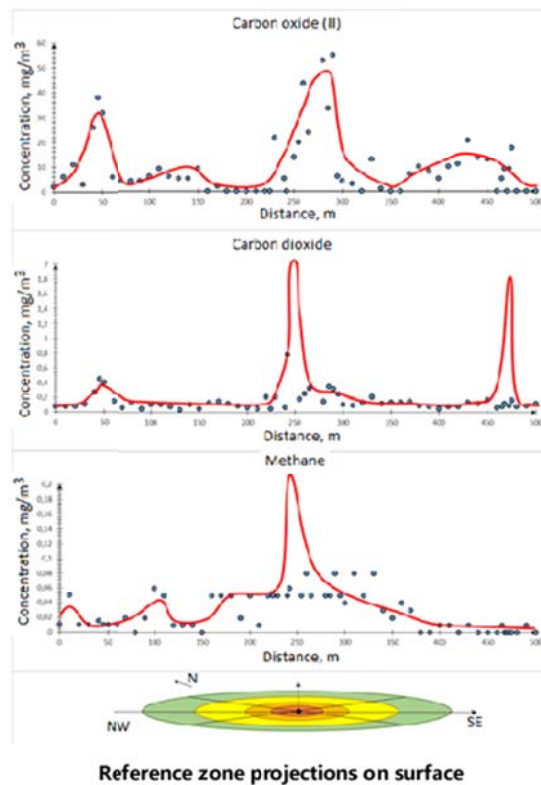
Figure 4. *UNEs zone projection to the daylight surface and distribution overlay of gas concentrations*

UNEs effects at warfare borehole 1315 were calculated based on works (Broud, 1971; Derlich, 1970; Duff and Shalit, 1971; Glasstone, 1971).

The figure shows projections onto the surface of reference zones. Calculations assumed that the explosion was made in a rock. The results are as follows: UNE cavity radius – 27 m, fragmentation zone – 27-54 m, zone of intense fracturing – 54-108 m, locally deformed zone of natural fracturing – 108-163 m. Thus, effects are limited by a circumference of 200 m radius around the warfare borehole head.

Sapling spacing is 10 m. It was advisable to determine zone projections of UNE effects in the rock by gas in the surface soil (about 1 m).

Maximum carbon oxide concentration of 55 mg/m^3 was obtained at point 29 (290 m). The data shows that there are three regions of elevated values in the profile – 50, 130 and 430 m. Peak concentration of carbon oxide is equal to 7.5 %. Zone configuration of carbon dioxide is different from that of carbon oxide. Peaks were registered at a virtually equal distance from the warfare borehole head. A bigger peak of 3.4% in the southeastern direction (470 m) and a smaller one of 0.45 % in the northwestern direction (45 m).

The central region of elevated values of 1.26 % (250 m) in the concentration profile for methane and two smaller regions of peak concentrations – 0.05 and 0.06 % are visible. Maximum concentrations were detected at the head of a warfare borehole. Regions of elevated concentrations exceed projections of schematic distribution zones of underground nuclear explosion effects. This can be explained by horizontal gas diffusion during their vertical migration to the daylight surface.

A significant factor for gas release is presence of tectonic disturbances in this region.

Assessing presence of thermal anomalies

Presence of hot cavities may be evidence of uncompleted post-explosive processes whose nature is unclear so far. Measurements of underground water temperature using a portable electro thermometer performed in hydrogeological wells in "Sary-Uzen" and "Balapan" testing areas. Measurement interval is 5 m. Temperature measurements were made in underground water at depths of 0.5 to 97 m.

a)   b)
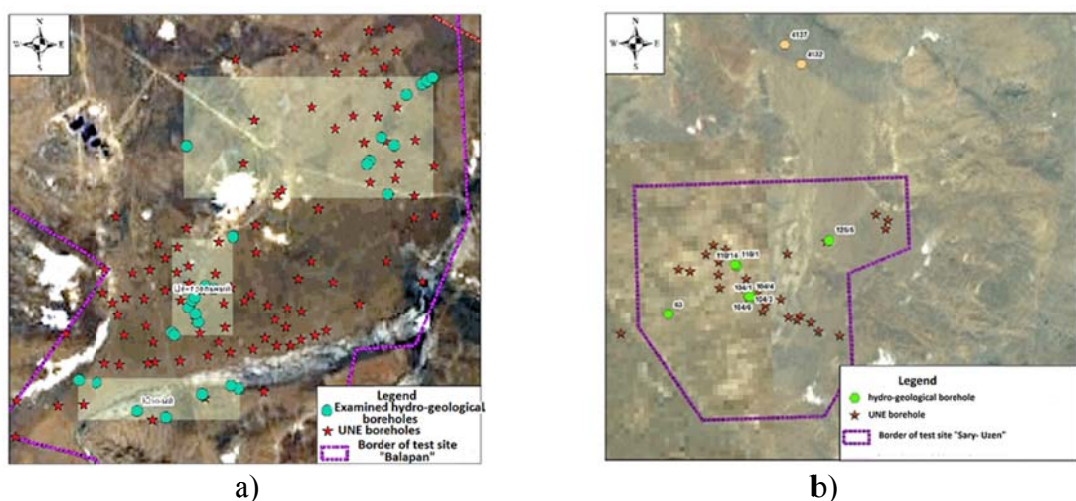
Figure 5. *Location diagram of hydrogeological wells in STS testing areas a) "Balapan", b) "Sary-Uzen"*

37 hydrogeological wells have been investigated (Romanenko et al, 2015). Average temperature values for underground water in "Sary-Uzen" and "Balapan" testing areas at a depth of 45 m – 8.4 and 8.7 °C respectively (Figure 5).

"Balapan" testing area. Northern region.

In this region, 10 hydro geological wells have been investigated (Figure 6).
Temperature range of underground water is 7.8-9.2 ℃ at a depth of 45 m. Temperature curves are mostly C-shaped except for 538 and 1053/1. Break-over point of curve is located at a depth between 30 and 40 m.
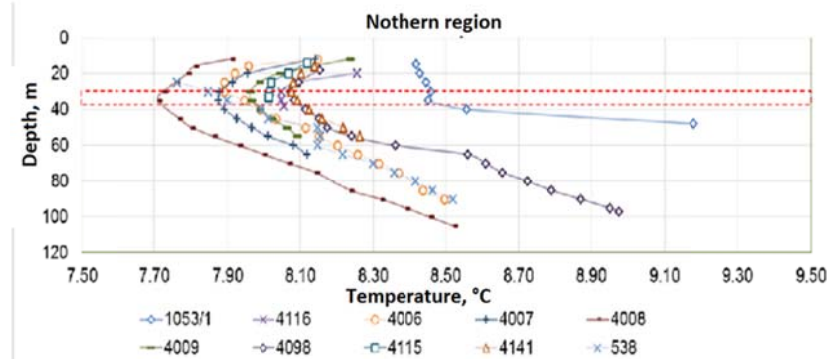
Figure 6. *Temperature of underground water in the northern region of "Balapan" area*

Relatively high water temperature of 9.2 °C with high temperature gradient was observed in hydrogeological well 1053/1. The thermal anomaly identified is possibly associated with presence of a very slowly cooling UNE cavity where a full camouflet explosion was conducted at a depth of 310 m in 1968 (Tleubergenov, 1997).
In hydrogeological well 4115, the temperature gradient at depths of 0-30 m was not observed.
In all other cases, temperature values ranges from 7.8-8.2 °C. Mean temperature of underground water in the region is 8.1 °C.

"Balapan" testing area. Central region.

In this region, 10 hydrogeological wells were investigated (Figure 7).
A significant thermal anomaly was observed in hydrogeological well 1061/1. Temperature gradient equal 49.5 mK/m, temperature at 40 m is 11.4 °C. UNE was conducted in warfare borehole 1061 at a depth of 340 m in 1972.
Temperature at a depth of 45 m ranged within 8.1 – 11.4 °C. Average temperature of underground water in this region – 8.7 °C.
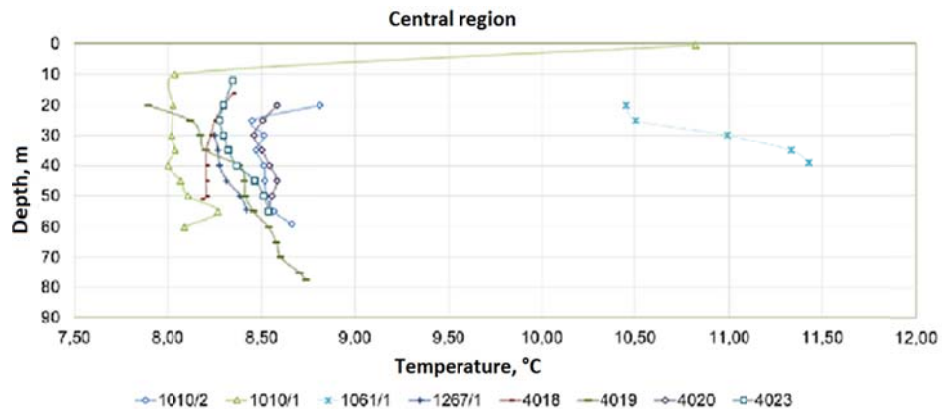
Figure 7. *Temperature of underground water in the central region of "Balapan" area*

"Balapan" testing area. Southern region.

In this region, seven hydrogeological wells were investigated (Figure 8).

Maximum temperature gradient was observed in hydrogeological well 4103 – 32 mK/m. Relatively mean values of average temperature and temperature gradient were observed in the rest of wells.

Temperature at a depth of 45 m – 8.2 – 8.7 °C. Average temperature value in this region is 8.4 °C.
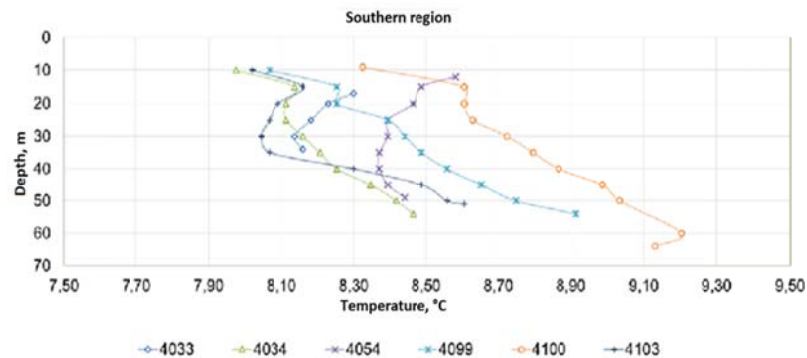
Figure 8. Temperature of underground water in the central region of "Balapan" area

"Sary-Uzen" testing area

Maximum temperature of underground water was observed in hydrogeological well 125/5 – 9.7 °C. The testing area has several hydrogeological wells of over 9 °C at a depth of 45 m – 125/5, 104/3, 104/1, 110/1.

The coldest water was in hydrogeological 63 – 7.1 °C.

Water temperature range at a depth of 45 m – 7.1 – 9.7 °C. Average temperature value in the area is 8.7 °C (Figure 9).
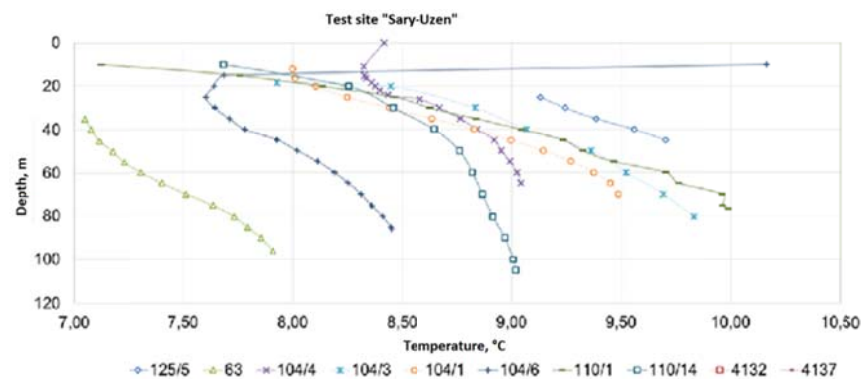
Figure 9. Temperature of underground water in the central region of "Balapan" area

Conclusions

As a result of work performed, a preliminary distribution pattern of underground water temperature has been obtained, heterogeneity of temperature field with anomalous regions of elevated temperature established in "Sary-Uzen" and "Balapan" areas. The hottest regions match venues of underground nuclear explosions. This phenomenon now is considered to be related to the residual energy release of nuclear fission reaction products.

Signs of long-term post-explosion processes were observed in the course of research. In the course of research, an effect of gas release was detected from heads and soil around warfare boreholes related to geological structure. Thermal anomalies in the temperature of underground water have been identified in UNE venues.

Thus, no one can currently be sure that UNEs cavities are stable while subsurface processes are running.

References

Bocharov et al, 1989 V.S. Bocharov, S.A. Zelentsov, V.N. Mikhailov
  Characteristics of 96 underground nuclear explosions at the Semipalatinsk test site
  Atomic energy. - 67 3 (1989) - p. 210e214.
Broud, 1971 G.L. Broud
  Nuclear explosion effect
  Moscow, 1971
Busygin et al, 1996 V.P. Busygin, A.I. Andreyev, M.V. Shipletsov
  Thermal radiation effects of many years by underground explosions and their environmental monitoring
  Abstracts of the international symposium Science and Society: history of the soviet atomic project", Dubna city, May14-17 , 1996. 253 p.
Busygin et al, 1997 V.P. Busygin et al.
  Residual thermo-radiation occurrences in the spalling zone of an underground nuclear explosion
  Report at the International Symposium "Detection and monitoring of underground nuclear explosions and earthquakes". M. 17-21, 1997.
Derlich, 1970 S. Derlich
  Underground Nuclear Explosion Effects in Granite Rock Fracturing
  Proc. Symp. on Engineer. with Nuclear Explosives, Las Vegas, Nevada, January 14-16, 1970. Washington, 1970, p. 505-518 (conf. 700101 (v.1)).
Duff and Shalit, 1971 Duff R.E., Shalit L.M.
  The Chemistry of Gassbuggy Chimney
  Nuclear Technology, 1971, v.11,N3, p. 390-399.
Glasstone, 1971 S. Glasstone
  Publish Safety and Underground Nuclear Detonations
  Washington, U.S. Atomic Energy Commis., 1971. – 276 p. (TID – 25708).
Izrael, 1974   Yu.A. Izrael
  Peaceful nuclear explosions and the environment
  Leningrad, Gidrometeizdat, 1974. – 136 p.
Logachyov, 1997 V.A. Logachyov
  Semipalatinsk test site
  Moscow, 1997. – 344 p.
Lukashenko et al, 2009   S.N. Lukashenko et al
  "Safety assurance at the former Semipalatinsk test site, Republican Budget program 011 "Radiation Safety Assurance"
  Information report of 2009, IRSE NNC RK, 2009
Lukashenko et al, 2010   S.N. Lukashenko et al
  Safety assurance at the former Semipalatinsk test site
  Information report of 2010, IRSE NNC RK, 2010
Mikhailov et al, 1997 V.N. Mikhailov et al
  Nuclear tests in USSR. Vol-1.,
  RFNC –VNIIEF, Sarov city, 1997
Nifontov et al, 1965 B. I. Nifontov et al.
  Underground nuclear explosions
  Moscow, Atomizdat, 1965
Romanenko et al, 2010 V.V. Romanenko, S.N. Lukashenko, S.B. Subbotin, L.V. Chernova
  Results of reconnaissance exploration of gas releases in "Sary-Uzen" area
  Proceedings of the Institute of Radiation Safety and Ecology over 2010 - Pavlodar : "Dom Pechati" Ltd, 2011. – 2
Romanenko et al, 2015 V.V. Romanenko, U.P. Koztayeva, S.B. Subbotin, D.Ye. Ayunov
  Research into temperature field of underground water in "Balapan" testing area
  NNC RK bulletin, issue 1, March 2015
Subbotin and Lukashenko, 2010   S.B. Subbotin, S.N. Lukashenko
  Assessing possible running processes of disastrous nature in "Balapan" area
  Proceedings of the Institute of Radiation Safety and Ecology over 2007-2009 - Pavlodar: "Dom Pechati" Ltd, 2010. – 2
Taylar, 1973   R.W. Taylar
  Thermal effects of underground nuclear explosions
  Nuclear Technology. V. 18. 1973. P. 185-193.
Tleubergenov, 1997 S.T. Tleubergenov
  Test sites of Kazakhstan
  Almaty: Gylym publishing house, 1997, - 745 p.

Results of areal radiological survey of the territory adjacent to the "Atomic" lake

Aidarhanov A.O.[1], Lukashenko S.N., Umarov M.A., Yakovenko Yu.Yu.

Institute of Radiation Safety and Ecology, National Nuclear Center of the Republic of Kazakhstan,
Krasnoarmeyskaya 2, 071100 Kurchatov, Kazakhstan

Abstract

The article gives research results of the nature and levels of radioactive contamination of the territory adjacent to the "Atomic" lake. Figures have been obtained on concentrations of technogenic radionuclides such as $^{239+240}$Pu, ^{241}Am, ^{137}Cs, ^{152}Eu, at a various distance from the "Atomic" lake.
The nature of areal surface contamination in the territory with technogenic radionuclides has been defined, several spots identified differing in radionuclide distribution in depth (crater bank, Shagan river flood plain, the near-shore area of the reservoir),. Some data presented were obtained by underwater gamma-spectrometric survey.

Introduction

The purpose of a pilot underground nuclear explosion conducted at the Semipalatinsk test site consisted in obtaining information on a possible use of such explosions to form deep craters thereby showing utility and, perhaps, necessity to employ nuclear charges to create water storages in arid regions of the country. This explosion was implemented on 15.01.1965 at the junction of Shagan and Ashisu rivers at Balapan natural boundary. The explosion was prepared and conducted under a special project with the action plan in radiation and seismic safety for the population.

After all the building operations were completed, two large reservoirs were formed: the internal one– in the crater and the external one – due to filling with water from the floodplain of Shagan and Ashisu rivers (Figure 1).
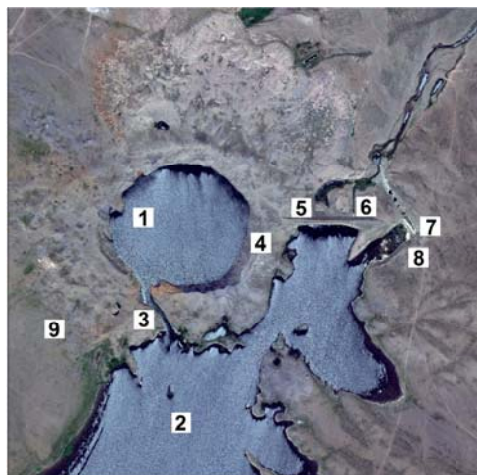
Figure 1. A scheme of man-made reservoir at Shagan river and its structure layout:
1 – Internal reservoir "Atomic" lake; 2 – External reservoir; 3 – Water supply channel; 4 – Soil bank; 5 – Rockfill dam; 6 – Bottom discharge; 7 –Flood trench discharge sluice with a side spillway; 8 – Remainders of a dam destroyed; 9 – Border of soil bank zone

---

[*] Corresponding author: Assan Aidarkhanov, Asan@nnc.kz

Nevertheless, available data analyzed by now has only shown the general nature of radioactive contamination in the territory mentioned. Findings do not allow information to be obtained which would characterize mechanisms and accurately delineate radioactive contamination, define features of radionuclide distribution or assume that one source or another contributes to contamination of the area.

Methodology of works

In order to assess present radiation situation in the region of the "Atomic" lake, a gamma-spectrometric pedestrian survey technique was applied as the main one. This survey technique allows it to obtain information on surface radioactive contamination of the area with three major nuclear "debris" – fission products from a nuclear charge (^{137}Cs), activation products from constructional materials and environmental elements (^{152}Eu) and the material itself in a nuclear charge (^{241}Am). In addition, this technique allows assessment of radioactive contamination of the area with virtually no environmental sampling, and, accordingly, no in-vitro sample analysis made.

Borders of the survey area were selected given the information available on the radioactive fallout plume that had extended in the north-eastern direction from the crater (of the "Atomic" lake), i.e. this work aimed at carrying out the areal gamma-spectrometric survey not only around the crater bank zone but also the plume zone. Thus, most of the survey territory was located north of the "Atomic" lake.

Pedestrian gamma-survey.

Lanthanum bromide (LaBr$_3$ (Ce)) scintillation detector-based field gamma-spectrometric systems were used in these works and ORTEC DigiBase pulse analyzers.
The whole territory was split into basic sectors of 240x240 m, and each sector is overlaid with a survey points grid of 20x20 m (with coordinates for all grid points). The distance accepted between survey points virtually ensures that radioactive fallout plumes are detected as well as comparatively small (20x20) radioactively contaminated spots, which is quite adequate for the goal of this kind of survey.

Sensitivity of the pedestrian gamma-spectrometric survey was:
- ^{137}Cs – 200 Bq/kg;
- ^{241}Am – 200 Bq/kg;
- ^{152}Eu – 300 Bq/kg.

Underwater gamma-survey.

Besides the technique to use gamma-spectrometric survey, underwater gamma-spectrometric survey was applied for bottom sediments in the reservoir, adjoining the "Atomic" lake on the southern side of the survey area.

A waterproof casing was made to use the technique, which held a detector. Detector submersion depth was 2-6 m. Measurements were made at fixed points, over the survey grid of 60x60 m, i.e. the distance between survey points was 60 m.

A survey point was approached by a waterborne vehicle (boat) using a satellite navigation device. Then the "operator" would lower the detector (cased) to the reservoir bottom, fix it with a conducting rope in vertical position and run spectral acquisition.

At the final survey stage all the spectra obtained and processed (during the pedestrian and underwater gamma-spectrometric survey) provided the basis for map document in areal distribution of artificial radionuclides in the region of the "Atomic" lake.

Drilling holes.

Three holes located within 25 m zone were drilled at a sloping spot to define the nature of man-made radionuclides distribution in depth at the bank of the "Atomic lake (Figure 2). The depth of boreholes drilled is 6 m. No ground water has been discovered at spots drilled in the bank.

Holes were drilled by means of LBU 50-07 drill rig on the basis of KamAZ motor vehicle. Mechanically rotational drilling method was employed to open up ground water horizons.

Soil sampling at a depth.

Soil was sampled at a depth of down to 50 cm to define the nature of radionuclide distribution in depth at various spots different in soil type. Sampling was made in the flood plain part of Shagan river in the near-bank area of the external reservoir. Sampling points are presented in the figure (Figure 2).
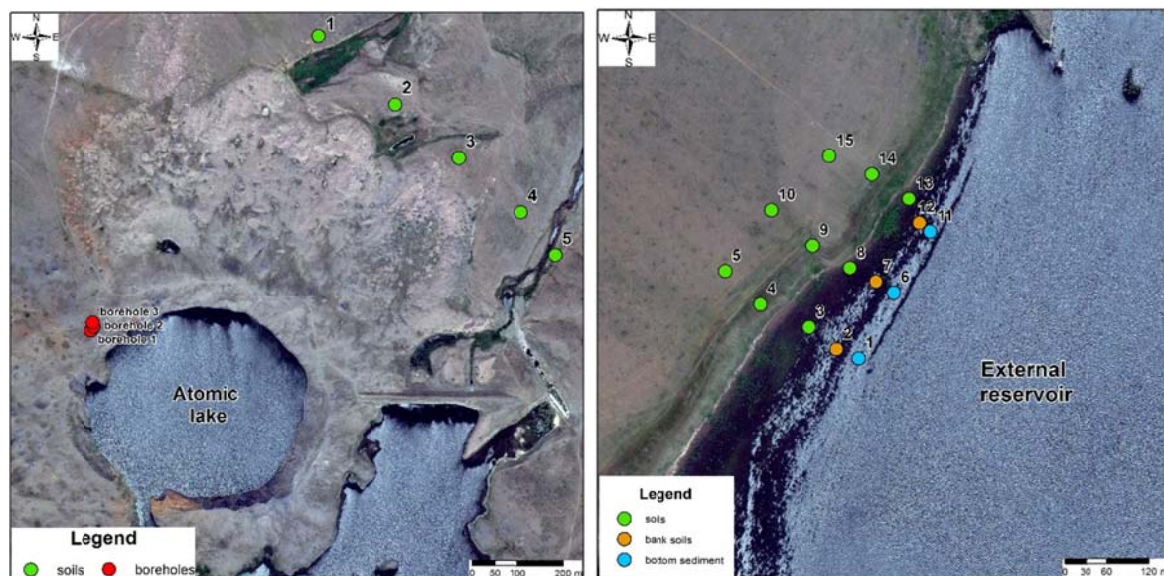
Figure 2. Soil sampling points by layers

Soil sampling (surface).

For the purpose of characterizing radioactive contamination and calibrating field gamma-ray spectrometers, soil surface samples have been collected. Sampling was made along 4 beams, from the crater of the "Atomic" lake and farther on (Figure 3).
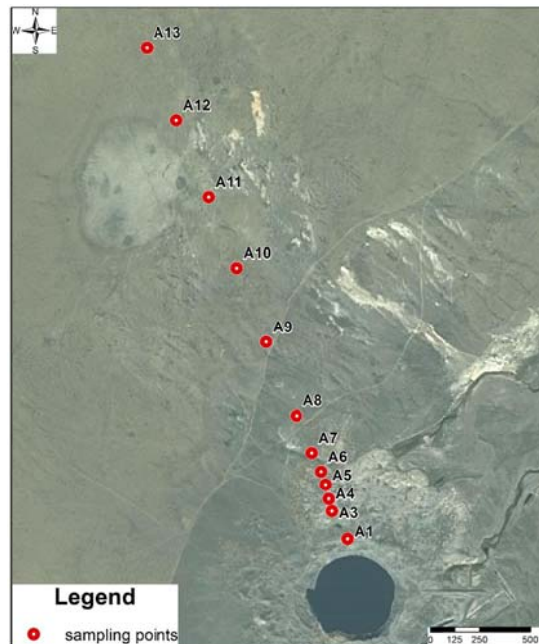
Figure 3. Sampling points by beams

Map construction for surface radionuclide distribution.

For the spatial analysis of available data with geoinformation systems, two software products Golden Software Surfer and Arc Gis were used.

In-vitro studies.

Pu and Sr were determined after radiochemical isolation was previously carried out. Canberra alpha-spectrometers were used to determine $^{239+240}$Pu, ^{238}Pu concentrations. An alpha spectrometer consists of vacuum chambers, α-rays detectors, a pulse analyzer and GENIE 2000 software. Detection limits were calculated based on a type of sample and measurement time.
Liquid-scintillation beta-spectrometer TRI-CARB 2900 TR from Hewlett Packard was used to determine specific activities of ^{3}H, ^{90}Sr and other β-emitting radionuclides in samples.
Canberra and Ortec gamma-spectrometers were used in order to determine concentrations of γ-emitting radionuclides in soil.

Working results

As a result of pedestrian gamma-spectrometric survey, a picture has been obtained that characterizes radioactive contamination of the territory adjacent to the "Atomic" lake. Overall, data obtained allowed detailing the picture of radioactive contamination and confirmed results from the previous research. The major radioactive contamination in soils and subsoils spreads in the northern direction. At that, maximum concentrations of radionuclides focused in the zone of crater bank and within a two-kilometer area.

Nature of areal distribution of radionuclides.

As shown by the analysis, ^{137}Cs contamination in the territory is the most extensive and occupies the area of some 27 km^2 The main detectable soil contamination with ^{241}Am is concentrated in the northern direction and does not exceed 20 km^2
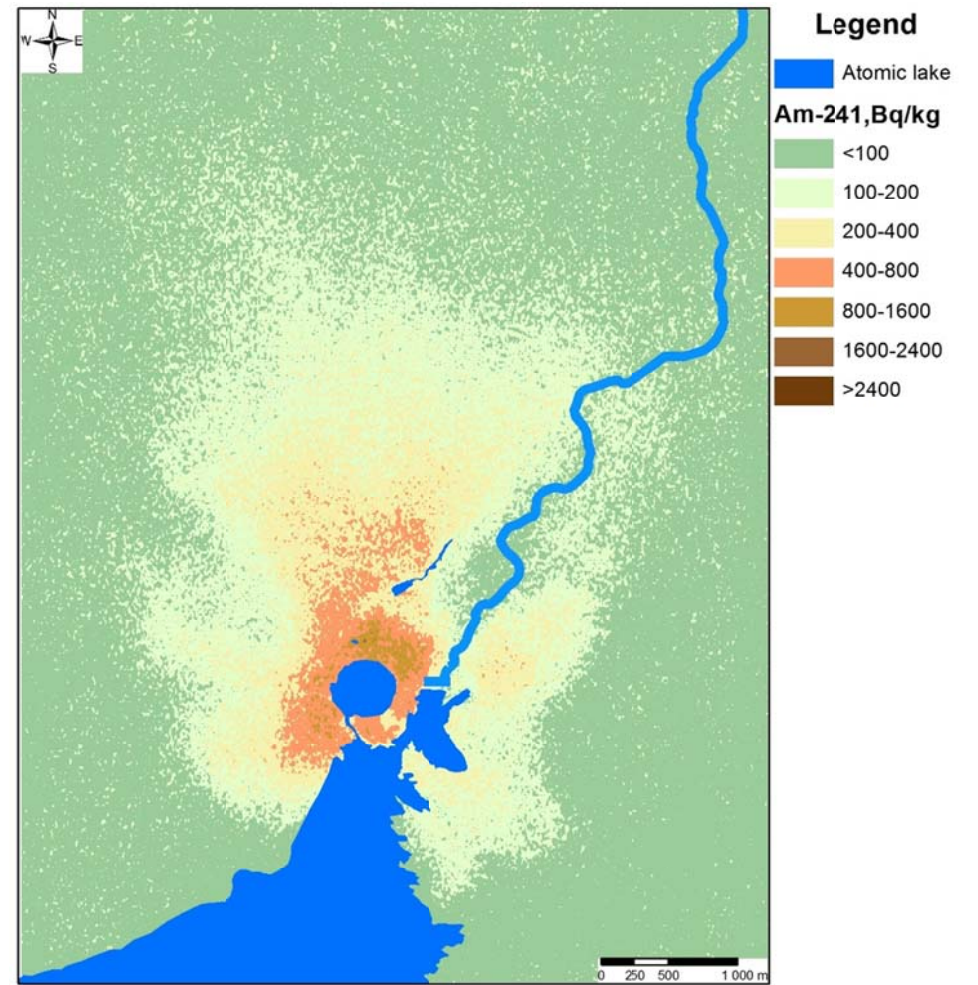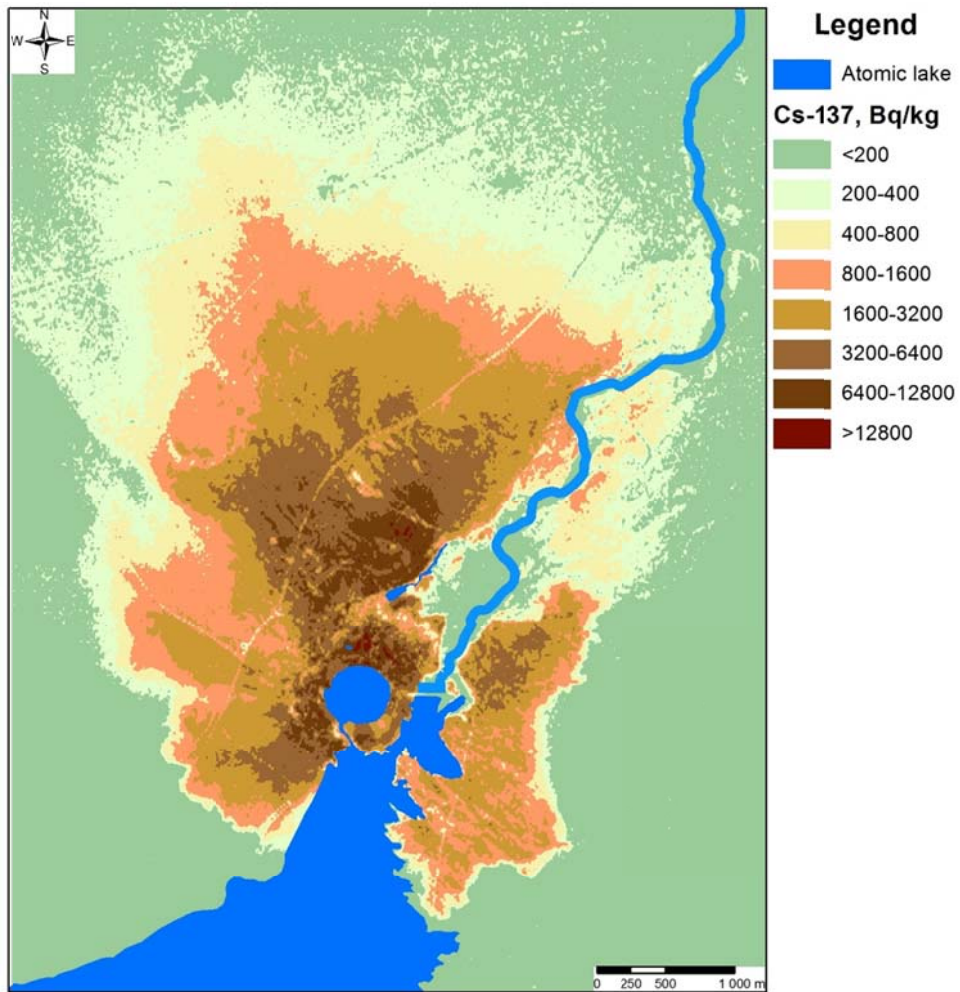
Figure 2. Distribution of ^{137}Cs and ^{241}Am

Nature of radionuclides distribution in depth in the crater bank.

Nature of man-made radionuclides distribution in depth of the "Atomic" lake crater bank is given in the Figure (Figure 5).
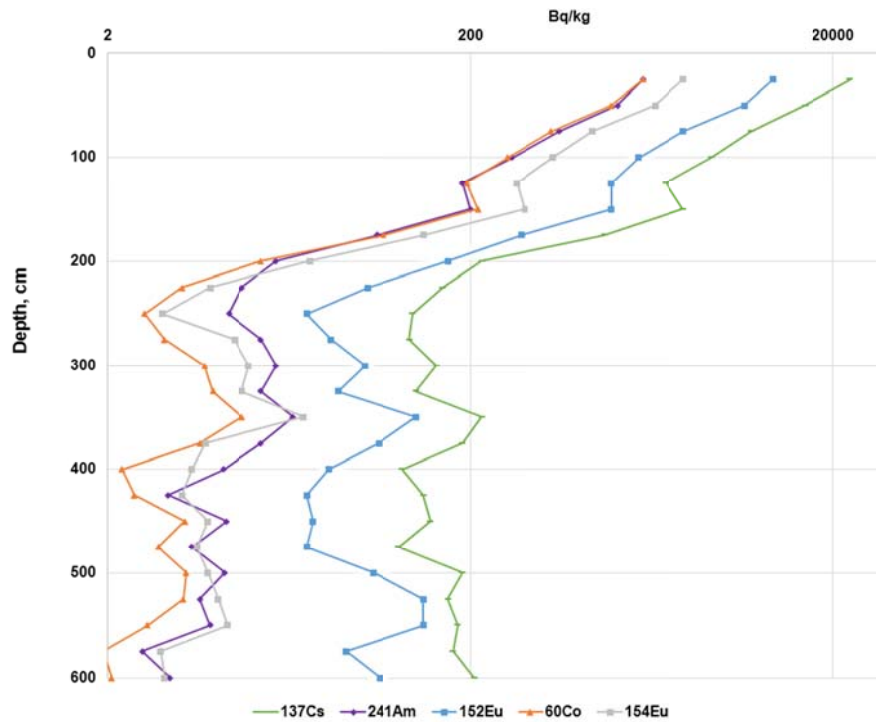
Figure 5. Nature of man-made radionuclides distribution in depth (bank)

Nature of man-made radionuclides distribution in depth at individual spots.

Nature of man-made radionuclides distribution in depth in the region of the external reservoir is presented in the Figure (Figure 6).
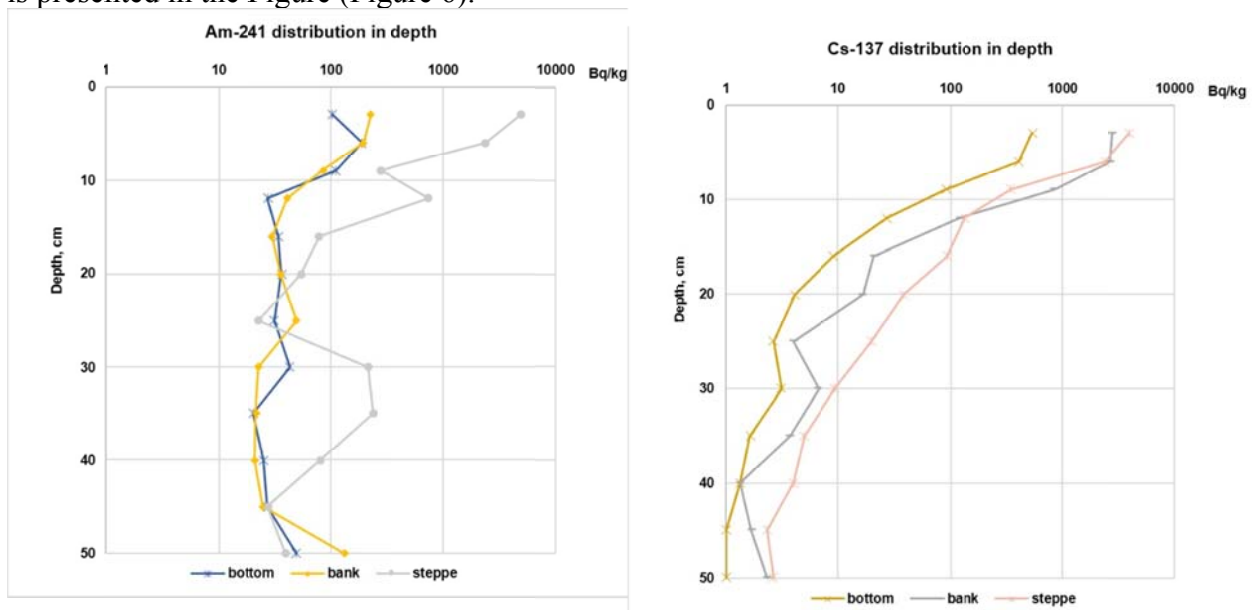
a)   b)

Figure 6. Nature of man-made radionuclides distribution in depth (external reservoir): a) ^{241}Am and b) ^{137}Cs

Nature of man-made radionuclides in depth in the region of Shagan river flood plain is presented in the Figure (Figure 7)
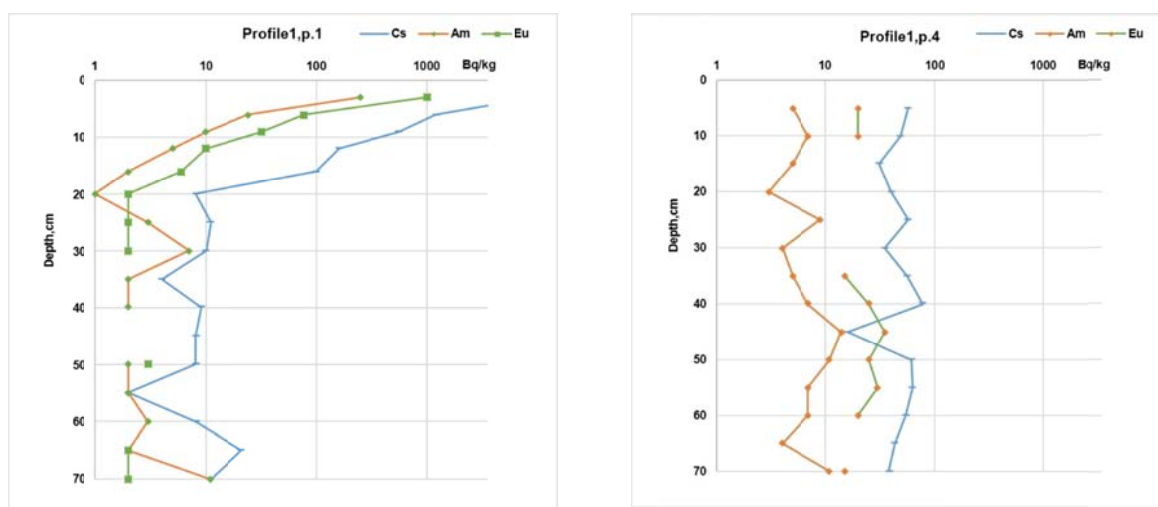
Figure 7. Nature of man-made radionuclides distribution in depth (Shagan river region)

Nature of 3H, $^{239+240, 238}$Pu, ^{90}Sr, ^{60}Co, ^{154}Eu contamination.

Determinations of ^{3}H, $^{239+240, 238}$Pu, ^{90}Sr, ^{60}Co, ^{154}Eu man-made radionuclides are presented in the Table (Table 1).

***Table 1.** In-vitro analysis results*

#	Sampling point	Sampling spot	H-3	^{90}Sr	$^{239+240}$Pu	^{238}Pu	^{60}Co	^{154}Eu
1.	A1	Bank ridge	150000	<2	17000	7500	<4,9	<11
2.	A2	100 m from the ridge	60000	7400	1800	710	500	760
3.	A3	160 m from the ridge	23000	2500	500	180	150	230
4.	A4	230 m from the ridge	57000	12000	2700	740	800	1200
5.	A5	300 m from the ridge	97000	11000	2500	710	680	1000
6.	A6	370 m from the ridge	9600	1500	200	60	240	360
7.	A7	470 m from the ridge	65000	8900	2100	840	590	890
8.	A8	670 m from the ridge	12000	2100	320	90	110	150
9.	A9	1070 m from the ridge	25000	4100	500	160	190	280
10.	A10	1470 m from the ridge	12000	4100	280	110	110	150
11.	A11	1870 m from the ridge	3600	1700	60	20	20	<40
12.	A12	2270 m from the ridge	2300	650	100	30	20	<40
13.	A13	2670 m from the ridge	4300	8500	90	30	30	40

Conclusions

It has been found as a result of research that radioactive contamination of the area studied is non-uniform. Maximum concentrations of radionuclides expectedly focus in the region of the crater bank. With increasing distance from the crater ridge, a sharp reduction of radionuclides concentration occurs down to background values at a distance of 10 km.

Nature of radionuclide distribution in depth also depends on the location of spots and their landscape and geographical properties. Maximum concentrations in the zone of the crater bank focus in the top soil of 0-100 cm. Then uniform distribution occurs in a 2 – 6 m layer. A different kind of radionuclide occurrence is observed at spots subjected to seasonal flooding. These have a virtually uniform radionuclide distribution across the depth. Otherwise, nuclide distribution in depth is classical, i.e. maximum concentrations are in the top 5 cm soil.

D – MARINE

Concentration of radionuclides in marine organisms

Fernando P. Carvalho

Laboratório de Protecção e Segurança Radiológica, Instituto Superior Técnico/ Universidade de Lisboa
Estrada Nacional 10, km 139, 2695-066 Bobadela LRS, Portugal
E-mail: carvalho@itn.pt

Abstract

The first measurements made of artificial radionuclides released into the marine environment did reveal that radionuclides are concentrated by marine biological species. The need to report radionuclide accumulation in biota in different conditions and geographical areas prompted the use of concentration factors as a convenient way to describe the accumulation of radionuclides in biota relative to radionuclide concentrations in seawater. Later, concentration factors would become a tool in modelling radionuclide distribution and transfer in aquatic environments and to predicting radioactivity in organisms. Many environmental parameters can modify the biokinetics of accumulation and elimination of radionuclides in marine biota, but concentration factors remained a convenient way to describe concentration processes of radioactive and stable isotopes in aquatic organisms. Revision of CF values is periodically undertaken by international organizations, such as the International Atomic Energy Agency (IAEA), to make updated information available to the international community. A brief commented review of radionuclide concentration processes and concentration factors in marine organisms is presented for key groups of radionuclides such as fission products, activation products, transuranium elements, and naturally-occurring radionuclides.

Keywords: radionuclides; marine organisms; biokinetics of radionuclides; accumulation; elimination; food chain transfer.

Introduction

Concentration of radionuclides in marine organisms, and in aquatic organisms in general, was noticed with the first measurements of radioactivity in marine biota made in the mid of 20th century (Polikarpov 1966; Shannon and Cherry, 1967). Using radiation detection techniques and instruments that are largely outdated today, were measured at that time very high concentrations of naturally occurring polonium-210 in marine plankton, and recorded artificial radionuclides such as caesium-137 and cobalt-60 from nuclear weapons fallout in fish, mollusc and crustacean (Polikarpov, 1966). When the 1st International Conference on Radioecological Concentration Processes was held in 1966, there were already a large number of scientific reports published on radioactivity in marine biota, and the conference enabled to consolidate at the highest international level the recently acquired knowledge on concentration of radionuclides in biota (Aberg and Hungate, 1967).

Since then, the concepts and the data base of radioactivity measurements relevant to the understanding of chemical and physiological processes that regulate the accumulation of radionuclides in marine biota have continuously expanded (Eisenbud and Gesell, 1997). This knowledge has been the basis for more recent attempts to model bio concentration and transfer of radionuclides in the environment in general, and in the marine environment in particular (e.g., Strand et al.,2000; Tateda et al., 2013; Tagami and Uchida, 2016). The development of such radioecological models is crucial to predict the concentration of radionuclides by marine biota and the transfer and dispersal of radionuclides in the environment in order to provide a sound basis for radiological risk assessment to man and to other biological species, as needed from enhanced radioactivity levels in the environment. This need has been highlighted in several circumstances and, especially, following the nuclear accident of Fukushima and subsequent radioactivity releases into the sea (Tagami and Uchida, 2016).

The correct understanding of bio concentration mechanisms and the harmonized use of concepts and terminology is very important to capture in computational models the parameters that underpin concentration and transfer of radionuclides in the environment. The better the radionuclide concentration mechanisms are understood, the better the radioecological models will be. With the purpose of better understanding the processes underlying biological concentration of radionuclides in the marine environment, some of the key concentration mechanisms in marine organisms are reviewed and summarized herein.

The concept of Concentration Factor

The Concentration Factor (CF), understood as the ratio of concentration of a contaminant substance in biota and the concentration of the same substance in surrounding water, was first introduced in aquatic toxicology. This concept was found useful to describe the uptake and accumulation of radionuclides in aquatic biota and it was adopted in environmental radioactivity and radioecology reports since the 1950s (Ancellin et al., 1979; Eisenbud and Gesell, 1997). However, in the 1st Radioecological Conference held 50 years ago, the expression CF was still in use side by side with others and it was not of generalized use yet (Aberg and Hungate, 1967). Gradually, the CF became of overwhelming use in the next decades in radioecology. This factor is usually represented in terms of a concentration in biota relative to that in ambient sea water. If both biological material and seawater concentrations are derived per unit mass, this term is dimensionless (IAEA, 2004). Then, CF (dimensionless) = Concentration per unit mass of organism (kg/kg or Bq/kg wet weight) /Concentration per unit mass of sea water (kg/kg or Bq/kg).

In data compilations, CF values originate both from laboratory experiments and from field measurements and generally are pooled together. These data compilations may display a considerable disagreement of CF values for the same species that occurs because in many laboratory experiments test organisms were exposed to contaminants dissolved in water only, and in the field the concentration of contaminants occur from the combined effect of uptake from water and from food with a significant effect on the CF value (Ancellin et al., 1979; Pentreath 1980). Some authors introduced a different terminology to distinguish values from laboratory experiments (Bio Concentration Factors, or BCFs) from values obtained from field studies (Bio Accumulation Factors, or BAFs). There is some value in this distinction, although some of the international data compilations, including those of the IAEA, do not make use of them.

Currently, CFs remain basic operational values which have been useful to enable comparison of the concentrations of several radionuclides in the same biological species, and comparison of the ability of different species in concentrating the same radionuclide from the marine environment. The clear advantage of using CFs resides in allowing rapid identification of species that will concentrate more the radionuclides from sea water, and, thus, the selection of those to be used as the best sentinel organisms in environmental monitoring programmes, providing early detection of radionuclides in the marine environment. Furthermore, in a given marine area the use of a selected biological species will enable to identify the radionuclides of major concern in the environment (critical radionuclides). This bio monitoring approach was introduced 40 years ago through the concept of Mussel Watch (Goldberg, 1975; Farrington et al, 2016). The mussel watch nowadays is used in many countries for monitoring radioactivity and other pollutants in coastal areas and allows monitoring the current status of contamination and the investigation of temporal and spatial pollution trends (Carvalho and Civili, 2001; Villeneuve et al., 1999; Carvalho et al, 2011a, 2011b).

Adsorption and absorption of radionuclides

For radionuclides in the marine environment two basic mechanisms have definite influence in their concentration by marine species: adsorption (i.e., uptake from sea water by physical-chemical

processes onto the organism's external surfaces) and absorption (i.e., uptake of radionuclides from the food through the gut wall into the internal tissues and organs of organisms; may also include uptake through the gills). Both adsorption and absorption may be very relevant in radionuclide concentration processes and, thus, in the build-up of CF values in marine organisms.

Adsorption is the key mechanism that intervenes in the concentration of transuranic radionuclides from sea water, particularly in organisms with hard and calcified external body surfaces, such as crustacean. Experimental results demonstrated that the uptake of plutonium, americium, neptunium, californium and other transuranic elements was mainly due to radionuclide sorption from sea water onto the external surfaces of organisms. For example, ^{237}Pu, ^{241}Am and ^{252}Cf concentrated in a marine isopod from sea water were mostly attached to the external body surface (exoskeleton) and were gradually loss by desorption when these crustacean isopods were transferred into non contaminated sea water (Carvalho and Fowler, 1985a; Fowler and Carvalho 1985; Fowler et al., 1986). In experiments with transuranics and marine macrophytic algae radionuclide sorption on algae blades was external and related to piston velocity across the blade boundary layer, and could vary amongst Pu and Am (Carvalho and Fowler, 1985b). In planktonic algae, Pu and Am from sea water were mainly adsorbed onto the cell wall (Fisher et al., 1983a).

Absorption is the key mechanism in concentrating radionuclides from the ingested food. This mechanism is particularly important when radionuclides are highly concentrated in the diet and when the gut transfer factor of radionuclides is high in the consumer species. Laboratory experiments have shown, for example, that for some radionuclides gut absorption may be low while for other radionuclides may be very high. For example, crustacean and fish fed with food contaminated with transuranium elements generally showed little absorption of these elements (few percent of ingested dose) through gut walls (Carvalho et al, 1983; Carvalho and Fowler, 1985a). Contrasting with this, absorption of other elements from food by marine biota, such as polonium (^{210}Po), can be very efficient and account for most of radionuclide concentrated from the environment being by large more important than ^{210}Po adsorption from sea water (Carvalho and Fowler, 1993, 1994). Experimental research on crustacean and fish using three polonium isotopes (^{208}Po, ^{209}Po, ^{210}Po) demonstrated through an elegant technique that Po from sea water practically did not contribute to ^{210}Po accumulated in internal tissues, while Po in ingested food explained most (>97%) of Po concentrated in internal organs (Carvalho and Fowler, 1994).

Marine organisms, such as for example those living in the epipelagic layer and in the deep layer of the oceans, are exposed to similar concentrations of ^{210}Po dissolved in seawater, about 1 mBq/L. Notwithstanding, in both environments there are fish displaying a wide range of ^{210}Po concentrations as shown by several authors (e.g., Cherry and Shannon, 1974; Carvalho 1988). Analyses of ^{210}Po in organisms from all layers of the ocean have documented this variation and ^{210}Po concentration in organisms was related to the energy transfer (protein) in marine food chains and trophic levels (Carvalho 1988, 1990, 2011). As a consequence, ^{210}Po CFs in marine organisms may vary, and has a reason to vary widely among species living in the same ecosystem. Furthermore, even closely related biological species, i.e., belonging to the same taxon as for example "Fish", may display very different CFs for ^{210}Po according to their trophic level (Figure 1). In current CF data compilations, this effect and differences in CF for "Fish" have not been taken into account yet.

CF values do not elucidate the concentration mechanisms and do not inform about the sites of radionuclide accumulation in organisms. The sites and type of binding (external adsorption by weak chemical bonds such as with transuranium elements, or internally accumulated and incorporated in organic molecules such as Po in ferritin, and cadmium and other metals in metallothioneins) may have a large influence to the subsequent radionuclide transfer in marine food chains (Galey et al., 1983; Durand et al., 1999). Indeed, it was experimentally demonstrated that the entry of some metals/radionuclides in the food chain starts at the lowest trophic levels with bacteria and microscopic plankton which easy their entrance in the first trophic level of marine food chains

(Fisher et al.,1983a, 1983b, 2000). In the next steps of food chains, the binding or incorporation of radionuclides in organic molecules may control their transfer to other organisms.
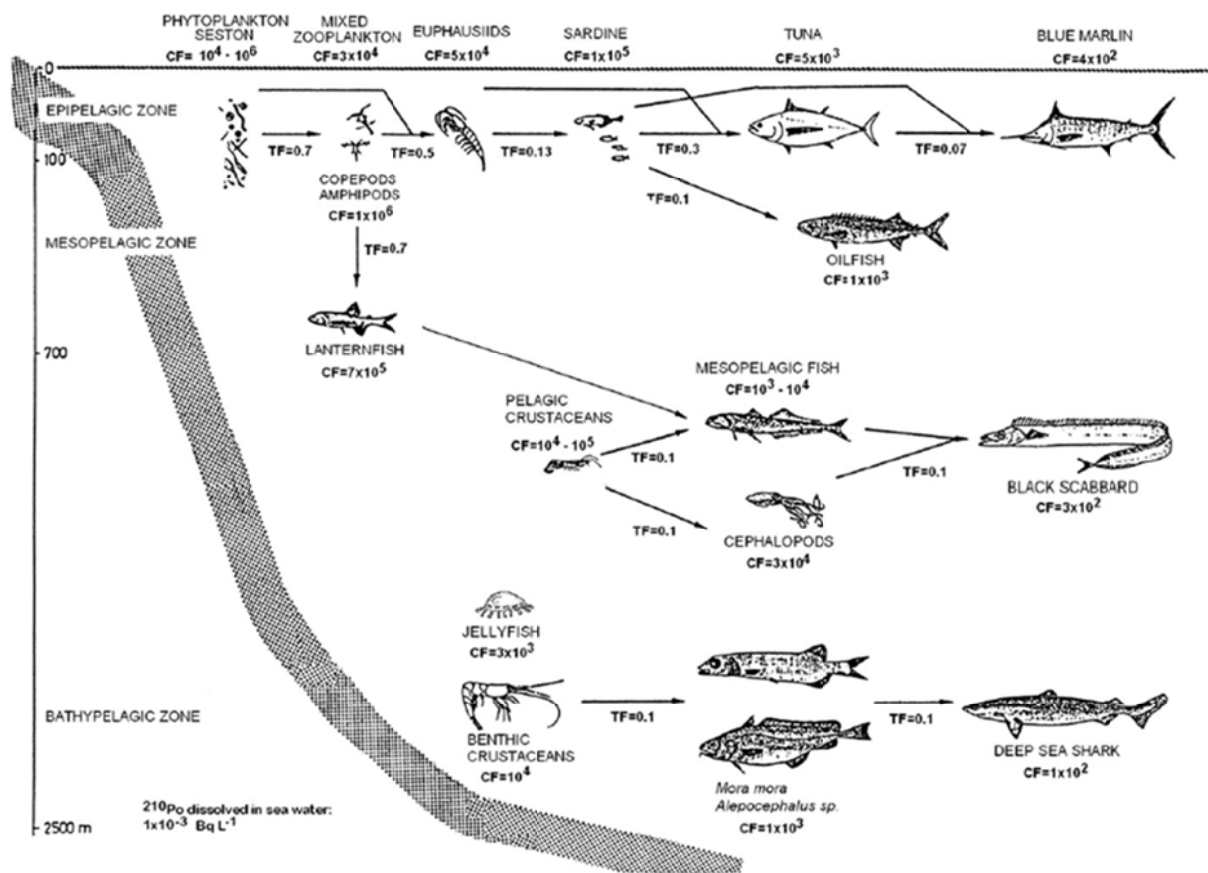
Figure 1. *Polonium 210 concentration in marine organisms and transfer in marine food chains (Reproduced from Carvalho 2011)*

Regulation of internal concentration of radionuclides

From decades of experimental research on the concentration of elements in aquatic organisms, it was observed that aquatic organisms do concentrate some elements to high levels and do not concentrate other elements despite their presence in the environment. Furthermore, the concentration of some elements in the internal medium is regulated and kept constant in many species, in spite of large fluctuations of their concentrations in the aquatic environment. For example mollusc, crustacean and fish are able to regulate the concentrations of Na and K in the intracellular and extracellular fluids, and to keep them at different levels compared to the environmental aqueous media. This ability is called homeostasis (Langston and Bebianno, 2013). In contrast to this, the concentration of other elements/radionuclides in biological species is not under metabolic regulation and the concentration of the element in the organism is proportional to the concentration in water, being the CF a constant value throughout very large ranges of environmental concentrations.

The homeostatic regulation mechanism is effective in the regulation of ionic concentrations of essential and quasi-essential elements. For radioactive isotopes often present in radioactive wastes from nuclear industry, such as ^{65}Zn, ^{54}Mn, ^{55}Fe, and ^{45}Ca, their biological concentration follows special kinetics. These radioactive ions released into the sea will dissolve in sea water and dilute in

the pool of stable isotopes of the element. In the uptake by biota, the CF may increase up to a certain level but, due to homeostasis, above a given value the concentration process will not increase further even in the case of continued increase of concentration in the sea water. In such condition the CF value will decrease, and the radionuclide concentration in the biological species will not be proportional to the radionuclide concentration in sea water. Therefore the use of CFs must be critically assessed taking into account the actual concentrations of radionuclides in sea water.

Another interesting group of radionuclides, that could be called mimetic chemical species, include Cs (that is chemically similar to K), Ba, Sr and Ra (that are chemically similar to Ca), Po (that is similar to S), etc. Radioactive discharges into the marine environment allow these elements, which generally are not essential to organisms, to become concentrated in marine species. Caesium (^{134}Cs and ^{137}Cs) is a monovalent ion similar to K and its concentration in biota depends on K concentration in the external water (Pentreath, 1980). ^{90}Sr and ^{226}Ra, that are common radionuclides from uranium nuclear fission and from natural origin respectively, have chemistries similar to Ca and, once mixed with Ca in the environment, are concentrated via calcium pathways in the organisms (Mauchline and Templeton, 1966). These radionuclides are accumulated and large fractions may be immobilized in calcium reservoirs, such as mollusc shells and bone tissue, but may be transferred also in the food chain accompanying the absorption of Ca ions from the food into the consumer's tissues.

Concentration of Inorganic and Organic forms of radionuclides

Concentration of radionuclides from sea water was found to vary substantially in the case of some metals and metalloids that may occur as inorganic ions and as organic ligand species. It has been shown that ionic species of Hg (metal) is little concentrated from sea water but, after methylation, the methyl-mercury is strongly concentrated by marine species, such as fish and marine mammals, and transferred to man with sea food. The methylation of Hg, stable or radioactive, takes place in the environment mainly by sediment bacteria (Langston and Bebianno, 2013).

Cobalt, in particular ^{60}Co that is often reported as an activation product present in radioactive effluents from nuclear power plants, is an ionic species whose concentration from sea water by molluscs and fish is generally low. However, Co is incorporated in cobalamine, an organic compound (vitamin) synthetized by bacteria, and important as an enzyme to the vertebrates, including man. The uptake of ionic cobalt from sea water is very low, but the gut transfer of cobalamine is very high in fish as well as in other biota (Nolan and Dahlgaard, 1991).

Tin and trybutil-tin follow the same concentration processes of other metal ions and metal ligands, and concentration of the trybutil tin have significant ecological impact on the marine fauna.

Another example is polonium (^{210}Po), that is weakly taken up and concentrated in marine biota from ^{210}Po soluble form in sea water, but easily and efficiently concentrated through food chain in association with organic molecules. For example, in marine fish and crustacean it was demonstrated that the organically bound ^{210}Po was absorbed through gut walls with an efficiency of 0.05 and 0.35, respectively, which corresponded approximately to the efficiency of protein absorption in the same species (Carvalho and Fowler, 1994).

Therefore, it seems a general trend in metal concentration that ionic species of metals do have low gut absorption, while organically bound ions of the same metals/radionuclides are efficiently absorbed into internal tissues of organisms. CFs of the inorganic and organic species of radionuclides do have different CF values that must be recognized.

Biokinetics of radionuclide concentration from water and from food

Concentration of radionuclides from the water (soluble fraction) on one side, and from the particulate fraction and ingested food on the other side, must be taken both into consideration for

most marine organisms. Concentration from water and food can be described by differential equations that take into account both pathways, the length of exposure, and turnover rates in the internal tissues. When contaminated organisms are transferred to a clean environment, and thus the exposure ceases, the rate of elimination is generally described by exponential rates and may involve several compartments (Figure 2).

For example, the uptake of polonium from food and water and its elimination from the body in crustacean was fit to exponential dynamic models that allowed computing biological half-lives of the radionuclide (Carvalho and Fowler, 1994). Similar models can be applied to other radionuclides and biological species and accurately describe the kinetics of bio concentration processes.

However, in the field, often the fluctuating rates of radionuclide discharges into the sea create non equilibrium concentrations and the CF values determined do not reflect steady state conditions. The time of exposure and other environmental variables are then paramount factors in the description of the kinetics of accumulation and elimination of radionuclides in biota (Tagami and Uchida, 2016; Tateda et al., 2013).

The development of models need to introduce more parameters that play a role in describing better the concentration and elimination processes of radionuclides in biota.
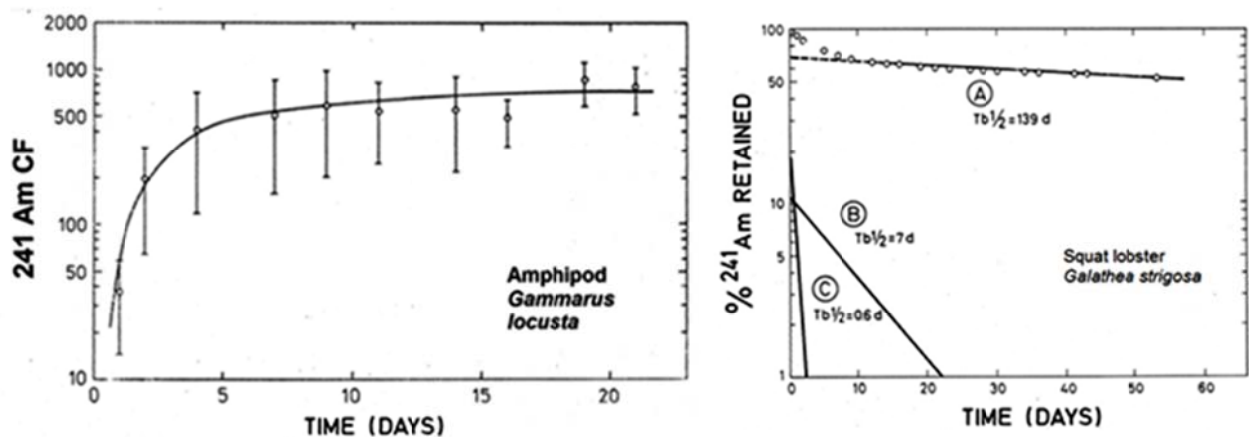
Figure 2. Examples of the kinetics of concentration and elimination of americium-241 by crustacean (Reproduced from Carvalho and Fowler, 1984).

Final remarks

Concentration Factors (CFs) have been used during the last decades in radioecology as a suitable descriptor of radionuclide concentration in marine organisms, enabling comparison among species and, for the same species, enabling comparisons among concentrations of different elements and radionuclides.

Currently, CFs are a tool used in food chain transfer models, dispersion models, and radiological risk assessment models. Nevertheless, it is still necessary to develop better models able to predict the radiecological consequences of radioactive discharges and nuclear accidents, particularly for the marine environment. The use of descriptors of concentration processes is required, but one needs to keep proper understanding of CFs in order to make a correct use in models. The CFs are not an absolute property of each radionuclide, and are not an absolute characteristic of biological species and thus cannot be an unequivocal descriptor from each species. As reviewed above, adsorption and absorption mechanisms may play important roles in the build-up of CFs, chemical similarity of some radionuclides to essential elements or oligoelements may facilitate the concentration of those

radionuclides, and the presence of radionuclides in inorganic and organic chemical forms is crucial to determine the concentration in biota and, thus, the CF values applicable.

Environmental parameters, such as temperature that has effect on metabolic rates, and ionic competition that may affect external sorption of ionic radionuclides for example, play a role on the CF value of radionuclides. Furthermore, biological growth and nutritional status of biota may play an additional role also in the build-up of the CF value for a given radionuclide (Carvalho, et al. 2011a, 2011b). Although relevant to the final CF, these are secondary parameters that act through influencing chemical and physiological variables.

Laborious compilations of CF values have been made and are currently available, but there is still work needed, for example, to differentiate CF values for organic and inorganic radionuclide forms, and to take into account the trophic transfer of radionuclides. In addition, there are data gaps yet for several taxonomic groups that should be filled. Moreover, a critical revision of CF data for radionuclides in the marine environment should be made in order to constraint the large ranges of values and to understand and reflect better the ecological and physiological reasons for such variability.

References

Aberg, A., Hungate, F.P. 1967. Radioecological Concentration Processes. Proceedings of an International symposium held in Stockholm, 25-29 April 1966. Pergamon Press.

Ancellin, J., Guegueniat, P., Germain, P.,1979. Radioécologie Marine, Editions Eyrolles, Paris.

Carvalho, F. P. 2011. Polonium (210Po) and lead (210Pb) in marine organisms and their transfer in marine food chains. J. Environ. Radioact. 102, 462-472.

Carvalho, F.P., 1988. Polonium-210 in marine organisms: a wide range of natural radiation dose domains: Rad. Prot, dosimetry 24: 113-117.

Carvalho, F. P., 1990. Contribution a l' étude du cycle du Polonium-210 et du Plomb-210 dans l'environnement. Thèse de Doctorat. Université de Nice Sophia-Antipolis, France, 398 pp.

Carvalho, F. P., Oliveira, J. M., Alberto , G., Vives i Batlle, J., 2011a. Allometric relationships of 210Po and 210Pb in mussels and their application to environmental monitoring. Marine Poll. Bull. 60, 1734-1742.

Carvalho, F.P., Oliveira, J.M., Alberto, G. 2011b. Factors affecting 210Po and 210Pb activity concentrations in mussels and implications for environmental bio-monitoring programmes. J. Environ. Radioact. 102, 128-137.

Carvalho, F.P., Civili, F. S., 2001. Monitoring of the Mediterranean Sea Pollution (MED POL) and Data Quality Assurance. Intern. J. Environ. Studies, B, 58, 139-158.

Carvalho, F.P., Fowler, S.W., 1984. Experimental studies on biokinetics of americium in benthic marine organisms. In: International Symposium on the Behaviour of Long-Lived Radionuclides in the Marine Environment, pp. 297-315. Ed. by A. Cigna and C. Myttenaere. Luxembourg, Comission of the European Communities.

Carvalho, F.P., Fowler, S.W., 1985a. Biokinetics of plutonium, americium and californium in the marine isopod Cirolana borealis with observations on its feeding and molting behaviour. Mar. Biol. 89, 173-181

Carvalho, F.P., Fowler, S.W., 1985b. Americium adsorption on the surfaces of macrophytic algae. J. Environ. Radioact. 2, 311-317.

Carvalho, F.P., Fowler, S.W., 1993. An experimental study on the bioaccumulation and turnover of polonium-210 and lead-210 in marine shrimp. Mar. Ecol. Prog. Ser. 102, 125-133.

Carvalho, F.P., Fowler, S.W., 1994. A double tracer technique to determine the relative importance of water and food as sources of polonium-210 to marine prawns and fish. Mar. Ecol. Prog. Ser. 103, 251-264.

Carvalho, F.P., Fowler, S.W., La Rosa, J., 1983. Assimilation, inter-organ transfer and excretion of americium in two teleost fish. Mar. Biol. 77, 59-66.

Cherry, L.D., Shannon L.V. 1974. The alpha radioactyivity of marine organisms, Atomic Energy Review, 12(19), IAEA, Vienna, pp. 3-45.

Durand, J.P., Carvalho, F.P., Goudard, F., Pieri, J., Fowler, S.W., Cotret, O., 1999. 210Po binding to Metallothioneins and Ferritin in Liver of Teleost Marine Fish. Mar. Ecol. Prog. Ser., 177, 189-196.

Eisenbud, M. and Gesell, T. Environmental Radioactivity.From Natural, Industrial, and Military Sources.

1997 (Fourth Edition). Elsevier.

Farrington, J.W., Tripp, B. W., Tanabe, S., et al., 2016. Edward D. Goldberg's proposal of "the Mussel Watch": Reflections after 40 years. Marine Poll. Bull. 110, 501–510.

Fisher, N.S., Burns, K., Cherry R.D., Heyraud, M., 1983a. Accumulation and cellular distribution of 241Am, 210Po, and 210Pb in two marine algae. Mar.Ecol. Prog. Ser., 11, 233- 237.

Fisher, N.S., Bjerregaard, P., Fowler, S.W., 1983b. Interactions of marine plankton with transuranic elements, 1. Biokinetics of neptunium, plutonium,americium and californium in phytoplankton, Limnol. Oceanogr. 28, 432.

Fisher, N.S., et al., 2000. Trace metals in marine copepods: A field test of a bioaccumulation model coupled to laboratory uptake kinetics data, Mar. Ecol. Prog. Ser. 194, 211.

Fowler, S.W., Carvalho, F.P., 1985. Americium biokinetics in benthic organisms as a function of feeding mode. Bull. Environ. Contam. Toxicol. 35, 826-834.

Fowler, S.W., Carvalho, F.P., Aston, S.R., 1986. Experimental studies on californium bioavailability to marine benthic invertebrates. J. Environ. Radioact. 3, 219.

Fowler, S.W., Carvalho, F.P., Aston, S.R., 1986. Experimental studies on californium bioavailability to marine benthic invertebrates. J. Environ. Radioact. 3, 219-243.

Galey, J., Goulard, F., Pieri, J., Fowler, S.W., Carvalho, F.P., 1983. Tissue and subcellular distribution of 252Cf and 241Am in the seastar Marthasterias glacialis. Mar. Biol. 75, 253-259.

Goldberg, E.D., 1975. The mussel watch: a first step in global marine monitoring. Mar. Pollut. Bull. 6, 111.

International Atomic Energy Agency, 2004. Sediment distribution coefficients and concentration factors for biota in the marine environment. Technical Reports Series No. 422, IAEA, Vienna.

Langston, W. J., Bebianno, M. J., (Ed.) 2013. Metal Metabolism in Aquatic Environments. Springer Science & Business Media. Ecotoxicology Series vol. 7, 448 pp.

Mauchline, J.,Templeton,W.L., 1966. Strontium, calcium and barium in marine organisms from the Irish Sea. J. Cons. Int. Explor. Mer. 30, 161.

Nolan, C.; Dahlgaard, H. 1991. Accumulation of metal radiotracers by Mytilus edulis. Mar. Ecol. Prog. Ser., Vol. 70, No. 2, p. 165-174.

Polikarpov, G. 1966. Radioecology of aquatic organisms: the accumulation and biological effect of radioactive substances. Moscow Academy of Sciences. Reinhold Book Division, 314 pp.

Pentreath R. J.. Nuclear Power, Man and the Environment. Publ. Taylor and Francis, London 1980.

Shannon L.V., Cherry R.D., 1967. Polonium-210 in marine plankton. Nature, 216 (5113), 352-353.

Strand, P., Brown, J.E., Woodhead, D.S., Larsson, C.M., 2000. Delivering a system and framework for the protection of the environment from ionising radiation. In: 10th Int. Congress IRPA, 14 – 19 May 2000, Hiroshima, Japan. pp.116.

Tagami, K., Uchida, S., 2016. Consideration on the Long Ecological Half-Life Component of 137Cs in Demersal Fish Based on Field Observation Results Obtained after the Fukushima Accident. Environ. Sci. Technol., 50, 1804−1811.

Tateda, Y., Tsumune, D., Tsubono, T., 2013. Simulation of radioactive caesium transfer in the southern Fukushima coastal biota using a dynamic food chain transfer model. Journal of Environmental Radioactivity 124: 1-12

Villeneuve, J.P., Carvalho, F.P., Fowler, S.W. Cattini, C., 1999. Levels and Trends of PCBs, chlorinated pesticides and petroleum hydrocarbons in mussels from the N.W. Mediterranean coast. Comparison of concentrations in 1973/74 and 1988/89. Sci. Total Environ. 237/238, 57-65.

Bioaccumulation and trophic transfer in marine food chains – An example from the northern Arabian Gulf

S. Uddin[a], M. Behbahani

Environment and Life Sciences Research Center, Kuwait Institute for Scientific Research, Kuwait

Abstract

This study presents the ^{210}Po concentration in marine biota and turnaround in marine environment. The ^{210}Po concentration was established in biota across the trophic levels from microalgae to top predators in the Arabian/Persian Gulf. The ^{210}Po was highly concentrated at the base of the food chain, among the primary producers.

The concentrations observed in green and brown algae were 15.1-26.0 and 38.4-56.3 Bq Kg^{-1} ww. The concentrations are typically in range of 1.1 – 1.6 Bq Kg^{-1} ww for *Sargassum boveanum* and 0.9 – 6.7 Bq Kg^{-1} ww for *Sargassum angustifolium.* The concentrations in shrimp specie *Paneus semisulcatus* were 0.25-0.65 and 0.45-0.63 Bq Kg^{-1} ww in muscle and shell. The clams and crockle showed high ^{210}Po concentrations *Marica marmorata* (84.20 – 92.88); *Circe intermedia* (30.72-35.79); *Marcia opima* (18.44-21.19); *Fulvia fragile* (16.52-20.08) Bq Kg^{-1} ww. Bryoza samples of *Schizoporella errata* showed high concentration of ^{210}Po. Those larger in size and older in age have ^{210}Po concentrations between 402.1-527.2 Bq Kg^{-1} wet weight and formed bigger colony, those smaller in size and younger have ^{210}Po concentrations between 283.1-356.7 Bq Kg^{-1} wet weight.

Tunicate samples of *Ascidiscea Phallusia nigra* showed very high ^{210}Po bio concentration, typically values observed were between 871.9-1012.3 Bq Kg^{-1} wet weight. The ^{210}Po concentration in male crab *Scylla serrata* was 102.40-111.96 Bq Kg^{-1} ww in the soft tissue; 490.34-564.04 Bq Kg^{-1} ww in the organs; 104.64-137.78 Bq Kg^{-1} ww in shell and 13.56-36.24 Bq Kg^{-1} ww in appendages; while in female *Scylla serrata* the concentration of ^{210}Po were 77.02-83.07 Bq Kg^{-1} ww in the soft tissue; 743.3-801.37 Bq Kg^{-1} ww in the organs; 54.78-163.53 Bq Kg^{-1} ww in shell and 25.80-32.60 Bq Kg^{-1} ww in appendages.

In blue crab *Portunus pelagicus* ^{210}Po concentration was 23.40-26.00 Bq Kg^{-1} ww in the soft tissue; 83.44-110.91 Bq Kg^{-1} ww in the organs; 17.33-24.09 Bq Kg^{-1} ww in shell and 3.75-3.95 Bq Kg^{-1} ww in appendages.

Fish from different trophic levels were analysed and showed a wide range of concentrations varying several orders of magnitude, typically the fish in trophic level 2 has ^{210}Po concentration between 0.05 – 2.5 Bq Kg^{-1} ww, in trophic level 3 the concentrations were 0.5 – 4.8 Bq Kg^{-1} ww and in the trophic level 4 between 0.5 - 500 Bq Kg^{-1} ww.

The ^{210}Po concentration in filtered seawater range between of 0.30 – 0.44 mBq L^{-1}. It has been observed that in all the fish samples, the ^{210}Po concentrations in gills were an order of magnitude lower than in the digestive system.

It is noteworthy that the ^{210}Po concentration in fecal matter was always higher than that in the digestive system which gives a strong indication that much of the ingested ^{210}Po is excreted back into the marine environment in a much more concentrated form which then becomes part of the bottom detrital material

as well as suspended particulates, both of which provide a higher exposure to both detritivore and pelagic fish. Among all the biota that were analyzed, the highest overall concentration of ^{210}Po was noted in Yellowfin tuna indicating significant ^{210}Po biomagnification in that particular species.

Introduction

The radioecological community has been actively engaged to quantify the radiation effects on biota. Over the past five decades, the natural radionuclide ^{210}Po has been extensively studied for its spatio-temporal variability and transfer and transport in the environment (Cherry and Shannon 1974, Cherry et al. 1975, Cherry and Heyraud 1981, Cherry and Heyraud 1982, McDonald et al. 1986, Carvalho 1988, Cherry and Heyraud 1988; 1991, Cherry et al. 1994, Stewart et al. 2005, Carvalho 2011, Fowler 2011, Uddin et al. 2012, Farber-Lorda et al. 2013, Uddin and Behbehani 2014, Uddin et al. 2015) due to its particle reactive nature and enhanced accumulation in various marine organisms (Fowler 2011), especially the microscopic phytoplankton at the base of the food chain.

Several initial studies have reported elevated uptake of ^{210}Po in phytoplankton and zooplankton (Shannon and Cherry 1967, Shannon et al. 1970, Folsom and Beasley 1973, Cherry et al. 1975, Beasley et al. 1978). However, to adequately understand bioaccumulation processes and trophic transfer through marine food chains, an in-depth knowledge of the behavior and fate of this radionuclide in a variety of marine species comprising the food web is necessary. Several earlier workers have studied experimentally ^{210}Po transfer in various marine food chains, but usually most experiments have selectively examined a single species or a very few species. Also, several bioaccumulation experiments have been conducted in controlled aquaria, by spiking radionuclides of interest in very high (non-environmental) concentrations, and as acute exposures usually for very short exposure times. We believe that this is not appropriate for defining concentration factors, Kd values, bioaccumulation and biomagnifications. There have been very few studies which have examined ^{210}Po bioaccumulation in organisms across several trophic levels (Uddin et al. 2016).

Methods

^{210}Po bioaccumulation in the local food web has been determined by analyzing market size fish and shell fish as well as several other biota species sampled from Kuwait territorial waters (Fig. 1). A large number of samples covering several trophic levels, ranging from microalgae to top predator sharks, were obtained.

The local, English, scientific names and fdry factors of the marine organisms sampled are given in Table 1. Most of these organisms were collected by making a series of net trawls during the period from February 2014 to April 2015. Approximately 250 g of phytoplankton (microalgae) were also sampled from Kuwait Bay by towing a 20-µm mesh size bongo net. All the biota samples were packed on ice and immediately transported to the special radionuclide- and metal-clean laboratory at KISR. In addition, there were also a few fresh frozen samples that were obtained commercially from the local food basket.

Standard protocols for sample collection, preparation, and radionuclide determination were followed (IAEA 1989). All the analyzed samples of fish, molluscs and seaweed were composite samples made by bulking 5 kg of a similar species.
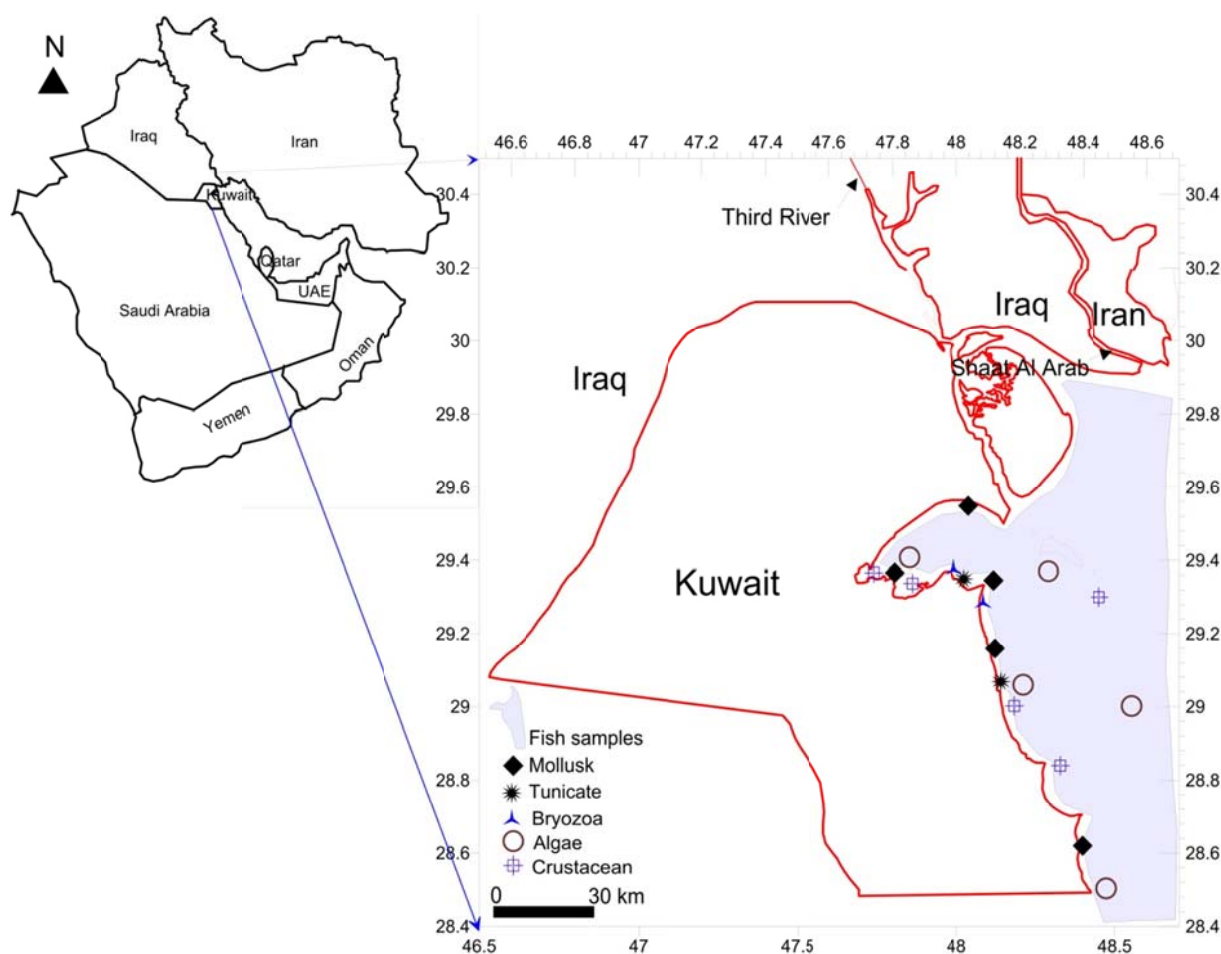
Figure 1. Map of the Kuwait coast showing the location of sampling sites and the types of organisms collected.

Fish samples were dissected and [210]Po concentrations were determined in edible tissues, gills, liver, and digestive system. Whenever noted, eggs were collected, and fecal matter was carefully removed from the terminal end of the intestinal tract. All the samples were dried at 105°C and pulverized.

Each sample was digested in concentrated nitric acid for at least 24 h with an addition of hydrogen peroxide to aid in oxidizing the organic materials, after which a clear solution was obtained and evaporated to near dryness. The resulting residue was then dissolved in 100 ml of 0.5-mol/l HCl and the solution heated on a magnetic stirrer at 80 $^{\circ}$C. The [210]Po in this solution was then spontaneously plated onto a 0.64mm-thick silver disc (1.2 cm dia) after iron reduction with ascorbic acid (Fisenne 1997, Al-Masri et al. 2000). All the samples (2 g dry) were spiked with 100 μL of [209]Po tracer at the beginning of the digestion process to ascertain the [210]Po recovery and efficiency. A Canberra twelve-chamber alpha spectrometry system with a passive ion-implanted silicon detector (active area of 300 mm^2, background count of 2.3 per day, and minimum depletion thickness of 90 µm) was used for the [210]Po determination, and the 5.305-MeV energy line was chosen for quantification.

As part of our quality assurance procedures, reagent blanks and IAEA certified materials were also analyzed with each batch of samples. Along with the fish samples, the Fish Certified

Reference Material (IAEA 414) was analyzed for ^{210}Po, and the concentration of ^{210}Pb (^{210}Po) was found to vary between 1.82 and 2.15 Bq kg^{-1} with a median value of 2.01 Bq kg^{-1}. This compared well with the certified ^{210}Pb (^{210}Po) information value of 2.1 Bq kg^{-1} and a 95% confidence interval of 1.8 to 2.5 Bq kg^{-1}.

Results and Discussion

Previous baseline analyses of seawater from this area have shown that the ^{210}Po concentrations in filtered seawater range between of 0.30 – 0.69 mBq L^{-1} .

At the base of the food chain, ^{210}Po was highly concentrated among the primary producers, i.e microalgal cells (both brown and blue green). The concentrations observed in brown microalgae were 38.4-56.3 Bq Kg^{-1} ww, substantially higher than those measured in the blue green microalgae (15.1-26.0 Bq Kg^{-1} ww), and are several orders of magnitude higher than the ^{210}Po concentrations in sea water. The macroalgae (Sargassum) displayed much lower concentrations compared to the microalgae. The shrimp *Paneus semisulcatus* was analyzed for ^{210}Po, with concentrations of 0.25-0.65 and 0.45-0.63 Bq Kg^{-1} ww measured in their muscle and shell, respectively. The reason for the similar concentrations in muscle and shell is not immediately evident from our initial measurements, however, we suspect the presence of subcutaneous tissues adhering to the shell might be responsible for these similar values. The clams and cockles all showed relatively high ^{210}Po concentrations in their soft parts, e.g., *Marica marmorata* (84.2 – 92.9), *Circe intermedia* (30.7-35.8), *Marcia opima* (18.4-21.2), and *Fulvia fragile* (16.5-20.1) Bq Kg^{-1} ww.

Bryozoan samples of *Schizoporella errata* displayed very high concentrations of ^{210}Po. Those larger in size and older in age had ^{210}Po concentrations between 402-527 Bq Kg^{-1} ww and formed a larger colony; those smaller in size and younger had lower ^{210}Po concentrations ranging between 283-357 Bq Kg^{-1} ww. Tunicate samples of *Phallusia nigra* also contained very high levels of ^{210}Po, with typical values ranging between 872-1012 Bq Kg^{-1} ww. Two varieties of crabs, *Scylla serrata* which is found in the muddy tidal flats and the free swimming blue crab *Portunus pelagicus*, showed a significant difference in ^{210}Po concentration.

There is large variability in ^{210}Po concentration in biota from different taxonomic groups across the trophic level. The values vary several orders of magnitude in different taxanomic groups, with lowest in muscle of red snapper (0.05 Bq Kg^{-1}) and highest in liver of yellowfin tuna (1692.6 Bq Kg^{-1}). The bioaccumulation of ^{210}Po increases in the following order: tunicates>bryoza>crustacean>mollusc>algae. Fish show a wide range of concentration in different tissues and species. The fish have also been classified according to their feeding regimes (Table 3). It is evident that predator fish have a very high concentration of ^{210}Po as well as high variability, indicating enhanced bioaccumulation and the potential for trophic transfer and biomagnification of this radionuclide.

Conclusions

The concentrations of ^{210}Po were established in a variety of marine biota across different trophic levels. The highest concentrations were observed in the order:

tunicate>bryozoa>mollusk>crustacean>algae>fish. The ^{210}Po concentrations in edible tissue of fish were extremely variable ranging from 0.04 – 44.93 Bq Kg^{-1} ww. The maximum concentration in trophic level 2 is an order of magnitude lower than trophic level 3 and two orders of magnitude than trophic level 4 (Table 2). It is also observed that the predator fishes have highest ^{210}Po concentrations.

It was observed that in all the fish samples, the ^{210}Po concentrations in gills were an order of magnitude lower than in the digestive system suggesting ingestion as more likely uptake pathway. It is noteworthy that the ^{210}Po concentration in fecal matter was always higher than that in the digestive system which gives a strong indication that much of the ingested ^{210}Po is excreted back into the marine environment in a much more concentrated form which then becomes part of the bottom detrital material as well as suspended particulates, both of which provide a higher exposure to both detritivore and pelagic fish. Among all the biota that were analyzed, the highest overall concentration of ^{210}Po was noted in Yellowfin tuna indicating a potential for enhanced ^{210}Po biomagnification in that particular species. This finding suggests that a more detailed study of top predator marine fish, such as tuna, and their prey is necessary to determine if food chain biomagnification is indeed occurring in these top trophic level species.

Table 1. Local, English and scientific names of marine biota along with the average percentage of dry weight.

English Name	Scientific Name	Muscle (% dw)	Gills (% dw)	Liver (% dw)	Digestive System (% dw)	Fecal matter (% dw)	Eggs (% dw)
King soldier bream	*Argyrops spinifer*	22.11	22.41	21.98	19.01		22.36
Red snapper	*Lutjanus malabaricus*	22.71			27.23		
Greater lizard fish	*Synodus intermedius*	25.73	24.54	39.04	25.51	27.19 (GC)	31.66
Daggertooth pike	*Muraenesox cinereus*	25.26		38.67	22.59		35.22
Yellowfin tuna	*Thunnus albacores*	31.99	24.92	25.50	25.53	21.51	
Spanish mackerel	*Scomberomrus guttalus*	22.10			20.87		
Bombay duck	*Harpadon nehereus*	16.23	16.75		12.45		
Longfin trevally	*Carangoides armatus*	22.68			20.72		
Fourfinger threadfin	*Eleutheronema tetradactylum*	25.08			23.65		
Sea catfish	*Arius spp.*	29.42	31.03	22.27	24.49	15.92	25.83(S)
Orange spotted grouper	*Epinephelus coioides*	24.96	34.92	37.72	23.17		
Arabian smoothhound	*Mustelus mosis*	32.02	23.65	38.37	27.11	27.00 (skin)	27.42 (head)
Delagoa threadfin bream	*Nemipterus bipunctatus*	21.94			20.96		
Spangled emperor	*Lethrinus nebulosus*	23.70	22.82		22.54		
Five lined snapper	*Lutjanus quinquelineatus*	22.06			24.05		
Tigertooth croaker	*Otolithes ruber*	28.83	24.37		30.54	19.03	
Bartail flathead	*Platycephalus indicus*	24.10			30.02		
Haffara seabream	*Rhabdosargus haffara*	31.83	33.61		30.03	27.13	
Soldier bream	*Argyrops filamentosus*	24.16			23.71		
Oriental sole	*Brachirus orientalis*	19.91			21.10		
Moonfish	*Mene maculate*	32.38	35.35		23.70		32.99
Javelin grunter	*Pomadasys kakaan*	24.55			27.65		
Yellowfin seabream	*Acanthopagrus latus*	30.65	30.25		33.27	32.62	
Yellowtip halfbeak	*Hemiramphus marginatus*	27.29	26.09		29.25		24.21
Gilthead seabream	*Sparidentex hasta*	25.30			34.77		
Shorthead anchovy	*Encrasicholina heteroloba*	17.80					
Southern pompano	*Trachinotus africanus*	37.96	27.74	29.93	24.88		35.05

English Name	Scientific Name	Muscle (% dw)	Gills (% dw)	Liver (% dw)	Digestive System (% dw)	Fecal matter (% dw)	Eggs (% dw)
Pomfret	*Pampus argenteus*	29.16			23.38		
Indian mackerel	*Rastrelliger kanagurta*	24.35	23.38	33.58	23.89		
White sardine	*Escualosa thoracata*	35.76	31.15		30.08		26.68
Persian Gulf cuttlefish	*Sepia Arabica*	22.26			27.74	31.81	34.88
Shrimp	*Paneus semisulcatus*	19.83	26.25 (SH)				
Spotted scat	*Scatophagus argus*	27.44	26.07	26.73	21.00		37.83
Spiny Lobster	*Panulirus versicolor*	18.11	25.10 (SH)				29.43
Black pomfret	*Parastromateus niger*	26.20			21.67		
Hilsa shad	*Tenualosa ilisha*	31.52	27.01		21.23		46.12
Klunzinger mullet	*Lisa klunzingeri*	25.72			30.54		
Greenback mullet	*Liza subyiridis*	27.76			28.77		
Aquacultured Redbelly tilapia	*Tilapia zillii*	25.13	29.19	23.65	21.90		42.01
Roho labeo	*Labeo rohita*	23.84	24.97		31.16		
Nile tilapia	*Oreochromis niloticus*	24.41			25.00		
Clam	*Marica marmorata*	15.70					
Clam	*Circe intermedia*	20.30					
Clam	*Marcia opima*	20.40					
Cockle	*Fulvia fragile*	22.50					
Crab	*Portunus pelagicus*	26.30	33.90 (A)	43.80 (SH)	33.20	42.10 (claws)	
Crab (male)	*Scylla serrata*	22.1	34.80 (A)	57.40 (SH)	21.20		
Crab (female)	*Scylla serrata*	22.6	34.20 (A)	52.30 (SH)	24.70		
Cheilostome bryozoan	*Schizoporella errata*	16.40 (soft tissue)		53.90 (SH)			
Cheilostome bryozoan	*Schizoporella errata*	16.44 (soft tissue)		53.95 (SH)			
Solitary ascidian	*Phallusia nigra*	24.80 (soft tissue)		9.20 (SH)			
Solitary ascidian	*Phallusia nigra*	25.00 (soft tissue)		16.33 (SH)			
Brown microalgae	n.i.	2.05 (whole body bulk concentrations)					
Blue-Green microalgae	n.i.	1.58 (whole body bulk concentrations)					
Sargassum	*Sargassum boveanum*	12.20 (whole body bulk concentration)					
Sargassum	*Sargassum angustifolium*	11.55 (whole body bulk concentration)					

G : Gills; S: Spleen; SH: Shell; A: Appendages; GC: Gut content; n.i. : Not identified.

Table 2. ^{210}Po concentration in marine biota from Kuwait waters (wet weight)

English Name	Scientific Name	Trophic Level	^{210}Po Bqkg^{-1} Muscle	^{210}Po Bq kg^{-1} Gills	^{210}Po Bq kg^{-1} Liver	^{210}Po Bq kg^{-1} Digestive Sys.	^{210}Po Bq kg^{-1} fecal matter	^{210}Po Bq kg^{-1} eggs
King soldier bream	*Argyrops spinifer*	4.5	0.63-0.96	3.29-3.61	27.22-28.26	20.72-38.04		2.49-2.83
Red snapper	*Lutjanus malabaricus*	4.5	0.05-0.11			1.64-2.11		
Greater lizard fish	*Synodus intermedius*	4.4	4.67-5.11	15.62-20.36	16.80-23.27	63.46-71.05	10.00-11.83 (feed)	52.00-58.03
Daggertooth pike	*Muraenesox cinereus*	4.4	4.22-4.67		20.91-27.84	42.47-43.96		21.10-24.39
Yellowfin tuna	*Thunnus albacores*	4.4	37.26-44.93	97.53-119.21	1511.3-1692.6	451.56-548.21	303.56-314.76	
Spanish mackerel	*Scomberomrus guttalus*	4.3	2.17-2.41			49.27-57.16		
Bombay duck	*Harpadon nehereus*	4.2	28.44-36.81	83.57-86.02		165.60-190.60		
Longfin trevally	*Carangoides armatus*	4.2	1.15-1.65			19.01-19.81		
Fourfinger threadfin	*Eleutheronema tetradactylum*	4.1	0.14-0.21			3.00-3.66		
Sea catfish	*Arius spp.*	4.0	0.31-0.35	1.01-1.11	4.76-5.49	13.08-15.38	18.86-23.18	3.99-4.66(S)
Orange spotted grouper	*Epinephelus coioides*	4.0	0.07-0.10	4.03-4.67	4.67-5.54	1.46-4.81		
Arabian smoothhound	*Mustelus mosis*	4.0	0.50-0.61	7.61-10.02	64.16-71.94	13.74-18.59	4.12-5.98 (skin)	2.29-2.84 (head)
Delagoa threadfin bream	*Nemipterus bipunctatus*	3.9	0.12-0.18			4.21-4.67		
Spangled emperor	*Lethrinus nebulosus*	3.8	0.14-0.16	6.41-7.51		8.97-9.67		
Five lined snapper	*Lutjanus quinquelineatus*	3.7	0.21-0.28			9.11-10.42		
Tigertooth croaker	*Otolithes ruber*	3.6	0.31-0.34	4.95-5.66		5.47-7.40	11.57-11.99	
Bartail flathead	*Platycephalus indicus*	3.6	0.51-0.67			11.63-14.85		
Haffara seabream	*Rhabdosargus haffara*	3.5	0.65-0.83	9.71-10.13		18.52-21.80	16.48-25.42	
Soldier bream	*Argyrops filamentosus*	3.5	1.57-2.22			31.38-33.13		
Oriental sole	*Brachirus orientalis*	3.5	0.17-0.21			6.87-8.20		
Moonfish	*Mene maculate*	3.5	0.44-0.72	6.54-7.66		42.82-46.47		5.03-5.85
Javelin grunter	*Pomadasys kakaan*	3.5	0.15-0.26			1.76-1.88		
Yellowfin seabream	*Acanthopagrus latus*	3.4	0.29-0.34	6.28-7.14		6.75-8.35	26.18-31.07	
Yellowtip halfbeak	*Hemiramphus marginatus*	3.4	0.37-0.41	1.94-2.13		7.40-8.01		23.75-31.34
Gilthead seabream	*Sparidentex hasta*	3.4	0.08-0.14			2.33-2.65		
Shorthead anchovy	*Encrasicholina heteroloba*	3.3	25.40-28.27					

English Name	Scientific Name	Trophic Level	^{210}Po Bqkg^{-1} Muscle	^{210}Po Bq kg^{-1} Gills	^{210}Po Bq kg^{-1} Liver	^{210}Po Bq kg^{-1} Digestive Sys.	^{210}Po Bq kg^{-1} fecal matter	^{210}Po Bq kg^{-1} eggs
Southern pompano	*Trachinotus africanus*	3.3	0.97-1.01	8.26-8.52	58.03-58.97	82.75-99.41		23.39-31.08
Pomfret	*Pampus argenteus*	3.3	0.98-1.11			23.07-23.62		
Indian mackerel	*Rastrelliger kanagurta*	3.2	0.69-0.95	5.89-6.83	737.21-821.30	10.02-11.48		
White sardine	*Escualosa thoracata*	3.2	6.92-8.25	18.78-22.53		44.67-46.43		17.59-19.82
Persian Gulf cuttlefish	*Sepia Arabica*	3.0	0.16-0.21			2.29-2.80	39.34-41.43	0.20-0.27
Shrimp	*Paneus semisulcatus*	3.0	0.25-0.65	0.45-0.63 (SH)				
Spotted scat	*Scatophagus argus*	3.0	0.37-0.42	1.25-1.53	3.21-3.55	16.00-18.11		1.11-1.53
Spiny Lobster	*Panulirus versicolor*	3.0	2.40-2.61	34.86-45.28 (SH)				6.10-9.72
Black pomfret	*Parastromateus niger*	2.9	0.49-0.65			16.68-19.61		
Hilsa shad	*Tenualosa ilisha*	2.9	1.28-1.67	3.72-6.04		18.12-19.84		8.07-10.25
Klunzinger mullet	*Lisa klunzingeri*	2.7	1.49-1.56			14.32-16.15		
Greenback mullet	*Liza subyiridis*	2.7	1.29-1.48			8.12-9.11		
Aquacultured Redbelly tilapia	*Tilapia zillii*	2.5	0.43-0.50	1.34-1.49	5.72-7.19	2.31-3.06		0.92-1.28
Roho labeo	*Labeo rohita*	2.2	0.04-0.06	0.09-0.11		0.37-0.53		
Nile tilapia	*Oreochromis niloticus*	2.0	0.07-0.11			0.40-0.60		
Clam	*Marica marmorata*	2.0	84.20-92.88					
Clam	*Circe intermedia*	2.0	30.72-35.79					
Clam	*Marcia opima*	2.0	18.44-21.19					
Cockle	*Fulvia fragile*	2.0	16.52-20.08					
Crab	*Portunus pelagicus*	2.0	23.40-26.00	75-3.95 (A)	17.33-24.09 (SH)	383.44-110.91.	2.05-2.71 (claws)	
Crab (male)	*Scylla serrata*	2.0	102.40-111.96		104.6-137.8 (SH)	490.34-564.04	13.56-36.24 (A)	
Crab (female)	*Scylla serrata*	2.0	77.02-83.07		54.78-163.53(SH)	743.3-801.37	25.80-32.60 (A)	
Cheilostome bryozoan	*Schizoporella errata*	2.0	402.1-527.2 (soft tissue)		206.4-256.5 (SH)			
Cheilostome bryzoan	*Schizoporella errata*	2.0	283.1-356.7 (soft tissue)		144.1-153.1 (SH)			
Solitary ascidian	*Phallusia nigra*	2.0	892.5-947.1 (soft tissue)		223.7-253.5 (SH)			
Solitary ascidian	*Phallusia nigra*	2.0	871.9-1012.3 (soft tissue)		183.9-212.4 (SH)			
Brown algae	n.i.	1.0	38.43-56.31 (whole body bulk concentrations)					
BlueGreen algae	n.i.	1.0	15.07-25.99 (whole body bulk concentrations)					
Sargassum	*Sargassum boveanum*	1.0	1.09-1.64 (whole body bulk concentration)					
Sargassum	*Sargassum angustifolium*	1.0	0.89-6.72 (whole body bulk concentration)					

G : Gills; S: Spleen; SH: Shell; A: Appendages; n.i. : Not identified.

Table 3. The feeding regieme of fish analyzed.

Code	Stands for :	Species included	
GSP	Grazer Scavenger Planktivorous	Nile Tilapia	2.2
		Greenback Mullet	2.7
		Klunzinger Mullet	2.7
		Hilsa shad	2.9
Aquaculture	Aquaculture	Redbelly tilapia	2.5
		Atlantic salmon	4.5
		Black pomfret	2.9
		Indian mackerel	3.2
		White sardine	3.2
		Pomfret	3.2
P	Planktivorous	Shorthead anchovy	3.3
		Spotted Scat	3.3
GSI	Grazer Scavenger Invertebrates-eater	Yellowtip halfbeak	3.4
PI	Predator of invertebrates	Southern pompano	3.3
		Haffara seabream	3.5
		Moon Fish	3.5
		Oriental sole	3.5
		Soldier bream	3.5
		Bartail flathead	3.6
PBI	Predator of benthic invertebrates	King Soldier bream	4.5
		Yellowfin seabream	3.4
		Jevelin Grunter	3.5
		Spangled emperor	3.8
		Arabian smoothhound	4.0
		Daggertooth pike	4.4
PBIF	Predator of benthic invertebrates and fish	Red Snapper	4.5
		Gilthead Seabream	3.4
		Tigertooth croaker	3.6
		Five lined snapper	3.7
		Delagoa threadfin bream	3.9
		Orange spotted grouper	4.0
		Fourfinger threadfin	4.1
		Longfin trevally	4.2
		Spanish Mackerel	4.3
		Greater Lizard Fish	4.4
PIF	Predator of invertebrates and fish	Yellowfin tuna	4.4
		Sea catfish	4.0
		Baracuda	4.0
PF	Predator of fish	Bombay Duck	4.2

GSP = Grazer Scavenger Planktivorous; FWPL=Freshwater plant; Aquaculture = Farmed species; P = Planktivorous; GSI=Grazer Scavenger Invertebrate-eater, PI=Predator of invertebrates; PBI=Predator of benthic invertebrates; PBIF=Predator of benthic invertebrates and fish; PIF=Predator of invertebrates and fish; PF=Predator of fish

References

Al-Masri, M.S., S. Mamish, Y. Budeir, and A. Nashwati. 2000. "^{210}Po and ^{210}Pb concentrations in Fish consumed in Syria." *Journal of Environmental Radioactivity* **49** (3):345-352.

Beasley, T.M., M. Heyraud, J.J.W. Higgo, R.D. Cherry, and S.W. Fowler. 1978. "^{210}Po and ^{210}Pb in zooplankton fecal pellets." *Marine Biology* **44**:325-328.

Carvalho, F. P. 1988. "^{210}Po in marine organisms: a wide range of natural radiation dose domains." *Radiation Protection Dosimetry* **24**:113-117.

Carvalho, F.P. 2011. "Polonium (^{210}Po) and lead (^{210}Pb) in marine organisms and their transfer in marine food chains." *Journal of Environmental Radioactivity* **102**:46-472.

Cherry, R.D. , and M. Heyraud. 1981. "Polonium-210 content of marine shrimp: Variation with biological and environmental factors." *Marine Biology* **65** (2):165-175.

Cherry, R.D., S.W. Fowler, T.M. Beasley, and M. Heyraud. 1975. "Polonium-210: its vertical oceanic transport by zooplankton metabolic activity." *Marine Chemistry* **3**:105-110.

Cherry, R.D., and M. Heyraud. 1982. "Evidence of high natural radiation doses in certain mid-water organisms." *Science* **218**:54-56.

Cherry, R.D., and M. Heyraud, eds. 1988. *Polonium-210 in selected categories of marine organisms: interpretation of the data on the basis of an unstructured marine food web model.* Edited by J.C. Guary, P. Guegueniat and R.J. Pentreath, *Radionuclides: a Tool for Oceanography.* London: Elsevier Applied Science Ltd.

Cherry, R.D., and M. Heyraud. 1991. " Polonium-210 and lead-210 in marine organisms: allometric relationships and their significance." In *Radionuclides in the Study of Marine Processes*, edited by P.J. Kershaw, Woodhead, D.S, 309 - 318. London: Elsevier Applied Science Ltd.

Cherry, R.D., M. Heyraud, and R. Rindfuss. 1994. "Polonium-210 in Teleost Fish and in Marine Mammals: Interfamily Differences and a Possible Association between Polonium-210 and Red Muscle Content." *Journal Environmental Radioactivity* **24**:273-291.

Cherry, R.D., and L.V. Shannon. 1974. "The alpha radioactivity of marine organisms." *Energy Reviews* **12**:3-45.

Farber-Lorda, J., S.W. Fowler, J-C. Miquel, A.R.Y. Baena, and R.A. Jeffree. 2013. "210Po/210Pb dynamics in relation to zooplankton biomass and trophic conditions during an annual cycle in northwestern Mediterranean coastal waters." *Journal of Environmental Radioactivity* **115**:43-52.

Fisenne, I.M. 1997. "Polonium in water and urine, Method Po-01-R C " *Environment measurement laboratory, USA.* **Vol. I.** (HAS L-300):1-5.

Folsom, T.R., and T.M. Beasley. 1973. "Contributions from the alpha emitter polonium-210 to the natural radiation environment of marine organisms." *In: Radioactive Contamination of the Marine Environment. IAEA, Vienna*:625-632.

Fowler, S.W. 2011. "^{210}Po in the marine environment with emphasis on its behaviour within the biosphere." *Journal of Environmental Radioactivity* **102** (8):448-461.

IAEA. 1989. "Measurement of radionuclides in food and the environment." *International Atomic Energy Agency, Technical Report Series* **No. 295**.

McDonald, P., S.W. Fowler, M. Heyraud, and M.S. Baxter. 1986. "Polonium-210 in nussels and its implications for environmental alpha-autoradiography." *Journal of Environmental Radioactivity* **3**:293-303.

Shannon, L.V., and R.D. Cherry. 1967. "Polonium-210 in marine plankton." *Nature* **216**:352-353.

Shannon, L.V., R.D. Cherry, and M.J. Orren. 1970. "Polonium-210 and lead-210 in the marine environment." *Geochim. Cosmochim Acta* **34**:701-711.

Stewart, G.M., S.W. Fowler, J.-L. Teyssie, O. Cotret, J.K. Cochran, and N.S. Fisher. 2005. "Contrasting transfer of polonium-210 and lead-210 across three trophic levels in marine plankton." *Marine Ecology Program Series* **290**:27-33.

Uddin, S., A. Aba, and M. Bebhehani. 2015. "Baseline concentration of ^{210}Po and ^{210}Pb in Sargassum from the northern Gulf." *Marine Pollution Bulletin* **90**:330-333.

Uddin, S., A. Al-Ghadban, M. Behbehani, A. Aba, A. Al-Mutairi, and Q. Karam. 2012. "Baseline concentration of 210Po in Kuwait's commercial fish species." *Marine Pollution Bulletin* **64**:2599-2602.

Uddin, S., and M. Behbehani. 2014. "Bioaccumulation of Po-210 in common gastropod and bivalve species from the northern Gulf." *Ecotoxicology and Environmental Safety* **104**:132-135.

Uddin, S., S. W. Fowler, M. Behbehani, and M. Metian. 2016. "210Po bioaccumulation and trophic transfer in marine food chains in the northern Arabian Gulf." *Journal of Environmental Radioactivity*.

Activity levels of ^{210}Po in marine organism consumed in south of Spain

I.Díaz-Francés, G.Manjón and R. García-Tenorio

University of Seville, Department of Applied Physics, Dept. of ApliedPhysics, ETSA, Avenida Reina Mercedes 2, 41012 Sevilla, Spain

Abstract

The distribution and behaviour of Polonium (^{210}Po) in marine organisms has been and is now a subject of great interest because of their relatively high concentrations in comparison with those in terrestrial organisms and its relatively high weight in the doses received by humans via ingestion. However, depending of the specimen analysed and its relative position along the marine food chain, the ^{210}Po activity levels can be quite different, even in several orders of magnitude. ^{210}Po is primarily absorbed from water and concentrated by phyto- and microzooplankton, and then is transferred to the next trophic level along the marine food chains.

In this work, the contribution of ^{210}Po to the committed effective dose via ingestion received by the Spanish population have been evaluated, by determining the ^{210}Po activity concentrations in an ample set of samples which can be considered representatives of the different marine organisms consumed in Spain. The obtained results show a quite high variability, preventing the possibility to fix a representative value for the ^{210}Po contribution to the ingestion doses received by the Spanish population, but in general these values, due exclusively to ^{210}Po, are higher than the average value assigned by UNSCEAR to the annual committed effective dose received by the worldwide population due to the ingestion of natural and anthropogenic radionuclides.

Introduction

Polonium-210 is a natural occurring radionuclide, belonging to the Uranium series, which is present in minute amounts in the different environmental compartments and that through its route along the trophic chain can finish incorporated in the human body via ingestion of waters and/or food. This radionuclide is highly radiotoxic, with the highest value between the natural radionuclides of the committed effective dose per unit intake via ingestion, and it is present in relatively high concentrations in the marine biota due to its enhanced bioaccumulation and its strong affinity for binding with certain internal tissues. Consequently, ^{210}Po it is an important contributor to the radiation dose received by the marine organisms as well as by the humans consuming seafood.

The high radiotoxicity of ^{210}Po is mainly due to the kind of emissions associated to this radionuclide (alpha particles) and, on the other hand, due to its behavior once it has been incorporated to the human body. According to the ICRP model (ICRP, 1992), for adults, 10% of the inhaled and 50% of ingested ^{210}Po enter the circulatory system while the remaining fraction stays at the gastro-intestinal system for 24-36 hours before being removed by the organism. The absorbed ^{210}Po tends to be accumulated in liver (30%), kidney (10%), spleen (7%) and the bone marrow (10%).
The Spanish population has the seafood as an important component in their diet. Higher committed effective doses via ingestion can be then expected in the Spanish population in relation with other European groups where the culture to include fish in their diet is not so much introduced, due to the higher intake of ^{210}Po associated to this food component. To confirm this fact, we have first estimated the contribution of this radionuclide to the annual committed effective dose by ingestion received by the Spanish population, by determining the ^{210}Po activity concentrations in an ample set of samples which can be considered representatives of the consumed in Spain.

To confirm the key role that the seafood can play for the explanation of the ingestion doses due to [210]Po, the levels of this radionuclide in the edible parts of a great variety of marine organisms were determined, with the peculiarity that the analyses were performed after their cooking, in order to check if cooking can alter the [210]Po content in the seafood and to refine the dose estimates to human consumers. With this end we have analyzed the [210]Po content in the edible parts of several seafood products bought in commercial markets of our town and cooked following the more common recipes in our country. The obtained results will be discussed and evaluated in this work.

Materials and Methods

Samples

The activity concentrations of [210]Po were determined in a group of 20 seafood samples purchased in different local markets in Seville (Spain). Also U-isotope determinations were performed in the same samples for comparison purposes. This group of samples was split up in three different subgroups: a) fishes, b) molluscs-crustaceous and c) fish canned preserves.

The fish species samples analyzed were: mackerel (*Scomberscombrus*), dabs (*Dicologoglossacuneata*), atlantic sardines (*Sardinapilchardus*), anchovies (*Engraulisencrasicolus*), europeangiltheads (*Sparusaurata*), hakes considering muscle and spawns (*Merlucciusmerluccius*), and tuna (*Thunnusobesus*), while the molluscs-crustaceous analyzed were: mussels (*Mytilusedulis*), purple dye (*Murex brandaris*), winkles (*Littorinalittorea*), clams (*Donaxtrunculus*),baby clams (*Chameleagallina*), white shrimps (*parapenaeuslongirostris*), king prawns (*Hymenopaenaeusspp*) and cuttlefish (*Sepia betheloti*). Finally, and regarding preserves the following species were analyzed; cockles (*Cerastodermaedule*), anchovies (*Engraulisencrasicolus*) and baby clams (*Chameleagallina*).

Most of these fish species were cooked in the usual way they are consumed for population focusing the posterior radionuclide analyses only in edible parts, with the exception of the preserves which were analyzed directly as they were taken from the can. After cooking, every sample was dried, milled and homogenized before applying a radiochemical procedure for U and Po isotopes isolation and determination.

Radiometric technique

The radiochemical procedure applied for [210]Po and U-isotopes determination in the seafood samples, after their pretreatment and after the addition of radiochemical-yield tracers ([209]Po and [232]U respectively), had three main steps: a) a wet digestion process, b) a separation process to isolate Po and U from interfering elements, and c) a source preparation process for alpha measurement.

The digestion process was carried out using a Multiwave 3000 Anton Paar microwave system. This device is equipped with a rotor mechanism with eight XF100 liners (independently guarded) that can work under controlled pressure up to 60 bar and temperatures up to 260 ºC. The liners are sealed in order to avoid any leak of gases during the digestion process, and particularly avoiding Po losses even if the evaporation temperature of this element is exceeded. The liners are made of Teflon and they are inlayed in vessel jacked ceramics making up a stiff reaction cell. The digestion process was performed following the protocol recommended by the manufacturer of the microwave.

The outgoing solution of the digestion process is submitted then to a process of U/Po separation using a well-established liquid solvent extraction with TBP (Holm and Fukai, 1977). Finally, from the resulting two independent solutions containing the U or the Po isolated, the needed thin sources for alpha-spectrometric measurements were performed: in the case of Po applying a self-deposition method onto copper planchets (Flynn, 1968), and in the case of U applying an electrodeposition method onto stainless-steel planchets (Hallstadius, 1984).

The measurement of both U and Po planchets were carried out in a AlphaAnalyst spectrometric (Canberra) system formed by eight separate chambers, each one equipped with a silicon detector (PIPS type) Model A450-18AM, and devoted exclusively to one of the mentioned radionuclides to avoid cross-contamination and for a better background control.

To assess the annual committed effective dose due to ingestion of a particular radioelement associated to each particular sample type, we have applied the following equation:

$$D_E = A \cdot F_C \cdot C$$

where "DE" is the annual committed effective dose (Sv/year) via ingestion of a given marine specie due to the radionuclide under consideration. "A" is the activity concentration of this radionuclide measured in the marine specie considered (Bq / kg wet weight), Fc is the corresponding committed effective dose per unit activity taken by ingestion (Sv/Bq), and C is the amount of the marine specie consumed per person and year, expressed as kg wet weight per year.

The value of Fc is dependent on the radionuclide considered and although it is also depending of the age of the population considered (ICRP, 1992), in this study the annual committed effective doses by ingestion have been determined only for adults. In this case, the values of Fc adopted in this work have been Fc (^{210}Po) = 1.2 10^{-6}Sv/Bq and Fc (^{238}U) = 4.5 10^{-8}Sv/Bq, following ICRP recommendations (ICRP, 1992).

The value of C for each marine specie was obtained from published Spanish statistics concerning food consumption (Ministerio Medio Ambiente, 2006), with the exception of three species, where a estimated consumption of 1 kg per year and person was adopted because no data were available.

Results and Discussion

The activity concentrations of ^{210}Po in the samples representatives of the marine organims consumed by the population of Seville are displayed in Table 1. It is possible to observe that the obtained values are quite variable with differences in some cases of near three orders of magnitude. Also in Table 1 are shown the ^{238}U activity concentrations determined in the same samples, being obtained relatively more uniform values over the time, but clearly lower than the obtained ones for ^{210}Po.
The ^{210}Po activity concentrations (expressed in wet weight) are, in most cases, one or several orders of magnitude higher than those determined for another radionuclide belonging to the same natural radioactive series as ^{238}U.

	^{210}Po (Bq/kg w.w.)	^{238}U (Bq/kg w.w.)
Merlucciusmerluccius (muscle)	2.4±0.7	<0.04
Sardina pilchardus	40±13	<0.07
Engraulisencrasicolus	140±37	<0.19
Thunnusobesus	3.4±1.3	<0.03
Scomberscombrus	17±7	0.03±0.01
Sparusaurata	0.15±0.04	NM
Dicoglosacuneata	28±7	0.03±0.01
Merlucciusmerluccius (roe)	11±3	0.04±0.01
Chamelea gallina	43±12	0.70±0.20
Mitylusedulis 1	84±23	NM
Mitylusedulis 2	115±3	NM
Sepia bethelothi	0.09±0.02	<0.02
Paranaeuslongirostris	21.0±0.5	<0.04
Hymenopaenaeusspp.	0.4±0.1	<0.02
Donaxtrunculus	64±16	0.43±0.11
Bolinusbrandaris	16±4	0.43±0.11
Litorinalittorea	5±1	0.72±0.17
Cerastodermaedule	27±6	0.71±0.15
Engraulisencrasicolus	1.3±0.5	0.07±0.3
Chamelea gallina	10.1±0.1	NM

Table 1. *Activity concentrations of ^{210}Po and ^{238}U (Bq/kg w.w.).*

It is noteworthy to remember that the measurements of ^{210}Po were made on seafood samples that had previously experienced the most characteristic cooking process applied in our geographical area (boiling of shellfish, grilled white fish, etc) since the objective is to perform a dosimetric evaluation as realistic as possible by taking into account the possible losses or redistribution of ^{210}Po between different parts or organs of the analyzed specie in the process of preparation for consumption. The Po activity concentrations obtained were particularly high in some species such as anchovies (140 Bq/kg w.w.), sardines (40 Bq/Kg w.w.), mussels (80-100 Bq/kg w.w.) and clams (60 Bq/kg w.w.).

In fact, and assuming an average value of 1 mBq/L of ^{210}Po in the Atlantic seawater, where the great majority of marine species were collected (Bolivar et al., 2000), concentration factors for ^{210}Po of 10^4- 10^5 can be assessed, indicating the high bioaccumulative behavior of this radionuclide along the marine food chain. The ^{238}U activity concentrations do not overpass, on the contrary, in any case the level of 1 Bq/kg wet weight (Table 1), with concentration factor (CF) several orders of

magnitude lower than the found ones for [210]Po. All the data shows the existence of a pronounced radioactive fractionation in the uranium series and indicates how wrong can be the simplification of assuming in the marine species secular equilibrium in the uranium series.

The results obtained in this work for [210]Po are, on the other hand, of the same order of magnitude to those found in the bibliography (Carvalho, 2011) (Cherry et al., 1994) (Connan et al., 2001) (Kannan et al., 2001) (Pietrzak-Flis et al., 1997) (Alonso-Hernandez et al., 2002) (Dahlgaard, 1996) (Heyraud and Cherry 1979) (Cherry and Heyraud, 1981) (McDonald et al., 1991)(Strok and Smodis, 2011) for the same marine species, although there is a general trend to observe some lower values in this work. This deviation could be due to the previous cooking procedure applied over the samples analyzed in this work, which is not the case in the determinations used from comparison and taken from the bibliography, which corresponds in each specie to edible fresh samples.

The assessment of annual committed effective doses for adults due to [210]Po and associated with the ingestion of the different marine species is shown in Figure 1. In this Figure it can be observed that the average annual intake of some of the species, leads to dose values that can be in the order, or exceeds, hundred microsieverts per year (sardines, anchovies, mussels, clams). Then, it can be followed that population having a varied diet rich in marine products could receive a dose due exclusively to [210]Po ingestion of seafood in the order of the mSv/year, by simply adding the dose contributions due to different species. This last value can be in a first instance evaluated as quite high, but can be put in context if ,having in consideration the determinations performed in this work, we indicate that simply a consumption of 1 kg of mussels (100 Bq/kg w.w. of [210]Po) imply a committed effective dose of 120 microsieverts.

The value of 1 mSv/year is close to that used generically as a global average dose received by people from all natural sources of radiation (2.5 mSv /year), and clearly higher that the average global dose value associated to the ingestion route.

All these facts highlights the importance of the route shown in this study related to the total dose received due to natural sources by the Spanish population. And, additionally, indicates that the above mentioned global average of 2.5mSv/year could underestimate the value of the dose received from all natural sources of radiation that should be associated with the population of Spain.
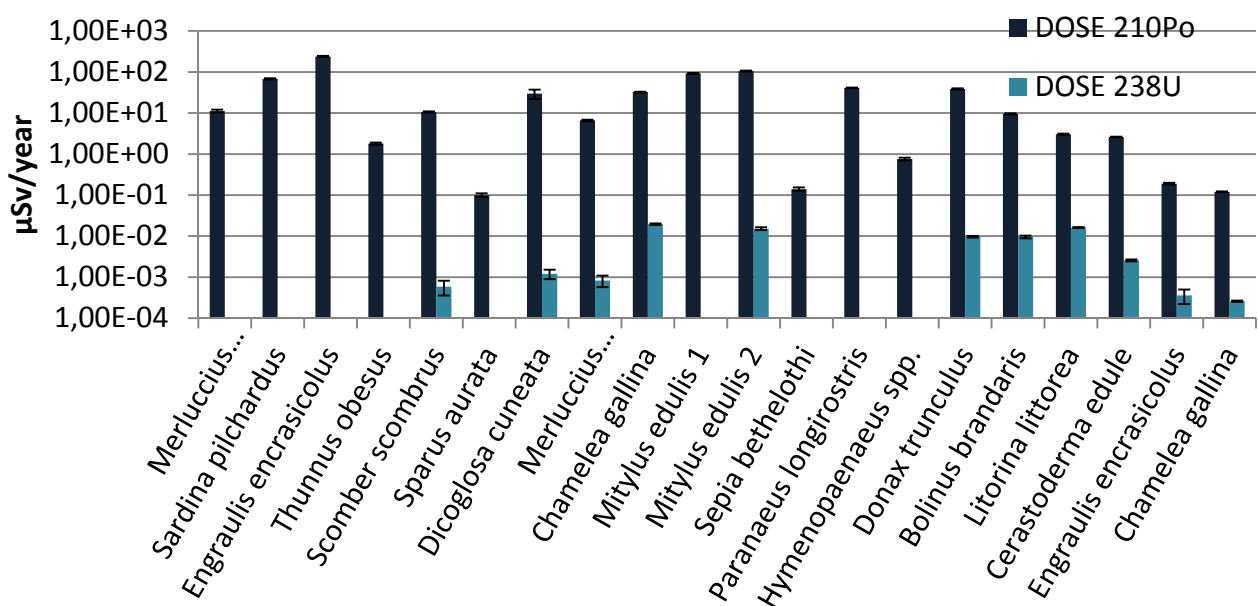

Figure 1. Doses of [210]Po and [238]U (μSv/year)

To put more in context the value of 1 mSv/year obtained for the annual committed effective dose due to ^{210}Po and associated to the ingestion of seafood by the Spanish population, is interesting to mention that this value is equal to the reference level indicated by the IAEA for the additional occupational doses that could be received in NORM industries without the adoption of countermeasures (IAEA 2006). It is then not surprising to find some industries where some countermeasures are taken in order to decrease the additional dose due to natural radionuclides received by the workers, while at the same time comparable doses can be received by them without any restriction due to their consumption habits.

Finally, and with comparison purposes, Figure 1 also shows the annual committed effective doses for adults due to ^{238}U and associated with the ingestion of the different marine species analyzed in this work. Due to the low activity concentrations found for this radionuclide in the analyzed samples and the low Fc value associated to this radionuclide, the annual committed doses are negligible in comparison with the determined ones for ^{210}Po (in general a factor of 10^4 to 10^5 lower), and in all the cases lower than 10^{-2}µsv/year. These data clearly shows the extremely different role that radionuclides belonging to the same natural radioactive series play along the marine food chain and in the assessment of the ingestion doses received by the population which have the seafood as an important component of their diet.

Conclusions

On the basis of the ^{210}Po determinations performed in composite samples representing the edible parts of an ample set of cooked seafood samples, purchased in the local markets, the annual committed effective dose received by Spanish population due to ^{210}Po and associated to the consumption of these products have been realistically assessed.

Having in consideration the well established culture in Spain for heavy consumption of seafood products, the mentioned annual committed effective dose due exclusively to ^{210}Po can even reach the value of 1 mSv/year, constituting a considerable fraction of the average annual dose received by the Spanish population due to all sources of natural radiation.

References

Alonso-Hernández C., Díaz-Asencio M., Munos-Caravaca A., Suarez-Morell E, Avila-Moreno R. 2002 .^{137}Cs and ^{210}Po dose assessment from marine food in Cienfuegos Bay (Cuba). Journal of Environmental Radioactivity 61, 203- 2011.

Bolivar J.P., García-Tenorio R., Vaca F. 2000.Radioecological study of an estuarine system located in the South of Spain. Water Research 32, 2941-2950.

Carvalho, F.P. 2011.Polonium (^{210}Po) and lead (^{210}Pb) in marine organisms and their transfer in marine food chains. Journal of Environmental Radioactivity 102, 462-472

Cherry R.D., Heyraud M. 1981. Polonium-210 content of marine shrimp: variation with biological and environmental factors. Marine Biology 65. 65-175

Cherry R.D., Heyraud M., Rindfuss R. 1994. ^{210}Po in teleost fish and in marine mammals: interfamily differences and a possible association between ^{210}Po and red muscle. Journal of Environmental Radioactivity 24, 273-291

Connan O., Germain P., Solier L., Gouret G. 2007. Variations of ^{210}Po and ^{210}Pb in various marine organisms from Western English Channel: contribution of ^{210}Po to the radiation dose. Journal of Environmental Radioactivity 97, 168-188

Dahlgaard H. 1996. Polonium-210 in mussels and fish from the Baltic North Sea Estuary. Journal of Environmental Radioactivity 32, 91-96.

Flynn W.W. 1968 The determination of low levels of polonium-210 in enviromental simples. Analytical Chemistry Acta 43, 221-227

Fowler S.W. 2011.^{210}Po in the marine environment with emphasis on its behaviour within the biosphere. Journal of Environmental Radioactivity 102,448-461

Hallstadius L. 1984. A method for the electrodeposition of actinides". Nuclear Instruments and Methods A 223, 266–267.

Heyraud M., Cherry R.D. 1979. Polonium-210 and lead-210 in marine food chains. Marine Biology 52, 227-236.

Holm E., Fukai R. 1977.A method for multielement alpha-spectrometry of actinides and its application to environmental radioactivity studies.Talanta 24, 659-664

IAEA 2006.International Atomic Energy Agency, Assessing the Need for Radiation Protection Measures in Work Involving Minerals and Raw Materials. Safety Report Series No. 49,Vienna

ICRP, 1992. Age-dependent Doses to Members of the Public from Intake of Radionuclides- Part 2. Ingestion Dose Coefficients. ICRP Publication 67. Ann.ICRP 22, 3-4

ICRP, 1992. Age-dependent Doses to Members of the Public from Intake of Radionuclides- Part 2. Ingestion Dose Coefficients. ICRP Publication 67. Ann.ICRP 22, 3-4

Kannan V., Iyengar M.A.R., Ramesh R., 2001. Dose estimates to the public from 210Po ingestion via dietary sources at Kappakarm (India). Applied Radiation and Isotopes 54, 663-674.

McDonald P., Cook G.T., Baxter M.S., 1991. Natural and artificial radioactivity in coatal regions of UK. In: Radonuclides in the Study of Marine Processes (Eds P.J. Kershaw and D.S. Woodhead). Elsevier Applied Science, London and New York, 286-298

Pietrzak-Flis Z., Chrzanowski E., Dembinska S., 1997. Intake of ^{226}Ra, ^{210}Pb and ^{210}Po with food in Poland. Science of the Total Environment 203, 157-165

Strok M., Smodis B., 2011. Levels of ^{210}Po and ^{210}Pb in fish and mollusks in Slovenia and the related dose assessment to the population. Chemosphere 82, 970-976.

A New Approach to Process Planktonic Foraminifera for Radiocarbon Measurements

Roberta Guerra[a,b]*, Francisco-Javier Santos Arévalo[c], Rafael García-Tenorio[c,d]

[a] University of Bologna, Department of Physics and Astronomy, Viale Berti Pichat 6/2, 40127 Bologna, Italy
[b] University of Bologna, Centro Interdipartimentale di Ricerca per le Scienze Ambientali, CIRSA, Via S. Alberto 163, 48123 Ravenna, Italy
[c] Centro Nacional de Aceleradores (Universidad de Sevilla, Consejo Superior de Investigaciones Científicas, Junta de Andalucía), Thomas Alva Edison 7, 41092 Seville, Spain
[d] University of Seville, Department of Applied Physics, ETSA, Avenida Reina Mercedes 2, 41012 Sevilla, Spain

Abstract

Carbonate shells from foraminifera are often analyzed for radiocarbon to determine the age of deep-sea sediments or to assess radiocarbon reservoir ages. The Centro Nacional de Aceleradores (CNA) is equipped for the AMS radiocarbon analysis with a MICADAS (MIni CArbon DAting System), and a sample processing line including vial flushing, carbonate dissolution and transfer of the evolved CO_2 from the septum sealed tubes to the automated graphitization equipment (AGE). In this work, we have tested a fully-automated setup from sampling the released CO_2 from small carbonate samples (i.e. foraminifera shells) for radiocarbon analysis, where the formed CO_2 is later flushed by helium flow by means of a double-wall needle mounted from the tubes to the zeolite trap of the existing AGE-2. This carbonate dissociation line essentially replaces the elemental analyser normally used for the combustion of organic samples to further reduce the effort involved for sample preparation. The automated method yields in low sample blanks of about 50,000 years. Results of the processed reference materials (IAEA-C1 and IAEA-C2) are in agreement with their consensus values. Using this automated dissociation line we were able to date samples of monospecific foraminifera shells (~10 mg) of ~ 1000 radiocarbon years.

Introduction

AMS ^{14}C dating measured on foraminifer shells provides an important means of age model development for proxy records from sediment cores when the reservoir age is known (Stuiver et al., 1998). In the marine environment, the reservoir age at a certain location and water depth is related to the ventilation age of the prevailing water mass [Stern and Lisiecki, 2013]. Yet several complications have been highlighted that may lead to significant uncertainties when attempting to interpret foraminiferal ^{14}C ages. These include the effects of bioturbation within the upper sediment column, faunal assemblage variations through time, secondary calcification, downslope transport and variations in atmospheric Δ14C (Peng and Broecker, 1984; Adkins and Boyle, 1997; Broecker et al., 2006).

Conventional AMS radiocarbon analysis of carbonate samples such as speleothems, foraminifera and corals, requires the extraction of about 1 mg C (ca. 10 mg $CaCO_3$). Most laboratories prepare samples by decomposition of carbonates by phosphoric acid in evacuated glass tubes, with the formed CO_2 requiring further cleaning and conversion to graphite, but the entire processing is labor intensive and time consuming. The enhancement of sample preparation throughput should be considered as a key issue for AMS ^{14}C measurements. Automation is a solution for the effective preparation of the samples, and some laboratories have actually carried out automation for the several steps in sample preparation (e.g., Longworth et al., 2013; Wacker et al., 2010a). Significant advances in the graphitization and accelerator mass spectrometry (AMS) dating of small samples

---

* Corresponding author, e-mail: roberta.guerra@unibo.it

have been made in recent years (e.g. Santos et al. 2007; Delqué-Količ et al. 2013), but few studies have specifically targeted small carbonate samples for use in oceanographic research (Wacker et al., 2013a,b; Freeman et al., 2016).

A fully-automated system to handle carbonates using wet chemistry directly connected with an AGE system for sample combustion and graphitization was installed at the Centro Nacional de Aceleradores (CNA), Seville in 2015. Here, we tested this automated system for a rapid acid decomposition of foraminifer shells to obtain CO_2 for conversion into AMS graphite targets by AGE. Yet, we describe the potential effects of another potentially complicating mechanism, that of dating foraminiferal shells within the sedimentary bioturbated zone or mixed layer.

Materials and Methods

Sampling and processing

Sediment cores were mainly collected in the southern basin of Mediterranean Sea, including the western part of the Algero-Balearic basin close to the Arboran Sea (V4B), the southern-central part of the Balearic abyssal plain (V3C) and the central Ionian abyssal plain (V7Cbis), during the oceanographic cruise VECTOR (TRANSMED). Oceanographic and sedimentological conditions have been described previously in detail (Barsanti et al., 2011; Kovačević et al., 2012). The sediment was dried at 50°C and disaggregated in 200 mL deionized water before wet sieving into <150 μm and >250 μm fractions using additional deionized water. Aliquots of ~10-20 mg of well-preserved monospecific planktonic foraminifera (~200-600 individuals) were hand-picked from the >250 μm size fraction of washed sediment samples from the 1-1.5 cm sections of cores V4B, V3C and V7Cbis.

Experimental procedure

The schematic automated setup to process carbonated samples is shown in Fig. 1. Primary and secondary standards were used at the CNA to test for sample dissolution with phosphoric acid and graphitization by the AGE as unknowns. Oxalic Acid II (Reference Material for Contemporary Modern Carbon-14, NIST 4990c) was the primary standard used for all ^{14}C measurements. Secondary Standards used in this study and their consensus pMC values were IAEA C-1 Marble, infinite age (0±0.002), and IAEA C-2 Travertine, 7135±5 yr (0.4114±0.0003) carbonate materials.

Aliquots of ~10 mg of carbonaceous material were weighted in 12 mL vials and closed with a screw cap containing a butyl septum (Exetainer® vials, Labco, UK). Air was removed from the vials with a He flow of 65ml/min using a double-walled needle (Thermo Fisher, Gasbench) inserted through the septum. Fast carbonate dissolution and a complete conversion to CO_2 was ensured by adding 1 mL analytical grade H_3PO_4 (85%) and heating the sample vials to 85°C in a Carbonate Handling System CHS, IONPLUS+ (ETH, Zurich, Switzerland). The formed CO_2 was then flushed with a He flow at 65 mL/min within 2 min to the AGE system by means of a commercial available auto-sampler syringe (PAL-GC, CTC, Switzerland) (Fig. 1). Any water was retained on a phosphorous pentaoxide trap (Merk Sicapent®), and the CO_2 was then absorbed on the zeolite trap (Supelco®, X13, -60 mesh, 200 mg) of the AGE-2 system within 2 min. Finally the pure CO_2 was thermally released (500 °C for 2 hours) into a selected reactor of the AGE-2, where it is converted with hydrogen to graphite on 4.5 mg iron powder (Alfa Aesar®, reduced iron 99%, -325 mesh) in about 2 hours.

All ^{14}C measurements were accomplished on the graphitized samples using a MICADAS (MIni CArbon DAting System) developed by the ETH Zurich (Synal et al., 2007; Wacker et al., 2010b), which was installed at the at the CNA, Seville in 2012 (Santos Arévalo et al., 2015).

Radiocarbon dates are reported as conventional ^{14}C age in ^{14}C year before present (^{14}C yr BP, present 1950) to obtain the reservoir-corrected age. The dates have been corrected for natural

isotopic fractionation by normalisation to $^{13}C = -25‰$ VPDB, and calibrated with the Marine13 radiocarbon calibration curves with associated ΔR (Reimer et al., 2013).
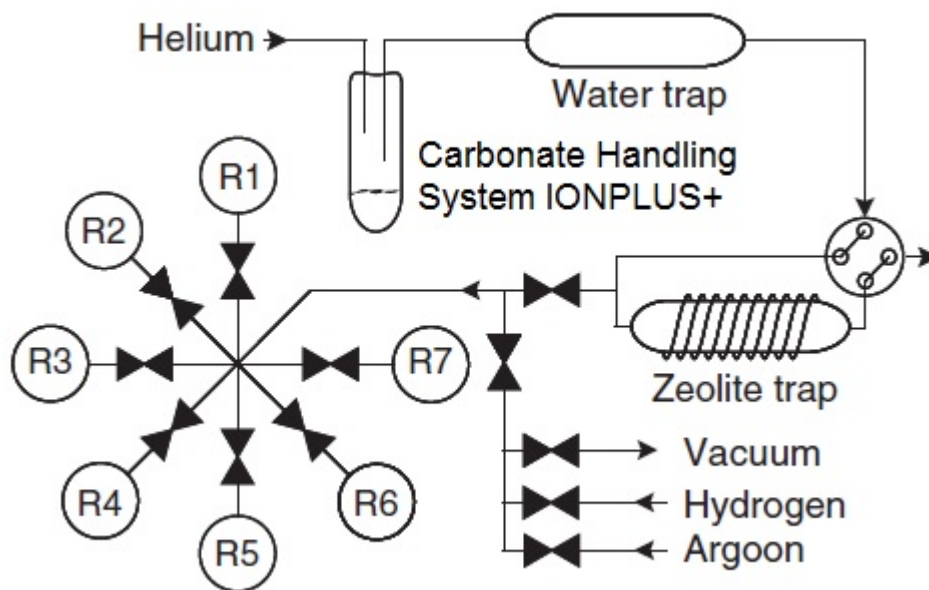
Figure 1. *A schematic representation of the automated setup with the carbon dissociation line connected to the AGE with the zeolite trap and the 7 reactors (R1-R7)(modified from Wacker et al., 2010a).*

Results and Discussion

A measurement procedure as usually performed at our MICADAS system for routine AMS measurements was applied with repeated analyses of samples, standards, and blanks to enable a statistical assessment of the dataset. During these measurements the overall ^{12}C transmission was 36-39%.

We used DBSP (Double Spar calcite) to quantify the contribution from the graphitization using the AGE-2 system and the automated carbonated dissolution line. Based on 3 experiments (30 and 60 minutes) with independent preparations and measurements, the mean blank pMC is 0.11±0.01, which translates to a ^{14}C age of ~ 55,000 years BP (Table 1). This shows that the combined system for sample dissolution and graphitization is able to reach old ages.

Based on six NIST 4990c Oxalic Acid II targets, the average pMC is 134.07 with a standard deviation of 0.01. These measured values agree with the standard value of 134.07 pMC (Table 1).

We also tested the influence of the time on carbonate decomposition (30 and 60 minutes) with phosphoric acid 85%. Radiocarbon measurements of processed reference carbonate materials (IAEA-C1 and IAEA-C2) are very well reproduced and in agreement with their consensus values (Table 1). The calculated means are 0.11 and 0.13 pMC (statistical spread: 0.01 and 0.02) for IAEA-C1 and 41.10 and 41.48 pMC (statistical spread: 0.04 and 0.05) for IAEA-C2, at 30 and 60 minutes decomposition time, respectively. A comparison of the results with the automated setup using the Carbonate Handling System IonPlus+ and the AGE-2 system showed that differences between the two treatments, tested by ANOVA, were highly significant for material IAEA-C2 ($p < 0.01$); post hoc comparison with SNK test showed significantly higher pMC values with a 60 minute dissolution time; conversely differences among the two treatments were not significant for reference material IAEA-C1.

Table 1. *Repetitive preparation and radiocarbon measurement of reference carbonate materials normalized to oxalic acid II Reference material. Results are given in percent modern carbon (pMC) for the Reference Quality Control Materials IAEA-C1 and IEAEA-C2 measured with AMS MICADAS.*

Sample label	Info	N analyses	Measured value ^{14}C (pMC)	Nominal value ^{14}C (pMC)
DBSP [a]		2	0.12±0.01	blank
DBSP [b]		2	0.11±0.01	
OX-II		6	134.07±0.37	134.07
IAEA-C1 [a]	Marble	3	0.11±0.01	0.00±0.02
IAEA-C1 [b]	Marble	3	0.13±0.02	0.00±0.02
IAEA-C2 [a]	Travertine	3	41.10±0.04	41.14±0.03
IAEA-C2 [b]	Travertine	3	41.48±0.05	

Dissolution time with 85% H_3PO_4 in the Carbonate Handling System CHS, IONPLUS+: a) 30 minutes, b) 60 minutes.

Monospecific planktonic foraminifera (*Globigerinoides inflata* and *Globigerinoides ruber*; size >250 μm diameter) from the deep Mediterranean Sea were pre-treated similarly following a 30 min dissolution time with the automated setup. This approach is less time consuming and requires a smaller amount of sample. However, it is necessary to convert radiocarbon age to calendar age because of the varying atmospheric ^{14}C content through time. For marine samples, this conversion requires an assumption about the 'reservoir age', or the offset in age between organisms that grow in the atmosphere and those that grow in a different carbon reservoir, such as the ocean (Stuiver et al., 1986). The Mediterranean Sea has a typical modern reservoir age (~ 400 yr), similar to that of the Atlantic Ocean in accordance with the modern oceanic circulation pattern, which is assumed to be constant through time during most of the past 18,000 carbon-14 years (Siani et al., 2001); however, larger variations in the Mediterranean ^{14}C reservoir ages have occurred in the past due to changes in the reservoir age of the North Atlantic water entering the Mediterranean Sea or fluctuations in continental runoff, which could introduce an additional source of uncertainty and potentially bias results by hundreds of years (Reimer and McCormac, 2002).

Table 2 lists the ^{14}C dating results of monospecific foraminifera samples from the Mediterranean Sea. Radiocarbon measurements are reported as percent Modern Carbon (pMC), and the dates are reported as conventional ^{14}C age to obtain the reservoir-corrected age. A ΔR value of 85±1 years was used to correct for regional differences in the reservoir age within the Algero-Balearic basin and the Algero-Balearic abyssal plain, whereas a ΔR of 158±40 was used for the Ionian Abyssal plain (Marine Reservoir correction Database; Reimer and Reimer, 2001).

Differences in radiocarbon age in the deep Mediterranean Sea (~2500 to ~4000 m depth) are recorded in planktonic foraminifers from the same depth interval between the Algero-Balearic basin and abyssal plain (core V4B and V3C), and the central Ionian abyssal plain (V7Cbis). Planktonic foraminifera from the Algero-Balearic basin (core V4B) with conventional negative radiocarbon ages (formed since mid 1950) cannot be calibrated, and highlighted an anomalous younger age probably reflecting the presence of bomb-produced atmospheric nuclear ^{14}C (Stuiver and Braziunas 1993; Reimer et al., 2004).

Although foraminifera shells are well suited for ^{14}C dating because the measured age marks the true time death of the organism, it is often difficult to distinguish between possible causes of observed

age anomalies as, e.g. downslope transport, secondary calcification, carbonate dissolution effects, or reworking in high-deposition rate deep-sea cores (Broecker et al., 1991, 2006).

Barsanti et al. (2011) indicated that bioturbation is the dominant processes responsible for sediment reworking in the deep areas of the Mediterranean Sea. The seafloor in the Algero-Balearic basin displayed a mixing depth of ~10 cm (SML) and a significant reworking activity (bioturbation coefficient, D_b ~ 0.15 cm^2 yr^{-1}). Conversely, the seafloor in the Balearic and the Ionian abyssal plains reported the lowest SML and D_b values (~ 2 - 6 cm and ~ 0.01 - 0.04 cm^2 yr^{-1}, respectively). The age anomaly detected in the seafloor of Algero-Balearic basin may be explained by a combination of factors, i.e. downward mixing of foraminifera shells carrying the bomb-^{14}C signature throughout the sediment mixed layer (SML). Conversely, the effect of bioturbation and related effects on our radiocarbon ages seems to be negligible in the Algero-Balearic and Ionian abyssal plains, and this is plausible considering the extremely high sedimentation rates recorded in these deep areas of the Mediterranean Sea (Zuniga et al., 2007; Garcia-Orellana et al., 2009). All evidence points to reworking of foraminifera and high sedimentation rates as the actual causes of the age discrepancies between the foraminifera from the same depth interval in sediments in the present case.

Table 2. Foraminifera samples were prepared with the automated method comprising acid decomposition under helium atmosphere using the Carbonate Handling System CHS, IONPLUS+. The graphite targets were measured together in one set with the same standards and blanks.

Sample label	Info/size	Measured value ^{14}C (pMC)	^{14}C conventional age (yr BP)	^{14}C calibrated age	δ^{13}C (‰)
V4B	*G. inflata*	105.66±0.42	-442±32	-	8.5
V3C	*G. inflata*	88.11±0.36	1017±32	1290-1530 BC	4.6
V7Cbis	*G. rubens*	92.69±0.37	610±32	1799-1949 BC	3.9

Conclusions

We are confident the new dedicated fully-automated line for carbonate samples will be far more accessible for radiocarbon analysis of users. It will put radiocarbon capabilities down to standard analytical techniques. Additionally, it has the advantage to target specific analysis of inorganic carbon from small carbonate samples only (i.e. foraminifera shells, speleotherms, corals, etc.), in contrast to the total carbon obtained when using an elemental analyzer. Quality assurance analyses of IAEA carbonate standards, which were processed by dissolution and graphitization, revealed good agreement between measured and consensus values.

Some radiocarbon age uncertainties remain due to reworking of foraminifer shells, as well as large and variable reservoir effects within the Mediterranean Sea. These age differences could have important implications for extrapolation of radiocarbon ages from different fractions to date palaeoceanographic records in deep sediments of the Mediterranean Sea. Future research will focus on: a) variations in regional reservoir ages as a function of water masses and circulation within the Mediterranean Sea, b) additional AMS ^{14}C dates on different monospecific foraminifera and other sedimentary components, and c) other geochemical proxies to constrain the tuning of chronological scales within the Mediterranean Sea.

References

Adkins, J. F., Boyle, E. A., 1997. Changing atmospheric D14C and the record of deep water paleoventilation ages, Paleoceanography 12, 337- 344.

Barsanti, M., Delbono, I., Schirone, A., Langone, L., Miserocchi, S., Salvi, S., Delfanti, R., 2011. Sediment reworking rates in deep sediments of the Mediterranean Sea. Sci. Total. Environ. 409, 2959-2970.

Broecker, W.S., Klas, M., Clark, E., Bonani, G., Ivy, S., Wolfli, W., 1991. The influence of CaCO3 dissolution on core top radiocarbon ages for deep-sea sediments. Paleoceanography, 6, 593-608.

Broecker, W. S., Barker, S., Clark, E., Hajdas, I., Bonani, G., 2006. Anomalous radiocarbon ages for foraminifera shells, Paleoceanography, 21, PA2008, doi : 1 0 .1029/2005PA001212.

Delqué-Količ, E., Caffy, I., Comby-Zerbino, C., Dumoulin J-P, Hain, S., Massault, M., Moreau, C., Quiles, A., Setti, V., Souprayen, C., Tannau, J-F, Thellier, B., Vincent, J., 2013. Advances in handling small radiocarbon samples at the Laboratoire de Mesure du Carbone 14 in Saclay, France. Radiocarbon 55, 648-56.

Freeman, E., Skinner, L.C., Reimer, R., Scrivner, A., Fallon, S., 2016 Graphitization of Small Carbonate Samples for Paleoceanographic Research at the Godwin Radiocarbon Laboratory, University of Cambridge. Radiocarbon 58, 89-97.

Garcia-Orellana, J., Pates, J.M., Masqué, P., Bruach, J.M., Sanchez-Cabeza, J.A., et al., 2009. Distribution of artificial radionuclides in deep sediments of the western Mediterranean Sea. Sci. Total Environ. 407, 887-898.

Kovačević, V., Manca, B.B., Ursella, L., Schroeder K., Cozzi, S., Burca, M., Mauri, E., Gerin, R., Notarstefano, G., Deponte, D., 2012. Water mass properties and dynamic conditions of the Eastern Mediterranean in June 2007. Prog. Oceanogr. 104, 59-79.

Longworth, B.E., Robinson L.F., Roberts M.L., Beaupre S.R., Burke A., Jenkins W.J., 2013. Carbonate as sputter target material for rapid ^{14}C AMS. Nucl. Instrum. Methods Phys. Res. B 294,328-334.

Peng, T.H., Broecker, W.S., 1984, The impacts of bioturbation on the age difference between benthic and planktonic foraminifera in deep-sea sediments. Nucl. Instrum. Methods Phys. Res. B 233, 346-352.

Reimer, P.J. Reimer, R.W., 2001. A marine reservoir correction database and on-line interface. Radiocarbon 43, 461-463.

Reimer, P. et al., 2013. INTCAL13 and MARINE13 radiocarbon age calibration curves 0-50,000 years cal BP. Radiocarbon 55, 1869-1887.

Reimer, P.J., McCormac, F.J., 2002. Marine radiocarbon reservoir corrections for the Mediterranean and Aegean Seas. Radiocarbon 44, 159-166.

Reimer, P.J., Brown, T.A., Reimer, R.W., 2004. "Discussion: Reporting and Calibration of Post-Bomb14C Data", Radiocarbon 46, 1299-1304.

Sanders, C.J., Santos, I.R., Silva-Filho, E.V., Patchineelam, S.R., 2006. Mercury flux to estuarine sediments, derived from Pb-210 and Cs-137 geochronologies (Guaratuba Bay, Brazil). Mar. Pollut. Bull. 52, 1085-1089.

Santos Arévalo, F.J., Gómez Martínez, I., Agulló García, L., 2015. ^{14}C SIRI samples at CNA: Measurements at 200 kV and 1000 kV. Nucl. Instrum. Methods Phys. Res. B 361, 322-326.

Santos, G.M., Southon, J.R., Griffin, S., Beaupre, S.R., Druffel, E.R.M., 2007. Ultra small-mass AMS 14C sample preparation and analyses at KCCAMS/UCI Facility. Nucl. Instrum. Methods Phys. Res. B 259(1), 293-302.

Siani, G., Paterne, M., Michel, E., Supizio, R., Sbrana, A., Arnold, M., Haddad, G., 2001. Mediterranean Sea Surface Radiocarbon Reservoir Age Changes Since the Last Glacial Maximum. Science 294, 1917-1920.

Stern, J.V., Lisiecki, L.E., 2013. North Atlanticcirculation and reservoir age changes over the past 41,000 years. Geophys. Res. Lett., 40, 3693-3697.

Stuiver, M., Pearson, G.W., Braziunas, T.F., 1986. Radiocarbon Age Calibration of Marine Samples Back to 9000 cal yr BP. Radiocarbon 28, 980-1021.

Stuiver, M., Braziunas, T.F., 1993, Modeling atmospheric 14C influences and 14C ages of marine samples back to 10,000 BC, Radiocarbon 35:137-189.

Stuiver, M., Reimer, P. J., Bard, E., Beck, J.W. G., Burr, S., Hughen, K.A., Kromer, B., McCormac, G., Van der Plicht, J., Spurk, M., 1998. INTCAL98 radiocarbon age calibration, 24,000 – 0 cal BP, Radiocarbon, 40, 1041-1083.

Synal, H.A., Stocker, M., Suter, M., 2007. MICADAS: a new compact radiocarbon AMS system Nucl. Instrum. Methods Phys. Res. B 259, 7-13.

Wacker, L., Nemeç, M., Bourquin, J., 2010a. A revolutionary graphitisation system: fully automated, compact and simple. Nucl. Instrum. Methods Phys. Res. B 268, 931-934.

Wacker, L., Bonani, G., Friedrich, M., Hajdas, I., Kromer, B., Nemec, M,., Ruff, M., Suter, M., Synal, H.-A., Vockenhuber, C., 2010b. MICADAS: routine and high-precision radiocarbon dating, Radiocarbon 52, 252-262.

Wacker, L., Fülöp, R.-H., Hajdas, I., Molnár, M., Rethemeyer, J., 2013a. A novel approach to process carbonate samples for radiocarbon measurements with helium carrier gas. Nucl. Instrum. Methods Phys. Res. B 294, 214-217.

Wacker, L., Lippold, J., Molnár, M., Schulz, H., 2013b. Towards radiocarbon dating of single foraminifera with a gas ion source. Nucl. Instrum. Methods Phys. Res. B 294, 307-310.

Zuniga, D., Garica-Orellana, J., Calafat, A., Price, N.B., Adatte, T., Sanchez-Vidal, A. et al., 2007. Late Holocene fine-grained sediments of the Balearic Abyssal Plain, Wetern Mediterranean Sea. Mar. Geol. 237, 25-36.

Acknowledgements

Pacific Proving Grounds radioisotope imprintin sediments from equatorial Western Pacific and Indonesian Throughflow

D. Pittauer[1,2], S. Tims[3], P. Roos[4], M. Froehlich[3], J. Qiao[4], H.W. Fischer[2]

[1] University of Bremen, MARUM - Center for Marine Environmental Sciences, Bremen, Germany
[2] University of Bremen, Institute of Environmental Physics, Bremen, Germany
[3] Australian National University, Department of Nuclear Physics, Canberra, Australia
[4] Technical University of Denmark, Center for Nuclear Technologies, Roskilde, Denmark

Abstract

Artificial radionuclides were studied in radiometrically dated deep sea short sediment cores taken in Philippine Sea and Bismarck Sea in equatorial Western Pacific and in Lombok basin in the Indonesian Archipelago. Plutonium activities and atom ratios were used to distinguish and quantify their origin, including the integrated global fallout, regional fallout from the Pacific Proving Grounds nuclear test site, as well as the radionuclide thermoelectric generator from the SNAP-9A satellite that burnt up in the atmosphere in 1964. Plutonium isotopes together with [241]Am are more suitable chronomarkers in the studied area than the more traditional [137]Cs.

Introduction

The United States conducted an extensive nuclear test programme at Bikini and Enewetak atolls, known as the Pacific Proving Grounds (PPG). Approximately 70% of the total yield of all U.S. atmospheric tests were performed in the PPG, and consequently it is an important regional source of anthropogenic radionuclides. Plutonium isotopes from the local fallout are known to be continuously distributed from the PPG by the North Equatorial Current and towards the Pacific Ocean marginal seas. However, there is a lack of knowledge on the transport of the PPG derived transuranics via the Indonesian Throughflow (ITF, Fig. 1), a complex array of passages that provide low latitude connection between the Pacific and Indian Oceans.
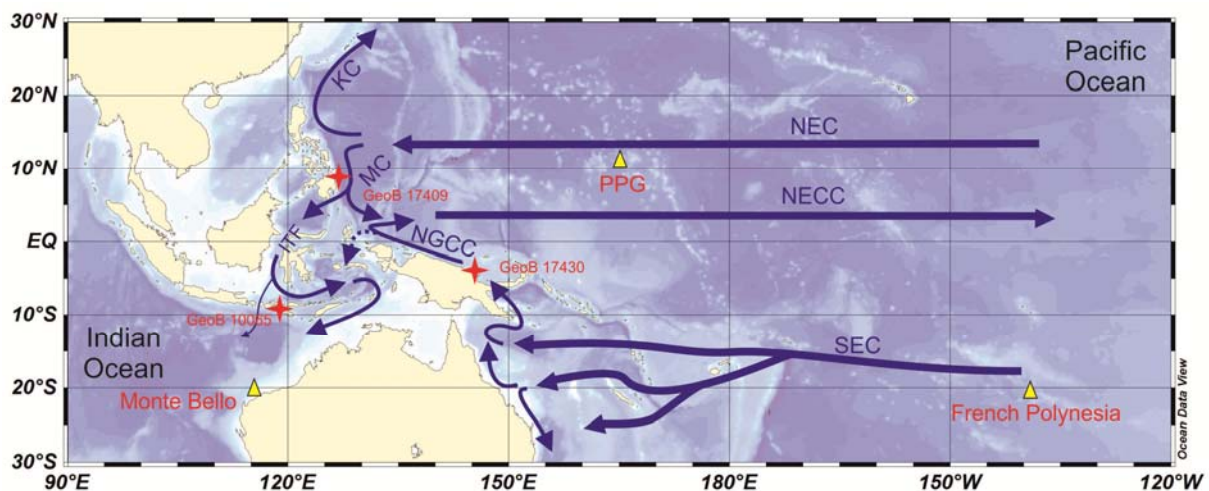
Figure 1.Map of the study area. NEC = North Equatorial Current, NECC = North Equatorial Countercurrent, SEC = South Equatorial Current, MC = Mindanao Current, KC = Kuroshio Current. NGCC = New Guinea Coastal Current. ITF = Indonesian Throughflow. PPG = Pacific Proving Grounds. The map was created using Ocean Data View: https://odv.awi.de.

Recently a sediment core GeoB10065 from Lombok Basin off the Indonesian island of Sumba, was found to contain high ^{241}Am inventories (Steinke et al., 2014). This work aims to find out if the high Am inventory in ITF is also related to high Plutonium inventories. Additionally, in this and other two locations in equatorial West Pacific, artificial radionuclides are studied to interpret their sources other than global stratospheric fallout, with PPG representing the likely additional contributor. It is also of high interest to evaluate, whether ^{241}Am and Pu isotopes provide useful chronomarkers to support sediment chronologies in the equatorial Western Pacific region.

Artificial radionuclides remain in the Pacific Ocean water column many years after the initial fallout. Availability of particles near the continental margin due to higher productivity and suspended particle load, supports particle-reactive radionuclides' (^{241}Am and plutonium isotopes) scavenging from the water column and their incorporation in the sediment (Vintró et al., 2005). Depth distribution of artificial radionuclides in fast depositing anthropogenic sediment layers can provide information about changes of radioisotopes' concentration in the overlying water column in time. Activity and atom ratios of anthropogenic radionuclides contain information about their origin.

Apart from the integrated global fallout and PPG, additional sources of anthropogenic radionuclides in the sediments in the tropical western Pacific and ITF can be SNAP-9A satellite (with a ^{238}Pu radioisotope thermoelectric generator on-board) burn-up in the atmosphere above the Indian Ocean in 1964. This has changed ^{238}Pu/$^{239+240}$Pu activity ratios in the southern hemisphere (Livingston and Povinec, 2000). High post-SNAP-9A ^{238}Pu/$^{239+240}$Pu values (up to 0.5) were reported for example from a New Zealand lake sediment (Hancock et al., 2011). French nuclear testing performed in French Polynesia (atolls Fangataufa andMururoa, 1966–1974) are another possible source in the Southern Pacific. Finally, British nuclear testing at Monte Bello Islands off NW Australia may be a minor source in that specific area.

Materials and Methods

Sampling

Short sediment cores in this study were taken during German R/V Sonnecruises SO-184 in 2005 and SO-228 in 2013 by a multi-corer and slice on-board to 1-5 cm depth increments. The sampling sites were selected in the Eastern Lombok Basin off Sumba Island, and from locations close to the inflow portals of the Pacific waters to the ITF: in the Philippines Sea east of Mindanao and the Bismarck Sea east of Papua New Guinea (Tab. 1).

Table 1. Sediment sampling sites

Location (year of sampling)	Sediment core	Latitude (+N, -S)	Longitude (E)	Water depth (m)
Lombok Basin off Sumba Island (2005)	GeoB10065	-9°13.41	118°53,55'	1284
Philippine Sea off E Mindanao (2013)	GeoB17409	+7°51.50'	126°33.28'	503
Bismarck Sea off E Papua New Guinea (2013)	GeoB17430	-4°13.04'	145°01.63'	1160

Radionuclide analyzes

Natural and anthropogenic radionuclides in sediments were analyzed by radiometric and mass spectrometric techniques. Gamma spectrometry was performed at Institute of Environmental Physics, University of Bremen (IUP). This provided mainly the information about excess ^{210}Pb used for sediment chronology, ^{137}Cs and ^{241}Am. Plutonium isotopes were measured by alpha spectrometry

only for cores GeoB17409 and GeoB17430 at IUP and Alfred Wegener Institute for Polar and Marine Research in Bremerhaven, Germany. Plutonium and [241]Am were additionally analyzed by mass spectrometric methods: accelerator mass spectrometry (AMS) at Department of Nuclear Physics, Australian National University (core GeoB10065) and Inductively coupled plasma mass spectrometry (ICP-MS) at Center for Nuclear Technologies, Technical University of Denmark (cores GeoB17409 and GeoB17430).

Results and Discussion

Sediment chronology

Decreasing activities of excess ^{210}Pb were found in the upper dozens of cm of all three studied cores (the depth profiles are not shown in this abstract). All three sites are characterized by high recent sediment accumulation rates, which make them suitable archives for the last Century. The sediment chronologies based on this isotope were determined and the ages calculated by Constant Rate of Supply (CRS) model are plotted at secondary axes (Figs. 2-4). The age models for stations GeoB17409 and GeoB17430 are not final, because several samples still need to be measured, which for the purpose of the preliminary model were interpolated.

Artificial radionuculides

High [241]Am and [239+240]Pu activity concentrations, as well as inventories, were found in the Lombok Basin sediment (Fig. 2), both showing a wide subsurface maximum. [137]Cs concentrations were lower than expected, given the high actinide activities. The [240]Pu/[239]Pu atom ratios increased with depth (and age) and were significantly higher than 0.18, a value considered representative for the integrated global fallout (Kelley et al., 1999).
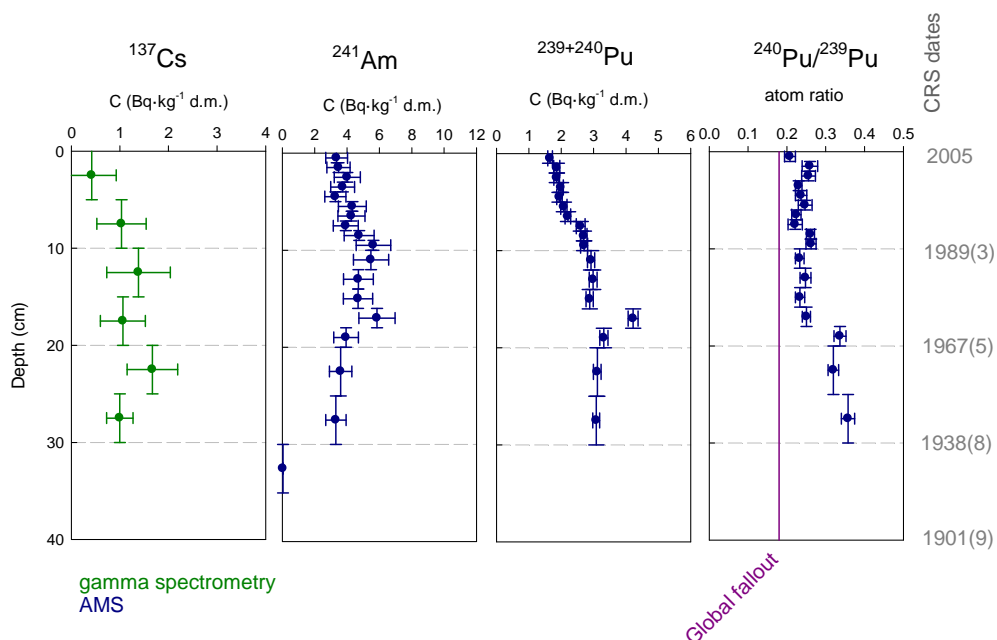
Figure 2. *Artificial radionuclide depth profiles at GeoB1006 – Lombok Basin.*
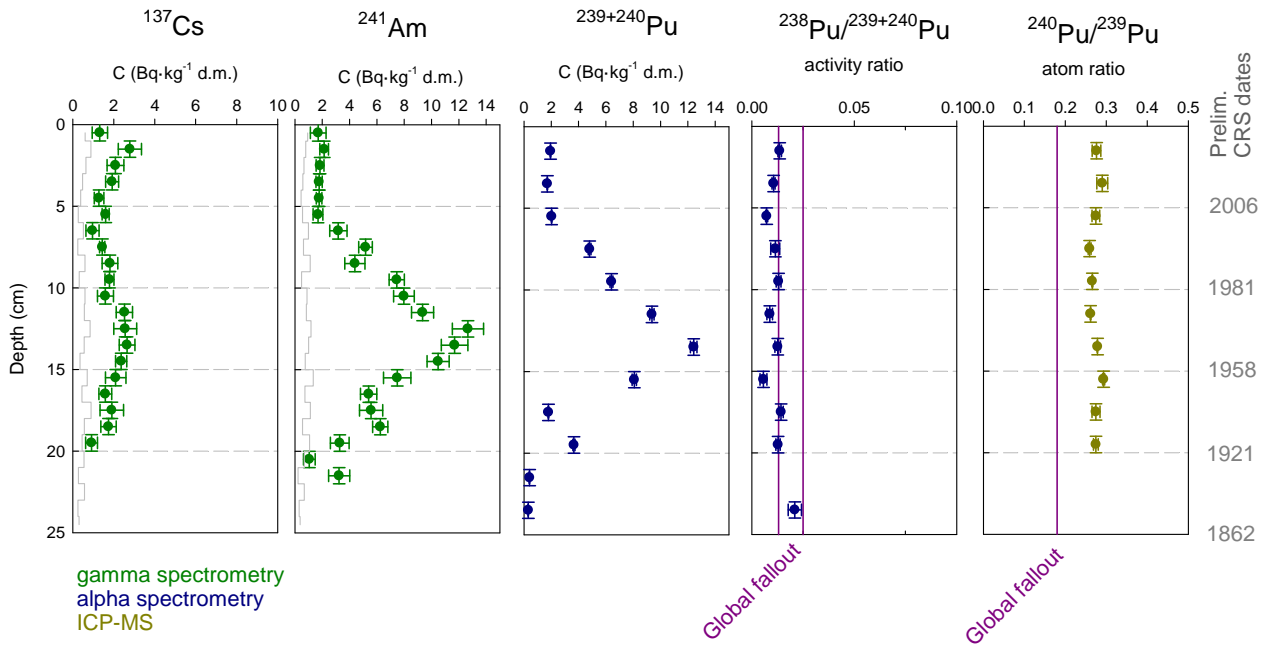
Figure 3. Artificial radionuclide depth profiles at GeoB17409 – Philippine Sea. The grey curve indicates decision thresholds for ^{137}Cs and ^{241}Am.
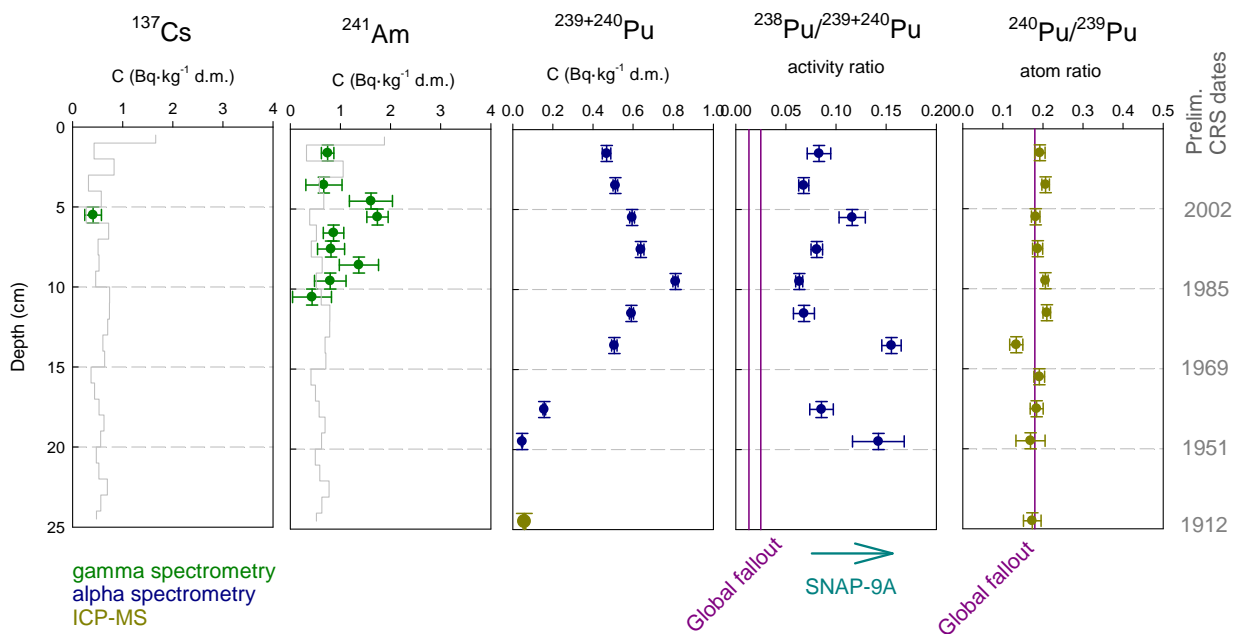
Figure 4. Artificial radionuclide depth profiles at GeoB17430 – Bismarck Sea. The grey curve indicates decision thresholds for ^{137}Cs and ^{241}Am.

Very high ^{241}Am and $^{239+240}$Pu activity concentrations and inventorieswere also found inthe Philippine Sea station (Fig. 3), with a distinct subsurface maximum. This site is located close to the bifurcation of the North Equatorial Current into Kuroshio Current to the north and Mindanao Current to the south (Fig. 1).^{137}Cs concentrations were low and did not vary significantly with depth.The ^{238}Pu/$^{239+240}$Pu activity ratios were close to values usual for the global fallout. The ^{240}Pu/^{239}Pu atom ratios were significantly higher than the global fallout ratio.

Comparatively lower ^{241}Am and $^{239+240}$Pu activity concentrations and inventories were found in the Bismarck Sea sediment (Fig. 4). A distinct subsurface maximum of $^{239+240}$Puwas located at 10 cm depth.^{137}Cs concentrations were below decision threshold in most analyzed samples. The ^{238}Pu/$^{239+240}$Pu activity ratios were significantly higher than values usual for the global fallout. The ^{240}Pu/^{239}Pu atom ratios were close to the global fallout ratio values.

Sources of plutonium

Very high ^{240}Pu/^{239}Pu atom ratios detected in the Philippine Sea and further along the ITF partway in Lombok Basin can likely be attributed to the PPG origin. The reported value from Enewetak Atolls of 0.363±0.004 (Diamond et al., 1960) is often used as the end-member for evaluating the portion of PPG derived fallout. However, recent Enewetak lagoon coral investigation showed a decrease of the ratio from 0.41 to 0.08 between years 1952-1958 (Froehlich et al., 2016). Therefore, for calculation of PPG portion of Pu in the studied cores, 0.36 is considered the upper limit, and the resulting portions are minimum estimates.

Two end-member mixing model (Krey, 1976) was used to assign portions of PPG versus integrated global fallout in the studied sediments. In the Lombok Basin site, the PPG portion is the highest during 1950's, with 100% PPG plutonium and decreases to about 90% during 1960's. From 1970's on, the PPG portion remains still significant with an average of 40% (Pittauer et al, submitted). The portion of PPG derived plutonium in the Philippine Sea station calculated from the mean ^{240}Pu/^{239}Pu atom ratio of 0.27±0.01 is (59±8)%.

While the ^{238}Pu/$^{239+240}$Pu activity ratios in Philippine Sea do not indicate any major contribution from the SNAP-9A fallout, the increased ratios in the Bismarck Sea sediments provide an evidence of stronger South Pacific water influence at this site. ^{238}Pu/$^{239+240}$Pu activity ratios in Bismarck Sea site are anti-correlated with ^{240}Pu/^{239}Pu atom ratios. This can be explained by mixing with North Pacific water masses due to a seasonal reversion of the New Guinea Coastal Current direction.

Conclusions

The artificial radionuclide study of sediment cores from equatorialWestern Pacific and Lombok Basin brings an evidence of significant on-going transport of PPG-derived plutonium with the Mindanao Current and through the Indonesian Throughflow towards the Indian Ocean. Another contributing source of plutonium in Bismarck Sea is the SNAP-9A satellite burn-up fallout. In this site it is likely that South Pacific and North Pacific signals are mixing due to ocean current seasonal reversals. Plutonium isotopes, together with ^{241}Am, appear to be better preserved in the sedimentary record than ^{137}Cs, and are therefore better suited as chronomarkers in this area.

References

Diamond, H., Fields, P.R., Stevens, C.S., Studier, M.H., Fried, S.M., Inghram, M.G., Hess, D.C., Pyle, G.L., Mech, J.F., Manning, W.M., Ghiorso, A., Thompson, S.G., Higgins, G.H., Seaborg, G.T., Browne, C.I., Smith, H.L., Spence, R.W., 1960. Heavy Isotope Abundances in Mike Thermonuclear Device. Phys Rev 119, 2000-2004.

Froehlich, M.B., Chan, W.Y., Tims, S.G., Fallon, S.J., Fifield, L.K., 2016. Time-resolved record of ^{236}U and ^{239,240}Pu isotopes from a coral growing during the nuclear testing program at Enewetak Atoll (Marshall Islands). J Environ Radioact 165, 197-205.

Hancock, G.J., Leslie, C., Everett, S.E., Tims, S.G., Brunskill, G.J., Haese, R., 2011. Plutonium as a chronomarker in Australian and New Zealand sediments: a comparison with ^{137}Cs. J Environ Radioact 102, 919-929.

Kelley, J.M., Bond, L.A., Beasley, T.M., 1999. Global distribution of Pu isotopes and Np-237. Sci Total Environ 238, 483-500.

Krey, P.W., 1976. Remote Plutonium Contamination and Total Inventories from Rocky Flats. Health Phys 30, 209-214.

Livingston, H.D., Povinec, P.P., 2000. Anthropogenic marine radioactivity. Ocean & Coastal Management 43, 689-712.

Pittauer, D., Tims, S., Froehlich, M., Fifield, K., Wallner, A., McNeil, S., Fischer, H. W. (Submitted). Continuous transport of Pacific-derived anthropogenic radionuclides towards the Indian Ocean.

Steinke, S., Mohtadi, M., Prange, M., Varma, V., Pittauerová, D., Fischer, H.W., 2014. Mid- to Late-Holocene Australian-Indonesian summer monsoon variability. Quaternary Sci Rev 93, 142-154.

Vintró, L.L., Mitchell, P.I., Smith, K.J., Kershaw, P.J., Livingston, H.D., 2005. Transuranium nuclides in the world's oceans, in: Hugh, D.L. (Ed.), Radioactivity in the Environment. Elsevier, pp. 79-108.

Acknowledgements

Health and environmental risk assessment of the dumped Russian submarine K-27 in the Arctic

Hosseini A.[1*1], Amundsen, I.[1], Bartnicki, J.[2], Brown, J.E.[1], Dowdall, M.[1], Dyve, J.E.[1], Karcher, M.[3], Kauker, F.[3], Klein, H.[2], Lind, O.C.[4], Salbu, B.[4], Schnur, R.[3], Standring, W.[1]

[1]Norwegian Radiation Protection Authority/CERAD CoE.
[2]Norwegian Meteorological Institute/CERAD CoE.
[3] O.A.Sys - Ocean Atmosphere Systems GmbH .
[4] Norwegian University of Life Sciences/CERAD CoE.

Abstract

Amongst dumped objects in the Arctic, the Russian submarine K-27, which was dumped in the Kara Sea in 1981, has received much attention due to particular concerns related to this vessel: it contains two reactors with highly enriched Spent Nuclear Fuel (SNF) and lies at a depth of about 30 m under water. A study was initiated in 2013 to examine the potential radiological consequences of this submarine for both humans and the environment. The study investigated different hypothetical accident scenarios and evaluated possible associated consequences of potential releases with particular focus on possible salvage operations. A major part of this study was related to the transport of radioactivity in the environment and its fate with regards to exposure situations relevant for environmental impact assessments. These components form the focus of this paper.

Introduction

There is increasing concern over potential radioactive contamination of the Arctic due to the presence of a wide range of nuclear sources within this region. Dumped radioactive waste contributes the greatest proportion to the total activity found in the Arctic followed by historic inputs from Sellafield and global fallout (Sarkisov et al., 2009). Of these, dumped objects containing Spent Nuclear Fuel (SNF) constitute the greatest potential radioecological hazard.

Figure 1. *Location of the dump-site of K-27 at Stepovogo Fjord, the intermediate site used for dispersion studies denoted Location B and the probable post-recovery location of the submarine at Gremikha. Dotted line indicates envisioned transport route after eventual recovery.*

---

[1] Corresponding author, E-mail: Ali.hosseini@nrpa.no

Amongst dumped objects in the Arctic, the Russian submarine K-27 has received much attention. This nuclear submarine is one of several objects with SNF which was dumped in Stepovogo Fjord (see Figure 1) of the Kara Sea in 1981, at an estimated depth of 30 m.

In 2013, the Norwegian Radiation Protection Authority (NRPA) initiated a study to examine the radiological consequences of the dumped submarine K-27 for both humans and the environment. The focus of the present paper will be on the part of the work related to the application of dispersion and food-chain transfer models and the results from these models. More details regarding this study can be found in Hosseini et al. (2015 & 2016).

Methods

The main starting point for the study was the derivation of different hypothetical accident scenarios for K-27. In general, three main scenarios related to three release locations (Stepovogo Fjord, Barents Sea (location B in Figure 1) and Gremikha Bay) were considered:
- Current and future impact; assuming no interventions.
- Accidental scenarios involving the raising of the submarine.
- Accidental scenarios related to the transportation of the submarine to land for defueling.

As changes in the reactor sub-criticality might occur, the occurrence of a spontaneous chain reaction (SCR) has also been considered.

Two major steps in the process of acquisition of data for conducting environmental and health impact assessments were the estimation of inventory of the submarine and the characterization of the concomitant source term. While the former aims at making an evaluation of the activity present in the K-27 reactors, the latter characterises the quantity and types of potentially released radionuclides (and also their physical and chemical properties) and associated release patterns. An up-to-date assessment indicated that the total inventory of the submarine is of the order of 3.7E+14 Bq (as of 2015), of which about 82% is formed by fission products which in turn are dominated by ^{137}Cs and ^{90}Sr.

Dispersion and transfer modelling

After characterization of the source term, the next step was to model the transport of hypothetically released radionuclides in the environment. Following the input of radionuclides to the environment, several immediate processes are likely to occur. A fraction of the radionuclide inventories will be diluted and dispersed away from the input point and the remaining fraction will undergo interaction with surrounding materials and / taken up by biota. The degree of interaction will depend on numerous factors including the physico-chemical form of the radionuclide, the availability of adsorption surfaces and chemical attributes of the receiving environment. It is thus convenient to model radionuclide behavior and fate in the environment by splitting the problem into two components namely (i) physical (abiotic) transport processes and (ii) biological transfer through marine food-chains.

To simulate the physical transport of potentially released radionuclides in the marine environment as a consequence of a possible recovery of K-27 as well as a prolonged stay under water a large scale numerical model called NAOSIM (North Atlantic/Arctic coupled Ocean Sea Ice Model) has been applied. To include most probable cases, 24 scenario experiments were considered. Each experiment was performed for 10 years duration. To evaluate atmospheric transport and deposition of hypothetically released radioactive debris to

Norwegian territory, a Lagrangian particle model called SNAP (Severe Nuclear Accident Program) was used.

An important output of the abovementioned dispersion models is the prediction of the spatial and temporal distribution of radionuclide concentrations in the environment.More details regarding modelling activities can be found in Hosseini et al. 2016.

With regards to exposure pathways for both human and environmental dose assessments there is an immediate requirement to simulate transfer of radionuclides through food-chains, i.e. simulating the biological transfer. There are commonly adopted standard methodologies used for implementing this based on the application of concentration ratios (or factors), aggregated transfer factors (see IAEA, 2004,IAEA, 2010) but the applicability of such parameters is evidently more suited to either planned exposure situations or conditions existing some time following a release of radioactivity when steady state conditions are more prevalent. For conditions under which environmental activity concentrations are changing rapidly with time, models which account for the dynamics of the situation are more appropriate (Vives I Batlle et al, 2008). For this reason, marine and terrestrial food-chain models have been applied in the analyses presented in this report. There is a clear commonality in the approachs in the sense that the assessment endpoints for the human and environmental assessment are often related. For example, for the environmental impact assessment with fish having been selected as a representative organism, the food-chain model should be developed to provide activity concentrations associated with this organism group. As fish form a large component of the diet of some relatively highly exposed human groups, the same data might then be used to derive doses to humans through the application of appropriate dosimetric models. Similar considerations hold for the modelling undertaken for the terrestrial environment.

Modelling transfer of radionuclides through food-chains

For the purpose of deriving activity concentrations in representative plants and animals and for human foodstuffs, food-chain models have been applied. For convenience these have been split into marine and terrestrial models. More details on modelling can be found in Hosseini et al. 2016.

Marine food-chain model description

For the marine assessment representative biota considered were; fish, seal and sea bird. A model, based on the work of Thomann (1981), Landrum et al. (1992), and Fisher (2002), was used to simulate the uptake of radionuclides via food and water by aquatic organisms and transfer through marine food-chains. An earlier version of the model is described in Brown et al. (2004). However, a condensed explanation is provided below:
For Zooplankton (prey species), steady state conditions between radionuclide activity concentrations in biota and water are assumed, allowing the application of concentration ratios[2]:

$$C_p = CR_p \cdot C_w \qquad\qquad (1)$$

Where:

C_p is the radionuclide activity concentration in prey species (Bq kg^{-1} f.w.);
CR_p is the concentration ratio for prey species (l kg^{-1}); and

---

[2] Concentration ratios =Activity concentration within an organism relative to that in (normally filtered) water.

C_w is the radionuclide activity concentration in sea water (Bq l^{-1}).

For Fish, accounting for radionuclide uptake via water and food, the following equation is applied:

$$\frac{dC_f}{dt} = AE_f \cdot IR_f \cdot C_P + k_{uf} \cdot C_w - C_f \cdot k_{ef} \qquad (2)$$

Where:

AE_f is the assimilation efficiency (dimensionless) for fish;
IR_f is the ingestion rate per unit mass of fish (kg f.w. d^{-1} per kg f.w.);
k_{uf} is the uptake rate of radionuclide to fish directly from water column (d^{-1});
C_f is the activity concentration in fish (Bq kg^{-1} f.w.);
k_{ef} is the depuration rate from fish (d^{-1}).

CR values (arithmetic means) for zooplankton were taken from IAEA (2014), Fish depuration rates (based on biological half-lives) from ICRP (2009), all other parameters were taken from Thomann (1981).One way to consider radionuclide transfer to seals, based on the work of Brown et al. (2004), is through Equation 3.

$$\frac{dC_s}{dt} = \sum_1^n (x_i.AE_s \cdot IR_s \cdot C_i) - C_s \cdot k_{es} \quad (3)$$

Where:

x_i is the fraction of the diet associated with dietary component "i"
$AE_{r,i}$ is the assimilation efficiency (dimensionless) for dietary component "i"
IR is the ingestion rate per unit mass of seal (kg f.w. d^{-1} per kg f.w.)
C_i is the activity concentration in the dietary component "i" (Bq kg^{-1} f.w.)
C_s is the "whole body" activity concentration in the seal (Bq kg^{-1} f.w.)
k_{es} is the effective loss rate from seal (d^{-1}) – incorporating both excretion rate and physical decay of the radionuclide

A similar approach can be adopted to model the time varying activity concentrations in seabirds, C_b, with a requirement to then provide specific values for the parameters IR_b (the ingestion rate per unit mass for seabirds), AE_b (the assimilation efficiency of radiocaesium for seabirds) and k_{eb} (the effective loss rate of radiocaesium for seabirds).

An ingestion rate, IR_s, of 0.072 kg f.w. day^{-1} per kg f.w. seal was derived by Gwynn et al. (2006) using allometric relationships (Nagy, 2001) for carnivora (Equation 4)

$$FMI = 0.348M^{0.859} \qquad (4)$$

where FMI is the fresh matter intake (g/day) and M is the mass of the seal (g).

In a similar way, Nagy (2001) provides the allometric relationship for marine birds (Equation 5):

$$FMI = 3.221M^{0.658} \qquad (5)$$

where FMI is the fresh matter intake (g/day) and M is the mass of the bird (g).

A representative mass of 1.26 kg, commensurate with the value used for marine birds in the ERICA Tool (Brown et al., 2008), was used as a default for calculations. This yields an IR_b of 0.28 kg f.w. day^{-1} per kg f.w. seabird.

An overview of all of the parameters used in the (bio-)kinetic models can be found in Hosseini et al. (2016).

Terrestrial food-chain model description

A terrestrial food-chain model was used to provide input for both the derivation of ingestion doses for humans and for the assessment of doses to wild plants and animals. The considered biota here were shrub, small burrowing mammal and deer.

Using a variant of the methodology given in UNSCEAR (2008, 2014), the activity concentration in flora (shrub in this study) can be derived from the total deposition using an expression accounting for interception by foliage, direct deposition onto soil, weathering losses of radionuclides from vegetation and uptake from soil to plant.

In the case of an acute deposition, the radionuclide content on vegetation at time 't', accumulated via direct deposition from the air, can be calculated (as outlined in Brown et al., 2003) as:

$$C_{flora,r}^{air} = \frac{f_{flora} \cdot D_{tot,r}}{b_{flora}} \cdot [e^{(-(\lambda_{flw,r} + \lambda_r) \cdot t)}] \tag{7}$$

where
$C_{flora,r}$ is the radionuclide activity concentration in flora from air deposition (Bq kg^{-1} f.w.)
f_{flora} is the interception fraction for a given flora (dimensionless)
$D_{tot,r}$ is the total deposition of radionuclide 'r' (Bq m^{-2})
$\lambda_{flw,r}$ is the weathering constant for a given flora for radionuclide r(d-1)
λ_r is the decay constant for radionuclide r (d^{-1})
b is standing biomass of the flora(kg m^{-2})
t is time (d)

For the same acute deposition, at time 't', there is also a component of contamination that arises from soil to plant transfer. In this case an assumption is made that for this fraction of the contamination in the plant attributable to root uptake, equilibrium exists between the activity concentration in the plant and the soil.

$$C_{flora,r}^{soil} = \left[\frac{D_{tot,r} \cdot \left[(1 - f_{flora}) + f_{flora} \cdot (1 - e^{-\lambda_{flw,r}t}) \right] \cdot e^{-\lambda_r t}}{\rho_{soil} \cdot d_{soil}} \right] . CR_{flora,r} \tag{8}$$

where
ρ_{soil} is the dry soil density (kg m^{-3} d.m.)d_{soil} is the depth of soil within which radionuclide r has become mixed (m) $CR_{flora,r}$ is the soil to plant concentration ratio for radionuclide r (dimensionless)

All other parameters have been described above in equation (7).Application of this model also allows for time varying deposition rates to be considered. For this more complex situation, the problem can be solved numerically.

In order to determine the transfer to deer/herbivorous mammal and burrowing mammal a similar model as the one given by Equation 3 was applied. For details see Hosseini et al. 2016.

Results and discussion

The dynamics of ^{137}Cs and ^{90}Sr activity concentrations in shrub, small mammal and deer at the location of maximum deposition in Finnmark, following releases from the Gremikha scenario are presented in Figure 2.
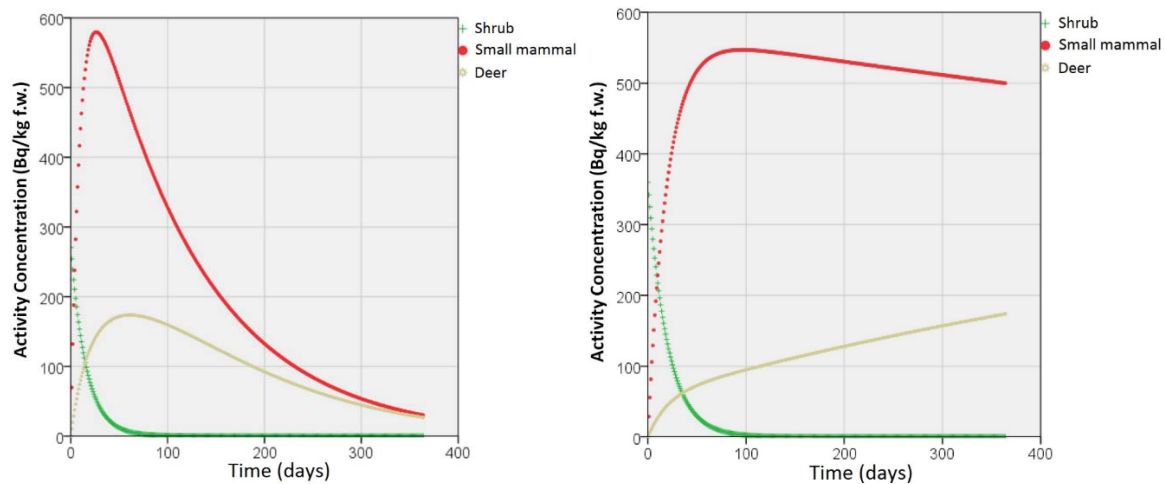
Figure 2.*Activity concentrations (Bq kg^{-1} f.w.) of ^{137}Cs (left) and ^{90}Sr (right) in shrub, small burrowing mammal (including game animals) and deer for the area of maximum deposition in Finnmark for the Gremikha release scenario.*

For shrub, the simulated levels of both radionuclides falls quite rapidly from levels of approximately 270 and 360 Bq/kg f.w. for ^{137}Cs and ^{90}Sr, respectively, in the initial days after fallout to levels of the order of 1 to 2 Bq/kg f.w. within a period of about 100 days.

For the case of small mammals, the simulated activity concentrations of both ^{137}Cs and ^{90}Sr increasesafter the initial deposition event with ^{137}Cs attaining a maximum activity concentration of ca. 580 Bq/kg f.w. within the first month before falling moderately rapidly to a level slightly in excess of 300 Bq/kg f.w. by 100 days.

The kinetics of ^{137}Cs and ^{90}Sr in deer (Figure 2), unsurprisingly, follow a similar pattern to those observed for small mammals with regards to an observed build up of activity with time following the initial deposition event. However, the biological half-lives characterising the retention of ^{137}Cs and ^{90}Sr in the whole body of deer are protracted compared to the much smaller burrowing mammal. This simply reflects the employment of allometric relationships in the derivation of biological half-lives for model parameterisation; the larger the animal, the longer the biological half-life (see Higley et al., 2003; Beresford & Wood, 2014).

The behaviour of ^{90}Sr contrasts to radiocaesium in the case of small mammal and deer; no equilibrium is attained over the 1-year simulation period. This may reflect poor parameterisation of the model. Although the output results for the period post 3 months are quite uncertain there is an expectation that ^{90}Sr will be lost relatively slowly from the body of mammals following assimilation because the radionuclide rapidly becomes associated with bone (see Coughtrey & Thorne, 1983). Once sequestered by bone the retention of radiostrontium within the animal's body can be protracted, reflecting the skeletal turnover of analogous elements such as calcium.

With regards to marine dispersion modelling, three release scenarios at each of the three locations (Stepovogo Fjord, Barents Sea and Gremikha Bay) were considered. Simulations for

the case of Stepovogo yielded the highest peak ^{137}Cs activity concentrations in biota with levels of approximately 150 Bq/kg f.w. and 340 Bq/kg f.w. derived for fish and seal respectively (Figure 3). These elevations undoubtedly reflect the protracted, relatively high concentrations of ^{137}Cs in seawater for the Stepovogo scenario. The maximum activity concentration of ^{137}Cs predicted forseabird fell slightly below 1000 Bq/kg f.w.

Although the ^{137}Cs activity concentrations predicted for fish were generally below the intervention limit (600 Bq/kg) by some margin, the levels are close enough to raise some concerns. In view of the uncertainties involved, not least those associated with the imposed degree of spatial averaging, the levels in fish for an actual pulsed release could conceivably exceed the intervention limit. Such an outcome would potentially require the imposition of fishing restrictions/fishery closures.
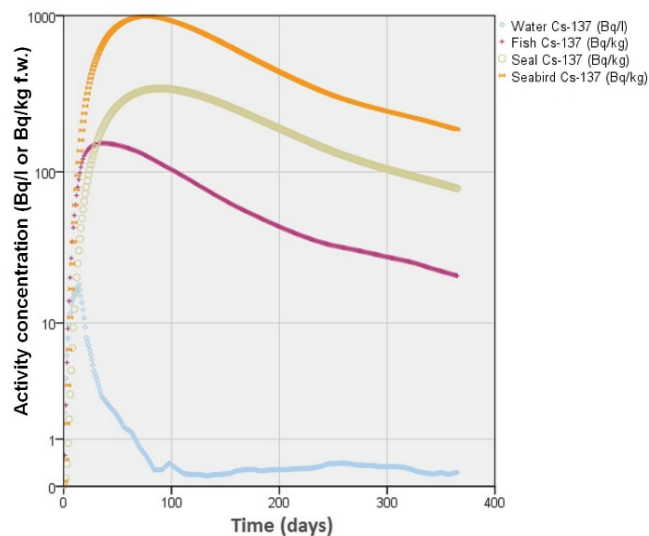
Figure 3. At surface activity concentrations of ^{137}Cs in sea water (Bq/l), fish (Bq/kg f.w.) seal (Bq/kg f.w.) and seabird (Bq/kg f.w.) based on releases to the marine environment for the Stepovogo scenario.

Conclusions

Radionuclide activity concentrations in biota predicted for marine and terrestrial environment are similar despite the fact that the source to receptor distance for the terrestrial simulations were much greater.
It should be emphasized that the release scenarios that have been considered are highly unlikely but if there is a release our predictions are likely to be conservative (mainly because of the conservative assumptions made regarding the source term).
Due to limitations associated with the use of concentration ratios, biokinetic models were preferred and applied but it was challenging to acquire the information and details needed for the parametrization of such models. This is clearly an extra source of uncertainty in the assessment. As a means to deal with uncertainty, conservatism has been introduced at various points in the assessment.

References

Beresford N.A., Wood M.D. (2014). A new simplified allometric approach for predicting the biological half-life of radionuclides in reptiles. Journal of Environmental Radioactivity, 138, 116-121.

Brown, J., Børretzen, P., Dowdall, M., Sazykina, T., Kryshev, I. (2004). The derivation of transfer parameters in the Assessment of Radiological Impacts to Arctic Marine Biota. Arctic, 57 (No.3), pp. 279-289.

Brown, J., Strand, P., Hosseini, A., Borretzen, P. (Eds.), (2003). Handbook for Assessment of the Exposure of Biota to Ionising Radiation from Radionuclides in the Environment (with 2 appendices). Deliverable 5, of the FASSET project (FIGE-CT-2000-00102). Norwegian Radiation Protection Authority, Østerås.

Coughtrey, P.J., Thorne, M.C. (1983). Radionuclide distribution and transport in terrestrial and aquatic ecosystems: a critical review of data. Volume 1. Rotterdam: A.A. Balkema, 1983.

Fisher, N.S. (2002). Advantages and problems in the application of radiotracers for determining bioaccumulation of contaminants in aquatic organisms. In: Børretzen P, Jølle T, Strand P (eds). Proceedings of the International conference on radioactivity in the environment, Monaco 1–5 September 2002. Østerås: Norwegian Radiation Protection Authority, 2002: 573–576.

Gwynn J.P., Brown J.E., Kovacs K.M., Lydersen C. (2006). The derivation of radionuclide transfer parameters for and dose-rates to an adult ringed seal (Phoca hispida) in an Arctic environment. Journal of Environmental Radioactivity 90 (2006) 197-209.

Higley, K.A., Domotor, S.L., Antonio, E.J. (2003). A kinetic-allometric approach to predicting tissue radionuclide concentrations for biota. Journal of Environmental Radioactivity, 66, 61–74.

Hosseini A, Amundsen I, Bartnicki J, Brown J, Dowdall M, Dyve JE, Harm I, Karcher M, Kauker F, Klein H, Lind OC, Salbu B, Schnur R, Standring W, 2016. Environmental modelling and radiological impact assessment associated with hypothetical accident scenarios for the nuclear submarine K-27. StrålevernRapport 2016:8. Norwegian Radiation Protection Authority, 2016.

Hosseini A, Amundsen I, Brown J, Dowdall M, Standring W, 2015. Inventory and source term evaluation of the dumped nuclear submarine K-27. StrålevernRapport 2015:6. Norwegian Radiation Protection Authority, 2015.

IAEA (2004). Sediment distribution coefficients and concentration factors for biota in the marine environment. Technical reports series 422. Vienna: IAEA, 2004.

IAEA (2010). Handbook of parameter values for the prediction of radionuclide transfer in terrestrial and freshwater environments. IAEA technical report series 472. Vienna: IAEA, 2010.

IAEA (2014). Handbook of parameter values for the prediction of radionuclide transfer to wildlife. Technical report series 479. Vienna: IAEA, 2014.

ICRP (2009). Transfer Parameters for Reference Animals and Plants. International Commission on Radiological Protection. Environmental Protection Publication 114. Annals of the ICRP 39(6), Elsevier, Oxford. 2009.

Landrum, P.F., Lee, H., Lydy, M.J. (1992). Toxicokinetics in aquatic systems: model comparison and use in hazard assessment. Environmental Toxicology and Chemistry 1992; 11(12): 1709–1725.

Nagy K.A. (2001). Food requirements of wild animals: predictive equations for free-living mammals, reptiles, and birds. Nutrition Abstracts and Reviews Series B Livestock Feeds and Feeding 2001; 71(10): 21R–32R.

Sarkisov A.A., Sivintsev Yu.V., Vysotskiy V.L. Nikitin V.S. (2009). Atomic Legacy of the Cold War at the Arctic Seabed. Radioecological Cosequences and Technical and Economic Problems of Radiation Remediation at the Arctic Seas. Nuclear Safety Institute, Moscow 2009.

Thomann, R.V. (1981). Equilibrium model of fate of microcontaminants in diverse aquatic food-chains. Canadian Journal of Fisheries and Aquatic Sciences 1981; 38(3): 280-296.

UNSCEAR (2008). Sources and effects of ionizing radiation, UNSCEAR 2008 report: Volume II:Annex E: Effects of ionizing radiation on non-human biota. New York: United Nations, 2008.

UNSCEAR (2014). Sources, effects and risks of ionizing radiation, UNSCEAR 2013 report: Volume I: Annex A: Levels and effects of radiation exposure due to the nuclear accident after the 2011 great east-Japan earthquake and tsunami. New York: United Nations, 2014.

Vives i Batlle, J., Wilson, R.C., Watts, S.J., Jones, S.R., McDonald, P., Vives-Lynch S. (2008). Dynamic model for the assessment of radiological exposure to marine biota. Journal of Environmental Radioactivity. 99(11): 1711-1730.

E – TERRESTRIAL/MARINE

FUKUSHIMA

Radioactive and stable cesium isotopes in Fukushima forests

V. Yoschenko[1]*, T. Takase[1], K. Nanba[1], Y. Onda[2], A. Konoplev[1]

[1]Institute of Environmental Radioactivity, Fukushima University, 1 Kanayagawa, Fukushima City, Fukushima Prefecture, 960-1296 Japan

[2]Center for Research in Isotopes and Environmental Dynamics, University of Tsukuba, 1-1-1 A-405 Tennodai, Tsukuba City, Ibaraki Prefecture, 305-8572 Japan

Abstract

Accident at Fukushima Daiichi NPP resulted in release into the environment of large amounts of radiocesium (^{134}Cs and ^{137}Cs) and in radioactive contamination of terrestrial and aquatic ecosystems. Up to 2/3 of the most contaminated territory in Fukushima prefecture is covered with forests; in differ to the agricultural areas where the extensive decontamination measures have been being implemented, the large-scale decontamination of the forests is not planned.

Our study is aimed to monitoring and modelling of the radiocesium redistribution in Fukushima forests at the stage of its root uptake from soil. It has been performed since May 2014 at several experimental sites equipped for monitoring of the radiocesium fluxes in the typical Fukushima forests (Japanese cedar, Japanese red pine) at the radioactive contaminated territory. Based on the extensive sampling program we obtained the current distributions of radiocesium in the studied ecosystems and estimated the numerical values of the fluxes which will redistribute it in the future (Yoschenko et al., 2016). In order to distinguish between the radiocesium activities in the ecosystem compartments caused by its root uptake and those remaining from the initial deposition intercepted by foliage etc., we also determined the stable cesium distributions.

In addition to the mentioned experimental sites, a part of our study was performed at the border of the FDNPP where we measured the radiocesium concentrations in soil and in the several typical tree species.

Introduction

Forests cover the main part (about 71%) of the whole area of Fukushima prefecture (Fukushima Prefecture, 2014). About 343,000 ha of the forests, or about 35% of their area are artificial plantations (MAFF, 2012) with the annual roundwood production of 655,000 m^3 in 2014 (MAFF, 2015). Contribution of the main forestry species, *Cryptomeria japonica* D. Don (also called Japanese cedar, or Sugi) was 450,000 m^3. Other important forestry species is *Chamaecyparis obtuse* (Japanese cypress, or Hinoki). At the roundwood prices of 11,400 ¥ m^{-3} and 18,500 ¥ m^{-3} (MAFF, 2012) for cedar and cypress, respectively, the annual income from the wood production can be roughly estimated as 9 billion ¥, which clearly demonstrates the important role of forestry in the prefecture economy.

On March 11th, 2011, 14:46 JST, the Great East Japan earthquake of magnitude 9.0, the worldwide fourth largest earthquake recorded in history, occurred off Tohoku region of Japan. The tsunami followed in 1 h caused to the severe damage to Units 1-4 of Fukushima Daiichi Nuclear Power Plant (FDNPP) that led to the release of large amounts of radionuclides into the environment (Atomic Energy Society of Japan, 2015). The International Atomic Energy Agency rated the accident at the FDNPP as Level 7 according to the International Nuclear Event Scale (IAEA, 2011); this was the second largest nuclear accident in history after the Chernobyl accident. In contrast to the Chernobyl accident, the Fukushima release consisted mainly of gas phase radionuclides, the only long-lived radionuclide released in significant amount was ^{137}Cs ($T_{1/2}$ 30.1 y). In general, the area contaminated by the Chernobyl accident is much larger (Steinhauser et al., 2014; Ohta, 2011); however, the ^{137}Cs deposition values in the near zones of the two accidents are similar.

---

* Corresponding author, E-mail: vasylyoschenko@gmail.com

In the Fukushima Prefecture, 42,800 ha of forests were contaminated with radiocesium (^{134,137}Cs) above 1 MBq m^{-2} (November 2011); the total amount of the aboveground biomass at this territory is estimated as 11,300,000 m^3 (Hashimoto et al., 2012). It should be noted that the planned capacity of the interim storages of the radioactive waste in the Fukushima Prefecture is 22,000,000 m^3 (Fukushima Minpo, 2016). Assuming the same percentage of the artificial plantations as at the rest of the prefecture territory, the total current price of the commercial wood at the radioactive contaminated territory can be roughly estimated as 50 billion ¥.

In order to prepare conditions for the population return, the extensive decontamination measures were carried out at the agricultural and residential areas in the evacuation zones. For some towns and villages the evacuation orders have already been lifted. However, the large-scale decontamination of the forests is not planned: decontamination activity in forests is aimed only on reduction of air doses to the population in the adjacent settlements and thus is performed at the limited areas (Fukushima Prefecture, 2015; JAEA, 2015a,b; IAEA, 2015). The total costs for removal and storage of the forest litter and humus surface exceed 22 million ¥ ha^{-1} (Yasutaka et al., 2013), which means that this decontamination option for the heavily contaminated plantations will require about 320 billion ¥, and almost 3 times more if decontamination is performed at the whole forest territory. Therefore, decontamination cost for the artificial plantation significantly exceeds the above-mentioned price of the commercial wood (even its estimate is very rough). Moreover, as we will show later, efficiency of this decontamination option at the present stage can be very low, while other decontamination options may create the huge amounts of the radioactive waste.

In absence of the large-scale decontamination, the strategy should be elaborated for the radioactive contaminated Fukushima forests. For evaluation of the forestry perspectives, the reliable prognosis of the long-term radiocesium distribution in the forest ecosystems, particularly, in the typical artificial forest plantations, is necessary. This should also include assessments of the possible spreading of radiocesium from the contaminated forests to the adjacent decontaminated areas due to the surface run-off and due to resuspension (i.e. during the forest fires), and identification of the radiation effects to the forest species (Watanabe et al., 2015; Yoschenko et al., 2016b).

Numerous studies revealed and quantified the key processes governing radiocesium redistribution in Fukushima forests at the early stage after the Fukushima accident (e.g. Kato et al., 2012, 2015; Kato and Onda, 2014; Loffredo et al., 2014; Endo et al., 2015). At this stage, the dominant process was removal of the initially intercepted radiocesium from the tree crowns to the to the soil profile with precipitation and litterfall. Similar processes were observed at the early stages after the Chernobyl and Kyshtym accidents (Bunzl et al., 1989; Tikhomirov and Shcheglov, 1994); however, later the radionuclide concentrations in the biomass compartments increased due to their root uptake from the soil profile (Tikhomirov and Shcheglov, 1994). Recent studies by the Ukrainian Institute of Agricultural Radiology show that in certain conditions the radiocesium inventories in the coniferous forest biomass and litter at the late stage after the Chernobyl accident may reach 20% and 50% of its deposition, respectively (Yoschenko et al., 2015).

Aims of our ongoing study are characterization of the radiocesium distribution at the beginning of the late stage and quantification of its fluxes for modelling of its long-term redistribution in the typical Fukushima forest ecosystems.

Materials and Methods

Experimental sites, monitoring equipment and sampling
Our monitoring program started in the spring of 2014 in the mature Japanese cedar artificial plantation located in Yamakiya district, Kawamata town, Fukushima prefecture (N37°35.2860' E140°42.6540'), in Area 2 of the Fukushima zone, approximately 34 km northwest of FDNPP. With time, we extent our study to other species, and to the moment it is performed at 7 experimental sites in the Fukushima prefecture (Fig. 1, Table 1).
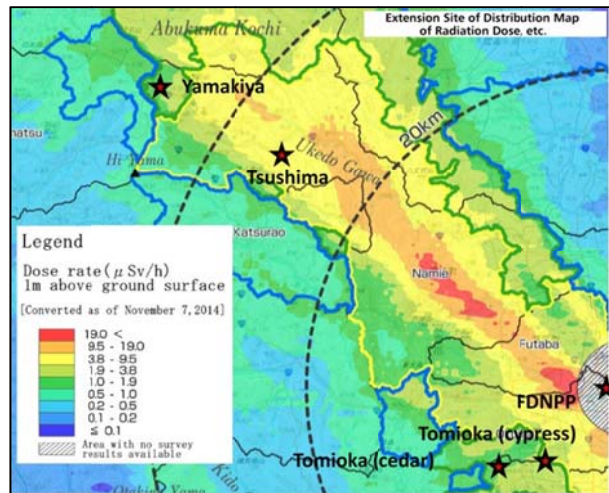
Figure 1. *Location of the experimental sites in the Fukushima zone. Background map: "Extension Site of Distribution Map of Radiation Dose, etc.,/GSI Maps" (http://ramap.jmc.or.jp/map/eng/about.html).*

Table 1. *Description of the experimental sites.*

Location	Type of forest	Plantation density (dominant species), ha⁻¹	Monitoring since
Yamakiya	Mature Japanese cedar (artificial plantation)	335	May 2014
Tsushima	Mature Japanese cedar (artificial plantation)	4430	Aug 2015
	Mature Japanese red pine and broadleaved species (natural)	900	Sep 2015
FDNPP	Mixed forest (Japanese cedar, Japanese cypress, Japanese fir, Japanese red pine and several broadleaved species)	-	March 2016
Tomioka	Mature Japanese cedar (artificial plantation)	1490	Nov 2016
	Mature Japanese cypress (artificial plantation)	3090	Nov 2016
	Young Japanese cypress (artificial plantation)	7230	Nov 2016

At all sites except the FDNPP site the same principal research scheme was used. The first step was characterisation of the forest stand based on the measurements of the tree diameters at the breast height (DBH), heights and plantation density. Then the group of the control trees (5-9) was selected at each site in such manner that the frequency distribution of DBH^2 in this group should be similar to that in the whole forest. At Yamakiya site collar-type stemflow (SF) collectors (Thimonier, 1998) were installed at each control tree. The collectors were connected to the 90-L plastic tanks equipped with the WT-HR loggers (Intech Instruments Ltd.) of the water level. SF samples were collected at intervals of 2 weeks to 2 months since June 2014 till the end of 2016 with recording of the total of stemflow based on the measured water levels. Similarly to other researchers (Kato et al., 2015), we found that stemflow provides the negligible contribution to the removal of radiocesium from the trees as compared to litterfall and throughfall, and in this reason we did not install SF collectors at other sites. Thoughfall (TF) was collected using the collectors each consisting of 10 L polyethylene tank, 21-cm-diameter funnel with the evaporation suppressor and polyethylene mesh filter, and WT-HR loggers. Finally, the litterfall (LF) was collected using 1 m² litter traps installed approximately at 1 m above the ground surface. The traps were constructed from the metal coated plant stake supports and garden mesh tissue. TF and LF samplers were randomly distributed within the experimental plots; in the case of the low plantation density, TF samplers were randomly relocated after each sampling.

At the beginning of the dormancy period, the biomass samples (outer and inner bark, last 3 sapwood annual rings (sapwood 1-3), rest of sapwood (sapwood 4+), heartwood, big branches, small

branches, current year foliage and old foliage were collected at the control trees. For characterization of the terrestrial contamination density and radiocesium vertical distribution in soil profile, at several locations chosen randomly within the experimental plots the litter samples (L, F and H horizons) were collected from area of 0.1 m^2 each, and after that, within these areas the soil core samples were collected using DIK-110C liner sampler (Daiki Rika Kogyo Co., Ltd.).

The aboveground biomass distributions at the sites were determined based on the measured distributions of DBH, literature data (Usoltsev, 2010) and measured weights of compartments of the cut trees.

More details on the sampling along with the discussion on the sampling reliability can be found in Yoschenko et al. (2016a).

At the FDNPP site we only collected the biomass samples from 1-2 trees of each recognised species, and several soil and litter samples.

Sample preparation and measurements

After measurements of weights at the natural moisture content (f.w.), samples of soil, litter and vegetation were dried at 105 °C till constant weight (d.w.). All measurement results below are presented for d.w. The samples were thoroughly homogenized; litter and biomass samples were grinded to 1-2 mm before homogenization.

Radiocesium activities in the samples were measured by means of γ-spectrometry using HPGe detectors GC-4020 (Canberra) and Lynx Digital Signal Analyzer in 100 mL U-8 containers (AS ONE, Tokyo, Japan) for soil, litter and biomass and in 2 L Marinelli containers for TF and SF.

Radiocesium flux calculations

For calculation of the radiocesium annual fluxes in the studied ecosystems, we used an approach that was successfully applied earlier for the Chernobyl Scots pine forest ecosystems (Goor and Thiry, 2004; Thiry et al., 2009). The approach specifies three main fluxes in the ecosystem: *Incorporation*, *Uptake* and *Translocation*. *Incorporation* is a total quantity of element (activity of radionuclide) associated with production of the new biomass. *Uptake* quantifies an annual absorption of element (radionuclide) from soil profile through the root system; it is calculated as a sum of the radiocesium annual *Immobilization* in perennial compartments and its annual *Return* to soil with TF, SF and LF. *Translocation* shows the annual internal remobilization of element (or relocation of radiocesium) from senescing organs to support production of the new biomass.

Results and Discussion

For the most of the experimental sites the sample measurements are in progress now, or the measurement results are analysed. Here we present the results obtained at the Yamakiya site in the monitoring campaign of 2014 (Yoschenko et al., 2016a) and some preliminary results of the monitoring campaigns of 2015 and 2016 for this site and for Japanese cedar at the experimental sites in Tsushima and at the FDNPP.

During the monitoring period we observed significant redistribution of radiocesium in the studied ecosystems. Its inventories decreased 2-3 times in the forest litter and increased in the 5-cm topsoil layer (Fig. 2), which reflects processes of the litter mineralization and leaching of radiocesium with precipitations, as well as decreasing of the radiocesium concentrations in the fresh litterfall. In general, at the both sites (Yamakiya and Tsushima, Japanese cedar forest ecosystems) the major fractions of radiocesium (up to 80% of its total inventory in soil profile) are found in the 0-5 cm soil layer. However, in 3-5 years after the deposition to the forest ecosystems the Fukushima-derived radiocesium has also migrated in the measurable amounts to the deeper soil layers, which can be likely caused by the high porosity of soil and large amount of precipitation.
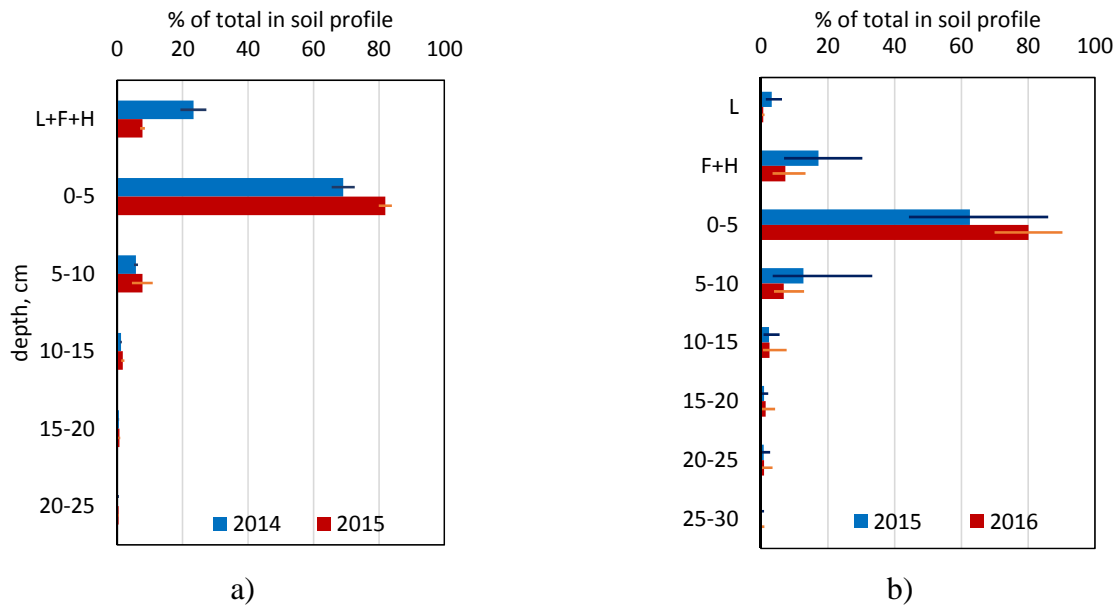
Figure 2. *Radiocesium distributions in soil profiles in the Japanese cedar forest ecosystems at the experimental sites in Yamakiya (a) and Tsushima (b).*

The radiocesium concentrations in the tree compartments in the Japanese cedar ecosystems are presented at Fig. 3. In all studied ecosystems the highest concentrations are found in the compartments that could intercept the initial deposition in March 2011: in outer bark and small branches at the experimental site in Tsushima, in outer bark at the site at the FDNPP, and in small branches and old foliage in 2014 in Yamakiya. Fig. 3a clearly shows removal of the residues of the initially intercepted radiocesium from the tree compartments during 2015: indeed, its concentrations significantly decreased in outer bark, small branches and old foliage. In general, at this site the radiocesium distribution in 2015 is rather similar to those at the other two sites. Some differences may be caused by the different initial distribution of radiocesium in the studied ecosystems after the deposition in March 2011 (e.g. due to the different plantation densities, weather conditions during deposition etc.), and also may reflect the different removal rates of the initially intercepted radiocesium from the tree crowns. It is important to note that at all sites the radiocesium concentrations in 2015-2016 in young foliage reached or exceeded those measured in old foliage, which may indicate increase of its root uptake. Another interesting feature is higher concentrations of radiocesium in heartwood as compared to sapwood. In the tree species heartwood serves as a source for the nutrients recycling to sapwood (during formation of the new annual rings of heartwood) and as a storage of toxic chemical substances (Bamber, 1987; Taylor et al., 2002), and the observed distribution requires the additional studies for clarification of the mechanisms involved in its formation. It should be noted that the similar radiocesium distributions in the Japanese cedar wood were reported by Ogawa et al. (2014) and by Coppin et al. (2016). Moreover, we found similar distribution of stable cesium in the wood compartments of Japanese cedar at the experimental site in Yamakiya (Fig. 4), which confirms reliability of the observed radiocesium distributions.

Fig. 4 also shows that in the studied forest ecosystem the equilibrium between the stable and radioactive cesium isotopes has not been reached yet. It concerns not only heartwood, for which one can expect the further relative increase of the radiocesium concentrations, but also other compartments that are not shown at the diagram: according to the stable cesium measurement results, the radiocesium concentrations should increase in the future in young foliage and decrease in outer bark and small branches. More detail prognosis can be provided on completion of the stable cesium measurements.
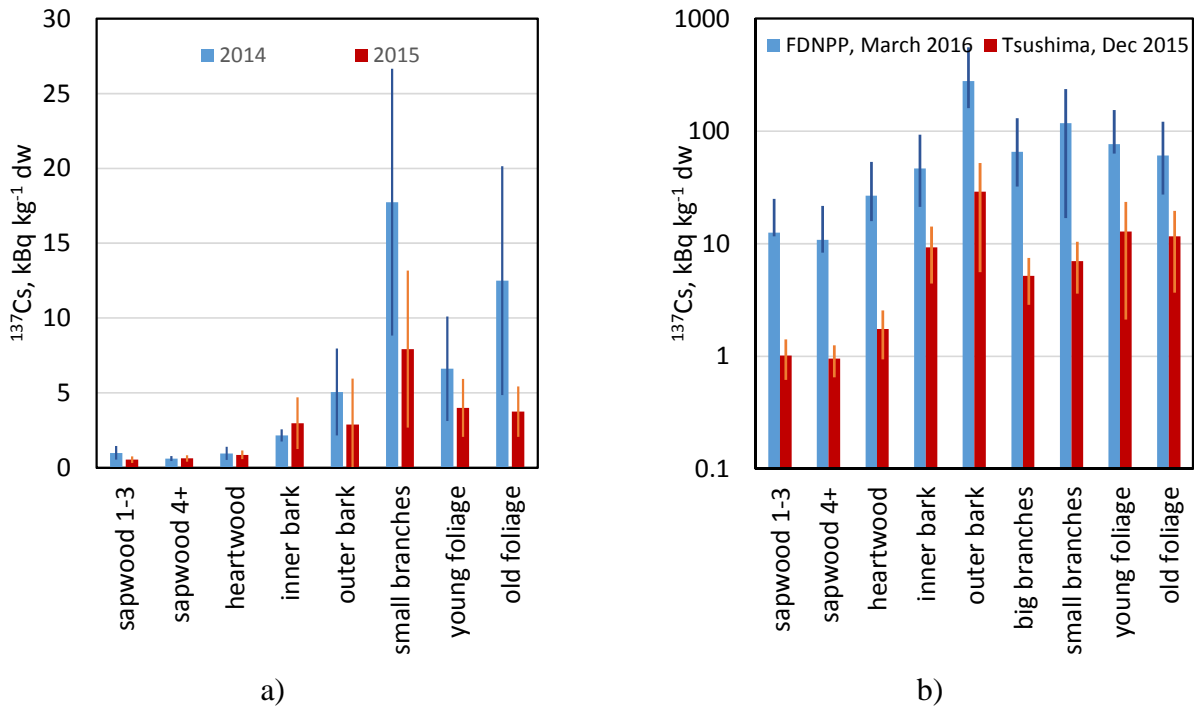
Figure 3. ^{137}Cs activity concentrations in the Japanese cedar forest ecosystem compartments at the experimental sites in Yamakiya (a) and at the FDNPP and in Tsushima (b).
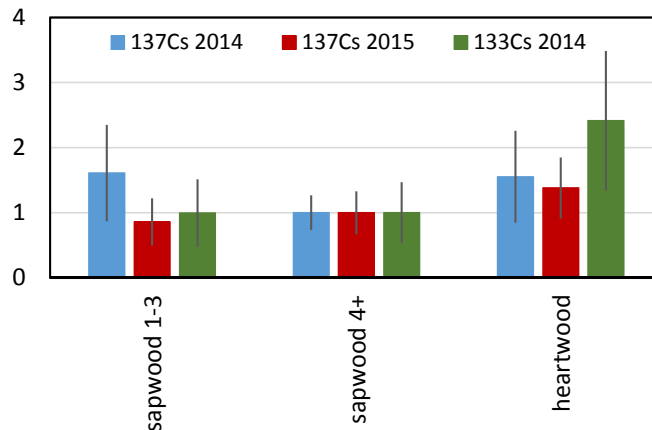
Figure 4. Radioactive (^{137}Cs) and stable (^{133}Cs) cesium isotopes distributions in the wood compartments of Japanese cedar at the experimental site in Yamakiya. The average concentrations normalized to the mean concentration of isotope in the sapwood 4+ compartment and STD are presented.

Based on the results of the monitoring campaign of 2014 in Yamakiya, we made the first estimates of the main fluxes in the Japanese cedar forest (Yoschenko et al., 2016a). It should be noted, however, that the above-described approach for the fluxes calculation works well if the radionuclide activities in the tree compartments are formed by the root uptake only (i.e. at the quasi-equilibrium stage) and gives the conservative (upper) estimates, especially for the *Uptake* flux, in case of presence of the residues of the initial deposition in some compartments, which was emphasized in the mentioned publication. *Uptake* was estimated as 4±3 % of the total radiocesium deposition in the ecosystem. With decrease of the initially intercepted fraction in 2015, this flux could be estimated as about 2 %, while the assessment based on the total inventories of radiocesium in the aboveground biomass in 2014 and 2015 with account of the activities removed with the litterfall, thoughfall and stemflow in the period between the sampling campaigns gives the value of *Uptake* about 1.4 %. More precise estimates of the radiocesium fluxes will be available after completion of measurements

of the samples collected in 2016. Also, the stable cesium flux estimates will be used for the modelling of the long-term radiocesium redistribution in the studied forest ecosystems.

Conclusions

The long-term monitoring campaign has been started at several experimental sites in the Fukushima zone in order to characterize the current distributions of radiocesium in typical Fukushima forests and to provide the prognosis of its future levels in the forest compartments. Main results to the moment have been obtained for the Japanese cedar forests. For this species we found that in 3 years after the accident the major part of the initially intercepted radiocesium has been removed from the aboveground biomass. During 2015, its inventories sharply decreases in the forest litter and in the biomass compartments containing the residues of the initial deposition (old foliage, outer bark and small branches). Based on the apparent absence of equilibrium between the radioactive and stable cesium in the studied ecosystem we expect that the radiocesium redistribution processes (removal and internal translocation of the initial deposition from the above-listed compartments, increase of the root uptake) will continue in the following period. The current annual root uptake of radiocesium from the soil profile is about 1% of its total activity in the studied forest ecosystem in Yamakiya. The further in-depth studies are necessary for the reliable prognosis of the further fate of radiocesium in Fukushima forests.

Acknowledgement

References

Atomic Energy Society of Japan (Ed.), 2015. The Fukushima Daiichi Nuclear Accident. Final Report of the AESJ Investigation Committee. Springer, Tokyo Heidelberg New York Dordrecht London. http://dx.doi.org/10.1007/978-4-431-55160-7.

Bamber, R.K., 1987. Sapwood and Heartwood. Forestry Commission of New South Wales, Tech. Publ. 2.

Bunzl, K., Schimmack, W., Kreutzer, K., Schierl, R., 1989. Interception and retention of Chernobyl-derived ^{134}Cs, ^{137}Cs and ^{106}Ru in a spruce stand. Sci. Total Environ. 78, 77-87.

Coppin, F., Hurtevent, P., Loffredo, N., Simonucci, C., Julien, A., Gonze, M.-A., Nanba, K., Onda, Y., Thiry, Y., 2016. Radiocaesium partitioning in Japanese cedar forests following the "early" phase of Fukushima fallout redistribution. Scientific Reports | 6:37618 |

Endo, I., Ohte, N., Iseda, K., Tanoi, K., Hirose, A., Kobayashi, N.I., Murakami, M., Tokuchi, N., Ohashi, M., 2015. Estimation of radioactive 137-cesium transportation by litterfall, stemflow and throughfall in the forests of Fukushima. J. Environ. Radioact. 149, 176-185.

Fukushima Prefecture, 2014. Agriculture, Forestry and Fishery Industries of Fukushima Prefecture. http://www.pref.fukushima.lg.jp/site/english/agriforesty-fish.html (accessed 29.10.15).

Fukushima Prefecture, 2015. Steps for Revitalization in Fukushima.

Fukushima Minpo, 2016. Full-fledged work begins to build interim nuke waste storage site in Fukushima http://www.fukushimaminponews.com/news.html?id=754

Goor, F., Thiry, Y., 2004. Processes, dynamics and modelling of radiocaesium cycling in a chronosequence of Chernobyl-contaminated scots pine (*Pinus sylvestris* L.) plantations. Sci. Total. Environ. 325, 163-180.

Hashimoto, S., Ugawa, S., Nanko, K., Shichi, K., 2012. The total amounts of radioactively contaminated materials in forests in Fukushima, Japan. Sci. Rep. 2, 416. http://dx.doi.org/10.1038/srep00416.

IAEA, 2011. Fukushima Nuclear Accident Update Log. Updates of 12 April 2011. https://www.iaea.org/newscenter/news/fukushima-nuclear-accident-updatelog-15 (accessed 29.10.15).

IAEA, 2015. The Fukushima Daiichi Accident. Technical Volume 5. Post-accident Recovery. International Atomic Energy Agency, Vienna.

JAEA, 2015a. JAEA-review 2014-051. Remediation of Contaminated Areas in the Aftermath of the Accident at the Fukushima Daiichi Nuclear Power Station: Overview, Analysis and Lessons Learned. Part 1: a Report on the "Decontamination Pilot Project". Japan Atomic Energy Agency.

JAEA, 2015b. JAEA-Review 2014-051. Remediation of Contaminated Areas in the Aftermath of the Accident at the Fukushima Daiichi Nuclear Power Station: Overview, Analysis and Lessons Learned. Part 2: Recent Developments, Supporting R&D and International Discussions. Japan Atomic Energy Agency.

Kato, H., Onda, Y., 2014. Temporal changes in the transfer of accidentally released ^{137}Cs from tree crowns to the forest floor after the Fukushima Daiichi nuclear power plant accident. Prog. Nucl. Sci. Technol. 4, 18-22.

Kato, H., Onda, Y., Gomi, T., 2012. Interception of the Fukushima reactor accident derived ^{137}Cs, [134]Cs and ^{131}I by coniferous forest canopies. Geophys. Res. Lett. 39, L20403.

Kato, H., Onda, Y., Hisadome, K., Loffredo, N., Kawamori, A., 2015. Temporal changes in radiocesium deposition in various forest stands following the Fukushima Dai-ichi nuclear power plant accident. J. Environ. Radioact. http://dx.doi.org/10. 1016/j.jenvrad.2015.04.016

Loffredo, N., Onda, Y., Kawamori, A., Kato, H., 2014. Modeling of leachable ^{137}Cs in throughfall and stemflow for Japanese forest canopies after Fukushima Daiichi nuclear power plant accident. Sci. Total Environ. 493, 701-707.

MAFF, 2012. Prefecture and Artificial Forest Ratios. http: //www.rinya.maff.go.jp/ j/keikaku/ genkyou/h24/pdf/shinrin_j_h24.pdf (accessed 29.10.15).

MAFF, 2015. Statistics of Agriculture, Forestry and Fisheries. http:// www.maff.go.jp /j/tokei/kouhyou/mokuzai/pdf/mokuzai_14.pdf (accessed 29.10.15).

Ogawa, H., Ito, H., Murakami, K., Kumata, A., Hirano, Y., Yokota, K., Yoshida, H., 2014. Radiocesium distribution in Japanese cedar trees at one year after Fukushima Dai-Ichi nuclear power plant accident. In: Proceedings of the 15th Workshop of Environmental Radioactivity. KEK, Tsukuba, Japan. March 6-8, 2014, pp. 252-260.

Ohta, H., 2011. Environmental Remediation of Contaminated Area by the Fukushima-Daiichi NPP Accident. https://www.iaea.org/OurWork/ST/NE/NEFW/WTShttps://www.iaea.org/OurWork/ST/NE/NEFW/WTS-Networks/IDN/idnfiles/IDN_AnnFor2011/Cleanup_activities-OHTA.pdfNetworks/IDN/idnfiles/IDN_AnnFor2011/Cleanup_activities-OHTA.pdf (accessed 29.10.15).

Steinhauser, G., Brandl, A., Johnson, T.E., 2014. Comparison of the Chernobyl and Fukushima nuclear accidents: a review of the environmental impacts. Sci. Total Environ. 470-471, 800-817.

Taylor, A.M., Gartner, B.L., Morrell, J.J., 2002. Heartwood formation and natural durability: a review. Wood Fiber Sci. 34 (4), 587-611.

Thimonier, A., 1998. Measurement of atmospheric deposition under forest canopies: some recommendations for equipment and sampling design. Environ. Monit. Assess. 52, 353-387.

Thiry, Y., Colle, C., Yoschenko, V., Levchuk, S., Van Hees, M., Hurtevent, P., Kashparov, V., 2009. Impact of Scots pine (Pinus sylvestris L.) plantings on long-term ^{137}Cs and ^{90}Sr recycling from a waste burial site in the Chernobyl Red Forest. J. Environ. Radioact. 100, 1062-1068.

Tikhomirov, F.A., Shcheglov, A.I., 1994. Main investigation results on the forest radioecology in the Kyshtym and Chernobyl accident zones. Sci. Total Environ. 157, 45-57.

Usoltsev, V.A., 2010. Eurasian Forest Biomass and Primary Production Data. Ural Branch of Russian Academy of Sciences, Yekaterinburg, Russia.

Watanabe, Y., Ichikawa, S., Kubota, M., Hoshino, J., Kubota, Y., Maruyama, K., Fuma, S., Kawaguchi, I., Yoschenko, V.I., Yoshida, S., 2015. Morphological defects in native japanese fir trees around the Fukushima daiichi nuclear power plant. Sci. Rep. 5, 13232. http://dx.doi.org/10.1038/srep13232.

Yasutaka, T., Naito, W., Nakanishi, J., 2013. Cost and Effectiveness of Decontamination Strategies in Radiation Contaminated Areas in Fukushima in Regard to External Radiation Dose. PLoS ONE 8(9): e75308. doi:10.1371/journal.pone.0075308

Yoschenko, V., Nanba, K., Konoplev, A., Takase, T., Kashparov, V., Levchuk, S., Protsak, V., 2015. Radionuclides distributions and fluxes in the forest ecosystems of Chernobyl and Fukushima. In: ICOBTE 2015 Fukuoka Abstract Book. 13th International Conference on the Biogeochemistry of Trace Elements, p. 213.

Yoschenko, V., Takase, T., Konoplev, A., Nanba, K., Onda, Y., Kivva, S., Zheleznyak, M., Sato, N., Keitoku, K., 2016a. Radiocesium distribution and fluxes in the typical Cryptomeria japonica forest at the late stage after the accident at Fukushima Dai-Ichi Nuclear Power Plant. J. Environ. Radioact. http://dx.doi.org/10.1016/j.jenvrad.2016.02.017

Yoschenko, V., Nanba, K., Yoshida, S., Watanabe, Y., Takase, T., Sato, N., Keitoku, K., 2016. Morphological abnormalities in Japanese red pine (Pinus densiflora) at the territories contaminated as a result of the accident at Fukushima Dai-Ichi Nuclear Power Plant. J. Environ. Radioact. 165, 60-67.

Effective half-lives of radiocesium in different Japanese tree species

K. Tagami[*], S. Uchida and N. Ishii

National Institutes for Quantum and Radiological Science and Technology (QST) -
National Institute of Radiological Sciences (NIRS), Anagawa 4-9-1, Inage-ku, Chiba 263-8555, Japan

Abstract

Due to the Fukushima nuclear accident occurred in 2011, trees were contaminated with radiocesium ($^{134, 137}$Cs) in Fukushima and surrounding prefectures in Japan. Although the radiocesium concentrations in leaves of trees have decreased with time, it was not clear whether or not the radiocesium decreasing rates observed after the Fukushima accident were similar to those observed after the Chernobyl accident.Therefore, we carried out literature survey to calculate the decreasing rates of ^{137}Cs, which is expressed as effective half-life (T_{eff}) for ^{137}Cs after both nuclear accidents. We also collected ^{137}Cs concentrations in leaves and fruits of *Citrus natsudaidai* from September 2011 to March 2015 at Chiba prefecture for comparison. The T_{eff} of ^{137}Cs was ca. 0.5-0.9 y for leaves and fruits flesh, respectively, at Chiba. In other areas, fruits of the same family tree, *Citrus unsiu*, showed the similar T_{eff} values of about 0.55 y after the Fukushima nuclear accident, and interestingly, similar value was observed after the Chernobyl accident. In leaves of the other plant species, i.e. Japanese black pine (*Pinusthunbergii*) and tea tree (*Camellia sinensis*), the T_{eff}s were also similar after both accidents. These results may indicate that the chemical form of ^{137}Cs deposited on these tree species were similar for both accidents.

Introduction

Since the accident at TEPCO's Fukushima Daiichi Nuclear Power Plant (FDNPP) in March 2011, many environmental studies have been carried out inside and outside Japan to clarify the fate of released radiocesium in the environment. IAEA published a large volume report on the FDNPP accident (IAEA, 2015) but the fate of radiocesium in the Japanese environment was not described in details. Because forests cover large areas in Japan (about 70% of the land area), changes of radiocesium concentrations in plants are of great concern to the public and thus food monitoring has been carried out for wild edible plants by Ministry of Health, Labour and Welfare since March 2011.

Previously, we reported the radiocesium concentration change with time in herbaceous plants and persimmon trees (Tagami & Uchida, 2015a, b). Comparison of such data with those observed after the Chernobyl accident would help us to understand the differences between the accidents. In this study, therefore, radiocesium decreasing rates, expressed as effective half-life (T_{eff}), observed in trees in Japan within 3-4 years after the Fukushima Daiichi and Chernobyl accidents was carried out. For this purpose, we measured ^{137}Cs concentrations in some tree species to provide T_{eff} data after the Fukushima accident, and also we did literature survey to obtain ^{137}Cs concentration changes in tree tissues for T_{eff} calculations. By using ^{137}Cs data observed only in Japan, the climate effect on ^{137}Cs fate would be ignored.

---

[*]Corresponding author, E-mail: tagami.keiko@qst.go.jp

Materials and Methods

Open source data

Data selected were ^{137}Cs concentrations in leaves of black pine (*Pinusthunbergii*) and tea tree (*Camellia sinensis*), and fruits of *Citrus unshiu* collected from 1985 to 2015 using the environmental radiation database (Nuclear Regulation Authority, 2016a). From the database, we found direct deposition effect from the Chernobyl accident (1986-1988) and the Fukushima accident (2011-2013). An example of the ^{137}Cs concentration data are shown in Figure 1 (Japanese black pine, 2-y old leaves @ Fukushima). In order to have more data on fruits of citrus species in Fukushima, we also used ^{137}Cs concentrations from food monitoring data reported by Ministry of Health, Labour and Welfare (2016) and environmental monitoring data of ^{137}Cs for pine trees by Nuclear Regulation Authority (2016b).
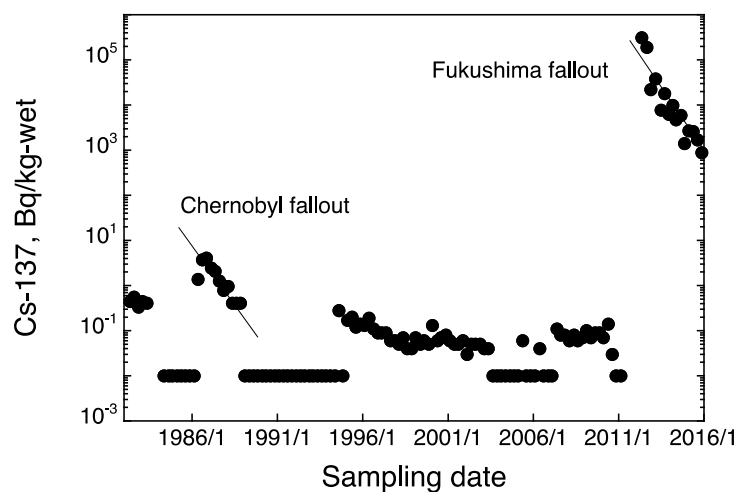
Figure 1. ^{137}Cs concentration data in two years-old leaves of Japanese black pine trees collected in OKM town, Fukushima Pref. (Data from Nuclear Regulation Authority, 2016)

Measurement of ^{137}Cs concentration change in Citrus natsudaidai

^{137}Cs concentrations in *Citrus natsudaidai* were measured from September 2011 to March 2015 at our institute campus in Chiba City, Japan. The collection site was the QST-NIRS campus in Chiba Prefecture located about 220 km south from the FDNPP and we found Fukushima fallout at this site (Ishii et al., 2013). Leaf and fruit samples were collected several times. Immediately after collection, samples (leaves and fruits) were transferred to a laboratory and weighed. Leaves and fruits were washed with tap water to remove dust from the surface, and then, finally, the samples were rinsed with reverse osmosis water. Fruit samples were separated into fruit flesh and skin. Each sample was oven-dried at 80°C for more than 2 days, and then the sample was pulverized and transferred into a plastic container. Measurements were carried out using a Ge detecting systems (Seiko EG&G).

Results and Discussion

^{137}Cs concentration change in pine tree leaves in 2011-2015

Pine tree leaves (2 y.o.) data for ^{137}Cs from Nuclear Regulation Authority (2016b) are plotted in Figure 2. Samples were taken from three sites located at 23-42 km north west from the FDNPP. In

all area, decreasing trend of ^{137}Cs concentrations 2 y.o.leaves have been changed after 2013, that is, the decrease was slower in 2013-2015 compared to that observed in 2011-2013. Probably, mobile radiocesium deposited on the above ground part of trees were taken up through the tree surface and translocated to new shoots in the first year (Tagami et al., 2012), but the concentration decreased with time by plant mass increase.In the following years, the radiocesium uptake became much smaller than the first year and radiocesium moved to more inner part of trees was expected according to the Japanese cedar tree results (Ogawa et al., 2016), which caused the slow radiocesium concentration decreasing rates.

According to these results, in this study, we used only 2011-2013 data to calculate short-term fractions of T_{eff}s of ^{137}Cs from the trees to compare the data with those observed after the Chernobyl accident. As shown in Figure 1, only a small effect from the Chernobyl fallout was found in Japan so that short time period changes were only available for Japanese datasets.
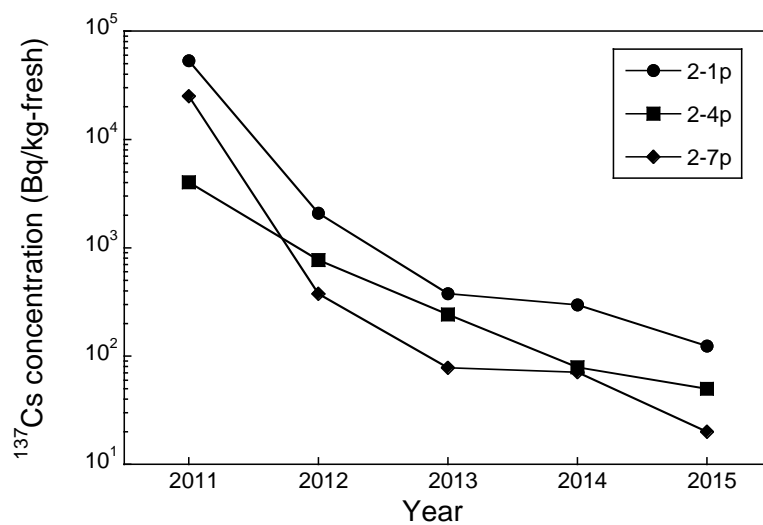
Figure 2.*^{137}Cs concentrations in 2 y.o.leaves of Japanese black pine collected at three sampling sites. Samples collected in 2011 was directly contaminated, but indirectly contaminated after 2012 samples.*

^{137}Cs concentrations in Citrus species in 2011-2015

Concentration changes of ^{137}Cs in a *C. natsudaidai* tree tissue sample are shown in Figure 3. Because ^{137}Cs concentration in leaves were affected by sampling seasons (Tagami & Uchida, 2015a), August-September sample data in 2011-2014 were used for calculation. The T_{eff}s were 0.87 y for fruits flesh, 0.60 y for fruits peel, and 0.49 y for leaves. The reason of the T_{eff} data differences among different tissue parts were not clear. Unfortunately, however, we did not measure the tree in 2012 and thus it was difficult to discuss further.

For comparison, using ^{137}Cs data in Yuzu (*Citrus junos*) fruits collected in Koriyama City, Fukushima Prefecture, $T_{eff}$was calculated and the value was 1.03 y, when 2011-2015 data were used. The T_{eff} was similar to those we reported previously for persimmon trees (Tagami & Uchida, 2015a).
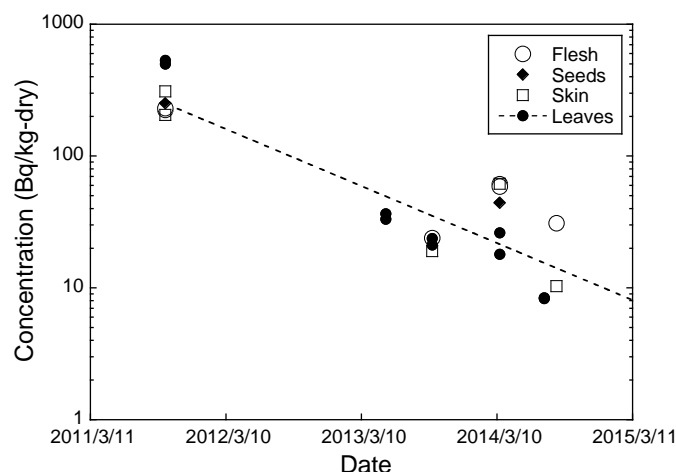
Figure 3. ^{137}*Cs concentrations in leaves and fruit parts (flesh, skin and seeds) of Citrus natsudaidai collected at QST-NIRS campus.*

T_{eff} comparison observed after the Chernobyl and Fukushima nuclear accidents in three plant species

Some of the calculated T_{eff} data of ^{137}Cs in trees are summarized in Table 1 with sampling prefecture. All T_{eff} data were used, there was no statistical differences of T_{eff}s observed after the Chernobyl and Fukushima accidents for *P. thunbergii* (n=28 for Chernobyl and n=18 for Fukushima accidents) and *Camellia sinensis*(n=11 for Chernobyl and n=11 for Fukushima accidents). For citrus species, not many data were available for the same species, however, in this classification, similar T_{eff}s were observed. These results may indicate that the chemical form of ^{137}Cs deposited on these tree species were similar for both accidents.

Table 1. *Effective half-lives(T_{eff}s) of ^{137}Cs observed after the Chernobyl and Fukushima nuclear accident in tree tissues observed in Japan.*

Species	Prefecture	Chernobyl accident		Fukushima accident	
		Observation period	T_{eff}, y	Observation period	T_{eff}, y
Pinusthunbergii	Miyagi		0.32		0.36
	Fukushima		0.60		0.33
	Shizuoka	1986-1988	0.37	2011-2013	0.31
	Ehime		0.44		-
Camellia sinensis	Shizuoka	1986-1988	0.42	2011-2013	0.38
Cistrusunsiu, fruits	Ehime	1986-1988	0.54	2011-2013	0.55
Citrus natsudaidai,					
leaves	Chiba	-		2011-2013	0.49
fruits					0.87
Citrus junos	Fukushima	-		2011-2014	1.03

Conclusions

In this study, we compared the T_{eff}s of ^{137}Cs in tree tissue parts using Japanese data observed after the Chernobyl and the Fukushima accidents. T_{eff}s calculated were similar for the leaves of Japanese black pine and tea tree. Although less data were available for citrus species, the T_{eff}s observed were similar observed after both accidents. The results may suggest that the chemical forms of ^{137}Cs deposited on trees were similar for both nuclear accidents. However, the released chemical forms of radiocesium from the Fukushima accident were not clear. Thus further studies are necessary to clarify the radiocesium fate in the environment especially after accidental releases.

Acknowledgement

References

IAEA, 2015. The Fukushima Daiichi Accident. STI/PUB/1710. 1254 pp. IAEA, Vienna.

Ishii, N., Tagami, K., Takata, H., Fujita, K., Kawaguchi, I., Watanabe, Y., Uchida, S., 2013. Deposition in Chiba Prefecture, Japan of Fukushima Daiichi nuclear power plant fallout.Health Phys. 104, 189-194.

Ministry of Health, Labour and Welfare, 2016.Levels of Radioactive Contaminants in Foods Tested in Respective Prefectures. Available at: http: //www.mhlw.go.jp/ english/topics/2011eq/ index_food_radioactive.html (accessed 14.10.16.).

Nuclear Regulation Authority, 2016a.Environmental Radiation Database. Available at: http://search.kankyo-hoshano.go.jp/servlet/search.top (in Japanese) (accessed 14.10.16).

Nuclear Regulation Authority, 2016b.Readings of environmental monitoring samples (Pine leaf). Available at: http://radioactivity.nsr.go.jp/ja/list/483/list-1.html (in Japanese) (accessed 14.10.16).

Ogawa, H., Hirano, Y., Igei, S., Yokota, K., Arai, S., Ito, H., Kumata, A., Yoshida, H., 2016. Changes in the distribution of radiocesium in the wood of Japanese cedar trees from 2011 to 2013.

Tagami, K., Uchida, S., Ishii, N., Kagiya, S., 2012. Translocation of radiocesium from stems and leaves of plants and the effecton radiocesium concentrations in newly emerged plant tissues. J. Environ. Radioact. 111, 65-69.

Tagami, K., Uchida, S., 2015a. Effective half-lives of ^{137}Cs from persimmon tree tissue parts in Japan after Fukushima Dai-ichi Nuclear Power Plant accident. J. Environ. Radioact. 141, 8-13.

Tagami, K. Uchida, S., 2015b.Effective half-lives of ^{137}Cs in giant butterbur and field horsetail, and the distribution differences of potassium and ^{137}Cs in aboveground tissue parts. J. Environ. Radioact. 141, 138-145.

^{90}Sr in Japanese soil samples after the Fukushima nuclear accident

N. Kavasi[*], S.K. Sahoo and T. Aono

National Institute for Quantum and Radiological Sciences and Technology,
4-9-1 Anagawa, Inage-ku, Chiba, 263-8555 Japan

Abstract

The radioactive fission product ^{90}Sr has prolonged biological half-life (about 18 y) in the human body. Because of its chemical similarity to calcium that easily accumulates in bones and irradiates the bone marrow, it causes high radio-toxicity. Therefore, accurate assessment of ^{90}Sr is a paramount task in case of a nuclear disaster.
The atmospheric emission of ^{90}Sr at the Fukushima accident was two orders lower than Chernobyl, negligible compared to the atmospheric global fallout caused by nuclear weapon tests.
Considering measurement results in the period between 2011-2016, significant ^{90}Sr contamination in extended areas has not yet been reported around the Fukushima Daiichi Nuclear Power PlantFDNPP. The typical ^{90}Sr contamination level is tens of Bq/kg or lower, however, the discovery of ^{90}Sr deposition hot spots cannot be ruled out.

Introduction

Radioactive strontium isotopes are generated by high cumulative fission yield (5-6 %) during thermal neutron fission in a nuclear reactor. The physical half-life of ^{89}Sr (50.52 d) is short but that of ^{90}Sr (28.8 y) is long enough to cause radioecological consequences (Vajda and Kim, 2010). ^{90}Sr has a long-lasting biological half-life (~18 y) in the human body due to its chemical similarity to calcium,therefore the importance of ^{90}Sr analysis is emphasized in case of a nuclear disaster.

The worldwide spreading of ^{90}Sr, as a background, is a result of the global atmospheric fallout attributed to the large-scale atmospheric nuclear weapons tests conducted from 1945 onwards (Mangano et al., 2003). In the case of local contamination, nuclear accidents are not the only source of ^{90}Sr isotope: underground nuclear weapons tests; improper handling of by-products of nuclear weapons production; or normal operation of nuclear facilities (e.g. reprocessing plants) should also be taken into account.

It is important to note that, with regard to the Fukushima accident, there have been a vast array of scientific papers published on gamma emitter radionuclides such us iodine, tellurium and cesium isotopes (Hirose, 2012; Hosoda et al., 2013; Kanai, 2012; Yamaguchi et al., 2014), while the number of papers on ^{90}Sr are limited (Sahoo et al., 2016; Steinhauser et al., 2013). The underlying reason can be found in the applied measurement methods: determining the gamma emitter radionuclides by using gamma spectroscopy, where the sample treatment is very simple, makes the procedure straightforward and swift. In contrast, analysing the pure beta emitter ^{90}Sr is more time-consuming and the process complicated. Since beta particle spectroscopy is not applicable to distinguishing the beta emitter isotope, the energy distribution of the emitted electrons in the beta decay is continuous. Therefore, a complex separation procedure is needed before calculating the radionuclide (Hou and Roos, 2008; Maekawa et al., 2012, December 14; Vajda and Kim, 2010).

---

[*]Norbert Kavasi, E-mail: kavasi.norbert@qst.go.jp

The current work provides a summary on ^{90}Sr measured in Japanese soil samples after the Fukushima nuclear accident.

Results and Discussion

The FDNPPdisaster in Japan released and dispersed a significant amount of radionuclides (~520 PBq) in the environment. Shortly after the catastrophe, volatile nuclides e.g. ^{137}Cs, ^{131}I and ^{132}Te were detected in the Northern Hemisphere and elevated rates were observed in most of Japan (Hirose, 2012).

Contamination of radiostrontium isotopes,since they have intermediate volatility, was delayed. The approximate^{90}Sr and ^{89}Sr emission into the atmosphere was 0.14 PBq and 2.0 PBq while the estimated ^{90}Sr release into the Pacific Ocean was 0.1-2.2 PBq. A significant part of the ^{90}Sr and ^{89}Sr - about 8.6 PBq and 70 PBq - remained in the stagnant water around the nuclear plant. In the vicinity of the plant, ground water contamination has been reported but could not be clearly identified(Casacuberta et al., 2013; Castrillejo et al., 2016; Povinec et al., 2013).

The estimated atmospheric emissions of ^{90}Sr after both the Fukushima and Chernobyl accidents are presented in Figure 1.along with the atmospheric global fallout. The ^{90}Sr emission at Chernobyl was higher than Fukushima by two orders of magnitude due to themore intensive damage to the reactors at the former. Regarding the Fukushima accident, the period of emission was shorter than Chernobyl and there were containment systems (Mark I) in place to isolate the radionuclides discharge in an emergency situation. However, these containment systems were also damaged during the accident.

The radioactive emission contributes to the terrestrial contamination via dry or wet fallout that was much more significant in the Chernobyl nuclear accident since 79 % of the terrestrial ^{90}Sr contamination density was more than 20 kBq m^{-2} (max. >20,000 kBq m^{-2}) within the 30 km zone, whereas for Fukushima the maximum contamination was 3 kBq m^{-2} (Kashparov et al., 2001; MEXT, 2012b). Comparing the Fukushima and global fallouts on the atmospheric scale, the difference appears to be slight (~0.02%). Therefore, it seems that the former is more restricted to local areas of Japan, namely Fukushima Prefecture.
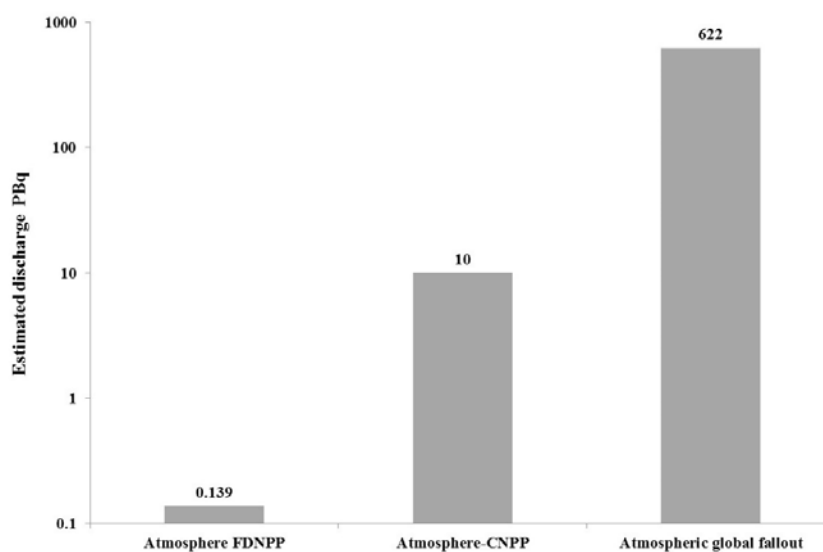

Figure 1.- *Estimated atmospheric emissions of ^{90}Sr after both the Fukushima and Chernobyl accidents along with the atmospheric global fallout*

Regarding the results of ^{90}Sr activity concentration measurement in Japanese soil between 2011 and 2016, more details are displayed in Figure 2.

The measurement results were collected from different reference sources and categorized according to their distance from the FDNPP. Few results appeared in scientific journals by independent scientists (Maekawa et al., 2012; Sahoo et al., 2016; Steinhauser et al., 2013; Takagai et al., 2014), the majority were published in official reports by Japanese governmental organizations such as MEXT and TEPCO (Japanese-Government, 2011; MEXT, 2012a, b; TEPCO, 2011a, b). Beyond the evacuation zone (a 30 km radius around the FDNPP), noteworthy contamination was not discovered, and only one value was above 10 Bq kg^{-1} (13 Bq kg^{-1}) within 100 km, excluding the results from Kashiwa (35 Bq kg^{-1}) and Yokohama (85 Bq kg^{-1}), where the samples were collected on the roof of a building and in a drain respectively and a high background sampling point in Fukushima Prefecture (21 Bq kg^{-1}) out of the 100 km radius.

Four years after the Chernobyl disaster it was possible to compose a map wherein the different ^{90}Sr contamination levels covered extended areas (thousands of km^2) that centred around the damaged Chernobyl Nuclear Power Plant (CNPP) (IAEA, 1991). For the Fukushima accident, composing a similar map is problematic as the activity concentration of ^{90}Sr changed within a wide range, from 1.4 to 1100 Bq kg^{-1} in the evacuation zone, proving that the distance from the FDNPP is an important but not adequate factor when gauging contamination levels because the fallout pattern is highly influenced by atmospheric transport processes such as wind and rain; geological forms such as mountains, flats, etc. Therefore, the results demonstrate that the probability of the presence of localized hot spots is higher than those of large, extended contaminated fields. However, the contamination level gradually decreases by the distance from the FDNPP.
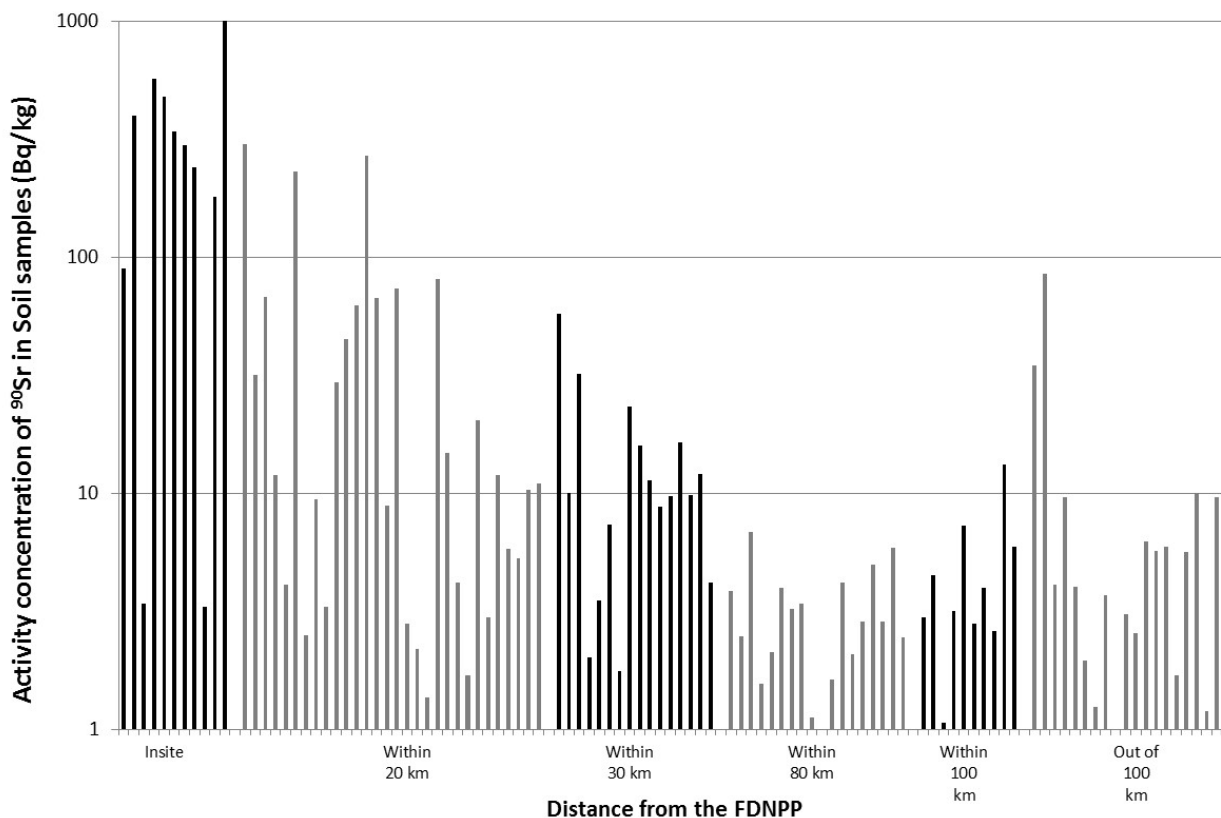
Figure 2.^{90}*Sr activity concentrations of soil samples collected at different distance from the FDNPP*

Conclusions

Damaged reactors ofthe FDNPP were mounted with protective containment systems (Mark I) and the emission period was relatively shorter than the Chernobyl accident.

Consequently, the atmospheric emissionsof ^{90}Sr at Fukushima were two orders lower than in Chernobyl and negligible compared to the atmospheric global fallout.

Significant ^{90}Sr contamination has not so far been reported around the FDNPP as the typical contamination level is some tens of Bq kg^{-1}or lower.

Funding

References

Casacuberta, N., Masqué, P., Garcia-Orellana, J., Garcia-Tenorio, R., Buesseler, K.O., 2013. 90Sr and 89Sr in seawater off Japan as a consequence of the Fukushima Dai-ichi nuclear accident. Biogeosciences 10, 3649-3659.

Castrillejo, M., Casacuberta, N., Breier, C.F., Pike, S.M., Masque, P., Buesseler, K.O., 2016. Reassessment of (90)Sr, (137)Cs, and (134)Cs in the Coast off Japan Derived from the Fukushima Dai-ichi Nuclear Accident. Environmental science & technology 50, 173-180.

Hirose, K., 2012. 2011 Fukushima Dai-ichi nuclear power plant accident: summary of regional radioactive deposition monitoring results. J. Environ. Radioact. 111, 13-17.

Hosoda, M., Tokonami, S., Akiba, S., Kurihara, O., Sorimachi, A., Ishikawa, T., Momose, T., Nakano, T., Mariya, Y., Kashiwakura, I., 2013. Estimation of internal exposure of the thyroid to (131)I on the basis of (134)Cs accumulated in the body among evacuees of the Fukushima Daiichi Nuclear Power Station accident. Environ. Int. 61, 73-76.

Hou, X., Roos, P., 2008. Critical comparison of radiometric and mass spectrometric methods for the determination of radionuclides in environmental, biological and nuclear waste samples. Analytica chimica acta 608, 105-139.

IAEA, 1991. The International Chernobyl Project. Assessment of radiological consequences and evaluation of protective measures, http://www-pub.iaea.org/MTCD/publications/PDF/Pub886_web/Start.pdf, Last access: October 26, 2016.

Japanese-Government, 2011. Report of Japanese Government to the IAEA Ministerial Conference on Nuclear Safety http://www.kantei.go.jp/foreign/kan/topics/201106/iaea_houkokusho_e.html, Last access: October 27, 2016.

Kanai, Y., 2012. Monitoring of aerosols in Tsukuba after Fukushima Nuclear Power Plant incident in 2011. J. Environ. Radioact. 111, 33-37.

Kashparov, V.A., Lundin, S.M., Khomutinin, Y.V., Kaminsky, S.P., Levchuk, S.E., Protsak, V.P., Kadygrib, A.M., Zvarich, S.I., Yoschenko, V.I., Tschiersch, J., 2001. Soil contamination with 90Sr in the near zone of the Chernobyl accident. Journal of environmental radioactivity 56, 285-298.

Maekawa, A., Momoshima, N., Sugihara, S., Tamari, T., 2012. Determination of radiostrontium released from Fukushima Daiichi Nuclear Power Plant through extraction chromatography and liquid scintillation counting. Conference proceedings, http://www.rri.kyoto-u.ac.jp/ anzen_kiban/ outcome/ Proceedings_for_Web/Topics_2-09.pdf, Last access: October 27, 2016.

Maekawa, A., Momoshima, N., Sugihara, S., Tamari, T., 2012, December 14. Determination of radiostrontium released from Fukushima Daiichi Nuclear Power Plant through extraction chromatography and liquid scintillation counting, International Symposium on Environmental monitoring and dose estimation of residents after accident of TEPCO's Fukushima Daiichi Nuclear Power Stations. Office KUR Research Program for Scientific Basis of Nuclear Safety, Research Reactor Institute, Kyoto University, Shiran Hall, Kyoto, Japan.

Mangano, J.J., Gould, J.M., Sternglass, E.J., Sherman, J.D., McDonnell, W., 2003. An unexpected rise in strontium-90 in US deciduous teeth in the 1990s. Sci. Total Environ. 317, 37-51.

MEXT, 2012a. Analysis Results Concerning (i) Gamma-emitting Nuclides and (ii) Sr-89 and Sr-90 (Second Distribution Survey) by MEXT http://radioactivity.nsr.go.jp/en/contents/ 6000/5636/ 24/338_Sr_0912018_e.pdf, Last access: October 27, 2016.

MEXT, 2012b. Results of the Radiation Monitoring of Soil in Fukushima Prefecture http://radioactivity.nsr.go.jp/en/contents/6000/5025/24/232_e_0409.pdf, Last access: October 27, 2016.

Povinec, P., Hirose, K., Aoyama, M., 2013. Fukushima Accident Radioactivity Impact on the Environment. Elsevier.

Sahoo, S.K., Kavasi, N., Sorimachi, A., Arae, H., Tokonami, S., Mietelski, J.W., Lokas, E., Yoshida, S., 2016. Strontium-90 activity concentration in soil samples from the exclusion zone of the Fukushima daiichi nuclear power plant. Scientific reports 6, 23925.

Steinhauser, G., Schauer, V., Shozugawa, K., 2013. Concentration of strontium-90 at selected hot spots in Japan. PloS one 8, e57760.

Takagai, Y., Furukawa, M., Kameo, Y., Suzuki, K., 2014. Sequential inductively coupled plasma quadrupole mass-spectrometric quantification of radioactive strontium-90 incorporating cascade separation steps for radioactive contamination rapid survey. Anal. Methods 6, 355-362.

TEPCO, 2011a. Fukushima Daiichi Nuclear Power Station: Strontium analysis result in the soil 2011.08, http://www.tepco.co.jp/en/press/corp-com/release/betu11_e/images/110903e12.pdf, Last access: October 27, 2016.

TEPCO, 2011b. Fukushima Daiichi Nuclear Power Station: Strontium analysis result in the soil 2014.04, http://www.tepco.co.jp/en/press/corp-com/release/betu11_e/images/110508e7.pdf, Last access: October 27, 2016.

Vajda, N., Kim, C.K., 2010. Determination of radiostrontium isotopes: a review of analytical methodology. Appl. Radiat. Isot. 68, 2306-2326.

Yamaguchi, M., Kitamura, A., Oda, Y., Onishi, Y., 2014. Predicting the long-term Cs distribution in Fukushima after the Fukushima Dai-ichi nuclear power plant accident: a parameter sensitivity analysis. J. Environ. Radioact. 135C, 135-146.

Behavior of radiocesium from arthropods in different trophic levels after the Fukushima Daiichi nuclear power plant accident: Chronological changes from 2012 to 2015

S. Tanaka[1], T. Adati[2], T. Takahashi[3] and S. Takahashi[1,3]*

[1] Graduate School of Agriculture, Kyoto University
[2] Tokyo University of Agriculture
[3] Research Reactor Institute, Kyoto University

Abstract

To understand the behavior of radiocesium after the Fukushima Daiichi nuclear power plant accident in the ecosystem, chronological changes of the radiocesium concentrations in arthropod species were investigated. From 2012 to 2015, arthropods species from different trophic levels were sampled and the air radiation dose rates at the sampling site was measured. The air radiation dose rate showed a significant and constant reduction over the 3 years at the sampling sites in Fukushima. The median radiocesium (^{134}Cs+^{137}Cs) concentration: the rice grasshopper, *Oxya yezoensis*, and the Emma field cricket, *Teleogryllus emma*, were 0.469 and 0.156 Bq/g fresh weight in 2012, respectively, and dropped continuously to 0.040 and 0.069 Bq/g in 2015. In contrast, no significant reduction in radiocesium concentration was observed in the Jorô Spider, *Nephila clavata*, in which the concentration was 0.310 Bq/g in 2012 and remained at 0.239 Bq/g in 2015.

Introduction

A large amount of radionuclides was released into the environment by the Tokyo Electric Power Company's Fukushima Daiichi nuclear power plant (FDNPP) on March 11th 2011. The radiocesium (^{134}Cs+^{137}Cs) has been concerned long-term ecological effects. In Fukushima, approximately 70% of the land is covered with forests, and most areas including farmland and residential areas are in hilly and mountainous regions (Fukushima Prefectural Government, 2010). Therefore, released radiocesium deposited mostly on these ecosystem as a fallout on the ground surfaces and forest canopies (Kato et al., 2012). Deposited radiocesium moved by the rainfall within a few months after the accident and then accumulated on soil surface including litter by ecological process. Once accumulated radiocesium on the soil surface has been decreased physical mobility with time (Nakanishi et al., 2014). These radiocesium transfer to the lower to higher trophic level organisms through the food chain (Murakami et al., 2014; Sakai et al., 2015). Therefore, to understand long-term behavior of radiocesium in the ecosystem, monitoring the ecological processes through the food chain is needed.

Arthropods have large biomass and distribution in environment. They maintain relationships between ecological processes, such as terrestrial herbivores, omnivores and carnivores, thorough the food chain. Therefore, monitoring the radiocesium in different trophic level species of arthropod lead to elucidate the long-term behavior of radiocesium in the ecosystem. In addition, there has a concern of the radiation effect on wildlife species after the FDNPP accident. Arthropods were reported the morphological abnormalities and a significant negative correlation between population density of arthropod and air radiation dose rate (Akimoto, 2014; Hiyama et al., 2012; Møller et al., 2013). To assess radiation effect on wildlife, the behavior of radiocesium through the food chain would also be provide important insight. From these perspective, the radiocesium concentrations of

---
[*] Corresponding author, E-mail: tanaka.sota.57s@st.kyoto-u.ac.jp

arthropods from three different trophic levels in hilly and mountainous area were investigated from 2012 to 2014 (Tanaka et al., 2016). This paper shows latest data in 2015 and analysed four-year chronological changes of radiocesium in arthropods from 2012 to 2015.

Materials and Methods
Sampling site
The site is 40.1km northwest from FDNPP (Fig. 1). Status of the sampling site is summarized in Table 1. The decontamination operation under the direct control of Ministry of Environment began in September 2012, and by the end of December 2014 included 14.4% of the target farmland and forest areas (Ministry of the Environment, 2014a; 2014b).

Air radiation dose rate
 The air radiation dose rate was measured at a height of 1 m above the ground surface using a NaI (TI) scintillation survey meter (Hitachi-Aloka TCS-172B). Five points of approximately 20 m intervals in distance were measured at the sampling site.

Arthropods
We collected three arthropod species at the sampling site which are the rice grasshopper, *Oxya yezoensis* Shitaki (Orthoptera: Catantopidae), the Emma field cricket, *Teleogryllus emma* (Ohmachi et Matsura) (Orthoptera: Gryllidae) and the Jorô Spider, *Nephila clavata* L. Koch (Araneae: Nephilidae). Those species are dominant in the sampling site and also common species in hilly and mountainous area in japan. All of the arthropods are univoltine species, having one generation per year. Arthropods were collected by sweep-net sampling and hand collection. Each arthropod species was collected from 20 to 200 individuals each year. Collected samples were preserved immediately in 70% ethanol at the field and refrigerated until sorted.

Radioactivity measurement
 Concentrations of radiocesium in arthropod samples were measured by gamma spectrometry using a high-purity germanium semiconductor detector (From 2012 to 2014: GC-2020, Canberra Industries. In 2015: GEM30-70, Ortec.) with a multichannel analyser for 3600 to 10800sec. When the measured values were under the detection limit, the concentration of radiocesium was regarded with equivalent to the detection limit. The detail of radioactivity measurement on arthropod described by Tanaka et al. (2016).

Statistical analyses
 For both the air radiation dose rate and the amount of radionuclides in the arthropod samples, the lower (Q_1) and higher (Q_3) quartiles and the interquartile range (IQR = $Q_3 - Q_1$) were calculated. Data points lying outside the range from ($Q_1 - 1.5 \times$ IQR) to ($Q_3 + 1.5 \times$ IQR) were identified as outliers and excluded (Tukey, 1977) (Fig. 2). Differences in the chronological change values were analyzed by a Kruskal-Wallis test using R version 2.15.3 (R core Team, 2013).

Results
Air radiation dose rate
  Air radiation dose rates from 2012 to 2015 are summarized in Table 1. In 2012, the median air radiation dose rate was measured at 3.74µSv/h with range from3.55 to 4.06µSv/h. The median air radiation dose rate showed significant and constant reductions from 3.74 to 1.35 µSv/h between 18 and 54 months (2012-2015) after the FDNPP accident (Kruskal-Wallis test: $H = 16.894$, $df = 3$, $P = 0.0007$; Fig. 3).

Chronological changes in radiocesium contamination in arthropods

The changes in radiocesium concentrations over a four-year period was investigated in samples of three arthropod species, and summarized in Table 2. In grasshoppers, the median concentration of radiocesium was significantly reduced from 0.469 to 0.040 Bq/g between 18 and 54 months after the FDNPP accident ($H = 13.746$, $df = 3$, $P = 0.003$; Fig. 4A). Field crickets also showed a significant reduction in radiocesium concentration, from 0.156 to 0.069 Bq/g ($H = 10.905$, $df = 3$, $P = 0.012$; Fig. 4B). In contrast, the median radiocesium concentration in Jorô spiders was estimated to be 0.310, 0.333, 0.204 and 0.239 Bq/g at 18, 30, 42 and 54 months after the accident; those radiocesium concentrations were not significantly differrent ($H = 3.970$, $df = 3$, $P = 0.264$; Fig. 4C). The decreasing rate of median radiocesium concentration form 18 to 54 months after accident was calculated to be 91.4%, 55.7% and 22.9% for grasshoppers, crickets and Joro spiders, respectively.
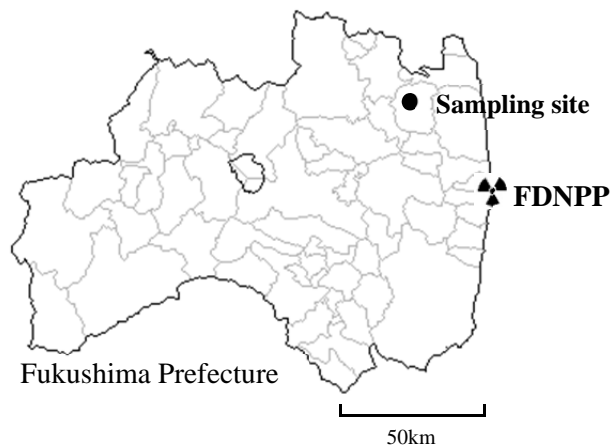
Fig. 1. The location of the sampling site and FDNPP.
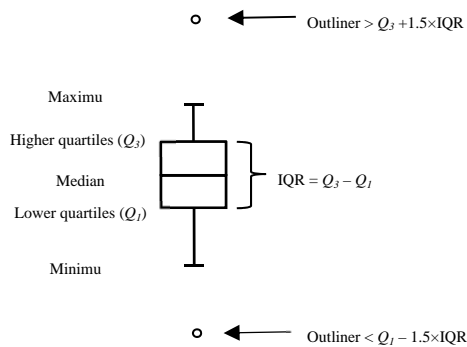
Fig. 2. Description of the box plot

Table 1 Location and status of the sampling site and air radiation dose rate at the site from 18 to 54 months (2012-2015) after the accident.

Site	Latitude, longitude and altitude	Distance from FDNPP	Description
	37°41'38" N 140°44'10" E 446 m	40.1 km	A high school campus, currently closed, equipped with sports fields, shrub gardens and experimental farms. Residents are not permitted to live in 2016.

Month after the accident	18		30		42		54	
Air radiatio dose rate (μSv/h)	n	Median (range)	N	Median (range)	N	Median (range)	n	Median (range)
	5	3.74 (3.55-4.06)	5	2.64 (2.47-2.83)	5	1.96 (1.84-2.06)	5	1.36 (1.25-1.54)

Table 2 Concentration of radiocesium in arthropods from 18 to 54 months (2012-2015) after the accident.

Month after the accident	18				30				42				54			

Concentarion of radionuclides(10^{-2} Bq/g fresh weight)

Species	No. of individuals/ sample	Radio-nuclide	n	Median (range)	No. of individuals/ sample	Radio-nuclide	N	Median (range)	No. of individuals /sample	Radio-nuclide	n	Median (range)	No. of individuals /sample	Radio-nuclide	n	Median (range)
Rice grasshopper	50	^{134}Cs	4	17.2 (14.8-9.9)	40	^{134}Cs	5	4.4 (3.9-4.8)	20	^{134}Cs	4	2.0 (1.2-2.8)[a]	20	^{134}Cs	5	1.9 (1.6-4.9)[a]
		^{137}Cs	4	29.5 (23.6-1.7)		^{137}Cs	5	10.0 (8.3-11.2)		^{137}Cs	4	5.7 (4.7-8.1)		^{137}Cs	5(1)	2.0 (1.6-2.5)[a]
		Total	**4**	**46.9 (38.4-51.3)**		**Total**	**5**	**13.9 (12.8-15.8)**		**Total**	**4(1)**	**8.0 (5.9-8.0)[a]**		**Total**	**5(1)**	**4.0 (7.1-3.3)[a]**
Emma field cricket	10	^{134}Cs	4	5.8 (5.0-6.4)	20	^{134}Cs	5	3.5 (3.0-4.8)	20	^{134}Cs	3	2.0 (1.6-4.8)	20	^{134}Cs	5(1)	1.4 (1.4-1.5)[a]
		^{137}Cs	4(1)	9.7 (9.2-16.2)		^{137}Cs	5	7.8 (6.1-10.1)		^{137}Cs	3	5.8 (3.9-6.3)		^{137}Cs	5(1)	5.4 (5.0-7.7)
		Total	**4**	**15.6 (14.1-22.6)**		**Total**	**5**	**11.3 (9.0-14.9)**		**Total**	**3**	**7.8 (5.5-11.1)**		**Total**	**5(1)**	**6.9 (6.5-9.2)[a]**
Jorô spider	20	^{134}Cs	4	12.4 (10.2-14.0)	20	^{134}Cs	5(1)	9.2 (4.6-10.4)[a]	20	^{134}Cs	3	4.9 (3.4-5.6)[a]	20	^{134}Cs	5(1)	3.5 (3.4-3.6)[a]
		^{137}Cs	4(1)	18.1 (16.9-19.4)		^{137}Cs	5	22.9 (7.4-35.1)		^{137}Cs	3	15.5 (10.3-16.7)		^{137}Cs	5	20.5 (16.3-30.2)
		Total	**4(1)**	**31.0 (28.3-31.1)**		**Total**	**5**	**33.3 (12.0-51.2)[a]**		**Total**	**3**	**20.4 (13.7-22.2)[a]**		**Total**	**5**	**23.9 (19.4-33.7)[a]**

Number in parentheses after the number of analysed samples (n) represent the number of outliners among the samples (see text).

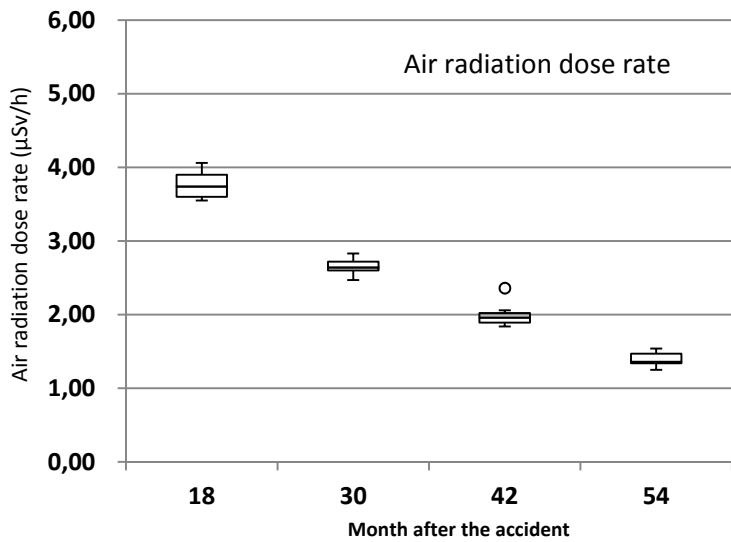[a] Data include detection limits since the measured amounts were below the limit (see text).

Fig. 3. Air radiation dose rate (µSv/h at 1m above ground), significantly differed with time after the FDNPP accident (Kruskal-Wallis test, $H = 16.894$, $df = 3$, $P = 0.0007$). Minimum and maximum dose rates are depicted by whiskers. The box signifies the upper and lower quartiles, and the median is represented by a horizontal line within the box for each year. The outlier, which is a value more than 1.5 times the interquartile range away from the top or bottom of the box, is represented by a circle.
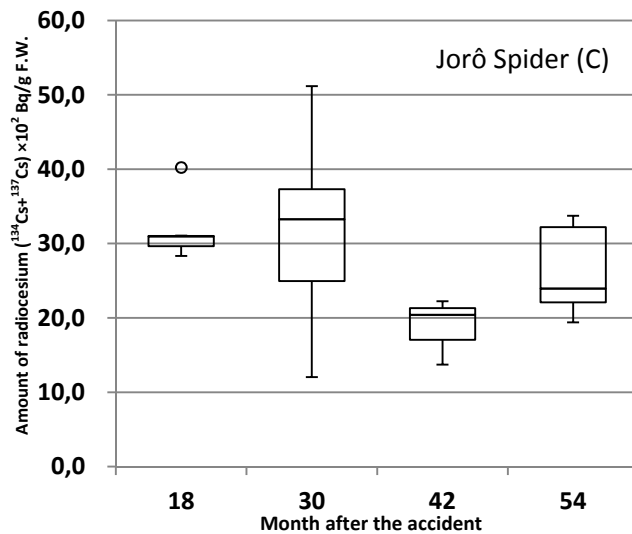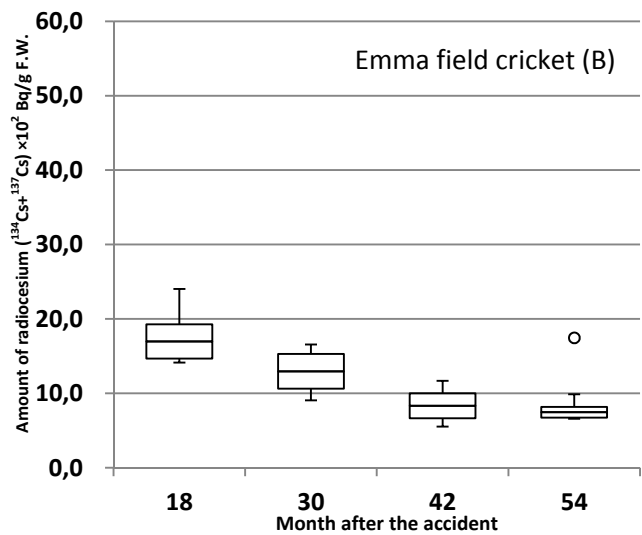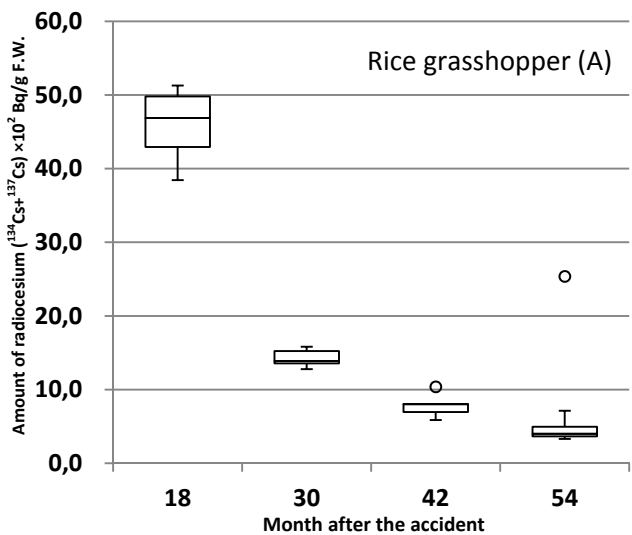
Fig. 4. Radiocesium concentration (Bq/g of fresh weight) in the rice grasshopper, *Oxya yeziebsus* (A) and the Emma field cricket, *Teleogryllus emma* (B) significantly changed over time after the FDNPP accident (A: $H = 13.746$, $df = 3$, $P = 0.003$; B: $H = 10.905$, $df = 3$, $P = 0.012$ using the Kruskal-Wallis test). However, no significant changes was observed in the Jorô spider, *Nephila clavata* (C: $H = 3.970$, $df = 3$, $P = 0.264$). Minimum and maximum concentrations are depicted by whiskers. The box signifies the upper and lower quartiles, and the median is represented by a horizontal line within the box for each year. The outlier, which is a value more than 1.5 times the interquartile range away from the top or bottom of the box, is represented by a circle.

Discussion

Four-year investigations of arthropods from different trophic levels demonstrated significant differences in the level of radiocesium contamination. The median concentrations of radiocesium in the grasshopper and field cricket showed a significant and constant reduction from 2012 to 2015. In contrast, no significant reduction of radiocesium concentration was observed in the Jorô spider. These radiocesium values include the decay of ^{134}Cs (half-life: 2.06 y). The median radiocesium in the Jorô spider showed a widely variation and 77.1% of the radiocesium still remained from 2012 to 2015. Main factor of these radiocesium values is likely due to the different food resource pathways at the respective trophic levels, such as grazing and detrital food chains (Polis and Strong, 1996). Grasshopper rely on the grazing food chain, feeding exclusively on green plants, while field cricket and spider make use of detritus food chain (ElEla et al., 2010; Shimazaki and Miyashita, 2005). Highly accumulated ^{137}Cs flows up to higher trophic levels through the detritus food chain (Murakami et al., 2014). Therefore, radiocesium in the grasshopper, herbivorous, showed rapid reduction at 91.4% from 2012 to 2015, followed by the field cricket, omnivorous, at 55.7%, and the Jorô spiders, carnivorous, no significant reduction at 22.9%. Web-making spiders such as Jorô spider, rely on prey such as saprophagous flies for their food more than herbivores, increasing the likelihood of transferring radionuclides through the detritus food chain (Rudge et al., 1993; Wood et al., 2009). Moreover, the accumulation of alkali metals in the Jorô spider is dependent on the type of prey it consumes, thus their predation is rely on the level of ^{137}Cs concentration (Ayabe et al., 2015). Therefore, higher trophic levels of the Jorô spider showed no significant reduction of radiocesium in this study period. This suggest that the dominant pathway of radiocesium in arthropods is the detritus food chain.

In 2015, however, the outliers of radiocesium concentrations were shown in the rice grasshopper (0.253 Bq/g) and field cricket (0.174 Bq/g) in Fig. 4. This has possibility that radiocesium re-transferred to the grazing food chain by the inflow of soil and organic matter with radiocesium from the surrounded high contaminated area such as mountainous forests. These factor might be caused by ecological character of hilly and mountainous area in this study site.

Conclusions

The chronological changes of radiocesium concentrations in arthropod from different trophic levels in hilly and mountainous area in Fukushima were investigated. The results showed that the radiocesium contaminations in the arthropods changed in different chronological patterns in each trophic levels. This likely caused by different food chain pathways as the grazing food chain and detritus food chain. The radiocesium in Jorô spider was no significant reduction from 2012 to 2015. This is suggested that the radiocesium transferred to higher trophic levels species through the detritus food chain in the ecosystem. Meanwhile, still high contamination were founded in 2015 at outliers of the grasshopper and field cricket, especially the grasshopper depend on the grazing food chain. This suggest that radiocesium is distributed ununiformity and re-transferred to organisms in the ecosystem such as hilly and mountainous area in Fukushima. Therefore, long-term investigation with a different trophic level species is needed to clarify the movement of radiocesium in the ecosystem. Cumulative data of these movement of radionuclides through the food chain would be lead to accurate assessment of radiation impact on non-human biota.

References

Akimoto, S., 2014. Morphological abnormalities in gall-forming aphids in a radiation-contaminated area near Fukushima Daiichi: selective impact of fallout? Ecol. Evol. 4, 355–369.

Ayabe, Y., Kanasashi, T., Hijii, N., Takenaka, C., 2015. Relationship between radiocesium contamination and the contents of various elements in the web spider Nephila clavata (Nephilidae: Arachnida). J. Environ. Radioactiv. 150, 228–235.

ElEla, S.A., ElSayed, W., Nakamura, K., 2010. Mandibular structure, gut contents analysis and feeding group of orthopteran species collected from different habitats of Satoyama area within Kanazawa City, Japan. J. Threat. Taxa 2, 849–857

Fukushima Prefectural Government, 2010. The Strategy for the Promotion of Depopulated Hilly and Mountainous Area in Fukushima Prefecture, Fukushima Prefectural Government, Fukushima.

Hiyama, A., Nohara, C., Kinjo, S., Taira, W., Gima, S., Tanahara, A., Otaki, J.M., 2012. The biological impacts of the Fukushima nuclear accident on the pale grass blue butterfly. Sci. Rep. 2, 570.

Kato, H., Onda, Y., & Gomi, T., 2012. Interception of the Fukushima reactor accident‐derived ^{137}Cs, ^{134}Cs and ^{131}I by coniferous forest canopies. Geophys. Res. Lett. 39, L20403.

Ministry of the Environment, 2014a. Progress of decontamination in the special target areas, Oct. 17, 2014. http://josen-plaza.env.go.jp/info/weekly/pdf/weekly_141017a.pdf (accessed 16.10.24).

Ministry of the Environment, 2014b. Progress of decontamination based on the special target area project, Oct. 17, 2014. http://josen-plaza.env.go.jp/info/weekly/pdf/weekly_141017c.pdf (accessed 16.10.24).

Møller, A.P., Nishiumi, I., Suzuki, H., Ueda, K., Mousseau, T.A., 2013. Differences in effects of radiation on abundance of animals in Fukushima and Chernobyl. Ecol. Indic. 24, 75–81.

Murakami, M., Ohte, N., Suzuki, T., Ishii, N., Igarashi, Y., Tanoi, K., 2014. Biological proliferation of cesium-137 through the detrital food chain in a forest ecosystem in Japan. Sci. Rep. 4, 3599.

Nakanishi, T., Matsunaga, T., Koarashi, J., Atarashi-Andoh, M. 2014. 137 Cs vertical migration in a deciduous forest soil following the Fukushima Dai-ichi Nuclear Power Plant accident. J. Environ. Radioac. 128, 9-14.

Polis, G.A., Strong, D.R., 1996. Food web complexity and community dynamics. Am. Nat. 147, 813–846.

R Core Team, 2013. R: A language and environment for statistical computing. R Foundation for Statistical Computing, Vienna. ISBN 3-900051-07-0, http://www.R-project.org (accessed 16.10.26).

Rudge, S.A., Johnson, M.S., Leah, R.T., Jones, S. R., 1993. Biological transport of radiocaesium in a semi-natural grassland ecosystem. 1. Soils, vegetation and invertebrates. J. Environ. Radioactiv. 19, 173–198.

Sakai, M., Gomi, T., Negishi, J.N., Iwamoto, A., Okada, K. 2016. Different cesium-137 transfers to forest and stream ecosystems. Environ. Pollut. 209, 46-52.

Shimazaki, A., Miyashita, T., 2005. Variable dependence on detrital and grazing food webs by generalist predators: aerial insects and web spiders. Ecography 28, 485–494.

Tanaka, S., Hatakeyama, K., Takahashi, S., Adati, T., 2016. Radioactive contamination of arthropods from different trophic levels in hilly and mountainous areas after the Fukushima Daiichi nuclear power plant accident. J. Environ. Radioact. 164, 104-112.

Wood, M. D., Leah, R. T., Jones, S. R., Copplestone, D., 2009, Radionuclide transfer to invertebrates and small mammals in a coastal sand dune ecosystem. Sci. Total Environ. 407, 4062–4074.

Measurement of environmental radioactivity using a cumulative gamma radiation dosimeter: A challenge in detecting regional characteristics of landscapes

Toshihiro Yoshihara*[1,3], Akari Kominato[3], Yuto Nagao[2], Naoki Kawachi[2], Shin-nosuke Hashida[1], Nobuo Suzui[2], Yong-Gen Yin[2], Shu Fujimaki[2]

1   Env. Sci. Lab., Central Research Institute of Electric Power Industry (CRIEPI),
1646 Abiko, Chiba, Japan; e-mail: yoshiha@criepi.denken.or.jp
2   Radiotracer Imaging Res. Project, Natl. Inst. Quantum Beam Sci. Tech. (QST),
1233 Watanuki, Takasaki, Gunma, 370-1292, Japan
3 Natl. Inst. Quantum Beam Sci. Tech. (QST), 4-9-1 Anagawa, Inage, Chiba, 263-8555, Japan
4 Dep. Biol. Sci. Tech., Grad.Schl. Ind. Sci. Tech., Tokyo Univ., Sci. (TUS),
6-3-1 Niijyuku, Katsushika, Tokyo, Japan

Abstract

A simple method of evaluating a specific environmental radioactivity was developed using a combination of personal cumulative gamma radiation dosimeter, a customized lead shield, and their holder. The customized lead shield could reduce the environmental radiation dose to approximately 56% of that measured without the shield and focused the detectable area to a circle with a radius of approximately 1 m under the dosimeter. The holder maintained the height of the dosimeter and the shield at 20 cm above the soil surface. Subsequently, a total of 12 sets of the apparatus were set up to detect landscape-dependent regional changes in environmental radioactivityfrom July 29, 2015, to March 9, 2016. The study site was located in a small forest in Abiko, Chiba, Japan (Laboratory of Environmental Science, CRIEPI), and contained a steep-walled semi-circular basin. Results demonstrated the following: 1. The method could clearly indicate specific middle- to long-term changes in radiation dose at each observation point. 2. The changes were possibly linked to an occasional event (e.g., heavy rainfall and falling leaves) at each point. Although further trials are required to establish a decisive link between events and changes in radiation dose, these trials demonstrate promise of using this method to detect changes in specific environmental radioactivity.

Introduction

The accident at the Fukushima Dai-ichi Nuclear Power Plant following the huge earthquake on March 11, 2011, dispersed radionuclides across large areas of northern Japan (Amano et al., 2012; Katata et al., 2012; Kato et al., 2012a; Gonze et al., 2014). Since then, many decontamination programs have been hurriedly implemented in both residential and agricultural areas (MOE, 2012). However, forested areas, except those in the vicinity of residential areas, have been excluded from these plans.Thus, monitoring of radionuclide deposition should be continued for prediction of the fate of these areas (Forestry Agency, 2014). The majority of current monitoring systems are based on non-invasive techniques using survey meters (MEXT, 1976, 1990). Such systems are easy to use but highly labor-intensive and not suitable to continuous stationary measurement. Additionally, invasive techniques using a Ge-semiconductor detector are common for determining radioactivity. Although such systems provide accurate data, they require physical samples for every measurement, disturbing the targeted trees and/or the environment. The cost of the measurements is also a significant problem.Thus, cheaper and more efficient alternative methods are needed.One proposed method is based on the measurement of cumulative gamma radiation doses using a recently commercialized personal dosimeter (D-shuttle, Chiyoda Technol. Corp., Japan; Fig. 1A). If the D-shuttle could separately detect radiation from a targeted object, it could be used to monitor the long-

term transition of radionuclides in the environment. Monitoring of environmental radiation using a dosimeter is an already established technology (De Planque& Gesell, 1986). For example, the dosimeter was used as a so-called "stationary monitoring post" to detect changes in dosage even before the Fukushima accident (Kitadate et al., 2014). However, although such monitoring posts can measure the entire dosage in the immediate vicinity, they cannot detect radiation from a specific object. With this in mind, Yoshihara et al. (2015) demonstrated the usefulness of such shielded measurements with a commercial dosimeter in elucidating the translocation of radionuclides from roots to the upper parts of some fruit plantlets grown in a greenhouse. Yoshihara et al. (2012) also demonstrated their usefulness in evaluating specific radiation dose from individual small section of bare ground in a baseball field.The results indicated sufficient correlation ($r^2 = 0.94$) with the surface dose measured by a GM survey meter and the radiation dose evaluated by a dosimeter.However, they also revealed a challenge in applying this method in forests with complicated landscapes because of the heterogeneous vertical dispersion of radionuclides in the soils and/or the tree canopy. Here, based on these previous results, we refined the shielded-measurement method using a high-performance dosimeter and applied it to the detection of changes in dosage over the middle to long term in a forest ecosystem.

Materials and Methods

Measurement apparatus

The measurement apparatus consisted of three parts: a recently commercialized personal dosimeter (D-shuttle, Chiyoda Technol. Corp., Japan; Fig. 1A), a customized lead shield (Fig. 1B, C), and their holder (Fig. 1D, E). The D-shuttle was outfitted to detect an energy peak of ^{137}Cs (i.e., 662 Kev) using a semi-conductor detector at very fine resolution (>0.01 μSv h^{-1}) and store the data for more than 12 months. The data were notably recorded as at least hourly cumulative doses and could be read for discretionary durations. Lead shields were 99.99% lead and were customized to cover five of six surfaces of the D-shuttle with at least 3 cm of thickness (Fig. 1B, C). Thus, each shield could theoretically blockat least 96% of unspecified radiation from the upper hemi-sphere of the D-shuttle and may have increased the detection efficiency of radiation from the soil surface of interest. In fact, the mean shielding effectwas $44 \pm 7\%$ in an open air environment in Abiko (data not shown). The exact size of the lead shield was L130 x W95 x D45 mm (outside) and L70 x W35 x D15 mm (inner pit), with a weight of 5.885 kg. The holder was made of stainless steel (Fig. 1D, E). Four legs and a box structurewere used to support the D-shuttle and shield. The legs were detachable with adjustable length to suit different soiltypes of fields, and 450-mm legs were used for the following experiments. In addition, the bottom of the holderbox had an opening to fit the size of the D-shuttle and prevent the holder from disrupting the measurements.
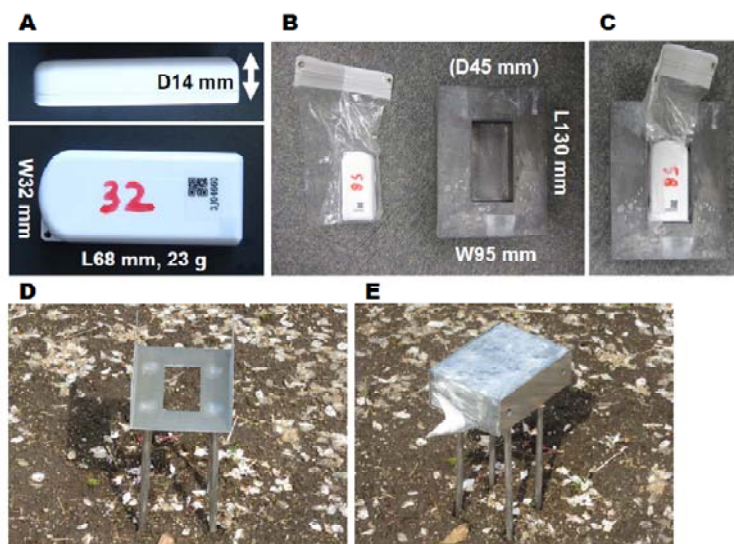

Figure 1.Measurement apparatus and settings
A) A close-up view of D-shuttle
B) A view from afar of the lead shield
C) D-shuttle set in the lead shield.
D) Aview from afar of the holder
E) D-shuttle and the lead shield were set into the holder. When the apparatus was used to measure soil contamination, the opening of the shield faced the soil and was set at a 20-cm distance from the soil surface.

Study site

The study site was in Abiko, Chiba, Japan (Laboratory of Environmental Science, CRIEPI; Fig. 2A−D). Abiko has a moderate monsoon climate. The average total annual rainfall and daily temperature between 2011 and 2016 were 1419.8 mm and 14.4 ºC, respectively (Fig. 3A, B; JMA, 2016). The basal soil type was pale Ando soil, which wascovered with an organic layer (NLA, 1983). The site was located at a steep-walled semi-circular basin in a small forest (Fig. 2C, D).
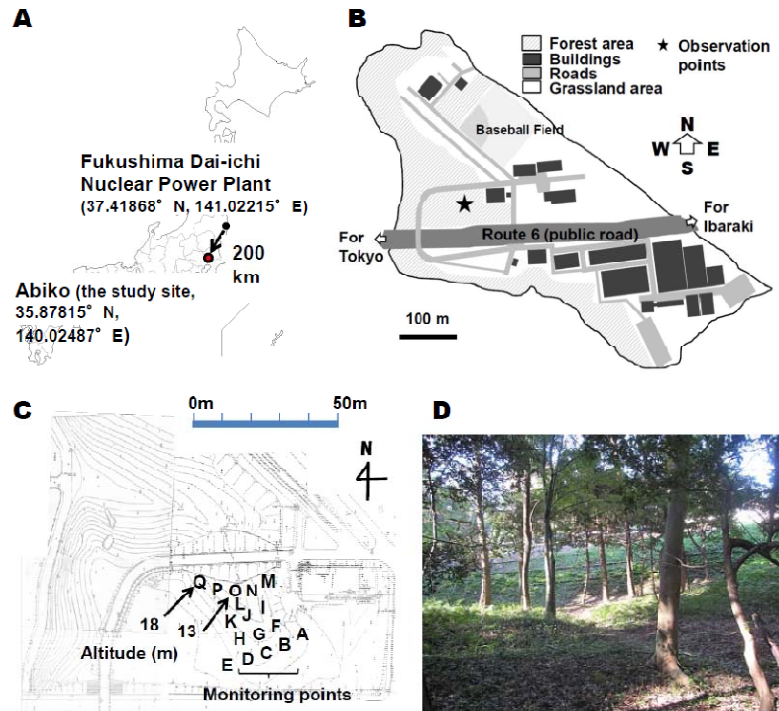
Figure 2.Study site and monitoring points.The study site was located in Abiko (35.87815ºN, 140.02487° E, Laboratory of Environmental Science, CRIEPI, with a total area of 17.3 ha), approximately 200 km SSW of the FDNPP. The majority of the fallout was observed on March 21, 2011, with rainfall. In total, 60–100 kBq m^{-2} of radiocesium (^{134}Cs, and ^{137}Cs) was recorded from Abiko following the aforementioned deposition event.
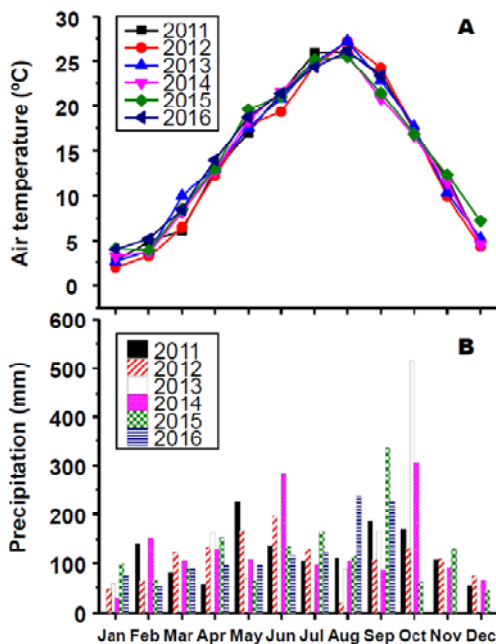
*Figure 3.Monthly air temperature andprecipitation in Abiko*
Average monthly air temperature (A) and cumulative monthly precipitation (B) in Abiko are shown by year from 2011 to 2016 (JMA, 2016). The temperatures were consistent from year to year, with the lowest temperature in January and the highest in August each year. On the other hand, the data for precipitation exhibited quite large differences among the observed years. In particular, anextraordinary amount of precipitation occurred in October in 2013.However, in general, the greatest amounts of precipitation occurred in June, September, or October, always caused by Baiu (Japanese usual rainy season) or typhoons.

Estimation of D-shuttle focus

Prior to the continuous observation of changes in specific environmental radioactivity, the focus of the D-shuttle was estimated. Normal-sized lead bricks (L200 x W100 x D50 mm) were arranged to enclose the measurement apparatus with several sizes of circles with radii of 10, 25, 50, 75, and 100 cm (Fig. 4).This was done to restrict the area of radiation emissions. Notably, this experiment was conducted on flat land in a separate forest from that in the following experiment. Observations without bricks were also conducted as controls. Results were generated as the daily dose rate (μSv d^{-1}) if otherwise no mentioned, and the averages of three independent sets of two-week-long observations were summarized as the **d**oses mainly **i**nfluenced by the **s**oils under the dosimeter against the control (DIS).

Continuous environmental measurements

From July 29, 2015, to March 9, 2016, a total of 12 sets of the D-shuttle, leadshield, and holder (Fig. 1A−E) were located on the ground in a forest in Abiko, CRIEPI (Fig. 2C; 12 points:A−E, G, J, and M−Q). The entire test site area was approximately 1000 m^2, although the actual observed areas were much smaller. Most areas of the site were covered with underbrush during summer (Fig. 2D). All sets were kept in the same position during the experimental period and continued to measure DIS. In addition, these data were compared with meteorological data (JMA, 2016) and data obtained 7.5 months after the deposition event (October 7, 2011) at similar points (Fig. 2C; 15 points, A−Q) by a similar method of observation (Yoshihara et al., 2012).
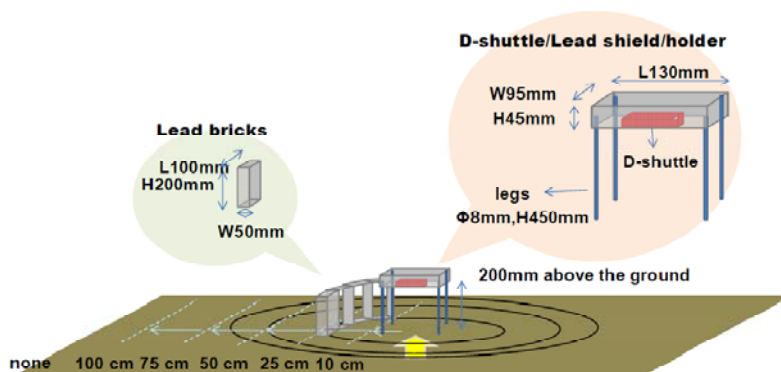

Figure 4. *A schematic for estimation of the focus of the D-shuttle*
Lead bricks were arranged to enclose the measurement apparatus by several sizesof circles.

Results and Discussion

Areas of focus of D-shuttle

DIS was estimated from doses in areas enclosed by lead bricks (Fig. 4). Generally, the doses gradually increased with expansion of the enclosed areas (Fig. 5).More specifically, the doses in circles of 0.1, 0.25, and 0.50 m in size were 1.05 ± 0.02, 1.19 ± 0.06, and $1.29 \pm 0.08\mu$Sv d^{-1}, respectively, and were significantly different from each other. However, all doses in circles of 0.5−1 m in radius were approximately 1.3 μSv d^{-1}and not significantly different from each other. On the other hand, the dose measured without bricks (i.e., control) was $1.87 \pm 0.22\mu$Sv d^{-1} and was significantly different from every dose from the tested enclosed areas. Thus, areas of the focus of D-shuttle likely primarily comprised the soils just under the D-shuttle. The ratio of DIS from the1-m-radius circle (= ca. 3 m^2) to that of the control (RDIS) was approximately 70%.In other words, approximately 70% of detected radioactivity by the D-shuttle was emitted from the area of 1-m circle (= ca. 3 m^2), even if the dose was measured without bricks for the circle. However, it is worth noting that the RDIS may depend on the distance of the D-shuttle from the soil surface (i.e., length
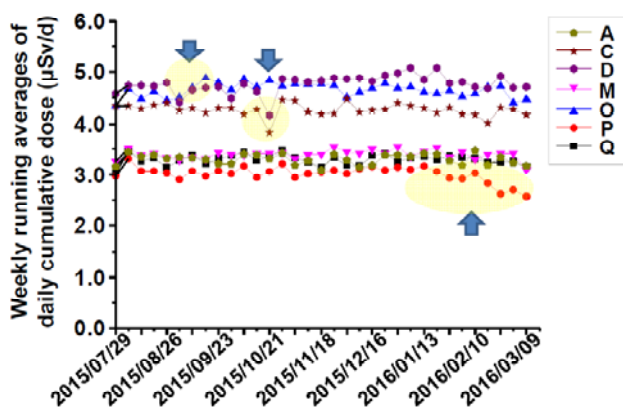
of holder legs). If the distance is greater than 20 cm, RDIS should decrease to less than 70%. In this regard, Yoshihara et al. (2012) demonstrated the usefulness of such shielded measurementsinnarrowing the target area. When the dosimeter was placed at 1-m height from the ground and put on theceiling of a lead shield box (L100 x W50 x D100 mm, inner size) in the shape of an up turned deep bowl, the target area was estimated to be 6.2 m^2.
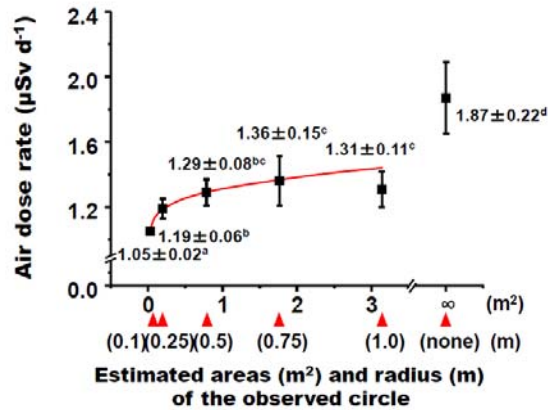
Figure 5.Areas of the focus of D-shuttle
The averages of three independent sets of two-week-long observations were summarized as the doses mainly influenced by the soils (and/orlitter)under the dosimeter against the control (DIS).Different lettersfor the standard deviations indicate significant differences (p ≤ 0.05) among data according toTukey's multiple comparison tests.

Changes in doses over the middle term

Doses werecontinuously measured at 12 observation points in a forest in Abiko (Fig. 2C;points A−E, G, J, and M−Q) from July 29, 2015, to March 9, 2016.The data were plotted as weekly running averages of daily cumulative dose (μSv d^{-1}; Fig. 6). In six of the 12 points (such as points A, M, and Q; Fig. 6), the doses changed in a comparatively stable manner in this duration. On the contrary, specific changes were observed in four of the 12 points (points C, D, O, and P; Fig. 6). More specifically, an obvious increase (approximately 0.8 μSv d^{-1}) in the dose was observed in points O at the beginning of September 2015, whereas two distinct patterns of decrease in dose were observed in points C and D in the middle of October 2015 (totalling approximately 1.3 μSv d^{-1}) and in point P between early January and the beginning of March 2016 (totalling approximately 0.8 μSv d^{-1}).As shown in Fig. 6, decreasing patterns in points C and D were somewhat temporal and levels rebounded quickly, while the pattern in point P was gradual and continuous over a longer duration.


Figure 6.Changes in doses observed between from July 29, 2015, to March 9, 2016
Results from seven (i.e., comparatively stable points A, M, and Q and obviously changed points C, D, O, and P) of the 12 observed points are shown as the weekly running average of daily cumulative dose (μSvd^{-1}). The arrows point to the obvious changes in C, D, O, and P.

Figure 7.Possible correlation between changes in dose and precipitation
Results at observation point O are shown with the data on precipitation. The dose is indicated as daily cumulative dose (μSvd^{-1}).The arrows point to obvious changes in point O with the extraordinarily heavy rain from the typhoon No. 18, 2015 (Etau; JMA, 2016).
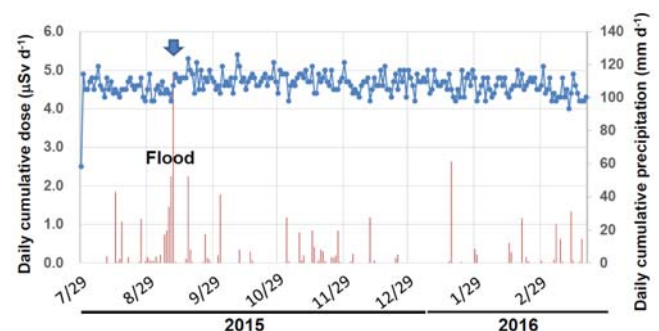
It is possible that a specific event (e.g., heavy rainfall) occurred in this period and influenced the dose. In fact, point O was located in the bottom of the basin, collecting runoff containing soil and/or organic particles, which would have been rich in radiocesium (Kato et al., 2012b; Nagao et al., 2013). In addition, a possible correlation was found between precipitation and dose at point O (Fig. 7).In the case of point P, a mechanical malfunction of the D-shuttle and/or unknown natural processes possibly induced the slow decrease. It is also noteworthy that the D-shuttles at points B and N were submerged and could not read out the data. Rain water seeping into the D-shuttle could have caused a malfunction. In addition, as a mechanical attribute of the D-shuttle, higher air temperatures decrease the detection efficiency ($\Delta 0.25\%/°C$, data not shown). If a point-specific increase in air temperature occurred, it may have reduced the reported dose. However, the decreasing of doses observed in points C and D were hard to understand. One explanation is a shielding effect of something covering the soil surface under the D-shuttle. For example, although the shielding effect of autumnal litterfall is expected to be quite low, contributing to the decrease might have been a wetted large mass of litterfall that temporarily covered the soil surface.

Changes in doses over a comparatively longer term

For investigating long-term changes in dose, the doses at the beginning (July 29, 2015) and the end (March 9, 2016) of the observation period were mapped as hourly cumulative doses in Figs.8B and C and compared with data obtained using a similar methodology at the same points on October 7, 2011 (Fig. 8A; Yoshihara et al., 2012). The data obtained at October 7, 2011, revealed a higher dose (more than 0.2 μSvh^{-1}) at point O, which was situated at the bottom of the basin. Some other points along the margin of the steepwall (i.e., points L, M, N, and P) showed a slightly higher dose (more than 0.12 μSvh^{-1}) than the other points situated on the comparatively gentle slope (i.e., points B−D and F−K; less than 0.12 μSvh^{-1}).
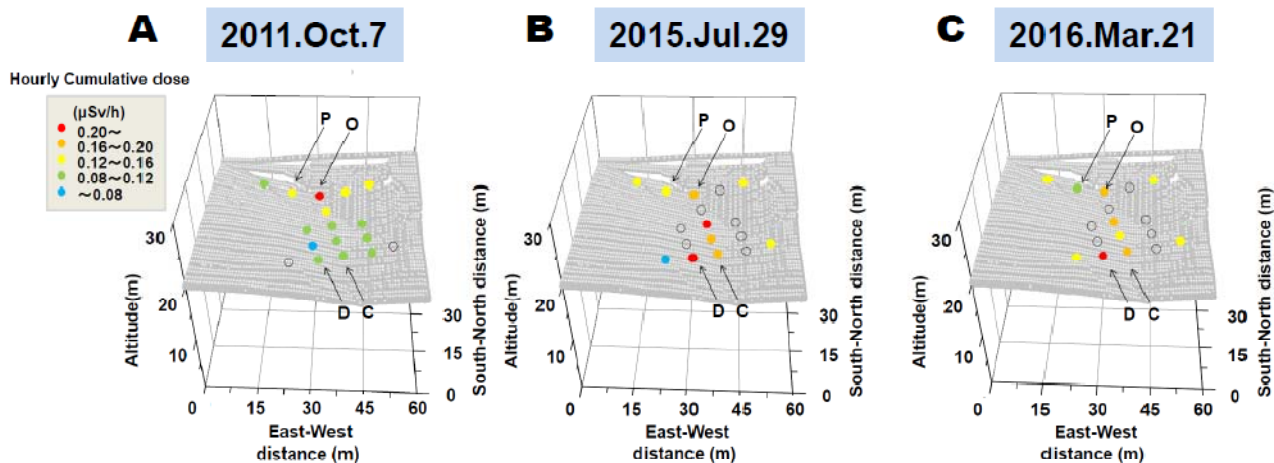
Figure 8.*Changes in doses observed onOctober 7, 2011 (A), July 29, 2015 (B),and March 9, 2016 (C) Data of July 29, 2015, and March 9, 2016, which measured in 12 of 17 points (A−E, G, J, and M−Q), and those of October 7, 2011, which measured in 15 of 17 points (A−Q; Fig. 2C), are shown as coloured circles plotted in 3D maps.Colour of the circles (Red to Blue) are indicating a visual classification of hourly cumulative doses. Non-coloured circles indicate losses of data by a mechanical malfunction or points not in measurement.*

In 2011, the majority of deposited radionuclide would have remained on the tree canopy, and comparatively less contamination was detected in the soils (Kato et al., 2013; Yoshihara et al., 2013). In addition, it is a well-known phenomenon that runoff, which contains radiocesium-rich soil and/or organic particles, accumulates at the geologically lowest point, which will therefore exhibit a higher dose (Nagao et al., 2013; Koarashi et al., 2014). Such tendencies were evident not only in our test

site as shown by the data of October 7, 2011, but also at Fukushima and other sites particularly during the so-called acute phase of deposition.On the other hand, the data of July 29, 2015,exhibited great changes from the data of October 7, 2011 (Fig. 8B). Specifically, all points exhibited greater doses (more than 0.12 μSvh^{-1}) except the point E. In addition, the contamination seemed to be dispersed. The highest dose shifted to points D and J from point O. It is also noteworthy that points D was situated at the midpoint of a gentle slope,where runoff may not have accumulated, although point J was near the geologically lowest point. It is possible that the contamination on the tree canopy dropped as throughfall and litter, remained there for a considerable period, and contributed to increasing the dose (Kato et al., 2013). In addition, as shown by Dörr and Münnich (1989), ^{137}Cs migration depends on the turnover and downward movement of soil organic material. Thus, the status of litter could also be an important factor affecting the dose. Furthermore, the data obtained after 7.5 months later (March 9, 2016) was similar for many points (Fig. 8C). However, in detail, the dose decreased at points G, J, and P but increased at point E. These data indicate that in addition to a drastic change in the acute phase of deposition, a noticeable change occurred after the acute phase and even within a half year of the observations. Such a change may have been dependent on seasonal variations. Even though a temperature-dependent mechanical attribute of the D-shuttle could affect data at each point, an overall tendency among all points would not be influenced by such an attribute. Rather, eco-physiological changes, such as vital activity of trees and microorganisms, may induce to seasonal differences (Chen et al., 1999). Further continuous observations may confirm this.

Conclusions

Measurements using a shielded D-shuttle clearly indicate specific middle- and long-term changes in radiation dose at each observation point. The changes may be linked to occasional events (e.g., heavy rainfall and falling leaves) and/or the landscape-dependent aspects of each point; however, the influence of unknown event (e.g., a mechanical malfunction of the D-shuttle and/or natural processes) also suggested. Although further trials are required to establish a decisive link between events and changes in dose, these trials showed a great potential for use of this method in monitoring the fate of radionuclides, and may contribute to the actual safety and peace of mind for the residents of disaster areas.

References

Amano H, Akiyama M, Chunlei B, Kawamura T, Kishimoto T, Kuroda T, Muroi T, Odaira T, Ohta Y, Takeda K, Watanabe Y, Morimoto T (2012) Radiation measurements in the Chiba Metropolitan Area and radiological aspects of fallout from the Fukushima Dai−ichi Nuclear Power Plants accident. J Environ Radioact 111: 42−52.

Chen J, Saunders SC, Crow TR, Naiman RJ, Brosofske KD, Mroz GD, Brookshire BL, Franklin JF (1999)Glenn D. Mroz, Brian L. Brookshire, and Jerry F. Franklin Microclimate in Forest Ecosystem and Landscape Ecology. BioScience, 49: 288−297.doi: 10.2307/1313612

De Planque G, Gesell TF (1986) Environmental Measurements with ThermoluminescenceDosemeters - Trends and Issues. RadiatProt Dosimetry, 17: 193−200.

Dörr H, Münnich KO (1989) Downward movement of soil organic matter and its influence on trace-element (^{210}Pb and ^{137}Cs) transport in the soil. RADIOCARBON, 31: 655−663.

Forestry Agency (2014) Forests/timbers and radionuclides – Revival of forests and forestry in Fukushima. https://www.pref.fukushima.lg.jp/uploaded/attachment/100065.pdf, In Japanese, Final access 2016/11/17.

Gonze M-A, Renaud P, Korsakissok I, Kato H, Hinton TG, Mourlon C, Simon-Cornu M (2014) Assessment of Dry and Wet Atmospheric Deposits of Radioactive Aerosols: Application to Fukushima Radiocaesium Fallout. Environ. Sci. Technol. 48: 11268−11276.

JMA (Japan Meteorological Agency) (2016)Tables of Monthly Climate Statistics. http://www.data.jma.go.jp/obd/stats/data/en/smp/index.html (Final access; 22 November, 2016)

Katata G, Ota M, Terada H, Chino M, Nagai H (2012) Atmospheric discharge and dispersion of radionuclides during the Fukushima Daiichi Nuclear Power Plant accident. Part I: Source term estimation and local-scale atmospheric dispersion in early phase of the accident. J Environ Radioact 109: 103−113.

Kato H, Onda T, Gomi T (2012a) Interception of the Fukushima reactor accident−derived ^{137}Cs, ^{134}Cs and ^{131}I by coniferous canopies. Geophysical Res Lett 39: L20403, doi:10.1029/2012GL052928.

Kato H, Onda Y, Teramage M. (2012b) Depth distribution of ^{137}Cs, ^{134}Cs and ^{131}I in soil profile after Fukushima Dai-ichi Nuclear Power Plant accident. J Environ Radioact, 111: 59-64.

Kato H, Onda Y (2013). Temporal changes in the transfer of accidentally released 137Cs from tree crowns to the forest floor after the Fukushima Daiichi Nuclear Power Plant accident.Prog.Nucl. Sci. Technol. 4: 18−22.

Kitadate S, Hasunuma J, Sato T, Ishida M (2014) Building of system to monitor environmental radioactivity level. Fujitsu Sci. Tech. J. 50: 52−58.

Koarashi J, Atarashi-Andoh M, Takeuchi E, Nishimura S (2014) Topographic heterogeneity effect on the accumulation of Fukushima-derived radiocesium on forest floor driven by biologically mediated processes. Sci Rep 4: 6853, DOI: 10.1038/srep06853

MEXT (Ministry of Education, Culture, Sport, Science, and technology) (1976) The manual for analysis of radiocesium, In; Issue No. 3 of a series of manuals for measurement of radiocesium concentration. pp.21−27, Japan chemical analysis center, Chiba, Japan, In Japanese.

MEXT (Ministry of Education, Culture, Sport, Science, and technology) (1990) The manual for analysis of radiocesium, In; Issue No. 20 of a series of manuals for measurement of radiocesium concentration. pp.161, Japan chemical analysis center, Chiba, Japan, In Japanese.

MOE (Ministry of the environment) (2012) Decontamination plans for forests, http://josen.env.go.jp/about/efforts/forest.html, In Japanese, Final access 2016/11/17.

Nagao S, Kanamori M, Ochiai S, Tomihara S, Fukushi K, Yamamoto M (2013) Export of 134Cs and 137Cs in the Fukushima river systems at heavy rains by Typhoon Roke in September 2011. Biogeosciences, 10: 6215–6223.

NLA (National Land Agency, Japan) (1983) Soil Map, Ryugasaki. http://dbx.cr.chiba−u.jp/ gdes/LUS/12chiba.html, In Japanese, Final access 2016/3/17.

Saito Kimiaki (2014) Mapping and modelling of radionuclide distribution on the ground due to the Fukushima accident.RadiatProt Dosimetry, 160: 283−287.doi: 10.1093/rpd/ncu011

Yoshihara T., Nagaoka T., Hashida S.-N., Wakamatsu T. 2012. Monitoring of radionuclides in the environment (Part 1); A mapping of ground surface radio contamination with measurement of a directive Gamma-ray dose rate. CRIEPI Report V11026. pp.14.

Yoshihara T, Matsumura H, Hashida S-N, Nagaoka T (2013) Radiocesium contaminations of 20 wood species and the corresponding gamma−ray dose rates around the canopies at 5 months after the Fukushima nuclear power plant accident. J Environ Radioact 115: 60−68.

Yoshihara T, Kominato A, Nagao Y, Kawachi N, Hashida S-n, Suzui N, YinY-G, FujimakiS (2015) Measurement of environmental radioactivity using a cumulative gamma radiation dosimeter; Fertilization-induced changes in young fruit trees. New challenges with new analytical technologies (Edit. A. Ioannidou and P.P. Povinec), Proc. Intl. Conf. Environ.Radioact.2015, Tessaloniki, Greecepp. 134−137.

Reconstruction of radiocesium levels in Fukushima coastal organisms: Best practice for planning emergency monitoring

Y. Tateda[1], D. Tsumune[1] and T. Aono[2]

1 Environmental Science Research laboratory, Central Research Institute of Electric Power Industry,
1646, Abiko. Chiba, Japan 270-1194
[2] National Institute for Quantum and Radiological Science and Technology,
4-9-1, Anagawa, Inage-ku, Chiba, Japan 263-8555

Abstract

The Regional Ocean Model System ROMS was used to simulate ^{137}Cs concentrations in coastal waters during March 2011 to September 2015 with the sources input from direct leaked radioactivity, atmospheric input and continuous release. For biota level, dynamic compartment model was applied using corrected seawater level by fitting simulated level to observed seawater concentration. Though the radioecological kinetic mechanism in some demersal fish and rockfish are not yet clarified, most of the biota levels were reconstructed along Pacific coastal waters of eastern Japan. The simulated levels for macro algae *Sargassum* sp. and bivalve as bio-monitor were used to examine effectiveness of emergent simulation associated with initial monitoring data. The best practice for planning emergency monitoring is proposed as associated application of model simulation and initial monitoring of bio-monitor during the initial stage of the accident of Fukushima case.

Introduction

Marine biota in coastal waters of Pacific Ocean along eastern Japan was contaminated by radiocesium ($^{134,\ 137}$Cs) which was introduced via atmospheric deposition and direct release from the accident of the Fukushima Dai-ichi Nuclear Power Plant (1FNPP) on March 2011. To clarify the radiocesium transfer and depuration mechanism in ecosystem, the concentrations in several biota at some study cites were simulated by the biological dynamic compartment model including food chain transfer using temporal seawater level simulation by Regional Ocean Model System (ROMS) (Tateda et al., 2013, 2015, 2016a, b). In these studies, fitting of simulated seawater levels to measured concentrations in seawater, e.g. deriving correction factor (CrF), was effective for reconstruction of biota level regardless of uncertainty of source used in simulation. As a result, contamination and depuration mechanism in algae, invertebrates, and fishes belong to planktonic food chain were clarified. However, the reconstructed radiocesium levels in the biota were limited to some study stations. To understand spatiotemporal contamination and depuration state in biota, reconstruction of successive temporal levels in all of the accident affected coastal area is necessary. In this study, by using approximation by CrF for all of the coastal areas along Pacific coast of eastern Japan, radiocesium levels in biota of well understood transfer mechanism were reconstructed in accident affected coastal waters. In addition, advantage of bio-monitor such as macro algae and open water mussel were examined by comparison between initial simulated levels and observed values in bio-monitor/seawater to find best practice for planning emergency environmental monitoring activity.

Materials and Methods

Simulation

The ^{137}Cs levels in seawater was simulated by ROMS using direct leakage source 3.5 PBq, atmospheric deposition 12 PBq and continuous release 0.1 PBq (Tsumune et al., 2013, Tateda et al., 2016). The ^{137}Cs levels in biota were simulated using dynamic biological compartment model (Tateda et al., 2013) during March 2011 to August 2015.

Reconstruction of biota level

Since simulated seawater levels were deficit compared to observed seawater concentrations at study sites in previous study (Tateda et al., 2016), the correction factors (CrF: (measured seawater concentration)/(simulated seawater level)) were derived for all of the coastal zone (off 10km, average water depth 30m) along the Pacific Ocean coasts in eastern Japan by least square method fitting. The corrected seawater levels (simulated levels × CrF) were used to calculate radiocesium levels in macro algae, sedentary bivalves, planktivorous fish and piscivorous fish. Total radiocesium ($^{134+137}$Cs) levels were derived by the decay correction of ^{134}Cs from initial emission at March.

Simulation for macro algae and mussels as bio-monitor

To derive good practice for planning of emergent monitoring, especially usage of bio-monitor, the radiocesium ($^{134+137}$Cs) levels in macro algae and sedentary bivalve were calculated by using emergent simulated seawater levels at initial accident phase (Tsumune et al., 2013), only by direct leakage total source 3.5 PBq as constant release (3×10^{14} Bq d^{-1}, 26/March to 6/April) and exponential decrease (to 3×10^{12} Bq d^{-1} at 25/April). To check the reality of the simulated seawater levels in seawater of 1FNPP port area by emergent model calculation, the calculated levels were compared with measured seawater concentration reported by TEPCO. In addition, to check that there was not absence of missing source in emergent simulation, calculated radiocesium levels in bio-monitor at three southern coastal study sites were compared with measured data of four macro algae species Scytosiphon, lomentarta, *Sargassum thunbergii, Sargassum muticumi, Sargassum macrocapm* and open water mussel *Septifer virgatus*,. (Tateda et al., 2016, Appendix) to derive CrFs from both of the seawater and bio-monitor.

Results and Discussion

Reconstructed radiocesium concentrations in biota

Derived CrF for seawater in Pacific coasts of eastern Japan was increased to approximately five especially in southern coastal area of 1FNPP. Using fitted CrF curve between St. 3 to St. 6, total deficit amount of ^{137}Cs were derived as unidentified source necessary to elevate simulated levels to measured levels in seawater (Fig.1). The deficit amount of additionally necessary source in coastal water was the largest at St. 4, however was decreased to both north and south, suggesting that the unknown source necessary to reproduce observed level is likely dependent to distance from 1FNPP. This result demonstrates that source uncertainty is probably in initial atmospheric deposition, being not likely from river run-off input during immediate after accident. Calculated sum of deficit inventory was 10 TBq in 200 km of whole coasts. This value (0.01 PBq) is equivalent to error 0.01 PBq of direct leakage 3.5 PBq (Tsumune et al., 2013). Therefore unidentified local source may not critical as total source introduced to ocean. However, in contrast, it was indispensable to explain level history in biota of all coastal waters. Thus correction of simulated seawater

level by using CrF is necessary to biota level reconstruction.

The $^{134+137}$Cs concentrations in macro algae, bivalve, planktivorous fish and piscivorous fish were calculated. Because of unknown mechanism of contamination and depuration of radiocesium in some demersal fish and rockfish, the biological simulations for these fish were not carried out. The spatiotemporal distribution of reconstructed radiocesium levels in macro algae at the end of March/2012 (Fig. 2 (a)), and coastal piscivorous fish at the end of August 2015 (Fig. 2 (b)) are shown. The result demonstrates that radiocesium levels in fish of this category was decreased to almost less than regulatory level for seafood safety (100 Bq kg-wet^{-1}) through almost all of the accident affected coastal area. The simulated result of coastal piscivorous fish agreed to the observed monitoring result of olive flounder *Paralichtys olivaceus* those were reported by

Figure 1. Necessary total ^{137}Cs amount at off shore water of 10km^2, to reproduce total ^{137}Cs concentration history of bio-monitor.

Japan Ministry of Agriculture, Forestry and Fishery (MAFF). The levels in biota were derived for individual those exposed to initial contamination at March/2011. Therefore the result of e.g. macro algae represents that of perennial species such as sea oak *Eisenia bicyclis*, while annual macro algae was exposed to decreased level of radiocesium in seawater after 2012 winter, resulting lower concentration of 1 Bq kg-wet^{-1} the order of magnitude (Tateda et al., 2016). Same for bivalve, planktivorous fish and piscivorous fish, thus the result in this study is for the organism exposed to initial contamination, and is consequently the maximum level for those organisms having such contamination history.

Bio-monitor simulation

Derived correction factors (CrF) by seawater and bio-monitor at three study sites of southern coast area from 1FNPP is shown in Fig.3 for each monitoring occasion. As a result, the result
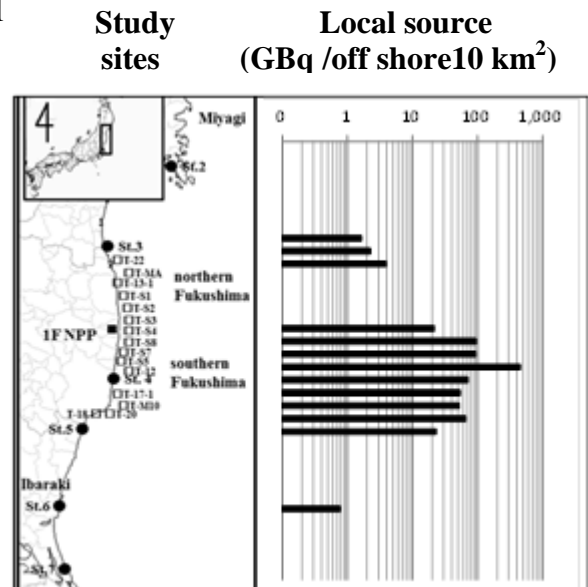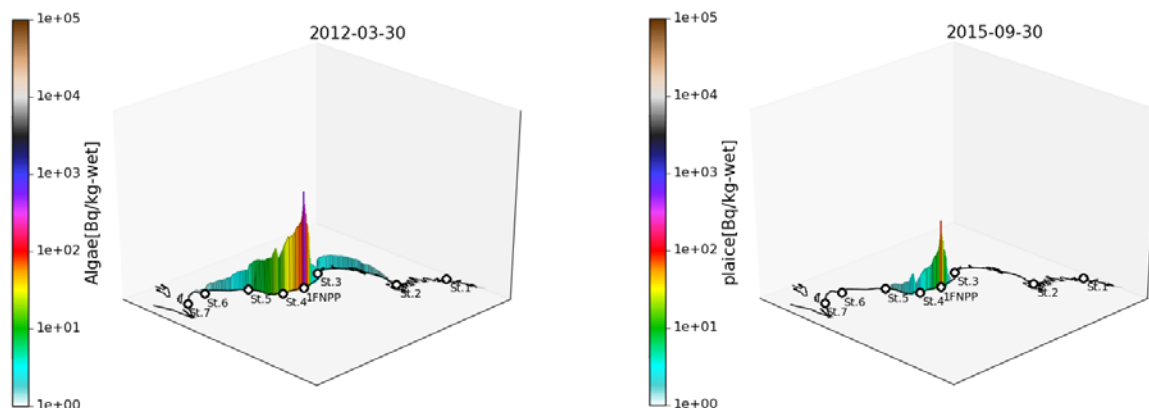

Figure 2. Spherical distribution of reconstructed $^{134+137}$Cs levels in (a) macro algae at the end of March/2012, and (b) piscivorous fish at the end of September 2015.

demonstrates that the first monitoring occasion at 7th April 2011 which 14 days after initial accidental leakage, is enough reliability for emergency use to derive spherical radiocesium seawater level by fitting methodology. In addition, the agreement between seawater derived CrF and bio-monitor derived CrF indicated that there was not missing source to be involved to determine seawater level along coastal waters. In case for preventing public access to swimming area by the threshold as 10 Bq l^{-1}, the off-limit period of swimming activity at St. 4 area can be calculated by reconstructed radiocesium time-series level in surface seawater as shown in Table 1. The information appeared by initial monitoring demonstrates 150 days, which is almost equivalent to 140 days calculated by the reconstructed seawater level time series derived by fitting simulated levels to two years monitoring result.
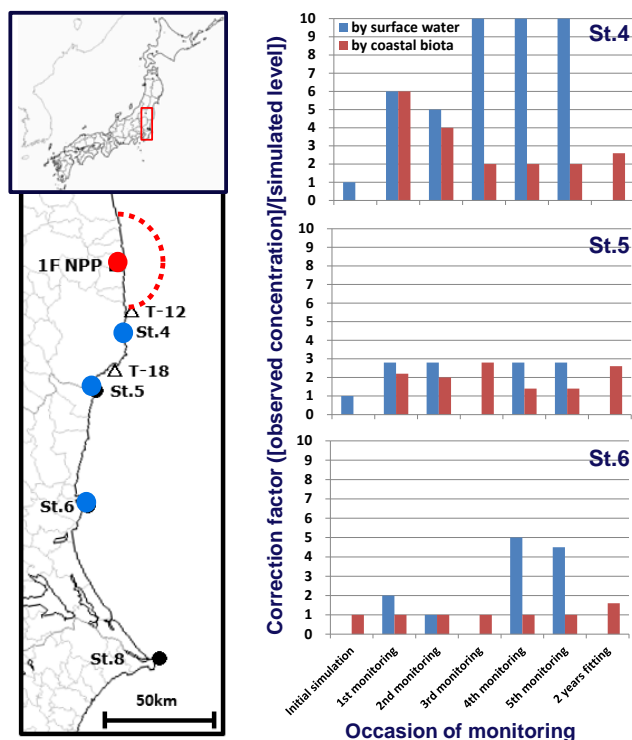
Figure 3. Correction factors derived by seawater (blue bar) and bio-monitor (red bar) in each occasion at southern coastal area (St. 4 to 6) during 7th April, 21st April, 6th May, 2nd June, 16th July 2011.

Table 1. Results for calculated off-limit period derived by the reconstructed $^{134+130}$Cs concentration in surface seawater and bio-monitor .

	Monitoring occasion	Off-limit period (days)	
		by surface water	by bio-monitor
St. 4	Initial	50	
	1st	150	150
	2nd	150	150
	3rd	260	140
	4th	260	80
	5th	260	80
	2 years fitting		140
St. 5	Initial	50	
	1st	90	50
	2nd	90	50
	3rd	90	90
	4th	90	50
	5th	90	50
	2 years fitting		80
St.6	Initial	30	
	1st	20	20
	2nd	20	20
	3rd	20	20
	4th	100	20
	5th	100	20
	2 years fitting		20

Conclusions

The radiocesium levels in coastal biota those exposed to initial contaminated seawater was reconstructed by fitting method. Approximation approach was useful to reconstruct spatiotemporal radiocesium concentrations for the organism of well-understood transfer mechanism. Confirmation by radiocesium content in bio-monitor to check missing source in seawater simulation, there was no significant additional source as total inventory. Trial examination demonstrated that initial seawater and bio-monitor monitoring associated with model simulation is effective to obtain information of spatiotemporal contamination state at initial coastal waters.

References

MAFF, 2015. Results of the Monitoring onRadioactivity Level in Fisheries Products. List of monitoring results, Cesium. Excel file. Japan Fisheries Agency. http://www.jfa.maff.go.jp/e/inspection/index.html.

Tateda, Y., Tsumune, D., Tsubono, T., 2013. Simulation of radioactive cesium transfer in the southern Fukushima coastal biota using a dynamic food chain transfer model. J. Environ. Rad. 124, 1-12.

Tateda, Y., Tsumune, D., Tsubono, T., Aono, T., Kanda, J., Ishimaru, T., 2015. Radiocesium biokinetics in olive flounder inhabiting the Fukushima accident-affected Pacific coastal waters of eastern Japan. J. Environ. Rad. 147, 130-141.

Tateda, Y., Tsumune, D., Tsubono, T. Aono, T., Kanda, J., Ishimaru, T. 2016. Status of ^{137}Cs contamination in matine biota along the Pacific coast of eastern Japan derived from a dynamic biological model two years simulation following the Fukushima accident. Journal of Environ. Rad. 151, 495-501.

Tateda, Y., Tsumune, D., Misumi, K. Aono, T., Kanda, J., Ishimaru, T. 2016. Biokinetics of radiocesium depuration in marine fish inhabiting the vicinity of the Fukushima Dai-ichi Nuclear Power Plant. Journal of Environmental radioactivity.http://dx.doi.org/10.1016/j.jenvrad.2016.02.028

TEPCO, 2015. Archive of the Result of Radioactive Substance Analyses Around the Fukushima Daiichi Nuclear Power Plant, Seawater CSV File. Tokyo Electric Power Company. http://www.tepco.co.jp/decommision/planaction/monitoring/index-j.html (in Japanese).

Tsumune, D., Tsubono, T., Aoyama, M., Uematsu, M., Misumi, K., Maeda, Y., Hayami, H., 2013. One-year, regional-scale simulation of ^{137}Cs radioactivity in the ocean following the Fukushima Dai-ichi Nuclear Power Plant accident. Biogeoscience 10, 5601e5617.

Concentration ratios of radionuclide in marine organisms around Japan

*Tatsuo Aono[*1], Miho Fukuda[1], Shinnosuke Yamazaki[1],
Yukari Ito[2], Takashi Ishimaru[2], Jota Kanda[2]*

[1]National Institute of Radiological Sciences (NIRS), National Institute for Quantum and Radiological Science and Technology(QST), Japan
[2]Tokyo University of Marine Science and Technology (TUMSAT), Japan

Abstract

The Fukushima Daiichi Nuclear Power Station (FDNPS) accident have caused environmental changes around Fukushima immediately. It is important to make the comparison between the pre-accident levels and the levels after and since the accident. This study aimed to examine the temporal and spatial variation of radionuclide activities and to discuss concentration ratio (CR) of marine organisms around Japan.

Introduction

Almost artificial radionuclides such as ^{137}Cs, ^{239}Pu and ^{240}Pu have been entered terrestrial and marine environments through radioactive fallout, and liquid and solid-state radioactive wastes before the Chernobyl and Fukushima accident, and the activity levels in marine environment were extremely lower than these in 1950-1960's. The Fukushima Daiichi Nuclear Power Station (FDNPS) accident have caused environmental changes around Fukushima immediately. Monitoring and surveying of radioactivity in seawater, sediments and organisms in the marine environment off the coast of Fukushima in the Pacific Ocean are important for understanding the dispersion and behaviour of artificial radionuclides after the FDNPS accident. The ^{137}Cs activities in seawater in the coastal area (less than the water depth of 100m) around Fukushima were gradually decreased from over 100 mBq/L to less than 10 mBq/L, although these in the offshore area were almost the same levels as before the accident (NRA, 2016; Fukuda et al., 2016). In contrast, the ^{137}Cs activities in sediment had decreased more slowly than those in seawater and have fluctuated widely around Fukushima (Fukuda et al., 2015). Furthermore, ^{134}Cs and ^{137}Cs (radioactive Cs) and ^{110m}Ag were observed in marine organisms, including not only fish and shellfish but also benthos, after this accident.This study aimed to examine the temporal and spatial variation of radionuclide activities and to discuss concentration ratio (CR) of marine organisms around Japan.

Materials and Methods

Marine samples such as seawater, sediment and organisms were collected with a plankton net, sediment sampler, and trawl during cruises of T/S Umitaka-maru, T/S Shinyo-maru, and some research and fishing vessels after this accident. Radioactive Cs in seawater were determined with the AMP/Cs method (Aoyama and Hirose, 2008) and the γ spectrometry using Ge detectors. Sediment samples were dried at 60°C, and radioactive Cs were measured with the Ge detector used for the seawater samples.In case of marine organisms, after being classified into species and weighed, each sample was dried with a vacuum drying machine, homogenized, and packed into a plastic container (U-8). Radioactivity was determined by gamma-ray spectrometry using a HP-Ge detector. The radionuclide activities of marine samples in the sampling date were calculated with the correction of

---

the decay and the coincidence-summing of ^{134}Cs. Detection limits of ^{134}Cs, ^{137}Cs, and ^{110m}Ag in marine organisms were estimated within 1 and 0.5 Bq/kg [wet weight (wet-wt)], respectively.

Results and Discussion

$^{239+240}$Pu and ^{137}Cs in marine biota before the FDNPS accident

The activities of $^{239+240}$Pu were less than the detection limit in the muscle part of many fishes, and ranged from less than 0.04 mBq/kg-wet in the enable part to 1.42 mBq/kg-wet in the bony parts of benthic fish. On the other hand, shellfish showed remarkably higher activity of $^{239+240}$Pu than fishes, 1.4 mBq/kg-wet to 21mBq/kg-wet. The activities of ^{137}Cs in fish and shellfish range from 40mBq/kg-wet to 290mBq/kg-wet. The activities of $^{239+240}$Pu and ^{137}Cs in algae ranged from 5mBq/kg-wet to 40mBq/kg-wet and from 110mBq/kg-wet to 360 mBq/kg-wet, respectively. The CR [= activity in biota (Bq/kg (wet wt)) /activity in seawater (Bq/kg or Bq/L)] is usually represented in terms of the concentration in biota relative to that of seawater for modeling purposes (IAEA, 1985). The activities of these showed great variation at the same location within one year. The pre-accident levels of ^{137}Cs activities in seawater and sediments were 1–2 mBq/L and 1 Bq/kg-dry, respectively. Based on these, the estimated CR-Cs values in fish, shellfish and algae ranged from 20 to 100, 10 to 50, 27to 120, respectively. the estimated CR-Pu in marine biota were higher than those of Cs, as the accumulation of Pu was greater than that for Cs. It seemed that the $^{239+240}$Pu and ^{137}Cs in marine biota was attributable to not only metabolism but also their food chain and habitat environment.

^{134}Cs, ^{137}Cs, ^{110m}Ag and $^{239+240}$Pu in marine biota after and since the FDNPS accident

^{134}Cs, ^{137}Cs, ^{110m}Ag and $^{239+240}$Pu were detected in fish and shellfish collected off Onahama (the southern area from FDNPS) in June and December 2011, and then ^{90}Sr were not detected in the bony part of fish and the $^{239+240}$Pu activities in visceral parts were almost same levels as before this accident. The radioactive Cs activities were less than 1 to 450mBq/kg-wet in benthos from 2011 to 2013 around Fukushima, and ^{110m}Ag were also detected in some parts of benthos. The variations of radioactive Cs activities were influenced by feeding habits and the sediment in their habitat. The estimated CR-Cs values in marine biota around Fukushima were higher than the reported values in TRS-422, and then similar to K_d-Cs value in TRS-422. It seemed that the particles such as suspend matter, settling particles and sediment led to high CRs-Cs after this accident.

Seawater and plankton net sample around off Fukushima after the FDNPS accident

The radioactive Cs monitoring in seawater and plankton net sample have been started off Fukushima in 2012. The radioactive Cs activities in seawater in the coastal area (less than the depth of 100m) were gradually decreased to less than 10 mBq/L near the coastal area, although these in the offshore area have observed the same levels as before the accident. The radioactive Cs activities were ranged from 1 Bq/kg-wet to over 100 Bq/kg-wet in the plankton net samples collected in the coastal area in autumn 2012, and these were higher than these in 2013-2016.

Estimation of concentration ratio (CR)-Cs in plankton net sample after the FDNPS accident

The apparent concentration ratios (CR)-Cs were ranged from 34 to 9,400, and their geomean was 420 (n=54). Sediment- seawater distribution coefficients K_d (L/kg) were observed to be from 1,900 to 25,000 in the same area in 2013. The estimated CR-Cs in plankton net sample in 2012-2016 was 10-70 times higher than those of plankton in 2005-2006. For CR-Cs values, it is necessary to consider the influence by the sediment and suspended particles in seawater than plankton, as plankton net samples was mixed plankton, caesium-rich particulate matter and sediment in the coastal area. It was suggested that the rapid change in radioactivity in seawater and the resuspension of particles from the sediments led to high CRs of Cs after the FDNPS accident.

Conclusions

The radioactive Cs activities in seawater and plankton net sample around off Fukushima after the FDNPS accident are gradually decreased until the background level before this accident. The estimated CR-Cs in plankton net sample and marine organisms in 2011-2016 were higher than those of plankton in 2005-2006 and marine organisms before this accident, but also similar to the K_d-Cs (IAEA, 1985).It was suggested that the particulate form Cs in marine environment, such as suspend and settling particles and sediment led to high CRs-Cs around off Fukushima after this accident.

References

Aoyama, M., Hirose, K., 2008. Radiometric determination of anthropogenic radionuclides in seawater, in: Analysis of Environmental Radionuclide, In P. P. Pavel (Ed.), Radioactivity in the Environment (pp. 137–162). Hungary: Elsevier.

Fukuda, M., Yamzaki, S., Aono, T., Yoshida, Ishimaru, T., Kanda, J., 2015. The distributions of radiocaesium in seawaters and sediments collected in the Niida River estuary, Fukushima Prefecture. Proceedings of International Symposium on Radiological Issues for Fukushima's Revitalized Future, 66–69.

Fukuda, M., Aono, T., Yamazaki, S., Nishikawa, J., Otosaka, S., Ishimaru, T., Kanda, J., 2016.Dissolved radiocaesium in seawater off the coast of Fukushima during 2013–2015. J. Radioanal. Nucl. Chem., DOI 10.1007/s10967-016-5009-9.

IAEA (1985) Sediment distribution coefficients and concentration factors for biota in the marine environment, vol. 422, Technical reports series. International Atomic Energy Agency, Vienna.

NRA (Nuclear Regulation Authority) (2016) Readings of sea area 340 monitoring. http://radioactivity.nsr.go.jp/en/list/205/list-1.html. 341 Accessed May 1 2016.

F – NORM

Identification and classification of key processes ruling environmental behaviour of radionuclides released from NORM industry

Bogusław Michalik

Silesian Centre for Environmental Radioactivity, Central Mining Institute (GIG), Katowice, Poland
e-mail: bmichalik@gig.eu

Abstract

According to the European BSS, graded system of authority control shall demonstrate that environmental criteria for long-term human health protection are met. Given the fact that all sources of radiation exposure should be fully integrated within the overall requirements this creates a specific challenge when natural radioactivity must be taken into account as a source of environmental burden. NORM activities cover broad industrial sectors of much diversified characteristics however, environmental burden imposed actually can be limited into three exposure scenarios: landfill site, discharge of liquids and stack emission that cover all NORM situations. In spite of these situations look like typical ones met in nuclear industry actually they are different in terms of appearance, which tend to have more in common with industrial waste than radioactive ones, total amount and ambient conditions when deposited at an unauthorised site. That is why methods of classical radioecology can not be applied directly to evaluate NORM impact, especially accounting that radioactive fallout is not the case here. In NORM industries the technology determines properties of residues and its way of release hence process identification must start just at a plant. Then, the crucial processes can be identified for each kind of NORM and structured assessment procedure can be developed independently on particular NORM industry. However, one should consider that a NORM site is usually contaminated by other pollutants and there is no need to evaluate radiation exposure at a site and only radionuclides migration to neighbouring areas must be assessed. For liquids radionuclides dilution or precipitation are the most important as well as deposition in case of a release from a stack. Finally, bottom sediments or soil are contaminated, usually. Then classical radioecology can move in to identify way of radionuclides migration from soil to biota. However, bearing in mind that NORM is always a suite of different elements the complexity of radionuclides speciation and fractionation is expected to be raised significantly. Moreover, considering that natural radionuclides are ubiquitous in environment, all processes identified should be categorised as leading to either accumulation or dilution when its final impact is evaluated.

Introduction

Natural radionuclides are present in natural environment since Earth has been created. Up to today natural radioactive elements were spread into all environmental compartments and they are present elsewhere. So called natural background radiation has been around since before the dawn of life on the earth and all living creatures are exposed into some amount of ionizing radiation. Hence natural radiation background usually is not considered to be harmful neither to humans nor to other organism. Therefore, from formal point of view this phenomenon is not subject to radiation protection. However, selective accumulation of radionuclides caused either by forces of nature or human activity often occurs leading to significant increase of amount of radioactive elements enclosed in some materials present in human neighbourhoods.

I such cases exposure to radiation can reach the level that cannot be neglected form radiation protection point of view. When consider physical properties of ionizing radiation and possible effect on biota there are no matter whether radionuclides present had resulted from human activity or they have entirely natural origin. Ionizing radiation always has the same properties and expected results do not depend on its source nature. This was reflected in the European BSS [1] requiring that protection against natural radiation sources, rather than being addressed separately in a specific title, should be fully integrated within the overall system of radiation protection. Special attention is paid to industries processing materials containing naturally-occurring radionuclides. Evidently, industries processing naturally occurring radioactive material extracted from the earth's crust mainly subject workers to increased exposure and this situation is usually accounted as planned exposure. However, if material is released into the environment, members of the public as well as non-human biota can be also exposed to enhanced level of radiation. According to the European BSS, graded system of authority control shall demonstrate that environmental criteria for long-term human health protection are met. Given the fact that naturally occurring radioactive materials usually occur in huge amount and industrial activities of concern cover broad sectors of much diversified characteristics this creates a specific challenge when natural radioactivity must be taken into account as a source of environmental burden. Therefore, developing of sufficient understanding of industrial processes either processing materials with enhanced natural radioactivity or leading to its concentration is expected by industry operators as well as authorities. To do this, one has to define basic terms reflecting possible exposure scenario and combine them with technological processes sequences typical for such industry involved in mineral resources exploitation, recycling and processing.

Definition of NORM vs. TENORM

In order to facilitate the development of an initial conceptual framework towards the identification a processes structure for a studied enhanced natural radioactivity-environment interaction proper definition of situations of concern must be formulated. Existing terms are rather prepared to reflect formal status of a materiel than to define real circumstances. Definition of NORM (that is usually used for description all cases of natural radioactivity occurrence) is provided by IAEA [2] as *"material designated in national law or by a regulatory body as being subject to regulatory control because of its radioactivity and containing no significant amounts of radionuclides other than naturally occurring radionuclides"* and does not give any suggestion concerning possible derived exposure scenario neither to humans nor to environment. The approach presented by EPA and relevant abbreviation TENORM (that means Technologically Enhanced Naturally Occurring Radioactive Material) that is defined as, *"naturally occurring radioactive materials that have been concentrated or exposed to the accessible environment as a result of human activities such as manufacturing, mineral extraction, or water processing"* are giving a clue where pitfalls with natural radioactivity are expected. In the contrary to IAEA definition, EPA defines NORM as *"materials which may contain any of the primordial existing from the beginning of time, naturally occurring radionuclides or radioactive elements as they occur in nature, such as radium, uranium, thorium, potassium and their radioactive decay products that are undisturbed as a result of human activities."* It is not clearly declared but this definition suggests that NORM, taking into account EPA definition, is not subject to authority control.

Apart from legal consequences and having a look at these abbreviations literal meaning both of them can be used for classification of industrial processes according to possible scenario of exposure to radiation. Namely, the term NORM should be used only towards materials with

elevated activity concentration of natural radionuclides, significantly above the average level of background, albeit not related to or caused by any type of either chemical or physical processes resulting from human activity. It has to be pointed out that NORM is treated as a component of the natural background unless they are present in the human's natural or work environment due to industrial activity. This definition limits exposure scenarios a subject to regulation to excavation, transport and storage of, usually, raw materials, where additional radiation risk is just caused by the presence of NORM with no regard what is its final form i.e. bulk, dust or effluents. Besides specific raw materials NORM e.g. uranium ore examples are radon exhaling into work places and formation water released due to mining activity.

The acronym TENORM is used for the description of any material, product, residue or waste, in which activity concentration of natural radionuclides has been altered (enhanced) as a result of technological processes involving either physical processing or chemical reactions to levels significantly above natural background. It doesn't matter if the enhancement is intentional or not, however European BSS set different legal contest for materials which natural radionuclides are processed for their radioactive, fissile or fertile properties [3]. The most important difference between NORM and TENORM from process identification point of view is that it's possible to create TENORM in processes where no NORM has been used as input materials. The crucial condition to get TENORM is significant mass reduction of either a product or residues resulting from a process in comparison to feed. One of the best examples depicting TENORM creation process is coal combustion where carbon is oxidised and all impurities enclosed in coal, including radioactivity, remain in coal combustion products (CCP). Other processes are physical (mechanical) as mineral dressing, extraction, concentration, beneficiation however, element specified chemical processes are by most efficient in natural radionuclides concentration. From radiation risk assessment point of view there is no significant difference between NORM and TENORM defined as above, however use of both terms facilitated identification of exposure situation that should subject to authority control. When initiating industry of concern identification the presence of either NORM or TENORM may be presumed at the level of every each generic process typical for mineral processing or recycling industry as:

- excavation,
- mechanical/physical treatment,
- chemical processes including combustion and metal smelting,
- transport,
- storage.

The differences between NORM and TENORM in the context of generic technological processes are depicted in fig.1. Per definitions, risk related to NORM may occur only during excavation, transport and storage. After processing raw materials may become TENORM (in case of processing NORM it is obvious) and all processes listed, besides excavation, should be considered in the context of possible radiation risk. As the properties of processed NORM are very well known people involved usually are cautioned about possible radiation risk and relevant prevention or mitigation methods are planned. To the contrary, TENORM often can be created where no NORM is used. Therefore, conditions necessary to create TENORM can be used for the preliminary selection of processes in industries not been regulated till now in term of radiation safety.
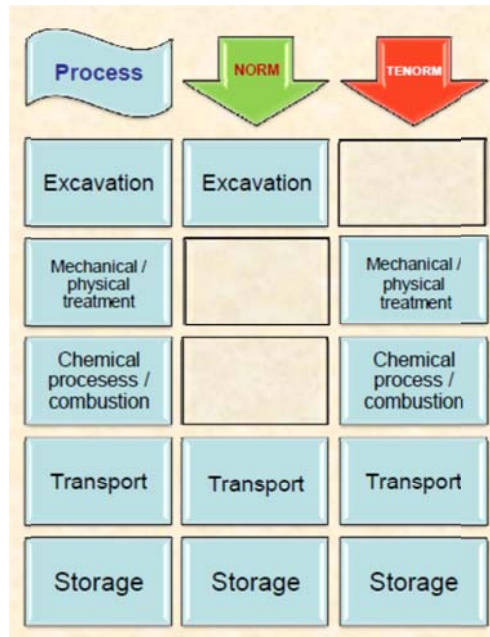
Fig.1. Main (primordial) technological processes in mining and mineral industry and possibility of NORM or TENORM presence

Identification of processes responsible for environmental burden

Releases

Experience gathered showed that NORM and TENORM, first is the source of exposure to workers involved and is observed inside borders of a plant. To assess real exposure to environment, all processes selected should be considered in the context of the release radioactive substances into environment. The sine qua non-conditions when NORM and TENORM may influence environment seriously, are:

- release of contaminated air/dust (PM).
- release of contaminated water,
- existence of enormous amount of residues or waste deposited directly into environment.

This approach limits many possible industry specific exposure scenarios to three typical situations that can be analyzed with no regard to industry type (fig. 2). Moreover, this facilitates identification process of industries (or only specific processes) that should subject to authority control in term of possible impact on environment. On the other hand, this approach also paves ground for adequate determination of authorized releases in case of already identified processes. Moreover, setting upside down it, basic knowledge about technology let one to identify processes leading to releases and then analyze them in terms of possible occurrence of either NORM or TENORM. The nature of existing releases gives also worthwhile suggestion on which radionuclide one should focus to classify them into relevant category, i.e. below or above clearance level.
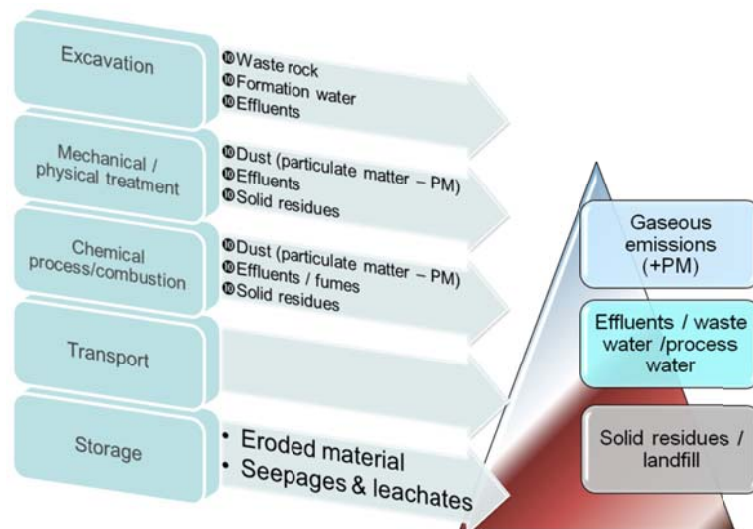
Fig.2. Generic industrial processes considered in terms of environmental burden

In majority cases of liquid and gaseous releases isotopic composition does not depend on the industry. Gaseous releases are dominated by volatile radionuclides ^{210}Pb, ^{210}Po and, radon isotopes to some extent. Liquids are mainly affected by radium isotopes presence. In case of disposal of solid waste its initial isotopic composition is specific to a technological process, however possible radionuclides suite undergone further migration is determined by their chemical properties and existing external circumstance.

Secondary processes responsible for radionuclides migration

Having identified technological processes and classified into three possible pathways of environmental exposure one can try to assess expected environmental effect with no regard to industrial process. However, three basic exposure scenarios must be analyzed in terms of secondary process determined by interaction of releases with the receiving environment. Since this moment, the term process concerns behaviour of a radionuclide in environment that is determined by its chemical properties. After release all subsequent processes first must be concerned with possible dilution or accumulation of natural radionuclides. Fumes and effluents are usually diluted and final activity concentration of natural radionuclides in receiving compartment of environment is lower than in released NORM or TENORM. This is sometimes used as a final solution for NORM or TENORM created in industries where other treatment of residues is not justified from economical and/or technical point of view, e.g. oil and gas industry, especially in case of off shore oil platforms. The opposite situation is created in case of solids residues when disposal can lead to radionuclides accumulation in a landfill site. In spite of that landfill often is concerned as justified final solution for NORM/TENORM as well. Apparently, in this case landfill site area is lost for environment however, proper construction of a landfill site can significantly limit burden of the environment in its neighbourhood. Currently, majority of industries generating NORM/TENORM finishes its activity focused on safe disposal of their residues at this level.

With no regard to kind NORM/TENORM and form of released material subsequent processes going on after primary dilution (or accumulation) should be considered to provide evidence that really environment is protected in the proper way. Keeping in the mind that NORM/TENORM usually contains a suite of natural radionuclides being different elements and subject to sequence decay, complexity of possible exposure situation may build up significantly. Moreover interaction with biota and human activity not related to the previous

industrial activity creates a number of additional processes influencing radionuclides migration in abiotic environment that are frequently element specific and determined by existing external circumstances. However, given that the environmental effect at the level of abiotic environment is usually assessed based on observed final activity concentration of a radionuclide the whole sequence of processes after release should be considered from dilution – accumulation balance point of view (Fig. 3.)
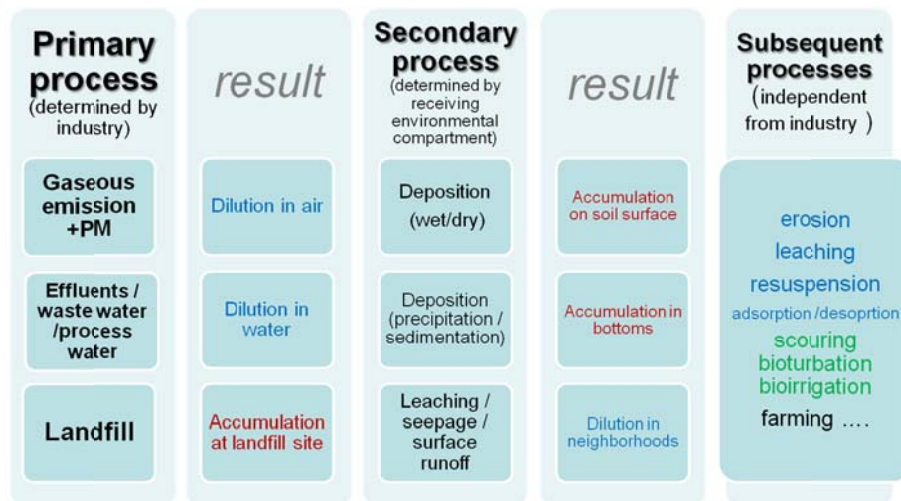

Fiure 3. Possible sequence of processes ruling radionuclide behaviour after release into environment.

Interaction with biota and migration in an ecosystem

Altered distribution of radionuclides concentration in environmental media influences exposure to external radiation scenario and, may be used as a measure of environmental effects, to some extent. However, migration into living matter as a primary source of internal exposure is usually crucial, taking into consideration that natural radionuclides are alpha emitters frequently, at least. Living organism acquires matter and energy from the external environment and converts it into different forms constituting its body. That is why identification of processes responsible for radionuclides transfer from biotope to biocenosis is crucial for proper exposure assessment. From the first point of view ingestion, inhalation and interception are the generic processes leading to accumulation of radionuclides in biota. However, looking into processes going on in an ecosystem (no matter what is its scale) it is easy to notice that actual migration from abiotic environment into biota is just going on at the level of the primary production controlled by photosynthesis. This fact is crucial not only for an organism (plant) that is just subject to this process but also for all other ones that are at the higher level in the trophic chain. In the contrast to direct ingestion of an abiotic matter that is only accidental, ingestion of organic one with already incorporated radionuclides is the main secondary process leading into radionuclides accumulation in biota, including humans. When radionuclides activity concentration in particular organisms occupying a trophic level are known their further migration is quite easy to be evaluated based on e.g. dietary pattern that usually is well recognized at each level of an ecosystem.

For description of soil-to-plant transfer a *transfer* or *concentration* factor (TF) is commonly used. However, it is not simple mechanistic process and, as a quantity should be rather expressed by a multivariable function instead of a simple factor such as it is usually done (except a specific case). Moreover the process that is responsible for the migration from soil to plant consists of two sub-processes that depend on different conditions/parameters and are ruled by different phenomena. The first one is migration from soil to soil solution and the

second one, is migration from soil solution to plant roots. What is going on inside a plant after that is completely another matter that is ruled by plant's metabolism. Up to now the radionuclides distribution among different plant tissues is not so important when the radiation dose is calculated (but it does not men that this information is not important). Dividing general transfer process into many sub-processes an additional advantage is created that also let one easily include in the effects analysis the presence of other than radioactive elements as a source of synergy as well as antagonism (e.g. ion competition effects). However this multiplicities number of processes subject to identification significantly and, in practice, the preliminary assessment of NORM/TENORM industry can be done based on available in literature TFs. However, reaching next level of processes influencing accumulation in biota as well as dispersion in abiotic environment but determined by an ecosystem all players' metabolism and biotope fine properties should be known to predict final radionuclide fate.

Discussion and conclusions

All deliberations presented let one to construct a structured approach to identification industries for which a possibility exists to affect natural environment in terms of radiation protection. All processes responsible for potential effect on environment can be grouped into five classes that consequently follow each other. Only two first are determined by industry, remaining are a radionuclide specific and are driven by properties of receiving environment compartment and external circumstances. Presented as inversed pyramid let one also conclude about the complexity of observed phenomena and then imagine the measure of resources necessary to monitor and control them (fig. 4.).
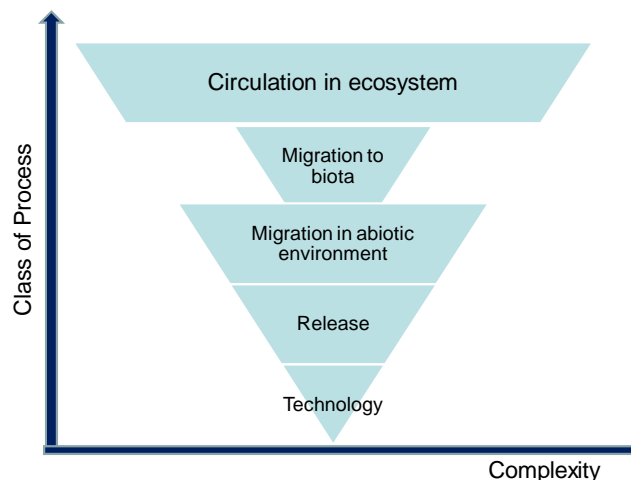

Figure. 4. Classes of processes responsible for potential effect on environment

Graded system of authority control can be applied based on identified structure of processes as well as relevant mitigation methods and necessary resources can be planed. It is clear that most efficient way to limit a potential effect on environment is to close all NORM/TENORM in the borders of a plant (or well prepared repository). This approach is commonly and successfully applied in nuclear industry. However, considering characteristic of NORM/TENORM generating industry, there is no possibility often to do this in the same way, due to total amount of NORM/TENORM, at least. Moreover, many technological processes in so called non-nuclear industry have been developed in this way that some releases are unavoidable, even BAT is applied, and accepted as the lesser from two evils, when compare with technical or chemical complications related to adequate technology improvement. Due these reason releases of NORM/TENORM are often observed. Evaluation

of potential environmental impact at this stage can be founded on clearance levels expressed as activity concentration (EU BSS). However, clearance levels are applicable only in case of solid residues and were set based on exposure to humans, not other biota. Hence, their direct use towards environment is not justified enough. Therefore, proper assessment of a NORM/TENORM generating industry in terms of environmental burden may reach level of processes ruling radionuclides migration to biota and circulation in environment. At this level processes are not only radionuclide specific but also properties of ecosystem must be considered that makes all assessments complex.

In order to facilitate the development of an initial conceptual framework towards the identification a processes structure (sequence) for a studied NORM/TENORM-environment interaction case useful tools as FEP and IM analyses already developed in the human safety assessments can be applied [4]. A FEP is defined as a feature, event, process or other factor that may be necessary to consider in the radiological risk assessment. This includes physical features, events and processes that could directly or indirectly influence the release and transport of radionuclides in the biosphere, the resultant radionuclide behaviour and subsequent radiation exposures to biota. The interaction matrix is a systematic approach that shows how FEPs are incorporated in the conceptual modelling process. The principle of IM is to represent in a square matrix the biosphere system components of interest and their interrelationships constituting the conceptual model. Visualising the main FEPs and their connections between wildlife and abiotic environment in a schematic way as done in an interaction matrix can also help with the identification of research needed to advance towards an integrated risk assessment approach and it also may improve the communication with and between stakeholders.

Discussed exposure scenarios do not contain use of NORM/TEORM product/tools, decommissioning (when demolition and land reclamation is applied) NORM/TENORM generating industry, and legacy sites. However, the use of NORM/TEORM product/tools in industry (e.g. abrasive materials or refractories) generates a stream of residues that are typical for particular process, hence can be treated as releases. Demolition and land reclamation can be treated as a separate processes and assessed according to presented scheme. Legacy site is a case of landfill site, the same approach can be applied, however lack of initial data concerning technological process (and consequently radionuclides and chemical composition) raise the evaluation to specific level of difficulty.

References

[1] Council Directive 2013/59/Euratom of 5 December 2013 laying down basic safety standards for protection against the dangers arising from exposure to ionising radiation, and repealing Directives 89/618/Euratom, 90/641/Euratom, 96/29/Euratom, 97/43/Euratom and 2003/122/Euratom
[2] IAEA Safety Glossary (version 2.0)
[3] art. 30 of Council Directive 2013/59/Euratom of 5 December 2013
[4] International Atomic Energy Agency, Safety assessment methodologies for near surface disposal facilities – Results of a co-ordinated research project, Volume 1: Review and enhancement of safety assessment approaches and tools, IAEA, Vienna, July 2004.

Environmental behavior of radionuclides from uranium mining and milling activities

F. P. Carvalho, J.M. Oliveira, M. Malta

Laboratório de Protecção e Segurança Radiológica, Instituto Superior Técnico/ Universidade de Lisboa, Estrada Nacional 10, km 139, 2695-066 Bobadela LRS, Portugal
E-mail: carvalho@itn.pt

Abstract

Uranium series radionuclides are present in waste from uranium mining and milling industries and in mine drainage, very often in high activity concentrations. When surface runoff from uranium waste piles and mine drainage are allowed to flow untreated into the environment, a significant radioactive impact will build up in the area over time. Results from research and environmental monitoring in the environment surrounding old uranium mines in Portugal showed that some radionuclides, such as [226]Ra, may be very mobile in the environment and may accumulate in soils and be transferred to horticulture products, while other radionuclides, such as [230]Th and [210]Po, are much less soluble and little accumulated by plants. A detailed report on the environmental distribution of these radionuclides in the uranium mine of Cunha Baixa is presented, including the accumulation of these radionuclides in horticulture products and farmed animals.

Keywords: uranium residues; solubility of radionuclides; accumulation in aquatic biota; soil to plant transfer.

Introduction

Uranium mining and milling was carried out in Portugal during most of the 20th century initially for radium production and later for uranium production (Carvalho 2010, 2014). After closure of the last mine in 2001, a large number of uranium legacy sites were inventoried in the Centre North of the country and the toxicological and radiological impact of abandoned waste on the environment was assessed during the years 2001-2007, leading to the approval of an environmental remediation programme currently being implemented (Carvalho 2014; EDM 2011).

As part of the environmental radioactivity assessment in the areas of old uranium mining and milling sites, several studies were carried out in the area of the Cunha-Baixa mine, near city of Mangualde, to evaluate the radioactive contamination of soils, irrigation waters, agriculture products, and animal products of this area (Carvalho et al., 2009a, 2009b; Pereira et al., 2014). This paper gives an account of the results on radionuclide concentrations and radionuclides transfer in that area.

Materials and Methods

Sampling

The old uranium mine of Cunha Baixa, that is located near the village with the same name, was exploited during about twenty years (Figure 1). The activities carried out in the mine area included ore production and ore transport to Urgeiriça facilities for uranium extraction, heap leaching of low grade ore by the mine, and in situ leaching of uranium from the rock in the underground mine. From the years of uranium production were left mining waste and milling tailings, radioactive mud from mine water treatment, and strong acidification of groundwater due to the use of sulphuric acid in in situ leaching. The mine was closed in 1986, but the acid mine water treatment plant was kept in

operation until present and modernized, while waste piles were reconfigured and the waste covered and confined on site.

In 2015 were obtained for radionuclide analyses samples of water, soils, and agriculture products from the area near the mine site and by Cunha Baixa village, as well as poultry and rabbits produced for local consumption. Similar products were sampled at a horticulture area in the same geological setting, near the city of Viseu, at a distance of 15 km from Cunha Baixa, for comparison purposes.
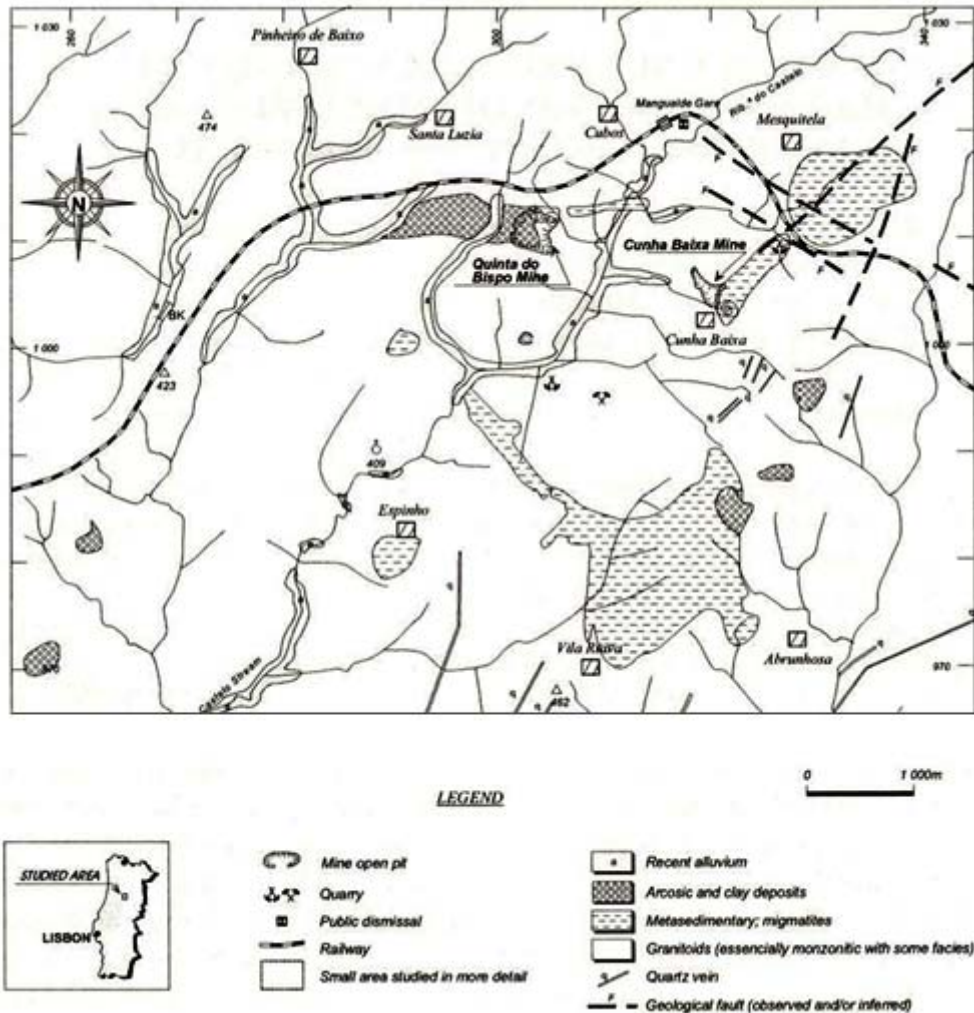
Figure 1. *Map of the area of Cunha Baixa village and uranium mine.*

Radiometric technique

Water samples were filtered, soils samples were sieved, and vegetables washed prior to analysesand as for consumption. The samples were analysed applying sampling preparation and analytical procedures currently in use in our laboratory and previously validated (Carvalho &Oliveira, 2007; Carvalho et al., 2009a, 2009b) Analytical quality of methods were tested through participation in international intercomparison analytical exercises with good results (Pham et al., 2014, 2016; Povinec et al., 2007). Radionuclides were determined by alpha spectrometry and Figure 2 shows examples of alpha spectrograms of radionuclides in environmental samples of this area.
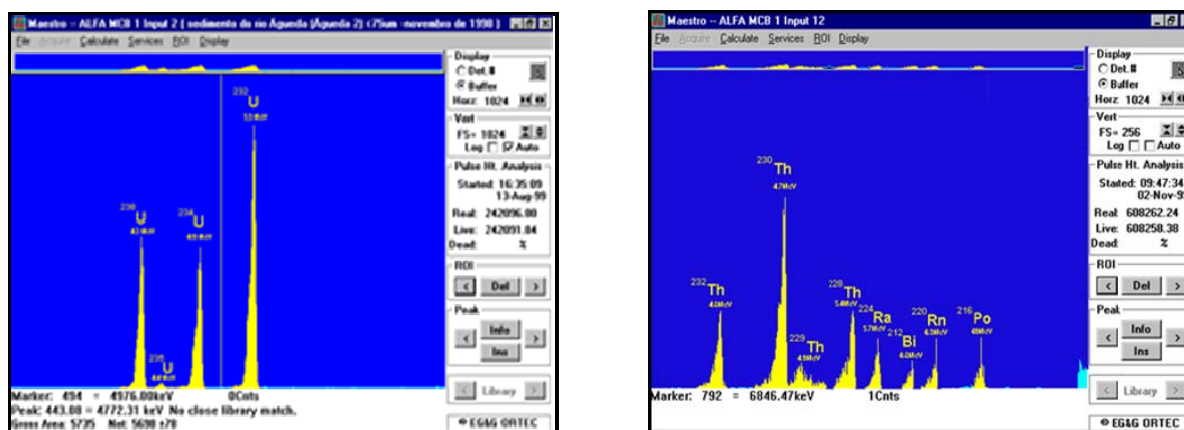
Figure 2. *Left: alpha spectrogram of uranium isotopes; Right: alpha spectrogram of thorium isotopes in environmental samples.*

Results and Discussion

Results of analyses of environmental samples and agriculture products from the Cunha Baixa area are shown in Table 1. The results of soil and well water analysis showed relatively high concentrations of uranium isotopes (^{238}U, ^{235}U, ^{234}U), plus ^{230}Th, ^{226}Ra, ^{210}Pb and ^{210}Po. In particular, the concentrations of ^{226}Ra, which exceeded those of the radium progenitors in the uranium series, i.e., ^{230}Th and ^{238}U, indicated that the agriculture soil in the area has soil radioactivity increased by adsorption and retention of ^{226}Ra and ^{210}Pb dissolved in water of the irrigation wells plus surface runoff waters. Indeed the agriculture area of Cunha Baixa village is located at lower altitude than the mine and waste heaps, and runoff and groundwater flowed into the agriculture fields over the years (Table 1; Figure 1).

Table 1 – *Radionuclide concentrations in water from an irrigation well and agriculture soil in a kitchen garden near the village and old uranium mine of Cunha-Baixa.*

Sample (Date: 2.10.2013)	^{238}U	^{234}U	^{230}Th	^{226}Ra	^{210}Pb	^{210}Po
Water, soluble phase (mBq/L)	389±15	370±14	7.2±0.4	273±11	60.5±3.4	20±1
Water, particulate phase (mBq/L)	285±8	273±7	38.1±2.1	86±6	238±13	82±4
Water, particulate phase (Bq/kg)	14401±394	13816±379	1926±106	4378±296	12027±668	4165±226
Soil, fraction <63µm (Bq/kg)	881±26	926±27	186±15	1126±115	1007±37	1007±37

The water from the garden well, used for periodic watering of vegetables, contained 389 ± 15 mBq/L of dissolved ^{238}U and 285 ± 8 mBq / L of ^{238}U in the particulate phase, and contained 273 ± 11 mBq/L and 86 ± 6 mBq/L of ^{226}Ra in the dissolved and particulate phases, respectively. Other radionuclides were present also in the water, but in lower concentrations (Table 1). The concentrations of radionuclides determined in this water (soluble phase) of the irrigation well were 5-10 times higher than other uncontaminated wells in the same region (Carvalho et al., 2005).

Vegetable products from this kitchen garden at Cunha Baixa, such as cabbages, lettuce, tomatoes, cucumbers and green beans, had concentrations of ^{226}Ra and ^{210}Pb several times higher than those of

uranium, although in the irrigation water there were higher concentrations of uranium than radium (Table 2). Concentrations of radionuclides in plants confirmed that ^{226}Ra and ^{210}Pb are generally more concentrated by plants than the U, Th, Po radionuclides (Table 2) (Carvalho et al., 2014 a,b,c; Fesenko et al., 2014). Lettuce is an exception and the higher concentration of ^{238}U and ^{230}Th in the leaves might be due to foliar deposition of radioactive dust particles.

Table 2 – *Radionuclide concentrations (mBq/kg wet weight) in horticulture products of Cunha Baixa area.*

Sample	DW/WW	^{238}U	^{234}U	^{230}Th	^{226}Ra	^{210}Pb	^{210}Po
Lettuce #10- 17.7.2013	0.072	1301±38	1277±38	1119±57	2719±141	937±16	3882±349
Onions #11- 17.7.2013	0.122	15.5±0.9	17.4±1.0	24.1±3.5	1222±92	69.2±4.7	8.68±1.35
Cabbages #8- 19.6.2013	0.126	112±6	124±6	175±14	30222±1544	603±22	540±2
Green bean #12- 17.7.2013	0.124	94.2±5.3	110±6	73.1±7.7	1593±83	244±11	5.53±0.59
Green pasture #9- 19.6.2013	0.435	88.2±5.6	104±6	97.1±11.7	9030±459	569±18	652±75
Cucumber #2-2.10.2013	0.072	6.8±0.7	8.2±0.8	2.9±0.4	376±30	38.8±2.8	25.9±2.0
Pepper #5- 2.10.2013	0.077	8.5±0.7	9.8±0.7	3.8±0.6	242±15	52.9±3.2	12.3±1.0
Tomato #1-2.10.2013	0.059	15.1±1.6	19.0±1.8	7.4±1.0	210±29	33.9±2.3	19.2±1.5

DW/WW= Dry Weight / Wet Weight ratio.

Rabbits and chicken reared in the Cunha Baixa at the family farm sampled for vegetables as reported above, displayed also enhanced concentrations of uranium series radionuclides when compared with similar species from the reference area (Tables 3). In these animals, radionuclide accumulation in internal tissues was differentiated, with generally higher concentrations in organs such as liver, bone and gonads than in muscle. For example, in the concentration of ^{238}U, ^{226}Ra and ^{210}Pb in rabbits' muscle was 33±2, 242±19, and 865±8 mBq/kg fresh weight, respectively. Concentrations of radionuclides in the tissues and internal organs of chickens grown in the same farm were also differentiated between organs. The organs with the highest activities were kidneys and liver, and the least contaminated was muscle tissue (Table 3). Radionuclide concentrations in these animals, fed with products from the local agriculture at Cunha Baixa, were also significantly higher (5-10 times) than the products from the reference area (to be reported). Significant differences in radionuclide concentrations were found also in tissues of sheep grazing around old uranium mines and sheep grazing outside mine areas (Carvalho et al, 2014 d).

Radionuclide concentrations in the soil and water of the irrigation well of the comparison family farm (for reference levels) at the city of Viseu, were much lower than those of the Cunha Baixa farm. For example, the concentrations of ^{238}U and ^{226}Ra dissolved in the water were 39 ± 1 and 88 ± 5 mBq/L, respectively,and this was an order of magnitude lower than in the water of the irrigation well at Cunha Baixa. The relative concentrations of radionuclides in Viseu's farm products also showed the preferential bioaccumulation of ^{226}Ra and ^{210}Pb in plants, well above the accumulation of U, Th, and Po, as at the Cunha Baixa site.

Table 3 – *Radionuclide concentrations (mBq/kg wet weight) in tissues of farmed animals.*

Sample (n=1)	DW/WW	^{238}U	^{235}U	^{234}U	^{230}Th	^{226}Ra	^{210}Pb	^{210}Po
Rabbit								
Kidney	0.224	42.7±3.7	2.1±1.2	45.6±3.9	-	1962±91	751±39	99±12
Liver	0.303	90.1±4.3	4.8±0.9	84.9±4.1	87.1±17.6	348±15	718±58	2178±13
Bone	0.628	186±22	10.2±9.5	86.6±13.3	410±77	93339±3443	12152±351	4225±65
Muscle	0.236	33±2	2.6±0.6	36.3±1.8	100±19	242±19	80±7	865±8
Gonad	0.287	65.3±10.5	7.1±5.2	72.4±11.8	132±43	210±26	646±85	-
Chicken								
Kidney	0.333	123±21	49.9±24.9	61.7±10.8	1542±221	82228±6378	1827±84	42322±1867
Liver	0.312	41.5±3.8	4.4±1.3	43.4±3.9	87.8±23.8	250±18	137±8	10471±1000
Bone	0.591	488±28	36.6±8.4	510±29	253±46	26333±946	11571±177	328±6
Muscle	0.267	32±2	2.1±0.8	24±2	119±24	110±12	82±8	855±85
Gonad	0.267	188±32	< 100	116±24	622±58	17972±2298	-	-

DW/WW= Dry Weight / Wet Weight ratio.

All the products of horticulture in Viseu consistently showed lower concentrations than the vegetable products of the same species from the farm by the Cunha Baixa mine area, underlining the impact of uranium mining and milling waste on the enhancement of natural radioactivity levels of this region. This has already prompted attempts to define reference levels useful to identify contaminated soils in the region of uranium mining (Caetano et al., 2014).

Conclusions

The concentrations of uranium and its decay products in horticultural productions, poultry and rabbits grown in the Cunha Baixa mine area confirmed that local families, producing under conditions similar to those described herein and consuming their products, ingested more significant activities of radionuclides of uranium series, in particular ^{226}Ra, ^{210}Pb and ^{210}Po. Enhanced dietary intake of these radionuclides may result in internal radiation doses exceeding the maximum recommended doses for members of the public.

In the previous year, it had been concluded through the analysis of family meals in the village of Cunha Baixa that the effective radiation dose through ingestion could reach 4mSv / year for some members of the population (Carvalho et al., 2014). Results reported herein confirm the significant accumulation of radionuclides in locally produced vegetables and animals. Therefore, ingestion of locally produced foods using contaminated soil and irrigation water constitutes a significant pathway of radionuclide transfer to the population.

Based on the comparative results of two family farms, one near the old uranium mine and other quite apart of mine area, the ingestion of radioactivity by a person of Cunha Baixa population consuming produces from their farm, could lead to exposure to ionizing radiation several times higher than in the members of the public in the city of Viseu.

Recent measures adopted to seal contaminated irrigation wells and to provide alternative clean water for irrigation of the agriculture farms near Cunha Baixa mine seem appropriate to reduce public exposure to radionuclides in the vicinity of old uranium mining and milling waste in the area of Cunha Baixa.

References

Caetano A. L., C. R. Marques, A. Gavina, F.P. Carvalho, F. Gonçalves, E. F. Silva, R.Pereira, 2014. Contribution for the Derivation of a Soil Screening Value (SSV) for Uranium Using a Natural Reference Soil.PLOS ONE: Volume 9 (10), 1-15 (6 October 2014, e108041).

Carvalho F. P., Oliveira J. M., 2007. Alpha emitters from uranium mining in the environment.J. Radioanal. Nucl. Ch. 274(1), 167–174.

Carvalho F. P., Oliveira J. M., Faria, I.,2009a. AlphaEmittingRadionuclides in Drainagefrom Quinta do Bispo and Cunha Baixa Uranium Mines (Portugal) and AssociatedRadiotoxicologicalRisk. Bull. Environ.Contam.Toxicol. 83, 668-673.

Carvalho, F.P, Oliveira, J.M., Malta, M., 2016. Radioactivity and Water Quality in Areas of Old Uranium Mines (Viseu, Portugal).Water Air Soil Pollut.227:252. DOI 10.1007/s11270-016-2948-2.

Carvalho, F.P, Oliveira, J.M., Malta, M., Lemos, E.,2014d. Radioanalytical assessment of environmental contamination around non-remediated uranium mining legacy site and radium mobility.J. Radioanal. Nucl. Chem. 299(1), 119-126.

Carvalho, F.P., 2010.Environmental remediation and the legacy of uranium mining waste in Portugal and Europe. Lessons to retain.Adv. Mater. Res. 107,157-161.

Carvalho, F.P., Oliveira, J.M., Libânio, A., Lopes, I., Ferrador, G., Madruga, J.M., 2005.Radioactivity in public water supplies in the uranium mining regions in Portugal. In: AIEA. Proceedings of the International Workshop on Environmental Contamination from Uranium Production Facilities and Remediation Measures, held in Lisbon 11–13 Feb 2004. Vienna, pp. 41–51.

Carvalho, F.P., Oliveira, J.M., Malta, M., 2009b. Analyses of radionuclides in soil, water and agriculture products near the Urgeiriça uranium mine in Portugal. . Radioanal. Nucl. Ch., 281, 479-484.

Carvalho, F.P., Oliveira, J.M., Malta, M., 2014a.Radioactivity in Iberian Rivers with Uranium Mining Activities in their Catchment Areas.Procedia Earth Planet. Sci. 8, 48–52.

Carvalho, F.P., Oliveira, J.M., Malta, M., 2014b. Radioactivity in Soils and Vegetables from Uranium Mining Regions.Procedia Earth Planet. Sci. 8, 38–42.

Carvalho, F.P., Oliveira, J.M., Malta, M., 2014c. Intake of Radionuclides with the Diet in Uranium Mining Areas.Procedia Earth Planet. Sci. 8, 43–47.

Carvalho, FP.,2014. The National Radioactivity Monitoring Program for the Regions of Uranium Mines and Uranium Legacy Sites in Portugal.Procedia Earth Planet. Sci. 8, 33–37.

EDM (2011).The Legacy of Abandoned Mines.Empresa de Desenvolvimento Mineiro, Lisboa, 2011. (ISBN: 978-972-95226-2-8)
http://www-pub.iaea.org/MTCD/publications/PDF/Pub1228_web.pdf

Pereira, R., Barbosa, S., Carvalho, F. P., 2014. Uranium mining in Portugal: a review of the environmental legacies of the largest mines and environmental and human health impacts. Environ.Geochem.Health 36, 285–301 (DOI 10.1007/s10653-013-9563-6).

Pham M.K., Benmansour M., Carvalho F.P., Chamizo E., Degering D., Engelerf C., et al., 2014. Certified Reference Material IAEA-446 for radionuclides in Baltic Sea seaweed.Appl. Ppl. Radiat.Isotopes 87, 468 –474. (Doi.org/10.1016/j.apradiso.2013.11.013).

Pham, M.K., VanBeek, P., Carvalho , F.P., Chamizo , E., Degering , D., Engeler, C., et al., 2016. Certified reference materials for radionuclides in Bikini Atoll sediment (IAEA-410) and Pacific Ocean sediment (IAEA-412).Appl. Radiat. Isotopes 109, 101–104.

Povinec, P.P., Pham, M., Bari-Funel, G., Bojanowski, R., Boshkova, T., Burnett, W., Carvalho, F.P. et al., 2007.Reference material for radionuclides in sediment, IAEA-384 (Fangataufa Lagoon sediment).J. Radioanal. Nucl. Ch. 273, 383–393.

Fesenko S., Carvalho, F.P., Martin, P., Moore, W.S., Yankovich, T.,2014. Radium in the environment.In: The Environmental Behaviour of Radium: Revised Edition. Technical Reports Series No. 476, pp. 33-105. International Atomic Energy Agency. Vienna.

Dispersion, Transfer and Risk of NORMandMetals due to Construction in U-bearing Minerals

L. Skipperud[*], H-C. Teien, K.E. Tollefsen,F.M. Wærsted

Center for Environmental Radioactivity (CERAD CoE), Norwegian University of Life Sciences, P.O. Box 5003, N-1432 Ås, Norway
Norwegian Institute for Water Research (NIVA), Gaustadalléen 21, N-0349 OSLO, Norway.

Abstract

Road- and tunnel construction in U-bearing minerals (alum shale) is one industrial process that has given large quantities of waste/debris containing a variety of contaminants such as NORM and metals. Impact assessment of multiple stressors has been highlighted as one of the major challenges by national and international research and regulatory communities. The work presented here focused on alum shale leaching from a road- and tunnel construction site where the bedrock is rich in U-bearing minerals, giving a high potential for environmental contamination of U alongside other metals. To assess the effects, consequences and risks to the environment associated with the intervention in alum shale and evaluate relevant measures for the protection of environment, it is important to include both Naturally Occurring Radioactive Materials (NORM) and metals in the survey program and research the effects and assess pollutants overall. Runoff of uranium and other metals are observed, even at high pH. Alum also contains a number of toxic metals, primarily cadmium, copper, nickel and zinc. Radionuclides and metals in such concentrations are potentially very harmful to aquatic and soil organisms.

Several fieldworks have been performed in the area together with a variety of exposure – effect laboratory experiments with both brown trout (*Salma trutta*) and crustaceans (Daphnia magna). Concentrations of U and other metals are varying but higher than the reference sites, and in certain cases above the threshold of regulatory concern (WHO's drinking water guideline and Environmental Quality Standards). Fractionation of the waters showed that uranium and several elements such as As, Cu, Mo, Zn, is present in the waters as low molecular forms, making these metals both potentially mobile and bioavailable. Risk assessments using the ERICA tool and cumulative risk assessment (CRA) using combined toxicity principles such as concentration addition, revealed that certain leachates can cause adverse effects in aquatic organisms in the receiving waters.

Introduction

Industrial processes involving U-bearing minerals such as alum shale, e.g. road- and tunnel construction, produce large quantities of waste that may contain a variety of contaminants such as Naturally Occurring Radioactive Material (NORM)and metals. Nationally and internationally, impact assessment of multiple stressors has been highlighted as one of the major challenges(Salbu et al. 2005).The work presented here, have been focusing on alum shale leaching from the road- and tunnel construction site in the Gran municipality on Highway Rv4 in Norway wherethe bedrock is rich in U-bearing minerals, giving a high potential for environmental contamination of U alongside other metals. In 2011, the Norwegian Pollution Control Act was amended to include naturally occurring radioactive materials (NORM) as contaminants. This amendment implicated that radioactive waste regulations were no longer exclusive to the nuclear industry, but also applied to natural radioactive material derived from non-nuclear industries.

To assess the effects, consequences and risks to the environment associated with the intervention in alum shale and evaluate relevant measures for the protection of environment, it is important to include both NORM and metals in the survey program and researching the effects and assess pollutants overall(Salbu and Skipperud 2007).

---

[*]Corresponding author, E-mail: lindis.skipperud@nmbu.no

The overall objective of the project was to consider the mobility, uptake, effects and risk of NORM and metals from alum shale, in order to predict potential environmental impact of road- and tunnel construction and the re-use of tunnel waste. This paper focus only on the exposure and risk assessment of radionuclide and metal contamination of the aquatic environment (water and aquatic organisms) from the construction of road and tunnel through U-rich alum shale minerals.

The following questions where sought to be answered:
1. What is the impact to the aquatic environment from new tunnel and road construction?
2. Is leaching from alum shale giving a multiple stressor scenario towards aquatic organisms?
3. How important is the speciation of radionuclides and metals for risk assessment?

Materials and Methods

Several fieldworks have been performed within the framework of this project. The fieldworks were performed during 2013, before the new road and tunnel construction started and in 2015 while the road and tunnel construction were ongoing. Fieldworks were performed both late spring and in autumn to count for seasonal variations.

Site description

At Gran (Hadeland), Norway the highway (Rv 4) has been rerouted and a tunnel has been built through U-rich alum shale minerals. The tunnel is situated just east of Gran and the tunnel masses enriched in U ($\geq$ 1 Bq/g) has been reused (filled in a bog) under parts of the new road at the southern entrance of the tunnel. River Vigga flows northwards on the west side of the landfill, and into Lake Jarenvannet. Several streams in the area flow into River Vigga or directly into Jarenvannet.
Sampling was performed at the following sampling points (Table 1):

Table 1. Sampling sites and expected impact from road and tunnel construction

Name/lokality	Station id	Expected impact 2013	Ecpected impact 2015
Bog/Alum shale deposit of tunnel masses	Station 1	Tunnel	Tunnel
Vigga uptsream from construction	Station 2	No impact	Road
Stream going into Vigga from construction area (Vøyenbekken)	Station 3	No impact	Road
Stream going into Vigga just before Jarenvannet	Station 4	No impact	Road
River Vigga just before running into Jarenvannet	Station 6	No impact	Road og tunnel
Stream north of Gran going directly into Jarenvannet (Nordtangen)	Station 7	No impact	Road
Jarenvannet	Station 8	No impact	Road og tunnel
Stream (Horgenbekken)going into Jarenvannet	Station 9	No impact	Road
Reference upstream Vigga	Station 10	No impact	No impact

Samples

The samples of importance for this paper, are:

<u>Water samples</u>: Total water and fractionated water. Fractionation were performed using *in situ* ultrafiltration identifying particles (> 0.45 μm), colloids (< 0.45 μm, > 10 kDa) and low molecular masses (LMM, < 10 kDa)(Salbu and Skipperud 2009; Skipperud et al. 2013).

<u>Fish</u>: *Salmo trutta* were sampled in Vigga. In Jarenvannet, *Rutilus rutilus, Perca fluviatilis and Esox lucius* were sampled. The fish was killed by a blow to the head and length, weight and dissection of organs (gills, kidney, liver, bones etc.) according to EMERGE protocol (Rosseland et al. 2001) were performed in the field.

<u>Benthos</u>: Macroinvertebrates were collected in Vigga and all streams included in the monitoring. The purpose of benthic samples were; 1) to survey the composition of the different groups and

species (preferably the larvae of mayflies (*Ephemeroptera*), caddis (*Trichoptera*) and stoneflies (*Plecoptera*)) and 2) to identify the levels of metals in benthic organisms(Engelstad 2016).

Methods
All samples were analysed using Agilent 8800 Triple Quadrupole ICP-MS to identify the levels of U, Th and different metals. Po-210 was determined in waters and fish bones using radiochemical separation and alpha-spectrometry.
Radiological risk to environmental organisms was performed using ERICA tool (http://www.erica-tool.eu/) and the cumulative risk of NORM and metals predicted by theNIVA risk assessment database (www.niva.no/radb).

Results and Discussion

Radionuclide and metal concentrations
Based on surface water samples collected on fieldwork in 2013 and 2015, the water quality at most sampling sites in the area satisfying with high pH, high Ca levels, moderate TOC and low metal concentrations. It was not possible to observe any significant increase in concentrations due to constructions work, because the seasonal variations were high. Continuous measurement of pH and conductivity gave no indication of altered water quality. The concentration of Fe, As, Co, Zn and Ni in the creek north of Gran (Station 7) are relatively high already before the tunnel work was commenced, which is likely due to impact from alum shale in the area and the old highway. Similarly results are seen for station 9 (Horgenbekken) who were only sampled in 2015, but showed the highest concentrations of uranium and other metals in this area, which indicates an influence from runoff from exposed alum shale surfaces such as road cuts, but also from fines from alum shale supplied from construction work. It is important to point out that the results of fieldworks represents a snapshot for the period, and that water quality can vary significantly throughout the year.
Concentrations of U and other metals are varying in the area but are higher in the affected area compared to the reference site, and in certain cases above the threshold of regulatory concern (WHO's drinking water guideline and Environmental Quality Standards, EQS). Examples of concentrations of radionuclides and metals in waters from the fieldwork in 2015 are given in table 2.

Speciation of radionuclides and metals
Fractionation of the waters are important to identify possibly mobile and bioavailable species of radionuclides and metals (Salbu 2009; Salbu 2015). Figure 1 presents the percentage distribution of U, Mo and Cd in the different size fractions in water from the different stations from the water sampling in 2015. Uranium and Mo are mainly present in the LMM fraction (around 90%) both in 2013 and in 2015 water samples, with small variations between stations and season. Cd varies in the different factions between stations, but are present mainly as either LMM or particulate fraction. Other element shows greater variation in speciation between stations and seasons in 2015 compared to 2013. In 2015 there is a greater colloidal transport and also more particles observed of the different elements compared to 2013 sampling.

Uptake in organisms and effects
Results from fish studies showed that there is uptake of trace metals in low concentrations in the fish where the distribution between the organs depended on trace metal and species. Uranium, Cd and Mo shows high uptake in gills, liver and kidney. For brown trout caught in Vigga is uranium concentration highest in the gills and kidney, for Cd concentration highest in kidney, while Mo concentration is highest in the liver. There is no difference in the concentration of these trace metals in fish caught in the lower part of Vigga in 2015 under ongoing road and tunnel construction, compared with fish caught in 2013, before the construction was begun.

Table 2. *Concentrations of radionuclides and metals in waters*

	Al µg/L	Ca mg/L	V µg/L	Mn µg/L	Fe mg/L	Co µg/L	Ni µg/L	Cu µg/L	Zn µg/L	As µg/L	Mo µg/L	Cd µg/L	Pb µg/L	Po-210 Bq/L	Th µg/L	U µg/L
Jun-15																
St. 2	420 ± 50	50 ± 0.9	1.2 ± 0.1	82 ± 9	0.98 ± 0.1	0.79 ± 0.1	3.9 ± 0.4	1.8 ± 0.2	9.6 ± 1	0.48 ± 0.1	1.2 ± 0.01	0.048 ± 0.005	1.6 ± 0.1	0.0022	0.046 ± 0.003	0.75 ± 0.01
St. 3	580 ± 400	49 ± 0.2	1.4 ± 1	99 ± 70	1.0 ± 0.7	0.98 ± 0.7	3.9 ± 2	5 ± 1	17 ± 6	0.47 ± 0.3	1.5 ± 0.01	0.028 ± 0.01	1.2 ± 0.8	0.0066	0.026 ± 0.01	0.75 ± 0.06
St. 4	410 ± 200	46 ± 1	1.1 ± 0.4	45 ± 20	0.52 ± 0.2	0.49 ± 0.2	2.8 ± 0.4	1.6 ± 0.3	13 ± 4	0.35 ± 0.1	1 ± 0.04	0.027 ± 0.006	0.53 ± 0.2	0.0004	0.016 ± 0.005	1.4 ± 0.01
St. 6b	96 ± 20	51 ± 1	0.32 ± 0.06	30 ± 10	0.20 ± 0.05	0.23 ± 0.08	3.1 ± 0.3	0.99 ± 0.01	11 ± 1	0.29 ± 0.02	5.8 ± 0.06	0.025 ± 0.005	0.22 ± 0.02	0.0011	0.013 ± 0.005	1.6 ± 0.03
St. 7	270 ± 40	71 ± 1	1.1 ± 0.2	1900 ± 400	1.3 ± 0.2	1.7 ± 0.2	15 ± 3	3.5 ± 1	23 ± 3	0.98 ± 0.04	5.4 ± 0.3	0.13 ± 0.009	0.67 ± 0.1	0.0033	0.028 ± 0.002	8.6 ± 0.2
St. 9	21 ± 0.7	110 ± 2	0.22 ± 0.02	110 ± 1	0.56 ± 0.02	3.1 ± 0.03	59 ± 0.5	1.1 ± 0.06	32 ± 1	0.35 ± 0.07	33 ± 0.2	0.31 ± 0.004	0.085 ± 0.008	0.0024	0.0083 ± 0.001	83 ± 1
St. 10	99 ± 30	41 ± 0.7	0.32 ± 0.08	19 ± 2	0.18 ± 0.05	0.19 ± 0.05	5.6 ± 3	5.3 ± 4	38 ± 10	0.28 ± 0.02	1.4 ± 0.08	0.049 ± 0.02	2.6 ± 2	0.0033	0.019 ± 0.006	0.61 ± 0.03
Sep-15																
St. 2	36	64	0.15	21	0.10	0.13	2.6	0.88	3.7	0.22	2.1	0.01	0.053	-0.0001	<0.016	1.1
St. 3	56	73	0.22	14	0.10	0.12	1.2	0.92	4.1	0.22	1.3	0.009	0.097	0.0002	<0.016	1.1
St. 4	41	65	0.25	16	0.078	0.12	1.4	0.88	2.2	0.21	1.5	0.012	0.053	0.0004	0.037	2.3
St. 6b	30	70	0.15	26	0.12	0.1	2.8	0.75	2.7	0.25	5.8	0.013	0.055	0.0006	<0.016	2.7
St. 7	41	110	0.29	730	0.70	0.76	5.1	1.2	3.4	0.67	6.4	0.039	0.1	0.0004	<0.016	8.5
St. 9	19	130	0.21	110	1.1	3.3	57	0.99	35	0.53	28	0.43	0.059	0.0031	0.036	92
St. 10	17	60	0.11	28	0.12	0.15	2.2	0.65	6.7	0.2	3.1	0.022	0.035	n.m.	<0.016	1

Colour coding: Blue – very good, Green – good, Yellow – less good, Orange – bad, Red – really bad. Yellow, orange and red values are all above EQS or WHOs drinking water limit.

Figure 1. *Fractionation results of U, Cd and Mo in waters in 2015.*
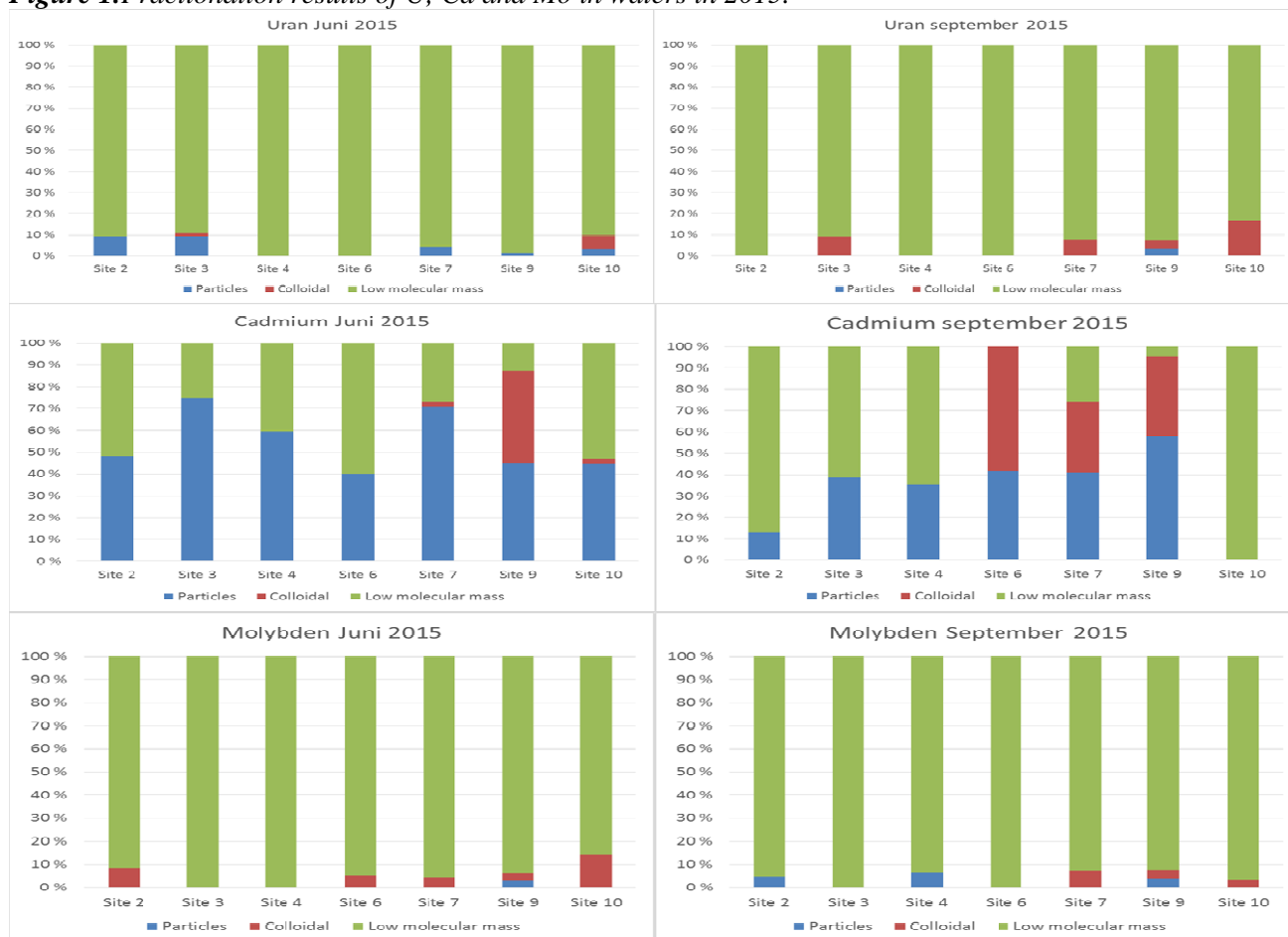
There are relatively large variations between individual fish, but there is a trend towards increased concentration of U, Cd and Mo in the kidney with increasing size of the fish. The same correlation between fish size and accumulation in gills is not found, but this is not expected as metal

accumulation on gills reflect the water quality at sampling time more than accumulation over a longer time period. For fish caught in 2015 there was a difference in gill concentration of Cd and Mo, where there was a higher concentration in the gills of fish caught downstream construction area compared with upstream reference site. This difference could be attributable to runoff of radionuclides and metals from the road and tunnel construction work.

The Po-210 concentrations (Table 3) are low, but the calculated concentration factors , Cf, are still higher than world average for freshwater fish (IAEA 2010).These higher Cf's however have been observed in other Scandinavian waters, and are mostly due to the water quality of the Nordic waters(NKS 2009). No effects were found in the fish, and this was due to good water quality, specially prevented by high pH and high levels of Ca. Had the waters been lower in pH and Ca levels, we would have expected much higher uptake of U and thereby also effects on the fish.

Table 3. Concentrations of Po-210 in fish bones and calculated concentration factors (Cf).

Fisk No	1	2	3	4	5	6	7	8	9	10	11	12	13	14
Po-210 i fiskebein (Bq/kg)	3 29	2 04	0 59	0 69	0 60	1 11	0 52	2 13	3 99	1 79	0 88	0 89	0 97	0 44
Cf	1317	817	223	275	323	445	249	852	395	703	353	355	386	175

Collection of benthos was performed in spring and autumn before and after the construction work, and the variation between seasons contributed to considerable variations. Even though, it was shown a generally lower richness and diversity of species and groups and a higher proportion of tolerant than sensitive species, i.e. lower pollution index (ASPT Index score) (Figure 2) and elevated levels of metals in mayfly during tunnel and road construction work.
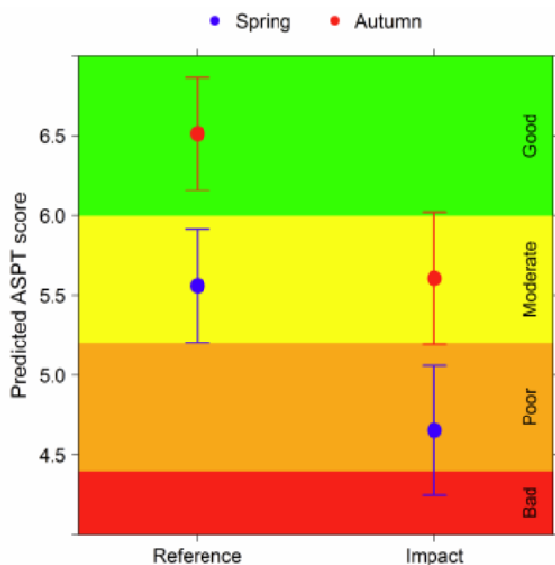
Figure 2. Predicted ASPT index score as a function of season and time (spring and autumn, before and under construction work).

Risk assessment

Radiological risks based on Erica Tool indicates that the radiological consequences are small, except in station 9 (Horgenbekken) where the level exceeds the dose rate of 10 µGy / h (screening dose rate value for the environment) (Figure 3).

Cumulative risks associated with metals (especially U, Al, Ni) varied widely between the various field stations. All stations proved to represent a risk for the three groups of species (algae, crustaceans, fish) tested (Figure 4). The differences in the risk was relatively similar for the three groups of species of station 6 (Vigga,), while the composition of the water from station 7 proved to give a higher cumulative risk to all species groups. Water from Station 9 (Horgenbekken) proved to represent high predicted risk to algae and crustaceans, and lower risk to fish. High predicted risk appears to match the observation of a possible change in species composition of the benthic community. The cumulative risk predictions represent an initial screening approach as uncertainty were potentially introduced by lack effect data for certain toxicity

endpoints. Using only the LMM concentrations, potentially representing the mobile and bioavailable fraction of NORM and metals, lead to risk identification by an exceedance factor of up to 40 for crustaceans at station 9. The use of total concentrations or colloidal fractions of NORM and metals, which is likely accounting also for non-bioavailable compounds, are likely overestimating the cumulative risk and was consequently omittedfrom the analyses.
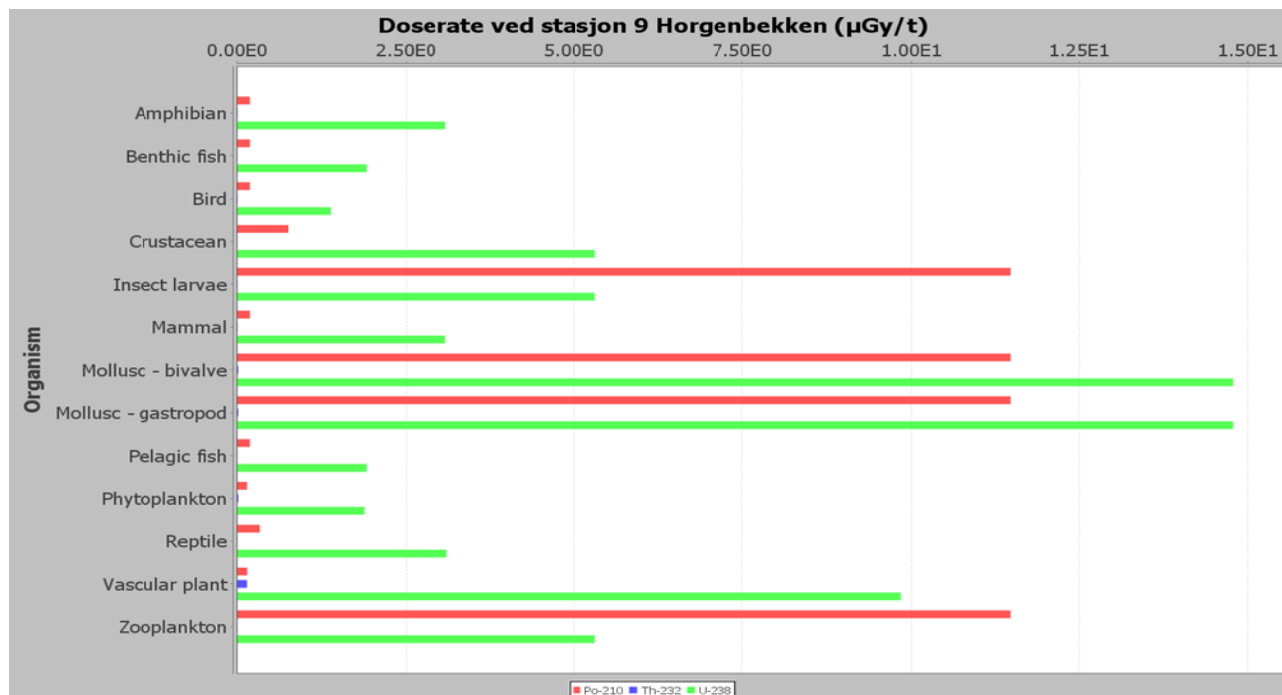

Figure 3. Predicted total dose rate (internally and externally) from NORM radionuclides using measured Po-210, U-238 and Th-232 concentrations at station 9 (Horgenbekken).

Conclusions

Due to seasonal variations, there were not observed any increase in metal or radionuclide concentrations or changes in speciation in the waters. The results shows, however, uptake of both radionuclides and metals into fish organs, especially towards gills, liver and kidney. An increase in the uptake can be seen from the fish samples taken during road and tunnel construction even though the seasonal variations is large. No effects were observed on the fish, but there is a clear effect on the benthic community in the area, and this community is significantly affected by the construction work. Therefore, the conclusion is that there is an impact on the biota of the aquatic environment because of leaching from the road and construction work.

Both ERICA and CRA showed risk towards crustaceans and the benthic community. This predicted risk includes both radiotoxicity (radionuclides) and chemical toxicity (metals) and therefore predicting a multiple stressor scenario.

When looking at the speciation of the radionuclides and metals, there are large differences in what elements that can be found in the LMM fraction – indicating the most mobile and bioavailable fractions. Comparing the risk assessment using both the results from dissolved fractions (colloidal and LMM) and the LMM fraction only, gave different results for the CRA. This indicates that it is important to take the actual radionuclide and metal species into account, when doing risk assessment. Only using total concentrations, might over overestimate the risk towards water living organisms.
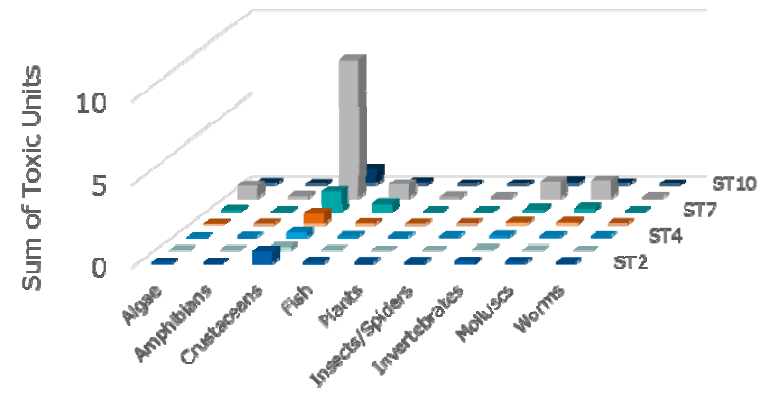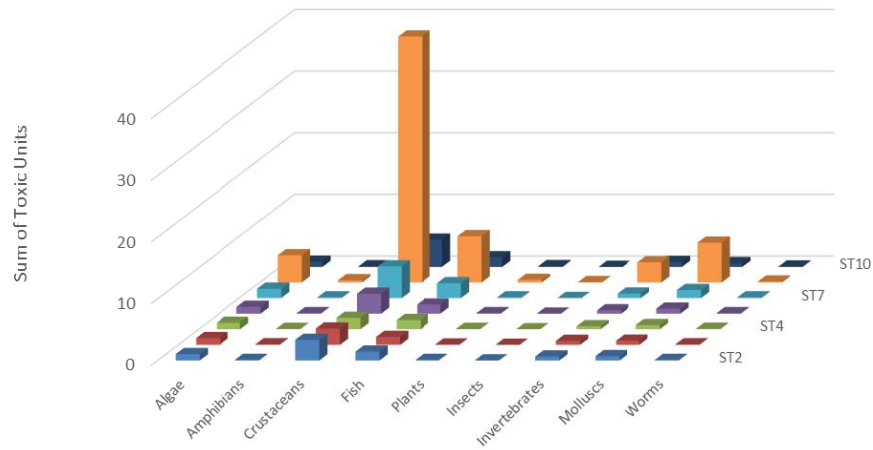
Figure 4. *Cumulative risk of chemical toxicity effects from the measured mix of radionuclides and metals size a)< 0.45 μm b)only LMM, in waters. The predicted risk is given as the sum of toxic units (STU) where more than 1 predicts significant risk of effects while STU above 10 gives high predicted risk.*

References
Engelstad, J. G. (2016). *Ecological Implications of Road Construction in an Alum Shale Bedrock Area - A State Highway (Rv4) Case Study*, NMBU, Ås.
IAEA. (2010). *Handbook of Parameter Values for the Prediction of Radionuclide Transfer in Terrestrial and Freshwater Environments*. International Atomic Energy Agency, Vienna.
NKS. (2009). *Po-210 and other radionuclides in terrestial and freshwater environments*. NKS, Oslo.
Rosseland, B. O., Massabuau, J. C., Grimalt, J., Hofer, R., Lackner, R., Raddum, G., Rognerud, S., and Vives, I. (2001). *Fish Ecotoxicology: European mountain lake Ecosystems Regionalisation, diaGnostic & socio-economic Evaluation (EMERGE). Fish sampling for live fish*. Norwegian Institut for Water Research, Oslo, Norway.
Salbu, B. (2009). "Challenges in radioecology." *Journal of Environmental Radioactivity*, 100(12), 1086-1091.
Salbu, B. (2015). "Environmental impact and risk assessments and key factors contributing to the overall uncertainties." *Journal of Environmental Radioactivity*, 151(2), 352-360.
Salbu, B., Rosseland, B. O., and Oughton, D. H. (2005). "Multiple stressors - a challenge for the future." *Journal of Environmental Monitoring*, 7, 1-2.
Salbu, B., and Skipperud, L. (2007). "Challenges in Radioecotoxicology." *The NATO Programme for Security through Science*(1), 3-12.
Salbu, B., and Skipperud, L. (2009). "Speciation of radionuclides in the environment." *Journal of Environmental Radioactivity*, 100(4), 281-282.
Skipperud, L., Stromman, G., Yunusov, M., Stegnar, P., Uralbekov, B., Tilloboev, H., Zjazjev, G., Heier, L. S., Rosseland, B. O., and Salbu, B. (2013). "Environmental impact assessment of radionuclide and metal contamination at the former U sites Taboshar and Digmai, Tajikistan." *Journal of Environmental Radioactivity*, 123, 50-62.

Environmental impact of some NORM industries in Mexico

D. Mandujano-García,[1,2,], M. Sosa[1], J. Mantero[2,3], R.García-Tenorio[2,4]*

[1] Department of Physical Engineering, DCI, University of Guanajuato, Mexico
[2] Department of Applied Physics II, ETSA, University of Sevilla, Spain
[3] Department of Radiation Physics, Sahlgrenska Academy, University of Gothemburg, Sweden
[4] Spanish National Accelerator Centre, University of Sevilla, Spain

Abstract

Industrial activities associated with metal mining, extraction and processing of oil and gas, power generation using fossil fuels, among others, may concentrate natural radionuclides in various products, by-products and wastes. Radiological implications of naturally occurring radioactive materials (NORM) generated by human activities need to be taken into account to control exposure to workers, public and the environment.

Concerning these types of industries in Mexico, in this work we present the radiometric characterization of different materials with naturally occurring radioactive contents; wastes generated by silver mining in Xichú, environmental soils affected by and an industrial complex (oil refining, power generation and manufacture of agrochemicals) in Salamanca and produced waters from the oil and gas industry in Monclova. The activity concentrations of radionuclides from the natural series ^{238}U and ^{232}Th, besides ^{40}K in the analysed samples have been determined by gamma-ray spectrometry and alpha-particle spectrometry.

The levels of radioactivity found in Xichú and Salamanca are of the order of the values found in soils not affected by human activities, indicating that the NORM environmental radiological impact of these industries is very low. On the other hand, the activity concentrations of natural radionuclides, mainly ^{226}Ra and ^{228}Ra, in produced waters from Monclova showed values up to a thousand times higher than those found in natural waters, with a variable radiological impact in the region. A periodic radiometric monitoring is required to ensure a proper control of the produced waters and limit the potential radiological environment contamination.

Introduction

For several decades, international studies have shown that exposure to natural radiation sources is modified by human practices. This has led to a growing interest in control of radioactivity in the environment around different industrial activities. Industrial activities associated with metal and non-metal mining, processing of ores, production of oil and gas, power generation using fossil fuels, among others, may generate Naturally Occurring Radioactive Materials (NORM), increasing the potential for exposure of workers, public and environment in comparison with the unaltered situation (IAEA, 2003).Therefore, these industrial activities are considered as NORM industries.

Natural radionuclides, including ^{40}K and decay products from the natural series of ^{238}U and ^{232}Th are presents in significant amounts in many raw materials used by NORM industries. When the levels of natural radionuclides are concentrated in products, by-products or wastes as a result of an industrial process, radiological implications need to be taken into account to control exposure to workers, public and the environment. The presence of technologically enhanced NORM at industrial activities may contribute to internal/external doses in humans, particularly during maintenance activities. Although each country establishes its own NORM regulations, exemption levels of 10 kBq/kg for ^{40}K and 1 kBq/kg for all radionuclides of the natural series of ^{238}U and ^{232}Th, are recommended for proper control of NORM (IAEA, 2014).

---

[*]Corresponding author, E-mail:cmandujano@fisica.ugto.mx

For example, in mining and processing of Cu in Arizona (United States of America), increases in natural radionuclide levels have been found in solutions and residues from solvent extraction processes, affecting surface water sources and underground mining near the mines (USEPA, 1999). Aluminum processing and refining (bauxite) generates several million tons worldwide of tailings (bauxite tailings) with a high content of natural radionuclides. Typical values of 232Th in tailings areof the order of 100 to 3000 Bq/kg (IAEA, 2013).However, NORM levels in the mining industry vary greatly according to the geological conditions of the region, the type of ore exploited, among others, so that a radiometric evaluation is necessary for each specific case.

Likewise, exploration, extraction and production of fossil fuels including oil, gas and coal are also considered NORM industries. In the deposits of these natural resources, rock formations usually contain significant amounts of natural radionuclides. In the oil industry, during the production processes a mixture of oil, gas and water is drawn through a piping system from a well. In the rock formations present in the production well are radionuclides of the ^{238}U and ^{232}Th series. Although uranium and thorium do not mobilize from the rock formations present in the rock formations, the decay products ^{226}Ra, ^{228}Ra and ^{210}Pb do have mobility and are thus extracted and concentrated in the produced water, sludge and crusts of the pipes. These NORM by-products and wastes usually contain high concentrations of radioactive content (NRPA, 2004; OGP, 2008).

Thus, it is important for industries and regulatory bodies to understand where and when high concentrations of NORM are present in a given process, to manage NORM generated in a way that ensures the protection of human health and the environment.

In Mexico there are important activities that can be classified as NORM industries. Globally, Mexico is one of the largest producers of oil, gas, silver, copper, gold, lead, zinc, among other natural resources. However, in the country there are few studies on the radiological impact that the NORM industries generate when exploiting these natural resources.In this work we present the radiometric characterization of different materials with naturally occurring radioactive contents; wastes generated by silver mining, produced water from the oil and gas industry and soils affected by an industrial complex.

Materials and Methods

Samples

In this work a total of 37 samples were collected, including, wastes, soils and sediments from three different regions of Mexico influenced by several NORM industries. In Figure 1 a map of the regions of Mexico where samples were collected is presented.
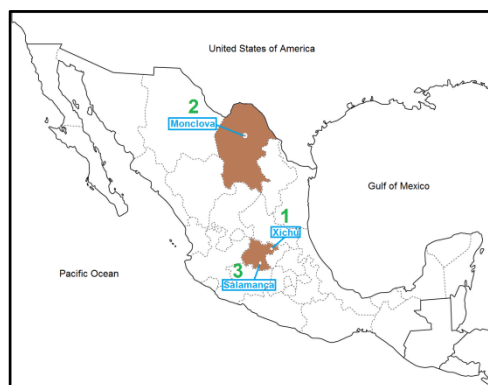
Figure 1.Map of the regions from Mexico where samples were collected.

The samples from each region are described below:

1. Mine wastes from Xichú. Samples of mine tailings generated by silver, gold and copper mining activities and also sediment from Xichú River in Guanajuato were collected. High amounts of mine wastes enriched with potentially toxic elements (As, Pb, Fe) are abandoned along Xichú River, representing a potential risk for environment and health from nearby population.

2. Produced water from Monclova. Samples of produced water from two different oil and gas water treatment stations were collected in Coahuila. Collected samples are a mixture produced waters obtained as a by-product after separation from oil and gas from several gas wells. In this region produced water is reinjected to depleted wells and may represent a radiological issue for workers during maintenance activities or potential releases to environment.

3. Soils from Salamanca. Samples of soils affected by an industrial complex were collected. Activities associated with oil refining, power generation by combustion of gas and fuel oil, and also manufacture of agrochemicals are carried out inside the industrial complex. Soils around the industrial complex have been influenced by contamination released from the industrial complex for several decades. Salamanca is considered as one of the most highly contaminated zones of the country (SEMARNAT, 2013).

All solid samples were collected form the first 10 cm in points selected randomly according to potential influence from NORM activities. About 1 kg of solid samples were transported in sealed plastic bags to laboratory, dried, grounded and sieved for further analysis. Liquid samples were transported in 5 L plastic bottles and kept in fresh environment (22 °C) until further analysis.

Radiometric techniques

Samples were characterized radiometrically by gamma-ray spectrometry and alpha-particle spectrometry.Proper aliquots of the samples were taken and treated according to the required methodology by each technique. A detailed description from the methods used in this work for the determination of the radionuclides of interest may be found elsewhere (Lehritani, 2012;Mantero, 2015; Mandujano-García, 2016). Briefly,

Samples were vacuum sealed in adequate containers. Solid samples were packed in Petri dishes and liquid samples were packed in 1 LMarinelly beakers. All samples were stored for 30 days before measurement. In this way, secular equilibrium between ^{226}Ra and their short half-life daughters was ensured.The samples were measured in a spectrometric system consisting of a Canberra hyperpure germanium detector HPGe type XtRa (extended range), with a relative efficiency of 37% and resolution of 1.77 keV for the 1.33 MeV photopeak of ^{60}Co. The detector is shielded by 10 cm of old lead, lined with a 5 mm layer of Cu, and, additionally, has an anticoincidence device (organic scintillator) to reduce background radiation levels and increase the sensitivity in the environmental gamma radiation measurements.

Efficiency calibration was performed for each type of geometry. For solid samples, reference standards materials: IAEA-RGU1 and IAEA-RGTH1, were used for energy peak efficiency determination. To determine the activity concentration of ^{226}Ra the values obtained from the main gamma emission of their descendants in secular equilibrium were averaged: ^{214}Pb (295 and 352 keV) and ^{214}Bi (609, 1120 and 1764 keV), which were consistent considering associated uncertainties (1-σ) throughout the measurement process. The effects of sum coincidence for efficiency determination can be neglected due to the use of reference materials with the same

radionuclides of interest. For the low energy emissions of [210]Pb (46.5 keV) corrections were applied due to differences in self-absorption between the real and reference samples, following the methodology described by Cutshall (Cutshall et al., 1983). In the case of liquid samples a CIEMAT mixed nuclides solution with multi-gamma emissions in the range of 59.5-1836.5 keV was used for efficiency calibration.

On the other hand, [238]U, [234]U, [230]Th and [232]Th radionuclides were determined by alpha spectrometry. In this technique, radionuclides of interest must be isolated from the matrix by applying a radiochemical process consisting of three stages: pre-concentration of actinides, separation and purification of the elements of interest, and preparation of alpha particle sources for measurement. The methodology of the radiochemical process followed in this work is well described by Lehritani (Lehritani et al, 2012).

Results and Discussion

Activity concentration values of radionuclides from [238]U and [232]Th natural series were measured via alpha spectrometry and gamma-ray spectrometry. Figure 2 shows the results obtained for the activity concentration of radionuclides from the U and Th natural series in the samples from Xichú.
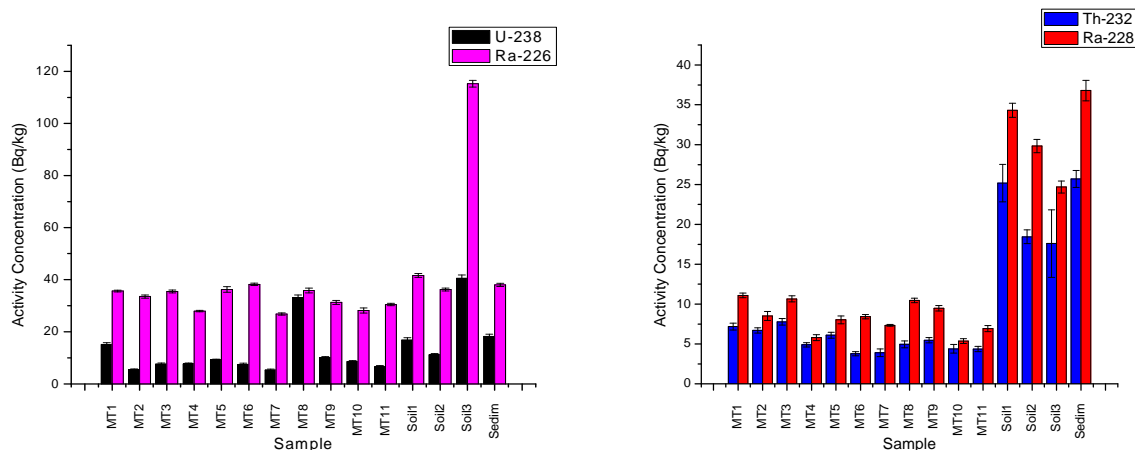
*Figure 2.*Activity concentrations (Bq/kg) of radionuclides from the U and Th natural series in mine tailings from Xichú. Uncertainties correspond to 1-σ.

Samples of mine tailings from Xichú (MT1-MT-11) presented levels of activity concentration in the range of 4-38 Bq/kg for both series. These levels are very similar to the values found in the soil and sediment collected in the surroundings. Also, the activity concentration levels of the analysed samples are in the order or lower than world average environmental soils: 20-40 Bq/kg(UNSCEAR, 2000). The low levels indicate that U-238 and Th-232 radionuclides mobilize to other stages of the mining activities. The results as a whole clearly indicates that mine wastes under analysis do not constitute any radiological problem either form a public or environmental point of view.

In the same way, the results of the activity concentration levels of natural radionuclides measured in soils from Salamanca are presented in Figure 3. Measurements of activity concentration of radionuclides from [238]U and [232]Th natural series presented values in the range of 10-82 Bq/kg for both series. Activity concentrations of [238]U are similar than the values found in unaltered soils from North America; mean natural radionuclide content in soils from United States of America and Costa Rica are 35 and 46 Bq/kg respectively. The obtained results indicated that there is not clear anthropogenic increments in the levels of NORM in the analyzed soils.
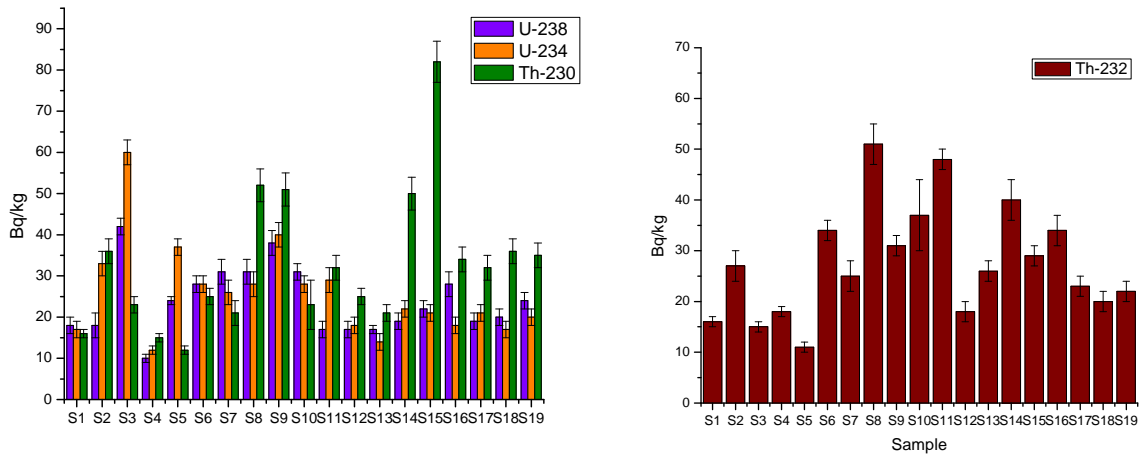
Figure 3.*Activity concentrations (Bq/kg) of radionuclides from the U and Th natural series in mine tailings from Xichú. Uncertainties correspond to 1-σ.*

Moreover, results of activity concentration levels measured in the samples of produced waters from Monclova are compiled in Table 1. The obtained activity concentration values in the analysed produced water samples are quite variable but in the order found in other oil and gas regions of the world: 0.002-1200 Bq/L for ^{226}Ra (OGP, 2008).

Table 1.*Activity concentrations (Bq/L) of radionuclides from the U and Th natural series in produced water from Monclova, Mexico. Relative uncertainties correspond to 10% .*

Radionuclide	Station A Activity Concentration (Bq/L)	Station B Activity Concentration (Bq/L)
^{238}U	0.046	0.001
^{234}U	0.074	0.005
^{226}Ra	1.0	15.5
^{210}Po	0.017	0.470
^{228}Ra	<0.30	2.4

The results of the analysed produced water samples show that both stations could be considered NORM due to the activity concentration levels clearly higher than the found ones in natural surface/ground waters. In particular, levels of Ra-isotopes are quite high, while U-isotopes are clearly lower. Produced water samples from Station B contain higher concentration activities of ^{226}Ra and ^{210}Po than Station A samples. Both samples present a high ^{234}U/^{238}U disequilibrium.

Conclusions

After all measurements of samples associated with NORM industries in Mexico, the results lead to the following conclusions:
The levels of radioactivity found in Xichú and Salamanca are of the order of the values found in soils not affected by human activities, indicating that the NORM environmental radiological impact of these industries is very low.
On the other hand, radiometrical characterization of produced waters from Monclova, shows that Ra isotopes presented a high activity concentration very depending from station to station, indicating that the radiological impact of the produced waters for the Mexican gas industry can be quite variable; a more extensive monitoring for each station is needed for a proper radiological management of the produced waters.

It is recommended to continue this kind of studies to other regions of the countries affected by these and other types of NORM industries, in order to increase the information about the levels of natural radionuclides and their radiological implications to environment and health population.

References

(IAEA, 2003)International Atomic Energy Agency.Extent of environmental contamination by naturally occurring radioactive material (NORM) and technological options for mitigation. IAEA Technical Reports Series 419 (2003).

(IAEA, 2013)International Atomic Energy Agency.Management of NORM Residues.IAEA-TECDOC-1712 (2013).

(IAEA, 2014)International Atomic Energy Agency.Radiation Protection and Safety of Radiation Sources".IAEA Safety Standards. No. GSR Part 3 (2014).

(Lehritani, 2012) Lehritani, M., Mantero, J., Casacuberta, N., Masqué, P. and García-Tenorio, R. Comparison of two Sequential Separation Methods for U and Th determination in environmental samples by alpha-particle spectrometry", RadiochimicaActa, Vol. 100, pp.431-438(2012).

(Mandujano-García, 2016) Mandujano-García, C.D., Sosa, M., Mantero, J., Costilla, R., Manjón, G. and García-Tenorio, R. Radiological impact of natural radionuclides from soils of Salamanca, Mexico. Applied Radiation and Isotopes 117: 91-95(2016).

(Mantero, 2015) Mantero, J., Gázquez, M.J., Hurtado, S., Bolívar, J.P. and García-Tenorio, R. Application of gamma-ray spectrometry in a NORM industry for its radiometricalcharacterizarion. Radiation Physics and Chemestry 115: 78-81 (2015).

(NRPA, 2004) Norwegian Radiation Protection Authority.Natural Radioactivity in Produced Water from the Norwegian Oil and Gas Industry in 2003.StralevernRapport 2005:2. Osteras (2004).

(OGP, 2008) International Association of Oil and Gas Producers.Guidelines for the Management of Naturally Occurring Radioactive Material (NORM) in the oil and gas industry. Report No. 412 (2008).

(SEMARNAT, 2013) Secretaría de Medio Ambiente y Recursos Naturales. http://www.semarnat.gob.mx/temas/gestion-ambiental/materiales-y-actividades-riesgosas/sitios-contaminados (in spanish, last consulted 23-dic-2016)

(USEPA, 1999) United States Environmental Protection Agency. Technologically Enhanced Naturally Occurring Radioactive Materials in the Southwestern Copper Belt of Arizona.USEPA Technical Report 402-R-99-002 (1999).

(UNSCEAR, 2000) United Nations Scientific Committee on the Effects of Atomic Radiation.Sources and effects of Ionizing Radiation. Report Vol. I, Annex B. New York: UNSCEAR(2000).

Radioactivity Levels in Scales Generated from Crude Oil Production in Ghana

R. García-Tenorio, J. Mantero, G.Manjón, I. Vioque

University of Seville, Department of Applied Physics II, ETSA, Avenida Reina Mercedes 2, 41012 Sevilla, Spain

D.Kpeglo

Radiation Protection Institute, Ghana Atomic Energy Commission, P. O. Box LG80, Legon-Accra, Ghanna

Abstract

Knowledge of accurate radio isotopic signatures is very necessary in assessing any potential radiological hazards and risks to members of the public and workers from exposure to NORM contaminated scales. In this work scales from crude oil production activities from Ghana have been assessed using alpha spectrometry after radiochemical separation, and non-destructive gamma spectrometry. Characterization and determination of activity concentrations of ^{234}U, ^{238}U, ^{210}Po, ^{230}Th, ^{232}Th, ^{226}Ra, ^{210}Pb, ^{228}Ra, ^{228}Th, ^{224}Ra and ^{40}K have been established. The average activity concentrations of 43.9 ± 8.1 kBq.kg^{-1}, 30.3 ± 5.1 kBq.kg^{-1}, 11.2 ± 2.8 kBq.kg^{-1} and 11.2 ± 2.6 kBq.kg^{-1} obtained for ^{226}Ra, ^{228}Ra, ^{228}Th, and ^{224}Ra respectively in scale samples in this study exceeded the IAEA Basic Safety Standards (BSS) exemption levels giving an indication that the scale samples could present significant future radiological risk for workers, the public and environment

Introduction

During the last decade some oil explorations and exploitation activities have started at different sites along the west coast of Ghana. Consequently, environmental concern has appeared in association with possible chemical pollution but, in addition, radiometrical characterization becomes relevant in oil extraction, which is a well-known NORM (Naturally Occurring Radioactive Material) activity.

A common problem in oil production is the accumulation of scale on the interior surfaces of production pipes. The scales are mostly composed of barium sulphate, barium carbonate, and/or calcium carbonate. NORM scale is produced when Ra dissolved in the formation water is co-precipitated with Ba, Sr, or Ca as mostly sulphates[1]. These materials form insoluble hard deposits inside the production equipment[2] and depending on the formation and age of the well, the management (removal, storage and disposal) of the scale can result in serious health and environmental risks if not handled properly, both for workers and the public.

The dominating radionuclides present in scales and other precipitates are ^{226}Ra and ^{228}Ra, with typical concentrations ranging from 1 to 1000 kBq kg^{-1}, although concentrations as high as 15,000 kBq kg^{-1} have been reported in literature [3]. Values for ^{228}Ra in scales are, in general, not much less than for ^{226}Ra.

Radiation protection considerations arise mainly from the removal of this scale during maintenance and decommissioning operations resulting in exposure to external gamma radiation and inhalation of dust, and from the subsequent disposal of such materials as waste. Individuals working close to heavily scaled pipes and vessels may also need to be subjected to radiation protection measures.

The primary aim of the study shown in this paper has been to determine and characterize the radioactivity levels of scale generated as a result of oil and gas production in Ghanna production oilfields in order to establish baseline data. The emphasis of this study is on the determination of the activity concentrations and distribution of several naturally occurring radionuclides of the U/Th decay series and ^{40}K using mainly alpha-particle and high-resolution gamma-ray spectrometric techniques. This work was necessary since no studies have been carried out on radioactivity levels in scales generated as a result of oil and gas exploration and production from the oilfields in Ghana and published data are not available.

Materials and Methods

Composite samples comprising of 5 scales were collected for this work from produced water pipes at the storage and maintenance facility onshore for the Ghana oilfields in January 2015.

The preparations for U, Th and Po determination by alpha-particle spectrometry were carried out in three main steps: pre-concentration, radiochemical separation and electrodeposition. The details of these procedures can be found in earlier presentation[4]. However, in this study the step involving calcination was excluded (due to our interest in Po for this work, the samples were wet-digested directly using aqua regia) and also a different radiochemical separation procedure using liquid – liquid solvent extraction (TBP + Xylene) according to a method described by Martinez-Aguirre [5,6] was applied to the samples. The Th fraction obtained by this separation was further purified using AGI-X8 ionic exchange resin (100-200 mesh). Source preparation for Po was done by self-deposition onto copper discs while U and Th were independently electrodeposited onto stainless steel discs by applying the well-known method of Hallstadius [7].

The measurement of the U and Th isotopes electroplated and Po self-deposited were done using 450 mm^2 active surface PIPS detectors installed in an 8- chamber Alpha analyst system (Canberra). In our laboratory, each chamber is devoted to the exclusive measurement of one element in order to avoid cross contamination. The measurements were carried out at a source to detector distance of 0.5 cm. The accumulation and analysis of Alpha spectra was done using Genie 2000 software with measurement time of 200,000s. The background spectra were also used to determine the minimum detectable activity (95% confidence level) of U, Th and Po (~0.1mBq) for a measuring time of 2-3 days. The mean recovery yields of the radiochemical procedure were 69% for U, 60% in the case of Th and 70% for Po.

For gamma-ray determinations, scale aliquots were air-dried and finally oven dried in some cases to remove any additional moisture from the samples. The dried samples were each transferred into measuring cylindrical containers (55mm diameter by 12mm height) without any treatment and vacuum sealed after sealing with silicone. All samples were non-destructively analysed by high-resolution gamma spectrometry using a p-type Extended Range Germanium coaxial detector (XtRa) with relative efficiency of 37.1% and with an energy resolution of 1.8 keV for gamma-ray energy of 1332 keV of ^{60}Co. The detector is housed in a 10 cm passive shielding of ancient lead with an active shielding made with an organic scintillation detector (Bicron BC-418) placed on the top of the lead shield and working in anticoincident mode with the Ge detector. This allows remarkable precision in the environmental gamma-radiation measurements due to the very low background. The counting time was 180000 seconds for each sample. The identification of individual radionuclides was performed using their characteristic gamma-ray energies and the quantitative analysis of radionuclides was performed using the Genie 2000 gamma acquisition and analysis software. Background spectra were acquired and used to correct the net peak area of gamma rays of the

measured isotopes and used to determine the minimum detectable activities of ^{226}Ra (0.11 Bq), ^{232}Th (0.13 Bq), and ^{40}K (1.10 Bq) at the 95% confidence level.

The IAEA reference materials IAEA-RGU-1(U-ore) and IAEA-RGTh-1 (Th-ore) with mean densities (1.33 ± 0.03 g/cm^3) similar to the mean densities of scale samples to be measured were prepared into same cylindrical containers as that of scale and sludge samples and were used to estimate the efficiencies for photo peaks of natural radionuclides measured and quantified in the samples.

The activity concentrations of ^{226}Ra were determined using the γ-ray emissions and the respective γ-yield of ^{214}Pb at 351.9 keV (35.8%) and ^{214}Bi at 609.3 keV (44.8%). The ^{228}Ra activity concentrations were determined through the gamma emissions of ^{228}Ac at 911 keV (26.6%), and the ^{228}Th activity concentrations were determined through the gamma emissions of ^{212}Pb at 238.6 keV (43.3%) and ^{208}Tl at 583 keV (30.1%) and 2614.7 keV (35.3%) taking into consideration a branching ratio of 33.7% from ^{212}Bi towards ^{208}Tl. The ^{40}K activity concentration was determined directly from its emission line at 1460.8 keV (10.7%) while the ^{210}Pb activity concentration was determined directly from the gamma emission line at 46.5 keV (4.3%). In calculating the activities, considerations of self-absorption correction factor for low energy photo peak ^{210}Pb was incorporated. All the energies and intensities of the different radiations mentioned were taken from a well-known library [8].

Air borne radon activity concentrations were measured directly with a Genitron Alpha Guard, Model PQ 2000/mp50. The measurements were carried out outdoor and indoor in the field at scale embedded pipes storage and maintenance facility. The temperature, atmospheric pressure and relative humidity were also recorded during the measurement. The Alpha Guard is provided with a large surface glass fibre filter, which allows only the gaseous ^{222}Rn to pass through whilst the radon progeny are prevented from entering the ionisation chamber. The data was evaluated using Alpha View/ Data Expert Software, which automatically transforms radon daughter concentrations from working level (WL) to equilibrium equivalent concentration (ECC) in Bqm^{-3}.

Results and Discussion

The results of radioactivity concentrations of radionuclides ^{226}Ra, ^{210}Pb, ^{228}Ra, ^{228}Th, ^{224}Ra and ^{40}K in scale samples determined by gamma spectrometry are presented in Table 1. The average value of the activity concentration of ^{226}Ra was 43.9 ± 8.1 kBq.kg^{-1} (in a range of 38.5–58.3kBq.kg^{-1}); for ^{210}Pb, the average was 0.36 ± 0.15 kBqkg^{-1}(in a range of 0.20–0.60 kBq.kg^{-1}); while for ^{228}Ra, the average activity concentration was 30.3 ± 5.1 kBq.kg^{-1} (in a range of 26.8 – 39.2 kBq.kg^{-1}); and for ^{228}Th, the average was 11.2 ± 2.8 kBq.kg^{-1} (in a range of 8.6–15.9 kBq.kg^{-1}). In the case of ^{224}Ra the average activity concentration was 11.2 ± 2.6 kBq.kg^{-1} (in a range of 8.8–15.4 kBq.kg^{-1}); whiles for ^{40}K, the average is 1.8 ± 0.4 kBq.kg^{-1} (in a range of 1.3–2.3 kBq.kg^{-1}).

Sample ID	Concentration (kBq.kg^{-1})					
	^{226}Ra	^{210}Pb	^{228}Ra	^{228}Th	^{40}K	^{224}Ra
SC1	38.5 ± 0.4	0.4 ± 0.01	26.8 ± 0.1	9.8± 0.8	1.8 ± 0.2	9.6 ± 0.9
SC2	41.5 ± 0.4	0.3 ± 0.01	28.2 ± 0.5	11.0 ± 0.6	1.8 ± 0.1	10.9 ± 0.8
SC3	40.7 ± 0.4	0.2 ± 0.01	27.6 ± 0.5	10.9± 0.5	1.3 ± 0.2	11.2 ± 0.7
SC4	40.7 ± 0.1	0.3 ± 0.01	29.9 ± 0.5	8.6 ± 0.6	2.0 ± 0.3	8.8 ± 0.6
SC5	58.3 ± 0.2	0.6 ± 0.1	39.2 ± 0.7	15.9 ± 1.2	2.3 ± 0.3	15.4 ± 0.9

Table 1. *Activity Concentration of ^{40}K, ^{238}U, ^{232}Th series radionuclides in Scales samples by Gamma Spectrometry.*

It is clear from the data shown in Table 1, that all radionuclides except ^{210}Pb compared for scale samples exceeded the IAEA Basic Safety Standards (BSS) exemption levels and hence there may be need to exert regulatory control of the NORM residues.

The results of ^{226}Ra and ^{228}Ra in scale were compared with data from other countries as shown in Table 2. The specific activities in general compare well with data from other countries around the world. The range of activity concentration of ^{226}Ra and ^{228}Ra in scale from Ghana (this study) was higher than the range of values reported in Scale from other studies carried out in other Oilfields in Norway, Congo, Egypt and Kazakhstan [9-12] and lower than those recorded in some other work undertaken in various oil fields in the United Kingdom, United States of America, Egypt, Tunisia, Algeria, Syria, Malaysia, Brazil and Australia [13-22]. The variation in activity concentration of natural radionuclide content in scales of different origins in the oil extraction industry can be attributed to factors such as the geochemical and geological characteristics of reservoir rocks, age, the type of hydrocarbons produced and operating conditions for the oilfields.

Country	^{226}Ra (kBq.kg^{-1})	^{228}Ra (kBq.kg^{-1})	Reference
Algeria	1 – 950	-	Hamlat et al., 2001
Australia	21 – 250	48 – 300	APPEA, 2002
Brazil	19.1 – 323	4.2 – 235	Godoy and Crux, 2003
Brazil	77.9 – 2110	101.5 – 1550	Gazineu and Hazin, 2008
Congo	0.097 – 0.151	-	Testa et al., 1994
Egypt	0.49 – 0.52	0.032 – 0.05	Abo-Elmagd et al., 2010
Egypt	7.5 – 143	35.46 – 368.654	Shawky et al., 2001
Ghana	38.5 – 58.3	26.8 – 39.2	Present study
Kazakhstan	0.51 – 51	0.2 – 10	Kadyrzhanov et al., 2005
Malaysia	114 – 188	130 – 207	Omar et al., 2004
Norway	0.3 – 32.3	0.3 – 33.5	Lysebo et al., 1996
Syria	147 – 1050	43 – 181	Al-Masri and Suman, 2003
Tunisia	4.3 – 658		Heaton and Lambley, 1995
UK	1 – 1000		E & P forum, 1987
USA	15 – 76		White and Rood, 2001

Table 2. *Comparison of ^{226}Ra and ^{228}Ra in Scale and Sludge from Ghanaian oilfields with others published in literature*

Table 3 presents specific activities of ^{234}U, ^{238}U, ^{210}Po, ^{230}Th and ^{232}Th determined using alpha spectrometry. The activities of ^{234}U were in the range 0.9–4.5 Bq.kg^{-1} with average 1.9 ± 1.5 Bq.kg^{-1}, the activities of ^{238}U in the range 1.6–4.6 Bq.kg^{-1} with average 2.5 ± 1.2 Bq.kg^{-1}, the activities of ^{210}Po in the range 66 – 166 Bq.kg^{-1} with average 99 ± 39 Bq.kg^{-1}, the activities of ^{230}Th in the range 1.2 – 3.9 Bq.kg^{-1} with average 1.9 ± 1.2 Bq.kg^{-1} and the activities of ^{232}Th in the range 0.9–4.5 Bq.kg^{-1} with average 1.9 ± 1.5 Bq.kg^{-1} respectively.

Sample ID	Concentration (Bq.kg^{-1})				
	^{234}U	^{238}U	^{210}Po	^{230}Th	^{232}Th
SC1	2.1 ± 0.2	1.6 ± 0.1	97 ± 4	1.3 ± 0.2	0.9 ± 0.1
SC2	2.9 ± 0.3	2.3 ± 0.5	66 ± 3	3.9 ± 0.3	4.5 ± 0.3
SC3	3.1 ± 0.3	2.4 ± 0.3	83 ± 5	1.3 ± 0.2	1.8 ± 0.3
SC4	5.5 ± 0.4	4.6 ± 0.4	82 ± 2	1.2 ± 0.1	1.1 ± 0.1
SC5	2.2 ± 0.2	1.8 ± 0.2	166 ± 7	1.7 ± 0.2	1.0 ± 0.1

Table 3. *Activity Concentrations of ^{238}U, ^{235}U, ^{234}U, ^{210}Po, ^{230}Th and ^{232}Th in Scales determined by alpha-particle spectrometry.*

The ^{210}Po level was highest in all the scales samples via alpha, an indication that ^{210}Po may contribute significantly to total alpha activity. This could be a significant source of exposure to workers via internal contamination by inhalation during maintenance, decommissioning operations and waste processing and disposal. However, generally activity concentrations of U and Th-isotopes as well as ^{210}Po for all scale samples in this study were much lower compared to that of radium isotopes discussed earlier above.

Finally, the ^{222}Rn concentrations were measured in air on the field from pipes at storage and maintenance facility and the results were 21 – 194 Bq.m^{-3} with average 113 ± 49 Bq.m^{-3} for outdoor and 200 – 548 Bq.m^{-3} with average 334 ± 94 Bq.m^{-3} for indoor. The airborne radon concentration measurements were made at average conditions of temperature, atmospheric pressure, and relative humidity with mean values of 34.5 $^{\circ}$C, 100.3 kPa and 90.4 % respectively. By comparison of results, it is observed that indoor concentrations were about 3 times higher than that of outdoor measurements as a result of diffusion and dilution outdoor. This indicates that, one of the most effective means of reducing radon exposure is to provide proper and effective ventilation when the levels are high in an enclosed area. The airborne radon concentrations are on the other hand within the ICRP recommended value of 200-600 Bq/m^3 in dwellings and below the value of 1000 Bq/m^3 for workers [23].

Conclusions

Radioactive characterization of NORM contaminated scale resulting from the crude oil production activities and waste generation from oilfields of Ghana have been investigated using alpha spectrometry after radiochemical separation and non-destructive gamma spectrometry. Characterization and determination of specific activities of ^{234}U, ^{238}U, ^{210}Po, ^{230}Th, ^{232}Th, ^{226}Ra, ^{210}Pb, ^{228}Ra, ^{228}Th, ^{224}Ra and ^{40}K for NORM residues have been established.

The specific activities of ^{226}Ra, ^{228}Ra, ^{228}Th, and ^{224}Ra for scale samples in this study exceeded the IAEA Basic Safety Standards (BSS) exemption levels and hence needs to be handled with care in the deciding its transport, removal, storage and disposal of the NORMs residues. It was also clear from this study that, ^{210}Po level was highest between the radionuclides measured via alpha spectrometry, an indication that ^{210}Po may contribute significantly to total alpha activity. This could be a significant source of exposure to workers via internal contamination by inhalation during maintenance, decommissioning operations and waste processing and disposal.

The airborne radon concentration measured at waste storage facilities in this study were within the ICRP recommended value of 200-600 Bq/m^3 in dwellings and below the value of 1000 Bq/m^3 for workers [29].

Overall, this study suggests that removal, storage and disposal of Scale and sludge could present significant future radiological risk for workers, the public and environment if not properly managed.

References

1.- White G. J., Rood A. S. (1999). 5th Intern. Petroleum Environmental Conf., University of Tulsa and others, Albuquerque, N. M., USA, Oct. 20-23.

2.-Smith, K.P., Blunt, D.L., Arnish, J.J., Williams, G.P., M. Pfingston, J. Herbert, R. A. Haffenden (1999). An Assessment of the Disposal of Petroleum Industry NORM in Nonhazardous Landfills, Final Report, Fossil Energy, National Petroleum Technology Office U.S. Department of Energy, Tulsa, Oklahoma, USA, p. 21

3.-USEPA (1993). Development Document for Effluent Limitations Guidelines and New Source Performance Standards for the Offshore Subcategory of the Oil and Gas Extraction Point Source Category. US Environmental Protection Agency EPA-821-R-93-003. Office of Water, Washington, DC, USA.

4.- Kpeglo DO, Mantero J, Darko EO, Emi-Reynolds G, Akaho EHK, Faanu A, Garcia -Tenorio R (2014). Radiological Exposure Assessment from Soil, Underground and Surface Water in Communities along the coast of a Shallow Water Offshore Oilfield in Ghana. Radiation Protection Dosimetry, Advance Access Publication, doi:10.1093/rpd/ncu197, 1-12.

5.- Martínez-Aguirre A (1991). Radiactividad natural en diversos compartimentos naturales de Andalucía. PhD Thesis. University of Sevilla.

6.- Lehritani M, Mantero J, Casacuberta N, Masqué P, García-Tenorio R (2012). Comparison of two Sequential Separation Methods for U and Th determination in environmental samples by alpha-particle spectrometry. Radiochimica Acta 100:431-438.

7.- Hallstadius L (1984). A method for electrodeposition of actinides, Nucl.Instrum.Methods 223, 226-238.

8.- Chu, SYF, Ekström LPY, Firestone RB (1999). The Lund/LBNL Nuclear Data Search, February (1999). http://nucleardata.nuclear.lu.se/nucleardata/toi/

9.- Lysebo J, Birovliev A, Strand T (1996) NORM in oil production – occupational doses and environmental aspects. In: Proc of the 11th Congress of the Nordic Radiation Protection Society, 26–30 August 1996, Reykjavik, p 137.

10.- Testa C, Desideri C, Meli MA (1994) Radiation protection and radioactive scales in oil and gas production. Health Phys 71:34–38.

11.-Abo-Elmagd M., Soliman H.A., Salman Kh.A., El-Masry N.M., (2010). Radiological hazards of TE-NORM in the wasted petroleum pipes, J. Envron. Radio. 101, 51-54.

12.- Kadyrzhanov K.K, Tuleushev A.Z, Marabaev Z.N (2005). Radioactive components of scales at the inner surface of pipes in oil fields of Kazakhstan. J Radioanal Nucl Chem 264:413–416.

13.- Hamlat M.S., Djeffal S., Kadi H. (2001). Assessment of radiation exposures from naturally occurring radioactive materials in the oil and gas industry. Applied Radiation and Isotopes 55, 141–146.

14.-Exploration & Production Forum, 1987. Low specific activity scale origin treatment and disposal. Report no. 6.6/127, Old Burlington Street, London WlX 1LB, pp. 25–28.

15.- White G. J. and Rood A. S. (2001). Radon emanation from NORM contaminated pipe scale and soil at petroleum industry sites. Journal of Environmental Radioactivity 54, 401-413.

16.- Shawky S., Amer H., Nada A.A., Abd El-Maksoud T.M., Ibrahiem N.M. (2001). Characteristics of NORM in the oil industry from Eastern and Western deserts of Egypt. Applied Radiation and Isotopes 55, 135-139.

17.-Heaton, B., Lambley, J., (1995). TENORM in the oil, gas and mineral mining industry. Applied Radiation and Isotopes 46, 577–581.

18.-Al-Masri,M.S., Suman, H. (2003). NORM waste in the oil and gas industry: theSyrian experience. Journal of Radio analytical and Nuclear Chemistry 256, 159-162.

19.-Omar M, Ali HM, Abu MP (2004) Distribution of radium in oil and gas industry wastes from Malaysia. Appl.Radiat Isot 60:779–782.

20.-Godoy, J.M., Crux, R.P. (2003). ^{226}Ra and ^{228}Ra in scale and sludge samples and their correlation with the chemical composition. Journal of Environmental Radioactivity 70, 199-206.

21.-Gazineu M.H.P., Hazin C.A., (2008). Radium and potassium-40 in solid wastes from the oil industry. Applied Radiation and Isotopes 66, 90–94.

22.- Australian Petroleum Production & Exploration Association Limited (2002). Guidelines for Naturally Occurring Radioactive Materials, APPEA, Australia.

23.- IAEA, (1996). International Basic Safety Standards for Protection against Ionizing Radiation and for the Safety of Radiation Sources, Safety Series No. 115, IAEA, Vienna.

Heavy mineral sand deposits and accumulation of radionuclides in foods

F.P. Carvalho, J.M. Oliveira, M. Malta

Laboratório de Protecção e Segurança Radiológica, Instituto Superior Técnico/ Universidade de Lisboa, Estrada Nacional 10, km 139, 2695-066 Bobadela LRS, Portugal
E-mail: carvalho@itn.pt

Abstract

Concerns with human exposure to ionizing radiation from radionuclides present in non-nuclear materials attracted attention to areas with high natural radioactivity and mining activities. We investigated several areas with heavy mineral sands deposits for determining the ambient radiation doses and the activity concentrations of radionuclides in raw sand and in segregated mineral fractions such as zircon, rutile, and ilmenite, as well as activity concentrations of radionuclides in food products from those areas. Although radionuclides from uranium and thorium series may be present in high activity concentrations, they are not mobile in the environment and are not absorbed and accumulated in aquatic biota and terrestrial plants. Therefore, in such areas radionuclide transfer by the food chain seems very limited. The exposure to ambient radiation, i.e., external radiation exposure, and radon inhalation are the main contributors to human exposure to radionuclides in heavy mineral sands.

Keywords: uranium residues; solubility of radionuclides; accumulation in aquatic biota; soil to plant transfer

Introduction

The production of zircon (Zr) and rare earth elements (REE) has been increasing worldwide to supply a growing demand of these elements for microelectronics and telecommunication industries (Jha, 2014). Those elements are often associated with naturally occurring radionuclides in heavy mineral sand deposits along coast lines around the globe, besides occurrence in other geological formations. The presence of naturally occurring radioactive elements originates a radiation exposure risk that is important to quantify in order to facilitate the adoption of safety and hygiene procedures to protect exploitation workers, members of local populations, non-human biota, and the environment in general (IAEA, 2006, 2007).

Currently, there is exploitation of heavy mineral sand deposits in coastal areas of countries in Asia, East and West Africa and South America. In many cases, the radiation protection regulations of countries are not updated to the point of including safety regulations adequate to the exploitation of naturally-occurring radioactive materials (NORMs) and thus radiation issues might be overlooked because of lack of scientific information.

In a preliminary study we analysed materials from two important coastal areas, Moma and Angoche on the Indian coast of Mozambique, both with extractive industries of heavy minerals from sand deposits. A preliminary assessment was made of naturally-occurring radioactive elements in heavy mineral sand deposits and environmental samples from these areas.

Materials and Methods

Sampling
The areas surveyed in the districts of Moma and Angoche, were visited and sampled jointly with inspectors of the Ministry of Mines of Mozambique and in collaboration with safety officers of the mining companies. In both areas radiation measurements were performed and samples collected for radioanalyses in the laboratory (Figure 1).

Measurement of ambient radiation doses were performed using a Thermo Scientific FH40 and a portable gamma spectrometer Flir, duly calibrated in a SSDL laboratory. Radiation dose surveys were carried out in the areas and triplicate radiation measurements were performed at specific spots, and recorded in conjunction with the GPS coordinates.

Figure 1.- Left: hydraulic separation plant of heavy minerals from coastal sand dunes at Angoche; Right: arrival of heavy minerals' wet concentrate at the magnetic separation plant in Moma coastal area.

Samples of soil materials, sand from coastal dunes, and segregated heavy mineral fractions as separated in the industrial facilities were collected into identified plastic bags. Later in the laboratory, these samples were dried in the oven at 60ºC to ensure standard drying, sieved through 63 µm Retsch sieves, and the fraction of grain size <63 µm retained for radioanalyses.

Radiometric analyses
Aliquots of the soil and sand samples were analysed by gamma spectrometry in the geometry of multi-source customized standards supplied by Eickert&Ziegler. Other aliquots were used for determination of alpha emitting radionuclides, by total dissolution with acids and microwave digestion, after addition of internal isotopic tracers according to analytical procedures described elsewhere (Carvalho et al., 2014b; Carvalho & Oliveira, 2009). Results are reported in Bq/kg dry weight (DW).

Results and Discussion

Ambient radiation doses measured over the sand dunes did not exceed 0.10 µSv/h and generally were below 0.8 µSv/h on the coastal dunes at Moma and Angoche. For comparison, the ambient radiation doses outside the coastal sand dune deposit, over clayey soils of the coastal plain in the Angoche area, were of 0.04 µSv/h and lower.

At the mineral separation plants (MSP) of both mining companies, in the area of minerals feed, the ambient radiation doses increased to about 2.5 µSv/h, and the highest radiation dose rates were measured by the piles of segregated minerals reaching about 4.80 µSv/h near the non-magnetic minerals pile and 2.05 µSv/h near the magnetic minerals fraction pile. The highest radiation dose rates were measured by the non-magnetic piles after extraction of silica, with 7.75 µSv/h. Elsewhere in the facilities, the external (ambient) radiation doses generally ranged between 0.10 and 3.10 µSv/h and radiation exposure at workplaces varied according to the location of work-post and accumulation of mineral dust nearby.

Analysis of radionuclides in the fine fractions (<63 µm) of all samples confirmed that they contain the three naturally-occurring radioactive series of uranium (^{238}U), actinium (^{235}U) and thorium (^{232}Th). Both in activity concentration and mass concentration, thorium series was much more

abundant than uranium and actinium series (Table 1). For example, in the unprocessed sand from dunes at Angoche, the thorium (^{232}Th) activity concentration was 122±9 Bq/kg (0.25±0.04 g/kg in mass concentration), while uranium (^{238}U) activity concentration was 40±1 Bq/kg (mass concentration of total uranium was 0.035±0.001g/kg).

It was interesting to observe that uranium and thorium elements were present in the same activity proportions in most fractions separated in the industrial process. In the final fraction, standard zircon,the uranium became more concentrated than thorium due to tight association with zirconium in the heavier oxides. Therefore, in the industrial facilities most of the external radiation dose above natural background that may be received by workers will be due mainly to exposure to uranium and thorium series radionuclides present in the heavy minerals.

In the industrial facilities, resuspension of ore particles creates a dusty atmosphere and workers may also inhale dust containing radionuclides. Radionuclides present in the fine fraction separated from sands were present in the concentrations shown in Table 1.

Table 1.Radionuclide concentrations (Bq/kg dry weight) in heavy mineral sand materials from coastal deposits in Mozambique.

Sample description	Site	^{238}U	^{230}Th	^{226}Ra	^{232}Th
Sand dune-top layer	Angoche #5	40 ± 1	39 ± 3	28 ± 2	122 ± 9
Sand dune-rich layer	Angoche #1	428 ± 16	326 ±48	324 ± 49	1001 ± 146
Rejected sand waste	Angoche #2	29 ± 2	18 ± 2	24 ± 2	23 ± 2
Wet mineral concentrate	Angoche #6	727 ± 22	904 ± 94	936 ± 110	3233 ± 331
Non-magnetic fraction	Angoche #8	2729 ± 83	330 ± 22	415 ± 42	1593 ± 103
Sand dune-top layer	Moma #1	9.3 ± 0.9	6.5± 0.5	7.5 ± 0.6	20 ± 1
Wet mineral concentrate	Moma #2	605 ± 22	356 ± 30	353 ± 34	1380 ± 114
Magnetic fraction	Moma #5	179 ± 5	151 ± 12	147 ± 13	846 ± 62
Non-magnetic fraction	Moma #4	1560 ± 48	1225 ± 283	1076 ± 254	4513 ± 1040
Standard zircon	Moma #11	1057 ± 30	898 ± 168	800 ± 152	221 ± 43

From the ambient radiation dose measurements made and reported above, there is a clear indication that at some working areas, especially those of storage of segregated metals, the occupational exposure to external radiation is high.

No air sampling and analysis of inhalable dust were performed. However, estimates can be made. In the dusty atmosphere of heavy minerals segregation, dust may reach 10 mg/m^3 in the air. Applying the radionuclide concentration determined for ^{210}Po, 2632±143 Bq/kg, the annual dose from inhaled dust may exceed 0.1 mSv/y. Inadvertent ingestion of dust may give rise to a similar dose from ingested radionuclides. Inhalation and ingestion will add to the radiation dose from exposure to external radiation.

While in the area outside facilities the ambient radiation dose would account for 350 μSv per year, (external radiation dose from natural background), in the average working conditions with an exposure of 1.5 μSv/h a factory worker may receive a dose of 3 mSv/y from external exposure plus 0.2 mSv/y from inhalation and ingestion. In areas with the highest radiation dose rates, e.g. by the mineral piles, the external radiation dose may reach 15.5 mSv/y for 2000 hours exposure. These

exposures would largely exceed the radiation dose limit above background for the non-radiation workers, adopted at1 mSv/year.

These results indicate that the operation of these heavy mineral sands exploitation industries involve occupational radiological risks. The hiring of a radiation protection officer and application of radiation protection methodologies should be mandatory and the protection measures should be inspected by radiation protection authorities according to the international safety standards (IAEA, 2014).

According to the International Basic Safety Standards for radiation protection of workers, the dose limit for radiation exposure added to radiation background by practices should not exceed 1 mSv/y, otherwise the facilities should be classified as radiation facilities and a radiation monitoring and radiation protection programme must be implemented (IAEA2006, 2007, 2014). Areas with higher radiation doses must be identified and monitored and safety and hygiene of workplaces must be managed to abate radiation doses. In particular, frequent cleaning for removal of accumulated dust and minerals in facilities will contribute to reduce radiation exposure. Due to the presence of dust in all areas of the factory, the use of respiratory protective gear must be enforced all times.

Several environmental pathways do exist around the factories that may transfer radionuclides from segregated heavy minerals to members of the public, such as water, suspended dust, and agriculture products (particularly leafy vegetables) and coastal fish (IAEA, 2014; Carvalho et al., 2014a).

Table 2. *Radionuclide concentrations (Bq/kg dry weight) in several foods from Angoche area.*

Designation	^{238}U	^{234}U	^{230}Th	^{226}Ra	^{232}Th
Dry marine fish	0.77 ± 0.05	0.83 ± 0.05	0.6 ± 0.1	2.5 ± 0.1	1.5 ± 0.2
Peanuts	0.033 ± 0.004	0.030 ± 0.004	0.14 ± 0.02	0.23 ± 0.01	0.14 ± 0.02
Manioc	0.009 ± 0.001	0.008 ± 0.001	0.48 ± 0.06	0.24 ± 0.03	0.41 ± 0.05
Sweet potato	0.052 ± 0.007	0.039 ± 0.006	0.6 ± 0.1	2.3 ± 0.2	0.25 ± 0.06

Results of analyses of samples collected in the area of Angoche town are presented in Table 2. The concentrations of ^{232}Th in these foods were significantly higher than the concentrations of ^{238}U, in line with the proportions of the same radionuclides in dust particles from the sand dunes. As thorium is an element much less taken up from soils by plants than radium and uranium, these results suggest that there is contamination of these aliments by atmospheric deposition of dust particles. Indeed, in the area it is a common procedure to sun dry sea foods in open air. Agriculture products, such as manioc and sweet potato with a close contact with soil particles, may carry contaminant particles if not properly washed. Regarding internal contamination of food products through root uptake, the uranium is always much less concentrated in plants than thorium, and radium (226Ra) concentrations are generally the highest among these radionuclides such as commonly observed in agriculture products around the world (Fesenko et al., 2014). Notwithstanding, the concentrations of these radionuclides in foods are comparable to concentrations of radionuclides in areas of slightly elevated natural radioactivity as, for example, in the uranium mining district of Sabugal in Portugal (Carvalho et al, 2016).

Conclusions

Thorium and uranium radioelements are associated with heavy mineral fractions in the coastal dune deposits of Mozambique, currently mined for zirconium and rare earth elements. On unmodified coastal sand dunes the averageradiation background displays normal radiation dose values, comparable to many other regions around the globe. However, in the areas of industrial facilities with the segregation of heavy mineral fractions, uranium and thorium also become concentrated and radiation doses are enhanced. At some workplaces, the external radiation doses may reach and exceed annual radiation dose limits adopted internationally. Occupational radiological risks associated with inhalation of dust and ingestion of dust particles are present and do not seem negligible. Therefore, application of the radiation protection basic safety standards is needed at workplaces in these industries. Concerning the risk to members of the population not occupationally exposed, there is the potential exposureto fine dust particles transported by the wind, although not quantified yet. Regarding the pathway of radionuclide ingestion through contaminated food, there is no clear evidence that radionuclides from the heavy mineral sands are concentrated by the agriculture and fishery products. A more extensive work should however be carried out in the area.

References

Carvalho F. P., Chambers, D., Fesenko, S., Moore, W.S., Porcelli, D., Vandenhov, E, H., Yan Kovich T., 2014a. Radium Environmental Pathways and Corresponding Models, in: The Environmental Behaviour of Radium: Revised Edition. Technical Reports Series No. 476, IAEA, Vienna, pp. 106 – 172.

Carvalho, F.P., Matine, O.F., Taímo, S., Oliveira, J.M., Silva L. , Malta, M., 2014b. Radionuclides and radiation doses in heavy mineral sands and other mining operations in Mozambique. Radiat. Prot. Dosimetry Vol. 158 (2), 181–186.

Carvalho F. P., Oliveira J. M., 2009. Performance of alpha spectrometry in the analysis of uranium isotopes in environmental and nuclear materials. J. Radioanal. Nucl. Ch. 281, 591–596.

Carvalho F. P., Oliveira J. M., Malta M. (2016). Preliminary assessment of uranium mining legacy and environmental radioactivity levels in Sabugal region, Portugal. International Journal of Energy and Environmental Engineering,7:399–408. DOI 10.1007/s40095-016-0219-z

Fesenko S., Carvalho, F.P., Martin, P., Moore, W.S., Yankovich, T., 2014. Radium in the environment. In: The Environmental Behaviour of Radium: Revised Edition. Technical Reports Series No. 476, pp. 33-105. International Atomic Energy Agency. Vienna.

International Atomic Energy Agency, 2006. Assessing the Need for Radiation Protection Measures in Work Involving Minerals and Raw Materials. Safety Reports Series No. 49, IAEA,Vienna.

International Atomic Energy Agency, 2007. Radiation Protection and NORM Residue Management in the Zircon and Zirconia Industries. Safety Reports Series No. 51, IAEA, Vienna.

International Atomic Energy Agency, 2014. Radiation Protection and Safety of Radiation Sources, International Basic Safety Standards - GSR Part 3, IAEA, Vienna.

Jha, A.R., 2014. Rare Earth Materials. Properties and applications. CRC Press

G – EMERGING ISSUES
Hot- Particles,
New radionuclides,
New technologies)

Particles as concentrated sources related to uptake and radiological dose in mammals

Mathew P. Johansen[1], Emily Caffrey[2], David P. Child[1], Richard Collins[3], Michael A.C. Hotchkis[1], Nicholas Howell[1], Timothy E. Payne[1], Atsushi Ikeda-Ohno[4], Lida Mokhber-Shahin[1]

[1] Australian Nuclear Science and Technology Organisation, Kirrawee, Australia Mathew.johansen@ansto.gov.au
[2] Oregon State University, Oregon, United States
[3] University of New South Wales, Sydney, Australia
[4] Helmholtz-Zentrum Dresden-Rossendorf, Dresden, Germany

Abstract

The radiological residues at the former weapons testing sites in Australia, at Maralinga, Emu and the Montebello Islands, often occur in particulate form ("hot particles"). The physical and chemical characteristics of these particles affect their mobility and availability for uptake into living organisms. At the Taranaki site, Maralinga, substantial body burdens of Pu were observed in mammals, likely due to the presence of respirable particles. However, larger-than respirable particles (e.g. > 7 µm) are also present and, due to the fact that they are in a less bioavailable form, dampen the effectiveness of Pu uptake such that the use of standard reference concentration ratios (CRs) would over-predict animal Pu body burdens.

For respirable-sized Pu-containing particles that can be inhaled and lodged in the lung, most of the alpha emissions escape the particle and are deposited in the surrounding tissue. For larger particle, which typically do not lodge in the lung but could be ingested, most of the alpha emissions do not escape the particle, but are instead captured within it (self-shielding). The type of emission is also important when considering dose rates from particles. We compared dose rates from particle vs. homogeneous sources (using the same tissue volume) and results indicate decreased dose rates for the particles, with small decreases for particles containing gamma emitters and substantial decreases for particles containing beta or alpha emitters.

Introduction

The radiological residues at the former weapons testing sites in Australia (Figure 1) often occur in particulate form ("hot particles"). Large numbers of these particles were emitted from nuclear test detonations and non-nuclear tests during the 1950s and 1960s. For example, autoradiography images on a composite soil sample suggests the presence of more than 3000 readily-identifiable particles per square meter, within a plume that extends for tens of kilometres, at the Taranaki site, Maralinga, Australia. A portion of these particles are of a size that is respirable by mammals (<0.7 µm).

The particles that are larger than respirable (<0.7 µm) can degrade/weather slowly over time, and thus can provide persistent sources of more biologically-available forms of radionuclides, for many thousands of years. The rates of this weathering, and thus the availability for uptake of radionuclides into living organisms, are largely determined by the physical and chemical characteristics of the particles (Lind et al., 2005; Salbu, 2001). Our study aims to better quantify particle characteristics related to radiological uptake by living organisms and explore particle effects on the resulting dose rates to mammals.
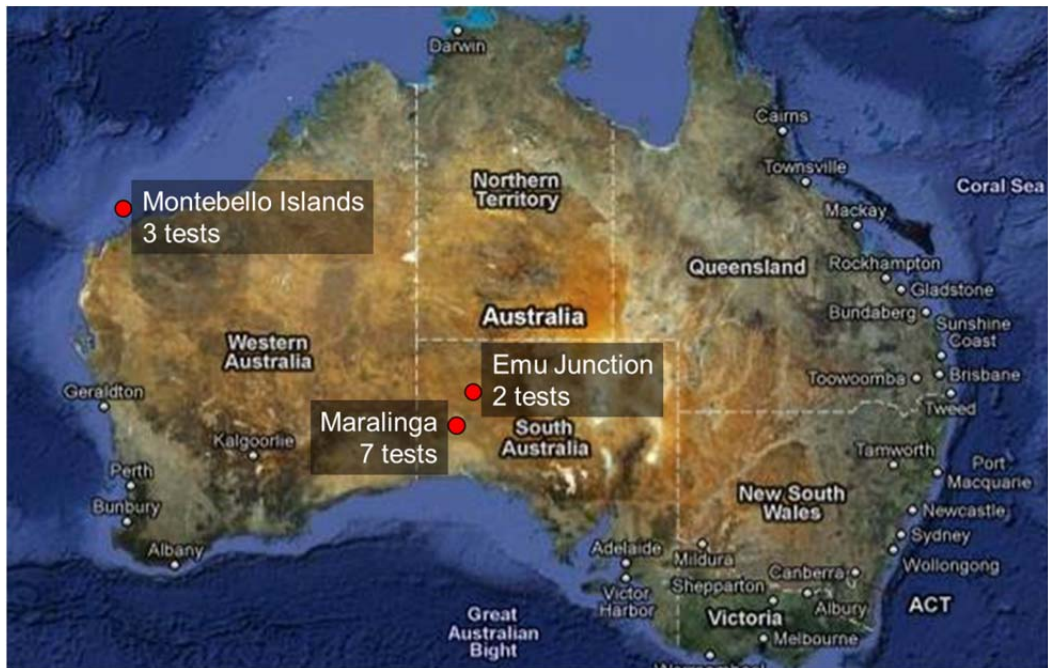
Figure 1. *Former weapons testing sites in Australia where twelve nuclear detonations were performed 1952-1957*

Materials and Methods

We have gathered a series of soil samples containing particles from the former Maralinga, Emu and the Montebello Island locations (Figure 1) where twelve major nuclear detonation tests took place, as well as where non-nuclear (e.g. high explosive) tests were conducted (e.g. Taranaki tests, Maralinga, Figure 2)(Child and Hotchkis, 2013; MARTAC, 2003).

It has now been more than fifty years since the initial formation and release of the particles. During this time, the particles, particularly their surfaces, may have been altered through interactions with the environment (e.g. infiltrated rainwater, physical disturbance by wind, water, and biological organisms) (Johansen et al., 2014).

To investigate their potential weathering and environmental behaviours, the particles are first isolated through repeated gamma counting on split soil samples to separate a small quantity (~5g) of soil that contains particles.The soil is then spread thinly over a plate and subjected to photostimulated luminescence (PSL) autoradiography from which an image is created (Figure 3). Individual particles can be identified and separated by placing an image transparency over the actual soil sample (Figure 4a and 4b).

Depending on the type of test release event, the particles may be large enough to be readily seen through a standard microscope and are relatively easy to manipulate using pipettes and micro-tools. The separated particles are evaluated using a range of methods including gamma spectrometry, PSL autoradiography, Accelerator Mass Spectrometry (AMS), PIXE, SEM-EDX, leaching studies, and synchrotron X-ray fluorescence microscopy(Ikeda-Ohno et al., 2016).
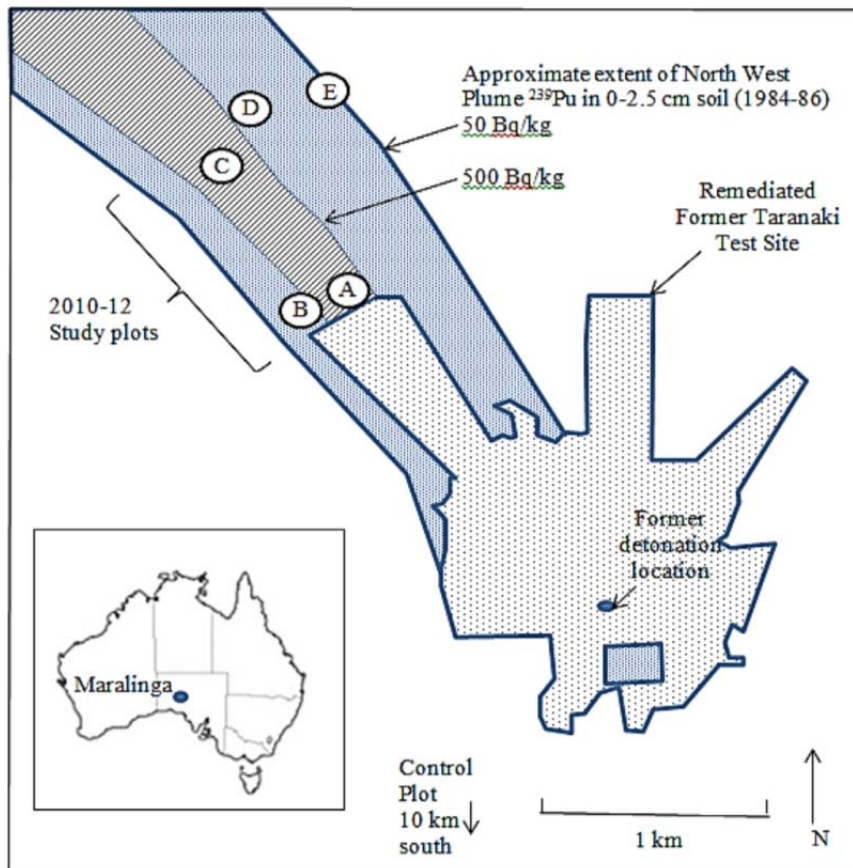
Figure 2. *Study plots within the northwest plume relative to the remediated former Taranaki Test Site, Maralinga, South Australia, where non-nuclear tests were performed 1961-1963(Johansen et al., 2014)*
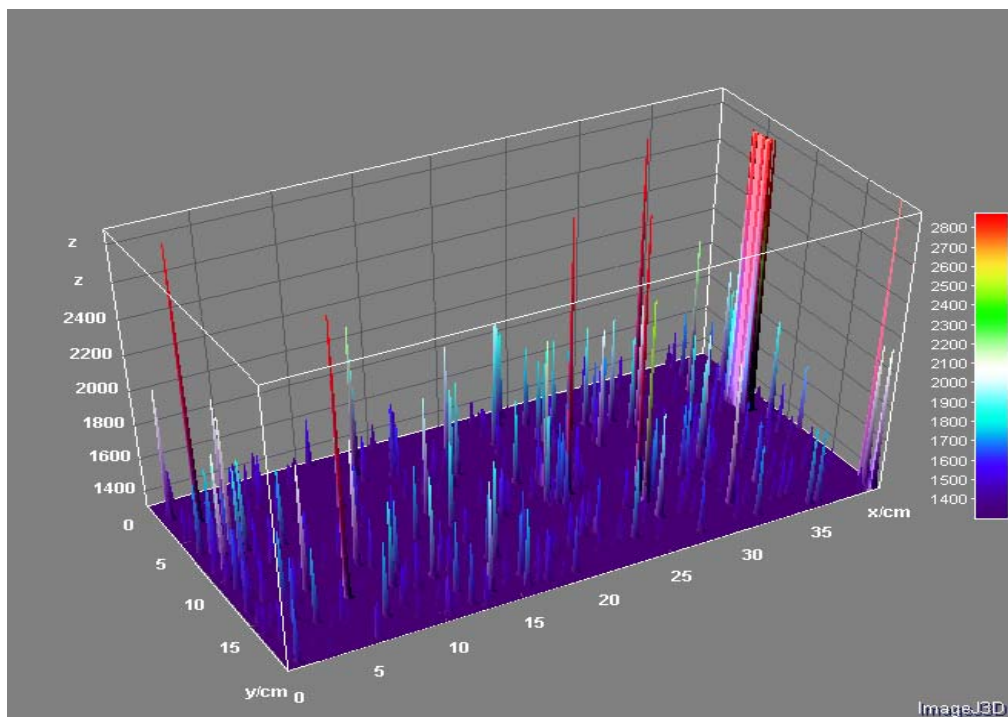
Figure 3. *Image from photostimulated luminescence (PSL) autoradiography of a typical soil sample of 5 g from the Taranaki, Maralinga site. The measurement bar is of relative intensity and generally reflects relative activities of the particles present*
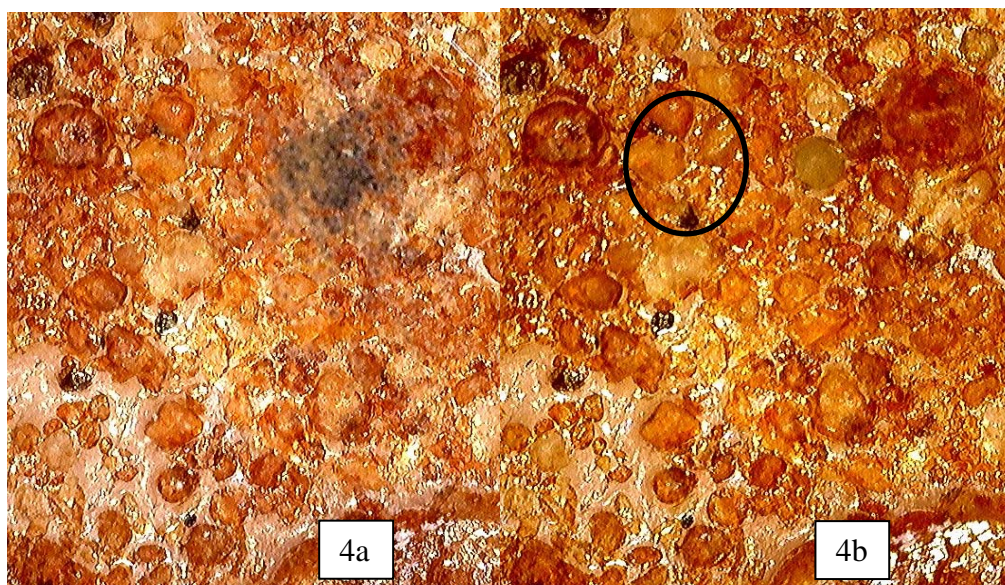
Figure 4. Example identification of a particle within the host soil, using(4a)a transparency copy of a PSL autoradiography image which includes the location of recorded energy emissions (dark circular pattern).The transparency is removed (4b) revealing the particle underneath (in this case a spherical particle of slightly green hue)

Results and Discussion

During investigation of the Taranaki, Maralinga site, it became apparent that the soil-to-animal uptake ratios (whole-organism Concentration Ratios, $CR_{wo-soil}$) were not consistent among rabbits captured from various plots within the plume, but rather indicated a distinct spatial pattern which appears to relate to the physical form of the Pu.

While the activity concentrations of Pu within rabbits was highest at plot A (Figure 1), which is closest to the test detonation location and has the highest soil activity concentrations, the effectiveness of transfer from soil-to-animal, as measured by $CR_{wo-soil}$values was lowest at this location. At plots located further awayin more marginal areas of the plume, the $CR_{wo-soil}$ values increased,approximately linearly, by three orders of magnitude (as measured between Plot A and the control site ten kilometres distant).

Similar uptake patterns have been observed at Nevada Test Site, USA(Gilbert et al., 1988), and Semipalatinsk, Kazakhstan (this conference). The most likely explanation is the increased density of larger unrespirable (e.g. >7µm), low-solubility particles at areas closer to the test detonation locations. Such particles contribute to the soil concentration in the denominator of the $CR_{wo-soil}$ calculation, but make a limited contribution to the numerator as they are not readily respired or absorbed. This effect dampens the effectiveness of Pu uptake such that the use of standard reference $CR_{wo-soil}$values would over-predict animal Pu body burdens where such particles are present (see (for further discussion, see Johansen et al., 2016; Johansen et al., 2014).
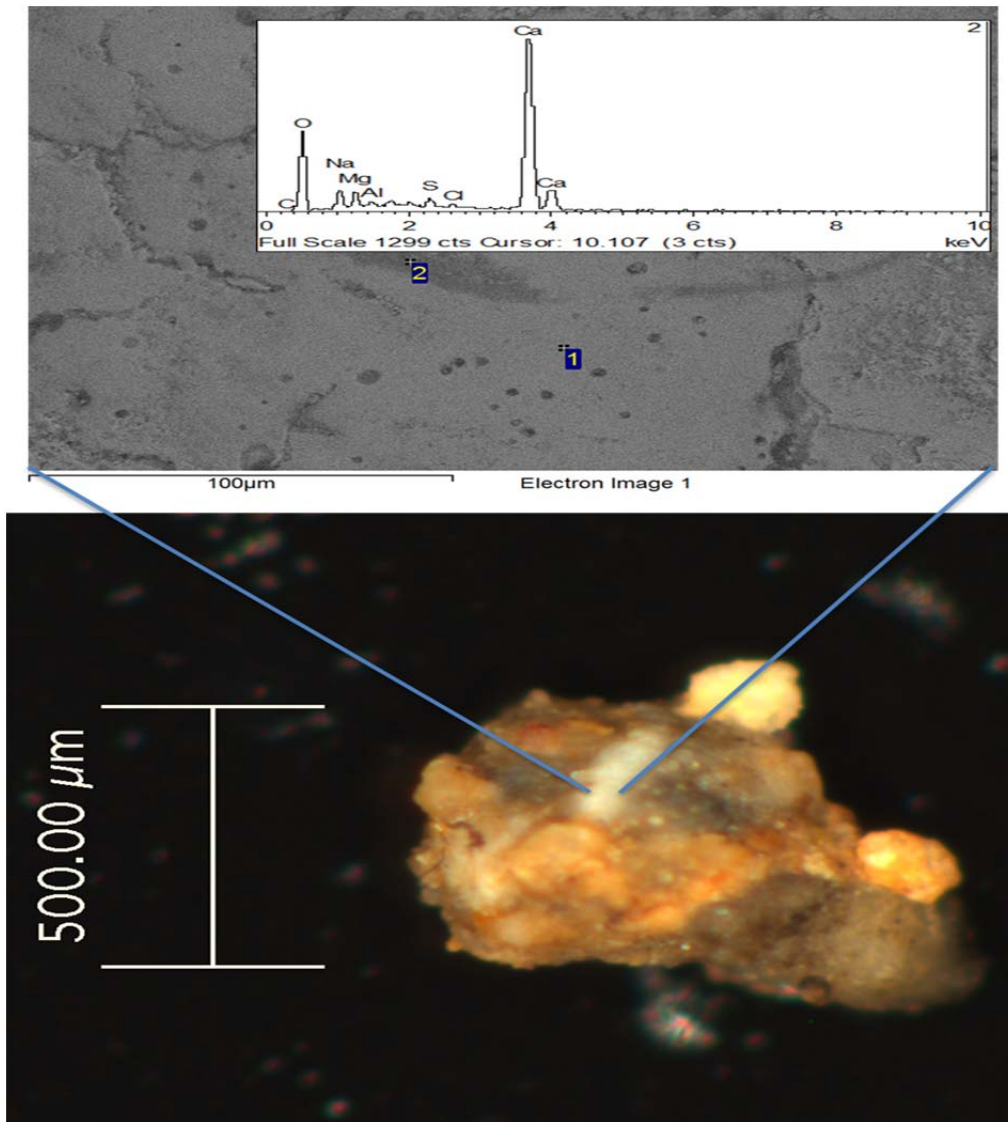
Figure 5. *Example SEM-EDX interrogation of the outer surface of a large particle indicating, in this instance, calcium and other light elements being dominant*

When considering potential absorption of radionuclides from an ingested or inhaled particle, of interest is the composition at, and near, the particle surface. The exterior surfaces of the glassy particles from nuclear detonations were often dominated by silicon, calcium, and other light elements as elucidated using SEM-EDX (Figure 5).A clear core-shell structure is sometimes evident in these particle (e.g. from Emu site, Figure 6).A core-shell structure is also indicated by XFM data on a particle from the non-nuclear testing at Taranaki, Maralinga(Figure 7)(Ikeda-Ohno et al., 2016).

Such core-shell structures have important implications as it is their external surface that interacts with the environment, or in the case of inhalation or ingestion, with potential lung or gastrointestinal tissues and fluids. In one glassy fission fragment from Maralinga, the ^{137}Cs was clustered on the exterior (more available for environmental interaction), while, in the same fragment, the ^{90}Sr occurred mainly in the interior (less available for environmental interaction and weathering processes). This structure also suggests the beta emissions from the ^{90}Sr may be largely self-shielded within the particle.
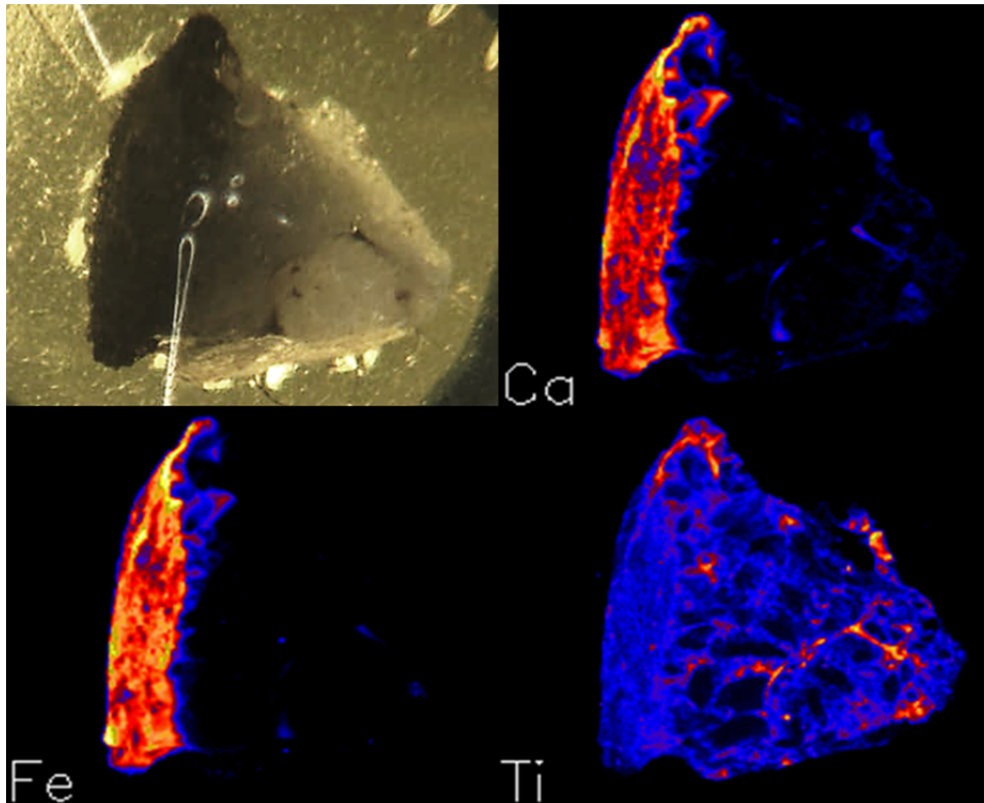
Figure 6. *Example of a particle fragment from the Emu detonation site in which the outer shell (to the left) is dominated by calcium and iron, while the titanium is spread throughout.*
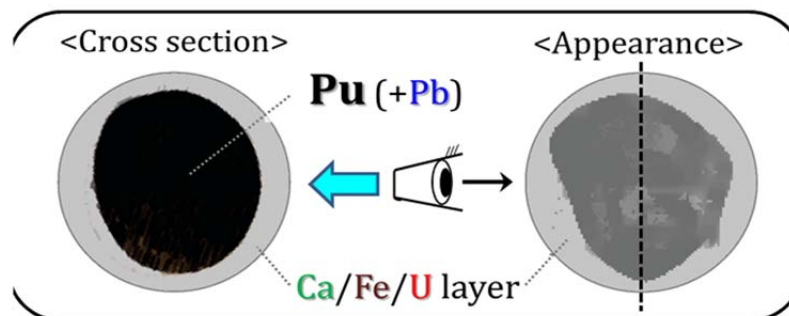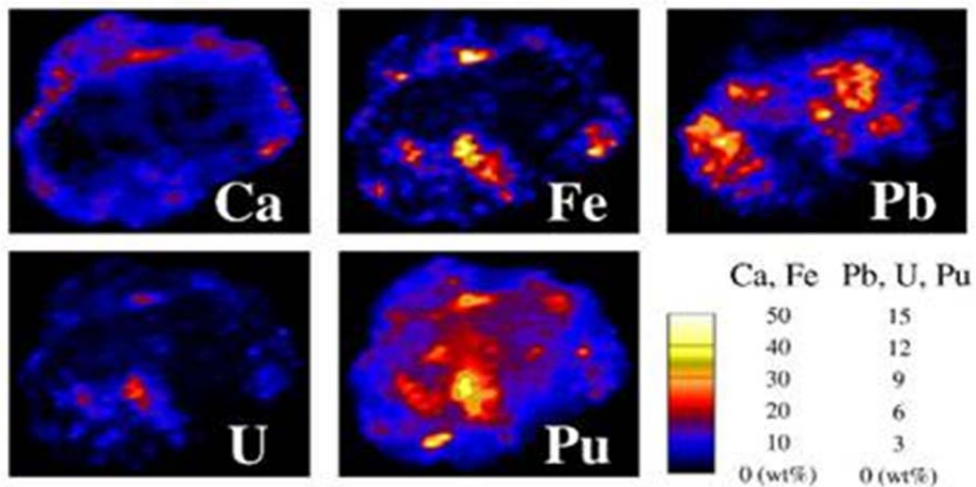
Figure 7. *Synchrotron XFM data suggesting a core-shell structure within a particle from the non-nuclear testing at Taranaki, Maralinga(image from Ikeda-Ohno et al., 2016)*

Such self-shielding has implications for radiological exposure. Figure 8 provides modelling results which estimate the percentage of alpha emission energy that is deposited within a Pu-containing particle (self-shielding), vs that deposited in surrounding tissue. The percentage deposited in tissue is highest for smaller particles of the respirable range (e.g. <0.7 µm) and the 50/50 percentage happens to occur at the ~3 µm diameter size. In this model, it was assumed that the Pu was distributed homogenously within the particle. However, for particles that have most Pu/U in the interior of a core-shell type structure (e.g. Figure 6), the percentage escaping to the surrounding tissue will be less and will be further influenced by the densities of the elements located in the shell (yet to be modelled).

These model results suggest that it is when the particles are of respirable sizes(e.g. <0.7 µm), or when the Pu exists on exterior surfaces, that a hot particle that has been internalised (e.g. lodged in a mammalian lung) may produce relatively intense dose rates to adjacent tissues, as well as providing an ongoing source available for absorption into the body.

This self-shielding discussed above is one factor to be considered when comparing dose rates to an organ (e.g. lung). Another factor is the effect of radionuclide being concentrated in a single particle (essentially a point source) vs. the equivalent amount that is homogenously distributed, as is assumed for organisms in the ERICA-Tool. We compared particle vs. homogeneous sources for an example organ (rabbit lung) using the MCNP6 computer code and results indicate decreased dose rates for particles, with small decreases for particles containing gamma emitters and substantial decreases for particles containing beta or alpha emitters (Caffrey et al., 2016; Caffrey et al., 2015).
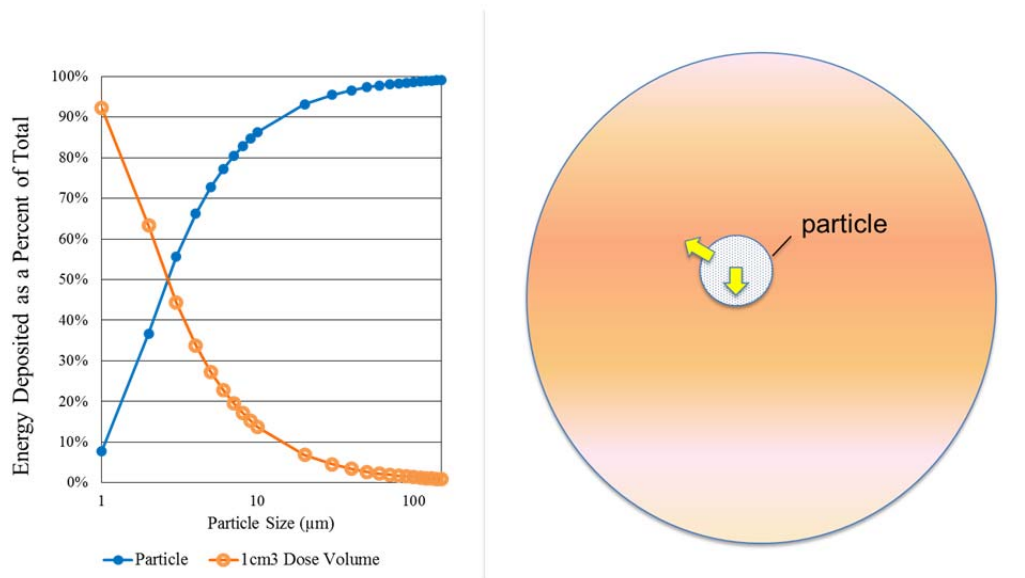
Figure 8. MCNP6 model data indicating percentage of alpha emission energy that is deposited within a Pu-containing particle (blue symbols), vs that deposited in surrounding tissue (orange symbols)(adapted fromCaffrey et al., 2016)

Conclusions

The radiological residues at the former weapons testing sites in Australia, at Maralinga, Emu and the Montebello Islands, often occur in particulate form. The physical and chemical characteristics of these particles affect their mobility and availability for uptake into living organisms. At the Taranaki site, Maralinga, substantial body burdens of Pu were observed in mammals, likely due to the presence of respirable particles. However, larger-than respirable particles (e.g. > 7 µm) are also present, and due to the fact that they are in a less bioavailable form, dampen the effectiveness of Pu uptake such that the use of standard reference concentration ratios (CRs) would over-predict animal Pu body burdens. Modelling results suggest that for respirable-sized Pu-containing particles (that can be inhaled and lodged in the lung), most of the alpha emissions escape the particle and are deposited in the surrounding tissue. For larger particles, (e.g. >7 µm), which typically do not lodge in the lung but could be ingested, most of the alpha emissions do not

escape the particle, but are instead captured within the particle itself (self-shielding).The type of emission is also important when considering dose rates from particles. We compared dose rates from particle vs. homogeneous sources (using the same tissue volume) and results indicate decreased dose rates for the particles, with small decreases for particles containing gamma emitters and substantial decreases for particles containing beta and alpha emitters.

References

Caffrey, E.A., Johansen, M., Higley, K., 2016. Comparison of Homogeneous and Particulate Lung Dose Rates for Small Mammals. Health Phys.

Caffrey, E.A., Johansen, M.P., Higley, K.A., 2015. Organ Dose-Rate Calculations for Small Mammals at Maralinga, the Nevada Test Site, Hanford and Fukushima: A Comparison of Ellipsoidal and Voxelized Dosimetric Methodologies. Radiat Res 184, 433-441.

Child, D.P., Hotchkis, M.A.C., 2013. Plutonium and uranium contamination in soils from former nuclear weapon test sites in Australia. Nuclear Instruments and Methods in Physics Research Section B: Beam Interactions with Materials and Atoms 294, 642-646.

Gilbert, R.O., Shinn, J.H., Essington, E.H., Tamura, T., Romney, E.M., Moor, K.S., O'Farrell, T.P., 1988. Radionuclide Transport From Soil to Air, Native Vegetation, Kangaroo Rats and Grazing Cattle on the Nevada Test Site. Health Phys. 55, 869-887.

Ikeda-Ohno, A., Shahin, L.M., Howard, D.L., Collins, R.N., Payne, T.E., Johansen, M.P., 2016. Fate of Plutonium at a Former Nuclear Testing Site in Australia. Environ. Sci. Technol. 50, 9098-9104.

Johansen, M.P., Child, D.P., Caffrey, E.A., Davis, E., Harrison, J.J., Hotchkis, M.A.C., Payne, T.E., Ikeda-Ohno, A., Thiruvoth, S., Twining, J.R., Beresford, N.A., 2016. Accumulation of plutonium in mammalian wildlife tissues following dispersal by accidental-release tests. J. Environ. Radioact. 151, Part 2, 387-394.

Johansen, M.P., Child, D.P., Davis, E., Doering, C., Harrison, J.J., Hotchkis, M.A., Payne, T.E., Thiruvoth, S., Twining, J.R., Wood, M.D., 2014. Plutonium in wildlife and soils at the Maralinga legacy site: persistence over decadal time scales. J. Environ. Radioact. 131, 72-80.

Lind, O.C., Salbu, B., Janssens, K., Proost, K., Dahlgaard, H., 2005. Characterization of uranium and plutonium containing particles originating from the nuclear weapons accident in Thule, Greenland, 1968. J Environ Radioact 81, 21-32.

MARTAC, 2003. Rehabilitation of the former nuclear test sites at Emu and Maralinga (Australia). Commonwealth of Australia, Canberra, Australia

Salbu, B., 2001. Actinides associated with particles, in: Kudo, A. (Ed.), Plutonium in the Environment; Proceedings of the Second International Symposium. Elsevier, pp. 121-138.

Characterisation of radionuclides in uranium mine tailings with synchrotron-based hard x-ray microprobe techniques

Steve Mihok[1]*, Karina Lange[1], Antonio Lanzirotti[2], Julie Brown[1]

[1] Canadian Nuclear Safety Commission, P.O. Box 1046, Station B, 280 Slater Street, Ottawa, On, Canada, K1P 5S9
[2] Center for Advanced Radiation Sources, University of Chicago, Argonne, Illinois 60439, USA

Abstract

The ultimate disposal of uranium (U) mine tailings containing long-lived radionuclides requires information on their solid form and potential for environmental transfer over time. Synchrotron X-ray micro-spectroscopy techniques (SXRMS) are useful for addressing this issue as these methods are able to simultaneously characterize the micro-scale distribution of multiple elements, as well as their incorporation and association with mineral phases. A study was therefore initiated at the US DOE Advanced Photon Source to test the ability of SXRMS to characterize the distribution and forms of U in tailings, with some exploratory work also done on thorium and radium. Tailings at different depths were obtained from the JEB pit at the McClean Lake mine in Canada. Mapping of uranium distribution by µXRF (X-ray fluorescence) showed that U was spatially dispersed and not just localized in high U particulates. Initial characterization of mineralogy in localized particles with high U by µXRD (X-ray diffraction) did not identify the presence of distinct, crystalline U minerals. The µXRD analyses showed that tailings contained abundant illite, hematite and gypsum. Uranium L3 XANES results (µX-ray absorption near edge spectroscopy) indicated that U was dominantly in the hexavalent state. Our preliminary work has shown that synchrotron applications can provide unique insights into the geochemistry and mineralogy of uranium in tailings. These findings can provide solid lines of evidence to inform long-term management strategies, and to support regulatory licensing decisions on the decommissioning and remediation of operating and legacy uranium mines in Canada.

Introduction

The management of uranium (U) mine tailings containing long-lived radionuclides requires information on their potential for environmental transfer. Synchrotron X-ray micro-spectroscopy techniques (SXRMS) can inform geochemical and mineralogical models used to predict contaminant behavior (Lanzirotti et al., 2016), but have not yet been applied to the study of U series radionuclides in tailings. These methods are able to simultaneously characterize the micro-scale distribution of multiple elements, as well as their incorporation and association with mineral phases. Here we report initial results from research by the Canadian Nuclear Safety Commission (CNSC) at the United States Department of Energy Advanced Photon Source (APS) exploring SXRMS for characterizing the distribution and forms of U and its key daughters in tailings (CNSC, 2016).

Materials and Methods

Uranium mill tailings were obtained from borehole samples of the Tailings Management Facility (TMF) at the McClean Lake mine in Saskatchewan, Canada in 2008; the TMF was constructed in a mined-out open pit called the JEB pit. Tailings solids from TMF elevations of 369 masl and 400 masl (with 369 representing the older tailings) were mixed with epoxy, mounted to quartz glass slides and doubly polished to a thickness of 30-60 microns. Our samples contained 41 to 649 ppm

---

* Corresponding author, E-mail:steve.mihok@canada.ca, smihok@bell.net

U (μg/g) in solids, data for thorium (Th) and radium (Ra) were unavailable. Associated porewater contained median concentrations of 5,692 μg/L natural U (equivalent to 70.3 Bq/L U-238 by specific activity), 3.2 Bq/L Ra-226, and 1.0 Bq/L Th-230 (AREVA, 2015). Samples were analyzed at the GSECARS beamline 13-ID-E at the APS, Argonne National Laboratory, Illinois (general methods in Lanzirotti et al. (2016), detailed methods in CNSC (2016)). High-resolution μXRF maps (1.5 x 1.5 mm) were examined for four samples (two at each depth) at incident beam energy of 19 keV. This was done by raster scanning continuously and bi-directionally with XRF energy dispersive spectra collected every 2 μm at 40 msec per pixel. Single point μXRD spectra (20 second exposure for a 2 μm beam spot) were then collected from 85 features of interest to evaluate if crystallographically distinct U bearing minerals were identifiable. These spectra were also used to explore whether U distribution was correlated with specific non-U mineral phases.

Representative areas (0.2 x 0.2 mm, 2 μm pixels) from the four large-scale maps showing contrasting features were also studied with coupled μXRD / μXRF (100 msec accumulation). Features of interest from all of these analyses were then examined by μXANES to unequivocally demonstrate the presence of U (n=31), Ra (n=11) or Th (n=4). Lastly, several particles with high and low U signatures were examined with μXAFS to evaluate both the oxidation state of uranium and to constrain potential molecular species. Analysis was conducted at the U L_3 edge, ~17166 eV by scanning from 17086-17156 eV in 5 eV steps, 17156-17179 eV in 0.25 eV steps and from 17179-17326 eV in 2 eV steps at 4 seconds per energy point. Uranium standards in the U^{6+} oxidation state measured under a similar configuration provide an E_0 of 17170.4 eV (Guo et al., 2016).

Results and Discussion

Detection of radionuclides by μXRF

Minimum detection limits (MDL) for U, Th and Ra (which have $L\alpha_1$ emission lines at 13.6, 13.0, and 12.3 keV respectively) were expected to be ~ 1-5 ppm for 300 msec accumulation time. These limits are based on calibration of our methods for Pb and U with NIST XRF thin film standards SRM1832 and 1833, and NBS uranium glasses K-0373, K-0375, and K-0546. In four representative XRF maps (Fig. 1), U was present at ~ 150 to 400 ppm, in agreement with ICP-MS analysis of solids (AREVA, 2015). Strong X-ray fluorescence K lines from Fe, Ni, As, and L lines from Pb were found in most samples (note log scale, Fig. 1). Other common K-lines were K, Ca, Ti, Cr, Mn, Cu, Zn, Rb and Sr. Other L-line emissions included U, Ba (overlap with Ti K), and Bi.

Uranium was detectable in all samples under our experimental conditions (U $L\alpha_1$ is separated from Rb Kα by only 218 eV). Attempts to detect Ra L emission were unsuccessful due to difficulties in resolving Ra emission lines from Pb, Bi, Zr and, at high Fe concentrations, the Fe K detector pileup (sum) peaks. Additional XRF maps were therefore generated by setting beam energy to bracket the Ra L3 and Ra L2 absorption edges for more sensitive evaluation of XRF fluorescence intensities for the Ra $L\alpha_1$ and $L\beta_1$ emission lines. Although likely present in sufficient quantities from porewater data (AREVA, 2015), detection of Ra L fluorescence was never confirmed with a reasonable effort. Further work would therefore not likely be informative in a uranium mine tailings matrix. Thorium fluorescence was also not detected in these samples, for similar reasons. The Th $L\alpha_1$ emission line strongly overlaps with the Lβ peaks of Pb and Bi, and includes overlaps with Fe Kα pileup peaks. The Th $L\beta_1$ peak suffers from fewer spectral overlaps, but the potential for detecting Th at the L2 edge was not fully explored since beam energies were kept below the Th L2 edge (19.693 keV). This could be tested with other tailings samples with higher amounts of Th.
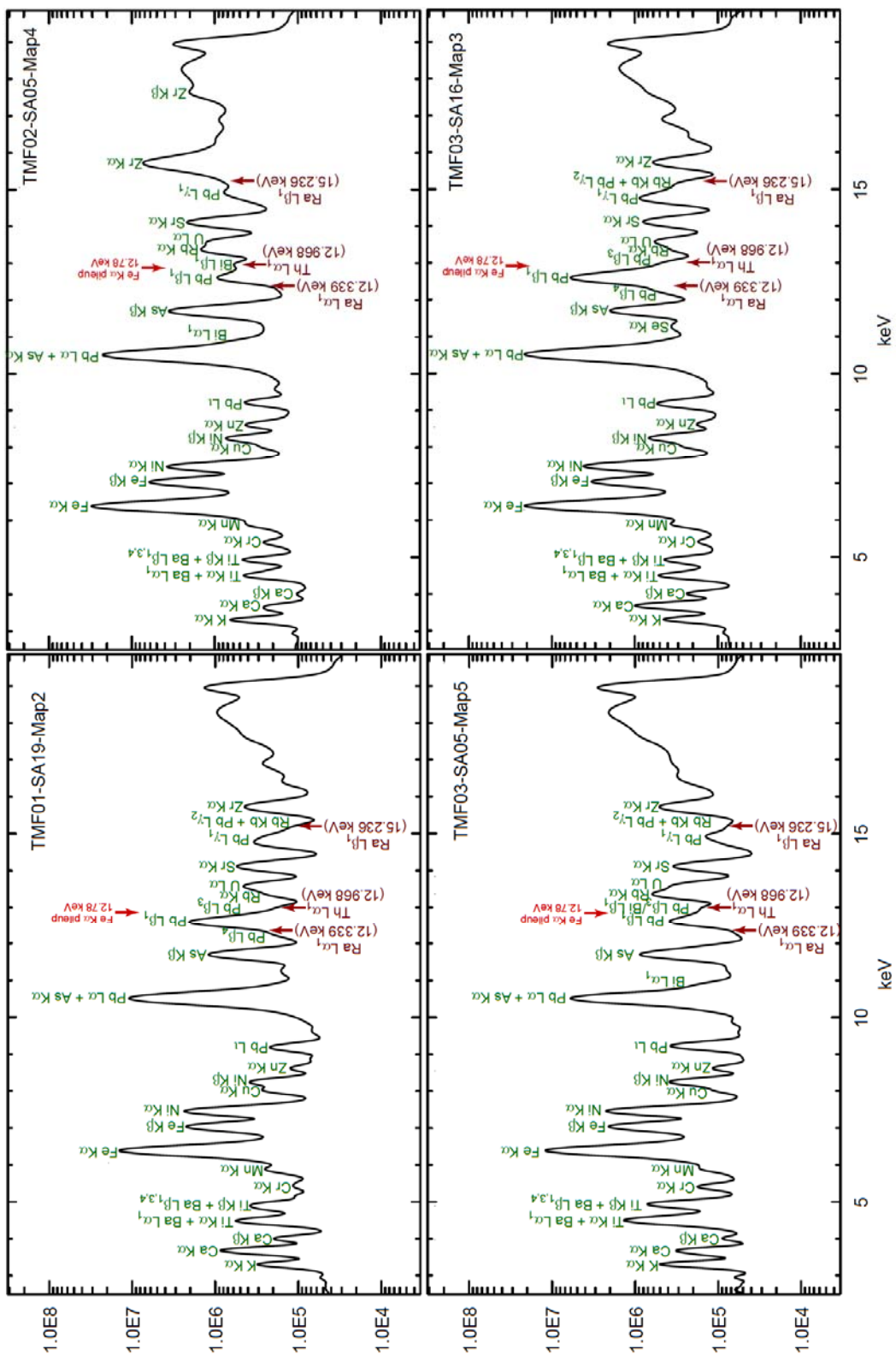
Figure 1. *Summed energy dispersive spectra from compositional maps of four samples from different boreholes and/or depths. These spectra represent roughly 0.2 x 0.2 mm areas extracted from the larger maps. Identified X-ray fluorescence emission lines are labeled. Where lines for Ra Lα₁, Ra Lβ₁, and Th Lα₁ could have been observed, they are in red. The energy at which the Fe Kα pileup peak would occur is also shown.*

Evaluation of U distribution and elemental associations by µXRF

Figure 2 shows binned fluorescence intensities for some common X-ray emission lines (Ni Kα, As Kβ, Pb Lβ₁ and U Lα₁) in grayscale maps for shallow (left panel) and deep tailings (right panel). Such maps can be used to visualize broad associations among elements. Here, the displayed counts are scaled so that the lowest 5% intensities are uniformly set to black and the highest 5% to white to avoid visualizing only very high concentrations. Scaling is defined relative to the counts for each element's X-ray emission, so maps cannot be used to interpret absolute differences in relationships between elements. Other data manipulations could nevertheless be used to explore/quantify associations, along with other data presentation approaches for visualization (e.g. colour coding of emission lines in one image).

In all four maps, K, Fe, As, Pb, Ni and U, were broadly distributed within particulates 100's of μm in size. These particulate masses were particularly well defined in TMF01-SA19-Map2 (Fig. 2 right panel) and to a lesser extent in TMF03-SA16-Map3 (not shown), the two samples with the highest U concentrations. Smaller particulates ten's of μm in diameter containing all these elements at higher concentration were also observed, along with small particulates enriched in Ca and Ti. Particles with high U abundance ten's of μm in size were common, e.g. with concentrations ten or more times higher than those observed in larger diffuse masses. Altogether, no clear elemental associations were visualized between U and other elements in this preliminary assessment. However, some spatially localized associations were found and could be further explored. For example in the map of TMF03-SA05-Map5 (not shown) an area of elevated Ti was associated with high U. The µXRD data collected for this area showed the presence of anatase (TiO_2) within the mineral and surrounding it, along with other minerals such as phengite (an As enriched area), hematite and illite.
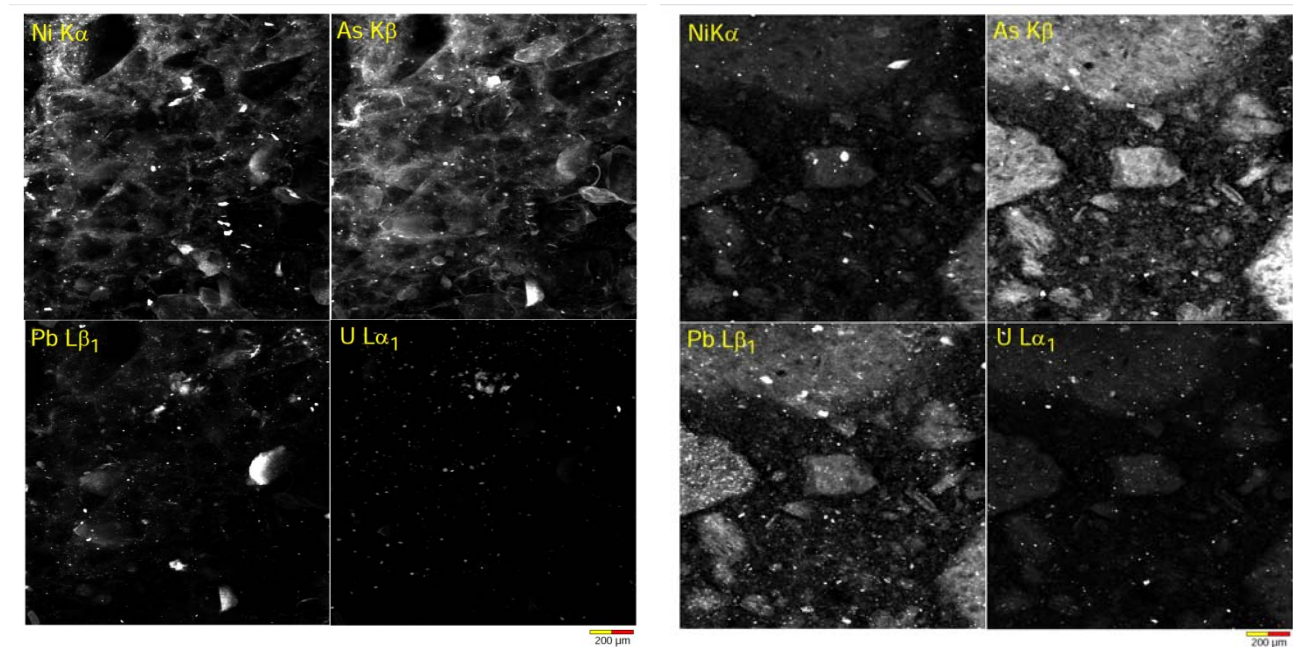
Figure 2. *X-ray fluorescence intensities from 1.5 x 1.5 mm compositional maps of section TMF02-SA05-Map4 (left panel, 400 masl) and TMF01-SA19-Map2 (right panel, 369 masl). Maps show Ni Kα, As Kβ, Pb Lβ₁ and U Lα₁ separately. All are displayed as two dimensional grayscales with white being the highest intensity, 40 msec accumulation time per 2 μm pixel.*

Constraints on sample mineralogy in relation to U distribution by µXRD

Our µXRD data indicated that all samples were dominated by three mineral phases, illite (with small structural variations), hematite, and gypsum. For example, Fig. 3 shows a matching µXRF map for TMF02-SA05-Map4 where Fe Kα, As Kβ and U Lα$_1$ are displayed simultaneously in red-green-blue (RGB) intensities rather than as simplified grayscale maps (Fig. 2, left panel). A small high U area analyzed by µXRD (Fig. 3 yellow arrow, Spot 58) is shown in the upper right panel (2θ vs intensity). Comparison of the µXRD pattern to reference illite shows that the only mineral identifiable by µXRD is this clay phase; illite was the most frequently identified mineral overall. In a similar RGB map for the large central particle in TMF01-SA19-Map2 (Fig. 2 right panel) a high U area was found to consist of a mixture of gypsum and illite. In both cases, no U bearing minerals were identified even though U concentrations were high. In some maps, µXRD of areas with high Fe showed the presence of hematite as the dominant mineral phase. Overall, of the 85 µXRD spectra collected, no distinct U minerals have been identified to date by diffraction. The lack of U-bearing minerals identifiable by µXRD does not preclude their presence, but implies that U is mostly bound or sorbed to other mineral phases, or that it exists as poorly crystalline or amorphous phases.
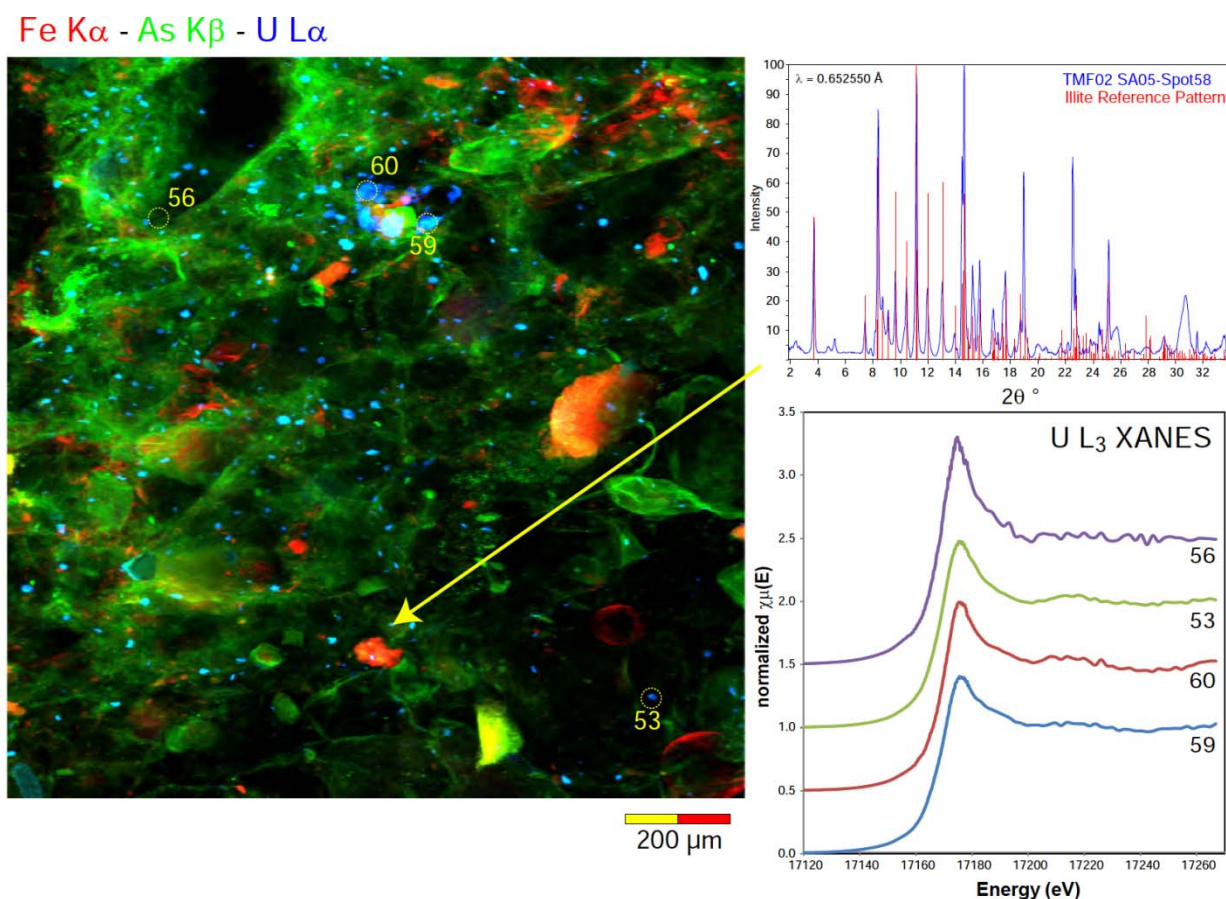
Figure 3. *Three color µXRF intensity map of Fe Kα (red), As Kβ (green) and U Lα$_1$ (blue) for sample TMF02-SA05-Map4. Yellow arrow shows where single point µXRD spectra were collected for Spot 58 with the integrated 2θ vs intensity plot shown in the upper right. Integrated diffraction pattern for this point is shown in blue. Reference pattern for illite is superimposed in red. Yellow numbered circles on the map show where U L3 µXANES spectra were collected. The measured, edge step normalized µXANES spectra are shown in the lower right. Edge positions are all consistent with U in the 6+ oxidation state.*

Constraints on U oxidation state and speciation by U L3 µXAFS

Uranium abundances were high enough, both in areas where U was diffusely distributed and in localized, high U particulates, to complete high quality U L_3 edge µXAFS. Spectra were examined to help define variations in U oxidation state, and more specifically to help characterize the potential long-term geochemical controls on U in tailings. Selected examples of the 31 spectra analyzed are shown for contrasting points of interest. For example, Figure 3 shows U XANES spectra from four points on map TMF02-SA05-Map4. The location of each point is shown with a dashed yellow circle. Data were collected from three points with high U (53, 59, 60) and one (56) with low U. Four additional spectra from a small fifth area of the same map are shown in Figure 4, again three from high U particles (1, 2, 3) and one with low U (spot 4). All eight spectra are essentially indistinguishable; and similar to other XANES spectra obtained for TMF03-SA16-Map3. The E_0 energies are all consistent with the presence of uranium in the U^{6+} oxidation state. They also show a distinct shoulder centered at 10 to 15 eV above the absorption maximum, often attributed to a multiple-scattering resonance within the linear O=U=O moiety. Figure 5 (left panel) shows an example of this shoulder in a uranyl acetate standard as compared to a uraninite standard (collected at beamline X26A, National Synchrotron Light Source, Brookhaven National Laboratory and adjusted to the energy calibration at 13-ID-E). This feature is less prominent in spot 56.

Such differences in the EXAFS portion of the spectra have been noted in other studies and may indicate that different U^{6+} species exist, or species with differing equatorial coordination. In a few cases, e.g. U associated with the anatase mineral in TMF03-SA05-Map5, we noticed differences in the EXAFS portions of spectra (Fig. 5, right panel). The E_0 energies of spectra were both consistent with U^{6+} in adjacent high and low U regions of this mineral particulate. However, variation in the shape of the EXAFS portion from XANES spectra obtained for some samples suggested that differences likely exist in the U species present. Altogether, our results are consistent with the presence of U mainly as a result of discharged process solutions, following efficient extraction of parent minerals, which are mainly U^{4+}. More XAFS analyses would be useful in terms of documenting minor U-phases to improve geochemical models for predicting the long-term stability of the U that remains in tailings. The large amount of SXRMS data collected here provides a useful resource for exploring the forms and relationships of various contaminants on a microscale in tailings from a modern operating U mine in Canada.

Other studies

These results for *in situ* tailings are generally consistent with our understanding of the nature of tailings as originally deposited from the McClean Lake Tailings Optimization and Validation Program (AREVA, 2015). Following U extraction by acid leach, the tailings consist of unreacted quartz and illite, with lesser amounts of kaolinite and chlorite. They are treated with ferric sulfate and barium chloride under specific pH and Eh conditions to control radium, arsenic and other metal concentrations in pore water. The final pH is adjusted to near neutral, then thickened to 30 to 50 percent solids by weight prior to being discharged. Several secondary mineral phases have been identified following treatment; they include gypsum, hydrobasaluminite, ferrihydrite and theophrasite. Elevated pore water concentrations of U in the older tailings have been hypothesized to occur in part due to the affinity for uranyl to form strong solution complexes with carbonate species. These species have increased in the tailings over time from the conversion of organic carbon (e.g. from kerosene, flocculants, and decay of phytoplankton and algae). However, to date we have not been able to demonstrate identifiable calcite in these tailing samples using *µXRD*.
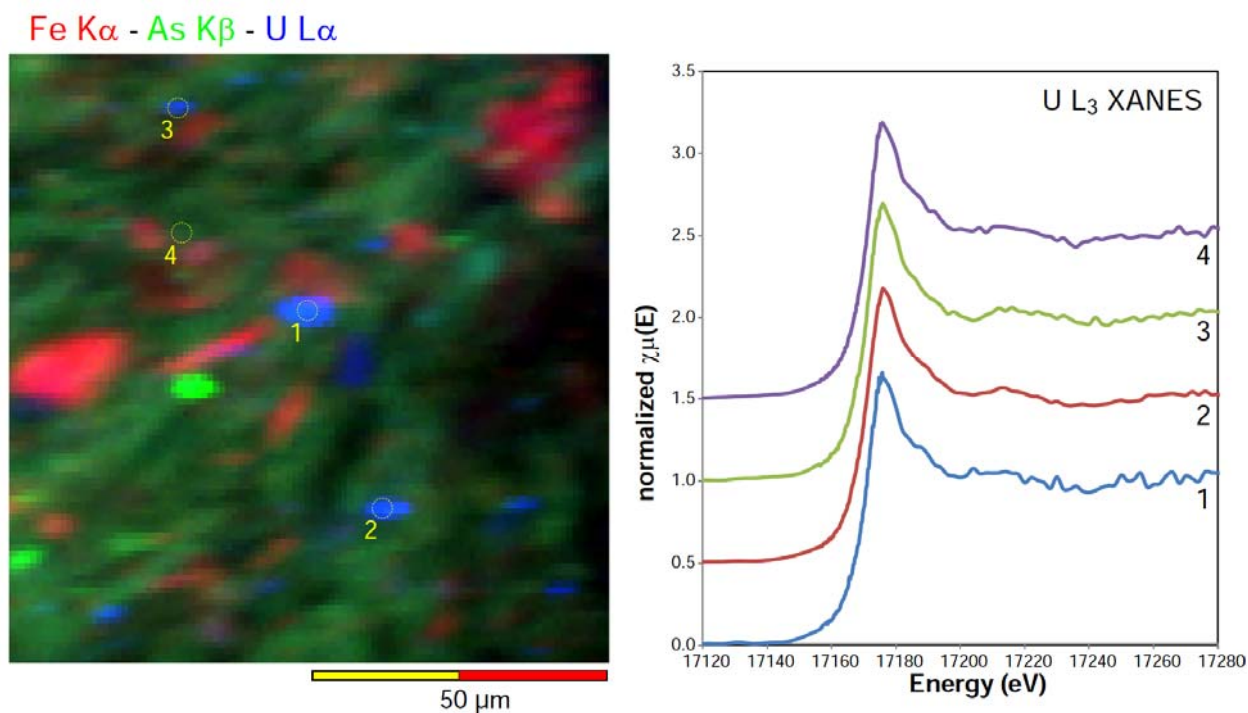
Figure 4. *Three color µXRF intensity map of Fe Kα (red), As Kβ (green) and U Lα₁ (blue) for a localized area of the sample TMF02-SA05-Map4 in Figure 3. Yellow numbered circles show where U L3 µXANES spectra were collected. The measured, edge step normalized µXANES spectra are shown to the right. Edge positions are consistent with U in the 6+ oxidation state.*
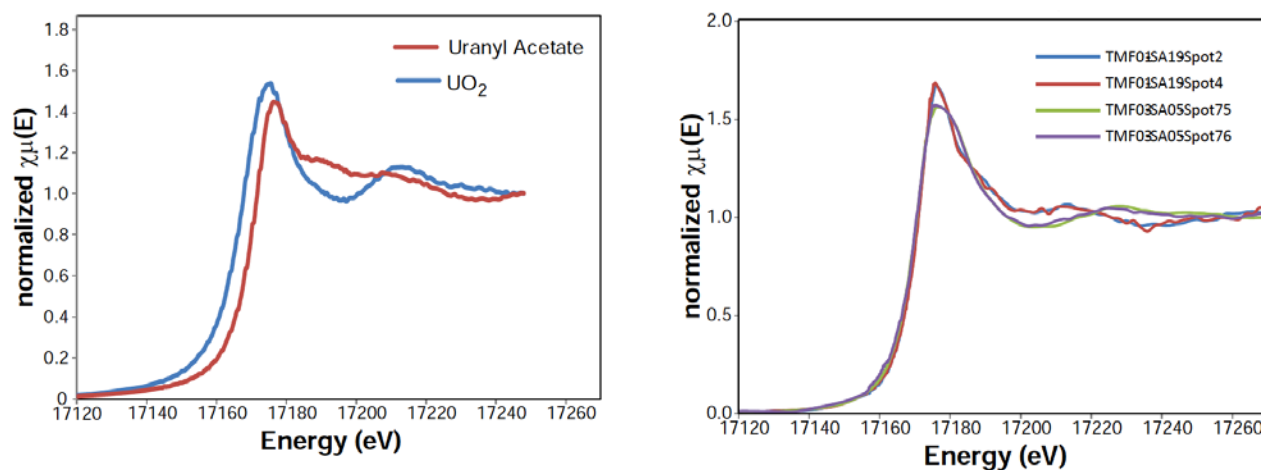
Figure 5. (Left) Comparison of U L3 µXANES spectra from UO_2 and Uranyl acetate standards. Note that the spectra for $U^{4+}O_2$ is shifted to lower energy than that for $(U^{6+}O_2(CH_3COO)_2 \cdot 2H_2O)$ and that uranyl acetate has a distinct shoulder at 10 to 15 eV above the absorption maximum. (Right) Comparison of U L3 µXANES spectra from sample TMF01-SA19 with two spectra from TMF03-SA05.

Recommendations

Our initial results suggest that further SXRMS studies of U in tailings will be both productive and informative, with caveats on further work only for Th/Ra. We recommend:

- µXRF analysis of thin sections to evaluate U distribution and concentration at µm scale to evaluate potential elemental associations, especially with quantitative approaches
- µXRD analysis for constraining sample mineralogy relative to ore minerals or phases formed during ore processing and after prolonged residence in the TMF
- µXAFS analysis to evaluate the oxidation state of U and to constrain potential molecular species relative to assumed geochemical controls on U solubility
- Further investigations of SXRMS techniques for Th; but not for Ra in tailings solids
- Further studies of radionuclides in porewaters, especially in terms of detecting Ra with less interference from other elements

Conclusions

Tailings management facilities are required to safely isolate remaining radioactive contaminants from their surrounding environment for very long periods of time. Our preliminary work has shown that synchrotron applications can provide unique insights into the geochemistry and mineralogy of uranium in tailings. These findings can provide solid lines of evidence to inform long-term management strategies, and to support regulatory licensing decisions on the decommissioning and remediation of operating and legacy uranium mines in Canada.

References

AREVA. 2015. McClean Lake Operation – Tailings Management Technical Information Document, AREVA Resources Canada Inc., Saskatoon, May 29, 2015.

CNSC. 2016. RSP-606.1 – Synchrotron X-ray microspectroscopy for detecting Ra-226 and its daughters in tailings and mill waste from uranium mining operations. Canadian Nuclear Safety Commission, Ottawa. PDF: www.nuclearsafety.gc.ca.

Guo, X., Tiferet, E., Qi, L., Solomon, J.M., Lanzirotti, A., Newville, M., Engelhard, M.H., Kukkadapu, R.K., Wu, D., Ilton, E.S. et al. 2016. U (v) in metal uranates: a combined experimental and theoretical study of $MgUO_4$, $CrUO_4$, and $FeUO_4$. Dalton Transactions 45, 4622-4632.

Lanzirotti, A., Newville, M., Manoukian, L., Lange, K. 2016. High-speed, coupled micro-beam XRD/XRF/XAFS mapping at GSECARS: APS beamline 13-ID-E. The Clay Minerals Society Workshop Lectures Series, v. 21, Chapter 5, 53-64. PDF: www.clays.org

Acknowledgements

Accelerator Mass Spectrometry (AMS) in Radioecology

M. García-León*

Universidad de Sevilla
Centro Nacional de Aceleradores
Avda. T. A. Edison
41092 Sevilla
Spain

Abstract

Accelerator Mass Spectrometry (AMS) provides with an excellent sensitivity for the determination of radionuclides in the environment. In fact, conventional radiometric techniques can hardly compete with AMS in the solution of many problems involving the measurement of very low levels of radioactivity in Nature. For that reason, during the last years AMS has become a powerful tool for Radioecology studies.
In this paper a review is done on the evolution of AMS applications to the measurement of environmental radioactivity and, therefore, its contribution to the understanding of radionuclide behavior in Nature.For that, the advantages of using AMS to determine key nuclides as ^{129}I, ^{14}C, Pu-isotopes and others in different natural compartments will be discussed. The content of the paper is illustrated with the contributions to these studies of the Spanish National Center for Accelerators (CNA) AMS systems.

Introduction

One of the main interest in Radioecology is the study of the dynamics and behaviour of radionuclides in the environment, their sources and fate. For that we need to measure radioactivity in Nature. In the majority of the cases at low or very low levels. Radiometric methods solve this problem by the direct mesurement of the radiations emitted by the radionuclides as a way of determining its activity. The basis for these methods is the well known Equation.

$$A = \lambda N \qquad\qquad (1)$$

Being A the activity of the sample, λ the disintegration constant and N the number of radioactive nuclei. There are many examples in the literature which show how these methods have succeeded all along the history of Radioecology. In many cases, however, they cannot give reasonably precise data, or it is simply impossible, due to the extremely low concentration of the radionuclide or its very long half-life, or both.In these situation is better to measure N instead of A.That is possible by using mass spectrometry techniques where the application of electric and magnetic fields to a charged beam that contains the radionuclide of interest produce a deviation of its trajectory according to its mass and energy.

Accelerator Mass Spectrometry (AMS) is a veteran mass spectrometry technique which consists of the coupling of a mass spectrometer to an accelerator of tandem type. Its sensitivity has made it a very competitive analytical technique.In fact very long lived radionuclides can be determined with sensitivities close or below one part in 10^{15}. A brief description of AMS is given in the next Section. After that its application to the measurement to key radionuclides in Radioecology are discussed.

Methods

AMS was proposed for the first time by *Alvarez and Cornog 1939* which used a cyclotron to identify ^{3}He in Helium. Under its actual form, however, AMS appears by 1977 (*Gove et al. 2010*) as a way to solve the limitations of conventional radiometric techniques for ^{14}C dating. After this moment it has rapidly evolved to find application in many disciplines. One of them, the measurement of Environmental Radioactivity.
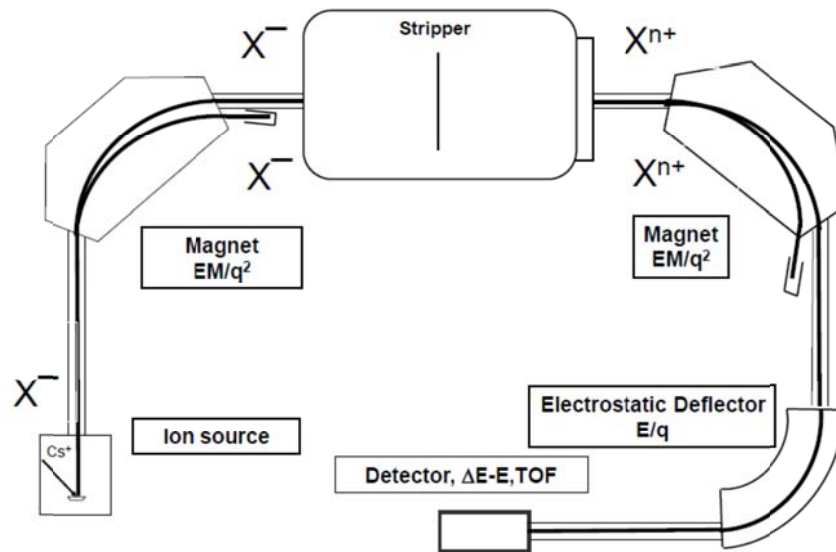
Figure 1.AMS typical system. It is a scheme of the CNA 1 MV Cockcroft-Walton spectrometer.

In Figure 1 we present a simplified scheme of an AMS system which is well representative of many working systems all along the world.The beam, containing the radionuclide of interest is extracted from the sample in the ion source at a charge state1⁻. In the low energy side of the system, the beam is analyzed for mass with a magnet. After that it is injected in the accelerator tank where it is accelerated in two steps. First, before the stripping and then, after the stripping process during which the beam becomes positively charged after its interaction with the stripper. The possitive beam is analyzed once more for mass and energy at the high energy side of the spectrometer with a magnet and a electrostatic deflector. The selected mass is then driven to the radiation detector where the number of radionuclides of interest are counted.

The advantages of AMS regarding conventional mass spectrometry come basically from two special features. First, the dramatic lowering of the molecular background as a consequence of the stripping process, since the majority of molecules are unstable under the resulting strong positive charge state. Second, since the beam is accelerated until energies of the order of MeV/nucleon, it is possible to use nuclear radiation detectors and, consequently, to add to the problem new boundary conditions that permit the discrimination of isobaric species. The use of ΔE-E telescopes make possible the measurement of stopping powers and the application of the Bethe-Bloch equation to distinguish isobars. Or the use of Time of Flight Spectrometers allows the measurement of different masses, even slightly different masses, at the same energy. As an additional advantage, the use of negative ions at the beginning of the process makes a previous selection of the ions injected in the system. This is very convenient for many radionuclides. In fact, the discovery of the unstability of ^{14}N⁻, the main interferent of ^{14}C, gives place to the development of a new radiocarbon dating technique based on AMS as described above (*Gove et al. 2010*).

At these conditions the sensitivity one can reach with AMS makes it a really powerful tool to afford many problems in Environmental Sciences and other disciplines. A good review on the sensitivity of AMS for many cases can be found in *Tuniz and Norton 2008*.

The main drawback of the technique has been the need of large facilities. Nevertheless, since the beginning of this century it has been developed the so called Low Energy AMS with uses low terminal voltage accelerators (below 1 MV) and small dimensions machines. An example is the National Center for Accelerators (CNA) AMS system based on1MV Cockcroft-Walton tandem accelerator. The dimensions of such spectrometer are relatively small, 3.8x6.3 m^2. Even smaller systems can be fairly competitive in AMS. An example is the Spanish MICADAS, 3x2.5 meters in

size, based on a 200 kV van de Graaff accelerator. This system is devoted in CNA to ^{14}C measurements. Both are described in *Chamizo et al 2015a*.

There is an ample documentation about how AMS can succesfully meet Radioecology problems. In practical terms the main adavantages of AMS is providing extremely good precision in the measurement for very small samples and using low counting times. Indeed, g or mg for solid samples or few L or fraction of L for liquid samples are very common in the majority of AMS experiments. Counting times of some 20 min for ^{129}I are enough to obtain precissions of< 10% forits determination with current methods. Another illustrative example is the case of the measurement of Pu-isotopes in environmental samples where some 15 min of counting gives results with a precission of 5% and the additional advantage of measuring ^{239}Pu and ^{240}Pu. This is simply impossible to achieve with conventional radiometric methods.

The application of AMS to the measurement of radionuclides in waters, sediments, biota, etc., i.e. to some relevant problems for Radioecology, needs new radiochemical methods for sample preparation. Indeed, the final chemical form of the radionuclide to be measured has to be compatible with the mass spectrometer ion source.

There are many examples in the literature about such developments. One of them is the procedure developed at CNA by *Chamizo et al. 2008* for the separation of Pu from different matrices basedon the use of TEVA resins. The main potential interferents in this case are ^{238}U and Dy isotopes. ^{238}U may reach the detector even in the case the spectrometer is tunned for ^{239}Pu, due to, for instance, instrumental unstabilities. ^{160}Dy^{2+} has the same M/q ratio that ^{240}Pu^{3+} and, therefore can also be counted by the detector. The method provides good decontamination factors that makes posible the measurement of ^{239}Pu down to fg levels. Pu is injected in the spectrometer as Pu oxide.

Another interesting example is that presented by *Gómez-Guzmánet al. 2010* also at CNA for the separation of ^{129}I from lichens based on a microwave digestion which significantly diminishes the processing time regarding the conventional leaching or combustion based methods. As a last step of the method, Iodine is precipitated as AgI.

Results

The range of applications of AMS and the number of radionuclides that can be measured with such a technique are still expanding. Nowadays, however, the most relevant radionuclides for Radioecology can be tried by AMS. A very brief summary of such applications are given in what follows.

^{14}C

In the case of ^{14}C, its main role in AMS is dating. In fact, as it was said before, AMS based on tandem machines was developed to overcomethe limitations of ^{14}C dating by radiometric methods. For that the discovery of the instability of ^{14}N$^-$ was a fundamental starting point (*Gove et al. 2010*). But the advantages of AMS can be used to determine ^{14}C in environmental samples.

A beautiful example is the use of ^{14}C to trace seawater masses movements. In *Gislefoss et al. 1994*, AMS was used to repeat several GEOSEC Nordic Seas water profiles previously measured by conventional radiometric techniques. AMS allowed to use 0.5 L water samples instead of 100 to 200 L needed for traditional techniques. That is very important in order to make the sampling in a cruise expedition and manage the samples after at the laboratory.The authors claim to obtain 6°/$_{oo}$precision or better with some 20 min counting time per sample. Interesting information is presented in the paper about the CO_2 uptake in the Nordic Seas and its transport into deep waters. Also the age of deep waters is estimated and the authors conclude that the meaurement of ^{14}C by traditional techniques in deep waters "has come to an end".

Radiocarbon is considered to be the most important contributor for the collective total dose received by the population from nuclear fuel processes (*UNSCEAR, 2008*). For that it is very important to know its behaviour and fate in affected environments. A typical study case is that

presented by *Tierney et al. 2016* on the presence of ^{14}C in the Irish Sea and West of Scotland as a result of Sellafield activities. The authors find a general ^{14}C enrichment of mussels and shell material above the background level. A time series study show that the enrichment level in mussels is decreasing as the Sellafield releases have decreased along the time. However, the enrichment is still increasing in sediments. A similar study is presented by the same group but for the Eastern UK coastal environment (*Muir et al. 2015*). Anomalous ^{14}C enrichment are found in the samples analysed, biota and sediments, and some possible ^{14}C sources are suggested. On the other hand, by dating the sediments with^{210}Pb, the authors find that the ^{14}C releases are being produced since1960 til the present days.

Inputs of radiocarbon from the Fukushima accident into the sea has been also investigated (*Povinec et al. 2016*). Impact has been determined but in general terms the contribution of Fukushima ^{14}C was only 9% above global fallout level. Interesting to say is that the amount of seawater sample to extract CO_2 for ^{14}C AMS analysis was typically of 20 mL. The uncertainty in the measurements were 5°/$_{oo}$.

The analysis of ^{14}C in tree rings is a good way to determine the environmetal impact from Nuclear Facilites in their close environment. An example of these type of works appears in *Janovics et al. 2016* where a study is carried out on the impact of a low to intemediate level radioactive wastes disposal installation on nearby trees. Radiocarbon is measured in rings from a tree situated close to the facility and from a tree far from the site in order to compare results. As expected, rings of the nearby tree shows a ^{14}C time pattern distribution unambiguously related to the radioactive wastes disposal plant.

A very complete analysis of the impact of a Nuclear Power Plant based on ^{14}C appears in *Wang et al. 2014*. Seawater, undergroundwaters, river waters and drinking waters, together with atmospheric samples are analysed for ^{14}C by AMS. Samples of some 1 L were enough to give ^{14}C with less than 1% uncertainty. The authors find that air samples present impact from the operation of the plant while seawaters give results which are not distinguishable from the background.

In CNA, ^{14}C measurements are mainly addressed to dating works (*Santos et al. 2009*). Nevertheless, environmental applications are also done. In *Beramendi-Orosco et al. 2015*, data are presented on the measurement of atmospheric samples at Mexico City. Specifically ^{14}C is determined in tree rings collected at a park within the metropolitan area of the city. The typical ^{14}C bomb pulse with a peak at 1964 is found, but a detailed studied of the results obtained in comparison with similar data taken at the Northern Hemisphere shows a ^{14}C depletion (up to 246‰ lower than the expected backgorund)atributted to the vast fossil fuel consumed in the area. Few mg samples and some half an hour of measurement is enough to get a very precise measurement of ^{14}C in each ring.

^{129}I

The development of AMS has been crucial for ^{129}I. It has a very long half-life and is very diluted in ^{127}I. Therefore, its measurement by conventional radiometric methods is only posible under very special circumstances. Pioneering works on AMS of ^{129}I dates back to *Elmore et al 1980* and later to *Kilius et al. 1990*. After this work the information on the presence of ^{129}I in the environment has increased outstandingly. The review by *Raisbeck and Yiou, 1999* is a good reference on how AMS benefited the ^{129}I "environmental science", specially in oceans, since ^{129}I is a well recognised tracer of water movements, as the authors themselves proposed. By that time, it was posible to measure ^{129}I in only 1L water sample volume with an uncertainty better than 10%. The authors analyze the vertical and horizontal distribution pattern of ^{129}I /^{127}I in North Atlantic Ocean and combine these data with those of ^{137}Cs and ^{99}Tc. Thus obtaining an ample oceanographic information on the area.

The sensitivity of AMS has made possible the measurement of ^{129}I in surface fresh waters. *Aldahan et al. 2006* studied its presence in rivers of the Baltic area. 1L samples were enough to obtain precise ^{129}I concentrations. The origin of ^{129}I in the rivers was attributed to atmospheric

inputs from the Baltic Sea which in turn is affected by Sellafield and La Hague nuclear fuel reprocessing plant. Being others contributions as global fallout or Chernobyl inputs negligible.

^{129}I in the amosphere has been also an important topic. A good review of ^{129}I in air can be found in *Jabal et al. 2013*. And it is a target of the CNA studies. AMS allowed a high time resolution analysis on its presence in Sevilla, Spain, an area not affected by nuclear facilities. Results presented in *Santos et al. 2006* gave information on ^{129}Iconcentration and the ratio ^{129}I/^{127}I of aerosol and rainwater samples. These measurements allowed the authors to conclude the influence of the atmospheric emissions of Sellafield and La Hague over the area and suggest the possibility that such discharges were done in an aerosol form or in a chemical form that associates rapidly to aerosol which facilitates the arriving to Sevilla.

More recently, measurements have been done of ^{129}I in aerosol samples and 0.5 L rainwater samples during March and April 2011 when the radioactive Fukushima plume arrived Spain (*Gómez-Guzmán et al. 2016*). ^{131}I was also measured. The analysis showed the ^{129}I impact in Sevilla and according to the data it is suggested to use it as a marker of ^{131}I radiological impact. The same conclusion is derived by *Muramatsu et al. 2015* that analysed both I isotopes in soils close to Fukushima.

Once more the sensitivity of AMS allowed to determine it in a sediment core taken at Huelva, SW Spain, a non affected place by direct emissions, during 1999 (*Santos et al. 2007*). Only 2 g of sediments were enough to clearly identify three sections in the profile. The older layers corresponding to the pre-nuclear era, a prominent peak corresponding to the 1964 bomb pulse and the more young layers which reflect the influence of Sellafield and La Hague in the area.

As said before, there is a wide scientific literature on the presence of ^{129}I in the marine environment. It has also been studied by the CNA group. Results in seaweed and water samples taken in the Baltic area were presented in *Gómez-Guzmán et al. 2013* and *Gómez-Guzmán et al. 2014*. It was possible to show that the main contributionsto this area comes from the releases of Sellafield and La Hague and that the contribution of ^{129}I from Chernobyl was not significant. An interesting comparison is done on the concentration of ^{129}I in the South and North Atlantic áreas (*López-Gutiérrez et al. 2016*).

The sensitivity of AMS has permitted to makespeciation studies of ^{129}I in waters from the Baltic Sea and in the surroundings of the Savannah River site contaminated by the Savannah atmospheric emissions. Speciation works are key studies in radioecology as it is known. For long half-life radionuclides it is only posible by very sensitive techniques, AMS in our case. Iodide and iodate forms for ^{129}I are identified in waters from the Baltic Sea in *Hansen et al. 2011*. The authors compare it with the same analysis for ^{127}I and do not find differences in this environmental context. In the case of waters from the Savannah (*Schwehr et al. 2014*) the authors find a clear dependency on pH of the ^{129}I/^{127}I isotopic ratio for each chemical species.

^{36}Cl

The determination of ^{36}Cl by AMS is a classic topic in this field. The first work was published in 1979 (*Elmore et al. 1979*) on the analysis of ^{36}Cl in natural water samples requiring only 1 to 5 L. In this pioneer paper the principles of ^{36}Cl detection by AMS were presented for the first time. Rejection of ^{36}S, its main interferent, was done with a gas ionisation based ΔE-E telescope. Uncertainties in measurements were < 10% in less than 1 h counting time.Since that paper many works have been producedon the determination of ^{36}Cl in different samples. The main application being dating groundwaters or tracing its dynamics. An interesting work on that issue was published by *Balderer and Synal 1997*. In this paper the authors carry out a detailed study of the presence and sources of ^{36}Cl in groundwaters and develop a model for the application of ^{36}Cl to understand the groundwater cycle. The extremely precise ^{36}Cl AMS measurements make possible to inform on residence times, age, evaporation porcesses, water-rock interactions etc.

^{36}Clhas been used also as a tracer of the environmental contamination provoked by contaminated Chernobyl material buried in trenches in the exclusion zone. Indeed, *Roux et al. 2014*studied the presence of ^{36}Cl in underground waters in the surroundings of one of these trenches. Results shown that ^{36}Cl is a suitable tracer in this context and ^{36}Cl/Cl ratios some 3 to 4 orders of magnitudes higher than foreseen at natural conditions were found. Once again the amount of sample needed for analysis was small, 1 to 6 L each. The choice of ^{36}Cl as a tracer was based in the assumption of its conservative behaviour in waters. A recent work describes, however, a ^{36}Cl non-conservative behaviour in the Great Lakes (*Poghosyan and Sturchio 2015*).

The presence of ^{36}Cl in the atmosphere has received attention from seveeral groups. ^{36}Cl in rainwater samples taken at Sevilla, Spain, during 1999 and 2000 was studied and results presented in *Santos et al. 2004*. Uncertainties < 10% in ^{36}Cl atom concentrations and ^{36}Cl/Cl isotopic ratios are obtained by analysisng no more than 5 L of water. Results revealed a seasonal time pattern variation with peaks during late spring-early summer. The influence of "dead" Cl carried by (SW) winds from the Atlantic ocean is also shown. Furthermore, the authors found that the ^{36}Cl total atmospheric deposition in the area was higher than expected from the known cosmogenic models for ^{36}Cl production. This effect was previously discovered by *Blinov et al. 2004*. The authors measured the atmospheric ^{36}Cl deposition worldwide and detected an systematic excess compared to the calculations from the known cosmogenic models. They attributed such effect to the retention of ^{36}Cl bomb produced in the biosphere ad its afterward reintroduction in the atmosphere.The seasonal time variation has been confirmed by *Tosaki et al 2014* with atmospheric samples taken at central Japan. In this publication measurements of ^{36}Cl monthly flux over Japan have been carried out from 2004 to 2009. The influence of the sea spray is also demonstrated on the Cl content in the atmosphere.

Pu-isotopes

The importance of Pu isotopes in Radioecology is well known. The determination of Pu isotope ratios, mainly ^{240}Pu/^{239}Pu is, on the other hand of paramount relevance to know the source term of Pu in a given environment. Efforts have been done to measure such ratios by α spectrometry but only in very special circumstances,and with the help of α- spectra deconvultion codes,it has been posible. In addition, α spectrometry is time consuming with days of counting often necessary to determine Pu in environmental samples. On the contrary, AMS is less time consuming and uses smaller amount of sample to get better precision. And, above all, it gives the ^{240}Pu/^{239}Pu isotope ratio. And without the need of large facilities in spite of the high mass of the Pu isotopic family. *Fifield et al. 2004* demonstrated the possibility of measuring Pu isotopes with 300kV terminal voltage accelerators.

In the CNA group an extensive development of methodology has been carried out for the determination of Pu isotopes in a variety of environmental samples.

This way Pu isotopes and ratios have been determined in the Palomares environment, SE Spain, affected by an accident occurred in 1966 when the fuel from two termonuclear bombs spread in it. Previous studies have been carried out in the site by measuring $^{239+240}$Pu activity or ^{238}Pu/$^{239+240}$Pu activity ratios but this has not shown to be enough to characterize and identify the dispersion of Pu originated in the accident. *Chamizo et al. 2006* measured ^{240}Pu/^{239}Pu isotope ratio in soil samples from Palomares by Low Energy AMS (LEAMS). Small, 1-2 g of soil samples were measured with low and high level of contamination and the results compared to those found in soils from Sevilla affected only by fallout. Typical values for the atom ratio of around 17% was found for the Sevilla samples while a typical atom ratio of (6.57 $\pm$ 0.06)% was measured for highly contaminated samples from Palomares, showing this way the utility of measuring the ratio to unambiguously assign the origin of Pu in the studied area. Later, *Chamizo et al. 2010a* were able to determine ^{240}Pu/^{239}Pu also by LEAMS in a sediment core taken offshore Palomares. Results shown that the sediment was affected by the releases from the accident since the ratio was found to be 11%

in the average along the profile. Ratios close to 6% were found in the first cm of the profile where as calculated the majority of Pu coming from the accident accumulated. Results confirmed a land to sea transport of contamination in this case.

The sensitivity of AMS made possible to measure the $^{240}Pu/^{239}Pu$ isotope ratio in soils samples from Southern Hemisphere, specifically from Chile (*Chamizo et al. 2011*). It was possible to detect the influence of French tests in some of the samples by measuring the isotope ratio which values close to 4%. In other cases, ratios of 18%, the fallout signal in the area, were obtained.

Also with the AMS sytem of the CNA, *Chamizo et al. 2010b* measured the temporal evolution of Pu-isotopes in surface air samples collected in Sevilla. On the average 6 g of aerosol, i. e. some 30.000 m^{3}of filtered air, were enough to obtain Pu concentrations with uncertainties of some few % using counting times of 30 min. A seasonal pattern was found with maximun activites corresponding to the dry summer and minimum corresponding to the following autumn rainy period, this in agreement with the hypothesis of a soil resuspension effect as the origin of Pu in this area. Correlation was found of Pu concentrations with the aerosol mass and the content of Ti and Al. This indicated a possible modulation of the Pu-isotpes activities in the air of Seville by Saharian dust intrusion. $^{240}Pu/^{239}Pu$ ratio was typically of 14%, close to the expected fallout ratio in the region of around 18%.

AMS has been shown to be a very important tool to meet, in a precise and realistic way, the measurement of ^{239}Pu in human urine samplesfor routine monitoring of exposed workers. Traditionally this work is done by analysing large volumes of urine samples. Moreover the whole measurement by α-spectrometry takes one week including the radiochemical separation of Pu. *Hernández- Mendoza et al. 2010* developed a method using the CNA AMS system to analyse Pu in urine samples using only 1-2 L. The whole measurement takes 10 h including chemical processing.

With regard also to the operation of nuclear power plants, it is important to have methodology for the classification of wastes in low, medium or high level. This is conventially done by studying the activites of long-lived radionulides in them by radiometric methods, which are time consuming, laborious and necessarily have to treat high volumeof samples, which means dangerous methods. As *López-Gutiérrez et al. 2013*demonstrated, AMS provides a fast and less laborious method using significantly less amount of sample. They measured $^{240}Pu/^{239}Pu$ and ^{129}I in wastes from Spanish Nuclear Power Plants including materials from the decommissioning of one of them. They showed that meauring activity ratios can be give additional information about the history of the residue.

Pu speciation studies are possible with AMS. *Skipperud et al. 2009* presented Pu speciation studies in waters and sediments from the Ob and Yenisey rivers and estuaries in Russia. Knowledge of chemical association of the Pu isotopes gives unvaluable information on their transfer, fate and environmental impact in the Baltic Sea in that case. The authors found that more than 80% of the Pu in the Yenisey river is very weakly bound, i.e. associated to organic compunds. This pattern changes when going from the riverine to estuarine area, where Pu is more strongly and irreversibly bound.

^{236}U

^{236}U is a very new member of the AMS family. In fact, only few years ago ^{236}U has been recognised as a good tracer for marine dynamics or others environmental processes. Nevertheless, the measurement of ^{236}U is impossible by radiometric methods and it is a very challenging isotope for AMS. In spite of that the amount of literature on AMS of ^{236}Uhas increased during the last years.

Sakaguchi et al. 2010 reported a study of the fallout from the Hiroshima bomb by using ^{236}U together with other nuclides. Its presence at the site was expected from the fast neutron activation reaction $^{235}U(n,\gamma)$ occurred during the detonation of the A-bomb.Data obtained shown that it was not posible to distinguish between global ^{236}U falloutand the current level found for it at the zone.

The authors concluded that less than 1% of the ^{236}U produced in the detonation deposited in the area.

The global ^{236}U fallout signal has been measured by *Srncik et al. 2011* in soils collected from a remote clean air area in the La Palma Isle in Canary Islands, Spain. Some few grams per sample were analyzed and counting times of around 30-60 min were typically used. ^{236}U concentrates in the first cm of the soil profile. The atom ratio ^{236}U/^{238}U ranges from 10^{-7} to 10^{-9}. The global fallout U-isotope ratio is sparce according to the authors in soils.

Eigl et al. 2013 measured ^{236}U in seawater and river waters (only 2 L). ^{236}U/^{238}Uratios were found of 10^{-9} in marine and 10^{-8} in river waters. The authors atributted to global fallout such results. More recently, *Srncik et al. 2014* were able to determine ^{236}U in soils of the Southern hemisphere from unaffected areas. The atuhors provide results on the ^{236}U inventory in the Southern Hemisphere, which is found to be 8.4×10^{11}, one order of magnitude lower than in the Northern Hemisphere. The ratio ^{236}U/^{239}Pu was 0.08 clearly lower than the ratio at the Northern Hemisphere, typically 0.2.Related to this work, *Froehlich et al. 2016* studied the uptake of ^{236}U by plants in the Southern Hemisphere by AMS. Compared to ^{239}Pu, ^{236}U seems to be uptaken preferentially by vegetation.

In *Chamizo et al. 2016a*, data are presented on ^{236}U in a peatbog core collected at Madagascar. Ratios ranging from 0.02 to 0.29 are found for ^{236}U/^{239}Pu which complete the datafile for these nuclides in the Southern Hemisphere.

Documentation is already published on the ^{236}U dynamics and presence in oceans. *Eigl et al. 2016*, presented results of ^{236}U depth water profiles from the Northeast Pacific Oceans. They obtain very precise data with only 1 L sample volumen. ^{236}U concentrations are higher in surface samples than in deep waters. This reflecting, according to the authors, the low vertical transport of waters in this region, and consequently the large age of deep waters. ^{236}U/^{238}U ratio is also higher at the surface, ranging from 10^{-9} at the surface to 10^{-10} at 1500 m and deeper. *Villa et al. 2016*, on the other hand, present in these Proceedings results on ^{236}U in the Equatorial area of the Pacific Ocean.Also based in measurements carried out in the AMS CNA system, *López-Lora et al. 2016*, have measured ^{236}U in South Atlantic water samples. ^{236}U/^{238}U ratios of some 10^{-10} are obtained lower than those presented by *Eigl et al. 2016* of 10^{-9} for North Atlantic samples which points to an influence in this region of a local contamination coming from the nuclear reprocessing plants.The same CNA group together with that from IAEA-Environment Laboratory at Monaco (*Chamizo et al. 2016b*) have determined ^{236}U in the Northwestern Mediterranean area. In this case the^{236}U/^{238}U atom ratio reached a value of 10^{-9} indicating that anthropogenic ^{236}U dominates the whole water column. Some 5 l samples were used and around 25 min was the counting time per sample. The ^{236}U inventory in the water column is 2 times higher than expected in this area. The authors consider that several additional sources to global fallout has to be taken into account to explain the ratio, such as French Nuclear Power Plants, remaining traces from Chernobyl and even Sahara dusts. Interesting to say is that the CNA measurements have been done by a Low Energy AMS (LEAMS). A full account of the method is given in *Chamizo et al. 2015b*. In fact, the possibility of measuring ^{236}U by LEAMS was proposed by *Vockenhuber et al. 2011*. It made available the technique to many groups.

Others
Non regular applications of AMS to interesting isotopes for radioecology can be found in literature.

^{99}Tc has been investigated by AMS. Its determination in the environment by AMS was reported by *Fifield et al. 2000*. A technical effort was done in the paper to separate ^{99}Tc from ^{99}Ru and AMS was shown to be able to determine it at fg levels. Some first measurements were done in seaweed intercalibration samples.The method was refined by *Wacker et al. 2004*. Close in the time *Bergquist et al. 2000* published another AMS ^{99}Tc method. Good separation from ^{99}Ru and molecular backgrounds was obtained by the authors with MeV beam energies. The method was

applied to fresh and sea waters, some 200 mL in volume, and arid soils, around 60 to 100 g. After these works, it seems, however, that no suystematic applications of AMS to Tc can be found in regular literature, although new approaches to the problem were presented by *Ming et al. 2007*.

^{90}Sr or ^{135}Cs has been meaured also by AMS in *Tumey et al. 2008* and *Mc Donald et al. 2015* respectively. In the first case the main challenge lies on the discrimination against^{90}Zr. In their work the authors wait to achieve a sensitivity of 10^{6}^{90}Sr atoms per sample after some expected developments. The case of ^{135}Cs is very special since Cs does not easily forms negative ions. In fact, it has to be injected into the accelerator as CsF_2^- and a Isobar Separator for Anions has to be used to reject the Ba contamination of the sample. The paper provides promising first results.

Very recently measurementsof Am and Cm isotopes by LEAMS has been carried out (*Christl et al. 2015*). Sensitivities of ~ fg or even ~10^{-1}fg for Am and Cm isotopes respectively are achieved by using a 500 kV terminal voltage tandem accelerator. The radionuclides are accelerated in oxide form.

^{237}Np is receiving an increasing attention within the AMS community. Radiochemical methodology can be found in *Hain et al. 2015* and *Levy et al. 2016*, both for small (fractions or few L as much) seawater. The work by *Wang et al. 2010* presents ^{237}Np standards for AMS.

AMS studies are being done for Pb isotopes, including ^{210}Pb (*Sookdeo et al. 2015*). The accelerated species is PbF_3^-.

Conclusions

Since 1977 tandem accelerator based AMS using negative ions has evolved enormously. Important improvements in precission and sensitivity have been achieved since which has converted AMS in an essential tool for many scientific disciplines. That is the case of Radioecology, where the possibility of analysing small samples, during short counting times together with the increasing number of detectable radionuclidesmake it a very useful analytical technique. As a consequence, the applications of AMS to Radioecology are exponentially increasing. Furthermore, the appearing of small and compact machines as aproduct of the development of the so-called Low Energy AMS (LEAMS) has made AMS available to many laboratories.Summing up the sensitivity one can reach with AMS makes it a really powerful tool to afford many problems in Environmental Sciences and Radioecology as it can be seen in Fig. 2
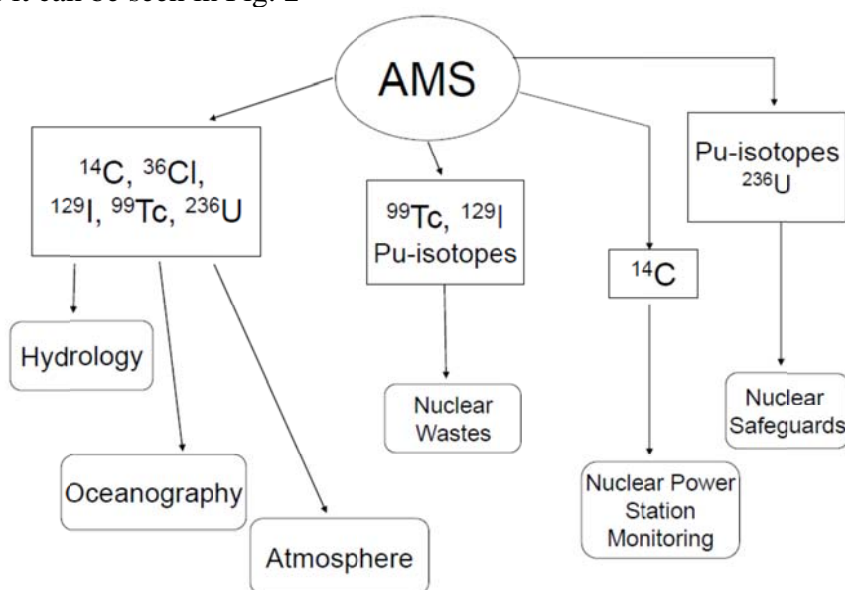
Figure 2.*AMS impact on Environmental Radioactivity and Radioecology studies through the measurement of relevant radionuclides.*

References

Aldahan A., Kekli A., Possnert G., 2006, Distribution and sources of ^{129}I in rivers of the Baltic region, J. Environ. Radioact. 88, 49-73.

Alvarez L. W., Cornog R., 1939, ^{3}He in helium, Phys. Rev. 56, 379.

Balderer W., Synal H. A., 1977, Use of chlorine-36 as tracer for the evolution of waters in geotermal and tectonically active areas in Western Turkey, Nuc. Instrum. and Meth. in Phys. Res. B123, 387-393.

Beramendi-Orosco L., Gonzalez-Hernandez G., Martinez-Jurado A., Martinez-Reyes A., Garcia-Samano A, Villanueva-Diaz J., Santos-Arevalo F. J., Gomez-Martinez I., Amador-Muñoz O., 2015, Temporal and spatial variations of atmospheric radiocarbon in the Mexico City metropolitan area, Radiocarbon, 57, 363-375.

Bergquist B. A., Marchetti A. A., Martinelli R. E., McAninch J. E., Nimz G. J., Proctor L. D., Southon J. R., Vogel J. S., 2000, Technetium measurements by accelerator mass spectrometry at LLNL,Nuc. Instrum. and Meth. in Phys. Res. B172, 328-332.

Blinov A., Massonet S., Sachsenhauser H., Stan-Sion C., Lazarev V., Beer J., Synal H. A., Kaba M, Masarik J., Nolte E., 2000, An excess of ^{36}Cl in modern atmospheric precipitation, Nuc. Instrum. and Meth. in Phys. Res. B172, 537-544.

Chamizo E., García-León M., Synal H.A., Suter M., Wacker L., 2006, Determination of the ^{240}Pu/^{239}Pu atomic ratio in soils from Palomares (Spain) by low-energy accelerator mass spectrometry, Nuc. Instrum. and Meth. in Phys. Res. B249, 768-771.

Chamizo E., Jiménez-Ramos M. C., Wacker L., Vioque I., Calleja A., García-León M., García-Tenorio R., 2008, Isolation of Pu-isotopes from environmental samples usingion chromatography for accelerator mass spectrometry andalpha spectrometry, Anal. Chim. Acta, 606, 239-245.

Chamizo E., Jiménez-Ramos M. C., Enamorado S. M., García-León M., García-Tenorio R., Mas J. L., Masqué P, Merino J., Sanchez-Cabeza J. A., 2010a, Characterisation of the plutonium isotopic composition of a sediment core from Palomares, Spain, by low-energy AMS and alpha-spectrometry, Nuc. Instrum. and Meth. in Phys. Res. B268, 1273-1276.

Chamizo E., García-León M., Enamorado S. M., Jiménez-Ramos M. C., Wacker L., 2010b, Measurement of plutonium isotopes, ^{239}Pu and ^{240}Pu, in air-filter samples from Seville (2001-2002), Atmospheric Environment 44, 1851-1858.

Chamizo E., García-León M., Peruchena J. I., Cereceda F., Vidal V., Pinilla E., Miró C., 2011, Presence of plutonium isotopes, ^{239}Pu and ^{240}Pu, in soils from Chile, Nuc. Instrum. and Meth. in Phys. Res. B24, 3163-3166.

Chamizo E., Santos F. J., López-Gutiérrez J. M., Padilla S., García-León M., Heinemeier J., Schnabel C., Scognamiglio G., 2015a, Status report of the 1 MV AMS facility at the Centro Nacional de Aceleradores, Nuc. Instrum. and Meth. in Phys. Res. B361, 1-9.

Chamizo E., Christl M., Fifield L. K., 2015b, Measurement of ^{236}U on the 1 MV AMS system at the Centro Nacional de Aceleradores (CNA), Nuc. Instrum. and Meth. in Phys. Res. B358, 45-51.

Chamizo E., López-Gutiérrez J. M., Holm E., García-Tenorio R., 2016a,^{129}I, ^{236}U, ^{239}Pu and ^{240}Pu profiles in a peatbog from the Southern Hemisphere. These Proceedings.

Chamizo E., López-Lora M., Bressac M., Levy I., Pham M. K., 2016b, Excess of ^{236}U in the northwest Mediterranean Sea, Sci. Total Environ. 565, 767-776.

Christl M., Dai X., Lachner J., Kramer-Tremblay S., Synal H. A., 2014, Low energy AMS of americium and curium, Nuc. Instrum. and Meth. in Phys. Res. B331, 225-232.

Eigl R., Srncik M., Steier P., Wallner G., 2013, ^{236}U/^{238}U and ^{240}Pu/^{239}Pu isotopic ratios in small (2 L) sea and river water samples, J. Environ. Radioact. 116, 54-58.

Eigl R., Steier P., Winkler S. R., Sakata K., Sakaguchi A., 2016, First study on ^{236}U in the Northeast Pacific Ocean using a new target preparation procedure for AMS measurements, J. Environ. Radioact. 162/163, 244-250.

Elmore D., Fulton B. R., Clover M. R., Marsden J. R., Gove H. E., Naylor H., Purser K. H., Kilius L. R., Beukens R. P., Litherland A. E., 1979, Analysis of ^{36}Cl in environmental water samples using electrostatic accelerators, Nature 277, 22-25.

Elmore D., Gove H.E., Ferraro R., Kilius L.R., Lee W., Chang K.H., Beukens R.P., Litherland A.E., Russo C.J., Murell M.T., Finkel R.C., 1980. Determination of ^{129}I using tandem accelerator mass spectrometry. Nature 286, 138-140.

Fifield L. K., Carling R. S., Cresswell R. G., Hausladen P. A., di Tada M. L., Day J. P., 2000, Accelerator mass spectrometry of ^{99}Tc, Nuc. Instrum. and Meth. in Phys. Res. B168, 427-436.

Fifield L. K., Synal H. A., Suter M., 2004, Accelerator mass spectrometry of plutonium at 300 kV, Nuc. Instrum. and Meth. in Phys. Res. B223/224, 802-806.

Froehlich M. B., Dietze M. M. A., Tims S. G., Fifield L. K., 2016, A comparison of fallout ^{236}U and ^{239}Pu uptake by Australian Vegetation, J. Environ. Radioact. 151, 558-562.

Gislefoss J. S., Nydal R., Donahue D. J., Jull A. J. T., Toolin L. T., 1994, Tracer studies of ^{14}C in the Nordic Seas by AMS measurements, Nuc. Instrum. and Meth. in Phys. Res. B92, 431-435.

Gómez-Guzmán J. M., López-Gutiérrez J. M., Pinto A. R., Holm E., García-León M., 2010, Analysis of ^{129}I in lichens by accelerator mass spectrometry through a microwave-based sample preparation method, Nuc. Instrum. and Meth. in Phys. Res. B268, 1171-1174.

Gómez-Guzmán J. M., Villa M., Le Moigne F., López-Gutiérrez J. M., García-León M., 2013, AMS measurements of ^{129}I in seawater around Iceland and the Irminger Sea, Nuc. Instrum. and Meth. in Phys. Res. B294, 547-551.

Gómez-Guzmán J. M., Holm E., Niagolova N., López-Gutiérrez J. M., Pinto-Gómez A. R., Abril J. M., García-León M., 2014, Influence of releases of ^{129}I and ^{137}Cs from European reprocessing facilities in Fucus vesiculosus and seawater from the Kattegat and Skagerrak areas, Chemosphere 108, 76-84.

Gómez-Guzmán J. M., López-Gutiérrez J. M., García-Tenorio R., Agulló L., Peruchena J. I., Manjón G., García-León M., 2016, Estimating the impact from Fukushima in Southern Spain by ^{131}I and Accelerator Mass Spectrometry detection of ^{129}I, J. Environ. Radioact. article in press, 1-9.

Gove H. E., Purser K. H., Litherland A. E., 2010, Accelerator Mass Spectrometry (AMS) 1977–1987, Nuc. Instrum. and Meth. in Phys. Res. B268, xvii–xxii.

Hain K., Faestermann T., Famulok N., Fimiani L., Gómez-Guzmán J. M., Korschinek G., Kortmann F., Lierse v. Gostomski Ch., Ludwig P., Shinonaga T., 2015, Analytical method for the determination of Np and Pu in sea water by AMS with respect to the Fukushima accident, Nuc. Instrum. and Meth. in Phys. Res. B361, 505-509.

Hansen V., Yi P., Hou X., Aldahan A., Roos P., Possnert G., 2011, Iodide and iodate (^{129}I and ^{127}I) in surface water of the Baltic Sea, Kattegat and Skagerrak, Sci. Total Environ. 412-413, 296-303.

Hernández-Mendoza H., Chamizo E., Yllera A., García-León M., Delgado A., 2010, Measurement of ^{239}Pu in urine samples at ultra-trace levels using a 1 MV compactAMS system, Nuc. Instrum. and Meth. in Phys. Res. B268, 1331-1333.

Jabbar T., Wallner G., Steier P., 2013, A review on ^{129}I analysis in air, J. Environ. Radioact. 126, 45-54.

Janovics R., Kelemen D. I., Kern Z., Kapitany S., Veres M., Jull A.J.T., Molnar M., 2016, Radiocarbon signal of a low and intermediate level radioactive waste disposal facility in nearby trees, J. Environ. Radioact. 153, 10-14.

Kilius LR, Baba N, Garwan MA et al., 1990, AMS of heavy ions with small accelerators. Nucl Instrum Methods B52, 357-365.

Levy I., Chamizo E., López-Lora M., Bressac M., 2016, Analysis of Pu isotopes and ^{237}Np in seawater by AMS. These Proceedings.

López-Gutiérrez J. M., Gómez-Guzmán J. M., Chamizo E., Peruchena J. I., García-León M., 2013, Long-lived radionuclides in residues from operation and decommissioning of nuclear power plants, Nuc. Instrum. and Meth. in Phys. Res. B294, 647-651.

López-Gutiérrez J. M., Ceballos-Romero E., Stinchcombe M., Vivó-Vilches C., Villa M., 2016, ^{129}I Concentrations in the Sputhern Hemisphere: North Atlantic versus Southern Ocean, These Proceedings.

López-Lora M., Chamizo E., Levy I., Rozmaric M., Louw D. C., Blinova O., 2016, First results of 236U in the South-Atlantic Ocean. These Proceedings.

MacDonald C. M., Charles C. R. J., Zhao X. L., Kieser W. E., Cornett R. J., Litherland A. E., 2015, Determination of ^{135}Cs by accelerator mass spectrometry, Nuc. Instrum. and Meth. in Phys. Res. B361, 554-558.

Ming H., Shan J., Bo P., Xiangdong R., Kejun D., Yongjing G., Shihong L., Shaoyong W., Jiuzi Q., Xinyi Y., Yanqiu D., 2007, ^{99}Tc measurements with accelerator mass spectrometry at CIAE, Nuc. Instrum. and Meth. in Phys. Res. B259, 708-713.

Muir G. K. P., Cook G. T., MacKenzie A. B., MacKinnon G., Gulliver P., 2015, Anomalous ^{14}C enrichments in the Eastern UK coastal environment, Radiocarbon 57, 337-345.

Muramatsu Y., Matsuzaki H., Toyama C., Ohno T., 2015, Analysis of ^{129}I in the soils of Fukushima Prefecture: preliminary reconstruction of ^{131}I deposition related to the accident at Fukushima Daiichi Nuclear Power Plant (FDNPP), J. Environ. Radioact. 139, 344-350.

PoghosyanA., Sturchio N. C., 2015, Temporal evolution of ^{36}Cl abundances in the Great Lakes, J. Environ. Radioact. 144, 62-68.

Povinec P. P., Liong Wee Kwong L., Kaizer J., Molnar M., Nies H., Palcsu L., Papp L., Pham M.K., Jean-Baptiste P., 2016, Impact of the Fukushima accident on tritium, radiocarbon and radiocesium levels in seawater of the western North Pacific Ocean: A comparison with pre-Fukushima situation, J. Environ. Radioact., article in press, 1-11.

Raisbeck G. M., Yiou F., 1999, ^{129}I in the oceans: origins and applications, Sci. Total Environ. 237/238, 31-41.

Roux C., Le Gal La Salle C., Simonucci C., Van Meir N., Fifield L. K., ASTER Team, Diez O., Bassot S., Simler R., Bugai D., Kashparov V., Lancelot J., 2014, High ^{36}Cl/Cl ratios in Chernobyl groundwater, J. Environ. Radioact. 138, 19-32.

Sakaguchi A., Kawai K., Steier P., Imanaka T., Hoshi M., Endo S., Zhumadilov K., Yamamoto M., 2010, Feasibility of using ^{236}U to reconstruct close-in fallout deposition from the Hiroshima atomic bomb, Sci. Total Environ. 408, 5392-5398.

Santos F. J., López-Gutiérrez J. M., García-León M., Schnabel Ch, Synal H. A., Suter M., 2004, Analysis of ^{36}Cl in atmospheric samples from Seville (Spain) by AMS, Nuc. Instrum. and Meth. in Phys. Res. B223/224, 501-506.

Santos F. J., López-Gutiérrez J. M., Chamizo E., García-León M., H.A. Synal, 2006, Advances on the determination of atmospheric ^{129}I by acceleratormass spectrometry (AMS), Nuc. Instrum. and Meth. in Phys. Res. B249, 772-775.

Santos F. J., López-Gutiérrez J. M., García-León M., Synal H. A., San Miguel E. G., 2007, ^{129}I record in a sediment core from Tinto River (Spain), Nuc. Instrum. and Meth. in Phys. Res. B259, 503-507.

Santos F.J., Gómez-Martínez I., García-León M., 2009, Radiocarbon measurement program at the Centro Nacional de Aceleradores (CNA), Spain, Radiocarbon 51, 883-889.

Schwehr K. A., Otosaka S., Merchel S., Kapland D. I., Zhang S., Xua C., Li H.-P., Ho Y.-F., Yeager C. M., Santschi P. H., ASTER Team, 2014, Speciation of iodine isotopes inside and outside of a contaminant plume at the Savannah River Site, Sci. Total Environ. 497/498, 671-678.

Skipperud L., Brown J., Fifield L. K., Oughton D. H., Salbu B., 2009, Association of plutonium with sediments from the Ob and Yenisey Rivers and Estuaries, J. Environ. Radioact. 100, 290-300.

Sookdeo A., Cornett J., Kieser W. E., 2015, Optimizing production of Pb beams for ^{205,210}Pb analysis by Accelerator Mass Spectrometry, Nuc. Instrum. and Meth. in Phys. Res. B361, 450-453.

Srncik M., Steier P., Wallner G., 2011, Depth profile of ^{236}U/^{238}U in soil samples in La Palma, Canary Islands, J. Environ. Radioact. 102, 614-619.

Srncik M., Tims S. G., De Cesare M., Fifield L. K., 2014, First measurements of ^{236}U concentrations and ^{236}U/^{239}Pu isotopic ratios in a Southern Hemisphere soil far from nuclear test or reactor sites, J. Environ. Radioact. 132, 108-114.

Tierney K. M., Muir G. K. P., Cook G. T., MacKinnon G., Howe J. A., Heymans J. J., Xu S., 2016, Accumulation of Sellafield-derived radiocarbon (^{14}C) in Irish Sea and West of Scotland intertidal shells and sediments, J. Environ. Radioact. 151, 321-327.

Tosaki Y., Tase N., Sasa K., Takahashi T., Nagashima Y., 2012,Measurement of the ^{36}Cl deposition flux in central Japan: natural background levels and seasonal variability, J. Environ. Radioact. 106, 73-80.

Tumey S. J., Brown T. A., Hamilton T. E., Hillegonds D. J., 2008, Accelerator mass spectrometry of strontium-90 for homeland security, environmental monitoring and human health,Nuc. Instrum. and Meth. in Phys. Res. B266, 2242-2245.

Tuniz C., Norton G., 2008, Accelerator mass spectrometry: New trends and applications, Nuc. Instrum. and Meth. in Phys. Res. B266, 1837-1845.

United Nations Scientific Committee on the Effects of Atomic Radiation UNSCEAR, 2008. Report to the General Assembly, Annex B: Exposure of the Public and Workers of Various Sources of Radiation, vol. 1, p. 247.

Villa M., Chamizo E., López-Lora M., Kenna T. Casacuberta N., Christl M., 2016, Measurement of ^{236}Uat the GEOTRACES East Pacific zonal transect. These Proceedings.

Vockenhuber C., Christl M., Hofmann C., Lachner J., Müller A. M., Synal H. A., 2011, Accelerator mass spectrometry of ^{236}U at low energies, Nuc. Instrum. and Meth. in Phys. Res. B269, 3199-3203.

Wacker L., Fifield L. K., Tims S. G., 2004, Developments in AMS of ^{99}Tc, Nuc. Instrum. and Meth. in Phys. Res. B223/224, 185-189.

Wang X., Jiang S., Dong K., He M., He G., Li Ch., Li S., Gong J., Lu L., 2010, Development of laboratory standards for AMS measurement of ^{237}Np, Nuc. Instrum. and Meth. in Phys. Res. B268, 1949-1953.

Wang Z.,Hu D., Xu H., Guo Q., 2014, ^{14}C distribution in atmospheric and aquatic environments around Qinshan nuclear power plant, China, Radiocarbon 56, 1107-1114.

^{129}I, ^{236}U, ^{239}Pu and ^{240}Pu profiles in a peatbog from the Southern Hemisphere

Elena Chamizo[1], Jose María López-Gutierrez[1],

Elis Holm[2] and Rafael García-Tenorio[1]

[1] *Spanish National Accelerator Centre, Sevilla, Spain*

[2] *Gothenburg University, Sweden*

Abstract

^{129}I, ^{236}U, ^{239}Pu and ^{240}Pu isotopes have been analyzed in the different layers of a peatbog core collected in Madagascar Island (South Hemisphere) and representing at least the last 100 years of atmospheric deposition. The determination of ultra-low levels of these isotopes has been possible by applying the Accelerator Mass Spectrometric Technique (AMS) by using the 1 MV Tandetrom AMS facility located at CNA (Seville, Spain). The elements of interest were extracted and isolated previous to the measurements by applying validated radiochemical procedures.

In this contribution, the behavior along the core of the different isotopes under analysis will be discussed, evaluating in particular the magnitude of their post-depositional retention/migration. In this sense, it will be highlighted the great mobility of the ^{129}I with a near uniform profile along the core, in opposition for example with the preservation for the Pu isotopes of the fallout bomb peak.

In the case of ^{236}U, the ^{236}U/^{239}Pu atomic ratios determined in a total of eight layers of the core are ranging in the interval 0.02 – 0.29 with an average value of 0.15. As far as we know, these are the first ^{236}U results seeing the light that were obtained in deposits as peatbogs collected in the southern hemisphere.

Experimental Set-up and Objectives

The main objective of the work was to obtain the profiles for several artificial radionuclides (^{239}Pu, ^{240}Pu, ^{129}I and ^{236}U) in a peatbog collected in the Southern Hemisphere (Madagascar) by Accelerator Mass Spectrometry (AMS). These determinations hardly can be done by radiometric techniques due to the low levels expected for the analyzed radionuclides.

The behavior of the mentioned radionuclides in the peatbog core has been analyzed, and information (scarce in the literature) about ^{240}Pu/^{239}Pu, ^{236}U/^{238}U and ^{236}U/^{239}Pu atom ratios in the environment of the southern hemisphere are given and briefly discussed.

The study have been done by using the SARA (Spanish Accelerator Radionuclide Analyses) system of 1 MV (LEAMS) located at the Spanish National Accelerator Centre in Seville, Spain. A schematic representation of the set-up is shown in Figure 1. Radiochemical and measurement procedures used at CNA with SARA for the radionuclides involved in this work, can be found in the following references: Santos et al. (2006), Chamizo et al. (2008), Gomez-Guzmán et al. (2012), Chamizo et al. (2015) and Scognamiglio et al. (20169. In addition, and in aliquots of the different layers of the profile, ^{238}U activity concentrations have been determined by alpha-particle spectrometry after applying a radiochemical method for isolation and conditioning for the measurement (Lehritani et al., 2012).
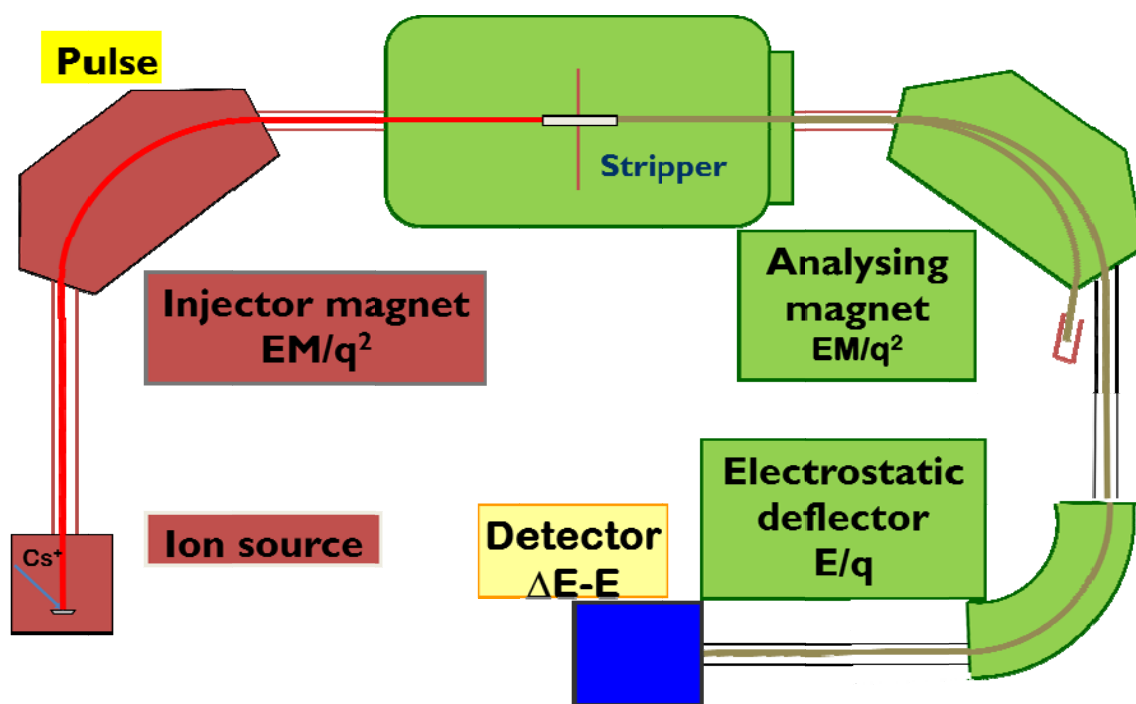
Figure 1.- Schematic representation of the SARA LEAMS system

Results

The ^{129}I, ^{239}Pu, ^{236}U and ^{238}U concentrations, expressed in atoms/g, in a total of eight layers from the analyzed peatbog are compiled in Table 1, while in Table 2 are compiled the ^{240}Pu/^{239}Pu, ^{236}U/^{238}U and ^{236}U/^{239}Pu atom ratios.

The corresponding ^{129}I and ^{236}U profiles, in the Figure 1, and the ^{240}Pu/^{239}Pu and ^{236}U/^{239}Pu atom ratios, in the Figure 2, are also represented. All the set of results are briefly commented and discussed in the following section.

CODE	DEPTH (cm)	^{129}I (atoms/g)	^{239}Pu (atoms/g)	^{236}U (atoms/g)	^{238}U (atoms/g)
TOT – 2	2 -4 cm	$(11.47 \pm 0.81)10^6$	$(264.5 \pm 5.7)10^6$	$(59.9 \pm 3.4)10^6$	$(16.3 \pm 1.2)10^{14}$
TOT – 5	8 – 10 cm	$(10.36 \pm 2.42)10^6$	$(187.9 \pm 5.2)10^6$	$(35.0 \pm 1.9)10^6$	$(35.4 \pm 2.1)10^{14}$
TOT – 7	12 – 14 cm	$(7.25 \pm 2.11)10^6$	$(28.6 \pm 1.7)10^6$	$(4.9 \pm 1.1)10^6$	$(19.3 \pm 1.4)10^{14}$
TOT – 9	16 – 18 cm	$(3.49 \pm 0.25)10^6$	$(27.1 \pm 1.6)10^6$	$(2.5 \pm 0.6)10^6$	$(26.7 \pm 1.6)10^{14}$
TOT – 10	18 – 20 cm	$(4.63 \pm 1.29)10^6$	$(163.9 \pm 4.3)10^6$	$(3.7 \pm 0.6)10^6$	$(22.3 \pm 1.6)10^{14}$
TOT – 11	20 – 22 cm	$(2.09 \pm 0.12)10^6$	$(28.9 \pm 1.5)10^6$	$(3.4 \pm 0.8)10^6$	$(25.5 \pm 1.6)10^{14}$
TOT – 12	22 – 24 cm	$(2.38 \pm 0.86)10^6$	$(12.2 \pm 1.0)10^6$	$(1.3 \pm 0.4)10^6$	$(24.3 \pm 1.2)10^{14}$
TOT – 13	24 – 26 cm	$(3.44 \pm 0.34)10^6$	$(6.5 \pm 0.7)10^6$	$(1.9 \pm 0.4)10^6$	$(22.3 \pm 0.7)10^{14}$

Table 1.- ^{129}I, ^{239}Pu, ^{236}U and ^{238}U concentrations (atoms/g) in the different layers of the analyzed peatbog

CODE	DEPTH (cm)	^{240}Pu/^{239}Pu	^{236}U/^{238}U	^{236}U/^{239}Pu
TOT – 2	2 -4 cm	0.150 ± 0.007	$(3.67 ± 0.34)10^{-8}$	0.23 ± 0.01
TOT – 5	8 – 10 cm	0.171 ± 0.010	$(0.99 ± 0.09)10^{-8}$	0.19 ± 0.01
TOT – 7	12 – 14 cm	0.173 ± 0.024	$(0.25 ± 0.06)10^{-8}$	0.17 ± 0.04
TOT – 9	16 – 18 cm	0.100 ± 0.018	$(0.09 ± 0.02)10^{-8}$	0.09 ± 0.02
TOT – 10	18 – 20 cm	0.069 ± 0.005	$(0.17 ± 0.04)10^{-8}$	0.02 ± 0.01
TOT – 11	20 – 22 cm	0.091 ± 0.014	$(0.13 ± 0.03)10^{-8}$	0.12 ± 0.03
TOT - 12	22 – 24 cm	0.105 ± 0.025	$(0.05 ± 0.02)10^{-8}$	0.11 ± 0.04
TOT - 13	24 – 26 cm	0.105 ± 0.037	$(0.09 ± 0.02)10^{-8}$	0.29 ± 0.07

Table 2.- ^{240}Pu/^{239}Pu, ^{236}U/^{238}U and ^{236}U/^{239}Pu atom ratios in the different layers of the analyzed peatbog.
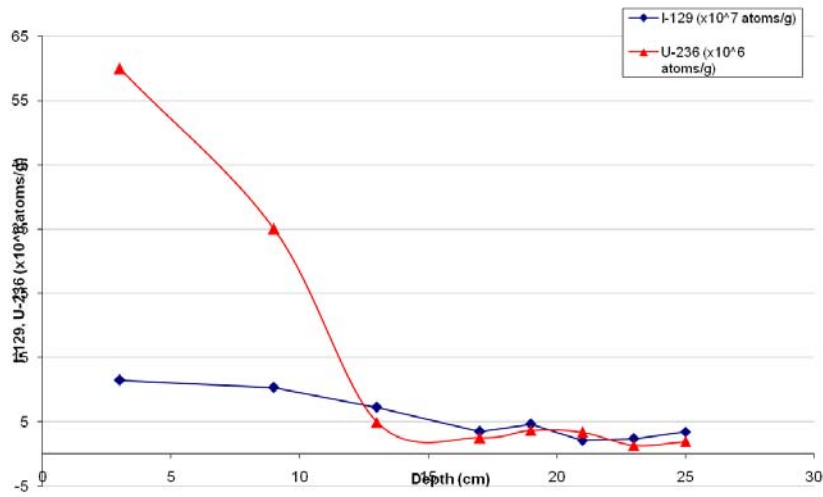
Figure 1.- ^{129}I and ^{236}U profiles in the analyzed core.
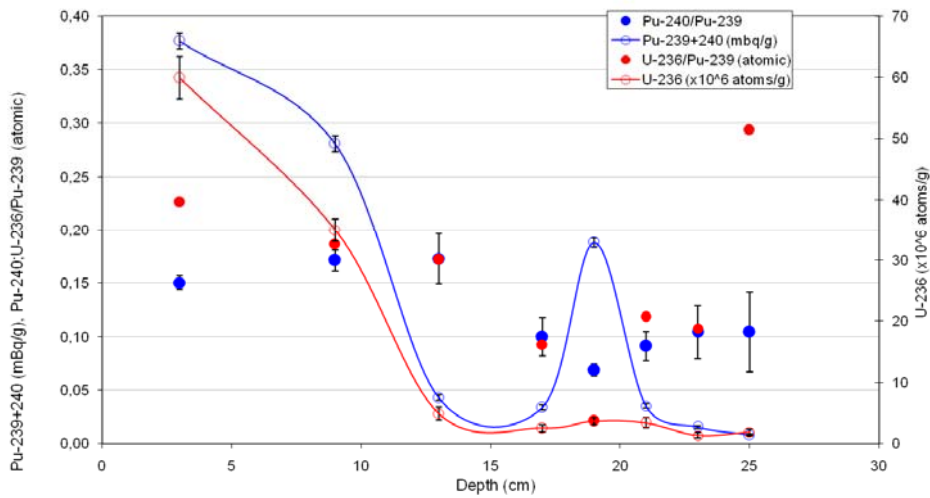
Figure 2.- $^{239+240}$Pu (mBq/g), ^{240}Pu/^{239}Pu and ^{236}U/^{239}Pu atom ratios profiles

Discussion

The set of obtained results deserve the following comments:

-The ^{129}I deposited historically is not preserved without translocation in the different layers of the peatbog, moving along the entire core. The levels of ^{129}I are on the other hand low, indicating the possible no accumulation of all the ^{129}I atmospherically deposited over time.

-The ^{239}Pu profile shows enhanced concentrations of this radionuclide in the uppermost layers indicating an upward mobilization of a fraction of the historical record of deposited ^{239}Pu over time. However, a clear peak is observed around 18-20 cm, which can be associated to the maximum deposition of global fallout in 1962-63. The chronology established by the ^{210}Pb method ratifies the mentioned age-depth association.

-The ^{236}U profile indicates that this radionuclide in the peatbog suffers its remobilization, being not preserved any historical information about its deposition. Its mobility is clearly higher than the observed one for Pu.

-The mean ^{240}Pu/^{239}Pu atom ratio is lower than the value for global fallout, but in a good number of the uppermost layers, the results are consistent with the average ratio of 0.17 ± 0.03 for the southern hemisphere. In the deepest layers, associated to the years 1950-1970, even lower values have been found, fact that can be an evidence of the deposition by local fallout of some ^{239}Pu with origin in the disintegration over the collection area of the SNAP-9A satellite at the beginning of the 60´s. NEVERTHELESS, MORE EVIDENCES ARE NEEDED.

-The ^{236}U/^{238}U atom ratios are at least three orders of magnitude higher than natural background . ^{236}U anthropogenic origin of this radionuclide in the southern hemisphere is global fallout, as ^{236}U is produced by nuclear or thermonuclear bombs.

-The values of the ^{236}U/^{238}U atom ratio are on the other hand clearly lower than the found one in the vicinities of reprocessing plants and nuclear facilities, because another fraction of anthropogenic ^{236}U in the environment is originated in the mentioned facilities.

Generation of similar profiles in other peatbog cores collected in the area are now under development with special emphasis in the analysis of the actinide nuclides (^{236}U, ^{239}Pu and ^{240}Pu) by AMS and the determination of ^{238}Pu by alpha-particle spectrometry. The objective is to evaluate the magnitude of possible local fallout existing in the area with origin in the accident of the SNAP-9A satellite.

Acknowledgements

References

E. Chamizo, S.M. Enamorado, M.García-León, M. Sutter and L. Wacker
Plutonium Measurements on the 1 MV AMS system at the Centro Nacional de Aceleradores (CNA)
Nuclear Instruments and Methods B 266 (2008) 4948-4954

E.Chamizo, M. Christi and L.K.Fifield
Measurement of ^{236}U on the 1 MV AMS system at the Centro Nacional de Aceleradores (CNA)
Nuclear Instruments and Methods B 358 (2015) 45-51

J.M.Gomez-Guzmán, J.M.Lopez-Gutierrez, A. R. Pinto, E.Holm
[129]I measurements on the 1MV AMS facility at the Centro Nacional de Aceleradores (CNA, Spain)
Applied Radiation and Isotopes 70 (2012) 263-268

M. Lehritani, J. Mantero, N. Casacuberta, P. Masqué and R. García-Tenorio
Comparison of two sequential separation methods for U and Th determination in environmental samples by alpha-particle spectrometry
Radiochimica Acta 100 (2012) 431-438

F.J. Santos, J.M.Lopez-Gutierrez, E. Chamizo, M. García-León and H. Synal
Advances on the determination of [129]I by accelerator mass spectrometry (AMS)
Nuclear Instruments and Methods B 249 (2006) 772-775

G. Scognamiglio, E. Chamizo, J.M.Lopez-Gutierrez, A.M.Muller, S. Padilla, F.J. Santos, M. López-Lora, C.Vivo-Vilches and M. García-León
Recent developments of the 1MV AMS facility at the Centro Nacional de Aceleradores
Nuclear Instruments and Methods B 375 (2016) 17-25

Survey of Iodine-129 in soil from South Korea

H. Kim[*], J. M. Lim, Y. Y. Ji, W. Lee, K. H. Chung, and M. J. Kang

Environmental Radioactivity Assessment Team, Korea Atomic Energy Research Institute,
111 Daedeok-daero 989, Yuseong-gu, Daejeon, 34057, Korea

Abstract

Ten samples in a surface soil were taken near nuclear facility in republic of Korea. The soil samples were combusted in Pyrolyzer and ^{127}I was then analysed using ICP-MS. Iodine-129 was extracted based on extraction and back-extraction using CCl_4, and then analysed by AMS (accelerator mass spectrometry) at the Xi'an AMS centre. The iodine isotopic ratio (^{129}I/^{127}I) near the nuclear facility ranges from 2.05×10^{-9} to 1.90×10^{-8}. The ^{129}I/^{127}I ratio depends on the concentration of ^{127}I in the soil. These are the first ^{129}I dataset in soil from Korea. The analysis of ^{129}I in soil is applicable for the retrospective dosimetry of the radiation exposure caused by ^{131}I, which cannot be detected after several months owing to its short half-life ($T_{1/2}$=8 d).

Introduction

Many studies reported the strong correlation between childhood thyroid cancer and thyroid exposure dose from ^{131}I ($T_{1/2}$=8 d) released from Chernobyl accident (Beral et al., 1992; Hou et al., 2003; Prisyazhiuk et al., 1991). The concentration of ^{131}I around an accident site has not adequately measured at that time. The concentration of ^{137}Cs ($T_{1/2}$= 30.1 y) in the radio-contaminated area was studied to reconstruct the ^{131}I deposited area. However, the results of the ^{137}Cs concentration is not completely correlated with the level of ^{131}I due to different chemical behaviour in the environment (Hou et al., 2003). ^{129}I ($T_{1/2}$= 1.57×10^7 y) is the proxy for ^{131}I because they are of the radioisotopes, and therefore identically behave in the environment after the nuclear accident.

^{129}I is naturally produced through the reactions of cosmic rays with xenon and the spontaneous fission of ^{238}U in the earth crust (Hou, 2004). The natural atomic ratio of ^{129}I/^{127}I is around 10^{-12} (Moran et al., 1998). It has been increased by at least 2 orders magnitudes resulting from nuclear weapon testing, nuclear accident, and routine nuclear activity including nuclear power plant (NPP) and reprocessing facilities. However, the concentration of ^{129}I in the environment is still extremely low, so general radiometric approach including gamma spectrometry or liquid scintillation counter is not applicable for the estimation of atomic ratios of ^{129}I/^{127}I in the environment. Neutron activation analysis or accelerator mass spectrometry (AMS) is mainly suitable for the determination of ^{129}I in environmental sample (Hou et al., 2001; Hou et al., 1999; Hou et al., 2013; Miyake et al., 2012).

In this study, we presented the first dataset of ^{129}I concentration in surface soil near the Singori NPP in Korea, republic of. The concentration of ^{129}I and ^{127}I in the surface soil was chemically separated from the soil, and analysed by AMS in Xian' AMS centre. The relationship between ^{129}I/^{127}I and ^{127}I in the soil can be used as the background level in the environment in Korea, and applicable to reconstruct the ^{131}I level released from the unexpected nuclear accident.

---

[*]Corresponding author, E-mail:hckim3@kaeri.re.kr

Materials and Methods

Sample and reagents

Surface soil samples (0-5 cm) were collected in Gijang (35° 16′ 42″ N, 129° 13′ 55 ″ E) of Busan, Korea in which NPPs have been operated since 1980.Fig. 1 shows the 10 sampling locations, which are within 40 km from Singori NPP. It was dried at 70°C for two days. And samples wereground and sieved to 150 um. All chemicals, including HNO_3, $NaHSO_3$, $CHCl_3$, $NaNO_2$ were of analytical grade (Sigma-Aldrich, USA) and all solutions were prepared using de-ionized water (DIW, MilliQ-Plus, 18 MΩ.).
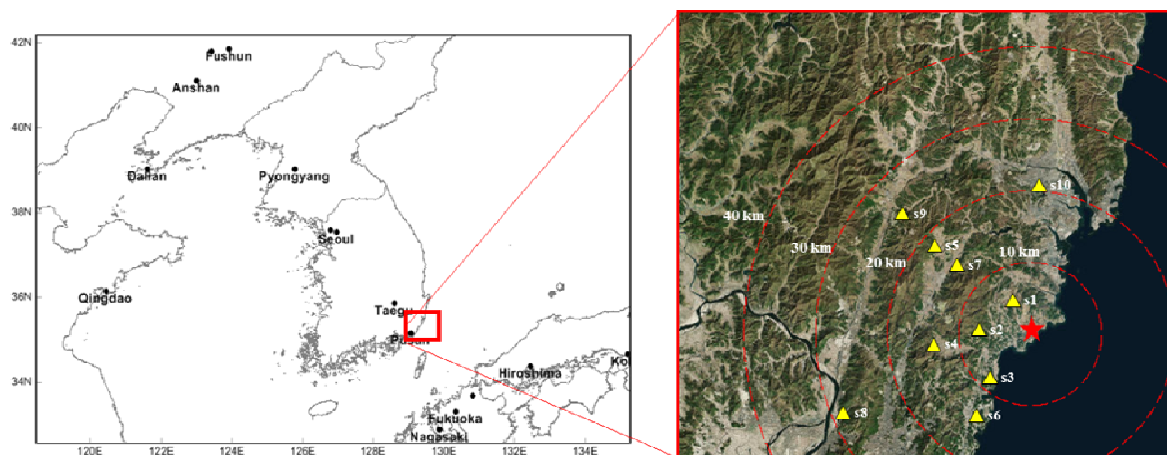
Figure 1. Sampling locationsnear Singori nuclear power plant

Pretreatment and chemical separation

Samples of 0.5 or 1 g were taken for the determination of ^{127}I and ^{129}I concentration. Each soil sample were placed into a boat for the combustion, then 100 Bq of ^{125}I was added with sample as a recovery tracer. It was combusted using Pyrolyzer (Raddec, UK), and the outgas was trapped in about 30 mL of alkali solution containing 1 M NaOH and 0.02 M $NaHSO_3$(Wang et al., 2010). After the combustion, 1 mLof the trapped solution was taken for the determination of ^{125} by gamma spectrometry and then it was used for the determination of^{127}I by ICP-MS. Then 1 mL of ^{127}I carrier (1 mg of I mL^{-1}) was added into the remaining sample to help the precipitation of ^{129}I as AgI.In remaining trap solution, all iodine existed as iodide (I$^-$) due to $NaHSO_3$ used as reducing agent. Iodide in the sample was converted into I_2 with addition of 1 mL of 0.5 M $NaNO_2$ at low pH, then I_2 was extracted by $CHCl_3$ solution. Then, I_2 in $CHCl_3$ solution was back-extracted with a $NaHSO_3$ solution as iodide (Fig. 2). These steps were repeated two times to purify the iodine(Zhou et al., 2013).The purified I$^-$ was precipitated as AgI with 1 mL of 1 M $AgNO_3$ solution. It was centrifuged to separate the precipitate from the solution, then dried at 60°C for several hours. The dried AgI was mixed with five times (by weight) niobium powder. It was used for prepare the ^{129}I target for AMS. The ^{129}I analysis was performed at Xian AMS centre ofChinese Academy of Science.
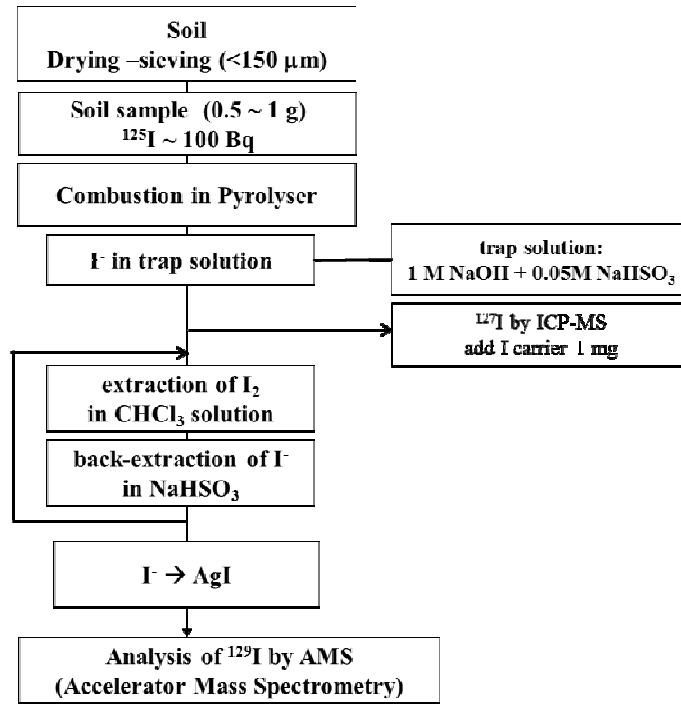
Figure 2. *Scheme of the chemical separation of ^{129}I from the soil*

Results and Discussion

The ^{129}I and ^{127}I concentration in the soil samples are listed in Table 1. The ^{127}I concentrations range from 2.1 to $17.3 10^{-6}$g g^{-1}. The ^{129}I concentrations range from 0.1 to 0.9 10^{-13}g g^{-1}. The atom ratio of ^{129}I and ^{127}I in samples ranges from 2.0×10^{-9} to 1.9×10^{-8}. It was reported that the ^{129}I concentration in surface soil collected from background area (far from nuclear facilities) ranged from 6.7×10^{-10} to 2.2×10^{-8} k. It showed the similar trend of the results of the atomic $^{129}I/^{127}I$ ratio in this study. The level of $^{129}I/^{127}I$ was not moderate correlation with the distance from the NPP. If the NPP was the source of ^{129}I, the atomic ratio of $^{129}I/^{127}I$ would be positively correlated with the distance from the NPP. However, Table 1 shows that $^{129}I/^{127}I$ was not any relationship with the distance, so the source of ^{129}I is not the NPP, the global fallout.

Table 1. *Analytical results of ^{129}I and ^{127}I in the soil*

Sample code	Distance (km)	^{127}I (10^{-6}g g^{-1})	^{129}I (10^{-13}g g^{-1})	$^{129}I/^{127}I$
Sample 01	<10	2.14	0.41	1.9×10^{-08}
Sample 02	< 10	3.01	0.14	4.5×10^{-09}
Sample 03	< 10	6.63	0.14	2.1×10^{-09}
Sample 04	10-20	17.3	0.79	4.5×10^{-09}
Sample 05	10-20	4.39	0.32	7.2×10^{-09}
Sample 06	10-20	9.94	0.58	5.7×10^{-09}
Sample 07	10-20	15.6	0.79	5.0×10^{-09}
Sample 08	20-30	8.80	0.84	9.4×10^{-09}
Sample 09	20-30	13.0	0.69	5.2×10^{-09}
Sample 10	20-30	3.70	0.65	1.7×10^{-08}

Fig.3 shows the relationship between $^{129}I/^{127}I$ and ^{127}I in samples. The ratio of $^{129}I/^{127}I$ is moderately negatively correlated with ^{127}I. This implies that the $^{129}I/^{127}I$ ratio depends on the ^{127}I concentration in the soil. It is similar with the previous studies on the relationship between $^{129}I/^{127}I$

and ^{127}I in the soil in Japan before Fukushima-Daichi nuclear power plant(FDNPP) accident(Miyake et al., 2012; Muramatsu et al., 2008). Before the FDNPP accident, $^{129}I/^{127}I$ showed the negative correlation with the concentration of ^{127}I in the soil, but $^{129}I/^{127}I$ was increased by several orders of magnitude regardless of the level of ^{127}I in the soil sample (Miyake et al., 2012).
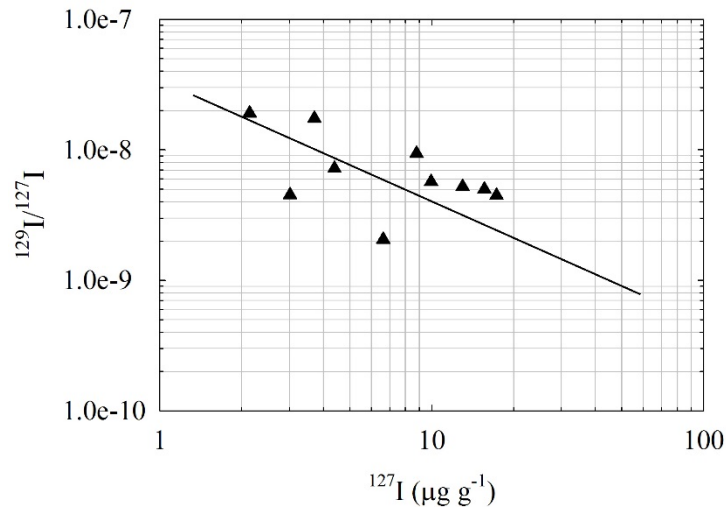
Figure 3.$^{129}I/^{127}I$ and ^{127}I in the soil

Conclusions

We presented the first dataset of ^{129}I concentration in surface soil collected around the NPP in Korea. The sampling locations is 40 km within the NPP. The analytical results of this study shows that $^{129}I/^{127}I$ ranges from 2.0×10^{-9} to 1.9×10^{-8}, and is negatively correlated with the concentration of ^{127}I. And the $^{129}I/^{127}I$ ratio has no relationship with the distance from the NPP. Its source of ^{129}I is global fallout, not the NPP. It is similar trend with $^{129}I/^{127}I$ ratio in Japanese soil before FDNPP accident. The analysis of ^{131}I in the initial stage of a nuclear accident is very important with respect to the radiation dosimetry considering the impact on human health. However, the survey of the area affected by deposition of ^{131}I can not sufficiently estimated owing to its short half life. As the background level of $^{129}I/^{127}I$ in Korean soil is estimated in this study, it can be applicable for reconstruction of the area contaminated by ^{131}I released from the nuclear accident.

Acknowledgement

References

Beral, V., Reeves, G., Shigematsu, I., Thiessen, J.W., 1992. Childhood thyroid cancer in Belarus. Nature 359, 680-681.
Hou, X., 2004. Application of 129I as an environmental tracer. J Radioanal Nucl Chem 262, 67-75.

Hou, X., Dahlgaard, H., Nielsen, S.P., 2001. Chemical speciation analysis of 129I in seawater and a preliminary investigation to use it as a tracer for geochemical cycle study of stable iodine. Mar Chem 74, 145-155.

Hou, X., Dahlgaard, H., Rietz, B., Jacobsen, U., Nielsen, S.P., Aarkrog, A., 1999. Determination of 129I in seawater and some environmental materials by neutron activation analysis. Analyst 124, 1109-1114.

Hou, X., Povinec, P.P., Zhang, L., Shi, K., Biddulph, D., Chang, C.C., Fan, Y., Golser, R., Hou, Y., Ješkovský, M., Jull, A.J.T., Liu, Q., Luo, M., Steier, P., Zhou, W., 2013. Iodine-129 in seawater offshore fukushima: Distribution, inorganic speciation, sources, and budget. Environ Sci Technol 47, 3091-3098.

Hou, X.L., Fogh, C.L., Kucera, J., Andersson, K.G., Dahlgaard, H., Nielsen, S.P., 2003. Iodine-129 and Caesium-137 in Chernobyl contaminated soil and their chemical fractionation. Sci Total Environ 308, 97-109.

Miyake, Y., Matsuzaki, H., Fujiwara, T., Saito, T., Yamagata, T., Honda, M., Muramatsu, Y., 2012. Isotopic ratio of radioactive iodine (129I/131I) released from Fukushima Daiichi NPP accident. Geochem J 46, 327-333.

Moran, J.E., Fehn, U., Teng, R.T.D., 1998. Variations in 129I/127I ratios in recent marine sediments: Evidence for a fossil organic component. Chem Geol 152, 193-203.

Muramatsu, Y., Takada, Y., Matsuzaki, H., Yoshida, S., 2008. AMS analysis of 129I in Japanese soil samples collected from background areas far from nuclear facilities. Quaternary Geochronology 3, 291-297.

Prisyazhiuk, A., Pjatak, O.A., Buzanov, V.A., Reeves, G., Beral, V., 1991. Cancer in the Ukraine, post-Chernobyl. The Lancet 338, 1334-1335.

Wang, Z., He, C., Li, H., Zhao, Y., Chen, N., Zhang, L., Liu, Q., Luo, M., Liang, W., Fan, Y., 2010. Measurement of 129I level around a nuclear power plant by Accelerator Mass Spectrometer, 18th International Conference on Nuclear Engineering, ICONE18, Xi'an.

Zhou, W., Chen, N., Hou, X., Zhang, L., Liu, Q., He, C., Fan, Y., Luo, M., Zhao, Y., Wang, Z., 2013. Analysis and environmental application of 129I at the Xi'an Accelerator Mass Spectrometry Center. Nucl Instrument Meth B 294, 147-151.

First results of Uranium-236 in the South Atlantic Ocean

Mercedes López-Lora[1,2]*, Elena Chamizo[1], Oxana Blinova[3], Martina Rožmarić[3], Deon C. Louw[4], Isabelle Levy[3]

[1]Centro Nacional de Aceleradores (CNA). Universidad de Sevilla. Junta de Andalucía. Consejo Superior de Investigaciones Científicas. Parque científico y tecnológico Cartuja. Thomas Alva Edison 7, 41092, Sevilla, Spain
[2]Dpto. de Física Aplicada I, Escuela Universitaria Politécnica, Universidad de Sevilla, Virgen de África 7, 41011 Sevilla, Spain
[3]International Atomic Energy Agency, Environment Laboratories, MC 98000 Monaco
[4]National Marine Information and Research Centre, PO Box 912, Swakopmund, Namibia

Abstract

In the last years, ^{236}U (T$_{1/2}$=2.34·10^7 y), which is essentially an anthropogenic radionuclide, has been established as a new oceanographic tracer thanks to its conservative behaviour in seawater. At the Centro Nacional de Aceleradores (CNA), in Seville (Spain), it has been recently demonstrated that ^{236}U can be determined at environmental levels on the 1 MV Accelerator Mass Spectrometry (AMS) system. In the framework of the existing collaboration between the National Marine Information and Research Centre (NatMIRC), in Namibia, and the IAEA Environment Laboratories in Monaco, ^{236}U has been analysed by AMS at CNA in a set of seawater samples collected in the northern Benguela upwelling system, on the Namibian coast. In surface samples, ^{236}U/^{238}U atom ratios at the level of 10^{-10} have been obtained, in agreement with the expected values for the so-called global fallout. The ^{236}U inventories reported up to now in seawater are discussed.

Introduction

The naturally occurring isotopes of uranium are the alpha emitters ^{238}U (T$_{1/2}$=4.51·10^9 y), ^{235}U (T$_{1/2}$=7.038·10^8 y) and ^{234}U (T$_{1/2}$=2.455·10^5 y), and their atomic abundances are, respectively, 99.2742%, 0.7204% and 0.0054%. These isotopes have been extensively measured in seawater for oceanographic studies because of their conservative behaviour in the seawater. Typical ^{238}U concentrations in the oceans are approximately 3.5 ppb (3.5 µg/L or 3.5 mBq/L), so they can be easily assessed by conventional radiometric and/or mass spectrometry (MS) techniques (Boulyga and Heumann 2006).In contrast, ^{236}U(T$_{1/2}$=2.342·10^7 y) has mainly an anthropogenic origin. It has been estimated that about 10^6 kg of ^{236}U has been produced by men since the onset of the nuclear age in the 1940´s (i.e. in atomic bombs mainly via the reaction ^{238}U(n,3n)^{236}U induced by fast neutrons; in nuclear reactors via the reaction ^{235}U(n,γ)^{236}U induced by thermal neutrons; and in minor amounts from the alpha-decay of its parent, ^{240}Pu (T$_{1/2}$=6524 y)). On the other hand, it has been estimated that about 35 kg of ^{236}U have a natural origin (i.e. produced by the neutron activation of the natural ^{235}U by cosmogenic and nucleogenic neutrons)(Christl et al. 2012). In recent years, several studies have been focused on the determination of ^{236}U in seawater (Casacuberta et al. 2014, Casacuberta et al. 2016, Chamizo et al. 2015b, Christl et al. 2012, Christl et al. 2013, Sakaguchi et al. 2012). ^{236}U is a powerful oceanographic tracer because of its long half-life and the fact that, unlike natural uranium isotopes, it has not reached steady-state in the oceans because it has been released to the general environment in the last 70 years(Sakaguchi et al. 2012, Christl et al. 2012). However, ^{236}U concentrations in the environment, and specifically in the oceans, are extremely small. For instance, surface waters from the Northern Hemisphere are strongly influenced by the so-called *fallout* (i.e. atmospheric debris produced in the nuclear explosions). However, their activity concentrations, which are at the fg/L or nBq/L level, cannot be assessed by radiometric counting techniques (Casacuberta et al. 2014, Sakaguchi et al. 2012). The

---

study of ^{236}U in environmental samples has recently become possible as a result of the high sensitivity reached by modern MS systems. When ^{236}U enters the environment, it is mixed with the existing ^{238}U and a wide range of ^{236}U/^{238}U atomic ratios arises. For instance, in surface seawater from the Northern Hemisphere only influenced by the so-called *global fallout* (i.e. particles injected into the stratosphere during the high-yield nuclear atmospheric tests), atomic ratios at the 10^{-9} level have been determined (Casacuberta et al. 2014, Sakaguchi et al. 2012), and in the Equatorial Pacific Ocean, ratios at the 10^{-10} level have been determined in surface seawater and at 10^{-12} level in deep waters(Chamizo et al. 2015b). The main limitation for the determination of ^{236}U by MS techniques is the presence of scattering events and/or molecular isobars produced by the abundant isotopes,^{235}U and ^{238}U, which cannot be chemically suppressed. MS techniques such as TIMS (*Thermal Ionization Mass Spectrometry*) and HR-ICP-MS (*High Resolution Inductively Couple Plasma Mass Spectrometry*) can only measure ratios down to the 10^{-10} level(Lee et al. 2015, Roos 2008). Accelerator Mass Spectrometry (AMS) features with the lowest ^{236}U/^{238}U background atomic ratios mainly thanks to the destruction of the molecular isobars in the so-called stripping process, which occurs in the terminal of an electrostatic tandem accelerator. In the last years, compact AMS systems, working at accelerator terminal voltages of 1 MV and below, have demonstrated their potential to measure ^{236}U at environmental levels(Christl et al. 2015, Chamizo et al. 2015).

However, because of the recent development of these high sensitive AMS techniques, there is still very few information about ^{236}U in the environment and, furthermore, these data are especially rare in the South Hemisphere. In this context, the first ^{236}U results in the South Atlantic Ocean have been obtained on the 1MV AMS system at the Centro Nacional de Aceleradores (CNA), in Seville, Spain. The studied area was the coast of Namibia, in the south eastern Atlantic Ocean, where the marine environment is strongly influenced by the northwards flowing, cold Benguela upwelling current (Sakko 1998).

Materials and Methods

Samples

Sampling was done along the Namibian coast, in the framework of the existing collaboration between the National Marine Information and Research Centre (NatMIRC), in Namibia, and the IAEA Environment Laboratories (IAEA-NAEL) in Monaco. The aim of the project was to establish a baseline study of marine radioactivity and offshore trace elements levels in this area (Fig. 1). Surface seawater samples (150 L) were collected for the determination of ^{90}Sr, ^{137}Cs, ^{241}Am and Pu isotopes and processed in the IAEA-NAEL following a sequential method for the simultaneous extraction of these elements(Lee et al. 2003, La Rosa et al. 2001, Lee et al. 2001, Povinec et al. 2001). In order to analyse ^{236}U in these samples, the residues produced throughout that procedure containing most of the uranium were further processed at CNA, following a similar strategy than the one described in (Chamizo et al. 2016).
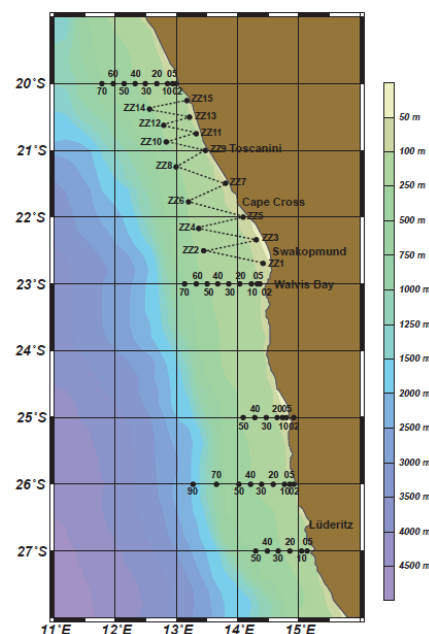
Figure 1.Map of the sampling location of the seawater samples collected by the IAEA-NAEL and the NatMIRC in the Namibia's coast, South Atlantic Ocean.

Radiochemical procedure

The radiochemical method performed in a first instance at IAEA-NAELis mainly constituted in three steps (Fig. 2). First, actinides are preconcentrated by two sequential MnO_2 and $Fe(OH)_2$ precipitations and separated from the Sr and Cs which are recovered from the first supernatant. Using an AG1-X8® resin, a first purification is performed and Pu and Am are separated. Finally, Pu and Am fractions are additionally purified. Following this method, U is not retained in the AG1-X8® resin, so the first eluates and the corresponding washings were combined and further processed. U was preconcentrated from these fractions by $Fe(OH)_3$co-precipitation, which, once dried, it was brought to the CNA for its final purification. The samples were dissolved in 8M HNO_3, spiked with 3 pg of [233]Uandloaded into TEVA resins, in order to remove the Pu traces. Finally, the U fractions were purified using UTEVA® resins. AMS cathodes were prepared by adding 1 mg of Fe(III) to the uranium solutions for their co-precipitation. Precipitates were transferred to quartz crucibles, dried and oxidized at $650^{\circ}C$. Finally samples were mixed with 3 mg of Nb powder and pressed into appropriated aluminum cathodes (Chamizo et al. 2015).
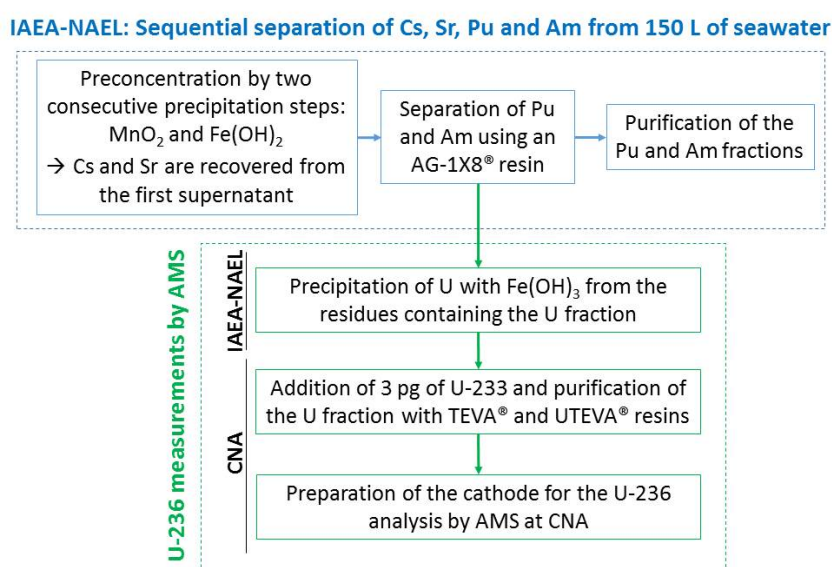
Figure 2. Radiochemical method followed in this work for the recovery of the uranium fraction from the residues obtained from the initial processing at IAEA-NAEL of 150L seawater samples. The first steps of the procedure were carried out at the IAEA-NAEL and the final uranium purification at the CNA.

Reagents and spikes

[238]U is an abundant natural radionuclide so it is important to minimize its presence in the samples. [238]U traces in reagents and laboratory equipment would underestimate the measured [236]U/[238]U atom ratios, which is the final result of an AMS measurement. To minimize its contamination, glassware was avoided when possible and, in the different $Fe(OH)_3$ co-precipitation steps, an Fe^{3+} solution provided by *High Purity Standards* (HPS, England), whose certified [238]U concentration is at the <0.5 ppb level, was used. Furthermore, in the purification of the uranium fraction at CNA, *Suprapur* grade reagents were used.
Ion chromatography extraction was performed in a vacuum box, and TEVA® and UTEVA® resins (Eichrom Industries, Inc.) in 2 mL cartridges with 100-150 µm particle size material were used.
[233]U spike was provided by the Laboratory of Ion Beam Physics, ETH Zürich (IRMM-051).

AMS measurements

AMS determinations were performed on the 1 MV AMS system at the Centro Nacional de Aceleradores (CNA, Seville, Spain). The current status of the facility is discussed in (Chamizo et al. 2015b) and (Scognamiglio et al. 2016). Briefly, uranium isotopes are extracted from the Cs^+ sputtering ion-source as negative oxide ions (UO^-). These anions are analysed by a first 90° sector magnet in the low-energy side and, then, they are accelerated along the first section of a tandem accelerator which contains the stripper gas (He) in its terminal. The molecular ions are broken up, stripped to positive charge states and the atomic breakup products undergo a second acceleration along the second acceleration tube. On the high-energy side, ions are selected first by a 90° sector magnet and later by a 120° electrostatic deflector. ^{238}U, an abundant isotope, is analysed by measuring the $^{238}U^{3+}$beam-current in an offset Faraday cup. The minor isotopes, ^{236}U and the tracer ^{233}U, are detected in a gas ionization chamber.(Chamizo et al. 2015a)

The final AMS results are the atom ratios. The main limitation to determinate the$^{236}U/^{238}U$ ratio, which characterizes the sample of interest, is the presence of ^{235}U. This abundant natural isotope may interfere to ^{236}U analysis, due to their very similar trajectories in the different cinematic filtersand to the formation of molecular isobars. The corresponding background (i.e. spurious ^{236}U counts coming from the ^{235}U in the sample) was subtracted from our results using the ratio between the counts on mass 239 and ^{238}U as a proxy, assuming no real ^{239}Pu is present in the sample (Chamizo et al., 2015), At CNA, the current$^{236}U/^{238}U$ background ratio is $9 \cdot 10^{-11}$(Scognamiglio et al., 2016).The $^{233}U/^{238}U$ and $^{236}U/^{233}U$ ratios can be used to quantify the ^{236}U and ^{238}U concentrations by using the so-called isotope-dilution method. However, for the samples studied in this work, ^{233}U was added in an intermediate step of the procedure as explained before(Fig. 2). In order to obtain the ^{236}U concentrations in the original sample, the radiochemical yield of the steps carried out at the IAEA-NAEL (i.e. before the addition of the ^{233}U spike) was estimated from the expected ^{238}U concentration in the original sample, which can be extrapolated using the empirical formulas based on the salinity data(Owens et al. 2011, Pates and Muir 2007).

Results and Discussion

The measured $^{236}U/^{238}U$ atomic ratios are at the level of 10^{-10} in all the surface samples. Regarding to the ^{236}U concentrations, the results are at the level of the nBq/L or 10^6 atoms/L. The average $^{236}U/^{238}U$ atomic ratio and ^{236}U concentration obtained from the samples located in the 20-24°S latitudinal band was $6.8 \cdot 10^{-10}$, and 5.3nBq/L, respectively, with a standard deviation of 30%. From samples located in the 24-28°S band, the average $^{236}U/^{238}U$ ratio was $6.1 \cdot 10^{-10}$ and the average ^{236}U concentration 4.7 nBq/L, with 12% standard deviation. Therefore, the average results are very similar in both cases but the obtained results are more homogenous in the band 24-28°S than in the 20-24°S. These values are considerably lower than the reportedones in surface samples from the North Atlantic Ocean, the Mediterranean Sea and the Japan Sea, which are at the level of $10^{-9}$and 10 nBq/L for $^{236}U/^{238}U$ atomic ratios and ^{236}U concentrations, respectively (Casacuberta et al. 2014, Chamizo et al. 2016, Sakaguchi et al. 2012).

The ^{236}U inventory was estimated from a depth profile studied in this area. In Fig. 3 a compilation of the different inventories published up to now in the oceans together with the one obtained from Namibian Coast is displayed. Due to the recent development of the analytical methods, there is only a few available results of the ^{236}U inventories in the oceans all around the world: Arctic Ocean (Casacuberta et al. 2016), North Atlantic Ocean (Casacuberta et al. 2014), Greenland Sea (López-Lora, 2014), Japan Sea (Sakaguchi et al. 2012) and Mediterranean Sea (Chamizo et al. 2016). Furthermore, the countries with operating Nuclear Power Plants (NPP) and the different places where the Atmospheric Nuclear Test were carried out are marked in the map*(Carter & Moghissi, 1977)*.

The main source of anthropogenic radionuclides in the environment and, most specifically, in the oceans, is the so-called *global fallout*. In the case of ^{236}U, this source has not been well defined yet because of the few available results in the different environmental compartments. Atmospheric nuclear tests were carried out mainly in the North Hemisphere (Fig. 3), the deposition of radionuclides was higher in that hemisphere, about 3.8 times the one in the South Hemisphere(Hardy et al. 1973). Furthermore, the atmospheric deposition depends strongly on the latitude: if we divide the hemisphere in three bands: 0-30° N (band 1), 30-60° N (band 2) and 60-90° N (band 3), more than 50% of this deposition happened in the band 3 (UNSCEAR, 2000). The expected ^{236}U inventories from the global fallout in the oceans from the Northern Hemisphere are $6 \cdot 10^{12}$ atoms/m^2, $13 \cdot 10^{12}$ atoms/m^2 and $5.8 \cdot 10^{12}$ atoms/m^2 in bands 1, 2 and 3, respectively (Casacuberta et al. 2014).

The NPP are potential sources of ^{236}U into the environment, highlighting, especially, the liquid effluents from the nuclear reprocessing plants (e.g. Sellafield, United Kingdom; La Hague, France) and the accidental releases(e.g. Chernobyl, Fukushima). Unlike the global fallout, these inputs of ^{236}U are local sources. From the Fig. 3, it is clear that the most of the NPP are situated in the North Hemisphere. Therefore, it is expected that this fact would contribute to increase the differences between Northern and Southern Hemispheres.
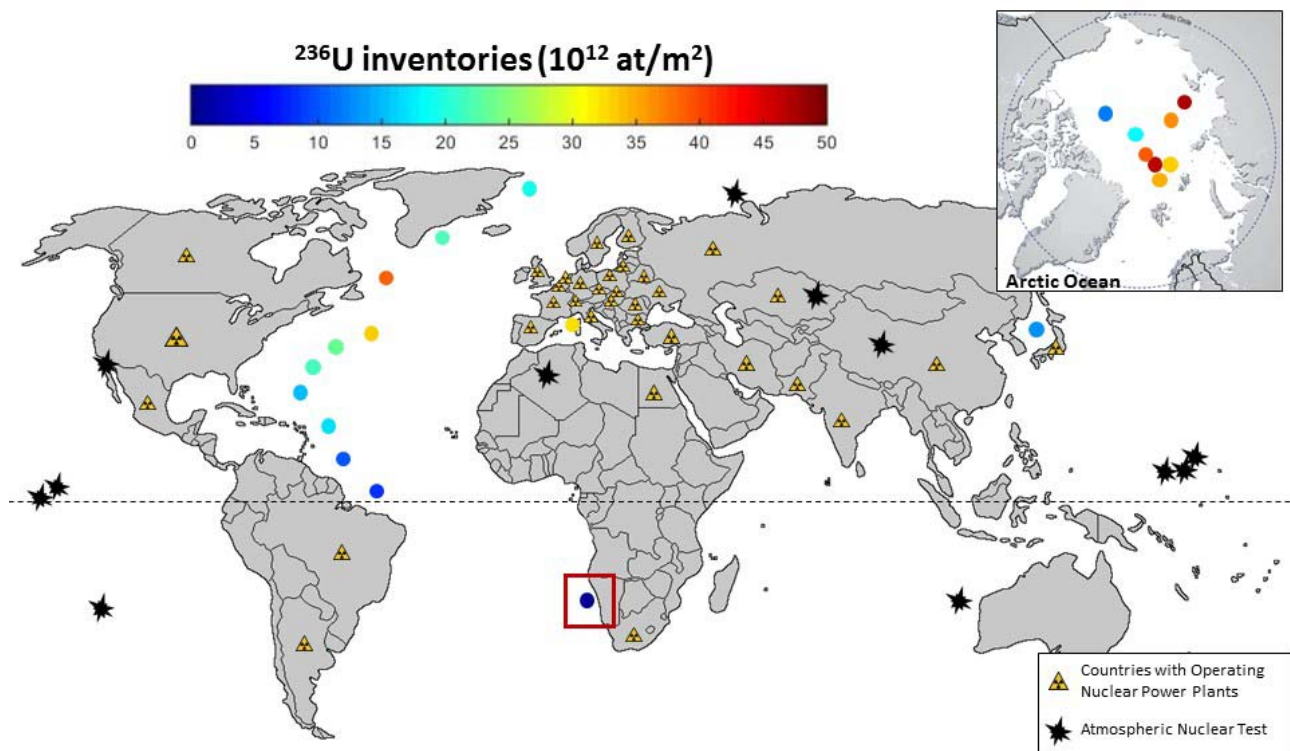
Figure3. ^{236}U *inventories reported in different studies: Arctic Ocean (Casacuberta et al. 2016), North Atlantic Ocean (Casacuberta et al. 2014), Greenland Sea (López-Lora, 2014), Japan Sea (Sakaguchi et al. 2012), Mediterranean Sea (Chamizo et al. 2016) and South Atlantic Ocean (this work). Countries with operating Nuclear Power Plants (NPP) and Atmospheric Nuclear Test locations are marked in the map(Carter & Moghissi, 1977).*

The ^{236}U inventories shown in the Fig. 3 are in agreement with the previous discussion of the main sources. The highest values of ^{236}U were obtained in the North Atlantic Ocean because of the strong influence of the nuclear reprocessing plants of Sellafield and La Hague, among others. The lowest value is the one presented in this work from the South Atlantic Ocean. As it was expected in

advance, the global fallout seems to be the main ^{236}U source in this region. Furthermore, the plutonium results from these samples also showed the influence of the global fallout. The obtained ^{240}Pu/^{239}Pu atomic ratios from the surface samples range from 0.19 to 0.20, which are the typical values of that source. Further studies are necessary to find out more information about other potential regional ^{236}U sources in the studied area.

Conclusions

This work extends the current data set of ^{236}U in seawater, presenting the first results in the South Atlantic Ocean. The results from a set of surface samples and from a depth profile showed the influence of the global fallout in this area. As it was expected because of the heterogeneous distribution of the ^{236}U released into the environment, the obtained values were lower than the ones reported in the North Hemisphere.

Acknowledgement

References

Boulyga, S. F. and Heumann, K. G. (2006) 'Determination of extremely low 236U/238U isotope ratios in environmental samples by sector-field inductively coupled plasma mass spectrometry using high-efficiency sample introduction', Journal of Environmental Radioactivity, 88(1), 10.

Carter, M. W.,Moghissi, A. A. (1977), Three decades of Nuclear Testing,Health Physics, 33, 55-71

Casacuberta, N., Christl, M., Lachner, J., van der Loeff, M. R., Masqué, P. and Synal, H. A. (2014) 'A first transect of 236U in the North Atlantic Ocean', Geochimica et Cosmochimica Acta, 133(0), 34-46.

Casacuberta, N., Masqué, P., Henderson, G., Rutgers van-der-Loeff, M., Bauch, D., Vockenhuber, C., Daraoui, A., Walther, C., Synal, H. A. and Christl, M. (2016) 'First 236U data from the Arctic Ocean and use of 236U/238U and 129I/236U as a new dual tracer', Earth and Planetary Science Letters, 440, 127-134.

Chamizo, E., Christl, M. and Fifield, L. K. (2015a) 'Measurement of 236U on the 1 MV AMS system at the Centro Nacional de Aceleradores (CNA)', Nuclear Instruments and Methods in Physics Research Section B: Beam Interactions with Materials and Atoms, 358, 45-51.

Chamizo, E., Santos, F. J., López-Gutiérrez, J. M., Padilla, S., García-León, M., Heinemeier, J., Schnabel, C. and Scognamiglio, G. (2015b) 'Status report of the 1 MV AMS facility at the Centro Nacional de Aceleradores', Nuclear Instruments and Methods in Physics Research Section B: Beam Interactions with Materials and Atoms.

Chamizo, E., López-Lora, M., Bressac, M., Levy, I. and Pham, M. K. (2016) 'Excess of 236U in the northwest Mediterranean Sea', Science of The Total Environment, 565, 767-776.

Chamizo, E., López-Lora, M., Villa, M., Casacuberta, N., López-Gutiérrez, J. M. and Pham, M. K. (2015) 'Analysis of 236U and plutonium isotopes, 239,240Pu, on the 1 MV AMS system at the Centro Nacional de Aceleradores, as a potential tool in oceanography', Nuclear Instruments and Methods in Physics Research Section B: Beam Interactions with Materials and Atoms, 361, 535-540.

Chamizo, E., Villa, M., López-Lora, M., Casacuberta, N., Christl, M. and Kenna, T. (2015b) 'First 236U results at the Equatorial Pacific Ocean', Annual report 2015, Ion Beam Physics, ETH Zurich.

Christl, M., Casacuberta, N., Lachner, J., Maxeiner, S., Vockenhuber, C., Synal, H.-A., Goroncy, I., Herrmann, J., Daraoui, A., Walther, C. and Michel, R. (2015) 'Status of 236U analyses at ETH

Zurich and the distribution of 236U and 129I in the North Sea in 2009', Nuclear Instruments and Methods in Physics Research Section B: Beam Interactions with Materials and Atoms, (0).

Christl, M., Lachner, J., Vockenhuber, C., Goroncy, I., Herrmann, J. and Synal, H.-A. (2013) 'First data of Uranium-236 in the North Sea', Nuclear Instruments and Methods in Physics Research Section B: Beam Interactions with Materials and Atoms, 294(0), 530-536.

Christl, M., Lachner, J., Vockenhuber, C., Lechtenfeld, O., Stimac, I., van der Loeff, M. R. and Synal, H.-A. (2012) 'A depth profile of uranium-236 in the Atlantic Ocean', Geochimica et Cosmochimica Acta, 77(0), 98-107.

Hardy, E. P., Krey, P. W. and Volchok, H. L. (1973) 'Global Inventory and Distribution of Fallout Plutonium', Nature, 241(5390), 444-445.

La Rosa, J. J., Burnett, W., Lee, S. H., Levy, I., Gastaud, J. and Povinec, P. P. (2001) 'Separation of actinides, cesium and strontium from marine samples using extraction chromatography and sorbents', Journal of Radioanalytical and Nuclear Chemistry, 248(3), 765-770.

Lee, C.-G., Suzuki, D., Esaka, F., Magara, M. and Song, K. (2015) 'Ultra-trace analysis of plutonium by thermal ionization mass spectrometry with a continuous heating technique without chemical separation', Talanta, 141(0), 92-96.

Lee, S.-H., La Rosa, J. J., Levy-Palomo, I., Oregioni, B., Pham, M. K., Povinec, P. P. and Wyse, E. (2003) 'Recent inputs and budgets of 90Sr, 137Cs, 239,240Pu and 241Am in the northwest Mediterranean Sea', Deep Sea Research Part II: Topical Studies in Oceanography, 50(17–21), 2817-2834.

Lee, S. H., Gastaud, J., La Rosa, J. J., Kwong, L. L. W., Povinec, P. P., Wyse, E., Fifield, L. K., Hausladen, P. A., Di Tada, L. M. and Santos, G. M. (2001) 'Analysis of plutonium isotopes in marine samples by radiometric, ICP-MS and AMS techniques', Journal of Radioanalytical and Nuclear Chemistry, 248(3), 757-764.

López-Lora, M. (2014) Medidas de Isótopos de Uranio y Plutonio por Espectrometría de Masas con Aceleradores de baja energía y sus aplicaciones en estudios oceanográficos, Trabajo Fin de Máster, Universidad de Sevilla

Owens, S. A., Buesseler, K. O. and Sims, K. W. W. (2011) 'Re-evaluating the 238U-salinity relationship in seawater: Implications for the 238U–234Th disequilibrium method', Marine Chemistry, 127(1–4), 31-39.

Pates, J. M. and Muir, G. K. P. (2007) 'U–salinity relationships in the Mediterranean: Implications for 234Th:238U particle flux studies', Marine Chemistry, 106(3–4), 530-545.

Povinec, P. P., La Rosa, J. J., Lee, S. H., Mulsow, S., Osvath, I. and Wyse, E. (2001) 'Recent developments in radiometric and mass spectrometry methods for marine radioactivity measurements', Journal of Radioanalytical and Nuclear Chemistry, 248(3), 713-718.

Roos, P. (2008) 'Analysis of radionuclides using ICP-MS' in Pavel, P. P., ed. Radioactivity in the Environment, Elsevier, 295-330.

Sakaguchi, A., Kadokura, A., Steier, P., Takahashi, Y., Shizuma, K., Hoshi, M., Nakakuki, T. and Yamamoto, M. (2012) 'Uranium-236 as a new oceanic tracer: A first depth profile in the Japan Sea and comparison with caesium-137', Earth and Planetary Science Letters, 333–334(0), 165-170.

Sakko, A. L. (1998) 'The influence of the Benguela upwelling system on Namibia's marine biodiversity', Biodiversity & Conservation, 7(4), 419-433.

Scognamiglio, G., Chamizo, E., López-Guitiérrez, J. M., Müller, A. M., Padilla, S., Santos, F. J., López-Lora, M., Vivo, C. and García-León, M. (2016) 'Recent developments of the 1 MV AMS facility at the Centro Nacional de Aceleradores', Nuclear Instruments and Methods in Physics Research Section B: Beam Interactions with Materials and Atoms.

UNSCEAR (2000) United Nations Scientific Committee on theEffects of Atomic Radiation (UNSCEAR). Sources and Effectsof Ionizing Radiation, United Nations, New York.

^{129}I in the environment

J.M. López-Gutiérrez

Universidad de Sevilla, Department of Applied Physics I, Escuela Politécnica Superior,
c/ Virgen de África, 7, 41011 Sevilla, Spain

Abstract

^{129}I is a long-lived radionuclide ($T_{1/2}$ = 15.7×10^6 years) whose presence in the environment has increased strongly since the beginning of the nuclear era. The main responsible for this are the nuclear fuel reprocessing plants of Sellafield and La Hague. Due to its tendency to enter the hydrological cycle, it has been strongly widespread especially over the Northern hemisphere. Besides, because of its biophilic behaviour, iodine can enter the food chain via the air as a result of aerial emissions. For these reasons, its importance from the point of view of Radioecology is extremely high. In this article we will present a short overview of some the traditional applications of ^{129}I in the environment.

Introduction

^{129}I is a long-lived cosmogenic radionuclide ($T_{1/2}$=15.7×10^6 years) for which the natural abundances have been altered in a significant way by human actions. Natural production processes lead to typical ^{129}I/^{127}I isotopic ratios between 10^{-12} (Kilius et al., 1992) and 6×10^{-13} (Roberts et al., 1997). The natural inventory of ^{129}I has been estimated to be ~230 kg, most of which resides in the deep oceans (Rao and Fehn, 1999). ^{129}I has also been produced anthropogenically during the last 60 years during fission processes associated with civil and military nuclear activities and accidents, such as Chernobyl (1986). An estimated 50–150 kg of ^{129}I were released to the atmosphere during the main period (1945–1964) of nuclear weapons testing (Wagner et al., 1996) and a further ~6 kg were released due to the Chernobyl accident (1986) (Gallagher et al., 2005).

However, the most significant contribution to the mobile ^{129}I inventory in the environment comes from succeeding activities of nuclear fuel reprocessing plants and, in particular, the liquid and gaseous releases from the two major European reprocessing facilities, namely NDA's plant at Sellafield (UK) and AREVA's plant at Cap de La Hague (France), which now account for >90% of the total global releases (Aldahan et al, 2007). Airborne releases from these facilities, and the fraction of their liquid ^{129}I releases volatilised from the ocean surface have been shown to be the main source of ^{129}I deposited over Europe.

The total annual ^{129}I discharge from both facilities remained below 20 kg year^{-1} (0.1 TBq year^{-1}) until the beginning of the 1990s. Later the discharge increased up to 300 kg year^{-1} (2 TBq year^{-1}) with 75% originating from La Hague facility (UNSCEAR, 2000). The ^{129}I discharges from these facilities account for >95% of the total inventory in the global ocean until 2000. This anthropogenic source thus predominated over all other sources including natural production, nuclear testing and other nuclear activities and accidents.

Detection and measurement

^{129}I decays by emitting β-particle with a maximum energy of 154.4 keV and γ-rays of 39.6 keV as well as X-rays (29–30 keV). It is possible to detect it by γ-spectrometry and β-counting by Liquid Scintillation Counting (Verrezen et al., 1992). However, these techniques show very low efficiency

because of its long half-life. A more sensitive method for the determination of ^{129}I is neutron activation analysis. In this method, the sample is irradiated with neutrons in a reactor to convert ^{129}I to short-lived ^{130}I ($T_{1/2} = 12.36$ h) by reaction ^{129}I(n, γ)^{130}I, which is then measured by γ-spectrometry. With this technique, better detection limits (1 μBq) were reported (Hou et al., 1999).

Mass spectrometry techniques have shown to be the most powerful tools for ^{129}I detection, especially in environmental samples. ICP-MS (Inductively Coupled Plasma Mass Spectrometry) has been used for ^{129}I detection. However, it shows some problems associated with low sensitivity, isobaric and molecular ions interferences (^{129}Xe, ^{127}IH$_2$, ^{89}Y^{40}Ar, ^{115}In^{14}N, ^{113}Cd^{16}O), memory effects, low abundance sensitivity of ICP-MS, especially isobar ^{129}Xe and tailing of ^{127}I (Hou et al., 2008).

Nowadays, the most widely used technique for ^{129}I detection is Accelerator Mass Spectrometry (AMS). In AMS, isotopic ratios ^{129}I/I are measured by mass spectrometry combined with the use of a tandem accelerator. This reduces strongly the possible background because molecules with the same mass as the isotope of interest are broken when they pass through the accelerator stripper, typically consisting on an Ar or He gas tube. Besides, the use of high energies also allows employing nuclear detectors, to discriminate between the isotope of interest and possible molecular fragments that arrive to the detector with the same m/q ratio. Even the presence of ^{129}Xe is not a problem for AMS, as ions are extracted from the ion source in charge state -1, in which Xe is not stable. As a result, the detection limit is very low, but it depends on the AMS facility, as different configuration can show different background levels. In any case, typical blank isotopic ratios of ^{129}I/I in the order of 10^{-14} and 10^{-13} are reported (Hou & Roos, 2008). Then, AMS is the only method for the determination of ^{129}I in the pre-nuclear age samples (^{129}I/^{127}I < 10^{-10}).

Applications

^{129}I in the marine environment

Most of the mobile iodine resides in oceans. For that reason, special attention has been paid to ^{129}I as a tracer of hydrological processes in the marine environment. However, in spite of the interest and the numerous publications on the presence of this radionuclide in the seas, the picture is not complete, and more data are needed to reconstruct the information on the sources and the ^{129}I activities, especially in the Southern Hemisphere.

A very good view of the scene was given in He et al. (2013). There, the authors compile a set of data published up to the moment on the presence and evolution of ^{129}I in the oceans. Figure 1 shows a summary of the ^{129}I concentrations in seawater samples taken all over the world as a function of latitude. It can be seen that the pre-anthropogenic level has been strongly surpassed due to the artificial discharges. While nuclear fallout due to nuclear weapons testing would be responsible of levels in the order of 10^7 atoms/l, concentrations of even 10^{12} atoms/l have been measured in the Northern Hemisphere, for example in the Irish Sea. The main responsible for this increase are the nuclear fuel reprocessing plants of Sellafield and La Hague, as described in the intriduction. Fortunately, good information on the history of the discharges is available.

Most of this ^{129}I follows a well-known path. The currents take it from La Hague to the North Sea along the English Channel where it meets the ^{129}I from Sellafield. This has a longer way as it surrounds the whole Scotland and the English coasts to the North Sea. Then, the currents carry this ^{129}I to the Arctic Ocean, following the Norwegian Coastal Current. For that reason, these zones have been extensively studied, as shown in figure 2.
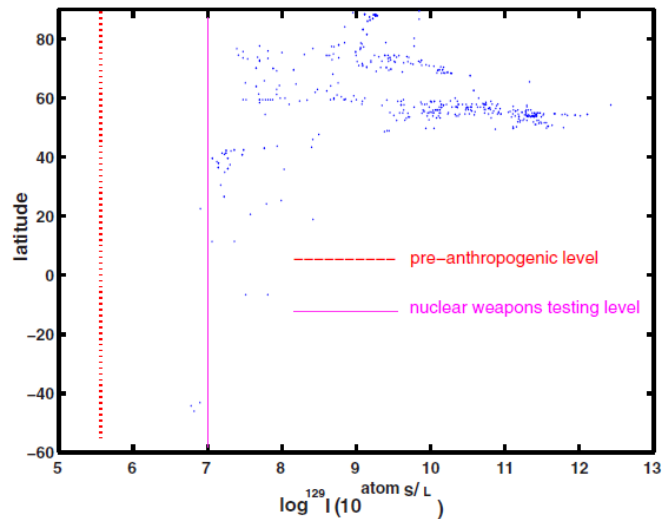
**Figure 1**. Global ^{129}I marine distribution as a function of latitude (He et al., 2013).
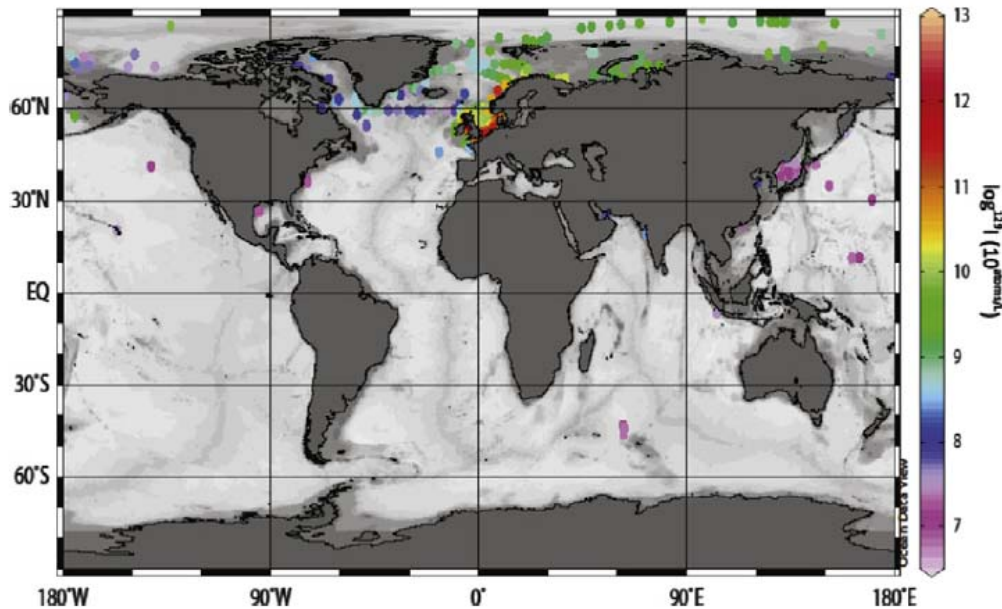
Figure 2. Sampling locations of published available ^{129}I data and the concentrations of ^{129}I in the surface water in the sampled sites (compilation by He et al., 2013).

As it can be seen, the amount of information on the presence of ^{129}I in the Southern hemisphere is, however, very scarce, and even in mid latitudes in the Northern hemisphere. For this reason, more information is needed to reconstruct the behaviour of ^{129}I in the global oceans.

^{129}I in sediments

As ^{129}I has been released to the marine environment in such large quantities, it is clear that part of has precipitated and can be found in the sediments, even when it is very conservative in water. This way, its presence in sediments can give us information not only on the amount of the contamination but also on the history of the sedimentation process and possibly on the source of the releases. An example was published by López-Gutiérrez et al. (2004), as shown in figure 3. In that work, a sediment core from the Kattegat area in the North Sea was analysed. The ^{129}I results were compared

to the ^{137}Cs activities measured in 1986. In both cases a strong increase at about 13 cm depth is consistent with the beginning of the operations at the nuclear fuel reprocessing plans of Sellafield and La Hague, in the 20th century. Thanks to the comparison with the history of the nuclear discharges from these plants, a lot of data on the transfer times and factors, sedimentation rates, residence time in water, and behaviour in the sediment column could be extracted.
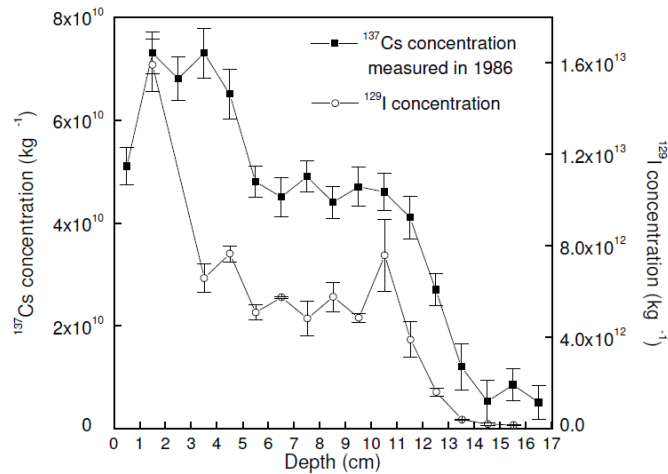

Figure 3. Depth profiles of ^{137}Cs and ^{129}I in a sediment core from Kattegat (López-Gutiérrez et al., 2004).

^{129}I in the atmosphere

Iodine is a very volatile element. Most part of the iodine in the atmosphere is evaporated from the oceans and it remains typically around 20 days both in gaseous or particulate forms. The oceans are also a very important source of ^{129}I to the atmosphere. For example, Krupp and Aumann (1999) measured isotopic ratios in the order of ^{129}I/^{127}I ~ 10^{-7} in Germany in 1994 and 1995, several orders of magnitude over the pre-nuclear level of 10^{-12}. ^{129}I discharge by the reprocessing plants in the North Sea was probably the main responsible of these high levels.

But ^{129}I is also released in a gaseous form by the nuclear fuel reprocessing plants, so the signal is very much affected by the evolution of the gaseous releases, which travel very fast long distances in a few days. Something similar happens in the case of accidental releases like the one in Fukushima in 2011. Figure 4 shows the evolution of different magnitudes in Sevilla (Spain) during the days after the accident (Gómez-Guzmán et al., 2017). It can be seen that both ^{131}I and ^{129}I were detected in air filters as well as in rainwater. However, the levels of ^{129}I before and after the accident were even higher than during the days that ^{129}I and ^{131}I from Fukushima arrived to Spain. As the authors showed, the prevalent winds during those days were favourable to the arrival of Fukushima contaminated air instead of the releases from Sellafield and La Hague.

A very relevant of ^{129}I in these cases, thanks to its long half-life, is that the analysis can be carried out many years after the samples were taken. In the previous example, ^{131}I was measured right after the sample collection but ^{129}I was measured by AMS in 2015. And then, ^{129}I can help reconstruct the ^{131}I impact (which, from the radiation protection is more relevant) long time after the emissions. An example of this can be seen on figure 5.
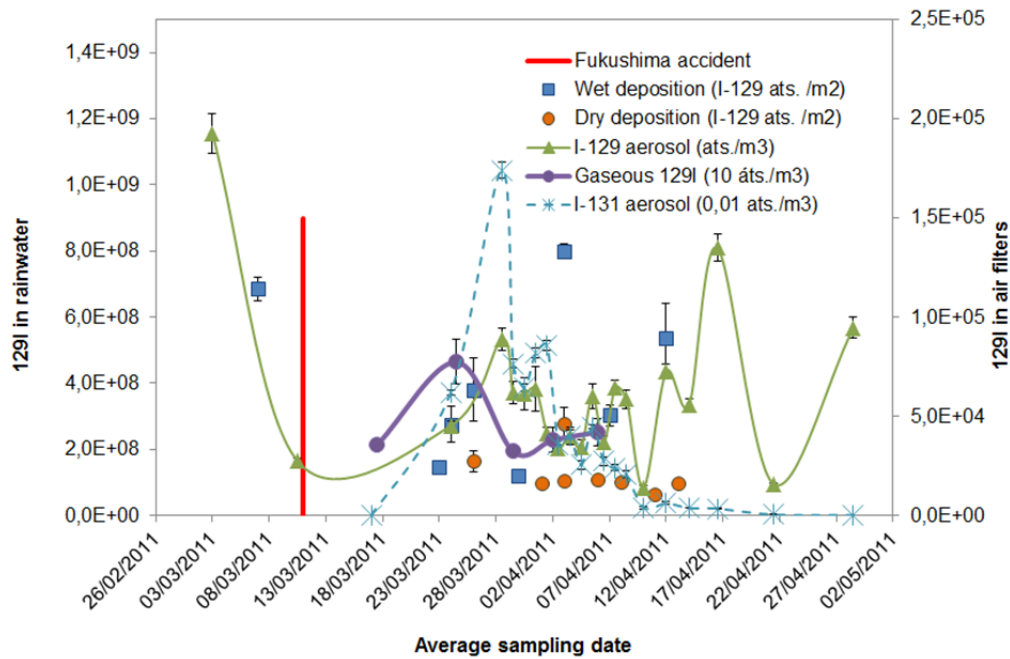
Figure 4. ^{131}I and ^{129}I detected in atmospheric samples in Sevilla (Spain) after the Fukushima accident (Gómez-Guzmán et al., 2017).
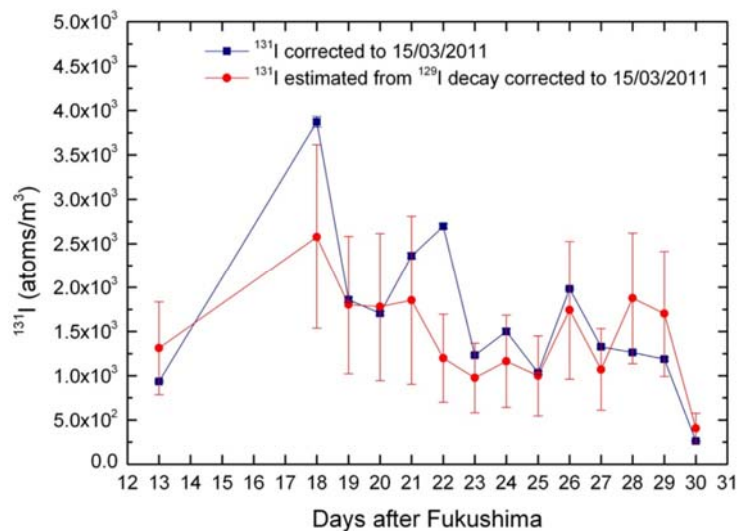
Figure 5. Comparison between the measured ^{131}I concentration in air in Sevilla after the Fukushima accident and the estimation made through the ^{129}I measurement (Gómez-Guzmán et al., 2017).

^{129}I in biota

As iodine is also a very biophilic element, ^{129}I is clearly also incorporated to the living organisms. This is relevant from the Radioecology point of view itself and also from the information that can be extracted on the sources and the ways it is transported.

Many examples can be found in the literature. In 2011, Gómez-Guzmán et al. (2011) measured the concentration of ^{129}I in lichens (*Cladonia alpestris*) from Sweden. These lichens are commonly part of the diet of reindeer, whose meat is afterwards eaten by humans. In figure 6, it is shown how ^{129}I is not uniformly distributed in the different layer of the lichens. Also, the concentrations measured

after the Chernobyl accident in 1986 increased strongly with respect to the ones detected before 1975.
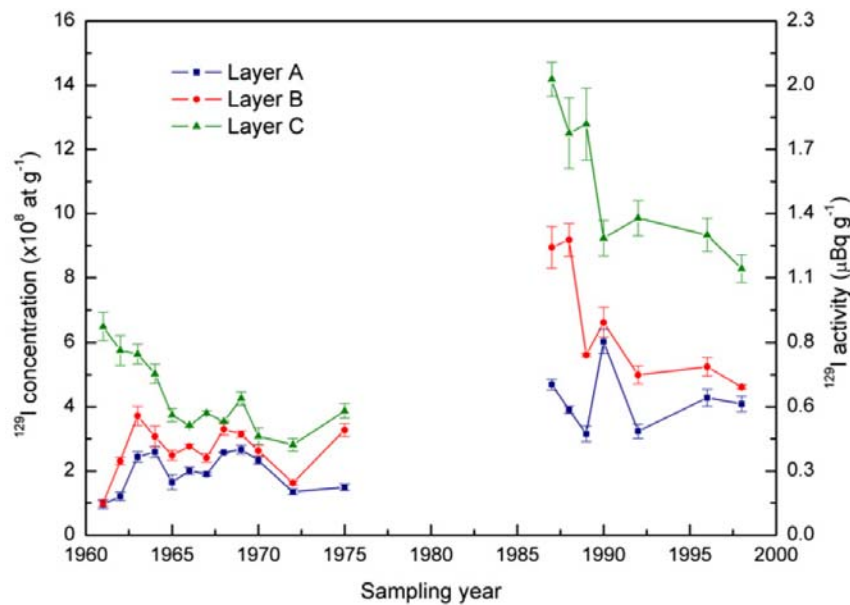
Figure 6. ^{129}I in the different layers of lichen *Cladonia alpestris* from Sweden (Gómez-Guzmán et al., 2011).

Another example can be found in Biddulph et al. (2006). The authors measured ^{129}I in coral skeletons from the Solomon Islands and Easter Island (figure 8), showing the increase of the levels due to the history of atmospheric nuclear weapons tests in this ocean in the 20th century and demonstrating that Coral skeletons preserve an iodine record in the tropical surface waters of the ocean.
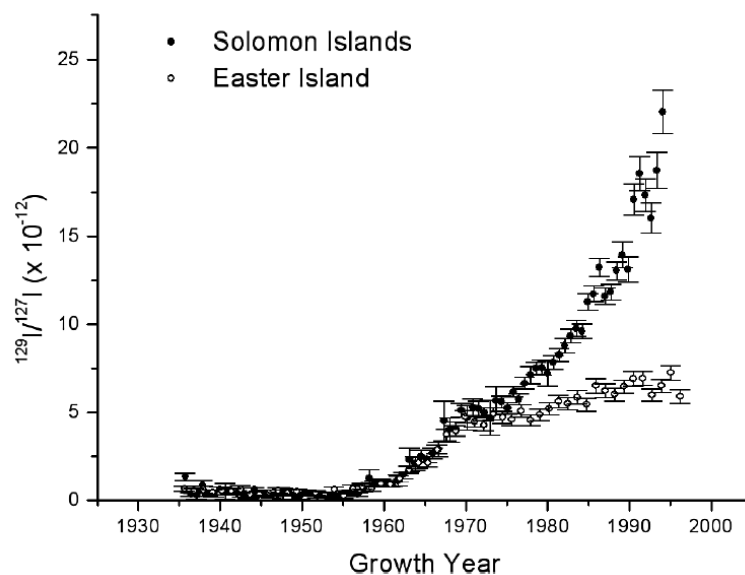
Figure 8. Isotopic ratio ^{129}I/^{127}I ratio in corals from the South Pacific (Biddulph et al., 2006).

As a summary, it has been shown how ^{129}I is a very interesting radionuclide from the environmental point of view. It strong value as radiological and environmental tracer is funded on a well-known history of the sources and its ability to disperse over many environmental compartments.

References

- Aldahan, A., Possnert, G., Alfimov, V., Cato, I., Kekli, A., 2007. Anthropogenic 129I in the Baltic Sea. Nuclear Instruments and Methods in Physics Research, Section B 259, 491-495.
- Biddulph, D.L., Beck, J.W., Burr, G.S., Donahue, D.J., 2006. Two 60-year records of 129I from coral skeletons in the South Pacific Ocean, In: P.P. Povinec and J.A. Sanchez-Cabeza, Editor(s), Radioactivity in the Environment 8, 592-598.
- Gallagher, D., McGee EJ, Mitchell PI, Alfimov V, Aldahan A, Possnert G., 2005. Retrospective search for evidence of the 1957 Windscale fire in NE Ireland using 129I and other long-lived nuclides. Environ. Sci. Technol. 39, 2927–2935.
- Gallagher, D., Mcgee, E.J., Mitchell, P.I., Alfimov, V., Aldahan, A., Possnert, G., 2005. Retrospective search for evidence of the 1957 Windscale fire in NE Ireland using 129I and other long-lived nuclides. Environmental Science and Technology 39, 2927-2935.
- Gómez-Guzmán, J.M., López-Gutiérrez, J.M., Holm, E., Pinto-Gómez, A.R., 2011. Level and origin of 129I and 137Cs in lichen samples (Cladonia alpestris) in central Sweden. Journal of Environmental Radioactivity 102, 200-205.
- Gómez-Guzmán, J.M., López-Gutiérrez, J.M., García-Tenorio, R., Agulló, L., Peruchena, J.I., Manjón, G., García-León, M., 2017. Estimating the impact from Fukushima in Southern Spain by 131I and Accelerator Mass Spectrometry detection of 129I. Journal of Environmental Radioactivity 166, 36-44.
- He, P, Aldahan, A, Possnert, G., Hou, X., 2013. A summary of global 129I in marine waters. Nuclear Instruments & Methods in Physics Research. Section B 294, 537-541.
- Hou, X., Dahlgaard, H., Rietz, B., Jacobsen, U., Nielsen, S.P., Aarkrog, A., 1999. Determination of chemical species of iodine in seawater by radiochemical neutron activation analysis combined with ion-exchange preseparation. Analytical Chemistry 71, 2745-2750.
- Hou, X., Roos, P., 2008. Critical comparison of radiometric and mass spectrometric methods for the determination of radionuclides in environmental, biological and nuclear waste samples. Analytica Chimica Acta 608, 105-139.
- Kilius, L.R., Litherland, A.E., Rucklidge, J.C., Baba, N., 1992. Accelerator mass-spectrometric measurements of heavy long-lived isotopes. Applied Radiation and Isotopes 43, 279-287.
- Krupp, G., Aumann, D.C., 1999. Iodine-129 in rainfall over Germany, Journal of Environmental Radioactivity 46, 287-299.
- Lopez Gutierrez, J., Garcia Leon, M., Schnabel, C., Suter, M., Synal, H., Szidat, S.., Garcia Tenorio, R., 2004. Relative influence of 129I sources in a sediment core from the Kattegat area. Science of the total environment 323, 195-210.
- Rao, U., Fehn, U., 1999. Sources and reservoirs of anthropogenic iodine-129 in western New York, Geochimica et Cosmochimica Acta 63, 1927-1938.
- Roberts, M.L., Caffee, M.W., Proctor, I.D., 1997. 129I interlaboratory comparison. Nuclear Instruments and Methods in Physics Research B 123, 367-370.
- UNSCEAR, 2000. United Nations Scientific Committee on Effects of Atomic Radiation. Sources and Effects of Ionizing Radiation Vol. 1: Sources. Report to the General Assembly. United Nations, New York, 654 pp.
- Verrezen, F., Hurtgen, C., 1992. The measurement of technetium-99 and iodine-129 in waste water from pressurized nuclear-power reactors. International Journal of Radiation Applications and Instrumentation 43, 61-68.
- Wagner, M. J. M.; Dittrich-Hannen, B.; Synal, H.-A.; Suter, M.; Schotterer, U., 1996. Increase of 129I in the environment, Nuclear Instruments and Methods in Physics Research Section B 113, 490-494.

H – AQUATIC SYSTEMS

Study of plutonium redistribution in a raised peat bog following a fire

M. Sáez-Muñoz[1], E. Holm[2], J. Mantero[2,3], R. Thomas[2],
S. Martorell[1], R. García-Tenorio[3]

1. Laboratorio de Radiactividad Ambiental of the Universitat Politècnica de València, MEDASEGI Research Group, Camino de Vera s/n, 46022 Valencia, Spain.
2. Department of Radiation Physics, University of Gothenburg, Gula stråket 2 b su/sahlgrenska, 41345 Göteborg, Sweden.
3. Department of Applied Physics II. E.T.S.A. University of Seville, Department of Applied Physics, Avenida Reina Mercedes 2, 41012 Sevilla, Spain.

Abstract

Peat lands are archives of past diversity, climate, and other environmental conditions. The redistribution of radionuclides in a peat bog after a fire consists of change in vertical distribution and releases/losses to the atmosphere through evaporation and resuspension. The study of different radionuclides such as plutonium isotopes will be important to understand the radiation exposures to man following fire on contaminated land.

In this work, a fast and sequential procedure for uranium, plutonium and americium determination in soil samples is presented. Together with the study of redistribution of uranium and plutonium isotopes in a raised peat bog located in the nature reserve of Vakö Mire (south of Sweden) following a big fire (1992).

The procedure is based on the four main steps of any radiochemical procedure: pre-treatment, isolation of radionuclides, source preparation and measurement via alpha spectrometry. The sequential separation of the radionuclides is performed by extraction chromatography, employing UTEVA resin in columns and DGA resin in cartridges.

Once the procedure was established, two cores of the Vakö Mire peat bog were studied (one from the burnt area and another from the not affected area). The first 10cm of each core sliced in 1 cm layers were analyzed. The results for plutonium in the burnt core show an increase in the $^{239+240}$Pu activity concentration (Bq/m^2) at the ash layer, while in the not affected area the concentration slightly increases with depth due to the global fallout. Regarding uranium isotopes, their behaviour in the peat bog is different from plutonium. The non-burnt area presents much higher values of activity concentration than the burnt one due to its higher inorganic content. The fire made this element easily movable via weathering conditions and as results the U content in the burnt core is hardly 10% of the total amount accumulated in the non-burnt area. Moreover, ^{234}U and ^{238}U isotopes were found in secular equilibrium.

Introduction

Peat lands are archives of past diversity, climate, and other environmental conditions. The upper layers of a peat land are an archive for recent environmental information, such as atmospheric deposition of natural and man-made radionuclides, and offer an opportunity to understand how environmental conditions have been recorded in peat profiles by relating the deposition to the peat to recent historical records.

The redistribution of radionuclides in a peat bog after a fire consists of change in vertical distribution and releases/losses to the atmosphere through evaporation and resuspension. Selected radionuclides such as ^{210}Pb, ^{137}Cs and $^{239+240}$Pu will be of major concern (among others). This is of importance to understand the radiation exposures to man following fire on contaminated land.

Materials and Methods

Samples

The nature reserve of Vakö Mire is located in the south of Sweden. The area of the peat bog is 13 km^2 and is one of the largest raised peatbogs in Sweden. Most of it was affected by the fire in 1992 but some areas remained intact (Hököns intresseförening, 2012). In the summer of 2015, through an expedition in this area, different peat bog samples were taken (Figure 1). The view of the reserve in 2015 is shown in Figure 2.
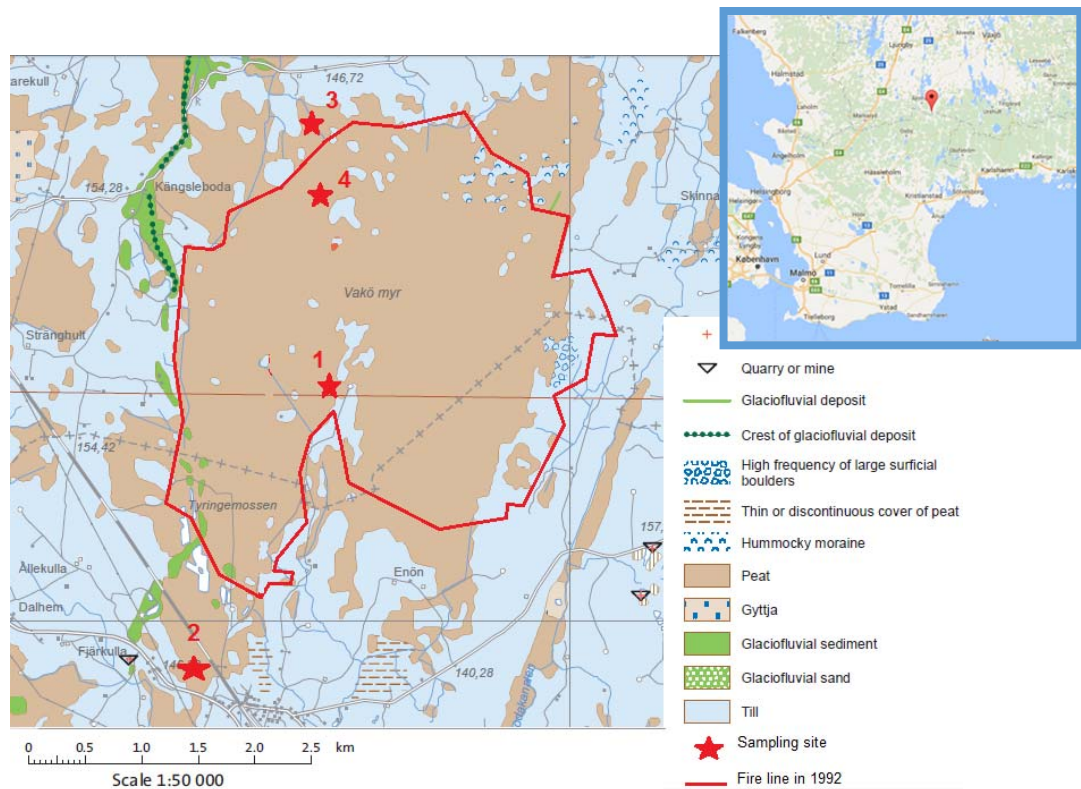
Figure 1. Nature reserve of Vakö Mire, sampling points and situation in Sweden.

Figure 2. View of Väko Mire in 2015.

In this expedition vertical cores were taken by a steel corer, with a diameter of 7.7 cm. Several cores were taken in the peat bog both in the area of the fire and outside the affected area (Figure 3). The cores were transported to the laboratory for further treatment.

The cores were sliced in 1 cm layers. Assuming a growth rate of 2 mm/year, the growth in the peat bog 24 years after the fire has been about 4-5 cm. Below this depth, we expect to find the "ash layer", as it is seen in the core from the burnt area (Figure 3).

Figure 3. Cores from the peat bog in the area subject to the fire (left), and from the unburnt area (right). The ash layer is seen at a depth of about 5 cm in the core from burnt area.

Radiometric technique

The procedure is based on the four main steps of any radiochemical procedure: pre-treatment, isolation of radionuclides, source preparation and measurement via alpha spectrometry.

Initially each 1cm slice was dried at 60-70 degrees for several days until the weight became stable, removing this way the moisture of the sample. Afterwards the dried fraction was calcined at 450 degrees for 24 hours, removing most of the organic fraction. Then a leaching digestion with aqua regia was applied. In order to carry out the sequential separation of the radionuclides, extraction chromatography employing UTEVA resin in columns and DGA resin in cartridges is performed. The complete procedure is shown in Figure 4.

After isolation, every fraction containing either U isotopes or Pu will be electroplated. The method of electrodeposition applied in this case follows strictly the method detailed in Hallstadius (Hallstadius, 1984).To maximize the chemical recovery of both actinides U and Pu sources are electroplated at 1.2 A during 1 hour in a 20mm diameter steel disk.

The measurement system is an Alpha Analyst from Canberra equipped with 12 PIPS detectors and the software used to analyze spectra was Genie 2000.

Sequential Pu, U and Am determination
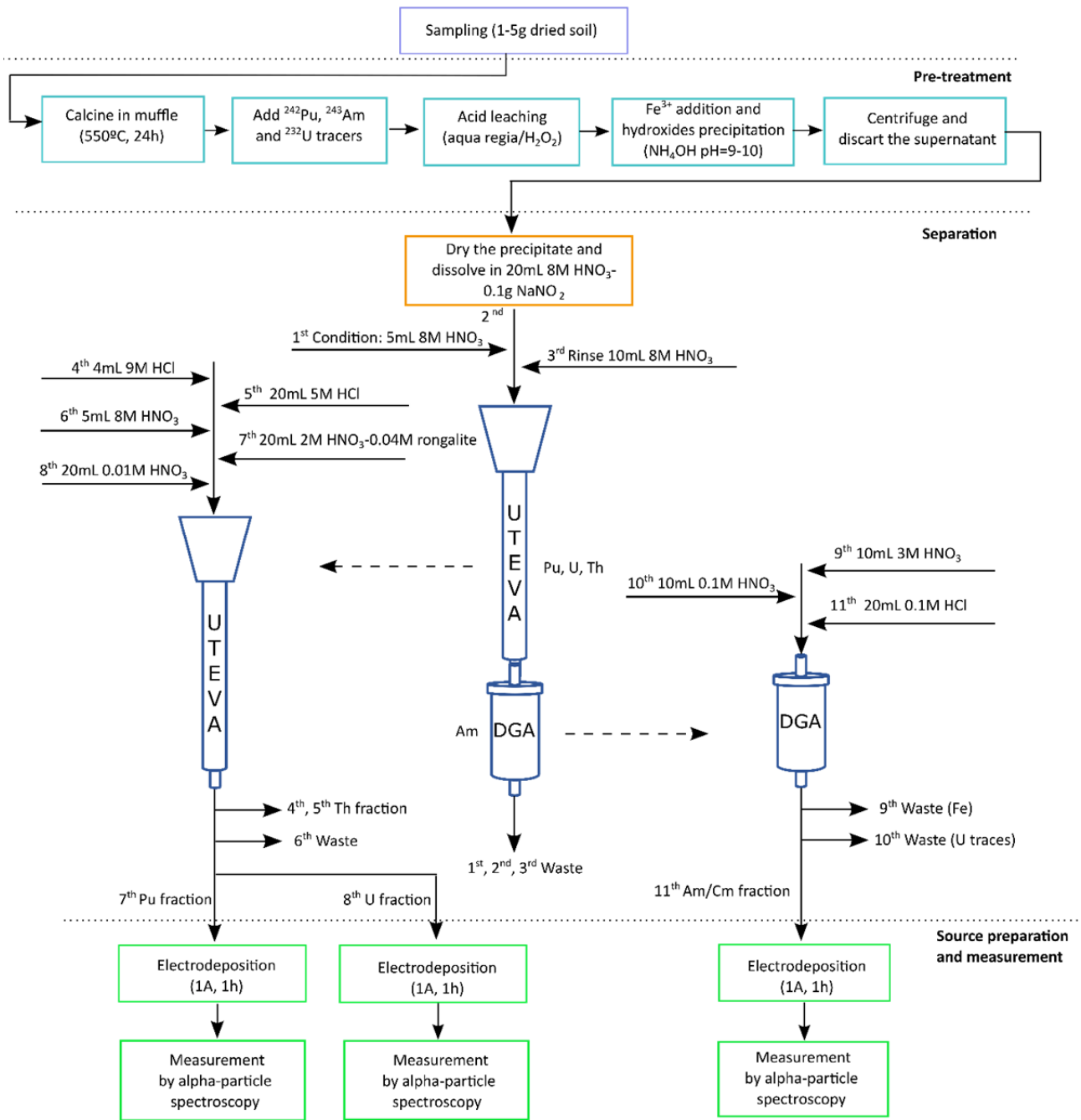
Figure 4. *Fast and sequential procedure for uranium, plutonium and americium determination in soil samples.*

Results and Discussion

Drying and Calcination

Core 12 from the burnt area (Site 4 in Figure 1), and Core 10 from the unburnt area (Site 3 in Figure 1), were analyzed in the laboratory. The 1cm slices of each core were dried and calcined. Figure 5 shows different behavior between the cores: while Core 12 is compound mainly (averaging 97%) by

organic matter, Core 10 (non affected by fire) shows a higher inorganic fraction, specially from 10cm and deeper, where it is compound around 75% by organic matter.
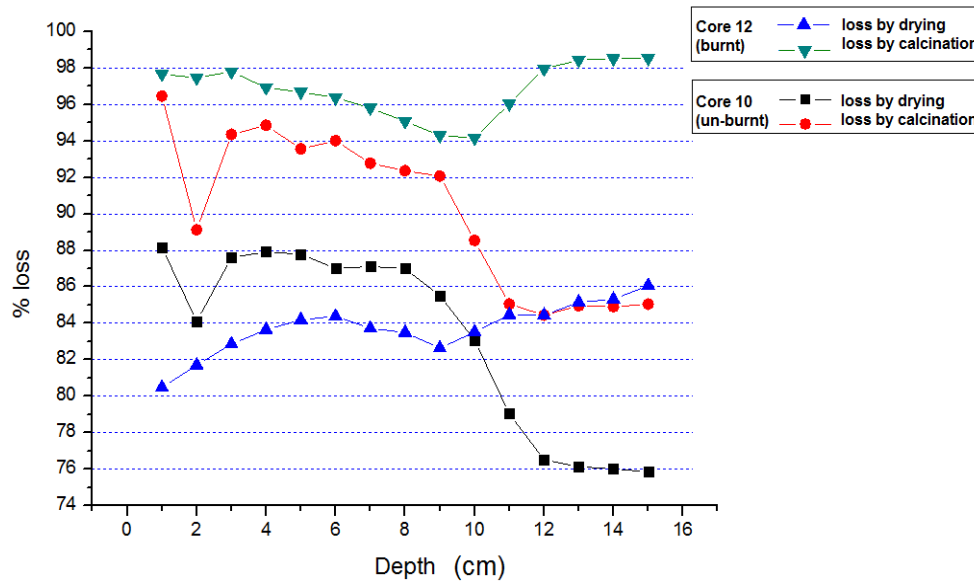

*Figure 5. Loss on every 1cm layer for both cores: after drying and calcination.*

Plutonium Redistribution

The first 10cm of each core sliced in 1cm layers were analyzed for plutonium and uranium determinations. The results for plutonium in the burnt core show an increase in the $^{239+240}$Pu activity concentration (Bq/m^2) at the ash layer (6cm depth), while in the non-affected area the concentration slightly increases. Assuming an annual growth rate of 2mm, we would expect the fallout of $^{239+240}$Pu from nuclear tests to be at 10cm depth in a general peat bog (Core 10). In Väko Mire the fire went deeper (until 20cm) and the organic matter turned into ashes, concentrating plutonium isotopes in the "ash layer".

The ^{238}Pu/$^{239+240}$Pu ratio in 1972 was 0.036 , 36% originated from the satellite failure SNAP 9A and the rest from the global fallout (Holm and Persson, 1975). The fallout from the Chernobyl accident was very patchy with an activity ratio of 0.47 which decreased to 0.37 in 2015. The increase of ^{238}Pu, expressed as Bq·m^{-2}, was only about 9% in Sweden following the Chernobyl accident and probably less in the studied area (Holm, 1991). In Core 12, the ratios are mainly situated around this line.

Uranium Redistribution

The behavior of uranium isotopes in the peat bog is different from plutonium (Figure 6). The non-burnt area presents much higher values of activity concentration than the burnt one due to its higher inorganic content. The fire made this element easily movable via weathering conditions and as results the U content in the burnt core is hardly 10% of the total amount accumulated in the unburnt area. Moreover, ^{234}U and ^{238}U isotopes were found in secular equilibrium.
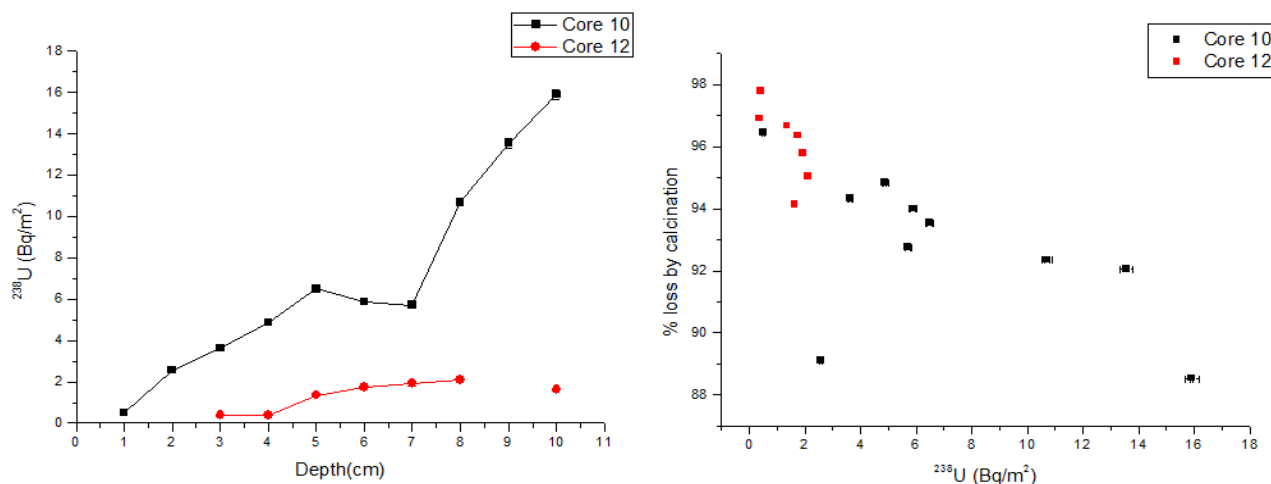
Figure 6. *Activity concentration (Bq/m^2) of ^{238}U as a function of depth (left), and content of organic matter (represented by % of loss by calcination) versus ^{238}U activity concentration (right) in two cores from Vakö mire.*

Conclusions

A fast and sequential procedure for Uranium, Plutonium and Americium determination in soil samples has been developed. The separation step is based on extraction chromatography, employing UTEVA resin in columns and DGA resin in cartridges.

Two peat bog cores of the nature reserve of Vakö Mire (south of Sweden) have been studied. One core of the area affected by the big fire of 1992, and one of the non-affected area. Plutonium isotopes experimented a redistribution in the peat bog due to the fire. The $^{239+240}$Pu activity concentration (Bq/m^2) increased at the ash layer, unlike in the non-affected core. The ^{238}Pu/$^{239+240}$Pu ratio is maintained constant due to the global fallout. The behaviour of Uranium isotopes differ from plutonium element. The fire made U easily movable via weathering conditions, and the activity concentration of the non-burnt area is much higher also due to its higher inorganic content. ^{234}U and ^{238}U isotopes were found in secular equilibrium.

References

Hallstadius L., 1984. A method for the electrodeposition of actinides, Nucl. Instrum. Methods 223, 266-267.

Hököns intresseförening, 2012. Den stora branden på Vakö myr.

Holm E., 1991. Fallout of Transuranium Elements in Sweden Following the Chernobyl Accident. In: The Chernobyl Fallout in Sweden. p. 67-81. The Swedish Radiation Protection Institute. Ed. Moberg L.

Holm E. and Persson R.B.R., 1975. Fallout plutonium in Swedish Reindeer Lichens, Health Physics 29, 43-51.

Acknowledgments

Depth distributions of bomb-derived and Chernobyl-derived radiocaesium in sediment sinks and their application in reconstructing changes in erosion rates

V. Golosov[1,2] *, D. Walling[3], M. Ivanov[2], A. Sharifullin[1]

[1] Kazan Federal University, Institute of Ecology and Environment, Department of Landscape Ecology, Kremlevskaya st., 18, 420000, Kazan, Russia
[2] Lomonosov Moscow State University, Faculty of Geography, Laboratory for Soil erosion and Fluvial processes, Leninskie Gory, 1, 119991, Moscow, Russia
[3] Geography, College of Life and Environmental Sciences, University of Exeter, Exeter, UK

Abstract

Vast areas of Europe were contaminated by Chernobyl fallout in April-May 1986. As a result, an additional time-marker appeared in the sediment profiles of many sediment sinks, including dry valleys, river floodplain, lakes and reservoirs. Recently, both bomb-derived and Chernobyl-derived ^{137}Cs have been used to reconstruct sedimentation rates for two time intervals, as a basis for interpreting changes in soil redistribution and sediment transport within terrestrial and fluvial environments. The work described here comprises three main components. Firstly, attention is directed to ^{137}Cs depth distributions in soils within different landscape zones of European Russia and with different levels of Chernobyl fallout. Evidence for vertical migration of ^{137}Cs and its influence on ^{137}Cs depth distributions and their interpretation is considered. Secondly, the advantages and limitations of ^{137}Cs as a tracer for investigating the dynamics of erosion processes within croplands and sediment redistribution in river basins of different scales are considered. Thirdly, new results associated with the application of ^{137}Cs depth distributions for reconstructing changes in erosion rates and sediment fluxes in different parts of European Russia are reported and compared with the results of similar studies undertaken in the UK. It is concluded that a knowledge and understanding of both erosion-deposition processes and the potential for vertical migration of ^{137}Cs are important for correct interpretation of ^{137}Cs depth distributions in sediment sinks, when reconstructing changes in erosion rates and sediment fluxes in terrestrial and fluvial environments.

Introduction

Large areas of Europe were contaminated by caesium-137 (^{137}Cs) fallout in April-May 1986 after the Chernobyl Nuclear Power Station (NPS) accident. As a result, recent studies aimed at estimating deposition rates in sediment sinks have made use of both bomb-derived and Chernobyl-derived ^{137}Cs. ^{137}Cs is often applied in combination with ^{210}Pb$_{ex}$ for dating sediment profiles from ponds, lakes, reservoirs and the coastal zone (San Miguel et al., 2003; Alvarez-Iglesias et al., 2007; Appleby, 2008; Porto et al, 2016 etc.). Recently the two radionuclides have also been used for estimating sedimentation rates on river floodplains (Golosov et al., 2010; Du & Walling, 2012 etc.). However, in some cases the approach used for selecting the sampling locations has been wrong and incorrect interpretations of the ^{137}Cs depth distribution have resulted. (Ciszewski et al.,2008; Lokas et al., 2010). The potential for using both Chernobyl-derived and bomb-derived ^{137}Cs in other sediment sinks, located along the pathways from cultivated slopes to the river channel in small agricultural catchments (SAC), including dry valley bottoms, has not been fully explored. One of reasons for this is the limited information available concerning the behaviour of ^{137}Cs in the soils of SAC with different levels of initial Chernobyl fallout, distant from the Chernobyl NPS (Panin et al.,

---

* e-mail: gollossov@gmail.com

2001). However, the sedimentation rates documented in the bottoms of the SAC valleys provide a very valuable indicator of the erosion rates of the cultivated slopes of the SAC (Golosov et al., 2013). The aim of this paper is to evaluate the features of ^{137}Cs depth distributions in areas with different levels of Chernobyl fallout, giving particular emphasis to sediment sinks, and to discuss the possibility of applying ^{137}Cs as a tracer for evaluating recent erosion rates at the scale of SAC and small river basin.

Materials and Methods

Study area

The southern half of the Russian Plain is the largest agricultural region in Europe and also the area with the greatest variability of Chernobyl-derived ^{137}Cs fallout. This ranged from 2 – 1600 kBq m^{-2}. Areas with fallout > 1600 kBq m^{-2} were not subsequently used for agriculture (Askbrant et al., 1996). Several study sites were selected within the forest-steppe zone and the zone south of the forest zone located ENE of the Chernobyl NPS in areas with different levels of ^{137}Cs contamination (Fig. 1). Some study sites were selected to assess the vertical migration of Chernobyl-derived ^{137}Cs at undisturbed locations. The other sites were located in various sediment sinks (dry valley bottoms, ponds, river floodplains). Both bomb-derived and Chernobyl-derived ^{137}Cs were used to evaluate sedimentation rates associated with the two associated time windows in most of the sediment sinks.
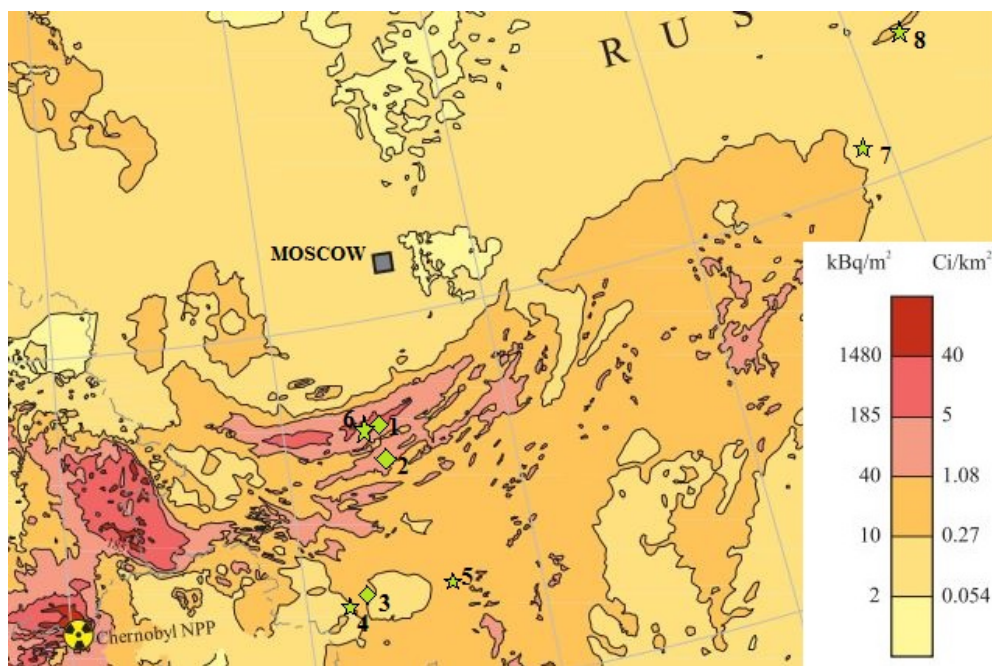
Figure 1. Map showing the ^{137}Cs contamination of the central part of the Russian Plain by Chernobyl fallout and the location of the study sites. Legend ◇ - reference sites (1 – Plavsk, 2 – Novosil; 3 – Kursk); ☆ - First order dry valleys (4 – Gracheva Loschina; 5 – Veduga; 6 – Verkhnaya Lokna; 7 - Temeva Rechka; 8 - Kuregovo

Information on the main characteristics of the study areas is presented in Table 1. The advantages of using the southern part of European Russia as a study area for comparing sedimentation dynamics in areas with different levels of Chernobyl-derived ^{137}Cs fallout include the following: 1) Most of the soils have developed on loess and colluvial deposits with similar grain size distributions: 2) The area is characterized by a high proportion of cultivated land. As a result the contribution of sediment produced by sheet and rill erosion is very high for SAC and small river basins; 3) Gully erosion

rates within the study area have decreased considerably during the last three decades. However, most of the sediment mobilised by active gullies is also derived from loess or colluvial deposits; 4) The gradient of annual precipitation across the study areas is relatively low (range 650-550 mm). Potential spatial variability of bomb-derived ^{137}Cs fallout and rainfall infiltration within the individual study sites is therefore relatively low.

Table 1. The main characteristics of the study sites

Area	Sites (see Fig.1)	[137]Cs contamination* kBq m[-2]		Annual precipita -tion, mm	Soil characteristic			Sampling periods
		Bomb-derived	Chernobyl-Derived		Parent material	Texture	Mean density, g cm^{-3}	
Plavsk	1,6	2.5-3	>200	614	Loess	Loam	1.3	2002-2013
Novosil	2	3-3.5	40-200	619	Loess	Loam	1.3	2003
Kursk	3,4	2-2.5	2-40	584	Loess	Loam	1.3	2005-2006
Voronezh	5	2-2.5	10-40	550	Loess	Loam	1.5	09.2015
Tatarstan	7	2.5-3	2-10	562	Colluvial	sandy-loam	1.6	08.2015
Udmurtiya	8	2.5-3	10-40	550	Colluvial	sandy-loam	1.6	06.2016

* level of contamination on May 1986.

Field sampling and radiometric measurements

The locations of the sampling points were selected after a detailed survey of each study site. For the reference sites, emphasis was placed on the geomorphological stability and undisturbed condition of the location. Available information regarding possible land use changes was collected from topographic maps and archive data for the period since 1986 and in most cases for the period since the 1950s. In the field, a description of the landscape position of each sampling point was undertaken before excavation of the soil profile. Particular attention was given to selecting sites where the soil surface was protected by grass. The selection of the sampling points for sediment sink sites was based on an analysis of the morphological characteristics of the different sections. Usually, between 2 and 9 sampling points were selected for depth incremental sampling in each sediment sink, depending on their morphological features. After selection of a sampling point, the soil profile was excavated and before the sampling was undertaken a very detailed description (including a photo) of the soil profile was recorded. The profile face with the lowest disturbance by bioturbation was selected for depth incremental sampling. Soil samples without grass and organic material were collected from an area 15x15 cm at 2-3 cm depth increments for the upper 60-70 cm and at 5 cm depth increments below 60-70 cm. Subsequent laboratory processing of the ^{137}Cs samples involved oven-drying at 105°C, grinding, sieving to <2 mm and homogenization of sub-samples for gamma-analysis. The ^{137}Cs activity was measured at 661.66 keV, using a high-resolution, low-background, hyperpure germanium coaxial gamma-ray detector with a maximum relative error of the isotope activity determination of ±5-7%. Sample preparation, treatment and ^{137}Cs activity measurements were carried out at the Laboratory of Soil Erosion and Fluvial Processes, Faculty of Geography, Lomonosov Moscow State University.

Results and Discussion

Examples of ^{137}Cs profiles from the reference locations are presented in Fig. 2. They can be split into two groups based on their basic shape. Profiles B and C have a clearly defined ^{137}Cs peak at or very close to the surface. Both of these sampling points are located on flat interfluve areas. Profile B from the Central Chernozem Reserve has a surface horizon of organic residue which extends to a

depth of 20 cm. It is therefore very similar to a profile from a peaty soil. Profile C has a different shape, with a much greater proportion of the ^{137}Cs found below a depth of 4 cm. This contrast can be linked to the thinner organic surface horizon associated with this profile and evidence of surface cracking. Profiles A and D again have similar shapes, but these differ from those associated with profiles B and C. In profiles A and D the maximum ^{137}Cs concentration is found below the surface in the 2-4 and 3-6 cm deep layers, respectively. Soil profile A was collected from the bottom of a slope hollow which has been under natural steppe vegetation for more than 100 years. The surface of the soil is protected by a deep organic layer, as well as the 100% grass cover. Profile D was collected from an area of meadow on a slope, again with a good vegetation cover. The slightly deeper position of the ^{137}Cs here could reflect a small amount of sediment deposition at this site since 1986. Because of its position in a hollow, it is likely that a greater amount of water infiltrates at profile A than profile D.

The shapes of the two groups of profiles are further compared in Fig. 3. In the case of profiles B and C depicted in Fig. 3B , 99% of the inventory is found above a mean depth of 22-23 cm. The ^{137}Cs is found to a greater depth in profiles A and D (Fig. 3A) and 99% of the inventory is found above a mean depth of 33-35 cm. Since there are no important differences in dry bulk density and grain size
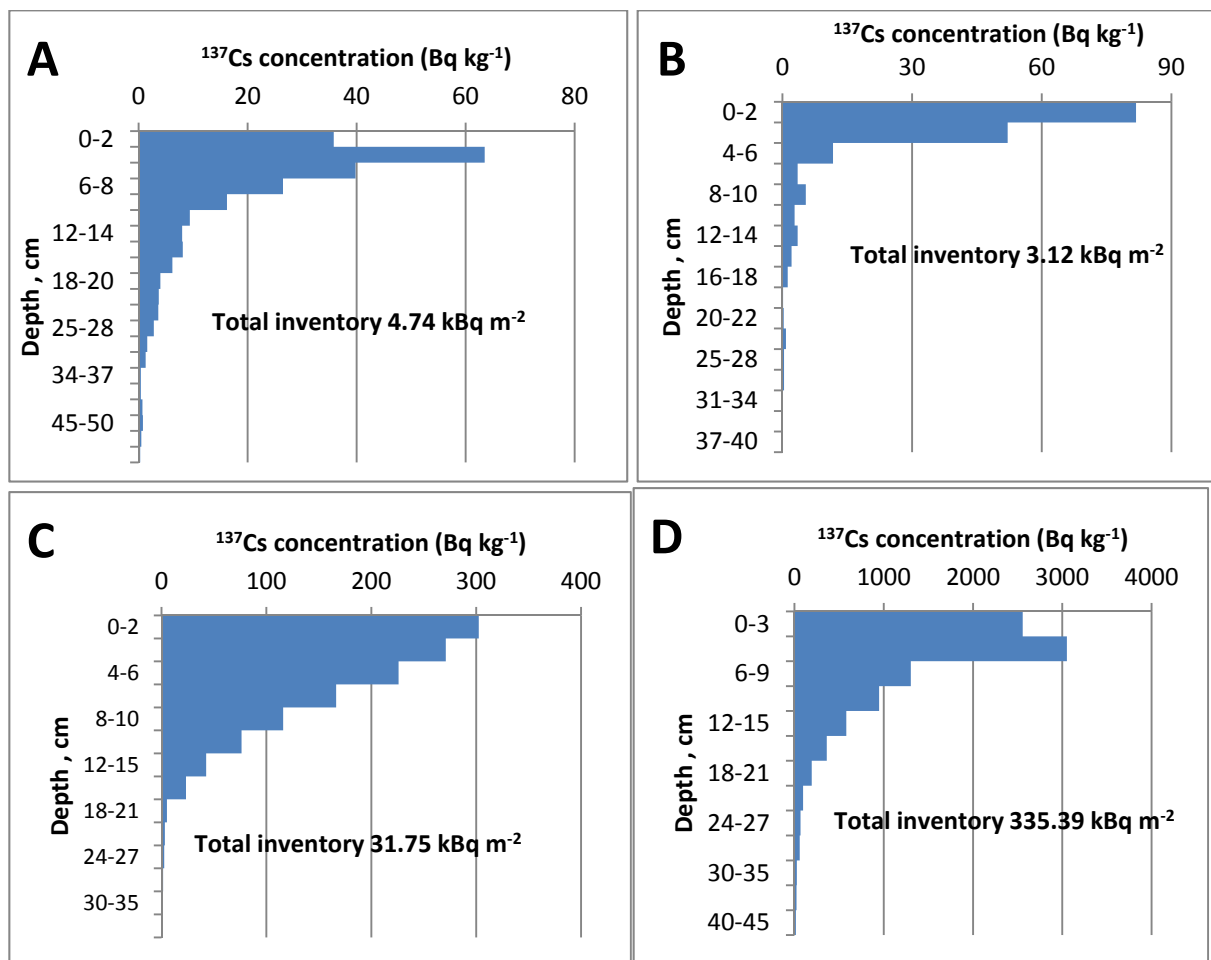
Figure 2. Depth distributions of ^{137}Cs s associated with soil cores collected from reference sites, located in areas with different levels of l Chernobyl-derived ^{137}Cs fallout: A and B –Central Chernozem Reserve, Kursk (site 1, Fig. 1); C – Novosil experimental station (site 2, Fig.1); D – Lokna river basin, central part, Plavsk (site 1, Fig.1). To avoid overcrowding of the plots, measurement precision has not been shown for individual depth increments.. This was typically ±5% at the 95% level of confidence.
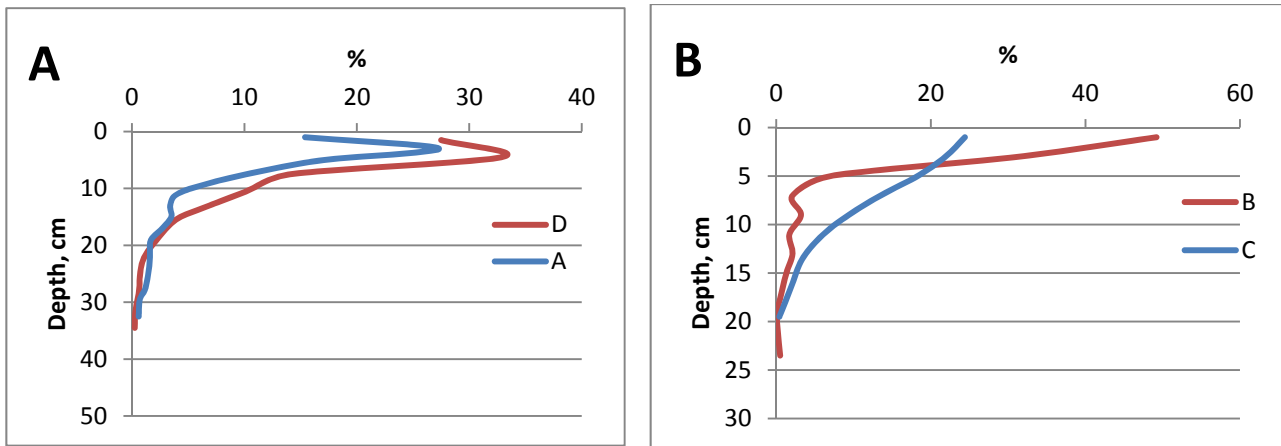
Figure 3. *Change in the proportion of* [137]*Cs found in different soil layers at reference locations with different morphological positions: A – hollow bottom, undisturbed steppe vegetation, Central Chernozem Reserve, Kursk; D – meadow on the slope with protection of soil by 95-98% vegetation cover, the Lokna River basin, Plavsk; B – flat interfluve area with natural steppe vegetation, Central Chernozem reserve, Kursk; C – meadow on flat interfluve area, Novosil experimental station.*

composition between reference profiles (see Table 1, sites 1-4), differences in the downward diffusion of ^{137}Cs are likely to reflect differences in topographic position, which will influence the amount of wáter infiltrating. The deeper diffusion in áreas experiencing greater infiltration needs to be taken into consideration when interpreting ^{137}Cs profiles in sediment sinks. In addition, possible downward migration of both the Chernobyl-derived and bomb-derived ^{137}Cs peaks by 1-3 cm must be seen as limiting the accuracy of sedimentation rate estimates.

Typical ^{137}Cs profiles for dry valley bottoms are given in Fig.4. Chernobyl peaks are evident for all the sampling points. Peaks of ^{137}Cs activity associated with maximum bomb fallout and which can be dated to 1963 are recognizable for only 3 of these profiles (Fig, 4 A,B,C). It is likely that the lack of bomb-derived ^{137}Cs at the Veduga site (Fig.4D) can be explained by active erosion in the lower part of the dry valley botom at the beginning of the 1960s. This suggestion is confirmed by the alternation of layers of a lighter colour not containing ^{137}Cs with layers of a darker colour containing ^{137}Cs, in the layer 60-105 cm below surface. Loamy sediment with a lighter colour represents sediment mobilised by erosion of channel banks and gully walls and bottoms. The darker sediment represents sedment mobilised from cultivated slopes by sheet and rill erosion. It is therefore likely that in this part of the valley bottom rapid sedimentation began during the second half of the 1960s. This is also confirmed by the morphology of the valley cross-section with its steep banks and relatively narrow flat bottom. At the Kuregovo site (Fig.4C) it is likely that maximum sedimentation rates occurred before 1963. An active deep bottom gully was formed upstream from the sampling point at this time and this provided additional sediment to that mobilized by sheet and rill erosion from the cultivated slopes. The shape of the ^{137}Cs profile from the Temev Ruchei site (Fig.4B) reflects the mechanism of sediment redistribution in the valley bottom, where active retreat of shallow (10-15 cm high) knickpoints within the bottom gullies was an important process during the mid 1960s. The remobilized sediment was generally redeposited no further than 50-100 m downstream. A fuller desription of this process can be found elsewhere (Panin et al., 2001). The shape of the ^{137}Cs profile at the Gracheva Loschina site (Fig. 4A) is more similar to those associated with with floodplain sediment profiles experiencing continuous sedimentation with a relatively uniform mix of sediment sources (Golosov et al., 2010; Du & Walling, 2012). It is necessary to emphasize that in areas with levels of Chernobyl-derived ^{137}Cs fallout >200 kBq m[-2], the bomb-derived ^{137}Cs peak representing 1963 can only be identified where
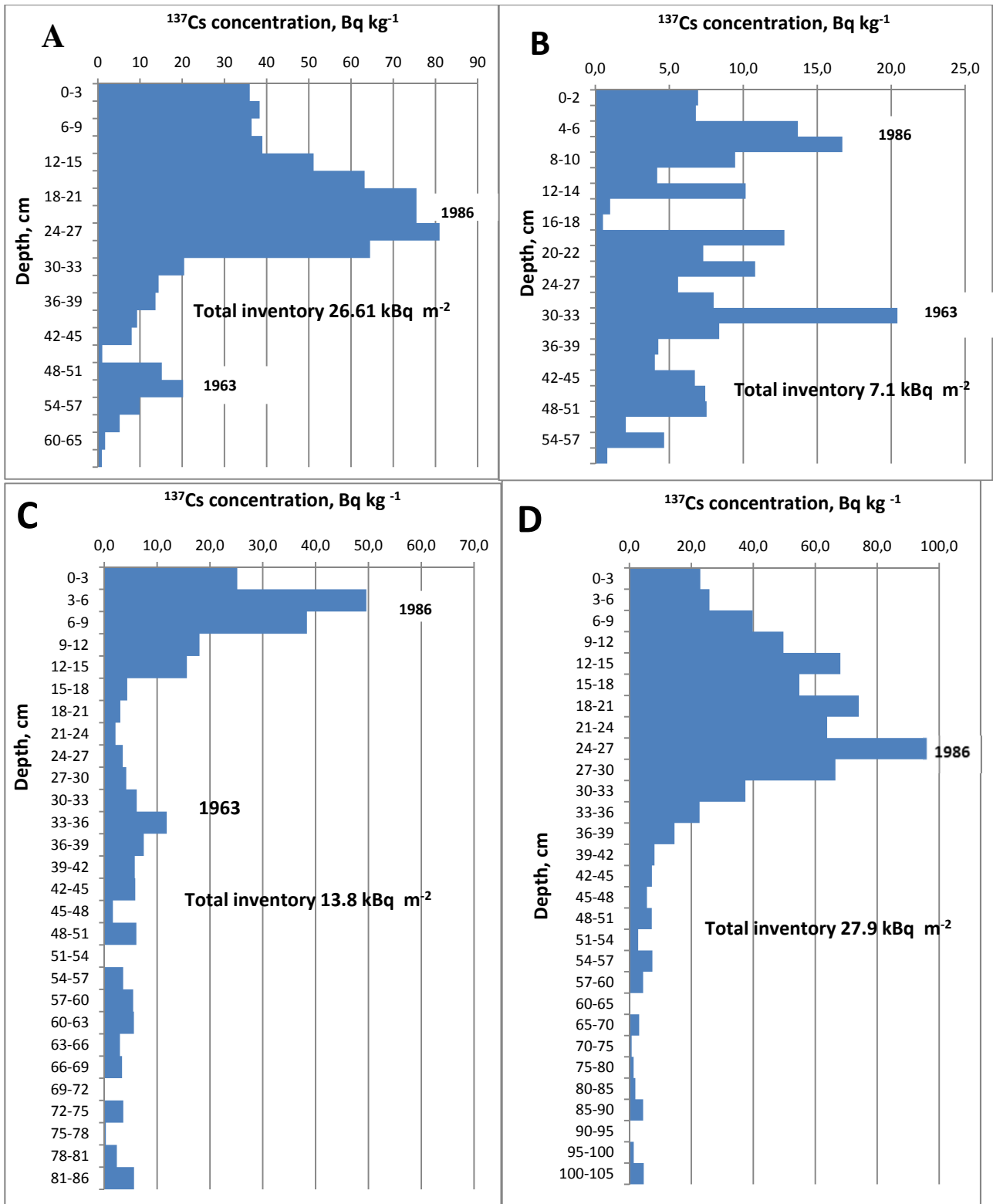
Figure 4. [137]Cs profiles associated with the sediment cores collected from the bottoms of the first order dry valleys in different parts of European Russia. A – Gracheva Loschina, Kursk (site 4, Fig.1); B – Temev Ruchei, Tatarstan (site 7, Fig.1); C – Kuregovo, Udmurtiya (site 8, Fig.1); D – Veduga, Voronezh (site 5, Fig.1).

the sedimentation rate at the sampling point has been > 2 cm yr^{-1}. Alternatively, it is possible to use [241]Am to identify this peak, if it can be detected (Bunzl et al., 1994). The dynamics of sedimentation

rates associated with individual sediment sinks may be determined based on several ^{137}Cs depth profiles. In the case of a small pond, only a small number of ^{137}Cs depth profiles are required, because the site will be characterized by continuous sedimentation (Appleby,2001). A minimum of 3-4 ^{137}Cs depth profiles located in typical cross-sections along the dry valley bottom have been used to document sediment accumulation rates in dry valley bottoms. This made it possible to establish more precise values for sedimentation rates during different periods (Table 2). It has been found that sedimentation rates decreased by a factor of 3-5.4 for different study sites. This is in good agreement with previous results, mostly obtained for dry valleys and small river floodplains in the Western part of European Russia (Golosov et al., 2010, 2013, 2014). A similar trend of decreasing overbank sedimentation rates was demonstrated by ^{137}Cs profiles collected from the floodplains of small rivers in England and Wales (Du & Walling, 2012), using a similar approach. Sedimentation rates in dry valley bottoms and on river floodplains are respectively good indicators of erosion rates on the adjacent cultivated slopes and in the local river basin, respectively, in areas with a high proportion of cropland. In areas which received Chernobyl fallout it is difficult to apply the ^{137}Cs technique to document soil redistribution rates on agricultural land, because of its high spatial variability (Golosov et al., 2013). As a result, use of ^{137}Cs for sediment dating in dry valley bottoms provides a valuable alternative for assessing minimum rates of soil loss from cultivated slopes. A more precise assessment of soil losses from a catchment based on ^{137}Cs dating can be obtained by evaluating the total sediment storage in small agricultural ponds with a known period of operation (Porto et al., 2016).

Table 2. Estimates of mean annual sedimentation rates in dry valley bottoms for different periods based on interpretation of ^{137}Cs depth profiles.

Dry valley name	Landscape zone	Co-ordinates	Mean annual sedimentation rates, mm yr⁻¹, for indicated time interval		Reduction of sedimentation rate
			1963-1986	1986 - 2015(2016)	
Veduga	Forest-steppe	51.760539N 38.602139E	2.0 ± 0.2	0.5 ± 0.05	x 4
Temev Ruchei	North of forest-steppe	55.645670N 49.646451E	1.4 ± 0.15	0.26 ± 0.03	x 5.4
Kuregovo	South of forest	56.549672N 52.910720E	1.0 ± 0.2	0.33 ± 0.03	x 3

Conclusions

The downward diffusion of Chernobyl-derived ^{137}Cs in soils of the Southern half of the European Russia depends on morphological position. It is higher for positions on slopes and in depressions than for flat interfluve areas. This should be recognized when interpreting ^{137}Cs depth profiles from different sediment sinks. The shape of ^{137}Cs profiles obtained from dry valleys bottoms will reflect the relative contributions of different sediment sources and can be used to interpret recent (post 1950s) sediment redistribution when studying small agricultural catchments (SAC). The Chernobyl ^{137}Cs peak is easily identifiable in most sediment sinks in areas with different levels of fallout. Where both erosion and sedimentation are active within depositional sinks, bomb-derived ^{137}Cs can be absent from the lower sections of sediment profiles collected from the middle and lower reaches of the dry bottom valleys and the lower levels of river floodplains, due to sediment remobilisation.

Analysis of ^{137}Cs depth distributions collected from different sediment sinks within small river basins in areas with different levels of Chernobyl-derived ^{137}Cs fallout can provide a basis for documenting sedimentation rates for two periods (1963-1986 and 1986-sampling date). In areas with

very high levels of Chernobyl fallout (> 200 kBq m^{-2}), bomb-derived ^{137}Cs peaks can only be identified if the sedimentation rate during the period 1963-1986 was > 2 cm yr^{-1}. A minimum of 3-4 ^{137}Cs profiles are required to characterize the different sections along the length of dry valley bottoms and quantify mean annual sedimentation rates. A decreasing trend of sedimentation rates was found for different dry valley bottoms within the Russian Plain, when using a small number of ^{137}Cs profiles to compare the periods 1963-1986 and 1986-2016 at each study site. This trend in agreement with results of previous investigation of sedimentation rates dynamic in the western part of Russian Plain and in England and Wales.

References

Askbrant, S., Melin, J., Sandalls, J., Rauret, G., Vallejo, R., Hinton, T., Cremers, A. , Vandecastelle, C. , Lewyckyj, N., Ivanov, Y.Y., Firsakova, S.K. Arkhipov, N.P. & Alexakhin R.M.. 1996. Mobility of radionuclides in undisturbed and cultivated soils in Ukraine, Belarus and Russia six years after the Chernobyl fallout. J. Environ. Radioact., 31, 287-312.

Alvarez-Iglesias, P., Quintana, B. Rubio & Pérez-Arlucea, M. 2007.Sedimentation rates and trace metal input history in intertidal sediments from San Simón Bay (Ría de Vigo, NW Spain) derived from ^{210}Pb and ^{137}Cs chronology. J. Environ. Radioact., 98, 229–250.

Appleby, P.G. 2001. Chronostratigraphic techniques in recent sediments. In: Last, W.M., Smol, J.P. (Eds.), Tracking Environmental Change Using Lake Sediments. Basin Analysis, Coring and Chronological Techniques, vol. 1. Kluwer Academic Publishers, Dordrecht, The Netherlands, pp. 171-203.

Appleby, P.G. 2008. Three decades of dating recent sediments by fallout radionuclides: a review. The Holocene, 15, 83-93.

Bunzl, K, Kracke, W. & Schimmack, W. 1994. Residence time of fallout ^{239,240}Pu, ^{238}Pu, ^{241}Am and ^{137}Cs in the upper horizons of undisturbed grassland soils, J. Environ. Radioactivity, 22, 11-27.

Ciszewski, D., Czajka, A. & Bażej, S. 2008. Rapid migration of heavy metals and ^{137}Cs in alluvial sediments, Upper Odra River valley, Poland. Environ. Geol., 55, 1577-1586.

Du, P. & Walling, D.E. 2012. Using ^{210}Pb measurements to estimate sedimentation rates on river floodplains. J. Environ.Radioact., 103, 59–75.

Golosov, V.N., Belyaev, V. R. & Markelov, M. V. 2013. Application of Chernobyl-derived ^{137}Cs fallout for sediment redistribution studies: lessons from European Russia. Hydrological Processes, 27, 807-821.

Golosov, V.N., Belyaev, V.R., Markelov, M.V. & Kislenko, K.S. 2010. Overbank sedimentation rates on the flood plains of small rivers in Central European Russia. In: Sediment Dynamics for a Changing Future (ed. by Banasik, K. *et al.*) (Proceedings of a Symposium held in Warsaw, Poland, June 2010), pp.129–136, IAHS Publ. 337. IAHS Press, Wallingford, UK.

Golosov, V. N. , Belyaev, V. R. , Shamshurina. E. N. & Kuznetsova, J. S. 2014. Use of an integrated approach for assessing soil redistribution in the River Vorobzha basin. Proceedings FAO-IAEA International Symposium on Managing Soils for Food Security and Climate Change Adaptation and Mitigation. FAO. Rome, 107–112

Lokas, E., Wachniew, P., Ciszewski, D., Owczarek, P., Dinh Chau, N. 2010. Simultaneous use of trace metals, ^{210}Pb and ^{137}Cs in floodplain sediments of a lowland river as indicators of anthropogenic impacts. Water Air Soil Pollut., 207, 57–71.

Panin, A.V., Walling D.E. & Golosov V.N. 2001. Fluvial transport of Chernobyl ^{137}Cs: Case study of the Lapky catchment, Central Russia. Geomorphology, 40, 185-204

San Miguel, E.G., Bolívar, J.P. & García-Tenorio, R. 2003. Mixing, sediment accumulation and focusing using ^{210}Pb and ^{137}Cs. Journal of Paleolimnology, 29, 1-11.

Acknowledgement

Redistribution of ^{137}Cs from an Ash Landfill to a Nearby Lake

Sara Ehrs, Mats Eriksson, Sofia Eriksson, Pål Andersson,
Marie Huss

Swedish Radiation Safety Authority, Department of Radiation Protection, SE-171 16 Stockholm

Introduction

The Swedish Radiation Safety Authority (SSM), which is a supervisory authority, has inspected a company that processes fertilizers and biofuel. The company has a facility with about 50 000 tons of ash that contains up to 5 kBq/kg ^{137}Cs. Rainwater and process water leach ^{137}Cs from the ash and this water is collected in dams around the site. The water is processed and cleaned from chemical pollution before it is released to the environment; however, ^{137}Cs is not removed through this process and has been found to reach a nearby lake. Between 2004-2013 the company's own calculations state that approximately 20 GBq ^{137}Cs has been released into the stream leading to the recipient lake. To get a second opinion SSM has investigated the situation by studying the lake and its surrounding areas. The site is located in an area affected by the fallout from Chernobyl. The deposition in the area has earlier been determined with airborne measurements performed by the Swedish geological survey, and was approximately 60 kBq/m^2 in 1986 (see map in e.g. Andersson et al., 2007).

Materials and Methods

Samples

Samples from the site were collected in proximity to the stream leading from the site and in the recipient lake, Skogssjön, which is located 0.3 km from the site (see, figure 1). The recipient lake has an area of 0.18 km^2 and a catchment area of ~6 km^2. As a reference, samples were also collected at a nearby lake, Neder-Våltjärnen, which does not receive runoff from the site. The reference lake is located 1 km from the site; it has an area of 0.1 km^2 and a catchment area of ~11 km^2.
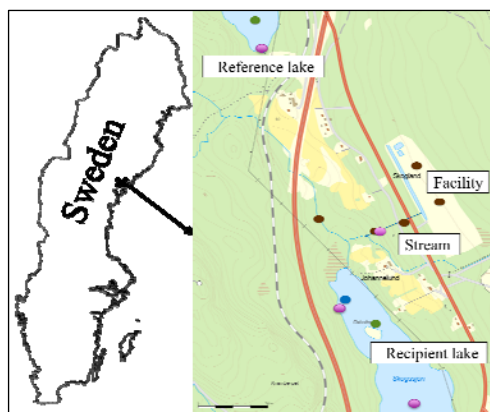
Figure 1. Area map of the studied area. To the left, a map of Sweden showing where the facility is situated and to the right a detailed map of where samples were taken. The reference lake is in the upper part and the recipient lake is in the lower part of the map. The landfill with the facility and the dams can be seen. Green spots are sediment sampling sites, purple spots are water sampling sites, the blue spot is the fish sampling site and brown spots are grass and soil sampling sites.

Water was sampled in the reference lake, in the stream, at one end of the recipient lake, where the water from the site enters, and at the outlet at the other end of the lake. Water was filtered in field (1 µm). Fish were caught in one spot with net. The sediments were taken with an HTH

gravity corer from Polonex with a diameter of 9 cm. The cores were sliced into 1 cm sections. The cores were taken at the deepest location in each lakes (~5 m in the recipient lake and ~8 m in the reference lake). The fish were cleaned from bone and stomach contents, dried and homogenized. Small fish were homogenized with head and scales. The soil was dried, cleaned from roots and homogenized. The other samples were dried and homogenized.

Radiometric technique
Samples were measured using an HPGe detector. The detector was calibrated for ^{210}Pb (46 keV) using an aquatic solution traceable to NIST as calibration source. The detector was calibrated for ^{137}Cs (661 keV) using calibration sources of density 1.0, 0.5 or 0.2 g/cm^3 traceable to NIST or PTB. Samples were measured for Cs-137 using the calibration obtained with the source with the density most similar to the sample's density. The sample spectra were analysed using a calibration curve with the Genie 2000.

Dating of core
The determination of the sedimentation rates was only done for the reference lake. The recipient lake is shallow and has been exposed to anthropogenic activities during the construction of a road along the west shoreline. The sediment was clearly mixed in this lake and the simple sedimentation model, based on the constant initial concentration (CIC) model (Appelby et al. 1979), could not be used. In the reference lake the model was applied by fitting the exponential function to the ^{210}Pb data in the statistical program R. The supported ^{210}Pb concentration, the initial ^{210}Pb concentration, and the sedimentation rate were fitted in the fitting procedure. The uncertainties of the fitted parameters and the sedimentation rate were calculated from the fitted results and the age of the measured slices were calculated.

Results and Discussion

The results from the measurement of the samples are shown in Table 1. There are higher activity concentrations in the samples from areas around the facility site compared to samples from the reference sites. The ^{137}Cs activity concentration in water is five times higher in the recipient lake, and twenty-five times higher in the stream, compared to the reference lake. The ^{137}Cs activity concentration in environmental samples from around the stream is also higher than in reference samples: soil (18-45 times higher), bushes (3-10 times higher), and grass (2-6 times higher). The ^{137}Cs area activity concentration in sediment samples from the recipient lake (57 kBq/m^2) is twice as high as that in sediments from the reference lake (31 kBq/m^2).

Table 1. Results of the ^{137}Cs activity concentration in samples, reference date 2015-05-27.

Sample type	Reference samples *	Stream	Recipient lake	Unit
Sediment	31	-	57	kBq/m^2
Predatory fish (1 pike, 2 perch)	-	-	350-650	Bq/kg fw**
Fish (other) n=3	-	-	100-150	Bq/kg fw
Grass n=4	160	410-960	-	Bq/kg dw**
Bushes (bird cherry) n=4	74	219-742	-	Bq/kg dw
Soil n=4	92	1700-4150	-	Bq/kg dw
Water n=5	<0.05	2.5	0.24-0.34	Bq/L

* Reflecting Chernobyl and global fallout
** Fresh weight (fw), dry weight (dw)

The results suggest that there has been a redistribution of ^{137}Cs from the facility site to the surrounding environment and the recipient lake. In order to determine the magnitude of activity that has been redistributed to the lake, the lake sediments were studied and compared. The sediments in the recipient lake were mixed and could not be dated using our simple model. The sedimentation rate in the reference lake was low: 0.09 ± 0.01 cm/y with the ^{210}Pb model and 0.12 ± 0.03 cm/y when using the ^{137}Cs peak (assumed to be from 1986). The differences can be due to attenuation corrections not being applied to the calculations of the ^{210}Pb concentrations.

As the recipient lake had mixed sediment profiles and ^{137}Cs originating from Chernobyl, the global test fallout and possible ^{137}Cs leaching from the facility site could not be distinguished. Instead it was assumed that ^{137}Cs from Chernobyl and global test fallout has the same integrated area activity (Bq/m^2) in the sediment of the reference lake and the recipient lake. We are aware that this is a rough approximation, which suggests comparable inflow and outflow and run off from the terrestrial areas into the lakes. The integrated area activity obtained from the reference lake was subtracted from the recipient lake and then multiplied by the area of the lake to gain the net activity originating from the leaching of the ash at the facility site. The calculation suggests that 5 GBq of the 20 GBq ^{137}Cs released from the facility can be found in the recipient lake, assuming a homogenized distribution of ^{137}Cs in the recipient lake. The remaining part of the released activity might be found in the stream and downstream the recipient lake.
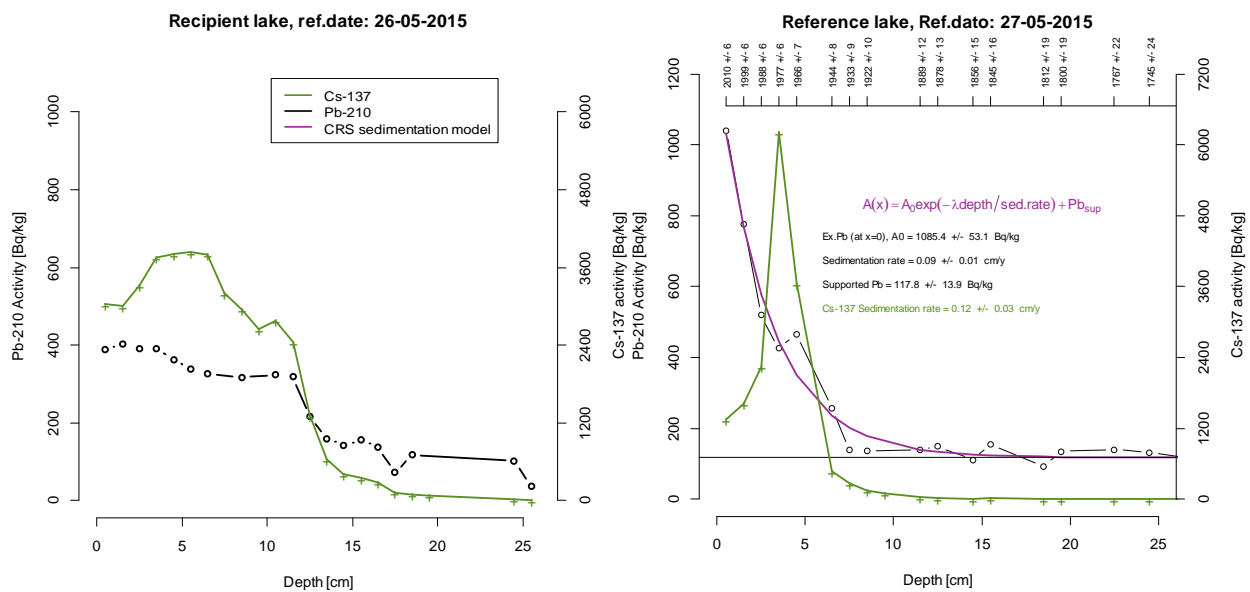
Figure 2. *^{137}Cs and ^{210}Pb activity concentration in sediment cores from recipient lake and reference lake.*

Conclusions

The results suggest that the facility has released ^{137}Cs and contaminated the surrounding environment to some extent. However, the release of ^{137}Cs might only contribute to a very minute dose to people living in the area. For example, none of the fish caught in the recipient lake contained Cs-137 activity that exceeded the Swedish National Food Agency guidance level of 1500 Bq/kg fresh weight.

References

Andersson P, Carlsson M., Falk R., Hubbard L., Leitz W., Mjönes L., Möre H., Nyblom L., Söderman A-L, Yuen Lasson K, Åkerblom G. and Öhlén E., 2007.Stålmiljön i Sverige/The radiation environment in Sweden SSI report 2007:02

Appleby P.G., Oldfield F., Thompson R., Huttunen P. & Tolonen K., 1979. ^{210}Pb dating of annually laminated lake sediments from Finland. Nature, 280:53-55.

Corresponding author: sara.ehrs@ssm.se

Uranium concentration in the sandy-clayey aquifer

A. Malov[*]

Federal Center for Integrated Arctic Research of Russian Academy of Sciences, 23 Severnoy Dviny Emb., Arkhangelsk, 163061, Russia

Abstract

This paper describes the occurrence and redistribution of U in the Vendian aquifer of the paleo valley at NW Russia. Sediments of the aquifer were accumulated in the coastal marine environment. In anoxic environments, early diagenesis conditions favour the reduction of U^{6+} into low solubility U^{4+}, which decreases U concentrations in overlying waters and sediment pore-waters. During these periods was the main flow of uranium to the study area. Transgressive era, in Middle Carboniferous-Permian led to formation of a cover of the terrigenous-carbonate deposits, however, during the long continental environmental interspace in the Mesozoic-Pliocene was formed the paleo valley. Its depth could reach 250-300 meters. Within its boundaries, Vendian deposits were brought to the surface. During this period occurred main redistribution of accumulated U. The inverse correlation between the concentrations of uranium and iron is typical for Vendian rock. It is a result of removal of U from the paleovalley slopes in oxidizing conditions and accumulation of U at the bottom in reducing conditions, and accumulation of Fe on the slopes and removal from bottom. As a result, significant part of the equilibrium U on the slopes of the paleovalley had been replaced by a newly formed hydrogenic U with a higher $^{234}U/^{238}U$ activity ratio about 3 and content about 2.6 ppm. Elevated concentrations of equilibrium U had been preserved in the unoxidized lenses at the paleo valley bottom. Now there is a hydrogenic U dissolution and desorption from the slopes of paleovalley. In general, its concentration in oxidized groundwater is correlated with the groundwater residence time in aquifer. The maximum U concentrations are characteristic of old waters with residence time from 17 to 33 ka, located close to the redox barrier. Behind the redox barrier, the U becomes restored to U^{4+} and precipitates, its concentration in the rocks reach 20 ppm, $^{234}U/^{238}U$ activity ratio decreases to 0.5-0.9.

Introduction

Uranium isotopes actively investigated as mechanistic or time scale tracers of natural processes (Porcelli, 2008; Baskaran, 2011). They may have application to determine the radiological suitability of groundwater for drinking purposes (Dhaoui et al., 2016; Wang et al., 2015; Yi et al., 2016; Manickum et al., 2014), ore bodies exploration (Hall et al., 2016; Cuvier et al., 2015; Keatley et al., 2015), assisting in understanding historical climates (Dosseto & Schaller, 2016; Jamieson et al., 2016; Wang et al., 2016). This justified the interest in uranium redistribution in the Vendian siltstones of the Northern Dvina Basin (NDB) – paleo valley at NW Russia (Fig. 1).

Materials and Methods

Study object is the Padun aquifer of the NDB. Sediments of the Padun Formation of the study area were accumulated in the coastal marine environment. The Padun Formation of the Vend 90-170-m-thick located above -150 m.a.s.l. is composed of siltstones and sandstones with intercalations of mudstones. The rocks are characterized by reddish brown color on the NDB slope and with light green lenses and spots under central part of the NDB (at the NDB bottom). Forty-four rock samples were collected from nine boreholes, and twenty-five groundwater samples (Fig. 1, Tables 1, 2).

---

[*] Corresponding author, malovai@yandex.ru:
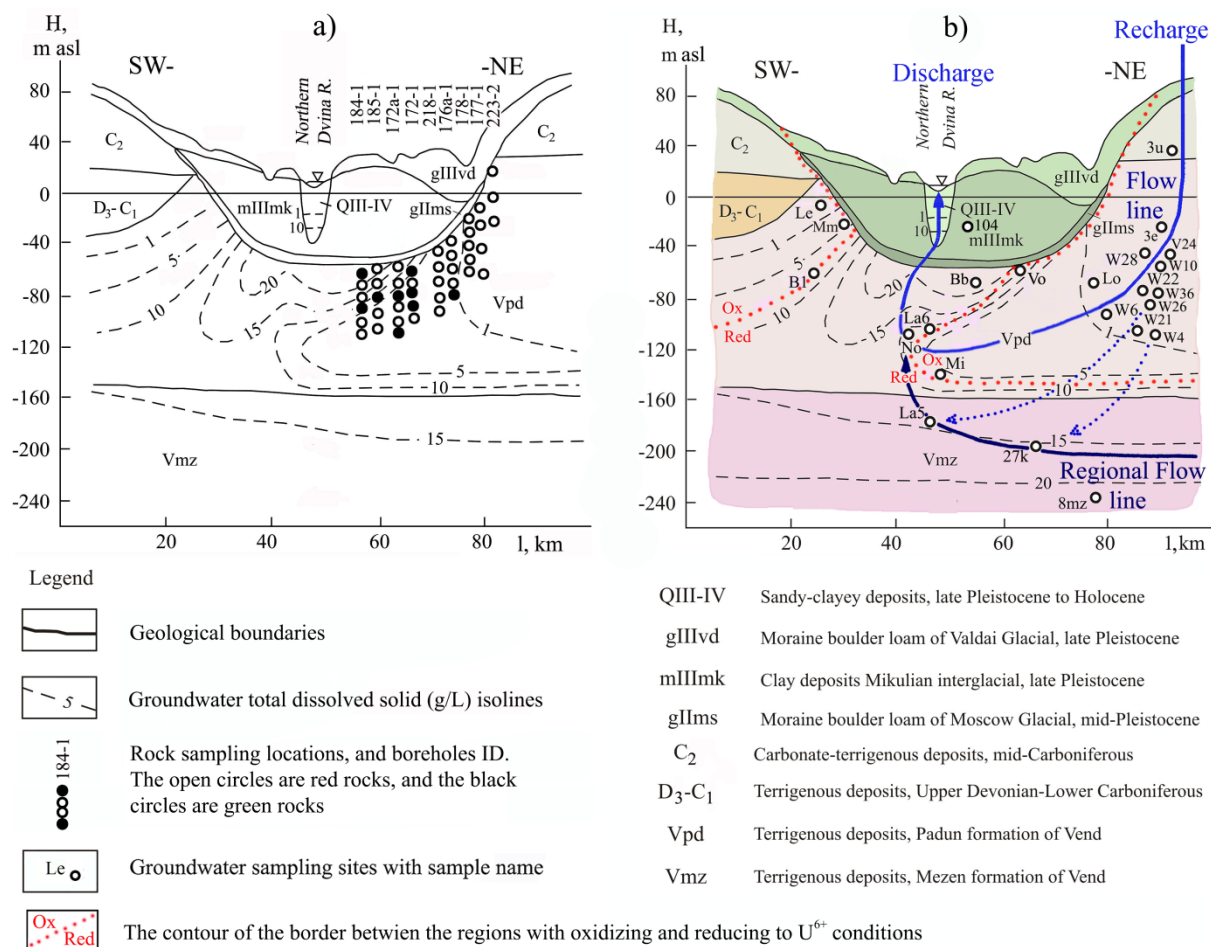
Figure 1. General location of the study site showing the rock sampling locations (a) and the groundwater sampling locations (b) on a conceptual schematic cross section of the groundwater system perpendicular to the main axis of the Northern Dvina Basin from the recharge area to the discharge in the river valley, including the location of the flow path of the water body in the aquifer (modified after Malov, 2016).

The water temperature, pH, Eh, DO, alkalinity, total dissolved solids (TDS), Fe concentrations (C_{Fe}^{W}), U concentrations (C_{U}^{W}), $^{234}U/^{238}U$ activity ratio (AR^{W}), ^{14}C, $\delta^{13}C$ were determined in the groundwater, as described by Malov (2016). The U content (C_{U}^{R}), $^{234}U/^{238}U$ activity ratio (AR^{R}), Fe content (C_{Fe}^{R}) in rock samples were determined, as described by Malov et al. (2015). We used the flow piston model to estimate the ^{14}C residence time of groundwater in an aquifer. This model takes into account both the exchange occurs predominantly between soil CO_2 and HCO_3^{-}, and the exchange occurs predominantly between HCO_3^{-} and solid carbonate minerals (Han & Plummer, 2016). We also used the mass-balance model (Malov, 2013, 2016) and model of the down-flow radioactive decay of ^{234}U excess in solution (Ivanovich et al., 1991) to estimate the ^{234}U-^{238}U residence time of groundwater in an aquifer under oxidizing and reducing conditions for U, respectively.

Results and Discussion

On the NDB slope groundwater (Fig.2b, d) with Eh from -68 to 106 mV, pH from 7.7 to 9.1 and alkalinity from 1.0 to 5.2 meq/L represents fresh water. The residence time this water in aquifer ranged from 0.3 to 16.4 ka. Accordingly very low C_{Fe}^{W} (4-203, average 41 ppb), medium AR^{W} (1.3-5.9, average 3.0) and high C_{U}^{W} (0.3-12.5, average 5.4 ppb) are characteristic of this waters. At the NDB bottom, around the redox barrier old salt water with residence time ranging from 17 to 33 ka,

TDS from 4 to 13 g/L, Eh from -38 to 2 mV, pH from 7.4 to 7.8 and alkalinity from 1.7 to 4.2 meq/L is located. The maximum C_U^W (7.2-15.4, average 12 ppb), and high AR^W (4.8-7.2, average 5.9) and C_{Fe}^W (0.4-1.9, average 0.8 ppm) are observed here. Behind the redox barrier exist the oldest (^{234}U-^{238}U age from 0.1 to 0.5 Ma) and the most salty (TDS from 9 to 22 g/L) waters. The Eh ranged from -23 to -151 mV, pH ranged from 7.6 to 9, alkalinity ranged predominantly from 0.2 to 0.9 meq/L. The minimum C_U^W (0.1-1.4, average 0.4 ppb) and maximum C_{Fe}^W (0.7-8, average 3.7 ppm) are observed here. AR^W decrease from 7.16±0.94 to 2.97±0.45.

Table 1. *Uranium content and $^{234}U/^{238}U$ activity ratio in the rocks of the Vendian (Ediacaran) Padun (Vpd) Formation at the Northern Dvina Basin (NDB)*

Borehole ID	Rock[a]	Depth (m)	^{238}U (ppm)	$^{234}U/^{238}U$	Borehole ID	Rock	Depth (m)	^{238}U (ppm)	$^{234}U/^{238}U$
Samples taken from rocks under the central part of the NDB (NDB Bottom)					Samples taken from rocks on the slope of the NDB (NDB Slope)				
184-1	GSi	106.0	3.15±0.33	0.65±0.10	218-1	RSi	72.8	1.02±0.19	1.12±0.19
	RSi	116.4	1.13±0.22	1.17±0.17		RM	82.5	1.26±0.21	1.19±0.20
	RSi	127.2	1.92±0.36	1.09±0.15		RSa	89.4	1.16±0.18	1.23±0.21
	GSi	127.2	20.9±3.52	0.54±0.08		RSi	108.1	0.63±0.11	1.07±0.18
	RSi	143.2	0.86±0.15	1.21±0.18		RSi	114	0.81±0.14	1.34±0.21
	RSi	156.0	0.63±0.11	1.14±0.16	176a-1	RSa	68.5	1.01±0.16	1.50±0.25
185-1	RSi	122.8	0.80±0.14	1.21±0.18		RSi	72.1	1.70±0.26	1.13±0.19
	RSi	133.0	0.68±0.11	0.81±0.12		RSi	85.6	1.69±0.25	1.02±0.18
	GM	144.1	1.52±0.28	1.03±0.15		RM	97.0	1.20±0.19	1.26±0.20
	VSi	153.4	2.16±0.37	1.21±0.18		GM	97.0	3.45±0.48	1.18±0.19
	RSi	160.0	0.11±0.03	0.99±0.15	177-1	RSS	52.0	0.58±0.12	1.30±0.21
172a-1	RSS	110.6	0.76±0.13	0.99±0.15		RSi	60.8	1.03±0.16	1.33±0.22
	VSi	120.0	1.11±0.22	1.30±0.19		RSi	78.1	1.79±0.27	1.17±0.19
	GSi	133.6	4.96±0.75	1.21±0.18		RM	89.0	1.26±0.21	1.07±0.18
	RSi	133.6	1.14±0.23	1.12±0.16	178-1	RSi	72.5	1.50±0.23	1.07±0.18
	RSi	150.9	1.45±0.27	1.18±0.17		RSa	79.4	1.74±0.27	1.17±0.19
	GSi	150.9	14.9±2.31	0.77±0.11		RSi	83.0	0.85±0.15	1.21±0.21
172-1	GSi	114.0	1.46±0.23	1.07±0.15		RSa	92.0	1.73±0.27	1.13±0.18
	RSi	119.6	1.57±0.25	0.97±0.15		RSa	101.5	0.84±0.15	1.25±0.20
	GSi	119.6	3.11±0.38	0.93±0.14	223-2	RSi	49.0	2.89±0.78	1.51±0.25
	GSi	131.6	2.10±0.35	0.90±0.14		RSi	70.0	0.83±0.15	1.16±0.19
	RSi	145.0	1.11±0.22	1.12±0.16		RSi	92.0	1.01±0.17	1.05±0.17
Average			3.07±0.50	1.03±0.16	Average			1.36±0.23	1.20±0.20

Total average ^{238}U = 2.22±0.36 ppm, $^{234}U/^{238}U$ = 1.12±0.18
Green rock average ^{238}U = 6.17±0.99 ppm, $^{234}U/^{238}U$ = 0.92±0.15
Red rock average ^{238}U = 1.20±0.20 ppm, $^{234}U/^{238}U$ = 1.16±0.19

[a] GSi - green siltstones, RSi – red siltstones, GM – green mudstones, RM – red mudstones, VSi - variegated siltstones, RSS – red siltstone-sandstone, RSa - red sandstones

Behind the redox barrier, the uranium changed to U^{4+} speciation and precipitates, its concentration in rocks reach 20 ppm, $^{234}U/^{238}U$ activity ratio in rocks decreases to 0.5-0.9 (Fig.2a, c). However, total precipitation does not occur because the process of recoil loss continues and ^{238}U enters into the water with ^{234}U. For every 1 atom of ^{234}U in rock, ~18,000 atoms of ^{238}U exist; therefore, recoil atoms inevitably encounter and knock other atoms from the crystal lattice, creating an area of disorder. The uranium atoms in the disordered zone are first transferred to water, resulting in a disturbance of the radioactive equilibrium in the water. Evidence that recoil atoms are not transferred into water alone but carry away a certain amount of ^{238}U atoms explains why AR^W under reducing conditions usually does not exceed 10-20. This is possible if 1000-2000 ^{238}U atoms are transferred into the water for every recoil atom.

Table 2. *Measured values of the chemical and isotopic compositions of the groundwater and the calculated values of the $^{14}C_0$ and ^{14}C ages, and U age (modified after Malov, 2016)*

Sample name	TDS (mg/L)	pH	DO	T°C	^{14}C (pmC)	δ^{13}C (‰)	Age (ka)	Eh (mV)	Alk. (meq/L)	Fe (µg/L)	C_8^W (ppb)	AR_t
Samples taken from groundwater under the central part of the NDB (NDB Bottom)										
8 mz[2014]	22,246	7.6	0	6.7	0	7.6	460±70[b]	NA	0.16	8097	0.2±0.004	2.97±0.45
27[2012]	15,724	7.9	1.1	5.9	NA	NA	160±25[c]	-23	0.92	826	1.39±0.03	5.45±0.81
La5[2012]	15,158	9	0	6.8	NA	NA	110±17[c]	-151	0.15	6031	0.12±0.002	6.19±0.93
La6[2012]	9065	8.4	0.3	6.3	NA	NA	90±15[c]	- 42	0.7	708	0.47±0.01	6.53±0.98
No[2014]	8954	8.3	1.2	6.8	0	NA	80±14[c]	-82	0.57	1352	0.28±0.01	6.72±1.05
Bb[2003]	20,619	NA	NA	NA	NA	NA	NA	NA	3.97	400	NA	NA
B1[2012]	8399	7.7	1.2	5.7	5.78±0.24	-16.6	27.3±0.6[a]	-38	4.18	1872	15.22±0.3	5.46±0.82
B1[2014]	9193	7.6	NA	5.8	5.79±0.19	-15.6	26.1±0.6[a]	NA	4.07	776	15.38±0.3	5.41±0.81
Vo[2012]	13,370	7.7	0	5.3	NA	NA	22.2±3.3[b]	NA	2.18	NA	13.84±0.3	4.75±0.71
Mi[2014]	5317	7.4	0	5	1.70±0.26	-14.6	33.0±2.3[a]	-25	1.74	439	9.86±0.2	7.16±0.94
MM[2012]	4362	7.8	NA	4.8	NA	NA	16.6±2.4[b]	2	3.75	443	7.24±0.14	6.4±0.96
Samples taken from groundwater on the slope of the NDB (NDB Slope)										
3e[2015]	138	8.7	3.5	4.8	34.18±0.59	-12.3	2.1±0.3[a]	-68	1.62	203	12.15±0.24	2.26±0.34
W10[2014]	387	9.1	1.4	4.1	NA	NA	11.7±1.8[b]	101	3.67	5.6	11.22±0.22	2.39±0.36
W6[2014]	738	8.9	0.6	4.5	25.30±0.64	-9.6	4.0±0.3[a]	99	3.75	9.5	5.21±0.92	2.86±0.42
W21[2014]	647	8.6	2.9	4.6	NA	NA	4.8±0.8[b]	23	3.44	18.2	7.55±0.15	1.99±0.3
W4[2012]	638	9	0	4.7	NA	NA	16.4±2.4[b]	106	3.97	3.9	7.0±0.14	4.76±0.72
V24[2012]	307	8.6	1.5	3.8	NA	NA	8.9±1.4[b]	-12	3.33	71.9	5.71±0.11	3.51±0.52
3u[2014]	285	7.7	NA	4.0	44.97±1.08	-8.7	1.3±0.2[b]	NA	3.21	65.7	4.01±0.84	1.46±0.22
3u[2015]	93	7.8	NA	4.9	NA	NA	NA	NA	1.02	94.9	0.25±0.01	1.28±0.21
W22[2014]	383	8.4	1.2	4.1	24.86±0.43	-10.1	4.6±0.4[a]	-8	3.02	14.3	6.37±0.13	1.63±0.24
W28[2014]	260	8.2	3.3	3.9	58.40±0.89	-11.0	2.0±0.3[b]	106	3.05	9.3	2.99±0.06	2.39±0.36
W26[2014]	365	8.1	0.8	4.4	NA	NA	2.8±0.4[b]	-34	3.61	10.8	2.38±0.05	3.04±0.45
W36[2014]	348	8.2	2.7	5.2	25.01±0.47	-11.7	5.8±0.4[a]	-62	3.56	59.1	2.0±0.04	4.81±0.62
Lo[2014]	790	9.0	1.8	4.7	37.03±0.67	-11.2	5.4±0.8[b]	NA	5.25	26.4	1.78± 0.04	5.94± 0.84
Le[2012]	209	8.2	6	5	51.67±0.63	-11.5	0.3±0.05[b]	-24	2.61	165	1.70±0.03	1.43±0.21

NA not analyzed; *NC* not calculated

[a] ^{14}C age, [b] ^{234}U-^{238}U age, [c] ^{234}U-^{238}U age of the regional and local flow systems mix groundwater (see Fig.1)
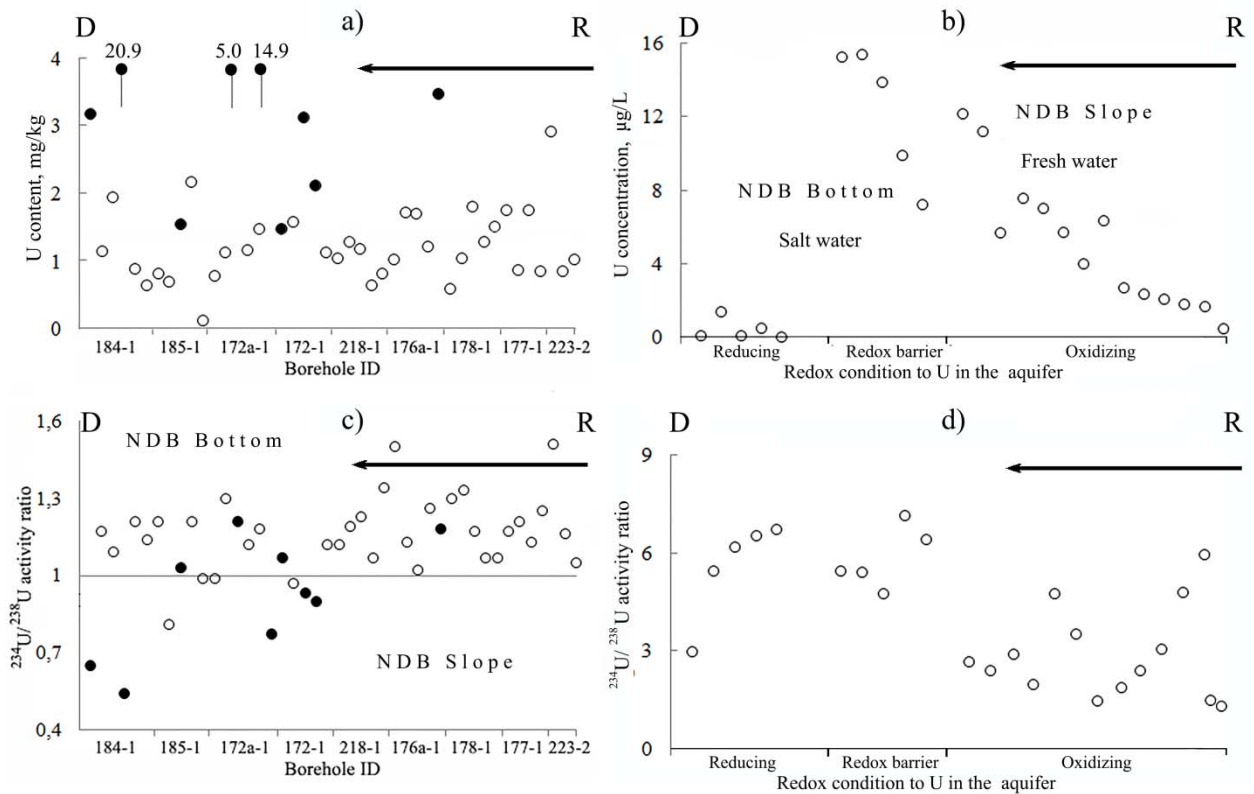
Figure 2. Uranium and its isotopes distribution in Padun aquifer of the NDB from the recharge area on the watershed («R» on the graphs) to the NDB slope and NDB bottom and discharge in the river valley («D» on the graphs): red (empty circles) and green (solid circles) rock samples (a, c) and groundwater samples (b, d). Arrows indicate the direction of groundwater flow path and uranium redistribution.

The maximum AR^W in groundwater directly close to the barrier is estimated to be 8.1 (sample Mi^{2014}). In other samples, the activity ratio is lower, namely, from 6.72±1.05 to 2.97±0.45, which suggests a greater age for the groundwater in these samples, in accordance with a simple model of the down-flow radioactive decay of excess ^{234}U in solution.

C_U^R in the red rock ranged from 0.11 ppm to 2.89 ppm, average 1.2 ppm. C_U^R in the green rock ranged from 1.52 ppm to 20.9 ppm, average 6.17 ppm. AR^R in the red rock ranged from 0.87 to 1.51, average 1.16. AR^R in the green rock ranged from 1.18 to 0.54, average 0.92 ppm. The average value of C_U^R on the slope of the NDB is 1.36 ppm, AR^R is 1.2; at the bottom of the NDB average values are 3.07 and 1.03, respectively.

The average value of C_{Fe}^R from 18 samples of red rocks on the slope of the NDB is 3.67%. In two samples from wells 184-1 on the NDB bottom C_{Fe}^R in the red rock is 2.33%, C_{Fe}^R in the green rock is 1.83%.

In Upper Vendian products of the rocks weathering were transferred to the study area with nearby eastern tip of the Baltic Shield and were deposited together with the buried organic matter. In subsequent geological periods (Upper Devonian-Lower Carboniferous) NDB was also in coastal marine and lake environment under hot humid climate (Grazhdankin et. al., 2005; Rozanov et. al., 1980). In such anoxic environments, early diagenesis conditions favor the reduction of U^{6+} into low solubility U^{4+}, which decreases U concentrations in overlying waters and sediment pore-waters (Barnes & Cochran, 1993). This period was the most favorable for the supergene ore formation (Mikhailov et al.,, 1998; Shore et al., 2005). During these periods, apparently, and was the main flow of uranium to the study area and its deposition as a result of hydrolysis, adsorption on natural sorbents and changes oxidizing conditions of the environmental in reducing conditions.

Transgressive period, in Middle Carboniferous-Permian led to the formation of a cover of the terrigenous-carbonate deposits, however, during the long continental environmental interspace in the Mesozoic-Pliocene was formed the NDB palaeo valley. Its depth could reach 250-300 meters. The depth of the valley and its Pliocene age are confirmed by the data of other paleovalleys of the East European platform (Goretsky, 1964; Kashtanov, 1954, 1956). Within its boundaries, most of the Palaeozoic sediments were destroyed, and Vendian deposits were brought to the surface.

The processes of chemical weathering of Vendian deposits led to the formation a strong oxidation zone, developed above -250 m.a.s.l. Deeper increased proportion of Fe^{2+} iron, is typical presence of bitumen, organic carbon, pyrite, and rock kept the gray-green color (Malov, 2004). During this period, probably occurred main redistribution of uranium accumulated in the Paleozoic in the Padun aquifer of the NDB. The inverse correlation between the concentrations of uranium and iron is typical for Padun rock (see above). It is a result of removal of U from NDB slopes in oxidizing conditions and accumulation of U at the bottom of the NDB in reducing conditions, and accumulation of Fe on the slopes and removal from bottom. As a result, significant part of the equilibrium U on the slopes of the NDB had been replaced by a newly formed hydrogenic U with an initial $AR_0 \approx AR^W$ of modern fresh groundwater = 3, and the initial U concentration of the rocks $C_0^R \approx C_U^R$ of modern siltstones of the region (2.6 ppm). Ending of the period of co-precipitation of hydrogenic uranium with iron hydroxide on NDB slopes can be estimated from the following equation (Ivanovich et al., 1991):

$$t_1 = \lambda_4^{-1} \ln\left[(AR_0 - 1)(AR_t - 1)^{-1}\right],$$

where λ_4 – decay constant for ^{234}U = 2.8263·10^{-6} (a^{-1}) (Cheng et al., 2000); AR_t – average AR^R of red rock = 1.16.

We get: t_1 = 0.9 Ma, which should roughly correspond to the period of a sharp cold snap in the region and filling of the paleo valley by clay material (Head & Gibbard, 2015; Azzaroli et al., 1988; Markova & Vislobokova, 2015; Muttonia et al., 2010). The duration of the subsequent removal of hydrogenic uranium from the NDB slopes can be estimated from the following equation (Malov, 2016):

$$t_2 = (C_8^W \cdot R)(R_d \cdot M_s \cdot C_8^R)^{-1},$$

where C_8^W – concentration of U was passed from the red siltstones to the water for a time t ($C_0^R - C_U^R$) = (2.6 – 1.2) = 1.4 ppm; M_s – solid mass to fluid unit volume ratio = 9.2; C_8^R – average concentration of U in solid phase for a time t: ($C_0^R + C_U^R$):2 = 1.9 ppm; $R:p$ = 24; and average $R_d:p$ = 3.6·10^{-6} a^{-1}.

We get: t_2 = 0.5 Ma. The difference ($t_1 - t_2$) should roughly correspond to the duration of glaciations and marine transgressions in the past 0.9 Ma, when the movement of groundwater in the Padun aquifer was significantly delayed or even absent (Ehlers et al., 2013; Lisitsyn, 2010; Molodkov & Bolikhovskaya, 2006; Glaznev et al., 2004). Removal of uranium was not appeared, but radioactive decay was continued.

Lower values of AR^R in the green siltstones can be explained by the fact that these deposits have reached a steady state AR_U that depends only on their size (AR_U = 0.92, the average grain size $d_p \approx$ 30 μm) (DePaolo et al., 2006), because were under reducing conditions over 1 Ma. Significantly higher content of uranium in them compared to red siltstones show considerable variability into the permeability values of the aquifer, whereby they were away from the paths of groundwater filtration and have retained uranium. A similar situation is typical for the preserved here iodine water lens (sample Bb[2003]), the source which are the iodine-containing seaweed from the Mikulinian interglacial Boreal sea.

Conclusions

The processes of chemical weathering of Vendian deposits led to the formation of a strong oxidation zone, developed above -250 m.a.s.l. The inverse correlation between the concentrations of uranium and iron is a result of removal of U from NDB slopes in oxidizing conditions and accumulation of U at the bottom of the NDB in reducing conditions, and accumulation of Fe on the slopes and removal from bottom. Almost all the U on the slopes of the paleo valley could be replaced by a newly formed hydrogenic U with a higher $^{234}U/^{238}U$ activity ratio. After that dissolution and desorption of hydrogenic U was occurred from the slopes of paleo valley during periods without any glaciations and marine transgressions. Elevated concentrations of U preserved in not oxidized lenses at the NDB bottom.

References

1.   Azzaroli, A., De Giuli, C., Ficcarelli, G., Torre, D., 1988. Late pliocene to early mid-pleistocene mammals in Eurasia: Faunal succession and dispersal events. Palaeogeogr. Palaeoclimatol. Palaeoecol. 66, 1-143.
2.   Barnes, C.E., Cochran, J.K., 1993. Uranium geochemistry in estuarine sediments: controls on removal and release processes. Geochim. Cosmochim. Ac. 57, 555-589.
3.   Baskaran M. (Ed), 2011. Handbook of Environmental Isotope Geochemistry. Springer, Berlin-Heidelberg.
4.   Cheng, H., Edwards, R.L., Hoff, J. et al., 2000. The half-lives of uranium-234 and thorium-230. Chem. Geol. 169, 17-33.
5.   Cuvier, A., Panza, F., Pourcelot, L., et al., 2015. Uranium decay daughters from isolated mines: Accumulation and sources. J Environ. Radioactiv. 149, 110-120.
6.   DePaolo, D.J., Maher, K., Christensen, J.N. et al., 2006. Sediment transport time measured with U-series isotopes: Results from ODP North Atlantic drift site 984. Earth Planet. Sci. Lett. 248, 394-410.
7.   Dhaoui, Z., Chkir, N., Zouari, K., Hadj Ammar, F., Agoune, A., 2016. Investigation of uranium geochemistry along groundwater flow path in the Continental Intercalaire aquifer (Southern Tunisia). J Environ. Radioactiv. 157, 67-76.
8.   Dosseto, A., Schaller, M., 2016. The erosion response to Quaternary climate change quantified using uranium isotopes and in situ-produced cosmogenic nuclides. Earth-Science Rev. 155, 60-81.
9.   Ehlers, J., Astakhov, V., Gibbard, P.L., Mangerud, J., Svendsen, J.I., 2013. GLACIATIONS | Middle Pleistocene in Eurasia. In: Reference Module in Earth Systems and Environmental Sciences. Encyclopedia of Quaternary Science (Second Edition) 172–179.
10.   Ehlers, J., Astakhov, V., Gibbard, P.L., Mangerud, J., Svendsen, J.I., 2013. GLACIATIONS | Late Pleistocene in Eurasia. In: Reference Module in Earth Systems and Environmental Sciences. Encyclopedia of Quaternary Science (Second Edition) 224–235.
11.   Glaznev, V.N., Kukkonen, I.T., Rajewsky, A.B., Ekinen, J., 2004. New data on the heat flow in the central part of the Kola Bay. Dokl. Earth Sci. 396, 102-104.
12.   Goretsky, G.I., 1964. Alluvium of the great anthropogenic paleorivers of the Russian Plain. Nauka, Moscow.
13.   Grazhdankin, D.V., Podkovyrov, V.N., Maslov, A. V., 2005. Paleoclimatic Environments of the Formation of Upper Vendian Rocks on the Belomorian-Kuloi Plateau, Southeastern White Sea Region. Lithol. Miner. Resour. 40, 232-244
14.   Hall, S.M., Mihalasky, M.J., Tureck, K.R., Hammarstrom, J.M., Hannon, M.T., 2016. Genetic and grade and tonnage models for sandstone-hosted roll-type uranium deposits, Texas Coastal Plain. Ore Geology Reviews, 2016 (in Press).
15.   Han, L.F., Plummer, N., 2016. A review of single-sample-based models and other approaches for radiocarbon dating of dissolved inorganic carbon in groundwater. Earth-Science Rev. 152, 119-142.
16.   Head, M.J., Gibbard, P.L., 2015. Early-Middle Pleistocene transitions: Linking terrestrial and marine realms. Quatern. Int. 389, 7-46.
17.   Ivanovich, M., Fröhlich, K., Hendry, M.J., 1991. Uranium-series radionuclides in fluids and solids, Milk River aquifer, Alberta, Canada. Appl. Geochem. 6, 405-418.

18. Jamieson, R.A., Baldini, J.U.L., Brett, M.J., et al., 2016. Intra- and inter-annual uranium concentration variability in a Belizean stalagmite controlled by prior aragonite precipitation: A new tool for reconstructing hydro-climate using aragonitic speleothems. Geochimica et Cosmochimica Acta (in Press).

19. Kashtanov, S.G., 1954. The geological data of Pliocene age of the Kazanka and Sviyaga rivers valleys. Uchenye Zapiski Kazanskogo Universiteta. 114, 155-163 (in Russian).

20. Kashtanov, S.G., 1956. New data to the history of the Paleo-Kama, 1956. Dokl. Earth Sci. 106, 708-711.

21. Keatley, A.C., Scott, T.B., Davis, S., Jones, C.P., Turner, P., 2015. An investigation into heterogeneity in a single vein-type uranium ore deposit: Implications for nuclear forensics. J Environ. Radioactiv. 150, 75-85.

22. Lisitsyn, A.P. (Ed.), 2010. The White Sea system. Nauchn. Mir, Moscow (in Russian).

23. Malov, A.I., 2004. Water-Rock Interaction in Vendian Sandy-Clayey Rocks of the Mezen Syneclise. Lithol. Miner. Resour. 39, 345-356.

24. Malov, A.I., 2013. The use of the geological benchmarks to assess the residence time of groundwater in the aquifer using uranium isotopes on the example of the Northern Dvina basin. Lithol. Miner. Resour. 48, 254-265.

25. Malov, A.I., 2016. Estimation of uranium migration parameters in sandstone aquifers. J Environ. Radioactiv. 153, 61-67.

26. Malov, A.I., Bolotov, I.N., Pokrovsky, O.S. et al., 2015. Modeling past and present activity of a subarctic hydrothermal system using O, H, C, U and Th isotopes. Appl. Geochem. 63, 93-104.

27. Manickum, T., John, W., Terry, S., Hodgson, K., 2014. Preliminary study on the radiological and physicochemical quality of the Umgeni Water catchments and drinking water sources in KwaZulu-Natal, South Africa. J Environ. Radioactiv. 137, 227-240.

28. Markova, A.K., Vislobokova, I.A., 2015. Mammal faunas in Europe at the end of the Early – Beginning of the Middle Pleistocene. Quatern. Int. In Press.

29. Mikhailov, B.M. (Ed), 1998. The forecast of the supergene zones at solid minerals. VSEGEI, St. Petersburg (in Russian).

30. Molodkov, A.N., Bolikhovskaya, N.S., 2006. Long-term palaeoenvironmental changes recorded in palynologically studied loess–palaeosol and ESR-dated marine deposits of Northern Eurasia: Implications for sea–land correlation. Quatern. Int. 152–153, 37–47.

31. Muttonia, G., Giancarlo Scardiab, G., Kentc, D.V., 2010. Human migration into Europe during the late Early Pleistocene climate transition. Palaeogeogr. Palaeoclimatol. Palaeoecol. 296, 79-93.

32. Porcelli, D., 2008. Investigating groundwater processes using U- and Th-series nuclides. Radioact. Environ. 13, 105-153.

33. Rozanov, A.Yu., Bessonova, V.Ya., Brangulis, A.P., Giants, V.A., 1980. Paleogeography and lithology of the Vendian and Cambrian of the western part of the Eastern European Platform. Nauka, Moscow (in Russian).

34. Shore, G.M., Starchenko, V.V., Myronyuk, E.P. et al., 2005. Requirements to maps of the ore-bearing of the supergene zones. VSEGEI, St. Petersburg (in Russian).

35. Wang, F., Tan, L., Liu, Q., Li, R., Li, Z., Zhang, H., et al., 2015. Biosorption characteristics of Uranium (VI) from aqueous solution by pollen pini. J Environ. Radioactiv. 150, 93-98

36. Wang, Q., Song, J., Li, X., Yuan, H., Li, N., Cao, L., 2016. Environmental evolution records reflected by radionuclides in the sediment of coastal wetlands: A case study in the Yellow River Estuary wetland. J Environ. Radioactiv. 162-163, 87-96.

37. Yi, Z. Yao, J, Chen, H-l, Wang, F, Yuan, Z., Liu, X., 2016. Uranium biosorption from aqueous solution onto *Eichhornia crassipes*. J Environ. Radioactiv. 154, 43-51.

38. Zverev, V.P., Malov, A.I., Kostikova, I.A., 2005. Geochemical state groundwater of the active water exchange zone at the Lomonosov diamond deposit. Geoecology 4, 298-303 (in Russian).

Acknowledgements

Factors influencing the distribution of weapon-test plutonium alpha-emitters on the whole-basin of a lake

I. Vioque[1]*, G. Manjón[1], R. García-Tenorio[1,2]

[1]Department of Applied Physics II, E.T.S. Arquitectura, Avenida Reina Mercedes 2, 41012-Sevilla, Spain.
[2]Centro Nacional de Aceleradores (CNA), Seville, Spain

Abstract

By analysing the $^{239+240}$Pu and ^{238}Pu content in a total of 32 sediment gravity cores, it has been possible to obtain quite rich information about the accumulation pattern of these radioactive pollutants on the basin of a small lake located in southwest Sweden. In fact, it has been observed that the traditional lacustrine models reflecting as expectations higher accumulation of pollutants at deeper water depths are not appropriate for describing the specific processes controlling the distribution of the Pu alpha-emitters isotopes in the analysed whole basin.

Additionally, and knowing the primary weapon-test atmospheric origin of the Pu-isotopes in the region where the lake is located, it has been possible to evaluate the magnitude of the Pu incorporated to the lake basin from the surrounding drainage area. This evaluation was based in the analysis of the Pu-isotopes profile in a twelve layers sediment core collected from the deepest part of the basin and in the comparison between the Pu cumulative depositions determined in the gravity cores and the expected direct-atmospheric inputs.

Introduction

The knowledge of the Pu-isotopes historical and integrated fallout incorporated to several compartments of the biosphere has allowed opening new fields of research and/or developing quite established tools. In this sense, new insights about the environmental behavior of these pollutants once they were incorporated to a particular environmental compartment (soils, sediments, vegetation, etc.) have been obtained, while the determination of the Pu profiles in some environmental archives (sediment and ice cores) have been used as a dating tool (Ketteret et al., 2004; Eriksson et al., 2001). In particular, the analysis and the determination of the spatial and temporal Pu-distribution on lake basins, located in places only affected by global sources of these nuclides, can give very rich information about the fate of these pollutants in lacustrine aquatic systems and in their surroundings drainage areas. In this sense, it is well known the extremely high reactivity of the transuranic elements to the particulate matter, which, in lakes with a not very short water residence time, should imply that the great majority of the fallout Pu incorporated to the waters finishes associated to the sediment beds (Eriksson et al., 2001).

In this paper, through the analysis of one twelve layers sediment core and thirty two integrated sediment cores collected from the basin of a small Swedish lake affected by acidification, it has been performed a complete study about the behavior of the Pu alpha-emitter pollutants in a lake of this type and in its catchment. All the plutonium determinations have been performed by applying the high-resolution alpha-particle spectrometric technique with semiconductor detectors.

* Corresponding author: ivioque@us.es

Materials and Methods

Site description

For this study it was selected the Lake Härsvatten, which is located at the southwest of Sweden, near the city of Gothenburg and at about 30 km of the North Sea coast (55º 03' N, 12º 02' E) (Figure 1). The lake is at 130 m over sea level and has an extension of 0.18 km². The average annual precipitation in the region is about 800 mm and the lake is covered by a consolidated ice-layer during the winter. In the summer, the lake is stratified with the interface between 10 and 15 m depth. Is an acidic clear-water oligotrophic lake (pH 4.4).
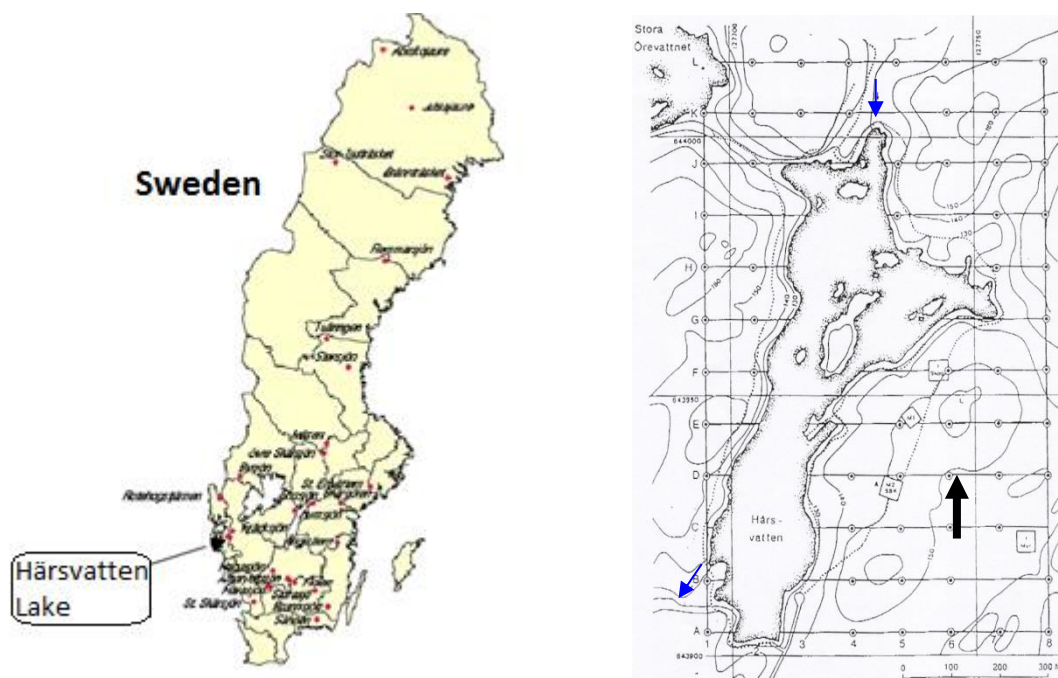
*Figure 1. Map of Sweden with the location of Lake Härsvatten and a map of the lake.*

From a bathymetric point of view, we can indicate that the lake shows a quite complex morphometry (see Figure 2). In the whole basin, it is possible to distinguish four different regions: a northern basin with a water maximum depth of 12 m, a shallow central zone with a depth ranging between 3 and 8 m, a southern basin, the largest one, with a maximum depth of 24.3 m, and an eastern basin, which is generally shallow although, in some points, it reaches a water depth of 10 m. The eastern basin is separated from the central north-south line of the lake by several islands and very shallow sills.

Sampling

A total of 32 sediment cores were collected at the places indicated in Figure 2, following this spatial distribution: 9 sediment cores were collected from the northern basin, 4 from the eastern basin, 2 from the shallow central zone of the lake and 17 from the southern basin (the largest one). Watching the southern and northern basin, the sampling strategy established allowed the collection of sediment

cores covering a wide range of water depths in order to study and analyse the use of a sediment focussing model for explaining the distribution of the Pu-isotopes cumulative depositions.). At every collection site, it was recorded the water depth from the ice surface. Once in the field, these cores where immediately sliced in two sections: the upper one corresponding to the upper 10 cm, and the lower containing the remaining part. This cutting strategy was adopted due to the knowledge gained in previous studies carried out in this lake, which indicate that the upper 10 cm of the collected integrated cores should contain all the Pu-isotopes inventories (which start to be deposited in the 50´s).

In addition to the integrated cores, it was collected in the deepest part of the south basin a twelve layers core (see Figure 2). This core had a length of 20 cm and was sliced also in the field in layers, 1 cm high each one, in order to obtain a Pu-isotope depth profile.
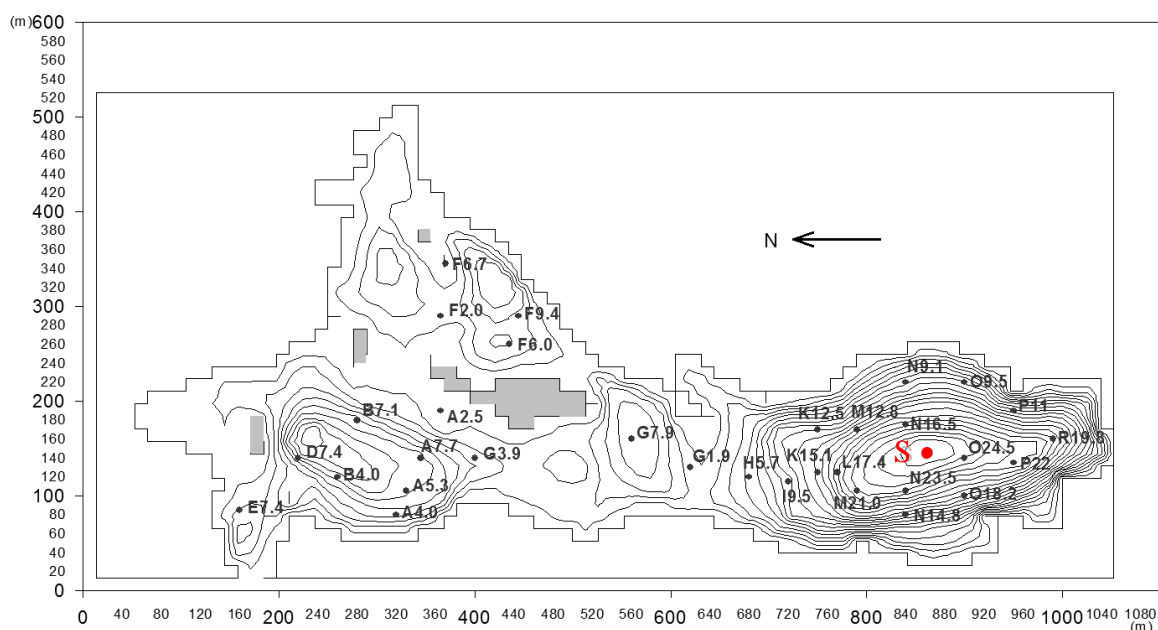
Figure 2. Bathymetric map of Lake Härsvatten. The place of collection of the 32 integrated cores and of the high-resolution core is marked (red).

The sediment fractions (either corresponding to the high-resolution or integrated cores), were placed in the field in a bag or container and stored at 4ºC. In the laboratory, the samples were weighed, freeze-dried, and reweighed to determine the water content and dry mass of the sediments.

Analytical methods

In order to proceed to the Pu-isotope alpha-emitters determination by alpha-particle spectrometry, a radiochemical procedure was applied to every sediment sample. According to the alpha-spectrometry requirements, plutonium was chemically isolated and deposited in thin layers to avoid interferences and to make sure a fine resolution. This radiochemical procedure can be found described in full detail in Vioque et al. (2002).
The detection system used for the measurements was an alpha spectrometer Alpha Analyst (Canberra) formed by eight independent chambers which can work in parallel. Each chamber is equipped with a 450 mm^2 passivated implanted planar silicon PIPS detector (18 keV nominal resolution), being
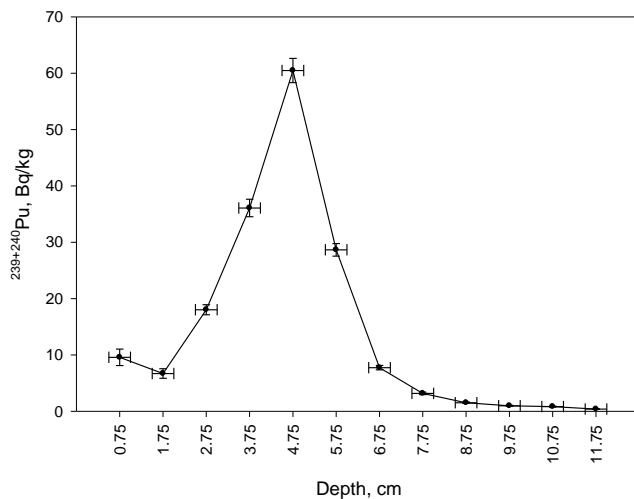
performed the measurements by placing the samples at a distance of 4 mm from the detector. In these conditions the counting efficiency is 0.34.

Results and Discussion

Twelve layers core

A total of 12 layers from a core, collected in the deepest part of the southern basin, were analysed for Pu-isotopes alpha-emitters ($^{239+240}$Pu, ^{238}Pu). The obtained $^{239+240}$Pu activity concentration profile (Bq kg^{-1}), with a resolution of 1 cm, is shown in Figure 3.

The shape of the profile is clearly affected by the historical evolution of the $^{239+240}$Pu concentrations in the lower layers of the atmosphere due to the weapons-tests fallout. Indeed, the maximum observed in the 5 cm depth layer could be associated with the years 1962-1963 (when the concentrations in the atmosphere of these Pu isotopes reached their maximum) as it was validated by the independent application of the ^{210}Pb dating method to the core (El-Daoushy et al., 1999). After these years the concentrations of Pu isotopes in the atmosphere decreased sharply to very low values in the 1970s and following years when weapons testing in the atmosphere decreased dramatically, fact that can be observed in the Pu sediment profile where the concentrations decrease sharply from the maximum at 5 cm until the surface. Additionally, the Pu with origin in the weapon tests fallout started to be detectable in the troposphere in the middle of the 50´s as is qualitatively reflected in the profile, because these dates correspond to the 8-9 cm sediment layer according to the ^{210}Pb dating method (El-Daoushy et al., 1999).

Figure 3. $^{239+240}$Pu activity concentration profile (Bq.kg^{-1}) in the high-resolution core collected in the south basin of lake Härsvatten.

In Figure 4, $^{239+240}$Pu deposition (Bq m^{-2}) and ^{137}Cs deposition (Bq m^{-2}), evaluated in the same samples, layers of core collected in the southern basin of lake Härsvatten, are shown for comparison. Indeed the highest value is in agreement for both elements. In the case of ^{137}Cs, the contribution of Chernobyl accident is clearly observed (El-Daoushy et al., 1999). Additionally, the $^{239+240}$Pu activity concentration (Bq kg^{-1}) is in agreement to SCP (g^{-1}) in the 12-layers core (Bindler et al., 2001). Similar patterns can be observed in Figure 5.
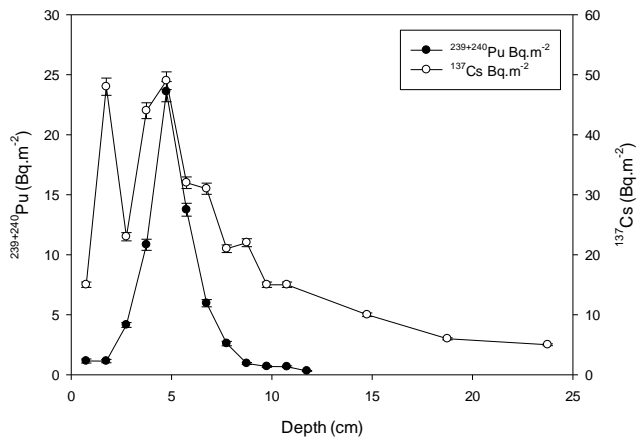
Figure 4. $^{239+240}Pu$ and ^{137}Cs deposition ($Bq.m^{-2}$) in the high-resolution core collected in the south basin of Lake Härsvatten.
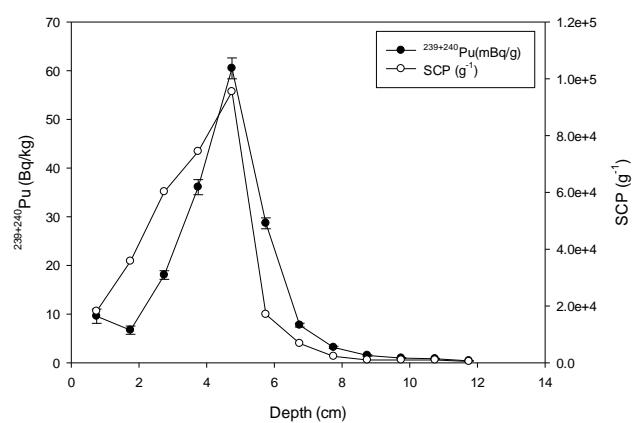
Figure 5. $^{239+240}Pu$ ($Bq.m^{-2}$) and SCP (g^{-1}) in the high-resolution core collected in the south basin of Lake Härsvatten.

Once the good correlation observed between the Pu profile in the analysed twelve layers sediment core and the historical evolution of the Pu concentrations in the atmosphere was shown, several conclusions can be proposed:

a) These results reflect the no existence of physical or biological mixing processes affecting this core, at least in the upper layers of sediment.

b) By other hand, the sharp decrease observed in the twelve layers sediment $^{239+240}Pu$ profile (Figure 4), from the maximum at 5 cm until the surface, as well as the comparatively low concentrations associated to these upper layers, is reflecting the quite small contributions of Pu originally deposited in the catchment area of the lake to the plutonium cumulative deposition in the core.

This last conclusion is in agreement with the fact that the integrated $^{239+240}Pu$ cumulative deposition found in the sediment core (65.5 ± 1.2 Bq m^{-2}) is in a rather good agreement with the expected value of the direct weapon-test atmospheric Pu deposition in the area.

Integrated cores

In Table 1 are compiled the $^{239+240}Pu$ cumulative depositions (Bq m^{-2}) determined in the 32 upper sections (0-10 cm) of the integrated cores collected at the places shown in Figure 2. These results have been arranged by dividing them into two main groups (one including the cores collected in the northern and eastern basins as well as in the central zone, the other one including the collected ones in the southern basin), and through its general analysis the following facts can be highlighted:

a) The $^{239+240}Pu$ cumulative deposition, according to the data obtained at the different places of the lake bottom, is not uniform. Furthermore deposition range, 10 to 103 Bq m^{-2}, is very wide for evaluating a representative average value of cumulative deposition.

b) It can be also observed that the higher $^{239+240}Pu$ cumulative deposition values are not found in sediments collected from the deepest parts of the different basins of the lake, and that the $^{239+240}Pu$ cumulative depositions in sediment cores collected in some shallow zones (A2.5, F 2.0 and G 3.9, for example) are higher that the determined in another cores taken in deeper

areas. It is evident that no correlation exists between the determined $^{239+240}$Pu cumulative depositions and the depth.

c) If we amalgamate the results obtained in the northern and eastern basin (northern zone of the lake) we found that its average $^{239+240}$Pu cumulative deposition (62 Bq m^{-2}) is higher than the determined one in the south basin (44 Bq m^{-2}), in spite of the fact of the higher water depths in the southern part of the lake.

North basin, central zone and east basin		South basin	
Samples	$^{239+240}$Pu(Bq/m^2)	Samples	$^{239+240}$Pu(Bq/m^2)
A 2.5	76 ± 7	H 5.7	43 ± 2
A 4.0	78 ± 4	I 9.5	22 ± 1
A 5.3	53 ± 3	K 12.5	10 ± 1
A 7.7	46 ± 2	K 15.1	28 ± 1
B 4.0	33 ± 2	L 17.4	34 ± 1
B 7.1	77 ± 2	M 12.8	52 ± 1
D 7.4	53 ± 1	M 21.0	41 ± 1
E 7.4	97 ± 3	N 14.8	53 ± 2
F 2.0	103 ± 5	N 16.5	50 ± 1
F 6.0	56 ± 6	N 23.5	53 ± 1
F 6.7	36 ± 1	N 9.1	62 ± 2
F 9.4	27 ± 2	O 18.2	46 ± 1
G 1.9	34 ± 2	O 24.5	40 ± 1
G 3.9	81 ± 3	O 9.5	36 ± 1
G 7.9	85 ± 3	P 11	14 ± 1
		P 22	66 ± 2
		R 19.8	55 ± 2

Table 1.- *$^{239+240}$Pu cumulative depositions (Bq/m^2) determined in the 32 upper sections of the integrated cores collected in lake Härsvatten*
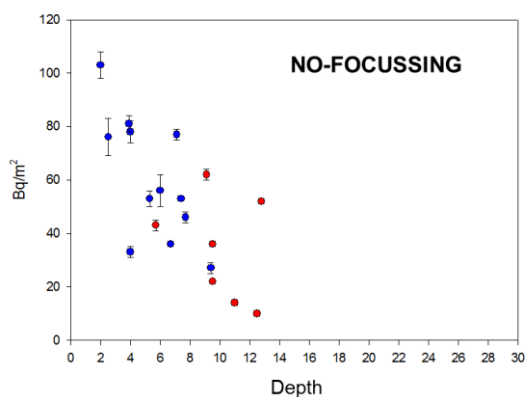
Figure 6. *$^{239+240}$Pu (Bq.m^{-2}) deposition in sampling point under 15m depth (blue, north and east basins; red, south basin).*
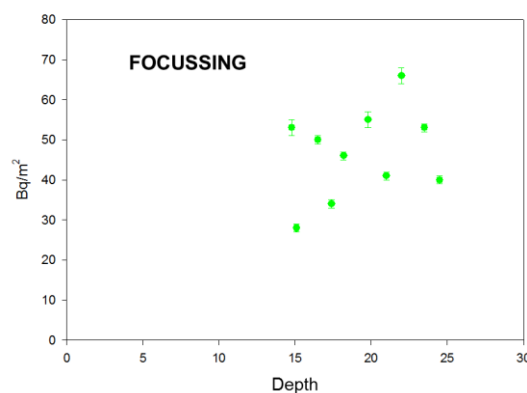

Figure 7. *$^{239+240}$Pu (Bq.m^{-2}) deposition in sampling point over 15m depth.*

The results shows that the basic model for sediment distribution and accumulation in lakes called "focussing", clearly cannot describe and explain the distribution of $^{239+240}$Pu. This model would predict a correlation between the $^{239+240}$Pu cumulative depositions and the depth, fact which is not observed at all in the lake analysed. But if we separated the deposition in the integrated cores collected at a depth under 15 m (Figure 6) and the collected over this depth (Figure 7) we can show that exits a correlation between the deposition and the depth in the samples over 15m depth (focussing) and an inverse correlation in samples under this depth (no-focussing).

As we have commented before, 15 m is the depth at were the lake is stratified in summer and it is also the depth from which it is possible to find algae mats in the bottom of the lake. The acidification of the waters can induce in this lake the expansion of algal mats on the lake bottom that prevent or interrupt sediment-focussing processes because the algae can act as efficient sediment traps, contributing to its uneven distribution across the lake bottom.

Additionally, from the data obtained through the analysis of the integrated cores some information can be ratified concerning the long-term and large-scale behaviour of plutonium in this lacustrine system. The weapon-test fallout origin of the accumulated Pu in the lake has been confirmed through the analysis of the $^{238Pu/239+240}$Pu activity ratios found in the analysed integrated cores (Figure 8). The average value of the activity ratios (0.034 + 0.008 with n=32) is in agreement with the expected value if the origin of these nuclides are the commented global ones (Hardy et al., 1973; Michel et al., 2002). There is non appreciable effect of Chernobyl (I.R.=0.47).
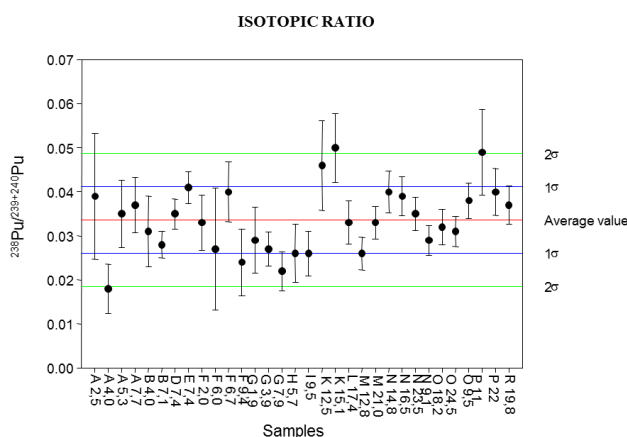
Figure 8. $^{239+240}$Pu activity concentration profile (Bq.kg^{-1}) in the high-resolution core collected in the south basin of lake Härsvatten.

In addition, the expected integrated atmospheric weapon-test fallout value in the region where is located lake Härsvatten can be evaluated to be in the range 45-60 Bq m^{-2} according to several data taken form the literature, which is in good agreement with the average cumulative Pu deposition on the whole lake basin (40-60 Bq m^{-2}). Indeed, being well known that the deposition of the Pu weapon-test fallout global source followed a latitudinal distribution, through the analysis of suitable soil cores, a general average deposition value of 58 Bq m^{-2} was fixed for the latitudinal band where the analysed lake is placed (UNSCEAR, 1982). Furthermore, some more refined studies performed at similar latitudes indicate that the integrated weapon-tests $^{239+240}$Pu deposition at regional scale is linearly correlated with the average annual precipitation in the different areas included in this region. Then, if we extrapolate the use of these correlations to the region of Lake Härsvatten, and we remember that the mean annual precipitation on the lake was 800 mm, the $^{239+240}$Pu cumulative weapon-test atmospheric deposition values obtained were in the range 45-60 Bq m^{-2}.

Conclusions

A detailed study about the spatial distribution of plutonium isotopes alpha-emitters have been performed on the whole basin of an acidified lake from southern Sweden, on the frame of an EU-financed project devoted to analyse the large-scale and long-term behaviour of transuranic elements in freshwaters systems and their surroundings catchment areas. The obtained results reflect the uneven distribution of this element which does not follow the pattern theoretically defined by the simple and ideal model of sediment focussing. Other factors like the lake hydrology or the influence of the acidification in the sedimentation processes can have influence in this distribution. On the other hand, through the average cumulative deposition value determined for the whole basin and through the analysis of the $^{239+240}$Pu profile in one high-resolution sediment core in the deepest part of the southern basin of the lake, it was deduced the no existence of appreciable inputs of Pu incorporated to the water body from the catchment area by erosion. In addition, the commented $^{239+240}$Pu-profile qualitatively reproduces the historical weapon-test deposition signal in the area, indicating that even under acidified conditions this signal can be well preserved in some areas of the lake bottom sediments.

References

Bindler, R., Renberg, I., Brännvall, M-L., Emteryd, O. and El-Daoushy, F. (2001). To whole-basin study of sediment accumulation using stable lead isotopes and fly-ash particles in an acidified lake, Sweden. *Limnology and Oceanography* 46, 178-188.

El-Daoushy, F. and others (1999).
"Large-scale and long-term environmental behaviour of transuranic elements as modelled through European surface water system"
European Commission, Nuclear Fission Safety, Final Report (Contract No. FI4P-CT96-0046), Uppsala University, Sweden.

Eriksson, M., Holm, E., Roos, P. and Dahlgaard, H. (2001). Plutonium in temperate and artic lakes. *Plutonium in the environment* (pp. 293 – 303). Ed. Kudo, A. In the series Radioactivity in the environment. Elsevier Science Ltd.

Hardy, E. P., Krey, P. W. and Volchek, H. L. (1973). Global inventory of fallout plutonium. *Nature*, 241, 444 – 445.

Ketteret M.E., Hafer K.M., Jones V.J. and Appleby P.G. (2004). Rapid dating of recent sediments in Loch Ness: inductively coupled plasma mass spectrometric measurements of global fallout plutonium. *Science of the Total Environment* 322, 221-229.

Michel, H., Barci-Funel, G., Dalmasso, J., Ardisson, G., Appleby, P. G., Haworth, E. and El-Daoushy, F. (2002) Plutonium and americium inventories in atmospheric fallout and sediment cores from Blelham Tarn, Cumbria (UK). *Journal of Environmental Radioactivity* 59, 127 – 137.

UNSCEAR (1982). Ionizing Radiation: Sources and Biological effects. *United Nations Scientific Committee on the Effects of Atomic Radiation, New York, United Nations.*

Vioque, I., Manjón, G., García-Tenorio, R. and El-Daoushy, F. (2002). Determination of alpha-emitting Pu isotopes in environmental samples. *The Analyst* 127, 530 – 535.

Wilson, T. A., Norton, S. A., Lake, B. A. and Amirbahman, A. (2008). Sediment geochemistry of Al, Fe and P for two historically acidic, oligotrophic Maine lakes. *Science of the Total Environment* 404, 269 – 275.

^{210}Pb and ^{137}Cs as tracers of recent sedimentary processes in two tropical water reservoirs

M. Díaz-Asencio[1][2], J.A. Corcho-Alvarado[3], H. Cartas-Aguila[1], A. Pulido-Caraballé[1], C. Betancourt[4], E. Alvarez-Padilla[1], Y. Labaut[1], C. Alonso-Hernández[1], M. Seisdedo-Losa[1]

[1] Centro de Estudios Ambientales de Cienfuegos, Carretera Castillo de Jagua km 1.5, Ciudad Nuclear, CP59350, Cienfuegos, Cuba
[2] Instituto de Ecología, Pesquería y Oceanografía del Golfo de México (EPOMEX), Universidad Autónoma de Campeche, México
[3] Spiez Laboratory, Federal Office for Civil Protection, CH-3700 Spiez, Switzerland.
[4] University of Cienfuegos "Carlos Rafael Rodríguez", Carretera a Rodas km 3, Cienfuegos, Cuba

Abstract

The Hanabanilla and Paso Bonito reservoirs are the main sources of fresh water for about half a million inhabitants in the central region of Cuba. Before this study, not precise information about the losses of storage capacity of both reservoirs was available. Sedimentation is the most important process that leads to changes on the water storage capacity. We investigated this process in both reservoirs by analyzing environmental radionuclides (e.g. ^{210}Pb, ^{226}Ra and ^{137}Cs) in sediment cores.

In the shallow Paso Bonito reservoir (PBR), we estimated a mean mass accumulation rate (MAR) of 0.4 (± 0.1) g cm^{-2} y^{-1} based on ^{210}Pb chronologies. ^{137}Cs was detected in the sediments but, due to the recent construction of this reservoir (1975), it wasn't possible to use it to validate the ^{210}Pb chronologies. The estimated MAR in this reservoir is higher than the typical values reported in similar shallow fresh water reservoirs worldwide. Our results highlight a significant loss of water storage capacity during the past 30 years. In the deeper and larger Hanabanilla reservoir (HR), the MAR was investigated in three different sites of the reservoir. The mean MARs based on the ^{210}Pb chronologies varied between 0.15 and 0.24 g cm^{-2}y^{-1}. The MARs calculated based on the ^{137}Cs profiles further validated these values. We show that the sediment accumulation did not change significantly over the last 50 years. A simple empirical mixing and sedimentation model, that assumes that ^{137}Cs in the water is originated from both direct atmospheric fallout and the catchment area, was applied to interpret the ^{137}Cs depth profiles. The model reproduced consistently the measured ^{137}Cs profiles in the tree cores (R^2> 0.9). Mean residence times for ^{137}Cs in the water and in the catchment area of 1 - 2.5 y and 35 – 50 y, respectively, were estimated. The model identified areas where the catchment component was higher, probably due to higher erosion in the catchment, and sites where the fallout component was quantitatively recorded in the sediments.

Introduction

Water reservoirs play a major role in water and energy supply all over the world. Their sustainable management requires a comprehensive knowledge of processes occurring within the reservoir and the catchment basin. One of the most important processes is sedimentation. This process has implications on water storage capacity and his quality (Baskaran et al., 2015).

Increased erosion in the catchment is commonly at the origin of an increased sedimentation in reservoirs. In the case of dams, as they interrupt the continuity of sediment through river systems, sediment trapping is as well important. A poor land use in the catchment basin and the expansion of human impacts into undisturbed areas are the most common causes of an accelerated soil erosion (Kondolf et al., 2014). A better understanding of the sedimentation rates and sediment dynamics is therefore essential for a better and sustainable management of the water reservoir.

Among the most commonly used techniques to determine recent sediment chronologies we have the radionuclides ^{210}Pb and ^{137}Cs. The combination of these two radionuclides have shown to be a powerful tool to investigate sediment deposition in lakes and reservoirs (Appleby, 2008). The

investigated reservoirs are used as sources of fresh water for the cities of Cienfuegos and Santa Clara (for about half a million inhabitants), they are therefore of strategic importance for the region. This paper focus on the determination of the sedimentation rates in two artificial freshwater reservoirs (Paso Bonito and Hanabanilla, Cienfuegos, Cuba). The paper deals with the determination of sediment chronologies in cores with incomplete inventories of ^{210}Pb and potentially of [137]Cs. A simple mixing and sedimentation model was applied to interpret the ^{137}Cs depth profiles in the sediment cores from the Hanabanilla reservoir.

Materials and Methods

Study area

The Hanabanilla and Paso Bonito reservoirs are located in the basin of the Arimao River, in the eastern of the Cienfuegos province (Fig. 1). Both reservoirs are used as a source of fresh water.

Figure 1. Study area in the Hanabanilla and Paso Bonito Reservoir. Sampling sites are indicated.
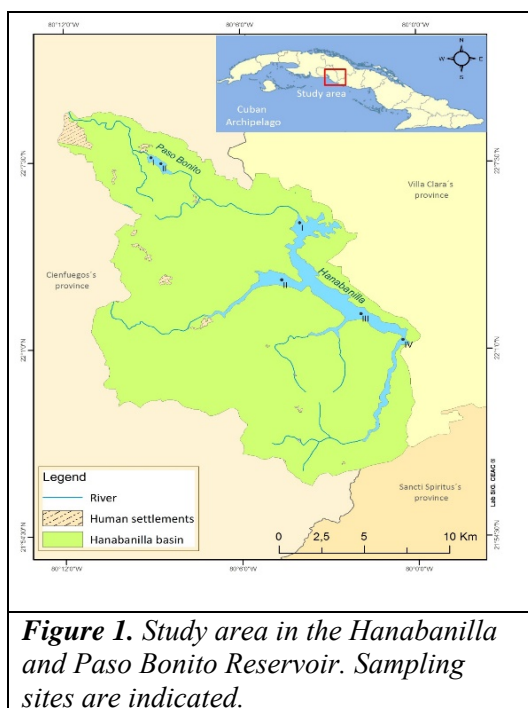
The HR was constructed between 1958 and 1962 by damming the Hanabanilla and Jibacoa rivers. At the outflow of the reservoir, three electric generators were installed. After the dam, waters are incorporated into the Hanabanilla River. The catchment of the Hanabanilla dam covers an area of 192 km^2 within the Guamuhaya Cordillera. This region has a complex geology, with an extensive area of metamorphic and igneous rocks. Intense rainfalls with short durations are typical in this area (Sánchez, 2000).

The PBR is located downstream of the Hanabanilla dam. The reservoir was constructed in 1975, to improve the water quality flowing out of the HR before its supply to the Cienfuegos and Santa Clara cities (Fig. 1).

A previous study in the PBR revealed that the accumulation of sediments was already reducing the storage volume of water storage (Laiz, 2009). The increase of the sedimentation was explained by the poor management of the soil in the watershed.

Sampling and sample preparation and texture analysis

In 2012, six sediment cores were collected in the reservoirs (Figure 1). An UWITEC corer with PVC liner (90 cm length, 8.6 cm inner diameter) was used. Two sediment cores were collected in the PBR. In the HR four cores were collected, one near to the dam and the rest in the principal basins formed by the inflow rivers. In order to define the sectioning thickness in each core, the length of the core and the date of construction of the reservoir were taken into account.

Texture analysis and radionuclides

Each section was freeze-dried and homogenized. Around 5 g was taken to determine the grain sizes. The percentage of mud (<63 μm) and sand (>63 μm) were determined by the gravimetric method. [210]Pb, [226]Ra and ^{137}Cs were analyzed by high-resolution gamma spectrometry using a low-background intrinsic germanium well detector (CAMBERRA, model EGPC100P15, with resolution of 2.1 keV at 1333 keV). Approximately 6 g of dry sediments were placed in sealed plastic

containers and stored for three weeks, in order to allow ^{226}Ra to reach equilibrium with its daughter nuclides. ^{210}Pb was analysed at 46.5 keV, ^{226}Ra was determined via the 352 keV (emitted by ^{214}Pb) and ^{137}Cs was determined at 662 keV. The efficiency calibration was performed using a Standard (IAEA-RGU-1).

^{210}Pb sediment dating

^{210}Pb$_{ex}$ in excess in each section was calculated from the difference between ^{210}Pb and ^{210}Pb$_{sup}$ supported (calculated from the ^{226}Ra activity in each layer). The MAR and the flux of ^{210}Pb in the recent sediments were determined through the Constant Flux Constant Sedimentation (CFCS) dating model (Robbins and Edgington, 1975). In sedimentary systems, where the sediment supply may vary, the Constant Flux (CF) model (Appleby and Oldfield, 1978) is preferentially used. To apply this model, it is necessary to know the total inventory of ^{210}Pb$_{ex}$ accumulated in the sediment core. As the reservoirs were constructed in the recent years (1968 and 1975), we have incomplete ^{210}Pb$_{ex}$ inventories in all the sediment cores. The "missing" inventory of ^{210}Pb$_{ex}$ has to be estimated before applying the CF model (Appleby, 2008).

Age validation with ^{137}Cs.

In order to better identify the depth horizon containing the ^{137}Cs peak in 1963, a model was used to reconstruct ^{137}Cs depth profiles in the HR (Fig. 2). The model assumes that ^{137}Cs in the water reservoir is rapidly scavenged into the sediments. Two sources of ^{137}Cs in the water column are considered. The first is the direct atmospheric deposition from global fallout, which is assumed to be after deposition well-mixed in the fresh water reservoir. The second source of ^{137}Cs in the water column is runoff/erosive transport from the catchment area (Porto et al., 2011). Assuming that the reservoir effect is described by an exponential function (Corcho-Alvarado et al., 2014), then the maximum annual flux of ^{137}Cs originated by direct fallout (first source) that can be transported to the sediment surface ($F_D(t')$, expressed in Bq/m^2/y), can be calculated as follows:

$$F_D(t') = \sum_{x=1952}^{x=t'} \frac{F_{in}(x_i) \cdot e^{-\frac{(t'-x_i)}{T}} \cdot e^{-\lambda(t'-x_i)} \cdot (x_i - x_{i-1})}{T}$$

Where F_{in} is the time-dependent atmospheric ^{137}Cs history (expressed in Bq/m^2/y), t' is the input year, T represents the mean residence time in the well mixed reservoir and λ is the ^{137}Cs decay constant. The time dependent atmospheric ^{137}Cs history in the investigated area (F_{in}) was estimated at 1.162 times the atmospheric deposition of ^{90}Sr for Miami. This multiplication factor accounts for *i)* the different atmospheric deposition of ^{137}Cs and ^{90}Sr (HASL, 1977) and *ii)* the latitudinal and rainfall amount effects between Miami and the study site (Alonso Hernández et al., 2004). The atmospheric deposition before 1950 was assumed to be negligible.

The output of ^{137}Cs from the catchment to the water reservoir is described by an exponential function which is defined by the readily available ^{137}Cs in the catchment area and the catchment/reservoir surface area ratio. The maximum annual flux of ^{137}Cs from the catchment area (second source) that can be transported to the sediment surface ($F_C(t')$, expressed in Bq m^{-2} y^{-1}) can be calculated:

$$F_C(t') = \sum_{x=1952}^{x=t'} \frac{\gamma \cdot F_{in}(x_i) \cdot e^{-\frac{(t'-x_i)}{T}} \cdot e^{-\lambda(t'-x_i)} \cdot (x_i - x_{i-1}) \cdot A_C}{T \cdot A_r}$$

Where A_r and A_c are the surface areas of the reservoir and catchment, respectively, and γ is an empirical parameter that describes the fraction of the annual fallout which is readily available for transport the following year. Several studies have shown that ^{137}Cs is strongly fixed to soil particles

with long effective half-lives. This fraction can very largely between 7 and 60 % depending on soils properties, slopes and others (Parsons and Foster, 2011). It is expected that ^{137}Cs has a long residence time in the catchment area compared to the scavenging time within the reservoir.
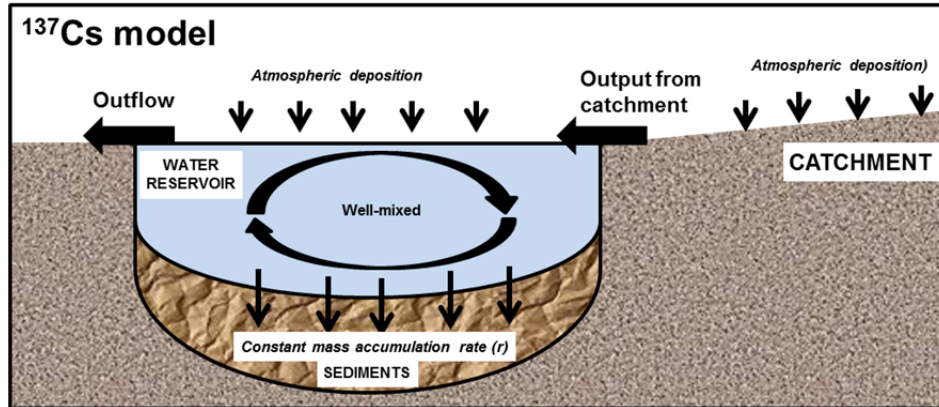
Figure 2. *Conceptual model used for the transport and deposition of ^{137}Cs in the investigated basin.*

Assuming a constant mass accumulation rate (r, kg/m^2/y), the activity of [137]Cs ($A_{(i)}$, in Bq/kg) incorporated into the sediment layer *(i)* can be calculated as:

$$A_i = \frac{(\alpha \cdot F_D(t') + \beta \cdot F_C(t'))}{r}$$

Where α and β are empirical parameters that quantify the fraction of the direct fallout and catchment fluxes (F_D and F_C) that are finally retained in the sediments. Both parameters are estimated by fitting the modelled data to the measured ^{137}Cs activities.

Results and Discussion

Sedimentation process in the Paso Bonito Reservoir
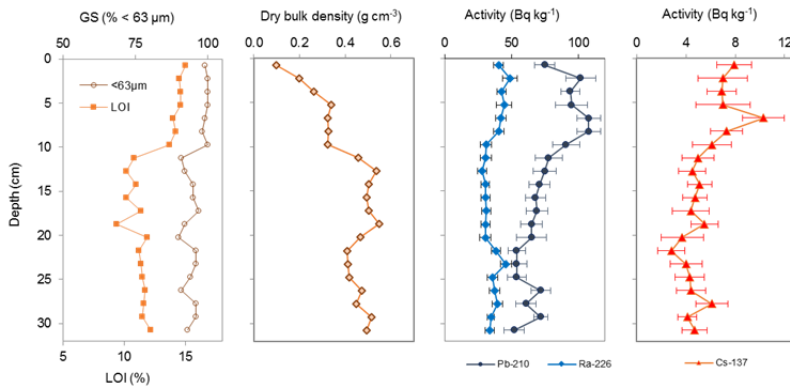
Figure 3. *Vertical profiles of grain sizes, loss of ignition, DBD and radionuclides in the core PB I.*

The content of fine particles (< 63 μm) was above 50 % in all the depth-sections of the sediment cores collected for this study. In the two cores of the PBR, the fraction of fine particles decreased below 10 cm depth. The dry bulk density (DBD), indicator of sediment compaction, increased with depth in the two cores, with values higher than 0.4 g/cm^3 after 10 cm of depth.

In both cores a rather constant activity of ^{210}Pb was observed at the top 10 cm and below this depth the activity decreased (Fig. 3). The secular equilibrium between [226]Ra and ^{210}Pb was not reached in both cores. [137]Cs was detected in all the depth sections of the cores; but in none of the cores a peak of ^{137}Cs is observed. In the core PB I, a lineal decrease of ln[210]Pb$_{ex}$ was observed in the upper 20 cm (80 kg/m^2) therefore the CFCS model was applied. This layer showed an apparent burial process in the past 20 years with a mean MAR of 0.40 ± 0.08 g/cm^2/y. Due to the irregular profile of ^{210}Pb in the core PB II the CFCS model was not used.

The mean SAR of 4.0 cm/y calculated with the CFCS ^{210}Pb dating model in the PBR is comparable to the value of 5.7 cm y^{-1} estimated from bathymetric studies (Laiz, 2009). Our study further

confirms a significant loss of water storage capacity in this fresh water reservoir during the past 30 years. The values of the sediment accumulation in the PBR were two times higher than the values calculated in the HR (see further below).

The mean MAR in the PBR is higher than the values reported for shallow fresh water reservoirs worldwide. Baskaran (2015) reported mean MAR values of 0.12 to 0.29 $g/cm^2/y$ for the Lake Union; and Waters (2015) estimated values of 0.08 to 0.30 $g/cm^2/y$ in the Lake Semiole.

Sedimentation process in the Hanabanilla Reservoir

In the Hanabanilla reservoir, the cores contained nearly 100% of fine particles. The content of OM varied in a narrow range from 10 to 15 % in all cores. In the core Hn I, OM was slightly higher than in the others cores. The DBD increased slightly with depth in the three cores. In Hn I and Hn II the higher values of DBD were observed in the bottom sections, which also showed a lighter colour. These features indicates that the bottom layers may contain pre-dam sediments (Waters et al., 2015).
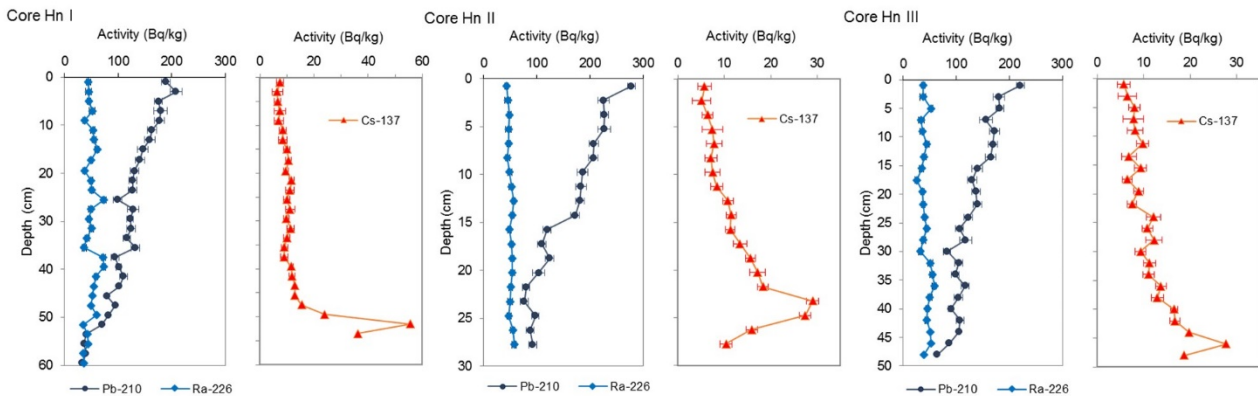
Figure 4. *Vertical profiles of radionuclides in three cores of Hanabanilla reservoir.*

In the cores of the HR, the ^{210}Pb activities showed a monotonous decrease with depth with values above 200 Bq/kg in the surface layers of the cores (Figure 4). In the cores, ^{226}Ra and ^{210}Pb didn't reach the secular equilibrium. ^{137}Cs was detected in all depth-sections of the three cores. The ^{137}Cs depth profiles have similar patterns in all the cores, with a maximum activity at the bottom part of the cores. In the core Hn I, the peak was more pronounced (circa 60 Bq/kg). In all the cores, the ^{137}Cs profiles depicted the same pattern observed for the ^{137}Cs global fallout (Robbins et al., 2000).

The CFCS model applied to the sediment cores of the HR showed two distinct burial layers in every core. Significant changes of the sedimentation process seem to have occurred at the same time (before 1990) in the three cores. The mean MAR was near to 0.15 $g/cm^2/y$ in the sites Hn I and II; and 0.24 $g/cm^2/y$ in the site Hn III. The mean MARs calculated based on the position of the ^{137}Cs peak are comparable to the ones resulting from the ^{210}Pb models. The mean MAR calculated based on the design characteristics of the reservoirs was estimated to be of 0.2 $g/cm^2/y$ (Sánchez, 2000). This design value is similar to MAR derived from the ^{210}Pb and ^{137}Cs data, and therefore it is confirmed that the design parameters are still valid. The range of the mean MAR in the HR is comparable to the values reported in other large and deep fresh water reservoirs worldwide. For example, Carnero-Bravo (2015) reported values in the range of 0.12 to 0.56 $g/cm^2/y$ for the Valle de Bravo Reservoir in Mexico; and Winston (2014) reported values of 0.2 to 0.8 $g/cm^2/y$ for the Beaver Reservoir in USA.

The MARs obtained with the CF model showed a large variability before 1990 and after this year remained constant. In the core Hn I, a clear peak in the MAR was observed around 1990. In June

1988, intensive rains with nearly 1000 mm in seven days affected the catchment area of the reservoir. This climatic event produced high floods in the region (Alonso-Hernandez et al., 2006).

The high accumulation in the site Hn III, located in the artificial channel that connect the two principal basins of the reservoir (the Hanabanilla and the Jibacoa river basins), produced a rapid decrease of the water depth in this area. Consequently, the water exchange between the two basins decreased with the increased resident time of the water in the Jibacoa basin.

Age validation with ^{137}Cs in the Hanabanilla reservoir
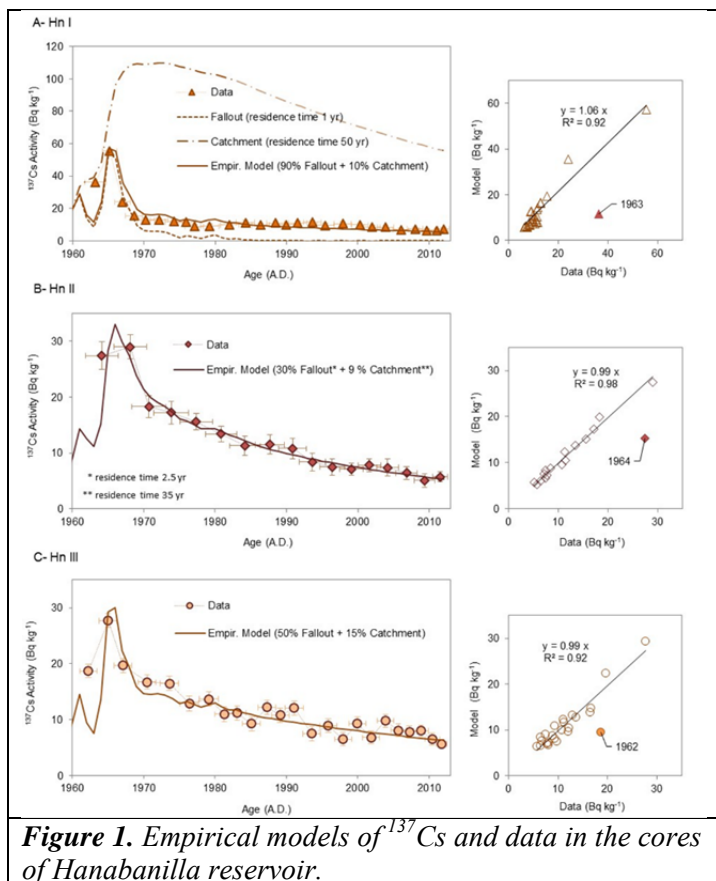
Figure 1. *Empirical models of ^{137}Cs and data in the cores of Hanabanilla reservoir.*

A simple empirical model was applied to interpret the ^{137}Cs depth profiles. Mean residence times (MRT) for ^{137}Cs in the water reservoir and in the catchment area of 1-2.5 and 35-50 years, respectively, best fitted the model to the measured data. The shorter MRT of ^{137}Cs in the reservoir may be explained by the scavenging process that additionally decreases the ^{137}Cs amount in the water column. The long MRT in the catchment is explained by its strong fixation in soil. In the three cores the empirical models reproduced the measured ^{137}Cs depth profiles ($R^2 > 0.92$).

In the Hn I core, the model indicates that sediments in this area captured about 90 % of the ^{137}Cs delivered by atmospheric fallout onto the corresponding reservoir surface. Additionally, a small fraction of the ^{137}Cs in the sediments was delivered by the catchment (10%).

In the core Hn II, the ^{137}Cs fallout component in the sediments represented only 30% of the total atmospheric fallout. In this core, the best fit was obtained for a MRT of Cs in the reservoir of 2.5 years. The catchment component was estimated at around 9% of the total ^{137}Cs in the catchment basin that is readily available for transport. The MRT of Cs in the catchment basin was estimated to be of 35 years, which suggest that soils in this local basin is more erodible than soils from other areas of the catchment.

In the sediment core Hn III, the ^{137}Cs fallout and catchment components were estimated to be of 50% and 15%, respectively. The model indicates that this area of the reservoir is more affected by the catchment. In fact, this core showed the highest MAR of the investigated cores. These results showed the principal characteristic of the sediment processes in each sampling areas and his local basin. In the site Hn I, the catchment has the lower relative importance on the sediment accumulation, that the others areas; on the contrary this component is higher in the site Hn III, that receive the influence of the major local basin (Jibacoa river). In the site Hn II, the local basin (Hanabanilla river) has a higher erosion process than the others zone of the reservoir.

Fluxes of ^{210}Pb$_{ex}$ and ^{137}Cs inventory in the Hanabanilla reservoir

The ^{210}Pb$_{ex}$ fluxes in the PBR and HR ranged from 235 to 372 Bq/m^2/y. These fluxes are higher than for example the fluxes reported by Binford & Brenner (1986) in the Florida lake (129 to 204

Bq/m^2/y), USA. Moreover, the ^{210}Pb$_{ex}$ fluxes in the PBR and HR are also slightly higher than the flux range reported by Carnero-Bravo (2015) in Valle de Bravo Reservoir (135 to 199 Bq/m^2/y) in Mexico.
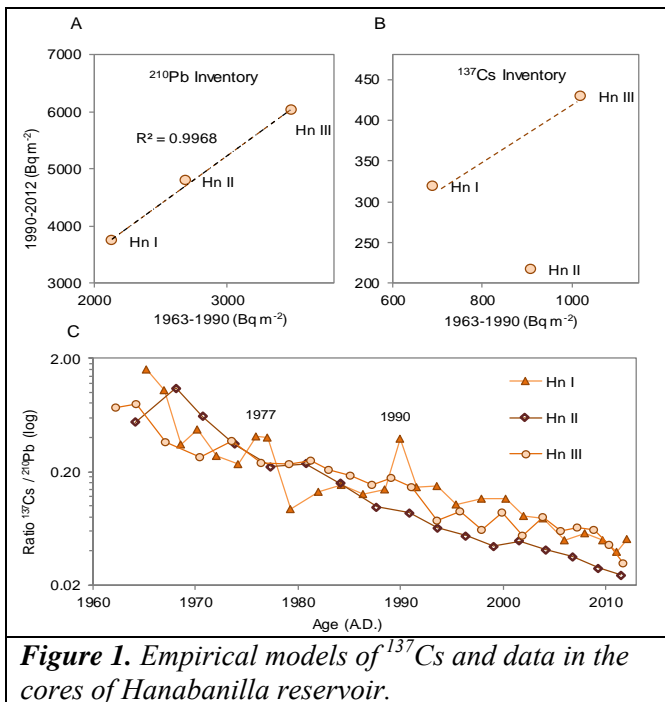
Figure 1. Empirical models of ^{137}Cs and data in the cores of Hanabanilla reservoir.

The inventories of ^{210}Pb$_{ex}$ and ^{137}Cs were calculated in the cores of the HR. Due to the recent construction date of the HR, incomplete inventories of ^{210}Pb$_{ex}$ and ^{137}Cs are expected in the sediment cores. The inventories of both radionuclides were calculated for the years between 1963 and 2012. The comparison of the ^{210}Pb inventories for the periods 1963-1990 and 1990-2012 showed that the ^{210}Pb supply didn't change significantly over the past decades. Although the atmospheric fallout of ^{137}Cs has changed significantly in the past 50 years, the 1963-1990 to 1990-2012 inventory ratios were similar in the cores Hn I and Hn III and lower in the core Hn II. The lower ratio in the core Hn II may be explained by the loss of ^{137}Cs by increased erosion in the catchment area during the period 1990-2012.

Moreover, in the core Hn II the ^{137}Cs/^{210}Pb$_{ex}$ ratio was lower than the other cores, after 1980. These results confirm than the local catchment of the site Hn II (Hanabanilla River) has higher erosion than the others of the reservoir. The ^{137}Cs/^{210}Pb$_{ex}$ ratio in core Hn I was higher during the intense rains in 1977 and 1988. The result could be explained for the intense erosion in the catchment during these exceptional events, causing the re-suspension and transport of old soils (with higher ^{137}Cs activities).

Conclusions

Sediment chronologies in the Paso Bonito and Hanabanilla fresh water reservoirs, obtained based on ^{210}Pb data, allowed to quantify the sediment accumulation process in the systems. Our results confirmed a significant loss of water storage capacity in the Paso Bonito reservoir during the past 30 years.

The accumulation of sediments in the Hanabanilla reservoir does seem to have changed significantly in the past 50 years. These results indicate that actual situation of this reservoir complies with the original design parameters of erosion and sedimentation. Nonetheless, our study identified areas of the reservoir which are more affected by sediment accumulation and by particle loading from the catchment. These results are indeed useful to improve the management of the reservoir and catchment to avoid major problems in the future. The results demonstrated that the geochronology with ^{210}Pb and ^{137}Cs are very useful to understand the effect of temporal environmental (and human) changes on aquatic systems, providing more information to improve the management activities.

References

Alonso Hernández, C.., Cartas Águila, H., Díaz Asencio, M., Muñoz Caravaca, A., 2004. Reconstruction of 137Cs signal in Cuba using 7Be as tracer of vertical transport processes in the atmosphere. J. Environ. Radioact. 75, 133–142. doi:10.1016/j.jenvrad.2003.11.007

Alonso-Hernandez, C.M., Diaz-Asencio, M., Munoz-Caravaca, A., Delfanti, R., Papucci, C., Ferretti, O.,

Crovato, C., 2006. Recent changes in sedimentation regime in Cienfuegos Bay, Cuba, as inferred from 210Pb and 137Cs vertical profiles. Cont. Shelf Res. 26, 153–167. doi:10.1016/j.csr.2005.08.026

Appleby, P.G., 2008. Three decades of dating recent sediments by fallout radionuclides: a review. The Holocene 18, 83–93. doi:10.1177/0959683607085598

Appleby, P.G., Oldfield, F., 1978. The calculation of lead-210 dates assuming a constant rate of supply of unsupported 210Pb to the sediment. CATENA 5, 1–8. doi:10.1016/S0341-8162(78)80002-2

Baskaran, M., Miller, C.J., Kumar, A., Andersen, E., Hui, J., Selegean, J.P., Creech, C.T., Barkach, J., 2015. Sediment accumulation rates and sediment dynamics using five different methods in a well-constrained impoundment: Case study from Union Lake, Michigan. J. Great Lakes Res. 41, 607–617. doi:10.1016/j.jglr.2015.03.013

Binford, M.W., Brenner, M., 1986. Dilution of 210 Pb by organic sedimentation in lakes of different trophic states, and application to studies of sediment-water interactions1. Limnol. Oceanogr. 31, 584–595. doi:10.4319/lo.1986.31.3.0584

Carnero-Bravo, V., Merino-Ibarra, M., Ruiz-Fernández, A.C., Sanchez-Cabeza, J.A., Ghaleb, B., 2015. Sedimentary record of water column trophic conditions and sediment carbon fluxes in a tropical water reservoir (Valle de Bravo, Mexico). Environ. Sci. Pollut. Res. 22, 4680–4694. doi:10.1007/s11356-014-3703-0

Corcho-Alvarado, J.A., Diaz-Asencio, M., Froidevaux, P., Bochud, F., Alonso-Hernández, C.M., Sanchez-Cabeza, J.A., 2014. Dating young Holocene coastal sediments in tropical regions: Use of fallout 239,240Pu as alternative chronostratigraphic marker. Quat. Geochronol. 22, 1–10. doi:10.1016/j.quageo.2014.02.001

HASL, 1977. Health and Safety Laboratory environmental quarterly: final tabulation of monthly 90Sr fallout data: 1954-1976. New York, USA.

Kondolf, G.M., Gao, Y., Annandale, G.W., Morris, G. regory L., Jiang, E., Zhang, J., Yongtao, C., Carling, P., Fu, K., Guo, Q., Hotchkiss, R., Peteuil, C., Sumi, T., Wang, H.-W., Wang, Z., Wei, Z., Wu, B., Wu, C., Yang, C.T., 2014. Sustainable sediment management in reservoirs and regulated rivers: Experiences from five continents. Earth' s Futur. 2, 256–280. doi:10.1002/2013EF000184.of

Laiz, O., 2009. ESTUDIOS CAPACIDAD DE ALMACENAJE EN EMBALSES CUBANOS. La Habana. Cuba.

Parsons, A.J., Foster, I.D.L., 2011. What can we learn about soil erosion from the use of 137Cs? Earth-Science Rev. 108, 101–113. doi:10.1016/j.earscirev.2011.06.004

Porto, P., Walling, D.E., Callegari, G., 2011. Using 137Cs measurements to establish catchment sediment budgets and explore scale effects. Hydrol. Process. 25, 886–900. doi:10.1002/hyp.7874

Robbins, J.A., Edgington, D.N., 1975. Determination of recent sedimentation rates in Lake Michigan using Pb-210 and Cs-137. Geochim. Cosmochim. Acta 39, 285–304. doi:10.1016/0016-7037(75)90198-2

Robbins, J. a., Holmes, C., Halley, R., Bothner, M., Shinn, E., Graney, J., Keeler, G., TenBrink, M., Orlandini, K. a., Rudnick, D., 2000. Time-averaged fluxes of lead and fallout radionuclides to sediments in Florida Bay. J. Geophys. Res. Ocean. 105, 28805–28821. doi:10.1029/1999JC000271

Sánchez, R., 2000. Características del agua del embalse Hanabanilla. Santa Clara.

Waters, M.N., Golladay, S.W., Patrick, C.H., Smoak, J.M., Shivers, S.D., 2015. The potential effects of river regulation and watershed land use on sediment characteristics and lake primary producers in a large reservoir. Hydrobiologia 749, 15–30. doi:10.1007/s10750-014-2142-8

Winston, B., Hausmann, S., Escobar, J., Kenney, W.F., 2014. A sediment record of trophic state change in an Arkansas (USA) reservoir. J. Paleolimnol. 51, 393–403. doi:10.1007/s10933-013-9762-2

[*] Corresponding author, E-mail: misaeldiazasencio1971@gmail.com

^{226}Ra, ^{228}Ra, ^{228}Th, ^{40}K and ^{137}Cs activity concentrations in a sediment core of a reservoir affected by acid mine drainage

E.G. San Miguel[1], C.R. Cánovas [2], M. Casas-Ruiz[3], J.P. Bolívar[1]*

[1]Dept Fisica Aplicada, Universidad de Huelva, Campus de Excelencia Internacional del Mar (CEIMAR), 21071 Huelva, Spain
[2]Dept of Geología, Universidad de Huelva, Campus de Excelencia Internacional del Mar, Huelva
[3]Dept Fisica Aplicada, Universidad de Cádiz, Campus de Excelencia Internacional del Mar (CEIMAR), Cádiz, Spain

Abstract

The present work shows the activity levels of ^{226}Ra, ^{228}Ra, ^{228}Th, ^{40}K and ^{137}Cs in a sediment core collected from the Sancho Reservoir (SW Spain). The acidity (pH 3–5), and high dissolved metal concentrations observed in the Sancho, together with the large volume stored (between 37 and 55 Mm^3), makes this reservoir an extreme case of surface water pollution worldwide.

^{40}K, ^{228}Ra and ^{226}Ra concentrations are nearly uniform from layer 20-22 cm to the bottom of the sediment core, whereas for sediment water interface to the layer 20-22 cm a clear decrease of the activities of these radionuclides can be observed. The significant variation in the activity levels of radionuclides from the top of the core to layer 20-22 cm might be due to their sorption/desorption processes onto the surface of sediments. These processes could have been enhanced as a consequence of the contamination of the Sancho Reservoir by Acid Mine Drainage. ^{226}Ra/^{228}Ra activity ratios range between 0.61-0.86 (Mean 0.72).

Similarly, low activity ratio (0.18) for ^{137}Cs/^{40}K r eflects the presence of very high content of ^{40}K in sediment due to presence of primary minerals in sediment. A significant positive correlation between ^{226}Ra and ^{228}Ra suggest a similar origin of their geochemical sources and identical behavior during transport in the sediment system.

The inventories and fluxes of these radionuclides in the sediment core show an important change in the layer 20-22 cm. The flux from the layer 22 cm to the bottom of the sediment core with respect to the flux for the first 22 cm of the sediment core range between 3.9 times for ^{226}Ra to 40 times for ^{228}Ra.

Introduction

Distribution of natural radionuclides in recent sediments could reflect terrigenous material input as well as anthropogenic influence, and is a useful tool for recognizing their possible sources and patterns along the investigated area. ^{40}K ($t_{1/2} = 1.248 \cdot 10^9$ yr) is a primordial natural radionuclide which is present in all rocks, sediments and soils. ^{40}K is considered as one of the classic radionuclides of lithogenic origin and may be applicable as a tool to differentiate between the contribution of lithogenic and biogenic fractions in marine sediments (Gulin et al., 2014). It is one of the most abundant naturally radioactive elements usually associated with clay minerals.

Radium isotopes, ^{226}Ra ($t_{1/2} = 1600$ yr) and ^{228}Ra($t_{1/2} = 5.75$ yr) are the most radiotoxic and dangerous element in case of ingestion due to their similarity in behavior to calcium, an element commonly fixed in bones (Martin Sanchez et al., 1999). Determination of Ra isotopes in environmental samples is important from the standpoint of health physics and environmental protection, because a large quantities of elevated Ra activities can be released by the phosphate industry, mining and processing industry of metal ores, oil and gas extraction industry, coal mining (Mas et al., 2006; Hierro et al., 2014). The source of ^{226}Ra and ^{228}Ra in the environment is the radioactive decay of naturally occurring ^{238}U and ^{232}Th found in the earth's crust. Thorium is mostly bound to the terrestrial/detritic material due to its low solubility in water. Thus, Th is rapidly

scavenged onto settling particles, removed from the water column and buried into the sediment. Since ^{40}K and ^{232}Th are associated with particles, they can be used as sediment tracers to study the origin of the sediment. ^{137}Cs ($t_{1/2}$=30.2 y) is an anthropogenic radionuclide originated from atmospheric nuclear weapons testing carried out from 1945 to 1972. Explosions lifted radionuclides into the stratosphere where they spread around the world. If the ^{137}Cs vertical profile in a sediment core has not been significantly affected by post-depositional processes, it will show a well defined peak corresponding to the years of maximum concentration in the atmosphere (1962-1963).

In Huelva province (SW Spain) important mining activities have been carried out since ancient times, especially during the mid-19th and 20th centuries, leaving an immense amount of sulfide-rich mine wastes in the area. The oxidation of sulfides contained in these wastes causes the release of high loads of sulfate, acidity and metals into the water bodies, a process commonly known as acid mine drainage (AMD), which is the cause of deterioration of extensive lengths of the Tinto and Odiel Rivers (Cánovas et al., 2016, and references therein). Acid mine drainage (AMD) is one of the main causes of water pollution worldwide.

The Sancho reservoir, located in the Odiel river watershed, is contaminated by acid mine drainage (AMD). A progressive acidification has been observed in the Sancho waters since 2003, as evidenced by decreasing pH values and increasing metal concentrations, especially noticeable after 2007. The increase in the net acidity in the reservoir originates from the higher input of metals and acidity due to the rebound effect after the closure of the Tharsis mine in 2001. The decrease of pH values from 4–5 to 3–4 has caused an increment of dissolved Fe and other metals (Cánovas et al., 2016).

The primary objective of this work is to report the behavior of different natural radionuclides from both U- and Th-series in a sediment core from this reservoir affected by AMD.

Materials and Methods

Description of the study area

The Sancho reservoir is located in the Iberian Pyrite Belt in the River Meca Valley. The Meca River basin has an area of 315 km^2 with the absence of steep slopes and a maximum height of 394 m (average of 149 m). The dry-Mediterranean climate promotes yearly mean rainfall close to 600 mm, with high intra- and inter-annual variability (Galván et al., 2009). The river flows shows a high variability, with average values of 0.84 m^{3}s^{-1} and maximum of 267 m^3 s^{-1} during extreme floods. On the other hand, the river usually dries up during the dry season (from June to September) until the arrival of the first rainfalls of autumn.

The Sancho Reservoir (58 Mm^3) was built in 1962 to supply water to a pulp mill factory and has been used as a domestic water supply after treatment. This water body has a surface area of 4.27 km^2, a maximum depth of 40 m and is mainly fed by the Meca River. In the headwaters of the Meca River are located several mining complexes. Due to the intense mining activities, the Meca River is currently deeply contaminated by AMD, transporting huge amounts of contaminants to the Sancho Reservoir (Galván et al., 2009). These pollutants are mainly transferred to the bottom sediments where high metal concentrations are observed in pore waters (Sarmiento et al., 2009). A more detailed description of the site can be seen elsewhere (Cánovas et al., 2016).

Sampling

In late 2011, a 1.4 m long sediment core was collected by scuba diving using a manual corer consisting of a 5.5 cm inner diameter cylindrical PVC tube. The sediment core was frozen in the laboratory and sliced in horizontal sections with a plastic cutter at 2.0 cm resolution excepting the most superficial layer that was sliced at 3.0 cm. Sediment samples were dried at 60 ºC to constant

weight, and then powdered and homogenized. From the wet and dry weights of the sediments, water content was determined.

Radionuclide determinations

An aliquot of about 4-5 g of each homogenized sample was sealed and stored in 5 mL cylindrical containers of polyethylene for at least a month for radionuclide determinations through gamma spectrometry. These containers were sealed and stored for more than one month in order to reach secular equilibrium between ^{228}Ra and its radioactive progenies ^{228}Ac, and ^{226}Ra and shorter half lives daughters of ^{222}Rn.

^{226}Ra, ^{228}Ra, ^{228}Th, ^{137}Cs and ^{40}K were determined by gamma-ray spectrometry using a Well Ge detector (Canberra), with a full-width at half-maximum (FWHM) of 1.33 keV at 122 keV (^{57}Co) and 2.04 keV at 1332 keV (^{60}Co), and a peak/Compton ratio of 56.2/1. The detector was coupled to a multichannel analyser and was shielded with 10 cm thickness lead shield. In order to avoid interferences from X-ray from the Pb of the shield, a layer of 2 mm thick of Cu layer is placed between the Pb shield and the detector. Spectra were collected for at least 80,000 s and analysed by Genie 2000 software (Canberra Industries).

The photopeaks used in the radionuclides determination were: ^{226}Ra (352 keV from ^{214}Pb), ^{228}Ra (911 keV from ^{228}Ac), ^{228}Th (583 keV from ^{208}Tl), ^{137}Cs (661 keV) and ^{40}K (1460 keV).

Efficiency calibration with self-absorption corrections were determined according to procedures detailed elsewhere (Appleby and Piliposian, 2004, and references therein).

Measurement uncertainties of ^{226}Ra, ^{228}Ra, ^{228}Th, ^{40}K and ^{137}Cs activity concentration expressed for 2 sigma were respectively in the range 2–15%, 2-20%, 2-20%, 1-6% and 2-40% for all samples, excepting for sample from depth 4.5–6.5 cm for whose uncertainties were 30%, 28%, 26%, 10% and 60% respectively. The minimum detectable activity (MDA) for the counting time of 80,000 s was about 50 mBq for ^{226}Ra, 70 mBq for ^{228}Ra, 20 mBq for ^{228}Th, 20 mBq for ^{137}Cs and 0.3 Bq for ^{40}K.

The quality of radiometric measurements are regularly ensured through participation in intercomparison exercises organized by the International Atomic Energy Agency (IAEA), as well as the periodic measurement of certified reference materials in our laboratory (IAEA-326 black soil; NIST-1646a estuarine sediment, etc.).

Results and Discussion

Fig. 1a shows the vertical profile of ^{226}Ra and ^{228}Ra activity concentrations in the sediment core from Sancho Reservoir. The ^{226}Ra activity concentrations ranged between 17.1 and 44.4 Bq kg^{-1} with an average 37.2 Bq kg^{-1} (S.D.: 5.7 Bq kg^{-1}). As can be seen from the vertical profile of ^{226}Ra, activity concentrations are lower than 20 Bq kg^{-1} in the first 10 cm of the sediment core whereas below 15 cm are higher than 30 Bq kg^{-1}. ^{226}Ra activities decrease gradually from 30 cm towards the surface of the sediment core.

In the case of ^{228}Ra, activity concentrations range between 26.7-61.9 Bq kg^{-1} (average: 51.4 Bq kg^{-1}, SD: 7.3 Bq kg^{-1}) in the whole sediment core. As can be seen from Fig. 1, the vertical profile of ^{228}Ra presents the same behavior than that of ^{226}Ra. There is a clear change in the trend of the activity concentrations about the layer 22 cm. The activity concentrations range between 26.7-47.0 Bq kg^{-1} (average: 36.1 Bq kg^{-1}) from the first to layer 22 cm.

A significant positive correlation between ^{226}Ra and ^{228}Ra has been found (linear correlation coefficient, R=0.80). This correlation suggests a similar origin of the geochemical sources of Ra-isotopes and identical behavior during transport in the sediment system.

a) ^{226}Ra and ^{228}Ra

b) ^{228}Th

c) ^{40}K

d) ^{137}Cs
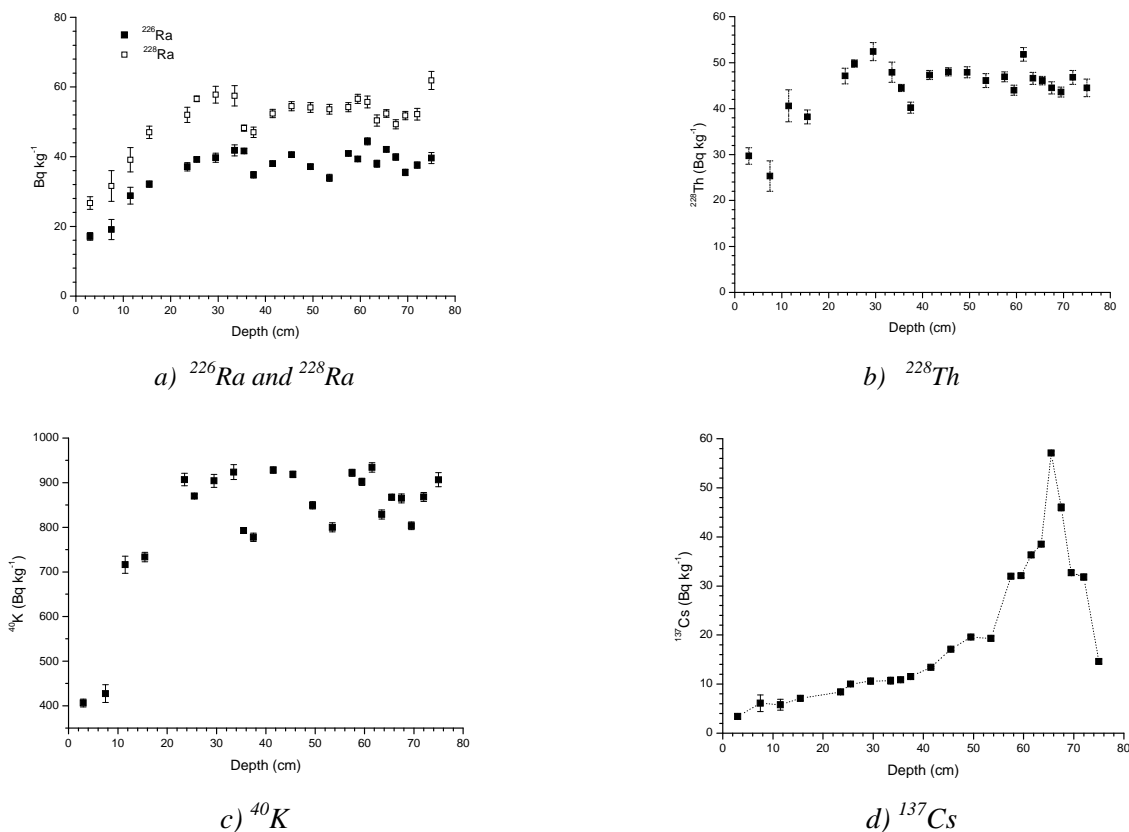
Figure 1.- *Vertical profiles of Radionuclides in Sancho Reservoir sediment core.*

In Fig. 1b the vertical profile of ^{228}Th activity concentrations is displayed. As can be seen from this figure, the change observed in layer 22 cm in the vertical profile ^{228}Th activity concentrations is less significant than in the case of Ra-isotopes. Nevertheless, a different trend can also been inferred in the two zones of the sediment core: the activity concentrations range between 25.3-52.4 Bq kg^{-1} (average: 45.2 Bq kg^{-1}, SD: 4.9 Bq kg^{-1}) in the whole sediment core whereas range between 25.3-40.6 Bq kg^{-1} (average: 33.5 Bq kg^{-1}) from the first to layer 22 cm.

In Fig. 1c the vertical profile of ^{40}K activity concentrations is plotted versus depth. As in the case of the others radionuclides, the vertical profile of ^{40}K shows a change in the trend in layer 22 cm. The differences between zones are even more marked in the case of ^{40}K. The activity concentrations range between 406.4-934.2 Bq kg^{-1} (average: 819.6 Bq kg^{-1}) in the whole sediment core although the lowest values were recorded from the sediment surface to the layer 22 cm (406.4-733.3 Bq kg^{-1}, average: 570.8 Bq kg^{-1}). This decrease may be related to the increasing pressure of AMD on the watershed of the Meca River and the Sancho Reservoir. Cánovas et al. (2016) reported increasing concentrations of AMD-related elements (e.g. Fe, S, Zn) in the first 20 cm of the Sancho sediments as a consequence of intense Fe and Al oxyhydroxisulfate precipitation. In addition, the higher transport of Fe and Al precipitates from the watershed, especially during high flood events, may have decreased the proportion of terrigenous material in the Sancho sediments, evidenced by the lower values of K and Mg observed by Cánovas et al. (2016).

The vertical profile of ^{137}Cs in sediment core is plotted in Fig. 1d. In the case of ^{137}Cs, since this radionuclide has an anthropogenic origin and is unhomogeneously distributed in the environment, the trend observed is not as clear as it was in the others radionuclides. Once it is introduced in the environment, ^{137}Cs behaves almost identically as ^{40}K. Close environmental behavior of ^{137}Cs and

^{40}K is expected since these two elements are chemical homologues (Avery, 1996). A positive correlation (R= 0.77) has been found between ^{137}Cs and ^{40}K in layers shallower than 40 cm. This depth was selected in order to avoid the layers of the sediment core that could be affected by the fallout corresponding to the years of maximum concentrations in the atmosphere. As can be seen from Fig. 1d, the vertical profile of ^{137}Cs shows a narrow peak which can be associated to the year of maximum concentration of this radionuclide in the atmosphere (1963). Taking into account that the peak appears in the layer 64.5-66.5 cm, an average sedimentation rate can be obtained by dividing the depth of the layer with maximum concentrations of ^{137}Cs and the time elapsed between 1963 (the year of maximum concentrations of ^{137}Cs in the atmosphere) and the year of collection of sediment core (2011 in this case). Therefore, an average sedimentation rate ranging between 1.34-1.39 *cm y^{-1}* can be estimated between 1963 and the year the sediment core was collected (2011).

Although ^{137}Cs is highly soluble and mobile (Avery, 1996), behaving as a conservative element, and thorium is mostly immobile and firmly bound to the particulate matter in the environment (Zhang et al., 2004), behaving as a non conservative element, their similar behavior is expected in the water bodies with high particulate fluxes (e.g. coastal waters, lakes, rivers). In such waters enriched in particulate matter, ^{137}Cs is easily scavenged from the water body in the same way as the thorium does. In this sediment core, ^{40}K and ^{228}Th show a similar behavior (linear correlation coefficient, R= 0.89) as can be inferred from their depth profiles. The similar pattern of the activity concentrations of these two radionuclides could suggest the increase of the terrigeneous silicate material input into the reservoir.

In Fig. 2a, the vertical profiles of ^{226}Ra/^{228}Ra and ^{137}Cs/^{40}K activity ratios are displayed. As can be observed from this figure the pattern of ^{137}Cs/^{40}K activity ratio is nearly identical to that of ^{137}Cs.
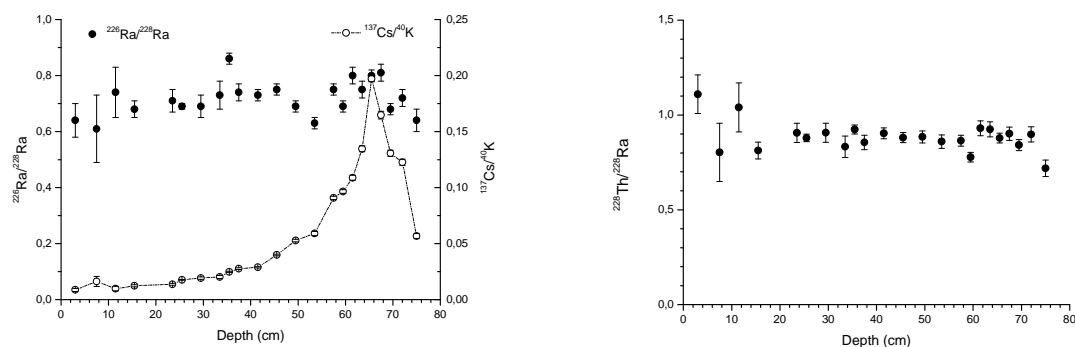
a) ^{226}Ra/^{228}Ra and ^{137}Cs/^{40}K   *b)^{228}Th/^{228}Ra*
Figure 2.- *Activity ratios of in Sancho Reservoir sediment core.*

^{226}Ra/^{228}Ra activity ratio ranges between 0.6-0.9 with average 0.7 in the whole sediment core and 0.6-0.7 (average: 0.7) from the first to layer 22 cm. There is no significant change between the zones of the sediment core. This is an indicative that the processes affecting the sediment core are influencing both Ra isotopes in the same way. Lower value of ^{226}Ra/^{228}Ra in the sediments is due to the relatively greater solubility and mobility of ^{238}U compared to ^{232}Th and as a consequence ^{232}Th activity concentrations are generally higher than ^{238}U in sediments. The enrichment of ^{228}Ra in estuarine and near-shore environments is often much greater than ^{226}Ra. This fact is due to a higher regeneration of ^{228}Ra from their insoluble thorium parents in bottom sediments. Although chemical behavior of ^{226}Ra and ^{228}Ra is virtually identical, the high solubility of ^{238}U, particularly in acids environments, make ^{226}Ra to be less concentrated in sediments. In contrast, ^{228}Ra shows high

binding capacity with sediment due to progeny of thorium, which is a particularly insoluble in natural waters and usually found associated with solid matter.

^{137}Cs/^{40}K activity ratio ranges between 0.009-0.197 in the whole sediment core and 0.009-0.016 from the first to layer 22 cm. The higher values of ^{137}Cs/^{40}K in the sediment core correspond to the layers more affected for the fallout in the years of maximum concentrations of ^{137}Cs in the atmosphere. The low activity ratio for ^{137}Cs/^{40}K observed indicates the presence of very high content of ^{40}K in sediment which is generally derived from the primary minerals.

In Fig. 2b, the vertical profile of ^{228}Th/^{228}Ra activity ratio is displayed. ^{228}Th/^{228}Ra activity ratio has been used for dating barite crystals (Noguchi et al., 2011) and it has been proposed for estimating plants ages (Chao et al., 2007). The problem with sediment dating with this activity ratio is the presence of parent nuclide ^{232}Th in sediments which is producing ^{228}Ra. In this sediment core ^{228}Th/^{228}Ra activity ratio range between 0.72-1.11 (Average: 0.89;S.D: 0,08).

Inventories and fluxes of radionuclides to the sediment

The inventories were calculated from the measured ^{226}Ra, ^{228}Ra, ^{40}K and ^{137}Cs activities and by extrapolation for those layers that were not measured by taking the average activities of the layers above and below the considered one.

The inventory of a radionuclide in a layer with mass depth (g cm^{-2}) comprised between m and $m + dm$ (this layer was formed between t and $t + dt$) is given by:

$$dA = C(m)dm = \phi e^{-\lambda t}dt$$

Where $C(m)$ is the activity concentration of the radionuclide in the layer (Bq kg^{-1}), ϕ is the flux of the radionuclide to the sediment (Bq m^{-2} yr^{-1}), λ is the radionuclide radioactive constant and dt is the time interval taken for the sediment layer to be formed. The inventory of the radionuclide from the surface to a given layer can be obtained by integration of the former equation:

$$A(m) = \int_0^m C(m)dm = \int_0^t \phi e^{-\lambda t}dt$$

Actually, sediment cores comprise a number finite of layers. This way, the inventory of a radionuclide in a given layer (i) can be obtained through the expression $\rho_i C_i \Delta z_i$ where ρ_i, C_i and Δz_i are the bulk density (g cm^{-3}), radionuclide activity concentration (Bq kg^{-1}) and the thickness (cm) of layer i respectively. Thus, the inventory from the surface to the layer n of the sediment core can be obtained as the sum of $\rho_i C_i \Delta z_i$ from the surface to the layer n. The whole inventory in the sediment core is obtained by extending the sum to the last layer of the sediment core, or the last layer the radionuclide can be detected in.

The average flux of radionuclides to the sediment in a time interval (τ) can be estimated through the expression:

$$\phi = \frac{A_\tau}{\int_0^\tau e^{-\lambda t}dt} = \frac{\lambda A_\tau}{(1 - e^{-\lambda \tau})}$$

Where A_τ is the inventory of the radionuclide from the surface of the sediment core to the layer formed τ years ago. The year of formation of each layer was estimated based on ^{137}Cs sedimentation rate.

In Table 1, the inventories (Bq m^{-2}) and fluxes (Bq m^{-2} yr^{-1}) of ^{226}Ra, ^{228}Ra, ^{40}K and ^{137}Cs in the sediment core are shown.

		^{226}Ra	^{228}Ra	^{40}K	^{137}Cs
Inventories	*z < 22 cm*	1417 ± 18	660 ± 60	33580 ± 181	317 ± 9
(Bq m^{-2})	*Whole core*	14977 ± 66	5150 ± 550	338349 ± 699	8472 ± 33
Fluxes	*z < 22 cm*	91 ± 1	94 ± 9	2140 ± 12	24 ± 1
(Bq m^{-2} yr^{-1})	*z > 22cm*	353 ± 2	3620 ± 450	7804 ± 18	453 ± 2

Table 1.- Inventories (Bq m^{-2}) and fluxes (Bq m^{-2} yr^{-1}) of radionuclides in the sediment core.

As it was previously shown, in this sediment core a change of the trend of the vertical profiles of activity concentration can be inferred at depth about 22 cm. The average fluxes of radionuclides in the different zones of the sediment core (from the surface to 22 cm depth and from 22 cm depth to the bottom of the sediment core) have been estimated. These fluxes are listed in Table 1.

As can be seen from this Table, the average fluxes of ^{226}Ra, ^{228}Ra, ^{40}K and ^{137}Cs suffer a clear decrease in the zone corresponding to the firsts 22 cm of the sediment core. If ϕ_1 is the flux from the surface to layer 22 cm and ϕ_2 is the flux from the layer 22 cm to the bottom of the sediment core, the ratio ϕ_2/ϕ_1 is 3.9; 38.5; 3.6 and 18.8 for ^{226}Ra, ^{228}Ra, ^{40}K and ^{137}Cs respectively. For ^{226}Ra and ^{40}K this ratio is similar which could mean that the processes affecting the sediment core are influencing both radionuclides in the same way.

It is worth noting that due to its short half-life (5.75 y), is probable that a significant fraction of the inventory of ^{228}Ra has been generated in situ. Therefore, a rough estimation of the ^{228}Ra derived from ^{232}Th decay in the sediment has been done. ^{232}Th was determined in several layers of another sediment core from Sancho Reservoir by alpha particle spectrometry (no reference to the method nor activities have been done because the results of ^{232}Th are not discussed here). ^{232}Th activity concentrations range between 35.9-55.7 Bq kg^{-1} (average 42 ± 5 Bq kg^{-1}). The ^{228}Ra derived from ^{232}Th decay is given by the expression:

$$a_{232}(0)(1 - e^{-\lambda t})$$

Where $a_{232}(0)$ is the ^{232}Th activity concentration (assumed to be the average 42 ± 5 Bq kg^{-1}), λ is the ^{228}Ra radioactive decay constant (0.121 yr^{-1}) and t is the age of the layer considered based on ^{137}Cs dating. By subtracting the ^{228}Ra derived from ^{232}Th to the ^{228}Ra determined in each layer, the inventory of ^{228}Ra has been determined and the results given in Table 1. As can be seen from this Table, the ^{228}Ra and ^{226}Ra flux for the first zone of the sediment core are in agreement.

According to thorium radioactive series, ^{232}Th and ^{228}Ra would be in equilibrium in environmental samples older than 30 years. This is not the case of the former layers of a sediment core. This fact should be taken into account when determining ^{232}Th through gamma spectrometry based on the gamma lines of one of its descendant.

Resume and Conclusions

In this work, the vertical profiles of activity concentrations of ^{226}Ra, ^{228}Ra, ^{228}Th, ^{40}K and ^{137}Cs have been analyzed in a sediment core collected from the Sancho Reservoir (SW Spain), which is affected by Acid Mine Drainage. The trend of the vertical profiles of these radionuclides shows a significant change in the

very same layer for all the radionuclides studied excepting for ^{137}Cs, something expected due to the artificial origin of this radionuclide.

The inventories and fluxes of these radionuclides to the sediment core have been estimated. They show an important change in the layer 20-22 cm. The flux from the layer 22 cm to the bottom of the sediment core with respect to the flux for the first 22 cm of the sediment core range between 3.9 times for [226]Ra to 40 times for [228]Ra.

References

Appleby, P.G., Piliposian, G.T., 2004. Efficiency corrections for variable sample height in well-type germanium gamma detectors. Nucl. Instr. Meth. Phys. Res. B 225, 423–433. doi:10.1016/j.nimb.2004.05.020

Avery, S.V., 1996. Fate of caesium in the environment: distribution between the abiotic and biotic components of aquatic and terrestrial ecosystems. J Environ. Radioactivity 30(2),139–171. doi: 10.1016/0265-931X(96)89276-9

Cánovas, C.R., Olías, M., Macias, F., Torres, E, San Miguel, E.G., Galván, L., Ayora, C., Nieto, J.M., 2016. Water acidification trends in a reservoir of the Iberian Pyrite Belt (SW Spain). Science of the Total Environment 541, 400–411. doi:10.1016/j.scitotenv.2015.09.070

Galván, L., Olías, M., Fernandez de Villarán, R., Domingo Santos, J.M., Nieto, J.M., Sarmiento, A.M., Cánovas, C.R., 2009. Application of the SWAT model to an AMD affected river (Meca River, SW Spain). Estimation of transported pollutant load. J. Hydrol. 377, 445–454. http://dx.doi.org/10.1016/j.jhydrol.2009.09.002.

Gulin, S.B., Gulina, L.V., Sidorov, I.G., Proskurnin, V.Yu., Duka, M.S., Moseichenko, I.N., Rodina, E.A., 2014. [40]K in the Black Sea: a proxy to estimate biogenic sedimentation. J. Environ. Radioact. 134, 21-26. http://dx.doi.org/10.1016/j.jenvrad.2014.02.011

Chao, J.H., Niu, H., Chiu, C.Y., Lin, C., 2007. A potential dating technique using [228]Th/[228]Ra ratio for tracing the chronosequence of elemental concentrations in plants. Appl. Rad. Isot. 65, 641–648. doi:10.1016/j.apradiso.2007.01.001

Hierro, A., Olías, M., Cánovas, C.R., Martín, J.E., Bolivar, J.P., 2014. Trace metal partitioning over a tidal cycle in an estuary affected by acid mine drainage (Tinto estuary, SW Spain). Sci. Total Environ. 497–498, 18–28. http://dx.doi.org/10.1016/j.scitotenv. 2014.07.070.

Martin Sanchez, A., Rubio Montero, M.P., Gomez Escobar, V., Jurado Vargas, M., 1999. Radioactivity in bottled mineral waters. Appl. Radiat. Isot. 50, 1049-1055. http://dx.doi.org/10.1016/S0969-8043(98)00126-2

Más, J.L., San Miguel, E.G., Bolívar, J.P., Vaca, F., Pérez-Moreno, J.P., 2006. An assay on the effect of preliminary restoration tasks applied to a large TENORM wastes disposal in the south-west of Spain. Sci. Tot. Environ. 364, 55-66. doi:10.1016/j.scitotenv.2005.11.006

Noguchi, T., Shinjo, R., Ito, M., Takada, J., Oomori, T., 2011. Barite geochemistry from hydrothermal chimneys of the Okinawa Trough: insight into chimney formation and fluid/sediment interaction. J. Mineral. Petrol. Sci. 106, 26–35. doi:10.2465/jmps.090825

Sarmiento, A.M., Olías, M., Nieto, J.M., Cánovas, C.R., Delgado, J., 2009b. Natural attenuation processes in two water reservoirs receiving acid mine drainage. Sci. Total Environ. 407, 2051–2062. http://dx.doi.org/10.1016/j.scitotenv.2008.11.011.

Zhang, L., Chen, M., Yang, W., Xing, N., Li, Y., Qiu, Y., Huang, Y., 2004. Size-fractionated thorium isotopes (228Th, 230Th, 232Th) in surface waters in the Jiulong River estuary China. J. Environ. Radioact. 78(2),199–216. doi:10.1016/j.jenvrad.2004.05.004

Distribution coefficients water sediment for uranium and polonium in the Moulouya River (eastern Morocco), a river affected by abandoned mines of lead and zinc

J. Galván[1], I. Díaz[1], G. Manjón[1], J. Mantero[1], I. Vioque[1], S. Chakiri[3], R. García-Tenorio[1,2]*

[1]Applied Nuclear Physics Group. University of Seville, Spain
[2] Centro Nacional de Aceleradores (CNA), Sevilla, Spain
[3]Université Ibn Tafail, Faculté des Sciences, B.P. 133, 14000 Kénitra, Morocco

Abstract.

The Upper Moulouya Lead district is a region of Morocco affected by the presence of mining deposits, pit lakes and other mining wastes, due to the former mining activities developed in the 20th century. The Middle Moulouya is a region not affected by human activities and is studied for a better comprehension of results obtained in the Upper Moulouya region.

Activity concentration of U-isotopes and [210]Po in water and sediments was determined in samples collected from the Moulouya River (Eastern Morocco) and two tributaries. These results were used for the evaluation of distribution coefficient in the river.

Some pit lakes resulting of former mining activities were also sampled and distribution coefficients were calculated for the mentioned radioisotopes. Sampling was made twice in different years. In the second sampling campaign a longer river area was studied.

Introduction

Determination of distribution coefficients for Uranium and Polonium (between water and sediment phases) is the main objective of this work. Natural radionuclides ([238]U, [234]U and [210]Po) were measured in water and sediment samples collected along the Moulouya River (Oued Moulouya) and in three pit lakes at abandoned mines of Zn and Pb located in the Upper Moulouya Mining District (Eastern Morocco). Mining activities generated waste material that can affect to natural conditions of this environment.

The Upper Moulouya Lead district is crossed by the Moulouya River (Oued Moulouya), which is the most important river in Morocco. The region is characterized by a low population density. The geological and geographical description of the area is presented in Ivazzo et al., 2012. In the Upper Moulouya Lead district there are three main Lead deposits: Zeida, Mibladen and Aouli (Figure 1) that were exploited from 1972 to 1985, 1936 to 1985 and 1926 to 1985 (Ivazzo et al, 2012). Mining activities have created abandoned mine sites comprising: waste deposits, pit lakes, processing plants and waste tailings. Erosion and transport of mining materials are experienced in this region and they could reach the Moulouya River and its tributaries where heavy metals and natural radionuclides could be increased.

Materials and Methods

Sampling

Two sampling campaigns (July 2007 and June 2010) were carried out. Water was directly collected from the Moulouya River, some tributaries and three pit lakes. These waters were transferred into 25 l plastic bottles and a few ml of HNO_3 were added to avoid adsorption by plastic walls. Sediment

samples were directly collected in the same points than waters were sampled and stored in plastic bags.
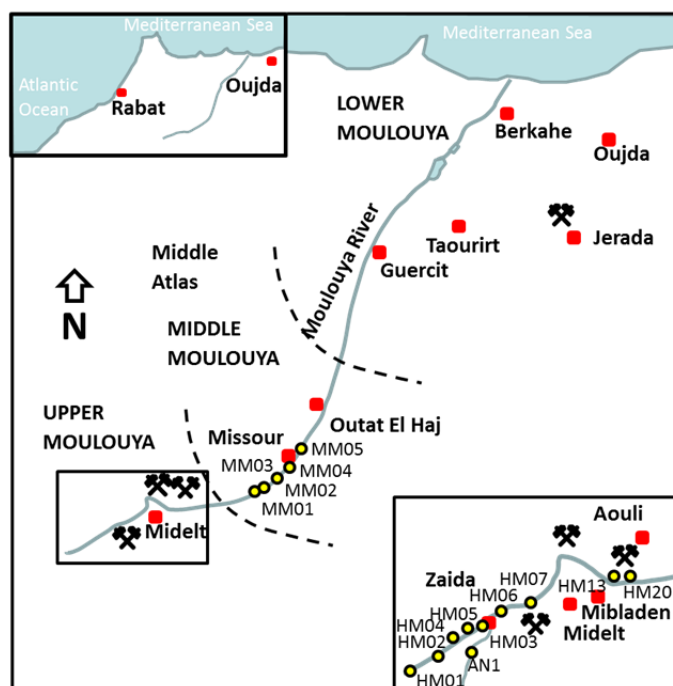
Figure 1. *Map of Morocco where Moulouya River and sampling area are remarked*

The sampling stations are shown in Figure 1. The sampling stations from the Upper Moulouya Lead District were the same in the two sampling campaigns, while the Middle Moulouya samples were collected only in the 2010 campaign.

The pH, of the water samples, shows slight alkalinity due to the presence of carbonates (Makhoukh, 2011). Higher pH values (around pH=9) were measured in pit lakes where the mineral is carbonated (Makhoukh, 2011; Ivazzo et al., 2012). The dominant mineral is Cerussite (Lead carbonate).

Analytical methods

The objective of the analytical method is to obtain both radioactive sources of U-isotopes and radioactive sources of ^{210}Po, which can be measured by alpha-spectrometry using an Alpha Analyst equipment based on PIPS semiconductor detectors. Although it is possible to obtain also radioactive sources of Th-isotopes, which is commented below, these results are not considered in this paper.

Concentration of actinides and polonium in water samples

An aliquot of 1 l of water, previously acidified, is taken for analysis. A well-known activity of ^{232}U, ^{229}Th and ^{209}Po is added for determination of radiochemical yield, and the actinides and polonium are co-precipitated with $Fe(OH)_3$ (Holm and Fukai, 1977). Precipitate is separated from aqueous solution by centrifugation, then dried and dissolved with 10 ml of 8M HNO_3.

Concentration of actinides and polonium in sediment samples

After collection, sediments are dried, powdered and sieved. If the polonium is not going to be measured the organic matter is eliminated by calcination of about one gram of sediment at 600 °C for 24 hours. The sieved soils or the resulting ashes are then traced with a well-known activity of ^{232}U, ^{229}Th and ^{209}Po and dissolved with acid (Lee and Lee, 2001). The dissolution is performed using first aqua regia with H_2O_2 and afterwards nitric acid 60 %, being the obtained solution conditioned in 8M HNO_3. From this solution, actinides are co-precipitated with Fe^{3+}, and the precipitate is separated from solution by centrifugation, dried and finally dissolved in 10 ml of 8M HNO_3.

Isolation of uranium, thorium and polonium

Two alternative methods have been used in this work for the sequential isolation of the Uranium-isotopes, the Thorium-isotopes, and ^{210}Po which are based either in the performance of solvent extractions with Tributyl-n-phosphate (TBP) or in the use of UTEVA (Uranium und TEtraValents Actinides, Eichrom trade mark) chromatographic resins.

The radiochemical procedure based in the use of TBP as solvent extract are described in Lehritani et al., 2012, and follows the original work performed by Holm and Fukai, 1977. The application of this procedure results in three aqueous solutions containing, respectively, the isolated Uranium, Thorium and Polonium. The purification of the isolated Thorium aliquot uses anion exchange resin (AG1×8, 100 – 200 mesh, Cl⁻ form) as described in Lehritani et al., 2012.

The radiochemical procedure based in the use of UTEVA chromatographic resins from Eichrom is described in Casacuberta et al., 2012, giving three aqueous solutions containing in isolated form the Uranium-isotopes, the Thorium-isotopes and the Po-210. In this procedure, no additional purification of any of the fractions is required.

Uranium source preparation for alpha-particle spectrometry

The Uranium sources for alpha-particle spectrometric measurements were prepared by electrodeposition of the elements onto stainless steel planchets following the method of Hallstadius (1984). The aqueous solutions containing the Uranium after application of the selected radiochemical procedure are evaporated until near dryness and conditioned as described in Mantero, 2010 then followed by electrodeposition.

The electrodeposition arrangement depends on the radionuclide of interest (Lehritani et al., 2012), using the electrical intensity 1.2 A in the case of Uranium.

Self-deposition of ^{210}Po

A well-established method (Flynn, 1968) based on the self-deposition of Polonium on several metal discs (Silver or Copper) is used for obtaining radioactive sources of ^{210}Po from the aqueous solutions containing this radionuclide. The adaptation of the Flynn method to our laboratory conditions is described in detail in Díaz-Francés et al., 2013.

Alpha-particle spectrometric measurements

Uranium-isotopes (^{238}U, ^{235}U, ^{234}U) and ^{210}Po activity determinations have been performed by applying the alpha-particle spectrometric technique using an Alpha-Analyst, spectrometer manufactured by Canberra Co. The system comprises eight independent chambers, each chamber being equipped with a 450 mm^2 PIPS detector, model A450-18AM. Only two chambers were used for ^{210}Po measurements, other two chambers for Thorium-isotopes measurements and the remaining four chambers have been used for Uranium-isotopes determinations. Activity determinations have been performed by applying the well-known isotope-dilution technique.

Results and Discussion

Activity concentration of U-isotopes

Activity concentrations of ^{238}U in water samples collected in 2007 and 2010 are presented in Figure 2. Higher activity concentrations correspond to pit lakes (HM04) or Moulouya water samples probably affected by mining wastes (HM06 and HM13). In the case of results of 2010, a different range of activity concentration is observed in the mining area (High Moulouya) and the rest of the river (Middle Moulouya). This fact can be also related to an enhancement due to mining wastes.
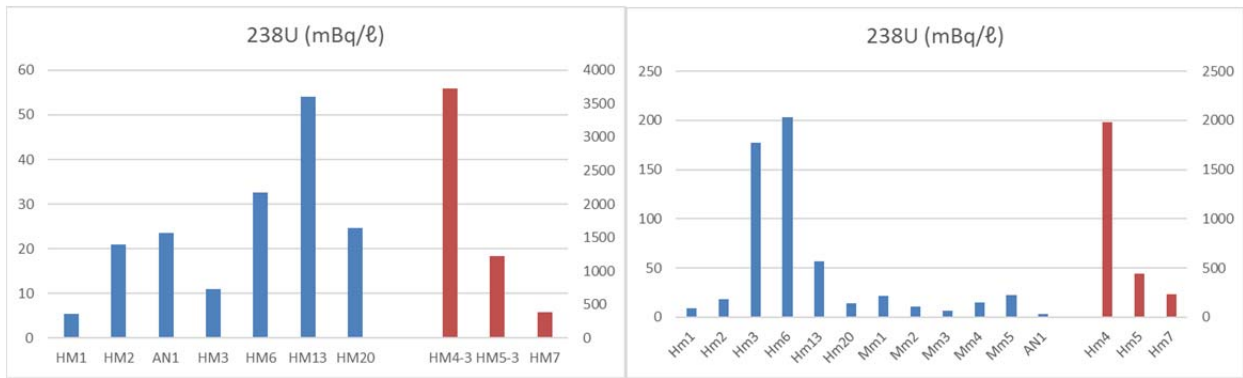
Figure 2. Activity concentration in river water (blue) and small lake water (red) samples collected in 2007 (left) and 2010 (right).

Figure 3 shows the $^{234}U/^{238}U$ activity ratio in water samples collected in 2010. A typical activity ratio around 2 can be inferred in water samples collected along the river. However, the activity ratio reaches more than 4 in water samples collected in the pit lakes.
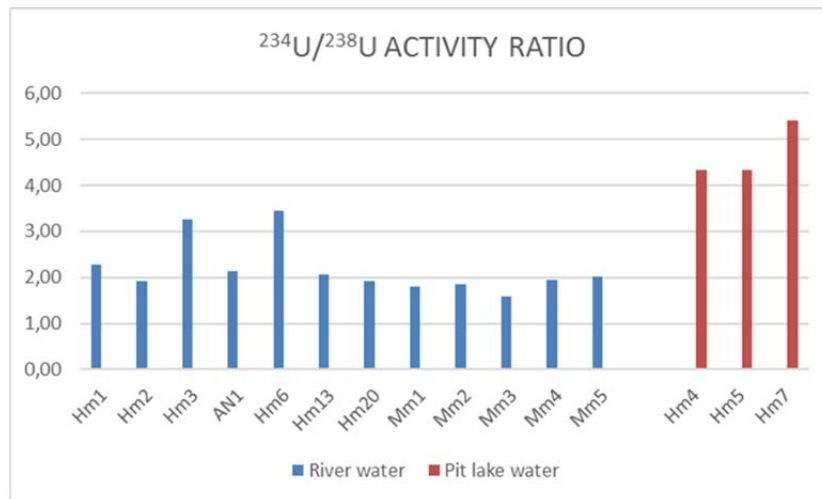
Figure 3. A ctivity ratio ($^{234}U/ ^{238}U$) in samples of water collected in 2010 in different sites along the Moulouya River (blue) and artificial lakes (red) caused by former air opened mines.

Sediment water distribution coefficient

The determinations performed at the same sampling point in both waters and sediments enable a discussion on the mobility of Uranium in the water – sediment system (Winde, 2002) using the distribution coefficients (K_d), defined as the quotient of ^{238}U activity concentration in sediment (mBq/kg) and water (mBq/l). Distribution coefficients of Uranium are compared with distribution coefficient of Polonium.

The values of distribution coefficients for Uranium and Polonium, in the samples collected in 2010 are shown in Figures 4 and 5. The following comments are made:

    a) as expected the K_d obtained for Po-210 are clearly higher than the K_d of Uranium due to the known tendency of the Po to bind to particulate matter in opposition to the more conservative behavior of Uranium,

    b) A good correlation is found between the $K_d(U)$ and the Uranium concentrations determined in the waters, as it is shown in Figure 4. K_d decreases when the Uranium concentrations in waters increase. The higher $K_d(U)$ values, in the order of 10^3, were determined in the sampling points less affected by the impact of the mining areas while values as low as 10^1

were determined in the pit lakes, indicating the tendency of the Uranium to be in dissolved form in environments rich in carbonates.

c) The K_d's of Po are less sensitive to the concentrations found for this radionuclide in the waters as can be observed in Figure 5.
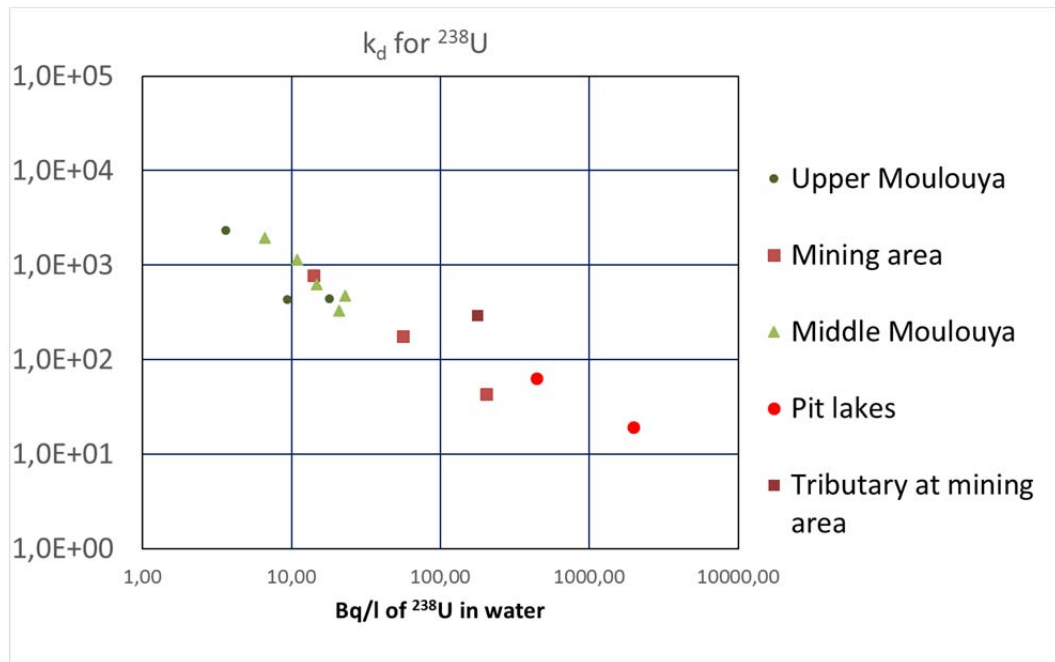
Figure 4. *Distribution coefficient kd for ^{238}U in samples collected along the Moulouya River and two pit lakes.*
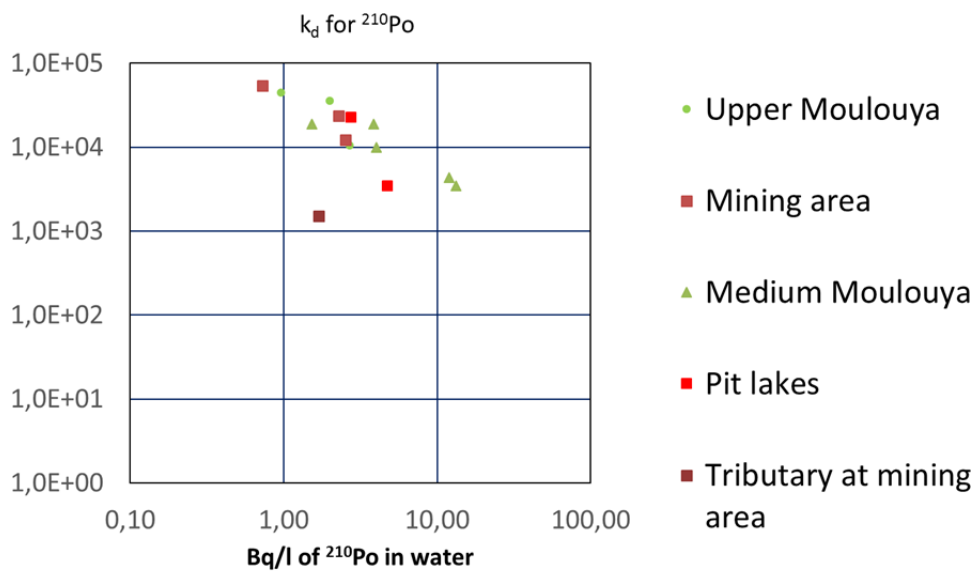
Figure 5. *Distribution coefficient kd for ^{210}Po in samples collected along the Moulouya River and two pit lakes.*

Conclusions

Environmental impact on Moulouya River, with origin in mining activities, has been observed through the determination of U-isotope levels in water and sediment samples.

Distribution coefficient, k_d, in Moulouya River and pit lakes has been calculated. In the case of ^{238}U, the distribution coefficient ranged from 10^1 to 10^3. This coefficient was between 10^3 and 10^5 for ^{210}Po.

References

N. Casacuberta, M. Lehritani, J. Mantero, P. Masqué, J. Garcia-Orellana, R. Garcia-Tenorio Determination of U and Th α-emitters in NORM samples through extraction chromatography by using new and recycled UTEVA resins. Applied Radiation and Isotopes, 70 (2012) 568-573.

I. Díaz-Francés, J. Mantero, G. Manjón, J. Díaz and R. García-Tenorio. ^{210}Po and ^{238}U isotope concentrations in commercial bottled mineral water samples in Spain and their dose contribution. Radiation Protection Dosimetry (2013) 1–7.

Flynn, W.W. The determination of low levels of polonium-210 in enviromental simples. Analytical Chemistry Acta 43 (1968) 221-227

Hallstadius, L., A method for the electrodeposition of actinides. Nuclear Instruments and Methods in Physics Research, 223 (1984) 266-267

Holm, E. and Fukai, R. Method for multi-element alpha-spectrometry of actinides and its application to environmental radioactivity studies. Talanta, 24 (1977) 659 – 664.

Iavazzo, P., Adamo, P., Boni, M., Hillier, S. and Zampella, M. Mineralogy and chemical forms of lead and zinc in abandoned mine wastes and soils: An example from Morocco. Journal of Geochemical Exploration 113 (2012) 56–67.

Lee, M. H. and Lee, C. W. Radiochemical analysis of uranium isotopes in soil and sediment samples with extraction chromatography. Talanta 54 (2001) 181 – 186.

Lehritani, M., Mantero, J., Casacuberta, N, Masqué, P. and García-Tenorio, R. (2012). Comparison of two Sequential Separation Methods for U and Th determination in environmental samples by alpha-particle spectrometry. Radiochimica 100 (2012) 431–438

Makhoukh, M., Sbaa, M., Berrahou, A. and Vanclooster, M. Contribution à l'étude de l'impact d'un site minier abandonné dans la haute Moulouya sur la qualité de l'Oued Moulouya, Maroc. Afrique Science 07(3) (2011) 33 – 48.

Mantero, J., Lehritani, M., Hurtado, S. and García-Tenorio, R. Radioanalytical determination of actinoids in refractory matrices by alkali fusion. Journal of Radioanalytical and Nuclear Chemistry 286 (2010) 557–563.

Winde, F. Stream pollution by adjacent deposits and fluvial transport of dissolved uranium – dynamics and mechanisms investigated in mining areas of Germany, South Africa and Australia. In the book: Uranium in the Aquatic Environment. Ed. Broder Merkel, Britta Planer-Friedrich, Christian Wolkersdorfe. Springer Science & Business Media, 2002 pp. 283 – 292.

Evidence of change in ^{210}Pb atmospheric flux in the Oualidia lagoon inferred from sediment radiometric dating

A. Laissaoui*[1], N. Mejjad[2], O. El Hammoumi[2], A. Benkdad[1], A. Fekri[2], M. Ghazi[1]

[1]*Centre National de l'Energie, des Sciences et Techniques Nucléaires–Rabat, Morocco*
[2]*Laboratoire de Géologie Appliquée, Géomatique et Environnement - Faculté des Sciences - Ben Msik, Casablanca, Morocco*

Abstract

Radiometric dating was carried out on sediment cores from the Oualidia Lagoon located in the north-western of Morocco. The objective of this study was to investigate recent environmental changes in this area, particularly the variation of ^{210}Pb atmospheric flux. Two sediment cores, Core-1 and Core-2, were collected from El Oualidia Lagoon lying in the Atlantic Ocean. Vertical distributions of radionuclides (^{226}Ra, ^{210}Pb and ^{137}Cs) were determined to carry out radiometric dating of sediment deposition in the studied sites within the Lagoon ecosystem. The profiles of excess ^{210}Pb showed an abrupt change in concentrations at specific depths along the cores, which reflected substantial variation in ^{210}Pb input to the sediment. A modified CRS (Constant Rate of Supply) was applied consisting of splitting the profile in two zones. As the CRS model requires the determination of the total inventory of ^{210}Pb, this ultimate was calculated as the sum of two inventories covering two superposed intervals. In this way, fluxes, accumulation rates and ages were obtained successfully. ^{137}Cs was used as independent tracer to validate the ^{210}Pb chronology using the modified CRS model. Core-1 displayed a peak of maximum concentration at a depth below 30 cm, in good agreement with the ages provided by the modified CRS Model.

Introduction

The Oualidia lagoon is a coastal aquatic environment located in the western Moroccan Atlantic Ocean coast. It is about a shallow inland body of seawater of about 7 Km length parallel to the coastline, separated from the ocean by a sand barrier. It is connected to the Atlantic Ocean by one permanent inlet of 150 m width and a small secondary inlet active in spring tides. The water in the lagoon is mainly seawater since it is about a lagoon without a river and the only freshwater inputs come from rainfall over the region, which constitute a small contribution during rainy seasons to the overall water budget in the Lagoon. Water currents are generally weak; the strongest currents during spring tides are about 1.25 m.s^{-1} registered near the entrance of the lagoon in the south, and decrease northward reaching values as low as 0.35 m.s^{-1}. On the other hand, currents during neap tides are extremely weak, not exceeding 0.2 m.s^{-1}. The bed channel exhibit a variety of sediment types with a predominance of sandy sediment in the centre of the main channel, while in most marginal areas sediments contain relatively high percentages of mud (silt/clay).

Coastal sediment has always been considered as a natural compartment in which records of environmental events are often stored. In this way, radiometric dating of sediment cores is a powerful tool in studies that require the age-depth relationships.

---

* Corresponding author, E-mail: laissaoui@cnesten.org.ma

The main objectives of this study is to assess the activity distribution of radionuclides (^{210}Pb, ^{137}Cs, ^{226}Ra, ^{228}Ra and ^{40}K) in two sediment cores collected from the Oualidia lagoon, and the use of excess ^{210}Pb profile to establish the relation age-depth in sediment, accumulation rates, inventory and rate of delivery.

Material and methods

Samples

Two sediment cores were collected at low tide from the right bank of the main channel of the Oualidia lagoon in May 2014 (Core-1: 52 cm, 32°45'12" N; 009°00'52" W and Core-2: 35 cm, 32°46'24'' N; 008°59'07" W) using PVC tubes of 10 cm internal diameter. The sampling locations (Figure 1) were selected on the basis of hydrodynamic conditions considerations (Hilmi et al., 2009); maximal tidal currents registered during neap tides are predominantly weak (<0.40 m/s), which may promote the settling of sediment particles.

Figure1. Map of study area showing the sampling locations.

The cores were sectioned into 2 cm slices immediately after retrieval to avoid particles redistribution, and then transported to the laboratory for pre-treatment and conditioning prior to radiometric analyses. Each one of the resulting sub-samples were dried in an oven at a constant temperature of 80°C during 24 h. Bulk densities were determined from weight and volume calculations.

Finally, dried sediment was gently ground in a mortar and homogenised for subsequent radionuclides determination. Organic matter content was calculated as the difference in weight between the dried sediment and the ash obtained following ignition at 550ºC for 24 h.

Radiometric technique

Gamma emitting radionuclides [^{228}Ac(^{228}Ra), ^{214}Bi(^{226}Ra), ^{210}Pb, ^{40}K and ^{137}Cs] were measured using gamma-ray spectrometer. The detector was a low background CANBERRA hyper-purity germanium p-type coaxial detector, surrounded by a cooper layer and housed in a 10-cm-thick high-purity lead shield. The detector is coupled through its associated electronic device to a PC running Maestro data acquisition software. The relative efficiency was 50% and the resolution was 1.9 keV for the 1332 keV ^{60}Co γ-peak. The range of energies is between 1 KeV and 10 MeV.

Weighed samples were introduced into 100 ml nalgene containers and sealed to trap the gaseous ^{222}Rn and ^{220}Rn emanating from *in-situ* ^{226}Ra and ^{224}Ra, respectively. The flasks were stored for more than 21 days and then counted for 24 hours each one. ^{226}Ra was obtained from ^{214}Bi photopeak at 609.3 keV. Energy and efficiency calibrations of the gamma spectrometer were carried out using a multigamma standard solution provided by Amersham in the same geometry as the samples. The activity concentration (in Bq.kg^{-1}) in each sample of all the studied radionuclides was determined from the net count rate under the photopeak of interest, detector efficiency, gamma intensity and sample weight.

Determination of ^{210}Pb activities involved a self-absorption correction factor. A disk source of ^{241}Am was measured on the empty sample vial, on the sample vial filled with tap water and finally on the sample vial filled with sediment. The corresponding attenuation factors obtained were used in the calculation of the self-absorption factor (Ramos-Lerate et al, 1998). The analytical procedure was checked using reference material (IAEA-327). Good agreement was found between measured and certified values, >90% in all cases.

Results and discussion

^{40}K and ^{228}Ra concentration profiles are shown in Figure 2. The values found for these naturally occurring radionuclides were of the same ranges of typical concentrations recorded in coastal environments (100 – 700 Bq.Kg^{-1} for ^{40}K and 10 – 50 Bq.Kg^{-1} for ^{228}Ra) UNSCEAR, 2000. Both radionuclides displayed quite similar vertical profiles along each core.

Sediment mineralogy variations throughout the core can be discussed using ^{40}K as proxy for clay content (Love et al., 2003). This radionuclide was not uniformly distributed over the sediment profiles (from 131 to 371 Bq.Kg^{-1} for Core-1 and from 130 to 380 for Core-2), but rather a visible minimum was registered at 38 cm depth in the Core-1 suggesting that there were substantial changes in sediment composition deposited throughout the years. This is in good agreement with results of granulometric analyses shown in Figure 3. A strong correlation was found between clay content and ^{40}K activities for both cores. Mud content in Core-1 presented an important decrease from 16 to 38 cm, accompanied by an increase in organic matter content, followed by a sudden increase reaching more than 90% of mud in the bulk sediment.
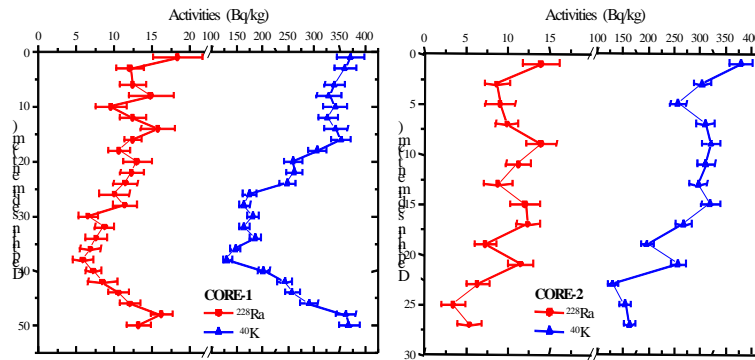
Figure 2. *Vertical distributions of ^{228}Ra and ^{40}K activities throughout the two cores collected from the Oualidia Lagoon.*
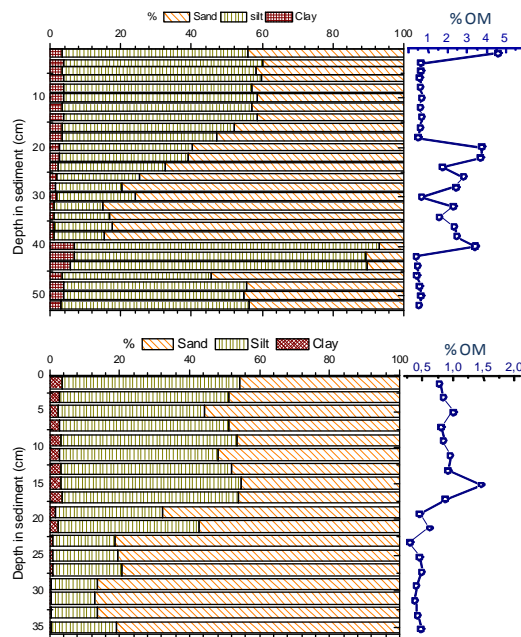
Figure 3. *Granulometric and organic matter distributions throughout the sediment cores.*

The total ^{210}Pb and ^{226}Ra activities throughout the two cores were determined (Figure 4) with the aim to carry out radiometric dating. ^{226}Ra concentrations were relatively uniform along the cores and the activities were in the range of those found in non-contaminated sediments (UNSCEAR, 2000), indicating that no ^{226}Ra enhancement has occurred during the period covered by the cores. On the other hand, ^{210}Pb concentrations decrease with depth to ^{226}Ra levels downcore.

Both ^{210}Pb profiles of Figure 4 showed a break at a certain depth in the sediment (24 cm for Core-1 and 4 cm for Core-2) indicating a substantial change in the flux of ^{210}Pb to the sediment starting from a specific period in time. Such increase has resulted in enhancing ^{210}Pb concentration in the sediment and, at the same time, altering the normal exponential decay throughout the cores. ^{210}Pb and ^{226}Ra were intended to be used for determining the age-depth relationship in the sediment cores by applying conventional dating models. Excess ^{210}Pb was determined by subtracting the supported ^{210}Pb, assumed to be in secular equilibrium with ^{226}Ra, from total measured ^{210}Pb at layer-by-layer basis. Nevertheless, in light of the limitation exposed above regarding the change detected in ^{210}Pb

flux, the most widely used dating model (CRS: Constant Rate of Supply) could not be applied due to the inconsistency of the model assumption of constant ^{210}Pb flux to the sediment. Alternatively, a modified CRS model taking into account the alteration of the ^{210}Pb flux has been developed and applied. As this model requires the determination of the total inventory of ^{210}Pb, this ultimate was calculated as the sum of two inventories covering two superposed intervals; the first one (Σ_1) includes the depth interval from the sediment-water interface until the breaking depth, and the second (Σ_2) covers the rest of the profile until the depth where no excess ^{210}Pb is detected.
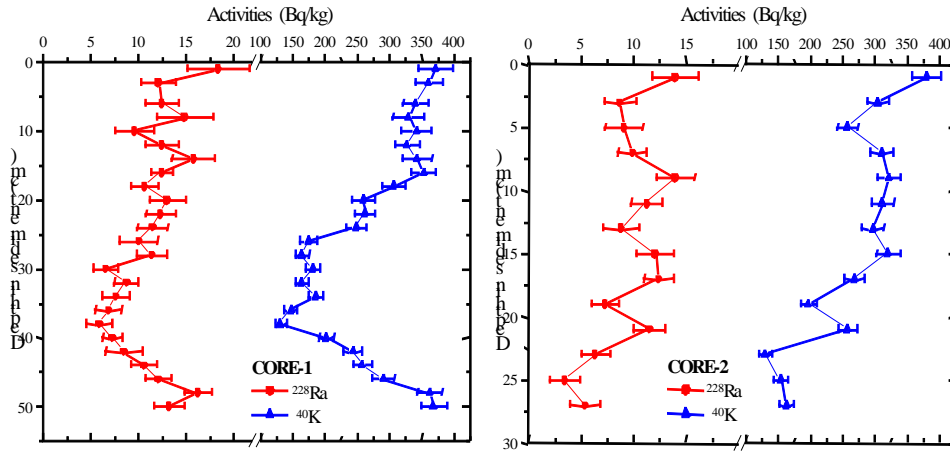
Figure 4. *Total ^{210}Pb and ^{226}Ra versus depth profiles in the two cores collected from El Oualidia Lagoon.*

The computed inventories and fluxes are given in Table 1. As a first result, the total inventory of Core-1 is higher by one order of magnitude than that of Core-2 due to the different hydrodynamic conditions prevailing in each sampling zone producing distinct sediment accumulation rates. Indeed, Core-2 was collected from the upper part of the Lagoon characterized by relatively low sediment accumulation rates (0.1 g.cm^{-2}.y^{-1} compared to 0.5 g.cm^{-2}.y^{-1} determined in Core-1). Partial inventories of ^{210}Pb and their corresponding fluxes presented different behaviour in each core; the inventory and flux calculated in the upper part of Core-1 (Σ_1 and F_1) were more than four-fold higher than those in the lower part (Σ_2 and F_2), attributed to the significant increase of the ^{210}Pb atmospheric flux. On the contrary, inventories in both parts of Core-2 were more or less similar and the flux in the upper part is larger by nearly two-fold than that in the lower part.

	Core-1	Core-2
Σ_{tot} **(Bq/m^2)**	$(11.7\pm1.4)\cdot10^4$	$(3.36\pm0.67)\cdot10^3$
Σ_1 **(Bq/m^2)**	$(9.6\pm0.14)\cdot10^4$	$(14.30\pm0.56)\cdot10^3$
Σ_2 **(Bq/m^2)**	$(2.20\pm0.04)\cdot10^4$	$(19.34\pm0.40)\cdot10^3$
Flux F$_1$	5115 ± 42	763 ± 30
Flux F$_2$	1628 ± 11	1432 ± 38
Mean Accum. Rate (g/(cm^2.y)	0.573 ± 0.082	0.109 ± 0.024

Table 1- *Calculated inventories and fluxes of ^{210}Pb to the sediment and mean accumulation rates for the two cores.*

The age of formation of each layer at depth z has been calculated and the obtained chronology is plotted in Figure 5 along with ^{137}Cs activities versus depth in the sediment for both cores. [137]Cs activities were of the same range of those measured in sediments collected from other coastal environments in Morocco (Laissaoui et al., 2013).
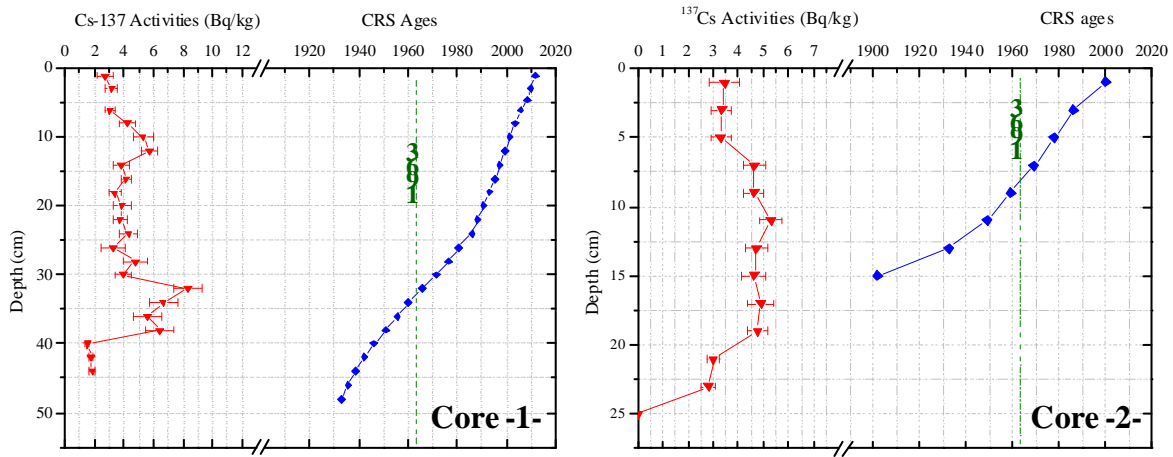
Figure 5. *[137]Cs profiles measured in both cores along with the ages provided by the modified CRS model.*

Regarding Core-1, a peak of maximum concentration is located at a depth of 33 cm with a broadening effect attributed to downward vertical migration. This result is in close agreement with the ages provided by the modified CRS model. The presence of ^{137}Cs in deep layers corresponding to the period before the beginning of nuclear atmospheric tests is attributable to post-depositional downward diffusion in sedimentary layers. This phenomenon has been previously reported in the scientific literature (Oughton et al. 1997; Foster et al. 2006). On the other hand, ^{137}Cs in Core-2 did not show any peak of maximal activity due to the relatively low accumulation rate (0.11 g.cm^{-2}.y^{-1}). It was therefore impossible to identify the depth of maximum ^{137}Cs fallout, which should be located at 8-10 cm below the sediment-water interface according to ^{210}Pb chronology. It should be noted that even in the presence of diffusion, the depth of ^{137}Cs peak would be preserved, but the peak would broaden significantly in the down direction when low accumulation rates prevail, which is the case of Core-2. In addition, and due to the poor core resolution (2-cm), the activity in the 8-10 cm layer is therefore the average value of activities of a number of thin layers formed during a period of about 8 years according to CRS model.

Conclusion

The levels of [228]Ra, [226]Ra, [40]K and ^{137}Cs concentrations in sediment cores collected from the El Oualidia Lagoon were all found similar to those of non contaminated sediments. The only exception is ^{210}Pb which exhibited specific activities relatively higher in the upper layers indicating a substantial change in the flux of ^{210}Pb to the sediment.

The application of the CRS dating model could not be possible without dividing the cores into two regions. In this way, radiometric dating of the sediment cores from the El Oualidia Lagoon has provided evidence that the atmospheric concentration of ^{210}Pb in El Oualidia surroundings has changed considerably in the last years.

References

Foster, I.D.L., Mighall, T.M., Proffitt, H., Walling D.E., Owens. P.N., 2006. Post-depositional 137Cs mobility in the sediments of three shallow coastal lagoons, SW England. J. Paleolimnol. 35, 881–895.

Hilmi, K., Koutitonsky, V.G., Orbi, A., Lakhdar Idrissi, J., Chagdali, M., 2005. Oualidia lagoon, Morocco: an estuary without a river. Afr. J. Aquat. Sci. 30, 1-10.

Laissaoui, A., Mas, J.L., Hurtado, S., Ziad, N., Villa, M., Benmansour, M., 2013. Radionuclide activities and metal concentrations in sediments of the Sebou Estuary, NW Morocco, following a flooding event. Environ. Monit. Assess. 185, 5019-5029.

Love, A., Esser, B., Hunt, J., 2003. Reconstructing contaminant deposition in a San Francisco Bay Marina, California. *J. Environ. Eng.* 129, 659-666.

Oughton, D.H., Børretzen. P., Salbu, B., Tronstad, E., 1997. Mobilisation of ^{137}Cs and ^{90}Sr from sediments: potential sources to arctic waters. Sci. Total Environ. 202: 155-165

Ramos-Lerate, I., Barrera, M., Ligero, R.A., Casas-Ruiz, M., 1998. A New Method for Gamma-efficiency Calibration of Voluminal Samples in Cylindrical Geometry. J. Environ. Radioactivity, 38. 47-57.

United Nations Scientific Committee on Effects of Atomic Radiation (2000) Exposures from Natural Radiation Sources, UNSCEAR Report, New York.

[234]Th as a proxy for determination of scavenging rates in a coastal zone: its measurement with a proportional counter

E. Cuesta[1], R.L. Lozano[1], E.G. San Miguel[1], M. Casas-Ruiz[2] and J. P. Bolívar[1]

[1]Dept Fisica Aplicada, Universidad de Huelva, Campus de Excelencia Internacional del Mar (CEIMAR), 21071 Huelva, Spain
[2]Dept Fisica Aplicada, Universidad de Cádiz, Campus de Excelencia Internacional del Mar (CEIMAR), Cádiz, Spain

Abstract

We are interested in determining particle-reactive scavenging rates in a highly polluted estuarine system. As it is well-known, these scavenging rates can be estimated by measuring disequilibria between naturally occurring, particle-reactive [234]Th and its generally soluble parent, [238]U. In this work, we show the calibration of a low background gas-flow proportional counter to determine low activity of [234]Th in coastal water samples. Electrodeposition was used to prepare calibration samples. Similar efficiencies were obtained in all detectors with an average of 0.401±0.004.

In this work, the procedure to obtain [234]Th activity in dissolution as well as in particulate matter is indicated. Two experiments have been designed in order to validate the calibration of the beta counter and the method to determine [234]Th in coastal waters with high concentration of particulate matter.

Introduction

[234]Th ($T_{1/2}$= 24.1 days) is a naturally occurring radionuclide present in the [238]U decay chain. [234]Th is a highly particle-reactive radionuclide that in seawater is continuously produced from its soluble parent, [238]U ($T_{1/2}$= 4.47·10[9] years).
[234]Th has been extensively used in a wide range of applications as tracer to determine the rate of nuclide's removal by any particular process (Cochran and Masqué 2003).
[234]Th emits gamma radiation immediately following its decay to [234m]Pa by beta emission. [234m]Pa ($T_{1/2}$ = 1.2 min) in turn decays by beta emission to [234]U. [234]Th can be measured in environmental samples either through gamma spectrometry, beta counting using gas-flow proportional (beta) counter and Cerenkov counting. The major problem associated with beta counting of [234]Th in natural samples is the unknown contribution of beta counts from the in-growth of beta producing progeny from [228]Th (and [229]Th, if added as tracer); and internal conversion electrons from the alpha decay of [228]Th, [229]Th, [230]Th, and [232]Th. Corrections for these non [234]Th + [234m]Pa beta counts are typically made in one of three ways defined as the immediate sample count method, the weak beta absorber method, and the multiple beta count method (Waples et al., 2003).
The main objective of this paper is to obtain the counting efficiency of a low background gas-flow proportional counter in order to determine [234]Th activity concentrations in water samples.

Theoretical fundamentals

Fig.1 shows a flowchart of the method used to measure dissolved and particulate-bond [234]Th fractions in seawater (coastal waters) samples. The procedure to determine [234]Th by beta counting in seawater samples consists of the followings steps: sampling, which is supposed to occur at time t_o; radiochemical procedure which in turn comprises pre-treatment, co-precipitation, separation of [234]Th

from ^{238}U; and finally, electrodeposition on stainless disk and counting. The time at which the separation ^{238}U-^{234}Th takes place is named as t_2, whereas electrodeposition and counting times are named as t_3 and t_4 respectively.
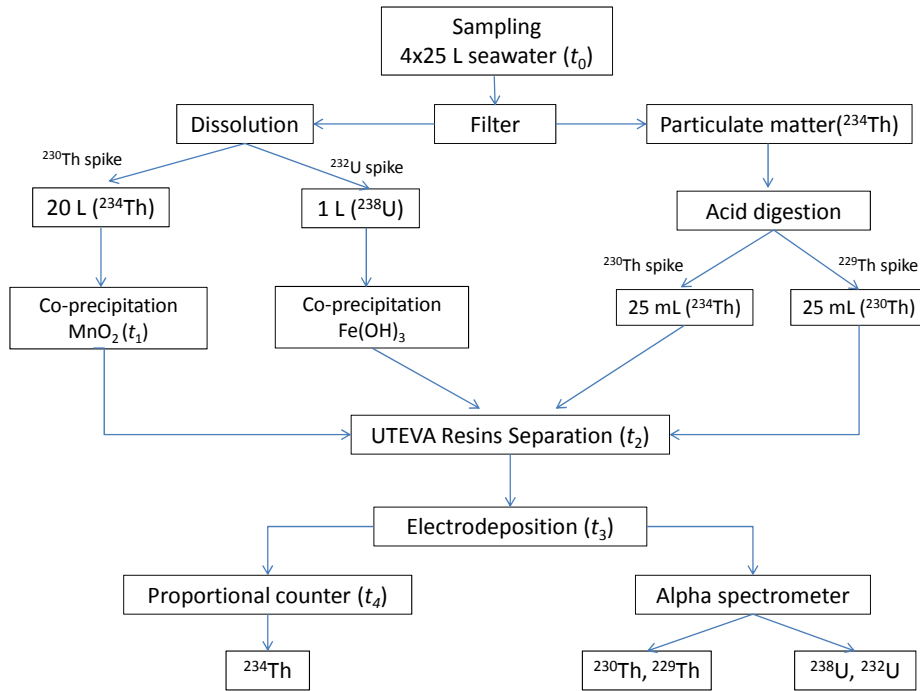
Figure. 1.- Procedure to measure ^{234}Th in seawater (dissolution and particulate matter).

As can be seen from Fig.1, the final step of the general procedure to determine Th and U isotopes in sea water samples is the counting of these planchets in both low background gas-flow proportional counters and alpha particle spectrometers (PIPS detectors). Recovery yield of the whole procedure (*R*) is determined by alpha spectrometry according to the equation:

$$A_{230} = \frac{n_{230}}{\varepsilon_\alpha R}$$

where n_{230} are the net counts per seconds (count rate) of ^{230}Th obtained in the alpha spectrometer, A_{230} is the activity of ^{230}Th added as tracer, and ε_α is the counting efficiency of the alpha spectrometer.

On the other hand, ^{234}Th is measured through the multiple beta count. According to the multiple beta count, the count rate in the proportional counter is given by:

$$n_\beta = be^{-\lambda t} + n_\beta^0$$

where λ is the ^{234}Th decay constant (λ= 28.76·10^{-3} d^{-1}), t is the time elapsed from the beginning of beta counting (t>15 days after electrodeposition), b is the slope in the fitting of the count rate versus $e^{-\lambda t}$ and n_β^0 is the count rate for $t \gg 145$ days which in turn represent the contribution other than ^{234}Th to the beta counting of the sample. The slope *b* and ^{234}Th activity at the beginning of the counting can be related by the expression (Waples et al., 2003):

$$b = \varepsilon_\beta A_{Th}(t_4)$$

^{234}Th activity at time of the sample collection (t_0), $A_{Th}(t_0)$, and the ^{234}Th activity at time of beginning of beta counting (t_4), $A_{Th}(t_4)$ are related by:

$$A_{Th}(t_0) = \frac{A_{Th}(t_4)}{R} e^{\lambda \Delta t_{40}} - A_U(t_0)\left(e^{\lambda \Delta t_{10}} - 1\right)$$

where Δt_{40}, Δt_{10} are the time elapsed between sampling and beta counting and sampling and co-precipitation respectively and λ is the [234]Th decay constant. Therefore by substituting the recovery yield and $A_{Th}(t_4)$ in the former equation, the [234]Th activity at the time of sample collection is given by:

$$A_{Th}(t_0) = b\, \frac{\epsilon_\alpha A_{230}}{\epsilon_\beta n_{230}} e^{\lambda \Delta t_{40}} - A_U(t_0)\left(e^{\lambda \Delta t_{10}} - 1\right)$$

Taking into account this equation, once the alpha-beta counting efficiency ratio ($\frac{\epsilon_\alpha}{\epsilon_\beta}$) has been determined, the [234]Th activity could be obtained for any sample. The method used to calibrate as well as the validation are described in the followings sections.

Materials and Methods

In this paper different set of samples have been used: calibration samples to obtain the counting efficiency of the low background gas proportional counter; validation samples to validate the efficiency calibration and "problem" samples, which have been collected from an estuarine system and applied the whole procedure to determine [234]Th in them. The whole procedure to obtain [234]Th and [238]U in particulate matter and in dissolution can be seen in full detail elsewhere (Cuesta et al., 2016)

Sample collection and pre-treatment

Seawater samples (4x25 L) were collected using a pump and immediately filtered with pre-weighed nitrocellulose Millipore filter (0.45 μm, 90 mm diameter). The filter is stored at 60^0 C until constant weigh is reached and the suspended matter content was calculate by subtracting the blank filter mass. The time of sampling is designed as t_0. The filtered water is homogenized in a 100 L container and 4 aliquots of 20 L and 1 L each are separated for [234]Th and [238]U analysis respectively.

Beta counting and alpha particle spectrometry

The planchet was first counted using a low background proportional counter (Berthold beta counter, LB 770-2 model) in order to determine [234]Th activity concentration. Every counting takes 1200 minutes in 4 cycles of 300 minutes each.
The disks were covered with an Al (41.13 ± 0.01 mg cm^{-2}) foil in order to prevent the weak beta emission of [234]Th and other contributions, and thus only counting the emission of [234m]Pa. [234]Th is measured through the multiple beta count which requires counting the sample beta source repeatedly (e.g., two to six times) over a period of up to six half-lives of [234]Th (about 145 days).
The alpha-emitting radionuclides such as U and Th isotopes have been determined using an EG&Ortec supplied alpha-particle spectrometry system with ion-implanted silicon detectors (PIP′s detectors) with an absolute efficiency about 25%. The quality assurance of radioanalytical measurements was regularly ensured through participation in intercomparison exercises organized by the International Atomic Energy Agency (IAEA), as well as the periodic measurement of certified reference materials (IAEA-326 black soil; NIST-1646a estuarine sediment, etc.).
The background contribution of the alpha detectors and beta counters used in this work ranged between $0.4 \cdot 10^{-5}$-$1.2 \cdot 10^{-5}$ cps and $1.4 \cdot 10^{-2}$-$1.5 \cdot 10^{-2}$ cps respectively. Reagent blanks were prepared separately. The results of the procedural blanks are of the same order of magnitude than background. From the blank samples a minimum detectable activity of 10 mBq has been estimated for the whole procedure based on the criteria suggested by Currie (2004).
The recovery of the process in all the samples analyzed ranged between 70-85%.

Reference materials

The Uranium reference material is the Uranium atomic absorption standard solution (code 207524 from Fluka) with 1000 ppm U in 1.06 wt. % HNO_3 (density 1.01 g/mL at 25 °C). The ^{230}Th reference material is the Thorium Standard 4342A from NIST. From these reference materials with high activity of ^{238}U and ^{230}Th, two standards of these radionuclides were prepared: The ^{238}U standard containing 244.1 ± 0.2 mBq·g^{-1} and the ^{230}Th 221.5 ± 0.9 mBq·g^{-1}. Details of preparation of standards can be seen elsewhere (Cuesta et al., 2016)

Calibration procedures

An electrodeposition of ^{238}U from high activities samples is carried out on the same kind of planchets as that used for the problem samples. The disks are stored the time needed for ^{234}Th to reach secular equilibrium with ^{238}U (>145 days). The ^{238}U and ^{234}Th activity in the stainless disks which is measured in the counters are obtained through the expressions:

$$A_{234Th} = \frac{N_{234Th}}{\epsilon_\beta t_\beta R} e^{\lambda t} \qquad\qquad A_{238U} = \frac{N_{238U}}{\epsilon_\alpha t_\alpha R}$$

where R is the recovery of the whole procedure of preparation of calibration samples, N_{234Th} and N_{238U} are the net counts of ^{234}Th and ^{238}U respectively, t_α and ϵ_α are the counting time and the counting efficiency for the alpha spectrometer and t_β and ϵ_β are the counting time and the counting efficiency for the beta counter. The exponential accounts the ^{234}Th decay between ^{238}U-^{234}Th separation and beta counting. Nevertheless, since in these set of samples ^{238}U and ^{234}Th are in secular equilibrium ($e^{\lambda t} \approx 1$), the ratio of counting efficiencies is given by:

$$\frac{\epsilon_\alpha}{\epsilon_\beta} = \frac{N_{238U} A_{234Th} t_\beta}{t_\alpha A_{238U} N_{234Th}} = \frac{cps_{238U}}{cps_{234Th}}$$

As can be seen from this equation, the ratio of counting efficiencies does not depend on the activity of the calibration samples because ^{238}U and ^{234}Th are in secular equilibrium in them.

Calibration samples

Four samples of water, 1L each, were recorded from a phosphogypsum waste disposal close to Huelva town. These samples present high levels of ^{238}U activity concentrations (Hierro et al., 2012.). The four samples (coded SB11, SB12, SB112 and SB411) were applied a pre-treatment procedure (Cuesta et al., 2016).

Results and Discussion

The ratio of counting efficiencies for a given alpha detector is shown in table 1.
As can be seen from this table, the ratios of counting efficiencies are not significant different at 2σ level.
Also, it is possible to observe that for a given pair of detectors alpha and beta, the ratio of counting efficiencies does not depend on the sample.

Table 2 shows the average ratios of counting efficiencies obtained for each sample.

			$\varepsilon_{\alpha4}/\varepsilon_{\beta n}$			
Sample	$\varepsilon_{\alpha4}/\varepsilon_{\beta2}$	$\varepsilon_{\alpha4}/\varepsilon_{\beta3}$	$\varepsilon_{\alpha4}/\varepsilon_{\beta4}$	$\varepsilon_{\alpha4}/\varepsilon_{\beta8}$	$\varepsilon_{\alpha4}/\varepsilon_{\beta9}$	Average
SB12	0.571 ± 0.008	0.568 ± 0.011	0.576 ± 0.008	0.586 ± 0.008	0.580 ± 0.008	0.576 ± 0.003
SB11	0.592 ± 0.007	0.586 ± 0.007	0.601 ± 0.007	0.613 ± 0.007	0.586 ± 0.007	0.596 ± 0.005
SB112	0.579 ± 0.006	0.588 ± 0.006	0.590 ± 0.006	0.586 ± 0.006	0.582 ± 0.006	0.5849 ± 0.0019
SB411	0.584 ± 0.014	0.591 ± 0.014	0.584 ± 0.013	0.585 ± 0.014	0.587 ± 0.014	0.5860 ± 0.0013
Average	0.582 ± 0.009	0.583 ± 0.010	0.587 ± 0.010	0.592 ± 0.014	0.583 ± 0.003	

			$\varepsilon_{\alpha5}/\varepsilon_{\beta n}$			
Sample	$\varepsilon_{\alpha5}/\varepsilon_{\beta2}$	$\varepsilon_{\alpha5}/\varepsilon_{\beta3}$	$\varepsilon_{\alpha5}/\varepsilon_{\beta4}$	$\varepsilon_{\alpha5}/\varepsilon_{\beta8}$	$\varepsilon_{\alpha5}/\varepsilon_{\beta9}$	Average
SB12	0.567 ± 0.010	0.564 ± 0.010	0.573 ± 0.010	0.582 ± 0.011	0.586 ± 0.011	0.576 ± 0.003
SB11	0.579 ± 0.009	0.573 ± 0.009	0.587 ± 0.009	0.599 ± 0.009	0.572 ± 0.009	0.582 ± 0.005
SB112	0.569 ± 0.005	0.578 ± 0.005	0.579 ± 0.005	0.575 ± 0.005	0.571 ± 0.005	0.5745 ± 0.0019
SB411	0.563 ± 0.009	0.570 ± 0.009	0.563 ± 0.009	0.564 ± 0.009	0.566 ± 0.009	0.5651 ± 0.0012
Average	0.570 ± 0.007	0.571 ± 0.006	0.575 ± 0.010	0.580 ± 0.015	0.571 ± 0.004	

			$\varepsilon_{\alpha16}/\varepsilon_{\beta n}$			
Sample	$\varepsilon_{\alpha16}/\varepsilon_{\beta2}$	$\varepsilon_{\alpha16}/\varepsilon_{\beta3}$	$\varepsilon_{\alpha16}/\varepsilon_{\beta4}$	$\varepsilon_{\alpha16}/\varepsilon_{\beta8}$	$\varepsilon_{\alpha16}/\varepsilon_{\beta9}$	Average
SB12	0.560 ± 0.007	0.557 ± 0.007	0.565 ± 0.007	0.575 ± 0.007	0.568 ± 0.007	0.565 ± 0.003
SB11	0.585 ± 0.008	0.579 ± 0.008	0.594 ± 0.008	0.605 ± 0.008	0.579 ± 0.008	0.588 ± 0.005
SB112	0.569 ± 0.006	0.577 ± 0.006	0.579 ± 0.006	0.575 ± 0.006	0.571 ± 0.006	0.5742 ± 0.0019
SB411	0.594 ± 0.013	0.600 ± 0.013	0.593 ± 0.013	0.594 ± 0.013	0.596 ± 0.013	0.5955 ± 0.0013
Average	0.577 ± 0.015	0.579 ± 0.018	0.582 ± 0.014	0.587 ± 0.015	0.579 ± 0.013	

			$\varepsilon_{\alpha17}/\varepsilon_{\beta n}$			
Sample	$\varepsilon_{\alpha17}/\varepsilon_{\beta2}$	$\varepsilon_{\alpha17}/\varepsilon_{\beta3}$	$\varepsilon_{\alpha17}/\varepsilon_{\beta4}$	$\varepsilon_{\alpha17}/\varepsilon_{\beta8}$	$\varepsilon_{\alpha17}/\varepsilon_{\beta9}$	Average
SB12	0.560 ± 0.009	0.557 ± 0.009	0.564 ± 0.009	0.575 ± 0.009	0.568 ± 0.009	0.565 ± 0.003
SB11	0.580 ± 0.010	0.574 ± 0.010	0.589 ± 0.010	0.600 ± 0.011	0.574 ± 0.010	0.584 ± 0.005
SB112	0.562 ± 0.004	0.570 ± 0.004	0.572 ± 0.004	0.568 ± 0.004	0.564 ± 0.004	0.5670 ± 0.0019
SB411	0.557 ± 0.011	0.563 ± 0.011	0.557± 0.011	0.558 ± 0.011	0.560 ± 0.011	0.5590 ± 0.0012
Average	0.565 ± 0.010	0.566 ± 0.008	0.570 ± 0.014	0.575 ± 0.018	0.566 ± 0.006	

Table1.- *Ratio of counting efficiencies obtained for the samples SB12, SB11, SB112, SB411. β_n is the number of the beta detector, and α_i is the number of the alpha detector, (uncertainties are expressed at 1 σ level, only counting uncertainties are considered).*

Detector	α_4	α_5	α_{16}	α_{17}
β_2	0.582 ± 0.009	0.570 ± 0.007	0.577 ± 0.015	0.565 ± 0.010
β_3	0.583 ± 0.010	0.571 ± 0.006	0.579 ± 0.018	0.566 ± 0.008
β_4	0.579 ± 0.011	0.575 ± 0.010	0.582 ± 0.014	0.570 ± 0.014
β_8	0.592 ± 0.014	0.580 ± 0.015	0.587 ± 0.015	0.575 ± 0.018
β_9	0.583 ± 0.003	0.571 ± 0.004	0.578 ± 0.013	0.566 ± 0.006

Table 2.- *Average ratios of counting efficiencies ($\varepsilon_{\alpha i}/\varepsilon_{\beta j}$) obtained for each sample.*

 As can be seen from this table, the ratios of counting efficiencies are not significant different. Finally, the counting efficiency of beta counter is determined after obtaining the alpha particle spectrometer efficiency with a standard reference material (MC9510, [241]Am, with certified activity of 276 ± 1 mBq g[-1]) with the same geometry of the disks used in this calibration method (and also in the problem samples which are routinely measured). From the former tables the counting efficiency of beta counters can be obtained. These results are shown in table 3.

As can be seen from this table, the counting efficiencies of beta counters are not significant different.

As can be seen from this table, the counting efficiencies of beta counters are not significant different.

Table 4 shows the average of counting efficiencies of beta counters for the 4 samples used.

From this table, it is possible to observe that the counting efficiencies of beta counters are not significant different. With these results, it is possible to assume that the efficiency for the beta proportional counter is 0.401 ± 0.004 for the five detectors.

ε_βn (ε_α4 =0.2365 ± 0.0013)						
Samples	$\varepsilon_{\beta2}$	$\varepsilon_{\beta3}$	$\varepsilon_{\beta4}$	$\varepsilon_{\beta8}$	$\varepsilon_{\beta9}$	**Average**
SB12	0.4140(23)	0.4162(23)	0.4108(23)	0.4032(22)	0.4079(22)	0.4104(23)
SB11	0.3993(22)	0.4033(22)	0.3935(22)	0.3860(21)	0.4037(22)	0.397(3)
SB112	0.4082(22)	0.4021(22)	0.4011(22)	0.4038(22)	0.4065(22)	0.4043(13)
SB411	0.4049(22)	0.4004(22)	0.4051(22)	0.4044(22)	0.4031(22)	0.4036(9)
Average	0.407(6)	0.405(7)	0.403(7)	0.399(9)	0.4058(23)	
ε_βn (ε_α5 = 0.2267 ± 0.0012)						
Samples	$\varepsilon_{\beta2}$	$\varepsilon_{\beta3}$	$\varepsilon_{\beta4}$	$\varepsilon_{\beta8}$	$\varepsilon_{\beta9}$	**Average**
SB12	0.3997(21)	0.4019(21)	0.3967(21)	0.3894(21)	0.3939(21)	0.3963(22)
SB11	0.3917(21)	0.395(21)	0.3860(20)	0.3786(20)	0.3961(21)	0.390(3)
SB112	0.3984(21)	0.3924(21)	0.3915(21)	0.3941(21)	0.3967(21)	0.3946(13)
SB411	0.4025(21)	0.3980(21)	0.4027(21)	0.4020(21)	0.4007(21)	0.4012(9)
Average	0.398(5)	0.397(4)	0.394(7)	0.391(10)	0.397(3)	
ε_βn (ε_α16 = 0.2331 ± 0.0013)						
Samples	$\varepsilon_{\beta2}$	$\varepsilon_{\beta3}$	$\varepsilon_{\beta4}$	$\varepsilon_{\beta8}$	$\varepsilon_{\beta9}$	**Average**
SB12	0.4161(23)	0.4184(23)	0.4129(23)	0.4053(23)	0.4101(23)	0.4126(23)
SB11	0.3984(22)	0.402(22)	0.3926(22)	0.3851(21)	0.4029(22)	0.396(3)
SB112	0.4099(23)	0.4037(23)	0.4028(22)	0.4055(23)	0.4084(23)	0.4060(13)
SB411	0.3927(22)	0.3883(22)	0.3929(22)	0.3922(22)	0.3910(22)	0.3914(8)
Average	0.404(11)	0.403(12)	0.400(10)	0.397(10)	0.403(9)	
ε_βn (ε_α17 = 0.2282 ± 0.0013)						
Samples	$\varepsilon_{\beta2}$	$\varepsilon_{\beta3}$	$\varepsilon_{\beta4}$	$\varepsilon_{\beta8}$	$\varepsilon_{\beta9}$	**Average**
SB12	0.4076(23)	0.4098(23)	0.4045(23)	0.3970(23)	0.4017(23)	0.4041(22)
SB11	0.3933(22)	0.397(23)	0.3876(22)	0.3802(22)	0.3977(23)	0.391(3)
SB112	0.4063(23)	0.4002(23)	0.3993(23)	0.4019(23)	0.4046(23)	0.4025(13)
SB411	0.4096(23)	0.4050(23)	0.4098(23)	0.4091(23)	0.4077(23)	0.4083(9)
Average	0.404(7)	0.403(6)	0.400(9)	0.397(2)	0.403(4)	

Table 3.- *Counting efficiency of beta counter obtained for the samples SB12, SB11, SB112 and SB411.*

Detector	$\varepsilon_{\alpha4}$ = **0.2365**	$\varepsilon_{\alpha5}$ = **0.2267**	$\varepsilon_{\alpha16}$ = **0.2331**	$\varepsilon_{\alpha17}$ = **0.2282**
β_2	0.407 ± 0.006	0.398 ± 0.005	0.404 ± 0.011	0.404 ± 0.007
β_3	0.405 ± 0.007	0.397 ± 0.004	0.403 ± 0.012	0.403 ± 0.006
β_4	0.403 ± 0.007	0.394 ± 0.007	0.400 ± 0.010	0.400 ± 0.009
β_8	0.399 ± 0.009	0.391 ± 0.010	0.397 ± 0.010	0.397 ± 0.012
β_9	0.4053 ± 0.0023	0.397 ± 0.003	0.403 ± 0.009	0.403 ± 0.004

Table 4.- *Average of counting efficiencies of beta counters obtained for each sample.*

Validation Procedures

Two experiments have been designed in order to validate the calibration.

Validation 1: Addition of ^{238}U natural in equilibrium with ^{234}Th

In this method, three dissolutions (D1, D2 and D3) are prepared by adding a known amount of ^{238}U standard reference material (244.1 ± 0.2 mBq·g^{-1}) and ^{230}Th tracer (221.5 ± 0.9 mBq·g^{-1}) to a solution of HNO$_3$ 3M. The samples are completed up to 25 mL with HNO$_3$ 3M. The activity added to validation samples are indicated in Table 5.
The electrodeposited sources are counted in the alpha spectrometer in order to obtain ^{230}Th counting rates and the recovery of the whole process. Afterwards, the planchets are counted in the low background gas-flow proportional counter through the multiple beta count method as it was previously mentioned.

As can be seen from this table, ^{234}Th activities show a good agreement with the values expected.

	Sample code	$^{238}U_{added}$(mBq)	$^{234}Th_{meas}$ (mBq)	$^{234}Th/^{238}U$
	Validation samples			
	D1	958.3 ± 0.8	1236 ± 22	1.29 ± 0.02
	D2	988.4 ± 0.8	1082 ± 19	1.10 ± 0.02
	D3	976.6 ± 0.8	1025 ± 19	1.05 ± 0.02
	VG1	1263 ± 18	1315 ± 52	1.04 ± 0.04
	VG2	1319 ± 18	1591 ± 42	1.21 ± 0.04
	VG3	1308 ± 18	1493 ± 40	1.14 ± 0.03
	Problem samples			
	Sample code	$^{238}U_{meas}$(mBq·L^{-1})	$^{234}Th_{meas}$ (mBq·L^{-1})	$^{234}Th/^{238}U$
Dissolution	**VM1**	37.1 ± 1.7	9.5 ± 2.5	0.26 ± 0.07
	VM2	33.8 ± 1.9	7.2 ± 2.0	0.21 ± 0.06
	VM3	33.9 ± 1.1	7.7 ± 1.2	0.23 ± 0.04
Particulate matter	**234a**	0.51 ± 0.04	4.2 ± 0.7	8.1 ± 1.6
	234b	0.51 ± 0.04	4.1 ± 0.7	8.0 ± 1.5
	234c	0.51 ± 0.04	4.4 ± 0.9	8.6 ± 1.8

Table 5.- *Activities of ^{238}U added (mBq) and ^{234}Th (mBq) determined in validation samples and activity concentrations of ^{238}U (mBq L^{-1}) and ^{234}Th (mBq L^{-1}) determined in problem samples. ^{234}Th/^{238}U activity ratios in the different set of samples are also shown. ($^{238}U_{meas}$ means ^{238}U measured; $^{234}Th_{meas}$ means ^{234}Th measured).*

Validation 2: 10 L water samples traced with natural Uranium

In this method, three samples (VG1, VG2 and VG3) of tap water 10 L each are acidulated with HNO$_3$ concentrated up to pH < 2, and spiked with ^{238}U and ^{230}Th reference materials. The activities added are indicated in Table 5. The samples are applied the general procedure of ^{234}Th determination in dissolution (Fig. 1).
As can be seen from this table both radionuclides are in secular equilibrium as it was expected.

Application: ^{234}Th determination in seawater samples

In this section, the ^{234}Th and ^{238}U activity concentrations are determined in three water samples (VM1, VM2 and VM3) of 20 L from the Estuary of Rio Odiel (Huelva, Southwest Spain) through the procedure previously indicated. This point (suspended particle concentration = 6.59 mg·L^{-1}) is affected by the acid mining drenage (AMD) of Odiel and Tinto River and by the fertilizer industry located in the estuary (Hierrro et al., 2013).

^{234}Th in dissolution

^{234}Th activity is determined once ^{238}U activity concentration has been obtained by alpha spectrometry. Table 5 shows the results obtained in samples VM1, VM2 and VM3. As can be seen from this table, ^{238}U activities in these samples are in agreement taking into account experimental uncertainties.

^{234}Th in particulate matter

As it was previously indicated, seawater samples of 20 L each were filtered and mixed in a 100 L container in order to determine ^{234}Th. Particulate matter corresponding to these 4 samples

were mixed and digested according to the procedure previously indicated. The final residue was diluted in 50 mL of HNO_3 (0.44 M) and six aliquots of 8 ml each were separated. In three of these aliquots, [234]Th was determined using [230]Th as tracer whereas in the rest, [230]Th of natural origin was determined using [229]Th as tracer. [230]Th of natural origin represents less than 1% of the [230]Th activity added as tracer in these samples. As can be seen from Table 5, [234]Th activity concentration in particulate matter is one magnitude order higher than its precursor, [238]U. This fact is well-known to happen in estuarine systems as a consequence of the scavenging processes in coastal areas (Bacon, 2004).

Conclusions

In this paper, a procedure to measure [234]Th, in dissolved and particulate phase, in coastal waters using a low-level beta counter has been developed. Also, a method based on using a disk with high [238]U activity electrodeposited to obtain the ratio ($\varepsilon_\alpha/\varepsilon_\beta$) of counting efficiencies by using [230]Th as tracer has been presented. The method does not depend on the activity of the samples used to calibrate. Similar efficiencies were obtained in all detectors, being found an average of 0.401 ± 0.004. The method to obtain the efficiency calibration as well as the procedure to determine [234]Th in seawater samples have been validated through several tests and applied to water samples collected from the Estuary of Rio Odiel (Huelva, Southwest Spain).

References

Bacon, M.P. 2004. Reactive radionuclides as tracers of oceanic particle flux. Marine Radioactivity. 139 – 165.

Cochran, J.K., Masqué, P., 2003. Short-lived U/Th Radionuclides in the Ocean: Tracers for Scavenging Rates, Export Fluxes and Particle Dynamics. In: Bourdon, B., Henderson, G.M., Lundstrom, C.C., Turner S.P., (Eds.), Uranium-series Geochemistry. Reviews in mineralogy and geochemistry, vol 52. Geochemical Society/Mineralogical Society of America, pp. 461 - 492.

Cuesta, E., Lozano, R.L., San Miguel, E.G. , Casas-Ruiz, M., Bolívar, J. P., 2016. Calibration of a low background gas-flow proportional counter to estimate [234]Th activity in coastal waters. Appl. Rad. Isot. 118, 201-210. http://dx.doi.org/10.1016/j.apradiso.2016.09.016

Currie, L.A., 2004. Detection and quantification limits: basic concepts, international harmonization, and outstanding (''low-level'') issues. Applied Radiation and Isotopes 61, 145–149.

Hierro, A., Bolivar, J. P., Vaca, F., and Borrego, J., 2012. Behavior of natural radionuclides in surficial sediments from an estuary impacted by acid mine discharge and industrial effluents in Southwest Spain. J. Environ. Radioact. 110, 13-23.

Hierro, A., Martín, J.E., Olías, M., Vaca, F., and Bolivar, J. P., 2013. Uranium behavior in an estuary polluted by mining and industrial effluents: The Ría of Huelva (SW of Spain). Water Res. 47, 6269 – 6279.

Waples, J. T., Orlandini, K. A., Weckerly, K. M., Edgington, D. N., and Val Klump, J., 2003. Measuring low concentrations of 234Th in water and sediment. Mar. Chem. 80, 265-281.

Acknowledgments

^{222}Rn Concentrations and dissolved ionic species in spring water from an arid region at the east of Chihuahua México

A. Cervantes-Trejo[1], A. Covarrubias-Muños[1], A. Pinedo-Álvarez[1], G. Manjon-Collado[2] and M. Rentería-Villalobos[1].

[1]Universidad Autónoma de Chihuahua, Periférico Francisco R. Almada km 1, 31415, Chihuahua, México.

[2]Universidad de Sevilla, Grupo de Física Nuclear Aplicada, ETSA, Avenida Reina Mercedes 2, 41012, Sevilla, España.

Abstract

^{222}Rn is a gas produced by radioactive decay of uranium. In the environment, the radon is found in zones with high concentration of uranium and/or radium. The radon is diffusing continuously by emanation from rocks and soils. In the arid zones of Chihuahua, Mexico, the main water supply to use and human consumption is from rivers, dams, and springs. The aim of this study was to obtain the concentrations of both ^{222}Rn and major ions to determine the quality of spring water. Six natural springs of area under study were sampled. ^{222}Rn concentrations were analysed by liquid scintillation, using a TRIATHLER HIDEX OY. The major ions were obtained using a spectrophotometer HACH DR 2010. ^{222}Rn in the 100% of the natural springs showed concentrations above of the allowable limits proposed by international regulations. Results showed that radon concentration decreases with the temperature increment. Furthermore, the water samples with the highest concentration of radon showed the highest concentrations of sulphates, fluorides and total dissolved solids. In conclusion, it is necessary to establish educational environmental programs for the local inhabitants as well as to apply pollutant removal techniques, to prevent any risk for human health

Introduction

Drinking water is usually provided by ground or surface water sources. Water naturally contain dissolved chemical species such as Ca^{+2}, Mg^{+2}, K^{+1}, Na^{+1}, HCO_3^-, CO_3^{-2}, SO_4^{-2}, Cl^-, F^-, NO_3^- and H_4SiO_4, that can negatively affect the water quality for both use and human consumption. In addition, the radioactive elements can be dissolved in water and contaminate this resource. The content of these natural radionuclides in groundwater can vary in several orders of magnitude and are influenced by physical (temperature), chemical (pH) and geological properties of the aquifer (Fonollosa, Peñalver et al. 2016). Radon (^{222}Rn), a decay product of ^{226}Ra, is a naturally occurring inert radioactive gas with a half-life of 3.82 days. When ^{226}Ra decays, ^{222}Rn atoms might be ejected from the soil grain by a-recoil and transferred to groundwater or air, where finally escape to surface (Abdallah, Habib et al. 2007, Tabar, Kumru et al. 2013). The primary health effect of ^{222}Rn is lung cancer, resulting from inhalation in indoor air. There is also evidence from epidemiology that ingestion of ^{222}Rn causes stomach cancer (UNSCEAR. 2000). Because of its potential public health hazard, the surveys of radon in water sources are necessary

The European Commission recommends for ^{222}Rn, that a reference level should be appointed above an activity concentration of 100 Bq l^{-1} (Commission) 2001). The present study attempts to analyze radon concentration and dissolved ionic species in spring water, in the state of Chihuahua, Mexico.

Materials and Methods

Study area

The state of Chihuahua is a semi-desert area, and virtually all the water for human consumption comes from well and dam, most of them more than 100 m depth. Around 50 uranium deposits are known in the state, many of them near the cities of Chihuahua and Aldama. In Aldama, a milling facility that processed uranium ore from the Peña Blanca mines operated during one decade, about 20 years ago. Therefore, it is reasonable to assume that high ^{222}Rn concentrations might be present in Chihuahua and Aldama waters, hence, in those intended for human consumption (Villalba, Colmenero Sujo et al. 2005).

Sampling

The study was carried out at the Luis L. León Dam, better known as El Granero (Figure 1). It is located in Aldama city, in the State of Chihuahua, Mexico. The dam was constructed from 1965 to 1968 for flood control and to take advantage of the waters of the Conchos River to irrigate 11,000 hectares in the municipality of Ojinaga. Its reservoir is located between 105°19´and 105°24´Latitute North and 28°52´and 29°00´Longitude East.
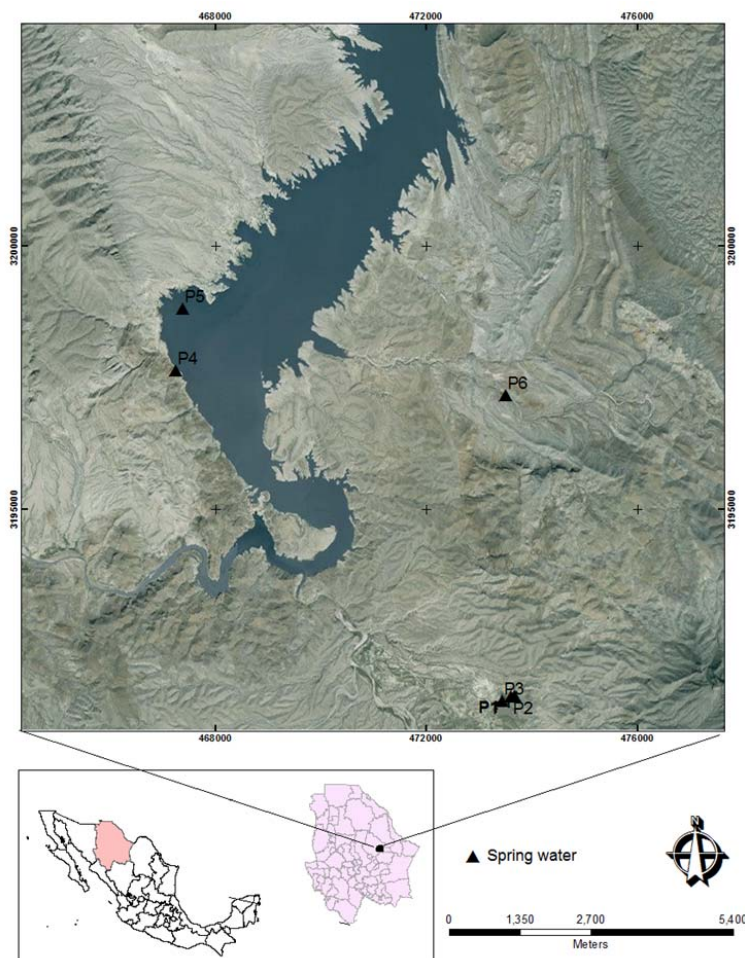
Figure 1. *Location of the Luis L. León Dam (El Granero) in the state of Chihuahua México and the spring sampling points.*

Sample locations of the analyzed natural spring waters (6 sampling points) were considered on the basis of the dam ¨El Granero¨. Natural spring water samples were collected directly in vials with a volume of 20 mL for the determination of ^{222}Rn. In addition, a second water sample was collected in

1 L polyethylene recipients with the capacity to determine fluorides, hardness, sulfates, nitrates, calcium, magnesium, and sodium. These samples were preserved on ice at a temperature of approximately 4   C.

Determination of dissolved ions

Dissolved chemical species were determined using different normative methods standardized in the Department of Water Quality of the Research Center of Advanced Materials (CIMAV). Anions were determined using the following methods: a) for sulfates the method proposed by HACH was used, using a HACH spectrophotometer, model DR 2010; and b) fluorides were analyzed using the ion-selective electrode method based on the operation procedure of the equipment Orion 1260. Cations such as Ca, Mg and Na were determined following Mexican regulations (CONAGUA 2001) using an atomic absorption spectrophotometer (Model GBC Avanta, Sigma). Total alkalinity was determined using the method proposed by the norm NMX-AA-036-SCFI-2001 (CONAGUA 2001). Because the hardness of the water is mainly influenced by the ions Ca^{+2} and Mg^{+2}, expressed in mg/L of $CaCO_3$ or meq/L, it was calculated using equation 1:

$$\text{Hardness (mg/L } CaCO_3) = (\text{meq Ca/L} + \text{meq Mg/L}) \times 50 \qquad (1)$$

Where, 1 meq/L CaCO3 is equivalent to 50 mg/L CaCO3

Radiometric technique

All samples were analyzed for radon concentrations, using the method described by (Chalupnik, Lebecka et al. 1994, Cook, Passo et al. 2003). Radon was extracted using a liquid scintillation cocktail and measured using a portable Hidex-Triathler liquid scintillation counter, with pulse-shape alpha–beta discrimination. The samples were counted for 50 min. For the relative analysis, a standard solution of ^{226}Ra (SRM-4965 certified by the US NIST) was used. The detection efficiency for α particles emitted by ^{226}Ra was $\varepsilon = 0.68$. The activity of ^{222}Rn was determined by assuming three successive decays until ^{210}Pb (a long-live progeny of ^{222}Rn). The activity concentration at the time of measurement was determined by:

$$A_{Rn} = cps_\alpha/(n*\varepsilon*V) \qquad (2)$$

where cps_α is a net count index in counts per second, registered for the region of detection alpha, ε is the detection efficiency, n is the number of alpha disintegrations of ^{222}Rn and its descendants ^{218}Po and ^{214}Po, and V is the water volume added to the vial in liters.

Results and Discussion

Table 1 shows the results of parameters measured in situ such as pH, temperature (T), redox potential (Eh), and total dissolved solids (TDS), as well as the geographic coordinates of each sampling point. Likewise, Table 2 shows the Parameters of water quality in spring water from the selected dam El Granero sampled.

In the samples taken from the spring waters of El Granero, the pH values varied from slightly acid to neutral. In addition, in the spring water the T was found to vary between 27.2 and 31.4 ^{0}C, whereas the results from Eh presented a slight variation from 132 to 158 mV, which indicates that the water is in sub-oxic conditions (Somaratne 2016). Furthermore, the values of TDS presented a high variability, with a concentration range from 270 up to 1180 mg/L.

Table 1. *Sample location and chemical parameters measured in situ of the different natural spring waters.*

Sample	Location		pH*	T(°C)*	Eh(mV)*	TDS(ppm)*
	Latitude	Longitude				
1	28°51'4.30"N	105°16'19.30"O	6.69	28.2	158	410
2	28°51'3.60"N	105°16'19.60"O	6.58	30.7	149	440
3	28°51'3.40"N	105°16'23.40"O	6.46	31.4	153	420
4	28°52'45.55"N	105°19'19.85"O	6.53	27.2	132	270
5	28°52'6.81"N	105°20'5.10"O	6.68	28.5	138	930
6	28°54'26.30"N	105°20'5.10"O	6.30	27.2	158	1180

* In situ measurements.

Table 2. *Parameters of water quality (mg/L) and ^{222}Rn concentrations (Bq/L) in the points sampled in spring water.*

Sample	Sulphate	Fluorides	Hardness	Ca	Na	K	Mg	Si	^{222}Rn
1	45	1.1	200	37.7	47.4	6.3	2.3	17.3	67.5
2	71	1.1	210	41.2	48.6	5.9	2.4	18.2	82.6
3	80	1.1	206	38.6	47.7	6.4	2.5	16.6	52.3
4	44	1.1	106	19.8	48.6	2.5	-	35.3	379.9
5	420	2.4	310	48.5	279.3	22.3	14.0	25.2	161.3
6	800	0.8	1350	196.7	72.6	6.7	12.5	17.7	229.3

In general, the highest concentrations were of Ca, Na, and Si, and the lowest concentrations of Mg and K, whereas sulfates were dominant in the analyzed water. From measured concentrations of Ca and Mg, the values of hardness ranged from 106 to 1350 mg $CaCO_3$/L. Thus, this water can be classified as moderately hard to hard (>100 mg/L $CaCO_3$). The pH measured in these water samples is slightly acid (<7), because of which the concentration of Mg, Ca, Al, Na, and K in the water can be attributed to this parameter and the geological conditions of the study area. From results, TDS in sampling points P5 and P6 are higher compared to the other sampling points. Likewise, the highest values for anions and cations were found in those sampling points, corroborating the results for the concentrations of TDS measured in situ. The anions with the highest concentrations were the sulfates, ranging from 44 to 800 mg/L.

Finally, ^{222}Rn concentration in the spring waters in the zone of El Granero showed concentrations ranging from 52 to 379 Bq/L. When ^{222}Rn is freed from ^{238}U decay chain, it is solubilized in the water of aquifers. Sampling points 4 and 6 presented the highest ^{222}Rn concentrations. It has been reported that in saturated soils with a porosity of 20%, with ^{226}Ra concentrations of 40 Bq/kg (world average in the earth crust), and with equilibrium conditions, radon concentrations in groundwater are around 50 Bq/L (UNSCEAR, 2000). ^{222}Rn concentrations are higher than that value, thereby it is suggested the presence of ^{226}Ra in rocks and groundwater in the study area, El Granero. The acceptable amount of radioactive substances present in drinking water is established by the Environmental Protection Agency (EPA, 2000). For ^{222}Rn the maximum acceptable limit is of 11Bq/L or 300 pCi/L. Considering this value, 100% of the spring waters in this study exceed this allowed limit.

Conclusions

In the present study the composition of the major ions and radon concentrations dissolved in spring waters were obtained. The spring waters with the highest concentrations of sulfates, fluorides, and total dissolved solids had the highest radon concentrations. It is suggested that anions and cations

are leaching from the geological substrate towards the spring waters. In addition, the salts that the water contains are mainly calcium fluorides, as well as sulfates of calcium and magnesium.

Although the region of El Granero does not present conditions of uranium mineralization, the high radon concentrations that were found can be attributed to the content of ^{226}Ra present in the groundwater. The water of all the springs evaluated showed values of ^{222}Rn that exceeded the maximum acceptable limit for water for human consumption.

The implementation of both environmental education strategies towards the population and technologies to remove the contaminants from the water may be the objectives to reduce the health risk for water consumers.

References

Abdallah, S. M., et al. (2007). "Radon measurements in well and spring water in Lebanon." Radiat Meas **42**(2): 298-303.

Commission), E. E. (2001). Commission recommendation of 20th December 2001 on the protection of the public against exposure to radon in drinking water. Official Journal of the European Commission. L. 2001/982/Euratom, European Commission.

CONAGUA (2001). NMX-AA-036-SCFI-2001. Water analysis - determination of acidity and alkalinity total in natural, wastewaters and wastewaters treated. Análisis de aguas. Determinación de acidez y alcalinidad en aguas naturales, residuales y residuales tratadas. México, DOF, Diario Oficial de la Federación.

CONAGUA (2001). NMX-AA-051-SCFI-2001. Water analysis - determination of metals by Atomic Absorption in natural, drinking, wastewaters and Wastewaters treated - test method. Análisis de agua - determinación de metales por Absorción atómica en aguas naturales, potables, Residuales y residuales tratadas. México, DOF. Diario Oficial de la Federación**: 1-47.

Cook, G. T., et al. (2003). Environmental Liquid Scintillation Analysis. Handbook of Radioactivity Analysis. M. F. L'Annunciata. New York, USA, Elsevier Science.

Chalupnik, S., et al. (1994). Determining radium in water: Comparison of methods. International Conference on Liquid Scintillation Spectrometry / 15th International Radiocarbon Conference, Glasgow, Scotland.

Environmental Protection Agency (EPA), National Primary Drinking Water Regulations; Radionuclides. 40 CFR Parts 141 and 142, 2000. 65(78): p. 21575-21628.

Fonollosa, E., et al. (2016). "Radon in spring waters in the south of Catalonia." J Environ Radioactiv, **151**(1): 275-281.

Somaratne, N. (2016). "Characterization of the effects of redox condition on Fe(III)/Fe(II) transformation in a small karstic aquifer: Poocher swamp freshwater lens, South Australia." Environ Nat Resour Res **6**(3): 134-145.

Tabar, E., et al. (2013). "Radiological and chemical monitoring of Dikili geothermal waters, Western Turkey." Radiat Phys Chem **91**: 89-97.

UNSCEAR. (2000). Report of the United Nations Scientific Committee on the Effects of Atomic Radiation to the General Assemby. Annex B: Exposures from natural radiation sources. New York, USA., UNSCEAR.

Villalba, L., et al. (2005). "Radon concentrations in ground and drinking water in the state of Chihuahua, Mexico." J Environ Radioactiv **80**(2): 139-151.

Behaviour of natural radionuclides in the karst aquifer system of Sierra de Gádor (Almería, SE Spain)

J.L.Guerrero[a,], A. Vallejos[b], J.C. Cerón[a], F. Sánchez-Martos[b], A. Pulido-Bosch[b] and J.P. Bolívar[a]*

[a]University of Huelva, Department of Integrated Sciences, Marine International Campus of Excellence (CEIMAR), 21071 Huelva, Spain

[b]University of Almería, Department of Biology and Geology, 04120, Almería, Spain

Abstract

Sierra de Gádor is a karst aquifer located in southeastern Spain. The main economic activities, agriculture and tourism, are supported by water resources from this aquifer system. The aim of this work is to study the behaviour of U-isotopes and ^{226}Ra in order to deep in the knowledge of the hydrogeochemical processes in this groundwater system. Both groundwater and surface water samples were collected, and their activity concentrations by alpha spectrometry were determined.

Activity concentrations of dissolved ^{238}U presented large variations, ranging from 1.1 to 65 mBq L^{-1}. The ^{234}U/^{238}U activity ratios (AR) were higher than unity for all samples (1.1-3.8; mean = median = 2.2). ^{226}Ra presented a wide range of activity concentrations in the waters, ranging from 0.8 up to about $4 \cdot 10^2$ mBq L^{-1} (median = 13 mBq L^{-1}; mean = 36 mBq L^{-1}). Most of the samples showed ^{226}Ra/^{234}U ARs lower than unity (median = 0.3), due to the greater mobility of U than Ra in the waters.

A Principal Component Analysis (PCA) was applied to the groundwater data. The natural U-isotopes are strongly correlated with sulphate concentrations, due to gypsum dissolution. The ^{226}Ra had a complex behaviour, showing a strong correlation with water salinity. The most saline samples showed in general the lowest ^{234}U/^{238}U ARs, and the greatest ^{226}Ra/^{234}U ARs.

Keywords: Uranium isotopes, ^{226}Ra, karst aquifer, radioactive disequilibrium

Introduction

Sierra de Gádor is a complex karst aquifer system located in southeastern Spain, in the province of Almería (Figure 1), which supports the two main economic activities in this arid area, agriculture and tourism (Vallejos et al., 2015).

This Triassic age karst macrosystem is mainly formed by limestones and dolomites with interbedded gypsum, and show an area of more than 900 km^2. It is hydraulically connected to the Campo de Dalías, supporting the aquifers of this important agricultural area (Pulido-Bosch et al., 2000).

The intense exploitation to which Sierra de Gádor has been subject, exceeding the annual average resource, has produced falls in the piezometric level, deterioration in water quality and seawater intrusion in some sectors of the southern edges (Molina et al., 2003).

---

[*]Corresponding author, E-mail: joseluis.guerrero@alu.uhu.es
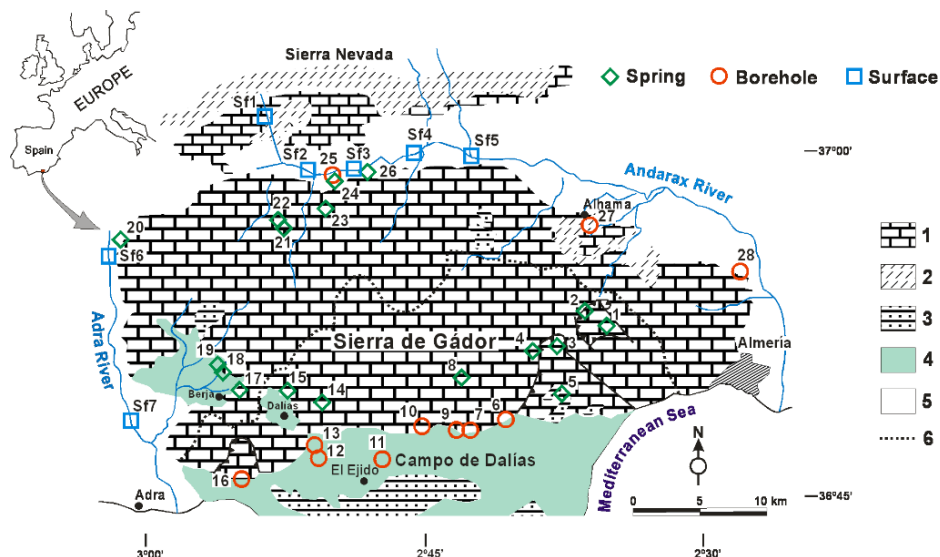
Figure 1. Hydrogeological scheme of the study area and sampling locations. 1: Limestones and dolomites; 2: Micaschists and phyllites; 3: Calcarenites; 4: Conglomerates, sandstones and silts; 5: Marls and silts; 6: Watershed.

Natural radionuclides have not been studied previously in this area. Such knowledge can be used to improve the understanding of the hydrochemical processes that regulate this complex system.

Taking into account the previous facts, the aim of this work is to study the behaviour of U-isotopes and [226]Ra in the aquifer system of Sierra de Gádor, in order to deep in the knowledge of the hydrogeochemical processes that regulate the composition of the waters.

Materials and Methods

During June 2012, 35 representative sampling points were selected: 28 groundwater points (from boreholes and springs) and 7 surface water points (5 from the Andarax River and 2 from de Adra River) (Figure 1). The surface samples were taken in points where groundwaters feed these rivers.

The main physicochemical parameters (pH, redox potential [Eh], dissolved oxygen [DO], temperature [T] and electrical conductivity [EC]) were determined in situ. Alkalinity (as HCO_3^-) was determined by titration at the time of sampling.

At each point, three samples were collected and stored in prewashed polyethylene bottles. Two 100 mL samples, the first one for the analysis of cations, and the second one for the analysis of anions. These samples were filtered in situ through 0.45 μm pore size Millipore filters and stored at 4 ºC.Another 6 L sample was collected at each point for the analysis of natural radionuclides (U-isotopes and [226]Ra). In the laboratory, these samples were filtered through 0.45 μm pore size Millipore filters, and acidified at pH = 1 - 1.5 using suprapure HNO_3.

Sample composition was determined by combination of ICP-MS and ICP-OES techniques at Acme Labs (Vancouver, Canada).The activity concentration of natural radionuclides (U-isotopes and [226]Ra) was determined by alpha spectrometry in the radiochemical laboratories of the University of Huelva (Spain), following the sequential method of tributilphosphate (TBP) combined with anion exchange resins. The application of this technique requires a previous radiochemical treatment, which consists in the isolation of the radioelements of interest and the final deposition on very thin film by electrodeposition (U and Ra).

Hydrogeochemical modelling of uranium speciation was performed using the code PHREEQC version 3. A principal component analysis (PCA) using XLSTAT (Version, 2015) was used to analyse the groundwater data.

Results and Discussion

Hydrogeochemistry

A statistical summary of the physicochemical parameters is listed in Table 1. The pH values are alkaline in all samples, with a mean value of 8.0 ± 0.1, due to the dissolution of limestones and dolomites. The uncertainty is shown as the standard deviation of the mean ($SD/N^{1/2}$).

Variable	Unit	Mean	Median	Min	Max	SD	CV (%)
pH	-	8	7.9	7.2	9	0.4	5.1
Eh	mV	467	467	374	557	46	9.9
T	°C	19.4	17.8	11.2	30.1	4.5	23
EC	µS cm^{-1}	697	531	154	2390	540	77.5
DO	mg L^{-1}	5.9	5.1	1	15.7	3.6	61.1

Table 1. *Statistical summary of the physicochemical parameters. SD: standard deviation; CV = coefficient of variation; N = 35.*

The positive redox potential (Eh) show the existence of oxidative conditions in the waters. The analysis of temperature (T) highlights the positive thermal anomalies that exist in the aquifer system, affecting most of the boreholes, with a maximum of 30.1 ºC near the thermal area of Alhama (sample 27). The electrical conductivity (EC), which indicates salinity, has a wide rangeand a great variability (CV = 77.5 %). Finally, dissolved oxygen (DO) shows relatively high values in the groundwaters, with similar values to surface water.

The concentration of the analysed ions is displayed as modified box and whisker plots (Figure 2). The existence of high extreme values for concentrations of most of these elements should be noted, resulting mean values far above the median.
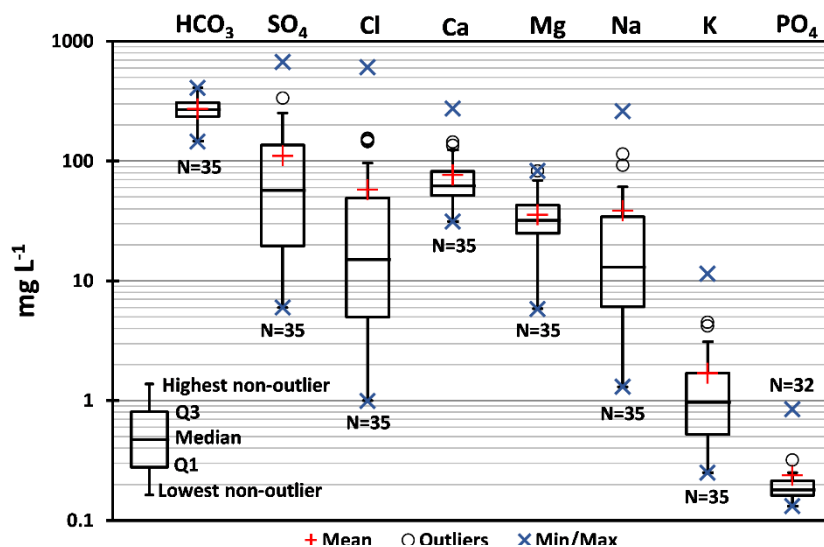
Figure 2. *Modified box and whisker plots of the ion concentrations (mg L^{-1}).*

The Shapiro-Wilk normality test results (not shown) indicated that, with the exception of HCO_3^-, these ions do not follow a normal distribution. Considering median values, the ions can be ordered from highest to lowest concentration: $HCO_3^- > Ca^{2+} > SO_4^{2-} > Mg^{2+} > Cl^- > Na^+ > K^+ > PO_4^{3-}$. The high HCO_3^-, SO_4^{2-}, and Ca^{2+} concentrations are related to carbonates and gypsum dissolution.

Natural radionuclides

The activity concentration of ^{238}U, ^{235}U, ^{234}U and ^{226}Ra is displayed as modified box and whisker plots (Figure 3). The activity concentration of ^{238}U, ^{235}U and ^{234}U show a mean value of 22 ± 2, 1.3 ± 0.2 and 43 ± 4 mBq L^{-1}, respectively. Shapiro-Wilk normality test results (not shown) indicated that ^{238}U and ^{234}U follow a normal distribution with mean values similar to the median. In the analysed samples, ^{226}Ra presents a mean value of 36 ± 12 mBq L^{-1} and follows a lognormal distribution with a mean value higher than the third quartile, due to the existence of high extreme values considered as outliers (Figure 3).
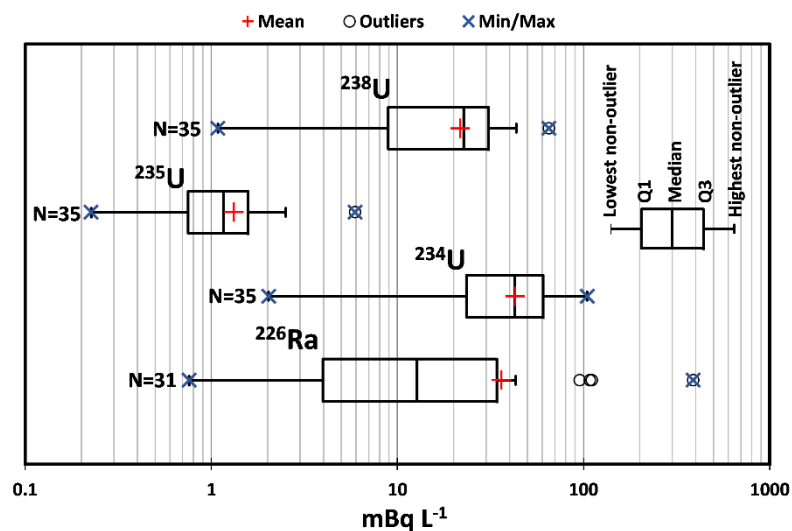
Figure 3. Modified box and whisker plots of natural U-isotopes and ^{226}Ra activity concentrations.

Uranium speciation modelling with the code PHREEQC confirms that all uranium is in the hexavalent state U(VI), as would be expected because of the redox potential values of the water. Uranyl carbonate complexes $[UO_2(CO_3)_3]^4$ and $[UO_2(CO_3)_2]^2$ are the dominant uranium dissolved species in the waters, with a mean of 90%, while the uranyl phosphate complex $[UO_2(HPO_4)_2]^2$ show a mean of 11% in relation to the total dissolved species.

The $^{234}U/^{238}U$ activity ratio is greater than unity (radioactive equilibrium) in all the studied samples (Figure 4A), ranging from 1.1 to 3.8 (mean value = 2.2 ± 0.1), showing the existence of ^{234}U significant preferential dissolution processes in the studied aquifer system.

Most of the samples show a $^{226}Ra/^{234}U$ activity ratio lower than unity (Figure 4B). This higher mobility of U than Ra in the majority of the samples could be related to the oxidising conditions of the waters, favouring dissolution of U, while Ra is very immobile under these conditions (U.S. EPA 1998; Martin et al., 2003), and/or the adsorption of Ra onto surfaces by cation exchangedue to the higher surface reactivity of Ra^{2+} than U complexes.
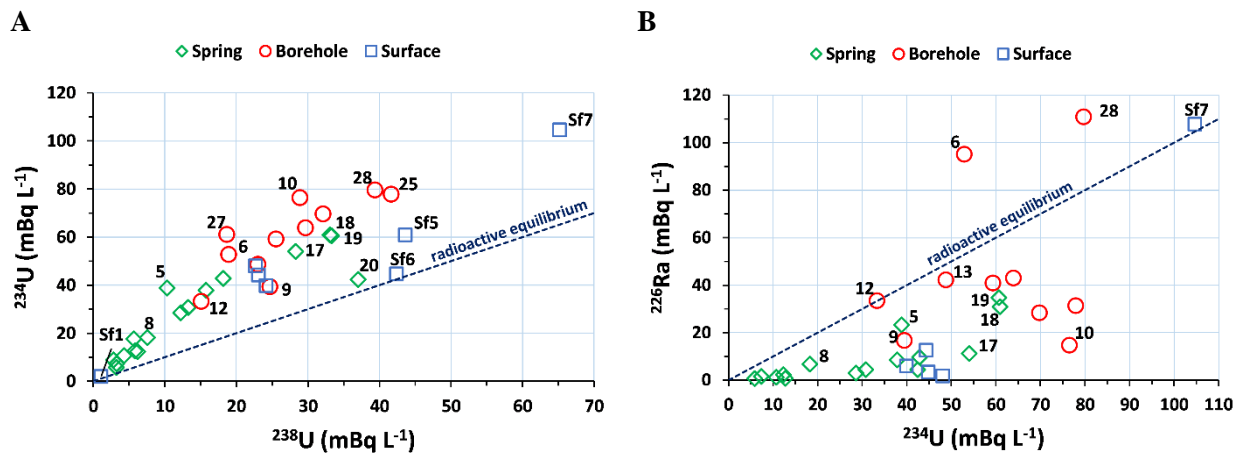
Figure 4. *Relation between (A)^{234}U and ^{238}U activity concentrationand (B)^{226}Ra and ^{234}U activity concentration (for better visualisation, sample 27 was not represented due to its high extreme ^{226}Ra value).*

Principal component analysis

The method used in this paper is based on the interpretation of the various factors as well as the correlation matrix obtained after processing the data. In this analysis, only groundwater samples were used to avoid the interferences in the correlations of the surface samples, mainly with the physicochemical parameters. Because many variables do not follow a normal distribution, the Spearman correlation coefficient was used. Concentration values of PO_4^{3-} below the detection limit (DL) were replaced with DL/2 for the statistical analysis, because the percentage of non-detects was below 15% (U.S. EPA, 2006). On the other hand, the ^{226}Ra activity concentration was replaced by the mean value in the two groundwater samples that were not measured.

Table 2 shows the calculated Spearman's correlation coefficients. ^{238}U shows high correlations with ^{234}U (0.92), SO_4^{2-} (0.80), Ca^{2+} (0.74) and Mg^{2+} (0.71). These correlations show the important influence that dissolution of sulphate evaporites, mainly gypsum, exert in the concentration of natural U-isotopes in the waters (Figure 5A).

Variables	pH	Eh	T	EC	DO	HCO$_3$	SO$_4$	Cl	Ca	Mg	Na	K	PO$_4$	^{238}U	^{235}U	^{234}U	^{226}Ra	^{234}U/^{238}U	^{226}Ra/^{234}U
pH	**1**																		
Eh	.34	**1**																	
T	-.08	-.33	**1**																
EC	**-.54**	**-.45**	**.71**	**1**															
DO	-.27	-.04	-.12	.17	**1**														
HCO$_3$	**-.42**	-.08	**.42**	.37	.00	**1**													
SO$_4$	**-.51**	**-.46**	**.51**	**.78**	.31	.16	**1**												
Cl	**-.43**	-.30	**.59**	**.82**	.07	.31	**.42**	**1**											
Ca	**-.63**	**-.45**	.36	**.74**	.39	.39	**.78**	**.44**	**1**										
Mg	**-.50**	**-.41**	**.76**	**.93**	.13	**.51**	**.75**	**.75**	**.72**	**1**									
Na	**-.48**	-.35	**.61**	**.85**	.11	.34	**.53**	**.98**	**.50**	**.79**	**1**								
K	**-.44**	-.34	**.71**	**.85**	.17	**.39**	**.75**	**.77**	**.58**	**.80**	**.80**	**1**							
PO$_4$	-.04	.04	.15	.20	-.02	-.30	.02	**.39**	-.21	.17	.32	.20	**1**						
^{238}U	**-.58**	-.37	**.51**	**.65**	.20	.30	**.80**	.36	**.74**	**.71**	**.42**	**.57**	.08	**1**					
^{235}U	**-.60**	-.25	.29	**.45**	.27	.20	**.55**	.18	**.48**	**.51**	.26	.35	.00	**.68**	**1**				
^{234}U	**-.46**	-.34	**.59**	**.70**	.07	.32	**.76**	.39	**.72**	**.75**	**.43**	**.55**	.09	**.92**	**.60**	**1**			
^{226}Ra	-.21	**-.40**	**.54**	**.64**	-.03	.24	**.46**	.30	**.56**	**.62**	.32	.35	-.03	**.48**	**.39**	**.64**	**1**		
^{234}U/^{238}U	.36	.05	-.12	-.16	-.12	-.14	-.35	-.08	-.21	-.21	-.13	-.29	-.10	**-.48**	-.30	-.19	.18	**1**	
^{226}Ra/^{234}U	-.10	**-.41**	**.47**	**.58**	.01	.15	.32	.31	**.40**	**.50**	.30	.30	.00	.22	.18	**.40**	**.92**	.25	**1**

Table 2. *Spearman correlation matrix. Significant correlations are denoted with bold text at significant level $p < 0.05$.*

^{238}U also shows a moderate positive correlation with EC (0.65) and T (0.51), and a moderate negative correlation with pH (-0.58), as is expected. In general, higher U concentrations are found in groundwater with lower pH values and higher salinity and temperature.
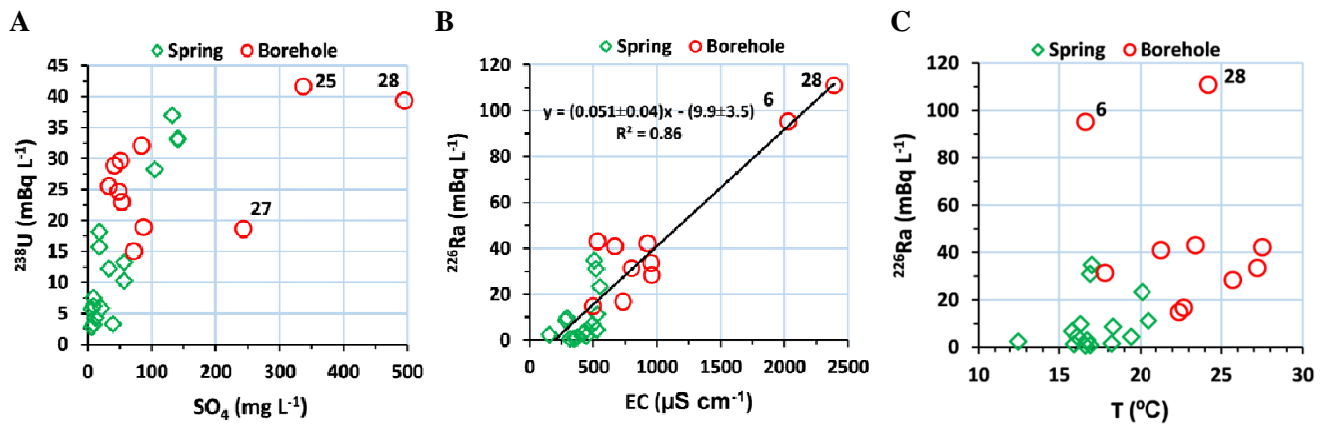
Figure 5. *Relation between (A) ^{238}U and SO$_4^{2-}$, (B) ^{226}Ra and EC and (C) ^{226}Ra and T (for better visualisation, sample 27 was not represented due to its high extreme ^{226}Ra value)*

On the other hand,^{226}Ra shows a high positive correlation with the ^{226}Ra/^{234}U activity ratio (0.92), showing that this ratio is mainly influenced by the ^{226}Ra concentration in the water, and a moderate positive correlation with EC (0.64), Mg^{2+} (0.62), Ca^{2+} (0.56) and T (0.54).These relatively low correlations show that ^{226}Ra has a more complex behaviour in this groundwater than the U-isotopes.

A good linear correlation (R^2 = 0.84) is observed between EC and ^{226}Ra in the samples (Figure 5B).Many studies have shown a positive correlation between radium and salinity (Sturchio et al., 2001; Tomita et al. 2014). Ra adsorbs onto mineral surfaces by cation exchange, therefore greater ionic strength (high salinity) means greater competition for exchange sites and possible liberation of Ra^{2+} due to its large ionic radius. The thermal samples, characterised by higher salinity values, generally shows the highest activity concentrations of ^{226}Ra (Figure 5C). The association of ^{226}Ra with Mg^{2+} and Ca^{2+} is probably due to the similar geochemical behaviour of these elements (Dickson, 1990).

In general, the studied activity ratios (^{234}U/^{238}U and ^{226}Ra/^{234}U) show low correlation values with the other variables, due to the complex process and various factors that generate this disequilibrium in the waters (alpha recoil, redox potential, thermalism, salinity etc.).

Graphs of the PCA results are shown in Figure 6, including both variable loadings (Figure 6A) and observation scores (Figure 6B). According to the PCA results, 58.4% of the total variance of the data set is accounted for by the two first components (F1: 47.0 and F2: 11.4%). This percentage is relatively low, which is probably due to the heterogeneity of the aquifer system and the complexity of factors controlling the water chemistry in the Sierra de Gádor.

The F1 component explains 47.0% of the total variance and is highly positively contributed by EC, T and most of the major ions. Therefore, F1 will be highly related to the bulk dissolution factor of the host rock. The U-isotopes and ^{226}Ra are also very regulated by this factor. The U-isotopes are near SO$_4^{2-}$ and Ca^{2+}, so they will be mainly associated with the dissolution of sulphate evaporites. On the other hand, ^{226}Ra appears to be strongly related to temperature (thermalism). It seems clear that thermalism has an important role in the ^{226}Ra activity concentrations (Table 2, Figure 5C).All samples from boreholes are situated in the positive part of this component because of the higher

salinity and temperature (thermalism), otherwise most of the spring samples are situated in the negative part.Obviously, this component is due to the sample salinity, affected by dissolution of evaporites and salts, which are favoured by the higher temperature of thermal samples.

A

B
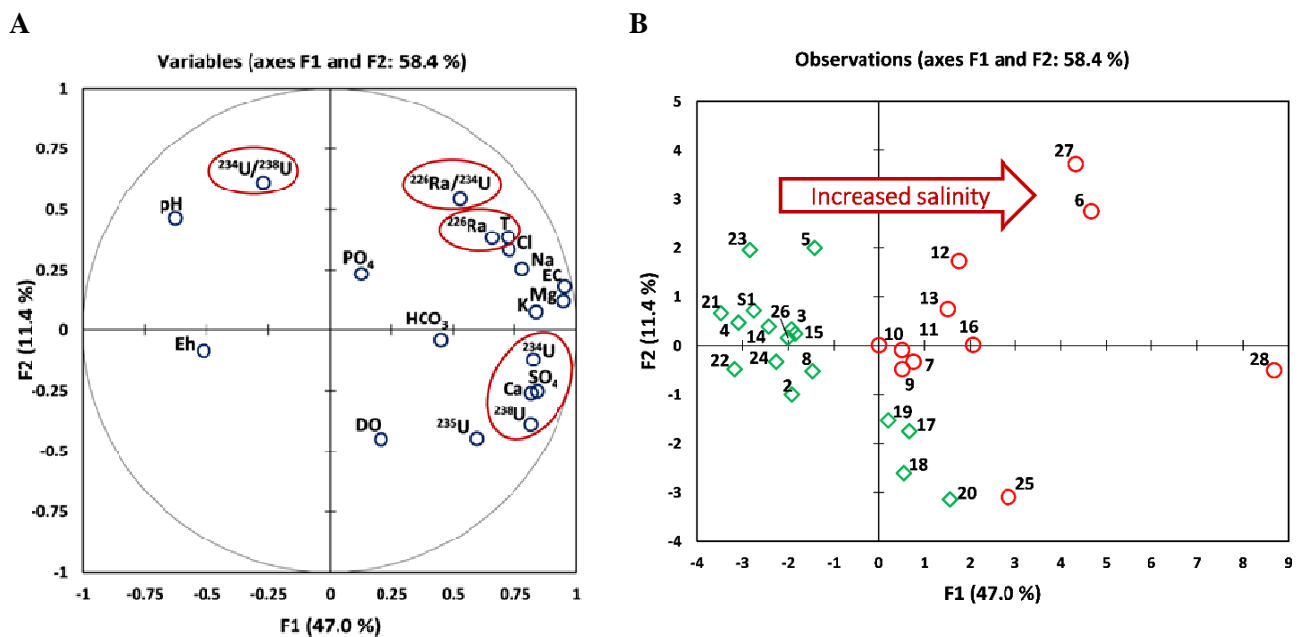
Figure 6. PCA results. A: Loading plot of variables and B: score plot of observations.

The location of the $^{234}U/^{238}U$ activity ratio in the F1 negative part show that the most saline samples (higher dissolution processes) present the lowest radioactive uranium disequilibriums. On the other hand, the $^{226}Ra/^{234}U$ activity ratio in the positive part shows that higher radioactive disequilibrium is produced in most saline samples.

The F2 component only explains 11.4% of the variance, being determined by the local characteristics of some samples. In this component, the $^{234}U/^{238}U$ activity ratio and the U-isotopes again appear at opposite poles due to higher dissolution processes producing generally lower radioactive disequilibriums. Both $^{234}U/^{238}U$ and $^{226}Ra/^{234}U$ activity ratios are located in the positive part of the F2 component.This component seems to be due to processes favouring radioactive disequilibrium between the studied activity ratios.

Conclusions

A complex karst aquifer system from an arid area (southeastern Spain) has been studied, which shows a great hydrochemical variability and heterogeneity.

The activity concentration of ^{238}U varied from around 1.1 to 65 mBq L^{-1} (mean = 22 ± 2 mBq L^{-1}). The $^{234}U/^{238}U$ activity ratios were higher than unity for all samples (mean = 2.2 ± 0.1), showing the existence of significant ^{234}U preferential dissolution processes in the studied aquifer system. Uranium speciation modelling with the code PHREEQC confirmed that in all studied samples uranium is in the hexavalent form U(VI), and uranyl carbonate complexes are the dominant dissolved species.

^{226}Ra presented a wide range of activity due to the existence of some high extreme values, with a maximum about $4 \cdot 10^2$ mBq L^{-1} in the thermal area of Alhama. Most of the samples showed ^{226}Ra/^{234}U activity ratios lower than unity, due to the higher mobility of U than ^{226}Ra in the waters.

The PCA showed that the concentration of the natural U-isotopes was closely correlated with the dissolution of sulphate evaporites (mainly gypsum). Also, a strong correlation between ^{226}Ra and the salinity of the waters was observed, which likely reflects the greater salinity in the thermal samples. In addition, this analysis demonstrated that the most saline samples show the lowest ^{234}U/^{238}U activity ratios, probably due to fast uniform bulk mineral dissolution that would reduce the tendency for ^{234}U-^{238}U fractionation and increase the tendency for ^{226}Ra/^{234}U ratios, fact expected by considering the comparatively higher solubility of Ra than U in saline conditions.

Acknowledgements

References

Dickson, B.L., 1990. Radium in groundwater. In: IAEA (International Atomic Energy Agency) (Ed.), The Environmental Behaviour of Radium. IAEA-Technical Reports Series 310, Vienna, 335–372.

Martin, A.J., Crusius, J., Mcnee, J.J., Yanful, E.K., 2003. The mobility of radium-226 and trace metals in pre-oxidized subaqueous uranium mill tailings. Appl. Geochem. 18, 1095-1110.

Molina, L., Sanchez-Martos, F., Pulido-Bosch, A., Vallejos, A., 2003. Origin of boron from a complex aquifer in Southeast of Spain. Environ. Geol. 44, 301-307.

Pulido-Bosch, A., Pulido-Loboeuf, P., Molina, L., Vallejos, A., Martín-Rosales, A., 2000. Intensive agriculture, wetlands, quarries and water management. A case study (Campo de Dalías, SE Spain). Environ. Geol. 40 (1-2), 163-168.

Sturchio, N.C., Banner, J.L., Binz, C.M., Heraty, L.B., Musgrove, M., 2001. Radium geochemistry of ground waters in Paleozoic carbonate aquifers, midcontinent, USA. Appl. Geochem. 16, 109-122.

Tomita, J., Zhang, J., Yamamoto, M., 2014. Radium isotopes (^{226}Ra and ^{228}Ra) in Na–Cl type groundwaters from Tohoku District (Aomori, Akita and Yamagata Prefectures) in Japan. J. Environ. Radioact. 137, 204-212.

U.S. EPA., 1998. Small system compliance technology list for the non-microbial contaminants regulated before 1996. Office of Water. EPA 815-R-98-002.

U.S. EPA., 2006. Data Quality Assessment: A Reviewer's Guide (EPA QA/G-9R). EPA/240/B-06/002.

Vallejos, A., Díaz-Puga, M.A., Sola, F., Daniele, L., Pulido-Bosch, A., 2015. Using ion and isotope characterization to delimitate a hydrogeological macrosystem. Sierra de Gádor (SE, Spain). J. Geochem. Explor. 155, 14-25

I – ATMOSPHERE

EURDEP AND REMdb TOOLS FOR THE SAKE OF RADIOECOLOGICAL SCIENCE OPPORTUNITIES

M.A. Hernández-Ceballos, K. Bogucarskis, , T. Tollefsen, G. Cinelli, L. De Felice, E. Nweke,P.V. Tognoli, S. Vanzo, M. De Cort[*]

European Commission, Joint Research Centre, Nuclear Safety and Security
Directorate, Knowledge for Nuclear Security and Safety Unit

Contact:
Marc De Cort; email: marc.de-cort@jrc.ec.europa.eu
Konstantins Bogucarskis, email: konstantins.bogucarskis@jrc.ec.europa.eu

Abstract

Under the terms of Article 36 of the Euratom Treaty, European Union Member States (MSs) shall periodically communicate to the European Commission (EC) information on environmental radioactivity levels, and at the same time, the EC was assigned 1) to bring together and store in a harmonized way environmental radioactivity data produced in the aftermath of the Chernobyl accident and 2) to provide an international data format and a network for the real-time exchange of radiation monitoring information in Europe. To achieve these mandates, the Radioactivity Environmental Monitoring Database (REMdb) and the EUropean Radiological Data Exchange Platform (EURDEP) were established in 1988 and in 1994 respectively. The purpose of this work is to describe and put in value the qualified information stored in these databases, and the potential use of this information in order to analyze and understand the levels of radioactive contamination of the various compartments of the environment (air, water, foodstuff) in Europe

1. Introduction

The severe Chernobyl NPP accident on 26 April 1986 contaminated large parts of the European continent as can be seen from the Chernobyl CS-137 Atlas of Europe (European Commission,1998). Much experience was gained in the European Union (EU), and in Europe more generally, following this accident, because of the European authorities became aware that:

a) there was lack of international coordination to reduce the effects of the accident,
b) that there did not exist a European-wide alerting system,
c) that there was no international harmonization regarding the application of countermeasures,
d) that most national monitoring networks were inadequate,
e) that appropriate international legislations were missing and
e) that there were no agreed standards and protocols to exchange monitoring data.

In order to avoid that the authorities would ever be unprepared again for similar future accidents, the EU defined and put in place a Council Decision that essentially obliges a country that implements or intends to implement widespread countermeasures for protecting its population, to inform the EC without delay. The resulting early notification and urgent information exchange system became known under the acronym ECURIE (European Community Urgent Radiological Information Exchange).

In this framework, the EC was assigned 1) to bring together and store in a harmonized way environmental radioactivity data produced in the aftermath of the Chernobyl accident and 2) to

provide an international data format and a network for the real-time exchange of radiation monitoring information in Europe. As a result of these mandates, the Radioactivity Environmental Monitoring (REM) (https://rem.jrc.ec.europa.eu/RemWeb/activities/Remdb.aspx) data bank was set-up in 1988 while the European Radiological Data Exchange Platform (EURDEP) (https://eurdep.jrc.ec.europa.eu/Entry/Default.aspx) was established in 1994, respectively.

Both databases are managed by the Radioactivity Environmental Monitoring (REM) group, being this group the responsible of providing support both for routine and emergency situations based on the information included in each one of the databases. E.g. routine measurements are managed in the REM database, and in the case of a nuclear or radiological/nuclear emergency, EURDEP system provides real-time monitoring information collected from automatic surveillance systems in 37 European Countries to the national and international competent authorities.

Nowadays, there is a growing concern with the general public about the radioactivity levels in the terrestrial and marine environment, as well about the potential risk of future nuclear accidents. To this context, and based also on the Council Decision 87/600/EURATOM, which specifies that also monitoring data have to be made available, a clear and transparent communication with the public is needed and in this sense, this work aims to contribute to widespread the existence of EURDEP and REMdb as valuable tools to understand and analyze the radioactivity levels in Europe. To this purpose, this paper describes the unique collection of measurements included in each database, as well as the potential use of the information already included in them to analyze and understand the levels of radioactive contamination in Europe.

2. EURDEP and REMdb: Description and applications

2.1. EURDEP system

A major trigger for the setup of radiological monitoring data on an international level was the Chernobyl NPP accident, as already anticipated in the introduction. After the accident, the EC and many European countries felt the need to setup activities headed to significantly improve the exchange of monitoring data between the European countries.

The resulting mechanism was EURDEP, having been proved the large interest and motivation in this system by the expansion registered in its use from its activation. From 1995, when 6 countries exchanged radiological monitoring data from some 300 stations all in different national formats once per week,to 2015 when 38 European countries exchange measurements of more than 5000 stations once per hour from their national radiological monitoring networks in almost real-time and in a standard data-format.

There are two ways of exchanging radiological data in EURDEP. During routine, the monitoring data is made available by the participating organizations at least once a day, while during an emergency, each organization makes data available at least once each two hours. In practice more and more organizations make their national data available on an hourly basis both during routine and during emergency conditions.

Based on the Council Decision 87/600/EURATOM, which specifies that also radiological monitoring data have to be made available,there are two web-sites to accomplish this requirement:

1) The public EURDEP web-site (Figure 1a). It makes available, few minutes after the transfer, most of the radiological data transferred. This map viewer can be accessed from any computer with an internet connection and does not require a license or subscription, and by default the map will show most of the latest Gamma Dose Rate aggregated averages from the approximately 5000 European gamma-dose stations as hexagons and discriminate these values as by colors. We use the term 'most of the data' because every participating organization can impose a delay (in hours) after which its data is made visible to the public. The purpose of this delay is to allow for the verification and correction of the data before making it public and should avoid that abnormally high values - that can be caused by exceptional meteorological situations, calibration activities or probe failures - unnecessarily cause concern and need subsequent explanation from the authorities.
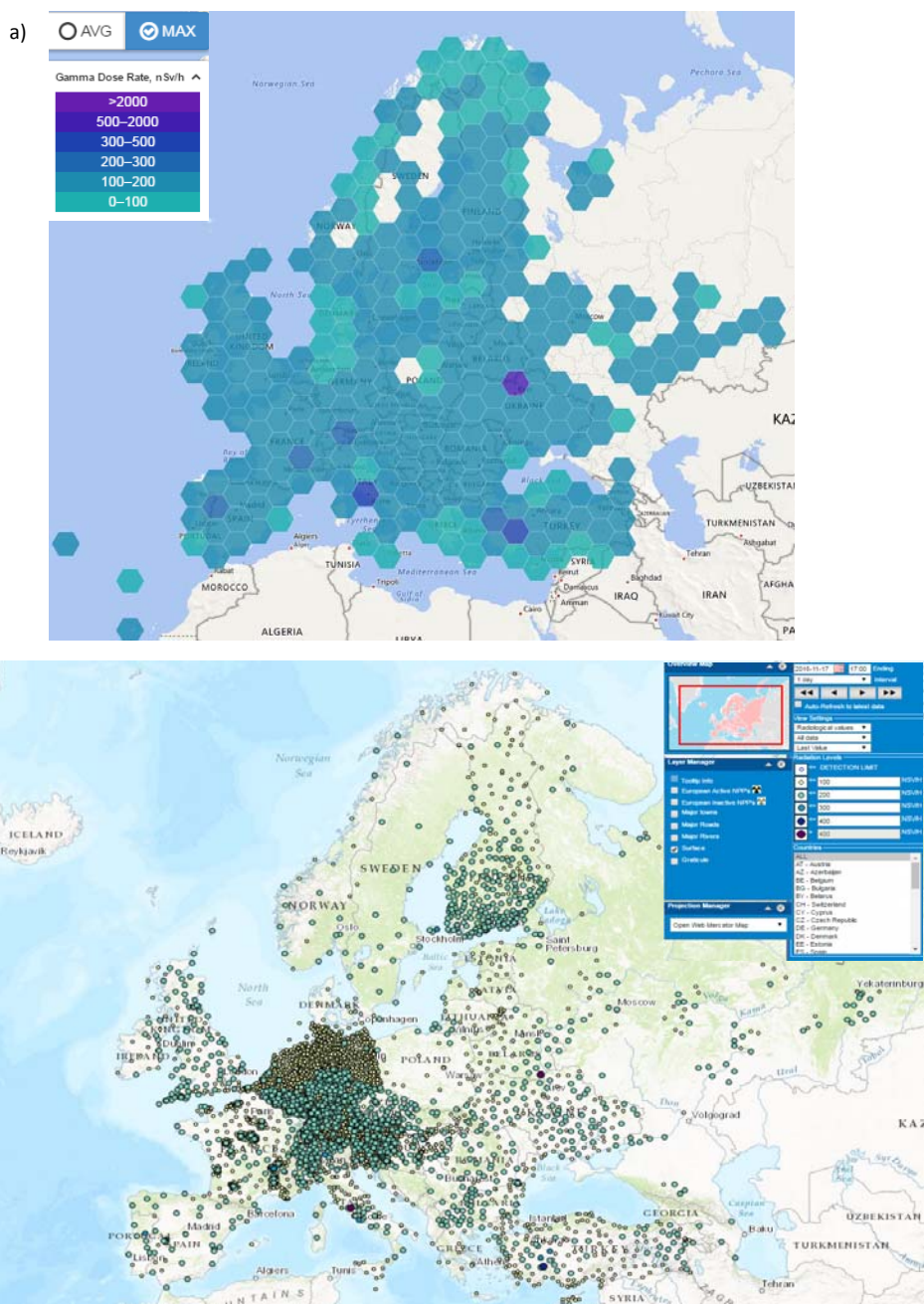

Figure 1. *a) Public and b) expert web-sites to make available the radiological monitoring data of EURDEP*

2) The private EURDEP web-site (Figure 1b). Password protected site to which only experts and data providers have access because they are supposed to be able to distinguish between higher readings caused by an accident from such values caused by other reasons. Therefore, the beforehand delay in the data is never applied for the private map.In this web-site, the time series collected in the stations can be downloaded by the expert users in order to analyze them and in case of an emergency, to take the countermeasures to limit its impact on the population.

In addition to the radiological information, the EURDEP system also allows the exchange of meteorological data from a monitoring station location. The scope of this exchange of meteorological information is to facilitate the interpretation of the radiological values, both during routine and emergency. To that purpose, information about pressure, temperature, wind-direction, wind-speed, precipitation, precipitation-occurrence, precipitation-duration, precipitation-intensity, relative humidity and solar-radiation is exchanged, although, not all countries deliver this kind of data yet.

Finally, and as an example of its usefulness, the collected data in EURDEP during the Fukushima crisis were used to analyze the spatial distribution of the contaminated air masses over Europe, identifying the movement of the plume and the temporal evolution of peak concentrations (e.g. Bossew et al., 2012, Kirchner et al., 2012). The analysis of the data revealed that the maximum concentration did not occur at the same time in all parts of Europe. In some parts the second maximum, around 5-6 April, was more pronounced than the first one, around 31March-1 April.The collected data showed that the maximum air concentration values were reached at the end of March over Poland: Iodine-131 (particulates) concentration values went up to 5-6 mBq/m³ whereas Cesium-137 values stayed below 1 mBq/m³. In normal conditions, air concentration levels for these isotopes stay below 1 µBq/m³. For comparison, the maximum values detected above Europe at the time of the Chernobyl accident were 1.000 to 10.000 times higher.

2.2. REMdb

Under the terms of Article 36 of the Euratom Treaty, Member States shall periodically communicate to the Commission information on environmental radioactivity levels. From 1984, the Radioactivity Environmental Monitoring database (REMdb) compiles the information received with two objectives:

- to keep a historical record of the Chernobyl accident, for further scientific study;
- to store the radioactivity monitoring data of the EC Member States in order to prepare the Monitoring Report. By means of this report the Member States are informed of the radioactivity levels in the environment in the European Community, as stated in art. 35 - 36 of the Euratom Treaty.

Nowadays, REMdb is an online database containing a unique collection of environmental radioactivity measurements from a wide number of different sources, media and countries, mainly the 28 EU Member States.In this sense, the sampling locations incorporated in REMdb are intended to be as representative as possible of regional or national situations.

The environmental radioactivity information stored in REMdbis referred to two networks; the dense one in which are included most of the sampling locations distributed all over the Member States' territories, and the sparse network in which high sensitivity measurements from a number of

representative locations selected by the Member States are stored. Table 1 shows the combination of sample and radionuclide categories included in REMdb.

Table 1. *Combination of sample and nuclide type in each network included in REMdb*

Sampling media	Radionuclide categories	
	Dense network	Sparse network
Airborne particulates	Gross β, ^{137}Cs	^{137}Cs, ^{7}Be
Surface water	Residual β, ^{137}Cs	^{137}Cs
Drinking water	^{3}H, ^{90}Sr, ^{137}Cs	^{3}H, ^{90}Sr, ^{137}Cs
Milk	^{90}Sr, ^{137}Cs	^{90}Sr, ^{137}Cs
Mixed diet	^{90}Sr, ^{137}Cs	^{90}Sr, ^{137}Cs

The current total number of environmental radioactivity data at the European scalestored in REMdb exceeds 2 million. This large amount of data, sentbythenationalcontactpoints of EU28 to the JRC, is on-line available to external users to be downloaded. Therefore, this information is totally available to analyze the levels of radioactive contamination of the various compartments of the environment (air, water, soil).

Among the research possibilities that this unique bank offers, all rely on environmental radioactivity being monitored at the European scale, are studies to assess ^{137}Cs deposition levels in Europe after the Chernobyl accident and, more recently, to describe the ^{7}Be activity concentrations in Europe have been performed.

As an example of this recent application, Figure 2a shows the annual average values of the ^{7}Be concentrations obtained for the REM network on a yearly basis from 1984 onwards (stations are listed from high to low latitudes and not all of thempresented the same number of years). This figure helps to confirm the impact of the latitude in the production of ^{7}Be, from high latitudes (low ^{7}Be concentration) to lower latitudes (high ^{7}Be concentrations), and also to observe how in central and southern Europe, this tendency is broken probably associated with the combination of different meteorological conditions and the geographical location of eachstation, which determines the impact of the regulating processes of the variability on activity of ^{7}Be in surface air. In addition to this, using this information the impact of the 11-y modulation on the^{7}Be air concentrations in Europe has been also demonstrated, by the yearly evolution from 1984 to 2011 of both ^{7}Be activity concentrations in air atsampling stations in the EU and sunspot number (Figure 2b).

Conclusions

This study has introduced to both the public and expert the existence of two environmental radioactivity databases at the European scales and it has been demonstrated the potentiality of them in the analysis and characterization the levels of radioactive contamination of the various compartments of the environment (air, water, soil).
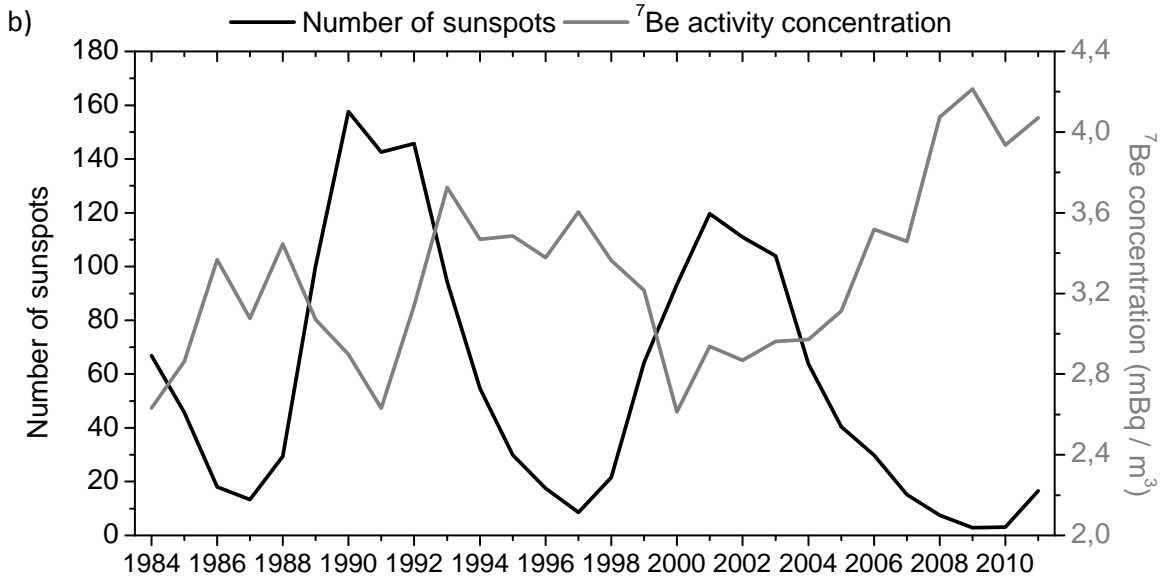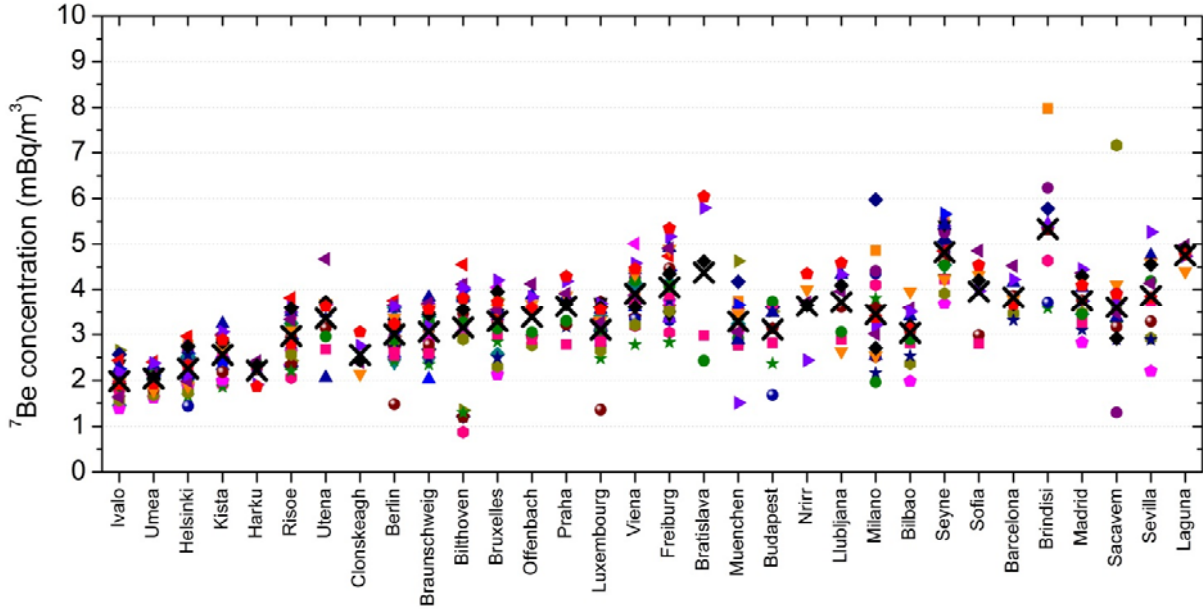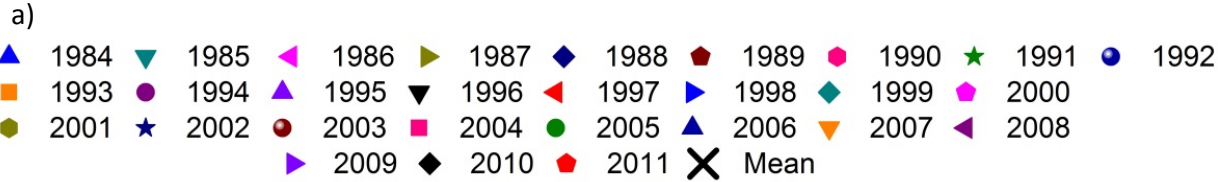
Figure 2.a) Average of the ^7Be at the different sites each year and the total average one (big black cross) and b)Yearly variations in the ^7Be activity concentration and sunspot number from 1984 to 2011 considering all sites(Hernández-Ceballos et al., 2015)

References

Bossew, P., Kirchner, G., De Cort, M., De Vries, G., Nishev, A., De Felice, L., 2012.Radioactivity from Fukushima Dai-ichi in air over Europe; part 1: spatio-temporalanalysis. Journal of Environmental Radioactivity, 114, 22-34.

European Commission (1998).The Atlas of caesium-137 contamination in Europe after the Chernobyl accident. In Kresson E (Ed) DG XII, Safety Programme for Nuclear Fission (Protection against Radiation), Joint Research Centre, Luxemburg.

Kirchner, G., Bossew, P., De Cort, M., 2012.Radioactivity from Fukushima Dai-ichi in air over Europe; part 2: what can it tell us about the accident?.Journal of Environmental Radioactivity, 114, 35-40.

Hernández-Ceballos, M.A., Cinelli, G., Marín Ferrer, M., Tollefsen, T., De Felice, L., Nweke, E., Tognoli, P.V., Vanzo, S., De Cort, M., 2015.A climatology of 7Be in surface air in European Union. Journal of Environmental Radioactivity, 141, 62-70.

DEPOSITION PATTERNS OF ATMOSPHERIC ^{7}Be, ^{210}Pb, AND ^{40}K INCOAST OF WEST MEDITERRANEAN SEA, MALAGA, SPAIN

C. Dueñas*[1], E. Gordo[2], S. Cañete[2], E. Liger[3], M. Pérez[4] and M. Cabello[1]

[1]University of Málaga, Department of Applied Physics I, Campus de Teatinos 29071Málaga, Spain
[2]University of Málaga, Central Research Facilities, Campus de Teatinos, 29071 Málaga, Spain
[3]University of Málaga,Department of Applied Physics II, Campus de Teatinos 29071 Málaga, Spain
[4]University of Málaga, Department of Radiology and Health Physics, Campus de Teatinos, 29071Málaga, Spain

Abstract

The deposition of radionuclides on the ground is an essential process to understand atmospheric transportation, sedimentation and geological process, being the major removal pathway for airborne particulates. To predict the long-term radiological consequences of an accidental deposition of the radionuclides to the ground, it is a prerequisite to know the environmental long-term behaviour of these radionuclides and a relatively large number of values are required for statistically meaningful conclusions. Nuclides of the natural decay chains, especially for ^{238}U decay chain, are widely applied into atmospheric research, oceanography and marine geology. Atmospheric depositional fluxes of ^{7}Be, ^{210}Pb and ^{40}K were simultaneously measured in monthly interval for eleven years (from January 2005 to December 20159 at Málaga (4 º28´ 8″W; 36º 43´40″N). The time variations of the different fluxes have been discussed in relation to various meteorological factors and the mean values have been compared to those published in recent literature for other sites located at different latitudes. Data of the atmospheric depositions of radionuclides in Málaga show clear seasonal variations which can be attributed to the meteorological conditions affecting the transport and deposition processes. The amount of rainfall controls mainly the depositional fluxes.There is a statistically relationship between ^{7}Be and ^{210}Pb fluxes indicating that removal behaviour from the atmosphere is relatively similar.

Introduction

The fluxes of radionuclides represents an important factor in environmental radioactivity monitoring and an important input parameter in radioecological models.It is well known that the main part of radioactivity deposition of natural as well as artificial radionuclides from the global nuclear weapons fallout takes place through wet precipitation and dry depositions. Precipitation scavenging is the removal of particulate matter and gases from the atmosphere through various types of precipitation.Following the deposition of ^{7}Be, ^{210}Pb and ^{40}K onto the Earth's surface is possible to study erosion, transportation and deposition of soils and sediments from episodic to continuous timescales with more details.

^{7}Be and ^{210}Pb are highly active particles and are easily scavenged by aerosols.Both have been used as aerosoltracers in studying the vertical transport and residence time of aerosols based on modified versions of the general circulation models.^{7}Be is produced in the upper troposphere and stratosphere and is removed from the atmosphere by radioactive decay and by wet and dry depositions.Most of the ^{210}Pb in the atmosphere is

---

[1]Corresponding autor, E-mail:mcduenas@uma.es

formed as a decay product of ^{222}Rn emanating from soil.^{40}K haslithogenic origin and is mainly originated from the suspension of soil.

The atmospheric fluxes of ^{7}Be, ^{210}Pb and ^{40}K for 11 years are continuously monitored in Málaga, discussing theirs temporal variations with the aim to better understand the influence of local meteorological conditions and the seasonal variations of mentioned fluxes are also discussed .Apart from simple methods of correlation analysis elements of multifactorial analysis were used for more precise investigation of their influence.Furthermore, scanty rainfall in the summer months will aid in quantifying the role of dry deposition of aerosols at the study site.

Material and methods

The study was carried out in the city of Málaga (4º 28′ 8″ W; 36º 43′ 40″N), in the south-east of the Iberian Peninsula, on the shores of the Mediterranean Sea and one of the provinces of the Andalusia Region, the southern-most region of Spain . The orography and climate of Málaga play an important role in the interpretation of the concentrations of aerosols.Due to the influence of the local topography, prevailing winds are from the SE and NW and these winds can be observed in the breezes of sea-land and land-sea, respectively. Málaga has a coastal Mediterranean climate with dry summers and mild winters generated under the intervention of three basic mechanisms: the influence of the sea, the South-facing coast which allows it to receive large number of hours of sunshine, and protection that give chains Béticas against Northern air masses. Due to its geographical vicinity with the African continent, our study area is frequently affected by intrusions of Saharan air with high concentrations of atmospheric particulate matter. Most of these Saharan dust plumes arrive in Spain between May and September. In the period January-June transport of Saharan dust toward Spain is mainly due to the cyclonic activities over the West or South of Portugal, while in the summer this transport is governed by the anti-cyclonic activities over the East or Southeast of Iberian Peninsula (Rodriguez et al., 2001).

Samples of bulk deposition were collected on a monthly basis from January 2005 to December 2015.Since the rain collector was exposed to the atmosphere continuously, the sum of the wet and dry fallout (bulk deposition) was collected. The sampling point is situated 14 m above the ground, on the flat roof of the SCAI building (University of Málaga) in an open area. The sample collection and processing procedures have been described elsewhere (Dueñas et al., 2011) .Briefly, a volume of 6L were reduced via evaporation to 1 L approximately and transferred to a Marinelli geometry container for gamma counting.

Gamma counting of the aerosols and bulk deposition samples was performed using an intrinsic germanium coaxial detector, Re-Ge-type (CANBERRA), to determine the radionuclides activities. Details of the efficiency and the low-background gamma-ray detection system used   have been previously described (Dueñas et al., 1999; 2011). The counting time was in the order of 90000-172000 s. The concentrations were corrected for decay to the mid-collection period using a 53 day half-life and 477.6 keV gamma-ray of ^{7}Be , 22.3 year half-life and 46.5 keV line of ^{210}Pb and $1.3 \cdot 10^{9}$ year half-life and 1460.81 keV line for ^{40}K .

The atmospheric fluxes are calculated using the expression:

$$F = A/St \ (Bq \ m^{-2} \ month^{-1}) \qquad\qquad (1)$$

Where A is the activity in the sample (Bq), S is the surface area of the collector and t is the duration of deployment (month).The activity of the sample is obtained from the gamma spectra.

Results and discussion

Table 1 provides some statistical information on atmospheric fluxes of ^{7}Be, ^{210}Pb and ^{40}K in Bq m^{-2}month^{-1} such as number of samples (N), average (AM), standard deviation (SD), geometric mean (GM), coefficient of variation (CV), Min, Max and standard error(SE).

Table 1.*Basic statistical parameters of atmospheric fluxes of ^{7}Be, ^{210}Pb and ^{40}K at the sampling station in the SCAY building of University of Málaga(January 2005-December 2015)*

	N	AM	SD	GM	CV	Min	Max	SE
^{7}Be	132	101.24	165.15	44.14	163.00	2.94	1284.01	14.37
^{210}Pb	132	12.10	16.22	6.93	134.11	0.90	102.30	1.41
^{40}K	67	5.59	11.31	2.78	202.17	0.47	81.06	1.38

The monthly depositional flux of ^{7}Be ranges from 2.94 to 1284 Bq m^{-2} month⁻1 (annual average = 1215 Bq m^{-2} year^{-1}). The lowest deposition occurring during the summer months (June, July and August) when in general there is no precipitation.The 20 % of measurement period (26 months) corresponds to months without precipitation and the depositional flux during these months is totally due to dry deposition. These dry periods occur more often duringJuly (11months), later June (8 months) and afterwards, August (7months). The average dry depositional fluxes for these dry months is approximately 12.6 Bq m^{-2} month^{-1}.If we assume that the dry deposition has remained constant throughout the period of measurement, the dry deposition would account for 12.5% of the bulk fallout.

The monthly depositional flux of ^{210}Pb varied between 0.90 and 102 Bq m^{-2} month^{-1} (annual average = 144 Bq m^{-2} year^{-1}).The average dry depositional flux of ^{210}Pb during dry months is 3.2 Bq m^{-2} month^{-1}. Likewise, ifwe assume that the dry deposition monthly has remained constant throughout the period of measurement, the dry deposition would account for 26.5 % of the bulk fallout. Thus, in our study, the dry deposition for ^{210}Pb is significantly higher than that for^7 Be and the differences are attributed to the differences in their sources, their half-lives and different contribution from resuspension dust particles .While ^{210}Pb in dust particles retains the memory of 32 years (the mean life of ^{210}Pb), ^{7}Be retains only for 77 days and hence the dry deposition removes higher proportions of ^{210}Pb relative ^{7}Be (Huch et al., 2006*).*Similar ranges of ^{7}Be and ^{210}Pbyearly deposition fluxes were found for western (Gonzalez Gomez et al. 2006; Garcia Orellana et al., 2006;Pham et al. 2013) and eastern (Ionannidou and Papastefanou, 2006) Mediterranean regions. For the inland sites the fluxes were generally higher(Winkler and Rosner, 2000;Mietelski et al.,2016) especially for ^{210}Pb due to the influence of continental air masses.

The Figure 1 reflects a strong correlation between monthly depositional flux of ^{210}Pb and monthly depositional flux of ^{7}Be (r = 0.91). Lead-210 and ^{7}Be in the atmosphere have distinct sources due to different modes of their production. This high correlation between these two radionuclides suggests that both radionuclides cannot be used as

independent atmospheric tracers at least for the areas similar to Málaga. This is also rather common observation (Baskaran et al., 1993; Kim et al., 2000; Caillet et al., 2001; McNeary and Baskaran, 2003) and suggest that deposition of both nuclides are largely governed by the same processes.

The monthly depositional flux of ^{40}K varied between 0.5 and 81 Bq m^{-2} month^{-1} (annual average = 67 Bq m^{-2} year^{-1}) .The average dry depositional flux of during dry months is 1.85 Bq m^{-2} month^{-1} (33% of bulk deposition).
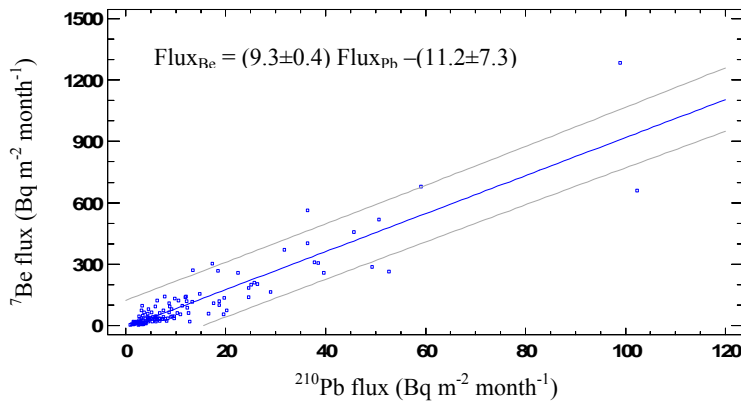
Figure1.Monthly depositional flux of ^7Be versus monthly depositional flux of ^{210}Pb in Málaga.

Figure 2 shows the seasonal patterns fluxes of ^7Be, ^{210}Pb and ^{40}K during four seasons:winter(January, February and March), spring (April, May and June), summer (July, August and September) andautumn (October, November and December)for the study period (2005-2011).The fluxes of ^7Be, ^{210}Pb and ^{40}K show a marked seasonal variation with higher values in winter and autumn months and lower values in spring and summer. In Málaga, the wet period comprises (approximately October-Abril) and the dry period (approximately May – September).There is several outliers for ^7Be and ^{210}Pb in all seasons while for^{40}K appear mainly in summer and autumn according to Figure 2.The seasonal results confirmed that most of the mentioned radionuclides were washout during months with generous precipitation amount
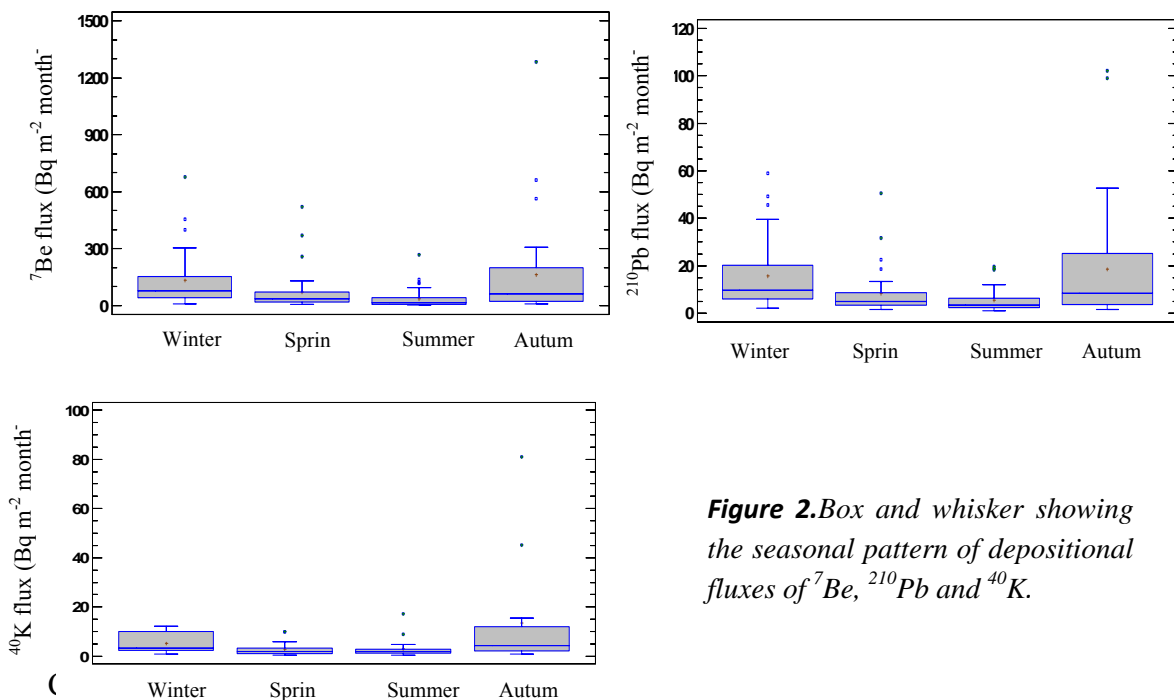
Figure 2.Box and whisker showing the seasonal pattern of depositional fluxes of ^7Be, ^{210}Pb and ^{40}K.

Correlation analysis is a useful technique to identify potential association between variables. We have performed a correlation study to identify parameters associated with fluctuations of fluxes of gamma radionuclides. Table 2 reports correlation coefficients values between fluxes of gamma radionuclides,meteorological variables (air temperature T, relative humidity RH, pressure P, distance travelled monthly by the wind Rv, amount of rainfall LL, duration of rainfall DL), and other variables such as number of African outbreaks and PM10.

Table 2._Correlation coefficients between radionuclides and different variables.Bold value denotes correlations significance level <0.05._

	^{7}Be	^{210}Pb	^{40}K	PM10	N°intr.	T	RH	P	Rv	LL	DL
^{7}Be	1	**0.91**	**0.50**	-0.06	-0.10	**-0.30**	**0.44**	-0.15	-0.13	**0.88**	**0.78**
^{210}Pb		1	**0.61**	-0.08	-0.13	**-0.33**	**0.48**	-0.16	-0.15	**0.90**	**0.81**
^{40}K			1	**0.33**	-0.08	-0.19	**0.47**	-0.24	-0.04	**0.66**	**0.60**
PM10				1	0.41	**0.46**	-0.12	-0.27	0.09	-0.09	-0.15
N° int.					1	0.70	-0.12	-0.27	0.21	-0.27	-0.15
T						1	**-0.52**	-0.37	0.16	**-0.43**	**-0.58**
RH							1	0.08	**-0.48**	0.54	0.56
P								1	-0.19	-0.13	-0.08
Rv									1	-0.18	-0.12
LL										1	0.92
DL											1

^{7}Be, ^{210}Pb and ^{40}K fluxes show the highest correlation with amount of rainfall as well as duration of rainfall. Also the fluxes of mentioned radionuclides show good relationship between them.All depositional fluxes of ^{7}Be, ^{210}Pb and ^{40}K show a poor correlation with other factors except the air temperature and relative humidity, with exception of ^{40}K flux with air temperature.Note that depositional flux of ^{40}K shows a good correlation with PM10 data (r = 0.33).

Conclusions

This work reports the results of a study focused on the temporal variations and statistical analysis for depositional fluxes of three natural radionuclides ^{7}Be, ^{210}Pb,^{40}K collected over the years 2005-2015 at the Spanish coastal station of Málaga. The monthly depositional flux of ^{7}Be, ^{210}Pb and ^{40}K ranged between 3 and 1284, between 1 and 102, and 0.5 and 81 Bq m^{-2} month^{-1} respectively.

- Both depositional flux of ^{7}Be and ^{210}Pb show seasonal trends and are linearly correlated indicating that atmospheric removal mechanism is relatively similar.The annual dry depositional flux is estimated to be 12.5%of the total flux for ^{7}Be, whereas for ^{210}Pb fraction of dry depositional flux appears to be

higher (24%). This could be explained because theresuspended soil dust is enriched in ^{210}Pb.

- The fluxes of radionuclides show a positive correlation with amount of rainfall as well as duration of rainfall and a poor correlation with other variables.

References

Baskaran, M., Coleman,C.H.,Santschi,P.H.,1993.Atmospheric depositional fluxes of ^{7}Be and ^{210}Pb at Galveston and College Station, Texas.*J. Geophys. Res*. 98 (20,555-20,571, doi: 10, 1029/93JD02182.

Caillet, S., Arpagaus,P., MonnaF, Dominik,J., 2001. Factors controlling ^{7}Be and ^{210}Pb atmospheric deposition as revealed by sampling individual rain events in the region of Geneva, Switzerland. J.Environ. Radioact., 53:241-256, doi.0.1016/S0265-931X(00900130-2

Dueñas, C., Fernández, M.C., Liger, E., Carretero, J. E., 1999. Gross-alpha, gross-beta activities and ^{7}Be concentrations in surface air: analysis of their variations and prediction model. Atmos. Environ. 33: 3705-3715.

Dueñas, C., Fernández, M.C., Gordo, E., Cañete S., Pérez M., 2011.Gross alpha, gross beta activities and gamma emitting radionuclides composition of rainwater samples and deposition to ground. Atmos. Environ. 45: 1015-1024.

Garcia-Orrellana, J., Sánchez-Cabeza, J.A., Masqué, P.,Avila, A.,Costa, E.,Loÿe-Pilot, M.D.,Bruach-Menchén,J.M.,2006.Atmospheric fluxes of ^{210}Pb to the Western Mediterranean sea and the Saharan dust influence.J. Geophys. Res., 1I11,D15305, doi1029/2005JD006660.

Gonzalez Gómez C., Azahra, M.,López-Peñalver, J.J.,Camacho-Garcia, A., Bardouni T.El.,Boukhal, H.2006.seasonal variability in 7Be deposition fluxes at Granada, Spain.Appl. radiat. Isotope,64:228-234.

Huch, C.A., Su C. C., Shiau L.J., 2006. Factors controlling temporal and spatial variations of atmospheric deposition of ^{7}Be and ^{210}Pb in northern of Taiwan. J. Geophys. Res. 111:D16304, doi: 10. 1029/2006JD007180.

Iannidou, A.,Pappastefanou, C.,2006.Precipitation scavenging of ^{7}Be and ^{137}Cs radionuclides in air. J. Environ. Radioact. 85:121-126.

Kim, G., N., Hussain,J.R., Scudlarrk and M. Church (2000).Factor s influencing the atmospheric depositinal fluxes of stable Pb, Pb-210 and Be-7 into Chesapeake Bay. *J. atmos. Chem.* 36, 65-70, doi:10.1023/A:1006383030362

McNeary,D., and Baskaran ,M., ,2003.Depositional characteristics of ^{7}Be and ^{210}Pb in southeastern Michigan, J. Geophys. Res., 108(D7), 4210, doi:10.1029/2002JD003021.

Mietelski, J.W., E. Nalichowska, E. Tomankiewicz, K. Burdecki, P.Janowski and R. Kierepko, 2016. Gamma emitters in atmospheric precipitation in Krakow (Southern Poland) during the years 2005-2015. *J. Environ. Radioct*. Doi.org/10.1016/j.jenvrad.2016.02.010

Pham, M.K., Povinec, P., Nies, H., Betti, M. 2013.Dry and wet deposition of ^{7}Be,^{210}Pb and ^{137}Cs in Mónaco air during 1998-2010:seasonal variations of deposition fluxes. J. Environ. Radioaact. 120:45-57

Rodríguez, S., X. Querol , A., Alastuey., G., Kallos,and O. Kakaliagou, (2001) Saharan dust contributions to PM10 and TSP levels in Southern and Eastern Spain. *Atmos. Environ*, 35,2433-2447

Winkler, R., and, G. Rosner (2000). Seasonal and long term variation of ^{210}Pb concentration in air atmospheric deposition velocity in south Germany. *Sci. Tot. Environ*. 263, 57-68.

Winter extremes of beryllium-7 surface concentrations in northern Europe

J. Ajtić[1,2,] V. Djurdjevic[3], M. A. Hernández-Ceballos[4] and E. Brattich[5]*

[1] Faculty of Veterinary Medicine, University of Belgrade, Bulevaroslobođenja 18, 11000 Belgrade, Serbia
[2] Institute for Research and Advancement in Complex Systems, Zmaja od Noćaja 8, 11000 Belgrade, Serbia
[3] Institute of Meteorology, Faculty of Physics, University of Belgrade, Studentskitrg 18, 11000 Belgrade, Serbia
[4] European Commission, Joint Research Centre, Knowledge for Nuclear Security and Safety Unit
Radioactivity Environmental Monitoring Group, Via Enrico Fermi 2749, I-21027 Ispra (VA), Italy
[5] Environmental Chemistry and Radioactivity Laboratory, Department of Chemistry "G. Ciamician", Alma Mater
Studiorum University of Bologna, Via Selmi 2, 40126 Bologna, BO, Italy

Abstract

Specific activity of cosmogenic [7]Be in surface air generally shows a spring-summer maximum. However, extremely high [7]Be concentrations in surface air also occur during winter. The aim of our analysis is to characterise temporal and spatial prevalence of winter extreme events, and to investigate the associated synoptic meteorological conditions in northern Europe. Four measurement sites, with an approximate weekly sampling rate over the 2001–2010 period, are selected from the online Radioactivity Environmental Monitoring (REM) Database. The extremes in the [7]Be surface concentration are defined as measurements above the 90th percentile in each location.The results indicate that at each measurement site, 10–20 % of the extremes occur during winter (November, December, January and February). Two types of [7]Be extremes are distinguished: 1) approximately half of these occurrences are isolated events detected in one or two stations, and 2) the other half are events grouped within four months, when at least three [7]Be extremes per month are observed. The monthly Scandinavia (SCAND) teleconnection index for isolated extreme events (type-1) is positive and, with only one exception, larger than 0.4, while in the case of type-2 events, the monthly SCAND is very high (larger than 1).This finding implies that in northern Europe during winter, the atmospheric conditions associated with a high SCAND index facilitate an occurrence of extreme [7]Be surface concentration.

Introduction

Cosmogenic beryllium-7 reaches the Earth's surface via vertical transport. This radioisotope is produced in spallation reactions that occur in the upper troposphere and lower stratosphere (UTLS region) (Lal & Peters, 1967), and is further transported through the atmosphere attached to fine aerosols (Dueñas et al., 2004; Heikkilä et al., 2008; Koch et al., 1996). The [7]Be downward transport to the Earth's surface is governed by the horizontal and vertical winds (Cristofanelli et al., 2006; Gerasopoulos et al., 2003).During this transport to the surface, high [7]Be specific activity typical of stratospheric air masses is decreased through radioactive decay, mixing with surrounding air of a lesser [7]Be concentration, and removal processes (Feely et al., 1989).

Due to arelatively long [7]Be half-life of 53.22 days, air masses that reach the Earth's surface in a fast subsidence from the UTLS region,can retain, to a certain extent, their signature of high [7]Be concentration (Husain et al., 1977). Since mixing diminishes the stratospheric properties of air within a few days (Appenzeller& Davies, 1992), the descent needs to occur fast enough so that the overall effect of mixing does not result in a complete loss of the [7]Be concentration gradient. Another condition that must hold is an absence of precipitation (Ajtić et al., 2013, 2016; Gerasopoulos et al., 2001), which has been shown to be the major removal mechanism of [7]Be from the atmosphere (Ioannidou& Papastefanou, 2006; Papastefanou &Ioannidou, 1991; Pham et al., 2011).

---

[*]Corresponding author, E-mail: jelena.ajtic@vet.bg.ac.rs

The [7]Be specific activity in surface air shows an annual pattern with a maximum in the spring-summer season, which has been attributed to an increased vertical transport from the UTLS. In spring, relatively frequent stratospheric intrusions (Cristofanelli et al., 2006; Elbern et al., 1997; Feely et al., 1989) enrich the troposphere with air masses of high [7]Be concentration, while in summer, efficient vertical mixing brings [7]Be-rich air from the upper troposphere down to the surface (Gerasopoulos et al., 2001, 2003; Feely et al., 1989;).

Cases of high [7]Be surface concentration have been previously investigated, mostly in alpine stations in Europe (Cristofanelli et al., 2006; Elbern et al., 1997; Gerasopoulos et al., 2001; Stohl et al., 2000; Zanis et al., 1999). In some studies, a fixed limit of 8 mBq/m^{3} (Cristofanelli et al., 2006; Hernández-Ceballos et al., 2016b; Stohl et al., 2000) was used as a threshold defining the events of high [7]Be concentration. However, the abundance of [7]Be in surface air depends on the latitude (Doering&Saey, 2014; Feely et al., 1989; Hernández-Ceballos et al., 2015, 2016a; Kulan et al., 2006; Persson& Holm, 2014) and some locations show frequent measurements above this threshold (Buraeva et al., 2007; Hernández-Ceballos et al., 2016b; Petrova et al., 2009). Hence, a relative threshold that is specific for each measurement site, as introduced by Ajtić et al. (2016), could be more suitable for investigation of extremely high [7]Be concentrations over an extended geographical region.

Elevated [7]Be specific activities at the surface have been shown to occur outside the warm season (Ajtić et al., 2016; Hernández-Ceballos et al., 2016b), and the aim of this paper is to characterise temporal and spatial prevalence of extremely high [7]Be surface concentrations that occur during winter in northern Europe. Northern Europe has been identified as one of three distinct regions of [7]Be behaviour in surface air (Ajtić et al., 2015; Hernández-Ceballos et al. 2015,2016c), and although this radionuclide's records in Scandinavia have been previously studied (Leppänen et al., 2010, 2012; Leppänen&Paatero, 2013), the extremes in the [7]Be records have only been investigated for Helsinki, Finland (Ajtić et al., 2016).

Materials and Methods

Datasets

Measurements of the [7]Be specific activity in surface air are a part of the data stored in the Radioactivity Environmental Monitoring Database (REMdb) that encompasses a wider collection of different environmental radioactivity measurements in a large number of environmental sample types in Europe. The REMdb contains measurements since 1984. The [7]Be activity concentrations in surface air used in this study are a part of the sparse network consisting of high-sensitivity measurements performed in 34representative locations in Europe.

The REMdb is supported by REM group of the DG Joint Research Centre (JRC). The [7]Be measurements prior to 2007 are public, while the access to the data corresponding to the 2007–2011 period can be granted only after explicit request. More details on the REMdb and [7]Be specific activity measurements can be found in Hernández-Ceballos et al. (2015) and the REMdb monitoring reports (https://rem.jrc.ec.europa.eu/RemWeb/Reports.aspx).

Monthly Scandinavia teleconnection indices (SCAND) were taken from the NOAA Climate Prediction Center (http://www.cpc.ncep.noaa.gov/data/teledoc/scand.shtml accessed 12 July 2016). The index values were standardised by the 1981–2010 climatology.

Study area

Four measurement sites, covering the northernmost region of Europe (55–69 °N; 12–28 °E), were chosen from the REM database. In these sites, approximately one measurement per week was

performed over the 2001–2010 period, thus giving a total of approximately500 data points per each site. Table 1 shows the details of the chosen locations.

Table 1. *Measurement locations with their latitude and longitude, total number of measurements over 2001–2010, value of the 90th percentile, total number of extremes and extremes during winter.*

Measurement location	Latitude and longitude (°N; °E)	Total number of samples	90 % threshold (mBq/m^3)	Number of extremes	Number of winter extremes
Ivalo	(68.64; 27.57)	486	3.09	48	7
Umea	(63.85; 20.34)	496	3.39	49	5
Kista	(59.40; 17.93)	512	4.54	51	6
Risoe	(55.69; 12.10)	517	4.96	51	10

Methodology

In this analysis, the winter season was extended to four months: November, December, January and February (NDJF). Extremes in the ^{7}Be surface concentration were defined as measurements above the 90th percentile. The percentiles were calculated for each measurement locationcovering the whole period considered, thus obtaining an extreme criterion specific to each site (Ajtić et al., 2016). Table 1 also presents the 90% thresholds, along with the total number of extremes and winter extremes for each station.

Back-trajectory calculations

Hourly kinematic 3D backward trajectorieswere calculated over a 120-h period and at final heights of 500 m, 1500 m and 3000 m above ground level,using the Hybrid Single ParticleLagrangian Integrated Trajectory (HYSPLIT) modeldeveloped by the NOAA's Air Resources Laboratory (Draxler et al.,2012). Model-calculated vertical velocities were used to compute backward trajectories, and the Global Data Assimilation System meteorological data set was used (information available online at http://ready.arl.noaa.gov/archives.php). These files have a spatial resolution of 1°x1° in latitude and longitude (111 km x 111 km), enough to resolve movement of air masses and its impact on the synoptic transport.
Since air masses with stratospheric properties, such as low temperature and low relative humidity, have been detected deep in the troposphere, at 3 km (Di Girolamo et al., 2009), we used this height as a tentative indication of stratospheric intrusion.

Potential vorticity anomaly calculations

Wind and temperature pressure level data from the NCEP/NCAR reanalysis (Kalnay et al., 1996) were used to calculate the potential vorticity (PV) anomalies at the 300 hPa level over the Northern Hemisphere. First, for each investigated month, November, December, January and February, long-term monthly mean PV over 1981–2010 was calculated, and then,for each day, the PV anomaly was obtained by subtracting daily PV field from the long-term mean for the corresponding month. For example, 31x30 (number of days in January x number of years over 1981–2010) anomaly PV fields were constructed for the month of January.
Further, for each grid point in the Northern Hemisphere and for each month, the 90th percentile in the PV anomaly series was calculated. This value was subsequently used in our analysis to separate areas with strong PV anomalies–a grid point was considered to have a "strong" PV anomaly if it was above the calculated 90th percentile for the given grid. This methodology enabled us to take into account the PV variability in the meridional direction, but also its month to month variability, as well as to avoid using a single fixed value as a threshold.

Results and Discussion

Table 1 shows the contribution of the winter extremes to the total number of extremes. The contribution rangedbetween 10 % in Umea, and 20 % in Risoe. Overall, for the four investigated measurements sites, there were 199 measurements above the 90th percentile, out of which 28 (14 %) occurred in (the four months of) winter.

The winter extremes were grouped according to the month in which they were registered,and two types of events were distinguished according to their spatial and temporal prevalence:

− type-1, when the number of extremes in a given month was less than three, and

− type-2,when at least three extremes occurred in a month – the extremes were either coincident (within a day) at three different sites, or consecutive extremesat one location with at least one extreme occurring elsewherein the region.

Table 2 shows the two types of the winter extremes and the corresponding monthly Scandinavia teleconnection index.

Table2. *Two types of winter ^{7}Be extremes and the corresponding monthly value of the SCAND index.*

Extreme type	Date (YYYYMM)	Site andthe end date of the measurement period in parenthesis	SCAND
Type-1	200502	Ivalo (13), Umea (28)	0.74
	200511	Risoe (14)	0.49
	200712	Kista (25), Risoe (21)	0.43
	200801	Ivalo (07), Kista (06)	0.46
	200901	Ivalo (19), Umea (12)	0.06
	200902	Ivalo (09), Umea (09)	0.53
	200911	Ivalo (09)	0.82
	200912	Kista (21)	0.86
Type-2	200302	Ivalo (23), Umea (24), Risoe (24)	1.55
	200601	Ivalo (23), Kista (23), Risoe (09, 23)	2.11
	201001	Kista (25), Risoe (18, 26)	1.23
	201002	Umea (01), Kista (01), Risoe (01, 08, 15)	1.04

It should be noted here that the end day of the ^{7}Be measurement period (the usual duration of the measurement periods for the four sites was six to eight days) was taken as the representative day of the whole period. In other words, a time stamp corresponding to the last day of the measurement period was given to the observed occurrence of extremely high ^{7}Be surface concentration. For example, three ^{7}Be extremes, in Ivalo, Umea and Risoe, were detected during February 2003 (Tab. 2), and we marked these events with the last day of the observation period for each of the sites, which was 23 February for Ivalo, and 24 February for Umea and Risoe.

The SCAND pattern consists of a primary circulation centre over Scandinavia, with weaker centres of opposite sign over western Europe and eastern Russia / western Mongolia (Barnston&Livezey, 1987). Over Scandinavia, the positive phase of the SCAND pattern is associated with: positive height anomalies, sometimes reflecting major blocking anticyclones; below-average temperatures; and below-average precipitation. These characteristics of the SCAND positive phase can be favourable for a stratospheric intrusion and an ensuing fast descent of air masses (Davies &Schuepbach, 1994; Di Girolamo et al., 2009; Kentarchos et al., 1998; Zanis et al., 2003).

For type-1 events (Tab. 2), except the one that occurred in January 2009, SCAND was close to or higher than 0.5 (the values of SCAND greater than 0.5 fall into the 66th percentile). For type-2 events, SCAND was above 1 (the 95th percentile). During February 2003, when a type-2 event was registered (Tab. 2), an extreme ^{7}Be occurrence was also noted in Helsinki, Finland (Ajtić et al., 2016).

Over 2001–2010, the winter SCAND index greater than 1 was observed in other two instances: in January 2001 and November 2003, when the SCAND index was 1.45 and 1.51, respectively. However, they were not accompanied by an extreme[7]Be occurrence.

We performed back-trajectory calculations to further analyse the transport conditions associated with the extreme [7]Be events. Figure 1 gives an example forthe type-2 event in February 2003, with 23 and 24 February taken as the representative days of the extremes (as briefly described above), and thus the starting days for the back-trajectory calculations.The trajectories for Umea and Risoe on 24 February 2003 had a clear anticyclonic movement, as expected in a situation with a high-pressuresystem over Scandinavia (corresponding to high values of SCAND), which further implied that sources of high [7]Be concentrations were located in a wider area on the edges of this high-pressure system. In each measuring location, there were trajectorieswith altitudes above 3000 m, some of which passed through grids of anomalously high PV values.
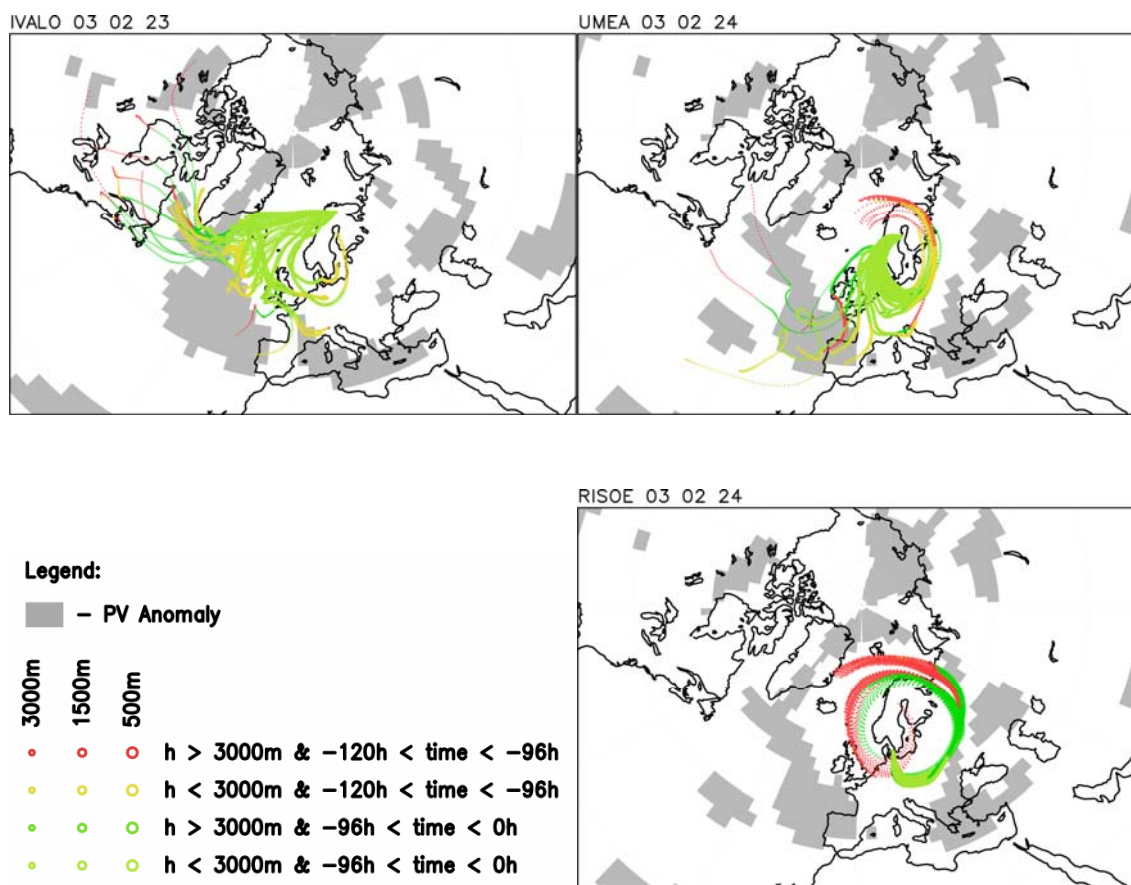
*Figure 1.*Back trajectories for Ivalo, Umea and Risoe. The trajectories started on therepresentative daysof the [7]Be extremes detected in February 2003, and were run backwards for five days. Three starting altitudes were chosen: 3000 m (small circles), 1500 m (medium-sized circles) and 500 m (large circles). The altitudes of the trajectories are colour coded: red and yellow if on the last day of calculations (between -96hours and -120hours), the altitude was higher or lower than 3000 m, respectively; dark and light green ifat any time during the first four days of calculations (between 0hours and -96hours), the altitude was higher or lower than 3000 m, respectively.Given in grey are areas whereinthe PV anomaly was above the 90th percentile threshold for the fourth (-96 hours) and fifth (-120 hours) day of the back-trajectory calculations in corresponding reanalysis grid points.

Although our approach needs a stricter statistical analysis of backtrajectories, their overall pattern for all the identified [7]Be extreme events showed a number of anticyclonictrajectories passing through fields of anomalously high potential vorticity above 3000 m.

Conclusions

Our results showed thatextremely high [7]Be surface concentrations in northern Europe occur over the November–February months. These winter extremes contributed between 10 % (in Umea) and 20 % (in Risoe) to the total number of extremes observed over the 2001–2010 period.

Two types of the [7]Be extremes were distinguished:isolated events detected in one or two stations (type-1), and extremes grouped within four months (February 2003, January 2006, and January and February 2010), when at least three [7]Be extremes per month were observed (type-2). In the case of type-1 extreme events, the monthly SCAND was positive and, with only one exception, larger than 0.4, while for type-2 events, the monthly SCAND was very high (larger than 1). This finding implies that in northern Europe during winter, the atmospheric conditions associated with a high SCAND index facilitate an occurrence of extreme [7]Be surface concentrations.The analysis of backtrajectories run for five days backwards from the representative dates of the extreme occurrences showed a prevailing pattern withanticyclonic trajectories passing through areas of anomalously high potential vorticity fields above 3000 m.

References

Ajtić, J.V., Todorović, D.J., Nikolić, J.D., Đurđević, V.S., 2013. A multi-year study of radioactivity in surface air and its relation to climate variables in Belgrade, Serbia. Nucl. Technol. Radiat. 28, 381–388.

Ajtić, J., Djurdjevic, V., Sarvan, D., Todorović, D., Nikolić J., 2015. Beryllium-7 and tropopause height: An analysis of correlations across latitudinal belts, in: Proceedings of XXVIII Symposium of the Radiation Protection Society of Serbia and Montenegro, Institute for Nuclear Sciences "Vinča" and Radiation Protection Society of Serbia and Montenegro, Belgrade, pp. 35–42, http://dzz.org.rs/wp-content/uploads/2013/06/2015-XXVIII-DZZSCG-Vrsac.pdf

Ajtić, J., Djurdjevic, V., Sarvan, D., Brattich, E., Hernández-Ceballos, M.A., 2016. Analysis of extreme beryllium-7 specific activities in surface air. Rad. Applic., in press.

Appenzeller, C., Davies, H.C., 1992. Structure of stratospheric intrusions into the troposphere. Nature 358, 570–572.

Barnston, A.G., Livezey, R.E., 1987. Classification, seasonality and persistence of low-frequency atmospheric circulation patterns. Mon. Weather Rev. 115, 1083–1126.

Bonasoni, P., Evangelisti, F., Bonafe, U., Ravegnani, F., Calzolari, F., Stohl, A., Tositti, L., Tubertini, O., Colombo, T., 2000. Stratospheric ozone intrusion episodes recorded at Mt. Cimone during the VOTALP project: case studies. Atmos. Environ. 34, 1355–1365.

Buraeva, E.A., Davydov, M.G., Zorina, L.V., Malyshevskii, V.S., Stasov, V.V., 2007. Content of cosmogenic [7]Be in the air layer at the ground at temperate latitudes. Atom. Energ. 102, 463–468.

Cristofanelli, P., Bonasoni, P., Tositti, L., Bonafè, U., Calzolari, F., Evangelisti, F., Sandrini, S., Stohl, A., 2006. A 6-year analysis of stratospheric intrusions and their influence on ozone at Mt. Cimone (2165 m above sea level). J. Geophys. Res., 111, doi: 10.1029/2005JD006553.

Davies, T.D., Schuepbach, E., 1994. Episodes of high ozone concentrations at the Earth's surface resulting from transport down from the upper troposphere/lower stratosphere: A review and case studies. Atmos. Environ. 28, 53–68.

DiGirolamo, P., Summa, D., Ferretti, R., 2009. Multiparameter Raman Lidar Measurements for the Characterization of a Dry Stratospheric Intrusion Event. J. Atmos. Oceanic Tech. 26, 1742–1762.

Doering, C., Saey, P., 2014. Hadley cell influence on [7]Be activity concentrations at Australian mainland IMS radionuclide particulate stations. J. Environ. Radioact. 127, 88–94.

Draxler, R.R, Stunder, B., Rolph, G., Taylor, A., 2012. HYSPLIT_4 User's Guide, via NOAA ARL Website. Silver Spring, MD: NOAA Air Resources Laboratory.

Dueñas, C., Fernández, M.C., Carretero, J., Liger, E., Cañete, S., 2004. Long-term variation of the concentrations of long-lived Rn descendants and cosmogenic [7]Be and determination of the MRT of aerosols. Atmos. Environ. 38, 1291–1301.

Elbern, H., Kowol, J., Sládkovic, R., Ebel, A., 1997.Deep stratospheric intrusions: A statistical assessment with model guided analyses. Atmos. Environ. 31, 3207–3226.

Feely, H.W., Larsen, R.J., Sanderson, C.G., 1989. Factors that cause seasonal variations in beryllium-7 concentrations in surface air. J. Environ. Radioact. 9, 223–249.

Gerasopoulos, E., Zanis, P., Stohl, A., Zerefos, C.S., Papastefanou, C., Ringer, W., Tobler, L., Hübener, S., Gäggeler, H.W., Kanter, H.J., Tositti, L., Sandrini, S., 2001. A climatology of [7]Be at four high-altitude stations at the Alps and the Northern Apennines. Atmos. Environ. 35, 6347–6360.

Gerasopoulos, E., Zerefos, C.S., Papastefanou, C., Zanis, P., O'Brien, K., 2003. Low-frequency variability of beryllium-7 surface concentrations over the Eastern Mediterranean. Atmos. Environ. 37, 1745–1756.

Heikkilä, U., Beer, J., Alfimov, V., 2008. Beryllium-10 and beryllium-7 in precipitation in Dübendorf (440 m) and at Jungfraujoch (3580 m), Switzerland (1998–2005). J. Geophys. Res. 113, doi:10.1029/2007JD009160.

Hernández-Ceballos, M.A., Cinelli, G., Marín Ferrer, M., Tollefsen, T., De Felice, L., Nweke, E., Tognoli, P.V., Vanzo, S., De Cort, M., 2015.A climatology of [7]Be in surface air in European Union. J. Environ. Radioact. 141, 62–70.

Hernández-Ceballos, M.A., Brattich, E., Cinelli, G., Ajtić, J., Djurdjevic. V., 2016a. Seasonality of [7]Be concentrations in Europe and influence of tropopause height. Tellus B 68, 29534, http://dx.doi.org/10.3402/tellusb.v68.29534

Hernández-Ceballos, M.A., Brattich, E., Lozano, R.L., Cinelli, G., 2016b. [7]Be behaviour and meteorological conditions associated with [7]Be peak events in Spain. J. Environ. Radioact. Available online 5 April 2016.

Hernández-Ceballos, M.A., Cinelli, G., Tollefsen, T., Marín Ferrer, M., 2016c. Identification of airborne radioactive spatial patterns in Europe – Feasibility study using Beryllium-7. J. Environ. Radioact. 155–156, 55–62.

Husain, L., Coffey, P.E., Meyers, R.E., Cederwall, R.T., 1977. Ozone transport from stratosphere to troposphere. Geophys. Res. Lett. 4, 363–365.

Ioannidou, A., Papastefanou, C., 2006. Precipitation scavenging of [7]Be and ^{137}Cs radionuclides in air. J. Environ. Radioact. 85, 121–136.

Kalnay, E., Kanamitsu, M., Kistler, R., Collins, W., Deaven, D., Gandin, L., Iredell, M., Saha, S., White, G., Woollen, J., Zhu, Y., Leetmaa, A., Reynolds, R., Chelliah, M., Ebisuzaki, W., Higgins, W., Janowiak, J., Mo, K. C., Ropelewski, C., Wang, J., Jenne, R., Joseph, D., 1996. The NCEP/NCAR 40-Year Reanalysis Project. Bull. Am. Meteorol. Soc. 77, 437–471.

Kentarchos, A.S., Davies, T.D., Zerefos, C.S., 1998. A low latitude stratospheric intrusion associated with a cut-off low. Geophys. Res. Lett. 25, 67–70.

Koch, D.M., Jacob, D.J., Graustein, W.C., 1996. Vertical transport of tropospheric aerosols as indicated by [7]Be and ^{210}Pb in a chemical tracer model. J. Geophys. Res. 101, 18651–18666, doi:10.1029/96JD01176.

Kulan, A. Aldahan, A., Possnert, G., Vintersved, I., 2006. Distribution of [7]Be in surface air of Europe. Atmos. Environ. 40, 3855–3868.

Lal, D., Peters, B., 1967. Cosmic ray produced radioactivity on the earth, in: Sitte, K. (Ed.), Cosmic Rays II. Springer Berlin Heidelberg, pp. 551–612.

Leppänen, A.-P., Pacini, A.A., Usoskin, I.G., Aldahan, A., Echer, E., Evangelista, H., Klemola, S., Kovaltsov, G.A., Mursula, K., Possnert, G., 2010. Cosmogenic [7]Be in air: A complex mixture of production and transport. J. Atmos. Sol.-Terr. Phys. 72, 1036–1043.

Leppänen, A.-P., Usoskin, I.G., Kovaltsov, G.A., Paatero, J., 2012. Cosmogenic [7]Be and [22]Na in Finland: Production, observed periodicities and the connection to climatic phenomena. J. Atmos. Sol.-Terr. Phys. 74, 164–180.

Leppänen, A.-P., Paatero, J., 2013. [7]Be in Finland during the 1999–2001 Solar maximum and 2007–2009 Solar minimum. J. Atmos. Sol.-Terr. Phys. 97, 1–10.

Papastefanou, C., Ioannidou, A., 1991. Depositional fluxes and other physical characteristics of atmospheric beryllium-7 in the temperate zones (40°N) with a dry (precipitation-free) climate. Atmos. Environ. 25A, 2335–2343.

Persson, B.R.R., Holm, E., 2014. [7]Be, ^{210}Pb, and [210]Po in the surface air from the Arctic to Antarctica. J. Environ. Radioact. 138, 364-374.

Petrova, T.B., Mikljaev, P.S., Vlasov, V.K., Afinogenov, A.M., Kirjukhin, O.V., 2009. Variations in the [7]Be Content in the Ground Layer of the Atmosphere at Middle Latitudes. Moscow Univ. Chem. Bull. 64, 317–321.

Pham, M.K., Betti, M., Nies, H., Povinec, P.P., 2011.Temporal changes of [7]Be, ^{137}Cs and ^{210}Pb activity concentrations in surface air at Monaco and their correlation with meteorological parameters. J. Environ. Radioact. 102, 1045–1054.

Stohl, A., Spichtinger-Rakowsky, N., Bonasoni, P., Feldmann, H., Memmesheimer, M., Scheel, H.E., Trickl, T., Hübener, S., Ringer, W., Mandl, M., 2000. The influence of stratospheric intrusions on alpine ozone concentrations. Atmos. Environ. 34, 1323–1354.

Zanis, P., Schuepbach, E., Gäggeler, H.W., Hübener, S., Tobler, L., 1999. Factors controlling beryllium-7 at Jungfraujoch in Switzerland. Tellus B 51, 789–805.

Zanis, P., Gerasopoulos, E., Priller, A., Schnabel, C., Stohl, A., Zerefos, C., Gäggeler, H.W., Tobler, L., Kubik, P.W., Kanter, H.J., Scheel, H.E., Luterbacher, J., Berger, M., 2003. An estimate of the impact of stratosphere-to-troposphere transport (STT) on the lower free tropospheric ozone over the Alps using [10]Be and [7]Be measurements. J. Geophys. Res. 108, doi: 10.1029/2002JD002604.

Acknowledgement:

EVENTS AFFECTING LEVELS OF GROSS ALPHA AND GROSS BETA ACTIVITIES AND HEAVY METALS COMPOSITION OF AIRBORNE PARTICULATE SAMPLES

E. Liger[1]*, C. Dueñas[2], E. Gordo[3], S. Cañete[3], M. Cabello[2] and M. Pérez[4]

[1]University of Málaga, Department of Applied Physics II, Campus de Teatinos, 29071 Málaga, Spain
[2] University of Málaga, Department of Applied Physics I, Campus de Teatinos, 29071 Málaga, Spain
[3] University of Málaga, Central Research Facilities, Campus de Teatinos, 29071 Málaga, Spain
[4] University of Málaga, Department of Radiology and Health Physics, Campus de Teatinos, 29071 Málaga, Spain

Abstract

The control of the atmospheric air quality is one of the most important tasks of environmental protecting programs. The air quality is a basic factor for the ecological balance and human health. Concentrations of radionuclides in air are continuously monitored in Málaga, a Mediterranean coastal city in South Spain located to receive pollution from different sources by means of air mass transport. Although gross-alpha and gross-beta measurements are generally made as a means of ''screening'' for unusual levels of radioactivity, these measurements are of interest since they allow establishing trends in radionuclide concentrations in the atmosphere and their measurements bring always new knowledge about exchange processes in the atmosphere, about its pollutants levels as well as the population exposures. Heavy metals in aerosol collected were determined as a complementary contribution to this study and was carried out using non-destructive wavelength dispersive X-ray fluorescence (WDXRF) analysis. Correlation analysis was carried out to examine dependences that may exist among the input variables. The effect of the long-range transported African dust on total alpha and beta activities together with metal concentrations, PM_{10} and other gaseous pollutants was also examined at our sampling coastal site.

Introduction

The association of particulate matter with adverse health effects has been recognized for a long time and plays a significant role in global climate and ecosystem cycling. Air quality and climate effects are not only dependent on the particle number concentration and size but also on their chemical composition. Information about aerosol composition and their sources especially during pollution events can be further used to establish strategies for the reduction of particulate matter concentration. The control of the atmospheric air quality can be considered one of the most important tasks of the environmental protecting programs as cleanness of the atmosphere is a basic factor for the ecological balance and human health (Landing and Paytan, 2010).

Knowledge of the total alpha and beta radioactivity in the ambient air is important in performing radiological impact assessment of various anthropogenic activities and aims to secure the increased standard of life in modern societies. Gross-alpha and gross-beta radioactivity measurements are generally made as a means of screening for unusual levels of radioactivity and are of particular interest for routine monitoring purposes. Nonetheless, these measurements are also of interest since they allow establishing trends in radionuclide concentrations in the atmosphere and the calculation of aerosol residence times. The concentrations of the atmospheric radionuclides and stable elements can vary substantially with location. Therefore their measurements bring always new knowledge about exchange processes in the atmosphere, air quality as well as the population exposures.

Among many pollutants, heavy metals are the most toxic component for all living organisms. Heavy metals are presented in the atmosphere in organic and also in inorganic forms, in the form of dust

---

*Corresponding author, E-mail: eliger@uma.es

and aerosols. They can be transported to large distances from their source and where they fall out they have a negative impact on the environment. Dust intrusions from deserts are also frequent sources of particles in different parts of the world (Alonso-Pérez et al., 2012; Huang et al., 2012; Sunnu et al., 2013; Varga et al., 2013). Dust intrusions from African desert regions have been recognized to have a non negligible impact on the particulate matter surface concentrations recorded in Europe (Querol et al., 2004, 2009).

The most common techniques for compositional analysis of particulate matter collected on filters include Atomic Absorption Spectroscopy (AAS) and Inductively Coupled Plasma techniques (ICP). These analyses require complete sample digestion that may be expensive and time-consuming. Because screening procedures are connected with an enormous number of samples to be analyzed, the development and application of cost-effective techniques are of particular interest. Non-destructive Wavelength-Dispersive X-Ray Fluorescence (WDXRF) analysis (Calzolai et al., 2008; Kavčič, 2012) has been successfully applied for the analysis of multi-element contents of atmospheric particulate matter requiring minimal sample preparation.

Concentrations of radionuclides in air are continuously monitored in Málaga, a Mediterranean coastal city in South Spain located to receive pollution from different sources by means of air mass transport (Dueñas et al., 1999; Gordo et al., 2015). The objective in the present study was to analyse variations in total suspended particle (TSP) mass concentration, gross-alpha and gross-beta activities and heavy metal components for evaluating the atmospheric loadings of substances with different sources and as well as to further examine the relationship between the occurrence of African dust intrusions and radionuclide activity concentrations.

Materials and Methods

Location of the area and the sampling station is shown in Fig. 1. Málaga, with a population around 600,000 inhabitants in the metropolitan area, is the southernmost large city in Europe. It lies on the shoreline of the Alboran Sea (Western Mediterranean), about 100 km east of the Strait of Gibraltar and about 130 km north of Africa. As a coastal city and as a result of its placing, the climate is typically Mediterranean with occasional heavy rains during the autumn-winter months and hot-dry weather persisting from June to October. The area is influenced by continental and maritime air masses, being influenced by westerlies from the Atlantic Ocean and easterlies from the Mediterranean. Due to its geographical proximity to the African continent, our study area is frequently affected by intrusions of air masses with high concentrations of atmospheric particulate matter.
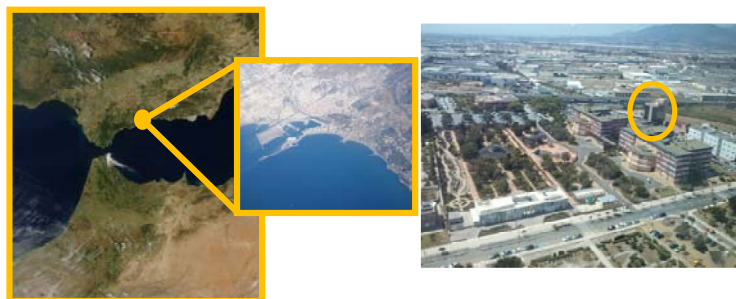
Figure 1. Map of the area and the sampling site in the University of Málaga, South Spain.

The sampling site is located on the North-West part of the city (36° 43′ 40″ N; 4° 28′ 8″ W), in an urban area away from specific local sources of heavy metals and 5 km away from the coastline. The sampling campaign for the present study was started on March 2014 and continued until February 2015. Aerosol samples (N=60) were collected on the roof of one of the buildings at the University Campus. Aerosol total suspended particulate (TSP) samples were periodically collected over 48-hour periods using a high-volume sampler (MCV, S.A.) at a flow rate of 30 m³/h using glass micro-

fibre filters (150 mm in diameter, type GF20, MCV) to ensure that sufficient amount of dust is collected for radioactivity analysis and for the determination of major metallic components. The pump maintains a constant flow rate independent of the dust load on the filter and around 1440 m^3 ambient air per sample were drawn through the filters for the sampling that has been performed. In addition to the normal operation, we added event samples collected according to various forecasts on dust concentration in the atmosphere and precipitation. Three to five filter samples were collected every month. The location and positioning of this aerosol pump was chosen to minimise the contamination of the filters by re-suspension of local soil particles. Dust content on the filter samples was calculated gravimetrically by weighting the filter before and after exposure under the same laboratory conditions using an electronic balance with the reading precision of 0.1 mg. Thereafter, 37 mm diameter circular representative sub-sample was removed from the active area of each filter, individually placed in a clean marked container and were kept in silicagel desiccators for moisture equilibrium before the subsequent radiometric analysis and non-destructive X-ray based techniques.

Gross-alpha and gross-beta measurements were carried out with a low background α/β proportional counter (CANBERRA LB4200) on the sub-samples with 37mm diameter. Since the levels of radioactivity encountered in environmental samples are low, long counting times were preformed, on the order of 1000 min sample^{-1} to increase the accuracy of measurement. The background of each detector was determined before and after use by 1000 min count with a clean unused filter. All the calculations have been made using the appropriate corrections for efficiencies to convert the gross-alpha (based on [241]Am) and gross-beta (based on ^{90}Sr/^{90}Y) measurements to specific activities in Bq m^{-3}. Rapid and simple determination of multi-elements in aerosol collected on the sub-samples was carried out using wavelength dispersive X-ray fluorescence (WDXRF) analysis without any further sample pre-treatment. UniQuant analysis package for standardless XRF analysis using intensities measured by a sequential X-Ray spectrometer (Thermo Scientific ARL WDXRF Spectrometers) was used. The program is highly effective for analyzing samples for which no standards are available. The content of Al, Ca, Cl, Cr, Cu, Fe, Mg, Mn, Px, Sx, Ni, Ti, V was determined in the filter piece reducing preparation, measuring time and sample flexibility. Sulphur present as sulfate is reported as Sx and the phosphor present as phosphate is reported as Px. Taking into account that filter paper materials may include various amounts of a variety of elements, ions and heavy metal impurities (Rizzio et al., 2000), for the accurate determination of trace amounts of heavy metals and common anions and cations in the air particulate matter on the filters, blank filters were also treated in the same manner as sample filters.

Additionally, data of daily concentrations of particulate matter fraction PM$_{10}$ and levels of gaseous pollutants (CO, NO$_2$, SO$_2$ and O$_3$) were also obtained from a monitoring station belonging to the regional Atmospheric Pollution Monitoring network managed by the Environmental Health Service of the Andalusian Government (De la Rosa et al., 2010). The identification of African events was confirmed by means of 3-day backward trajectories computed using the HYSPLIT model (http://www.arl.noaa.gov/ready/hysplit4.html), BSC-/DREAM dust maps (http://www.bsc.es/projects/earthscience/BSC-DREAM/) and aerosol maps from the Marine Meteorology Division of the Naval research Laboratory, USA (NRL) (http://www.nrlmry.navy.mil/aerosol).

Results and Discussion

Atmospheric particulate matter (PM) is a complex mixture of chemical components including metals, elemental carbon, other organic carbon, polycyclic aromatic hydrocarbons, sulfate and nitrate salts, and water. Among air pollutants are trace elements associated with PM from a variety of pollution emission sources. Atmospheric PM may be generated by various natural processes or human activities, such as soil dust, diesel trucks, and industrial. Table 1 provides some statistical

information on atmospheric PM mass concentration, gross-alpha and gross-beta activities on TSP aerosols and major elements and heavy metals concentrations during the sampling period at our site. The annual average concentrations of TSP and PM_{10} during the study period were 48.3±51.9 µg m^{-3} and 32.0±15.4 µg m^{-3}, respectively. Throughout the entire sampling period, PM10 levels recorded were within the range of 10.1–104.0 µg m^{-3}. The values for alpha-activity oscillated between 0.071 mBq/m^3 and 1.88 mBq/m^3 and between 0.078 mBq/m^3 and 1.87 mBq/m^3 for gross beta activity.

Table 1. Basic statistical parameters of mass concentration, gross-alpha and gross-beta activities and element concentrations on TSP aerosols at the sampling station in the University of Málaga (March 2014-February 2015).

	Valid N	Mean	Std.Dev.	Min.	Max.
Mass (mg/m^3)	60	4,83E-02	5,19E-02	1,39E-02	3,92E-01
Gross α (Bq/m^3)	60	5,60E-04	3,68E-04	7,12E-05	1,88E-03
Gross β (Bq/m^3)	60	6,92E-04	4,47E-04	7,81E-05	1,87E-03
Al (µg/m^3)	32	1,72E+00	3,38E+00	3,22E-01	1,93E+01
Ca (µg/m^3)	60	1,65E+01	1,81E+01	3,72E+00	1,20E+02
Cl (µg/m^3)	59	3,26E+00	3,38E+00	1,18E-01	1,51E+01
Cr (µg/m^3)	25	4,68E-02	3,23E-02	1,61E-02	1,93E-01
Cu (µg/m^3)	36	3,35E-01	3,52E-01	5,78E-02	1,14E+00
Fe (µg/m^3)	60	6,96E+00	1,24E+01	1,52E+00	9,70E+01
Mg (µg/m^3)	60	1,35E+00	1,23E+00	3,50E-01	8,32E+00
Mn (µg/m^3)	36	1,38E-01	2,51E-01	3,04E-02	1,55E+00
Ni (µg/m^3)	4	7,95E-02	8,87E-03	6,73E-02	8,82E-02
Px (µg/m^3)	60	1,02E-01	5,65E-02	3,84E-02	3,51E-01
Sx (µg/m^3)	60	2,24E+00	1,46E+00	5,53E-01	9,16E+00
Ti (µg/m^3)	59	4,46E-01	8,61E-01	6,68E-02	6,63E+00
V (µg/m^3)	30	1,04E-01	4,89E-02	3,59E-02	1,95E-01

WDXRF analysis was successfully applied for the determination of metallic species such as Al, Cr, Cu, Fe, Mn, Ni, Ti and V on these aerosol filters. The most abundant of these detected metallic elements in this sampling site were Fe (1.52-97.0 µg m^{-3}), Al (0.32-19.3 µg m^{-3}), Ti (0.067-6.63 µg m^{-3}), Mn (0.030-1.55 µg m^{-3}) and Cu (0.05-1.14 µg m^{-3}) reflecting influences of natural geochemical behaviour and urban activities. Metal-bearing aerosols in the ambient atmosphere are produced by various anthropogenic (particles generated from road traffic, industrial and construction activities) and natural sources (sea salt spray, forest fires, Saharan dust) in the area.

Table 2. Summary of Spearman rank correlation results among mass concentrations, gross-alpha and gross-beta activities and different elements determined in TSP samples. Bold value denotes correlations significance level <0.05.

	Mass Conc.	Gross α	Gross β
Mass Conc.	1,00	**0,53**	**0,53**
Gross α	**0,53**	1,00	**0,91**
Gross β	**0,53**	**0,91**	1,00
Al	**0,62**	0,18	0,29
Ca	**0,59**	0,25	0,12
Cl	0,11	**-0,34**	-0,24
Cr	**0,52**	0,27	**0,47**
Cu	0,18	-0,07	0,13
Fe	**0,68**	**0,53**	**0,60**
Mg	**0,65**	**0,28**	0,20
Mn	**0,74**	0,27	**0,47**
Px	**0,63**	**0,55**	**0,55**
Sx	**0,48**	**0,72**	**0,60**
Ti	**0,85**	**0,47**	**0,57**
V	0,19	**0,46**	0,34

In order to know the relationships between the studied variables, Spearman correlation coefficient, a nonparametric parameter which measures the strength of association between two ranked variables, was computed. The quantified results on total activity and elements concentrations in TSP samples, gaseous pollutants and PM_{10} concentrations were statistically analyzed. The values presenting a

significance level of 95% ($p < 0.05$) are shown in bold in Tables 2 and 3. The strong correlations found between these total activities and the concentrations of different elements imply that they are similarly affected by transport and by physical and chemical interaction processes in the atmospheric environment. Additionally, clear correlations between the increase of particle matter PM_{10} concentrations and gross-alpha and gross-beta activities were observed as well as with other gaseous pollutants in the city of Málaga such as carbon monoxide, sulphur dioxide and nitrogen oxides.

Table 3. *Spearman correlation coefficients among mass concentrations, gross-alpha and gross-beta activities in TSP and PM_{10} and other gaseous pollutants in the city of Málaga during the studied period. Bold value denotes correlations significance level <0.05.*

	Mass Conc.	Gross α	Gross β	PM10	CO	NO₂	SO₂	O₃
Mass Conc.	1,00	**0,53**	**0,53**	**0,62**	**0,25**	**0,37**	0,13	-0,03
Gross α	**0,53**	1,00	0,91	**0,61**	**0,48**	**0,44**	**0,37**	0,07
Gross β	**0,53**	**0,91**	1,00	**0,68**	**0,46**	**0,53**	0,25	-0,17

African episodes

Aeolian dust impacts the global climate by scattering and absorbing solar radiation, changing cloud properties, and affecting bio-geochemical cycles (e.g. Sassen et al., 2003; Maher et al., 2010). It also impacts human health through its effect on air quality. As the Saharan dust events have been recognized to have a non negligible impact on the particulate matter surface concentrations recorded in Europe, research on African dust has not only scientific but also social implications. The African dust outbreaks take place throughout the year and may induce particulate matter levels to increase simultaneously in large areas of the Iberian Peninsula. Their contribution is added to the local production, mostly due to local resuspension processes. This local production is viewed as a 'background' contribution, regular in time and mainly depending on the season. Moreover, the long range transport of dust coming from the Saharan region is more sporadic and intense, but it was shown that even far from the sources, it may contribute significantly to the local particulate matter budget. During the study period, 26 filters were collected under the influence of African dust intrusions (Fig. 2). 3-day atmospheric back-trajectories confirmed the African origin of the air masses during the dust intrusions and located the most probable aerosol source area within the Sahara region. The intrusion of African air masses produces dust "pulses" that could last for several days, taking place the longest events during the summer months.
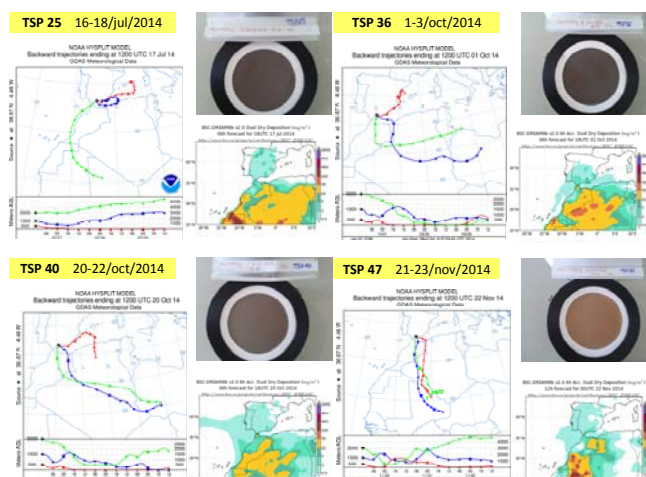
Figure 2. *Several samples collected on days affected by African dust outbreaks including: 3-day backward trajectories at 500 m (red triangles), 1500 m (blue squares) and 3000 m (green circles); BSC-/DREAM dust maps are shown at bottom right.*

The samples collected were sorted depending on the presence or not of African dust intrusions and comparison of average values at Málaga site during African and non-African dust events showed higher values specially in the set of samples collected under the influence of African episodes for total alpha and beta radioactivity, together with PM_{10} and other elements concentrations found in TSP samples (Table 4). To explore differences between them, total activities and concentrations of elements and gaseous pollutants in days affected or not by African dust intrusions were compared using the Mann-Whitney U test (Table 4). Results of the test showed that there were highly significant differences in gross-alpha and gross-beta concentrations and similarly, a highly significant difference was also observed in Al, Fe, Mg, Ti, PM_{10} and NO_2 data sets.

Table 4. *Mean values for the gross-alpha and gross-beta activity concentrations and for the different elements and gaseous pollutants in days affected or not by African dust intrusions during the studied period (March 2014 – February 2015). Significant differences on the basis of Mann-Whitney U test are marked in bold.*

	YES	NO	Z	p-level
Mass Conc. (mg/m3)	6,88E-02	3,36E-02	**4,0109**	**0,0001**
Gross α (Bq/m3)	7,25E-04	4,42E-04	**2,6165**	**0,0089**
Gross β (Bq/m3)	8,93E-04	5,49E-04	**2,8564**	**0,0043**
Al (µg/m3)	2,78E+00	7,82E-01	**2,0203**	**0,0434**
Ca (µg/m3)	2,25E+01	1,22E+01	1,8218	0,0685
Cl (µg/m3)	4,00E+00	2,64E+00	1,2220	0,2217
Cr (µg/m3)	5,25E-02	3,66E-02	1,5852	0,1129
Cu (µg/m3)	2,67E-01	3,97E-01	-0,4278	0,6688
Fe (µg/m3)	1,05E+01	4,44E+00	**2,4815**	**0,0131**
Mg (µg/m3)	1,88E+00	9,70E-01	**3,0213**	**0,0025**
Mn (µg/m3)	1,86E-01	8,41E-02	1,0932	0,2743
Px (µg/m3)	1,16E-01	9,14E-02	0,6972	0,4857
Sx (µg/m3)	2,76E+00	1,87E+00	1,6419	0,1006
Ti (µg/m3)	7,29E-01	2,51E-01	**3,3484**	**0,0008**
V (µg/m3)	1,11E-01	9,77E-02	0,7673	0,4429
PM10 (µg/m3)	4,02E+01	2,60E+01	**3,8460**	**0,0001**
CO (µg/m3)	6,48E+02	5,60E+02	0,9521	0,3410
NO2 (µg/m3)	2,92E+01	2,23E+01	**2,0767**	**0,0378**
SO2 (µg/m3)	1,22E+01	1,14E+01	0,6223	0,5338
O3 (µg/m3)	5,98E+01	5,93E+01	0,2774	0,7815

Spearman's rank correlation examining the association among the different variables during African and non-African dust events was also tested during this study (Table 5). Significant correlations were found for gross-alpha and gross-beta activities with different metals and gaseous pollutants during non-dusty days. Under the influence of African dust outbreaks, correlations among the different variables changed. Total alpha was positively correlated with Fe, sulfur species and CO while total beta was better correlated with Mn, phosphorus species and PM_{10} during days affected by African dust episodes. Interestingly, a significant correlation between the increase of particle matter PM_{10} concentrations during dust episodes was only then observed for the gross-beta activity.

Table 5. *Results for the Spearman correlation among the input variables computed under the influence or not of African in the city of Málaga during the studied period. Bold value denotes correlations significance level <0.05.*

Intrusion	YES			NO		
	Mass Conc.	Gross α	Gross β	Mass Conc.	Gross α	Gross β
Mass Conc.	1,00	0,37	0,37	1,00	**0,46**	**0,48**
Gross α	0,37	1,00	**0,87**	**0,46**	1,00	**0,91**
Gross β	0,37	**0,87**	1,00	**0,48**	**0,91**	1,00
Al	**0,80**	0,32	0,39	0,22	-0,17	-0,06
Ca	**0,65**	0,31	0,15	**0,57**	0,11	0,03
Cl	**0,60**	-0,25	-0,14	**-0,39**	**-0,53**	**-0,48**
Cr	**0,64**	0,07	0,30	-0,27	0,39	0,55
Cu	**0,68**	-0,08	0,10	-0,11	-0,11	0,17
Fe	**0,76**	**0,63**	**0,61**	**0,55**	0,31	**0,46**
Mg	**0,74**	0,28	0,16	**0,50**	0,08	0,02
Mn	**0,80**	0,32	**0,55**	**0,60**	0,17	0,24
Px	**0,66**	**0,62**	**0,63**	**0,70**	**0,44**	**0,47**
Sx	**0,39**	**0,74**	**0,50**	**0,49**	**0,64**	**0,65**
Ti	**0,81**	0,28	0,37	**0,79**	**0,39**	**0,51**
V	0,11	0,28	0,16	0,34	0,48	**0,51**
PM10	**0,59**	0,25	**0,48**	**0,48**	**0,69**	**0,69**
CO	0,11	**0,48**	0,35	0,32	**0,48**	**0,51**
NO2	0,34	0,26	0,35	0,29	**0,51**	**0,56**
SO2	-0,09	**0,41**	0,31	0,25	**0,38**	0,25
O3	-0,19	0,21	-0,02	0,04	-0,03	-0,24

Research with a higher temporal resolution is imperative in the future to deepen our understanding of the contribution of these natural events on the concentrations of radioactive matter. Further work is currently undertaken to establish the origin of the radionuclides transported during these events and to quantify the consequences of intensive dust outbreaks may have on the air quality of this coastal site.

Summary and Conclusions

Particulate matter pollution is a serious environmental issue mainly due to the presence of toxic substances and trace metals in the atmosphere. PM was routinely collected on filters and following characterized with several non-destructive and rapid analytical techniques. WDXRF appears particularly promising for environmental analysis, especially when heavy metals must be detected at low concentrations. From this preliminary data set and analysis on the levels of total alpha, total beta activities and different pollutants at this coastal station:

- Studies of total alpha and beta activities in aerosol particles are valuable to have a better insight of the behaviour of radionuclide labeled aerosols and atmospheric processes and provide a means for evaluating the atmospheric loadings of substances with different sources.
- WDXRF analysis can be used for monitoring major components as a fast pre-analysis of totally unknown samples prior to decide on further analyses. It simplifies the filter sample preparation procedure, avoiding contamination and material loss, and reducing preparation, measuring time and sample flexibility.
- WDXRF is concluded to be a powerful, non-destructive yet easily applicable tool to supply detailed elemental information of particles collected on filters. The further development and future potential of the method for detailed analysis of aerosol particles is currently undertaken.
- Since the variation of aerosol composition is very high depending on measurement site and season, long-term measurements (≥ 1 year) are needed. Nevertheless, this work clearly highlights the importance of multidisciplinary monitoring campaigns and the need to include radionuclides measurements in atmospheric studies. These preliminary results provide valuable insights for planning future monitoring and controlling strategies for airborne PM pollution in this area of the Western Mediterranean Sea.

References

Alonso-Pérez, S., Cuevas, E., Querol, X. Guerra, J. C. and Pérez, C., 2012. African dust source regions for observed dust outbreaks over the Subtropical Eastern North Atlantic region, above 25^0N. J. Arid Environ., 78, 100-109.

Calzolai, G., Chiari, M., Lucarelli, F., Mazzei, F., Nava, S., Prati, P., Valli, G., Vecchi, R., 2008. PIXE and XRF analysis of particulate matter samples: an inter-laboratory comparison. Nuclear Instruments and Methods in Physics Research Section B: Beam Interactions with Materials and Atoms 266, 2401-2404.

De la Rosa, J.D., Sánchez de la Campa, A.M., Alastuey, A., Querol, X., González-Castanedo, Y., Fernández-Camacho, R., Stein, A.F., 2010. Using PM10 geochemical maps for defining the origin of atmospheric pollution in Andalusia (Southern Spain). Atmos. Environ. 44 (36), 4595-4605.

Dueñas, C., Fernández, M.C., Liger, E., Carretero, J., 1999. Gross alpha, gross beta activities and ^{7}Be concentrations in surface air: analysis of their variations and prediction model. Atmos. Environ., 33,3705-3715.

Gordo, E., Dueñas, C., Fernández, M.C., Liger, E., Cañete, S., 2015. Behavior of ambient concentrations of natural radionuclides ^{7}Be, ^{210}Pb, ^{40}K in the Mediterranean coastal city of Málaga (Spain). Environ. Sci. Pollut. Res. http://dx.doi.org/10.1007/s11356-014-4039-5.

Huang, K., Zhuang, G., Lin, Y. et al., 2012. Typical types and formation mechanisms of haze in an Eastern Asia megacity, Shanghai. Atmos. Chem. and Phys., 12, 105-124.

Kavčič, M., 2012. Application of Wavelength Dispersive X-Ray Spectroscopy in X-Ray Trace Element Analytical Techniques, X-Ray Spectroscopy, Dr. Shatendra K Sharma (Ed.), ISBN: 978-953-307-967-7, http://www.intechopen.com/books/x-ray-spectroscopy/application-of-wavelengthdispersive-x-ray-spectroscopy-in-x-ray-trace-element-analytical-techniques.

Landing, W.M. and Paytan, A., 2010. Marine chemistry special issue: Aerosol chemistry and impacts on the ocean. Mar. Chem., 120 (1), 1-3.

Maher, B.A., Prospero, J.M., Mackie, D., Gaiero, D., Hesse, P.P., and Balkanski, Y., 2010. Global connections between aeolian dust, climate and ocean biogeochemistry at the present day and at the last glacial maximum. Earth-Sci. Rev., 99, 61-97.

Querol, X., Alastuey, A., Viana, M.M., Rodríguez, S., Artiñano, B., Salvador, P., Santos, S.G.D., Patier, R.F., Ruiz, C.R., Rosa, J.D.L., Campa, A.S.D.L., Menéndez, M., Gil, J.I., 2004. Speciation and origin of PM_{10} and $PM_{2.5}$ in Spain. J. Aerosol Sci. 35, 1151-1172.

Querol, X., Pey, J., Pandolfi, M., et al., 2009. African dust contributions to mean ambient PM_{10} mass-levels across the Mediterranean basin. Atmos. Environ. 43 (28), 4266-4277.

Rizzio, E., Giaveri, G., Gallorini, M. 2000. Some analytical problems encountered for trace elements determination in the airborne particulate matter of urban and rural areas. Sci. Total Environ., 256, 11-22.

Sassen, K., DeMott, P.J., Prospero, J.M., and Poellot, M.R., 2003. Saharan dust storms and indirect aerosol effects on clouds: CRYSTAL-FACE results. Geophys. Res. Lett., 30(12), 1633, doi: 10.1029/2003GL017371.

Sunnu, A., Resch, F. and Afeti, G., 2013. Back-trajectory model of the Saharan dust flux and particle mass distribution in West Africa. Aeolian Research, 9, 125-132.

Varga, G., Kovács, J. and Újvári, G., 2013. Analysis of Saharan dust intrusions into the Carpathian Basin (Central Europe) over the period of 1979–2011. Global and Planetary Change, 100, 333-342.

Soil CO$_2$ monitoring under a cool-temperate forest site in winter in Hokkaido,Japan

Taichi Nakamura[*], Kazumasa Okamoto, Kikuo Umegaki, Ryoko Fujiyoshi

Faculty of Engineering, Hokkaido University, Sapporo, Japan

Abstract

Concentration of soil CO$_2$ and its carbon isotopic composition (δ^{13}C, Δ^{14}C) have been measured in cool-temperate semi-natural woods on the campus of Hokkaido University, Sapporo, Japan from 2013 to 2016. There were good positive correlations between CO$_2$ concentration and soil temperature from early spring to early summer with similar CO$_2$ increasing rate (ppm $^{-1}$). Monthly CO$_2$ concentration showed cyclic patterns with soil temperature. Concentration of CO$_2$ decreased with certain time lag after decreasing soil temperature from September. In winter, drastic changes in soil CO$_2$ were observed, whensnow was partly melted at air temperature higher than 0 , then the CO$_2$ level decreased with melting snow and rainfall, and the CO$_2$ concentration was kept low during snowmelt season. The values of Δ^{14}C indicate that the sources of soil CO$_2$ were atmospheric CO$_2$, and decomposition of humic substance and contemporary C3 plants. Moreover, the values of Δ^{14}C increased from February to June. It means that older soil organic matter decomposed in winter season than that in early summer.

Introduction

Global warming has been regarded as one of the most serious problems resulting in sea level rise, ice melting in polar regions, frequent and severe heat waves and more. The amount of CO$_2$ in the atmosphere, a major greenhouse gas, has increased from 280 ppm before industrial revolutionto 400 ppm in 2013 at Mauna Loa in Hawaii (Betts et al., 2016).

The carbon cycle consists of three carbon pools, atmosphere, sea and continental biosphere including soil. Carbon has been transferred among the three pools as CO$_2$, and the largest proportion of carbon is exchanged between the atmosphere and continental biosphere (IPCC 4th assessment report, 2007). In the cycling, forests play an important role, in whichcarbon in the atmosphere is absorbed by forest plants as CO$_2$. And, the carbon is transferred to soil with falling leaves and withering of plants. Thus, great amount of the carbon reaches the soil floors in forest sites. Soils and surface litters store 2-3 times higher the amount of carbon than that in the atmosphere(Trumbore et al., 2009).

On the other hand, CO$_2$ is emitted by soil respiration. Great many studies have been conducted to elucidate forests as sinks or sources of CO$_2$. However, there are not enough data on soil CO$_2$especially in winter season. It's important to evaluate the effects of snow on CO$_2$ dynamics in soil air, since many forests area are distributed at higher latitude and higher altitude..

Almost all studies about soil CO$_2$ have focused only on the upper soils ($\sim$ 30 cm) with higher microbial activity, and measurement period has been no more than 3 months. However, when we focus onlong term carbon cycle like global warming, we also havetoconsider the contribution of lower soils, and to conduct measurement for a long time.

In addition, it is important to clarify the sources of soil CO$_2$ and their variability. Isotopes of carbon(δ^{13}C, Δ^{14}C) provide inevitable information on the source and dynamics of CO$_2$ in soil. The purposes of this study is) evaluating factors affecting seasonal variability of CO$_2$ in soil air including winter season, and)estimating emission source(s) of CO$_2$ in a forest soil.

---

[*]Corresponding author, E-mail: fpr-v5-kttd-nadt@eis.hokudai.ac.jp

Materials and Methods

Site description

The observation site was located in semi-natural woods on the campus of Hokkaido University, Sapporo, Japan(43.08°N, 141.38°E). The stand consists of a mixture of cool-temperate deciduous trees (*Populus, Betula sp., Quercuscrispula*). Geology of the site is alluvial sediments from Kotoni River, a tributary of Ishikari River. A dark-green clay layer appeared at a depth of 40-50 cm. Mean annual temperature and precipitation are reported to be 8.9℃ and 1100 mm, respectively. Maximum snow depth is around 100 cm in February.

Figure 1.*Schematic representation of setting a CO_2 probe (TESTO, Germany) in soil*

Soil CO_2 monitoring

Soil CO_2 monitoring was conducted from 2013 to 2016, in which a CO_2 probe (TESTO, Germany) in a polyvinyl chloride pipe (Length; 100cm, $\Phi = 4$ cm) was set in a hole at a depth of 100 cm. The pipe was open only in the bottom (Figure 1). The detector measures CO_2concentration and temperature in the hole every ten minutes. Other meteorological data (air temperature, precipitation, snow fall, and snow depth) have been measured at Odori park every one hour (about 1.5 km from the observation site) by Sapporo District Meteorological Observatory.

Carbon isotope ($\delta^{13}C$, $\Delta^{14}C$) analysis

Soil CO_2 samples were collected every 1 month at depths of 1 m(Apr–May, 2015 and Feb‑Jun, 2016) and 0.3 m (Apr – Jun, 2016). Soil CO_2 was dissolved into NaOH solution (1 M, 100 cm^3) through pumping soil air out from the soil at a rate of 0.3 $Lmin^{-1}$for 2 hours via a column of drying agent (Drierite). In the laboratory, small amount of $CaCl_2$(1M) was added to the alkaline solution. The solution became turbid to white suspension ($CaCO_3$). The mixture stood for several hours was filtered. After drying at 60 for 1 day, it was transferred to a small vial for carbon isotope analyses with acceleratormass spectrometry (AMS) at the Mutsu office of the JapanAtomic Energy Agency (JAEA).

Results and Discussion

Soil CO_2 monitoring

Time series plots of CO_2 concentration in soil air (Figure 2) and soil temperature (Figure 3) showed similar increasing patterns in each year. Good positive correlations between them from April to mid-June when the CO_2 concentration reached the highest limit of quantification of the probe (~1.4 %). These correlations were explained by increasing biological activity in this season. Soil temperature stimulated decomposition of soil organic matter and plant growth. Increasing rate of
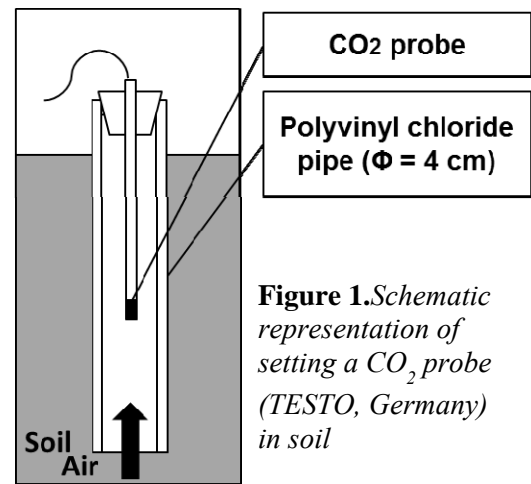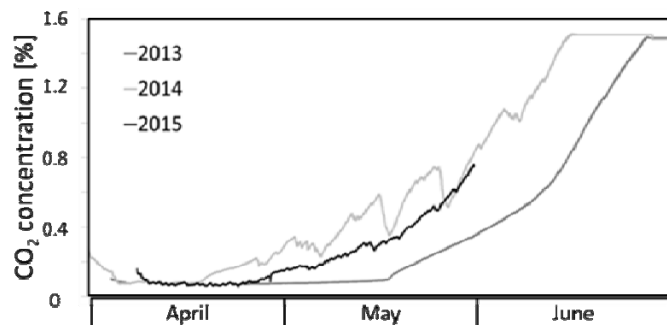
Figure 2. *Time series plots of CO_2 concentration from April to June in 2013-2015*
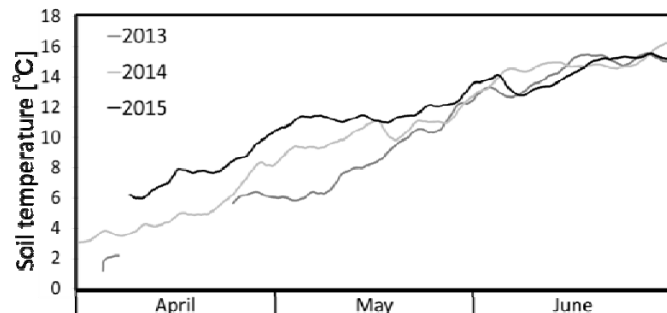
Figure 3. *Time series plots of soil temperature from April to June in 2013-2015*

CO_2 with soil temperature was calculated to be 0.14, 0.12, and 0.26 % $^{-1}$ in 2013, 2014, and 2015, respectively. Relatively high rate ($\sim$0.26 % $^{-1}$) in 2015 was reflected by warmer winter and earlier melting snow than usual; date of snow disappearance was about 2 weeks earlier, monthly mean temperature in April was high in 2015, but it was not high in May, and low in June compered to other two years. It means that rising temperature was very slow in 2015. Figure 4 (a, b, c) shows relationships between monthly means of CO_2 concentration in soil air and mean soil temperature at a depth of 100 cmin the period from January 2013 till December 2015. As explained above, CO_2 concentration increased from spring to early summer, and decreased from fall season . In March and April, CO_2 concentration was kept low, probably due to melting snow water to which CO_2 was dissolved. The results in Figure 4 were different from those reported in southern Poland (Gorczyca et al., 2003). They measured CO_2 and temperature at ground surface in the centre of a large mixed forest complex (*oak, hornbeam, pine*) resulting in lower CO_2 concentration in low temperature region (-3~10).It should be noted that cyclic patterns of the plots in Figure 4 indicate that biological activity would have decreased with certain time lag after decreasing soil temperature from September. Drastic changes in soil CO_2 were actually observed in winter as shownFigure 5. The figure gives time series plots of CO_2 and soil(air) temperature from Jan.1 to Mar.30 in 2016.Concentration of CO_2 varied drastically, while soil temperature was virtually kept
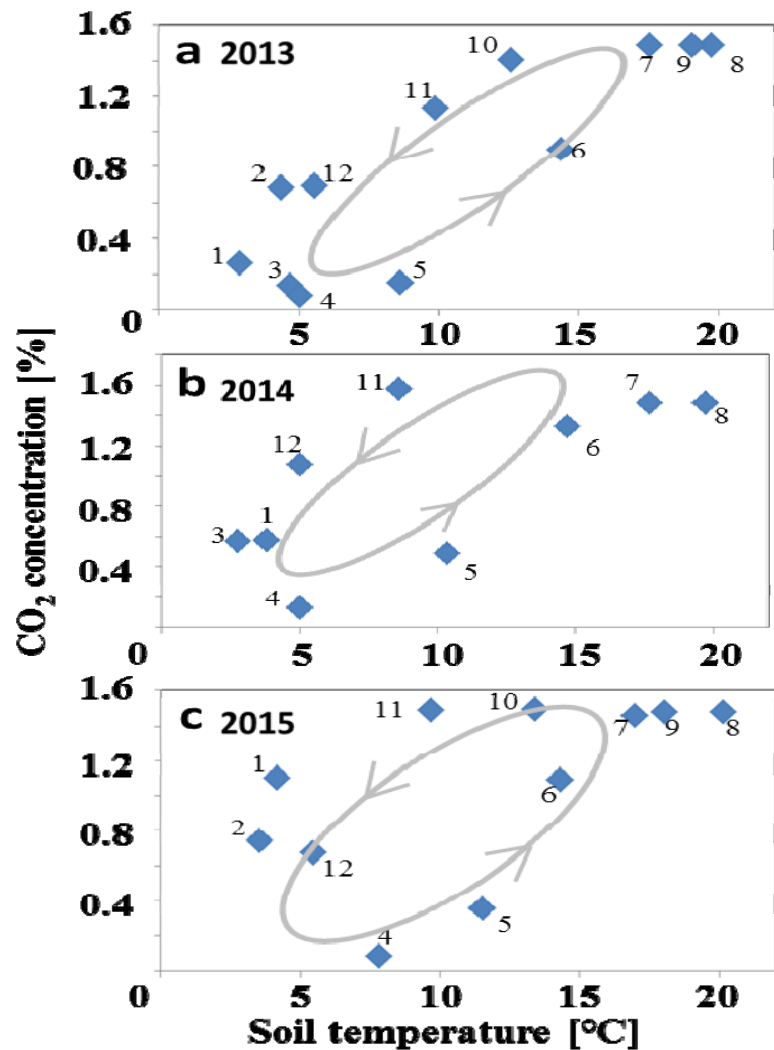
Figure 4. *Plots of monthly means of CO_2 concentration in soil against soil temperature from January 2013 till December 2015 except for missing data in February, November, and Decomber in 2014, and March 2015. From July to October in 2013 and from July to November in 2014 and 2015, CO_2 concentration exceed measuring range (1.4 %). Small number means month.*
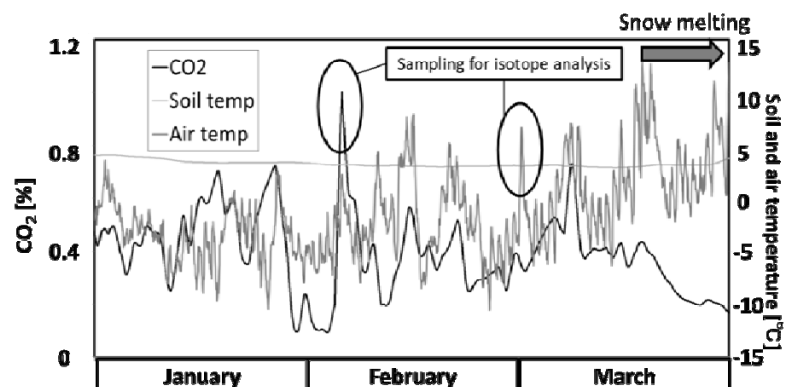
Figure 5. *Time series plots of CO_2 and soil(air) temperature from January 1st to March 30th in 2016. Time interval of measurements was 10 min. Two peakes dipicted in the figure appeared after the CO_2 sampling for carbon isotope analyses.*

constant (~4). In winter, there was much snow accumulated at the site (~ 100 cm). The snow was partly melted when air temperature exceeded 0 , thenthe CO_2 level decreased with melting snow and rainfall. The CO_2 concentration was relatively low (0.2 %) during snowmelt season (from mid-March, Figure 5). As mentioned above, soil CO_2 variation depends on the amount of soil moisture content.

Figure 6 shows distribution of $\delta^{13}C$ and $\Delta^{14}C$ of soil CO_2 obtained in this study with those of the literature values with atmosphere ($\delta^{13}C$; -8.5 ‰, $\Delta^{14}C$; 110 ‰), humic substnce ($\delta^{13}C$; -25 ‰, $\Delta^{14}C$; -160 ‰), and contemporary C3 plants ($\delta^{13}C$; -27 ‰, $\Delta^{14}C$;70 ‰) (Mayorga et al., 2005). The result indicates the sourses of CO_2 to be atmospheric CO_2 and decomposition of both contemporary C3 plants and humic substans.

Figure 7 shows time series plots of $\Delta^{14}C$ from February to June in 2015 and 2016. From winter to early spring in 2016, values of $\Delta^{14}C$ in CO_2 increased from -128 ‰ to 8 ‰, -94 ‰ to -7 ‰ at depths of 100 cm and 30 cm from the ground surface, respectively. In 2015, $\Delta^{14}C$ increased from -100 ‰ to -75.6 ‰ at a depth of 100 cm. In any case, the values of $\Delta^{14}C$ increased during this term. It's likelythat older soil organic matter was predominantly decomposed in winter season. A difference between data sets of 2015 and 2016 at

Figure 6. *Relationship between $\delta^{13}C$ and $\Delta^{14}C$ of soil CO_2*
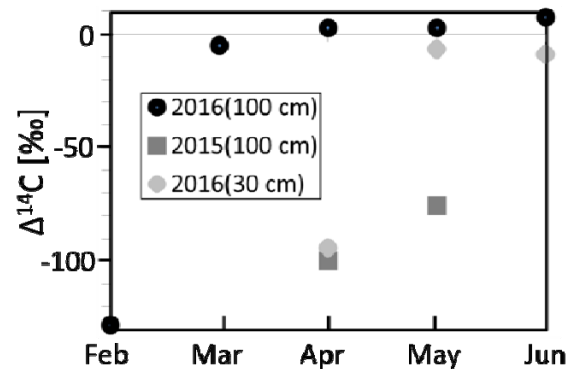
Figure 7. *Time series plots of $\Delta^{14}C$ from February to June in 2015 and 2016*

depth of 100 cm may due to different meteorological conditions, in which spring came earlier in 2016 than in 2015.

Conclusions

Concentration of soil CO_2 had been monitored for four years since 2013 including winter seasons with much snow and seasonal variation of carbon isotopic ratio.

From April to mid-June, CO_2 concentration increased with increasing soil temperature at a similar rate(from 2013 to 2015). Increasing rate of $CO_2$with temperature was calculated to find the rate in 2015 higher than the other two years. This was caused by warmer winter and earlier melting snow than usual. Meteorological conditions in winter and early spring affect to soil CO_2 dynamics in later season.

The variations of monthly CO_2 concentration with soil temperature showed cyclic patterns, suggesting that biological activity would have decreased with certain time lag after decreasing soil temperature from September.

It was also found that concentration of CO_2 varied drastically in winter season, and its variation was totally different from that in other seasons predominantly controlled by soil temperature.CO_2 concentration in winterwas affected by soil moisture.

The sources of CO_2 in soil air were estimated to be atmospheric CO_2, and decomposition of both contemporary C3 plants by carbon isotope analyses($\delta^{13}C$, $\Delta^{14}C$). The values of $\Delta^{14}C$ increased from February to June. The fact indicates that older soil organic matter was also decomposed in winter.

Soil CO_2 dynamics in winter should be consider when carbon dynamics in forest area include soil is discussed, especially in areas, in which has snow accumulation.

References

1. Richard A. Betts, Chris D. Jones, Jeff R. Knight, Ralph F. Keeling & John J. Kennedy, 2016, El Niño and a record CO2 rise, Nature Climate Change 6:806-810.
2. IPCC 4th assessment report, 2007, Intergovernmental panel on Climate Change.
3. Trumbore Susan, 2009, Radiocarbon and Soil Carbon Dynamics, Annual Review of Earth and Planetary Sciences 37:47-66.
4. Z.Gorczyca, K. Rozanski, T. Kuc, B. Michalec, 2003, Seasonal variability of the soil CO_2 flux and its isotopic composition in southern Poland, NUKLEONIKA 48(4):187-196.
5. Mayorga. E, Aufdenkampe. AK, Masiello. CA, Krusche. AV, Hedges. JI, Quay. PD, Richey. JE & Brown. TA, 2005, Young organic matter a source of carbon dioxide outgassing from Amazonian rivers, Nature 436(28), 538-541.

Acknowledgments

J – MODELLING

An overview of marine modelling activities in IAEA MODARIA program: lessons learnt from the Baltic Sea and Fukushima scenarios

R. Periáñez[a], R. Bezhenar[b], I. Brovchenko[c], C. Duffa[d], M. Iosjpe[e], K.T. Jung[f], T. Kobayashi[g], F. Lamego[h], V. Maderich[c], B.I. Min[k], H. Nies[m], I. Osvath[n], I. Outola[p], M. Psaltaki[q], K.S. Suh[k], G. de With[s]

[a]Dpt Física Aplicada I, ETSIA, Universidad de Sevilla, Ctra Utrera km 1, 41013-Sevilla, Spain. rperianez@us.es. [b]Ukrainian Center of Environmental and Water Projects, Glushkov av., 42, Kiev 03187, Ukraine. [c]Institute of Mathematical Machine and System Problems Glushkov av., 42, Kiev 03187, Ukraine. [d]IRSN, BP 330, 83507 La Seyne sur Mer, France. [e]NRPA, Grini naeringspark 13, NO-1332, Osteras, Norway. [f]KIOST, 787 Hean-ro, Sangnok-gu, Ansan-si, Gyeonggi-do, 426-744, Rep. of Korea. [g]JAEA, 2-4 Shirakata Shirane, Tokai, Ibaraki 319-1195, Japan. [h]IEN, Rua Hélio de Almeida 75, Ilha do Fundao CEP 21941-906 Rio de Janeiro, Brasil. [k]KAERI, Daedeok-Daero 989-111, Yuseong-Gu, Daejeon, Rep. of Korea. [m]Bundesamt fuer Seeschifffahrt und Hydrographie, Bernhard-Nocht-Str. 78, 20359 Hamburg, Germany. [n]IAEA, 4a Quai Antoine 1er MC-98000, Monaco. [p]STUK, Laippatie 4, 00880 Helsinki, Finland. [q]National Technical University of Athens, Iroon Polytexneiou 9, 15780 Zografou, Greece. [s]NRG, Utrechtseweg 310, 6800 ES Arnhem, Netherlands

Abstract

State-of-the art dispersion models were applied to simulate 137-Cs dispersion from Chernobyl nuclear power plant disaster fallout in the Baltic Sea and from Fukushima Daiichi nuclear plant releases in the Pacific Ocean after the 2011 tsunami. Models were of different nature, from box to full three-dimensional models, and included water/sediment interactions. Agreement between models was very good in the Baltic. In the case of Fukushima, results from models could be considered to be in acceptable agreement only after a model harmonization process consisting of using exactly the same forcing (water circulation and parameters) in all models. It was found that the dynamics of the considered system (magnitude and variability of currents) was essential in obtaining a good agreement between models. The difficulties in developing operative models for decision-making support in these dynamic environments were highlighted.

Introduction

The International Atomic Energy Agency (IAEA) has organized programmes on radioactivity dispersion model testing since the VAMP (Validation of Model Predictions) program in 1988. The most recent effort is the MODARIA (Modelling and Data for Radiological Impact Assessments) project, launched in 2012. Ten working groups were organized in four main topics: Remediation of Contaminated Areas, Uncertainties and Variability, Exposures and Effects on Biota, and Marine Modelling. Working Group 10 (Modelling of marine dispersion and transfer of radionuclides accidentally released from land-based facilities) was defined within MODARIA. It included experts from the following institutes and countries: Instituto de Engenharia Nuclear (IEN/CNEN, Brasil), Institut de Radioprotection et de Sûreté Nucléaire (IRSN, France), National Technical University of Athens (NTUA, Greece), Japan Atomic Energy Agency (JAEA, Japan), Korea Institute of Ocean Science and Technology (KIOST, Republic of Korea), Korea Atomic Energy Research Institute (KAERI, Republic of Korea), Norwegian Radiation Protection Authority (NRPA, Norway), University of Seville (USEV, Spain), Institute of Mathematical Machines and System Problem (IMMSP, Ukraine) and Ukrainian Centre of Environmental and Water Projects (UCEWP, Ukraine).

Models showing different characteristics and levels of complexity, from those based on a box-type approach to those making use of the shallow-water and advection/diffusion equations were tested in two different environments: deposition and subsequent dispersion of 137-Cs on the Baltic Sea from

the Chernobyl nuclear power plant disaster in 1986 and the dispersion of 137-Cs released from Fukushima Daiichi nuclear power plant in the Pacific Ocean after the earthquake and tsunami in March 2011 (originating from both liquid releases into the ocean and from atmospheric deposition on the sea surface). The performed exercises provided the opportunity to learn more about the appropriate usage of models for the management of complex environmental problems in view of the uncertainty and, often, of the vagueness of the input data, the uncertainty of the model parameters and the compatibility of different kinds of models applied to a specific contamination scenario.

A brief description of the scenarios and modelling exercises which were carried out is given in section 2. A discussion on what we have learnt from these modelling exercises is presented in section 3.

Materials and Methods

Models which participated in the exercises are listed in Table I, where appropriate references for detailed descriptions are included. They range from box models to finite difference and finite element numerical models solving simultaneously the Navier-Stokes equations for water circulation together with a sediment transport model and the radionuclide dispersion model including adsorption/release of radionuclides between water and the solid phases (suspended matter in the water column and bed sediments). Also, both Eulerian and Lagrangian dispersion models were tested.

Table I: Models participating in the exercises.

Institute	Model	Scenario	Reference
NRPA	Box model	Baltic Sea	Iospje et al. (2009)
IMMSP	POSEIDON	Baltic Sea	Lepicard et al. (2004)
IMMSP	THREETOX	Baltic Sea	Maderich et al. (2008)
IMMSP/KIOST	I/K-E, I/K-L	Fukushima	Roland et al. (2012)
USEV	USEV-2D	Baltic Sea	Periáñez et al. (2013)
KAERI	LORAS	Fukushima	Min et al. (2013)
NTUA	PHOENICS	Fukushima	Psaltaki et al. (2010)
IEN	SisBahia	Fukushima	Lamego (2013)
JAEA	SEA-GEARN	Fukushima	Kobayashi et al. (2007)
USEV	USEV-3D	Fukushima	Periáñez et al. (2012)
IFREMER	MARS3D	Fukushima	Bailly du Bois et al. (2014)
Univ. Toulouse	SYMPHONIE	Fukushima	Estournel et al. (2012)

In the case of the Baltic Sea four models were applied. They were two box-models: NRPA and POSEIDON; a 2D depth-averaged model forced by annual mean wind: USEV-2D; and a full 3D model including thermodynamics: THREETOX. In the case of Fukushima box models were not applied. Instead, all models were Eulerian or Lagrangian three dimensional dispersion models. The origin of the water circulation fields required to force Fukushima models is different for each model, i.e., water circulation is imported from different operative oceanographic models (Periáñez et al., 2015b). All models applied in both scenarios included water/sediment interactions.

For the Baltic Sea, models were started 6 months after Chernobyl deposition and when the first comprehensive investigation on the fallout distribution in the entire Baltic Sea was carried out, in October 1986. A map of 137-Cs in surface water over the Baltic obtained from measurements was

used as initial conditions. This date is t=0, and five year long simulations were carried out. The same information was extracted from all the models to allow intercomparisons and comparisons with field data from HELCOM (Helsinki Convention on the Protection of the Marine Environment of the Baltic Sea Area) database. These data were annual 137-Cs concentrations in the water column and bed sediments (mean values over several Baltic Sea sub-basins) and annual inventories in the water column and bed sediments estimated from measurements. Additionally, time series of 137-Cs concentrations in water and bed sediments were produced for some locations in the Baltic, which are used for further model intercomparisons.

The overall idea in the Fukushima scenario was to harmonize models, making them run with the same forcing in a step-by-step procedure, in such a way that the main agent in producing discrepancy between models can be found. This type of model intercomparison exercise was never carried out before for the marine environment. This was motivated since a simple preliminary exercise consisting of simulating the dispersion of a perfectly conservative radionuclide released at a constant hypothetical rate from Fukushima led to considerable differences in model results (concentrations in surface water some tens of km offshore Fukushima expanding over several orders of magnitude).

Results and Discussion

The four models applied to the Baltic Sea produced very consistent results for the temporal evolution of 137-Cs inventories in the water column and bed sediments over the Baltic, time series of radionuclide concentrations in water and sediment at some fixed points and time series of averaged 137-Cs concentrations in water and sediment over several sub-basins of the Baltic for five years following Chernobyl deposition on the sea surface. These averaged concentrations were also in good agreement with those obtained from measurements and reported in HELCOM (www.helcom.fi) database.

The Baltic Sea is a complex semi-enclosed marine environment. We may mention that it presents vertical stratification which reduces towards the north, horizontal density gradients and significant freshwater supplies. It is also partially covered by ice, especially in the north and during the winter. THREETOX model includes all these processes, but they are completely neglected in USEV-2D, for instance. In spite of this, there is a remarkable agreement between these models, as well as between these two models and the box models. Surprisingly, it seems that these processes are not too relevant for radionuclide transport in the Baltic Sea after the Chernobyl accident since similar results are obtained with models which include them and models which do not. Even in the case of bed sediments the agreement between all models is good (Periáñez et al., 2015a), in spite of the fact that each model is using its own description of water/sediment interactions. Nevertheless, it should be kept in mind that radionuclide transport could have been different if the accident occurred in winter, when a significant ice cover would exist.

The situation is completely different in the case of Fukushima releases. A first set of calculations consisting of simulating the dispersion of a perfectly conservative radionuclide (remaining dissolved, without interacting with suspended matter and bed sediments) released at a constant hypothetical rate from Fukushima led to considerable differences in model results (concentrations in surface water some km offshore Fukushima expanding over several orders of magnitude). A further chain of simulations was then carried out to investigate the reason for these significant model discrepancies. Model results when all of them use the same description of hydrodynamics (from the same circulation model), bathymetry and diffusion coefficients are now significantly closer than before. The produced signals are similar and results are within the same order of magnitude. From the set of simulations, it could be concluded that the main factor in producing differences between models was the use of different water circulation (Periáñez et al., 2015b). It did not seem possible to

achieve a further agreement between the applied models. Differences in model outputs are now attributed to intrinsic differences between them: a) Lagrangian vs. Eulerian models and b) the different numerical schemes which may be applied for each model category mentioned in a). The particular method used to reconstruct radionuclide concentrations from the density of particles in Lagrangian models may be relevant as well.

A comparison of model results with 137-Cs measurements in water and sediments was also carried out. Realistic source terms for both direct releases and atmospheric deposition were used. Direct releases were reconstructed by Kobayashi et al. (2013). Atmospheric dispersion modelling was used to obtain 137-Cs deposition maps over the ocean (Periáñez et al., 2015b). Model-data comparisons may be seen in Periáñez et al. (2015b).

The natural question which arises is why models with very different natures (from box to full 3D models) and parameterizations led to very coherent results in a complex marine environment like the Baltic Sea while, on the other hand, a drastic model harmonization was required in Japan coastal waters to have a reasonable agreement between rather similar models. Two marine environments have been studied: a highly dynamic system (Fukushima coastal waters) and a semi-enclosed basin (Baltic Sea). The description of the hydrodynamics is much more critical in the case of a dynamic system, since in the case of the Baltic Sea results of models are in good agreement in spite of the different approaches and simplifications applied by models. In the case of Fukushima, even similar hydrodynamic models lead to different current fields which, in turn, lead to very different radionuclide dispersion patterns. Given the intensity and variability of currents in this area, as well as the presence of unsteady eddies due to current convergence here, small differences in the hydrodynamics produce different dispersion patterns. These differences tend to be amplified with time. Results from the present exercises highlight the difficulties of developing operative modelling systems for supporting decision-making in cases of emergencies in highly dynamic environments: the output of the system will be very dependent on the ocean model which has been used for the prediction of currents. Further research on this type of emergency models is clearly required.

It seems evident that dispersion models are robust tools, providing consistent results. But the problem is located in the hydrodynamic forcing in energetic regions characterized by strong current variability, like Fukushima waters. Although applied hydrodynamic models may be providing a coherent general picture of water circulation in the area of interest, small differences in current magnitude and/or direction in the area of release cause that initial transport pathways are different.

The question then is how to proceed to develop a reliable model to be used to support decision-making after an emergency. A multi-model approach, as described by Monte et al. (2008), may be of interest when environmental processes are complex. Through this approach, the conclusions that obtain the greatest degree of consensus among modellers are made evident and the aspects that are subject to dispute and which should therefore be handled carefully also become clear. Nevertheless, a multi-model application is not the perfect choice when an emergency is involved and a rapid response from the model is required. In any case, it may help (in the model development stage) to select the most adequate characterization of water circulation to be used in the operational dispersion model. Care should be taken in any case: there may be cases when an "outlier model" is closer to observations than the "consensus". An example is provided in IAEA (1995) -pages 26-28.

We could define three stages, characterized by increasing spatio-temporal scales, after a nuclear accident in a coastal facility, each of them requiring a specific kind of model to give a response to decision makers. It must be noted that an "ideal" model which could be applied for all spatio-temporal scales does not exist. Of course physical-chemical processes are the same, but depending on the scales in which we are interested the numerical realization and involved simplifications are different. This leads to the different modelling approaches: from box models to full 3D coupled

hydrodynamic-dispersion models. The three stages which should be considered after an emergency are the following:

-Emergency phase: The temporal scale of the simulation extends from hours to a few days and the spatial scale to be solved from tens to a few hundred km. In this case a very rapid response (in matter of seconds to a few minutes) should be given by the model to decide, for instance, if swimming must be immediately banned in a beach, or the area where fishing should be banned. This rapid response may be achieved using data on forecast of currents and diffusivity from operational marine models and using Lagrangian models to predict the transport of radioactivity. The temporal horizon of such water current prediction is limited by the temporal scale of weather forecasts, which is about 7-10 days. Examples of this approach are given by Perianez and Pascual-Granged (2008), Duffa et al. (2016) and Maderich et al. (submitted). The marine product contamination can also be estimated using biota dynamic models, as it was done by Duffa et al. (2016). In this initial stage, the model output would also help to develop sampling strategies for monitoring.

-Post-emergency: the temporal scale extends to a few weeks and the spatial one to the order of 10^2-10^3 km. We may imagine that a desalination plant produces fresh water for irrigation a few hundred km from the nuclear facility. It should be decided if taking sea water should be stopped. Now there is more time to provide an answer than in the first stage. In this phase the use of short-term ocean forecasts is not viable. The potential solution is using data from analogous periods of previous years and formation of ensemble of radioactivity predictions to estimate future contamination of water, sediments and biota. With respect to the dispersion model, both Lagrangian and Eulerian approaches could be used (for instance Kawamura et al., 2011, and Periáñez et al., 2012, respectively).

-Long-term: this phase would imply the assessment of the long-term consequences of the accident, including transfers of radionuclides to sediments and biota, as well as evaluating the potential role of sediments as a source of contamination once radionuclide concentrations in seawater have decreased (Periáñez, 2003). This assessment may be carried out with Eulerian models, in which these complex processes are more easily included than in Lagrangian ones, and coupled dynamic biota models (Vives i Batlle et al., 2016). Water current fields are obtained from time-averaging of ocean circulation model outputs. Simulations over several months may be carried out for spatial scales of some hundred km. For even longer-term assessments (years to decades and thousand km), box models should be used (Lepicard et al., 2004; Iosjpe et al., 2009).

In any case, for highly dynamic environments, we have found that model output is extremely sensitive to the ocean model which is used to obtain circulation. Thus, the ocean model should be selected with great care and after a detailed comparison with local measurements of currents. In this sense, Duffa et al. (2016) indicated that local forecasts of marine circulation should be used for emergency modelling. Although global ocean models produce realistic pictures of the general circulation in the ocean, their outputs differ in the local scale in dynamic environments, as it has been found. This may be, at least in part, attributed to their relatively coarse spatial resolution.

Overall, models to be used for emergencies in the marine environment should be carefully tuned for each particular location, i.e., for each nuclear facility for which it is decided to have a modelling tool to support decision-making after a potential emergency occurring there. In other words, we cannot be a priori confident in generic models which import ocean forecasts of currents if a highly dynamic environment is involved.

Conclusions

State-of-the-art models were applied to simulate the dispersion of 137-Cs coming from Chernobyl fallout in the Baltic Sea and Fukushima releases in the Pacific Ocean. The basic components of

models which solve the transport of radionuclides in the abiotic compartments of a marine system are the hydrodynamic sub-model, which provides water circulation, and the dispersion sub-model, which includes advection/diffusion as well as a description of water/sediment interactions.

It was found that the energetics of the considered system (magnitude and variability of currents) is essential to obtain a good agreement between different models. Good agreement can be achieved between models of very different nature in environments characterized by weak currents. However, even similar models lead to rather different results in highly dynamic systems characterized by strong and variable currents.

This fact highlights the difficulties in developing operational models for emergency management and decision-making support (which is one of the main application of numerical modelling) in these dynamic environments. For this purpose, coastal nuclear facilities should put a significant effort in selecting the most appropriate hydrodynamic model for their specific location after a detailed and careful comparison of model results and observations.

References

Bailly du Bois, P., Garreau, P., Laguionie, P., Korsakissok, I., (2014). Comparison between modelling and measurement of marine dispersion, environmental half-time and 137-Cs inventories after the Fukushima Daiichi accident. Ocean Dynamics 64, 361-383.

Duffa, C., Bailly du Bois, P., Caillaud, M., Charmasson, S., Couvez, C., Didier, D., Dumas, F., Fievet, B., Morillon, M., Renaud, P., Thebault, H., (2016). Development of emergency response tools for accidental radiological contamination of French coastal areas. Journal of Environmental Radioactivity 151, 487-494.

Estournel, C., Bosc, E., Bocquet, M., Ulses, C., Marselaix, P., Winiarek, V., Osvath, I., Nguyen, C., Duhaut, T., Lyard, F., Michaud, H., Auclair, F., (2012). Assessment of the amount of 137-Cs released into the Pacific Ocean after the Fuskushima accident and analysis of its dispersion in Japanase coastal waters. Journal of Geophysical Research 117, C1014.

IAEA, (1995). Validation of models using Chernobyl fallout data from the Central Bohemia region of the Czech Republic. Scenario CB. First report of the VAMP Multiple Pathways Assessment Working Group. IAEA-TECDOC-795, Vienna.

Iosjpe M., Karcher, M., Gwynn, J., Harms, I., Gerdes, R., Kauker, F., (2009). Improvement of the dose assessment tools on the basis of dispersion of the 99-Tc in the Nordic Seas and the Arctic Ocean. Radioprotection 44(5), 531-536.

Kawamura H., Kobayashi T., Furuno A., In T., Ishikawa Y., Nakayama T., Shima S., Awaji T., (2011). Preliminary numerical experiments on oceanic dispersion of 131-I and 137-Cs discharged into the ocean because of the Fukushima Daiichi nuclear power plant disaster. Journal of Nuclear Science and Technology 48, 1349-1356.

Kobayashi, T., Otosaka, S., Togawa, O., Hayashi, K., (2007). Development of a nonconservative radionuclides dispersion model in the ocean and its application to surface cesium-137 dispersion in the Irish Sea. Journal of Nuclear Science and Technology 44(2), 238-247.

Kobayashi, T., Nagai, H., Chino, M., Kawamura, H., (2013). Source term estimation of atmospheric release due to the Fukushima Dai-ichi Nuclear Power Plant accident by atmospheric and oceanic dispersion simulations. Journal of Nuclear Science and Technology 50, 255-264.

Lamego, F.F., (2013). Advanced Nuclear Reactors and Tritium Impacts: Modeling the aquatic pathway. Progress in Nuclear Energy 68, 9-22.

Lepicard S., Heling R., Maderich V. (2004). POSEIDON/RODOS model for radiological assessment of marine environment after accidental releases: application to coastal areas of the Baltic, Black and North seas. Journal of Environmental Radioactivity 72, 1-2, 153-161.

Maderich V., Heling R., Bezhenar R., Brovchenko I., Jenner H., Koshebutskyy V., Kuschan A., Terletska K.. (2008). Development and application of 3D numerical model THREETOX to the prediction of cooling water transport and mixing in the inland and coastal waters. Hydrological Processes 22, 1000-1013.

Maderich, V., Brovchenko, I., Dvorzhak, A., Ievdin, Y., Koshebutsky, V., Periañez, R., (submitted). Integration of 3D model THREETOX in JRODOS-HDM, implementation studies and model validation on marine Fukushima scenarios. Radioprotection. Special issue.

Min, B.I., Periáñez, R., Kim, I.G., Suh, K.S., (2013). Marine Dispersion Assessment of 137-Cs Released from the Fukushima Nuclear Accident. Marine Pollution Bulletin 72, 22-33.

Monte, L., Boyer, P., Brittain, J., Goutal, N., Heling, R., Kryshev, A., Kryshev, I., Laptev, G., Luck, M., Periáñez, R., Siclet, F., Zheleznyak, M., (2008). Testing models for predicting the behaviour of radionuclides in aquatic systems. Applied Radiation and Isotopes 66, 1736-1740.

Periáñez, R., (2003). Redissolution and long-term transport of radionuclides released from a contaminated sediment: a numerical modelling study. Estuarine, Coastal and Shelf Science 56, 5-14.

Periáñez, R., Pascual-Granged, A., (2008). Modelling surface radioactive, chemical and oil spills in the Strait of Gibraltar. Computers and Geosciences 34, 163-180.

Periáñez, R., Kyung-Suk Suh, Byung-Il Min, (2012). Local scale marine modelling of Fukushima releases. Assessment of water and sediment contamination and sensitivity to water circulation description. Marine Pollution Bulletin 64, 2333-2339.

Periáñez, R., Casas-Ruíz, M., Bolívar, J.P., (2013). Tidal circulation, sediment and pollutant transport in Cádiz Bay (SW Spain): a modelling study. Ocean Engineering 69, 60-69.

Periáñez, R., Bezhenar, R., Iosjpe, M., Maderich,V., Nies,H., Osvath, I., Outola, I., de With, G., (2015a). A comparison of marine radionuclide dispersion models for the Baltic Sea in the frame of IAEA MODARIA program. Journal of Environmental Radioactivity 139, 66-77.

Periáñez, R., Bezhenar, R., Byung-Il, Min, Duffa, C., Jung, K., Kobayashi, T., Kyung-Suk, Suh, Lamego, F., Maderich,V., Nies,H., Osvath, I., Psaltaki, M., (2015b). A new comparison of marine dispersion model performances for Fukushima releases in the frame of IAEA MODARIA program. Journal of Environmental Radioactivity 150, 247-269.

Psaltaki, M., Florou, H., Trabidou, G., Markatos, N.C., (2010). Modelling and assessment of pollutant impact on marine environments. 2nd WSEAS International Conference on Computer Engineering and Applications (CEA '10) Harvard University, Cambridge USA, p.p.176-180, January 27-29, 2010.

Roland A., Zhang Y.J., Wang H.V., Meng Y, Teng Y.C., Maderich V., Brovchenko I., Dutour-Sikiric M., Zanke U., (2012). A fully coupled 3D wave-current interaction model on unstructured grids. Journal of Geophysical Research 117, C00J33, p. 1-18 doi:10.1029/2012JC007952.

Vives i Batlle, J., Beresford, N., Beaugelin-Seiller, K., Bezhenar, R., Brown, J., Cheng, J.J., Cujic, M., Dragovic, S.S., Duffa, C., Fievet, B., Hosseini, A., Jung, K.T., Kamboj, S., Keum, D.K., Kryshev, A., Le Poire, D., Maderich, V., Min, B.I., Periáñez, R., Sazykina, T., Suh, K.S., Yu, C., Wang, C., Heling, R., (2016). Inter-comparison of dynamic models for radionuclide transfer to marine biota in a Fukushima accident scenario. Journal of Environmental Radioactivity 153, 31-50.

Radioecological Informatics and Modelling of Polonium-210 and Caesium-137 in top predators.

B.R.R. Persson[1*], R. Gjelsvik[2], J.A. Kålås[3], J. Åsbrink[4], E. Holm[5]
:
Department of Medical Radiation Physics, Lund University, Lund, Sweden[1*]
Norwegian Radiation Protection Authority, NRPA, Norway[2]
Norwegian Institute for Nature Research, NINA, Norway[3]
National Veterinary Institute, Sweden[4]
Department of Medical Radiation Physics, Gothenburg University, GothenburgSweden[5],

Abstract

The results of ^{210}Po and ^{137}Cs in wolf, wolverine and Lynx have previously been published (Gjelsvik et al., 2014). In the present work these data are analysed with multivariate data processing methods such as Principal Component Analysis PCA, and modelled with the method of Projection to Latent Structures, PLS, or PLSR Partial Least Square Regression.

Introduction

Partial least squares was introduced by Herman Wold (Wold, 1982). His son Svante Wold, who was a chemist has then developed the method to be used in chemometrics, and according to him, the *projection to latent structures* should be the correct name of the method (Wold et al., 2001).Partial least square regression modelling (PLS-r) has previously been used to predict missing data of air concentration of ^{7}Be, ^{210}Pb and ^{210}Po at locations where only deposition values are available, and vice versa. In the PLS-r modelling, air concentration and deposition, values are used as dependent Y-variables, and height, latitude, longitude, and geometric average of time-period (GAT) as explanatory X-variables (Persson, 2016). Details about partial least square regression modelling (PLS-r) are given in the following references: Tenenhaus et al., 2005; Wold et al., 1996; and XLSTAT, 2015).The results of ^{210}Po and ^{137}Cs in wolf, wolverine and lynx have previously been published (Gjelsvik et al., 2014). The aim of the present work is to analyse and model these data with multivariate data processing methods such as Principal Component Analysis PCA, and modelling with the method of Projection to Latent Structures, PLS, or PLSR Partial Least Square Regression.

Materials and Methods

Samples
Wolves: In 2010, January-March, 9 wolves were obtained through traffic accident. In 2011, January 19 animals were sampledby regulated hunting.
Lynx: 16 animals were killed during regular hunting period, February-March 2011
Wolverine: 16 animals were obtained through hunting or trapping, February-march 2011

Multivariate analyses and modelling
A multidimensional variable databaseare created that is handled by using multivariate statistics. In radioecological informatics modelling the Principal component analyses PCA and clustering is used to study the quality and structure of the original database. PCA can also be used to find outliers and to find out if the data can be divided into various classes. In order to find an equation to predict the dependent variables from the descriptors, the model of Projection to Latent Structures, PLS-regression PLSR was used (XLSTAT, 2015).

---

*Corresponding author, E-mail: Bertil_r.persson@med.lu.se

Results and Discussion

Polonium-210 in wolf
In the first run the [210]Po data for wolf samples were analysed and it was found that they could be divided in 3 classes.
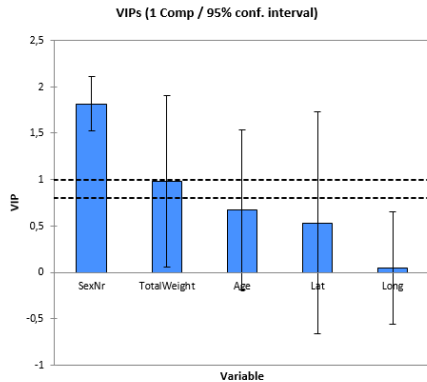
Figure 1. *Variable Importance of the various independent variables (descriptors) in the Projection (VIP).*
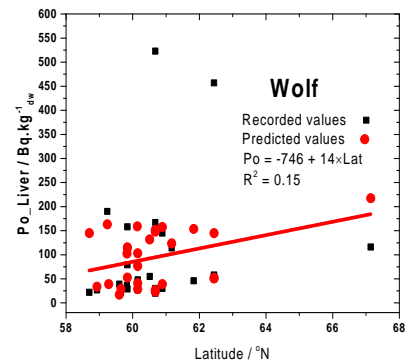
. **Figure 2.** *Recorded and predicted values of [210]Po activity concentration in liver from wolf sampled at various latitudes along longitude 14,4± 1,7 °E.*

The variable importance in the Projections (VIP) in the PLSR analysis of the activity concentration of [210]Po on wolf samples with sex, weight, age, longitude and latitude is shown in Figure 1.
The sex of the wolf (male =1, female=2) seems to be of great importance, which indicate that the male intake is larger.

The Equations of the model for prediction of activity concentration i the various organs of wolves:

Po_Liver = -360.5 - 0.610*Long + 7.80*Lat - 85.0*SexNr – 7.99*Age+3.32*TotalWeight

Po_kidney = -487.7 - 0.804*Long + 10.28*Lat – 112.1*SexNr – 10.53*Age+4.38*TotalWeight

Po_Muscle = -25.77 - 0.042*Long + 0.532*Lat – 5.798*SexNr – 0.545*Age+0.226*TotalWeight

Po_Blood = -40.15 - 0.072*Long + 0.916*Lat – 10.0*SexNr – 0.934*Age+0.390*TotalWeight

Recorded and predicted values of [210]Po activity concentration in liver from wolf sampled at various latitudes along longitude 14,4 ± 1,7 °E are displayed in Figure 2. The two high values are in liver samples fromHärjedalen 457 Bq/kg$_{dw}$ and Malung 523 Bq/kg$_{dw}$ are included in the analysis.

Polonium-210 in wolverine
A PLS modeling of [210]Po activity concentration in wolverine liver as depending variable and with [210]Po in precipitation, age, sex and total weight as predictors, resulted in the equation:

Po_Liver = -5.116 + 0.499*SexNr - 0.473*Age - 0.140*TotalWeight + 13.777*PoPrec

The variable importance in the Projections (VIP) in the PLSR analysis of the activity concentration of [210]Po on wolverine samples with sex, weight, age, longitude and latitude is shown in Figure 3.
Total body weight and sex of the wolverineis of less importance than in wolves. For wolverine, location seems to be most important. Recorded and predicted values of [210]Po activity concentration

*Corresponding author, E-mail: Bertil_r.persson@med.lu.se

in liver fromwolverine sampled at various latitudes sampled along longitude 16,2 ± 7,3 °Eis displayed in **Figure 4**.
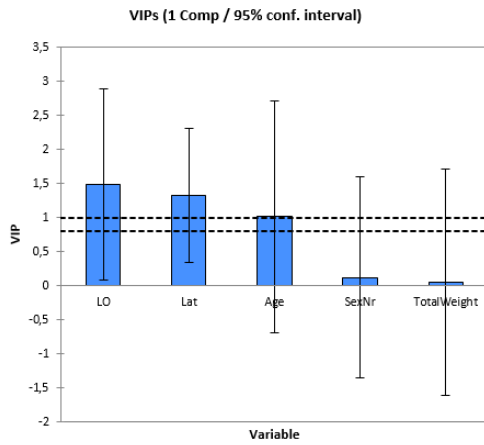
Figure 3 Variable Importance for the dependent variables (descriptors) in the Projection (VIP):
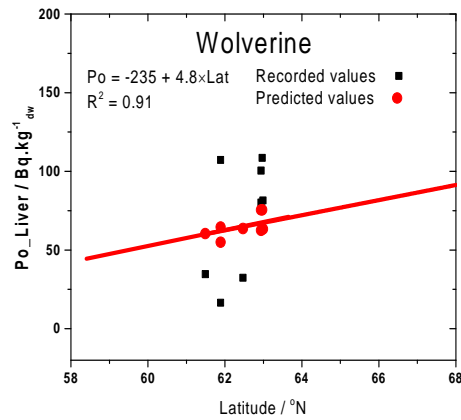
Figure 4 Recorded and predicted values of ^{210}Po activity concentration in liver from wolverine sampled at various latitudes sampled along longitude 16,2 ± 7,3 °E

The Equation of the model for prediction of activity concentration of ^{210}Po in wolverineis as follow:

Po_Liver = -67.9 + 1.22*LO + 2.16*Lat - 1.42*SexNr - 3.24*Age + 0.136*TotalWeight

Polonium-210 in lynx

A PLS modeling of ^{210}Po activity concentration in lynx liver as depending variable and with ^{210}Po in precipitation, age, sex and total weight as descriptors, resulted in the equation:

Po_Liver = 10.5 - 4.18*SexNr+0.497*Age-0.846*TotalWeight+14.1 *Poprec
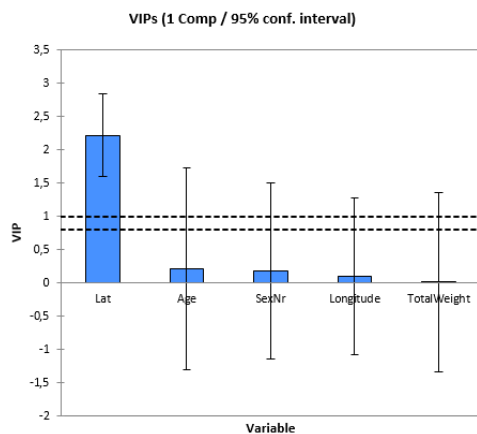
Figure 5 Variable Importance for the dependent variables (descriptors) in the Projection (VIP) for lynx.
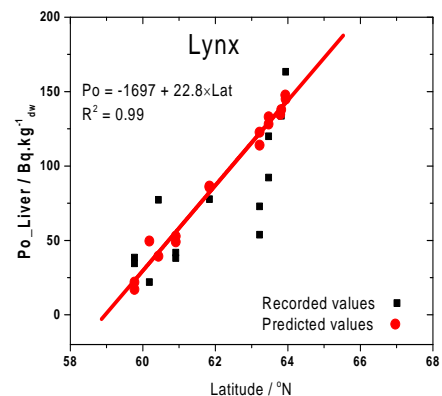
Figure 6 Recorded and predicted values of ^{210}Po activity concentration in liver from lynx sampled at various latitudes sampled along longitude 10,7 ± 0,6 °E

*Corresponding author, E-mail: Bertil_r.persson@med.lu.se

A PLS modeling of ^{210}Po activity concentration in lynx liver as depending variable, and with longitude, latitude, age, sex and total weight as descriptors, resulted in the equation:

Po_Liver = -1645 - 3.19*Longitude + 28.6*Lat - 7.03*SexNr + 1.948*Age - 0.0573*TotalWeight

Caesium-137 in wolf
By k-means clustering of the ^{137}Cs data for wolf samples it was found that they could be divided in 4 classes.
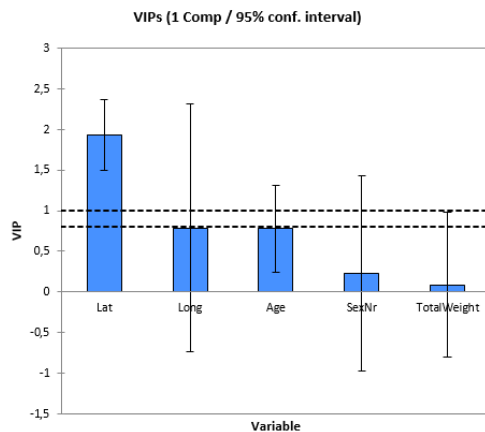
Figure 7 Variable Importance for the dependent variables (descriptors) in the Projection (VIP) for ^{137}Cs in wolf
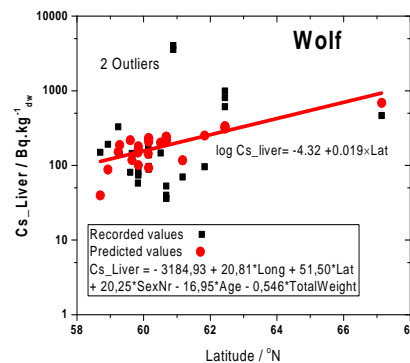
Figure 8 Recorded and predicted values of ^{137}Cs activity concentration in liver from wolf sampled at various latitudes sampled along longitude *14,4 ± 1,7 ^{o}E*

The variable importance in the Projections (VIP) in the PLSR analysis of the activity concentration of ^{137}Cs on wolf samples with sex, weight, age, longitude and latitude is shown in Figure 7. The sex of the wolf seems to be of less importance for ^{137}Cs than for ^{210}Po.

The Equations of the model for prediction of activity concentration in various organs:

Cs_Liver = - 3184.93 + 20.81*Long + 51.50*Lat + 20.25*SexNr - 16.95*Age - 0.546*TotalWeight

Cs_Kidney = - 2192.14 + 14.40*Long + 35.63*Lat + 14.01*SexNr – 11.73*Age - 0.378*TotalWeight

Cs_muscle = - 4123.65 + 27.02*Long + 66.86*Lat + 26.30*SexNr – 22.01*Age - 0.709*TotalWeight

Cs_blood = 70.15 - 0.300*Long – 0.743*Lat - 0.292*SexNr + 0.244*Age + 0.008*TotalWeight

Caesium-137 in wolverine
By k-means clustering of the ^{137}Cs data for wolverine samples it was found that they could be divided into 3 classes.
Model equations for prediction of activity concentration in Wolverine liver with sex, age, weight and ^{137}Cs precipitation in the area as descriptors:

Cs_Liver = -259.0 - 16.45*SexNr + 30.12*Age - 0.196*TotalWeight + 52.8 *CsPrec
Cs_Muscle = -289.7 - 24.685 *SexNr + 42.05 *Age + 0.0830 *TotalWeight + 74.0 *CsPrec

*Corresponding author, E-mail: Bertil_r.persson@med.lu.se

The variable importance in the Projections (VIP) in the PLSR analysis of the activity concentration of ^{137}Cs on wolverine samples with sex, weight, age, longitude and latitude is shown in Figure 9.

The Equations of the model for prediction of activity concentration in the liver and muscle of wolverine:

Cs_Liver = 4310-17.096*LO-50.368*Lat+245.0*SexNr+38.96*Age-55.42*TotalWeight

Cs_Muscle = 6513-25.75*LO-75.86*Lat+369.0*SexNr+58.67*Age-83.46*TotalWeight
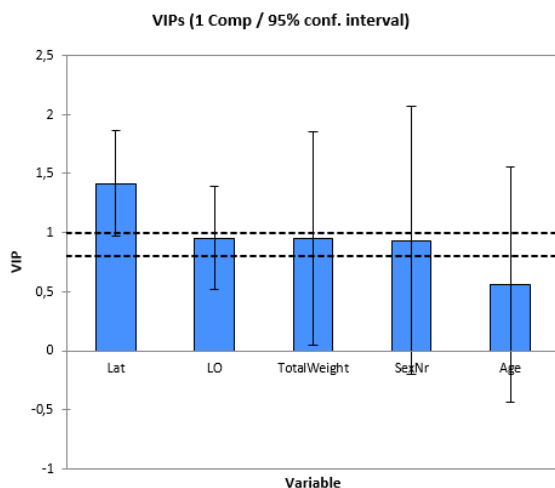
Figure 9 Variable Importance for the dependent variables (descriptors) in the Projection (VIP) for ^{137}Cs in wolverine
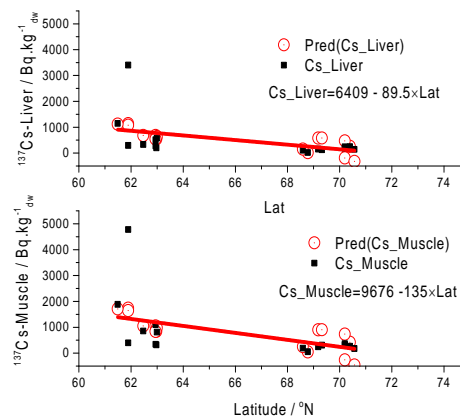
Figure 10 Recorded and predicted values of ^{137}Cs activity concentration in liver from wolverine sampled at various latitudes sampled along longitude $16,2 \pm 7,3$ °E

*Caesium-137 in Lynx*
By k-means clustering of the ^{137}Cs data for lynx samples it was found that they could be divided into 3 classes.

Model equations for prediction of activity concentration in lynx liver with sex,age, weight and ^{137}Cs precipitation in the area as descriptors:

Cs_Liver = -107.25 - 34.9*SexNr + 4.6*Age + 0.438*TotalWeight + 56.8*CsPrec

Cs_Muscle = -160.17 - 25.6*SexNr + 40.02*Age + 8.848*TotalWeight + 61.7*CsPrec

The variable importance in the Projections (VIP) in the PLSR analysis of the activity concentration of ^{137}Cs inlynx samples with sex, weight, age, longitude and latitude is shown in Figure 11.

The Equations of the model for prediction of activity concentration i the liver and muscle of lynx:

Cs_Liver = -40612+ 810*Long + 547*Lat+1173*SexNr + 230*Age - 175*TotalWeight
Cs_Muscle = -31168 + 629*Long + 425*Lat + 911*SexNr + 179*Age - 136*TotalWeight

5

*Corresponding author, E-mail: Bertil_r.persson@med.lu.se
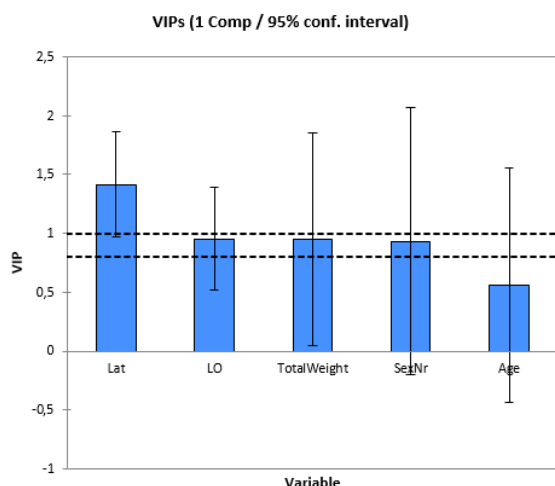
Figure 11 Variable Importance for the dependent variables (descriptors) in the Projection (VIP) for ^{137}Cs in wolverine
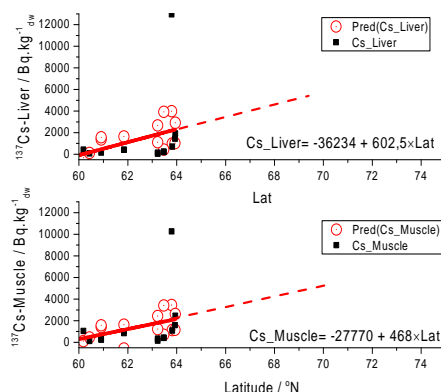
Figure 12 Recorded and predicted values of ^{137}Cs activity concentration in liver of wolverine sampled at various latitudes sampled along longitude $10,7 \pm 0,6$ ^{o}E,

Conclusions

The results of ^{210}Po and ^{137}Cs in wolf, wolverine and lynx have been analysed and modelled with multivariate data processing methods such as PCA and PLSR togenerateregression equations for ^{210}Po and ^{137}Cs activity concentrations in various tissues as dependent variables andsex, weight, age, longitude and latitude as from the descriptors.

References

Gjelsvik, R., Holm, E., Kålås, J.A., Persson, B., Åsbrink, J., 2014. Polonium-210 and Caesium-137 in lynx (*Lynx lynx*), wolverine (*Gulo gulo*) and wolves (*Canis lupus*). Journal of Environmental Radioactivity 138, 402-409.

Persson, B.R.R., 2016. Global distribution of ^{7}Be,^{210}Pb and, ^{210}Po in the surface air (with Appenix A-E). Acta Scientiarum Lundensia 2015, 1-51.

Tenenhaus, M., Pages, J., Ambroisine, L., Guinot, C., 2005. PLS methodology to study relationships between hedonic judgements and product characteristics. Food Quality and Preference 16, 315-325.

Wold, H., 1982. Soft modelling: the basic design and some extensions,*Systems under indirect observation, Part II*, 36-37.Wold, S., Kettaneh, N., Tjessem, K., 1996. Hierarchical multiblock PLS and PC models for easier model interpretation and as an alternative to variable selection. Journal of Chemometrics 10, 463-482.

Wold, S., Kettaneh, N., Tjessem, K., 1996. Hierarchical multiblock PLS and PC models for easier model interpretation and as an alternative to variable selection. Journal of Chemometrics 10, 463-482.

Wold, S., Sjostrom, M., Eriksson, L., 2001. PLS-regression: a basic tool of chemometrics. Chemometrics and Intelligent Laboratory Systems 58, 109-130.

XLSTAT, 2015. Data analysis and statistics with MS Excel®. Web: www.xlstat.com, Addinsoft,, 40 rue Damrémont 75018, Paris, France

*Corresponding author, E-mail: Bertil_r.persson@med.lu.se

Considerations of application of ecological thermodynamics to radionuclide transfer parameters

V. Kangasniemi[*] and A. T. K. Ikonen

EnviroCase Ltd., Hallituskatu 1 D 4, 28100 Pori, Finland

Abstract

Transfer of radionuclides into biota is clearly regulated by the availability and uptake/intake and the respective levels also by the losses from the organisms. Conceptually, this can be addressed also with allometric scaling, phylogeny and ecological stoichiometry. These have been studied also for their applications in radioecology, but the ecological niches and food webs as entireties have attracted less attention. This contribution considers some basic ideas of utilising ecological thermodynamics –energy balance of the ecosystem in and between its components – combined with stoichiometry to study processes affecting the radionuclide transfer in food webs usually represented in a much stylised manner through the use of concentration ratios aggregating over the trophic relationships and other factors.

Thermodynamic balance at the level of organisms comprises of consumption (uptake or intake) and the equalling sum of production (growth), respiration and excretion. Due to the typically high losses, the output flux available for the higher trophic levels (production) must be clearly less than the consumption. For the balance, the system considered should be closed in respect of the energy fluxes, at least so that reliable boundary conditions can be established – one must consider a whole ecosystem. Whereas the thermodynamic principles are the same for all, the rates of resource uptake, transformation and allocation vary (largely with temperature and body size), but also the availability of the resources and their elemental composition do vary. Despite of the complicated appearance, ecological thermodynamics and stoichiometry, especially when combined, could help in recognising features and processes explaining observed characteristics of concentration ratio data. Such deeper understanding would also benefit sufficient description of the ambient environmental conditions in field and laboratory work, allowing further analysis of the theoretically expected regularities.

Introduction

Modelling the transport of radionuclides in the environment and through food webs is needed for many applications, not the least for assessing the exposure of people and wildlife in various situations. Many such models employ simple concentration ratios (i.e., ratios of the radionuclide concentration in the organism and in its living medium) (e.g., Brown et al., 2016; Howard et al., 2013), but some models use biological half-lives of the radionuclides together with the food-chain transfer from the diet of an organism (e.g., USDOE, 2004). Often the input data is lacking to an extent (e.g., Howard et al., 2013), and surrogate values need to be assumed in a way or another, for which several methods have readily been tested to fill these gaps and reduce uncertainties (e.g., Beresford et al., 2016). These, of course, include approaches also used in other areas of ecology (e.g., Allen &Gillooly, 2009; Brown et al., 2004; Cresswell et al., 2014). However, the discussion on the theoretical background of the rationales understandably remains brief in connection of the various applications. This paper aims at contributing to such reasoning of the mechanisms underlying the regularities observed in the bulk radionuclide transfer data.

---

[*]Corresponding author, E-mail: ville.kangasniemi@envirocase.fi

Materials and Methods

This contribution is based on the literature referred to in the text.

Results and Discussion

In the following, first some remarks are made on thinking in terms of ecosystems, that is, ecological components and interactions. Then, fundamental thermodynamic principles and their application in terms of bioenergetics of organisms are briefly described. The discussion on the ecological stoichiometry after that adds the role of the different elements and their relationships into the picture, before some remarks on the overall setting from the viewpoint of food webs and ecosystems as a whole.

Ecosystem context

The transport of the radionuclides in the environment occurs on one hand driven by physical (and chemical) phenomena such as water exchange, sedimentation and erosion, and on the other hand in the biological cycling through food webs (for example, Figure 1):an organism consumes another one and finally gets consumed itself. However, finally all is returned, in a form or another, to decomposers and mineralised back to the abiotic matter, to be harvested again by the primary producers. This is to say the obvious: except for laboratory conditions, usually all organisms are in interaction with others and with their constantly changing abiotic environment and extract resources, that is energy, often also called food. When deriving aggregated parameters such as concentration ratios that integrate the effect of several trophic transfers, in times it may be difficult to appreciate the multiple interactions that take their role in promoting and regulating the transfers between the trophic compartments. Some of these interactions and regularities are discussed further in the following subsections.
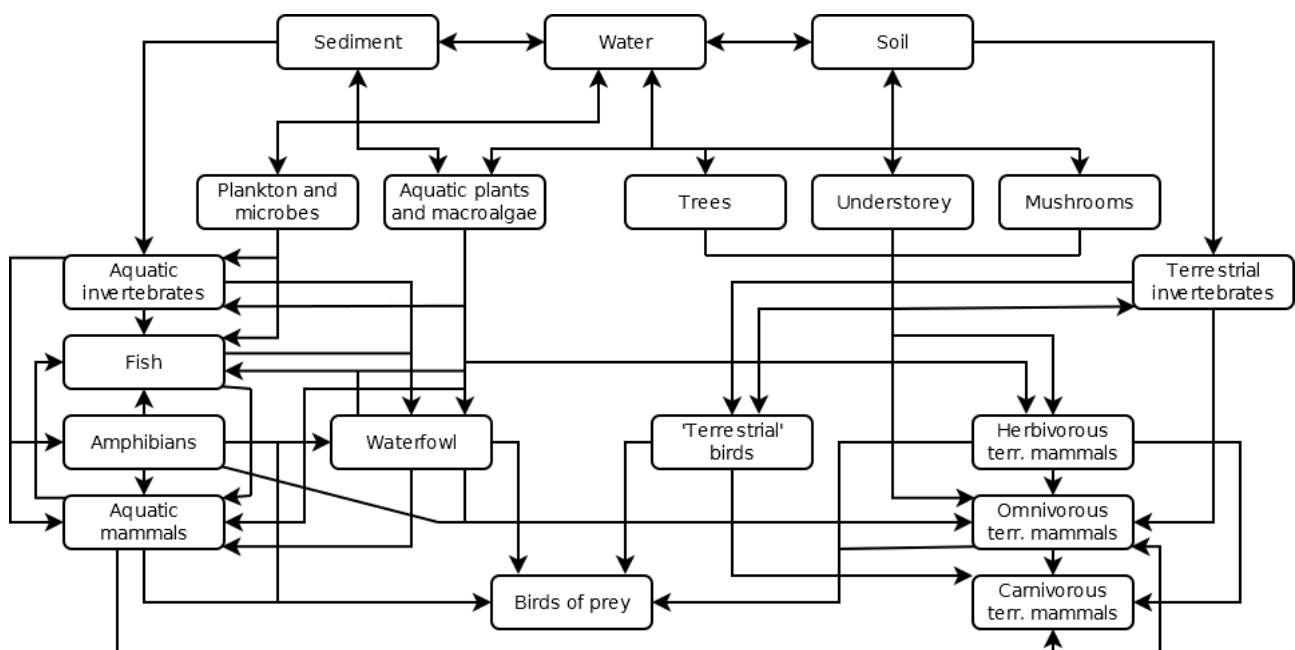
Figure 1.*An example of a food web at northern latitudes (modified from Verkhovskaja et al., 1967). The decomposers are not shown in the graph, but they process the 'left-overs' from all the other components.*

Thermodynamic principles

In general, the living organisms follow the same biochemistry and, universally, nothing can escape the fundamental laws of thermodynamics: when considering a closed system (or a semi-enclosed onetaking the sufficient boundary conditions into account), the amount of energy remains constant, and when converted from a form to another (e.g., from solid food to metabolic energy), losses inevitably occur in the fluxes of energy, and matter, through ecosystems (e.g., Brown et al., 2004; Pimm, 2002; Sterner &Elser, 2002).More practically, everyone needs to eat and rid of the extra, and loose energy (the efficiency of energy transfer between trophic levels, the so-called Lindeman efficiency, is generally about 10%; Brown et al. 2004; Lindeman 1942). At the ecosystem level, an output of an entity is another's input.This pattern is exemplified in Figure 2. These thermodynamic rules work at all levels of organisation and can link the individuals to the ecology of populations, communities and ecosystems (Brown et al., 2004), which makes the 'bioenergetics' also a common basis in several ecological modelling approaches(e.g., Pauly et al., 2000).
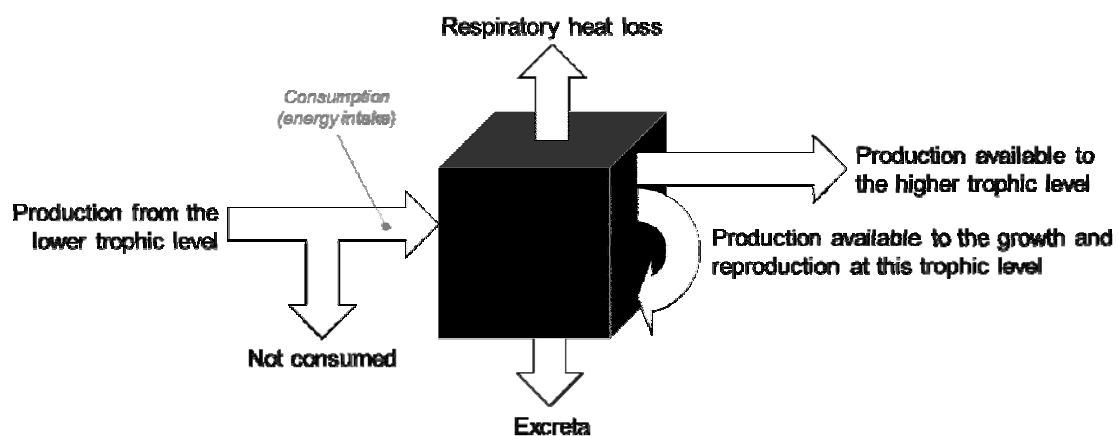
Figure 2.General pattern of energy flow through a heterotroph compartment in an ecosystem. For autotrophs, there is no loss by excreta and the energy intake is directly the input for the photosynthesis, that is light and CO_2. (Developed based on the examples of, e.g., Pauly et al., 2000; Townsend et al., 2008).

Metabolic theory

Whereas the basic thermodynamic principles are the same for all, and nearly all the organisms utilise the same basic biochemistry, the rates of resource uptake, transformation and allocation vary (Brown et al., 2004).The metabolic rateis largely governed by the Boltzmann factor (i.e., the temperature dependence of biochemical processes) and the quarter-power allometric dependency of biological rates on the body size (Brown et al., 2004; Gillooly et al., 2001; West et al., 1997). As a consequence, also the consumption rate scales with the animal size due to the metabolic demand, and also the losses and thus the trophic transfer are dependent on the body size. In radioecology, such allometric scaling methods are used, and there has been discussion on the variability in the scaling parameter values for certain biota groups and elements (radionuclides) mainly from the viewpoint of fitting to experimental data (e.g., Beresford et al., 2016), as well as in the field of bioenergetics in general, although there more prominently based on more theoretical considerations of the underlying mechanisms (e.g., Brown et al., 2004; West et al., 1997).The allometric methods are usually applied to homeothermic vertebrates and poikilothermic reptiles and amphibians, and but they have been tested also for some other biota groups (see the summary by Beresford et al., 2016).

It is usually well appreciated that there is an effect of ambient temperature on the metabolic ratefor poikilotherms, but usually less attention is paid on similar effect with homeotherms: what remains for production after the need of maintaining body functions depends on the ambient temperature. Also other environmental conditions (e.g., Lee & Lee, 2005; Rasmussen & Vander Zanden, 2004), or simply weather in general (e.g., over the growing season, as observed by Weih et al., 2016, for winter wheat), have an effect. Actually, most organisms can vary the metabolic rate and pathways to an extent to adjust for fluctuations in resource supply or demand, latter comprising factors such as reproduction or environmental change (Brown et al., 2004). This implies that the differences between different places and seasons, or longer periods of time, may bear significance to the element concentrations sometimes even at the level of the sampled individuals, even though in many radioecological contexts the interest lies rather in the longer-term averages.

Ecological stoichiometry and regulation by organisms

Ecological stoichiometry studies the balance of chemical elements in ecosystems (Sterner &Elser, 2002), and the closely related ionomics studies the total element composition of an organism (Salt et al., 2008), but these approaches have not been widely used in radioecology (Beresford et al., 2016). This is somewhat surprising when considering the common tendency towards conceptualising the ecosystems as trophic and other compartments, since – as phrased by Sterner &Elser (2002) – "the stoichiometric approach considers whole organisms as if they were single abstract molecules" and this approach has proved to have the capacity to "correctly predict very macroscopic phenomena using its very microscopic principles". In our view, this may be partly explained by the challenge of "interesting effects" arising from the driving mechanisms and constraints behind the stoichiometric variability across organisms, nutritional modes, and trophic levels (Sterner &Elser, 2002).

The stoichiometric approach is, coarsely, based on the principle that the composition of the consumer would follow that of the material consumed, but the food is not always exactly what is desired: "Creatures are, generally, *not* what they eat", but they do depict the residual of what they eat, "egest, defecate, excrete, lactate, exhale, or otherwise release back to the external world" (Sterner &Elser, 2002). Organisms tend to take up the necessary amounts of elements from their food so that they ensure essential levels but avoid toxic concentrations in the body (Hopkin, 1989, cited by Beresford et al., 2016) and pass the rest.

Elemental homeostasis (the ability of organisms to maintain constant body concentration despite changing concentrations in the environment and/or their supply; Sterner &Elser, 2002) means, in the strict sense, that the consumer stoichiometry does not vary with the resource stoichiometry (Sterner &Elser, 2002). However, in practice the degree of homeostasis varies depending whether the element is a macronutrient, an essential micronutrient or a non-essential element (Beresford et al., 2016, and references therein). Both macro- and micronutrients are necessary for the growth and normal development of organisms, and their function cannot be taken on by any other element. Even though the division into essential and non-essential elements is useful in many contexts, it is not always appropriate if broader groups of organisms are considered asa bulk, since certain types of life are more dependent on certain elements than others, or can utilise some elements in the available resources better. Also, the classic determination of essentiality of an element solely based on its high content in the organism is not always correct:A more accurate classification of the organism's need for an element can be built on 'structural elements' that are necessary for cell metabolism (proteins, lipids, carbohydrates, etc.) and for supporting or reinforcing the body (e.g., Ca, Si), 'electrolytic elements' that are important for physiological processes and maintaining osmotic relationships, and 'enzymatic elements' that exercise a catalytic function in cell metabolism

as metal complex compounds.It is to be noted, though, that some elements can act in several such roles (e.g., Ca as a structural and electrolytic element). (Markert et al., 2000; Sterner &Elser, 2002).

When considering the element ratios in the ecosystem, it should be borne in mind that not all food is alike (cf. calorific content of different foodstuffs, a concept applied most commonly to human nutrition) and that anyway the elemental composition varies within a group of individuals (with age, life stages, sexes etc.; Sterner &Elser, 2002). For example, since the body composition of fish is known to vary even considerably with age, it has been proposed that the growth should be expressed in terms of the body energy content (i.e., summation of mineral, protein, fat and carbohydrate fractions) rather than as the ordinary change in the live weight (Chapman, 1978). A more recent example is that variation has been shown to exist in concentrations of a number of nutrients in winter wheat over the life cycle of the plants, bearing a certain systematics (Weih et al., 2016). It is to be also noted, though, that photoautotrophic organisms, such as vascular plants and especially algae, generally "can exhibit a very wide range of physical plasticity in elemental composition", whereas for example multicellular animals have a nearly strict homeostasis (Elser&Kuang, 2012). However, this is not necessarily always the case in a local scale (e.g., Bradshaw et al., 2012).

In addition to the variability in the composition of the available resources as such, one should consider also the physical/chemical form (e.g., elements tightly bound in molecules or adsorbed by particles).It is known that, for example, some organic components in plant litter (e.g., lignin) are not easily available for higher trophic levels (e.g., Liski et al., 2005). However, usually these considerations have readily been resolved by the nature through the specialisation of the different organisms in respect of their food source, albeit some effects through environmental changes hardly can be ruled out as the amount of consumable resources may be limited (or, more rarely, satiation can be observed), when the consumers are forced to either use sub-optimal resources or perish.

Especially in lack of required elements, but to a certain extent also otherwise, biochemically similar elements mimic the required ones in the stoichiometry. For example, concentrations of Sr and Ca, Cs and K, and Ra and Ba are known to correlate with each other to the extent that some radioecological approaches base on this. There is apparently even stronger association between the radionuclide and carbon concentrations, which has been used for radioecological modelling as well. (For a brief summary, see Beresford et al., 2016).

In the context of applying allometric scaling to radionuclide transfer, Beresford et al. (2016) suggest that the apparent difference in the value of the allometric exponent for certain elements (such as Am, Ce, Eu, Pu and Th) could be, perhaps, related to that these elements do not play a biological role. In our view, this seems to be, indeed, related to the biological role of the elements as touched on in the discussion above, but not necessarily so that the exponent as such would change.Their observation that in the aquatic environment the allometric exponent would not vary perhaps due to the strong association of the particle-reactive elements in the food, or passive attachment on body surfaces, seems to support the notion.

Food web considerations

In the overall ecosystem, there is also transfer further along the food chain over several trophic positions, but there are limitations in the availability of the resources and in the transfer rates. As exemplified in Figure 1 above, there are differences in the type of organisms consumed towards upper trophic levels and, consequently yet not obviously, also difference in the body composition of the food items, enhancing the differences in the stoichiometry especially for the elements that are

not homogeneously distributed in the body. Basically, the more there are trophic transfer steps in the system, the more there are opportunities for focusing to extract the needed elements and also filtering-out of the unnecessary or harmful substances. On the other hand, the species occupying the higher trophic positions tend to be larger and to roam in a larger area, leading to variability not only in the environmental conditions experienced but also a higher variability in the type and element content of the food – and further possibly reflecting more integrated response and apparent weakening of the stoichiometric relationships (Bradshaw et al. 2012). However, in some cases biomagnification is observed: Introduction of a harmful substance into the system could mean that the individual having higher concentrations (and thus affected more by the substance) would be more susceptible to get eaten by the predators and to pass the substance forward, the more so the more specialised the predator is or the scarcer theprey available (when hungry, and top predators often are, also normally disfavoured food goes).For radionuclides and the respective elements, biomagnification would rarely be the situation, but there is a connection to the level of the concentrations.

Further aspects appearing rather at levels wider than a species or a group of species relate to the phylogenetic approaches to address the transfer (for a summary, see Beresford et al., 2016). As the phylogeny is associated to the evolutionary development, it should be noted that results seen from such approaches may, to an extent, reflect the differences in the evolutionary time scale to 'perfect' the biogeochemical use of the environmental resources for the needs of the specific organism. This may be related to the observation that predictions made on the basis of phylogenetic relationships worked in a case study better than grouping the species by their feeding group (Beresford et al., 2016, and references therein), even though there are, coarsely and in general, certain correlating tendencies between the phylogenetic and trophic positions.

Conclusions

In this paper, some of the most prominent principles and leading ideas in ecological thermodynamics, bioenergetics and stoichiometry have been briefly presented. The common observations that the radionuclide transfer to an organism as such (i.e., when the effect of the rate of food intake varying mainly with the animal size has been removed) is similar across not too dissimilar species (e.g., Beresford et al., 2016) seem to be explainable by the mechanisms and rules touched upon in this paper, albeit considerable further effort would be needed to build solid enough overall reasoning. Also, a higher variability observed between trophic levels (e.g., Bradshaw et al., 2012) seems logical for elements not evenly distributed in the organisms consumed.Similarly, many other observations derived by statistical treatment of various datasets appear somewhat more expected than in the original studies that often have considered the organisms rather in isolation, or plainly the aggregated transfer over several trophic levels, than the perspective of the ecosystem-level energy fluxes and their drivers and constraints.

Considering the high site-dependency of concentration ratios, the considerations of the biological drivers and controls discussed in this paper provide means to better analyse existing and forthcoming datasets, in addition to the statistical methods applied for this (e.g. the residual maximum likelihood method (REML; e.g., Beresford et al., 2016) or regression approaches). It needs to be borne in mind, though, that analysing data as a bulk across different site conditions may mask out some regularities and hinder generalisationsdue to the factors related to the ambient environmental conditions and the availability of the elements to be taken up.Of course, obtaining actual empirical data should always be prioritised over extrapolation methods, but the field (and laboratory) data should also be analysed for indications or absence of general patterns and attention should be paid to sufficiently describing the prevailing environmental conditions.

References

Allen, A.P., Gillooly, J.P., 2009. Towards an integration of ecological stoichiometry and the metabolic theory of ecology to better understand nutrient cycling. Ecol. Lett. 12, 369–384.

Beresford, N.A., Wood, M.D., VivesiBatlle, J., Yankovich, T.L., Bradshaw, C., Willey, N., 2016. Making the most of what we have: applications of extrapolation approaches in radioecological wildlife transfer models. J. Environ. Radioact. 151, 373–386.

Bradshaw, C., Kautsky, U., Kumblad, L., 2012. Ecological stoichiometry and multi-element transfer in a coastal ecosystem. Ecosystems 15, 591–603.

Brown, J.H., Gillooly, J.F., Allen, A.P., Savage, V.M., West, G.B., 2004. Toward a metabolic theory of ecology. Ecology 85, 1771–1789.

Brown, J.E., Alfonso, B., Avila, R., Beresford, N.A., Copplestone, D., Hosseini, A. 2016. A new version of the ERICA tool to facilitate impact assessments of radioactivity on wild plants and animals. J. Environ. Radioact. 153, 141–148.

Chapman, D.W., 1978. Production, in: Bagenal, T. (Ed.), Methods for Assessment of Fish Production in Fresh Waters. IBP Handbook No. 3. Blackwell Scientific, Oxford, pp. 202–218.

Cresswell, T., Simpson, S.L., Smith, R.E.W., Nugegoda, D., Mazumder, D., Twining, J., 2014. Bioaccumulation and retention kinetics of cadmium in the freshwater decapod *Macrobrachiumaustraliense*. Aquat. Toxicol. 148, 174–183.

Elser, J.J., Kuang, Y., 2012. Ecological stoichiometry, in: Hastings, A., Gross, L.J. (Eds.), Encyclopedia of Theoretical Ecology. University of California Press, Berkeley, pp. 718–722.

Gillooly, J.F., Brown, J.H., West, G.B., Savage, V.M., Charnov, E.L., 2001. Effects of size and temperature on metabolic rate. Science 293, 2248–2251.

Hopkin, S.P., 1989. Ecophysiology of Metals in Terrestrial Invertebrates. Elsevier Applied Science, London.

Howard, B.J., Beresford, N.A., Copplestone, D., Tellaria, D., Proehl, G., Fesenko, S., Jeffree, R.A., Yankovich, T.L., Brown, J.E., Higley, K., Johansen, M.P., Mulye, H., Vandenhove, H., Gashchak, S., Wood, M.D., Takata, H., Andersson, P., Dale, P., Ryan, J., Bollhöfer, A., Doering, C., Barnett, C.L., Wells, C., 2013. The IAEA handbook on radionuclide transfer to wildlife. J. Environ. Radioact. 121, 55–74.

Lindeman, R.L., 1942. The trophic-dynamic aspect of ecology. Ecology 23, 399–417.

Markert, B., Kayser, G., Korhammer, S., Oehlmann, J., 2000. Distribution and effects of trace substances in soils, plants and animals, in: Markert, B., Friese, K. (Eds.), Trace Elements – Their Distribution and Effects in the Environment. Trace Met. Environ. 4. Elsevier Science, Oxford, pp. 3–32.

Lee, J-S., Lee, B-G., 2005. Effects of salinity, temperature and food type on the uptake and elimination rates of Cd, Cr, and Zn in the Asiatic clam *Corbicula fluminea*. Ocean Sci. J. 40(2), 79–89.

Liski, J., Palosuo, T., Peltoniemi, M., Sievänen, R., 2005. Carbon and decomposition model Yasso for forest soils. Ecol. Model. 189, 168–182.

Pauly, D., Christensen, V., Walters, C. 2000. Ecopath, Ecosim, and Ecospace as tools for evaluating ecosystem impact of fisheries. ICES J. Mar. Sci. 57, 697–706.

Pimm, S.L., 2002. Food Webs. University of Chicago Press, Chicago.

Rasmussen, J.B., Vander Zanden, M.J., 2004. The variation of lake food webs across the landscape and its effect on contaminant dynamics, in: Polis, G.A., Power, M.E., Huxel, G.R. (Eds.), Food Webs at the Landscape Level. University of Chicago Press, Chicago, pp. 169–182.

Salt, D.E., Baxter, I., Lahner, B., 2008. Ionomics and the study of the plant ionome. Annu. Rev. Plant Biol. 59, 709–733.

Sterner, R.W., Elser, J.J., 2002. Ecological Stoichiometry: The Biology of Elements from Molecules to the Biosphere. Princeton University Press, Princeton.

Townsend, C.R., Begon, M., Harper, J.L., 2008. Essentials of Ecology, third ed. Blackwell, Malden, USA.

USDOE, 2004. RESRAD-BIOTA: A Tool for Implementing a Graded Approach to Biota Dose Evaluation – User's Guide, Version 1. DOE/EH-0676. United States Department of Energy.

Verkhovskaja, I.N., Vavilov, P.P., Maslov, V.I., 1967. The migration of natural radioactive elements under natural conditions and their distribution according to biotic and abiotic environmental components, in: Åberg, B., Hungate, F. P. (Eds.), Radioecological Concentration Processes, Proceedings of an International Symposium held in Stockholm 25–29 April, 1966. Pergamon, Oxford, pp. 313–328.

Weih, M., Pourazari, F., Vico, G., 2016. Nutrient stoichiometry in winter wheat: Element concentration patterns reflects developmental stage and weather. Sci. Rep. 6, 35958.

West, G.B., Brown, J.H., Enquist, B.J. 1997. A general model for the origin of allometric scaling laws on biology. Science 276, 122–126.

Acknowledgement

Implementation of a food chain sub-module into a model for radioecological assessments in the coastal waters around Iceland

*M. Iosjpe[*1], M. Isaksson[2], R. Thomas[2], Ó. Halldórsson[3], P. Roos[4], K. Logemann[5], G. Jonsson[3], H. P. Joensen[6], V. Suolanen[7]*

[1]Norwegian Radiation Protection Authority, Norway,[2]University of Gothenburg, Sweden; [3]Geislavarnir Rikisins, Iceland; [4]Technical University of Denmark, Denmark; [5]University of Iceland, Iceland; [6]University of the Faroe Islands, Faroe Islands;[7]Technical Research Centre of Finland Ltd, Finland

Abstract

Modelling tools of radioecological assessments for the coastal waters around Iceland are developed on the base of the NRPA model for the Arctic and Nordic Seas and the CODE operational ocean model. The present approach includes the kinetic modelling of bioaccumulation of radionuclides in biota. The comparison with experimental data shows that dynamic modelling of bioaccumulation processes can improve accuracy for description of the concentration of radionuclides in biota. This is due to the more realistic approach when using kinetic modelling compared to the equilibrium assumption when using concentration ratios factors. Further, estimations of radionuclide concentration in marine organisms and dose assessment with the implementation of the kinetic bioaccumulation model clearly demonstrate that there is a significant quantitative difference between the kinetic modelling approach and the approach based on the assumption of constant concentration ratios. Also, kinetic modelling of bioaccumulation processes leads to a better harmonisation between the different calculations (for example, between doses to the critical group and concentrations in marine organisms for short-life radionuclides) and also to better logical explanations of the results.

Introduction

Radioecological assessment covers complex processes such as dispersion of radionuclides in oceanic space, transfer of radioactivity between seawater and sediments, uptake of radionuclides by biota and, finally, dose calculations for man and biota.

The analysis of the consequences of some hypothetical accidents in the coastal Nordic marine environment shows conclusively that it is possible to improve the present evaluation by a more detailed modelling of the key processes for radioecological assessment (COSEMA, 2014; Iosjpe, 2011; Iosjpe & Liland, 2012).

The main hypotheses, which aretested in the present project, can be described with following expressions: Is it true that the description of the bioaccumulation process, which is based on the use of constant concentration ratios/factors, can be significantly improved by involving a food chainmodelling approach? Is it especially important during the initial dynamic phase of an accident when no equilibrium conditions exist?

Materials and Methods

Brief description of the model for radioecological assessments in the coastal waters around Iceland

The present compartment model is based on two models: (i) the NRPA box model, which is detailed in Iosjpe et al. (2002), and Iosjpe et al. (2009), and (ii) the hydrodynamic ocean model CODE (Logemann& Harms, 2006; Logemann et al., 2010).

---

[*]Corresponding author, E-mail: mikhail.iosjpe@nrpa.no

The surface box structures with transfer parametersare shown in Figure 1.Additionally, two compartments surrounding the Iceland boxes were developed on the basis of the NRPA box model.
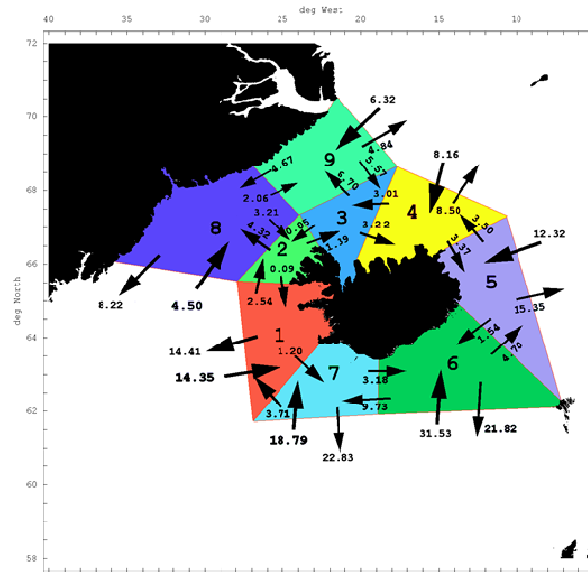
Figure 1. The structure of the surface compartments with flow rates between boxes in Sverdrup (Sv)

The present model adopts the sediment structure from the NRPA model, including the surface, mid-depth and deep sediment compartments for all water regions. Water-sediment interactions include sedimentation, diffusion of radioactivity through pore water in sediments, resuspension, mixing due to bioturbation, particle mixing and a burial process for radionuclides in deep sediment layers. Radioactive decay is calculated for all compartments. The contamination of biota is further calculated from the known radionuclide concentrations in filtered seawater in the different water regions. Doses to the man are calculated on the basis of seafood consumptions, in accordance with available data for seafood catches and assumptions about human diet in the respective areas.

Validation of the model is based on the global fallout of the $^{239+240}$Pu after the testing of nuclear weapons in the atmosphere (UNSCEAR, 2000). The contamination by $^{239+240}$Pu of the considered marine regions is strongly dominated by the global fallout, when compared to other sources of contamination (Green et al., 2013). Therefore, we have chosen to consider global fallout as a single source of $^{239+240}$Pucontamination in the present project. Figure 2 shows results of the model simulations for $^{239+240}$Pu contamination compared with the experimental data (MARINA II, 2003) for the marine regions surrounding Iceland. The circles show the average values, while the error bars show the minimum and maximum values of the experimental data. Figure 2 demonstrates that the model predictions are reasonably accurate.

Modelling of the bioaccumulation process

Figure 3 shows the schematic of the biokinetic model, which was used in the present paper. The model has been chosen after an analysis of existing models (Thomann, 1981; Heling et al., 2002; Brown et al., 2004; VivesiBatlle et al., 2008; Maderich et al., 2013). Parameters for the fish submodel for 137Cs and 239Pu are selected from (Thomann, 1981) with an additional assumption about the possibility of an uptake of radionuclides via zooplankton for large fish.

---

*Corresponding author, E-mail: mikhail.iosjpe@nrpa.no
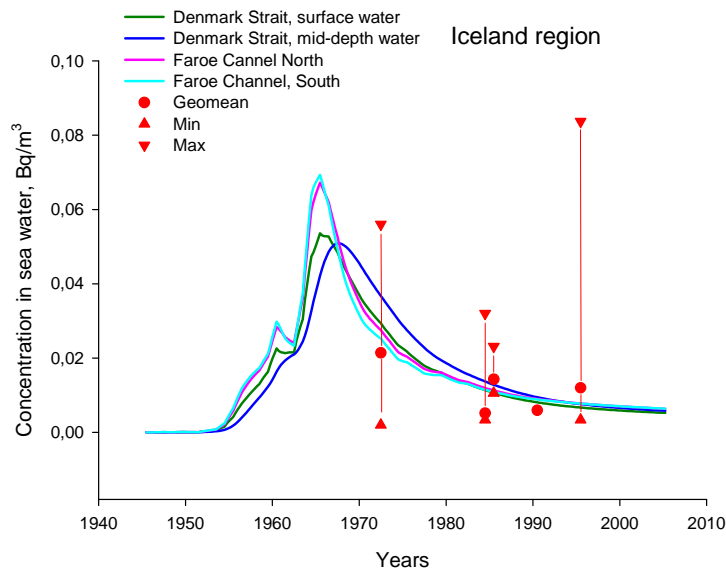
Figure 2.*Results of the model simulations (lines) in comparison with experimental data (dots and triangles).*
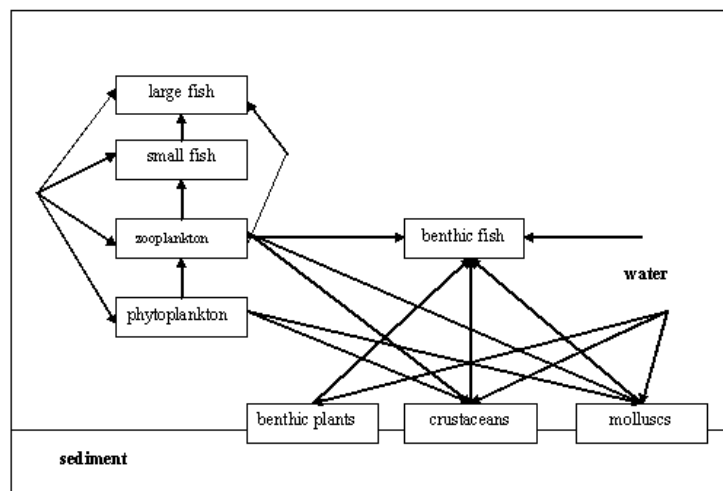
Figure 3.*Schematic of the biokinetic model.*

The system of equations for the biokinetic model can be described by the followingexpressions:

$$(1)\frac{dC_i^{(tl)}}{dt} = AE_i \cdot IR_i \cdot C_{i-1}^{(tl)} + k_{u,i} \cdot C_w - C_i^{(tl)} \cdot k_{e,i}$$

Here $C^{(tl)}_i$ and $C^{(tl)}_{i-1}$ – concentrations of radionuclide in trophic levels "i" and "$i-1$"; C_W – concentration of radionuclide in water column; AE_i– the assimilation efficiency for trophic level "i", IR_i – ingestion per unit mass for trophic level "i"; $k_{u,i}$ – rate of the direct uptake of activity from water column for trophic level "i"; $k_{e,i}$ – the excretion rate for trophic level "i". Where the consumption for species in trophic levels "i" includes "m" different species in trophic levels "$i-1$", parameter $C^{(tl)}_{i-1}$can be described as

$$C_{i-1}^{(tl)} = \sum_{j=1}^{m} w_{j} \cdot C_{i-1,j}^{(tl)}$$

---

*Corresponding author, E-mail: mikhail.iosjpe@nrpa.no

Here the consumption for species in trophic level "*i*" includes *m* species in trophic levels "*i-1*" with concentration of radionuclide in species *j* (*j*=1,...,*m*) of $C^{(tl)}_{i-1,j}$; w_j is a fraction of species *j* of all *m* species, where

$$\sum_{j=1}^{m} w_j = 1$$

Results of biokinetic modelling approach were compared with experimental data on the basis of an improved version of the NRPA box model for the Baltic Sea (see Figure 4).
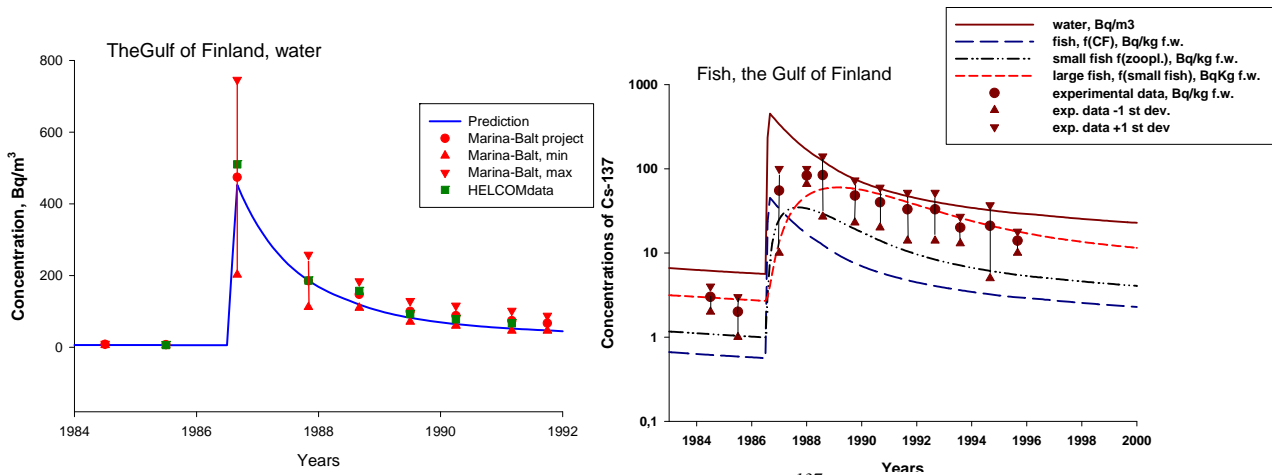
Figure 4. *. Comparison of the prediction of the concentration of ^{137}Cs in seawater (left) and in fish (right) with experimental data for the Gulf of Finland for the Chernobyl accident.*

Plots for concentrations in water and fish (with constant concentration factor approach) have the same shape. Biokinetic modelling describes the "delay" with the changing of concentration of radionuclides in water. It is a clear demonstration that the dynamic modelling of the bioaccumulation processes provides a more correct description of the concentration of radionuclides in biota (up to an order of magnitude) and, therefore, these results support one of the main ideas of the present paper, namely that the biokinetic modelling approach is important when evaluating the consequences after accidental releases of radionuclides into a marine environment.

It is interesting to note that the results in Figure 4 demonstrate that present modelling predictions are borne out by the experimental data after Chernobyl accident (1986) because the modelling parameters correspond to data from 1981 (Thomann, 1981).

Results and Discussion

The present simulations correspond to release scenario for the hypothetical accident with the nuclear reactor of the operative Russian submarine in the Icelandic coastal waters (Reistad, 2008; Iosjpe & Liland, 2012).

Caesium

Parameters for equation (1) for ^{137}Cs for zooplankton, small fish and large fish have been adopted from Thomann (1981). Parameters for molluscs and crustaceans have been adopted from Bezhenar et al.(2016). Phytoplankton and benthic plants have been calculated on the basis of the concentration factor (IAEA, 2004).

The excretion rate of trophic level "i" ($k_{e,i}$) for ^{134}Cs is calculated by expression (2):

---

*Corresponding author, E-mail: mikhail.iosjpe@nrpa.no

$$k_{e,i} = k_{e,i}^{(0)} + \ln 2 \left[\frac{1}{T_{1/2,i}} - \frac{1}{T_{1/2,i}^{(0)}} \right], \tag{2}$$

where $k_{e,i}^{(0)}$ is an excretion rate of trophic level "i" for ^{137}Cs, $T_{1/2,i}$ and $T_{1/2,i}^{(0)}$ are radionuclide half-life for ^{134}Cs and ^{137}Cs, correspondently.

Expression (2) has used an assumption that difference between excretion rates for ^{134}Cs and ^{137}Cs is based on differences of radionuclides physical half-life components in the biological half-life for marine organisms with the same physiology and metabolism for caesium isotopes.

Figure 5 shows calculation of ^{137}Cs and ^{134}Cs concentrations in seawater and fish according to the present scenario, corresponding to the accident location box. The results in Figure 5 show the same shape for the water concentration plots with a maximal value at the initial time and all kinds of fish, calculated on the basis of the constant concentration factor, whereas the use of the biokinetic model leads to another shape of the curves with a gradual increase followed by adecrease of the fish concentration similar to the results in Figure 4.
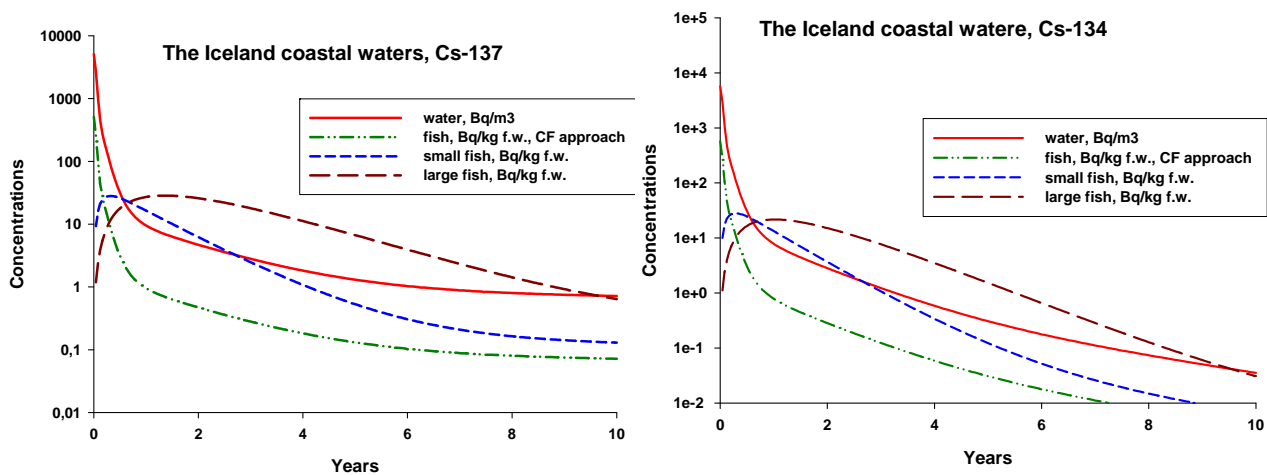
Figure 5. Concentrations of ^{137}Cs and ^{134}Cs in seawater and fish.

The results regarding the ^{137}Cs and ^{134}Cs concentrations with the constant concentration ratio approach leads to different dose distribution for the critical group (the group of high consumption of seafood) compared to the biokinetic modelling approach. Results in Figure 6 shows that when the concentration ratio approach is used, the maximum is reached in the first year (26 and 50 μSv for ^{137}Cs and ^{134}Cs, respectively) and the concentration becomes almost in significant in subsequent years. The use of the biokinetic approach for doses to the critical group for large fish, results in a distribution with the maximum dose corresponded to the second year (16 and 27 μSv for ^{137}Cs and ^{134}Cs, respectively), with slight decreases in subsequent years.

At the same time, the total dose after ten years for the concentration ratio approach and for the biokinetic modelling approach are equal to 27 μSv and 60 μSv for ^{137}Cs and 50 μSv and 75 μSv for ^{134}Cs, respectively.

*Corresponding author, E-mail: mikhail.iosjpe@nrpa.no
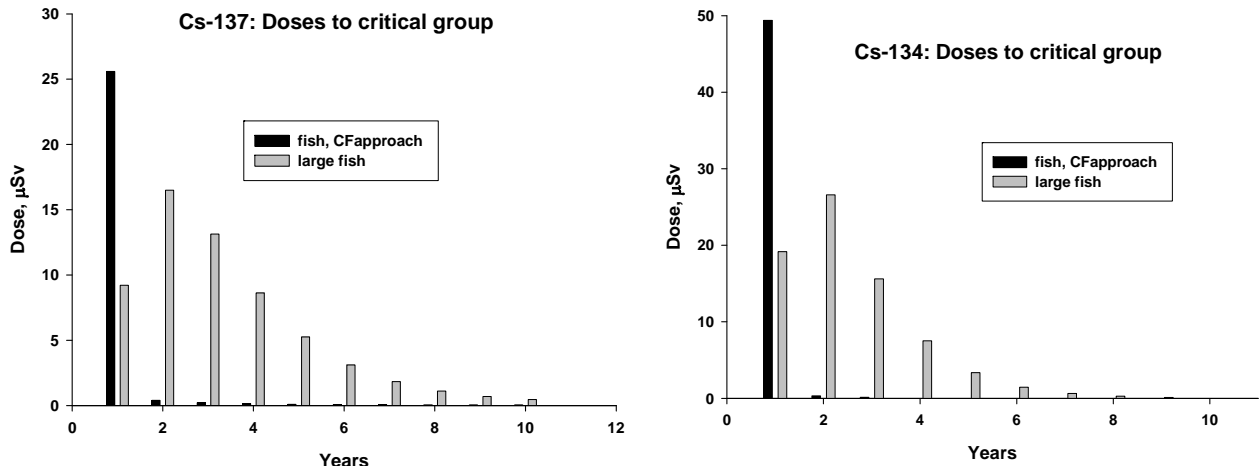
Figure 6. *Doses the critical group from fish consumption.*

Tellurium -132

Calculations of concentration of ^{132}Te in biota based on concentration factor approach indicates that results significantly exceed (up to two orders of magnitude) the guideline level for for the maximum permissible concentration of radionuclides in foods (CAC, 2006) during an initial time of radionuclide release. At the same time dose to the critical group from ^{132}Te is negligible. Therefore, a hypothesis that evaluation of concentration of radionuclides in biota on the basis of the concentration factor approach is too conservative for ^{132}Te has to be evaluated.

Unfortunately, information, which can be used for evaluation of kinetic coefficients, is very poor. There is limited information in ICRP (1993) that assimilation rates for tellurium isotopes for several animal species can lies within the range between 0.2 and 0.5. Additionally, values of 0.3 and 0.6 may be adopted for adults and infants, respectively. For following calculations, the value of 0.2 is selected for the zooplankton assimilation rate because this value corresponds to water soluble fractions of radionuclide (ICRP, 1993). For all other biota, it is selected conservative value of 0.6 for assimilation rates. The selection of conservative value can potentially lead to the faster accumulation process.

There is no information concerning excretion rates or biological half-life for ^{132}Te, but we can again select a conservative approach and define excretion rates as

$$k_{e,i} = \frac{\ln 2}{T_{1/2}^{(*)}},$$

where $T_{1/2}^{(*)}$ is radioactive half-live for ^{132}Te (3.26 d).

Further, assume that equilibrium state provided by equation (1), when $t \rightarrow \infty$ corresponds to average concentration in biota, which can be defined due the concentration factor.

When $t \rightarrow \infty$ equation (1) can be written as

$$0 = AE_i \cdot IR_i \cdot C_{i-1} + k_{u,i} C_w - k_{e,i} \cdot C_i \,. (3)$$

---

[*]Corresponding author, E-mail: mikhail.iosjpe@nrpa.no

Input parameters for ingestion rates $\{IR_i\}$ could be adopted from Thomann (1981) and rates of the direct uptake of activity from water $k_{u,i}$ can be defined from equation (3).

Figure 7(left) shows concentration of ^{132}Te in fish, where the concentration in water is of 1Bq/l. According to present modelling approach, concentrations in water and fish come to equilibrium after ten days, approximately. Figure 7 (right) shows calculation of ^{132}Te concentration in seawater and fish according to the submarine accident scenario.
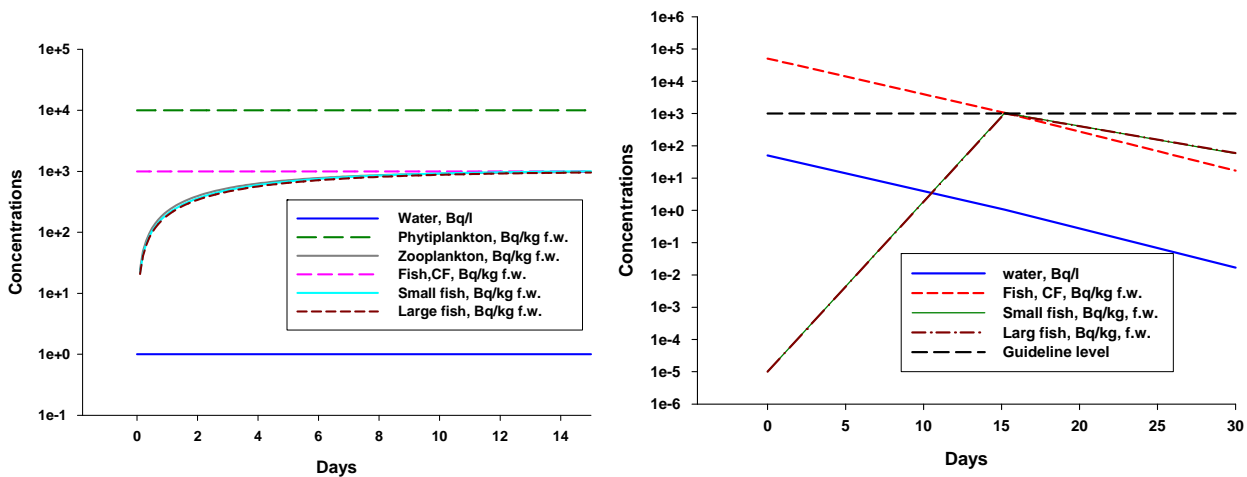
Figure 7. *Comparison of the concentration of radionuclides in biota for ^{132}Te.*

Results show the same shape for the graphs for water concentration and concentration in fish, calculated from the constant concentration factor, whereas the use of the biokinetic model leads to another shape of the curves with a dramatic decreasing of ^{132}Te concentration in fish (up to orders of magnitude). Small and large fish have very similar shape under this selection of parameters. It is important to note that concentration in fish according to the present approach does not exceed the Guideline level for the ^{132}Te. Such results can be important for decision makers, have better harmonisation with doses to humans and, in spite of lack of information for closer approximation of necessary parameters, provide more logical description of the bioaccumulation processes than approach based on use of constant concentration factors.

Conclusions

The results of the implementation of the kinetic model for bioaccumulation processes into the model for radioecological assessments clearly demonstrated that there is a significant quantitative difference between the kinetic modelling approach and the approach based on the constant concentration rates.

It shows also that dynamic modelling of the bioaccumulation processes can provide a more correct description of the concentration of radionuclides in biota.

It is important to note that kinetic modelling of bioaccumulation processes leads to a better harmonisation between the different calculations (for example, between doses to the critical group and concentrations in marine organisms for short-life radionuclides) and also to better logical explanations of the results.

*Corresponding author, E-mail: mikhail.iosjpe@nrpa.no

Acknowledgement

References

Bezhenar R., Jung K. T., Maderich V., Willemsen S., Govert de With, Qiao F., 2016. Transfer of radiocaesium from contaminated bottom sediments to marine organisms through benthic food chain in post-Fokushima and post-Chernobyl periods. Biogeosciences, 13,3021-3034.

Brown J., Børretzen P., Dowdall M., Sazykina T., and Kryshev I., 2004. The derivation of transfer parameters in the assessment of radiological impacts on Arctic marine biota. Arctic, 57, No. 3, 279-289.

CAC, 2006. Codex Alimentarius Commission: Joint FAO/WHO Food Standards Programme. Appendix 31. ftp://ftp.fao.org/codex/Alinorm06/al29_41e.pdf (09.01.07)

COSEMA, 2014. Consequences of severe radioactive releases to Nordic marine environment. Final report forthe NKS-B COSEMA activity 2013, Contract AFT/B(13)3.

Green N.W., Skogen M., Aas W., Iosjpe M., Måge A., Breivik K., Yakushev E., Høgåsen T., Eckhardt S., Ledant A.B., Jaccard P.F., Staalstrøm A., Isachsen P.E., Frantzen S., 2013. Tiførselprogrammet 2012. Overvåkning av tilførsler og miljøtilstand i Barentshavet og Lofotenområdet. Klima og forurensningsdirektoratet, ISBN 978-82-577-6279-7 (in Norwegian).

IAEA, 2004. Sediment distribution coefficients and concentration factors for biota in the marine environment. IAEA Technical reports series no. 422. Vienna: International Atomic Energy Agency, IAEA.

Iosjpe M., 2011. A sensitivity analysis of the parameters controlling water-sediment interactions in the coastal zone: consequences to man and environment, Journal of Marine Systems 88, 82-89.

Iosjpe M., Brown J. & Strand P., 2002. Modified Approach for Box Modelling of Radiological Consequences from Releases into Marine Environment, Journal of Environmental Radioactivity, Vol. 60, No 1-2, 91-103.

Iosjpe M. and Liland A., 2012. Evaluation of environmental sensitivity of the marine regions. Journal of Environmental Radioactivity 108 (2012) 2-8.

Iosjpe M., Karcher M., Gwynn J., Harms I., Gerdes R. and Kauker F., 2009. Improvement of the dose assessment tools on the basis of dispersion of the ^{99}Tc in the Nordic Seas and the Arctic Ocean. Radioprotection, vol. 44, no 5, 531-536.

Logemann, K. and Harms, I., 2006. High resolution modelling of the North Icelandic Irminger Current (NIIC), Ocean Sci., 2, 291-304,

Logemann, K., Olafsson, J., and Marteinsdóttir, G.,2010. The ocean model CODE and its application to Icelandicwaters, MARICE E-report MER-10-2010, University of Iceland, pp. 93, http://www.marice.is/ereports/MER-10-2010.pdf.

Maderch V., Bezhenar R., Heling R., G. de With, Jung K.T., Myoung J.G., Cho Y.-K., Qiao F., Robertson L., 2013. Regional long-term model of radioactivity dispersion and fate in the Fukushima Dai-ichi accident. Journal of Environmental Radioactivity 2013, www.elsevier.com/locate/jenvrad.

MARINA II, 2003. Update of the MARINA Project on the radiological exposure of the European Community from radioactivity in North European marine waters, European Commission, Radiation Protection 132, Contract B3-4305/2000/304957/MAR/C4.

Reistad O., 2008. Analyzing Russian naval nuclear safety and security by measuring and modeling reactor and fuel inventory and accidental releases. Doctoral thesis at NTNU, 2008:14.

[*]Corresponding author, E-mail: mikhail.iosjpe@nrpa.no

Thomann R.V., 1981. Equilibrium model of fate of microcontaminants in diverse aquatic food-chains.
Canadian Journal of Fisheries and Aquatic Sciences 38:280-296.
UNSCEAR, 2000. Sources and effects of ionizing radiation. UNSCEAR 2000 Report to the General Assembly
with Scientific Annexes. Volume I: Sources. UN, New York.
Vives i Batlle J., Wilson R.C., Watts S.J., Jones S.R., McDonald P., Vives-Lynch S., 2008. Dynamic model
for assessment of radiological exposure to marine biota. Journal of Environmental Radioactivity 99,
1711-1730.

---

*Corresponding author, E-mail: mikhail.iosjpe@nrpa.no

*Corresponding author, E-mail: mikhail.iosjpe@nrpa.no

Radioecological sensitivity of Aegean Sea

G.Eleftheriou[1,2]* and M. Iosjpe[1]

[1] Norwegian Radiation Protection Authority, Department of Monitoring and Research, Grini næringspark 13, 1361 Østerås, Norway
[2] Hellenic Centre for Marine Research, Institute of Oceanography, 46.7 km Athens-Sounio Ave., 19013 Anavyssos, Greece

Abstract

A radiological box model of the Aegean Sea has been developed simulating the dispersion and faith of radionuclides in the marine environment. The model incorporates all transfer processes within abiotic and biotic compartments in combination with appropriate site-specific information. The model's performance has been validated with the simulation of ^{137}Cs dispersion after the Chernobyl accident based on empirical data. Environmental sensitivity analysis has been carried out based on Chernobyl ^{137}Cs fallout, in terms of doses to representative marine organisms (fish, crustacean and molluscs) and human population. Comparison of the results with guideline levels and other models' sensitivity estimations for shallow marine environments has been performed in order to reveal the vulnerability of each sub-region. The main characteristics and parameters controlling the radioecological processes are also discussed.

Introduction

The environmental sensitivity of the marine regions under radionuclides' stress is of great interest, since it is valuable information for the improvement of radioecological assessments and development of proper radioprotection strategies (IAEA, 2013). Radiological modeling is an effective tool that can provide significant information about the environmental sensitivity of different environments or particular ecosystems after contamination by radionuclides. A number of models simulating the marine environment have been developed in order to predict the dispersion after the release of radionuclides into the sea and the radiological consequences to biota. The value of such models and the reliability of their predictions have been established and are reinforced through several international intercomparison projects (e.g. IAEA, 2012; Periáñez et al., 2015).

Due to the extent and complexity of the marine environments, box models are considered to be suitable for radioecological assessment. Box models are based on the parameterization of the marine space in compartments with uniform characteristics for the quantitative evaluation and balance of radionuclide activity concentrations in the aquatic system components (water and sediment), by accounting for radionuclides transfer between these components. Therefore, box model approach is recommended for radiological assessments of marine environment since it can be used for modeling radiological consequences with spatial and temporal scales of several thousand kilometers and millenniums, respectively (Iosjpe, 2006).

In this frame, the Aegean Sea model has been developed for the dispersion and fate of radionuclides in the marine environment (Eleftheriou & Iosjpe, 2016). The modeling approach includes terms describing the radionuclide dispersion into oceanic space with time, while the model's algorithms cover whole processes of radionuclides' transfer, bioaccumulation and doses assessment (Iosjpe et

---

al., 2002; Iosjpe, 2006; 2011). Empirical data of ^{137}Cs initial dispersion and activity concentration in abiotic and biotic components due to the Chernobyl accident were used for the model calibration.

Sensitivity analysis for the Aegean Sea sub-regions was undertaken based on the model estimations of the radioecological effect that the ^{137}Cs from Chernobyl had to humans and marine biota. The model performance was externally validated though intercomparison with analogous estimations for other marine regions (Tracy et al., 2013), as well as with previous models from the same study area (Psaltaki et al, 2010; Eleftheriou et al., 2015).

Materials and Methods

Aegean Sea box model

The Aegean Sea box model integrates all necessary and available site specific information, including morphological, hydrological, sedimentological, biological and radiological data. Taking into account the collected datasets, the Aegean Sea was parameterized into 20 marine regions including in total 50 marine and sediment boxes (Fig. 1). The model structure was based, in principal, on the morphology and the water circulation representation; and, secondarily, on the fish production and human population distribution.
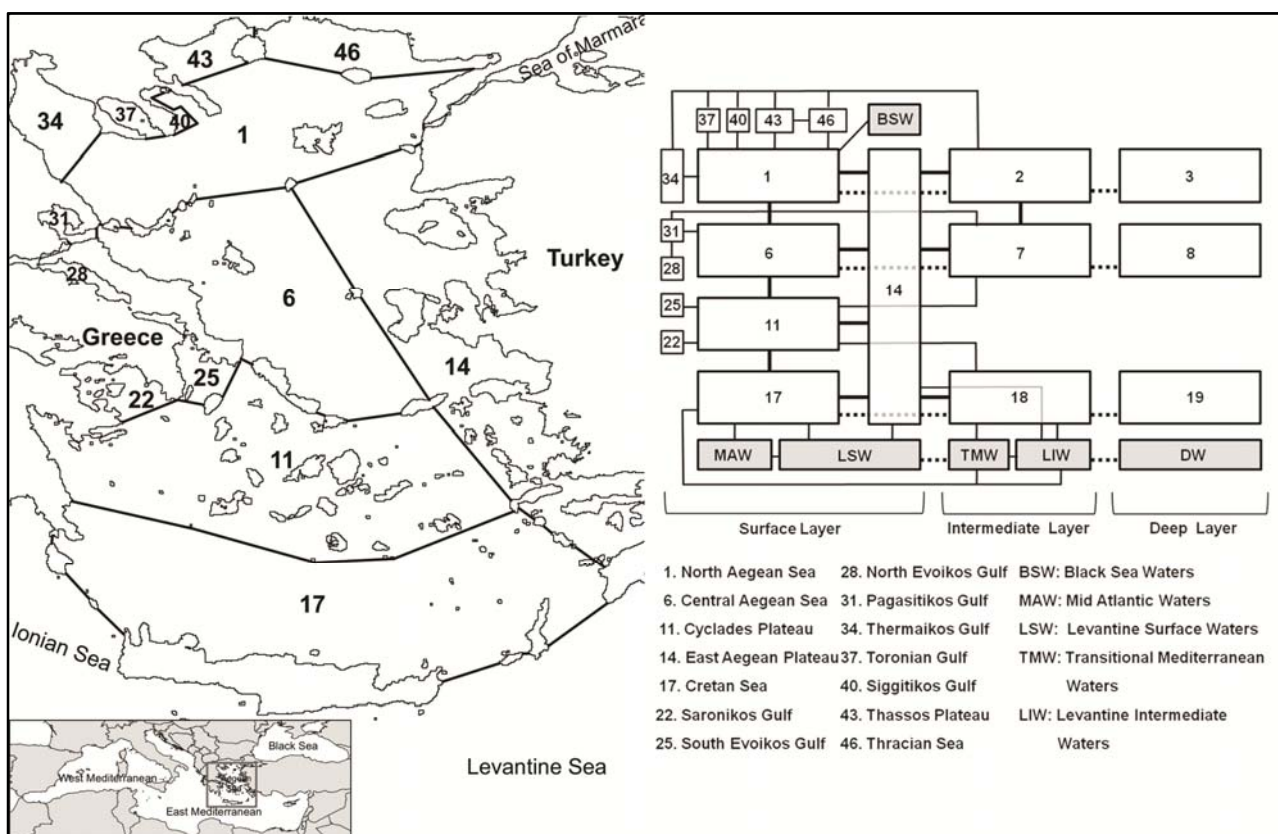
Figure 1. Aegean Sea box model and schematic structure of the water boxes (white boxes: marine regions; gray boxes: external water masses; solid lines: horizontal water fluxes; das lines: vertical water fluxes).

Key feature of the modeling approach is that the equations describing transfer k (in y^{-1}) of the radionuclide activity concentration A (in Bq) between boxes i and j under an external input source Q (in Bq y^{-1}), includes terms γ (unit function) describing the radionuclide dispersion into oceanic space with time Ta$_i$ (in y):

$$\frac{DA_i}{dt} = \sum_{j=1}^{n} k_{ij}A_j - \sum_{j=1}^{n} k_{ij}A_i\gamma\left(t \geq Ta_j\right) - k_iA_i + Q_i, \qquad t \geq Ta_i$$
$$A_i = 0, \qquad\qquad\qquad\qquad\qquad\qquad\qquad\qquad\qquad\qquad t < Ta_i$$

where $\quad \gamma\left(t \geq Ta_j\right) = \begin{cases} 1, & t \geq Ta_i \\ 0, & t < Ta_i \end{cases}$

The availability times Ta_i are calculated as a minimized sum of the weights for all paths from the initial box with discharge of radionuclides to the box i. This non-instantaneous mixing modeling approach can predict the different time trends for water transport within the marine compartments, fact particularly important for dynamic marine environments as Aegean Sea.

The model algorithms cover all aspects related with the fate and impact of the radionuclides to marine environment, including processes of advection of radioactivity between compartments; diffusivity of radioactivity through pore water; sedimentation and resuspension; mechanical mixing due bioturbation and molecular mixing of particles; and activity burial in deep sediments. Radioactive decay is also included in all compartments. The contamination of biota is further calculated from the radionuclide concentrations in filtered seawater in different water layers. Doses to man are calculated on the basis of data for the catch of seafood and assumptions concerning human diet.

Model calibration

Aegean Sea model was calibrated with the simulation of the ^{137}Cs dispersion following the Chernobyl accident (April 26, 1986), taking into account all the available experimental data. Starting point of the simulation was the estimated total ^{137}Cs fallout, considering also annual flux of ^{137}Cs from the Black Sea for the years after the accident. The predicted values for ^{137}Cs activity concentration in the biotic and abiotic components of the Aegean Sea boxes were compared with the empirical data. Adjustment of particular parameters was performed to improve the simulation results and the reliability of the model, always within physical acceptable limits (Fig. 2).
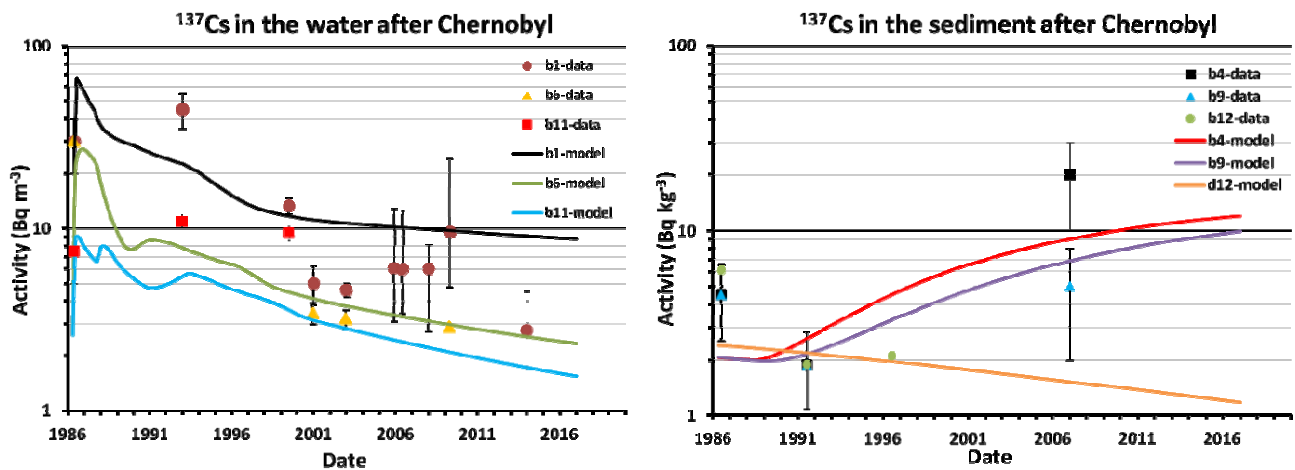
Figure 2. *Model estimations and experimental data of* [137]*Cs activity concentration in water and sediment.*

From the optimization process it was revealed that the availability times was the most influential parameter, while significant was the affect of the selection of the surface sediment thickness and the initial ^{137}Cs fallout for each boxes. The overall uncertainty for ^{137}Cs concentrations is considered to be less than one order of magnitude in all the calculations.

Impact assessment

Dose assessment calculations have been performed in order to estimate the impact of ^{137}Cs from the Chernobyl accident to the population and the marine biota of Aegean Sea. The radiation doses to population were calculated assuming that their entire food intake from the marine pathway comes from the local environment. Values for the mean fish production from the last 20 years were classified into three groups (fish, crustacean and mollusc), including mussels and fish aquaculture production and all fishing catches according the volume of each sub-region. The habitant's density (number of persons per prefecture) was also included and the total population was distributed to each box taking into account topological and social characteristics. Additional data concerning the sea food consumption and the marine occupancy by representative individuals and critical groups have been also considered in order to calculate the external and internal dose received by the population (EC, 1995). Concerning the radiological coefficients for the doses estimation (Dose Conversion Factor, Conversion Ratios and Sediment Distribution Coefficient) the recommended values have been adopted (ICRP, 2012; IAEA, 2014), while the values of the marine biota conversion factors came form the EPIC framework database (Brown et al., 2003).

Results and Discussion

Doses estimations

The dose rate evolution calculated for two groups of population (average residence and critical individual) for the years after the releases of ^{137}Cs. The annual dose received by a representative individual at the most populated marine compartments, as well as the total minimum, maximum and arithmetic mean values from all model's boxes, are illustrated in Fig. 3.
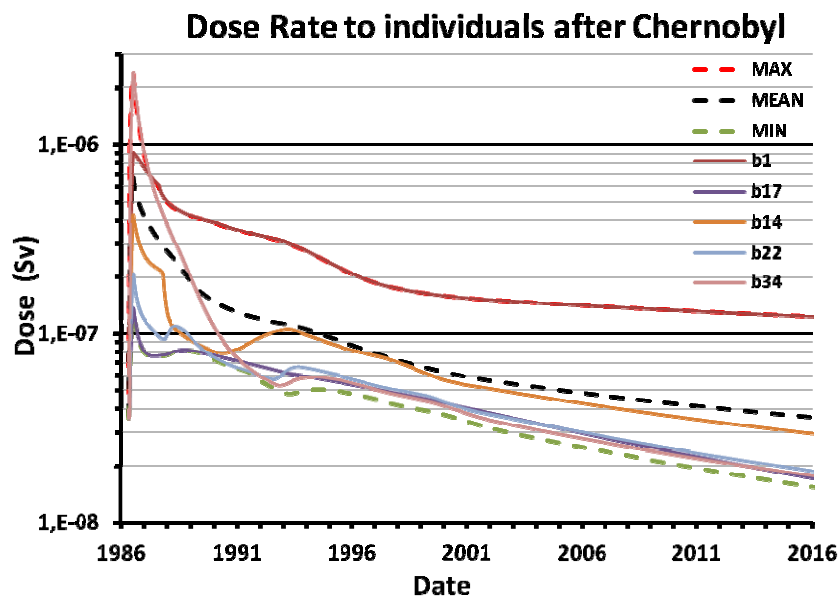
Figure 3. Dose rates to representative individual for the five most populated regions of Aegean Sea.

Maximum dose rates for all boxes appeared in the first year after the deposition, and in any case did not exceed the 3 μSv y^{-1}. According to UNSCEAR (2000), the annual exposure from natural sources can be expected to be in the range of 1-10 mSv, with an average annual exposure of 2 mSv. An additional exposure rate to the natural sources in the range of 1-10 μSv per year constitutes a negligible component of the annual effective dose from natural sources. This means that the effect to the individuals from the Chernobyl ^{137}Cs was negligible, concerning the marine pathways. However,

the maximum value for a critical individual (i.e. fisherman) was 54 μSv y^{-1}, value significantly lower than the average annual dose from nature sources but five times higher than the range for the negligible component to the annual individual dose. Therefore, it has to be under consideration during evaluation of the accident consequences.
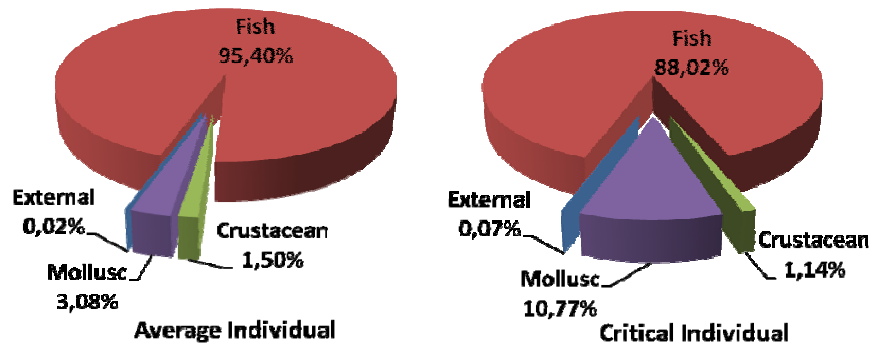
Figure 4. Contribution of different marine pathways to the doses to representative and critical individuals.

Collective doses have also been calculated, since the cumulative dose to the population is a more appropriate quantity for the estimation of the vulnerability of different regions. The total collective dose for all Aegean Sea 30 years after the initial deposition is estimated to be 982 manSv, while the collective doses in each region are illustrated in Fig. 5.
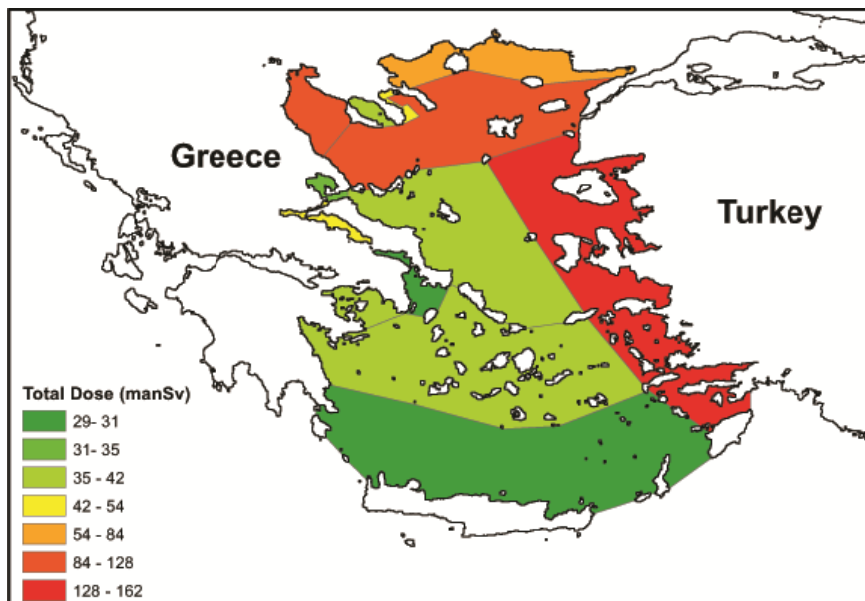
Figure 5. Estimated collective doses in the sub-regions of Aegean Sea at the year 2016.

Following the international recommendations for the concentration of radionuclides in foods, when contaminated after an accidental release of radionuclides, the model calculations for maximal concentrations in fish, crustaceans and molluscs (14.5, 9.2 and 8.7 Bq kg^{-1}, respectively), found 2 months after the accident in Thermaikos Gulf (box 34), are by orders of magnitude below the guideline level of 1000 Bq kg^{-1} for ^{137}Cs (CAC, 2006). As expected, the dose rates in fish, crustaceans and molluscs vary similarly with time, since the external and the internal doses are directly and exclusively, in the modelling frame, related to the concentration of radionuclide in water. The most affected specie is fish with dose rates reaching up to $2.5 \cdot 10^{-3}$ μGy h^{-1}, value far below the screening dose rate limit of 10 μGy h^{-1} that is considered to be not harmful to marine biota (Brown et al., 2003).
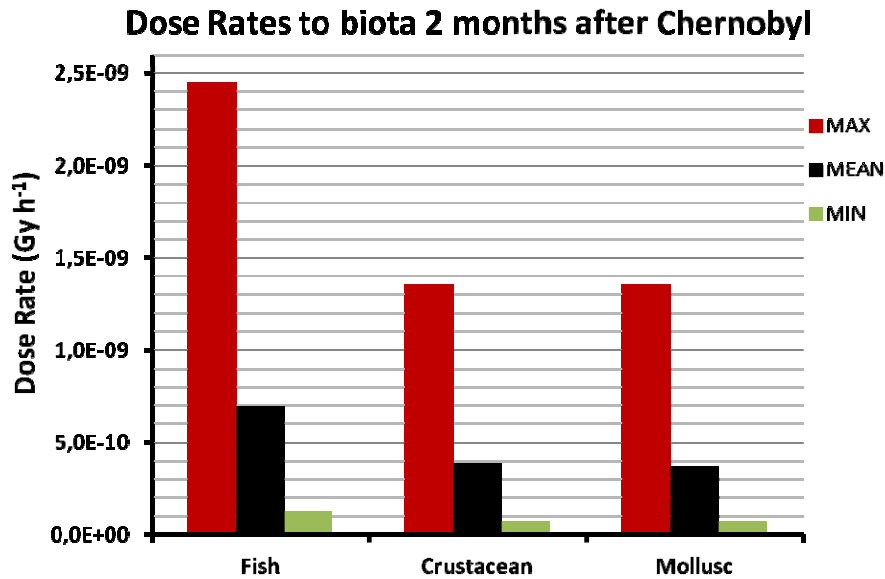
Figure 6. *Range of dose rate values for marine biota of Aegean Sea, 2 months after Chernobyl accident.*

Sensitivity analysis

Based on the Aegean Sea model estimations, the collective dose and the dose rate to representative individual have been selected as indicators of the collective and individual sensitivity, respectively, of the model's sub-regions. The calculated doses were dived by the initial ^{137}Cs deposition in each box. The sensitivity results for the 1st and the 30th year after the Chernobyl accident are presented in Table 1.

Table 1. *Sensitivity analysis results for the regions of Aegean Sea model.*

Box	Initial Deposition ^{137}Cs (Bq m^{-2})	Sensitivity (Measure of the effect / initial deposition)			
		Collective Dose (manSv per Bq m^{-2})		Individual Dose Rate (Sv y^{-1} per Bq m^{-2})	
		1st year	30th year	1st year	30th year
1	1.30E+04	1.03E-03	1.83E-04	1.32E-09	2.34E-10
6	4.00E+03	1.34E-03	1.42E-04	1.92E-09	2.03E-10
11	2.33E+03	1.22E-03	2.60E-04	1.09E-09	2.32E-10
14	7.33E+03	2.88E-03	3.18E-04	8.99E-10	9.93E-11
17	4.00E+03	5.21E-04	1.03E-04	5.31E-10	1.05E-10
22	2.33E+03	1.51E-03	2.25E-04	1.32E-09	1.97E-10
25	2.33E+03	1.09E-03	1.66E-04	1.32E-09	2.02E-10
28	5.00E+03	1.95E-03	5.99E-05	2.80E-09	8.60E-11
31	5.00E+03	1.42E-03	5.14E-05	2.36E-09	8.54E-11
34	1.33E+04	3.42E-03	5.29E-05	2.11E-09	3.26E-11
37	1.00E+04	1.04E-03	2.83E-05	1.39E-09	3.79E-11
40	1.00E+04	6.82E-04	6.88E-05	9.81E-10	9.90E-11
43	6.67E+03	2.28E-03	1.71E-04	2.10E-09	1.57E-10
46	5.00E+03	1.67E-03	2.65E-04	2.78E-09	4.41E-10

The differences in the two sensitivity indexes indicate that regions with high individual sensitivity can have comparatively very low collective sensitivity and vise versa. This is due the fact that

individual sensitivity is mainly affected by the radionuclides' concentrations in the marine components, while the collective sensitivity is strongly related with the population density. Moreover, from the sensitivity evolution it is derived that, in long term, the regions of South Aegean are becoming more vulnerable as the population suffer the contamination late effects due to the downstream dispersion of ^{137}Cs, following the general Aegean Sea circulation pattern.

The concept of environmental sensitivity, in terms of radioecological effect normalized to the initial stress, can give a measure of comparison within different natural environments. In this context, considering common basic initial assumptions (i.e. the conversion factors), the results of a given model can be compared and validated with other models' estimations, even if the examined contamination scenario is not exactly the same. Based on that, the measure of sensitivity of Aegean Sea was consequently compared with the results of the EMRAS II intercomparison exercise, where the contamination scenario of a uniform and spontaneous radionuclides fallout deposition of 1000 Bq m^{-2} was applied to various marine regions (IAEA, 2012).
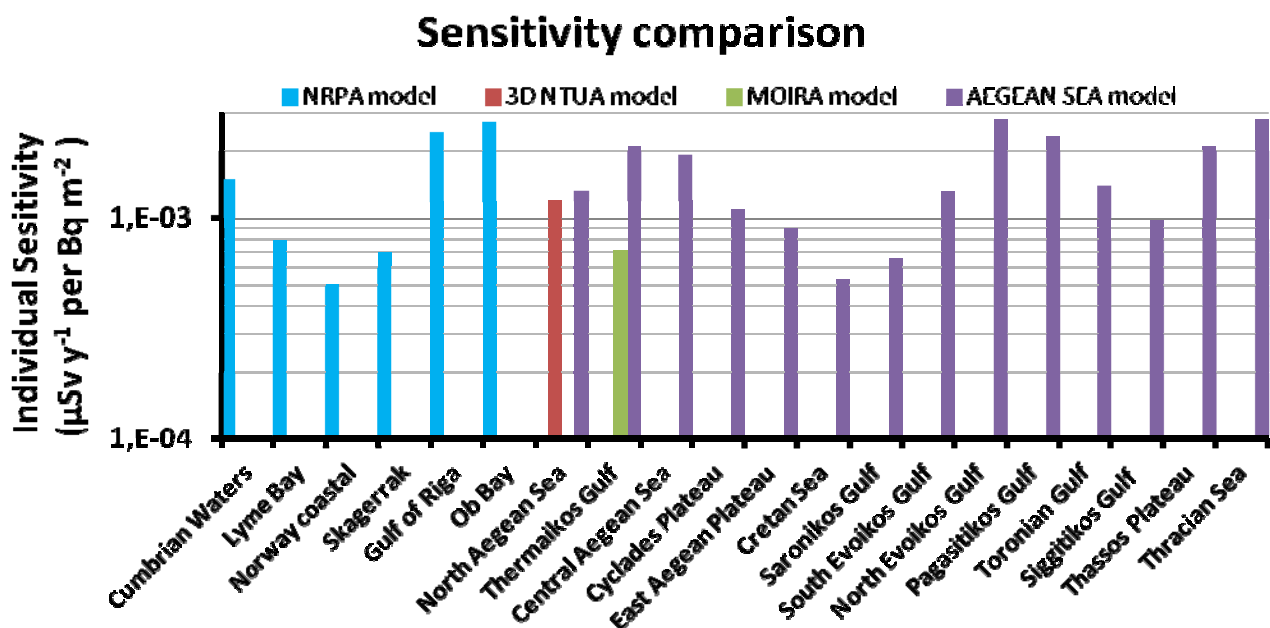
Figure 7. *Environmental sensitivity for various marine regions, calculated by different radiological models.*

Although the initial deposition is not uniform for the Aegean Sea model simulation, the results are consistent, since the effect of the BSW is negligible and the circulation is dominated by the water masses form the adjusted boxes with close concentrations. Moreover, considering the complexity of the environment, the different modeling approaches and the significantly wider spatial resolution of the Aegean Sea model, the satisfactory agreement with the 3D NTUA hydrodynamic model (Psaltaki et al, 2010) and the MOIRA box model (Eleftheriou et al., 2015) for the regions of North Aegean Sea and Thermaikos Gulf, respectively, underlines the fact that the developed model can be consider reliable and robust.

Conclusions

The radieological box model of Aegean Sea has been used for the investigation of the radioecological sensitivity of the region. Both model optimization and sensitivity analysis were undertaken with the simulation of the ^{137}Cs dispersion after the Chernobyl accident, based on empirical data. The radiological consequences have been estimated in terms of doses assessment. Calculated collective doses to man as well as dose rates to individuals found significantly lower

than the doses from natural sources, while the doses to critical individuals exhibited the negligible component to the annual individual dose from natural sources, during the first months after the accident. The estimations for the marine organisms indicate that doses to fish, crustacean and mollusc were much lower than the screening levels. The individual and collective sensitivity indexes reviled the spatial and temporal variation of the doses significantly affected by the water circulation pattern and the population distribution.

References

Brown, J.E., Thørring, H., Hosseini, A., 2003. The ''EPIC'' impact assessment framework. Deliverable Report for EC Inco-Copernicus project EPIC. ICA2-CT-2000-10032. Norwegian Radiation Protection Authority, Østeras, Norway.

CAC, 2006. Codex Alimentarius Commission: Joint FAO/WHO Food Standards Programme. Appendix 31. Food and Agriculture Organisation, United Nations.

EC, 1995. Methodology for assessing the radiological consequences of routine releases of radionuclides to the environment. EUR-15760-EN. European Commission, Luxembourg.

Eleftheriou, G., Iosjpe, M., 2016. Towards the development of a radiological box model for Aegean Sea: considerations and perspectives, Proceedings at the 25th Symposium of the Hellenic Nuclear Physics Society, 3-4 June 2016, Athens, Adv. Nucl. Phys. 25 (in press).

Eleftheriou, G., Monte, L., Brittain, J.E., Tsabaris, C., 2015. Modelling and assessment of the impact of radiocesium and radiostrontium dispersion in the Thermaikos Gulf. Sci. Tot. Environ. 533. 133-143.

IAEA, 2012. A Summary Report of the Results of the Environmental Modelling for Radiation Safety (EMRAS) Programme (2003–2007). TECDOC-1678. International Atomic Energy Agency, Vienna.

IAEA, 2013. Environmental sensitivities in nuclear emergencies and semi-natural environments. TECDOC-1719. International Atomic Energy Agency, Vienna.

IAEA, 2014. Handbook of the parameter values for the prediction of radionuclide transfer to wildlife. TRS-479. International Atomic Energy Agency, Vienna.

ICRP, 2012. Compendium of dose coefficients based on ICRP Publication 60. Annals of the ICRP, Publication 119. ICRP 41(Suppl.). International Commission on Radiological Protection.

Iosjpe, M., 2006. Environmental modelling: Modified approach for compartmental models, in: Povinec, P.P., Sanchez-Cabeza, J.A. (Eds), Radioactivity in the Environment, Volume 8, Elsevier, 463-476.

Iosjpe, M., 2011. A sensitivity analysis of the parameters controlling water-sediment interactions in the coastal zone: Consequences to man and environment. J. Mar. Syst. 88, 82-89.

Iosjpe, M., Brown, J., Strand, P., 2002. Modified approach to modelling radiological consequences from releases into the marine environment, J. Environ. Radioact. 60, 91-103.

Periáñez, R., Bezhenar, R., Iosjpe, M., Maderich, V., Nies, H., Osvath, I., Outola, I., de With, G., 2015. A comparison of marine radionuclide dispersion models for the Baltic Sea in the frame of IAEA MODARIA program. J. Environ. Radioact. 139, 66-77.

Psaltaki, M., Florou, H., Trabidou, G., Markatos, N., 2010. Modelling and assessment of pollutant impact on marine environments, 2nd WSEAS International Conference on Computer Engineering and Applications (CEA '10), Harvard University, Cambridge, USA, 27–29 January 2010, pp. 176–180.

Tracy, B.L., Carini, F., Barabash, S., Berkovskyy, V., Brittain, J.E., Chouhan, S., Eleftheriou, G., Iosjpe, M.,Monte, L., Psaltaki,M., Shen, J., Tschiersch, J., Turcanu, C., 2013. The sensitivity of different environments to radioactive contamination. J. Environ. Radioact. 122, 1–8.

UNSCEAR, 2000. Sources and effects of ionizing radiation. UNSCEAR 2000 Report to the General Assembly with Scientific Annexes. Volume I: Sources. United Nations Scientific Committee on the Effects of Atomic Radiation. New York.

Acknowledgements

A three-dimensional numerical model describing the ^{137}Cs behaviour in coastal waters: model verification and validation

Vito Bacchi

IRSN – Institut de Radioprotection et de Sûreté Nucléaire
France
vito.bacchi@irsn.fr

Pablo Tassi

EDF R&D and Saint-Venant Laboratory for Hydraulics
France
pablo.tassi@edf.fr

Abstract

The objective of this work is to present the implementation, verification and validation of a three-dimensional model capable to reproduce the propagation of the caesium-137 radionuclide in coastal waters and its interaction with suspended sediments, in the framework of the open-source TELEMAC-MASCARET modelling system. The mathematical model is based on the non-conservative transport of radionuclides, where the interaction with the particulate matter is considered. The resulting numerical model is verified by comparisons between numerical and analytical solutions of selected test cases. Finally, the model is validated with the Fukushima Dai-ichi case by comparing numerical results with field measurements of radionuclides concentration in the Japan Sea.

Introduction

On March 11, 2011, a devastating earthquake of magnitude 9.0 and a tsunami struck the Tohoku area, Japan, causing major damage to the cooling systems of reactors in the Fukushima Dai-ichi Nuclear Power Plant (NPP), operated by Tokyo Electric Power Company (TEPCO). In order to cool the reactor cores and the spent fuel in storage pools, large amounts of seawater and freshwater were used. A significant part of this radioactivity-contaminated water was discharged into the Pacific Ocean close to the power plant. In addition, between March 12 and 15 2011, several hydrogen explosions resulted in the release of significant radioactivity into the atmosphere, some of which was deposited onto the sea surface over a wide area of the Pacific Ocean. Consequently, high concentrations of iodine (^{131}I), strontium ($^{90}S_r$) and caesium-137 ($^{137}C_s$) were found in seawater and seabed sediments along the coastline of Fukushima Prefecture [25]. Moreover, radionuclides were detected in marine debris caught near Fukushima Prefecture [7]. The human and non-human populations of the nearby regions were exposed temporarily or permanently to the substances, either by external irradiation or by ingesting plants growing in the local area.

A significant number of modelling studies on the dispersion of radionuclides released from Fukushima into the Pacific Ocean have been recently published in the scientific literature. Recently, in the framework of the MODARIA project, supported by the International Atomic Energy Agency (IAEA), different models were applied to the accidental releases and discharges from Fukushima Dai-ichi NPP accident. A brief description of these models is given below. The reader is referred Periáñez et al. [19] for a detailed description of these models.

The model developed by IMMSP/KIOST (Institute of Mathematical Machine and System Problems, Ukraine, with the Korea Institute of Ocean Science and Technology, Republic of Korea) for radionuclide transport proposes two approaches: Eulerian and Lagrangian, and water circulation and sediment transport are obtained from the hydrodynamic SELFE model [22], [29]. The oceanic dispersion model named LORAS (Lagrangian Oceanic Radiological Assessment System) has been developed by Korea Atomic Energy Research Institute (KAERI) to evaluate the transport characteristics of the radionuclides released into the sea for a nuclear accident [13]. A particle random-walk model (SEA-GEARN) has been used by the Japan Atomic Energy Agency (JAEA) to simulate radionuclide transport in the Pacific Ocean. This model is based on the three-dimensional advection/diffusion dispersion equations. The SisBAHIA model [1] was developed by the Instituto de Engenheria Nuclear in Brazil and solves the transport of contaminants with the Eulerian and Lagrangian approaches. Finally, the USEV model, developed by the University of Sevilla (Spain), is based on the three-dimensional advection/diffusion dispersion equations. For these models, water circulation has been obtained from JCOPE2 hydrodynamic model [17], [18].

The numerical experiments of the MODARIA project were carried-out for a perfectly conservative radionuclide (Exercises 1 and 2) and for $^{137}C_s$, including water/sediment interactions (Exercises 2, 3 4a and 4b), using different hydrodynamic forcings and numerical and physical parameters (Exercises 1 and 4b). The model outputs were also compared with TEPCO measurements of radioactivity in water and sediments [25]. As a conclusion, it was found that the main reason of discrepancies between the model results was due to the differences between the numerical schemes and parameterizations used among these models.

The common point of all these models is the size of the computational domain (35°N–38.5°N, 140.5°E–144°E, covering approximately 670 km long and 620 km wide) and the need of employing a realistic reproduction of oceanic conditions

such as ocean current, temperature, salinity, and sea surface height (SSH) for performing accurate numerical simulations on the oceanic dispersion of radionuclides. In general, these models use the hydrodynamics obtained with general circulation models based on data assimilation techniques (NCOM, JCOPE2) or variation method, as for the JAEA model which uses the three-dimensional variational (3D-VAR) data assimilation system [28], Meteorological Research Institute (MRI) Multivariate Ocean Variational Estimation (MOVE) with the eddy-resolving ocean general circulation model, MRI Community Ocean Model (www.mri.com; [27]) at the Japan Meteorological Agency (JMA), which makes it possible to adjust the numerical results with field observations.

It can be considered that these models should be useful and powerful tools in post-emergency situations, when the estimation of future contamination of water, sediments and biota rely on data from analogous periods of previous years [21], or for the assessment of the long-term consequences of the accident, including transfers of radionuclides to sediments and biota, as well as evaluating the potential role of sediments as a source of contamination once radionuclide concentrations in seawater have decreased [15]. However, a model should be capable of providing quick-responses to emergency situations [21]. Rapid responses can be achieved using meteorological data or tide conditions from operational numerical models in order to accurately predict the radioactivity transport. In this case, the accuracy of the model could be improved by a refined spatial discretization and the model extension could be limited to the coastal area in the vicinity of the NPP.

In this context, the objective of this study is to develop a three-dimensional (3D) numerical tool able to reproduce the dispersion of radionuclides in coastal waters in an emergency situation such as the Fukushima Dai-ichi NPP accident. With this aim, the developed model has been forced only with data available immediately after (or during) the accident, as the weather conditions (wind, pressure, temperature) and/or the harmonic components of tides, and the model domain was limited to the coastal area near Fukushima and refined in the coastal area nearby the NPP.

The model was developed within the open source TELEMAC-MASCARET system, which is an integrated modelling tool for use in the field of free-surface flows. The various simulation modules use efficient algorithms based on the finite-element or finite volume methods. Space discretization is performed with unstructured triangular elements, which means that it can be locally refined in particular areas of interest. The mathematical model for radionuclides transport was built based on previous studies on non-conservative radionuclides [11], [16], where the interactions with the particulate matter has been considered. To account for these processes, a module that solves three-phase interaction has been implemented and described in the next section. This newly developed module was coupled with the 3D Reynolds-Averaged Navier-Stokes hydrodynamics module TELEMAC-3D of the TELEMAC-MASCARET system. Details on the 3D hydrodynamics model can be consulted in [5] and are not presented hereafter.

Radionuclides transport model

Conceptual Model

The radionuclides transport model is based on previous studies on non-conservative radionuclides propagation in sea waters, e.g. [11], [14], [16]. In particular, the model implemented in this work is a three phase's model with the following characteristics: (*i*) dissolved phase consists of radionuclides that are dissolved and adsorbed onto fine particles without settling velocity (diameter < 0.8 mm is preferred, according to Kobayashi et al. [9]), (*ii*) the large particle matter (LPM) phase consists of radionuclides that are adsorbed with the LPM which has settling velocity, (*iii*) active bottom sediment phase consists of radionuclides that are adsorbed with the LPM which deposit on the seabed, and the particle re-suspends according to the bottom velocity. For sediments, it is assumed that the LPM is an aggregate which has a single radius and density and the movement of each particle is characterized by velocity, diffusivity and settling velocity of the particle itself. A detailed description of this formulation can be found in [16], [17].

Governing Equations

The radionuclide transport model describes the water-sediment sorption processes. It includes the advection-diffusion equations for dissolved C_s^w and adsorbed by suspended sediment C_p^w radioactivity in the water column, and the equations for concentration of the dissolved C_s^b and adsorbed C_p^b radioactivity in the bottom deposits, expressed in [Bq/l], [Bq/m^3] or [kg/m^3]. The transport of radionuclides dissolved (or absorbed by sediments) in water can be written as a classic advection-diffusion equation, by considering as an additional source term the exchange between the solid and the dissolved phases:

$$\frac{\partial C_s^w}{\partial t} + \frac{\partial U C_s^w}{\partial x} + \frac{\partial V C_s^w}{\partial y} + \frac{\partial W C_s^w}{\partial z} =$$
$$\frac{\partial}{\partial x}\left(\nu_h \frac{\partial C_s^w}{\partial x}\right) + \frac{\partial}{\partial y}\left(\nu_h \frac{\partial C_s^w}{\partial y}\right) + \frac{\partial}{\partial z}\left(\nu_v \frac{\partial C_s^w}{\partial z}\right) -$$
$$\lambda C_s^w - a_{1,2}^w (S_d^w K_d^w C_s^w - C_p^w) + P_s^w \tag{1}$$

$$\frac{\partial C_p^w}{\partial t} + \frac{\partial U C_p^w}{\partial x} + \frac{\partial V C_p^w}{\partial y} + \frac{\partial (W - w_s) C_p^w}{\partial z} =$$
$$\frac{\partial}{\partial x}\left(\nu_h \frac{\partial C_p^w}{\partial x}\right) + \frac{\partial}{\partial y}\left(\nu_h \frac{\partial C_p^w}{\partial y}\right) + \frac{\partial}{\partial z}\left(\nu_v \frac{\partial C_p^w}{\partial z}\right) -$$
$$\lambda C_p^w - a_{1,2}^w (S_d^w K_d^w C_s^w - C_p^w) + P_p^w \tag{2}$$

where U, V, W [m/s] are the velocity field components along the $x, y, z-$directions, respectively, ν_h and ν_v [m^2/s] are respectively the horizontal and vertical diffusion coefficient for radionuclides, λ [s^{-1}] is the radionuclide decay constant, P_s^w and P_p^w are the input of the dissolved radionuclides from the source point and the input of the radionuclides which adsorbed to the LPM from the source point [kg/m^{2}s], respectively, S_d^w [kg/m^3] or [g/l] is the sediment concentration and w_s [m/s] is the sediment settling velocity. Above, the distribution coefficients K_d^w and K_d^b [m^3/kg] are defined under steady hydraulic conditions as:

$$S_d^w K_d^w = \lim_{t \to \infty}\left(\frac{C_p^w}{C_s^w}\right), \quad \frac{S_d^b}{\epsilon} K_d^b = \lim_{t \to \infty}\left(\frac{C_p^b}{C_s^b}\right) \tag{3}$$

with ϵ [-] the bed porosity.

In Equations (1–2), the radionuclides are treated as passive tracer, and the exchanges between the different phases are described by diffusion, sorption, and sedimentation-resuspension processes. The adsorption and desorption of radionuclides between liquid and solid phases are described by the radionuclide exchange rates $a_{1,2}^w$ [day^{-1}] and $a_{1,2}^b$ [year^{-1}], usually considered as constants for practical applications [11]. The variation of the dissolved ($m_s^b = C_s^b Z_b$) and adsorbed ($m_p^b = C_p^b Z_b$) mass of radioactivity in the bottom deposits can be written as follows:

$$\frac{\partial m_s^b}{\partial t} = \frac{F_{dif}}{Z_b}\left(C_s^w - \frac{C_s^b}{\epsilon}\right) - \lambda m_s^b - a_{1,2}^b \left(\frac{S_d^b}{\epsilon} K_d^b C_s^b - C_p^b\right) Z_b \tag{4}$$

$$\frac{\partial m_p^b}{\partial t} = \left(\frac{C_p^w D}{S_d^w} - \frac{C_s^b E}{S_d^b}\right) - \lambda m_p^b - a_{1,2}^b \left(\frac{S_d^b}{\epsilon} K_d^b C_s^b - C_p^b\right) Z_b \tag{5}$$

Above, F_{dif} [m^2/s] is the diffusion coefficient describing the exchange between the bed and the water at the bottom and Z_b [m] is the thickness of the bottom layer.

Boundary conditions

The boundary condition for C_s^w and S_d^w at the free surface Z_s is a no-flux condition, expressed as:

$$\left(\nu_v \frac{\partial S_d^w}{\partial z} + w_s S_d^w\right)_{z=Z_s} = 0, \quad \left(\nu_v \frac{\partial C_s^w}{\partial z} + w_s C_s^w\right)_{z=Z_s} = 0 \tag{6}$$

where Z_s is the z-coordinate of the free surface. The boundary condition for C_s^w, C_p^w and S_d^w at the bed describes the exchange of radionuclides and of sediments with the bed. The fluxes into the bottom are induced by the diffusion of radioactivity (desorption) between the bed sediments and water, and the flux of radioactivity associated to the depositional and erosional rates, as follows:

$$\nu_v \frac{\partial C_s^w}{\partial z} = \frac{F_{dif}}{Z_b}\left(C_s^w - \frac{C_s^b}{\epsilon}\right),$$
$$\nu_v \frac{\partial C_p^w}{\partial z} + (W - w_s) C_p^w = \frac{C_p^w}{S_d^w} D - \frac{C_p^b}{S_d^b} E, \tag{7}$$
$$\left(\nu_v \frac{\partial S_d^w}{\partial z} + w_s S_d^w\right)_{z=Z_s} = D - E.$$

For cohesive sediments, the deposition rate equation is described by the empirical Krone law [4]:

$$D = \begin{cases} w_s S_d^w (1 - \tau/\tau_{cd}) & \text{if } \tau < \tau_{cd} \\ 0 & \text{otherwise} \end{cases}$$

where τ_{cd} [N/m^2] is the deposition critical bed shear stress, w_s [m/s] the mud settling velocity near the bed and τ [N/m^2] is the bed shear stress. The erosion rate follows the empirical Partheniades law [4]:

$$E = \begin{cases} M(\tau/\tau_{ce} - 1) & \text{if } \tau > \tau_{ce} \\ 0 & \text{otherwise} \end{cases}$$

where τ_{ce} [N/m^2] is the erosion critical shear stress of the mud layer and M the Partheniades coefficient (kg/sm^2). For a single layer bed with a concentration S_d^b [kg/m^3], the mass conservation equation for the bed evolution is given by:

$$S_d^b \frac{\partial Z_b}{\partial t} = D - E. \tag{8}$$
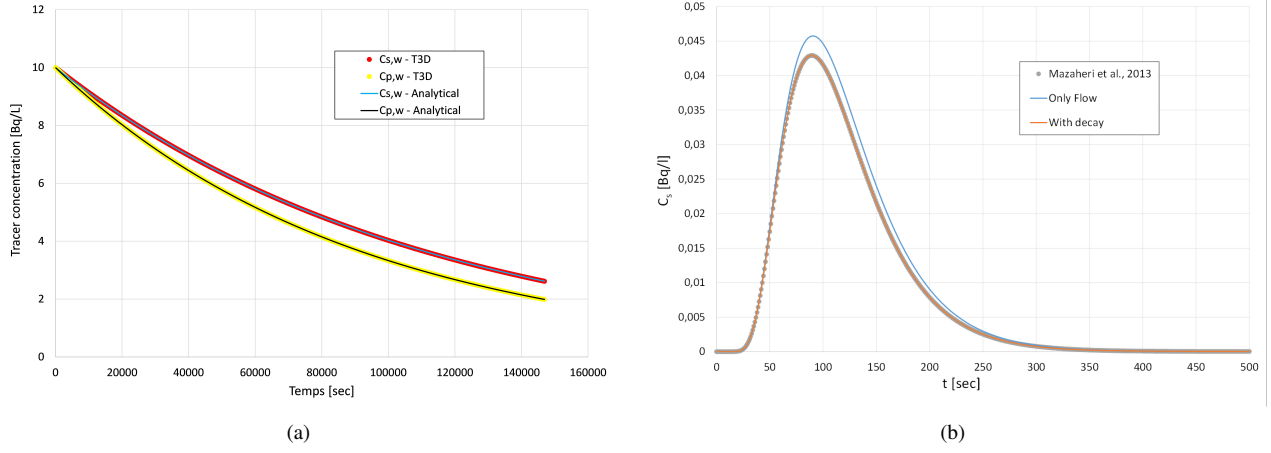
Fig. 1: (a) Comparison between the numerical results and the analytical solution for the kinematic exchange of radioactivity between water and suspended sediment in a basin, see section -A. (b) Time evolution of the tracer decay in a permanent flow field test, see section -B.

Model verification

In this section, the capability of the model at reproducing the advection and dispersion of radionuclides and its interactions is assessed by comparisons between numerical and analytical solutions.

Kinematic exchange of radioactivity between water and suspended sediment in a basin

The objective of this test case is to assess the ability of the model to reproduce the kinematic exchange of radioactivity between suspended sediments and water. A square basin $\Omega = [5 \times 5]$ [m^2] with constant water depth $h = 2$ [m] is considered, zero flow velocity $\vec{U} = (U, V, W) = (0, 0, 0)$ [ms^{-1}] and solid boundaries. The initial distribution of the dissolved $C^w_{s,0} = C^w_s(t = 0)$ and adsorbed by sediments $C^w_{p,0} = C^w_p(t = 0)$ radioactivity is uniform and equal to 10.0 [Bq/l] and the value of the diffusion coefficient of the tracers $K = 10$ [m^{2}s^{-1}]. The decay constant $\lambda = 0.00001$ [s^{-1}] and the radionuclide exchange rate $a_{1,2} = 0.000001$ [day^{-1}]. For these conditions, Equations (1–2) simplify into:

$$\frac{\partial C^w_s}{\partial t} + \lambda C^w_s = a^w_{1,2} C^w_p, \quad \frac{\partial C^w_p}{\partial t} + \lambda C^w_p = -a^w_{1,2} C^w_p \tag{9}$$

Analytical solutions of Equations (9) are:

$$C^w_s(t) = (C^w_{s,0} + C^w_{p,0}) \exp^{-\lambda t} + C^w_p(t), \tag{10}$$

$$C^w_p(t) = C^w_{p,0} \exp^{-(\lambda + a^w_{1,2})t} \tag{11}$$

For this test case we use an unstructured mesh and a time step of 10 [s]. Figure 1a shows the good agreement between the numerical and the analytical results for both the dissolved and adsorbed radioactivity.

Tracer decay in a permanent flow field

The purpose of this test case is to assess the ability of the numerical model to reproduce the physical behavior of radionuclides dissolved in water, when transported by an uniform flow field in a rectangular domain $\Omega = [1 \times 500]$ [m^2] with initial constant water depth $h = 1.0$ [m] and flow velocity $\vec{U} = (U, V, W) = (0, 0, 0)$ [ms^{-1}]. At boundaries $x = 0$ and $x = 500$ m, a constant water discharge $Q(0, t) = 1.0$ [m^{3}s^{-1}] and water depth $h(500, t) = 1.0$ [m] were imposed, respectively. No friction is considered at the bottom of the channel. At $t = 0$ [s], an initial triangular distribution of the dissolved radioactivity is considered between $x = 95$ [m] and $x = 105$ [m], with a peak value equal to 1.0 Bq/l at $x = 100$ [m]. At the inflow and outflow boundaries, a constant zero radioactivity and a Neumann-like boundary condition are imposed, respectively. An unstructured mesh with typical element size equal to 0.5 [m] and time step of 0.5 [s] was used. The decay constant $\lambda = 0.0007$ [s^{-1}]. For a uniform and unidirectional flow field, the analytical solution of the tracer transport equation is reported in detail in [12]. In Figure 1b, numerical results show that the temporal variation of the tracer concentration at the middle of the channel (orange line) is accentuated by the radioactivity decay, in comparison with a reference situation without decay (blue line). This result confirms that the simulated behavior of the dissolved radioactivity is physically based and in agreement with the analytical solution.

4
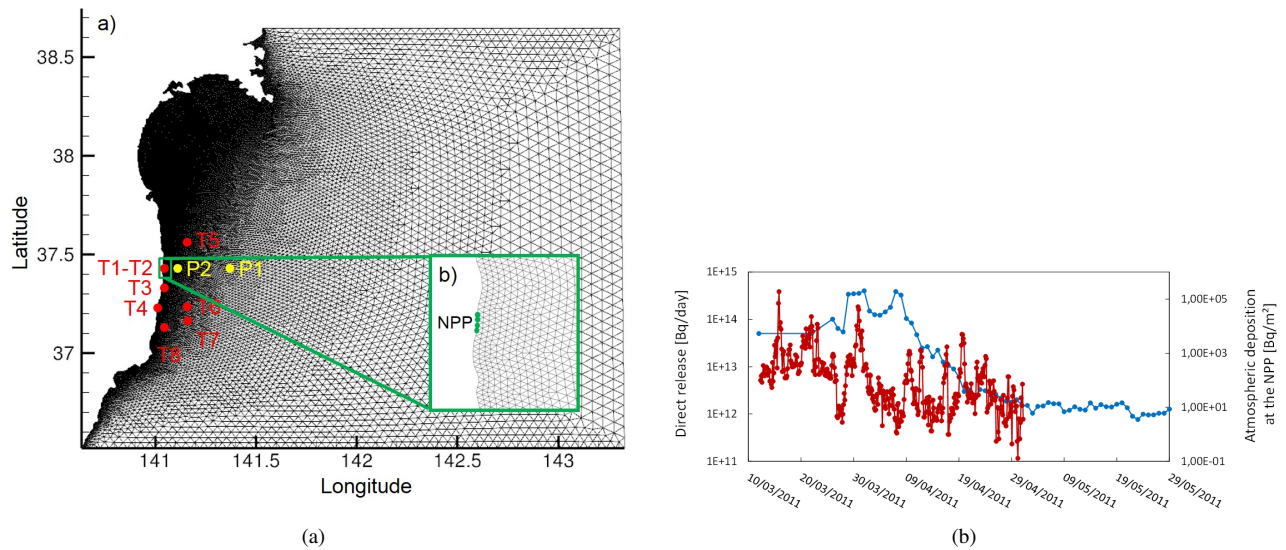
Fig. 2: a) Computational grid and sampling points where calculated $^{137}C_s$ concentrations in surface water have been compared with measurements. Points $P1$ and $P2$ are issued from the MODARIA project Exercice 1. The grid points employed for reproducing the NPP are indicated in green; b) Source term of caesium $^{137}C_s$ used in the numerical simulations, see section -B.

Application to the Fukushima Dai-ichi accident

Model construction

This study covers the oceanic coastal area nearby the Fukushima Dai-ichi NPP: 36.5°N–38.5°N, 140.6°E–143.4°E (covering an extension of c. 300 km to 300 km), see Figure 2a. The computational domain was discretized with 62,451 triangular elements, followed by extruding each triangle along the vertical direction into linear prismatic columns spanning the water column from the bottom to the free-surface. Each column is composed of a fixed number of prismatic elements, that number being chosen during the simulation set-up. The horizontal mesh size varied from 200 [m], near to the Fukushima Dai-ichi NPP to 10 [km] off-shore, depending on the resolution of the bathymetrical data (derived from the Japan Oceanographic Data Center) and the water depth. The vertical resolution of the layered mesh is 5 layers, resulting in elements with a height of the order of 50 [m] in the coastal area of the NPP and the computational time step was equal to 10 [s]. The simulations were performed for a total time of 90 days (from the March 1st 2011 to May 30th 2011). The model was initialised and forced at the oceanic boundary with tides (surface elevation and the currents). The tides are provided as complex amplitudes of earth-relative sea-surface elevation for eight primary ($M2$, $S2$, $N2$, $K2$, $K1$, $O1$, $P1$, $Q1$), two long period (Mf, Mm) and three non-linear harmonic constituents ($M4$, $MS4$, $MN4$), computed with the methodology reported in [2], [3]. The tidal constituents were extracted from the Oregon State University Tidal Prediction Software (OTPS/TPXO). These data are available on line (http://volkov.oce.orst.edu/tides/OhS.html). Current velocity and water surface elevation values were used to initialise the model the March 1st 2011. At initial time, the dissolved radionuclides concentration was set to zero. On the free surface, the model was also forced by wind and atmospheric parameters computed from the European Centre for Medium-Range Weather Forecasts (ECMWF) model.

Source terms

The amount of $^{137}C_s$ released directly into the ocean was given by [19]. According to Kobayashi et al. [10], this quantities correspond to the data of $^{137}C_s$ released directly into the ocean from the Fukushima Dai-ichi NPP. Four releases points were defined in the mesh along the coast between the northern discharge channel and the southern discharge channel of the Fukushima Dai-ichi NPP and it was assumed that the direct release into the ocean started on March 26th, see Figure 2b. Discharges were assumed to continue until June 30. The blue line in Figure 2b shows the temporal variation of the released amount of $^{137}C_s$ used in the numerical simulations. These data were estimated based on the concentrations of radionuclides at the northern and southern discharge channels of the Fukushima Dai-ichi NPP, which were monitored almost twice a day. This source term estimation led to a total $^{137}C_s$ release of 3.5 PBq from March 26th to June 30.

In [19], the authors used the ensemble average values of wet deposition of $^{137}C_s$ on the free surface issued from two atmospheric dispersion models. These models were developed by KAERI [23], [24] and JAEA [26]. Both are particle tracking dispersion models and permit to model the dispersion of radionuclides released to the atmosphere and evaluate the subsequent deposition on the sea surface. In this work, this dataset was projected onto the computational domain. An example of wet deposition in the proximity of the NPP is reported in 2b.

5

In this section, numerical simulations were performed from March 1st to June 1st 2011. Time series of calculated $^{137}C_s$ concentrations obtained with TELEMAC-3D were first compared to the measured concentrations obtained by TEPCO (T1 to T8, red points in Figure 2a). These measurements were reported in regular press releases [25]. As showed in Figure 3, TELEMAC-3D reproduces well the concentration values at the measurements points. Particularly, nearby the NPP (points T1 to T4), good agreement between numerical results and observations is found from March 28th, two days after the beginning of the direct release into the ocean. As observed in Figure 3, numerical results match well the measurements captured in the offshore zone, both in the south zone (points T6 to T8) and in the north zone (point T5) of the Fukushima Dai-ichi NPP. For these points, there is no evidence that the numerical results are improved starting from March 26. Conversely, the model is able to correctly reproduce the order of magnitude of the measured concentration of $^{137}C_s$ during the simulation period. The model is therefore able to reproduce the propagation and diffusion of the released $^{137}C_s$ in the vicinity of the NPP.
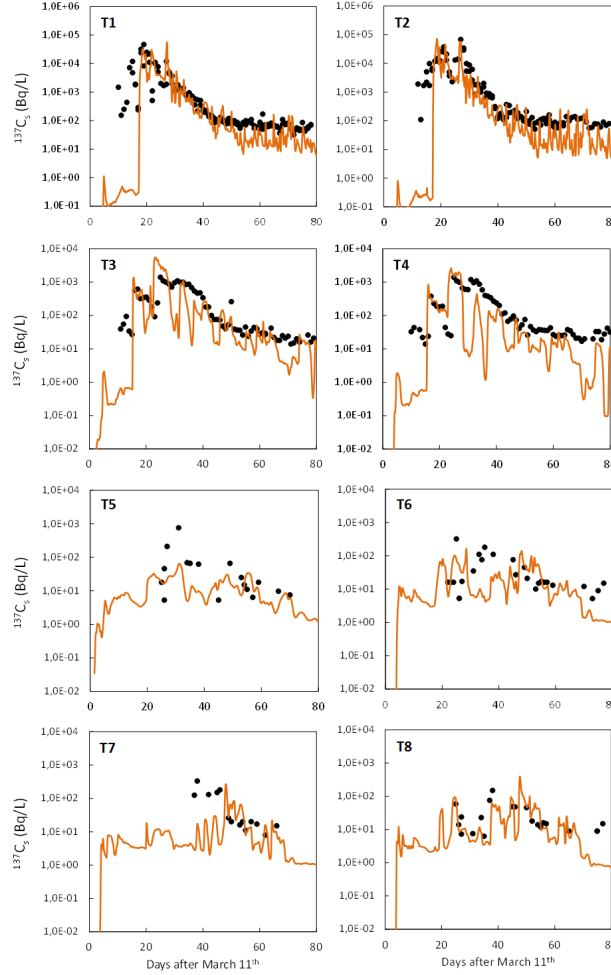
Fig. 3: Comparison between computed and measured $^{137}C_s$ concentration on the water surface, collected by TEPCO [25].

Maps of calculated $^{137}C_s$ distributions in surface water are presented in Figure 4. Corresponding maps obtained from interpolation of measurements are shown in Inomata et al. [6]. The calculated distributions, corresponding to the concentrations of the dissolved fraction of $^{137}C_s$ reflect the water circulation performed by the model. We observe that our model tend to produce an elongated patch in the North-South direction (Figures 4a-c) and, later, leading to offshore transport of radionuclides (Figures 4d-f). An accumulation of radionuclides is also observed along-shore and especially in the coastal zone of the numerical model, indicating that the main current direction is from South to North and, in a second time, toward the North/East direction.

Numerical results at coastal scale obtained with TELEMAC-3D are slightly different from the general path of an isotropic dispersion of radionuclides around the Fukushima Dai-ichi NPP reported by Inomata et al. [6]. Many reasons can explain these discrepancies. Firstly, the measured path has to be attributed to the small number of measurements and different sampling times used to produce these maps by an optimal interpolation method. Secondly, large scale models have showed the presence of a large anticyclonic eddy south of Fukushima, which plays a central role in the transport of radionuclides and which can affect the hydrodynamics near the coastal area around Fukushima, see [8]. Given the intensity and variability of currents in this area,
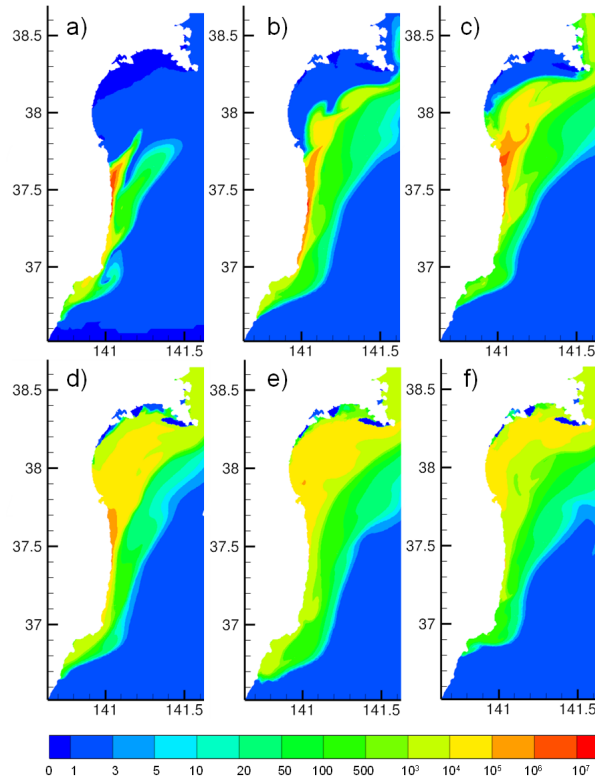
Fig. 4: Numerical results of the $^{137}C_s$ distribution on the water surface: a) April 1, b) April 6, c) April 11, d) April 21, e) May 1 and f) May 11, 2011.

as well as the presence of unsteady eddies due to current convergence here, small differences in the hydrodynamics can produce different dispersion patterns [19], [21].

Conclusions

The main objectives of this work were (*i*) to present the implementation, verification and validation of a three-dimensional model able reproducing the propagation of $^{137}C_s$ radionuclide in coastal waters and its interaction with suspended sediments, in the framework of the open-source TELEMAC-MASCARET modelling system and (*ii*) to evaluate the performances of the validated mode in an emergency situation as the Fukushima Dai-ichi NPP accident.

The mathematical model was based on the non-conservative transport of radionuclides, where the interaction with the particulate matter is considered, see e.g. [11], [14], [16]. This process was accounted for by solving a three-phase interaction problem, where the transfer of radionuclides from the liquid (water) to the solid phase (sediments) is governed by kinetic transfer coefficients. The resulting numerical model was first verified by comparisons between numerical and analytical solutions of selected test cases. We observed that the agreement between the analytical and numerical solution was satisfying for the performed tests, showing that the spatial and temporal distribution of the tracer concentration was well reproduced by the model. Moreover, both the kinematic exchanges of radionuclides between water and sediments and the radioactive decay were well reproduced.

The validation of the model with the Fukushima Dai-ichi case was realized by comparing numerical results with field measurements of radionuclides concentration in the Japan Sea (TEPCO measurements performed after the accident of 2011). The numerical results show that the model is able to reproduce the propagation and diffusion of the released $^{137}C_s$ in the vicinity of the NPP. Therefore, numerical results obtained with a small scale model with a simple forcing are consistent, at a coastal-scale, with models which employed general circulation model based on data assimilation techniques or variation method for hydrodynamics, see e.g. [20]. As a consequence, this kind of model could be employed in an emergency situation, when the dissolved radioactivity is considered.

References

[1] Cunha, C.L.N., Rosman, P.C.C., 2005. *A semi-implicit finite element model for natural water bodies*. Water Res. 39, 2034e2047.

[2] Egbert, G. D., Bennet, A., F., Foreman, M. G. G., 1994. *TOPEX/POSEIDON tides estimated using a global inverse model*. Journal of Geophysical Research. Vol. 99, Issue C12.

[3] Egbert, G. D., Erofeeva, S. Y., 2002. *Efficient Inverse Modeling of Barotropic Ocean Tides*. Journal of Atmospheric and Ocean Technology. Vol. 19. pp. 183-204.

[4] García, M. (2008) Sediment Transport and Morphodynamics. Chapter 2 of *Sedimentation Engineering: Processes, Measurements, Modeling, and Practice* pp. 21-163. doi: 10.1061/9780784408148.ch02

[5] Hervouet, J-.M., 2007. *Hydrodynamics of Free Surface Flows: Modelling with the Finite Element Method*. ISBN: 978-0-470-03558-0, 360 pp.

[6] Inomata, Y., Aoyama, M., Tsubono, T., Tsumune, D., Hirose, K., 2016. *Spatial and temporal distributions of 134Cs and 137Cs derived from the TEPCO Fukushima Daiichi Nuclear Power Plant accident in the North Pacific Ocean by using optimal interpolation analysis*. Environ. Sci. Process. Impacts 18, 126136.

[7] Kawamura, H., Kobayashi, T. and Furuno, A., In, T., Ishikawa, Y., Nakayama, T., Shima, S. and Awaji, T. 2011. *Preliminary numerical experiments on oceanic dispersion of 131-I and 137-Cs discharged into the ocean because of the Fukushima Daiichi nuclear power plant disaster*. J. Nucl. Sci. Technol., 48: 13491356.

[8] Kawamura, H., Kobayashi, T., Furuno, A., Usui, N., Kamachi, M., 2014. *Numerical simulation on the long-term variation of radioactive cesium concentration in the North Pacific due to the Fukushima disaster*. J. Environ. Radioact. 136, 64-75.

[9] Kobayashi, T, Otosaka, S., Togawa, O., and Hayashi, K.: *Development of a non-conservative radionuclides dispersion model in the ocean and its application to surface cesium-137 dispersion in the Irish Sea*, J. Nucl. Sci. Technol., 44, 238247, 2007.

[10] Kobayashi, T., Nagai, H., Chino, M., and Kawamura, H.: *Source term estimation of atmospheric release due to the Fukushima Daiichi Nuclear Power Plant accident by atmospheric and oceanic dispersion simulations*, J. Nucl. Sci. Technol., 50, 255 264, 2013.

[11] Margvelashvily, N., Maderich, V., Yuschenko, S., Zheleznyak, M., 2000. *3-D numerical modelling of mud and radionuclide transport in the Chernobyl Cooling Pond and Dnieper–Boog Estuary*. Fine Sediments Dynamics in the Marine Environnement Proceedings of INTERCOH-2000. Ed. J.C. Winterwerp and C. Kranenburg, Elsevier, p. 595-610.

[12] Mazaheri, M., Samani, J.M., Samani, M.V., 2013. *Analytical Solution to One-dimensional Advection-diffusion Equation with Several Point Sources through Arbitrary Time-dependent Emission Rate Patterns*. J. Agr. Sci. Tech., 15: 1231-1245.

[13] Min, B.I., Periáñez, R., In-Gyu, Kim, Kyung-Suk, Suh, 2013. *Marine dispersion assessment of 137Cs released from the fukushima nuclear accident*. Mar. Pollut. Bull. 72, 22e33.

[14] Periáñez, R., 1998. *A three dimensional $r-$coordinate model to simulate the dispersion of radionuclides in the marine environment*. Ecological Modelling 114, 5970.

[15] Periáñez, R., 2003. *Redissolution and long-term transport of radionuclides released from a contaminated sediment: a numerical modelling study*. Estuar. Coast. Shelf Sci. 56, 514.

[16] Periáñez, R. 2005. Modelling the dispersion of radio nuclides in the marine environment: An introduction. Springer, Berlin, ISBN: 3-540-24875-7.

[17] Periáñez, R., Suh, K.S. and Min, B.I. 2012. *Local scale marine modelling of Fukushima releases. Assessment of water and sediment contamination and sensitivity to water circulation description*. Mar. Pollut. Bull., 64(11): 23332339.

[18] Periáñez, R., Suh, Kyung-Suk, Min, Byung-Il, 2013. *Should we measure plutonium concentrations in marine sediments near Fukushima?* J. Radioanal. Nucl. Chem. 298, 635e638.

[19] Periáñez, R., Brovchenko, I., Duffa, C., Jung, K-T., Kobayashi, T., Lamego, F., Maderich, V., Min, B-I., Nies, H., Osvath, I., Psaltaki, M., Suh, K.S., 2015. *A new comparison of marine dispersion model performances for Fukushima Dai-ichi releases in the frame of IAEA MODARIA program*. J. Environ. Radioactivity, 150: 247-269.

[20] Periáñez, R., Suh, K.S. and Min, B.I. 2015. *Numerical Modeling as a Tool for Managing Nuclear Accidents: The Fukushima Daiichi Case*. Energy Vol. 4: Nuclear Science.

[21] Periáñez, R., Bezhenar, R., Brovchenko, I., Duffa, C., Iosjpe, M., Jung, K-T., Kobayashi, T., Lamego, F., Maderich, V., Min, B-I., Nies, H., Osvath, I., Outola, I., Suh, K.S., de With, G. 2016. *Modelling of marine radionuclide dispersion in IAEA MODARIA program: Lessons learnt from the Baltic Sea and Fukushima scenarios*. Science of the Total Environment, In press.

[22] Roland, A., Zhang, Y.J., Wang, H.V., Meng, Y., Teng, Y.C., Maderich, V., Brovchenko, I., Dutour-Sikiric, M., Zanke, U., 2012. *A fully coupled 3D wave-current interaction model on unstructured grids*. J. Geophys. Res. 117, 1e18.

[23] Suh, K.S., Jeong, H.J., Kim, E.H., Hwang, W.T., Han, M.H., 2006. *Verification of the Lagrangian particle model using the ETEX experiment*. Ann. Nucl. Energy 33, 1159e1163.

[24] Suh, K.S., Han, M.H., Jung, S.H., Lee, C.W., 2009. *Numerical simulation for a dispersion of a pollutant using Chernobyl data*. Math. Comput. Model. 49, 337e343.

[25] TEPCO (Tokyo Electricity Power Corporation). 2011. Available at: `http://www.tepco.co.jp/en/`.

[26] Terada, H., Katata, G., Chino, M., Nagai, H., 2012. *Atmospheric discharge and dispersion of radionuclides during the Fukushima Dai-ichi Nuclear Power Plant accident. Part II: verification of the source term and analysis of regional-scale atmospheric dispersion*. J. Environ. Radioact. 112, 141e154.

[27] Tsujino, H., Motoi, T., Ishikawa, I., Hirabata, M., Nakano, H., Yamanaka, G., Yasuda, T., Ishizaki, H., 2010. Reference Manual for the Meteorological Research Institute Community Ocean Model (MRI.COM) Version 3. Technical Reports of the MRI. 59. Meteorological Research Institute, Tsukuba, Japan.

[28] Usui, N., Ishizaki, S., Fujii, Y., Tsujino, H., Yasuda, T., Kamachi, M., 2006. *Meteorological Research Institute multivariate ocean variational estimation (MOVE) system: some early results*. Adv. Space Res. 37, 806e822.

[29] Zhang, Y., Battista, A.M., 2008. *SELFE: a semi-implicit Eulerian-Lagrangian finite-element model for cross-scale ocean circulation*. Ocean. Model. 21 (3e4), 71e96.

Modeling ^{131}I distribution in a tidal river

Maria-Evangelia Souti and Helmut W. Fischer

Institute of Environmental Physics, University of Bremen, Otto-Hahn-Alle 1, D-28359 Bremen, Germany

Abstract

This paper presents and evaluates a 3 compartment numerical model for water flow, radionuclide transport and sedimentation in a tidal river originating from the local sewage plant under routine releases. The model solves the hydrodynamic equations and the radionuclide dispersion equations including deposition of sediments. The assessment of the model is done by comparing simulated and experimental data on ^{131}I activity concentrations in the Weser River water and banks. The model provides realistic radionuclide distributions in water and bank sediments and the simulated currents and ^{131}I activity concentrations in the system are, in general, in agreement with observations.

Introduction

River flow and sedimentation are among the most complex processes in nature. The river Weser, located in NW Germany flows through the city of Bremen and discharges into the North Sea. It is influenced by the North Sea tides, which lead to a tidal range close to 4 m in the city and an inversion of flow direction about 4 times in 24 h. In its tidal part, about 8 km downstream of the city center of Bremen the sewage treatment plant (WWTP) is located, which routinely releases in the river water medically used radionuclides. Our study is focused on ^{131}I, the most used radioisotope in nuclear medicine with a half life of 8.02 days. In the vicinity of the WWTP, ^{131}I is detectable in both river water and sediments with varying activity concentrations of 0.8-200 mBq/l and 0.5-40 Bq/kg (d.m.) respectively (Souti, 2015),(Fischer et al.,2009), in both down and upstream directions. This wide range of concentrations is caused not only by the varying WWTP outflow activity concentration but also due to the tidal effects.

The aforementioned ^{131}I routine releases allow the use of this radionuclide as a readily available tracer for complex hydrological processes with the aim of obtaining a better understanding by simulating its distribution in the water-sediment system. However the majority of existing radionuclide distribution and transport models in rivers are applicable in short duration releases and/or in distances with uniform distribution of the contaminant over the river section downstream a source, unsuitable to our case. This spured the need for developing and assessing a model for predicting the dispersion of ^{131}I in Weser River applicable also eg. in emergency situations.

Materials and Methods

The mathematical model consists of 2 major coupled sub-models: the hydrodynamic and the radionuclide transport, which is subdivided for the components of river water and bank sediments. Due to the complexity of the partial differential equations (PDEs) the solution for the hydrodynamic and radionuclide transport in river water is approached with the numerical method of the finite elements, implemented in Matlab with the aid of the IFISS software package (Silvester et al.,2015).

Tidal related parameters are calculated by fitting measured data from the nearby Oslebshausen station, acquired from the Waterway and Shipping administration of the federal government (WSV), using the HAMELS method (Harmonic Analysis, Method of Least Squares) with the aid of the Tidal fitting toolbox (Grinsted, 2008). Maximum current speed and water level are calculated for standing waves, taking into consideration a mean river depth of 10 m.

In advance of the numerical calculations of the river flow velocity and activity concentration in river water and sediments it is of importance to define the domain by a grid which provides information (specifically, node point coordinates and element connectivity information) as an approximation of the actual region, as seen in figures 1 and 2. The grid is a sum of 10 rectangles with length between 125 m to 2.5 km and width of 250 m to 1 km. In the longitudinal direction (min 0, max 7.5km) the resolution is 65.5 m and in the lateral (min 0, max 1 km) 31.25 m. At coordinate x=0 km, the inflow boundary is located and at x=7.5 km the outflow. On the outflow, Neumann boundary conditions are applied, while for the inflow, banks and remaining boundaries Dirichlet boundary conditions are set. The domain is approximated by biquadratic finite elements with 9 nodes per element. In total the grid consists of 7000 (2x2 macro) elements with more than 28.000 nodes.

Figure 1. *Weser River in the vicinity of the WWTP. (Google maps)*
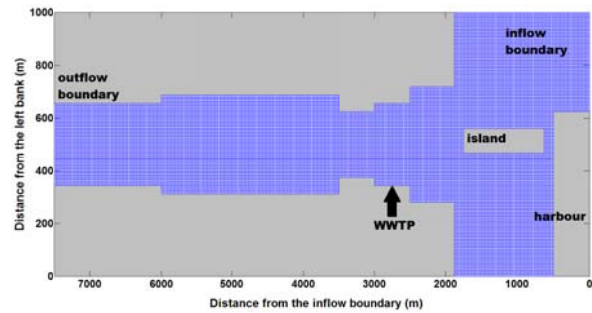
Figure 2. *Weser domain discretization.*

Hydrodynamic sub-model

The steady state Navier-Stokes equation system is the basis for the calculation of the flow of an incompressible fluid. Its solution is a flow velocity field, defined at every point in a region of space.

$$-v\nabla^2\vec{u} + \vec{u}\cdot\nabla\vec{u} + \nabla p = \vec{f} \qquad\qquad eq.1$$
$$\nabla\cdot\vec{u} = 0 \qquad\qquad eq.2$$

where v>0 the kinematic viscosity, $\vec{u}$ the flow velocity in the longitudinal and lateral directions, p the pressure and $\vec{f}$ a forcing term with Dirichlet conditions on boundary $\partial\Omega = \partial\Omega_D \cup \partial\Omega_N$

$$\vec{u} = \vec{w} \quad on\ \partial\Omega_D \qquad\qquad eq.3$$
$$v\frac{\partial\vec{u}}{\partial n} - \vec{n}p = \vec{0} \quad on\ \partial\Omega_N \qquad\qquad eq.4$$

where $\vec{n}$ denotes the outward-pointing normal to the boundary.

The Navier-Stokes are nonlinear partial differential equations and mixed approximation methods, namely Picard and Newton iterations, are used in order to reach a solution.

Radionuclide transport sub-model

The most important physical and chemical processes influencing the behaviour of radionuclides include adsorption, desorption, sedimentation of suspended particles, scour and resuspension from the active sediment layer, radioactive decay for the radionuclide and activity transfer between the pore water of the bed and overlying water. These processes can be expressed, as suggested by (Schnoor, 1996), as a system of 2 differential equations which describe the transport of activity in the river water and in sediments, by making the following assumptions: instantaneous equilibrium for the kinetics of transformation and sorption and steady state conditions for solids concentrations during the period of interest.

Convection-Diffusion in River water

The steady state convection-diffusion equation (eq. 5) describes the process of a pollutant, with C concentration, being transported along a stream moving with flow velocity $\vec{u}$, also subject to diffusive effects regulated by the diffusive parameter ε. For most practical problems the diffusion is less significant physical effect than convection (Elman et al., 2014).

$$-\varepsilon\nabla^2 C + \vec{u}\cdot\nabla C = f \qquad\qquad eq.5$$

with boundary conditions
$$C = g_D \quad on\ \partial\Omega_D \qquad\qquad eq.6$$
$$\frac{\partial C}{\partial n} = g_N \quad on\ \partial\Omega_N \qquad\qquad eq.7$$

The term *f* denotes "sources" or "sinks" for the quantity C, in our case it would include terms of radioactive decay, sedimentation, resuspension and pore-water diffusion, however since the time scales of these processes are much larger than the time period considered for the simulation, these terms are omitted.

Sedimentation sub-model

The activity concentration in the bank sediments (r[Bq/kg(d.m.)]) is calculated through an unsteady state one-dimensional equation (eq. 8) which includes first order processes of radioactive decay (λ radioactive decay constant), sedimentation (k_s sedimentation rate constant) and resuspension (α scour rate constant). Pore-water diffusion is based on the concentration difference between the pore water and the overlying water (k_L mass transfer coefficient between water column and pore water of bed sediment).

$$\frac{\partial r}{\partial t} = \left(-\lambda\frac{r}{1+k_{pb}S_b}\right) + \frac{k_s k_{pw} S_w \gamma}{\left(S_b+\frac{1}{k_{pb}}\right)}C + \left(-a\frac{S_b}{\left(S_b+\frac{1}{k_{pb}}\right)}r\right) + \left(\frac{-k_L}{\left(S_b+\frac{1}{k_{pb}}\right)d}\frac{r}{k_{pb}}\right) + \left(\frac{k_L}{\left(S_b+\frac{1}{k_{pb}}\right)}\frac{C}{(1+k_{pw}S_w)}\right) \quad eq.8$$

Additional parameters considered are the solid concentration in the water column/bed (S_w/S_b), partition coefficient in water/sediment (k_{pw}/k_{pb}), depth of active bed sediment (d) and its ratio to water depth (γ).

Results and Discussion

Hydrodynamic sub-model simulation results

For the simulation of the water flow in Weser River under steady state conditions, Poiseuille flow is imposed on the inflow boundary, a no-flow (zero velocity) is imposed on the walls and the natural outflow condition is satisfied. The kinematic viscosity, regulated by the Reynolds number is set to $1/100$ m^2/s. As suggested by (Elman et al.,2014), a hybrid method is selected with Picard and Newton iterations until the nonlinear convergence test with tolerance of 10^{-8} is satisfied.

The introduction of the tidal velocity factor based on the maximum speed of the current, allows us to calculate the longitudinal velocity in different tidal conditions and observe a simplistic approach of the inversion of the current. The results are illustrated in figures 3 and 4 for the longitudinal components of the flow velocity and the tidal factor, respectively.
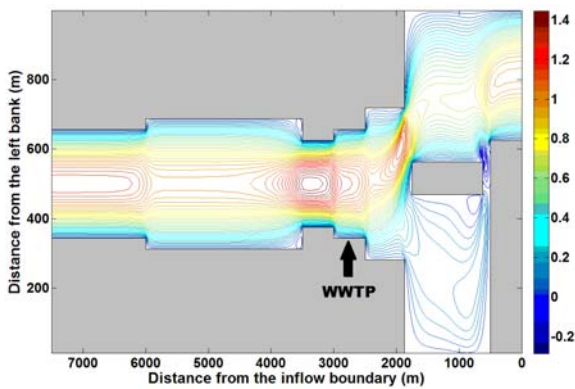
Figure 3. Longitudinal component of velocity. Negative values indicate flow in the upstream direction.
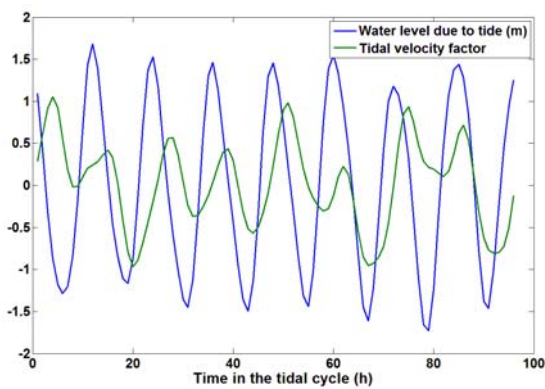
Figure 4. Water level and tidal velocity factor for a 4 day simulation period.

The tidal velocity factor led to fluctuations of maximum velocity values between 0 m/s (slack) to maximum values of 1.4 m/s (ebb and flood currents). As expected, maximum values of water flow are located in the central part of the river, while the flow diminishes to zero close to the banks. Current inversion is also present in locations south of the island with velocities reaching 0.2 m/s.

The results are consistent with measurements done in the area (Schuchardt et. al, 1993) and simulations (Stoschek&Matheja, 2001). However the lack of hydrological data during our study period hampers direct assessment of the simulated data.

Convection-Diffusion in River water sub-model simulation results

For the convection -diffusion model a diffusion coefficient of 0.015 m^2/s is selected (EPA, 2016), while the flow velocity is taken as an input from the hydrodynamic sub-model multiplied with the appropriate tidal velocity factor. The boundary conditions imposed are set to zero in the river banks and a maximum normalized value of 1 in the source location, i.e., the WWTP, with a lateral velocity of 0.006 m/s (Souti, 2012). In order to avoid node to node oscillations, the element Peclet number is calculated and for values greater than 1, the SUPG (Streamline-Upwinded Petrov-Galerkin) stabilization is applied (Elman et. al,2014). Simulation results of normalized (according to the original input concentration) [131]I activity concentrations in different times in the tidal cycle are presented in figure 5 and a comparison of experimental and simulated data for the periods of 3 to 4 hours after

high and low water for 5 locations across a river section in 7 distances up and downstream of the WWTP are shown in figure 6.
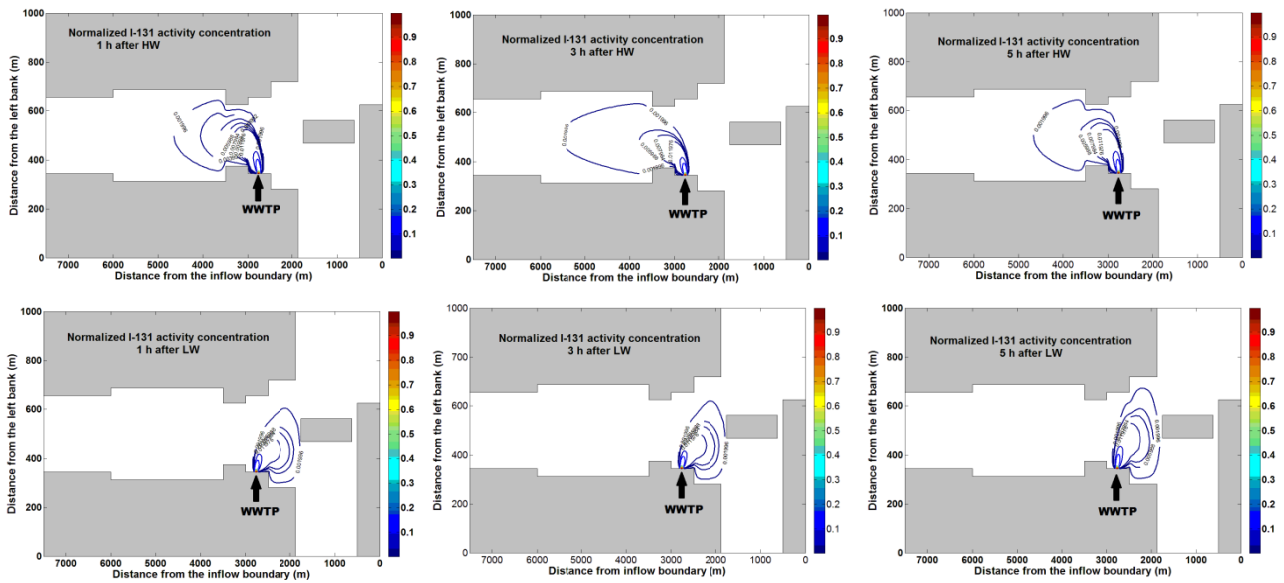
Figure 5: Simulated normalized ^{131}I activity concentration during different times in the tidal cycle.
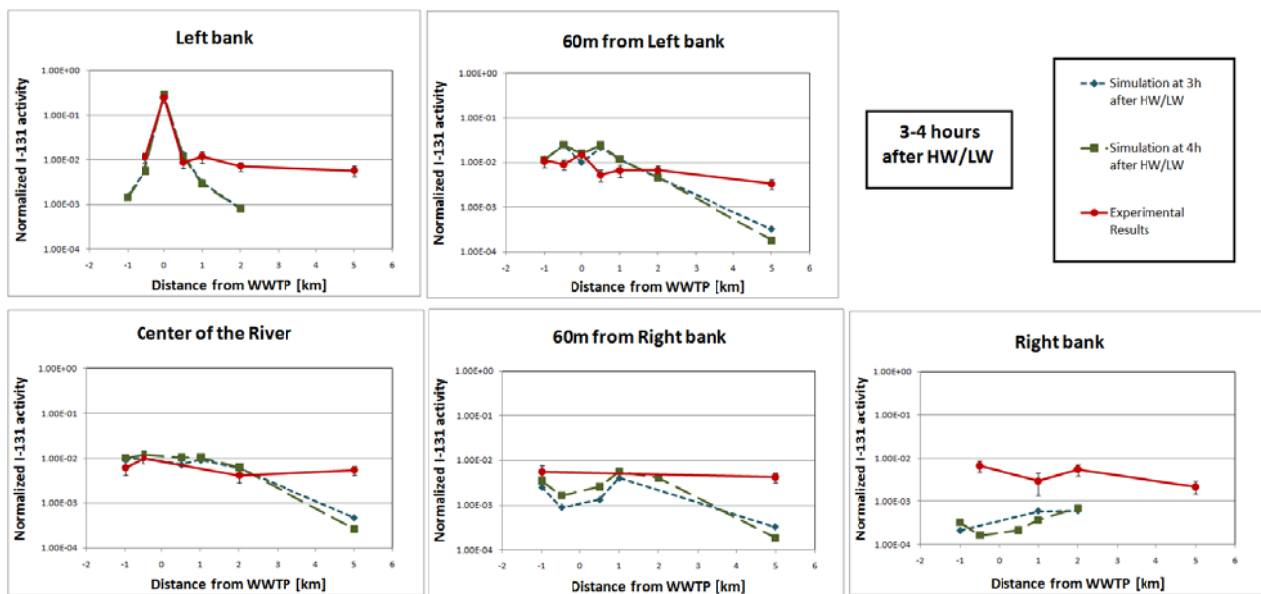
Figure 6: Comparison of simulated and measured ^{131}I activity concentrations 3 to 4 hours after high and low water in 5 locations across each river section located -1, -0.5, 0, 0.5, 1, 2 and 5 km from the WWTP.

Close to the WWTP outflow (left bank, -0.5 to 0.5 km distances) the experimental (Souti & Fischer, 2015) and simulated results are in complete agreement. The further away we get from the outflow, the larger are the discrepancies between simulated and measured data. There is a systematic underestimation of ^{131}I in distances larger than 2 km downstream of the WWTP and in the lateral direction, notably in the right bank.

These discrepancies could be attributed to several processes not taken into account in our simulations. Additional turbidity in the region, due to discharges from tributaries, breakwaters,

shipping, more complex geometry of the domain, differences in salinity and temperature, bottom shear and wind stress influence the mixing of the ^{131}I in the outflow plume (salinity: 0.2-0.4 ppt) and the river water (salinity: 0.5-0.7 ppt). These mixing processes force the outflow plume in deflecting towards the left bank, resulting in higher values 0.5 and 1 km downstream from the left bank than 60 m away from it, in contrast to our simulations in which the plume appears to be centrally located. An improper selection of the diffusion coefficient should not be excluded, which plays a crucial role in forming our results, especially since the program does not differentiate the coefficient value to longitudinal and lateral directions.

Another important factor not considered is the transport time of water parcels, which affected by the diurnal tide influence the activity concentration in both upstream and downstream direction. According to (Grabemann et. al, 1996) the retention time of a water parcel for the inner part of the estuary (app. 65 km length) can vary from 3 to 27 days depending on the river discharge. This forward/backward movement of the plume, creates a background value of ^{131}I activity concentration, present in locations as far as 5 km downstream and 1 km upstream from the source reaching also the other bank of the river (Souti, 2015),(Fischer et al.,2009).

Sediment sub-model simulation results

By contrast to the other PDEs, the unsteady state one dimensional equation describing the activity concentration in the bank sediments has an analytical solution. In addition, 2 particle sizes for the sediments are considered, as proposed by (Stoschek&Matheja, 2001), which produce different sedimentation velocities.

The simulation is run for a 24 day period (624 h), which corresponds to approximately 3 ^{131}I half lives, with the activity concentration in water as an input from the aforementioned sub-model in water, however due to discrepancies with experimental results, a varying background normalized concentration of 0.001-0.005 is taken into account for locations influenced by the reversing tidal current and for downstream locations with activity concentrations underestimated from the convection-diffusion in water sub-model.

The activity concentration of the source (outflow of the WWTP) is no longer normalized to one, rather selected in the range of 40-640mBq/l with the restrictions of value variance up to 30% for a 3 hour period and 60 % for a day (Hormann & Fischer,2016). For the time period 2 hours before or after low tide no sedimentation in the river banks is possible. The remaining parameter values are approximated similar to (Souti, 2012). The simulation results are illustrated along with the experimental values in the corresponding locations for varying conditions in the following figure.

The simulation results appear to describe relatively well our experimental data, with noticeable discrepancies in locations 0 km from the left bank and a systematic underestimation of the values in the downstream direction. The activity concentration of sediments in the outflow location is strongly influenced from the WWTP factor, creating more than 20% difference in the simulation results. Since there was no routine sampling of the outflow in the period before the sediment sampling campaign, the true activity concentration of the outflow is unknown and only approximations in the aforementioned range can be made, which can rise in both overestimated and underestimated values. The underestimated simulation results in the downstream direction, as a result of the low activity concentrations in the convection-diffusion in water sub-model, are improved by considering a background normalized activity of 0.005.
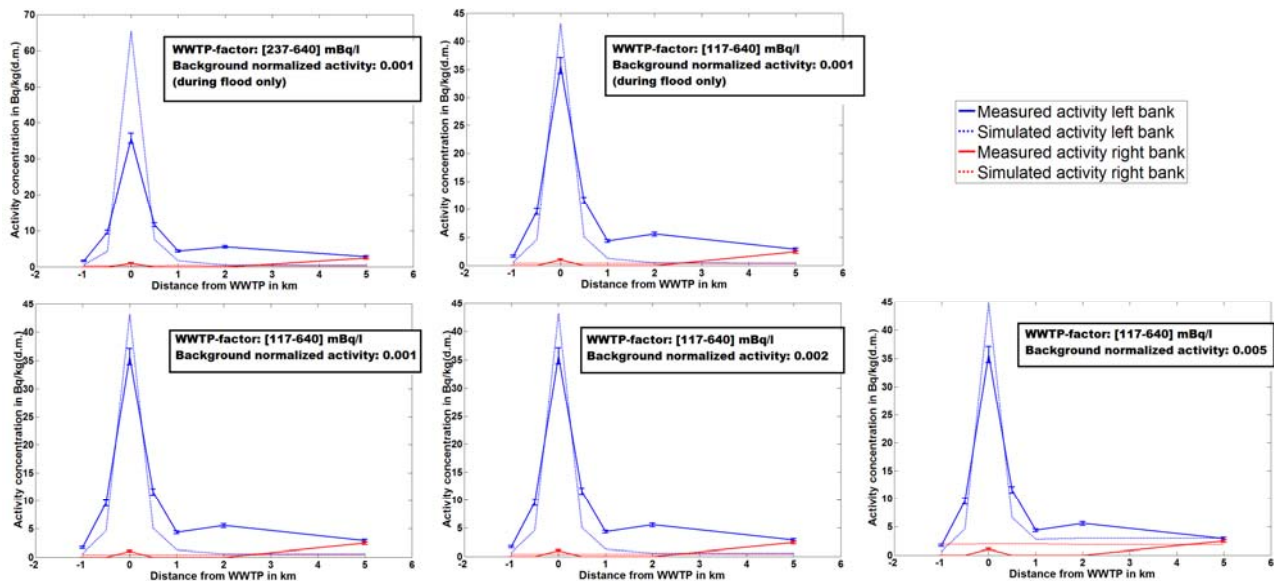
Figure 7: Sedimentation sub-model simulation results and comparison with experimental values under different parameter approximations.

The possibility of faulty parameter approximation and assumptions should not be excluded. As mentioned before, the water residence time can significantly vary depending on the discharge conditions and strong flood and ebb currents could make the assumption of slow kinetics of sorption compared to kinetics of transformation reactions or the time of transport (advection, dispersion, sedimentation, resuspension) no longer valid. Furthermore the assumption of a steady state condition during the simulation period for the solids concentrations may not hold, since the suspended particulate matter concentration is correlated with the river discharge, although with relatively low average concentration (Schuchardt et. al, 1993).

Moreover, the likelihood of additional processes able to influence, not considered, such as biological uptake of ^{131}I by aquatic biota, should not be eliminated.

Lastly, other sources of ^{131}I in the upstream direction could have an impact in our experimental values (Souti, 2015).

Conclusions

This paper presented a 3 compartment model which computes the ^{131}I behaviour in a tidal river for routine releases with hourly time steps. The complexity of the physical and chemical processes involved rule out completely simplistic approaches and analytical solutions for the problem. As a result a computational method (FEM- in the IFISS software) is utilized by making the appropriate adjustments for the domain, the tidal process (HAMELS method-tidal toolbox), for coupling the hydrodynamic and radionuclide in water and sediments submodels and for computing the ^{131}I activity concentration in bank sediments.

Despite the simplifications considered, the comparison between simulated and experimental data indicates the model capability of predicting the dispersion of medically derived iodine, originating from the WWTP, in the water body and banks of Weser River, possibly also in emergency situations.

References

Elman H., Silvester D., WathenA., 2014.Finite Elements and Fast Iterative Solvers with Applications in Incompressible Fluid Dynamics. Oxford Science Publications, Oxford.

EPA Watershed & Water Quality Modeling Support Center ,2016. Dispersion and Exchanges (PowerPoint slides).Retrieved from https://www.epa.gov/exposure-assessment-models/wasp7-course.

Fischer H.W., Ulbrich S., Pittauerova D., Hettwig B., 2009. Medical radioisotopes in the environment – following the pathway from patient to river sediment. J. Environ. Radioact. 200,1079-1085

Grabemann I., Kuehle H., Kunze B., Mueller A., 1996. Studies on Transport Times and Water Quality in the Weser Estuary (Germany). Coast. Estuar. Stud. 50, 291-301.

Grinsted A., 2008. Tidal fitting toolbox (MATLAB files). Available from https://de.mathworks.com/matlabcentral/fileexchange/19099-tidal-fitting-toolbox?requestedDomain=www.mathworks.com

Hormann V., Fischer H.W., 2016. Adynamic model for the transport of I-131 through a municipal wastewater treatment plant. Paper presented at the 2nd International Conference on Radioecological Concentration Processes. Seville, Spain.

Schnoor J., 1996. Environmental Modeling: Fate and transport of Pollutants in Water, Air and Soil. John Wiley and Sons. New York.

Schuchardt B., Haesloop U., Schirmer M., 1993.The Tidal Freshwater Reach of the Weser Estuary: Riverine or Estuarine? Neth. j. aquat. Ecol., 27,215-226.

Silvester D., Elman H., Ramage A., 2016. Incompressible Flow & Iterative Solver Software. Available from http://www.maths.manchester.ac.uk/~djs/ifiss/

Souti M., 2012. Medical ^{131}I in Weser water. (Master's thesis, University of Bremen, Bremen,Germany). Retrieved from http://www.pep.uni-bremen.de/research/masterthesis/index.html

Souti M. & Fischer H., 2015.Medical 131I in River Water and Sediments: Case Study of Weser River in NW Germany. Poster session presented at Envira 2015 International Conference on Environmental Radioactivity, Thessaloniki, GR.

Stoschek O. &Matehja A.,2001. Simulation von Sedimenttransportprozessen in tidebeeinflussten Hafengebieten. Mitteilungen des Franzius-Institut fuer Wasserbau und Kuesteningenieurwesen der Universitaet Hannover,Heft 86 (in German).

Wu W., 2008. Computational River Dynamics. Taylor&Francis Group.London.

Comprehensive and systematic knowledge quality assessment as a tool for model qualification

A. T. K. Ikonen[*] and V. Kangasniemi

EnviroCase Ltd., Hallituskatu 1 D 4, 28100 Pori, Finland

Abstract

In many applications, especially in safety cases for nuclear facilities, objective evidence-based confirmation that models and data are fit for the purpose is warranted. In addition to the numerical uncertainty and sensitivity analyses, various other approaches have been used for example in nuclear waste disposal, pharmacology and environmental management to evaluate also aspects that are not directly quantifiable. Such examples include protocol-based approaches and assessment of the knowledge base of model formulation and input data ('pedigree analysis'). The models and data also need to be understandable and credible as well as transparently described in a sufficient degree. To sufficiently cover all relevant aspects of such qualification, this paper presents examples of readily available approaches, recognising that the extent they would be useful to be employed varies case by case. These examples provide an effective means to demonstrate that a sufficient confidence in the outcome of the modelling and in its quality has been reached. The same methods can be useful also in model development and data selection in a wide range of applications, as well as for determining the appropriate level of detail in the modelling or for systematic and wide comparison of implementation or management options in various types of projects.

Introduction

Objective, evidence-based confirmation that models and data meet the requirements (verification) and are fit for the purpose (validation) is warranted in many applications, especially in licensing assessments for nuclear facilities (e.g., IAEA, 2009, 2012), alongside of identifying, addressing, bounding and reducing uncertainties being in general a major part of safety assessments (e.g., IAEA, 2011, 2012). Also, the uncertainties, approximations made in the models, and shortcomings in the models and in the underlying basis of data, and how these are to be taken into account in the safety analysis, all should be identified and specified (IAEA, 2009). Regarding radioecological modelling in general, such direct requirements and recommendations seem to be lacking, but also in some applications similar comprehensiveness should be strived for, a need indicated by approaches employing such components becoming more and more frequent for example in assessing environmental hazards and criteria (e.g., Cooper et al., 2016; Bardos et al., 2016; Queirós et al., 2016). However, as exemplified further below, these approaches employ tools beyond traditional, rather technical, verification and validation procedures in order to systematically grasp qualifications that are not directly quantifiable.

Verification, in principle, is rather straightforward and close to quality control and assurance procedures. It can be understood as solving test problems designed to show that the mathematical model solves accurately the equations that constitute the model (IAEA, 2011), or more broadly, studying whether the computational model correctly implements the intended conceptual or mathematical model (IAEA, 2009).This may include also the provision of similarly objective evidence that the valid input data and other settings have been correctly input to the model, and also

---

[*]Corresponding author, E-mail: ari.ikonen@envirocase.fi

that the model and the data meet the regulatory and possible other requirements. Calibration of the model with site data (IAEA, 2011) seems to lie somewhat between the verification and validation.

Validation, however, is usually a broader topic (sometimes also called 'model qualification'; e.g., Friedlich, 2016), although the boundary between verification and validation is somewhat movable within different sets of definitions.In contrast to calibration, which is a more site-specific model adjustment process, validation has more to do with producing credible results under a wide range of conditions (IAEA, 2011), or, specifically determining whether a mathematical model is an adequate representation of the real system being modelled (IAEA, 2009). This, of course, cannot always be completely done – for example, for models addressing very long time frames in the context of geological disposal of radioactive waste (IAEA, 2011) as, basically, the validation is the assessment of the accuracy of values predicted by the system code against relevant experimental data for the important phenomena expected to occur (IAEA, 2009), and for very long time frames into the future such experimental data cannot be obtained, not at least directly. Thus, other evidence of fitness for the purpose is needed for building of a sufficiently convincing case, but this often leads into less straightforward approach and adds challenge in keeping the entirety of the arguments consistent and logically as intact as possible.

This paper aims at presenting an approach to systematically and comprehensively assess the quality of the knowledge underpinning the models and data in order to support arguments for their validity, or 'fitness for the purpose'. It is to be noted, though, that the approach and the tools can well be utilised also in more straightforward cases as well. The various components have earlier been applied in the areas of, for example, nuclear waste disposal (e.g., SKB, 2004; Ikonen, 2006; Smith et al., 2010; Posiva, 2014), contaminated land management (e.g., Bardos et al., 2016), environmental policy (e.g., Petersen et al., 2013; Queirós et al. 2016), and pharmacology (e.g., Friedrich, 2016) – as well as in the multipurpose NUSAP methodology (www.nusap.net; e.g., van der Sluijs et al., 2005), parts of which many of these other approaches have successfully adopted.

Materials and Methods

This contribution is based on the literature referred to in the text.

Results and Discussion

Aside of the direct technical aspects of validation (and verification), the issues inqualification of models and data revolve around relevance, uncertainty, variability, and reliability of the data (Friedrich, 2016) and the meaning of the uncertainties and the robustness of the outcome to identify the main uncertainties and their sources and implications, and to consider what could be done to reduce the uncertainties (Petersen et al., 2013). In broader approaches, attention is paid also on how to frame the problem studied in general and who should be involved and to which degree – but regardless – also on whether the knowledge base is sufficiently large and how to communicate the reliability in a credible and convincing manner (e.g., Bardos et al., 2016; Petersen et al., 2013). Further, the knowledge base is often characterised in terms of quality criteria found or considered relevant, existence of any controversies or major deficiencies or limitations, and how these controversies, deficiencies and limitations could affect the decision making and how the situation could be improved (e.g., Petersen et al., 2013). Interestingly, the importance of the knowledge base is reflected also in standard reporting requirements aiming at conciseness of presentation for the various audiences, as they gradually elaborate from the basic knowledge to process knowledge, input data, mathematical implementation and evaluation of the model (NSAI, 2015).

Purpose, context and evaluation criteria

For a clear assessment of the validity, the purpose and scope, goals, indicators and outcomes (both qualitative and quantitative),and constraints in the process should be made clear (Bardos et al., 2016), and it should be evaluated whether the model scope is relevant for the research context (Friedrich, 2016). It has also been found useful to set the assessment protocols and evaluation criteria beforehand, the more so the wider is the audience and number of stakeholders involved; when stakeholders are to be involved, it also should preferably be planned (e.g., Bardos et al. 2016; Petersen et al. 2013). In the planning of the assessment process, it should be taken into account that whilst a graded approach (e.g., Bardos et al., 2016; IAEA, 2012) with iteration is often warranted, there should be also an adequate amount of exit points allowing the necessary decisions be made. For example, a pre-defined graded approach can take into account the urgency of decision-making in what kind of methods need and can be employed (e.g., Thayer &Schünemann, 2016).

Overall protocols developed for the context of geological disposal of radioactive waste include those presented by Posiva (2005) and Ikonen (2006) that are largely based on an earlier assessment (SKB, 2004), latter also adopting elements of the extensive NUSAP methodology (e.g., van der Sluijs et al., 2005) that has seemingly been a basis for Petersen et al. (2013) and associated further guidance. These have been further adjusted and used for a specific contexts, for example by Posiva (2014). On the side of the overall protocols, there are also tool catalogues available to further feed in with approaches to address specific issues (see, e.g., Petersen et al., 2013, and references therein).

Model formulation and implementation

First establishing a conceptual model that reasonably represents the behaviour of the system modelled and then translating it into an adequately matching mathematical model implemented in a computer code is an approach adopted, for example, in the IAEA guidance (IAEA, 2012). The conceptual model should provide a consistent description of the components of the system and the interactions between these components, including the chemical, physical, hydrogeological, biological and mechanical behaviour (IAEA, 2012).

As mentioned above, there are standards for describing the models (e.g., NSAI, 2015) that are applicable to radioecological and radionuclide transport models as well. To demonstrate compliance with regulatory assessments, at least in the case of geological disposal of radioactive waste, the descriptions should include a thorough discussion of the conceptual model and the physical basis for the model (IAEA, 2011). There is also a need to demonstrate sufficient comprehensiveness of, for example, interactions, transport processes and exposure pathways, so that there are no contributions to the radiation risk that have not been taken into account (e.g., IAEA, 2009). More generally, it should be reasoned out that the model captures the relevant known pathway variabilities (Friedrich, 2016, fig. 2) and the relevant (biological) mechanisms (Friedrich, 2016). Also the basis for scenarios and pathways is to be documented (IAEA, 2011), for which often a bottom-up or top-down analysis of features, events and processes (FEPs) is employed (e.g., IAEA, 2003, 2012). For demonstrating the comprehensiveness in terms of the FEPs, interaction matrices have been found useful (e.g., IAEA, 2003). There is guidance also on systematic exposure pathway analyses readily available (e.g., ATSDR, 2005).

In addition to the abovementioned approaches, multi-criteria scoring of the strength of the process understanding/parameterisation can be applied to highlight the weaker and stronger areas of the representation of process understanding. Such 'pedigree analysis' is optimally performed by a group of experts individually judging a set of criteria such as the degree of theoretical understanding,

empirical evidence, degree of using proxy representation (i.e., exactness of parameterisation), robustness against temporal changes and changes in external conditions, and the degree of collegial consensus. For example, the degree of the parameterisation can be scored on a scale ranging from crude simplifications to an exact description of the actual process in great mechanistic detail, and that of the theoretical understanding can scale, for example, from crude speculation to a well-established theory. (Ikonen, 2006; based on the NUSAP method, e.g., van der Sluijs et al., 2005). Similar approaches have been employed also, for evaluating environmental indicators proposed for the implementation of the EU Marine Strategy Framework Directive (Queirós et al., 2016).

A comprehensive and systematic quality evaluation of the modelling of the FEPs is helpful also for confirmation that the important features of the conceptual model have been translated into the mathematical model with an appropriate level of detail. A good system understanding is needed for a satisfactory simplification unavoidable in the models (IAEA, 2011) and demonstrating this is important also since the level of detail and the balance between realism and conservativeness in the modelling needs to be shown fit for purpose, given the assessment context and the level of existing knowledge (IAEA, 2012). In many applications rather elaborate models are justified, but there should also be efforts made to supplement the sophisticated modelling approach with a less complex model for explanatory purposes (IAEA, 2011). Satisfactory simplification also requires (and thus demonstrates) a good system understanding (IAEA, 2011).For this discussion, a protocol has been outlined (Ikonen, 2006) to consider evaluating at which level the conservativeness is, which are the rationales and evidence for the need and implementation, whether alternative approaches and interpretations could be employed, and whether the effect of the conservative choices on the outcome has been quantified or evaluated.

Main modelling assumptions

In addition to describing the conceptual and mathematical models and evaluating their strength as such, a discussion of alternative models and the reasons for disregarding such models, as well as a documentation of the assumptions and justifications of simplifications used, is needed (IAEA, 2011; IAEA, 2012). This can also help, through iteration, addressing the degree of conservativeness.

Protocols for addressing main uncertainties in models and potential for alternative interpretations or models have been developed, for example, by SKB (2004), Posiva (2005) and Ikonen (2006). In addition, a scheme for categorisation of the main assumption has been presented by Nagra (2002) and further adopted and applied by, for example, Ikonen (2006) and Posiva (2014). These classifications identify, among a few other types, conceptual assumptions corresponding to the likely or expected characteristics and evolution of the system, pessimistic conceptual assumptions within a reasonably expected range of possibilities, assumptions within the range of possibilities but with likelihood not possible to directly evaluate, and stylised conceptualisations of the system characteristics and evolution. Also for the assumptions, pedigree evaluation can be utilised (van der Sluijs et al., 2005). The quality criteria can then consider, for example, plausibility, inter-subjectivity (how commonly the same assumption would be made among peers and other stakeholders), choice space (possibilities for alternative assumptions), influence of situational resource limitations, sensitivity to view and interests of the analyst, and the potential to influence the results.

Data sources and main uncertainties

For the radioactive waste disposal, there are requirements that the actual data used, together with their source and justifications need to be documented, both for the choice of the deterministic ('best estimate') values and the probability distributions of the parameter values (IAEA, 2011, 2012), and

this is useful also in other purposes for gaining sufficient confidence. Appropriate and unbiased use of all relevant data is important also, for example, in terms of systematic reviews used for health risk assessments, where being aware of the various aspects of the data quality is important especially when bridging between laboratory experiments and real-world applications (e.g., Cooper et al., 2016). Also for addressing whether all data have been appropriately considered and understood, protocols have been developed (SKB, 2004; Posiva, 2005; Ikonen, 2006; Posiva, 2014). These include description of the data that have been used (also where and how, including possible pre- and post-processing), available data that have not been used and the rationales for their omission (e.g., not relevant to the context, poor quality, lack of time, etc.), potential impact if the unused data were used, means to establish the data accuracy (e.g., quality assurance procedures), and consideration of whether bias in the outcome would be introduced as a consequence using or not using the data. Of course, it needs to be acknowledged that not all unused datasets can be identified, but these considerations prompt improving the definitions of not only data selection but also data exclusion criteria.

A related item in a comprehensive evaluation process of the knowledge base is to address also such uncertainties in the input and result data that cannot readily be quantified, in addition to the quantified uncertainty and sensitivity analyses (see below). The different aspects that should be considered also qualitatively include (e.g., IAEA, 2012; Petersen et al., 2013; van der Sluijs et al., 2005) the contextual uncertainties (e.g., those related to the identification of the system boundaries and definition of the endpoints), scenario uncertainties, model uncertainties (e.g., model structure, process understanding, parameterisation, and numerical implementation),and data uncertainties of the deterministic values, distributions and correlations). It is also useful to identify whether the nature of the uncertainties is aleatoric or epistemic (e.g., IAEA, 2009, 2012) — that is, whether they are related to the statistical variability in the parameter values describing the system (in principle irreducible uncertainties, once studied well enough) or are rather a consequence of incomplete knowledge (at least in principle reducible through further research) — even though this is not always a straightforwardselection.

The scenario uncertainties refer to the uncertainty in the future states of the system that are usually dealt with assessing a range of systematically derived scenarios. The modelling uncertainties arise from the unavoidably imperfect knowledge of the processes, which first least to an imperfect conceptual model and then arise from the necessary simplifications in the mathematical and imprecision in the numerical implementation of the model. Such uncertainties are often dealt with performing comparisons across alternative models and between model predictions and empirical observations. Data uncertainties refer to the uncertainty in the values of the parameter values or the distributions of values used in the modelling, and they are often addressed with numerical uncertainty analysis (see below). (IAEA, 2012).

In addition to the methods mentioned above, protocols developed for verbal description of the uncertainties consider, for example identification of the main uncertainties in the input data and produced in the modelling process, determination of their cause (e.g., data inaccuracy, information density, uncertainty in other model or process understanding), quantification of the uncertainty (if possible), potential for alternative interpretations and whether alternatives have been developed (where and how), effect on the outcome, and possible means to reduce the uncertainty (SKB, 2004; Posiva, 2005; Ikonen, 2006; Posiva, 2014). However, this needs to be done iteratively with the other parts of the knowledge quality assessment and assessment rounds to find the main ones, since an exhaustive listing of all uncertainties is "virtually impossible" (Posiva, 2014).

Quality criteria considered in pedigree analyses applied for the model input data (van der Sluijs et al., 2005; Ikonen, 2006; Posiva, 2014; Queirós et al., 2016) include empirical, statistical and methodological rigour, relationship of the data to the parameterisation of the model, possibilities and results of comparison with independent datasets, appropriateness to the site, and spatial variability of the parameter values and their robustness against time scales and external conditions. It is to be noted also that the pedigree scoring could be used also to guide the data selection (e.g., van der Sluijs et al., 2005).

Evaluation of consistency

If several specific models are needed to represent the system components, processes or scenarios, their integration process with the necessary simplifications need to be properly justified and managed (e.g., IAEA, 2012). Also the consistency of the results of different levels of model complexity should be demonstrated, especially in respect of that the simplification has actually focused the assessment on the critical factors relating to the system safety (IAEA, 2011). When evaluating the consistency conceptual and methodological differences, differences in the mathematical model, results and endpoint quantities, and significance of the differences in the context should be considered (Ikonen, 2006; Posiva, 2014).In protocols for systematically evaluating the consistency the following items can be included (SKB, 2004; Posiva, 2005; Ikonen, 2006; IAEA, 2011; Friedrich, 2016), all including also rationales and evaluation of the significance of the findings:

- interaction and consistency between different modelling stages – which aspects are necessary, which have been implemented and how, and which have not been, why, and what is the impact of the omission;
- consistency with understanding of past evolution of the system;
- consistency with observations on analogous systems ('natural analogues');
- consistency with previous model versions;
- consistency with other similar models (model–model comparisons, benchmarking); and
- consistency with independent test data (model–data comparisons, i.e., conventional model validation).

Quantification of the meaning of assumptions and uncertainties

It is rather common to evaluate the performance of the model with numerical uncertainty and sensitivity analyses, quantifying the uncertainty in the outcome resulting from a given uncertainty in the inputs and the relative importance of the parameters to the outcome, respectively. Results of both the types of analyses are conditional to the given variability of the inputs, though, and the correlations between the parameters should be duly considered (e.g., IAEA, 2012). Uncertainty analysis can also be used to demonstrate that a relevant outcome variability is reproduced (Friedlich, 2016). Qualitative analyses should also be employed, though (e.g., IAEA, 2009). A full suite of related ways to analyse how the model responds to the uncertainties, and to quantify the uncertainties at least to an extent, includes also deterministic analyses (e.g., scenario analysis), bounding calculations and use and comparison of alternative models (see also the discussion above on evaluating the consistency aspects).

Establishing an overall view

An overall synthesis is important for the credibility and communication of the results and the uncertainties. It should be also identified where and how reduction of safety-relevant uncertainties is possible and to characterise the residual uncertainties (IAEA, 2001).For this, plotting the strength

indicator of the pedigree analysis against the sensitivity of the model to the parameter has been found a useful tool (e.g., van der Sluijs et al., 2005; Smith et al., 2010). A more elaborate approach that can more easily utilise also qualitatively aspects and verbal descriptions is to compile an 'uncertainty matrix' (e.g., Petersen et al., 2013) where the uncertainties in the various components of the assessment (e.g., uncertainties in the assumptions of the system boundaries, scenarios, model structure, data and outputs) are mapped, for example, against their seriousness (level of uncertainty), nature (aleatoric, epistemic) and backing by the knowledge base (strength of the knowledge).

On the basis of the outcome of the overall evaluation, it should be considered whether and in which part iteration is needed, or whether "assessment is judged to be adequate for its purpose" (IAEA, 2012). In some cases, depending for example on the maturity of the radioactive waste disposal programme, open issues may remain, but plans for addressing the unresolved issues should be presented to enhance the confidence.Regardless of the development stage of the assessment, any lessons learned in applying the models and interpreting results should be used to revisit assumptions and decisions made in the course of model development where deemed necessary. (IAEA, 2012).

Conclusions

The knowledge quality assessment toolbox presented in this contribution provides an effective means to demonstrate that a sufficient confidence in the outcome of the modelling and in its quality has been reached. Whilst the sound scientific basis of the evidence, the justification and rationales behind key assumptions, and the assumptions and uncertainties impacting most on the outcome should be clearly, traceably and transparently described (IAEA, 2011, 2012), it should be recognised also that "a complex hierarchy of documents and lack of attention to brevity can cause increasing problems" (IAEA, 2011). Thus, the aim should be to produce as solid evidence of the reliability of the modelling as possible.

It is recognised that the ensemble of approaches considered in this paper represent a developing field in assessment methodologies, reflected by the increasing number of applications and other considerations that have recently been published. Thus, this contribution is not intended to be an exhaustive account, but to demonstrate the possibilities of the frameworks and methodologies available. The methods that are applied need anyway to be tailored, especially the pedigree and uncertainty matrices (e.g., van der Sluijs et al., 2005).For example, it should be evaluated whether the verbal descriptions used for scoring schemes can be used constructively or whether the tendency of them being interpreted differently by individual persons would rather complicate reaching a solid overall picture. This highlights the importance of setting the scope and methodology already in the beginning, especially if a number of stakeholders are to be engaged.

References

ATSDR, 2005. Public Health Assessment Guidance Manual (Update), January 2005. Agency for Toxic Substances and Disease Registry, U.S. Department of Health and Human Services, Atlanta.

Bardos, R.P., Bone, B.D., Boyle, R., Evans, F., Harries, N.D., Howard, T., Smith, J.W.N., 2016. The rationale for simple approaches for sustainability assessment and management in contaminated land practice. Sci. Total Environ. 563–564, 755–768.

Cooper, G.S., Lunn, R.M., Ågerstrand, M., Glenn, B.S., Kraft, A.D., Luke, A.M., Ratcliffe, J.M., 2016. Study sensitivity: Evaluating the ability to detect effects in systematic reviews of chemical exposures. Environ. Int. 92–93, 605–610.

Friedrich, C.M., 2016. A model qualification method for mechanistic physiological QSP models to support model-informed drug development. CPT Pharmacometrics Syst. Pharmacol. 5, 43–53.

IAEA 2003. "Reference Biospheres" for Solid Radioactive Waste Disposal. IAEA-BIOMASS-6. International Atomic Energy Agency, Vienna.

IAEA, 2009. Safety Assessments for Facilities and Activities. General Safety Requirements Part 4, No. GSR Part 4. International Atomic Energy Agency, Vienna.

IAEA, 2011. Geological Disposal Facilities for Radioactive Waste. Specific Safety Guide No. SSG-14. International Atomic Energy Agency, Vienna.

IAEA, 2012. The Safety Case and Safety Assessment for the Disposal of Radioactive Waste. Specific Safety Guide No. SSG-23. International Atomic Energy Agency, Vienna.

Ikonen, A.T.K., 2006. Posiva Biosphere Assessment: Revised Structure and Status 2006. POSIVA 2006-07. Posiva Oy, Olkiluoto, Finland.

Nagra, 2002. Project Opalinus Clay: Models, Codes and Data for Safety Assessment. NTB-02-06. Nagra, Wettingen, Switzerland.

NSAI, 2015. Standard Documentation of Chemical Exposure Models. S. R. CWA 16938:2015. The National Standards Authority of Ireland.

Petersen, A.C., Janssen, P.H.M., van der Sluijs, J.P., Risbey, J.S., Ravetz, J.R., Wardekker, J.A., Martinson Hughes, H., 2013. Guidance for Uncertainty Assessment and Communication. 2nd edition. PBL Netherlands Environmental Assessment Agency, The Hague.

Posiva, 2005. Olkiluoto Site Description 2004. POSIVA 2005-03. Posiva Oy, Olkiluoto, Finland.

Posiva, 2014. Safety Case for the Disposal of Spent Nuclear Fuel at Olkiluoto: Data Basis for the Biosphere Assessment BSA-2012. POSIVA 2012-28. Posiva Oy, Eurajoki, Finland.

Queirós, A.M., Strong, J.A., Mazik, K., Carstensen, J., Bruun, J., Somerfield, P.J., Bruhn, A., Ciavatta, S., Flo, E., Bizsel, N., Özaydinli, M., Chuševė, R., Muxika, I., Nygård, H., Papadopoulou, N., Pantazi, M., Krause-Jensen, D., 2016. An objective framework to test the quality of candidate indicators of good environmental status. Front. Mar. Sci. 3, 73.

SKB, 2004. Preliminary Site Description of the Forsmark Area (Version 1.1). R-04-15. Swedish Nuclear Fuel and Waste Management Co., Stockholm.

Smith, K., Robinson, C., Jackson, D., De La Cruz, I., Zinger, I., Avila, R., 2010. Non-Human Biota Dose Assessment: Sensitivity Analysis and Knowledge Quality Assessment. Working Report 2010-69. Posiva Oy, Eurajoki, Finland.

Thayer, K.A., Schünemann, H.J., 2016. Using GRADE to respond health questions with different levels of urgency. Environ. Int. 92–93, 585–589.

van der Sluijs, J.P., Craye, M., Funtowicz, S., Kloprogge, P., Ravetz, J., Risbey, J., 2005. Combining quantitative and qualitative measures of uncertainty in model-based environmental assessment: The NUSAP system. Risk Anal. 25(2), 481–492.

Acknowledgement

Developing operational models to trace marine radioactive contamination of lower- and mid-trophic level organisms

Inna Senina*, Patrick Lehodey, Anna Conchon

Collecte Localisation Satellites, Toulouse, France,
31520Ramonville-St-Agne, France

Abstract

We present a modeling approach that allows tracing the propagation of radioactive elements through the oceanic food web. The SEAPODYM modelling framework includes a representation of the dynamics of functional groups of zooplankton and pelagic micronekton, which comprise the species of the lower- and mid-trophic levels respectively. The model computed the production of these groups starting from the primary production and describing the development linked to the temperature and the spatial transport by oceanic currents. Then, the biomass of these groups was predicted taking into account diel vertical migration and natural mortality linked to the time of development. Coupling this model with Thomann's radioecological equation provides a tool to quantify the contamination by radionuclides of the lower- and mid-trophic levels. Outputs of these coupled models can be used to compute indicators of contaminated habitat of top predators such as tunas. Realistic physics is necessary to force SEAPODYM model, which is highly sensitive to ocean currents input. The preliminary results of modeling transfer of ^{137}Cs were validated qualitatively using published data collected after Fukushima accident. An operational version of SEAPODYM model is currently developed to provide realtime and forecast outputs. This operational model configuration coupled with radioecological models can be used in the post-accident scenario to quickly produce contamination maps for zooplankton and micronekton communities and to provide the indicators of risk of contamination for top predator species.

Introduction

Following the accident at Fukushima nuclear power plant in March 2011, multiple radioactive elements, mainly radioactive isotopes of iodine 131, 132, 133, Caesium 134, 137 and Tellurium 129, 132, were released into the ocean and in the atmosphere. The impact of these accidental releases on the marine food web is difficult to monitor, especially at basin-scale. Contamination can potentially cascade through the pelagic food web until large and migrating fish. For instance, weak concentration of ^{137}Cs originated from Fukushima was found in Pacific bluefin tuna captured off California in August 2011 (Madigan et al. 2012). For food security reason, costly monitoring needed to be deployed for the control of wild fish caught in the vicinity but also at some distances of the contamination source. Therefore, realistic operational real-time modeling of the dynamics of the propagation of radioactive elements and their accumulation in the oceanic food web would be extremely useful for the understanding and monitoring of contamination.

To achieve such an objective, we use the Spatial Ecosystem and Population Dynamics Model (SEAPODYM) Eulerian framework that simulates the dynamics of oceanic ecosystem with functional groups at low and mid-trophic levels (Lehodey et al 2010; 2015), and more detailed population dynamics for valuable exploited species (Lehodey et al. 2008; Senina et al. 2008; 2016), most often at higher trophic levels. Physical (ocean temperature and currents) and biogeochemical (primary production, euphotic depth, dissolved oxygen concentration) environmental variables are provided independently. The mid-trophic level (MTL) includes six functional groups of epipelagic,

and upper and lower mesopelagic micronekton, which are prey fields of tuna and other large pelagic predators. These functional groups are characterized by their vertical migration behaviour, that is, with or without occurrence of diel migration between three vertical layers defined between surface and ~1000m. Dynamics of the functional groups relies on an energy transfer from the primary (phytoplankton) production modulated by a temperature-linked time of development and mortality coefficient. The model has a few parameters, which facilitates coupling and parameterization of a coupled radio-ecological model.

Bio-acoustic data, especially at 38 kHz are used to optimize and validate the parameterization of the model (Senina et al 2008; Lehodey et al. 2015). Fishing and tagging data are used for the exploited (tuna) species (Senina et al 2016). But to evaluate the radio-ecological model outputs, there is a need to collect more field data allowing to construct, validate and improve the modelling tool.

Materials and Methods

SEAPODYM model requires physical and biogeochemical variables in order to describe the dynamics of modelled species. For the radio-ecological model application, the primary source of the radionuclide in marine biota is also needed. It is provided byhydrodynamic dispersion modelling of sea water contamination by ^{137}Cs (e.g. see Rossi et al., 2013). Finally, data from published studies used to parameterize and validate the model are described below.

Model Input

An operational global ¼°xweek configuration of the SEAPODYM model was developed to provide real-time weekly forecast of lower and mid-trophic levels functional groups as well as tuna population dynamics. 2D fields of ocean currents and temperature were derived from the outputs of MERCATOR-OCEAN operational (PSY3V3R3) model at a resolution ¼ degree, weekly. Satellite-derived primary production and euphotic depth were obtained using empirical VGPM model (Behrenfeld & Falkowski, 1997) and Morel's formula (Morel & Berthon, 1989) correspondingly.

Concentrations of ^{137}Cs in sea water were obtained from a simulation produced at IFREMER using the ocean circulation model MARS-3D, with a spatial resolution of 1 nautical miles (nmi). These inputs are available for the period 2011-03-05 to 2011-07-21. Since physical forcing data (ocean currents and temperature) were available at a resolution 15 nmi and 7 days, the ^{137}Cs fields were aggregated to match the same spatiotemporal resolution (Fig. 1).

Pre-operational simulations

Due to computational constraints and the need to simulate long historical time series to provide realistic initial conditions to the operational model, a first series of parameter optimization experiments was conducted at coarse resolution of typically 1° or 2° and a monthly time step. Physical (temperature and currents) and biogeochemical (primary production, euphotic depth and dissolved oxygen concentration) variables were provided by a coupled ocean physical-biogeochemical model. We used a hindcast simulation (1972- 2011) of the NEMO ocean model (www.nemo-ocean.eu/) forced by the ERA40-INTERIM atmospheric reanalysis and coupled to the biogeochemical model PISCES (Aumont et al. 2015).

Once the optimal solution has been achieved at coarse resolution, it was used to generate the initial conditions for the operational global model. The change in resolution from the first configuration

required a downscaling approach for adapting the first set of optimal parameters to the new environmental model configuration.
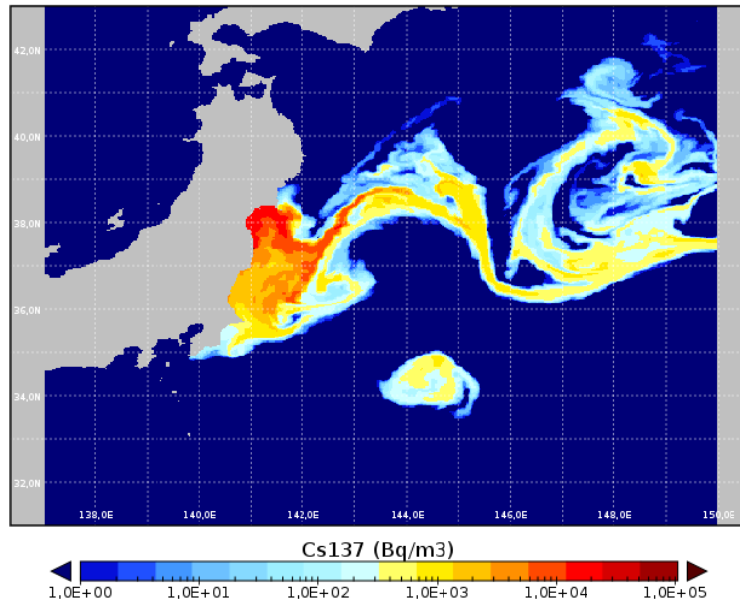
Figure 1.*Weekly average of ^{137}Cs in sea water predicted by MARS-3D model used as input forcing data for a coupled SEAPODYM radio-ecological model.*

SEAPODYM-REM: the coupled SEAPODYM and radio-ecological model of LTL and MTL dynamics

Let $Cs_p(t, \mathbf{x})$ be the ^{137}Cs activity concentration (Bq/gww) in the primary production. Hereafter we will omit time and space dimensions for brevity. Knowing Cs_w, activity concentration of a radionuclide in sea water, we can apply simple formula to compute the related activity concentration in primary production:

$$Cs_p = CF_{eq} \cdot Cs_w$$

where CF_{eq} is equilibrium concentration factor of a radionuclide for phytoplankton. Thus, the variable Cs_w is the source of LTL or MTL contamination by ^{137}Cs through the water and Cs_p is the source of the radionuclide contamination through the food web.

In SEAPODYM the biomass of the trophic level is modeled in two steps: 1) once the primary production is being recruited into the system as the source of trophic level (TL) biomass at 'age' 0, the dynamics of TL production is described explicitly in space, time and age dimensions; 2) when time of development that is necessary to reach the TL is attained, the production is then recruited into the system describing dynamics of species biomass. In the coupled system we have followed the same steps while linking the radionuclide concentration Cs_w and the production and the biomass and coupling the production-biomass system with Thomann radioecological equation (1981) describing the dynamics of radionuclide activity concentration in the species biomass.

Two TL functional groups are modelled – zooplankton (LTL, trophic position 0.5) and micronekton (MTL, trophic position 2.5). The 2D dynamics of the contaminants associated with the production of

LTL (n=1) or MTL (n=1..6) functional groups is described by the following system of equations with initial and boundary (Neumann type) conditions:

$$\frac{\partial S_n}{\partial t} + \frac{\partial S_n}{\partial a} = D\left(\frac{\partial^2 S_n}{\partial x^2} + \frac{\partial^2 S_n}{\partial y^2}\right) - \frac{\partial}{\partial x}(uS_n) - \frac{\partial}{\partial y}(vS_n)$$

$$S_n(t, a = 0, x, y) = \left(c\, E_n^{TL} P\right) \cdot Cs_p$$

$$\mathbf{n} \cdot \mathbf{v}\big|_{\mathbf{x} \in \partial\Omega} = \mathbf{n} \cdot \nabla S\big|_{\mathbf{x} \in \partial\Omega}$$

where $S_n(t, a, x, y)$ is the ^{137}Cs concentration of (Bq/km^2/day) associated with the production of n-th LTL or MTL groups at different time of development a (age); P – primary production (mmolC/m^2); c – conversion factor from mmolC/m^2 to gww/m^2 and E_n^{TL} is the energy transfer coefficient, which depends on the trophic level TL and that is unique for every functional group. To derive and compute the dynamics of the radionuclide activity concentration A in the production of organisms that comprise the trophic level functional groups we need to know the actual production F'. It is predicted by SEAPODYM model. Then dynamics of radionuclide concentration in TL production is described as follows:

$$\forall t_k, a, n \quad A_S = S_{t_k ij} \big/ F'_{t_k ij}$$

$$\frac{dA_S}{dt} = k_{uS} Cs_w - k_{dS} A$$

where k_{uS}, k_{dS} are the accumulation rate and decay (biological depuration) rate by the organisms between primary production and target TL (should be TL-dependent).

Finally, once the production is recruited to the targeted TL the dynamics of contaminants $C_n(t, x, y)$ associated with the TL biomass is modelled with help of the following equation:

$$\frac{\partial C_n}{\partial t} = D\left(\frac{\partial^2 C_n}{\partial x^2} + \frac{\partial^2 C_n}{\partial y^2}\right) - \frac{\partial}{\partial x}(\hat{u}C_n)\frac{\partial}{\partial y}(\hat{v}C_n) - \lambda C_n + R_{n,\tau_r}$$

where $R_{n_r} = \int_{\tau_r}^{a_{max}} S_n(t, a, x, y)\, da$ - the new source of contaminants arriving through the food web.

The dynamics of radionuclide concentration if TL biomass, A_F, is then modelled as follows :

$$\forall t, n \quad A_F = C_F \big/ F$$

$$\frac{dA_F}{dt} = k_u Cs_w + AE\left(IR_p Cs_p + IR_z Cs_z\right) - k_{dd} A_F$$

where k_u, k_{dd} are the accumulation rate and biological depuration rate by the TL functional groups and AE, IR_p, IR_z are the assimilation efficiency and ingestion rates of phyto- and zooplankton species respectively.

The above equations are approximated by finite differences and solved numerically with help of an implicit alternate direction method on the model domain (130E-180E; 25N-50N) and the resolution of 0.25 degree and 7 days. The coupled model outputs are i) the ^{137}Cs activity concentration (Bq/kgww) in zooplankton and micronekton, and ii) the biomass (g/m^2) of zooplankton and micronekton. Even though the radionuclide concentration in sea water was traced until July 2011,

the SEAPODYM-radio model simulations span until 31/12/2012 to allow tracing the propagation of ^{137}Cs through the food web, which would have different rate depending on the environment and the time of development of modelled organisms.

Habitats and top predator contamination risks maps

Once the activity concentration in MTL biomass is known we may calculate the contamination risks for the top predators such as tunas and billfishes. All we need to know is the amount of ^{137}Cs present in the micronekton biomass, that is accessible to top predators. This quantity is described by the model variable $C_n, n = 1..6$, which we can write as a matrix to facilitate the formula of the contamination index:

$$I_a = \boldsymbol{\Theta}_a \times \left(\tau \, \mathbf{C} \mathbf{e} + (1 - \tau) \mathbf{C}^{\mathbf{T}} \mathbf{e} \right);$$

$$\text{where } \mathbf{C} = \begin{pmatrix} C_{11} & 0 & 0 \\ C_{21} & C_{22} & 0 \\ C_{31} & C_{32} & C_{33} \end{pmatrix} \begin{matrix} \text{epi} \\ \text{meso} \\ \text{lmeso} \end{matrix} \text{ and } \Theta_{a,l} = f\left(O_{2l}; \boldsymbol{\theta}_{O_2}\right) \cdot g\left(T_l; \boldsymbol{\theta}_{T,a}\right)$$

where $\Theta_{a,l}$ is the accessibility of the top predator of age a to the pelagic layer l, τ is the day length, $\boldsymbol{\theta}$ isa vector of parameters defining the preference (age dependent) of the top predator to water temperatures T_l and tolerance to low dissolved oxygen concentrations O_2, f and g are the functions describing the dependence of species accessibility on temperature and oxygen respectively.

Results and Discussion

The parameters of SEAPODYM-REM coupled model were calibrated based on the findings of previous studies (Bryan, 1963; Tateda and Koyanagi, 1994; Zhao et al., 2001; Behrens et al., 2012; Doi et al., 2012; Wada et al., 2016; Belharet et al., 2016). Then, the Cs activity in zooplankton and micronekton biomass was simulated with the coupled model. The dynamics of radionuclide concentration in zooplankton is shown for three coastal areas near Fukushima and for micronekton in Fukushima prefecture (see Figure 2). The peak of ^{137}Cs in zooplankton biomass is attained very quickly in coastal areas, i.e. as soon as in six weeks after the accident (Chiba and Ibaraki) and the latest in 2.5 months (Iwate), while in offshore area the maximal concentrations are predicted to occur in September. Not surprisingly, the maximal concentrations are predicted for the prefectures that are closest to the contamination source: 132 Bq/kgww for Miyagi, 299 Bq/kgww in Fukushima and 629 Bq/kgww in Ibaraki (see Figure 2).

Activity concentrations of ^{137}Cs in micronekton are shown to peak at least twice with the first peak explained by the rapid contamination through water and the second peak occurring due to contamination through consumption of contaminated prey and accumulation of radionuclide in the tissue. The maximal concentrations are delayed in the deep water species (lower mesopelagic). It should be noted that Cs_w was not available for the vertical dimension that is why the concentrations were assumed homogeneously distributed in depth and hence impacted all functional groups equally. The latter is not realistic and should be revised in the future studies.

Regarding predictions in the coastal waters (Figure 3) there is also north-south and surface-depth changes in the concentrations and their maxima. Basically, it takes more time for the species inhabiting waters with colder temperatures (so having longer time of development and longer life

span) to accumulate the contaminants. Also, while the contamination through the water is prevailing for surface (epi-pelagic) species, this effect seems to be inversed (higher and occurring much later maximum) for the deeper (lower mesopelagic) species.
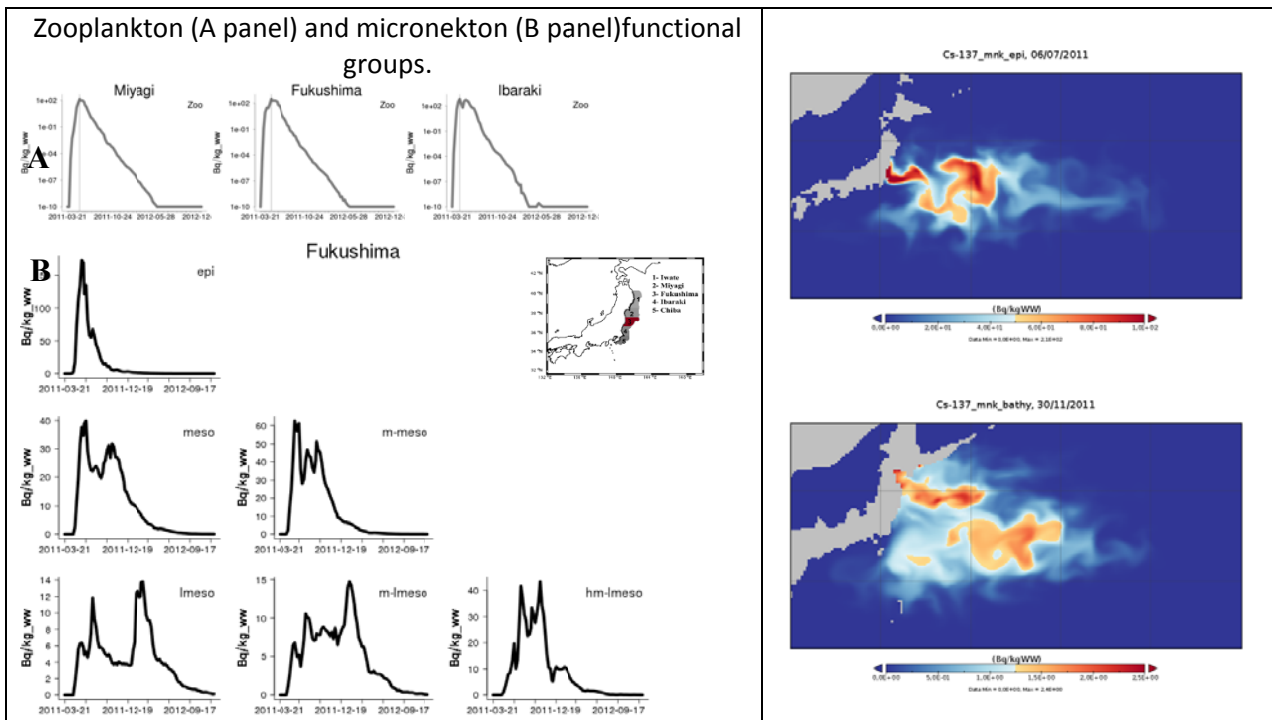
Figure 2. *Left: temporal dynamics of ^{137}Cs in the biomass of zooplankton (grey lines, shown on logarithmic scale) for three Prefectures and micronekton functional groups (black lines) in Fukushima Prefecture waters. Right: distributions of ^{137}Cs in epipelagic and lower mesopelagic micronekton during their respective predicted maximum (July for epi- and November for lower mesopelagic forage).*

These results are still preliminary as we were not able to validate the predictions quantitatively in the absence of field data. However, the qualitative convergence with the results obtained in other studies (Buesseler et al., 2012; Belharet et al., 2016) such as consistent delays between the accidental release of ^{137}Cs and its maximal concentrations observed in fish from different pelagic communities and similar order of magnitude of predicted and observed activity concentrations, is encouraging.

An application of this modeling to the estimation of skipjack tuna habitat is illustrated on Figure 3 with the resulting risk contamination map.

Operational model

The chain of operations starts with the delivery of physical and biogeochemical raw data once per week. Once physical and biogeochemical variables have been delivered, a phase of preprocessing reduces the number of vertical layers by averaging the values according to the definition of vertical boundaries (linked to the euphotic depth; see e.g., Lehodey et al 2015). Then the micronekton model runs in parallel to simulate production and biomass of the functional groups, and finally, it is the tuna model. As a result, once per week the SEAPODYM global model provides the simulation outputs for micronekton and tuna species for a period of 3 weekly time steps including one week of hindcast, one week of nowcast and one week of forecast. The hindcast is archived to produce a

historical series since the starting date of the operational model. The forecast is based on the physical ocean forecast and the persistence of last primary production map.
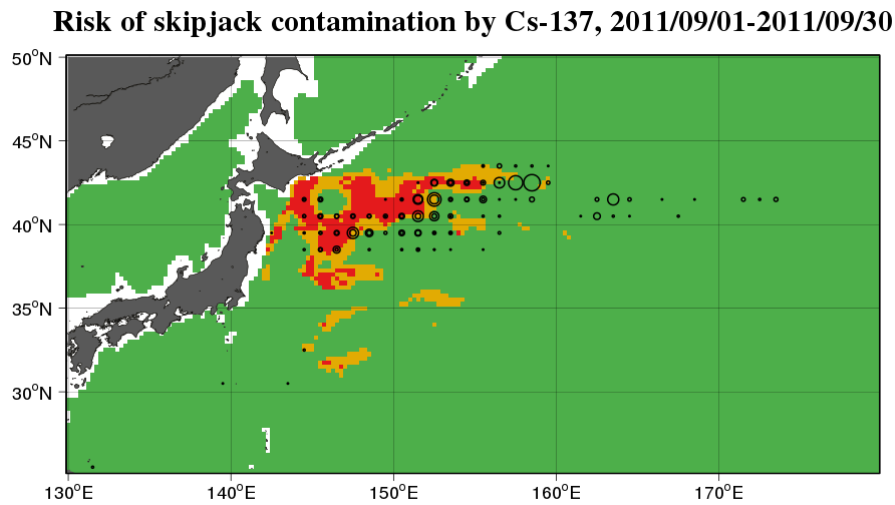
Figure 3. *Contamination index computed for skipjack tuna in September 2011(red = high risk; orange = medium risk; green = no risk). The circles show the distribution of skipjack catches in September 2010 (the catch data for Sep 2011 were not available).*

The model production is now running without any technical issue. The coupling with the radioecological model still needs to be implemented with one additional forcing (sea water ^{137}Cs concentration) and tested (Figure 2). Obviously, there are still a few more key challenges to achieve in order to provide a fully operational monitoring tool. The main one will be to validate the model outputs and to revise the parameterization based on the most diverse sources of observations, including fishing data (catch and size), tagging data of fish, acoustic biomass estimates of micronekton, biomass estimates of zooplankton and concentrations of 137Cs in the different functional groups and target species.

Conclusions

An approach is proposed and implemented to couple the lower and mid-trophic levels SEAPODYM model components with a radioecological model. The initial calibration of parameters (accumulation and elimination rates, assimilation efficiency, ingestion rates by low trophic level and mid-trophic level groups) has been achieved based on the data published in the scientific literature (Bryan, 1963; Tateda and Koyanagi, 1994; Zhao et al., 2001; Behrens et al., 2012; Doi et al., 2012; Wada et al., 2016; Belharet et al). Additional observations are sought to evaluate the model predictions, and to further improvethe model calibration, e.g., the biological decay should be linked to the ambient temperature. In addition to field data, we need also to update the simulation using a longer time series of forcing data on ^{137}Cs in sea water, in order to improve the spatiotemporal coverage of the model predictions.Finally, using these predicted concentrations and habitat modeling, real-time and forecast indicators of contamination risk for top predator species could be produced.

References

Behrenfeld, M. J., and Falkowski, P. G. 1997. A consumer's guide to phytoplankton primary productivity models. Limnology and Oceanography, 42: 1479–1491.

Behrens, E., Schwarzkopf, F. U., Lubbeck, J. F., Böning, C. W. 2012. Model simulations on the long-term dispersal of 137Cs released into the Pacific Ocean offFukushima. Environ. Res. Lett. 7 : 034004 (10pp). doi:10.1088/1748-9326/7/3/034004

Belharet, M., Estournel, C., Charmasson, S. 2016. Ecosystem model-based approach for modeling the dynamics of 137 Cs transfer to marine plankton populations: application to the western North Pacific Ocean after the Fukushima nuclear power plant accident. Biogeosciences, 13 : 499–516. doi:10.5194/bg-13-499-2016.

Bryan, G. W. 1963. The Accumulation of radioactive caesium by marine invertebrates. J. Mar. Biol. Ass. U. K. 43: 519-539.

Buesseler, K. O., Jayne, S. R., Fisher, N. S., Rypina, I. I., Baumann,H., Baumann, Z., Breier, C. F., Douglass, E. M., George, J., Mac-donald, A. M., Miyamoto, H., Nishikawa, J., Pike, S. M., andYoshida, S.: Fukushima-derived radionuclides in the ocean andbiota off Japan, Proc. Natl. Acad. Sci. USA, 109, 5984–5988,2012.

Doi H., Takahara. T., Tanaka K. 2012. Trophic position and metabolic Rate Predict the Long-Term Decay Process of Radioactive Cesium in Fish: AMeta-Analysis.

Lehodey P., Senina I., Murtugudde R. 2008. A Spatial Ecosystem And Populations Dynamics Model (SEAPODYM) - Modelling of tuna and tuna-like populations. Progress in Oceanography,78: 304-318.

Lehodey, P., Murtugudde, R., and Senina, I. 2010. Bridging the gap from ocean models to population dynamics of large marine predators: a model of mid-trophic functional groups. Progress in Oceanography, 84: 69–84.

Lehodey, P., Conchon, A., Senina, I., Domokos, R., Calmettes, B., Jouanno, J., Hernandez, O., and Kloser, R. 2015. Optimization of a micronekton model with acoustic data. – *ICES Journal of Marine Science*, 72(5): 1399-1412. doi: 10.1093/icesjms/fsu233.

Madigan,D. J.,Baumann, Z., Fisher, N.S.2012. Pacific bluefin tuna transport Fukushima-derived radionuclides from Japan to California. Proc Natl Acad Sci USA. vol. 109(24), 9483–9486, doi: 10.1073/pnas.1204859109

Morel, A, J-F Berthon. 1989. Surface pigments, algal biomass profiles, and potential production of the euphotic layer: Relationships reinvestigated in view of remote-sensing applications. Limnol. Oceanogr., 34: 1545-1562.

Rossi, V., Sebille, E. V., Sen Gupta, A., Garcon, V., England, M.H. 2013. Multi-decadal projections of surface and interior pathwaysof the Fukushima Cesium-137 radioactive plume. Deep-Sea Research I. 80: 37-46.

Senina, I., Sibert, J., Lehodey, P. 2008. Parameter estimation for basin-scale ecosystem-linked population models of large pelagic predators: application to skipjack tuna. Progress in Oceanography, 78: 319-335.

Senina, I., Lehodey, P., Calmettes, B., Nicol, S., Caillot, S., Hampton, J. and P. Williams. 2016. Predicting skipjack tuna dynamics and effects of climate change using SEAPODYM with fishing and tagging data. WCPFC, 12th Regular Session of the Scientific Committee, Bali, Indonesia 3–11 August 2016, WCPFC-SC12-2016/EB WP-01: 71 pp. http://www.wcpfc.int/node/27443

Tateda Y., Koyanagi T. 1994. Concentration factors for Cs-137 in Marine Algae from Japanese coastal waters. J. Radiat. Res., 35: 213-221.

Wada, T., Fujita, T., Nemoto, Y., Shimamura, S., Mizuno, T., Sohtome, T., Kamiyama, K., Narita, K., Watanabe, M., Hatta, N., Ogata, Y., Morita, T., Igarashi, S. 2016. Effects of the nuclear disaster on marine products in Fukushima: An update after five years. Journal of Environmental Radioactivity 164: 312-324.

Zhao X., Wang W.-X., Yu, K. N., Lam, P. K. 2001. Biomagnification of radiocesium in a marine piscivorous fish. Mar. Ecol. Prog. Ser. 222: 227-237.

Acknowledgements

New approach for simulation of particle dynamics and trace metal interactions in the ocean

Elena Ceballos-Romero1*, María Villa-Alfageme[1], Feliciano de Soto [2]

Universidad de Sevilla, Department of Applied Physics II, ETSA, Av. Reina Mercedes 2, 41012 Sevilla, Spain
Universidad Pablo de Olavide, Department of Physical, Chemical and Natural Systems, Carretera de Utrera km 1, 41013 Sevilla, Spain

Abstract

We present a stochastic computational model of particle dynamics in the ocean. The model simulates the processes of particle creation, sinking and remineralization in the ocean in order to describe the observed degradation, solubilisation and destruction that particles experience in their way out from the surface layers where they are produced- i.e. particle flux attenuation in depth. Unlike previous models, we explicitly include creation and attenuation processes time-dependent and interpret them probabilistically: particles are randomly created and destroyed. Once particles are created, sinking particles are let evolve independently as separated boxes that appear and disappear dynamically and interact with the dissolved and particulate phases of radionuclides in their way down through adsorption and desorption processes. Such interactions influence the biogeochemistry of the ocean and earth system as a whole.

The model describes the geochemical behaviour of radionuclides- from both natural and anthropogenic sources- in the marine environment. Factors as different particle sizes, particle concentration, or external sources such as Saharan dust, or other inputs can be easily included in more developed models.

Among naturally present radionuclides, ^{234}Th and ^{210}Po are especially important in radioecology due to their radioecological, especially for polonium. It is important to describe its behaviour in sea-water in order to predict and control potential releases (such as releases from the phosphate industry or phosphogyspsum stacks). The study we present here is focused on ^{238}U-^{234}Th and ^{210}Pb-^{210}Po radioactive pairs. Experimental published depth profiles were employed to validate the model. Vertical distributions were found to be the result of the balance between adsorption and desorption and attenuation processes.

One of the most relevant potential of this model is its applicability to simulate the chemical behaviour of particulate radionuclides in water. In the field of radioecology, we will be able to investigate and predict the functioning of radionuclides present in the ocean due to fallout and/or accidental releases or discharges from nuclear reprocessing plants to the sea.

Introduction

Marine ecosystems are strongly affected by toxic pollutants derived from human activities. Organic (such as pesticides and oils) and inorganic (e.g. heavy metals and radionuclides) toxic substances from land-based sources contaminate marine food chains in coastal areas and have an impact on the marine environments (Islam and Tanaka, 2004). The assessment of the behaviour and fate of these pollutant elements is therefore crucial to identify uptake and retention mechanisms in marine biota (Olaniran et al., 2013). In this sense, radiotracer techniques are a major non-destructive tool to investigate the effects of these environmentally-important contaminants.

Vertical distributions of radionuclides are depth dependent and geographically changing. They reflect the influence of a combination of several processes that include external and internal inputs, physical, chemical and biological removal, and recycling (Aparicio-González et al., 2012). Inventories in depth are essential to understand ocean biogeochemistry and to improve global models of carbon cycling and its response to climate change (Aparicio-González et al., 2012). The bioaccumulation of co-occurring contaminants in marine biota is a key issue in the field of radioecology nowadays.

In the present study, we focus on scavenged radioisotopes, i.e. elements which depth profiles result from adsorption onto particle surfaces, such as clay minerals and organic matter. They are characterised by concentrations that are lowest in surface waters- where the concentration of particles is typically higher and therefore, are highly assimilated by phytoplankton and/or adsorbed by particles-, and concentrations that increase at depth as sinking particles undergo remineralisation in subsurface waters.

Here we present a stochastic computational model for particle dynamics: creation, sinking and attenuation (i.e. degradation, solubilisation and destruction) in the ocean that includes particle-radionuclide interactions of radionuclides to sinking particles through adsorption and desorption processes (De Soto et al., submitted). Sinking particles are the major vehicle for exporting radionuclides from the sea surface to the ocean interior. The observed patterns of particle flux attenuation in depth are described by using creation and attenuation probabilistic functions time-dependent for sinking particles, which allow us to obtain the time evolution of radionuclides activities in both water and sinking particles through time. It is possible to reproduce the geochemical behaviour of a given radionuclide in the marine environment. Vertical profiles for both dissolved and particulate phases are obtained for any desired ocean scenario.

With this study we aim to provide a numerical tool to improve our knowledge of the biogeochemical and radioecological behaviour and distribution of natural and artificial radionuclides and trace elements in the oceans and to analyse the possible factors that contribute to the metals scavenging in the water column and their environmental dependence (focused in ^{234}Th and ^{210}Po).

Materials and Methods: stochastic model

To study the radionuclides profiles in the ocean through modelling techniques, we first have to model the particle dynamics, namely creation, sinking and attenuation; and secondly the trace metals/radionuclides interactions to these sinking particles (i.e. the particles scavenging).

We propose a microscopic model of particle creation, sinking and attenuation that takes into account both time and depth dependencies of these processes. With this approach, seasonal changes in the physical environment- temperature, hydrographic conditions or mixed layer depth among others - and ecosystem conditions- community structure and particles size, composition, lability and sinking velocity- that affect the amount of particles created and destroyed are qualitatively reproduced. Furthermore, particle properties such as sinking speed and attenuation rate are allowed to vary with depth, in order to potentially take into account different factors, e.g. ballast effect or particle recycling in the upper waters.

Particle dynamics

In the particles modelling, the time and depth evolution of the concentration of sinking matter (n) depends on the rates of creation, sinking and destruction of particles according to the continuity equation,

$$\frac{\partial n}{\partial t} = \sigma(z,t) \cdot N - \beta_{-1}(z,t) \cdot n - \frac{\partial P(z,t)}{\partial z} \tag{1}$$

Where the first term accounts for the rate of creaction of particles, with N the source term of total sinking mass (mg m^{-3} d^{-1}) and $\sigma(z,t)$ the normalized depth profile- in the sense that $\int dz \cdot \sigma(z,t) = 1$ - (m^{-1}); the second term accounts for the attenuation of particles, with $\beta_{-1}(z,t)$ rate of destruction (d^{-1}); and the third term accounts for the sinking particle flux, with $P = \int n(z,t) \cdot v(z,t)$ (mg m^{-2} d^{-1}), and v sinking velocity (m d^{-1}).

Figure 1. Schematic representation of the model.
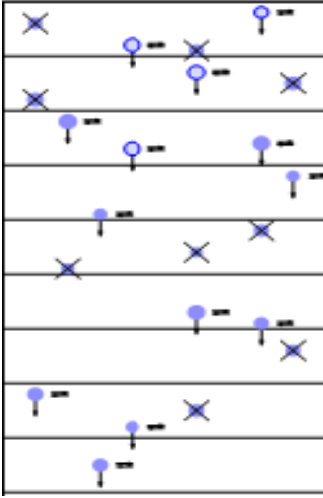
The standard approach (e.g. Burd et al. (2000)) resolves this equation numerically bydiscretising it in time and depth and resolving it iteratively in small steps. Additionally, creation and attenuation processes are consideredconstant over time.

On the contrary, our novel approach gives astochastic resolution to the master equation: the terms of creation and destruction are ruled by time-dependent probabilistic functions. This way, as schematically shown in Figure 1, particles are: i) randomly created with a probability distribution$\sigma(z,t)$ (light-blue circles), ii) moved in depth with$v(z,t)$ (downward arrows), and iii) randomly destroyed with a probability distribution$\beta_{-1}(z,t)$ (crossed circles).

In such a way, we mimic the randomness of nature, where creation and destruction of sinking particles is the result of a combination of random events rather than a continuous phenomenon.

The output of the simulation is a concentration profile of *sinking units* and flux in depth.

Radionuclide interactions

Regarding radioisotope modelling, radionuclide activities are partitioned between its dissolved phase and the particles. Once we have a simulation for particles dynamics, interactions with radioisotopes, both naturally and artificially present in the ocean, are easily included by adsorption and desorption first order processes (schematically shown by the horizontal arrows in Figure 1). This feature of the model is crucial since radioactive disequilibrium inventories are extensively used for the study of the biogeochemistry and multiple processes in the oceans. The time-evolution of the activity concentration of the particulate(a^P) and dissolved phases(a^D) is given by the equation,

$$\frac{\partial a_P}{\partial t} = -\overline{k_-} \cdot a_P + \overline{k_+} \cdot a_D = -\frac{\partial a_D}{\partial t} \tag{2}$$

Where $\overline{k_+}$ and $\overline{k_-}$are the effective adsorption and desorption coefficients respectively for each radionuclides desired that account for the effective scavenging of the radionuclides by particles. For simplicity in this study we do not distinguished by size, but it is important to note that the model allows it. In the case of different particles sizes, particle concentration would be partitioned between the small particles (P_S) and the large particles (P_L) and aggregation of small particles and the disaggregation of large particles would also be part of the process.

In a simulation with different particle sizes, $\overline{k_+}$ and $\overline{k_-}$ may depend on particle size, as discussed in detail in Burd et al. (2000). Note that the adsorption coefficient $(\overline{k_+})$ in the simulation is per *sinking unit*, so that for a given layer, the effect of adsorption is proportional to the concentration of *sinking units* at that depth. On the contrary, the desorption coefficient $(\overline{k_-})$ is independent of the concentration of matter at a given layer.

The algorithm for the radionuclide interactions starts by setting initial conditions for radioisotope activities in water for all radionuclides. The adsorption and desorption processes would add a fourth step by applying Eq. (1) to each *sinking unit*. This way, we need to compute the dissolved phase activity at each depth during the simulation, and the the time and depth evolution of the total concentration of radionuclides is given by:

$$\frac{\partial a_2(z,t)}{\partial t} = \lambda \cdot [a_1(z,t) - a_2(z,t)] - \frac{\partial a_2(z,t)}{\partial z} \tag{3}$$

Where a_1 is the father activity, and a_2 and λ the daughter activity and half-life.

Results and Discussion

In the sunlight euphotic zone, the autotrophic organisms- also known as primary producers-synthesize organic compounds and biomass (mainly O_2 and particulate organic carbon) from carbon dioxide through the process of photosynthesis, which constitutes the base of the food chain and creates matter. Since such process is light limited, the creation of particles is confined to a surface region of depth E_z that varies greatly with season and latitude. In the stochastic model, this depth within particles are created is fixed by the function $\sigma(z,t)$ of Eq. (1), which creates N particles randomly distributed within E_z with a probability that decreases with depth. Furthermore, the process of photosynthesis also relies on the amount of Chlorophyll (Chl-a) available in the surface ocean, which generally peaks during the spring bloom and declines in summer. Therefore, the rate of particles creation varies along the season. In the model, satellite-derived Chl-a seasonal data are used as a proxy for particle creation rate along productive seasons in each geographical scenario simulated. Thus, both the vertical and temporal dependence of the process of particle creation is described by the source function $\sigma(z,t)$.

Once biomass is created, a small fraction of this matter becomes large enough to attain high sinking velocities and survive all the process that undergo in the way out of the euphotic zone that result in its degradation, solubilisation and destruction (namely attenuation). This fraction sinks down to depth as dead phytoplankton cells, aggregates of carbon into particles and zooplankton faecal pellets constituting a sinking flux $P(z,t)$ (Eq.(1)). In the model, all the process involved in the attenuation of particles are encompassed on the attenuation function $\beta_{-1}(z,t)$, which works in a similar way as the creation function: it randomly destroys particles with a probability time- and depth-dependent. The time dependence takes into account the seasonal changes in the physical environment and ecosystem previously mentioned, while the depth dependence describes the geographical variations of in the vertical distributions of sinking particles experimentally reported (e.g. Marsay et al. (2015)).

Attenuation function: depth dependence

Any parametrization of the function $\beta_{-1}(z)$ in Eq. (1) can be used to describe the experimentally observed patterns in particle flux. The most relevant parametrizations considered in literature are those suggested by Martin et al. (1987) and Lutz et al. (2002), which propose respectively an attenuation rate inversely proportional to the depth ($\beta_{-1}(z) = v \cdot b/z$) that leads to a power law flux ($f_z = f_{z_0} \cdot (z/z_0)^{-b}$); and a constant attenuation rate ($\beta_{-1}(z) = v \cdot z^*$) that gives an exponential flux dependence ($f_z = f_{z_0} \cdot \exp\left[-(z-z_0)/z^*\right]$). The former one relates the flux at any depth to the flux measured at a reference depth z_0, and b quantifies flux attenuation; while the second one quantify particle attenuation via the remineralisation length scale z^*, which is defined as the depth interval over which the flux decreases by a factor of 1/e and is not affected by the relative depth used. However, despite all the attempts that have been made to mathematically define the vertical attenuation of particles in oceanic waters, the controlling mechanisms are still poorly understood. For this reason, we propose here a novel parametrization of the attenuation function $\beta_{-1}(z)$:

$$\beta_{-1}(z) = \beta_{-1}^0 \cdot e^{-z/z_0} \qquad (4)$$

Where β_{-1}^0 and z_0 are the attenuation rate (in d^{-1}) and the depth at which attenuation weakens (in m). This way, the attenuation is finite in the euphotic zone and goes to zero at very large depths ($z\,3z_0$ and therefore the flux stabilizes.

Model performance: particle dynamics inputs

The complete set of the model here presented therefore requires as inputs a) the data related to sinking particles: the profile (depth dependence) of the particle creation ($N \cdot \sigma$), the attenuation rate (β_{-1}) and the sinking speed (v), which are all geographically dependent; and b) the data related to radionuclides: the adsorption and desorption rates ($\acute{k}_{\pm}$), which are characteristic of each nuclei.

For the present study, we have chosen the sampling that took place during summer 2009 at the Porcupine Abyssal Plain (PAP) Site reported by Le Moigne et al. (2013) for two reason: PAP Site is a multidisciplinary moored observatory and intensively studied area that provides time-series datasets that could be used for the discussion; and a very exhaustive sampling took place during cruise D341 in summer 2009 and numerous biogeochemical parameters were obtained.

As previously explained, the model requires the euphotic zone depth and the production rate as an input for particle creation. Values of the euphotic zone reported by Le Moigne et al. (2013) were used to fix the particles creation interval depth; while Chl-a data of year 2009 from NASA MODIS satellite, downloaded from http://oceancolor.gsfc.nasa.gov/, (black point of Figure 2) were fit to the best fit curve and used as a proxy for the creation rate of the model (green line of Figure 2).

Figure 2.*Satellite-derived primary production profiles over time for the PAP site in year 2009* (Le Moigne et al., 2013) *in black points, and modelled profiles for the best Gaussian curve fitting in green line. The Day Of the Year (DOY) has been rescaled to match the maximum of the production.*
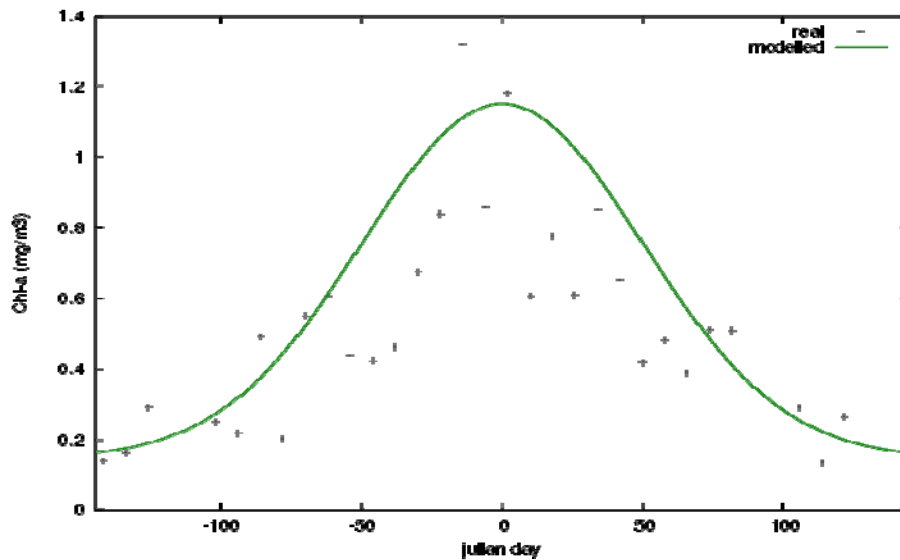
Furthermore, the sinking speed (v) was chosen in agreement with average values reported by Villa-Alfageme et al. (2016) for fast sinking particles during cruise D341 (100 m d^{-1}), who compiled data of sinking rates in the temperate and oligotrophic North Atlantic daring different bloom stages using inverse modelling of ^{210}Pb-^{210}Po disequilibrium; and the attenuation rate (β_{-1}^{0}) was chosen following the values reported by Marsay et al. (2015) (0.6 d^{-1}), who collected data from sediment traps along the North Atlantic and estimated attenuation following both Martin et al. (1987) and Lutz et al. (2002) approaches.

Particle and radionuclide concentration depth profiles

In this section with present the primary output results using the stochastic approach above described for the parametrization of the attenuation function here proposed (Eq. 4) and the creation rate depicted in Figure 1.

The primary output of the simulation is the depth concentration profile over time for both sinking particles and radionuclides. Although the methodology presented is general, for simplicity reasons we will focus here on the ^{238}U-^{234}Th pair. ^{234}Th is highly interesting for oceanography studies and process related to the Biological Carbon Pump (Volk and Hoffert, 1985) due to ^{234}Th suitable half-life ($T_{1/2}$ = 24.1 d) and high particle affinity, in contrast to the conservative distribution of ^{238}U is seawater. Furthermore, it will provide key information of the behaviour of the sinking thorium, due to natural or anthropogenic releases, in the ocean. Thorium's chemical toxicity and radiological hazard are especially important because of the short half-lives of many of its decay products.

The so called bloom in the ocean consist on a sudden production of phytoplankton in surface water, with the subsequent growing of zooplankton that produce abundant sinking particles that scavenge dissolved elements and radionuclides. This cycle is crucial to understand the process of sinking of natural and anthropogenic radionuclides in the ocean.

Figure 3 shows the vertical distribution of sinking particles and ^{234}Th activity for different moments of the bloom in relation to the maximum in the production (chosen as DAY 0, Figure 2). It evidences that, while particle concentration reacts rapid to changes in production (within a characteristic time: $t = z/v$), ^{238}U-^{234}Th disequilibrium reacts slower than particle concentration to changes in production due to the influence of the radioactive decay (Eq. 3), which prolong the persistence of ^{234}Th deficits in water column proportionally to its half-life.

Figure 3. *Temporal evolution of the modelled vertical distribution of a) sinking particles, b) ^{234}Th concentration in particles, and c) ^{284}U-^{234}Th disequilibrium in the PAP Site during summer 2009 (Le Moigne et al., 2013) for a creation rate that follows the Gaussian fit of the satellite-derived Chl-a data depicted in Figure 1 from 100 days before and 100 days after the maximum in the production. ^{238}U was calculated as A_U = 0.0686 x salinity normalised to a salinity of 35* (Chen et al., 1986).
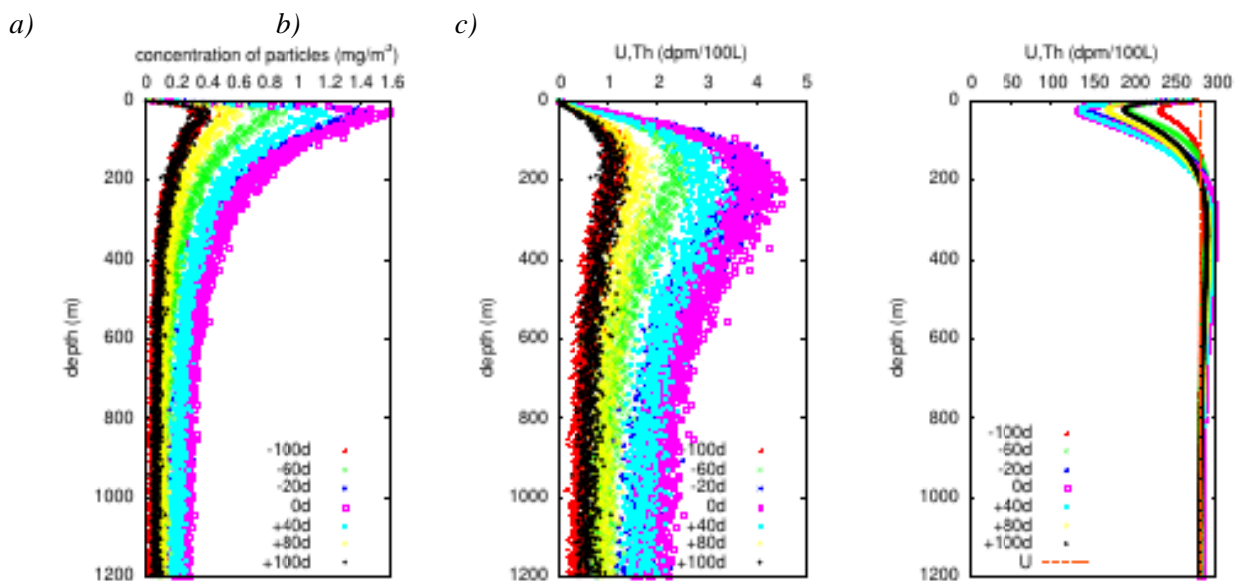
The range of adsorption and desorption effective coefficients valid for each radionuclide can be inferred by comparison to experimental data (Figure 3). In the case of ^{234}Th, large values for the desorption (around 10 d^{-1}) and adsorption values in the order of ~ 10^5 cm^3 g^{-1} d^{-1} were found to be necessary in order to match the experimental typical profiles of ^{234}Th (e.g. Coale and Bruland (1987); Le Moigne et al. (2013); Owens et al. (2015) among others). Once this rates are known, the radionuclide depth profile in the both the dissolved and particulate phase can be computed for any geographical scenario desired by adjusting the attenuation rate as previously mentioned (e.g. using data compiled by Marsay et al. (2015)) as shown in Figure 4.

Figure 4. Experimentally measured and modelled activity concentration (in dpm 100L^{-1}) in depth at the PAP site in the post-bloom of year 2009 (Le Moigne et al., 2013) *for the (b) dissolved phase, and the (c) particulate phase; for a model parameters of 100 m d^{-1} for the sinking speed* (Villa-Alfageme et al., 2016) *and 0.6 d^{-1} for the attenuation rate1* (Marsay et al., 2015). *A desorption rate of 10 d^{-1} and adsorption rate of 2·10^5 cm^3 g^{-1} d^{-1} were employed for the adjustment.*
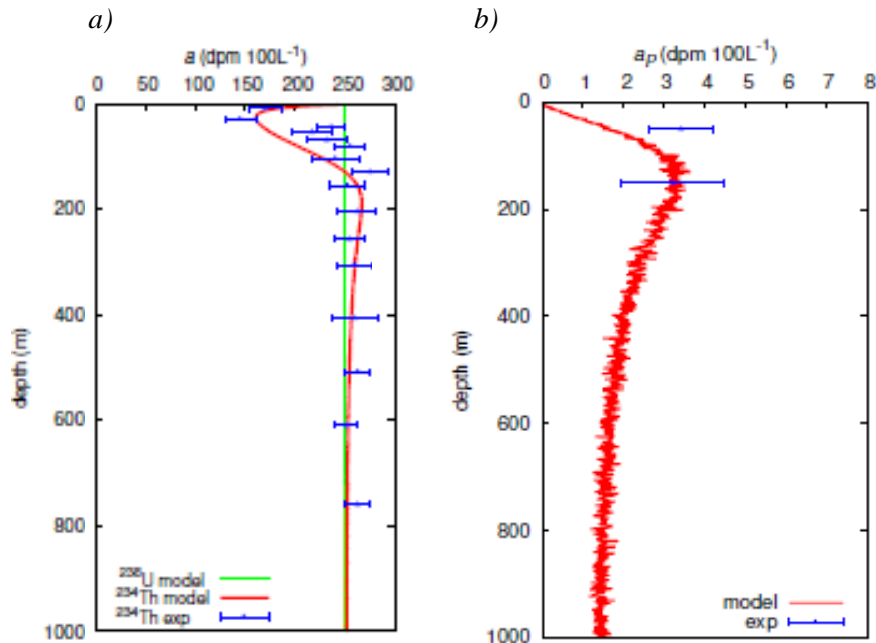
These results points out that the profile of ^{234}Th in depth results from the balance of the adsorption process and the action of both desorption and attenuation. This is clearly illustrated by Fig. 4b, which shows that the concentration of ^{234}Th in particles increases in depth until an equilibrium between these processes is reached. Once adsorption and desorption effects counteract (around 200 m in our results), the concentration of ^{234}Th in depth is exclusively determined by the attenuation process. This would explain why in temperate regions -characterised by low attenuation rates (Marsay et al., 2015)-^{234}Th-^{238}U disequilibrium persists deeper in the water column (around 150-200 m as found by e.g. Owens et al. (2015)) in comparison with subtropical latitudes, where ^{234}Th-^{238}U reach equilibrium at shallower depths (around 75 m, as shown by e.g. Buesseler et al. (2009) and Coale and Bruland (1987)). Equally, it would explain why equilibrium depth in winter deepens in relation to spring and summer (e.g. Kim and Church (2001)).

Conclusions

We show that our modelling approach provides a powerful computational tool to better understand the transient regimes of the adsorption and desorption particle-water process ongoing in the oceanic environment. We aim to assess the accuracy of the current experimental estimates and to predict the fate of possible radionuclide releases to the ocean. It allows a great variety of applications to the fields of both radioecology and oceanography and ocean biochemistry such as the study of particle interactions with the radioisotopes both naturally and artificially present in the oceans; the clarification of issues related to general circulation and mixing of radionuclides in the ocean, removal and input processes; the prediction of vertical distribution of any desired radionuclide through determination of its adsorption and desorption coefficients; or the study of the Biological Carbon Pump and the sinking carbon flux attenuation.

As a future work, we aim to increase model complexity by implementing several particles classes/sinking velocities and interaction between particle classes (aggregation/disaggregation process, as well as water mixing and geographical turbulence and most important, to include different radionuclides. Additional analysis regarding open questions in the science community such as the assessment of the influence of the temporal variability attenuation process in the radionuclides profiles, evaluation of the metric for the choice of a normalized export depth, or the accurate quantification of carbon export to the mesopelagic are also allowed by the model. In the field of radioecology, we can investigate/predict the functioning of radionuclides present in the ocean due to fallout or accidental releases or discharges from nuclear reprocessing plants to the sea.

References

Aparicio-González, A., Duarte, C.M., Tovar-Sánchez, A., 2012. Trace metals in deep ocean waters: A review. J. Mar. Syst. 100, 26–33. doi:10.1016/j.jmarsys.2012.03.008

Buesseler, K.O., Pike, S., Maiti, K., Lamborg, C.H., Siegel, D.A., Trull, T.W., 2009. Thorium-234 as a tracer of spatial, temporal and vertical variability in particle flux in the North Pacific. Deep Sea Res. Part I Oceanogr. Res. Pap. 56, 1143–1167.

Burd, A.B., Moran, S.B., Jackson, G.A., 2000. A coupled adsorption–aggregation model of the POC/234Th ratio of marine particles. Deep Sea Res. Part I Oceanogr. Res. Pap. 47, 103–120. doi:http://dx.doi.org/10.1016/S0967-0637(99)00047-3

Chen, J.H.H., Lawrence Edwards, R., Wasserburg, G.J.J., Edwards, R.L., Wasserburg, G.J.J., 1986. 238U,234U and232Th in seawater. Earth Planet. Sci. Lett. 80, 241–251. doi:10.1016/0012-821X(86)90108-1

Coale, K.H., Bruland, K.W., 1987. Oceanic stratified euphotic zone as elucidated by 234Th : 238U disequilibria. Limnol. Oceanogr. 32, 189–200. doi:10.4319/lo.1987.32.1.0189

De Soto, F., Ceballos-Romero, E., Villa-Alfageme, M., 2016. Modeling of particles flux attenuation in the ocean water column using a microscopic simulation approach. Submitt. to Geochim. Cosmochim. Acta.

Islam, M.S., Tanaka, M., 2004. Impacts of pollution on coastal and marine ecosystems including coastal and marine fisheries and approach for management: a review and synthesis. Mar. Pollut. Bull. 48, 624–49.

Kim, G., Church, T.M., 2001. Seasonal biogeochemical fluxes of 234 Th and 210 Po in the Upper Sargasso Sea: Influence from atmospheric iron deposition. Global Biogeochem. Cycles 15, 651–661. doi:10.1029/2000GB001313

Le Moigne, F.A.C., Villa-Alfageme, M., Sanders, R.J., Marsay, C., Henson, S., García-Tenorio, R., 2013. Export of organic carbon and biominerals derived from 234Th and 210Po at the Porcupine Abyssal Plain. Deep Sea Res. Part I Oceanogr. Res. Pap. 72, 88–101.

Lutz, M., Dunbar, R., Caldeira, K., 2002. Regional variability in the vertical flux of particulate organic carbon in the ocean interior. Global Biogeochem. Cycles 16, 11–18. doi:10.1029/2000GB001383

Marsay, C.M., Sanders, R.J., Henson, S.A., Pabortsava, K., Achterberg, E.P., Lampitt, R.S., 2015. Attenuation of sinking particulate organic carbon flux through the mesopelagic ocean. Proc. Natl. Acad. Sci. 112, 1089–1094.

Martin, J.H., Knauer, G.A., Karl, D.M., Broenkow, W.W., 1987. VERTEX: carbon cycling in the northeast Pacific. Deep Sea Res. Part A, Oceanogr. Res. Pap. 34, 267–285. doi:10.1016/0198-0149(87)90086-0

Olaniran, A.O., Balgobind, A., Pillay, B., 2013. Bioavailability of heavy metals in soil: impact on microbial biodegradation of organic compounds and possible improvement strategies. Int. J. Mol. Sci. 14, 10197–228. doi:10.3390/ijms140510197

Owens, S.A., Pike, S., Buesseler, K.O., 2015. Thorium-234 as a tracer of particle dynamics and upper ocean export in the Atlantic Ocean. Deep Sea Res. Part II Top. Stud. Oceanogr. 116, 42–59. doi:http://dx.doi.org/10.1016/j.dsr2.2014.11.010

Villa-Alfageme, M., de Soto, F.C., Ceballos, E., Giering, S.L.C., Le Moigne, F.A.C., Henson, S., Mas, J.L., Sanders, R.J., 2016. Geographical, seasonal, and depth variation in sinking particle speeds in the North Atlantic. Geophys. Res. Lett. doi:10.1002/2016GL069233

Volk, T., Hoffert, M.I., 1985. Ocean carbon pumps: Analysis of relative strengths and efficiencies in ocean-driven atmospheric CO2 changes. American Geophysical Union, pp. 99–110.

K– RADIOCHEMISTRY AND INSTRUMENTATION

Application of modern AC system in HPGe γ-spectrometry for the detection limit lowering of the radionuclides in air filters

M. Długosz-Lisiecka[*]

Technical University of Lodz, Institute of Applied Radiation Chemistry, Wróblewskiego 15, 90-924 Łódź

Abstract

In the present study, shielding made from very low radioactivity lead, combined with air displacement by nitrogen gas inflow, have been used for the effective passive reduction of the natural background in a gamma spectrometry system. The use of the active shield as a detector, operating in anticoincidence mode with the primary HPGe detector, substantially reduced the Compton region of the spectrum. Passive and active setups provided a sensitive and effective method to quantify the trace activities of radionuclides, e.g. ^{210}Pb, ^{234}Th, ^{235}U and ^{226}Ra, present in small environmental samples. However, the size and geometry of the samples, detection efficiency control, and other issues lead to limitations in routine measurements.

Introduction

In radiochemical measurements, the desired very low detection limits can be achieved if the background level of the system is very efficiently reduced. The background spectrum of a germanium detector depends on the level of environmental gamma radiation, the radioactivity of the construction materials of the detector and its shield, the intensity of cosmic rays, and the radon content of the air (Bem et al. 2002).

HPGe detectors can identify a wide range of peaks of specific energy, while retaining good resolution. Photon detection is based on the photon's interaction with the material by the photoelectric effect, Compton scattering, and pair creation. The photoelectric effect and pair creation also play a significant role in nuclide identification. Compton scattering of γ photons in the volume of detectors leads to a high background continuum, and therefore disturbs the analyzed spectra, especially in the intermediate gamma energy range.

Absorption and self-absorption of low energy photons in the samples and a high background are the most troublesome problems in routine gamma spectrometry measurements. The first phenomenon involves the energy loss of photons in the tested samples. The attenuation cross-sections for photoelectric absorption and Compton scattering vary in relation to the effective Z^{4-5} and Z of the detector material, respectively. The degree of photon self-absorption depends on the thickness of the samples, material density, and the chemical composition of the samples.

As a result of Compton scattering, only part of the initial photon energy is absorbed within the active volume of the germanium counter. A scattered photon can escape from the germanium counter detector, and can be detected in coincidence by the surrounding scintillation counter. Therefore, when the anticoincidence settings for both detectors are used, the Compton background spectrum is greatly reduced. In the performed measurements, the detector configurations were based mainly on HPGe as the primary detector, due to its excellent energy resolution and high Z value. In general, the electronic configuration can be adjusted for coincidence and anticoincidence modes of work.

---

[*]Corresponding author, E-mail: mdlugosz@mitr.p.lodz.pl

The use of the anticoincidence system allows for significant suppression and a decrease in the detection limits of the gamma spectrometry technique. Parus (2003) reported a factor of 12 for background reduction in the regions of ^{214}Pb and ^{214}Bi radionuclide peaks. The anticoincidence mode, as the most common system, has been studied previously (Długosz-Lisiecka 2016, Długosz-Lisiecka , Bem 2013, Długosz-Lisiecka Ziomek 2014).

A careful selection of the construction materials for detectors, and the use of passive shields with a low content of uranium series nuclides, seem to be significant factors for low-level activity measurements (Dragounován and Rulík, 2013; Wershofen et al., 2008; Sivers et al., 2014). The presence of ^{222}Rn in the laboratory air can also generate additional detector background. For good quality measurements of low activity and low energy radionuclides, all these problems need to be addressed. The ^{210}Pb radionuclide, with its characteristic photon energy of 46.5 keV, frequently occurs in environmental samples. Therefore, this radionuclide seems to be the best choice for checking the influence of different counting geometries on the activity analysis. The Minimum Detectable Activity (MDA) is defined as the level of activity that results in 5 % false negatives below the decision level, and is one of several important performance measures that determine the effectiveness of spectrometric systems.

The aim of this study was to improve the Minimum Detectable Activity for natural radionuclides in low activity environmental samples, and to conduct an assessment of all restrictions to the use of the constructed anticoincidence system. The selection of construction materials, detector geometry, sample size, and other limitations were taken into account.

Materials and Methods

Samples

In these experiments three types of the air dust sample collectors with different types of the filters have been used.

A- fractionated dust samples collected on a quartz filter by means of an aerosol collector (TISCH, USA),

B- total suspended particles collected on a Petrianov filter a high volume sampler ASS-500, implemented in the national monitoring system,

C-nitrocellulose filters with fractionated dust collected by the cascade impactor (Andersen)

The air dust samplers were working with different flow-rates: 85 m^3/h; 500 m^3/h; and 0.08 m^3/h for systems A, B and C respectively, The TISCH and Petrianov filters from ASS-500 station with the average mass of solid particulate matter about 20 mg and 2 g, respectively were compressed to the cylindrical pastille forms, with diameters: 12mm and 52 mm, respectively. The filters C, from cascade impactor diameters 70 mm were measured in the thin, one disc geometry. The standard radioactivity counting time of 80 000s were sufficient to determine the activity of the chosen radionuclides even in the filters from the cascade impactor containing milligram amounts of the dust, only.

Radiometric technique

The low-level gamma spectrometry laboratory was located in the basement of a three story building. The cosmic radiation, composed of charged particles, muons and their activation products, can be shielded by the building's material and the massive lead housing. The housing was designed using 2 cm of steel and 10 cm of 'spectrometric' lead, additionally augmented with a 5 mm layer of low activity (< 6 Bqkg^{-1})^{210}Pb (Plombum, Poland), and 5 mm of high purity electrolytic copper for the attenuation of X-rays generated in the lead shielding. The selection of construction materials was made carefully, to give descending layers of decreasing natural radioactive background.

In the continuously ventilated laboratory room, the concentration of low-level ^{222}Rn and its progeny were measured. The ^{222}Rn activity measured by a SARAD EQF 3020 detector over 7 days did not exceed 30 Bqm^{-3}. In order to obtain a further decrease of the concentration of the progeny of ^{222}Rn

inside the lead shield, a gas flow system flushing its inner space with pure nitrogen gas evaporating from a Dewar vessel wasinstalled[12].

An HPGe detector (model GX3020, Canberra), with a relative efficiency equal to 30%, along with an offset preamplifier (model 2002CLS,Canberra),were used together as a basic detector.

For a more convenient sample exchange, a 9 inch NaI(Tl) crystal assembly with two movable parts was used as a guard detector. The anti-Compton veto system manufactured by SCIONIX (Netherlands) consists of a left and a right half shell and an end cap. Such a construction of the guard detector provided for the convenient replacement of samples. Each part of this unique shield contained scintillating crystal NaI(Tl) in the aluminum housing, with three 3" photomultiplier tubes (PM) for collecting scintillation light pulses, and one central PM for the end cap. All PMTs (ELT 2' – 9266 type) were coupled with the NaI(Tl) crystals via quartz light guides. Careful selection of electronic components and optimization of the system's operation are necessary steps in the design and use of the equipment (Britton et al, 2012 and 2015).The Compton Suppression system can also be used in anticoincidence and coincidence modes of work.

Results and Discussion

The comparison of the background spectra for two modes of operation of the spectrometric system, showing both normal (black color) and low-background systems (gray color), with the full passive and active shield spectrum, is shown in Fig. 1. In the Compton Suppression mode, it is evident that a higher total number of coincidence events are rejected, especially in the low-energy part of the spectrum.
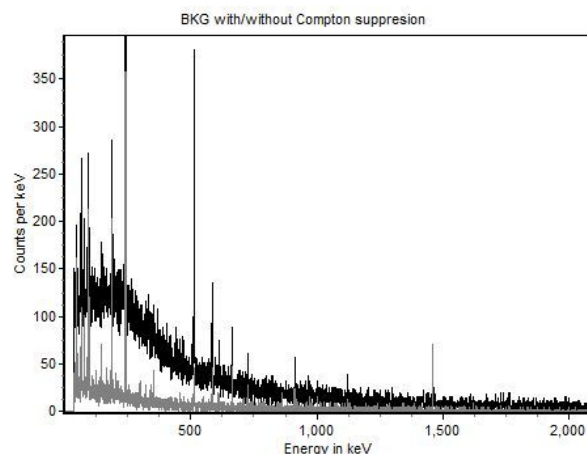
Fig. 1 Background energy spectrum (normal and Compton suppressed) recorded for 80,000 sec.

The most important reduction occurs for energies below 600 keV. For background measurement, the counting rate in this range is about 0.11 count/sec/keV. The Compton Suppression Factor (CSF), defined as Peak to Compton (P/C), the ratio for unsuppressed and suppressed spectra of the background in the region below 600keV, was equal 7.7, while in the overall range it was equal 3.7.In this study, for the ^{60}Co spectrum the CSF in region below 600 keV was 10.5 and in the total spectrum 8.1. For comparison, the CSF for the ^{60}Co spectrum noted in Fukuda's work (1996) was equal to 29.0 and 6.0keV respectively, and in Mauerhofer's work (1996) it was equal to 8.5 and 8.7 keVfor each region respectively.

The lowering of the background in Fig. 1 is primarily due to the suppression of cosmic-ray muons, especially for energies below 200 keV (Camacho et al.,2014; Duch et al., 2016). A significant reduction was achieved for short-lived[222]Rn progeny (Hurtado et al., 2006) by means of filling the interior of the lead housing with nitrogen vapor. Also, placing the spectrometer in the laboratory

with low concentrations of [222]Rn, carefully tightening the serried lead shield walls, and directing nitrogen vapor to the interior of the lead housing reduced the photo peaks of short-lived gaseous [222]Rn progeny by almost 15 times. The low background gamma spectrometry setup seems to be a perfect tool for short-lived[222]Rn progeny, [214]Pb,and also[214]Bi in air filter analyses.

For effective Compton region reduction, setting detectors close together seems to be necessary. The disadvantage of the AC system is connected with the significant reduction of the measurement volume. The air gap between both types of detectors allows measurements only for small volume samples. Geometry is probably the most important aspect of the CS system's design (Semkow et al., 2002, Radulescu et al., 2013; Khan et al., 2014; Kohler et al., 2009). Inadequate shielding or non-optimized detector material can dramatically alter the performance of the system. Various disc geometry types have been analyzed to optimize the geometry for measurements in the existing system. The diameter and thickness of the applied samples should not exceed 7.6 cm and 1 cm respectively.

Thin air-filter samples show a low self-absorption factor and sufficient yield of gamma measurements by HPGe detectors in the range of low energy photons. For all measurement geometries, the detection efficiency has been estimated on the basis of the LabSOCS application, taking into account the self-absorption correction factor and the coincidence summing correction. The MDA (Currie, 1968) values are related to the square root of the background counting rate, as is evident in equation 1. The use of passive and active methods resulted in a significant reduction of MDA for low energy photons ranging from 35 to 200 keV, emitted by the radionuclides listed in Table 1.

Table 1. Gamma energy lines and photon emission yields of ^{210}Pb, [235]U, [234]Th, [226]Ra radionuclides

Radionuclide	Energy of photons E [keV]	Y [%]
[210]Pb	46.5	4.05
[234]Th	63.3	3.82
[235]U	143.8	10.5
[226]Ra	186.3	3.28

Passive and active shields provided good quality measurement of ^{210}Pb and other specified radionuclides, even for 5 mg of fractionated dust on an air filter, or 2 grams of total dust samples, as well as for larger 30 g soil samples, using an 80,000 sec. measurement time. Use of the LabSOCS application allowed for the self-absorption correction of samples with various densities and chemical composition, however, it doesn't guarantee a correct detection efficiency estimation in the anticoincidence mode of work. Additional correction for coincidence summing in this mode of work should be done by using reference materials. An instrumental analysis of environmental samples' radioactivity, based on a single HPGe detector equipped with LabSOCS, can be a fast procedure, and the measurement does not require reference material as an external or internal standard. Modern software enables measurements of each sample in completely different geometries.

A thickness of the lead shield equal to 10 cm is sufficient for an effective background reduction by 99.5 %, even if no cosmic veto shield is used[18]. An additional increase of the passive shield's thickness, and an increase of the NaI size, had no significant influence on MDA improvement. An initial study of quantitative measurements in the anticoincidence counting mode was performed with thirteen air-filter samples with fractionated dust in 12 mm diameter disc geometry, ten samples of total dust collected on a Petrianow filter with a 51 mm diameter thin disc geometry, and soil samples

collected on a filter with a disc geometry of 55mm diameter. Table 2 presents the values of MDA calculated on the basis of equation 1 for the following low γ-energy radionuclides: [210]Pb, [235]U, [234]Th, and [226]Ra. Each sample is presented using two modes of counting: normal with the HPGe detector and using the Compton suppression system.

The MDA (Britton et al. 2015; Currie,1968; Zhang and Chatt, 2014) values, which were used as a one of the criterions are related to the square root of the background counting rate, as is evident in equation 1.

$$MDA = \frac{2.71 + 4.65 * \sqrt{N}}{t * \varepsilon_T}$$ (1)

where:

$\varepsilon_T = \varepsilon(\text{det}) \cdot \varepsilon(\gamma) \cdot \varepsilon(abs)$

t- counting time in sec – 80 000 sec.,

ε- detector efficiency,

N- counts for the background,

ε(det)- detection efficiency,

ε(γ)- efficiency of photon emission

ε(abs)- selfabsorption efficiency.

The another generally accepted criterion used for optimal choice of the detection methods is a Figure of Merit FOM parameter defined by equation 2 (Długosz-Lisiecka 2016).

$$FOM = \frac{\varepsilon_{(x)}^2}{I_{BKG(x)}}$$ (2)

The comparison of passive and active shielding methods on the MDA and FOM values for various type of air-filter samples geometry named A, B,C. is presented in the table 2.

Table 2. MDA and FOM values for ^{210}Pb, [235]U, [234]Th and [226]Ra nuclides counting in various geometries.

	sample type	Total detection efficiency AC system	MDA [mBq]		FOM at AC mode	FOM at single HPGe mode
			AC system	single HPGe detector		
[210]Pb	A	0.290	55.6	58.2	0.0972	0.0882
	B	0.256	62.9	65.8	0.0761	0.0690
	C	0.204	79.0	82.8	0.0481	0.0436
[234]Th	A	0.294	43.5	46.1	0.1649	0.1458
	B	0.270	47.3	50.1	0.1395	0.1233
	C	0.210	60.8	64.4	0.0844	0.0746
[235]U	A	0.234	10.3	11.4	3.3830	2.6938
	B	0.218	11.1	12.2	2.9314	2.3342
	C	0.173	13.9	15.4	1.8517	1.4745
[226]Ra	A	0.181	138	161	0.0154	0.0112
	B	0.161	155	180	0.0123	0.0090
	C	0.146	171	199	0.0100	0.0073

The relative MDA and FOM improvements for two modes of counting are shown in the Table 2.

As it is evident from Table 2, for A, B and C geometries the radionuclide MDA values for given radionuclide depends on the detection efficiency and the mode of the applied spectrometry system. Since particulate radionuclide detection efficiencies for both methods were basically the same, the MDA improvement for the AC system is a result of background reduction and it is constant for all three geometries.

The observed values of relatively the improvement in FOM values changed from 10 to 37% and depended on the energy of the gamma radiation.

It should be underlined that even small relative improvement in ^{210}Pb counting in AC mode is important for single filter measurements C geometry, where total mass of the collected dust is in the order of single mg and observed ^{210}Pb activities are extremely low. These two methods of counting were used for checking of the their accuracies for artificially deposited Standard Reference Materials (SRM's) on the filters.

As the most convenient standard reference materials for environmental analysis purposes the IAEA Soil-327 and IAEA Phosphogypsum-434 reference materials were chosen.

The instrumental analysis of such prepared experimental samples, for a single HPGe detector equipped where based on the LabSOCS software. It is a fast procedure, and the measurement does not require reference material as an external or internal standard (19,21). Use of the LabSOCS application allowed for the self-absorption correction of samples with various densities and chemical composition, however, it doesn't guarantee a correct detection efficiency estimation in the anticoincidence mode of work. In case of possible gamma coincidences discrimination use of a set reference materials or simulation methods (GEANT4 Monte-Carlo calculations software) is required.

The disadvantages of Compton suppression systems are limitation in sample size (limited by the internal and external size of the guard detector), and as a result a reduction in the types of materials that can be measured by this unique spectrometry system.

Detection efficiency reduction, which is the result of coincidence photons' discrimination. The problem seems to be serious for radioactive sources with a complex decay scheme in a cascade series, which has been considered elsewhere

As a result of detection efficiency reduction, for proper activity measurement external reference materials (calibration sources) are necessary. The LabSOCS software applied for detection efficiency does not guarantee correct results of activity for all measured radionuclides.

Because of the background count rate being proportional to detector size, smaller detectors are preferable for low activity measurement, typical for environmental samples. On the other hand, larger detectors provide better detection efficiency.

Smaller samples are counted more efficiently, but the need for coincidence summing correction is more probable for them

All the limitations are a result of a unique spectrometry system using highly specialized equipment. Improving the limit of detection is associated with a number of difficulties for the user. Buying an HPGe detector with a higher detection efficiency can probably give a similar improvement in the quality of measurement, without the effect of limiting the system's applications[26]

Conclusions

Special care should be taken for analysis low-energy gamma emitters such as ^{210}Pb ^{235}U, ^{234}Th, and ^{226}Ra by gamma spectrometry system. A comparison of the results obtained with the single HPGe detector spectrometer and the gamma anticoincidence counting mode of the spectrometer show

improved capabilities for detecting the low energy of natural radionuclides in air filters. AC mode provides from 5 to 16% of improvement for MDA and from 10 to even 37% for FOM coefficient. For a suitable determination of a low-energy natural radionuclides as ^{210}Pb, ^{235}U, ^{234}Th, and ^{226}Ra in air filters the use of a calibration standards is necessary.

References

Bem, H., Bem E.M., Krzemińska M., Ostrowska M., 2002. Determination of radioactivity in air filters by alpha and gamma spectrometry, Nukleonika 47, 2, 87–91.

Britton, R., 2012. Compton suppression systems for environmental radiological analysis, J. Radioanal. Nucl. Chem. 292; 33–39.

Britton, R., Davies, A.V., Burnett, J.L., Jackson, M.J., 2015. A high-efficiency HPGe coincidence system for environmental analysis, Journal of Environmental Radioactivity 146, 1-5.

Camacho, A., Laubenstein, M., Vargas, A., Serrano, I., Vallés, I., Plastino, W., Duch M.A. 2014. Validation of aerosol low-level activities by comparison with a deep underground laboratory Applied Radiation and Isotopes 87, 66–69

Currie, L., 1968. Limits for qualitative detection and quantification determination. Analytical Chemistry 40, 3, 587-593.

Długosz-Lisiecka, M., 2016. Comparison of two spectrometric counting modes for fast analysis of selected radionuclides activity, Journal of Radioanalytical and Nuclear Chemistry, J Radioanal Nucl Chem. 309, 941–945.

Długosz-Lisiecka, M. and Ziomek, M., 2015. Direct determination of radionuclides in building materials with self-absorption correction for the 63 and 186 keV γ-energy lines, Journal of Environmental Radioactivity, 150; 01; 44-48.

Długosz-Lisiecka, M. and Bem, H., 2013. Fast procedure for self-absorption correction for low γ energy radionuclide 210Pb determination in solid environmental samples. J Radioanal Nucl Chem, 298; 495–499.

Dragounován, L. and Rulík, P., 2013. Low level activity determination by means of gamma spectrometry with respect to the natural background fluctuation, Applied Radiation and Isotopes 81, 123–127.

Duch, M.A., Serrano, I., Cabello, V., Camacho, A. 2016. Comparison of different sampling methods for the determination of low-level radionuclides in air Applied Radiation and Isotopes, 109, 456–459.

Fukuda, K., Ohkuma, J., Asano, T., Satoh, Y., 1996. Performance of a Ge-BGO Comptonsuppression spectrometer and its application to photon activation analysis, Nuclear Instruments and Methods in Physics Research Section B: Beam Interactions with Materials and Atoms, 114, 3–4, 1, 379-386.

Hurtado, S., García-Leon, M., García-Tenorio, R., 2006. Optimized background reduction in low-level gamma-ray spectrometry at a surface laboratory, Applied Radiation and Isotopes 6; 1006–1012.

Khan, A.J., Semkow, T.M., Beach, S.E., Haines, D.K., Bradt, C.J., Bari, A., Syed, U.F., Torres, Marrantino, J., Kitto, M.E., Menia, T., Fielman, E. 2014. Application of low background gamma-ray spectrometry to monitor radioactivity in the environment and food, Applied Radiation and Isotopes 90; 251–257.

Kohler, M.., Degering, D., Laubenstein, M,Quirin, P, Lampert M.O., Hult, M., Arnold, D., Neumaiere, S., Reyss, J.L. 2009. A new low-level g-ray spectrometry system for environmental radioactivity at the underground laboratory Felsenkeller, Applied Radiation and Isotopes 67; 736–740.

Mauerhofer, E., Tharun, U., Denschlag, H.O., Schmidt, R., Kratz, J.V. 1996. A Compton suppression spectrometer for neutron activation analysis, Nuclear Instruments and Methods in Physics Research A 371;465-471.

Parus, J., Kierzek, J., Raab, W., Donohue, D. 2003. A dual purpose Compton suppression spectrometer, J Radioanal. Nucl. Chem., 258, 123–13.

Radulescu, I., Blebea-Apostu, A.M., Margineanu, R.M., Mocanu, N. 2013. Background radiation reduction for a high-resolution gamma-ray spectrometer used for environmental radioactivity measurements, Nuclear Instruments and Methods in Physics Research A: 1, 112–118.

Semkow, T.M., Parekh, P.P., Schwenker, C.D., Khan, A.J., Bari, A., Colaresi, J.F., Tench, O.K., David, G., Guryn, W., 2002. Low-background gamma spectrometry for environmental radioactivity, Applied Radiation and Isotopes 57; 213–223.

Sivers, M., Hofmann, M., Mannel, T., Feilitzsch, F., Oberauer, L., Potzel, W., Schönert, S. 2014. Low-level γ-ray spectrometry at the underground laboratory Garching, Applied Radiation and Isotopes 91, 49–56.

Wershofen, H., Bieringer, J., Frenzel, S., Kanisch, G., Katzlberger, C., Steinkopff, Th., Tschiersch, J., Volke, H., 2008. An inter-laboratory comparison of low-level measurements in ground-level aerosol monitoring, Applied Radiation and Isotopes 66, 737–741.

Zhang, W., Chatt, A., 2014. Anticoincidence counting further improves detection limits of short-lived products by pseudo-cyclic instrumental neutron activation analysis. Journal of Radioanalytical and Nuclear Chemistry 302, 3, 1201 – 1211.

Acknowledgements

Fully automated system for monitoring ^{99}Tc in radioactive residues using a selective resin and UV-Vis on-line detection

Marina Villar[1], Antoni Borràs[2], Fernando Vega[1],
Víctor Cerdà[3], Laura Ferrer[2]*

[1]*Radiopharmacy Service, Son Espases Hospital, Cra. Valldemossa 79, 07120 Palma de Mallorca, Spain.*
[2]*Laboratory of Environmental Radioactivity - LaboRA, University of Balearic Islands Cra.Valldemossa km 7.5, 07122 Palma de Mallorca, Spain.*
[3]*Laboratory of Environmental Analytical Chemistry – LQA, University of the Balearic Islands, Cra.Valldemossa km 7.5, 07122 Palma de Mallorca, Spain.*
corresponding author: laura.ferrer@uib.es

ABSTRACT

^{99}Tc is an artificial beta emitter, widely used in nuclear medicine for diagnostic tests, which has created great concern because of its long half-life (2.111×10^5 years) and its distribution in the environment. In order to help with the management of hospital residues, an automated and rapid system for monitoring ^{99}Tc was developed. Combination of flow analysis techniques, i.e. Lab-on-valve (LOV) and multisyringe flow injection analysis (MSFIA), with a selective resin (WBEC-resin) enables the analysis to be performed in a short time, achieving high selectivity and sensitivity levels. After elution with NH_4OH 3 mol L^{-1}, ^{99}Tc is derivatized with 1,5-diphenylcarbohydrazide (DPC) and finally detected by a miniaturized fiber optic CCD spectrophotometer at 520 nm, exploiting a long path-length liquid waveguide capillary cell (LWCC) of 100 cm path length. The proposed method was optimized by experimental design, achieving a LOD of 4 ng of ^{99}Tc (2.5 Bq), a reproducibility of 6%, and a resin durability of 80 injections. The microcolumn allows to preconcentrate up to 100 mL of sample without deteriorate the analytical signal. The automated system was successfully applied to hospital residues, attaining recoveries between 90-98%.

Keywords: ^{99}Tc; hospital residues; flow techniques; spectrophotometric detection.

1. INTRODUCTION

Technetium is an artificial radioactive element, in fact the first element to be produced artificially [1]. ^{99m}Tc is used in nuclear medicine for a wide variety of diagnostic tests because of its short half-life, the low γ-ray energy it emits, and its stability to chemically bind to many active biomolecules. ^{99m}Tc decays to ^{99}Tc which is a pure β-emitter (βmax= 294 keV). ^{99}Tc is considered a very important dose contributor in environmental risk assessment because of its long half-life, high abundance and high mobility [1,2]. In recent years, the use of ^{99m}Tc for medicinal purposes as a diagnostic tool has considerably increased and consequently the waste generation of ^{99}Tc.

In order to perform the ^{99}Tc monitoring, hospitals either estimate ^{99}Tc activities through calculations or perform tedious manual analytical protocols usually using liquid scintillation detection, which implies time-consuming in giving results to make the radioactive residue management. To help with the ^{99}Tc monitoring, we have developed a fully automated system, which is able to monitor very low levels of ^{99}Tc in residues samples in a simple a fast way. The proposed system incorporates the extraction and pre-concentration of ^{99}Tc from matrix sample, the derivatization to form a colored

complex, until the online UV-Vis detection. All these steps are possible thanks to the hyphenation of flow analysis techniques, a selective resin and a long path-length liquid waveguide capillary cell (LWCC) connected with a miniaturized spectrophotometer.

Flow analysis techniques have allowed the automation of a huge number of analytical protocols, providing the partial or complete automation of the analytical methods leading to simplicity, reliability, significant decrease in time of analysis, reduction of sample and reagent consumption, and minimal handling of samples and standards, improving the safety of the analyst [3]. Particularly, in the radiochemical field various methodologies dedicated to determine specific radionuclides or screening tests to find radioactive elements were automated [4].

Thus, the main objective of this work is to develop a fully automated system for monitoring ^{99}Tc in a simple and fast way to become a sensitive and inexpensive tool for helping in the management of radioactive residues.

2. EXPERIMENTAL

2.1. Reagents and equipment

All solutions were prepared from analytical grade reagents (HNO$_3$ 60%, H$_2$O$_2$ 30%, H$_2$SO$_4$ 96%, acetonitrile (AcN), ammonia solution 25%, 1,5-diphenylcarbohydrazide) with Milli-Q water. Besides, WBEC resin 50–100 μm (Triskem International, France)and glass fiber prefilters from Millipore were used.

The Radiopharmacy Service of the Son Espases Hospital receives weekly a ^{99}Mo/^{99m}Tc generator (Ultra-Technekow™ DTE- Technetium ^{99m}Tc Generator of Mallinckrodt), in order to assume the programmed explorations. The arrival day, a resulting vial of 5 mL with an average activity of 77.7 GBq, from the elution of the generator, was kept aside during a month to be sure that all ^{99m}Tc had decayed into its daughter ^{99}Tc. Previously to the decay process, the eluates from generator were measured by a dose calibrator, Capintec CRC-25R, to ensure the activity content, and it were taken as working standard solutions. These solutions were prepared by dilution in 0.1 mol L^{-1} HNO$_3$.

2.2. Samples

Nuclear Medicine residues. Liquid residues from Nuclear Medicine Service of Son Espases Hospital are collected into three-leaded container of 35 hectolitres until its activities decays below the exemption value which means that this radioactivity is negligible. These residues are composed by urine of the treated patients and cleaning water from the Radiopharmacy area, which not always contains radioactivity.

Laboratory waste. Radiopharmacy laboratory of Son Espases Hospital has a waste drum for discarding all non-radioactive solvents and solutions with decayed radioisotopes.

Technegas filter. Technegas Generator is able to heat up to 2550°C under ultrapure argon in the presence of ^{99m}TcO$_4$Na producing an aerosol of carbon microparticles labeled to ^{99m}Tc called Technegas[5]. Then, the patients inhale these particles to carry out a study that provides information about the pulmonar perfusion quality of the patient The cotton filter captures the exhaled Technegas so, after it decays, ^{99}Tc is supposed to be there in a high concentration because each filter is use for approximately fifty times before replacing it. To extract ^{99}Tc from the filters, they were submerged in 0.1 mol L^{-1} HNO$_3$for 21 hours.

All final solutions have a HNO$_3$ concentration of 0.1 mol L^{-1}. When oxidation to Tc(VII) was necessary, 6% (v/v) of H$_2$O$_2$ 30% was added.

2.3. Manifold and software

The LOV-MSFIA system is shown in Figure 1. The LOV microconduit (Sciware Systems, Bunyola, Spain), fabricated from methacrylate encompassing ten integrated microchannels was mounted atop of an ten-port multiposition selection valve (SV) (Multiburette 4S; Crison Instruments, Spain). The central port of the LOV unit connects to the syringe pump, via a holding coil, in order to address the liquids toward the peripheral ports of the unit (1–10), through the sequential aspiration mode. The flow network was constructed with 0.8 mm i.d. PTFE tubing, except for the holding coil (HC) connected to the LOV, which was constructed with 1.5 mm i.d. PTFE tubing. All connections were made by means of polyvinylidene fluoride (PVDF) connectors, except cross-junctions, which were made of methacrylate.

The detection system is composed of a deuterium–halogen light source (Mikropack, Germany), two optical fibers of 600 μm i.d. (Ocean Optics, USA), a flow cell made from type II Teflon AF long path-length liquid core waveguide capillary cell (World Precision Instruments, FL, USA) (internal diameter 550 μm, effective path length 100.0±0.5 cm, internal volume 240 μL), and a USB 2000 miniaturized optical fiber spectrometer (Ocean Optics), connected to a computer via an USB interface. The absorbance was measured at 520 nm.

Instrumental control, data acquisition and processing were performed using the software package AutoAnalysis 5.0 (Sciware Systems). The distinguished feature of this software based on dynamic link libraries (DLLs) at 32 bits is the viability to use a single and versatile application without further modification for whatever instrumentation and detection system needed. It involves a basic protocol, which allows the implementation of specific and individual DLLs attending the configuration of the assembled flow analyser.
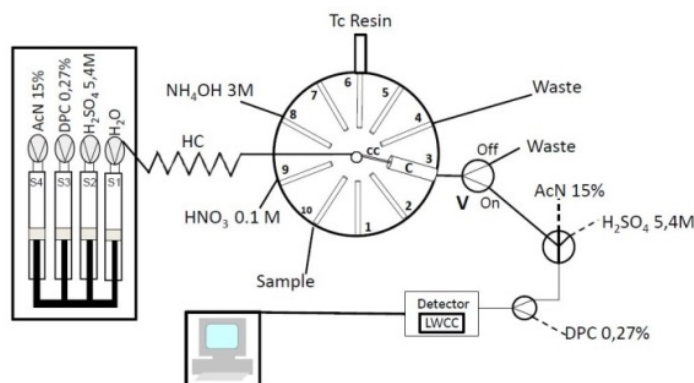
Figure 1. *Diagram of LOV-MSFIA system for ^{99}Tc on-line spectrophotometric determination. C: connector; CC: central conduit; HC: holding coil; LOV: lab-on-valve; LWCC: long wave capillary cell; RC: reaction coil; V: solenoid valve.*

2.4. Analytical procedure

Briefly, at a first step, the resin is loaded into channel 3 of the LOV that serves as microcolumn and then it is conditioned prior the sample loading. Afterwards, sample solution in a final HNO$_3$ concentration of 0.1 mol L^{-1} is passed through the column. Then, ^{99}Tc is eluted in a basic medium, which must be subsequently acidified with H$_2$SO$_4$ in order to form the ^{99}Tc–DPC complex. Since the kinetic reaction is slow, and to achieve a good sensitivity, a 5 min wait was necessary. Finally, the complex is sent to UV-Vis detector propelled by AcN. The microcolumn was rinsed with water after each elution in order to ensure the ^{99}Tc retention in the next run by avoiding any trace of eluent on it. Likewise, the LWCC was cleaned with AcN 15% (v/v) between samples.

3. RESULTS AND DISCUSSION

3.1. Optimization of system-variables

WBEC resin was selected to extract and preconcentrate ^{99}Tc because it is able to separate Tc, Pu and to a certain extent of tetravalent actinides, being its selectivity similar to TEVA resin. According to the manufacturer recommendation, Tc is eluted with 1 mol L^{-1} NH$_4$OH allowing a high degree of Tc selectivity [6].

The elution process from WBEC resin was studied in a multivariate approach. First, a screening test of volume (range: 0.5 – 1 mL) and concentration (range: 1 – 4 mol L^{-1}) of NH$_4$OH was made indicating that both variables are significant and also its interaction. Thus, a Central Composite Design was carried out varying the ammonia concentration and volume to obtain optimized values.

The derivatization conditions were optimized in a multivariate approach. First, a screening of H$_2$SO$_4$ concentration (range: 3 – 5 mol L^{-1}) required to develop the reaction between Tc and DPC, and concentration of DPC (range: 0.1 – 0.5 %) was made. The obtained results, i.e. ANOVA table, Pareto chart and predicted vs observed values, indicated that both variables affected significantly the reaction of derivatization. Therefore, a Doehlert design was carried out taking into account the screening results, i.e. since the DPC concentration had an effect more higher than H$_2$SO$_4$ concentration, experimental matrix was constructed with 5 and 3 levels, respectively.

Optimal values as are listed in Table 1.

Table 1. *Optimized values.*

Variable	Optimized values
Eluent concentration, NH$_4$OH	3 mol L^{-1}
Eluent volume, NH$_4$OH	0.65 mL
DPC concentration	0.27 %
H$_2$SO$_4$ concentration	5.4 mol L^{-1}
Reaction time	5 min

3.2. Analytical parameters

Mass calibration curves (net absorbance versus mass in ng of Tc(VII)), with a statistically satisfactory fit were obtained (y = 0.0015±0.0001x - 0.011±0.003, r²=0.9962, n=5). Under optimum conditions described above, calibration curves are linear over the concentration range 0–500 ng Tc(VII).

The limit of detection calculated from three times thestandard deviation of ten replicates of the blank divided bythe slope of the calibration curve, resulted of 4.1 ng (2.5 Bq).

Durability and repeatability parameters are related and both report the number of consecutive analyses feasible without changing the column packing. Thus, the repeatability of 6.0% expressed as RSD (n=10) was obtained. A durability up to 78 consecutive extractions, giving recoveries about 98%, was observed, which allow the reduction of cost per analysis.

The reproducibility was also evaluated during five different working days, changing the column packing and using the same Tc-working standard solution, giving 6.1% expressed as RSD (n=5).

Analytical parameters are summarized in Table 2.

Table 2.*Analytical parameters.*

Analytical parameter	Value
Detection Limit (ng)	4.1
Quantification Limit (ng)	13.5
Regression Coefficient (r^2)	0.9914
Repeatability (%) (n=10)	6.0
Reproducibility (%) (n=5)	6.1
Resin durability (injections)	78
Pre-concentration volume (mL)	Up to 100
Extraction frequency (h^{-1})*	4 – 9
Linear working range (ng)	0–500

*depending on the sample volume to pre-concentrate.

3.3. Application to real samples

This method was evaluated by analysing different residues samples. Excepting the Technegas filter sample, the rest of samples contained not only technetium, since they are very complex matrices that were taken in hospital waste-containers. Therefore, by using a selective resin the analyte of interest is isolated prior detection avoiding interferences and at the same time pre-concentrated. All samples were spiked with known ^{99}Tc activities. Results have shown good recoveries, between 90-98% (Table 3).

Table 3.[99]*Tc determination by a fully automated system applied to hospital residues samples (n=3).*

Sample	Add (ng)	Found (ng)	Recovery (%)
Nuclear Medicine liquid residues	0	281 ± 1	--
	328	575 ± 17	90
Laboratory waste	0	76 ± 1	--
	183	255 ± 3	98
Technegas filter	0	15 ± 2	--
	142	145 ± 9	91

4. CONCLUSIONS

The hyphenation of two multicommuted flow analysis techniques, i.e. Lab-on-valve (LOV) and multisyringe flow injection analysis (MSFIA), has allowed the development of analytical system to monitoring ^{99}Tc in complex matrix samples with a high degree of automation. The fully automated system is capable to carry out all analytical steps of extraction, preconcentration, elution, adjust the acidity, detection,

renewal of the microcolumn, system cleaning and data acquisition and processing. The advantages reached by the proposed system, compared with other systems to determine ^{99}Tc, are: the short time-response which allows a fast management of the residues; a good selectivity due to the use of selective resin that ensure the results obtained with a non-selective detector; a good sensitivity thanks to the pre-concentration step and the employ of a long path-length liquid waveguide capillary cell (LWCC) which allows to determine above 4.1 ng of ^{99}Tc (2.5 Bq) enough to make a responsible waste management; a good reproducibility due to the automatic packing of the microcolumn and the precision of the flow techniques used; the low cost of implementation and use of the system thanks to the decrease in reagents volumes and the use of a CCD spectrophotometer as detector; the compactness and miniaturization of the system that allows its assembly in a little place, near the waste warehouses; and finally the full automation that ensures the minimization of handling by the analyst and increases their safety. All these characteristics make the proposed system a very good tool to monitor ^{99}Tc in radioactive residues.

Acknowledgements

References

[1] Hu, Q. Wiley & Sons, 2010, pp 217-224.
[2] Shi, K. et al., 2012.
[3] Cerdà, V. et al., 2014.
[4] Fajardo, Y. et al., 2010.
[5] Data sheet of PULMOTEC^{TM}.Spanish Drugs Agency.
[6] Triskem International. WBEC resin product sheet (Last access November 2016). http://www.triskem.com/iso_album/ft_resine_wbec_en_151210.pdf

Study of the dynamic lixiviation of ^{226}Ra from phosphogypsum by an automatic system previous radiometric detection

Melisa Rodas Ceballos[1], Antoni Borràs[1], R. García-Tenorio[2], José Manuel Estela[3], Víctor Cerdà[3], Laura Ferrer[1]*,

[1]Environmental Radioactivity Laboratory (LaboRA), University of the Balearic Islands, 07122 Palma de Mallorca, Spain.
[2] Department of Applied Physics, University of Seville, ETSA, Av. Reina Mercedes 2, 41012 Seville, Spain.
[3] Environmental Analytical Chemistry Laboratory (LQA2), University of the Balearic Islands, 07122 Palma de Mallorca, Spain.

Abstract

The phosphogypsum (PG) is a by-product from phosphate fertilizer industry, it is produced in large amount, and contains naturally radionuclides, principally ^{226}Ra and these decay products. The lixiviation study of the radionuclides from PG has great industrial and environmental importance due to the reutilization possibilities. A study of dynamic lixiviation of ^{226}Ra in PG samples was carried out with an automatic system composed by a lab-on-valve and multisyringe flow injection analysis. Artificial rainwater at two different pH (5.4±0.2 and 2.0±0.2), was used as leaching agent. The PG sample was placed in a designed column, and the leaching agent passed through the column at a flow rate of 3.5 mL min^{-1}.Eightleaching fraction of 30 mL each one were recollected. Each leaching fraction was analyzed in an automatic system for the extraction/pre-concentration of ^{226}Ra, which is absorbed on manganese dioxide formed on cellulose beads. Then, ^{226}Ra is eluted with hydroxylamine and finally co-precipitated with barium sulfate. The ^{226}Ra activity was measured with a low background proportional counter. The specific activities of the leaching are between 28 and 12 Bq Kg^{-1} from artificial rainwater at pH 2, and in the range of 16 and 10 Bq Kg^{-1} at pH 5.4. The sum of eight fractions reached up to 52% of the total ^{226}Ra content in the PG sample, which is to highlight considering that re-absorption processes not occur in dynamic lixiviation. This methodology was validated by analyzing a PG reference material (MatControl CSN-CIEMAT 2008).

Introduction

The phosphogypsum (PG) is produced in large amount through acid phosphoric production by the wet process (Aguado et al., 2005; Haridasan et al., 2002) The PG contains natural radionuclides, mainly ^{226}Raand its decay products (Al-Hwaiti et al., 2010; Gázquez et al., 2009). After the wet process, between 80-90% originally present in phosphate rock stays in PG (Aguado et al., 2005; Bolívar et al., 1998; EPA, 1992). Much of the PG produced is stored in stockpiles exposed to meteorological process (Villa et al., 2009) causing damage to the environment.^{226}Ra is alpha emitter with a long half-life (1600 y), that increase its environmental control (Atwood, 2010). ^{226}Ra activity in PG varies if the sample is collected in different basins within the same geographic area and if collected at different points within the same raft (EPA, 1992).The study of radionuclide leaching from PG is of great environmental and industrial importance because of their reusability. The leaching of ^{226}Ra from PG has been studied mainly in a static approach, i.e. using a large amount of sample and leaching agent, and maintaining the contact time between the sample and the leaching agent for a long time (Aguado and Bolívar, 1999; Aguado et al., 2005; Azouazi et al., 2001; Haridasan et al., 2002; May and Sweeney, 1984). The conventional method of lixiviation has some limitations, including the ^{226}Ra reabsorption which can be up to 89%of the leaching content (May and Sweeney, 1984). To solve these inconvenient, a dynamic lixiviation of ^{226}Ra exploiting flow

---

analysis techniques is proposed. Continuous leaching agent flow through the sample allows the constant renewal of leaching agent, disfavoring the reabsorption process by continuously varying the equilibrium liquid-solid (Bacon and Davidson, 2008). The combination of the multysiringe flow technique analysis (MSFIA) (Cerdà et al., 1999) and lab-on-valve (LOV) (Ruzicka, 2000)combines the advantages of both techniques in one system.The main objective of this work is the evaluation of dynamic lixiviation of [226]Ra in PG samples, using artificial rainwater as leaching agent by an automatic system (MSFIA-LOV) previous radiometric detection.

Materials and Methods

Samples
PG samples were obtained from inactive deposits from Fertiberia in Huelva, Spain. The PG reference sample material MatControl CSN-CIEMAT 2008 was used to validate the proposed methodology. The samples were dried at 55±5ºC, until constant weight. The digestion of the PG samples and the residual fraction was carried out with 10 mL of HNO_3 (69%) in a microwave (Multiwave Go, Anton Paar) following the EPA 3052 method. After the digestion process, the HNO_3 concentrated was evaporated to dryness and the residual was diluted in 25 mL with Milli-Q water, finally the solution was filtered through a 0.45 µm filter and the pH was adjusted to 7.0±0.5.

Analytical procedure
The leaching, extraction and pre-concentration of [226]Ra was carried out with an MSFIA-LOV system presented in Figure 1.
1) PG sample was placed in the leaching column and 30 mL of artificial rainwater passed through the column. 0.22 mol L^{-1}NaOHwas dispensed to the PG leaching recollected, adjusting the pH at 7.0±0.5. The leaching was stirred for its homogenization.
2) Macroporous bead cellulose (MBC) column (port 8) was conditioned with hot deionized water (70ºC). Subsequently, $KMnO_4$ was dispensed on MBC column, keeping the contact for 2 min to help the formation of MnO_2.The sample was loaded into the MBC column at 1.5 mL min^{-1}.
3) Elution of [226]Ra was performed by dispensing$NH_2OH·HCl$ through the MBC column. Then,[226]Ra was co-precipitated with Na_2SO_4 and acetate/Ba^{+2} buffer. A wait of 30 minutes was necessary for the formation of $Ba(Ra)SO_4$.
4) The MBC column was automatically regenerated replacing the old beads by new ones, which are on the reservoir (port 4) in 20:80 methanol:water (v/v).
5) Finally, [226]Ra co-precipitated formed was filtered through a 0.22 µm nylon filter and was dried to dryness on a steel planchette under the infrared lamp. The alpha activity of each sample was determined in a low background proportional counter Canberra LB4200.

Results and Discussion

Optimization of the experimental conditions
The optimization of the PG leaching variables were studied by a multivariate approach. The independent factors were: PG sample weight and the leaching flow rate. A full factorial design 2^2 was performed into the range 200-600 mg of sample and 2 – 5mL min^{-1} flow rate. The range of the sample weight was according to the quantity of PG packed into the cell, without causing an impediment in the flow during the leaching process. The results (ANOVA table, Pareto chart) indicate that variables have not shown significant effects into the experimental domain studied, with 95% of confidence level. The central point of assays (0.400 mg and 3.5 mL min^{-1}) were used in further assays, since the results shown the lower RSD.
The optimal pH value of the sample, e.g. leached fraction, residual fraction and entire sample, to introduce in the extraction/pre-concentration manifold was studied between pH 6 – 8. The best

results were obtained between pH 6.5 to 7.5. The automatic system for extraction and pre-concentration of ^{226}Ra had been previously optimized (Rodríguez et al., 2016).

Validation of the method
The validation of the method was performed with a PG reference sample material (MatControl CSN-CIEMAT 2008). Eight fractions of 30 mL of artificial rainwater at pH 2.0±0.2 were analyzed. After the lixiviation process, the residual fraction was dried at 55±5ºC until constant weight. Finally, the digestion process was performed on the residual fraction and total sample. The results were validated with the z-score value, being satisfactory with a z-score less than 2 (Table 1).

^{226}Ra dynamic lixiviation in PG samples
The studied of the dynamic leaching of ^{226}Ra was carried out with artificial rainwater at pH 5.4±0.2 as leaching agent, and also with a pH 2.0±0.2 in order to study the behavior of the radium release in an acid medium (Table 2). Eight leaching fractions were analyzed, because the ninth fraction overlapped with the minimum detectable activity (MDA, 7 Bq Kg^{-1}) (Figure 2).Using artificial rainwater at pH 5.4, the released ^{226}Ra reached 37%, which is higher than those obtained in static studies. Between 0.24–16% of the ^{226}Ra total content in PG sample was lixiviated in static conditions (Aguado and Bolívar, 1999; Aguado et al., 2005). A 24% of lixiviation was the higher release achieved with 24 h contact time (Haridasan et al., 2002).For assays with artificial rainwater at pH 2.0, the released ^{226}Ra reached up to 50% of the total content in PG sample. These higher ^{226}Ra contents in the leached fractions, both in the dynamic vs. static processes and using a more acidic extractant, are due to direct dependence on the leaching conditions such as pH of the extractant and the contact time between sample and extractant (Haridasan et al., 2002). In this sense, in the dynamic approach, the contact time between the sample and the extractant is given by the lixiviation flow rate used. In this work, taking into account the cell capacity and the flow rate of 3.5 ml min^{-1}, the contact time is of 9 min since the agent enters the cell until it leaves. Thus, it can be considered that the leaching agent is renewed constantly and the equilibrium is displaced to benefit the extraction. In addition to the leaching process itself, ^{226}Ra determined in each fraction partially comes from the dissolution of PG. In order to quantify such contribution, the remanent sample together with the filters that help to contain it into the cell, were dried in oven at 55ºC up to constant weight after each lixiviation cycle, and weighted. Results indicate that PG solubility reaches between 18–20%, in accordance with previously reported values(Aguado et al., 2005; Haridasan et al., 2002; Rutherford, P. M., Dudas, M. J., Arocena, 1995).

Conclusions

- A dynamic lixiviation of ^{226}Ra was carry out in PG samples through an automatic system, including the lixiviation, and extraction/pre-concentration steps.
- Up to 37% of the total of ^{226}Ra was leached using artificial rainwater as leaching agent at pH 5.4. Meanwhile, a 50% of the total content of ^{226}Ra present in the PG samples was leached at pH2.0.
- Dynamic leaching avoids reabsorption process of ^{226}Ra in the PG.
- Between an 18-20% of PG is dissolved at the end of the leaching process.
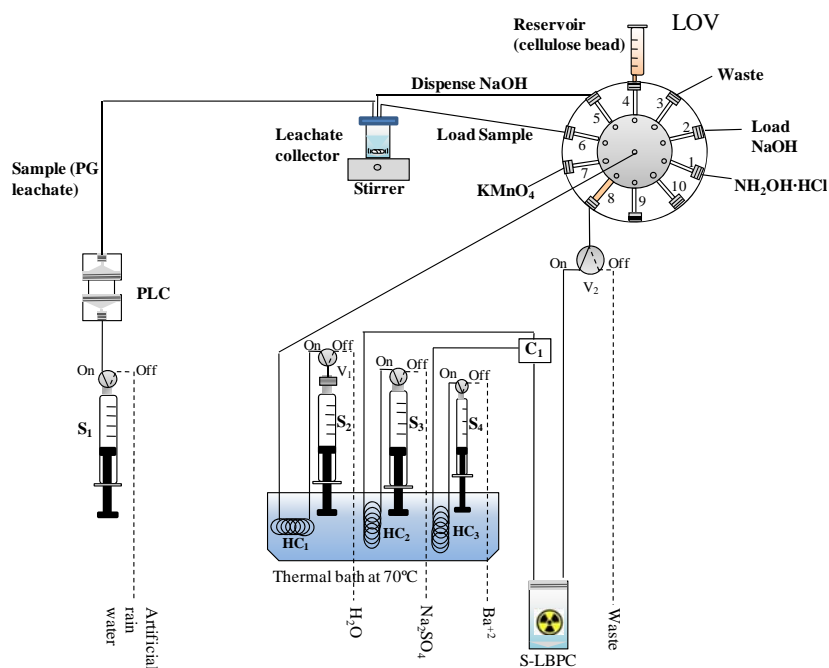
Figure 1. *Automatic system for the dynamic leaching, extraction/ pre-concentration and co-precipitation of ^{226}Ra from PG samples. C: Three-way connector, HC: holding coil, LOV: Lab-on-valve; MSFIA: multisyringe module, PLC: phosphogypsum lixiviation column, S: syringe, V: external solenoid valve.*
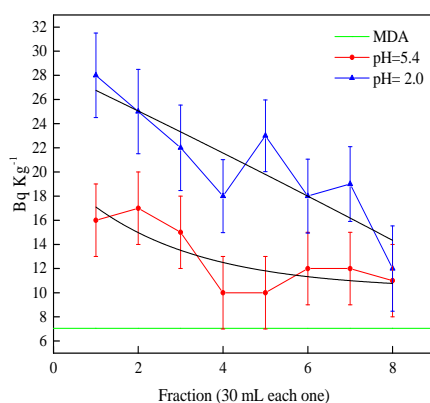
Figure 2. *^{226}Ra specific activiy for leached fractions with artificial rainwater. The results are expressed as weighted average ± uncertainly (n=3).*

Table 1. *Validation results of reference PG material (MatControl CSN-CIEMAT 2008).*

	Specific activity (Bq Kg^{-1}d.w.)	^{226}Ra (%)	Z-score
$\sum_{F=1}^{8}$ F (sum of leached fractions)	295±14	52	
Residual fraction	276±13	48	
Sum of fractions (leached+ residual)	571±14	100	-0.03
Total digestion	585±8		0.13
Reference value	573±115		--

4

Table 2. *Specific activity of [226]Ra in the leached fractions and the residual fraction in samples of phosphogypsum, using artificial rainwater as extracting agent at pH 5.4 and 2.0.*

	pH5.4±0.2		pH2.0±0.2	
	Specific activity (Bq Kg^{-1}d.w.)	[226]Ra (%)	Specific activity (Bq Kg^{-1}d.w.)	[226]Ra (%)
Fraction 1	16±3	6	28±4	9
Fraction 2	17±3	6	25±3	7
Fraction 3	15±3	5	22±3	5
Fraction 4	10±3	4	18±3	5
Fraction 5	10±3	4	23±3	9
Fraction 6	12±3	4	18±3	6
Fraction 7	12±3	4	19±3	4
Fraction 8	11±3	4	12±3	3
$\sum_{F=1}^{8} F$ (sum of leached fractions)	104±3	37	166±3	50
Residual fraction	177±36	63	163±18	50
Sum of fractions (leached+ residual)	280±25	100	329±13	100

References

Aguado, J.L., Bolívar, J.P., 1999. 226 Ra determination in phosphogypsum by alpha-particle spectrometry. Czechoslov. J. Phys. 49, 439–444.

Aguado, J.L., Bolívar, J.P., San Miguel, E.G., García-Tenorio, R., 2005. Ra and U isotopes determination in phosphogypsum leachates by alpha-particle spectrometry. Radioact. Environ. 7, 160–165.

Al-Hwaiti, M.S., Ranville, J.F., Ross, P.E., 2010. Bioavailability and mobility of trace metals in phosphogypsum from Aqaba and Eshidiya, Jordan. Chemie der Erde - Geochemistry 70, 283–291.

Atwood, D.A., 2010. Radionuclides in the environment, First edit. ed. Chichester, West Sussex, United Kingdom.

Azouazi, M., Ouahidi, Y., Fakhi, S., Andres, Y., Abbe, J., Benmansour, M., 2001. Natural radioactivity in phosphates, phosphogypsum and natural waters in Morocco. J. Environ. Radioact. 54, 231–42.

Bacon, J.R., Davidson, C.M., 2008. Is there a future for sequential chemical extraction? Analyst 133, 25–46.

Bolívar, J.P., García-Tenorio, R., Mas, J., 1998. Radioactivity of Phosphogypsum in the South-West of Spain. Radiat. Prot. Dosimetry 76, 185–189.

Cerdà, V., Estela, J.., Forteza, R., Cladera, A., Becerra, E., Altimira, P., Sitjar, P., 1999. Flow techniques in water analysis. Talanta 50, 695–705.

EPA, 1992. Potential uses of phosphogypsum and associated risks. Background information document for 40 CFR 61 Subpart R National Standard for Radon emissions from phosphogyspum stacks. U.S. Environmental Protection Agency Office of Radiation Programs, Washington, D.C. 20460.

Gázquez, M.J., Bolívar, J.P., García-Tenorio, R., Galán, F., 2009. Natural occurring radionuclide waste in Spain: the Huelva phosphogypsum stacks case, in: 1st Spanish National Conference on Advances in Materials Recycling and Eco – Energy. pp. 75–78.

Haridasan, P.P., Maniyan, C.G., Pillai, P.M.B., Khan, A.H., 2002. Dissolution characteristics of 226Ra from phosphogypsum. J. Environ. Radioact. 62, 287–294.

May, A., Sweeney, J.W., 1984. Evaluation of radium and toxic element leaching characteristics of Florida phosphogypsum stockpiles.

Rodríguez, R., Borràs, A., Leal, L., Cerdà, V., Ferrer, L., 2016. MSFIA-LOV system for 226Ra isolation and pre-concentration from water samples previous radiometric detection. Anal. Chim. Acta 911, 75–81.

Rutherford, P. M., Dudas, M. J., Arocena, J.M., 1995. Radium in phosphogypsum leachates. J. Environ. Qual. 24, 307–314.

Ruzicka, J., 2000. Lab-on-valve: universal microflow analyzer based on sequential and bead injection. Analyst 125, 1053–1060.

Villa, M., Mosqueda, F., Hurtado, S., Mantero, J., Manjón, G., Periañez, R., Vaca, F., García-Tenorio, R., 2009. Contamination and restoration of an estuary affected by phosphogypsum releases. Sci. Total Environ. 408, 69–77.

SedActiv 1.0:A cosmicveto gamma spectrometry setup for sediment samples

D. Pittauer[1,2], D. Höweling[2,3], M. Pérez Mayo[2], B. Hettwig[2] and H.W. Fischer[2]

[1]University of Bremen, MARUM - Center for Marine Environmental Sciences, Bremen, Germany
[2]University of Bremen, Institute of Environmental Physics, Bremen, Germany
[3]Carl von Ossietzky University of Oldenburg, Institute of Physics,Oldenburg, Germany

Introduction

Down-core activities of the fallout radionuclide ^{210}Pb are widely used for deriving chronologies in recent (Anthropocene) sediment profiles. Using HPGe gamma spectrometry is a preferred technique for their determination for some important reasons: many different natural and artificial radionuclides can be determined within a single spectrum, including the amount of supported ^{210}Pb (^{226}Ra is responsible for in-situ ^{210}Pb production), and the analysis is non-destructive. At the same time, the detection limits are comparatively higher for ^{210}Pb than by alpha spectrometry. Technical solutions, like special detectors, underground laboratories, active shielding or a combination of several measures, can improve the detection performance of gamma spectrometry systems.

Cosmic radiation at sea level consists mostly (about 75%) of muons. Muons interact weakly with the lead shielding, because of low specific energy loss rates, but can cause several secondary effects like bremsstrahlung that increases the background continuum.

At the recently installed cosmic veto gamma spectrometry setup an experiment was performed using low activity environmental samples with an aim to answer three basic questions regarding the application of the active shield in comparison to the passive shield only:

- How does the spectrum continuum change?
- Does the efficiency stay the same?
- How does the decision threshold change?

Materials and Methods

Cosmic veto setup

The Radioactivity Measurements Laboratory at the University of Bremen installed cosmic veto guard plastic scintillation detectors (Höweling, 2015a, Höweling, 2015b) on top of the passive shielding in the ground level laboratory to improve the performance of one of the gamma spectrometry systems. The system is similar to that used by Hurtado et al. (2006).

The system uses a 50% HPGe detector with carbon front window housed in a 10 cm Pb shielding with Cu, Cd and plastic inner linings and operated by Genie 2000. Efficiencies are generated by LabSOCS software.

This setup, frequently used for studies of **Sed**iment radio**Activ**ity (SedActiv 1.0), was tested.

Figure 1: The SedActiv setup is intended to be used for low activity environmental samples, including sediments.

Sediment samples (Tab. 1) including two reference sediments and three real samples from German lakes were measured with veto detectors off and on, and the net areas of photopeaks in the spectra were analyzed.Decision thresholds were calculated according to ISO 11929.

Table 1. *List of samples used for the comparison of counting with the veto setup on and off. Measurement geometry: pressed pellets, diam. 35 mm (mass and height given in the table).*

Sample	Description	Mass (g)	Height (mm)	Live-time (s)
IAEA-385	Reference material (marine sediment, Irish Sea)	9.92	5.05	86400
IAEA-384	Reference material (marine sediment, Fangataufa)	9.85	10.22	86400
Wol 225	Lake sediment, Wollingster See, Germany	9.79	7.50	63813
Teg 6	Lake sediment, Tegeler See, Germany	3.62	3.25	85884
Teg 28	Lake sediment, Tegeler See, Germany	4.82	3.85	86261

Results and Discussion

How does the spectrum continuum change?

The total background count rates (empty detector housing) have been reduced by a factor of 2 from 1.30 cps to 0.66 cps (Höweling, 2015a). Fig. 2 shows a comparison of sediment sample spectra measured with veto detectors off and on. The total count rate was reduced by a factor of 1.55 from 1.94 cps to 1.25 cps. A decrease in the continuum is obvious.
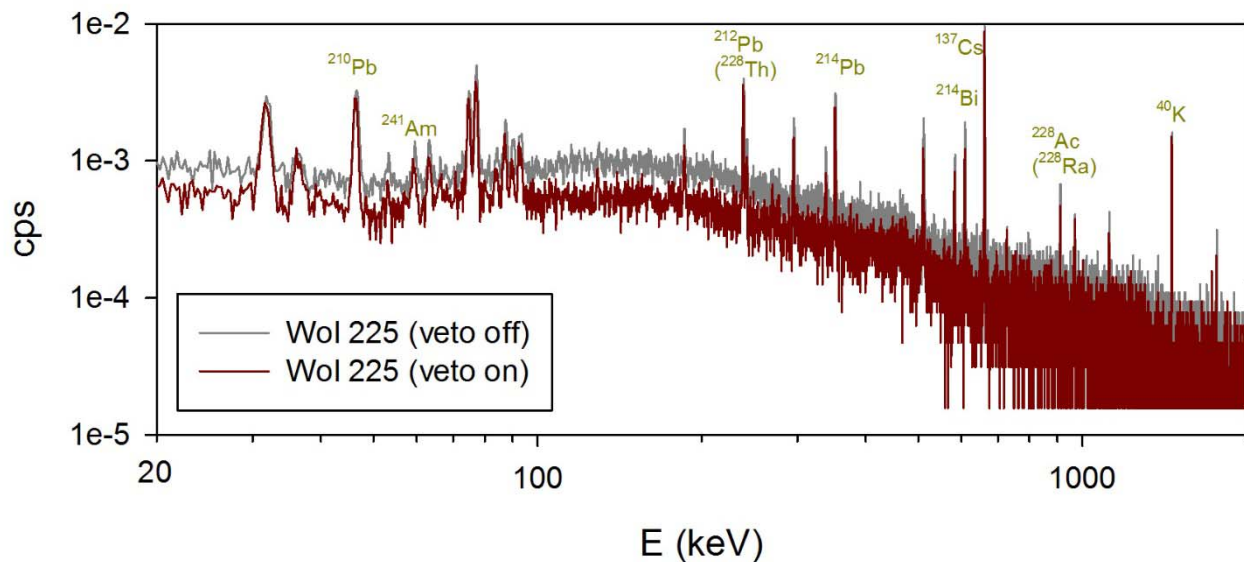
Figure 2. *Sample Wol 225 measured without (grey) and with (red) cosmic background suppression. The total count rate was reduced from 1.94 cps to 1.25 cps.*

Does the efficiency stay the same?

The areas o fthe photopeaks (net peak areas) were calculated for lines with counting error lower than 20%. A value of normalized difference *d_norm* was calculated for each line as

$$d\_norm = \frac{(area_{off} - area_{on})}{area_{off}},$$

Where *area_{off}* and *area_{on}*s tand for net peak areas with the veto off and on, respectively. If the efficiency at given energy stays constant, *d_norm* values are close to 0.
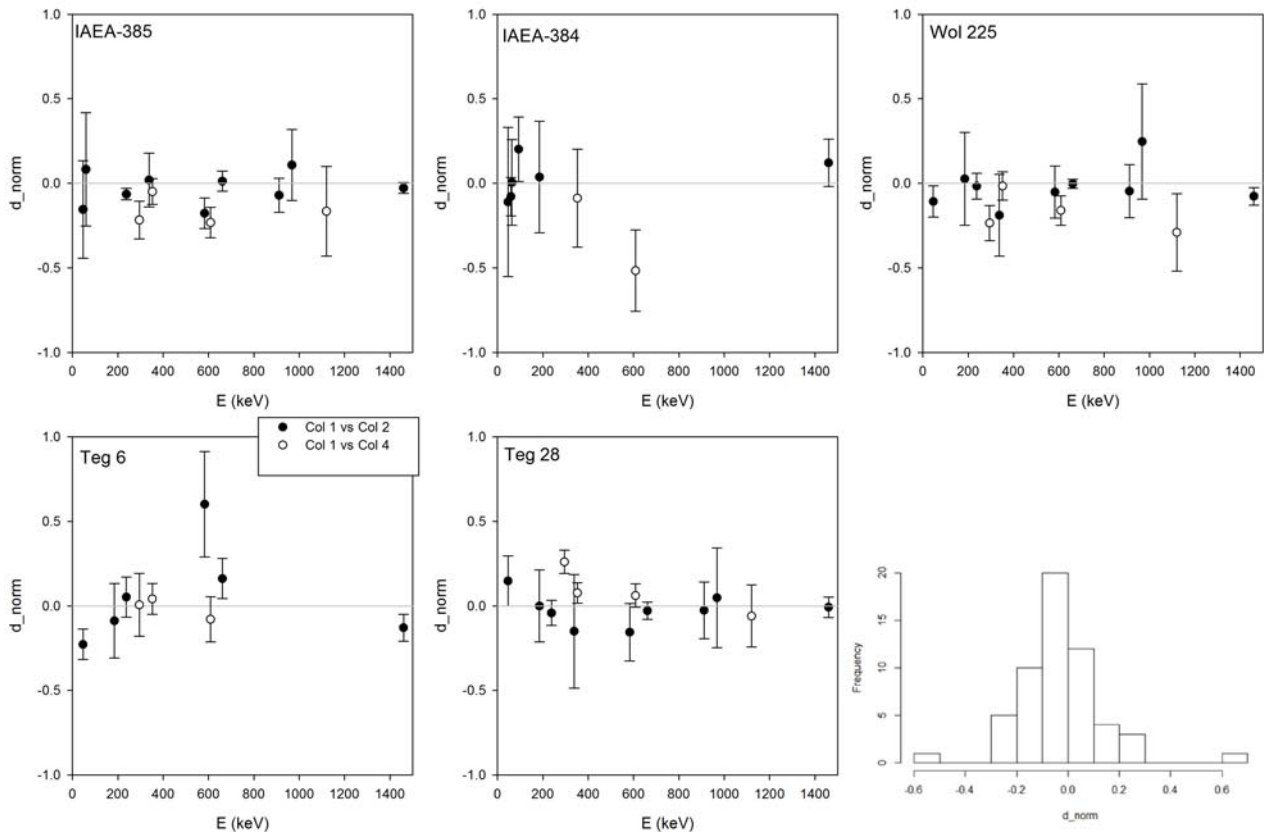
Figure 3.*Normalized difference of photopeak areas measured with veto off and on, for 5 sediment samples. Rn daughter products are marked with empty circles (as they might be a subject to varying background in the detectors). The error bars represent the counting errors.*
Bottom right: a histogram of all collected d_norm values.

In Fig. 3, the results are plotted for individual samples. The lines of the ^{222}Rn daughter products (^{214}Bi, ^{214}Pb) were plotted separately, as there is a possibility of their greater variability due to fluctuations in the background of the detector. Additionally, the histogram of all measured values is added, showing a distribution of values around 0. The mean d_norm value is -0.032. A t-test shows that the value does not vary significantly from 0 (t = -1.5094, df = 55, p-value = 0.1369).

How does the decision threshold change?

The decision thresholds were calculated for selected radionuclides with a major interest for sediment chronology studies. They included natural isotopes ^{7}Be, ^{40}K, ^{210}Pb, ^{214}Bi, ^{214}Pb, ^{228}Ra (detected via ^{228}Ac) and ^{228}Th (detected via ^{212}Pb), as well as artificial radionuclides ^{134}Cs, ^{137}Cs and ^{241}Am.

The relative improvement of decision thresholds are plotted in Fig. 4 as a mean value from all 5 samples. Overall, the improvement is a decrease to 83% on average.
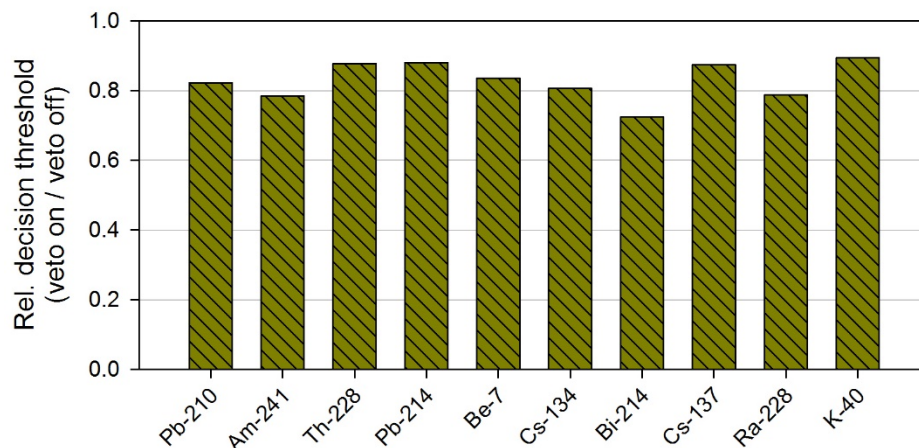
Figure 4. A relative improvement in decision threshold values for different isotopes (means from all 5 samples). The isotopes are ordered by increasing gamma energy of their photopeak.

Conclusions

An improvement in performance was achieved with the SedActiv 1.0 system used for low activity sediment samples with active anticosmic shielding in comparison to a passive shielding only.
The spectrum continuum was reduced.The system seems to have comparable efficiency for low-activity samples.Reduction of decision threshold was achieved to 83% on average.More extensive testing with other types of samples will continue.

References

Höweling, D., 2015a. Installation and test of an active muon veto shield for gamma-spectroscopy. Master Thesis, University of Bremen.
Höweling, D., 2015b: Background reduction in a gamma spectrometer with an active shielding. ENVIRA Conference Sept. 21-25 2015, Thessaloniki, Greece (poster presentation).
Hurtado, S., Garcia-Leon, M., Garcia-Tenorio, R., 2006.Optimized background reduction in low-level gamma-ray spectrometry at a surface laboratory.Appl. Radiat. Isot. 64, 9, 1006–1012.

Acknowledgements

Testing a CeBr$_3$ γ ray spectrometer for radiological environmental monitoring

R.Idoeta[*]*, M. Herranz, N. Alegría and F. Legarda*

Dpto. de Ingeniería Nuclear y Mecánica de Fluidos, ESI de Bilbao, Universidad del País Vasco UPV/EHU, Alda. Urquijo s/n, 48013 Bilbao, Spain

Abstract

The monitoring of radioactivity in the environment, as a complementary activity of radioecology, is an application of gamma ray spectrometry dealing with low and very low level gamma ray activities. Cerium bromide (CeBr$_3$) is part of a new bromide scintillators group that can be particularly attractive for radiological environmental monitoring as it can bridge the gap between the cheap, high efficiency but low energy resolution of room temperatures NaI(Tl) scintillator detectors and the more expensive, high energy resolution and cryogenically cooled semiconductor detectors like HPGe, this being always chosen for the finest gamma ray spectrometry. This work tests the suitability of a 1.5" CeBr$_3$ detector for the aim of radiological environmental monitoring and states the measurement conditions under which it can serve for measuring different environmental matrices used for monitoring purposes.

Introduction

Low gamma ray activity sources are a common problem for many gamma ray spectrometry applications. Radiological environmental monitoring is one of these applications, as environmental sources of radioactivity are usually of very low level, and becomes of particular importance for radioecology, as their actions are complementary.

In recent years there has been a growing interest in the development of new scintillator materials, pressed by the increasing number of industrial, medical and scientific applications looking for scintillation crystals with high luminosity, short decay time, high density and low cost for gamma ray analysis. The new bromide scintillators can be particularly attractive as they meet those requirements. In the case of radiological environmental monitoring, this type of detectors could bridge the gap between the cheap, high efficiency but low energy resolution NaI(Tl) scintillator detectors and the more expensive, high energy resolution and cryogenically cooled semiconductor detectors like HPGe, this being always chosen for the finest gamma ray spectrometry needed in environmental monitoring.

In particular, cerium bromide (CeBr$_3$) has recently become a crystal of interest in the pursuit of high energy resolution gamma-ray spectrometry at room temperatures (Shah et al, 2005).

In order to address the likelihood of this type of detectors for the aim of environmental monitoring, we have tested the suitability of a 1.5" CeBr$_3$ detector. We have tested it with different environmental test samples (different matrices in specific geometries) used for monitoring purposes. Appropriate calibrations for those test samples have been done, so that their uncertainties and detection limits are calculated and compared. This way, the ability and conditions of the measurements made with this scintillator to cope with the detection limits required Spanish Nuclear Regulatory Authority for radiological environmental monitoring is established.

---

[*] Corresponding author, E-mail: raquel.idoeta@ehu.eus

Materials and Methods

Samples

We have tested the CeBr$_3$ detector performance with different environmental test samples used for monitoring purposes. That is, three different types of samples commonly found in radiological environmental monitoring for air and water sampling have been tested. With regard to air sampling, it has been done with a system that allows circulating 300 m^3 a week. In this sampling system, two type of filters are put: a radioiodine collection filter cartridge (RADēCO model CP-100 47 mm effective diameter and 26 mm height) and a plain cellulose nitrate membrane filter (Whatman 7188-004 WCN, pore Size: 0.8 μm, diameter: 47 mm but 40 mm effective diameter). For water sampling, 2 liter water samples are evaporated on a polyethylene film folded to 50 x 30 mm size.

A 1.5" CeBr$_3$ detector from Scionix, with a 2" Hamamatsu photomultiplier, surrounded by 10 cm Pb shield has been used for this study. It has a nominal energy resolution of 4.3% at 662 keV (^{137}Cs). It has a 0.5 mm thick Al metal body housing and an external 45 mm diameter.

512 channels have been selected for the digital multichannel analyzer.

Method

Samples were measured placing them centred on the scintillator window with different counting times to study the influence of counting time on the detection limit.

Appropriate calibrations for those matrix-container configurations have been done. These calibration sources were prepared from a standardized certified solution containing 10 radionuclides, having 12 different gamma ray energies with an energy range between 59.54 and 1836.05 keV (see table 1). The calibration sources were prepared with the same procedure as that used for samples, so three different source geometries were measured. They were measured placing them centred on the detector window for energy and efficiency calibration. From the samples data it is observed that the active areas of the sources were larger than that of the detector.

1.5" CeBr$_3$ detector			60%HPGe
Radionuclide	Energy, keV	FWHM, keV	FWHM, keV
Am241	59.54	8.02	1.01
Cd109	88.03	10.27	1.00
Co57	122.06	11.59	1.01
Ce139	165.86	13.61	1.03
Hg203	279.2	18.94	1.07
Sn113	391.7	22.64	1.16
Sr85	514	25.85	1.26
Cs137	661.66	30.75	1.35
Y88	898.04	35.11	1.45
Co60	1173.23	38.76	1.58
Co60	1332.49	42.66	1.74
Y88	1836.05	48.56	1.81

Table 1. *List of radionuclides used for the calibration of the detector together with their energies and the FWHM observed for them. FWHM observed for a 60% coaxial HPGe is also shown for comparative purposes.*

Counting times for the calibration sources were selected according to their activities so that statistical uncertainties under the photo-peak would have a minor contribution on the final results. That is, photo-peak areas contained at least 10^5 counts for every nuclide.

As also seen in table 1 the different energies of the calibration sources were well resolved by the scintillator. The Full Width at Half Maximum (FWHM) values shown in table 1, although with rather large values compared with those typical found in HPGe detectors, are sufficiently small to allow correct separation of the calibration peaks. The energy resolutions obtained are similar to those reported by other authors with detectors of the same scintillator but different volumes (García-Toraño, 2016, Guss et al., 2009).

Peak efficiencies obtained in the calibration of the detector (see figure 1) with cellulose nitrate membrane filter calibration source have values between 21% at 88 keV ([109]Cd) and 1.3% at 1836 keV ([88]Y). In the case of the cartridge calibration source, efficiencies rank between 11% and 1.3% at the same energies, and, finally, for the polyethylene film folded calibration source, efficiencies found are between 11% and 1.7% at the same energies.
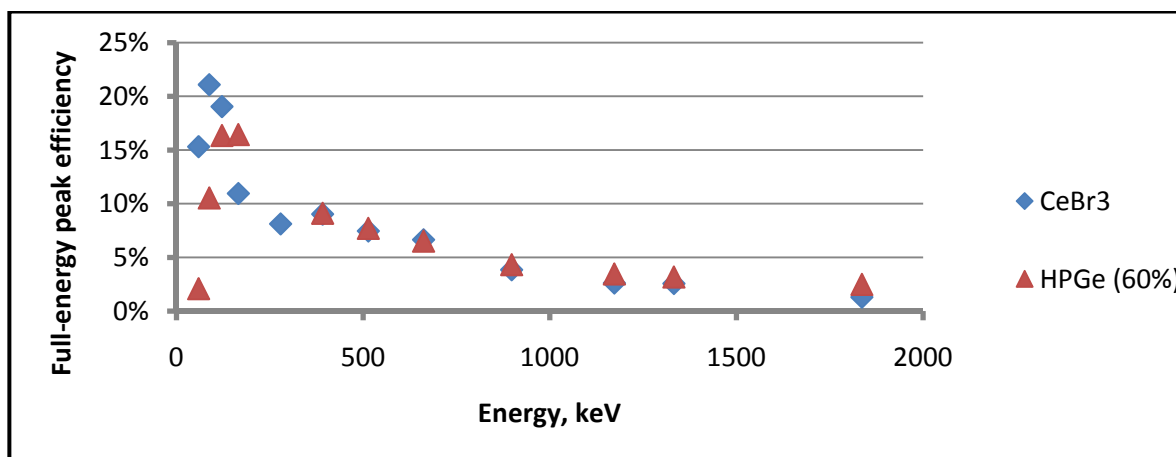
Figure 1. *Comparison of peak efficiency calibration of the CeBr$_3$ and 60% coaxial HPGe detectors obtained for the cellulose nitrate membrane filter calibration source.*

Background measurements were also done with blank samples. CeBr$_3$ scintillation detectors are known not to suffer from the intrinsic background typical for other new detectors like LaCl$_3$:Ce or LaBr$_3$:Ce. It must be considered that the detector is in the centre of a 10 cm lead shield. Background counting time is the same used for samples: 1 day.

In the background measurements there were found peaks from [40]K, [214]Pb and [214]Bi, with counting rates between 0.015-0.019, 0.0046-0.011 and 0.0029-0.0071 cps, respectively. For comparison reasons, the same peaks observed in standard coaxial HPGe detectors give the following results: 0.011-0.012, 0.0024-0.0035 and 0.0025-0.0028 cps, respectively for a 40% relative efficiency detector and 0.020-0.021, 0.0072-0.0084 and 0.0059-0.0083 cps, respectively for a 60% relative efficiency detector. Both HPGe detectors have a 10 cm lead shield. So, in this respect, the 1.5" CeBr$_3$ detector would have an intermediate background count rate between those of coaxial HPGe detectors with relative efficiencies of 40% and 60%.

Results and Discussion

The efficiency calibration of the detector done with the set of prepared calibration sources reveal that the peak efficiencies found for the radioiodine filter cartridge and for the polyethylene film folded are similar to those found for a 40% relative efficiency standard coaxial HPGe detector at 662 keV (^{137}Cs) whereas for the cellulose nitrate membrane filter the efficiency at that energy is similar to the one of a 60% relative efficiency standard coaxial HPGe detector as seen in figure 1. At lower energies, the CeBr$_3$ detector can show even higher efficiencies than those found in the case of semiconductor detectors but, at higher energies, lower efficiencies are found.

These differences obtained in the comparison with standard coaxial HPGe detectors of different sizes come mainly from the fact that the calibration sources have different active areas and, in some cases, they are larger than the radiation entrance window of the detector. In the case of the cellulose nitrate membrane filter, its area is slightly larger than that of entrance window of the detector, whilst the two other calibration sources have areas that are significantly larger than the 1.5" (38.1 mm) corresponding to the window of the detector. However, this does not happen in the case of 40% and 60% relative efficiency standard coaxial HPGe detectors as they have a crystal window diameter of 68 mm, bigger than all sample areas.

With respect to background, it is seen that it can be a problem in some radionuclide assessment. The main peak of [214]Pb at 352 keV found in the background spectra together with the energy resolution for the main peak (364 keV) of [131]I (FWHM = 21.5 keV) hinders the assessment of ^{131}I activity (see figure 2) and increases the counts under its peak, consequently increasing the detection limit. Their deconvolution of this gamma-ray peak doublet becomes really difficult. Anyhow, [214]Pb activity could be established from the 295 keV peak and its respective counts at 352 keV subtracted from the ^{131}I and [214]Pb full peak to assess ^{131}I activity.

In contrast, this problem does not arise in the case of HPGe detectors due to the great difference between [214]Pb and ^{131}I main photo-peaks compared to their respective FWHM values for this detector (table 1).
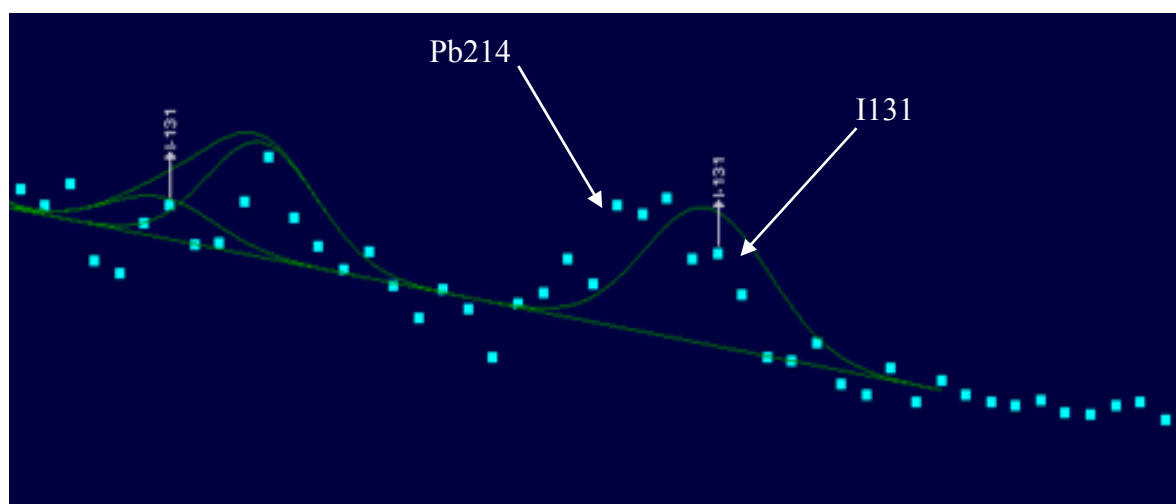
Figure 2. Spectrum obtained from the measurement of a radioiodine filter cartridge.

Luckily, ^{137}Cs with the main peak at 662 keV is sufficiently well separated from the main peak of [214]Bi at 609 keV for the CeBr$_3$ detector.

With the measurements done with the different test samples, activities, uncertainties and detection limits have been calculated. As no activities are found in the samples, only detection limits have been reported. Detection limits have been calculated using the ISO standard 11929 method (ISO, 2010).

In the air filter cartridges measured, ^{131}I is found under detection limit, being this value between 1.1-1.2 10^{-3} Bq/m^3. This value is slightly above the required detection limit for radioiodine of 1.0 10^{-3} Bq/m^3 established by the *Consejo de Seguridad Nuclear*, which is the Spanish Nuclear Safety Council, (CSN, 1993). As established before, the ^{214}Pb contribution to the counts under ^{131}I photo-peak causes a relatively high detection limit. However, measurement of the sample during a counting time of two days would allow achieving the detection limit required, as, in this case, the detection limit found is 6.5 10^{-4} Bq/m^3, well below the mandatory value.

In the case of cellulose nitrate air filters, the measurement of ^{137}Cs gives a detection limit of 1.5 10^{-3} Bq/m^3, below the required value of 2 10^{-4}Bq/m^3 established by the Spanish Nuclear Safety Council, (CSN, 1993). So, one day of measurement with this type of detector is sufficient to achieve the requirements of ^{137}Cs for air monitoring purposes.

Finally, for water samples, the detection limit for the measurement of ^{137}Cs is 90 Bq/m^3 below the required value of 100 Bq/m^3 (CSN, 1993). So, again, one day of measurement with this type of detector and a 2 liter sample is sufficient to achieve the requirements of ^{137}Cs for water monitoring purposes.

Conclusions

Energy resolution is the key factor for gamma ray spectrometry and this is the case for this new bromide scintillator, a 1.5" CeBr$_3$ detector. Background from the 352 keV from ^{214}Pb and its relatively high FWHM value produces large detection limits for ^{131}I assessment in air filter cartridges. But, fortunately, larger counting times, like a couple of days, are able to attain smaller detection limits, below those required by Nuclear Safety Councils. ^{137}Cs assessment in air filters and in water is possible with this small detector as its required detection limits are also achieved with standard one day counting time.

So, this small detector that operates at room temperature and is cheaper than traditional HPGe detectors could be considered as an option for simple routine tasks associated to radiological environmental monitoring as it can have an excellent performance in assessing highly important selected radionuclides that must be continuously monitored in the environment.

References

CSN, 1993. Guía de Seguridad no 4.1 Diseño y desarrollo del programa de vigilancia radiológica ambiental para centrales nucleares, Madrid.

García-Toraño E., Caro, B., Peyrés V. and Mejuto M., 2016. Characterization of a CeBr$_3$ detector and application to the measurement of some materials from steelworks. Nucl. Instr. Meth. In Phys. Res. A 837, 63-68.

Guss P., Reed M., Yuan D., Reed A. and Mukhopadhyay S., 2009. CeBr$_3$ as a room-temperature, high-resolution gamma-ray detector. Nucl. Instr. Meth. In Phys. Res. A 608, 297-304.

ISO, 2010. Determination of the characteristic limits (decision threshold. detection limit and limits of the confidence interval) for measurements of ionizing radiation -- Fundamentals and application, ISO 11929. International Standards Organization, Geneve.

Shah K. S., Glodo J., Higgins W., van Loef E. V. D., Moses W. W., Derenzo S. E. and Weber M. J., 2005. CeBr3 scintillators for gamma-ray spectroscopy. IEEE Trans. Nucl. Sci. 52, 4278-81.

Evaluation of radiochemical methods for thorium-isotopes determination in environmental and industrial samples by alpha-spectrometry

J.C.Lozano(1), M. Herranz(2) *, J.P.Bolivar(3) and R.García-Tenorio(4)

(1) University of Salamanca, Faculty of Science, c/ Casas del Parque, 1, 37008 Salamanca, Spain
(2) University of the Basque Country (UPV/EHU), Dept. Nuclear Engineering, alda. Urquijo s/n, 48013 Bilbao, Spain
(3) University of Huelva, Dept. of Applied Physics, Campus de El Carmen s/n, 21071 Huelva, Spain
(4) University of Seville, Dept. of Applied Physics, Avda. Reina Mercedes2, 41012 Sevilla, Spain

Abstract

Thorium is a very sensitive element to matrix effects that appear at different stages of its preparation to be measured by alpha-particle spectrometry. These effects are particularly important for inorganic solid samples from environmental and industrial origin. To deal with this problem and to define the most suitable method, not only from a technical point of view but also considering cost, time and chemical reagents used, a research project was started. In this work, the main results of this project are shown.

Introduction

Alpha spectrometry is the most widely used methodology to obtain the contents of Thorium isotopes (^{232}Th, ^{230}Th, ^{228}Th) in environmental and industrial samples. This technique involves a set of steps: sample pre-treatment to obtain a solution containing the thorium contents in the sample; radiochemical separation to isolate the thorium contents in the sample solution from other interfering chemicals, electrodeposition to obtain a test sample ready to be measured by alpha spectrometry, and finally, alpha measurement.

For each one of the first three steps there are different methods that could be applied, so, the most suitable methodology should be a proper and coherent selection of a method for each step. To define this most suitable methodology, and with the financial support of the Spanish Nuclear Safety Council (CSN), a research project was developed and a resume of its results is presented here.
To improve the quality of results, four working groups (WG) belonging to four different universities had participated in this project.

Materials and Methods

Materials

The 4 WG used the same material: alpha-spectrometer, from Canberra, equipped with passivated implanted silicon (PIPS) type, with an active area of 450 mm^2 and a nominal background of 0.1389 s^{-1}m^{-2}. Thorium tracers, ^{229}Th and ^{230}Th, provided by NIST and class PA chemicals reagents.

---

* Corresponding author, E-mail: m.herranz@ehu.eus

Methodology

Calculus:

Formulae for activity concentration, uncertainties and characteristics limits have been developed, following GUM (ISO, 1995) and ISO 11929 (ISO, 2010), respectively, to make results comparable. The total yield of the process is the product of its chemical yield (sample pre-treatment plus radiochemical separation) and electrodeposition yield. It is calculated as:

$$R = \frac{(r_{gt} - r_{0t})}{A.\ \varepsilon}$$

Where A is tracer activity added; r_{gt} and r_{0t} are the tracer gross counts rate in the sample test spectrum and background spectrum, respectively, and ε is the detector efficiency.

Developed experiments:

Experiment 1: Selection of radiochemical separation method.

The objective of the first experiment is the choice, among those methods implemented in the laboratories, of the most suitable and robust one to be used, for all the WG, when the capability of the sample pre-treatment methods will be compared.
To achieve this goal, four different radiochemical methods, TBP+II-anionic, II-anionic, and specific chromatographic resins type UTEVA and TEVA were analyzed, starting from a HNO_3 sample solution obtained by different pre-treatment methods.
These four methods have been applied to the following samples: phosphate rock (FR), ilmenite (ILM), sediments (SED), sludge coming from water plant treatment (SLG), ground water with high saline contents, blank water and reference samples of ^{232}Th (MR232) and ^{230}Th (MR230). Solid samples were previously dissolved (pre-treated) and each one of the 4 WG applied one of the methods described to 5 aliquots of these dissolved samples. At the beginning of the radiochemical process ^{229}Th tracer were added to the sample.
The solutions, containing Thorium, obtained from the radiochemical separation processes, were electrodeposited in 1 in diameter stainless steel disk, all the WG followed the method provided by Hallstadius (Hallstadius, 1984), to obtain the test samples to be measured by alpha spectrometry. The selected measurement times were always 300000 sec and the source-detector distance 5mm. Then, the total (separation+ electrodeposition) yield of the process was obtained.

Experiment 2: Performance of pre-treatment methods.

The objective of this experiment was to analyze the performance of four different pre-treatment methods: acid attack in a closed container (DAHC), acid attack in an open container (DAPA), microwave oven ((DAMO) and alkaline fusion (PIRO).
To deal with this objective, these four methods have been applied by the four WG to the following samples: uranium ore (MU), ilmenite (ILM), tionite (TIO), soil (SU), sludge from a water plant treatment (SLG), and ashes from vegetal origin (CE). Each WG's have been applied the aforementioned pre-treatment methods in 3 aliquots of each sample type, and after dissolution, all the WG applied the radiochemical isolation method selected in Part 1 as the most robust and suitable for all types of samples, II-anionic.
After that, test samples were prepared and measured in the same way than in Experiment 1, obtaining the activity concentration, uncertainties and detection limits of the samples.
The differences among the activities concentrations obtained for the same sample, when different methods are used, allow the comparison of the ability of the different sample pre-treatment methods

to provide a representative dissolution from the original sample. In addition, samples will be characterized for ^{232}Th, ^{230}Th and ^{228}Th activity concentration contents.

Experiment 3: Factors that affect the variability of the total yield.

From the results obtained in Exp. 1 and also in Exp. 2 it can be seen that total yields show a high variability; not only among the different type of samples, but also among the different analyses carried out in the same sample. So, the objective of this third experiment is to analyze if this variability is due to the separation methods or to the electrodeposition one. Also, if needed, which factors affect electrodeposition yields are analyzed.

To carry out this experiment the same samples than those used in the Exp.2, now characterized for ^{230}Th, ^{232}Th and ^{228}Th, were dissolved and divided in aliquots. In one of these aliquots conventional chemical analyses were carried out. The other aliquots were used to apply the four radiochemical separation methods, without using ^{229}Th tracer. After separation, the obtained solutions were divided in two aliquots; in one of them the conventional chemical analyses were carried out once again; so, the ability of each one of the radiochemical methods to clean up chemicals from the original sample was stated. The other aliquot was traced with ^{229}Th before to be electrodeposited and measured by alpha spectrometry; so, the electrodeposition yield is obtained using Eq. 1 and therefore, radiochemical separation yield.

A flow chart of this Experiment is show in Fig. 1.
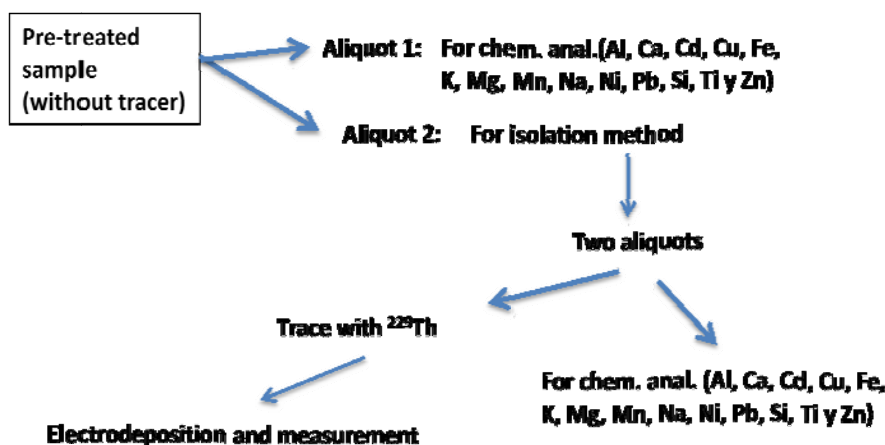
Figure 1. *Flow-chart of Experiment 3*

Results and Discussion

Experiment 1:

Results obtained for the Th isotopes activity concentration are shown in Figure 2 for the samples with highest activity contents.

In this Figure it can be seen that results obtained are very similar for all samples regardless of the separation method used. Also, there is a good coincidence on isotopic relations. So, it can be concluded that, all the analyzed methods work properly and in a similar way.
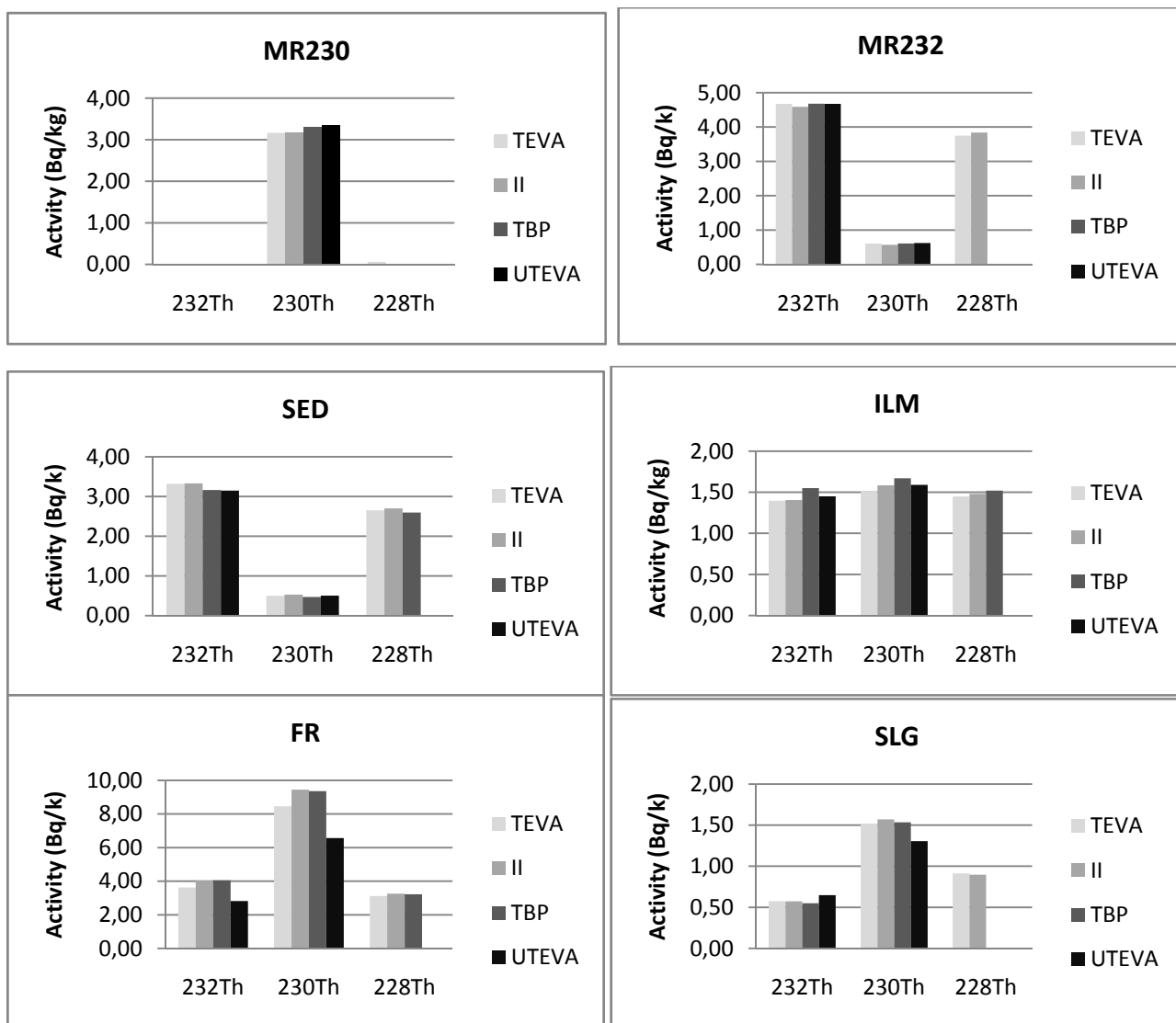
Figure 2. Five aliquots mean values of Th radioisotopes activity concentration of samples, obtained by the four radiochemical separation methods.

In Table 1, the mean values of the 5 aliquots obtained for the total yields are showed for all measured samples by the four separation methods. Values appear with its standard deviation (k =1).

SAMPLE	Radiochemical separation method			
	TEVA	II	TBP	UTEVA
MR230	0.77 ± 0.05	0.69 ± 0.07	0.88 ± 0.03	0.52 ± 0.10
MR232	0.73 ± 0.10	0.93 ± 0.06	0.80 ± 0.04	0.60 ± 0.12
ILM	0.68 ± 0.08	0.60 ± 0.09	0.72 ± 0.06	0.30 ± 0.04
FR	0.78 ± 0.08	0.64 ± 0.12	0.55 ± 0.15	0.45 ± 0.14
SED	0.82 ± 0.06	0.83 ± 0.11	0.53 ± 0.08	0.77 ± 0.07
LDF	0.87 ± 0.01	0.97 ± 0.03	0.35 ± 0.15	0.38 ± 0.08
ZAPR	0.11 ± 0.01	0.61 ± 0.08	0.77 ± 0.12	0.73 ± 0.11
H2O	0.90 ± 0.02	0.91 ± 0.01	0.54 ± 0.13	0.78 ± 0.05

Table 1. Five aliquots mean values of total yields. In %.

Following the results showed in this Table 1, it can be concluded that all radiochemical isolation methods were comparable among them, providing comparable mean values of total yields. Anyway, taking into account not only yields obtained but also its standard deviation, it can be concluded that the II-anionic methods are those that supply the highest and most reproducible yield results for all type of samples. However, the standard deviations obtained imply that total yield is not stables, not even for the same sample when the same method is used.

Experiment 2:

Mean values of the experimental data for activities concentrations for ^{228}Th, ^{230}Th and ^{232}Th for each type of sample and for each pre-treatment method are shown in Table 2. Data are provided with its uncertainty obtained following GUM method (ISO, 1995). Detection limits are not given, but in most cases, they are close to E-04 Bq/kg.

MUESTRAS		^{232}Th A (Bq/kg)	U (Bq/kg)	^{230}Th A (Bq/kg)	U (Bq/kg)	^{228}Th A (Bq/kg)	U (Bq/kg)
SUELO	DAPA	43.4	0.7	43.9	0.2	44.9	0.8
	DAHC	39.6	3.3	40.9	1.9	43.1	5.6
	DAMO	42.3	1.5	56.3	0.8	48.2	2.1
	PIRO	44.7	0.3	45.0	2.1		
FANGOS	DAPA	50,5	1.5	58,3	1.7	73,0	1.1
	DAHC	52.1	3.0	55.3	3.1	76.6	4.1
	DAMO	50.5	1.4	56.3	1.6	76.3	1.0
	PIRO	52.0	2.5	54.7	3.4		
MIN URANIO	DAPA	503.7	13.1	3055.0	35.1	517.2	14.4
	DAHC	513.2	11.6	3144.0	51.1	548.7	20.2
	DAMO	531.5	4.5	3174.0	56.5	561.2	4.7
	PIRO	508.0	16.2	3188.0	82.4	--	
CENIZAS	DAPA	5.24	0.08	8.17	1.64	9.53	0.43
	DAHC	5.09	0.17	13.8	8.56	6.05	4.39
	DAMO	--		--		--	
	PIRO	4.67	0.333	6.33	0.88	--	
TIONITE	DAPA	117.3	1.0	77.8	2.4	651.1	45.4
	DAHC	105.9	11.7	168.0	16.7	191.0	17.2
	DAMO	122.0	4.1	105.1	5.0	884.6	180
	PIRO	93.3	5.8	107.0	4.0		
ILMENITA	DAPA	330.9	4.6	105.1	3.4	318.0	6.9
	DAHC	310.4	47.0	112.6	6.1	376.3	14.3
	DAMO	334.6	4.7	125.7	1.9	373.3	7.0
	PIRO	342.3	8.4	124.7	2.0	--	

Table 2. *Mean activity concentration values for the 3 aliquots for each sample and each attack method, with its uncertainty (k=1)*

In this Table 2 it can be seen that the different data provided by the WG for the samples analyzed are very similar. Dispersions from the sample-mean values are in most cases lower than 10%. Tionite, which shows noticeable deviation in ^{232}Th and ^{230}Th and huge deviations in ^{228}Th, is an exception and also some data from ashes are. In the case of Tionite, it should be considered that ^{228}Th activity can be in continuously evolving over time depending on the relation ^{228}Ra/^{232}Th; this fact can be the cause of the huge deviation. In any case, there is not a tendency that allows us to decide which pre-treatment method provides better results. In the case of ashes samples it should be considered that the activities concentration were smaller than on the other samples; uncertainties

reported when DAHC method was used were much higher than 50%, and so these values should be discarded for statistical reasons.

So, considering that all the WG have been used the same radiochemical separation method and the same electrodeposition procedure, it can be concluded that all the pre-treatment methods work properly for the samples analyzed. Regarding total yields the mean value was higher than 65%, higher for the most conventional samples, soil and ashes, than for the most complexes ones, tionite and ilmenite.

At the same time, all the WG have been used their own methods to asses thorium values to these samples, results are not provided here, but together with those on Table 2 have been used to assess the activity concentration reference values to these samples.

Experiment 3:

Comparisons between the conventional chemicals present in the samples before and after radiochemical separation processes allow us to obtain the ability of these methods to remove chemical interferences for each type of sample. Results are shown in Figure 3, where mean values, for the samples analyzed, are shown for each separation method used and each chemical analyzed.
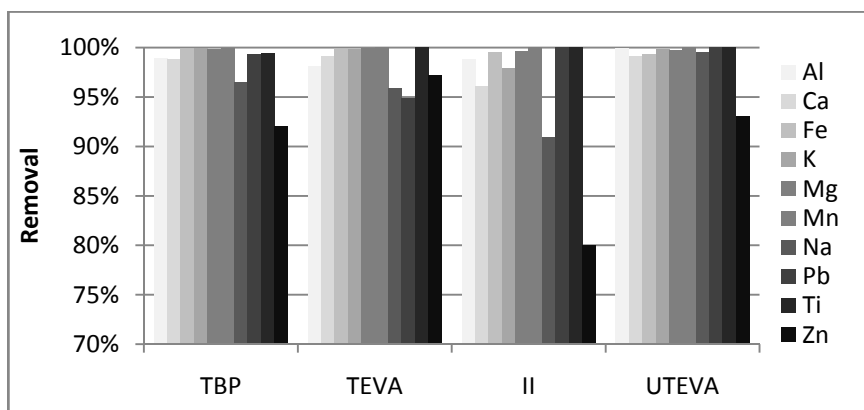
Figure 3. *Mean values of the removal percentage of chemical interferences when the four radiochemical separation methods are used in the different samples.*

Following the information contained in this Figure 3 it can conclude that all the separation methods are able to remove more than 90% of chemicals from the solution containing the dissolve sample, regardless of the sample type, being UTEVA resins those that provide the highest values.

It can be also seen that Zn shows values always higher than 80% but lower than the other chemicals, this behavior is due to Zn is quite an interchangeable element that appears in most of plastic made laboratory equipments.

Radiochemical separation yields were obtained for all samples and methods and data are shown in Figure 4

Regarding this Figure 4, it can be seen that the II-method is that which provide the more stable separation yields for the samples analyzed, with values higher than 70 %; biological ashes samples are the only exception, with separation yields close to 50%. The other separation methods provide yields that in some cases are higher than those from II-method but more variables depending on sample types. Regarding type of sample, it can be conclude that, being all of them very complexes, uranium ores is that in which thorium is separated with the highest and most stable yields regardless the separation method used.
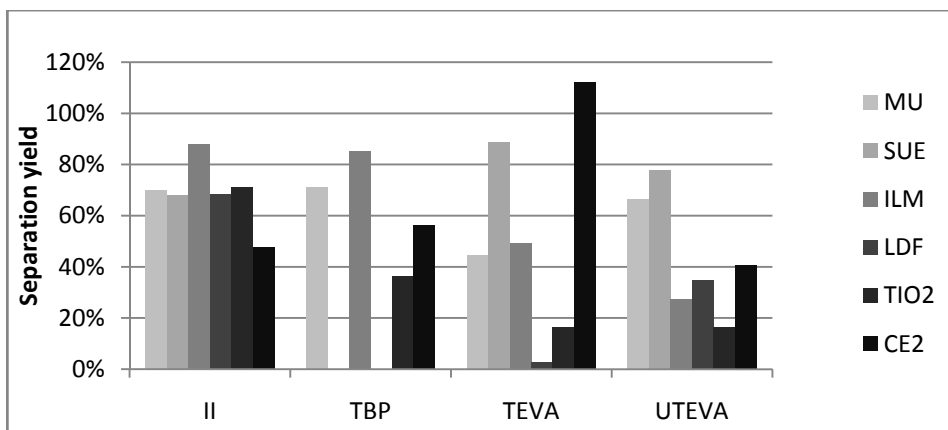
Figure 4. *Mean values of the radiochemical separation yield when the four methods are used in the different type of samples. In %.*

Finally, electrodeposition yields were obtained for all samples and methods; data are shown in Figure 5.
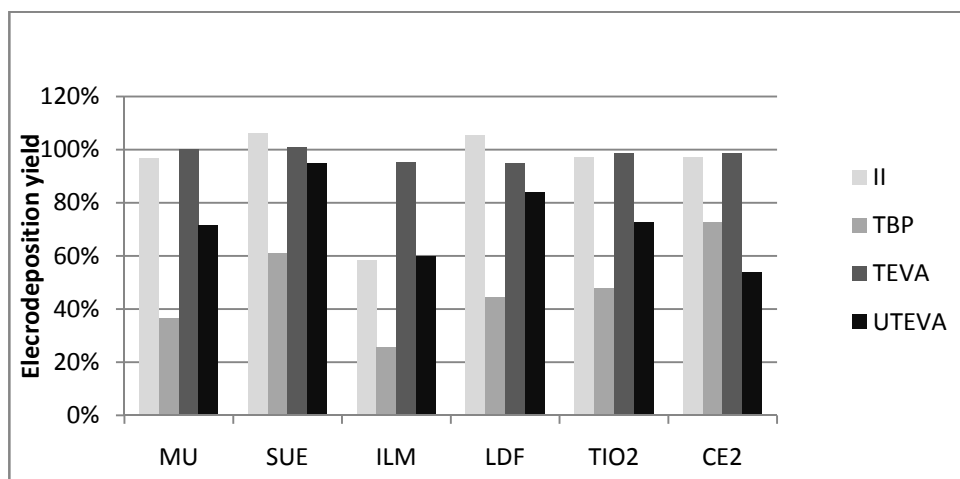
Figure5. *Mean values of the electrodeposition yield when the four radiochemical separation methods are used in the different type of samples. In %.*

Regarding this Figure 5, it can be seen how variables are the results obtained for every type of samples. A multivariate analysis has been carried out looking for a statistical relationship among the traces of chemicals remaining in the solution to be electrodeposited and the electrodeposition yield obtained. This analysis was no significant. So, it can be conclude that this huge variability is related to the physical parameters that can be varied during the electrodeposition process.

Conclusions

The four radiochemical separation methods analyzed: TBP+II-anionic, II-anionic, and specific chromatographic resins type UTEVA and TEVA, work properly and are able to preserve the isotopic equilibrium in the samples. However, the method II-anionic shows more stable results regarding total yield and also standard deviation of the activity concentration values obtained for different aliquots.
It can be also conclude that all the radiochemical separation methods are able to remove more than 90% of chemicals from the solution containing the dissolve sample, regardless of the sample type.

UTEVA resins are those that provide the highest values and II-method, the lowest one, being in any case, higher than 80%.

According to the results obtained it should be stated that all the pre-treatment methods studied: acid attack in on open container, acid attack in a close container, micro wave system and fusion method, are able to dissolve all the thorium contained in the sample.

The II-anionic radiochemical separation method is that which provide the more stables separation yields for the samples analyzed. The other separation methods provide yields that in some cases are higher than II method but more variables depending on samples types. Regarding type of sample, it can be conclude that, being all of them very complexes, uranium ores is that in which thorium is separated with the highest and most stable yields regardless the separation method used.

And finally, results obtained for electrodeposition yields are very variable for all type of samples. There is not a significant statistical relation between this variability and the traces of chemicals remaining in the solution to be electrodeposited. So, it can be conclude that this huge variability is related to the physical parameters that can be varied during the electrodeposition process.

References

Hallstadius, L., 1984. A Method for the Electrodeposition of Actinides. Nuclear Instruments and Methods in Physic Research 223.

ISO 11929, 2010. Determination of the Characteristic Limits (Decision Threshold, Detection Limit and Limits of the Confidence Interval) for Measurements of Ionizing Radiation. Fundamentals and Application. International Organization for Standardization, Geneva.

ISO/IEC Guide 98, 1995. Uncertainty of Measurement. International Organization for Standardization, Switzerland.

Acknowledgments

L – MISCELLANEOUS

Aspects of caesium-137 transport by microalgae Chlamydomonas reinhardtii related with potassium

José Alberto Gil Corisco *

*Instituto Superior Técnico, Centro de Ciências e Tecnologias Nucleares, Campus Tecnológico e Nuclear 2695-066 Bobadela, Portugal

Abstract

Uptake rate, concentration factor and loss rate of $^{137}Cs^+$ in green algae *Chlamydomonas reinhardtii* (Chlorophyceae) depend on the external concentration of potassium ($[K^+]_{ext}$). In a micromolar range, $1 - 50$ µM $[K^+]_{ext}$, the uptake rate (v_0) and concentration factor (CF) dependencies are non-lineal, with a significant decrease in v_0 from 21 to 5 pmol $^{137}Cs^+$ $ml^{-1}_{cell\ volume}$ h^{-1}, and in CF from 48388 to 4568, when $[K^+]_{ext}$ was increased from 1 to 5 µM, respectively. With a $[K^+]_{ext}$ range 0.1 mM – 10 mM, v_0 was less than 1 pmol $^{137}Cs^+$ $ml^{-1}_{cell\ vol.}$ h^{-1}, and CF less than 500. With $[K^+]_{ext} \leq 0.1$ mM, the $^{137}Cs^+$ equilibrium potential ($E^N_{137_{Cs}}$) ranged between -158mV (0.1mM $[K^+]_{ext}$) and -276mV (1 µM $[K^+]_{ext}$), more negative than the membrane potential ($E_m = -135\ mV$) of *C. reinhardtii* estimated by Malhotra and Glass (1995) using the equilibrium distribution of $[^3H]TPP^+$. In such conditions the electrochemical potential gradient would tend to push the $^{137}Cs^+$ ions out of the algal cells, therefore uptake would require an active transport mechanism. With $[K^+] > 0.1$ mM, $E^N_{137_{Cs}}$ practically equals the E_m values estimated by Malhotra and Glass (1995), apparently rendering the driving force virtually null. This paradox may result from an underestimation (less negative) of E_m based on the equilibrium distribution of $[^3H]TPP^+$, as pointed out by Rodriguez-Navarro (2000). Loss rate was less than 1 pmol $^{137}Cs^+$ $ml^{-1}_{cell\ vol.}$ h^{-1} with 1µM and 10µM $[K^+]_{ext}$ and increased significantly with $[K^+]_{ext} \geq 0,1$ mM up to 15 pmol $^{137}Cs^+$ $ml^{-1}_{cell\ vol.}$ h^{-1}. The modulation exerted by $[K^+]_{ext}$ on the $^{137}Cs^+$ efflux is consistent with the hypothesis that $^{137}Cs^+$ is liberated through K^+ outward channels (White and Broadley, 2000). In K^+ deficiency $^{137}Cs^+/Cs^+$ uptake is mediated by a saturable transport mechanism (low K_M), significantly more efficient than the uptake mechanism operating in K^+ sufficiency (higher K_M). Results are consistent with the proposed hypothesis of K^+ active transporters and K^+ ion channels mediating the transport of $^{137}Cs^+$, depending on the external K^+ concentration.

Introduction

A fraction of ^{137}Cs dispersed in Nature by human action ends up in aquatic ecosystems. Autotrophic planktonic organisms may absorb this radioactive element while it remains in solution. Unicellular green algae represent a broad group of species within the division Chlorophyta (Lewis and McCourt, 2004), making part of the planktonic community of primary producers in freshwater ecosystems (Margalef, 1983). The transport of ^{137}Cs by *Chlamydomonas reinhardtii* is here studied considering the energetic aspects and mechanisms of ion transport in plant cells (Maathuis and Sanders 1999; Fernández and Maldonado 2000; Rodriguez-Navarro, 2000). Membrane potential (E_m), equilibrium or Nernst potential (E^N), and electrochemical potential gradient are some of the concepts of ion transport here referred. Estimations of E_m associated with K^+ fluxes in *C. reinhardtii* by Malhotra and Glass (1995), based on the equilibrium distribution of lipophilic cation tetraphenilphosphonium labelled with tritium ($[^3H]TPP^+$), were used as reference values. Here are evidenced some relevant aspects of the relation between potassium and the absorption/desorption processes of ^{137}Cs by green algae *C. reinhardtii*. K^+ channels and K^+ active transporters are considered as putative mediators of $^{137}Cs^+/Cs^+$ transport (Zhu and Smolders, 2000).

Materials and Methods

Experimental procedures

A wild strain of unicellular green algae *C. reinhardtii* (CCAP 11/45) from Culture Collection of Algae and Protozoa, Institute of Freshwater Ecology, Ambleside, UK, was used. Potassium deficiency and sufficiency were induced in two separate lines by adapting algae to K^+ external concentrations ($[K^+]_{ext}$) of 1µM and 0.1mM. The simplified culture medium was supplemented with 0.1 mM $CaCl_2$ and 0.1mM NaCl. The solution pH=7.3 was buffered with 5mM HEPES and CAPSO (sodic salt).

In the experimental trials algae were suspended in fresh medium with a composition according to the specified treatment to be applied. Three replicates of 150 mL batch cultures for each treatment were spiked with 5.4×10^{-5} µM $^{137}CsCl$, corresponding to an activity concentration of 5.4 Bq ^{137}Cs mL^{-1}. Non-labeled replicates were used for the monitoring of culture density and biovolume (total volume of algae per unit volume of medium). Replicates were kept in glass vials with rubber stoppers, orbital agitation, continuous light (85 µmol m-2 s^{-1}) and room temperature at 20°C (Figure 1).

Culture density (n^{er} cells mL^{-1}) was estimated by cell counting with a Neubauer chamber. Biovolume ($mL_{cell\ volume}$) estimation was based on image analysis of 200 algal cells with software program VIDS IV (Analytical Measuring Systems) and assuming an ellipsoidal 3D geometry of cells.

Uptake trials lasted until apparent stability of the ^{137}Cs concentration in algae and filtrate solution were achieved. Elimination trials lasted until no more than a residual radioactivity in algae was measured. Algae in 20mL aliquots of contaminated cultures were separated from radioactive solution with Millipore membranes (0.45Ø, 25mm), by gentle vacuum pressure. Measurements of ^{137}Cs activity in algae and filtrate solution were made by gamma spectrometry (NaI, Tl).

Treatment of data

Uptake and elimination time course data were fitted to buildup and loss functions and their derivatives at time = 0 were used as estimators of uptake rate (v_0) and elimination rate ($-v_0$). Rates were expressed in mol units of Cs^+ $mL^{-1}_{cell\ vol.}$ h^{-1}. Dimensionless concentration factor (CF) was computed as the quotient of the asymptotic values of buildup functions for algae (Bq $mL^{-1}_{cell\ vol.}$) and loss functions for the radioactive solution (Bq $mL^{-1}_{sol.}$). Rationale as follows:

Build up function (algae) - $A_t = A_\infty(1 - e^{-\beta t})$; Loss function (solution) - $A_t = A_\infty + A_0 e^{-\delta t}$; Two compartment loss function (algae) $- A_t = a_1 e^{-\varphi_1 t} + a_2 e^{-\varphi_2 t}$, with A_t, time course (h) activity in algae (Bq $ml^{-1}_{cell.vol.}$) or solution (Bq $ml^{-1}_{sol.}$); A_∞, assymptotic values; A_0, initial activity; β, growth constant (h^{-1}); δ, decay constant ; a_1, a_2, sum components of the starting activity of algae; φ_1, φ_2, decay constants.

Nernst potential for $^{137}Cs^+$ was estimated by the Nernst equation applying the CF's determined experimentally. Rationale as follows:

$E_j^N = \frac{RT}{z_j F} \ln \left[\frac{C_j^o}{C_j^i} \right]$, with E_j^N, Nernst potential of ion j (mV, negative); C_j^o, external concentration of j; C_j^i, internal concentration of j; R,T,F, thermodynamic constants; z, ion electric charge. The quotient

$\left[\frac{c_j^o}{c_j^i}\right]$ expresses the asymmetry of j concentrations and is the inverse of CF. For a monovalent cation and at 20°C the equation is simplified to $E_j^N = 59 \log CF^{-1}$.

Using the enzyme kinetics approach expressed by the Michaelis-Menten model, the uptake kinetics of Cs$^+$ by *C. reinhardtii* shows the changes in its initial uptake velocity (i.e. uptake rate) by changing the external [Cs$^+$] and using a constant concentration of tracer ^{137}Cs$^+$. Linearization of data using the double inverses (Lineweaver-Burk) method helped estimating the maximum uptake rate (V_{max}) and the affinity constant of ^{137}Cs$^+$ transport (K_M). Rationale as follows:

Adaptation of Michaelis-Menten model: $v_0 = \frac{V_{max}[Cs^+]}{K_M + [Cs^+]}$; with v_0 – initial velocity of Cs$^+$ uptake; V_{max} – maximum velocity; K_M – affinity constant; [Cs$^+$] - cesium concentration in solution.

Lineweaver-Burk double inverses linearization: $\frac{1}{v} = \frac{1}{V_{max}} + \frac{K_M}{V_{max}} \times \frac{1}{[Cs^+]}$; where $1/V_{max}$ is the *yy* intercept and -1/K_M is the *xx* intercept of the fitted straight line.

Results and Discussion

^{137}Cs uptake and accumulation have been gradually reduced in K$^+$ deficient and K$^+$ sufficient algae, by increasing [K$^+$]$_{ext}$ (Fig. 1). The most significant effect was a dramatic decrease in v_0 and CF when [K$^+$]$_{ext}$ changed from 1 µM to 5 µM (Table 1).
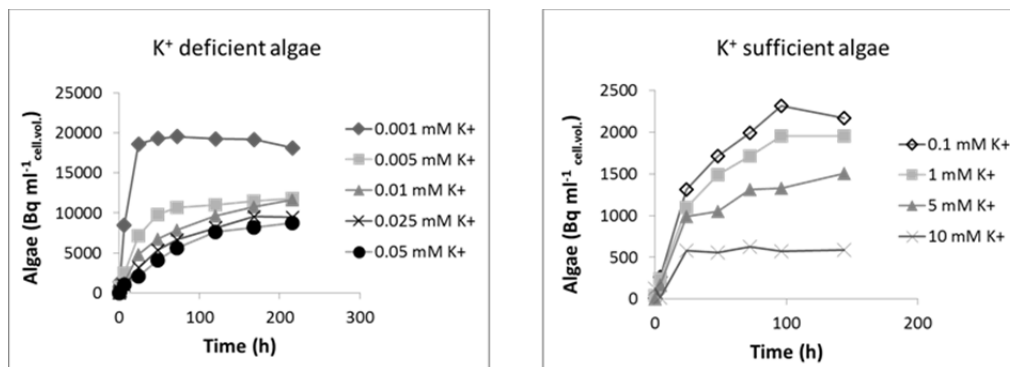
Figure 1. *Time course of ^{137}Cs uptake by K$^+$ deficient and K$^+$ sufficient microalgae in K$^+$ supplemented cultures (1µM K$^+$ and 0.1mM K$^+$ are the control cultures for deficiency and sufficiency; data are the mean of 3 replicates)*

With [K$^+$] ≤ 0.1 mK, the absolute value of ^{137}Cs$^+$ equilibrium potential (E^N_{137Cs}) clearly exceeds the absolute value of membrane potential (E_m) of *C. reinhardtii* estimated by Malhotra and Glass (1995). This means that in such conditions the driving force (electrochemical potential gradient) would tend to push the ^{137}Cs$^+$ ions out of the algal cells, therefore uptake would require an active transport mechanism. With [K$^+$] > 0.1 mM, E^N_{137Cs} practically equals the E_m estimated by Malhotra and Glass creating a situation where theoretically the net flux of ^{137}Cs$^+$ would be null. Once there was in fact a measured uptake of ^{137}Cs$^+$, this apparent paradox may be a consequence of the underestimation of E_m using the equilibrium distribution of [^{3}H]TPP$^+$ as was pointed out by Rodriguez-Navarro (2000).

Table 1. *Estimated values of uptake rate (v_0, pmol $^{137}Cs^+$ $ml^{-1}_{cellvol}$ h^{-1}), concentration factor (CF, dimensionless) and equilibrium potential (E^N_{137Cs}, mV) of $^{137}Cs^+$ under different K^+ concentrations (mM). Potential membrane (E_m, mV) according to the estimations of Malhotra and Glass (1995). Where applied data are mean±standard deviation, n=3*

$[K^+]_{ext}$	v_0	CF	E^N_{137Cs}	E_m
0.001	20.9±3.96	48388±3975.4	-276.3±2.139	-135
0.005	4.82±0.55	4567.7±583.29	-215.8±3.173	"
0.01	2.17±0.23	4246.0±529.41	-213.9±3.320	"
0.025	1.66±0.45	3593.6±796.80	-209.4±5.399	"
0.05	1.20±0.17	3340.9±309.48	-207.8±2.365	"
0.1	0.81±0.07	491.9±136.	-158.2±6.752	"
1	0.66±0.07	405.9±15.59	-153.9±0.974	-156
5	0.59±0.15	279.2±43.54	-144.1±4.202	-140
10	0.45±0.05	112.5±5.969	-121.1±1.353	-120

When contaminated algae were transferred to nonradioactive solutions, a stronger retention of the accumulated radionuclide was observed in the algae raised in solutions with the lowest K^+ concentrations. Loss of $^{137}Cs^+$ was enhanced with $[K^+]_{ext} \geq 0.1$ mM (Fig.2).
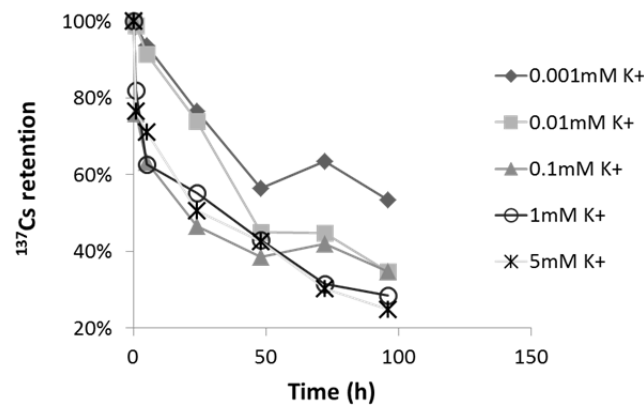
Figure 2. *Time course of $^{137}C^+$ retention after algae being transferred to nonradioactive solutions with different K^+ treatments (data are mean of three replicates).*

Loss rate was less than 1 pmol $^{137}Cs^+$ $mL^{-1}_{cell\ vol.}$ h^{-1} with $[K^+]_{ext} \leq 10\mu M$ and increased significantly with $[K^+]_{ext} \geq 0,1$ mM up to 15 pmol $^{137}Cs^+$ $mL^{-1}_{cell\ vol.}$ h^{-1}. The modulation exerted by $[K^+]_{ext}$ on the $^{137}Cs^+$ efflux is consistent with the hypothesis that $^{137}Cs^+$ is liberated through K^+ outward rectifying channels (White and Broadley, 2000). These have low activity when plant cells are under K^+ deficiency. By increasing $[K^+]_{ext}$, the cell membrane becomes depolarized (E_m less negative) and repolarization happens by the activation of outward K^+ channels, increasing K^+ efflux and presumably $^{137}Cs^+$ as well. As a consequence, in *C. reinhardtii* $^{137}Cs^+$ loss rates ($-v_0$) increase and biological periods ($Tb_{1/2}$) decrease significantly (Table 2).

Table 2. *Estimated values of loss rate (-v_0) and biological half life (Tb$_{1/2}$) of $^{137}Cs^+$ in C. reinhardtii under different K^+ treatments ([K^+]$_{ext}$, mM; -v_0, pmol $^{137}Cs^+ml^{-1}_{cellvol}$ h^{-1}; Tb$_{1/2}$, h. Data are the mean of three replicates±standard deviation).*

[K^+]$_{ext}$	-v_0	Tb$_{1/2}$
0.001	0.74±0.12	60.1±9.27
0.01	0.30±0.01	45.8±5.34
0.1	9.24±2.60	21.0±9.53
1	11.6±0.94	30.3±13.1
5	15.2±5.00	30.7±3.23

In K^+ deficiency, algal cells exhibited an evident saturable Cs^+ uptake kinetics. A saturation profile was not evident in K^+ sufficiency within the tested range of [K^+]$_{ext}$ (Figs. 3A, B, C, D).
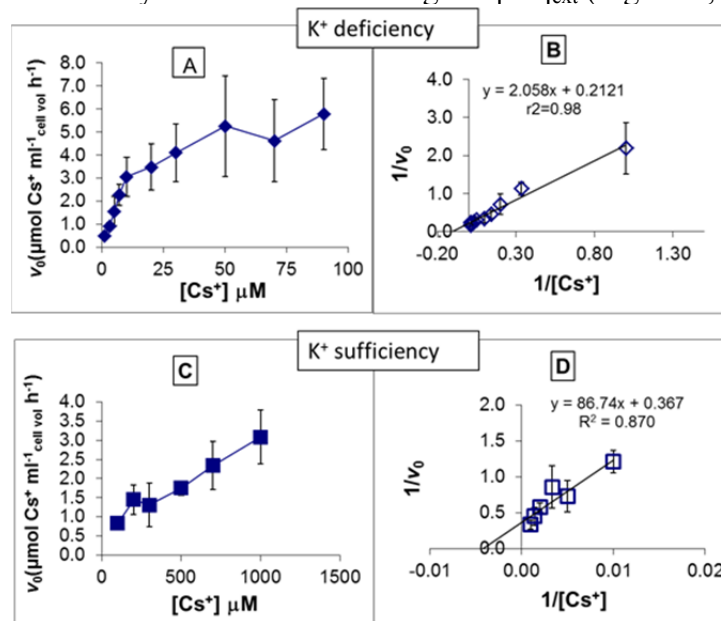
Figure 3. *Kinetics of Cs^+ uptake by K^+ deficient (A) and K^+ sufficient (C) microalgae. B and D represent the Lineweaver-Burk plots.*

In K^+ deficiency $^{137}Cs^+/Cs^+$ uptake was mediated by a saturable transport mechanism with a low constant affinity K_M = 9.7 µmol $Cs^+ml^{-1}_{cellvol}$ h^{-1}, significantly more efficient than the uptake mechanism in K^+ sufficiency with a higher K_M= 236.5 µmol $Cs^+ml^{-1}_{cellvol}$ h^{-1} (Table 3).

Table 3. *Kinetic parameters of Cs^+ uptake in K^+ deficient and K+ sufficient microalgae C. reinhardtii.*

	L.-Burk parameters		M.-Menten parameters		Uptake efficiency
	$1/V_{max}$	$-1/K_M$ (xx intercept)	V_{max}	K_M	V_{max}/K_M
K^+ deficiency	2.058	-0.103	4.715	9.665	0.488
K^+ sufficiency	86.74	-0.004	2.726	236.5	0.012

V_{max}, µmol Cs^+ $ml^{-1}_{cellvol}$ h^{-1}; K_M, µM Cs^+; Efficiency, $ml^{-1}_{cellvol}$ h^{-1} $l_{solution}$.

Conclusions

Results are consistent with the proposed hypothesis of K^+ active transporters and K^+ ion channels mediating the transport of $^{137}Cs^+$ in C. *reinhardtii*, with external K^+ conditions modulating uptake and loss. Any attempt to model the accumulation of $^{137}Cs^+$ by green microalgae in an environmental contamination context, should take into account the physiological aspects involved in the uptake and loss of the free cation and the modulation exerted by the environmental concentration of K^+ on the transport mechanisms.

References

Fernández, J.A., Maldonado, J.M. . 2000. Absorción y transporte de nutrientes minerales, in: Azcón-Bieto, J., Tallón, M. (Eds.), Fundamentos de Fisiología Vegetal. Edicions Universitat de Barcelona, pp. 99-112.

Maathuis, F.J.M., Sanders, D., 1999. Plasma membrane transport in context – making sense out of complexity. Curr. Opin. Plant Biol. 2, 236 – 243.

Lewis, L.A., McCourt, R.M., 2004. Green algae and the origin of land plants. Am. J. Bot. 100, 1535 – 1556.

Malhotra, B., Glass, A.D.M., 1995. Potassium fluxes in Chlamydomonas reinhardtii. (I) Kinetics and electrical potentials. Plant Physiol. 108, 1527 – 1536.

Margalef, R., 1983. Productores primarios del plankton, in: Limnología. Ediciones Omega, pp.203-246.

White, P.J., Broadley, M.R., 2000. Mechanisms of caesium uptake by plants. New Phytol. 147: 241-256.

Rodriguez-Navarro, A., 2000. Potassium transport in fungi and plants. Biochim. Biophys. Acta. 1469: 1-30.

Zhu, Y-G., Smolders, E., 2000. Plant uptake of radiocesium: a review of mechanisms, regulation and application. J. Exp. Bot. 51: 1635 -1645.

Influence of radioecological parameters on the dose rate in urban environments after a release of radioactive substances

Y. Hinrichsen[*] and K. G. Andersson

Technical University of Denmark, Center for Nuclear Technologies, DTU Risø Campus, Frederiksborgvej 399, 4000 Roskilde, Denmark

Abstract

In radiological emergency management many radioecological parameters are used for making decisions about e.g. evacuation or decontamination due to natural post deposition mobility of radiocontaminants. These applied parameters almost exclusively relate to radiocaesium contamination in soluble (cationic) form, as it has been of primarily concern in connection with the past large accidental releases from nuclear power plants. Secondary radiological parameter studies have mainly focused on rural areas so far. But apart from this scenario other radionuclides or physicochemical forms (e.g. particles) might be relevant for specific areas or in other radiological events. The effects on urban areas should also be considered.

Therefore a simple house geometry was used to calculate the air kerma in various parts of the house caused by different source areas. Those values were compared with previous calculations to show their influence of modelling parameters to the final results. Additionally for different scenarios already existing parameters were used to estimate the deposition and the mobility of the radiocontaminants on the different surfaces. By changing of parameters the influence of the physicochemical form of different radioactive substances on the resulting air kerma is shown.

Introduction

In radiological emergency management many radioecological parameters are used for making decisions about e.g. evacuation or decontamination due to natural post deposition mobility of radiocontaminants. They are included in the current European standard decision support systems ARGOS and RODOS. So far events like the past large accidental releases from nuclear power plants were of primarily concern. But apart from this scenario also other events could result in a dispersion of radioactive substances like accidents with highly radioactive sources, transport accidents or radiological terrorism. Other radionuclides or physicochemical forms (e.g. particles) might be relevant for specific areas after an accident at a nuclear power plant, too. In addition some of these scenarios are more likely to happen in an urban area.

The following calculations are based on a release of radionuclides to urban environments in which the gamma radiation from deposited radioactive substances contributes to the radiation exposure of the population. For the evaluation of this exposure pathway, three main model requirements are needed: (i) the calculation of the air kerma per photon emitted per unit source area, based on Monte Carlo calculations; (ii) the deposition distribution of contaminants on the different urban surfaces; and (iii) their post-deposition migration.

Materials and Methods

Air kerma from contaminated urban surfaces

Most of the air kerma for different types of buildings were calculated in the late eighties at the GSF (now Helmholtz Zentrum München - German Research Center for Environmental Health) (Jacob & Meckbach, 1987; Meckbach et al., 1988; Meckbach & Jacob, 1988). On the basis of the published data the model of a semi-detached house (Fig. 1) was calculated again using the transport code MCNP6 (Goorley et al., 2012) using the cross section data set ENDF/B-VII.0 (Chadwick et al., 2006).
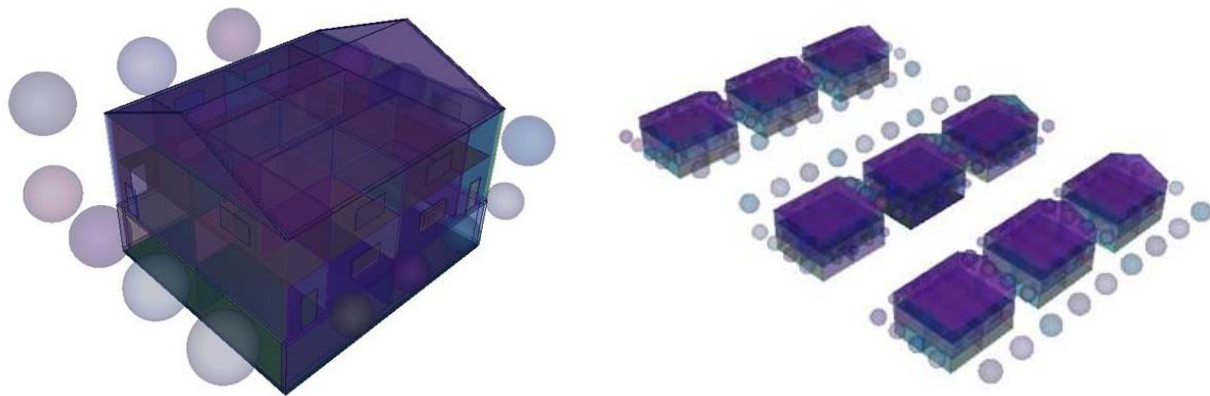
Figure 1. Birds-eye view of the semidetached house without (left) and with (right) neighbouring buildings. The spheres indicate the position of the trees.

Among others processes the MCNP code accounts for photon creation and loss through bremsstrahlung, p-annihilation, fluorescence, Compton scattering, pair production and photon capture that were most relevant in these calculations. The code allows the definition of complex three-dimensional geometries through a combinatorial geometry technique. The regions in space were constructed by logical combination (union, intersection, difference) of elementary geometric bodies and surfaces. The materials densities were assigned to the input data for the different building structures and environmental regions by using the data published by GSF (Meckbach et al., 1988) added by atomic composition data that were compiled by Pacific Northwest National Laboratory (McConn et al., 2011).

The source and detector regions were defined according to the data given by GSF (Meckbach et al., 1988). The number and energies of gamma particles passing through the detector regions were scored and by using conversion coefficients (ICRP, 2010) transferred to the air kerma free-in-air at the end of the calculation.

The calculated air kerma values per photon emitted per unit source area were compared to those published at GSF (Meckbach et al., 1988). The deviations were calculated for different source and detector areas and averaged over three different photon energies (Tab. 1).

From the results for the source areas on the house can be assumed that the highest differences of the shielding capability are the walls of the house. This effect can also be seen for the other source regions.

		Detection area		
		Basement	Ground floor	First floor	Attic
	On the house:				
	Windows	12%	59%	22%	32%
	Walls and doors	64%	59%	84%	77%
Source	Roof	5%	18%	8%	6%
	Without neighbouring buildings:				
	Ground	49%	63%	73%	19%
	With neighbouring buildings:				
	Ground	58%	64%	87%	87%
	Neighbouring buildings	65%	78%	65%	47%
	Trees	53%	25%	76%	10%

Table 1. *Deviation of kerma calculations to previous ones (Meckbach et al., 1988) according to source and detection area.*
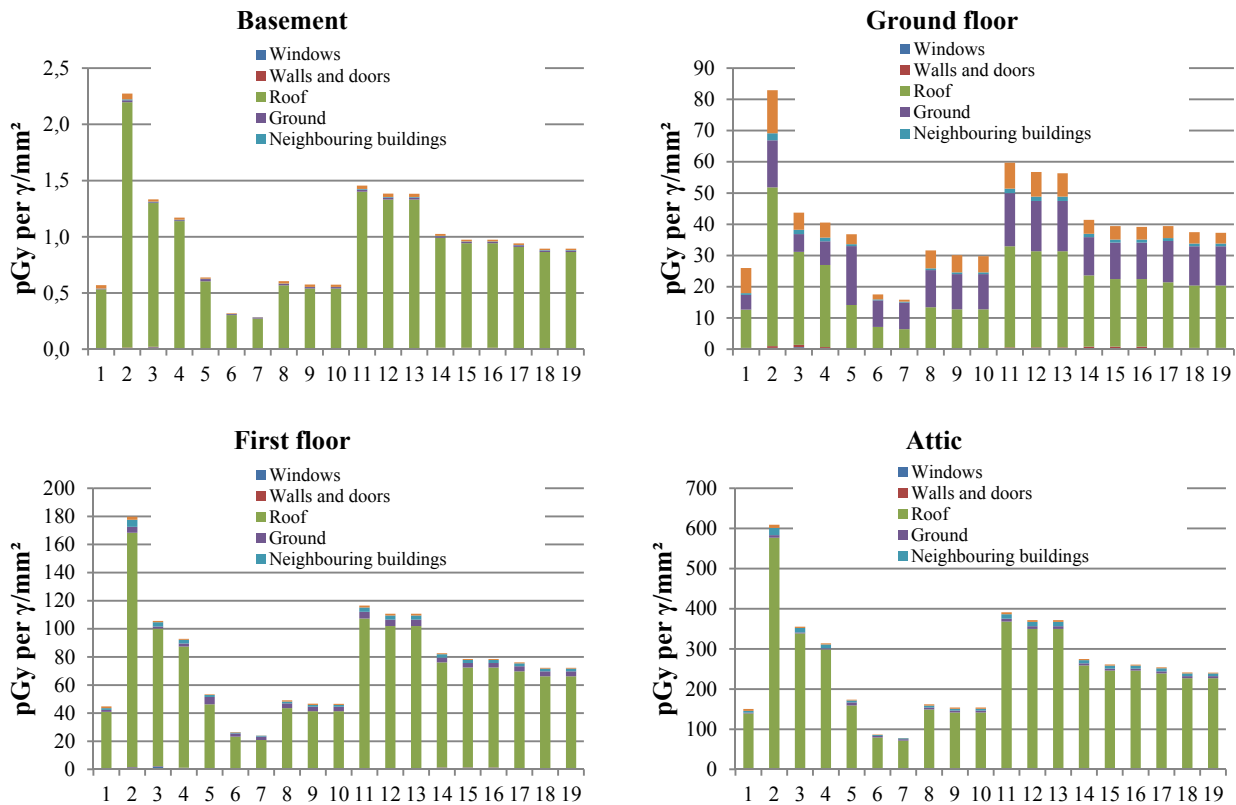
Figure 2. *Initial air kerma after deposition in parts of a semi-detached house distributed on different source areas. Bars 1-4 represent dry, bars 5-7 wet and bars 8-19 an equal amount of dry and wet deposition. Different particle sizes as activity median aerodynamic diameter (AMAD) are represented for <2 μm in bars 1 and 8-10, for 2-5 μm in bars 2 and 11-13, for 5-10 μm in bars 3 and 14-16 and for 10-20 μm in bars 4 and 17-19. The first run-off of rain water is represented in bars 6, 9, 12, 15, 18 for caesium cations and in bars 7, 10, 13, 16, 19 low solubility particles. The results are given in pGy per emitted photon of 0.662 MeV on a grassed reference surface of 1 mm².*

Distribution of contaminants on urban surfaces

As a next step the initial deposition to the different surfaces have to be considered. A grassed reference surface is used in combination with information on relative deposition to different surfaces to give an initial deposition on all surfaces considered in the model being used. The

relative deposition of particles depends on different weather conditions, the types of surfaces and the characteristics of the contaminants. The values applied are average values based on various publications (Alexander & Cresser, 1994; Andersson, 1991; Andersson et al., 2002; Carini & Bengtsson, 2001; Carlyle-Moses, 2004; Frank & Tschiersch, 1992; Freer-Smith et al., 2003; Gravenhorst & Höfken, 1982; Hirose et al., 1993; Horn et al., 1988; IAEA, 1994; Jacob & Meckbach, 1987; Jacob et al. 1987; Jacob et al., 1990; Kammann et al., 2005; Karlberg, 1986; Karlberg, 1992; Manfroi et al., 2004; McMahon & Denison, 1979; Müller & Pröhl, 1993; Neal et al., 1993; Nicholson, 1989; Pryor & Barthelmie, 2005; Rodriguez et al., 1999; Roed, 1985; Roed, 1987a; Roed, 1987b; Roed, 1988; Roed, 1990; Roed & Jacob, 1990; Ronneau et al., 1987; Rulik et al., 1989; Sandalls & Gaudern, 1988; Schell et al., 1996; Schimmack et al., 1991; Schwartz, 1986; Sehmel, 1973; Trautner et al., 1991; Tschiersch et al., 1995; Underwood, 1988; Watterson & Nicholson, 1996; Xiao et al., 2000).

In combination with the determined air kerma from different surfaces the initial air kerma after deposition was calculated for the different detector areas and different deposition conditions (Fig. 2). The ground was assumed to be paved.

The bars show that apart from the ground floor the highest air kerma in the house is caused by deposition of particles on the roof. Particles of AMAD >2 µm are causing the highest initial air kerma, especially those of AMAD 2-5 µm.
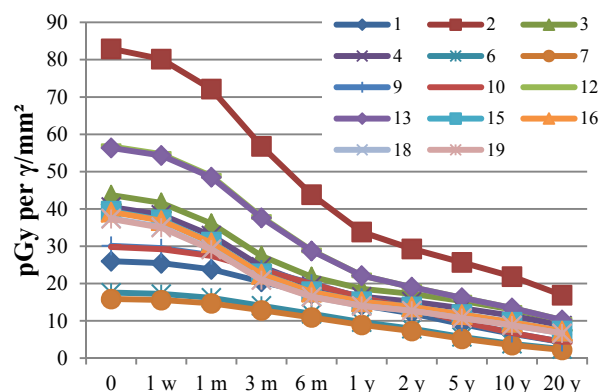
Figure 3. Air kerma development over different time scales at the ground floor of a semi-detached house. Graphs 1-4 represent dry, bars 6 and 7 wet and graphs 9-19 an equal amount of dry and wet deposition. Different particle sizes as activity median aerodynamic diameter (AMAD) are represented for <2 µm in graphs 1, 9 and 10, for 2-5 µm in graphs 2, 12 and 13, for 5-10 µm in graphs 3, 15 and 16 and for 10-20 µm in graphs 4, 18 and 19. The first run-off of rain water is represented in bars 6, 9, 12, 15, 18 for caesium cations and in bars 7, 10, 13, 16, 19 low solubility particles. The results are given in pGy per emitted photon of 0.662 MeV on a grassed reference surface of 1 mm² at the time of the initial deposition.

Migration of contaminants after deposition on urban surfaces

Following its deposition, material is transferred by a number of processes which modify the relative deposition to different surfaces. The migration of deposited particles depends on the types of surfaces and the characteristics of the contaminants and the retention of contamination is commonly described using a double exponential equation. The applied values for the retention parameters are based on various publications (Andersson, 1991; Andersson et al., 1995; Andersson et al., 1996; Andersson et al., 2002; Bender & Terstriep, 1984; Bunzl et al., 1997; Jacob et al., 1987; Jacob et al., 1990; Karlberg, 1986; Karlberg, 1992; Roed, 1987a; Roed, 1988; Roed, 1990; Roed & Andersson ,1996; Roed et al., 1998; Sandalls & Gaudern, 1988; Sartor et al., 1974, Sartor & Gaboury, 1984;

Warming, 1982; Warming, 1984; Wilkins, 1987). In combination with the pervious results the development of air kerma was calculated over different time scales for the ground floor as several source areas are relevant for it (Fig. 3).

As all graphs seem to develop similarly over time the development of all the contributing source areas is shown in Fig. 4 for the scenarios with dry deposition and different AMADs.
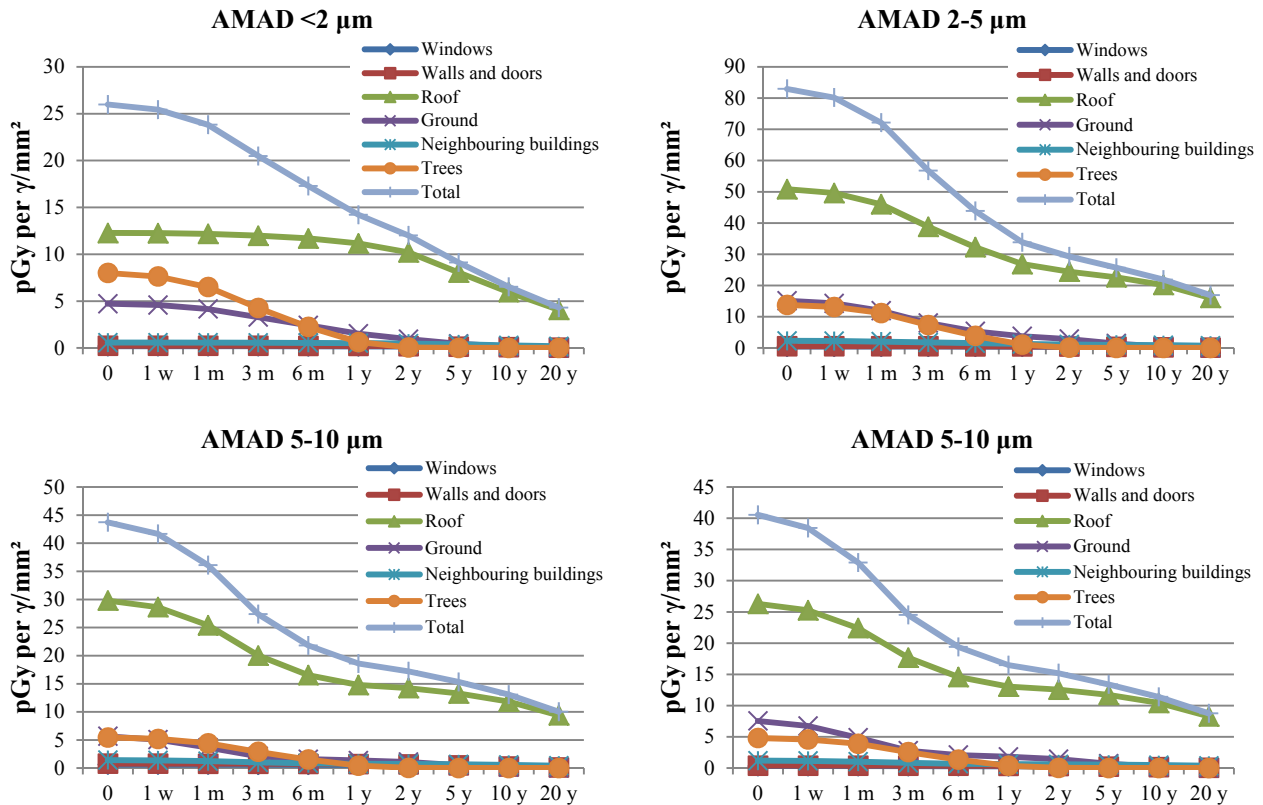
Figure 4. Air kerma development caused by different source areas over different time scales at the ground floor of a semi-detached house. The results are given in pGy per emitted photon of 0.662 MeV on a grassed reference surface of 1 mm² at the time of initial deposition.

The graphs show regardless of AMAD that after ca. 1 year apart from the roof the other source areas that contribute air kerma to the ground floor become more and more negligible.

Results and Discussion

From the calculations of the air kerma per photon emitted per unit source area could be concluded that different characteristics of walls could have a high impact on the total air kerma inside a house. But as seen from the deposition distribution of contaminants and their post-deposition migration the effect is almost negligible compared to the high contribution of a contaminated roof to the total air kerma inside a semi-detached house caused by its rather low shielding factor.

Conclusions

As pointed out the contamination of roofs seem to have an high influence on the air kerma inside houses. Therefore further radiological parameter studies on the behaviour of contaminants on different types of roofs as well as further Monte Carlo calculations are of major interest in radiological emergency management.

References

Alexander, C. E., Cresser, M. S., 1994. An assessment of the possible impact of expansion of native woodland cover on the chemistry of Scottish freshwaters. Forest Ecology and Management 73, 1-27.

Andersson, K.G., 1991. Contamination and decontamination of urban areas. Ph.D. Thesis, Riso National Laboratory.

Andersson, K. G., Roed, J., Paretzke, H. G., Tschiersch J., 1995. Modelling of the radiological impact of a deposit of artificial radionuclides in inhabited areas. in: Deposition of radionuclides, their subsequent relocation in the environment and resulting implications (Tschiersch J, Editor) EC report EUR 16604

Andersson, K.G., Roed, J. Jacob, P., Meckbach, R., 1996. Weathering of ^{137}Cs on various surfaces in inhabited areas and calculated location factors. in: Deposition of radionuclides, their subsequent relocation in the environment and resulting implications, J. Tschiersch (editor) EUR 16604 EN, ISBN 92-827-4903-7, pp. 47-57.

Andersson, K. G., Roed, J., Fogh, C. L., 2002. Weathering of radiocaesium contamination on urban streets, walls and roofs. Journal of Environmental Radioactivity 62 (1), 49-60.

Bender, G. M., Terstriep, M .L., 1984. Effectiveness of street sweeping in urban runoff pollution control. Science of the Total Environment 33, 185-192.

Bunzl, K., Jacob, P., Schimmack, W., Alexakhin, M., Arkhipov, N. P., Ivanov, Y., Kruglov, S. V., 1997. ^{137}Cs mobility in soils and its long-term effect on the external radiation exposure. Radiation and Environmental Biophysics 36, 31-37.

Carini, F. & Bengtsson, G., 2001. Post-deposition transport of radionuclides in fruit. Journal of Environmental Radioactivity 52, 215-236.

Carlyle-Moses, D.E., 2004. Throughfall, stemflow, and canopy loss fluxes in a semi-arid Sierra Madre Oriental matorral community. Journal of Arid Environments 58(2), 181-202.

Chadwick, M. B., Oblozinsky, P., Herman, M., Greene, N. M., McKnight, R. D., Smith, D. L., Young, P. G., MacFarlane, R. E., Hale, G. M., Frankle, S. C., Kahler, A. C., Kawano, T., Little, R. C., Madland, D. G., Moller, P., Mosteller, R. D., Page, P. R., Talou, P., Trellue, H., White, M. C., Wilson, W. B., Arcilla, R., Dunford, C. L., Mughabghab, S. F., Pritychenko, B., Rochman, D., Sonzogni, A. A., Lubitz, C. R., Trumbull, T. H., Weinman, J. P., Brown, D. A., Cullen, D. E., Heinrichs, D. P., McNabb, D. P., Derrien, H., Dunn, M. E., Larson, N. M., Leal, L. C., Carlson, A. D., Block, R. C., Briggs, J. B., Cheng, E. T., Huria, H. C., Zerkle, M. L., Kozier, K. S., Courcelle, A., Pronyaev, V., van der Marck, S. C., 2006. ENDF/B-VII.0: Next generation evaluated nuclear data library for nuclear science and technology. Nuclear Data Sheets 107 (12), 2931–3060.

Frank, G., Tschiersch, J., 1992. Parameterisation of below cloud scavenging at low precipitation intensities by using a fluorescent tracer method. Journal of Aerosol Science 23, S885-S888.

Freer-Smith, P. H., El-Khatib, A. A., Taylor, G., 2003. Capture of particulate pollution by trees: a comparison of species typical of semi-arid areas (Ficus Nitida and Eucalyptus Globulus) with European and North American species. Water, Air and Soil Pollution 155 (1-4), 173-187.

Goorley, T., James, M., Booth, T., Brown, F., Bull, J., Cox, L. J., Durkee, J., Elson, J., Fensin, M., Forster, R. A., Hendricks, J., Hughes, H. G., Johns, R., Kiedrowski, B., Martz, R., Mashnik, S., McKinney, G., Pelowitz, D., Prael, R., Sweezy, J., Waters, L., Wilcox, T., Zukaitis, T., 2012. Initial MCNP6 Release Overview. Nuclear Technology 180, 298–31.

Gravenhorst, G., Höfken, K. D., 1982. Concentration of aerosol constituents above and beneath a beech and a spruce forest canopy, in H. W. Georgii & J. Pankrath: Deposition of Atmospheric Pollutants, D. Reidel, Dordrecht, the Netherlands.

Hirose, K., Takatani, S., Aoyama, M., 1993. Wet deposition of radionuclides derived from the Chernobyl Accident. Journal of Atmospheric Chemistry 17(1), 61-71.

Horn, H. G., Maqua, M., Bonka, H., 1988. Nasse und trockene Ablagerung radioaktiver Stoffe auf die Vegetation und den Erdboden. Schriftenreihe Reaktorsicherheit und Strahlenschutz, BMU 199 –195, ISSN 0724-3316.

IAEA, 1994. Modelling the deposition of airborne radionuclides into the urban environment. First report of the VAMP Urban Working Group, IAEA TECDOC 760, International Atomic Energy Agency, Vienna.

ICRP, 2010. Conversion Coefficients for Radiological Protection Quantities for External Radiation

Exposures. ICRP Publication 116, Annals of the ICRP 40(2–5).

Jacob, P., Meckbach, R., 1987. Shielding factors and external dose evaluation. Radiation Protection Dosimetry 21 (1/3), 79-85.

Jacob, P., Meckbach, R. & Müller, H.M., 1987. Reduction of external exposure from deposited Chernobyl activity by run-off, weathering, street cleaning and migration in the soil. Radiation Protection Dosimetry 21(1/3), 51-57.

Jacob, P., Meckbach, R. Müller, H. M., Meimberg, K., 1990. Abnahme von künstlicher Radioaktivität nach Deposition in städtischer Umgebung. Abschlussbericht zum Forschungsvorhaben, Förderkennzeichen St.Sch.1051, GSF, Neuherberg, Germany.

Kammann, C., Grünhage, L., Gruters, U., Janze, S., Jäger, H. J., 2005. Response of aboveground grassland biomass and soil moisture to moderate long-term CO2 enrichment. Basic and Applied Ecology 6 (4), 351-365.

Karlberg, O., 1986. Avrinning och retention av Chernobyl nedfallet i stadsmiljö – Fält-mätningar med gamma spectrometer. Technical Note (6 pages), Studsvik AB, Nyköping, Sweden.

Karlberg, O., 1992. The environmental behaviour of Chernobyl deposition in a high fallout region of Sweden – Measurements and analysis of the urban programme 1986-1989, Studsvik Nuclear, Stockholm, Sweden, Report NS-92/1, ISBN 91-7010-184-1.

Manfroi, O. J., Koichiro, K., Nobuaki, T., Masakazu, S., Nakagawa, M., Nakashizuka, T., Chong, L., 2004. The stemflow of trees in a Bornean lowland tropical forest. Hydrological Processes 18(13), 2455-2474.

McConn Jr, R. J., Gesh, C. J., Pagh, R. T., Rucker, R. A., Williams III, R.G., 2011. Radiation Portal Monitor Project - Compendium of Material Composition Data for Radiation Transport Modeling. Pacific Northwest National Laboratory, PIET-43741-TM-963; PNNL-15870 Rev. 1.

McMahon, T. A., Denison, P. J., 1979. Empirical atmospheric deposition parameters – a survey. Atmospheric Environment 13, 571-585.

Meckbach, R., Jacob, P., Paretzke, H. G., 1988. Gamma exposures due to radionuclides deposited in urban environments. Part I: kerma rates from contaminated urban surfaces. Radiation Protection Dosimetry 25, 167-179.

Meckbach, R., Jacob, P., 1988. Gamma exposures due to radionuclides deposited in urban environments. Part II: location factors for different deposition patterns. Radiation Protection Dosimetry 25, 181-190.

Müller, H., Pröhl, G., 1993. ECOSYS-87: A dynamic model for assessing radiological consequences of nuclear accidents. Health Physics 64(3), 232-252.

Neal, C., Robson, A. J., Bhardwaj, C. L., Conway, T., Jeffery, H. A., Neal, M., Ryland, G. P., Smith, C.J., Walls, J., 1993. Relationships between precipitation, stemflow and throughfall for a lowland beech plantation, black-wood, Hampshire, Southern England – Findings on interception at a forest edge and the effect of storm damage. Journal of Hydrology 146(1-4), 221-233.

Nicholson, K. W., 1989. The dry deposition of small particles – a review of experimental measurements. Journal of Radiological Protection 9(2), 113-119.

Pryor, S. C, Barthelmie, R. J., 2005. Liquid and chemical fluxes in precipitation, throughfall and stemflow: Observations from a deciduous forest and a red pine plantation in the midwestern USA. Water Air and Soil Pollution 163 (1-4), 203-227.

Rodriguez, D., van Oijen, M., Schapendonk, A. H. M. C., 1999. LINGRA-CC: a sink-source model to simulate the impact of climate change and management on grassland productivity. New Phytologist 144, 359-368.

Roed, J., 1985. Dry deposition of urban surfaces, Risø Report R-515, ISBN 87-550-1069-5.

Roed, J., 1987a. Run-off from and weathering of roof material following the Chernobyl accident. Radiation Protection Dosimetry 21(1/3), 59-63.

Roed, J., 1987b. Dry deposition in rural and urban areas in Denmark, Radiation Protection Dosimetry 21(1/3), 33-36.

Roed, J., 1988. The distribution on trees of dry deposited material from the Chernobyl accident. paper NKA/AKTU-245 (88)2, presented at the Joint CEC/OECD (NEA) Workshop on Recent Advances in Reactor Accident Consequence Assessment, Rome, Italy, 25-30 January 1988.

Roed, J., 1990. Deposition and removal of radioactive substances in an urban area, ISBN 87 7303 514 9, NORD 1990:111.

Roed, J., Jacob, P., 1990. Deposition on urban surfaces and subsequent weathering. 335 - 356 in: Proc Seminar on methods and codes for assessing the off-site consequences of nuclear accidents. Athens 1990, EUR 13013.

Roed, J., Andersson, K.G., 1996. Clean-up of urban areas in the CIS countries contaminated by Chernobyl Fallout. Journal of Environmental Radioactivity 33(2), 107-116.

Roed, J., Andersson, K.G., Barkovsky, A.N., Fogh, C.L., Mishine, A.S., Olsen, S.K., Ponomarjov, A.V., Prip, H., Ramzaev, V.P., Vorobiev, B.F., 1998. Mechanical Decontamination Tests in Areas Affected by the Chernobyl Accident. Risø National Laboratory, Risø-R-1029, ISBN 87-550-2361-4.

Ronneau, C., Cara, J. & Apers, D., 1987. The deposition of radionuclides from Chernobyl to a forest in Belgium. Atmospheric Environment 21 (6), 1467-1468.

Rulik, P., Bucina, I., Malatova, I., 1989. Aerosol particle size distribution in dependence on the type of radionuclide after the Chernobyl accident and in the NPP effluents. Proceedings of the XVth Regional Congress of IRPA, Visby, Gotland, Sweden, 102-107, ISBN 3-88585-668-9, TÜV Verlag Rheinland GmbH, Köln.

Sandalls, F. J. & Gaudern, S. L., 1988. Radiocaesium on urban surfaces in West Cumbria five months after Chernobyl. Journal of Environmental Radioactivity 7, 87-91.

Sartor, J. D., Boyd, G. B., Agardy, F .J., 1974. Water pollution aspects of street surface contaminants. Journal WPCF, Water Pollution Control Federation, January 1974, 456-467.

Sartor, J. D., Gaboury, D. R., 1984. Street sweeping as a water pollution control measure: lessons learned over the past ten years. Science of the Total Environment 33, 171-183.

Schell, W. R., Linkov, I., Myttenaere, C., Morel, B., 1996. A dynamic model for evaluating radionuclide distribution in forests from nuclear accidents. Health Physics 70(3), 318-335.

Schimmack, W., Bunzl, K., Kreutzer, K., Rodenkirchen, E., Schierl, R., 1991. Einfluss von Fichte (Picea abies L. Karst) und Buchte (Fagus sylvatica L.) auf die Wanderung von radiocaesium im Boden. Fortwiss Forsch. 39, 242-251 (as referenced by Schell et al., 1996).

Schwartz, G., 1986. Deposition and post-deposition radionuclide behaviour in urban environments. Proc. Workshop on methods for assessing off-site radiological consequences of nuclear accidents, CEC, Luxemburg, Report EUR 10397 (EN), 533-558.

Sehmel, G. A., 1973. Particle eddy diffusitivities and deposition velocities for isothermal flow and smooth Surfaces. Journal of Aerosol Science 4, 125-138.

Trautner, F., Frank, G. & Tschiersch, J., 1991. Deposition of particle bound substances by fog and dew. Journal of Aerosol Science 22, S529-S532.

Tschiersch, J., Trautner, F. & Frank, G. (1995). Deposition of atmospheric aerosol by rain and fog, in Tschiersch et al.: Deposition of radionuclides, their subsequent relocation in the environment and resulting implications, EC Report EUR 16604 EN, European Commission, Brussels, Belgium, ISBN 92-827-4903-7.

Underwood, B. Y., 1988. Deposition in foggy condition. Safety and Reliability Directorate, UKAEA, Wigshaw Lane, Culcheth, Warrington WA3 4NE, report SRD R 487.

Warming, L., 1982. Weathering and decontamination of radioactivity deposited on asphalt surfaces. Risø report M-2273, ISBN 87-550-0903-4.

Warming, L., 1984. Weathering and decontamination of radioactivity deposited on concrete surfaces. Risø report M-2473, ISBN 87-550-1068-7.

Watterson, J. D., Nicholson, K. W., 1996. Dry deposition and interception of 4-22 μm diameter particles to a lettuce crop, Journal of Aerosol Science 27(5), 759-767.

Wilkins B. T., 1987. The retention behaviour of radiocaesium on common building materials under natural conditions. Radiation Protection Dosimetry 21 (1-3), 69-73.

Xiao, Q., McPherson, E. G., Ustin, S. L., Grismer, M. E., Simpson, J. R., 2000. Winter rainfall interception by two mature open-grown trees in Davis, California. Hydrological Processes 14, 763-784.

Analysis of transgenerational alterations in mitochondrial activity in three generations of crustacean *Daphnia magna* flowing acute parental exposure to γ-irradiation

E.I. Sarapultseva[1]*, D.V. Uskalova[2] and N.B. Savina[2]

[1] National ResearchNuclearUniversity "MEPhI", KashirskoeHighway, 31, Moscow 115409, Russian Federation
[2]Department of Biology, Institute of Nuclear Power Engineering NRNU MEPhI, Studgorodok,1, Obninsk, Kaluga Region 249040, Russian Federation

Abstract

Purpose: To analyze radiation-induced alterations in mitochondrial activity in the directly exposed crustaceans *Daphnia magna* and their non-exposed progeny.

Material and methods: One-days-old *Daphnia* from the F_0 generation were exposed to acute ^{60}Co γ-rays at doses of 10, 100, 1000 and 10000 mGy (2.8 – 96 cGy/min). The first- (F_1) and second- (F_2) generation offspring of exposed parents were not irradiated. In our study, the MTT-assay was first applied for the analysis of the *in vivo* mechanisms of transgenerational effects of radiation and developmental of stress in multicellular crustaceans *D. magna*. The MTT-test has been traditionally used for the analysis of drug cytotoxicity *in vitro*. The MTT-assay is a colorimetric assay that measures the activity of enzymes that reduce MTT (a yellow tetrazolium bromide) in living cells. The test allows measuring the activity of mitochondrial dehydrogenases, primarily succinate dehydrogenase and other oxidases that catalyze free radical processes in the electron transport chain with the formation of short-lived superoxide anion radical, as well as wide range of long-lived reactive oxygen species (ROS). MTT-assay was held in 4-day-old *Daphnia* in three generations. In each sample were 50 individuals.

Results: According to our data, the level of toxicity was significantly increased in the three groups of *Daphnia* exposed to 100, 1000 and 10000 mGy of gamma-rays ($LD_{50/30} \sim 60$ Gy). The toxic effects were not detected at a dose of 10 mGy. The effects of parental irradiation also manifested in the F_1 offspring, whereas in the F_2 generation the levels of toxicity were close to those in controls.

Conclusion: Given the results of our recent studies the decreased survival and life span are attributed to the persistently elevated level of toxicity in the directly exposed crustaceans and their F_1 offspring. The results of our studies suggest that: (i) radiation is the inductor, exposure to which perturbs metabolic processes at doses of $100 - 10000$ mGy in the directly exposed *D. magna* and their F_1 offspring; (ii) metabolic activity of *Daphnia* is restored in the second generation (F_2); (iii) toxic effects of radiation correlate with decreased survival and life span of the exposed *Daphnia* and their F_1 The results of our study also demonstrate that the MTT assay represents a useful biomarker of survival effects at *D. magna*.

Introduction

The number of papers published on the effects of ionizing radiation on aquatic invertebrates has increased in the last decade. The crustaceans *Daphnia magna* are ubiquitous in aquatic ecosystems. We have previously shown that parthenogenetic crustacean *Daphnia magna* represents a useful and very sensitive experimental model for the analysis of long-term effects of exposure to ionising radiation (Sarapultseva E.I. et al., 2008, 2011; Sarapultseva E.I. & Malina, 2009; Sarapul'tseva E.I. et al., 2013, 2014; Sarapultseva & Dubrova, 2016).

Most of the studies on the effects of ionizing radiation on aquatic invertebrates focus on mortality as the main parameter. Metabolic test is one of the important diagnostic parameter for

---

* Corresponding author, E-mail: helen-bio@yndex.ru

understanding the mechanisms underlying the effects of irradiation on mortality. It provides an opportunity to evaluate the oxidative stress that occurs in the body as a result of exposure.

Metabolic test have been widely used for the analysis of cytotoxic *in vitro* effects of anticancer chemotherapeutic agents, as well as other drugs. They allow to evaluate the effect of test compounds on cellular metabolism, including the generation of reactive oxygen species (ROS), cells and DNA structure, determination of viability and cell proliferative activity (Repetto et al., 2008; Shaukat et al., 2011).

From the literature known methods for evaluating the cytotoxicity of radiation exposure to change the permeability of cell membranes to different dyes, biochemical methods for determining the activity of lactate dehydrogenase, fluorescence methods for evaluating the integrity of mitochondrial ATP synthesis, the generation of ROS and lipid peroxidation radical products (O'Dowd C et al., 2009; Wu & Zhou, 2012).

The methyl thiazol-diphenyl-tetrazolium bromide (MTT) cell viability assay is widely used in determining drug sensitivity profiles and in primary screening of potential efficacy of chemotherapeutic drugs in cell lines (Hayon et. al., 2003; Hatok et al, 2009; Cancer Cell Culture, 2011). The MTT (3-[4,5-dimethylthiazol-2-yl]-2,5 diphenyl tetrazolium bromide) assay is based on the conversion of MTT into formazan crystals by living cells, which determines mitochondrial activity. Since for most cell populations the total mitochondrial activity is related to the number of viable cells, this assay is broadly used to measure the in vitro cytotoxic effects of drugs on cell lines or primary patient cells. Thus, any increase or decrease in viable cell number can be detected by measuring formazan concentration reflected in optical density (OD) using a plate reader at 540 and 720 nm.

In the cited articles was shown that the *in vitro* MTT assay has been extensively applied to predict drug sensitivity *in vivo*. However, to date this test has seldom been used for the analysis of in vivo effects. Earlier MTT-assay was first applied for the investigation *in vivo* of the mechanisms of non-targeted effects of radiation and development of stress in multicellular crustaceans *Daphnia magna* (Sarapul'tseva et al., 2013). In this paper we analyzed the radiation-induced transgenerational alterations of mitochondrial activity at acute exposed in D. magna and their non-exposed offspring.

Materials and Methods

Daphnia maintenance
The strain of *Daphnia magna* Straus used in our experiments was originally collected in the pond of the Moscow Zoo and maintained for several years at the laboratory in continuous parthenogenetic reproduction following the OECD guideline 211 (OECD, 2012) with modifications. D. magna were reared at density of 20 animals per 500 mL in aerated dechlorinated filtered tap-water (pH 7.5 – 8.2, O_2 ~9.0 mg/l; hardness: 128 mg L^{-1}, Ca:Mg 4:1, Fe 0.3 mg/l, Mn 0.1 mg/l) renewed a week. *Daphnia* were fed with green algae suspension (*Chlorella vulgaris*) at daily ration of 90 – 100 μg C *Daphnia*$^{-1}$. D. magna were incubated at 20 °C (±0.5°C) on a 12h/12h light/dark cycle photoperiod at light intensity 700-1200 lux (Climate Control model R2, LLC Omicron, Krasnoyarsk, Russia). Neonates were removed every weekday.

Irradiation
One-day-old *Daphnia* from the third broods of at least five females were γ-irradiated at the Lutch Facility (^{60}Co source, Lutch Irradiator, Latenegro, Latvia) at doses of 10 mGy (28 mGy min^{-}^{1}), 100 mGy (170 mGy min^{-1}), 1000 and 10,000 mGy (1000 mGy min^{-1}). During irradiation, D. magna were kept in the plastic tubes containing 15 ml of water with 10 individuals. All corresponding sham-treated (control) groups were placed in the same conditions but without irradiation.

To analyse the effects of parental exposure to the successive generation (F_1), one-day-old neonates from the third broods of generation F_0 were randomly taken from at least three females of irradiated or control groups and transferred to glass vials with 500 mL of water (20 *Daphnia* per vial). Using the same protocol, a group of second-generation offspring (F_2) was also established. Following generations F_1 and F_2 were maintained as the original samples but without exposure to γ-irradiation.

MTT-assay

The modified in vitro MTT-assay (Cancer Cell Culture, 2011) was used in this study. Four-days-old daphnids from at least fird broods were used in the MTT assay. 200 µl of MTT solution (Sigma, St. Louis, USA) (0.5 mg/ml) was added to an Eppendorf tube containing 50 *Daphnia.* After 10-min incubation, Daphnia were homogenized. The optical density was measured at 492 and 630 nm on tablet immunoassay analyzer StatFax 2100 (Awareness Technology, USA, VIS-model) and corrected for background noise. The 630 nm OD background were subtracted from the 492 nm OD total signal. The average OD of the blank control wells (homogenized Daphnia in DMSO without MTT) was subtracted.

Data analysis

All statistical analyses were conducted using SYSTAT 13 version (Systat Software Inc. San Jose, CA, USA). Two-way analysis of variance was performed to assess the effects of exposure on different generations. The homogeneity of quantitative traits within a group, and the significance of differences with appropriate controls was estimated using Kruskal-Wallis test with Bonferroni correction for multiple comparisons (Hosmer et al., 2008).

Results and Discussion

Within all control groups the values of MTT-test did not significantly differ (Kruskal-Wallis test 3.47, $P=0.06$). Therefore further analysis was performed on the combined control. Evaluation of radiation contribution in effect was carried out using two-factor analysis of variance. Table 1 shows the results of this analysis.

Table 1. Results of two-way analysis of variance for the effects of irradiation on the values of MTT-test

Factors	F (df)[*]	P[†]
Dose	50.73 (4.470)	1.27×10^{-11}
Generation	3.79 (1.470)	0.0521
Interaction	4.09 (4.470)	0.0029

* The value of Fisher test and the number of degrees of freedom (df)
† probability

The data on cytotoxic effects of parental irradiation provide a plausible explanation for the compromised fitness of directly exposed *Daphnia* and their F_1 offspring. The results shown in Table 1 suggest that γ-irradiation has a strong toxic effect as to the parental samples, as to the non-exposed offspring of *Daphnia* from F_1 generation. At the same time there are also significant differences between the effects directly irradiated generation and their offspring. Table 2 shows the changes in optical density in samples. They demonstrated the changes in mitochondrial activity in cells of control and irradiated *D. magna* from the F0 generation as well as effects in F1 generation. The table shows significant effect of irradiation at dose of 100 mGy on mitochondrial daphnids from the F0 generation. This dose is 50 times lower than the semi-lethal for *D. magna* (medial lethal dose for an adult *Daphnia* is about 50-60 Gy (Sarapul'tseva & Malina, 2009).

Table 2. The changes in optical density in samples of irradiated *D. magna* and their offspring from F0, F1 and F2 generations

	Generation F_0	Generation F_1	Поколение F_2
Dose, mGy	Mean ± sem		
Control	0.23±0.007 (n=52)	0.19±0.006 (n=52)	0.22±0.01 (n=44)
10	0.2174 ± 0.0149 (n=43, P^*=0.5780)	0.16±0.007 (n=67, P^*=6.33 x10^{-7})	0.21±0.01 (n=24, P^*=0.691)
100	0.1310 ± 0.0081 (n=53, P^*=3.00 x 10^{-15})	0.1450 ± 0.0059 (n=43, P^*=3.00 x 10^{-15})	0.21±0.02 (n=17, P^*=1)
1000	0.1244 ± 0.0078 (n=40, P^*=3.00 x 10^{-15})	0.1511 ± 0.0057 (n=49, P^*=6.66 x10^{-15})	0.17±0.03 (n=13, P^*=1)
10000	0.11±0.015 (n=20, P^*=1.23 x 10^{-6}	0.0969 ± 0.0180 (n=19, P^*=1.82 x10^{-8})	0.16±0.02 (n=17, P^*=0.062)
$P^\dagger$	9.99 x 10^{-16}	9.99 x 10^{-16}	0.13

* Bonferroni corrected probability of difference from control (Kruskal-Wallis test).
† Probability of Kruskal-Wallis test for homogeneity of all groups.

Fig 1 shows that the optical density, reflecting changes in mitochondrial activity and expressed as a percentage of the total control, was lower in exposed *Daphnia* from F_0 generation than in control samples with the exception of irradiated at a dose of 10 mGy.
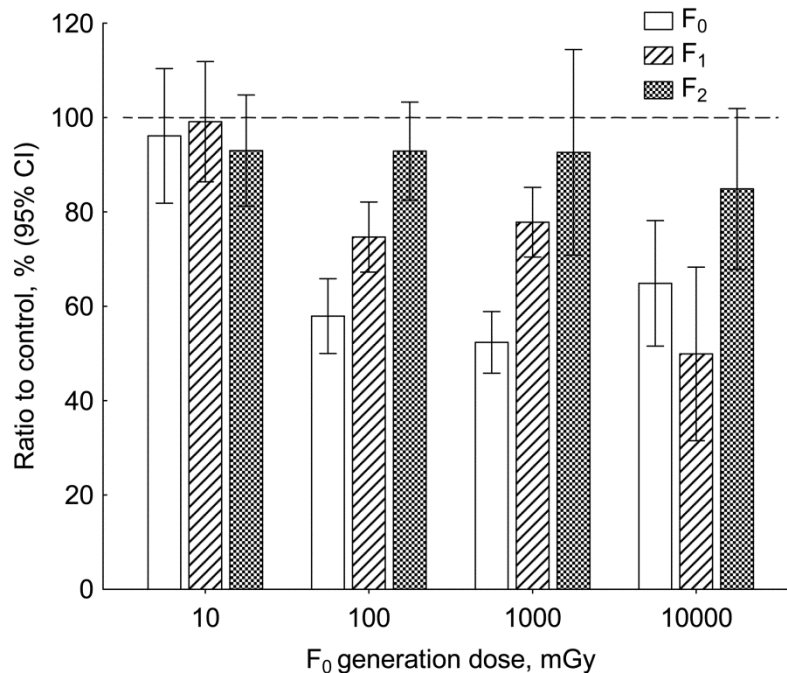
Figure 1. *The direct and transgenerational effects of parental irradiation on mitochondrial activity in two generations of D. magna.*

The same result was observed in the F1 generation of daphnids.

Thus, the MTT test showed that irradiation at doses of 100, 1000 and 10 000 mGy causes the cytotoxic effect in the directly exposed *Daphnia* and their non-exposed offspring of the first generation. The toxic effect is relatively weak after exposed *Daphnia* at a dose of 10 mGy. Apparently, some of the cells are killed, but the viability of *Daphnia* was not affected.

This assumption is based on the results of our earlier studies of radiation-induced effects of survival and life span of *Daphnia* in multigenerational study (Sarapultseva et al, 2009; 2011;

Sarapultseva & Dubrova, 2016). In these studies, the high sensitivity of neonates of *D. magna* was found to exposure at low and medium doses, which was reflected in the primary response − levels of ROS (Sarapultseva et al, 2014) and later − in increasing the mortality of directly exposed *Daphnia* and their first generation offspring. As shown in Fig. 2, a decrease in survival was observed only after exposure at doses of 100 and 1000 mGy, whereas exposure to smaller dose of 10 mGy did not affect their survival.
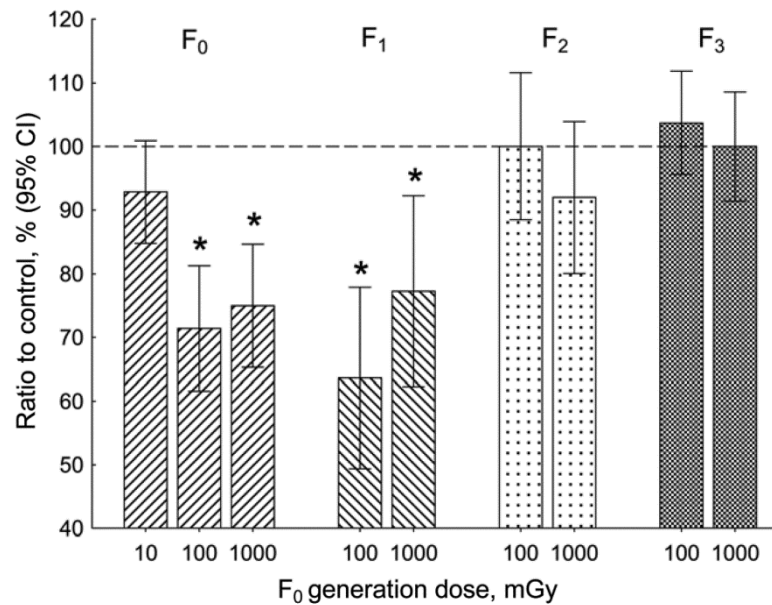
Figure 2*. The direct and transgenerational effects of parental exposure to γ-rays on survival in Daphnia*

There is a good correlation between the survival and the results of MTT-test (r = 0.92 in generation F0 and *r* = 0.80 in F1). For two generations, the correlation was *r* = 0.63, *p* = 0.09. Fig.3 shows the relationship between the survival and MTT-data.
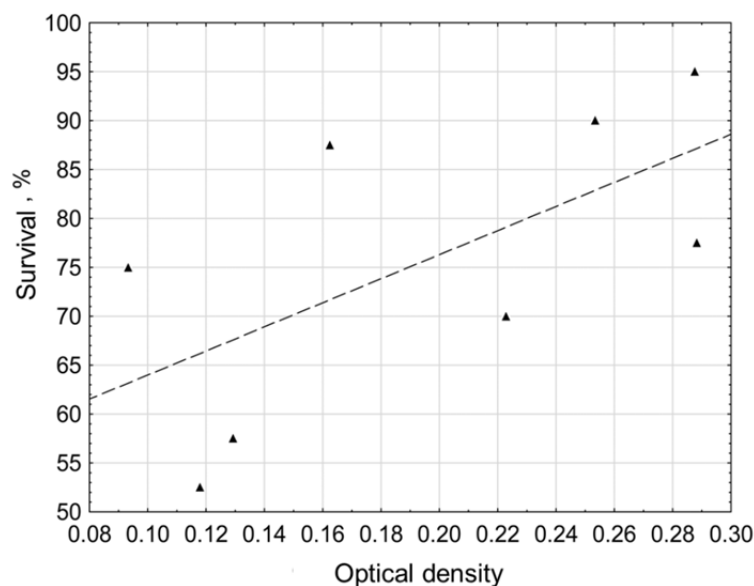
Figure 3. The relationship between the survival and cytotoxic effects of γ-irradiation in two generations of D. magna

Conclusions

Given the results of our recent studies it would appear that the decreased survival and life span is attributed to the persistently elevated level of toxicity in the directly exposed crustaceans and their offspring from the generation F_1. In particular, the results of our studies suggest that: (i) radiation is the inductor, exposure to which perturbs metabolic processes at doses of $100 - 10000$ mGy in the directly exposed *D. magna* and their F_1 offspring; (ii) metabolic activity of *Daphnia* is restored in the second generation (F_2); (iii) toxic effects of radiation correlate with decreased survival and life span of the exposed *Daphnia* and their F_1 The results of our study also demonstrate that the MTT assay represents a useful biomarker of survival effects at *D. magna*.

In conclusion, our data show that the increased cytotoxicity can shorten the life span of exposed Daphnia and their F1 offspring. Moreover, we have recently shown that parental irradiation can also affect the fertility of directly exposed *D. magna* and their F_1 offspring (Sarapultseva & Dubrova, 2016).

It may be explained that the same cytotoxic effects manifest in the parthenogenetic germline. It therefore remains to be established why relative low-dose acute parental irradiation is substantially cytotoxic, particularly whether these effects are attributed to apoptosis and/or necrosis. Future studies should address this important issue.

References

Cancer Cell Culture. Methods and Protocols. / Ed.I.A. Cree. Second ed. – Springer New York Dordrecht Heidelberg London: Human Press, 2011. pp. 237−244.

Hayon T., Dvilansky A., Shpilberg O., Nathan I., 2003. Appraisal of the MTT-based Assay as a Useful Tool for Predicting Drug Chemosensitivity in Leukemia. Leukemia & Lymphoma. 44 (11): 1957–1962.

Hatok J., Babusikova E., Matakova T., Mistuna D., Dobrota D., Racay P., 2009. *In vitro* assays for the evaluation of drug resistance in tumor cells. Clin Exp Med. 9. 1–7.

Hosmer D.W., Lemeshow S., May S. Applied survival analysis: Regression modelling of time-to-event data, 2nd ed. Hoboken, New Jersey: Willey, 2008.

Loed L.A., Wallace D.C., Martin G.M., 2005. The mitochondrial theory of aging and its relationship to reactive oxygen species damage and somatic mtDNA mutations. PNAS. 102 (52): 18769−18770.

Melekhova O.P. Svobodnoradical'nye prosessy v razvitii genomnoy epiregulyacii [Free radical processes in the development of genomic epiregulation]. − Moscow, Nauka Publ., 2010. 324 p. (in Russian).

Moskalev A.A., Aliper A.M., Smit-McBride Z., Buzdin A., Zhavoronkov A. 2014. Genetics and epigenetics of aging and longevity. Cell Cycle. 13(7): 1063-1077.

O'Dowd C., Mothersill C.E., Cairns M.T., Austin B., Lyng F.M., McClean B., Talbot A., Murphy J.E., 2009. Gene expression and enzyme activity of mitochondrial proteins in irradiated rainbow trout (Oncorhynchusmykiss, Walbaum) tissues *in vitro*. Radiat. Res. 171 (4): 464–473.

OECD, 2011. Organisation for Economic Co-operation and Development. In: TestNo. 202: Daphnia Sp. Acute Immobilisation Test. OECD Publishing, Paris.

Repetto G., del Peso A., Zurita J.L. 2008. Neutral red uptake assay for the estimation of cell viability/cytotoxicity. Nature Protocols. 3 (7): 1125–1131.

Sarapultseva E.I., Dubrova Y.E. 2016. The long-term effects of acute exposure to ionising radiation on survival and fertility in *Daphnia magna*. Environmental Research. 150. 138−143.

Sarapultseva E.I., Fedortseva R.F., Bychkovskay I.B. 2008. Nonstochastical Reduction of Organism Viability after the Low-Dose Irradiation. The Model Experiments on *Daphnia magna.* Medical radiology and health physics. 5. 3-7.

Sarapultseva E.I., Gorski A.I., Malina J.J., 2011. Radiation risk of mortality and reduced lifespan of daphnids gamma-irradiated at low doses. Bulletin of the National Radiation and Epidemiological Registry "Radiation & Risk". 20. N1. P.32-38.

Sarapultseva E.I., Melekhova O.P., Kossova G.V., Igolkina J.V., Alexeeva N.V., 2014. Free Radical Reactions in *Daphnia* after Low Doses of γ-Irradiation *in vivo*. Radiation biology. Radioecology. 54 (3): 305−308.

Sarapultseva E., Malina J., 2009. Change of *Daphnia magna* viability γ-irradiation at low doses. Radiat. Biology. Radioecology. 49 (1): 82-84.

Sarapul'tseva E.I., Ryabchenko N.I., Igolkina J.V., Ivannik B.P. 2013. Methyltetrazolium Bromide (MTT) was Applied for Bioassay of Environmental Radioactivity *in vivo*. Radiation biology. Radioecology. 53 (6): 634−638.

Shaukat A., Harald G.J. van Mil, Michael K.R. 2011. Largescale assessment of the zebrafish embryo as a possible predictive model in toxicity testing. PLOS ONE. 6 (6): 1–117.

Wu Y., Zhou Q. 2012. Dose and time related changes in aerobic metabolism, chorionic disruption, and oxidative stress in embryonic medaka (*Oryzias latipes*): Underlying mechanisms for silver nanoparticle developmental toxicity. Aqua. Toxicol. 15 (124–125): 238–246.

Plant bioassays for environment monitoring around facilities for radioactive waste treatment

A.A. Oudalova[1,2,], S.A. Geras'kin[2], S.V. Pyatkova[1] and S.M. Kiselev[3]*

[1] Obninsk Institute for Nuclear Power Engineering, National Research Nuclear University MEPhI, 249034 Obninsk, Russia
[2] Russian Institute of Radiology and Agroecology, Kievskoe shosse, 109 km, 249030, Obninsk, Russia
[3] Federal Medical Biophysical Center A.I. Burnazyan, Zhivopisnaya Str, 46, 123182, Moscow, Russia

Abstract

Contamination of territories through human civil and military activities such as nuclear facilities operation, mining sites, radioactive waste management involves a complex impact on the environment so that a mixture of radionuclides is supplemented by other potentially hazardous substances. There is still a large lack of knowledge on actual hazard of such combined contamination for biota and human health. This study was aimed at an environment assessment using biological monitoring approach in a vicinity of facilities for radioactive waste treatment, located in different regions of Russia: Central Russia, the Far-East and the Kola Peninsula. Two main technologies were used: bioindication of plant populations growing in the impacted environment, and a laboratory-based bioassay of soils and waters collected from the sites. As test-organisms, higher plants were used. For bioassay studies, cyto- and genotoxicity of soils and waters were estimated through the *Allium*-test; namely, as biological endpoints mitotic activity and frequency and spectrum of chromosome aberrations and mitotic abnormalities in *Allium cepa* root tips were used. In natural ecosystems, a fluctuating asymmetry of leaves and pollen fertility were studied as indexes of the environmental well-being. Findings obtained could be applied for an optimization of environment monitoring and decision-making process relating to rehabilitation measures and mitigation of impact on the environment and public from radiation hazardous facilities and activities.

Introduction

As a result of industrial and other man-made activities, many different stressors regularly come into the environment. Generally, of special concern are radioactive substances appeared in the environmental media (air, soils, waters, biota) as well as possible consequences of their biological effect on living beings. Among traditionally referred sources of radiation and other ecological hazards is nuclear industry which in Russia comprises about 400 enterprises and facilities. In regions where enterprises for radioactive waste storage, utilization and management are located, a significant attention is being paid for radiation-hygienic and radioecological monitoring.

Many surveys have been carried out to specify and justify constraints for radionuclide discharges and chemical substances releases into environment compartments, but a development of strategies for regulatory decision-making is still a challenge for specialists in radiation and chemical protection of the environment and the public. In the environment, there is an essentially complex impact so that a mixture of radionuclides is often supplemented by other potentially hazardous substances (e.g. heavy or alkali metals, organic compounds, etc.). An actual hazard of such combined contaminations is difficult to estimate and predict correctly because of a lack of knowledge about relationships between various types and combinations of environmental pollutants and consequences for biota and human health.

To mitigate the problem, bioassay-based approaches have been propagated to assess toxicity of unknown mixtures and environmental contaminants (Sharma, 1983; Grant, 1999; Geras'kin et al., 2011). Basic approaches applied in biomonitoring are typically classified into bioindication –

specially organized in-field observations of biota organisms, species or their communities, and bio-assays (or bio-testing) – a procedure for laboratory-based toxicity assessment of on-site collected soils, waters, etc. with use of sensitive test-organisms or test-endpoints. Higher plants are recognized as good indicators of the environment conditions because of many of advantages. Among the standardized bioassays, the *Allium*-test has been developed as a laboratory-based, single-species method for rapid screening of chemicals and environmental samples to assess their toxicity and genotoxicity (Grant, 1982; Fiskesjo, 1985; Rank & Nielsen, 1993).

In this paper findings are rewieved from a series of studies aimed at an application of plant-based techniques of the environment monitoring within and around several Russian facilities for radioactive materials management.

Material and Methods

Study sites

Study site No. 1 is located in the European part of Russia at a territory where a radioactive waste storage facility (RWSF) used to operate. The facility was built in the beginning of 1960th, radioactive wastes disposal had continued 8 years. Since 1998, there had been detected a leakage of ^{90}Sr from one of the storage tanks, and an increase of ^{90}Sr specific activity (up to 40 Bq/l) in one of the monitor boreholes was registered (Starkov et al., 2003). Maximum concentration of radioactivity occurred in a vicinity of the leaking storage tank (up to 180-210 Bq/l). To estimate consequences for the environment and population, a comprehensive radioecological survey was completed which included biological monitoring of the environment as one of the components. In a few years, the leakage was fixed, and a full-scale countermeasure program was implemented. By now, the RWSF has been decommissioned.

Study site No. 2 is the site for temporary storage (STS) of radioactive wastes (RW) and spent nuclear fuel (SNF) in the Far-East of Russia where a military coastal technical base of the nuclear fleet of the former USSR used to operate. From previous studies (Shandala et al., 2011), gamma dose rate within the STS ranges from 0.1 to 65 µSv/h, at regional natural background level of 0.10-0.15 µSv/h. The main source of exposure is radiation penetrating walls of specialized containers and buildings where radioactive materials are stored. Radioactive contamination of territory is mainly formed by ^{137}Cs and ^{90}Sr; their specific activities in soil vary significantly within the site.

Study site No. 3 is also associated with a former military coastal technical base (FTB) of the USSR nuclear fleet but it is situated in the Kola Peninsula, in the North of Russia. Here the preliminary study results are presented.

Sampling

Water samples from a territory impacted by the RWSF were collected in 2004 (Oudalova et al., 2014). They were taken from 7 monitor boreholes (Samples 5-7) and nearby waterbodies (Samples 3, 4, 8, 9). Water from a forest brook was considered as control (Sample 1), also distilled water was tested (Sample 2).

From a territory within the STS underground water samples were collected in 2013 from 7 monitor boreholes. Tap water was taken as control.

Also for a bioindication study, at study site No. 2 higher plants of three species (five-finger, violet, white clover) were sampled in five plots. Tree plots (R1 and R2 – ravines as well as RTGs – an area along a storage for radioisotope thermoelectric generators) were located within the STS territory; two other plots were in the sanitary zone (SanZone) and the observation zone (ObsZone). The last was considered as the reference plot. Dose rates between the plots ranged from 0.05 to 6.0 µSv/h.

At the FTB territory, underground waters were also samled from 14 monitor boreholes in 2014 with tap water as a control.

Bioassay with Allium-test

To test cyto- and genotoxicity of waters collected from all three study sites, the *Allium*-test was applied as one of standard bioassays. General procedure is described in (Grant, 1982; Fiskesjo, 1988), detailed description is also given in (Oudalova et al., 2014, 2016). Bulbs of onion, *Allium cepa* L., were germinated on water samples under testing. Squashed slides of *A. cepa* root tips were prepared and examined by optical microscopy. Cytotoxicity was estimated based on root proliferation that was quantified via mitotic index value. Geno-toxicity was assessed as a frequency of aberrant cells in root meristem of *A. cepa*.

Bioindication with wild plants

A fluctuating asymmetry (FA) of leaves and pollen fertility were used as indexes of the environmental well-being. To estimate the FA, 136, 119 and 131 leaves of clover, five-finger and violet plants were collected. They were scanned fresh. Five paired measurements (left and right parts of a leaf) were taken using computer imaging analysis system, and FA indexes were calculated. Pollen fertility was assessed for five-finger and violet flowers using routine procedure; clover had not reached blossoming by the time of the survey. Fertility was estimated for about 70 000 pollen grains.

Results and Discussion

Cyto- and genotoxicity testing via Allium-based bioassay

At study site No. 1 ^{90}Sr specific activities in the most contaminated waters were about 10 times of the intervention level (IL = 5.0 Bk/kg) adopted in Russia for drinking water. Concentrations of some heavy metals (Mn, Zn, Ni) exceeded the Russian guideline values for the maximum permissible content (MPC) in waterbodies. In all samples except control heavy metals concentrations were increased, especially for Zn and Mn (70-250 times of the MPCs), Ni (18-30 times of the MPC) (Oudalova et al., 2014).

The bioassay results obtained at the onion bulbs germination in the water sampled at study site No. 1 are shown in Table 1. The mitotic activity in root meristem changed from 55 to 190% of the control level. The inhibitory effect was observed for water collected from a small bog (Sample 3) and distilled water (Sample 2); both these samples could obviously been expected unfavorable for higher plant ontogenesis. Sample 4 that also inhibited the mitotic index (Table 1) was taken from a brook flowing close to the RWSF fence; this sample contained high amounts of ^{90}Sr, Zn and Cu. Comparing to Sample 1 (control), an increase of mitotic activity was found in Samples 8, 5 and 6. Interesting that these samples had got rather high concentrations of chemicals (Oudalova et al., 2014), and it was difficult to relate the increased mitotic index to chemical contamination.

For cytogenetic disturbances, a transparent effect of water contamination was shown for all water samples taken from and nearby the territory of the RWSF since the aberrant cells occurrence in root meristem of *Allim cepa* was significantly over the control (Table 1), which indicated a potential adverse impact on the natural environment in a vicinity of the storage. The main contribution to the genotoxic impact was given by laggard chromosome occurrence, which frequency significantly enhanced the control level in many samples (Oudalova et al., 2014). Remarkable role was also played by such severe disturbances as chromosome bridges and tripolar mitoses.

Table 1. *Mitotic index (MI) and aberrant cell (AC) frequency in root tip cells of Allium cepa bulbs germinated in waters sampled from three study sites.*

Study site No. 1 (RWSF)			Study site No. 2 (STS)			Study site No. 3 (FTB)		
Sample	MI, %	AC, %	Sample	MI, %	AC, %	Sample	MI, %	AC, %
1 (contr)	10.8±0.8	10.83±0.79	control	11.0±0.2	2.04±0.42	control	12.7±0.3	1.23±0.31 [a]
2	7.3±0.6 [a]	7.34±0.56	6	16.2±0.3 [a]	1.08±0.24	4077	10.0±0.2 [a]	5.54±0.85 [a]
3	5.9±0.4 [a]	5.94±0.40 [a]	12	16.6±0.3 [a]	1.75±0.35	4085а	10.5±0.2 [a]	3.65±0.64 [a]
4	8.7±0.7 [a]	8.69±0.65 [a]	13	10.1±0.2 [a]	3.72±0.58 [a]	4085б	10.8±0.2 [a]	3.15±0.60 [a]
5	12.7±1.3	12.66±1.30 [a]	14	16.8±0.3 [a]	0.69±0.21 [a]	4092a	11.6±0.2 [a]	3.40±0.59 [a]
6	20.7±2.1 [a]	20.69±2.10 [a]	15	16.7±0.3 [a]	0.78±0.23 [a]	4092б	10.7±0.2 [a]	2.61±0.48 [a]
7	10.8±1.2	10.82±1.17 [a]	16	10.0±0.2 [a]	3.96±0.58 [a]			
8	11.5±1.4	11.48±1.38 [a]	21	9.8±0.2 [a]	5.01±0.66 [a]			
9	8.4±1.0	8.36±1.01 [a]						

[a] Difference from the corresponding control sample, p < 0.05.

In waters sampled from study site No. 2, concentrations of some chemicals (ranged to the third hazard category) were over the permitted limits (Oudalova et al., 2016). Activities of ^{137}Cs и ^{90}Sr in waters amounted up to 3.8 and 16.2 Bq/l, correspondingly. In the *Allium* test for the STS samples, there were also found changes in mitotic activity of root meristem cells of both types: an inhibition and stimulation (Table 1). Mitotic index decreased below the control in Samples 13, 16 and 21. It was statistically significant, but in absolute value the decrease amounted only to 10-13% of the control level; it could be considered as a small cytotoxic effect. In other water samples (6, 12, 14, 15) from the STS an essential increase of mitotic activity up to 50-60% of the control level was observed. There could be two reasons: a stimulation of growth or a delay of mitotic cells at a stage of prophase induced by contaminants presenting in the water at intermediate concentrations.

Mutagenicity of the underground water from the STS estimated through the aberrant cells occurrence in root meristem was high in the same samples (13, 16, 21) which showed the inhibition effect on the proliferative activity (Table 1). Moreover, there was a close correlation between mitotic index and aberrant cell occurrence ($r = -0.88$, $p = 0.008$). In other samples, genotoxicity was not different from the control level, and in two samples (14 and 15) a significant, 3-fold decrease was detected. Chromatid aberrations recognized as damage of moderate severity were prevailing type in aberration spectrum in most samples (Oudalova et al., 2016). However, in cyto- and genotoxic waters in Samples 13, 16 and 21, there were found an appreciable fraction of genomic disturbances such as laggings and conglutinations.

At study site No. 3 underground waters contained significant amounts of different pollutants, including Be and Hg. All samples were turbid, colored from bright-yellow to brown and contained precipitates. In seven samples, there were either odor. Specific activity of ^{137}Cs was over the IL (up to 14 times) in 11 samples; the most contaminated waters were in Samples 4092a, 6092, 6097. Radioactive contamination with ^{90}Sr was small in most samples except for Samples 4092a and 4092b, where the IL for this radionuclide was enhanced up to 200 times.

The bioassay confidently reveled negative impact of the highly-contaminated waters from the FTB on plant cells. Although an experimental data analysis is not yet complete, but the preliminary findings (Table 1) show significant toxic and genotoxic effect of all water samples tested from study site No. 3. Especially pronounced is the mutagenic impact since the aberrant cell occurrence exceeds the control level by a factor of 2-4.

Summarizing findings obtained in the bioassay studies of environmental samples taken from territories with different scenarios of mixed radioactive and chemical contamination it could be concluded that the *Allium* test-system is an effective tool for toxicity and cytotoxicity testing. In all study sites, there were reveled sampling points where the water could be harmful for higher plants and, possibly, for other living beings, inducing statistically significant alterations of both the mitotic

activity and aberrant cells frequency in actively dividing plant tissues. When the proliferative activity in root meristem of *Allium cepa* L. is considered as an indicator, a wide spectrum of responses (from inhibition to stimulation) could be found which is often difficult to link to contaminants concentrations. While the level of cytogenetical disturbances in root tips seems to be the more reliable indicator which could effectively reveal most dangerous cases and help locating sites where additional surveys or rehabilitation measures are needed.

Bioindication within and nearby the STS

Fluctuating asymmetry of leaves was analyzed in three plant species inhabiting the STS (Gorshkova et al., 2014). A statistically significant increase in the FA index was found in white clover on the RTGs plot (Figure 1A) where the external dose rate enhanced the background level by a factor of 50–60. In the same white clover population, a rare morphological anomaly was found (Figure 1B): instead of a normal leaf with three leaflets there were noted leaves with 4 and 5 leaflets.
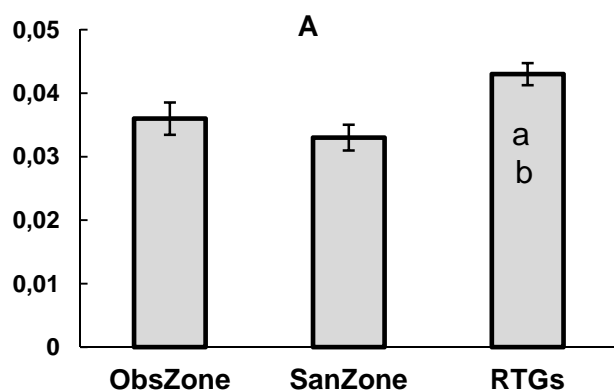
Figure 1. *Findings from white clover survey in study site No. 2. A – fluctuating asymmetry index in leaves (relative units); B – picture of a plant bearing morphological anomaly.*
[a], [b] Difference from ObsZone and SanZone is significant, $p < 0.05$.

Reproductive indicators, among which are fertility and sterility of pollen grains, are usually the most sensitive characteristics of natural populations' health. In the study at the STS, a relationship between pollen sterility and technogenic impact was found for violet plants (Gorshkova et al., 2014). At the same time, reproductive potential depends on many environmental conditions such as weather and soils, a species ecological strategy, neighboring species, etc. At low pollution levels, the environmental conditions could appear more significant. Thus, in five-finger population at the ObsZone plot (reference) an enhanced pollen sterility was found; we suspect that local environment and weather were responsible for this result.

Thus, in a pilot bioindication study conducted in study site No. 2, some alterations in developmental stability and reproductive indexes were revealed in some plant species in plots with the highest radiation impacts. It is desirable to repeat a bioindication survey in this study site as well as undertake similar studies in other sites to get data on possible influence of facilities for RW and SNF management on natural populations and ecosystems.

Conclusions

In this work, biological monitoring data are presented and reviewed that were obtained in three study sites impacted by Russian facilities on the RW and SNF storage and management. An administered or accidental intake of chemicals and radionuclides into the environment appeared

during the facilities operation. Concentrations of chemical and radioactive substances in natural waters at the study sites were measured with traditional instrumental techniques. As a rule, there were found enhanced concentrations of some contaminants in technical areas or around the facilities that could pose a risk both to human health and to biotic components of natural ecosystems.

There are differences in ecological and radioecological conditions at the study sites since they are located in various climatic zones and geographical regions, and these regional aspects make difficult a correct estimation of the environment well-being from data based solely on contaminants levels. Bioassays have an advantage in contrast to routine measurements since they are able of quantifying biological impact of mixtures independently of their composition.

In all the study sites, the same plant bioassay (*Allium* test) was completed to test the quality of natural (mostly, underground) waters. This bioassay has been used in many studies to test genotoxicity of wastewater, contaminated soils, remediation techniques, new substances, etc. (Grant, 1982; Rank & Nielsen, 1993; Fiskesjo, 1988; Leme & Marin-Moralis, 2009). But it was not so extensively exploited at testing of media contaminated with radionuclides or radionuclide-chemical mixtures, and this gap has been partly fulfilled by the surveys applied. The *Allium* test appeared an effective tool for toxicity testing in case of combined radioactive-chemical contamination. Indeed, in all three cases it identified water samples bearing high genotoxicity potential. The positive results obtained in the bioassay should be considered as a warning and also an indication that the tested environments may be of risk to both human health and biological components of natural ecosystems.

The other biological monitoring technique – a bioindication in natural conditions – was applied in one study site. Again, the higher plants were used as test species. Interesting results were obtained that implied negative consequences for developmental stability and reproductive potential of some wild plant species at plots with high levels of radiation exposure.

Findings obtained indicate that bioassays and bioindicaion should be considered as a promising method for primary screening the environment under technogenic, including radioactive, impacts. Information gained in this way can help in optimizing monitoring and rehabilitation activities. An effectively linking of bioassay-screening assays to the well-established environmental pollution monitoring approach is a way of improving and upgrading an existing system of the public and the environment protection.

Acknowledgements

References

Fiskesjo, G., 1985. The *Allium* test as a standard in environmental monitoring. Hereditas. 102, 99–112.

Fiskesjo, G., 1988. The *Allium* test – an alternative in environmental studies: the relative toxicity of metal ions. Mutat. Res. 197, 243–260.

Geras'kin, S.A., Evseeva, T.I., Oudalova, A.A., 2011. Plants as a tool for the environmental health assessment. In: Nriagu, J.O. (Ed.). Encyclopedia of Environmental Health. Burlington: Elsevier, pp. 571–579.

Gorshkova, T.A., Oudalova, A.A., Geras'kin, S.A., Kiselev, S.M., Ahromeev, S.V., 2014. Bioindication of the environment in the vicinity of the Far-Eastern center for radioactive waste treatment. Nuclear Energetics. 4, 130–139. (in Russian)

Grant, W.F., 1982. Chromosome aberration assays in *Allium*. A report of the US Environmental Protection Agency Gene-Tox program. Mutat. Res. 99, 273–291.

Grant, W.F., 1999. Higher plant assays for the detection of chromosomal aberrations and gene mutations – a brief historical background on their use for screening and monitoring environmental chemicals. Mutat. Res. 426, 107–112.

Oudalova, A.A., Geras'kin, S.A., Dikarev, V.G., Dikareva, N.S., 2014. Assessment of cyto- and genotoxicity of natural waters in the vicinity of radioactive waste storage facility using *Allium*-test. Radiat. Biol. Radioecol. 54, 97–106. (in Russian)

Oudalova, A.A., Pyatkova, S.V., Geras'kin, S.A., Kiselev, S.M., Akhromeev, S.V., 2016. Assessment of cyto- and genotoxicity of underground waters from the Far-Eastern center on radioactive waste treatment site. Radiat. Biol. Radioecol. 56, 208–219. (in Russian)

Rank, J., Nielsen, M.H., 1993. A modified *Allium* test as a tool in the screening of the genotoxicity of complex mixtures. Hereditas. 118, 49–53.

Shandala, N.K., Kiselev, S.M., Lucyanec, A.I., Titov, A.V., Seregin, V.A., Isaev, D.V., Akhromeev, S.V., 2011. Independent regulatory examination of radiation situation in the areas of spent nuclear fuel and radioactive wastes storage in the Russian Far East. Radiat. Prot. Dosimetry. 146, 129–132.

Sharma, C.B.S.R., 1983. Plant meristems as monitors of genetic toxicity of environmental chemicals. Current Science. 52, 1000–1002.

Starkov, O.V., Vaizer, V.I., Bogdanovich, N.G., Kozmin, G.V., 2003. Ecological problems of urbanized territories in regions with nuclear industry enterprises on an example of Obninsk region. Nuclear Energetics. 2, 67–73. (in Russian)

Polonium ^{210}Po and radiolead ^{210}Pb in calcium and magnesium supplements

D.I. Strumińska-Parulska[*], B. Skwarzec

University of Gdańsk, Faculty of Chemistry, Environmental Chemistry and Radiochemistry Department, Wita Stwosza 63, 80-308 Gdańsk, Poland

Abstract

The aim of this pioneer study was to investigate the most popular calcium and magnesium supplements as a potential additional source of polonium ^{210}Po and radiolead ^{210}Pb in human diet. The analyzed Ca and Mg pharmaceutics contained their organic or inorganic compounds; some from natural sources as shells, fish extracts, or sedimentary rocks. The objectives of this research were to investigate the naturally occurring ^{210}Po and ^{210}Pb activity concentrations in calcium and magnesium supplements, find the correlations between ^{210}Po and ^{210}Pb concentration in medicament and the element chemical form, and calculate the effective radiation dose connected to analyzed supplement consumption.

The study showed ^{210}Po and ^{210}Pb were present in analyzed calcium and magnesium supplements and could be an additional source of ^{210}Po and ^{210}Pb for the consumers. Inorganic samples were richer in ^{210}Po in comparison to organic. Also natural origin supplements, especially those made from sedimentary rocks, were richer in polonium and radiolead in comparison to the rest of analyzed samples.

Introduction

Polonium ^{210}Po ($T_{1/2}$=138.376 days) and radiolead ^{210}Pb ($T_{1/2}$=22.2 years) appear at the end of the decay-chain of uranium ^{238}U and are radio-ecologically interesting natural elements to investigate due to their high radiotoxic characteristics (Persson and Holm, 2011). Polonium is transferred to man mainly by dietary intake; the fraction of polonium taken up is 20-80% (Henricsson et al., 2012). Lead enters the human body similarly, mainly with food and much less by inhalation of contaminated aerosols (Pietrzak-Flis, 1997). Both ^{210}Po and ^{210}Pb radionuclides are, together with radon, the natural radioactive material delivering the highest natural dose to living organisms (Pietrzak-Flis, 1997). The data on its concentrations in daily foods showed they depended on the climate, geological- and agricultural conditions (Henricsson and Persson, 2012).

Calcium is one of the most essential elements in living organisms. Adult human body contains about 1.2 kg of Ca and 99% of this amount is located in bones and teeth (Ziółko, 2006). Dietary Reference Intakes (DRI) recommendations for Ca are from 0.8 to 1.5 g (Ross et al., 2011). The research showed calcium intake among Polish inhabitants covered 58-60% of the recommended values (Dybkowska et al., 2004). Thus calcium has become extremely popular, especially amongst older women, in the hope that it will prevent osteoporosis (Czerwiński et al., 2015).

Magnesium takes part in important interaction with phosphate ions mainly, is essential to the basic nucleic acid chemistry (Graczyk, 2008). An adult contains 22–35 g of magnesium (about 0.05% of the total body mass), with 60% in the skeleton, 29% in skeletal muscles, 10% intracellular, and 1% extracellular. The DRI value is 350-400 mg of Mg for adults (Ross et al., 2011). Magnesium deficiency is common: it is found in 2.5–15% of the general population (Ayuk and Gittoes, 2014). In Poland, magnesium deficiency was estimated at 30-77% of the population, while the biggest was found in adolescent girls (13-15 years of age) (Graczyk, 2008).

---

[*] Corresponding author, E-mail: dagmara.struminska@ug.edu.pl

Materials and Methods

Samples

In this study calcium and magnesium supplements available in Poland were analyzed. The pharmaceutics were bought in commercial pharmacies and contained different inorganic and organic calcium and magnesium compounds; some of them were natural origin: shells, mineral fish extracts, or sedimentary rocks. Analyzed Ca supplements samples were from 4 to 35 g, while Mg sources were from 4 to 31 g and contained from 17 to 375 of pure elementary Mg (Table 1-4).

Radiometric technique

The ^{210}Po analysis covered the samples mineralization, polonium autodeposition and ^{210}Po activity measurements (Skwarzec, 1995, 2010). Before radiochemical analysis, to each 10 mBq of ^{209}Po was added as a yield tracer. Further, 65% HNO_3 was added and the samples were slowly warmed until the HNO_3 was completely decomposed and evaporated. Further 35% HCl were added and the samples were warmed again. When the light clear solvent solution was reached, the samples were ready for polonium autodeposition (Skwarzec, 1995, 2010). The activities of polonium isotopes (^{209}Po and ^{210}Po) were measured in alpha spectrometer (Alpha Analyst S470, Canberra-Packard). The activities of ^{210}Po were corrected for decay to the day of polonium deposition (time of separation ^{210}Po from ^{210}Pb).

The ^{210}Pb analysis was connected to polonium ^{210}Po analysis. The samples after the first ^{210}Po deposition were stored for 6 months to allow for ^{210}Po increment from ^{210}Pb. Activities of ^{210}Pb were measured indirectly via its daughter ^{210}Po knowing that these two radioisotopes should reach secular equilibrium after a sufficient period of time since the first ^{210}Po deposition. Each sample was treated with 10 mBq of ^{209}Po again. The deposition of ^{210}Po on silver disc was repeated and the activities of ingrowing polonium isotopes (^{209}Po and ^{210}Po) were measured in alpha spectrometer (Alpha Analyst S470, Canberra-Packard). The activities of ^{210}Po were corrected for decay to the day of polonium deposition (time of separation ^{210}Po from ^{210}Pb) and further ^{210}Pb activity at the time of sample collection in analyzed samples were calculated (Skwarzec, 1997).

The accuracy and precision of the radiochemical method were evaluated using IAEA reference materials (IAEA-384, IAEA-385, IAEA-414) and estimated at less than 4%. The polonium yield in the analyzed samples of Ca and Mg supplements ranged from 90 to 99%. The results of ^{210}Po and ^{210}Pb concentration were given with standard deviation (SD) calculated for 95% confidence intervals.

Results and Discussion

^{210}Po and ^{210}Pb activity concentrations in calcium and magnesium supplements

The results of ^{210}Po and ^{210}Pb analysis in calcium and magnesium supplements were much differentiated and the average values of analyzed activity concentrations were presented in Table 1-4. The highest ^{210}Po and ^{210}Pb activity concentrations in Ca pharmaceutics were measured in mineral tablets made from sedimentary rocks, sample Ca7 (dolomite) – 3.88±0.22 and 2.97±0.18 mBq·g^{-1} respectively (Table 1, 3). The results obtained for natural origin calcium supplements (shells, sedimentary rocks) were much higher than the other analyzed samples. Also the results of ^{210}Po analysis obtained for inorganic forms of calcium supplements in comparison to organic were significantly higher. Similarly, the highest ^{210}Po and ^{210}Pb activity concentrations in magnesium supplements were measured in dolomite pills – 3.84±0.15 mBq·g^{-1} and 2.97±0.18 mBq·g^{-1}

respectively (Table 2, 4). The differences, mainly in [210]Po activities, are representatives of the individual supplement and its raw material properties as well as technological processes. If high temperature during supplement production is used, significant part of polonium can volatilize due to low sublimation point of polonium. Also time influences polonium activity decrease in the supplements.

Obtained data had consequences in further calculations. According to Dietary Reference Intake (DR) (Ross et al., 2011) the daily dose of calcium for adults should be 1 g. It means, the highest [210]Po and ^{210}Pb activity concentrations in 1 g of Ca per supplement were measured in dolomite pills (sample Ca7): 28.9±1.60 and 22.13±1.34 mBq per 1 g of Ca respectively (Table 1, 3). According to DRI the average daily dose of magnesium for adults should be 0.35-0.4 g (Ross et al., 2011). The results showed, the highest [210]Po and ^{210}Pb activity concentrations in 0.4 g of Mg per supplement were measured in dolomite sample again – 19.3±0.7 and 14.9±0.90 per 0.4 g of Mg respectively (Table 2, 4).

Effective doses

On the basis of previously calculated [210]Po and ^{210}Pb content in analyzed calcium and magnesium supplements, the annual effective radiation doses were estimated – for daily intake of 1 pill of pharmaceutic or DRI value of pure element (Table 1-4). The effective dose conversion coefficient from [210]Po ingestion for adult members of the public recommended by ICRP is 1.2 $\mu Sv \cdot Bq^{-1}$ and from ^{210}Pb ingestion is 0.69 $\mu Sv \cdot Bq^{-1}$ (ICRP, 2012). In both cases, for each supplement, the highest annual effective radiation doses calculated for DRI value were calculated for natural origin supplements – sample of dolomite (sedimentary rocks). In case of 1 g of pure Ca: 12.7±0.70 $\mu Sv \cdot year^{-1}$ from [210]Po and 5.57±0.34 $\mu Sv \cdot year^{-1}$ from ^{210}Pb; in case of 0.4 g of pure Mg: 3.38±0.13 $\mu Sv \cdot year^{-1}$ from [210]Po and 3.72 ± 0.02 $\mu Sv \cdot year^{-1}$ from [210]Pb (Table 1-4). Obtained results of the annual effective radiation dose in case of the highest [210]Po activity in dolomite supplement (sample Ca7) (12.7 $\mu Sv \cdot year^{-1}$) would be similar to Polish fish consumption that was estimated at 12 $\mu Sv \cdot year^{-1}$ (Skwarzec, 1997).

According to Polish conditions, the annual effective dose from [210]Po and ^{210}Pb total intake with different foodstuffs and water was estimated at 54 μSv per year for each isotope (Pietrzak-Flis et al., 1997) and the total annual effective dose from all sources was estimated at 2.1-2.6 mSv (Jagielak et al., 1997; Dobrzyński et al., 2005). It means if consumers would choose dolomite supplement as Ca or Mg source, they would receive additional value of radiation dose at level close to 25% of the total effective radiation dose from [210]Po and close to 10% of the total effective radiation dose from ^{210}Pb from typical dietary intake. But the impact of [210]Po with the consumption of dolomite supplement is small when compared with [210]Po and ^{210}Pb inhalation connected to cigarette smoke – 157 μSv and 314 μSv respectively (Skwarzec et al., 2001). However, they could be an additional source of [210]Po and ^{210}Pb for the consumers.

Conclusions

The idea behind this study was to investigate [210]Po and ^{210}Pb activity concentrations in Polish calcium and magnesium supplements. The results showed [210]Po and ^{210}Pb were present in analyzed supplements and could be their additional source for the consumers. The values of [210]Po and ^{210}Pb activities concentration in analyzed Ca and Mg pharmaceutics ranged from 0.07 to 3.97 mBq·g^{-1} respectively, and the maximum annual effective radiation dose from Dietary Reference Intake value of 1 g of Ca consumption was calculated at 12.7 μSv from [210]Po and 8.44 μSv from [210]Pb. As it turned out, samples containing inorganic Ca and Mg compounds were richer in [210]Po in comparison to their organic compunds. Also natural origin supplements, especially those made from sedimentary rocks, were richer in polonium and could increase the total annual effective dose from

^{210}Po ingestion by almost 25%. The results showed, some of analyzed supplements could be an insignificant source of ^{210}Pb for consumers and increase the total annual effective dose from ^{210}Pb ingestion by 10%.

Acknowledgments

References

Ayuk, J., Gittoes, N.J., 2014. Contemporary view of the clinical relevance of magnesium homeostasis. Ann. Clin. Biochem. 51 (2), 179–88.

Czerwiński. E., Osieleniec. J., Borowy. P., 2015. OSTEOPOROZA – choroba milionów złamań. http://www.kcm.pl/_files/File/PDF/Osteoporoza-fakty_2_2011-10-18kb.pdf

Dobrzyński, L., Droste, E., Trojanowski, W., Wołkiewicz, R., 2005. Spotkanie z promieniotwórczością, IPJ Świerk.

Dybkowska, E., Świderski, F., Waszkiewicz-Robak, B., 2004. Mineral components intake in average diet of Warsaw adult inhabitants in the comparison with polish diet. Ann. Universitatis Mariae Curie-Skłodowska, LIX, SUPPL. XIV, 97, 14-18, SECTIO D.

Graczyk, A., 2008. Magnez - król życia, Jak uzupełniać braki, czego unikać, PTMag, http://www.ptmag.pl/pl/32073/0/Magnez-krol_zycia.html

Henricsson, C.F. Persson, R.R.B., 2012. Polonium-210 in the bio-sphere: Bio-kinetics and biological effects, http://www2.msf.lu.se/b-persson/097_2012_Henricsson_Polonium-210.pdf

Henricsson, C.F., Ranebo, Y., Hanson, M., Raaf, C.L., Holm, E., 2012. A biokinetic study of 209Po i man. Sci. Total Environ. 437, 384-389.

ICRP - The International Commission on Radiological Protection, 2012. Compendium of Dose Coefficients based on ICRP Publication 60, ICRP Publication 119, Ann. ICRP 41(Suppl.), Elsevier.

Jagielak, J., Biernacka, M., Henschke, A., Sosińska, A., 1997. Radiologiczny Atlas Polski, PIOŚ, CLOR, PAA, Biblioteka Monitoringu Środowiska, Warszawa.

Persson, B.R.R., Holm, E., 2011. Polonium-210 and lead-210 in the terrestrial environment: a historical review. J. Environ. Radioact. 102, 420-429.

Pietrzak-Flis, Z., Chrzanowski, E., Dembińska, S., 1997. Intake of ^{226}Ra, ^{210}Pb and ^{210}Po with food in Poland. Sci. Total Environ. 6, 203 (2), 157-165.

Ross, A.C., Taylor, C.L., Yaktine, A.L., Del Valle, H.B., 2011. Dietary Reference Intakes for Calcium and Vitamin D, Institute of Medicine, The National Academy Press, Washington DC.

Skwarzec, B., 1995. Polon, uran i pluton w ekosystemie południowego Bałtyku – Rozprawy i monografie, Instytut Oceanologii PAN, Sopot.

Skwarzec, B., 1997. Polonium, uranium and plutonium in the southern Baltic Sea. Ambio, 26 (2), 113-117.

Skwarzec, B., 2010. Determination of radionuclides in aquatic environment, [in:] Analytical measurement in aquatic environments, J. Namieśnik and P. Szefer (eds), Tylor&Francis PE. 241-258.

Skwarzec, B., Ulatowski, J., Strumińska, D.I., Boryło, A., 2001. Inhalation of ^{210}Po and ^{210}Pb from cigarette smoking in Poland. J. Environ. Radioact. 57, 221-230.

Ziółko, E., 2006. Podstawy fizjologii człowieka. Oficyna Wydawnicza PWSZ w Nysie, Nysa, 2006.

Table 1. *Analyzed calcium supplements samples characteristic as well as average values of ^{210}Po activity concentration and annual radiation doses from ^{210}Po intake*

Supplement	Chemical form	Mass of Ca in 1 pill [mg]	^{210}Po concentration [mBq·g^{-1} dw]	^{210}Po activity in 1 pill [mBq ± SD]	^{210}Po activity per 1 g** of Ca [mBq ± SD]	Annual effective dose from ^{210}Po (1 pill a day) [µSv·year^{-1}]	Annual effective dose from ^{210}Po (1 g** of Ca a day) [µSv· year^{-1}]
Ca1	Calcium gluconate	45	0.17 ± 0.01	0.09 ± 0.01	2.06 ± 0.16	0.04 ± 0.01	0.90 ± 0.07
Ca2	Calcium lactate*	350	1.31 ± 0.04	5.16 ± 0.18	14.7 ± 0.50	2.26 ± 0.08	6.45 ± 0.22
Ca3	Calcium carbonate	500	0.36 ± 0.02	0.53 ± 0.03	2.65 ± 0.14	0.23 ± 0.01	1.16 ± 0.06
Ca4	Calcium pantothenate	15	1.24 ± 0.09	0.20 ± 0.02	13.2 ± 1.00	0.09 ± 0.01	5.78 ± 0.44
Ca5	Calcium carbonate*	300	0.40 ± 0.02	1.58 ± 0.07	2.63 ± 0.12	0.69 ± 0.03	1.15 ± 0.05
Ca6	Calcium diglycynate	280	3.04 ± 0.13	3.65 ± 0.16	13.0 ± 0.56	1.60 ± 0.07	5.71 ± 0.24
Ca7	Calcium carbonate (dolomite)	108	3.88 ± 0.22	3.12 ± 0.17	28.9 ± 1.60	1.37 ± 0.08	12.7 ± 0.70
Ca8	Calcium carbonate (mussels shells)	600	2.45 ± 0.15	4.90 ± 0.29	8.17 ± 0.48	2.15 ± 0.13	3.58 ± 0.21
Ca9	Calcium lactate*	180	0.07 ± 0.02	0.17 ± 0.04	0.94 ± 0.23	0.07 ± 0.02	0.41 ± 0.10
Ca10	Calcium carbonate*	300	0.26 ± 0.02	0.57 ± 0.03	1.91 ± 0.12	0.25 ± 0.02	0.84 ± 0.05
Ca11	Calcium carbonate	250	0.32 ± 0.02	0.41 ± 0.03	1.64 ± 0.12	0.18 ± 0.01	0.72 ± 0.05
Ca12	Calcium carbonate, calcium lactate*	260	0.12 ± 0.01	0.87 ± 0.08	3.36 ± 0.30	0.38 ± 0.03	1.47 ± 0.13
Ca13	Calcium carbonate	500	1.64 ± 0.07	2.46 ± 0.11	4.92 ± 0.21	1.08 ± 0.05	2.16 ± 0.09
Ca14	Mineral extract from fish	120	0.88 ± 0.09	0.55 ± 0.06	4.15 ± 0.45	0.24 ± 0.03	2.01 ± 0.21
Ca15	Calcium lactate*	180	0.14 ± 0.01	0.35 ± 0.03	3.13 ± 0.29	0.15 ± 0.01	0.85 ± 0.07
Ca16	Calcium carbonate (chalk)	400	3.36 ± 0.10	5.75 ± 0.17	14.4 ± 0.43	2.52 ± 0.07	6.29 ± 0.19
Ca17	Calcium carbonate (oyster shells)	500	0.57 ± 0.05	0.82 ± 0.07	1.64 ± 0.13	0.36 ± 0.03	0.72 ± 0.06

* soluble; ** Recommended Daily Intake for adults - 1 g of Ca

Table 2. *Analyzed magnesium supplements samples characteristic as well as average values of ^{210}Po activity concentration and annual radiation doses from ^{210}Po intake*

Supplement	Chemical form	Mass of Mg in 1 pill [mg]	^{210}Po concentration [mBq·g^{-1} dw]	^{210}Po activity in 1 pill [mBq ± SD]	^{210}Po activity per 0.4 g* of Mg [mBq ± SD]	Annual effective dose from ^{210}Po (1 pill a day) [μSv· year^{-1}]	Annual effective dose from ^{210}Po (0,4 g* of Mg a day) [μSv· year^{-1}]
Mg1	Magnesium carbonate	300	0.020 ± 0.002	0.078 ± 0.006	0.105 ±0.009	0.034 ± 0.003	0.046 ± 0.004
Mg2	Magnesium dioxide	375	0.361 ± 0.025	0.275 ± 0.019	0.294 ± 0.020	0.121 ± 0.008	0.129 ± 0.009
Mg3	Magnesium chloride	64	1.68 ± 0.07	1.57 ± 0.07	9.83 ± 0.43	0.689 ± 0.030	4.31 ± 0.19
Mg4	Magnesium carbonate	120	0.105 ± 0.011	0.068 ± 0.007	0.228 ± 0.023	0.030 ± 0.003	0.100 ± 0.010
Mg5	Magnesium dioxide	375	0.638 ± 0.064	0.470 ± 0.047	0.501 ± 0.050	0.206 ± 0.021	0.220 ± 0.022
Mg6	Magnesium heavy oxide	150	0.073 ± 0.010	0.061 ± 0..008	0.162 ± 0022	0.027 ± 0.004	0.071 ± 0.010
Mg7	Magnesium lactate	51	0.023 ±0.003	0.018 ± 0.003	0.144 ± 0.020	0.008 ± 0.001	0.063 ± 0.009
Mg8	Magnesium lactate	51	0.186 ± 0.008	0.143 ± 0.006	1.12 ± 0.05	0.062 ± 0.003	0.490 ± 0.022
Mg9	Magnesium citrate	60	0.024 ± 0.003	0.021 ± 0.003	0.137 ± 0.019	0.009 ± 0.001	0.060 ± 0.009
Mg10	Magnesium chelate	100	0.150 ± 0.010	0.105 ± 0.007	0.421 ± 0.028	0.046 ± 0.003	0.185 ± 0.012
Mg11	Magnesium chelate	94	0.088 ± 0.007	0.049 ± 0.004	0.209 ± 0.018	0.022 ± 0.002	0.092 ± 0.008
Mg12	Magnesium aspartate	17	0.349 ± 0.021	0.245 ± 0.015	5.77 ± 0.35	0.107 ± 0.006	2.53 ± 0.15
Mg13	Magnesium aspartate, Magnesium carbonate	18	0.157 ± 0.011	0.063 ± 0.004	1.34 ± 0.09	0.027 ± 0.002	0.609 ± 0.041
Mg14	Magnesium aspartate	17	0.891 ± 0.047	0.624 ± 0.033	14.1 ± 0.8	0.273 ± 0.014	6.43 ± 0.34
Mg15	Magnesium aspartate	40	0.117 ± 0.011	0.081 ± 0.008	0.814 ± 0.077	0.036 ± 0.003	0.357 ± 0.034
Mg16	Magnesium dioxide (from the Dead Sea)	375	0.365 ± 0.026	0.294 ± 0.021	0.313 ± 0.022	0.129 ± 0.009	0.137 ± 0.010
Mg17	Magnesium carbonate (dolomite)	64	3.84 ± 0.15	3.08 ± 0.12	19.3 ± 0.7	1.35 ± 0.05	8.44 ± 0.33
Mg18	Magnesium dioxide	56	1.53 ± 0.04	2.31 ± 0.07	16.5 ± 0.5	1.01 ± 0.03	7.23 ± 0.21

* Recommended Daily Intake for adults – 0.4 g of Mg

Table 3. *Analyzed calcium supplements samples characteristic as well as average values of ^{210}Pb activity concentration and annual radiation doses from ^{210}Pb intake*

Supplement	Chemical form	^{210}Pb concentration [mBq·g^{-1} dw]	^{210}Pb activity in 1 pill [mBq ± SD]	^{210}Pb activity per 1 g** of Ca [mBq ± SD]	Annual effective dose from ^{210}Po (1 pill a day) [µSv· year^{-1}]	Annual effective dose from ^{210}Po (1 g** of Ca a day) [µSv· year^{-1}]
Ca1	Calcium gluconate	0.20 ±0.01	0.11 ± 0.01	2.46 ± 0.17	0.028 ± 0.002	0.620 ± 0.043
Ca2	Calcium lactate*	1.17 ± 0.03	4.71 ± 0.13	13.45 ± 0.39	1.19 ± 0.03	3.39 ± 0.09
Ca3	Calcium carbonate	0.15 ± 0.02	0.22 ± 0.03	1.13 ± 0.13	0.057 ± 0.007	0.284 ± 0.034
Ca4	Calcium pantothenate	1.21 ± 0.06	0.19 ± 0.01	12.93 ± 0.69	0.049 ± 0.003	3.26 ± 0.17
Ca5	Calcium carbonate*	0.19 ± 0.03	0.78 ± 0.11	1.30 ± 0.18	0.197 ± 0.027	0.328 ± 0.046
Ca6	Calcium diglycynate	2.69 ± 0.25	3.22 ± 0.30	11.51 ± 1.08	0.812 ± 0.076	2.90 ± 0.27
Ca7	Calcium carbonate (dolomite)	2.97 ± 0.18	2.39 ± 0.14	22.13 ± 1.34	0.602 ± 0.036	5.57 ± 0.34
Ca8	Calcium carbonate (mussels shells)	1.95 ± 0.12	3.89 ± 0.23	6.48 ± 0.39	0.980 ± 0.059	1.63 ± 0.09
Ca9	Calcium lactate*	0.08 ± 0.01	0.19 ± 0.02	1.05 ± 0.09	0.047 ± 0.004	0.263 ± 0.023
Ca10	Calcium carbonate*	0.39 ± 0.03	0.87 ± 0.06	2.91 ± 0.19	0.220 ± 0.014	0.73 ± 0.05
Ca11	Calcium carbonate	0.32 ± 0.02	0.41 ± 0.02	1.64 ± 0.09	0.103 ± 0.006	0.41 ± 0.02
Ca12	Calcium carbonate, calcium lactate*	0.11 ± 0.01	0.78 ± 0.04	3.02 ± 0.15	0.198 ± 0.010	0.760 ± 0.038
Ca13	Calcium carbonate	1.37 ± 0.13	2.06 ± 0.20	4.12 ± 0.40	0.519 ± 0.050	1.04 ± 0.10
Ca14	Mineral extract from fish	0.92 ± 0.04	0.58 ± 0.02	4.82 ± 0.19	0.146 ± 0.006	1.21 ± 0.05
Ca15	Calcium lactate*	0.13 ± 0.01	0.34 ± 0.02	1.88 ± 0.09	0.085 ± 0.004	0.472 ± 0.024
Ca16	Calcium carbonate (chalk)	2.32 ± 0.06	3.97 ± 0.09	9.93 ± 0.24	1.00 ± 0.02	2.50 ± 0.06
Ca17	Calcium carbonate (oyster shells)	0.61 ± 0.04	0.88 ± 0.05	1.77 ± 0.11	0.223 ± 0.014	0.445 ± 0.027

* soluble; ** Recommended Daily Intake for adults - 1 g of Ca

Table 4. *Analyzed magnesium supplements samples characteristic as well as average values of ^{210}Pb activity concentration and annual radiation doses from ^{210}Pb intake*

Supplement	Chemical form	^{210}Pb concentration [mBq·g^{-1} dw]	^{210}Pb activity in 1 pill [mBq ± SD]	^{210}Pb activity per 0.4 g** of Mg [mBq ± SD]	Annual effective dose from ^{210}Po (1 pill a day) [µSv· year^{-1}]	Annual effective dose from ^{210}Po (0,4 g* of Mg a day) [µSv·year^{-1}]
Mg1	Magnesium carbonate	0.020 ± 0.002	0.079 ± 0.006	0.11 ± 0.01	0.020 ± 0.002	0.027 ± 0.0002
Mg2	Magnesium dioxide	1.87 ± 0.25	1.75 ± 0.24	10.9 ± 1.49	0.442 ± 0.060	2.76 ± 0.04
Mg3	Magnesium chloride	0.053 ± 0.005	0.034 ± 0.003	0.11 ± 0.01	0.009 ± 0.001	0.029 ± 0.0003
Mg4	Magnesium heavy oxide	0.053 ± 0.005	0.260 ± 0.037	0.69 ± 0.10	0.066 ± 0.009	0.175± 0.0025
Mg5	Magnesium lactate	0.047 ± 0.006	0.037 ± 0.005	0.29 ± 0.04	0.009 ± 0.001	0.074 ± 0.0009
Mg6	Magnesium lactate	0.059 ± 0.005	0.046 ± 0.004	0.36 ± 0.03	0.011 ± 0.001	0.090 ± 0.0008
Mg7	Magnesium citrate	0.029 ± 0.003	0.025 ± 0.003	0.16 ± 0.02	0.006 ± 0.001	0.041 ± 0.0005
Mg8	Magnesium chelate	0.110 ± 0.007	0.077 ± 0.005	0.31 ± 0.02	0.019 ± 0.001	0.077± 0.0005
Mg9	Magnesium aspartate	0.283 ± 0.017	0.199 ± 0.012	4.69 ± 0.27	0.050 ± 0.003	1.18 ± 0.007
Mg10	Magnesium aspartate, Magnesium carbonate	0.126 ± 0.015	0.050 ± 0.006	1.12 ± 0.14	0.013 ± 0.002	0.281 ± 0.003
Mg11	Magnesium aspartate	0.697 ± 0.039	0.488 ± 0.028	11.5 ± 0.65	0.123 ± 0.007	2.84 ± 0.02
Mg12	Magnesium aspartate	0.118 ± 0.006	0.082 ± 0.004	0.82 ± 0.04	0.021 ± 0.001	0.207 ± 0.001
Mg13	Magnesium carbonate (dolomite)	2.97 ± 0.18	2.39 ± 0.14	14.9 ± 0.90	0.602 ± 0.036	3.72 ± 0.02
Mg14	Magnesium dioxide	1.37 ± 0.13	2.06 ± 0.19	14.7 ± 1.41	0.519 ± 0.050	3.71 ± 0.03

* Recommended Daily Intake for adults – 0.4 g of Mg

HOW TO GET 16-19 YEARS OLD STUDENTS INTERESTED IN RADIATION PHYSICS

Per Törnquist[1], Håkan B.L. Pettersson [2]

[1]Linköping University, Linköping, Sweden, e-mail: per.tornquist@liu.se
[2]Radiation Physics Department, Linköping University Hospital, Sweden, e-mail: hakan.pettersson@regionostergotland.se

Abstract

We have initiated a project where one of the main goals is to increase the student's interest in physics, especially in radiation physics and radioecology. Another important goal is to make the students realise that physics is of great importance in a modern society and is closely connected to other school subjects, such as history, biology, chemistry, social science and ethics in addition to attract students to continuing in the area when they continuing the academic carrier in the universities. The used case scenario used in our classes show that physics can be used in multidisciplinary studies and are a tool to study history of pollutions were its possible to see the impact of political decisions in environmental archives. We also show that it often takes political action to decrease the amount of environmental pollution.

Introduction

As a teacher in physics in upper secondary school I meet a lot of students. All students learn in different ways. This project is a different approach of learning. After this project the students should know how to write a scientific report, they should know how to be critical to the sources of their report and they should also know what to think of as an opponent. Besides they also learn natural science and social science in a practical way. The project also works as a common reference for the future when we study more advanced physics.

Materials and Methods

Collecting samples

In the project, the students are taken on a sample excursion to a peat bog. The samples are then sliced and sample prepared in the schools laboratory facility. The measurements are conducted in close collaboration with the radiation physics department in Linköping were gamma-spectrometric measurements are performed. That make the students connect to the project even more, since the studied area and results relates to the vicinity of their home. The students become aware of that pollution concerns everyone and that those particles actually fall down everywhere. On location they get a question; "Is it possible to detect traces from the cold war in our immediate

Figure 1. Students collecting a core sample.

environment?" They also get a short outdoor lesson on how to answer that question and the role of Cs-137. A peat bog is a biotope which is very interesting to investigate for a scientist and the students also applies to the sensation of walking on the peat bog as it is wet and the surface is unstable. The peat bog consists mostly of sphagnum moss and grows annually upwards. Everything that the peat bog consists of originates from the air, such as water and all

Figure 2. *The core is being revealed.*   Figure 3. *This core has the surface to the right.*   Figure 4. *The core is sliced.*

other elementals, for instance carbon, sulphur and caesium. Since the condition below surface are both anaerobic and slightly acid the organic material is very slowly converted to soil. Very few insects and worms live below the surface, so the bioturbation process is negligible. This means that the peat bog works as an environmental archive i.e. a sort of diary of what has fallen down on the earth's surface. The age of the layers in the bog is a function of the depth. The students are teenagers and this is perhaps their first contact with a scientific question where they play a practical role. The more the students are able to do themselves, the more they feel connected to the project and they feel an ownership of the project and take more responsibility for the results. Therefore, we let them take a core in the peat bog under our supervision. The core is taken with an aluminium cylinder with a diameter of 10,00 cm and a length of 60 cm. As we only wish to go back to the 1940s it is enough with a depth of ca 30 cm in this peat. This particular peat bog has an actual depth of 4,5 m and the bottom layers are ca 10 000 years old.

Radiometric technique

The core is then taken to the laboratory where the students cut the core in slices. Each slice is being weight. The number of the slices is adequate for the time resolution and has to been put against the time consuming measurements. If you are very accurate you should not use the outer part of each slice, since the cylinder could have moved the outer layer and/or polluted the core. The slices are being freeze-dried. If you don´t do these preparations in connection with the taking of the sample, it is best to store the core in a regular freeze. For the radiometric analyses we collaborate with the Radiation Physics Department of our university hospital, which give the students insights into the
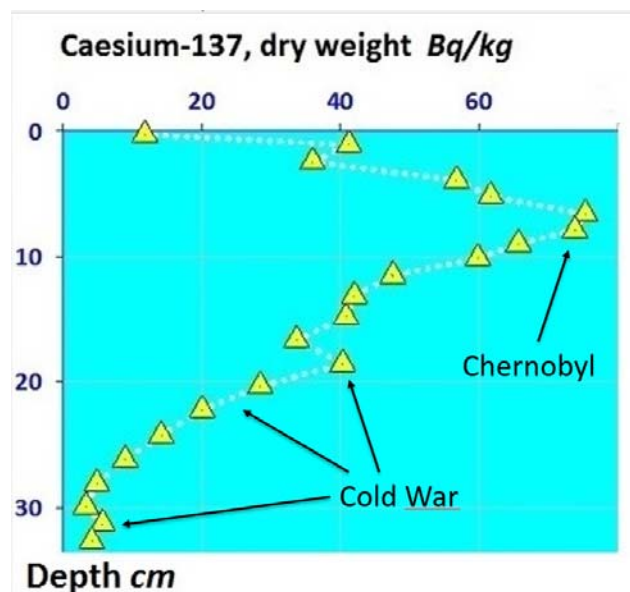

Figure 5. *The activity as a function of the depth of the core. Traces of the Chernobyl accident are present and traces from the cold war might also be present.*

work tasks of radiation physicist and knowledge about gamma spectrometry. The Radiation Physics Department uses a HP-Ge 42% detector and each slice takes about 48 hours to measure. We then plot the Cs γ-activity as a function of depth.

History of pollution

By using the fallout peak originating from the Chernobyl accident, 1986, the peak from the 1963 test ban treaty and that it was not until the1950s atmospheric nuclear test fall out were
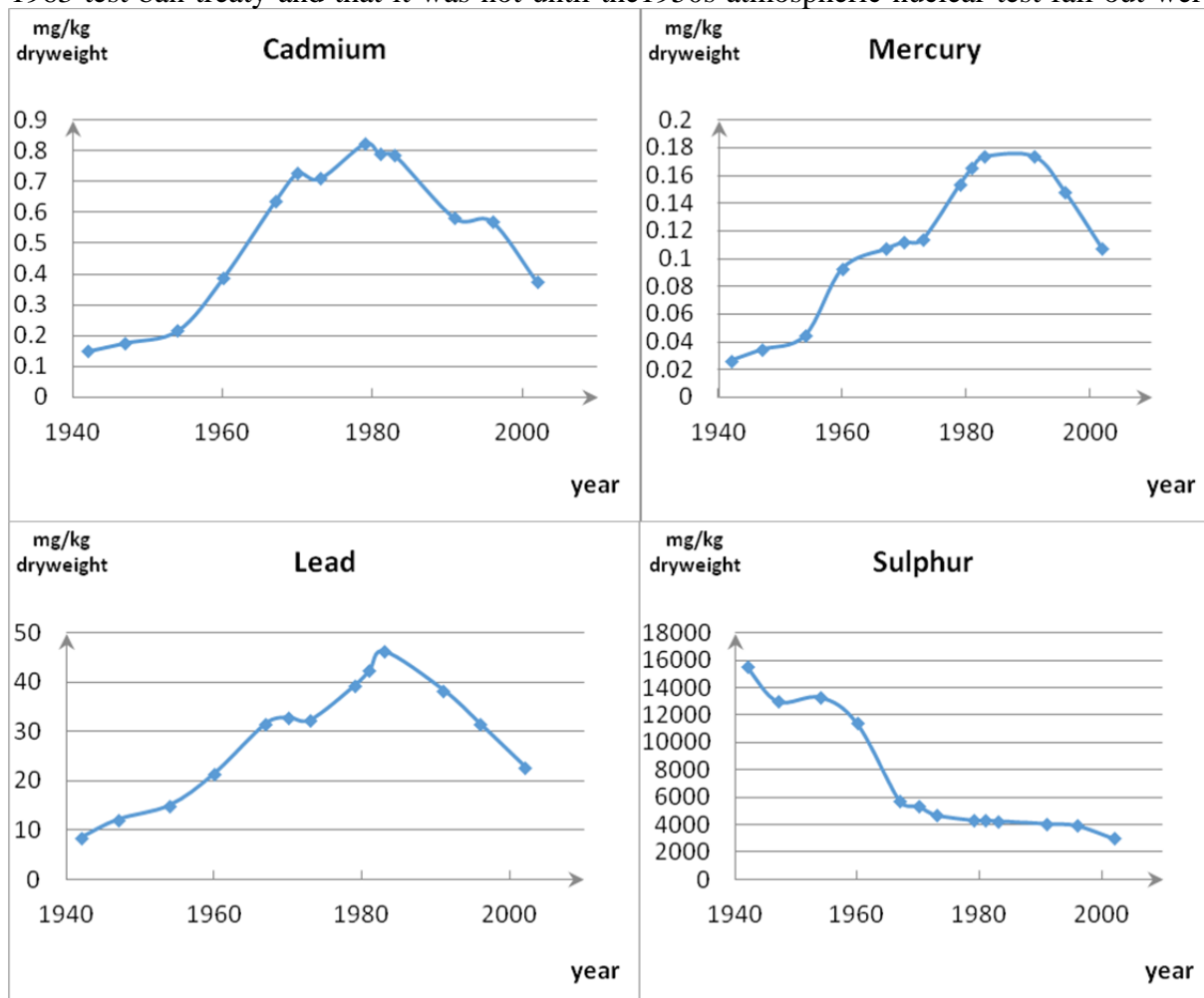

Figure 6. Examples of graphs showing the history of pollution of some of the elementals. For instance, you can easily see when we started using NiCd-batteries and what happened when we started to collect used batteries.

common, we can estimate the age of each slice. It is a rough method but for our purposes the accuracy is enough. Once the slices are dated with Cs-137, we let a commercial company made ICP-MS analyses of the slices in order to detect other contaminants than Cs-137. We measured the rate of As, Cd, Co, Cr, Cu, Hg, Mn, Ni, P, Pb, S, Zn and PCB in each slice. We got several nice graphs showing the modern history of pollution. Those graphs and the Cs graph show in a direct way that it is possible to decrease pollution with political action. We then divide the class into small groups and give each group a different element. A task for the students is to explain the shape of the distributions and to write a scientific report concerning their element. The students shall keep several aspects in mind, such as historical, biological, political aspects et cetera. Then they read each other's reports and give each other feedback following a kind of receipt we have found appropriate.

Results and Discussion

For the students the findings and results that they have detected caesium atoms that can be traced back to the nuclear tests and to the release from the Chernobyl accident are usually "a wakeup call". Detecting these atoms in our own environment raises questions about responsibilities, as well as the detrimental regional and more global biological implications. Another dimension is that we can date the slices with Cs-137 and get an extremely useful set of data that can be used in many different ways. An important advantage is if the students themselves perform the tests and are in charge of the results and its interpretations. It's a different thing when you are a part of a process, than if you only read and analyse other people's data. The facts become more real, hands on, if you can recall the smell and the feeling of the peat bog. One important experience is that science take time.

Our student case study is limited in time; however it could be extended to include Pb-210 dating methods if a longer project is planned. This would require more resources in terms of measuring equipment and analysing skills. An alternative to peat bog would be to sample undisturbed sediments that can be used as environmental archives. The case studies has been conducted the last four years involving over 200 students. This is the first year we have scaled up the project involving 160 students each year. Of the ca 50 students who have left our school at least one student has start to study radiation physics at the university.

Conclusions

The students like this project a lot. "When are we going to do it next?" is a common question. At our school we now have an agreement with the Radiation Physics Department to do this sampling campaign on an annual basis involving 160 students each year. Five classes take one core each. We encourage other schools to use similar case studies in their programs as at least in our opinion it's making highly motivated students in your classrooms. It would be interesting to start a joint exchange program for natural science students to conduct similar case studies and to enlarge the concept and look at other local pollutions in specific areas. They would notice similarities and differences and could discuss them.

References

Hattie, J.A.C (2009). Visible learning. A synthesis of over 800 meta-analyses relating to achievement. London: Routledge.

Sjöberg, S (2009). Naturvetenskap som allmänbildning: en kritisk ämnesdidaktik. Studentlitteratur.

M – LAST SUBMISSIONS

The dissolved polonium in groundwaters from southeast Brazil

D. M. Bonotto[*] and A. M. M. A. de Oliveira

UNESP-São Paulo State University, IGCE-Geosciences and Exacts Science Institute, DPM-Dept. of Petrology and Metallogeny, Av. 24A No. 1515, 13506-900 Rio Claro (SP), Brazil

Abstract

This paper describes a study focusing the presence of the radionuclides ^{210}Po and ^{210}Pb in spas groundwaters occurring at São Paulo and Minas Gerais states, Brazil, that are extensively used for drinking in public places, bottling and bathing purposes, among other. The water samples (75) for this study were taken from springs and pumped tubular wells drilled at different aquifer systems that are inserted in Paraná and Southeastern Shield hydrogeological provinces. The results of the measurements for samples collected in duplicate yielded a maximum ^{210}Po activity concentration of 0.4 Bq/L and a maximum ^{210}Pb activity concentration of 0.05 Bq/L. All ^{210}Pb levels were lower than the guidance level of 0.1 Bq/L established by the WHO for its presence in drinking water, whereas the ^{210}Po values reached or were above the same reference level for ^{210}Po in four samples from spas at Minas Gerais State: two of them provided from the Poços de Caldas alkaline massif that is a Early-Cretaceous to Eocene alkaline igneous province surrounding the Paraná sedimentary basin and the remaining two provided from Caxambu area where the gneissic rocks are cut by mafic dykes and alkaline breccias, constituting important recharge areas of the fractured aquifers.

Introduction

^{210}Pb and ^{210}Po are progenies in the natural mass number (4n+2) ^{238}U decay series that finishes at the stable ^{206}Pb and are produced continuously in minerals from rocks as uranium is an important radioelement contributing to the natural terrestrial radioactivity, concentrating preferentially in acid igneous rocks compared with intermediate, basic, and ultrabasic varities (crustal average ~2.5 µg/g; Bowie & Plant, 1983). Some ^{210}Pb and ^{210}Po atoms escape the rocks and soils to the surrounding fluid, such as groundwater during interactions between the liquid and solid phases. Both ^{210}Pb and ^{210}Po in water are well-documented radionuclides for health risk, as WHO (2011) proposed a guidance level of 0.1 Bq/L for their activity concentration in drinking water in order to not exceed the reference dose level of the committed effective dose equal to 0.1 mSv from 1 year's consumption.

Analyses of several natural waters have shown that ^{210}Po and ^{210}Pb occur at different levels, depending on factors like lithology, acidity, etc. (see, for instance, Laul et al., 1987; Benoit & Hemond, 1987; El-Daoushy & Garcia-Tenorio, 1988; Harada et al., 1989; Narita et al., 1989; Nozaki et al., 1990, 1991, 1997; Dickson & Herczeg, 1992; Ivanovich & Harmon, 1992; Hong et al., 1999; Peck & Smith, 2000; Kim et al., 2001, 2005; Vesterbacka et al., 2005; Godoy & Godoy, 2006; Ruberu et al., 2007). In the last few decades, the consumption of natural drinking water, either spring or mineral (bottled or not), increased in several countries. Despite drinking water has been used mostly as the tap water accessible in every household, many people believe that the naturally occurring waters are healthy and/or can be utilized for health cures, thus, exhibiting better quality than the tap water. Additionally, economic reasons have also favored their use as bottled waters so that the commercialization of mineral waters has widely increased, inclusive in Brazil where circa 20 million consumers are involved (SEBRAE, 2012).

---

[*] Corresponding author, E-mail: danielmarcosbonotto@gmail.com

The Brazilian Code of Mineral Waters (BCMW) was established by Register 7841 published on 8 August 1945 (DFPM, 1966). It classifies the mineral waters for spas and bottling uses, as well the potable waters for bottling, including several parameters like the radioactivity due to dissolved ^{222}Rn (radon) and ^{220}Rn (thoron) (DFPM, 1966). DNPM-National Department of Mineral Production manages in Brazil the production and commercialization of mineral waters. The amount of bottled mineral waters at SP in 2007 was higher than 1.5 billion liters (34% of the total in the country) (CPRM, 2012). Previous studies held by Oliveira et al. (2001) and Godoy et al. (2001) reported ^{226}Ra, ^{228}Ra and ^{210}Pb in 17 and 28 brands of bottled mineral waters, respectively. However, the actual accentuated consumption of spring and mineral waters for drinking purposes in Brazil has requested additional understanding of their radionuclides composition. They are widely exploited from spas located at SP and MG due to historical reasons and the generation of a consistent ^{210}Pb and ^{210}Po database from the use of the same experimental steps allowed new insights and a comparison with other analysis for dissolved radionuclides.

Materials and Methods

The groundwater samples (75) were taken from springs and pumped tubular wells from 14 spas located in SP and MG (Fig. 1) at various geological contexts: Águas de São Pedro (3), Águas da Prata (7), Águas de Lindóia (7), Serra Negra (8), Lindóia (2), Termas de Ibirá (5), Águas de Santa Bárbara (1), Lambari (6), São Lourenço (8), Cambuquira (6), Caxambu (10), Poços de Caldas (6), Pocinhos do Rio Verde (4) and Araxá (2). The water sources were from different aquifer systems in the Paraná and Southeastern Shield hydrogeological provinces as reported by Bonotto (2014, 2015, 2016a, 2016b). They corresponded to the same springs and pumped tubular wells analyzed in terms of physico-chemical parameters, major constituents, radium isotopes (^{226}Ra and ^{228}Ra) and dissolved gases (^{222}Rn, ^{220}Rn, O_2, CO_2, S^{2-}). The codes adopted by Bonotto (2014, 2015, 2016a, 2016b) for their identification will be also used in this paper.
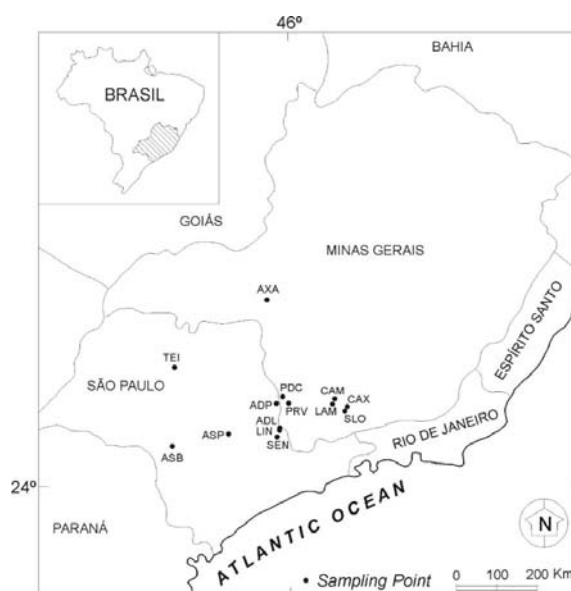
Figure 1. Sketch map of the research region in Brazil and location of the groundwater sampling points in the following spas of São Paulo and Minas Gerais states: ASP = Águas de São Pedro, ADL = Águas de Lindóia, SEN = Serra Negra, LIN = Lindóia, TEI = Termas de Ibirá, ASB = Águas de Santa Bárbara, ADP = Águas da Prata, PDC = Poços de Caldas, PRV = Pocinhos do Rio Verde, LAM = Lambari, SLO = São Lourenço, CAM = Cambuquira, CAX = Caxambu, AXA = Araxá.

Different methods have been used for characterizing ^{210}Pb and [210]Po in waters, for instance, γ-rays spectrometry with HPGe detector (Ivanovich and Harmon, 1992), gas-flow proportional counting (Peck & Smith, 2000), liquid scintillation counting (Kim et al., 2001), ICP-MS technique (Godoy & Godoy, 2006), electrochemical separation (Narita et al., 1989) or measurement of the α-particles (energy = 5.3 MeV) emitted by [210]Po (Laul et al., 1987; Benoit & Hemond, 1987; El-Daoushy & Garcia-Tenorio, 1988; Ivanovich & Harmon, 1992). In this study, the theoretical approach described by Bonotto et al. (2009) was adopted for generating the ^{210}Pb and [210]Po activity concentration data. Because [210]Bi grows into equilibrium with ^{210}Pb in about 25 days, a good approximation of the relationship between the [210]Po and ^{210}Pb activity concentrations after sampling (separation from the interaction with the host rock in the aquifer) is to wait at least a time (t_1) of about 20 to 30 days (several half-lives of [210]Bi) after sampling, extract [210]Po and measure its activity concentration. Then, the following equation (Froehlich, 2008) expresses the [210]Po and ^{210}Pb activity concentrations:

$$A_{Po}(t_1) = A_{Pb} + (A_{Poi} - A_{Pb}) \; exp \; (-\lambda_1 t_1) \tag{1}$$

where: A stands for activity concentration of the respective radionuclide and λ_1 is the decay constant of [210]Po. In order to avoid assumptions based on the condition of radioactive equilibrium to determine both radionuclide concentrations, a second groundwater sample from the same site was again analyzed by the same procedure, implying in another equation for a different time (t_2) that would permit unequivocally determine the two unknowns A_{Poi} and A_{Pb} (=A_{Pbi}, the initial ^{210}Pb activity concentration), i.e.:

$$A_{Po}(t_2) = A_{Pb} + (A_{Poi} - A_{Pb}) \; exp \; (-\lambda_1 t_2) \tag{2}$$

Such an approach was applied for the groundwater samples collected in duplicate (75), despite the time consuming of the analysis and costly laboratorial procedures. However, under the usual time scale of laboratorial experiments like one year, the decrease of the initial [210]Po activity (A_{Poi}) is high (84%) and, therefore, the [210]Po activity concentration measured at instant t in eqs. 1 and 2 is mainly related to the ^{210}Pb activity concentration. Consequently, the initial ^{210}Pb activity concentration may be found from measured [210]Po activity concentration according to the simplified equation (A_{Poi} is disregarded in eqs. 1 and 2):

$$A_{Po}(t) = A_{Pb} - A_{Pb} \; exp \; (-\lambda_1 t) \tag{3}$$

where: A is the activity concentration of the respective radionuclide, λ_1 is the [210]Po decay constant, and t is the time elapsed between the sample collection and counting date. The results obtained from applying simplified eq. 3 were compared with those using eqs. 1 and 2.

The duplicated groundwater samples were stored in polyethylene flasks, filtered through 0.45 μm Millipore membrane, acidified to pH ≅ 2 with 8M HCl, and a known amount (133.2 mBq) of [209]Po spike (α-particles emitting radionuclide, energy = 4.9 MeV; Karraker et al., 1951) was added to each one in order to assess [210]Po recovery. About 500 mg of $FeCl_3$ was also added to them, and [210]Po plus ^{210}Pb co-precipitated with $Fe(OH)_3$ by increasing the pH to 7-8 through addition of concentrated NH_4OH solution. The precipitated was recovered, dissolved in 8M HCl and Fe^{3+} was extracted into an equal volume of isopropyl ether. Then, it was added 5 mL of 20% hydroxylamine hydrochloride and 2 mL of 25% sodium citrate solution to the acid solution containing [210]Po and ^{210}Pb, being the pH adjusted to 2 with concentrated ammonia solution (Flynn, 1968). Polonium was subsequently plated onto a copper disc (1-in diameter) suspended in the solution placed on a hot plate magnetic stirrer, which was heated to 85-90°C, and stirred during 75-90 min with a Teflon stirrer. Then, the disc was removed, washed with demineralized water, dried in a heating lamp, and inserted in an evacuated chamber for α-counting.

The α-particles were counted by conventional alpha spectroscopy with four 450 mm^2 area, 100 μm depletion depth, 26 keV resolution PIPS detectors that were coupled to EG&G ORTEC multichannel buffer. The MAESTRO software provided 1024 channels to plot the alpha spectrum containing the [209]Po and [210]Po peaks. The system was calibrated in energy through a radioactive source prepared at the *Centre de Faibles Radioactivités*, CNRS-CEA, Gif-sur-Yvette, France, that

contained 0.91 Bq of ^{238}U (α-particles energy = 4.2 MeV), 0.91 Bq of ^{234}U (α-particles energy = 4.8 MeV), and 0.17 Bq of ^{232}U (α-particles energy = 5.3 MeV) (Lederer et al., 1967). The ^{209}Po peak (energy = 4.9 MeV) situated close to that of ^{234}U and the ^{210}Po peak in the ^{232}U channel region. The isotope dilution technique was used to generate the ^{210}Po activity concentration values from ^{209}Po and ^{210}Po peaks, whose statistical uncertainty was generally between 5 and 10%, within 1σ standard deviation.

Results and Discussion

Table 1 reports the ^{210}Po and ^{210}Pb activity concentrations determined from eqs. 1 and 2 in the groundwater samples collected in duplicate. The time elapsed between the sampling and counting date ranged from 25 to 2776 days. Each measured ^{210}Po activity concentration reported in Table 1 [$A_{Po}(t_1)$ and $A_{Po}(t_2)$] is not the initial ^{210}Po activity concentration in the groundwater sample (A_{Poi}), but it is a value produced from two opposite processes: a) ^{210}Po decrease according to its decay constant of 0.005 days^{-1}; b) ^{210}Po ingrowth from its grandparent ^{210}Pb that decays more slowly (decay constant of 8.55 × 10^{-5} days^{-1}). The initial ^{210}Po activity values are within the range of 0.09-401.5 mBq/L, whereas the ^{210}Pb activity concentration varied between 0.07 and 54.8 mBq/L (Table 1). The whole data set for the activity concentrations of both radionuclides (^{210}Po and ^{210}Pb) was submitted to a statistical treatment, considering class intervals arranged in geometric progression, due to the great variability of the values obtained. Table 2 indicates lognormal distribution of the data, as also observed for other radionuclides (^{222}Rn, ^{226}Ra, ^{238}U and ^{234}U) analyzed in the same water sources (Bonotto, 2014, 2015, 2016a). Median, modal, and mean values corresponding to 2.90, 14.93, and 6.58 mBq/L were obtained for the ^{210}Po activity concentration, respectively, whereas values of 2.60, 8.34, and 4.66 mBq/L for the ^{210}Pb activity concentration, respectively.

Equation 3 was applied to the measured ^{210}Po activity concentration in the water sources whose minimum time elapsed between the sampling and counting corresponded to 140 days. The estimated ^{210}Pb activity concentrations corresponded to maximum values as the use of eq. 3 implies that the contribution of the initial ^{210}Po to the measured ^{210}Po activity concentration has been disregarded. The mean ^{210}Pb activity concentration from such dataset was 12.64 mBq/L. Bonotto et al. (2009) also applied eq. 3 for GAS (Guarany Aquifer System) groundwaters, reporting a mean ^{210}Pb activity concentration of 1.95 mBq/L. The average value found in this study is 6.5 times higher certainly because of the presence of lithologies enriched in natural radionuclides in the spas investigated.

Table 1. ^{210}Po and ^{210}Pb activity concentrations in spas groundwaters from southeastern Brazil. Analytical uncertainties ±5-10% at 1σ standard deviation.

Sample Code	Volume (L)	Δt$_1$ (days)[1]	Meas. (1) ^{210}Po (mBq/L)	Volume (L)	Δt$_2$ (days)[1]	Meas. (2) ^{210}Po (mBq/L)	^{210}Po (mBq/L)	^{210}Pb (mBq/L)	^{210}Po/^{210}Pb activity ratio
ALS	13.5	420	1.48	19.7	36	8.15	9.69	0.33	29.4
GIO	21.7	69	32.88	20.6	500	4.03	46.32	0.25	185.3
JUV	9.4	269	2.14	9.7	471	1.43	5.31	1.02	5.2
PLA	16.9	68	4.22	20.6	35	4.80	5.53	0.99	5.6
POL	16.6	61	1.20	20.5	35	1.23	1.28	0.98	1.3
VIT	23.1	190	4.95	10.8	37	10.15	12.13	0.42	28.9
BOI	17.7	39	5.46	5.3	454	27.25	0.09	30.38	0.003
PTA	24.0	90	1.12	20.0	35	1.40	1.62	0.24	6.8
VIL	20.7	62	13.54	10.8	400	6.52	16.67	4.93	3.4
PDE	25.7	69	2.73	19.2	266	5.60	0.84	7.31	0.1
SIL	20.4	67	2.06	11.6	432	5.82	0.28	6.54	0.04
FIL	13.5	76	2.94	9.0	429	1.08	3.98	0.70	5.7

BEL	14.5	76	3.78	11.0	184	5.06	2.36	6.85	0.3
SRE	13.2	76	1.98	10.8	39	1.25	0.32	5.57	0.06
COM	20.0	61	0.92	10.7	197	1.89	0.22	2.89	0.08
LIN	22.5	61	33.25	10.4	184	19.58	43.86	3.49	12.6
CUR	23.7	120	2.98	10.9	438	1.39	4.62	0.98	4.7
SJO	13.6	120	2.42	19.0	249	2.92	1.56	3.47	0.4
SCA	4.9	120	4.66	11.2	440	5.38	3.92	5.56	0.7
ITA	14.8	50	8.33	16.4	264	25.49	0.91	34.45	0.03
SLU	19.2	265	16.60	11.7	540	4.48	61.41	0.38	161.6
SAT	19.6	270	30.07	7.5	413	25.80	53.96	21.71	2.5
BRU	5.2	427	3.66	9.7	497	2.60	30.43	0.07	434.7
LAN	5.0	412	2.49	6.0	502	1.89	13.82	0.83	16.6
SAA	14.0	20	3.17	18.2	269	23.71	0.14	32.02	0.004
SBE	22.7	120	10.56	17.2	268	11.39	9.26	12.15	0.8
BIO	16.8	263	2.39	11.6	429	2.70	0.89	2.94	0.3
JOR	19.5	251	7.74	6.4	523	2.75	24.58	1.03	23.9
ADB	19.2	60	20.92	19.5	400	3.97	28.18	0.18	156.6
CGO	12.2	90	6.80	18.0	252	3.10	10.59	0.14	75.6
SRC	14.6	54	4.47	18.0	274	3.82	4.77	3.50	1.4
SEI	6.2	258	3.74	6.4	453	3.46	4.92	3.29	1.5
BMU	10.0	111	3.23	10.6	350	1.17	5.42	0.28	19.4
LA1	20.1	90	22.66	17.8	267	9.67	35.23	0.54	65.2
LA2	20.5	167	4.59	10.0	472	4.94	4.00	5.04	0.8
LA3	17.2	274	20,54	9.5	447	20.10	22.77	19.78	1.2
LA4	9.4	273	7.65	5.1	469	5.17	19.22	3.68	5.2
LA5	15.5	90	3.57	8.7	288	7.21	0.28	9.36	0.03
LA6	20.4	168	5.14	17.5	273	6.24	1.59	7.83	0.2
SL7	22.3	173	2.60	15.0	28	3.58	3.86	1.68	2.3
SL5	19.6	140	1.99	15.2	28	1.01	0.67	3.30	0.2
SL6	20.4	173	3.58	15.8	28	1.27	0.60	5.75	0.1
SL3	19.6	173	5.76	14.6	78	4.20	2.23	8.32	0.3
SL4	18.8	146	3.65	16.2	78	4.95	7.10	0.44	16.1
SL1	14.8	155	3.16	1.0	90	3.57	4.41	2.09	2.1
SL10	16.4	154	5.32	16.0	28	2.32	1.36	8.74	0.2
SL9	17.5	260	2.27	15.8	78	4.75	6.73	0.60	11.2
ROR	24.2	156	12.70	6.5	470	3.14	26.96	0.63	42.8
REW	5.7	240	3.46	7.2	469	3.85	2.13	4.03	0.5
CAF	24.4	134	2.98	5.9	281	3.56	1.92	4.09	0.5
FEP	13.1	75	9.70	5.8	280	23.09	0.20	30.58	0.006
MAR	22.4	95	7.66	6.4	275	14.88	0.26	19.83	0.01
SLI	13.8	35	3.64	15.8	83	3.54	3.73	3.17	1.2
GFL	20.7	118	11.92	13.2	268	13.65	9.28	15.20	0.6
VEN	21.8	117	17.76	18.0	650	1.52	31.64	0.30	105.5
MAY	10.1	273	34.20	9.8	468	21.58	93.28	13.94	6.7
EGU	23.4	140	29.29	18.2	286	42.52	3.40	54.83	0.06
VIO	10.1	282	36.45	10.3	470	20.10	119.52	9.62	12.4
DPE	21.7	155	41.32	20.5	266	46.18	27.96	52.73	0.5
BZA	8.0	259	111.46	7.3	470	40.15	401.49	2.06	194.9
DXE	12.8	121	11.65	19.6	281	16.32	4.60	20.13	0.2
LEO	12.8	155	14.92	9.1	273	10.34	26.95	4.64	5.8
ISA	20.6	272	17.90	11.2	470	17.09	21.63	16.61	1.3
QUI	13.6	39	6.20	4.6	1422	3.34	6.82	3.34	2.0
NOV	24.3	53	12.62	10.8	186	11.42	13.37	10.15	1.3
MAC	24.1	82	13.31	11.0	300	4.85	19.77	0.56	35.3
SIN	19.8	185	49.45	5.2	431	25.10	101.81	15.04	6.8

FRA	18.6	82	8.00	11.6	560	0.88	11.97	0.16	74.8
PEB	13.9	77	3.69	10.4	186	2.79	4.70	1.55	3.0
RIV	17.3	68	24.86	7.6	265	20.62	27.60	18.09	1.5
SMA	7.8	264	10.43	10.0	453	7.37	24.16	5.42	4.4
SJO	7.5	257	6.56	9.2	454	6.71	5.93	6.80	0.9
AMO	19.2	260	52.85	1.4	2776	7.04	175.13	7.04	24.9
DBJ	10.0	811	25.48	9.3	26	9.97	7.77	25.79	0.3
AJU	10.0	811	12.07	9.7	25	8.30	7.79	12.14	0.6

[1] time elapsed between sampling and mid-counting date

Table 2. *Statistical evaluation of the data obtained for the activity concentrations of ^{210}Po and ^{210}Pb in groundwaters from spas at southeastern Brazil.*

Range of ^{210}Po activity conc. (mBq/L)	Average activity conc. (mBq/L)	Frequency	Frequency percentage (%)	Cumulative percentage (%)
0.06 – 0.23	0.09	4	5.3	5.3
0.23 – 0.92	0.36	9	12.0	17.3
0.92 – 3.75	1.48	11	14.7	32.0
3.75 – 15.20	6.01	27	36.0	68.0
15.20 – 61.67	24.39	19	25.3	93.3
61.67 – 250.22	98.96	4	5.4	98.7
250.22 – 1015.23	401.49	1	1.3	100.0

Range of ^{210}Pb activity conc. (mBq/L)	Average activity conc. (mBq/L)	Frequency	Frequency percentage (%)	Cumulative percentage (%)
0.05 – 0.14	0.07	2	2.7	2.7
0.14– 0.43	0.21	9	12.0	14.7
0.43 – 1.30	0.64	12	16.0	30.7
1.30 – 3.95	1.96	14	18.7	49.4
3.95 – 12.00	5.95	20	26.6	76.0
12.00 – 36.44	18.06	16	21.3	97.3
36.44 – 110.65	54.83	2	2.7	100.0

Plotting the ^{210}Pb activity concentrations acquired from eqs. 1 and 2 and estimated from eq. 3 indicates that several water sources fit the equiline, however, many of them indicate that eq. 3 yields ^{210}Pb values higher than those evaluated from the use of eqs. 1 and 2. In these cases, there is failure on the premise of disregarding the initial ^{210}Po activity on the measured ^{210}Po activity concentration value. As a consequence, the overestimation of the ^{210}Pb activity concentration may cause false decision on the evaluation of the drinking water quality due to the presence of dissolved ^{210}Pb. For instance, it may be pointed out the need of bores sealing or the closure of taps exploiting springs whose waters were previously available for human consumption. Therefore, eqs. 1 and 2 are recommended for providing the ^{210}Po and ^{210}Pb activity concentrations data, despite the time consuming of the analysis in duplicate and costly laboratorial tasks. Such procedure implies on avoiding occasional inconvenient decision for members of the public.

Conclusions

Statistical tests of correlation were realized between the ^{210}Po and ^{210}Pb activity concentrations in the water sources and the following parameters reported elsewhere: temperature, pH, electrical conductivity, redox potential Eh, dissolved gases (O_2, CO_2, H_2S), dry residue (~TDS, total

dissolved solids), alkalinity (bicarbonate, carbonate, hydroxide), major cations (Na, K, Ca, Mg), major anions (sulfate, chloride, nitrate, fluoride, phosphate), silica, iron (total Fe, Fe^{2+}), and radionuclides (^{222}Rn, ^{220}Rn, ^{226}Ra, ^{228}Ra, ^{238}U, ^{234}U). However, none significant value was found, indicating the complexity of the processes involving the transfer of both radionuclides ^{210}Pb and ^{210}Po into the liquid phase after their production in the minerals occurring in the various lithologies. Such situation has been also identified in other contexts, for instance, in Nordic drinking water from drilled wells, where it was found poor correlation to both aquifer geology and bedrock radioactivity. Some possible factors that also could justify the lack of correlation obtained in this study are: a) parameters involved on the generation of ^{210}Pb and ^{210}Po in host rocks and transfer to water that are very difficult or impossible to measure practically, i.e. microscopic properties (surface roughness, inhomogeneous radionuclides distribution in the solid), network of 100-200 Å wide nanopores in rocks and minerals, and radionuclides enrichment in grain boundaries or crevices; b) ^{222}Rn solubility dependent on the temperature, implying on the ^{210}Pb generation from the ^{222}Rn decay that may be largely removed from the water to bedrock surfaces of the aquifer, where could contribute to enhance the polonium activity in the water; c) relationship between ^{210}Po, hydrogen sulfide and bacteria growth that indicates a decline of sulfide and soluble ^{210}Po during the bacterial growth; d) systematic particulate polonium increase with time, reflecting the decreasing amount of soluble polonium that could be related to the adsorption of polonium and/or growth of polonium-bearing bacteria; e) association of some non-"Fe-scavengable" ^{210}Po in water with sulfide-oxidizing bacteria in the particulate rather than dissolved phase, therefore, drastically reducing the amount of soluble ^{210}Po. Co-variations among the ratios $^{210}Pb/^{226}Ra$, $^{210}Po/^{226}Ra$, $^{210}Pb/^{222}Rn$, $^{210}Po/^{222}Rn$, $^{210}Pb/^{238}U$ and $^{210}Po/^{238}U$ in the water sources analyzed indicated great deviation from the radioactive equilibrium condition as also verified for the $^{210}Po/^{210}Pb$ activity ratios. The ratios $^{210}Pb/^{226}Ra$ and $^{210}Pb/^{222}Rn$ always pointed out accentuated ^{210}Pb depletion in the waters relatively to its ancestors ^{226}Ra and ^{222}Rn, whereas the ratios $^{210}Pb/^{238}U$ and $^{210}Po/^{238}U$ were above unity in many cases. Radiation dose calculations permitted integrate the activity concentration data obtained for both radionuclides, ^{210}Pb and ^{210}Po, allowing estimate a total Committed Effective Dose (CED) range of 0.0015-0.35 mSv/yr. Four springs exhibiting high ^{210}Po levels possessed CED values equivalent or above of the WHO guideline reference level of 0.1 mSv from 1 year's consumption of drinking water. Two of these springs are located at the Poços de Caldas alkaline massif that is a well-known suite of alkaline volcanic and plutonic rocks enriched in natural radionuclides and rare-earth elements (REEs). Such finding confirms the results of some previous studies held there.

References
Benoit, G., Hemond, H.F., 1987. A biogeochemical mass balance of ^{210}Po and ^{210}Pb in an oligotrophic lake with seasonally anoxic hypolimnion. Geochim. Cosmochim. Acta 51 (6), 1445-1456.
Bonotto, D.M., 2014. ^{222}Rn, ^{220}Rn and other dissolved gases in mineral waters of southeast Brazil. J. Environ. Radioact. 132, 21-30.
Bonotto, D.M., 2015. ^{226}Ra and ^{228}Ra in mineral waters of southeast Brazil. Environ. Earth Sci. 74, 839-853.
Bonotto, D.M., 2016a. The dissolved uranium concentration and $^{234}U/^{238}U$ activity ratio in groundwaters from spas of southeastern Brazil. J. Environ. Radioact. doi: 10.1016/j.jenvrad.2016.03.009
Bonotto, D.M., 2016b. Hydrogeochemical study of spas groundwaters from southeast Brazil. J. Geochem. Explor. 169, 60-72.
Bonotto, D.M., Caprioglio, L., Bueno, T.O., Lazarindo, J.R., 2009. Dissolved ^{210}Po and ^{210}Pb in Guarani aquifer groundwater, Brazil. Radiat. Meas. 44, 311-324.
Bowie, S.H.U., Plant, J.A., 1983. Natural radioactivity in the environment. In: Thornton, I. (Ed.) Applied Environmental Geochemistry. Academic Press, London, 481-494.
CPRM (Brazilian Geological Survey), 2012. A indústria brasileira de água mineral, <http://www.cprm.gov.br/>.
DFPM (Division for Supporting the Mineral Production), 1966. The mining code, the mineral waters code and how applying research in a mineral deposit, 8th ed., DFPM, Rio de Janeiro.

Dickson, B.L., Herczeg, A.L., 1992. Naturally-occurring radionuclides in acid-saline groundwaters around Lake Tyrrell, Victoria, Australia. Chem. Geol. 96 (1-2), 95-114.

El-Daoushy, F., Garcia-Tenorio, F., 1988. Speciation of Pb-210/Po-210 in aquatic systems and their deposits. Sci. Total Environ. 69, 191-209.

Flynn, W.W., 1968. The determination of low levels of polonium-210 in environmental materials. Anal. Chim. Acta 43, 221-227.

Froehlich, K., 2008. Determination of the ^{210}Po and ^{210}Pb activity concentration in groundwater. Technical Information, IAEA-International Atomic Energy Agency, Vienna, 5 pp.

Godoy, J.M., Godoy, M.L., 2006. Natural radioactivity in Brazilian groundwater. J. Environ. Radioact. 85 (1), 71-83.

Godoy, J.M., Amaral, E.C.S., Godoy, M.L.D.P., 2001. Natural radionuclides in Brazilian mineral water and consequent doses to the population. J. Environ. Radioact. 53, 175-182.

Harada, K., Burnett, W.C., LaRock, P.A., Cowart, J.B., 1989. Polonium in Florida groundwater and its possible relationship to the sulfur cycle and bacteria. Geochim. Cosmochim. Acta 53 (1), 143-150.

Hong, G., Park, S., Baskaran, M., Kim, S., Chung, C., Lee, S., 1999. Lead-210 and polonium-210 in the winter well-mixed turbid waters in the mouth of the Yellow Sea. Cont. Shelf Res. 19 (8), 1049-1064.

Ivanovich, M., Harmon, R.S., 1992. Uranium Series Disequilibrium: Applications to Environmental Problems, 2nd edn. Clarendon Press, Oxford.

Karraker, D.G., Ghiorso, A., Templeton, D.H., 1951. Alpha-decay energies of polonium isotopes. Phys. Rev. 83, 390-393.

Kim, Y., Kim, C., Lee, J., 2001. Simultaneous determination of ^{226}Ra and ^{210}Pb in groundwater and soil samples by using the liquid scintillation counter - suspension gel method. Appl. Radiat. Isot. 54 (2), 275-281.

Kim, G., Kim, S., Harada, K., Schultz, M.K., Burnett, W.C., 2005. Enrichment of excess ^{210}Po in anoxic ponds. Environ. Sci. Technol. 39 (13), 4894-4899.

Laul, J.C., Smith, M.R., Thomas, C.W., Jackson, P.O., Hubbard, N., 1987. Analysis of natural radionuclides from uranium and thorium series in briney groundwaters. J. Radioanal. Nucl. Chem. 110 (1), 101-112.

Lederer, C.M., Hollander, J.M., Perlman, I., 1967. Table of isotopes, 6th edn. Wiley, New York.

Narita, H., Harada, K., Burnett, W.C., Tsunogai, S., McCabe, W.J., 1989. Determination of ^{210}Pb, ^{210}Bi and ^{210}Po in natural waters and other materials by electrochemical separation. Talanta 36 (9), 925-929.

Nozaki, Y., Ikuta, N., Yashima, M., 1990. Unusually large ^{210}Po deficiencies relative to ^{210}Pb in the Kuroshio current of the East China and Philippine Seas. J. Geophys. Res. 95, 5321-5329.

Nozaki, Y., Zhang, J., Takeda, A., 1997. ^{210}Pb and ^{210}Po in the equatorial Pacific and the Bering Sea: the effects of biological productivity and boundary scavenging. Deep Sea Res. II 44 (9-10), 2203-2220.

Nozaki, Y., Tsubota, H., Kasemsupaya, V., Yashima, M., Ikuta, N., 1991. Residence times of surface water and particle-reactive ^{210}Pb and ^{210}Po in the East China and Yellow seas. Geochim. Cosmochim. Acta 55, 1265-1272.

Oliveira, J., Mazzilli, B.P., Sampa, M.H.O., Bambalas, E., 2001. Natural radionuclides in drinking water supplies of São Paulo State Brazil and consequent population doses. J. Environ. Radioact. 53, 99-109.

Peck, G.A., Smith, J.D., 2000. Determination of ^{210}Po and ^{210}Pb in rainwater using measurement of ^{210}Po and ^{210}Bi. Anal. Chim. Acta 422 (1), 113-120.

Ruberu, S.R., Liu, Y., Perera, S.K., 2007. Occurrence and distribution of ^{210}Pb and ^{210}Po in selected California groundwater wells. Health Phys. 92(5), 432-441.

SEBRAE (Service for Supporting the Small Businesses in São Paulo State), 2012. Comércio de água mineral, <http://www.sebrae-sc.com.br/ideais/default.asp?vcdtexto= 31586&%5E%5E>.

Vesterbacka, P., Hämäläinen, K., Lehto, J., 2005. The effect of water treatment on the presence of particle-bound ^{210}Po and ^{210}Pb in groundwater. Radiochim. Acta 93 (5), 291-296.

WHO (World Health Organization), 2011. Guidelines for drinking water quality, 4th ed. WHO Press, Geneva.

Measurement of ^{236}U at the GEOTRACES East Pacific Zonal Transect

M. Villa-Alfageme[1]*, E. Chamizo[2], M. López-Lora[2], T. Kenna[3], N. Casacuberta[4], P. Masqué[5], M. Christl[4]

[1]Applied Physics Dept.II, ETSIE. Universidad de Sevilla. 41012 Sevilla, Spain
[2]CentroNacional de Aceleradores (CNA). Universidad de Sevilla. Junta de Andalucía. Consejo Superior de Investigaciones Científicas. Sevilla, Spain
[3]Lamont-Doherty Earth Observatory. Columbia University. NY. USA
[4]Ion Beam Physics.ETH Zürich. Switzerland
[5]School of Natural Sciences. Centre for Marine Ecosystems Research. Edith Cowan University. Joondalup. WA. Australia

Abstract

During October-December 2013 U.S. GEOTRACES sampled the East Pacific Zonal Transect (EPZT). The transect went from Peru (12°S, 77°W) to Tahiti (17°S, 149°W) and included the in-depth analysis of the Peru Margin upwelling and oxygen minimum zone (OMZ), and the large hydrothermal plume (HP) originating from the southern East Pacific Rise. Respectively St. 11 (12°S,94°W) and St. 18 (15°S,113°W). That area might have been influenced by the US and French nuclear weapon testing sites at the Pacific Ocean.Several water profiles were collected for the analysis of ^{236}U. Surface samples, i.e. above 400 m, were measured on the1 MV AMS system at the Centro Nacional de Aceleradores (CNA, Sevilla, Spain) because the ^{236}U/^{238}U atom ratio (AR) was at the order of 10^{-10}, and the maximum sensitivity achieved on this system is 7×10^{-11}. In deeper samples the expected AR was at the 10^{-12}-10^{-11} level, and for that reason they were measured on the 600 KV Tandy facility at the ETH Laboratory of Ion Beam Physics (Zürich,Switzerland), with a lower background (at the order of 10^{-14}).

We present here the results for stations 11 and 18. Our results show that: i) Samples above 1000 m presented ^{236}U concentrations from $0.02\cdot10^6$ to $7\cdot10^6$ at kg^{-1}, lower than the activity concentrations at the Equatorial North Atlantic (NA), from $2\cdot10^6$ to $6\cdot10^6$ at kg^{-1}, above 1000 m. The data indicated the presence of anthropogenic ^{236}U, but no additional sources than global fallout were identified here. In contrast,deep samples in the North Atlantic showed the presence of ^{236}U from European nuclear reprocessing plants. ii) Most of the samples between 600 and 2000 m presented very low values, close to the lithogenic/natural ratios (i.e. at the 10^{-12} level). To the best of our knowledge, these ratios are the lowest ones measured so far in seawater. Below 2000 m it might detected a slight increase in the ^{236}Uconcentration in both OMZ and HP stations.iii) Regarding the biogeochemical behaviour, similar ^{236}U/^{238}U profiles were obtained in the upper 1300 m in both OMZ and HP. The analysis of other radionuclides sampled during the cruise, e.g. ^{237}Np and ^{129}I, and of additional EPZT profiles will provide insights of the origin of ^{236}U fluctuations in depth.

Introduction

Uranium-236 is a long-lived radioisotope ($T_{1/2}$=2.35$\cdot10^7$ y) that decays by alpha emission to ^{232}Th. It is mainly produced in nuclear reactors through the capture of a thermal neutron by ^{235}U or ^{239}Pu (followed by alpha decay of ^{240}Pu). It is also naturally produced in much more inferior amounts by neutrons associated to cosmic radiation and by the so-called nucleogenic component (i.e. neutrons produced by the spontaneous fission of ^{238}U or in the (α, n) reactions on light elements). These processes lead to natural abundance levels that range from 10^{-14} to 10^{-10} ^{236}U/^{238}U atom ratios[*Steier*

et al., 2008]. However, ^{236}U in the environment mainly has an anthropogenic origin, leading to isotopic ratios in seawater between 10^{-9} and 10^{-6} in the environment ([*Steier et al.*, 2008; *Wendel et al.*, 2013; *Winkler et al.*, 2012] and references therein).

A total amount of 35 kg of mobile ^{236}U coming from natural sources has been estimated ([*Casacuberta et al.*, 2014; *Christl et al.*, 2015; *Steier et al.*, 2008] and references therein).It is estimated that about 10^6 kg of ^{236}U has been produced in nuclear reactors worldwide. Atmospheric nuclear weapons tests contributed to the total inventory with a quantity that has been calculated to range between 900 and 1400 kg [*Casacuberta et al.*, 2014; *Sakaguchi et al.*, 2009]. The nuclear fuel reprocessing plants (NFRP), Sellafield and La Hague, carried out important liquid releases discharges, approximately between 115-250 kg of ^{236}U, to the North Sea. The contribution of these sources is not well defined, but they dominate some areas of the Atlantic Ocean [*Christl et al.*, 2015].

Up to now, due to the difficulties in the measurement of low ^{236}U/^{238}U ratios, the availability of data on^{236}U in the environment was limited. After the improvement of the analytical detection techniques, AMS [*Marsden et al.*, 2001], ICP-MS [*Ketterer et al.*, 2003]or TIMS [*Richter et al.*, 2010], ^{236}U concentrations data in several environmental compartments have become available in recent years. Furthermore, recent studies demonstrated the potential use of ^{236}U as an oceanic circulation tracer [*Casacuberta et al.*, 2016; *Christl et al.*, 2012; *Sakaguchi et al.*, 2012], and to study the signal of fallout in corals [*Winkler et al.*, 2012] , peats [*Quinto et al.*, 2013]and ice cores[*Wendel et al.*, 2013].

However, it is uncertain the contribution of specific sources as Sellafield and La Hague in different areas and depths of the Atlantic Ocean. Thus, it is important to build a database that provides data of ^{236}U distribution in order to broad the information of the different sources to the Ocean. In this context, very few data from the Pacific Ocean waters are available [*Sakaguchi et al.*, 2009].

In this work, we present ^{236}U data from the Equatorial Pacific. This area is not expected to be affected by releases from nuclear fuel reprocessing plants, but it might be potentially affected by the past US and French nuclear tests carried out in the Marshall islands and Mururoa and Fangataufa atolls during the Pacific Proving Grounds (PPG) and the French Nuclear Weapons Testing, respectively [*Nomura et al.*, 2017].


Materials and Methods

Samples

The U.S. GEOTRACES East Pacific Zonal Transect (EPZT) was occupied from October-December 2013. The transect from Peru to Tahiti included the Peru Margin, upwelling and oxygen minimum zone (OMZ), St. 11 (12°S,94°W), and the large hydrothermal plume (HP), St. 18 (15°S,113°W), originating from the southern East Pacific Rise (Fig. 1). 125 samples were collected.

Radiometric technique

In a first step, 3 pg of ^{233}U ($T_{1/2}$= 1.59·10^5 y) spike were added to the samples to quantify the ^{236,238}U concentrations by the isotope dilution. Actinides were co-precipitated at Lamont-Doherty Earth Observatory (LDEO) as follows. 4 L of seawater samples were acidified with 1 mL of HNO_3 (65%) per litre of sample, mixed and let settled for, at least, one hour for their homogenisation. Fe^{3+} was

then added to the samples and uranium was extracted from the bulk of the sample by rising the pH to about 8.5 adding 45% NH_3. After complete precipitation and settling of the $Fe(OH)_3$ particles, the supernatant was discarded and the resulting precipitate taken to dryness. Subsequently, at CNA-Universidad de Sevilla,$Fe(OH)_3$ precipitate was dissolved with 8M HNO_3 and UTEVA® resins in a vacuum box were used for the final uranium purification following the method described in *López-Lora et al.* [In review]. AMS sources were prepared by adding 1 mg of Fe^{3+} to the uranium solutions for its coprecipitation with $Fe(OH)_3$. Precipitates were transferred to quartz crucibles, dried and heated at 650ºC to get iron oxides. Finally samples were mixed with 3 mg of Nb powder and pressed into suitable aluminium cathodes.
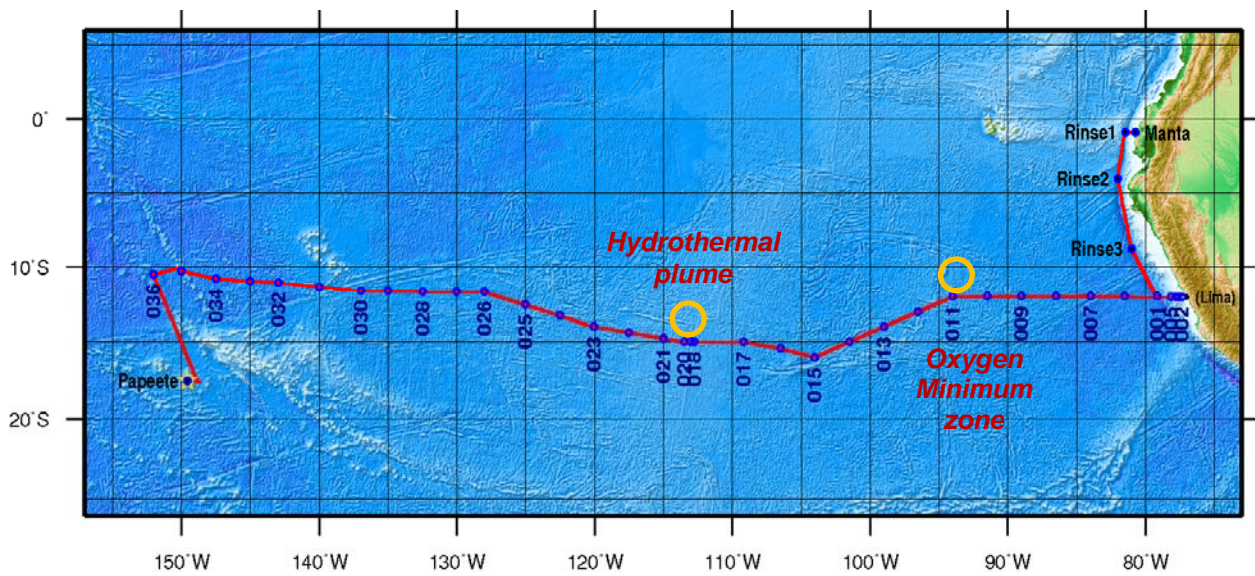
*Figure 1.*U.S. GEOTRACES East Pacific Zonal Transect. Geographical distribution. Discussed sections, 11 (Oxygen Minimum Zone) and 18 (Hydrothermal Plume), are marked in yellow.

Measurement

AMS determinations were performed on the 1 MV CNA AMS system and on the 600 kV ETH AMS facility. Details about the technique can be found in [*Chamizo et al.*, 2015].Briefly, uranium isotopes are extracted from the Cs^+ sputtering ion-source as negative oxide ions (UO-). These anions are analysed by a first 90º sector magnet and directed to the terminal of the tandem accelerator, which contains the stripper gas (He gas in both facilities). Negative oxide ions brake up and are stripped to 3+ charge state in the so-called stripping process. These ions are analysed by additional cinematic filters at the exit of the accelerator. Finally, the minor isotopes ($^{233,236}U^{3+}$) are counted from the total energy signal provided by a gas ionization chamber. The abundant natural isotope ^{238}U is measured as a beam-current in a Faraday Cup.

Surface samples, i.e. above 400 m, were measured at the CNA because the $^{236}U/^{238}U$ atom ratio (AR) was at the order of 10^{-10}, and the maximum sensitivity achieved on this system is $7x10^{-11}$. In deeper samples the expected AR was at the 10^{-12}-10^{-11} level, and for that reason they were measured at the ETH facility, which features with a lower background (at the order of 10^{-14}) obtained with an additional sector magnet before the final detection system. Details about the current status of the 1 MV CNA system are given in *Scognamiglio et al.* [2016]and about the 600 kV ETH facility in *Christl et al.* [2013]

Results and Discussion

Figure 2 shows that samples above 1000 m presented ^{236}U concentrations from $0.02 \cdot 10^6$ to $7 \cdot 10^6$ at kg^{-1}, which are lower than the concentrations at the Equatorial North Atlantic (NA), from $2 \cdot 10^6$ to $6 \cdot 10^6$ at kg^{-1}. The data indicated the presence of anthropogenic ^{236}U, but no additional sources than global fallout were identified here. In contrast to the deep samples in the North Atlantic, that showed the presence of ^{236}U from nuclear reprocessing plants. The inventories are presented in Table 1 and compared for both Pacific and Atlantic Ocean for similar latitudes, these data in the Pacific Ocean are lower that at North Atlantic Ocean, and seem to correspond exclusively to fallout.

The profiles and inventories show that at 94º and 113º western longitude there is no contribution of the local fallout from the Pacific Proving Grounds (PPG) and the French Nuclear Weapons Testingthat were carried out by US at the Marshall islands and by France at Mururoa and Fangataufa atolls.
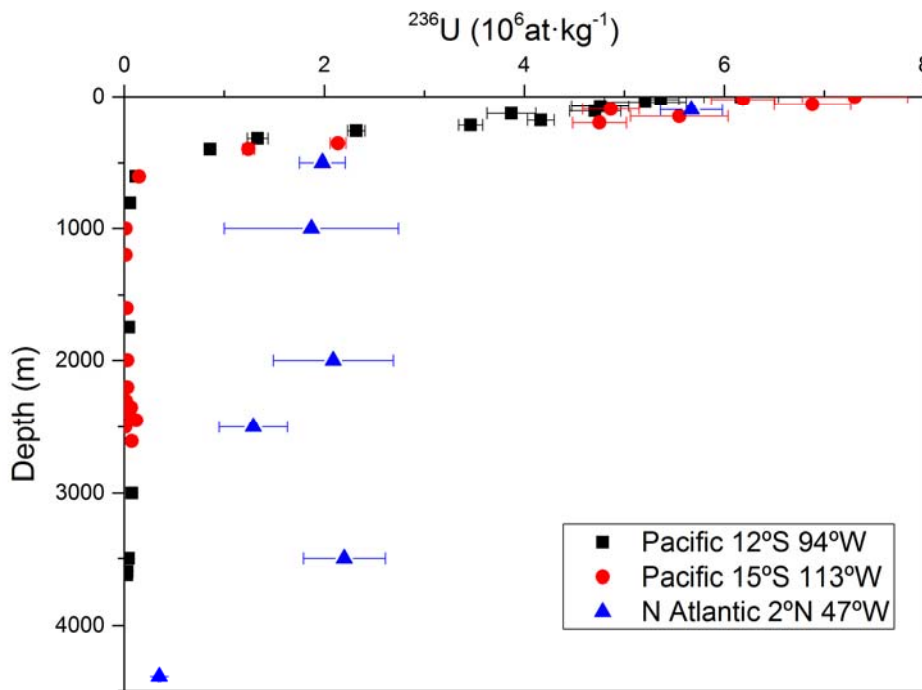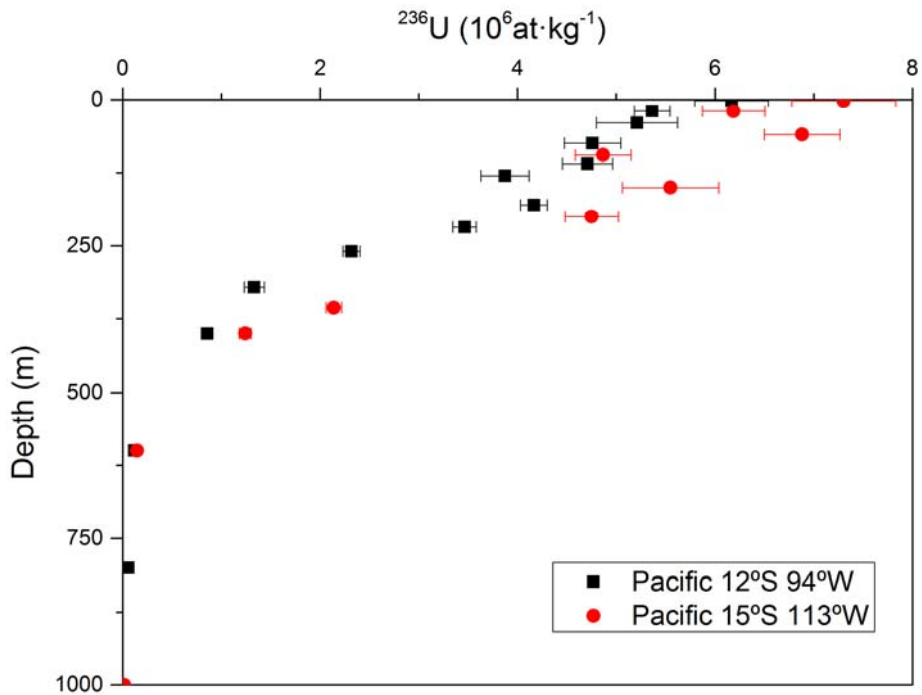

Figure 2.^{236}*U concentrations in i) the two stations from the EPZT. Station 11 (12ºS 94ºW) and station 18 (15ºS 113ºW) and ii) a North Atlantic Station at a close latitude (2ºN 47ºW).*

Figures 3 and 4 showed that most of the samples between 600 and 2000 m presented very low ^{236}U/^{238}U atom ratios, close to the lithogenic/natural ratios (i.e. at the 10^{-12} level). To the best of our knowledge, these AR are the lowest ones measured so far in seawater.

Below 2000 m Figure 4 shows the differences between the Hydrothermal Plume, 113º longitude station, in contrast to the Oxygen Minimum Zone, 94º longitude station.Figure 6 shows the bathymetric profile of the transect and the topography of the bottom ocean in both locations. The hydrothermal plume is originated from a sharp peak around 2500 m; whereas the ocean bottom at the Oxygen minimum zone is flatter and deeper.

Site	LAT ºN	LONG ºW	at m⁻²	Uncert
PacificOcean	12	94	1.45E+12	1E+11
	14.9	113	1.72E+12	1E+11
North Atlantic	18.6	58	1,57E+13	2,94E+12
	2.5	41	7,21E+12	1,68E+12

Table 1. ^{236}U inventories deep depths in two stations from the EPZT, station 11 (12ºS 94ºW) and station 18 (15ºS 113ºW) [this work] and in two stations from the North Atlantic at similar latitudes [Casacuberta et al., 2014].

Figure 4. ^{236}U concentrations in the first 1000 m in two stations from the EPZT. Station 11 (12ºS 94ºW) and station 18 (15ºS 113ºW).
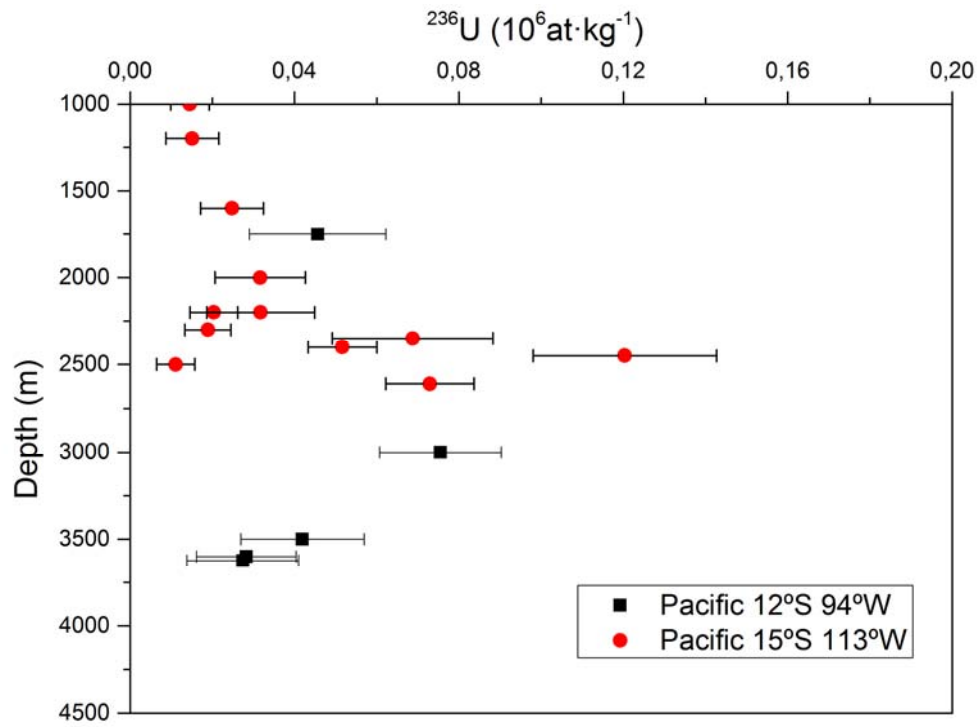
Figure 5. ^{236}U concentrations in deep depths in two stations from the EPZT. Station 11 (12ºS 94ºW) and station 18 (15ºS 113ºW).

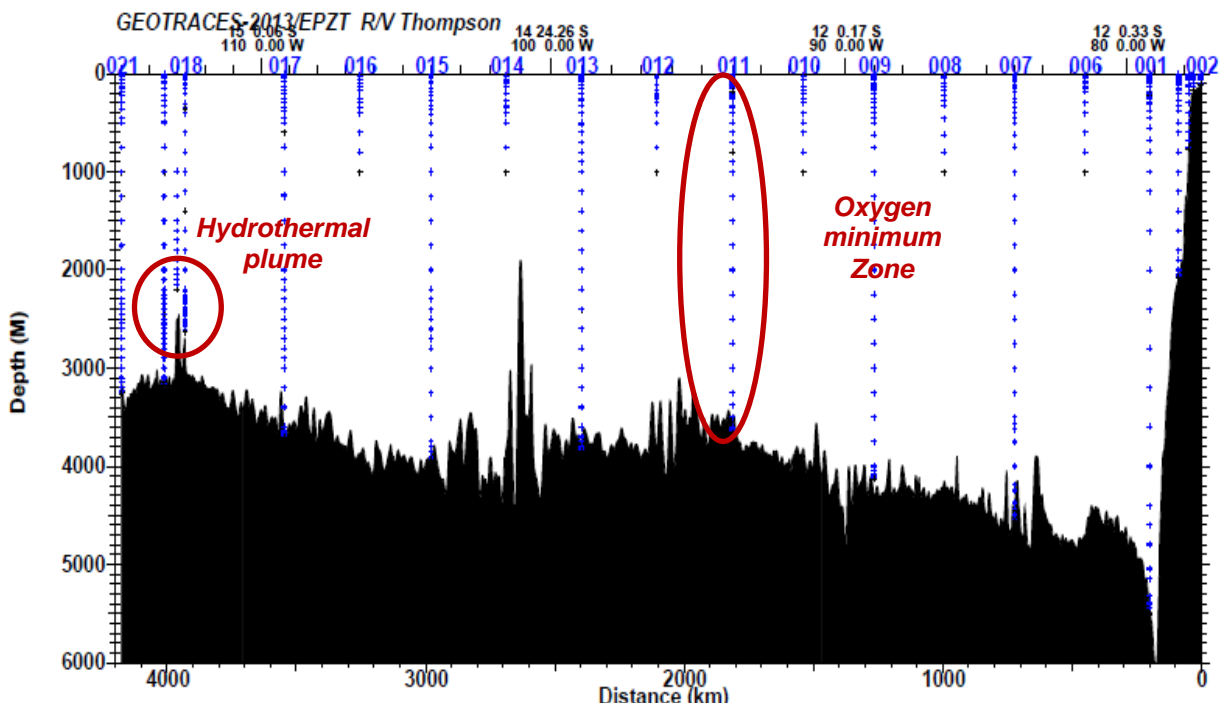**Figure 6.** U.S. GEOTRACES EPTZ Sample distributions: Stations 1-21.

Conclusions

These results show that the AMS ^{236}U technique allows the measurement of ^{236}U/^{238}U down to the lithogenic AR. In the profiles analyzed from the EPZT around the Equatorial Pacific, ^{236}U concentrations and inventories show that the main source of ^{236}U in these locations is global fall-out and no additional sources were identified. These results are key because the profiles are not affected by anthropogenic contributions from the nuclear reprocessing fuel plants (NRFP) and allow the examination of ^{236}U typical water conservative profiles.

References

Casacuberta, N., M. Christl, J. Lachner, M. Rutgers van der Loeff, P. Masqué, and H.-A. Synal (2014), A first transect of ^{236}U in the North Atlantic Ocean, *Geochim Cosmochim Ac*, *133*, 34-46.

Casacuberta, N., P. Masqué, G. Henderson, M. Rutgers van-der-Loeff, D. Bauch, C. Vockenhuber, A. Daraoui, C. Walther, H. A. Synal, and M. Christl (2016), First ^{236}U data from the Arctic Ocean and use of ^{236}U/^{238}U and 129I/236U as a new dual tracer, *Earth Planet Sc Lett*, *440*, 127-134.

Chamizo, E., M. Christl, and L. K. Fifield (2015), Measurement of ^{236}U on the 1 MV AMS system at the Centro Nacional de Aceleradores (CNA), *Nuclear Instruments and Methods in Physics Research Section B: Beam Interactions with Materials and Atoms*, *358*, 45-51.

Christl, M., J. Lachner, C. Vockenhuber, O. Lechtenfeld, I. Stimac, M. R. van der Loeff, and H. A. Synal (2012), A depth profile of uranium-236 in the Atlantic Ocean, *Geochim Cosmochim Ac*, *77*, 98-107.

Christl, M., C. Vockenhuber, P. W. Kubik, L. Wacker, J. Lachner, V. Alfimov, and H. A. Synal (2013), The ETH Zurich AMS facilities: Performance parameters and reference materials, *Nuclear Instruments and Methods in Physics Research Section B: Beam Interactions with Materials and Atoms*, *294*, 29-38.

Christl, M., et al. (2015), Status of 236U analyses at ETH Zurich and the distribution of 236U and 129I in the North Sea in 2009, *Nuclear Instruments and Methods in Physics Research Section B: Beam Interactions with Materials and Atoms*, *In Press, Corrected Proof*.

Ketterer, M. E., K. M. Hafer, C. L. Link, C. S. Royden, and W. Hartsock (2003), Anthropogenic U-236 at Rocky Flats, Ashtabula river harbor, and Mersey estuary: three case studies by sector inductively coupled plasma mass spectrometry, *J Environ Radioactiv*, *67*(3), 191-206.

López-Lora, M., E. Chamizo, M. Villa-Alfageme, S. Hurtado, N. Casacuberta, and M. García-León (In review), Sequential separation of uranium and plutonium and application to 236U and 239Pu-240Pu measurement in low-volume seawater samples by AMS, *Talanta*.

Marsden, O. J., F. R. Livens, J. P. Day, L. K. Fifield, and P. S. Goodall (2001), Determination of U-236 in sediment samples by accelerator mass spectrometry, *Analyst*, *126*(5), 633-636.

Nomura, T., et al. (2017), Reconstruction of the temporal distribution of 236U/238U in the Northwest Pacific Ocean using a coral core sample from the Kuroshio Current area, *Mar Chem*, *190*, 28-34.

Quinto, F., E. Hrnecek, M. Krachler, W. Shotyk, P. Steier, and S. R. Winkler (2013), Measurements of U-236 in Ancient and Modern Peat Samples and Implications for Postdepositional Migration of Fallout Radionuclides, *Environ Sci Technol*, *47*(10), 5243-5250.

Richter, S., A. Alonso, Y. Aregbe, R. Eykens, U. Jacobsson, F. Kehoe, H. Kuehn, A. Verbruggen, and R. Wellum (2010), Certification of a new series of gravimetrically prepared synthetic reference materials for n(U-236)/n(U-238) isotope ratio measurements, *Nucl Instrum Meth B*, *268*(7-8), 956-959.

Sakaguchi, A., A. Kadokura, P. Steier, Y. Takahashi, K. Shizuma, M. Hoshi, T. Nakakuki, and M. Yamamoto (2012), Uranium-236 as a new oceanic tracer: A first depth profile in the Japan Sea and comparison with caesium-137, *Earth Planet Sc Lett*, *333*, 165-170.

Sakaguchi, A., K. Kawai, P. Steier, F. Quinto, K. Mino, J. Tomita, M. Hoshi, N. Whitehead, and M. Yamamoto (2009), First results on (236)U levels in global fallout, *Sci Total Environ*, *407*(14), 4238-4242.

Scognamiglio, G., E. Chamizo, J. M. López-Guitiérrez, A. M. Müller, S. Padilla, F. J. Santos, M. López-Lora, C. Vivo, and M. García-León (2016), Recent developments of the 1 MV AMS facility at the Centro Nacional de Aceleradores, *Nuclear Instruments and Methods in Physics Research Section B: Beam Interactions with Materials and Atoms*.

Steier, P., et al. (2008), Natural and anthropogenic (236)U in environmental samples, *Nucl Instrum Meth B*, *266*(10), 2246-2250.

Wendel, C. C., D. H. Oughton, O. C. Lind, L. Skipperud, L. K. Fifield, E. Isaksson, S. G. Tims, and B. Salbu (2013), Chronology of Pu isotopes and U-236 in an Arctic ice core, *Sci Total Environ*, *461*, 734-741.

Winkler, S. R., P. Steier, and J. Carilli (2012), Bomb fall-out U-236 as a global oceanic tracer using an annually resolved coral core, *Earth Planet Sc Lett*, *359*, 124-130.

Levels of natural radionuclides in water and sediments from mining lakes in sweden

Mantero J. [1,3,]*, *Thomas R.* [1] , *Isaksson M.* [1], *Rääf C.* [2], *Perez-Moreno S.* [4], *Forssell-Aronsson E.* [1], *Holm E.* [1], *García-Tenorio R* [3,5]

[1] Dept. of Radiation Physics. Institute of Clinical Sciences. Salhgrenska Academy at University of Gothenburg, Gothenburg, Sweden
[2] Medical Radiation Physics, Department of Translational Medicine, Lund University, Malmö, Sweden
[3] Department of Applied Physics II, E.T.S.A., University of Seville, Seville, Spain
[4] Group of Radiation physics and Environment, University of Huelva, Huelva, Spain
[5] Spanish National Accelerator Centre, University of Sevilla, Spain
*Author for correspondence: manter@us.es

1. Introduction

The effect of mining activities in a country as Sweden (the major metal mining country in the European Union) implies enormous quantities of generated mining wastes. Historically, more than 2700 mines gather around 30000 sites that have been minor mines and quarries (according to the database of Geological Survey of Sweden, SGU [Norlin, 2016]). In 1950, there were around 100 active mines while nowadays no more than 15 active mines still remains with ongoing extractions. Many of these sites had opencast mines. During exploitation by open-pit mining, the water table is suppressed to avoid the flooding of active mines. However, when mining activity ceases, the water table recovers its original position, flooding the open pits and giving rise to mine pit lakes.

The environmental problem arises because these waters can be affected by Acidic Mine Drainage (AMD), having high/very high concentration of heavy metals in solution. Apart from the impact to the ecosystem, many of these places are nearby populated areas and most of these water bodies are usually used for recreational purposes (swimming, fishing, diving...) by inhabitants of these former mining areas.

Many works have been conducted to investigate the limnological and geochemical features of a pit lake [Castro, 1998; Stevens and Laurence, 1998; Shevenell, 2000; Ming Lu, 2004] measuring several parameters in waters (pH, temperature, conductivity, dissolved oxygen (DO) or redox potential among others), and the metal concentration. Another group of works with pit lakes are devoted to the study of the remediation of its acid/contaminated waters [Fischer and Guderitz, 1996; Lewis et al., 2003] where the neutralization of lakes is obtained by addition of bases, such as lime, caustic soda or alkaline material. However, really little bibliography can be found about pit lakes all over the world focusing their attention on naturally occurring radionuclides, coming mainly from ^{238}U and ^{232}Th series.

Based on previous experiences in Spanish pit lakes [Manjón et al., 2013; Manjón et al., 2014], it was shown that an enhancement on levels in natural radionuclides can occur at these sites. As an example, a non affected water should have around 15 to 30 mBq/L of ^{238}U while in these sites there was ^{238}U ranging from 14 to 1110 mBq/L what implies up to 50 times higher than environmental level. This was directly related to the AMD processes at these sites.

This work will try to add more data to this framework, through the measurement of levels of activity concentration in waters and sediments from these special water bodies.

2. Materials and Methods

Samples

There were two sampling campaigns (Figure 1. Left). During the 1st sampling (March 2015), a set of 23 sites in Central and Southern Sweden (mainly old mines/quarrels from 18th and 19th century) were sampled. A total of 25 superficial waters and 23 sediment/rocks were sampled in this stage. A second sampling (July 2015) in Northern Sweden (with bigger pit lakes in mining areas from the 20th century with less interaction of humans) a total of 20 sites provided 46 superficial waters and 34 sediment/rocks.

The radiometric characterization was carried out via Alpha spectrometry (to be applied in water and sediment) and Gamma spectrometry (to be applied in sediments).

Radiometric technique: alpha spectrometry

In order to apply this technique, samples need to be pretreated to isolate the element of interest and finally, alpha sources are produced in steel disks for U/Th and copper for Po measurements. U isotopes will be ^{238}U, ^{235}U and ^{234}U. Th ones are ^{232}Th and ^{230}Th while ^{210}Po is the only measured isotope of Po.

Depending on the matrix, samples will require different process:
Water samples (~ 0.5 L) were firstly acidified at pH ~2 and spiked with a known amount of tracers (^{232}U, ^{229}Th and ^{209}Po). Pre-concentration of radionuclides in water samples was carried out through the iron hydroxide precipitation. Then the isolation process was performed using UTEVA resins and finally U, Th fractions were electroplated separately in steel disks while Po fraction followed an instant deposition process using silver disk. For more details about this treatment check [Lehritani et al, 2012].

Sediment/rock samples (~ 1 g) were digested using a microwave (Multiwave 3000), from Anton Paars, equipped with a rotor (eight closed vessels) which allows us to work under controlled pressure until 260ºC without the losses of any volatile element during the digestion process. Once the samples were digested, solutions follow an iron hydroxide precipitation process. Separation process was performed via TBP and finally alpha sources prepared in the same way than for water samples.
Measurement were performed with a Canberra Alpha-Analyst system using Passivated Implanted Planar Silicon (PIPS) detectors with independent counting chambers for U, Th and Po. In 240000s measurements, this system provide a MDA (Minimum Detectable Activity) of 0.5 mBq for most of the isotopes.

Radiometric technique: gamma spectrometry

The radionuclides to be measured by γ-spectrometry are, belonging to ^{238}U series: ^{210}Pb (45.6 keV), ^{234}Th (63.3 keV), ^{226}Ra will be determined by secular equilibrium using the γ-ray emissions of ^{214}Pb (351.9 and 295.2 keV) and ^{214}Bi (609.3, 1120.3, 1238.1 and 1764.5 keV). Also ^{234}Pa (1001.0 keV) will be measured when possible (due to its very low gamma yield). Regarding ^{232}Th series: ^{228}Ra can be obtained via ^{228}Ac (338.3, 911.2 and 968.9 keV). ^{228}Th activity concentrations will be determined through emissions of ^{212}Pb (238.6 keV), ^{212}Bi (727.3 keV) and ^{208}Tl (583.2, 860.6 and 2614.5 keV). Isotopes from ^{235}U series, with an activity concentration around 20 times lower than

isotopes from the ^{238}U one, will be seldom detected, but in such a cases, the γ-lines used for its measurements are: ^{227}Th(50.1 and 235.9 keV), ^{235}U (163.4, 205.3 keV). Also, the ^{40}K activity concentration was determined directly from its emission line at 1460.8 keV and the anthropogenic ^{137}Cs from 661.67 keV.

In case of Sediment/rocks, samples were dried, grinded and then packaged in Petri disk. Samples were sealed and storaged for 3/4 weeks before being measured in order to reach secular equilibrium between ^{226}Ra and its daughter. Measurements were carried out with an extended range Germanium coaxial detector (XtRa) of 37.1% relative efficiency and 1.76 keV resolution. This system has a 10 centimetres passive shielding of ancient lead and an active shielding made with an organic scintillation detector (Bicron BC-418) that works in anti-coincident mode with the Ge detector resulting in very low background level [Hurtado et al., 2007]. In 200000s measurements, this system provide a MDA of 0.55Bq for ^{210}Pb (45.6 keV), 0.38 Bq for ^{214}Pb (351.9 keV), 0.30 Bq for ^{214}Bi (609.3 keV) or 1.62 Bq for ^{40}K (1460.8 keV) among others radionuclides of interest.

In situ measurements

Once at the different sites, an external dose measurement was performed at every place with two independent detectors that were placed 1 m above the ground during the sampling time. The final result was an average over 15 to 20 minutes for each site. The equipment was a Rados SRV 2000 Compensated GM-tube with an energy range: 50 keV - 3 MeV and a dose rate range: 0.05 µSv/h - 10 Sv/h.

Also a physicochemical characterization was carried out immediately after superficial water was collected. Measurement of temperature (T), pH, Dissolved Oxygen (DO), Oxidation-Reduction Potential (ORP), Specific Conductivity (spC), Total Dissolved Solids (TDS) and Salinity where performed just after superficial water collection using a Hydrolab M5 multiparametric probe.

Results and Discussion

The environmental external gamma dose measurements average 0.11±0.06µSv/h ranging from 0.05 to 0.37 µSv/h. The external exposure rates from terrestrial gamma radiation in Sweden according to [Unscear 2000] is 0.056 µSv/h with a range 0.04 to 0.50 µSv/h. In this sense, our measurements are within the expected values, however, several sites were identified for having external dose values three times above the average.

Results in waters

Regarding pH in superficial waters, values ranging from 4.4 to 9.33 with an average of 7.46±0.94 (one sigma criteria for standard deviation) were found, what implies neutral waters and not many problems due to ADM. It is worth to mention here that, due to several remediation projects in acid/contaminated waters [Boliden, 2015], the neutralization of lakes is obtained by addition of bases, such as lime, caustic soda or alkaline material. This has changed the chemistry of many of these water bodies, especially in the Northern areas.

In pit lakes in Spain [Manjón et al., 2013; Manjón et al., 2014], pH was in the range 2 to 3.5 (extremely acidic waters) finding up to 1110 mBq/kg of ^{238}U. In Morocco [Mantero et al, 2015] it was found a pH range from 8 to 9.5 (alkaline waters) in former mining lakes, with values of ^{238}U up to 1037mBq/kg. Alkaline pH values and elevated bicarbonate concentrations favour the stabilization

and mobilization of uranium as uranyl-carbonate complex, [Abdelouas et al.1998]. In contrast, the predominant species in acid, oxygenated waters are the uranyl ion and uranyl-sulfate complex [Wanty et al. 1999]. Attending to Figure 1.Right, it has been found moderate levels of ^{238}U up to 1183 mBq/kg (pH 5.9) in Sweden what implies different uranium chemistry more associated to bicarbonate complexes.
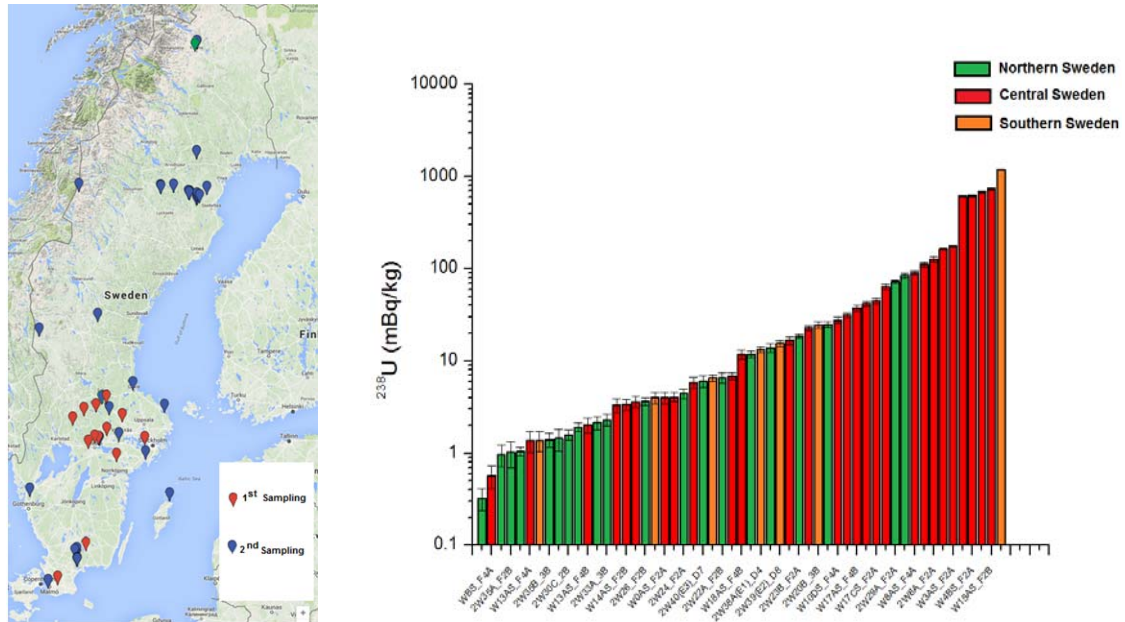
Figure 1. *(Left) Sampling map. (Right) ^{238}U activity concentration in superficial waters from pit lakes in Sweden.*

The 74% of the studied pit lakes have environmental levels regarding U isotopes, however 26% are above 50mBq/kg having some enhancement in U elements. It is observed a clear ^{234}U/^{238}U ratio higher than one, typical of water bodies interacting with underground waters.

Table 1 summarizes the values obtained by alpha spectrometry in these waters finding out environmental levels for Th and Po isotopes in all cases. It is well-known the tendency of U for being in mobile phases while Th and Po remains into the original matrices fixed to the bedrock. This behaviour is reflected in these data.

Radionuclide	Average (mBq/kg)	Range (mBq/kg)
^{238}U	94	0.3-1183
^{234}U	125	0.3-1700
^{230}Th	3.1	MDA-26
^{210}Po	5.9	1.1 -22

Table 1. *Summary of results in superficial waters for radionuclides belonging to ^{238}U series.*

Regarding ^{232}Th activity concentration in superficial waters, results were even lower that the ones of ^{230}Th. The MDA for this nuclide is 0.5 mBq/kg being 46% of the samples below this threshold. ^{232}Th ranges from MDA to 8.8 ±2.7 mBq/kg.

Results in sediments and rocks

Secular equilibrium in natural series was measured (via gamma spectrometry) in 93% of sediments and 100% of the rocks. In case of ^{238}U series: ^{234}Th, ^{234}Pa, ^{214}Bi, ^{214}Pb and ^{210}Pb had the same activity concentration. The same results among ^{228}Ac, ^{212}Pb, ^{212}Bi and ^{208}Tl from ^{232}Th series and also secular equilibrium between ^{235}U and ^{227}Th. These results have been summarized in Table 2 where also ^{137}Cs and ^{40}K are added.

According to [Unscear 2000] the natural radionuclide content (Bq/kg) in soils in Sweden is: ^{226}Ra from 12-170, ^{232}Th from 14-94 and ^{40}K from 560-1150. All these ranges include most of the results for sediments of Table 2 except for one site with higher U and Th values. At this site, there was collected a rock having 467±35 Bq/g for ^{238}U series, 22±3 Bq/g for ^{232}Th series, 16±3 Bq/g for ^{235}U series and 1.43±0.2 Bq/g for ^{40}K.

(Bq/kg)	SEDIMENTS (n=12)		ROCKS (n=13)	
	Average	**Range**	**Average**	**Range**
^{238}U serie	277	10-1518	54*	3-467000
^{232}Th serie	63	7-173	52*	4-22000
^{235}U-serie		MDA-79		MDA-16000
^{137}Cs		MDA-6		MDA
^{40}K	710	56-1405	826	2-2443

Table 2. Activity concentration (Bq/kg) in sediments for natural radionuclides (and ^{137}Cs) via gamma (n represents the number of analyzed samples).
(*)For these averages, the rock with 467Bq/g for ^{238}U and 22Bq/g for ^{232}Th was not included.

Several sites have been identified for having moderate levels of natural radionuclides and one of them require a more detailed study due to very high activity concentration values and because it's a well known place where local inhabitants.

Conclusions

A study on the levels of natural radionuclides in pit lakes in Sweden has been carried out in places where local inhabitants interact with former mining lakes. Regarding water samples, Th and Po isotopes were found at environmental levels in these water bodies while several sites in central Sweden were found with enhanced levels of U isotopes. These sites require further investigations mainly focused in U isotopes in order to carry out dose assessments. Concerning sediments/rocks, most of the results are included within the range of typical values in Sweden except for several sites. In one particular place (frequently used by local people for recreational purposes) very high levels were found of natural radionuclides.

Acknowledgement

References

[Allan, 1995] Allan,R.,1995 Introduction: sustainable mining in the future. Journal of Geochemical Exploration, 52:1-4

[Allgaier, 1997] Allgaier, F. K., 1997 Environmental Effects of Mining.In: Marcus, J.J. (Editor), Mining Environmental Handbook-Effects of Mining on the Environment and American Environmental Controls on Mining. Imperial College Press, Singapore, pp. 132-189. ISBN: 1-86094-029-3

[Boliden, 2016] Personal communication with Boliden stuff during 2016.

[Castro, 1998] Castro, J.M.,1998 Pit Lakes: Their Geochemistry and the Potential for their Remediation. PhD Thesis, University of Montana.

[Castro et al., 1999] Castro, J.M., Wielinga, B. W., Gannon, J. E. and Moore, J., 1999. Stimulation of sulfate-reducig bacteria in lake water from a former open-pit mine hrough addition of organic wastes. Water Environment Research, 71(2): 218-223

[Fischer and Guderitz, 1996] Fischer, R. and Guderitz, T., 1996. Concepts of chemical and biological remediation of acidic iron-containing lakes in mining areas. Wiss Z Tech Univ Dresden, 45:85-89.

[Gustaffsson et at, 1999] Gustaffsson, H. E., M., L., Lindahl, L. A., Eriksson, N., Jönsson. H., Broman, P. G. and Göransson, T., 1999. The Swedish acid mine drainage experience: Research, development and practice. In: Azcue, J. M. (Editor), Environmental Impacts of Mining Activities: Emphasis on Mitigation and Remedial Measured. Springer-Verlag, Berlin, Germany, pp. 203-228.

[Lewis et al., 2003] Lewis, N. M., Wangerud, K. W., Park, B. T., Fundingsland, S. D. and Jonas, J. P., 2003. Status of in situ treatment of Anchor Hill Pit Lake, Gilt Edge mine superfund site, South Dakot, USA. In: Proceedings of 6th International Conference Acid Rock Drainage. Caims, Aueensland, Australia, The Australasian Institute of Mining and Metallurgy, 779-788, ISBN: 1-875776-98-2.

[Logan et al., 2003] Logan, M., Ahmann.D. and Figueroa, L., 2003. Assessment of microbial activity in anaerobic columns treating synthetic mine drainage. In: Proceedings of 2003 Natural Meeting of the American Society of Mining and Reclamation and the 9th Billins Land Reclamation Symposium. Billings, MT, ASMR.

[Ming Lu, 2002] Lu, M., 2002. Aqueous Geochemistry of Pit Lakes- two Cases Studies at Rävlidmyran and Udden, Sweden. Licentiate, ISSN: 1402-1757 ISRN: LTU-LIC—02/59—SE Thesis, Lulea University of Technology, Lulea.

[Ming Lu, 2004] Lu, M., 2004. Pit Lakes from Sulphide Ore Mining, Geochemical and Limnological Characterization before Treatment, after Liming and Sewage Sludge Treatments. PhD Thesis, Lulea University of Technology, Lulea.

[Manjon et al., 2013] G.Manjón, J.Galván, J. Mantero, I. Díaz and R.García-Tenorio. NORM levels in pit lakes located in south-west of Spain. 7th International Symposium on naturally Occurring Materials (NORM VII), Beijing (China), 22-26 Abril 2013. ORAL communication

[Manjon et al., 2014] G. Manjón, J. Galván, J. Mantero, I. Díaz and R. García-Tenorio. "NORM levels in Spanish pit lakes and their impact in neighboring environments". International Conference on Radioecology & Environmental Radioactivity (ICRER), Barcelona (Spain), 7–12 September 2014. Poster communication.

[Norlin, 2016] Lars Norlin, SGU (Swedish Geological Survey), personal communication, 2016.

[Shevenell, 2000] Shevenell L. A.,2000. Water quality in pit lakes indisseminated gold deposits compared to two natural, terminal lakes in Nevada. Environmental G39(7): 807-815

[Stevens and Lawrence, 1998] Stevens, C. L. and Lawrence, G. A., 1998. Stability and meromixis in a water-filled mine pit. Limnology and Oceanography, 43(5): 946-954.